The copyright of this thesis vests in the author. No quotation from it or information derived from it is to be published without full acknowledgement of the source. The thesis is to be used for private study or non-commercial research purposes only.

Published by the University of Cape Town (UCT) in terms of the non-exclusive license granted to UCT by the author.

University of Cape Town

HYDRAULIC CONVEYANCE OF SOLID CAPSULES

A THESIS

FOR THE DEGREE OF

DOCTOR OF PHILOSOPHY

by

J.H. Lazarus, B.Sc.(Eng.), M.Sc.(Eng.)

The copyright of this thesis is held by the University of Cape Town.
Reproduction of the whole or any part may be made for study purposes only, and not for publication.

Copyright by the
University of Cape Town
April 1972

A C K N O W L E D G E M E N T S

I wish to express my gratitude to Associate Professor F.A. Kilner, Supervisor of this thesis, for his most valuable and enthusiastic criticism and encouragement, as well as his helpful suggestions and interest in the project.

I should also like to show my appreciation to Professor M.F. Kaplan for his interest and help in raising funds for equipment, and to Professor G. v.R. Marais for his consistent encouragement.

Dr. J.L.N. Besseling helped with the design of a differential transformer for clearance measurement.

Mr. E.A.Mitchley, Mr. R.F. Beverton and Mr. P.W. Duxbury, technicians in the department of Civil Engineering, helped with the manufacture of experimental equipment.

I should also like to thank Mrs. M.I. Cousins, Miss B. Spalding and Miss L. Jennings who typed the manuscript and had to contend with my hand writing and spelling.

This work could not have been accomplished without the help of the Univac 1106 computer, to whom I have come to attribute anthropomorphic qualities, occasionally malevolent.

D E C L A R A T I O N

The work for this thesis represents the research activities of the author from 1967 to 1972 and was performed in the Hydraulics laboratory of the University of Cape Town. It embodies only the original work of the author, except where otherwise stated, and no part of it has been presented to any other University.

Signed by candidate

J.A. Lazarus
20 April 1972

ABSTRACT

The hydraulics of two phase flow of capsule - liquid mixtures is investigated experimentally and analytically.

The technology of hydraulic transportation of solid capsules in pipes is advanced to the point of practical feasibility by the development and successful operation of experimental equipment in the laboratory. This involves the innovation of aspects of the technology concerned, such as novel booster pumps, injectors and metering equipment.

The effect of independent variables such as capsule geometry, density, roughness and concentration as well as mean water velocity and pipe inclination are investigated. It is shown to what extent these variables affect the dependent variables.

A theoretical analysis is presented for the determination of dependent variables, such as capsule velocity, excess energy and power dissipation.

Flow conditions around static capsules are shown to be amenable to analysis, supplemented by experimentally determined coefficients.

Energy dissipation at the inlet and outlet of static concentric and eccentric capsules is investigated for the first time, and empirical formulations are presented which are simple and consistent with all the data.

A correlation involving a pseudo hydraulic mean radius for analysing the friction head loss in eccentric annuli is presented. There have been numerous investigations concerned with friction head losses in concentric annuli. However, the correlation presented in this thesis is simpler than those given by other investigators and incorporates a wide range of experimental data satisfactorily.

A theoretical analysis for flow in annuli of varying eccentricity is also presented in a novel manner and agreement with experiment is evidenced.

A study is presented of incipient conditions of capsule motion which indicates a form of empirical equation for excess energy dissipation when capsules are moving.

The incipient analysis also yields the velocity at which capsules begin to move. Experiments with mobile capsules support this formulation and, in addition, yield a linear relation between mean water velocity and capsule velocity. When extrapolated, the line confirms the water velocity at incipient capsule motion, previously obtained by analysis of the static case.

A non-dimensional method of correlating the parameters involved in capsule kinematics is presented.

Laminar flow in the annulus of a concentric mobile capsule is analysed, and the shear stress and mean annular velocity are found to consist of two components; a pressure component due to flow through the static annulus, and an additional Couette component due to the motion of the capsule relative to the pipe wall.

The theory is extended to eccentric annuli and laminar or laminar-turbulent flow by the introduction of a finite element method of analysis.

The concept of curved cylindrical Couette flow is introduced and this component is analysed by the finite element method and quasi concentric polar co-ordinates, which is a method introduced for analysing the flow in eccentric annuli with stationary or mobile capsules.

The analysis is further extended to cover capsules of finite length.

An alternative analysis for eccentric mobile capsules is also presented, wherein the shear stress on capsule and pipe walls are considered separately.

The effect of eccentricity, diameter ratio and other parameters on the force components exerted on static and mobile capsules is analysed.

The distribution of shear stress and velocity components around the perimeter of the capsule is determined theoretically.

It is shown that at high velocities capsules (of density greater than the liquid) lift off the pipe bottom, and capsule to wall clearance is determined as a function of diameter ratio, capsule density and velocity. The mechanisms of capsule lift are discussed.

As well as an analytical determination of excess energy dissipation

across mobile capsules, an empirical formulation is presented, which is justified by considering ratios of forces on capsules.

The non-dimensional parameters for excess energy and capsule velocity are developed into a power equation.

The effect of independent variables on power dissipation for mobile capsules, as well as incipient power, is determined.

The power requirements for a capsule transportation system are optimised and a ψ-parameter is introduced, representing the energy per kg m, which is minimised for design purposes. Examples of design charts are presented.

Capsule transportation is compared with two phase particulate flow and the energy dissipation for capsule conveyance is shown to be less than for heterogeneous flow in the most economical zone and comparable with pseudo-homogeneous and non-Newtonian flow.

In conclusion, the contributions made in this thesis to the science and technology enable a capsule transportation system to be designed with confidence.

HYDRAULIC CONVEYANCE OF SOLID CAPSULES

LAYOUT OF THESIS

P A R T I *Survey of the field of capsule transportation*

CHAPTER 1 INTRODUCTION
CHAPTER 2 LITERATURE REVIEW
CHAPTER 3 TECHNOLOGY

P A R T II *Experimental Equipment*

CHAPTER 4 APPARATUS
CHAPTER 5 EXPERIMENTAL PROCEDURE
CHAPTER 6 MEASUREMENTS AND ERRORS

P A R T III *Theoretical considerations*

CHAPTER 7 THEORETICAL ANALYSIS OF FLOW AROUND CAPSULES
CHAPTER 8 FORCES ON CAPSULES

P A R T IV *Experimental Results and Discussion*

CHAPTER 9 HEAD LOSSES ACROSS STATIC CAPSULES
CHAPTER 10 CAPSULE KINEMATICS
CHAPTER 11 ENERGY DISSIPATION ACROSS MOBILE CAPSULES
CHAPTER 12 CAPSULE TO WALL CLEARANCE

P A R T V *Comparison of experimental and analytical results*

CHAPTER 13 STATIC CAPSULES
CHAPTER 14 INCIPIENT CAPSULE MOTION
CHAPTER 15 MOBILE CAPSULES

P A R T VI *Power considerations*

CHAPTER 16 POWER REQUIREMENTS
CHAPTER 17 OPTIMISATION
CHAPTER 18 COMPARISON OF SEDIMENT AND CAPSULE TRANSPORTATION

CHAPTER 19 CONCLUSIONS

APPENDIX I CAPSULE FREE PIPE TESTS
APPENDIX II DISCUSSION OF SOME OF THE MAIN COMPUTER PROGRAMMES

BIBLIOGRAPHY

C O N T E N T S

	page
ACKNOWLEDGEMENTS	ii
DECLARATION	iii
ABSTRACT	iv
LAYOUT OF THESIS	vii
CONTENTS	viii
NOTATION	xvii

P A R T I SURVEY OF THE FIELD OF CAPSULE TRANSPORTATION

CHAPTER 1 INTRODUCTION (pp 1.1 - 1.9)

1.	Statement of the problem	1.1
2.	Definition of capsule	1.2
3.	Validation of the study	1.3
3.1	Sediment transport : Existing schemes	1.3
3.2	Type of material transported	1.4
4.	Advantages of hydraulic transport of solids	1.5
5.	Disadvantage of transportation in slurry form	1.6
6.	The advantages of capsule transportation	1.7
7.	Objectives	1.9

CHAPTER 2 LITERATURE REVIEW (pp 2.1 - 2.34)

CHAPTER 3 TECHNOLOGY (pp 3.1 - 3.15)

1.	The preparation of capsules	3.1
2.	Injection of capsules	3.3
2.1	Injection under positive pressure	3.3
2.2	Injection at atmospheric pressure	3.6
3.	Recovery of capsules	3.7
4.	The pumping of capsules	3.8
5.	Pipeline layout systems	3.13

P A R T II EXPERIMENTAL EQUIPMENT

CHAPTER 4 APPARATUS FOR EXPERIMENTS (pp 4.1 - 4.33)

1.	The open and closed system	4.1
2.	Merits of the two systems	4.1
3.	Advantages of the closed system	4.2
4.	The open circuit	4.2

		page
4.1	The pipeline	4.3
4.2	The injector	4.3
4.3	Recovery box	4.6
4.4	The support system	4.6
4.5	Flow measuring device	4.7
4.6	Veriflux flow meter	4.8
4.7	Differential pressure measurement	4.10
4.8	The timer	4.14
5.	The closed circuit	4.15
6.	Description of the closed circuit	4.17
6.1	The pump	4.18
6.2	Pipe bends	4.19
6.3	Flow measurement	4.19
6.4	Pressure transients and capsule velocity	4.19
6.5	Orientation	4.19
6.6	Cooling water	4.20
7.	Apparatus for static capsule tests	4.20
8.	Other pipelines used	4.21
9.	Apparatus for measuring capsule clearance	4.23
10.	Capsules tested	4.25

CHAPTER 5 EXPERIMENTAL PROCEDURE (pp 5.1 - 5.13)

1.	Procedure when using the open circuit	5.1
2.	Calibration of flowmeter	5.2
3.	Calibration of differential pressure meter	5.2
4.	The digital timer	5.4
5.	Levelling the support beam	5.4
6.	Procedure for performing a test run in the open circuit	5.5
7.	The closed circuit	5.8
8.	Procedure for determining the coefficient of friction between capsule and pipe wall	5.8
9.	Procedure for determining incipient velocity	5.9
10.	Procedure for carrying out acceleration experiments	5.9
11.	Procedure for clearance measurement	5.11
11.1	Calibration of differential transformer	5.11
11.2	Experimental procedure for clearance measurement	5.12

CHAPTER 6 MEASUREMENTS AND ERRORS (pp 6.1 - 6.13)

1.	The mean flow velocity in the pipe	6.2
2.	Capsule velocity	6.3
3.	Friction head loss due to water alone	6.4
4.	Excess head loss due to presence of capsule	6.4
5.	Real hydraulic grade line transient	6.5
6.	Real hydraulic grade line transient due to capsule - second definition	6.7
7.	Accuracy of measuring excess head loss due to capsule	6.9
8.	The measurement of clearance	6.12

P A R T III THEORETICAL CONSIDERATIONS

CHAPTER 7 THEORETICAL ANALYSIS OF FLOW AROUND CAPSULES (pp 7.1 - 7.127)

		page
1.	Introduction to the analysis of the flow of solid capsules in a pipeline	7.1
1.1	Statement of the problem	7.3
1.2	Flow in the annulus of a mobile capsule	7.4
1.3	Layout of the rest of the chapter	7.7
2.	Geometry of the eccentric annulus	7.7
2.1	Bi-polar co-ordinates	7.8
2.2	Quasi concentric polar co-ordinates	7.10
2.3	Comparison of bi-polar co-ordinates with quasi-concentric polar co-ordinates	7.13
3.	Static capsules	7.14
3.1	Applicability	7.14
3.2	The object of studying static capsules	7.15
3.3	Definition of energy loss for a static capsule	7.16
4.	Flow in the annulus	7.18
4.1	Applicability to the capsule problem	7.18
4.2	Dimensional analysis	7.19
4.3	Conventional approach and reasons for inapplicability	7.19
5.	Shear distribution in concentric annulus due to pressure flow	7.21
6.	Laminar flow in a pipe with a stationary concentric annulus	7.23
6.1	Theory of laminar flow in concentric annulus	7.23
6.2	Rate of flow through the annulus	7.27
7.	Laminar flow in eccentric annulus	7.28
7.1	Annalysis of laminar flow in eccentric annulus	7.31
8.	Turbulent flow in annuli	7.31
9.	Turbulent flow in concentric annuli (Review)	7.32
9.1	Friction factor	7.32
9.2	Radius of maximum velocity	7.41
9.3	Radius of maximum velocity in eccentric annulus	7.44
9.4	Velocity distribution in annuli	7.44
9.5	Velocity distribution in concentric annuli	7.45
10.	Turbulent flow in eccentric annular ducts	7.53
10.1	Friction factor in eccentric annuli	7.54
10.2	Velocity profile in eccentric annuli	7.56
10.3	Circumferential pressure variation and entrance lengths	7.58
10.4	Summary	7.58
11.	Present experiments and analysis of flow in the annulus	7.59
11.1	Empirical approach from present experimental results	7.60
12.	Analytical verification of annular head loss relations	7.61
12.1	Determination of radius of maximum velocity	7.62
12.2	Determination of velocity distributions	7.63
12.3	Flow in eccentric annulus	7.64
13.	Reynolds number in annular flow	7.64
14.	Procedure for analysing turbulent flow in the eccentric annulus	7.66
15.	End effects	7.69
15.1	Static capsule-inlet energy loss	7.69
15.2	Energy losses at outlet	7.70
16.	Incipient motion	7.70
16.1	Momentum and energy principles applied to incipient conditions	7.71
16.2	Equation for determining the incipient velocity ($\overline{V}_i$)	7.74
16.3	Incipient motion in vertical pipes	7.75
17.	Mobile capsules	7.76

		page
18.	Laminar flow in a concentric annulus with a moving core	7.77
18.1	Discharge in the annulus of an infinitely long concentrically orientated capsule in laminar flow	7.18
19.	Couette flow	7.82
19.2	Plane Couette flow	7.83
19.3	Velocity profiles in turbulent plane Couette flow	7.87
19.4	Wall shear in turbulent plane Couette flow	7.89
19.5	The point where $u_c = V_c/2$ in curved Couette flow	7.94
19.6	Curved Couette flow in an eccentric annular section	7.96
19.7	Results of curved Couette flow analysis	7.100
20.	Continuity equation for mobile capsule water system	7.106
21.	Analysis of general case of mobile capsule water system	7.107
21.1	Pressure component	7.109
21.2	Couette component	7.109
22.	Total force equation	7.111
23.	Gross method of determining the total excess head loss across a mobile capsule	7.115
23.1	Inlet and outlet losses	7.115
23.2	Annular head losses	7.116
24.	Method of determining the total drag and lift force on a mobile capsule	7.118
25.	Finite element method of analysis	7.121
25.1	Method of analysing the mobile capsule water system by finite elements	7.121
25.2	Outline of finite element analysis for mobile capsule water system	7.122

CHAPTER 8 FORCES ON CAPSULES (pp 8.1 - 8.87)

1.	Normal forces	8.2
2.	Tangential forces	8.2
3.	Solid to solid friction forces	8.3
3.1	Surface cleanliness	8.3
3.2	Roughness	8.4
3.3	Capsule velocity	8.4
3.4	The mechanism of friction	8.4
3.5	Fluid lubrication	8.6
4.	Combination of the above forces	8.7
5.	Lift, drag and buoyancy forces	8.7
6.	Drag forces	8.8
7.	Form drag for static capsules	8.9
8.	Skin friction drag due to Couette flow	8.11
8.1	Effect of capsule velocity on Couette shear stress	8.13
8.2	Effect of eccentricity on Couette shear distribution around capsules	8.15
8.3	Effect of eccentricity on average Couette shear on capsules	8.15
8.4	The effect of diameter ratio on Couette shear stress distribution around capsules	8.18
8.5	Effect of diameter ratio on the average shear stress on pipe and capsule wall	8.23
8.6	Effect of pipe diameter on average Couette shear	8.23
9.	Skin friction drag due to pressure flow	8.26
9.1	Effect of pressure flow velocity component ($\overline{V}_{ap}$)	8.26
9.2	Effect of eccentricity on pressure shear around capsule	8.32

page

9.3 Effect of diameter ratio on shear stress distribution and average forward drag on the capsule due to pressure flow 8.35
9.4 Effect of pipe diameter on capsule force due to pressure flow 8.35
10. Interaction of total drag forces on capsule 8.38
10.1 Form drag 8.39
10.2 Net skin friction drag 8.42
10.3 Distribution of net shear stress on capsule 8.49
10.4 Velocity distribution in annulus 8.53
10.5 Friction drag 8.57
10.6 Relative values of the drag forces 8.57
10.7 Effect of length to diameter ratio on drag force components 8.61
11. Lift forces on capsules 8.61
11.1 Streamline patterns around static capsules 8.64
11.2 Mechanisms of lift 8.66
11.3 Calculation of lift ratio neglecting secondary flow and lubricating film effects 8.78
12. Modes of travel of capsule 8.80
12.1 Capsule and pipe wall in contact 8.83
12.2 Travelling free 8.84

P A R T IV EXPERIMENTAL RESULTS AND DISCUSSION (pp 9.1 - 9.21)

CHAPTER 9 HEAD LOSSES ACROSS STATIC CAPSULES

1. Hydraulic Grade lines and energy lines 9.1
2. Inlet head losses for static capsules 9.1
3. Outlet energy loss for static capsules 9.12
4. Annular losses for static capsules 9.16

CHAPTER 10 CAPSULE KINEMATICS (pp 10.1 - 10.83)

1. The kinematics of mobile capsules 10.1
2. Acceleration 10.1
3. Dimensional analysis 10.4
4. Velocity ratio 10.5
5. The specific gravity effect on the capsule velocity 10.8
6. Kinematic correlation 10.13
7. The effect of diameter ratio 10.24
8. The effect of length to diameter ratio on the capsule velocity 10.33
9. The effect of pipeline slope on capsule velocity 10.41
9.1 Observed features 10.41
9.2 Explanation of the foregoing 10.44
9.3 Kinematics of capsule flow in a vertical pipe 10.49
10. The effect of roughness 10.52
11. The effect of capsule spacing 10.59
12. The slope of the $V_c : \overline{V}$ line (m) 10.67
13. The effect of pipe diameter 10.78

CHAPTER 11 ENERGY DISSIPATION ACROSS MOBILE CAPSULES (pp 11.1 - 11.75)

page

1. The effect of mean water velocity 11.1
2. The effect of specific gravity 11.6
3. The effect of diameter ratio 11.8
4. The effect of capsule length 11.16
5. The effect of pipe slope 11.30
5.1 The most prominent effects of slope on excess head loss 11.36
5.2 Vertical pipes 11.52
6. The effect of capsule roughness 11.59
7. The effect of capsule spacing 11.65
8. The effect of pipeline diameter on ΔH_c 11.71

CHAPTER 12 CAPSULE TO WALL CLEARANCE (pp 12.1 - 12.19)

1. A priori evidence of lift 12.1
2. Friction factor 12.3
3. Four regimes of lift 12.3
4. Results of experiments on capsule lift 12.4
4.1 Effect of capsule velocity 12.5
4.2 Incipient capsule velocity for lift 12.7
4.3 Maximum clearance 12.11
4.4 Relation of velocity ratio to clearance 12.15

P A R T V COMPARISON OF EXPERIMENTAL AND ANALYTICAL RESULTS

CHAPTER 13 STATIC CAPSULES (pp 13.1 - 13.19)

1. Comparison of experimental inlet head losses with sudden contraction losses for conventional concentric pipes 13.1
2. Comparison of experimental outlet losses with sudden expansion losses in concentric pipes 13.3
3. Comparison of analytical and experimental results - pressure flow in the annulus of static capsules 13.5
3.1 Concentric annuli 13.5
3.2 Eccentric annuli - complete laminar flow 13.8
3.4 Comparison of conventional friction factor and hydraulic mean radius with pseudo values 13.7

CHAPTER 14 INCIPIENT CAPSULE MOTION (pp 14.1 - 14.32)

1. Effect of length and diameter ratio 14.2
1.1 Correlation 14.4
1.2 Experimental incipient velocity at different L_c/d ratios 14.4
1.3 Experimental incipient excess head loss at different L_c/d ratios 14.6
2. Effect of capsule density 14.9
2.1 Correlation 14.12
2.2 Experimental incipient velocities and excess head loss at different capsule densities 14.12
3. Effect of pipeline slope 14.18
3.1 Correlation 14.22

page

3.2 Experimental incipient velocity at different pipeline slopes 14.24
3.3 Incipient excess head loss at different pipeline slopes 14.24
3.4 Vertical pipeline orientation 14.28
3.4.1 Effect of diameter ratio, SG and L_c/d 14.28
4. Comparison of incipient and mobile correlations 14.30

CHAPTER 15 COMPARISON OF ANALYTICAL AND EXPERIMENTAL RESULTS FOR MOBILE CAPSULES (pp 15.1 - 15.72)

1. Definition of terms used 15.1
1.1 "Empirical m" analysis 15.1
1.2 "Experimental m" analysis 15.3
1.3 "Couette m" analysis 15.3
1.4 Gross analysis 15.3
2. The effect of capsule velocity on ΔH_c 15.3
2.1 Effect of SG 15.7
3. Predicted analytical values of ΔH_c for D = 150 mm for a range of diameter ratios and capsule densities 15.11
4. Effect of L_c/d ratio 15.19
5. The individual components of excess head loss : gross analysis 15.22
6. The individual components of excess head loss in the finite element analysis 15.25
6.1 Inlet head loss (Δh_i) 15.27
6.2 Outlet head loss (Δh_o) 15.32
6.3 Annular head loss (Δh_{fa}) 15.32
7. Assumptions inherent in the analysis 15.33
7.1 Geometry 15.34
7.2 Results of plane Couette flow used in curved Couette flow 15.34
7.3 Static friction coefficient equal to kinetic friction coefficient 15.34
7.4 No lift at incipience 15.35
7.5 The addition of velocity and shear stress components due to pressure and Couette flow 15.35
7.6 Energy dissipation at inlet and outlet of a static capsule applies in the mobile capsule case 15.35
7.7 Lines of neutral shear occur along quasi-concentric radii 15.36
7.8 Change from laminar to turbulent flow may occur at different positions around the annulus for pressure and Couette flow 15.36
7.9 Reynolds number criterion 15.37
7.10 Force on capsule wall equals force on pipe wall for Couette flow 15.37
7.11 Shear stress on capsule wall equals shear stress on pipe wall in pressure flow 15.38
7.12 Velocity profiles in concentric annuli assumed to apply to quasi concentric annuli 15.38
7.13 Fully developed flow assumed in the annulus 15.38
7.14 Capsule axis parallel to pipe axis 15.39
7.15 No account taken of wedging action 15.39
7.16 No account taken of primary streamline curvature and secondary flow 15.40

		page
7.17	Irregularities and distortion	15.40
8.	Empirical correlation of excess energy loss	15.40
8.1	Other methods of non-dimensional plotting	15.53
8.2	Ratio of forces acting on the capsule	15.56
8.3	Correlation to include pipeline slope	15.62
8.4	Percentage of data differing by more than 15% from the correlation line for different pipe diameter	15.67
8.5	Comparison with the correlation of Ellis and Kruyer	15.70

P A R T VI POWER CONSIDERATIONS

CHAPTER 16 POWER REQUIREMENTS (16.1 - 16.52)

1.	Definitions	16.1
2.	Effect of mean water velocity on power	16.4
3.	Effect of θ and L_s	16.6
4.	Effect of diameter ratio	16.8
5.	Effect of capsule density	16.13
6.	Effect of capsule length	16.16
7.	Effect of slope	16.20
7.1	Dissipated power	16.24
8.	Power requirements at incipience	16.29
8.1	Definitions	16.31
8.2	Effect of capsule spacing	16.32
8.3	The effect of diameter ratio	16.36
8.4	Effect of capsule SG	16.40
8.5	Effect of capsule length	16.41
8.6	Effect of pipe slope	16.45
9.	The relation between startup power and minimum mobile power requirements	16.48

CHAPTER 17 OPTIMISATION OF A CAPSULE TRANSPORTATION SYSTEM (pp 17.1-17.25)

1.	Economics of capsule transportation	17.1
1.1	Investment costs	17.2
1.2	Overhead costs	17.2
1.3	Operating costs	17.2
2.	Analysis	17.3
3.	Definitions	17.4
3.1	Capsule mass delivery rate	17.4
3.2	ψ-parameter	17.7
3.3	Efficiency	17.8
4.	Optimisation of flow velocity and power requirement	17.9
4.1	The optimum mean water velocity	17.9
4.2	Complete optimisation of ψ-parameter	17.11
4.3	Constraints	17.11
4.4	Optimum capsule diameter	17.12

CHAPTER 18 COMPARISON OF SUSPENDED SEDIMENT FLOW AND CAPSULE TRANSPORTATION IN PIPELINES (pp 18.1 - 18.29)

1.	Flow regimes	18.1
2.	Homogeneous flow	18.1

		page
2.1	Non-Newtonian flow	18.1
2.2	Pseudo homogeneous flow	18.6
3.	Heterogeneous flow	18.6
4.	The deposit regimes	18.8
5.	Volumetric concentration and voids ratio for capsules	18.8
6.	Comparison of capsule transportation with homogeneous suspension	18.10
	Case I - no voids in capsule	18.10
	Case II - voids present in the capsule	18.13
7.	Comparison of capsule transportation with heterogeneous suspensions	18.17
	Case III - no voids in capsule	18.17
	Case IV - voids present in the capsule	18.19
8.	Comparison of capsule transportation with non-Newtonian flow	18.24
9.	Example of a numerical comparison of hydraulic transportation of iron ore encapsulated and in suspension	18.24

CHAPTER 19 CONCLUSIONS (pp 19.1 - 19.19)

APPENDIX I CAPSULE FREE PIPE TESTS

APPENDIX II DISCUSSION OF SOME OF THE MAIN COMPUTER PROGRAMMES

BIBLIOGRAPHY

NOTATION

A_A = annular area.

A = constant in logarithmic velocity distribution law.

A_c = frontal area of capsule.

A_c = constant in logarithmic velocity distribution law for the capsule.

A_p = area of pipe.

A_p = constant in logarithmic velocity distribution law for the pipe.

A_{Tp} = constant in logarithmic velocity distribution law for the pipe (transition zone).

A_{Tc} = constant in logarithmic velocity distribution law for the capsule transition zone.

ΔA = elemental area of slice in quasi-concentric annulus.

ΔA_c = part of elemental area of slice between capsule radius and maximum velocity radius.

ΔA_p = part of elemental area of slice between radius of maximum velocity and pipe radius.

ΔA_i = ΔA at particular polar position.

Δa = sub-elemental area.

Δa_{mi} = sub-elemental area at specific position (m) in radial direction and (i) in angular direction.

b = distance between moving and fixed wall in Couette flow.

b_1 = half distance between moving and fixed wall Couette flow.

b_p = distance from pipe wall to position where $u = V_c/2$.

b_c = distance from capsule wall to position where $u = V_c/2$.

b_i = distance between moving and fixed wall ($b_i = C_{rmi} - C_{r1i}$) at position (i) around annulus.

b_{ci} = distance from capsule wall to position where $u = V_c/2$ at position (i) around annulus.

b_{pi} = distance from pipe wall to position where $u = V_c/2$ at position (i) around annulus.

B = constant in logarithmic velocity distribution law

B_c = constant in logarithmic velocity distribution law for the capsule.

B_p = constant in logarithmic velocity distribution law for the pipe.

B_{Tc} = constant in logarithmic velocity distribution law for the capsule, transition zone.

B_{Tp} = constant in logarithmic velocity distribution law for the pipe, transition region.

C = clearance between capsule and pipe wall at bottom.

C^* = maximum clearance reached by capsule.

C_f = local skin friction coefficient in Couette flow.

C_L = linear concentration of capsules in pipe.

C_r = quasi-concentric radius.

C_D = particle drag coefficient.

C_{rc} = quasi-concentric capsule radius.

C_{rp} = quasi-concentric pipe radius.

C_{rni} = general value of quasi-concentric radius of pipe at location (i).

C_{r1i} = general value of quasi-concentric radius of capsule.

C_{rmi} = general value of quasi-concentric radius (i.e. $C_{rmi} = C_{r1i} + b_i(m/n)$).

C_{rmidmi} = quasi-concentric radius to the mid-point of a sub-elemental area Δa

C_o = coefficient for veriflux flow meter.

C_v = volumetric concentration.

C_{vt} = volumetric concentration in transport (spatial).

C_{vd} = delivered volumetric concentration.

$(C_{vd})_{sc}$ = delivered volumetric concentration of solids in capsules.

$(C_{vt})_{sc}$ = transport volumetric concentration of solids in capsules.

d = capsule diameter.

d_p = equivalent diameter of solid particle.

D = pipe diameter.

D_f = form drag.

D_F = solid friction drag.

D_T = total drag forward or backward.

D_{Tf} = total forward drag.

D_{Tb} = total backward drag.

D_N = net drag.

D_{sf} = skin friction drag.

D_{sfp} = skin friction drag due to pressure flow.

D_{sfc} = skin friction drag due to Couette flow.

D_{ep} = equivalent diameter in Reynolds number for region of flow between r_c and r_{max}.

D_{ec} = equivalent diameter in Reynolds number for region of flow between r_c and r_{max}.

e = eccentricity = $2p$

e = void ratio

E = factor in Couette flow velocity profile equation.

f = friction factor in Darcy's equation.

f_p = friction factor for pipe wall in annulus based on average velocity in annulus.

f_c = friction factor for capsule wall in annulus based on average velocity in annulus.

f'_p = friction factor based on average velocity between r_m and r_p.

f'_c = friction factor based on average velocity between r_c and r_m.

f_{aw} = friction factor in annulus for pipe based on $\bar{V}_{am}$.

f_{ac} = friction factor for capsule based on V_r.

$\bar{F}_{cc}$ = mean drag force on capsule due to Couette flow per metre length of capsule.

$\bar{F}_{cp}$ = mean drag force on capsule due to pressure flow (N/m).

$\bar{F}_{pc}$ = mean drag force on pipe due to Couette flow (N/m).

$\bar{F}_{pp}$ = mean drag force on pipe due to pressure flow (N/m).

F_{pw} = pressure force in capsule-free pipe.

F_{pm} = pressure force on capsule water mixture.

F_{im} = inertial force on capsule water mixture.

F_{iw} = inertial force in capsule-free pipe.

ΔF_c = excess force acting across capsule water system.

G = gap between capsule and pipe wall at bottom assuming pipe and capsule axes parallel.

g = gravitational constant.

Δh_a = excess friction head loss in annular section of static capsule.

Δh_f = fluid friction head loss.

h_f = fluid friction head loss.

Δh_{fa} = total friction head loss in annular section of static capsule.

Δh_{f1} = time average value of friction head loss in capsule-free pipe.

Δh_{f2} = reduced time average value of friction head loss in capsule-free section due to presence of capsule elsewhere (in open circuit),

Δh_i = inlet head loss.

Δh_c = outlet head loss.

ΔH_p = total head dissipated in pipeline, of length L_p, containing capsule.

ΔH = total head loss between two tapping points with capsule in line.

ΔH_c = excess head loss across mobile capsule.

$\Delta H_c'$ = apparent value of excess head loss across capsule.

ΔH_m = total head loss for capsule water mixture per capsule length L_c.

$(\Delta H_c)_s'$ = total excess head loss in non-horizontal pipe.

$(\Delta H_c)_i$ = excess head loss at incipience.

$(\Delta H_c)_s = (\Delta H_c)_s' - (d/D)^2 |S_c - 1| L_c \sin \phi$.

ΔH_{cs} = excess head loss across static capsules.

Δh_{shc} = head loss over length (L_c) due to shear on capsule wall.

Δh_{shp} = head loss over length (L_c) due to shear on pipe wall.

$\Delta H_c''$ = $\Delta H_c + iL_c$, i.e. head loss across capsule when h_f acts over part of pipeline not including a capsule.

$(\Delta H_c)'_{is}$ = total excess head loss in sloping pipe at incipience.

$(\Delta H_c)_{is}$ = $(\Delta H_c)'_{is} - (d/D)^2 |S_c - 1| L_c \sin \phi$.

$\Delta H_c'''$ = excess head loss across mobile capsule with no capsule to pipe wall contact.

I = injection rate (capsule/s).

I = excitation current.

i = integer varying from 1 to n in quasi-concentric annulus analysis.

i = hydraulic gradient in capsule-free pipe.

i_c = hydraulic gradient in annulus.

i_m = hydraulic gradient for solid liquid mixture measured in units of water.

k_p = average pipe roughness size.

k_c = average capsule roughness size.

K = head loss coefficient for a sudden contraction in a pipe.

k'_e = head loss coefficient for sudden eccentric annular contraction.

k'_c = head loss coefficient for sudden concentric annular contraction.

k_{oe} = head loss coefficient for sudden eccentric annular expansion.

k_{oc} = head loss coefficient for sudden concentric annular expansion.

K = constant in equation = K/χ^q.

K' = measure of fluid consistency.

L = length of pipeline.

L_c = capsule length.

L_1, L_2 = length over which curvilinear flow takes place upstream and downstream of capsule.

L_p = total pipeline length.

L_F = lift force on capsule.

L_r = lift ratio = L_F/W'.

L_s = spacing length, centre-to centre, between successive capsules.

m = slope of $\bar{V} : \bar{V}_c$ line

M_c = mass of capsule.

n = number of capsules in pipe of length L_p.

n = number of elemental slices per half annulus in quasi-concentric annulus analysis.

n' = flow behaviour index.

O_p = pipe centre.

O_c = capsule centre.

O = centre point between O_p and O_c.

p = half distance between pipe centre (O_p) and capsule centre (O_c).

P_1, P_2 = average pressure at a section in the capsule-free pipe, upstream and downstream of a capsule.

P_1', P_2' = average pressure in annulus at an upstream and downstream section.

ΔP = pressure difference.

$\Delta P'$ = pressure difference in annulus.

P = total power dissipated.

P_T = total power utilised $P_T = P$ in horizontal pipe.

$(P_i)_T$ = total power at incipience.

P_i = total power dissipated at incipience.

ΔP_{ex} = excess power dissipated.

$(\Delta P_i)_{ex}$ = excess power dissipated at incipience.

P = percentage of full scale deflection on Veriflux converter.

P_m = mean pressure for lubricating film analysis.

Q = flow in capsule-free pipe.

Q_a = flow in the annulus.

Q_{ac} = flow in the annulus due to Couette component.

ΔQ_{ac} = Couette flow component in an elemental slice.

Δq_{ac} = Couette flow in sub-slice of an elemental area.

Q_c = volume flow of capsule.

q = index in $\Gamma = K/\chi^q$.

ΔQ = reduction in water flow due to presence of capsule in pipeline.

r = radius to arbitrary point in the annulus.

r_c = capsule radius.

r_p = pipe radius.

r_m = radius of maximum velocity in pressure flow.

r_{mt} = r_m for turbulent flow.

r_{ml} = r_m for laminar flow.

R = hydraulic mean radius.

R_p = pseudo-hydraulic mean radius.

R_{rp} = hydraulic mean radius for annulus between r_m and r_p.

R_q = hydraulic mean radius for quasi-concentric annular area.

R_{rc} = hydraulic mean radius for annulus between r_c and r_m.

R_e = Reynolds number = $2b\,\bar{V}_a/\nu$.

R_{eq} = Reynolds number for quasi-concentric annular area.

R_{ea} = Reynolds number for the annulus.

R'_{ec} = Reynolds number in region between r_c and r_m in pressure flow based on $\bar{V}_c$ and D_{ec}.

R'_{ecc} = R'_e for capsule zone = $V_c/2(b_c/\nu)$ in Couette flow.

R'_{ecp} = R'_e for pipe zone = $V_c/2(b_p/\nu)$ in Couette flow.

R'_e = $u_c\,b_1/\nu$ for Couette flow.

R_{ep} = Reynolds number based on $\bar{V}_a$ and D_{ep}.

R_{ec} = Reynolds number based on $\bar{V}_a$ and D_{ec}.

R'_{ep} = Reynolds number in region between r_m and r_p in pressure flow based on $\bar{V}_p$ and D_{ec}.

R'_{ec} = Reynolds number in region between r_c and r_m in pressure flow based on $\bar{V}_c$ and D_{ec}.

R_c = ratio of forward drag force on capsule to submerged weight of capsule.

R_i = ratio from empirical correlation = $2Kf$.

R_m = ratio of forward drag force on capsule water mixture to submerged weight of capsule.

R_{epw} = Reynolds number for the pipe region in the gross method based on $\bar{V}_{am}$.

R_{ecw} = Reynolds number for the capsule region based on V_r.

S_c = specific gravity of capsule.

S_s = specific gravity of solid particles.

ΔS_c = elemental arc length along capsule walls.

ΔS_p = elemental arc length along pipe wall.

u = point velocity in Couette flow.

u_c = velocity in Couette flow where $u = V_c/2$.

u_* = $\sqrt{\tau/\rho}$ for plane Couette flow.

u_{*c} = $\sqrt{\tau/\rho}$ for Couette shear at capsule wall.

u_{*p} = $\sqrt{\tau/\rho}$ for Couette shear at pipe wall.

v = point velocity in pipe.

$\bar{V}$ = mean velocity in pipe.

V_L = limit deposit velocity.

$\bar{V}_L$ = average water velocity across capsule area.

$\bar{V}_a$ = mean velocity in annulus of static capsule.

$\bar{V}_i$ = mean velocity in pipe at incipience.

V_c = capsule velocity.

V_2 = mean velocity in smaller pipe at sudden contraction in circular pipes.

V_t = terminal settling velocity of particles in still water.

$\bar{V}_{am}$ = mean velocity in annulus of mobile capsule.

$\bar{V}_{ac}$ = mean velocity in annulus due to Couette flow.

V_m = mixture velocity in suspended sediment flow.

V_m = velocity reading on Veriflux converter.

$\bar{V}_i'$ = pseudo-incipient velocity from back projection of $V_c : \bar{V}$. curve to intercept $\bar{V}$ axis.

$\bar{V}_{ap}$ = mean velocity in annulus due to pressure flow.

$\bar{V}_{api}$ = mean velocity in quasi-concentric annulus at a particular location.

v_{ap} = laminar flow velocity in quasi-concentric annular area (pressure flow).

V_{ac} = mean velocity in quasi-concentric annular area (Couette flow).

v_{*c} = $\sqrt{\tau_{cp}/\rho}$ at capsule wall, for pressure flow.

v_{*p} = $\sqrt{\tau_{pp}/\rho}$ at pipe wall, for pressure flow.

v_c^+ = v/v_{*c}.

v_p^+ = v/v_{*p}.

$\overline{V}_p$ = average velocity between r_m and r_p.

$\overline{V}_c$ = average velocity between r_c and r_m.

$\overline{V}_{SL}$ = water velocity at which capsule first starts to lift.

V_{cil} = capsule velocity at incipient lift.

v_o = point velocity for $r_m < r_c < r_p$.

v_i = point velocity for $r_m > r > r_c$.

V^+ = modified value of v^+.

w = specific weight of water.

W' = submerged weight of capsule.

W = capsule weight in air.

y_c, y_p = distance from pipe or capsule wall.

y^+ = $y_p\, v_{*p}/\nu$.

y_c^+ = $y_c\, v_{*c}/\nu$.

Y^+ = modified value of y^+.

Z_1, Z_2 = elevation of pipe centre line above horizontal datum.

Z = ratio R_p/R.

α = angle of incline pipe for determining μ_f.

β = $(v_{*c}/v_{*p})^2$.

γ = d/D.

λ = $(d/D)^2\, |S_c - 1|\, L_c \sin \phi$.

Γ = $\Delta H_c/L_c\ (L/h_f)(D/d)^2$.

Γ'' = Γ using $\Delta H_c''$.

$(\Gamma)_s$ = Γ on slope using $(\Delta H_c)_s$.

$(\Gamma)'_s$ = Γ on slope using $(\Delta H_c)'_s$.

Γ_i = Γ at incipience.

$(\Gamma_i)'_s$ = Γ in non-horizontal pipe.

$(\Gamma_i)_s$ = $(\Gamma_i)'_s$ involving $(\Delta H_c)_{is}$.

ϵ = eccentricity ratio.

η = axis used in bi-polar co-ordinate system.

η = efficiency factor for capsule transportation.

θ = angle around quasi-concentric annulus.

θ = capsule mass delivery rate.

θ_p = angle around quasi-concentric annulus with 0_p centre.

θ_c = angle around quasi-concentric annulus with 0_c centre.

$\Delta\theta$ = elemental angle around quasi-concentric annulus.

κ = von Karman's constant.

μ = dynamic viscosity of water.

μ_f = coefficient of solid to solid static friction.

ν = kinematic viscosity of water.

$\xi = \dfrac{\Delta H_c}{L_c} \Big/ \dfrac{h_f}{L}$

ξ = axis used in bi-polar co-ordinate system.

$\xi'' = \dfrac{\Delta H''_c}{L_c} \Big/ \dfrac{h_f}{(L_p - L_c)}$

ρ = density of water.

ρ_c = bulk density of capsule.

τ = shear stress on wall.

τ_{cc} = shear stress on capsule wall due to Couette flow.

τ_{cp} = shear stress on capsule wall due to pressure flow.

τ_{pc} = shear stress on pipe wall due to Couette flow.

τ_{pp} = shear stress on pipe wall due to pressure flow.

$\bar{\tau}_{cc}$, $\bar{\tau}_{cp}$, $\bar{\tau}_{pc}$, $\bar{\tau}_{pp}$ are average values of the above shear stresses.

τ_p = shear stress on pipe wall.

τ_c = shear stress on capsule wall.

$\bar{\tau}_p$ = shear stress on pipe wall for gross analysis, or average shear stress on pipe wall.

$\bar{\tau}_c$ = shear stress on capsule wall for gross analysis, or average shear stress on capsule wall.

$\bar{\tau}_{oc}$ = mean shear stress on wall of pipe in the curvilinear flow region just upstream and downstream of the capsule, for incipient capsule motion.

τ_{oc} = mean shear stress on wall of pipe in the curvilinear flow regions for the mobile capsule.

τ_o = shear stress in annulus between r_m and r_p.

τ_i = shear stress in annulus between r_c and r_m.

$\bar{\tau}_o$ = average shear stress in pipe and capsule walls.

ϕ = angle of inclined pipeline.

ϕ = electro-magnetic flux.

ϕ_c = angle subtended at capsule wall in quasi-concentric annulus.

ϕ_p = angle subtended at pipe wall in quasi-concentric annulus.

ϕ = a non-dimensional parameter in sediment transportation.

ϕ_c = a non-dimensional parameter in capsule transportation.

χ = $\sqrt{gD\,|S_c - 1|}$.

χ_L = χ - value using $\bar{V}_L$.

χ_i = χ - value using $\bar{V}_i$.

ψ = performance factor.

ψ_W = non-dimensional ψ - parameter.

ψ_{min} = minimum ψ - parameter.

ψ_{opt} = optimum ψ - parameter.

ψ_{ex} = excess ψ - parameter.

PART I

SURVEY OF THE FIELD OF CAPSULE TRANSPORTATION

"I have less difficulty to establish the movement of planets irrespective of their distance from the earth than to explore the movement of water in front of my eyes."

G. Galileo

CHAPTER 1

INTRODUCTION

1. Statement of the problem

The hydraulic conveyance of capsules in pipelines is a two phase system of transportation consisting of a liquid and solid component.

The liquid component may be a vehicle for the solid, or may be a creditable component in its own right. The solid component is the capsule which may be formed of the solid material to be transported or enclose the material as a container (encapsulation). This is a novel method of transportation and at present (1972) has not yet been utilised on a large commercial scale.

This thesis is concerned with a wide ranging investigation as to the viability of the concept. The purpose of the investigation is to examine the fluid mechanics of the flow of capsule water mixtures. Experiments are performed with a view to the formulation of correlating parameters for the dependent variables involved, such as, capsule velocity, energy and power requirements. This was essentially successful and the formulation, although empirical in nature, is substantiated in form by analysis.

After analysing the problem by various methods, the effect of the many independent variables involved in the flow of capsules in pipelines is discussed with particular reference to the effect on dependent variables.

The problem of hydraulic transportation is, in general, essentially one of minimising the energy required to transport a specified quantity of material at a fixed rate between two points, and apart from favourable energy requirements, capsules offer distinct advantages over other forms

of transporting solids in suspension in pipes.

2. Definition of capsule

A "capsule" is defined as a solid with rigid boundaries which enclose or containerise the material to be transported. The term capsule may also be extended to cover rigid (or even non-rigid) cylinders or spheres formed of the material to be transported in billetted, sintered or extruded form. Characteristically, material can be cast into spheres or cylinders from the molten state and transported with or without a protective coating, depending on whether contamination is to be avoided or not. Examples are steel, aluminium or other metals. The preparation of capsules will be discussed in Chapter 3.

Essentially, the capsule to pipe diameter ratio is envisaged as being large, of the order of one half to as near unity as is practicable.

The capsules do not touch the pipe all round, as pistons, but are free flowing either fully suspended or touching the bottom (or top) of the internal pipe surface.

This investigation is restricted to rigid cylindrical capsules. Spherical shapes were rejected on the following grounds.

2.1 In a sloping pipeline, whatever the slope, they would roll into a valley, if the pipeline were closed down.

2.2 Restarting is difficult because the spheres experience friction on one another, preventing rotation.

2.3 More containers of a chosen diameter are required for the same volume. The cost and handling problems are thus greater for spheres than cylinders.

2.4 From the manufacturing viewpoint, the cylinder is a more conventional method of containerisation.

3. Validation of the study

The remoteness of most raw material sources, and the fact that this country's prosperity could depend on vast untapped mineral resources, leads to a great need for more economical forms of transportation for various commodities.

It is estimated, for example, that by 1975, 12 million tonnes of ore will have to arrive at the steel producing contres of Pretoria, Vanderbijl and Newcastle every year. To this quantity must be added another 15 million tonnes - the amount estimated, that can be transported annually by 1980.

All this ore transportation would choke the existing railway system, and transporting ore by railway is expensive.

Alternative methods of transportation will have to be found, and it has been shown by Nolan and Drust (reference 43) as well as various other authors, that suspended solids, such as iron ore, can be conveyed, in certain instances, more economically in a pipeline than by rail or road.

In order to validate the study of hydraulic conveyance of solids in capsule form, it is necessary to make a brief digression into the field of hydraulic transportation of solids in particulate form, and then discuss the advantages displayed by capsules.

3.1 Sediment transportation : Existing schemes

The hydraulic transport of solids in sediment, or slurry form, in pipelines is no new concept and a patent for pumping solid slurries was issued in the United States as early as 1821. However, the first operating solids pipeline is generally assigned to G.G. Bell. A 200 mm diameter pipeline carried coal as a slurry from barges on the Thames to Hammersmith Power Station.

Not until 1957 was the method applied to long distance transportation

of solids. The Consolidated Coal Company built a 250 mm diameter line from Cadiz, Ohio to a power plant at Eastlake, 173 km away. The solids concentration was 50 per cent by weight and 3200 tonnes per day of coal were transported until 1963 when the company discontinued operation, because of lowered railway tariffs.

Many products have successfully been transported in suspension in many countries of the world; for example, 3 to 4 million tonnes per year of iron ore in Tasmania, a distance of 84 km through a 225 mm pipe at a concentration of 60 per cent by weight. Also 500 000 tonnes per year of mine tailings in Japan are conveyed a distance of 70,6 km through a 318,5 mm diameter pipe - a scheme initiated in 1968. The largest scheme yet is 5 million tonnes per year of coal from the Black Mesa coalfield in Arizona to Nevada, a distance of 440 km, through a 457 mm diameter pipeline.

In South Africa coal has been transported hydraulically from the Koornfontein Colliery to Komati Power Station at the rate of 120 tonnes per hour, from 1963 to 1968, over a distance of 2,4 km. Also, quartzite fines are raised a vertical distance of 2,194 km at Vaal Reef mines at the rate of 300 000 tonnes per annum.

3.2 Type of material transported

Some of the products already being transported hydraulically are cement, coal, concrete, fly ash, gilsonite, iron ore, iron ore tailings, phosphate slurry, uranium-bearing gold slurry, gunpowder rods, diamond-bearing rocks and fish. Products envisaged for the future include wood in chip form for the paper industry, canned food, kaolin, potash, sulphur, coke, foodstuffs and domestic refuse.

Are there limits to the type of material that could be hydraulically transported in pipelines? One might imagine that any product susceptible to contamination by a conveying medium or which should be kept dry would

be excluded. However, if the cargo were encapsulated, products such as chemicals, machine parts, canned foods, textiles or solid waste from cities could also be conveyed through pipelines.

4. Advantages of hydraulic transport of solids

There are certain advantages in transporting solids in pipelines.

4.1 Pipes are easier to install than roads, railways or conveyer belts. Difficult terrain, such as natural and man-made obstacles, is overcome more readily with pipelines.

4.2 Pipelines have smaller personnel requirements. The labour force for operation and maintenance is far less than for railways and roads. The "vehicle" has no driver.

4.3 All moving mechanical parts are grouped at the pumping station. The vehicle, being a fluid requires no maintenance or mechanical parts.

4.4 The system can readily be automated.

4.5 The vehicle, as well as the cargo or load, may be utilisable. Where large quantities of oil or water have to be conveyed as well as the load, then the system becomes even more economically attractive. For example, transporting carnalite from Sdom, in Israel, to Ashdod (125 km); the liquid contains a rich mixture of magnesium and salt.

4.6 The process is continuous as opposed to the batching of road or rail transport.

4.7 Strategically, the risk of sabotage is reduced since a pipeline is usually buried.

4.8 For mine hoisting, a small shaft space is required; for example, 9000 tonnes per day can be hoisted through a 250 mm diameter pipe.

4.9 The low operating costs are particularly attractive. Cement slurry is transported in England a distance of 113 km through a 250 mm diameter

pipe at the rate of 194 million tonnes per annum and the cost is about 2c per tonne as compared (in this case) with R2 per tonne by rail. The larger the pipeline the lower the cost per tonne km.

4.10 Change in directions is simply achieved by pipe bends. It is easy, for example, to combine hoisting with horizontal transport.

4.11 Compared with roads and railways, the space occupied by pipelines is small.

4.12 Aesthetically, there are advantages over other methods since nearly all facilities are buried and out of sight.

4.13 Slurry pipelines have a high degree of reliability and are thus capable of high operating factors. The Consolidation Coal Company pipeline had an operating factor of 98 per cent, for example.

4.14 Pollution is less of a by-product with pipelines than with roads or railways.

5. Disadvantages of Transportation in slurry form

There are certain disadvantages to transporting solids by pipelines in particulate form.

5.1 Pipeline wear is a problem, particularly with large irregular heavy particles.

5.2 Grinding and dewatering costs can be considerable. The most economical method of transporting a slurry particularly if the specific gravity is high, is to grind it down as much as possible and de-water at the delivery point. This can be expensive.

5.3 The degrading of particles during transportation may be objectionable, but in certain instances may be an advantage.

5.4 There are still design problems. The science is very much in the experimental stage and there are conflicting methods of design.

5.5 The disposal of the vehicle, if the fluid has no value at the downstream end, may be difficult if it is not clean.

5.6 Restarting a blocked line may prove difficult. When the specific gravity is high (e.g. iron ore) the ore tends to settle down and enough area of cross-section must remain in the pipe above the solids to enable clear water to pick up particles.

5.7 Only one commodity can be transported at a time.

6. The advantages of capsule transportation

The hydraulic conveyance of solids in capsules is one way in which these difficulties can be overcome. Capsule transportation has the following advantages when compared with sediment transportation.

6.1 Energy requirements

With large, heavy particles and heterogeneous flow the energy requirements are high. Low density materials, such as coal, sand, gilsonite or wood chips can be transported in pipelines as a suspension. High density materials, such as iron ore, zinc or other heavy ores can only be transported when velocities are high enough to provide turbulent suspension or when the material is ground fine enough to act as a non-Newtonian fluid.

Either case, i.e. large hydraulic gradients (in the former circumstance) or extensive grinding and dewatering (in the latter) may prove uneconomical over long distances.

If iron ore, for example, is transported in capsule form, as opposed to a suspension, the energy requirements are lower and the encapsulating or sintering costs may well offset the grinding and dewatering costs.

The pumping power for slurries increases rapidly with particle size and density increase.

6.2 Contamination

Contamination of the conveyed material by the conveying medium or vice versa can be prevented by means of encapsulation.

This opens up a whole new range of applications of pipeline transportation and different commodities which may be conveyed, such as foodstuffs, powders, textiles, machine parts, electronic components, radioactive material etc.

In fact, the only commercially encapsulated material transported to date is radioactive ore in France through four 122 m long lines in capsules which are 77 mm in diameter, 1,37 m long and have a mass of 20 kg. This is not a long distance application and design was probably by trial and error.

6.3 Abrasion

A serious problem in sediment lines, particularly with coarse, heavy particles, is wear of the pipeline. The life can be extended by rotating the pipe.

In gravel handling and dredging plant (where most wear is expected) the pipe may last a year or more if rotated periodically. Bends may last six months.

Experimental investigations have revealed negligible wear of the pipeline when conveying capsules.

6.4 Attrition

The attrition of the solid load during transportation may also pose problems since dewatering and separation procedures at the delivery point are aggravated. In capsule form there is no attrition and ore, for example, can be conveyed as mined.

6.5 Grinding and dewatering

For sediment transportation, the processes of grinding the solids to be transported, as well as dewatering at delivery, are costly, particularly for finely graded material, if complete drying is required. The costs incurred involve both capital outlay and energy requirements. Settling tanks, filters, centrifuges and hot air drying would be necessary.

These costs have to be compared with encapsulation or sintering costs. The separation of the solid material from the carrier fluid is fairly simple and inexpensive in the case of capsules.

7. Objectives

The object of the research project was as follows:

7.1 The design and development of hydraulic model experiments, together with the associated measuring equipment to investigate experimentally the effects of all the variables considered.

7.2 Development of the technology insofar as it was required for the experimental investigation. This involved the conception and design of an injection device for capsules, a workable method for capsule retrieval and the design of booster pumps.

7.3 The development of a theory to account for the phenomena and the formulation of relations suitable for extrapolation and design purposes.

CHAPTER 2

LITERATURE REVIEW

Apart from the present thesis, the most significant, in fact the only, work has been carried out by a team from the Research Council of Alberta in Canada.

When the present study was started by the author at the University of Cape Town the only literature available from the Research Council of Alberta were Parts 1 to 8 of the series which will be discussed below, and no experiments had been reported which dealt with pressure losses, sloped pipelines, capsule trains, correlation of data or power requirements.

The first mention of pressure losses and correlating parameters was given at the 1970 conference, (Hydrotransport I, B.H.R.A. Warwick University) and this coincided with the incipient theory together with kinematic and energy correlations and power requirements presented by the present author. No known work has been done on pipeline slope variation (including the vertical case) apart from that of the present author.

A large number of papers have been published by various groups of members of the team in Canada. Many of these contributions have been of a non-specialist descriptive nature and repetitive.

The scientific papers from Alberta have been designated the Pipeline Flow of Capsules and were numbered 1 to 9. Recently, papers in the same series numbered 10 to 11 have been written, Part 10 being published at the First International Conference on the hydraulic transport of solids in pipes, September 1970, and Part 11, at the time of writing, unpublished.

The paper by Lazarus and Kilner (reference 31) is not reviewed here since it represents a summary of some of the work done by the author and is largely reproduced in the course of this thesis.

The eleven papers in the Canadian series will be reviewed in detail below.

Other literature of relevance to the annular flow of water is reviewed under the section on static capsules (in Chapter 7).

Hodgson and Charles (reference 21) in Part 1 of the series deals with "The concept of capsule Pipelining." The idea is advanced, in the paper, that capsule pipelining is a natural evolution of fluid pipelining (first generation) and slurry pipelining (second generation).

First generation pipelining is thought of as encompassing situations, from the flow of a single fluid in a conduit, to situations as complex as the multiphase flow of two or more immiscible fluids. The bulk of the paper is concerned with describing flow situations observed during the course of an investigation dealing with the horizontal pipeline flow of oil in the presence of water.

Two types of capsules are considered, viz. cylindrical and spherical, both of which correspond to slug and bubble flow of oil globules in a water pipeline.

By observing the flow of oil and water certain observations were made which are summarised below.

1. For equal density oil and water mixtures the following flow patterns were observed when the mean mixture velocity was increased; oil drops in water, oil bubbles in water, oil slugs in water, concentric oil in water and water drops in oil.

2. The viscous (oil) phase was completely surrounded by the much less viscous (water) phase.

3. The diameter of oil form within the water annulus, varied from 60% to 90% of the pipe diameter.

4. At high average velocities the bubbles and slugs became distorted due to the higher degree of turbulence.

5. The velocities of the slugs were inferred (no measurements of slug velocities were made) to be greater than average mixture velocities. This is readily understood since oil bodies occupy the region of the pipe where the velocity is significantly greater than the mean velocity for the pipe flow as a whole.

The average oil velocity exceeded the overall velocity of the combined flow by 5% to 18% depending on the input ratio. This was deduced from calculations utilising the experimental input and in situ ratios for the concentric oil water systems.

6. From an examination of the pressure gradients recorded for bubble and slug flow, predictions were made for the magnitude of pressure gradients under capsule flow conditions. The experimental data obtained for the flow of different oils were presented in the form shown in Figure 2.1.

The ordinate; pressure gradient ratio, is defined as the ratio of experimentally determined pressure gradient for the flow of water and oil to the calculated pressure gradient for the flow of water alone at the same overall velocity. The effect of replacing part of the original water stream with semi-rigid bodies of oil is illustrated.

From this figure it is evident that, in general, the pressure gradient is reduced by the insertion of oil slugs or bubbles.

The water was always in turbulent flow, for the range of velocities considered. It was thus concluded that the presence of semi-rigid oil bodies eliminates the turbulence within the portion of the stream occupied by the oil as well as suppressing turbulence in the water phase, at least to the extent of the formation of a laminar sublayer adjacent to the water oil interface.

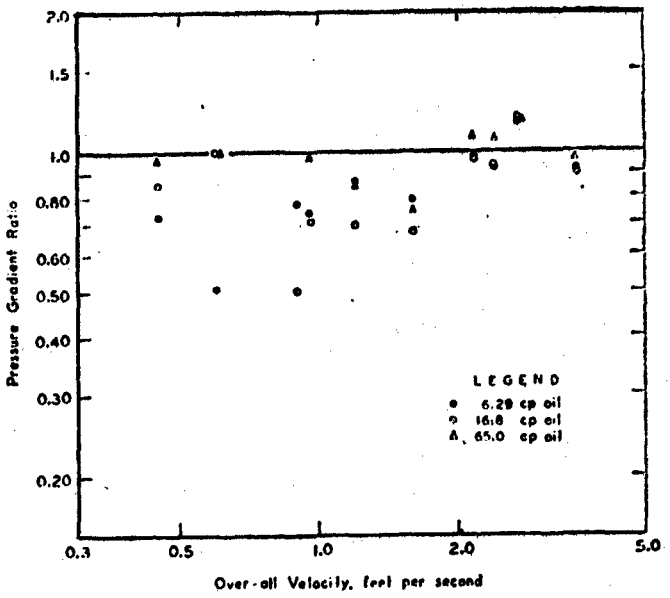

Pressure gradient ratio as a function of the over-all velocity for the oil-water system. The ratio is defined as the ratio of the experimentally determined pressure gradient for the flow of water and oil to the calculated pressure gradient for the flow of water alone at the same over-all velocity.

Fig 2.1 from Hodgson and Charles (ref. 21)

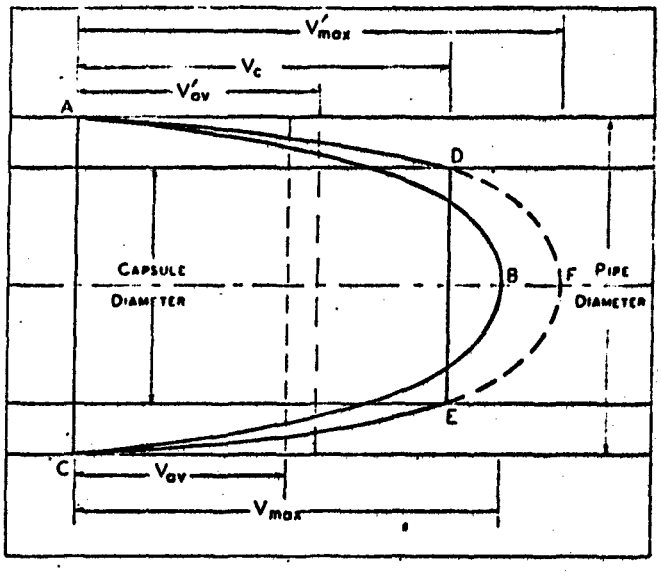

Velocity profiles in the capsule and capsule-free systems.

Fig 2.2 from Charles (ref. 10)

note: $V_{av} = \overline{V}$

It is also apparent that up to Reynolds numbers of about 15 000 the pressure gradient ratio is less than unity and after 15 000 the ratio is approximately unity.

The oil viscosity had no definite effect on the pressure gradient.

The opinion was also expressed that for laminar conditions (Reynold's number presumably based on the mean mixture velocity) the replacement of part of the water stream by oil slugs would increase the pressure gradient because of the necessary increase in the velocity gradient in the water phase between the oil bodies and pipe wall.

Note: All the above is based on a "capsule" of approximately the same specific gravity as water. No attempt was made to predict the behaviour of considerably heavier capsules in a water medium.

Charles (reference 10) in Part 2 considers a "Theoretical Analysis of the Concentric flow of Cylindrical forms." The theoretical model assumed in this paper was a cylindrical capsule aligned centrally in the pipe in a concentric position. This was recognised as an idealised situation, but one which represents the flow of capsules having the same density as the fluid. The capsule was assumed to be sufficiently long to ignore end effects. Both pipe and capsule surfaces were assumed smooth.

The capsule velocity was evaluated in terms of the average flow velocity and the capsule diameter to pipe diameter ratio for both laminar and turbulent conditions. Subsequently, estimates were made of the factor by which the pressure gradient is altered by the presence of the capsule.

Capsule velocity

The velocity profile assumed by Charles for the flow of pure fluid through a smooth pipe and the distortion due to the presence of a capsule are shown in Figure 2.2. It will be shown later, in Chapter 7, that such a profile is hardly likely to exist, except for neutrally buoyant capsules.

Laminar flow

The basic differential equation for unidirectional motion under steady state conditions (in cylindrical polar coordinates) is:

$$\partial^2 v/\partial r^2 + (1/r)\partial v/\partial r = 1/\mu\ (\Delta P/L)_c \qquad (2.1)$$

where v = velocity at radius r

μ = fluid viscosity

$(\Delta P/L)_c$ = pressure gradient.

A long cylindrical capsule flowing in a concentric position relative to the pipewall in laminar flow is considered and integrating twice gives the fluid velocity and capsule velocity when the appropriate boundary conditions are inserted.

The water flow in the annulus is given by a further integration, and combining the equations yields a relation between the capsule velocity and the average velocity under laminar conditions, viz:

$$V_c = (2/(1 + (d/D)^2)\overline{V} \qquad (2.2)$$

or

$$V_c = 2\ \overline{V}'\ (1 - (d/D)^2) \qquad (2.3)$$

where $\overline{V}'$ is the hypothetical average velocity based on the profile in Figure 2.2

$$\therefore \qquad \overline{V}' = (1/(1 - (d/D)^4))\overline{V} \qquad (2.4)$$

Note that the notation of all papers reviewed has been replaced by the notation used by the writer of this thesis.

Note also that from equation (2.2), since $0 \leq d/D \leq 1{,}0$; the capsule velocity always exceeds the average velocity.

Turbulent flow

The following is the only analysis given in the literature for turbulent flow, and it will be seen that this is a gross over-simplification dealing only with concentrically flowing neutrally buoyant infinitely

long capsules.

Using Prandtl's 1/7th power law for the turbulent flow of a single fluid in a circular pipe an equation is obtained correlating the maximum and local velocity, i.e.

$$v = v_{max}\{(r_p - r)/r_p\}^{1/7} \qquad (2.5)$$

This equation represents the velocity profile in the central part of the pipe (where $r < 0,85\ r_c$).

The assumption is made that the presence of the capsule has no effect on the velocity profile. In other words Charles theorised that a capsule attains a velocity both in turbulent and laminar flow such that V_c equals the point velocity in a free pipe velocity profile at the radial position in the pipe corresponding to the capsule boundary.

The profile used for turbulent flow in the capsule-pipe annulus is according to Prandtl's 1/7th power law for pipes (equation 2,5)

$$v = v'_{max}((r_p - r)/r_p)^{1/7} \quad \text{for} \quad r_c < r < r_p \qquad (2.6)$$

where v'_{max} is the hypothetical maximum velocity of the profile at the pipe axis as shown in Figure 2.2.

The capsule velocity is

$$V_c = v'_{max}((r_p - r_c)/r_p)^{1/7} \qquad (2.7)$$

From equation (2.4) the velocity ratio was calculated by summing the average velocity in the annulus and the capsule velocity which gives the overall average velocity of the system. Thus for turbulent flow

$$V_c = \overline{V}/\{\tfrac{7}{4}\gamma(1-\gamma) + \tfrac{49}{60}(1-\gamma)^2 + \gamma^2\} \qquad (2.8)$$

where $\gamma = d/D$

and $$\overline{V}' = 0,82\overline{V}/\{(1-\gamma)^{1/7}(\tfrac{7}{4}\gamma(1-\gamma) + \tfrac{49}{60}(1-\gamma)^2 + \gamma^2\} \qquad (2.9)$$

From plots of these equations (Figure 2.3) it can be seen that for diameter ratios of 0,5 to 0,9 under laminar conditions the capsule

velocity is 10% to 60% greater than the average velocity, while for turbulent flow the capsule velocity would be expected to be some 2% to 12% greater than the average velocity.

The pressure gradient ratio was defined as (see the discussion on Part 1) the ratio of the pressure gradient for capsule flow to the pressure gradient which would exist if fluid alone flowed in the same pipe at the same average velocity.

Four possible concentric flow models exist.

1. Laminar flow exists in both the annulus and in the capsule free pipe.
2. Turbulent flow exists in both the annulus and capsule free pipe.
3. Laminar flow in the annulus and turbulent flow in the capsule free pipe.
4. Turbulent flow in the annulus and laminar flow in the capsule free pipe.

The fourth model was only applicable in a small region and was not considered for analysis.

To calculate pressure ratios Charles used the relation $(\Delta P/L)_{water} \propto \overline{V}$ (laminar flow) and replaced the average velocities in equation (2.4) by the respective pressure gradients.

For turbulent flow the same approach was used except

$$(\Delta P/L)_W \propto \overline{V}^{1,75}$$

and

$$(\Delta P/L)_C \propto \overline{V}'^{1,75}$$

The pressure ratios calculated on this basis for the three models were

1) $$(\Delta P/L)_{CL} = (1/(1-\gamma^4))(\Delta P/L)_{WL} \qquad (2.10)$$

where subscript C = capsule

L = laminar flow

T = turbulent flow

W = water

2) $$(\Delta P/L)_{CT} = 0,82(\Delta P/L)_{WT}/\{(1-\gamma)^{1/7}(\tfrac{7}{4}\gamma(1-\gamma) + \tfrac{49}{60}(1-\gamma)^2 + \gamma^2\}^{1,75} \qquad (2.11)$$

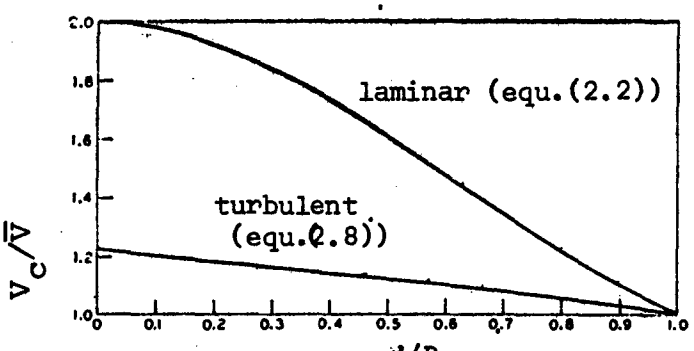

The relationship between the capsule velocity and the average flow velocity.

Fig 2.3 from Charles (ref 10)

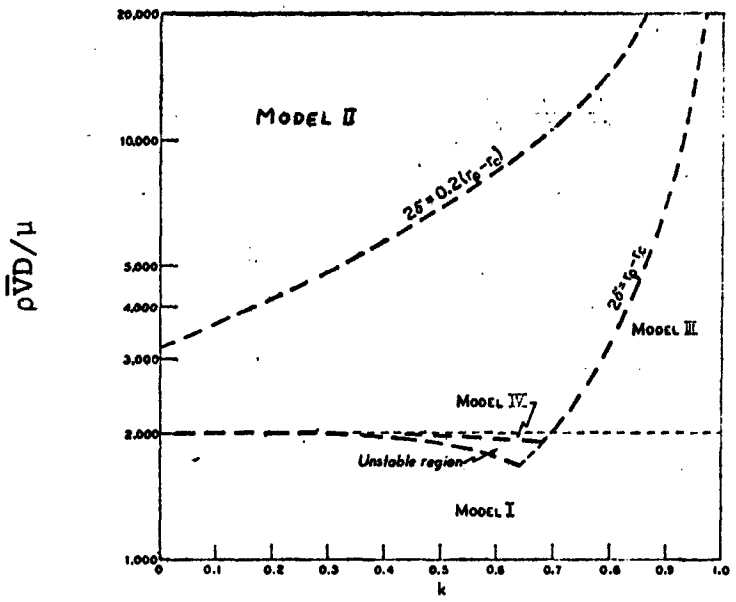

Regimes of applicability of the different models.

Fig 2.4 from Charles (ref 10)

3) $$(\Delta P/L)_{CL} = 202/((1-\gamma^4)(\rho\overline{V}D/\mu)^{\frac{3}{4}})(\Delta P/L)_{WT} \qquad (2.12)$$

The applicability of the various models is shown in Figure 2.4.

In this figure "k" is the diameter ratio. The dotted curve marked $2\delta = (r_p - r_c)$ is the locus of points for which the laminar sub-layers of the pipe and capsules just join.

The curve $2\delta = (r_p - r_c) \times 0{,}2$ is the locus of points for which the combined thickness of the laminar sub-layer is 20% of the thickness of the annulus. Model 4 is shown to be applicable to only a very small area in Figure 2.4.

For model 1 the pressure gradient ratio varies from unity at $d/D = 0$ to infinity at $d/D = 1{,}0$.

For model 2 the same phenomenon as above occurs but the increase in pressure gradient due to the capsule for a given diameter ratio is less than in the laminar case.

For model 3 both increases and decreases in pressure gradient are possible.

Both the laminar and turbulent flow analysis of Charles has been over-simplified as will be seen in Chapter 7.

For example one error made by Charles was to neglect the laminar sub-layer that should exist adjacent to the capsule wall in order to transfer shear from the water to the capsule.

Ellis (reference 15) in Part 3 considers "An experimental investigation of the transport by water of single cylindrical and spherical capsules with density equal to that of water."

This is the first experimental investigation of the series and is limited solely to neutrally buoyant capsules in a horizontal pipe. The investigation was carried out in a 35 ft (10,4 m) horizontal length of 1¼ in (32 mm) diameter plastic pipe.

The purpose of the investigation was to compare the magnitudes of the velocity of capsules recorded in the horizontal laboratory pipeline with those predicted in Part 2, and to determine the effect of length and end shape of cylindrical capsules.

In this paper only the effects on capsule velocity were considered (and not the pressure gradient).

The variables were capsule shape and size. The density was maintained as the density of water which was used throughout as the transporting medium. The pipe diameter was constant and the slope horizontal.

The results were presented as plots of velocity ratio versus average water velocity, and these were regarded as characteristic curves for capsule flow, illustrating the effects of different independent variables on the velocity ratio over a range of water velocities.

The characteristic curves are of the same general shape as shown on Figure 2.5.

The velocity ratio for the two capsules is greater than unity for all values of the average water velocity. This is in accordance with the theoretical predictions in Part 2. A feature of Figure 2.5 is that for a given capsule the velocity ratio is practically independent of average water velocity over a wide range.

Below 2 ft/s (0,608 m/s) the average water velocity is extremely critical and curves show a sharp rise of velocity ratio to a maximum of about 1 ft/s (0,305 m/s), followed by a precipitious drop and a further sharp rise. This sensitivity of velocity ratio, to average water velocity is, however, of no commercial significance since these low velocities are easily avoided.

Figure 2.6 shows the variation of velocity ratio with average water velocity for all the diameters of capsules 7 in (178 mm) long.

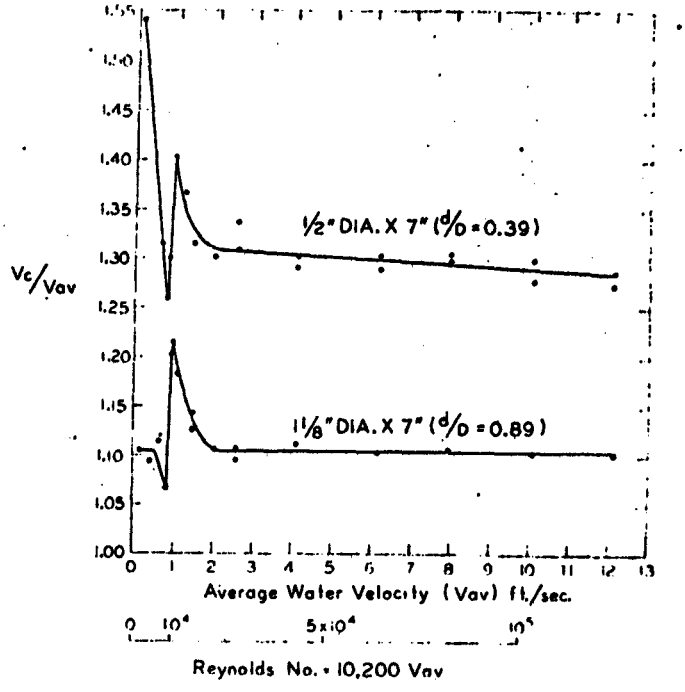

The variation of velocity ratio with average water velocity; two diameters of flat-ended capsules 7 in. long.

Fig 2.5 from Ellis (ref 15)

note: $V_{av} = \bar{V}$ and $R_e = \rho \bar{V} D/\mu$

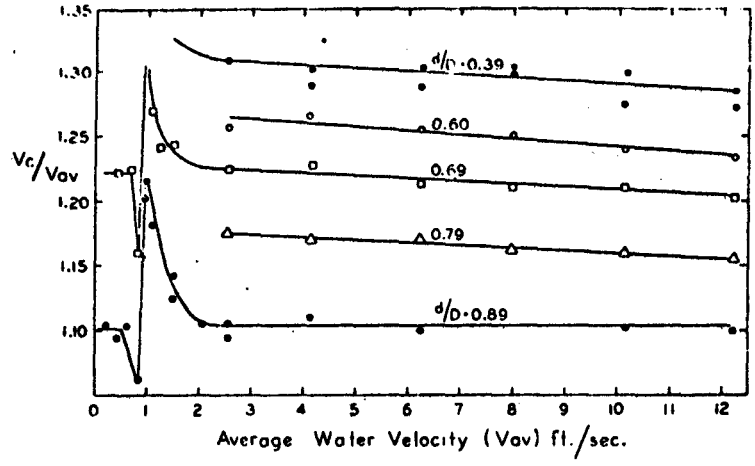

The variation of velocity ratio with capsule/pipe diameter ratio; (1) over the range of water velocities (flat-ended capsules 7 in. long).

Fig 2.6 from Ellis (ref 15)

Capsule velocity increases as diameter ratio decreases at a given capsule length and water velocity (note that these are neutrally buoyant capsules).

Figure 2.7 compares the results with the theoretical predictions for long cylinders. As diameter ratio decreases the results approach the curve for turbulent flow. At $d/D = 0,89$ although the flow conditions are turbulent in the pipe the results agree with the case of laminar flow in the annulus. The velocity ratio was found to increase with increasing length to diameter ratio, and the effect increases as capsule diameter decreases.

The effect of end shape was also tested. The effect of an ellipsoidal nose tended to be small but beneficial for all diameter ratios.

The adverse effect of an ellipsoidal rear grew progressively larger as diameter decreased.

The end effects are shown on Figure 2.8. Much of the apparent advantage of the ellipsoid-nosed capsules appears to be due to the increased length of these capsules, especially at smaller diameter ratios.

The capsules with both ends flat generally gave velocity ratio values intermediate between those with ellipsoidal fronts and flat rears, and the reverse configuration.

Ellis (reference 16) in Part 4 "An experimental investigation of the transport in water of single cylindrical capsules with density greater than that of water" extends the investigation to capsules of density greater than that of water.

The investigation was as presented in Part 3 except for the capsule density.

The same 32 mm diameter plastic pipe was used as for the tests in Part 3. Measurements were confined to the capsule velocity and average liquid velocity. Experimental data was again presented in the form of

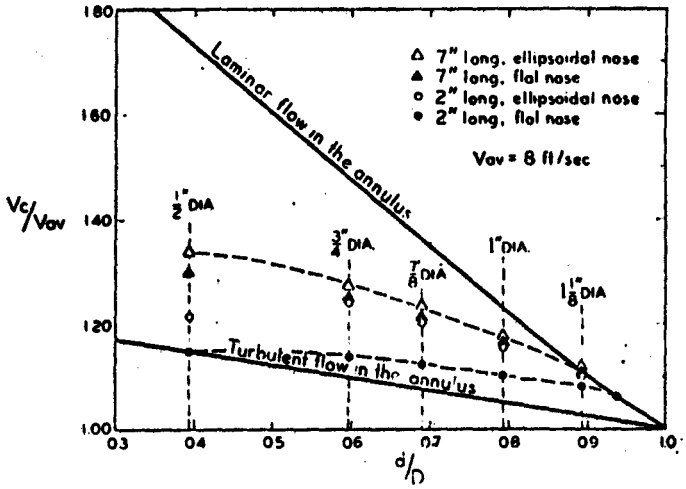

The variation of velocity ratio with capsule/pipe diameter ratio; (3) comparison with theory for long concentric cylinders, average water velocity 8 ft./sec.

Fig 2.7 from Ellis (ref 15)

note: $V_{av} = \overline{V}$

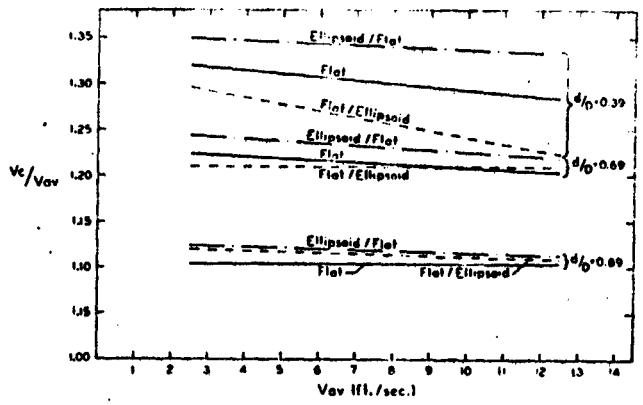

The effect of capsule end-shape: velocity ratio plotted against average water velocity.

Fig 2.8 from Ellis (ref 15)

velocity ratio against average water velocity. Some curves from this paper were used by the present author and these are re-presented as curves of capsule velocity versus mean water velocity in Chapter 10. Tests were performed exclusively with single capsules. The experimental data showed the following essential points.

1. Figure 2.9 shows a typical test result and it can be seen that a constant velocity ratio is attained, at high flows, which is greater than unity, but not as high as observed for the concentric equal density capsules.

2. The effect of increasing capsule length was to decrease the velocity ratio at low fluid velocities but to increase the velocity ratios at high fluid velocities.

3. The effect of increasing the diameter ratio was, in general, to increase the velocity ratio except for small diameter ratios at high velocities where the reverse was true.

The effects of diameter ratio and length to diameter ratio can both be seen on Figure 2.10. This figure will be discussed in more detail with relevance to the present thesis in a later chapter.

4. Increase in density ratio decreased velocity ratio at low velocities. All density ratios tend to the same velocity ratios at higher velocities.

5. The effect of end shape was slight. There was little or no advantage to be gained in fitting an ellipsoidal nose to large diameter capsules. An ellipsoidal rear was definitely disadvantageous.

A significant observation was that made regarding the presence of a liquid film between the capsule and pipe bottom. Particularly for the smaller diameter capsules it was noted that capsules lifted clear off the pipe bottom, first in tail up positions and at higher velocities nose-up positions. It was observed that at sufficiently high velocities this visible lift-off would occur for larger diameter ratios and heavier capsules.

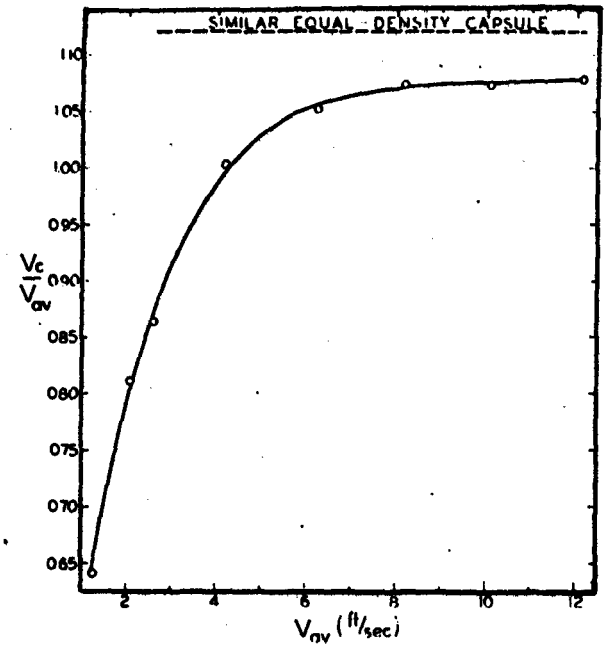

The effect of varying average water velocity: diameter ratio 0.89, 8 3/16 in. long with ellipsoidal nose and flat rear.

Fig 2.9 from Ellis (ref. 16)

note: $V_{av} = \overline{V}$

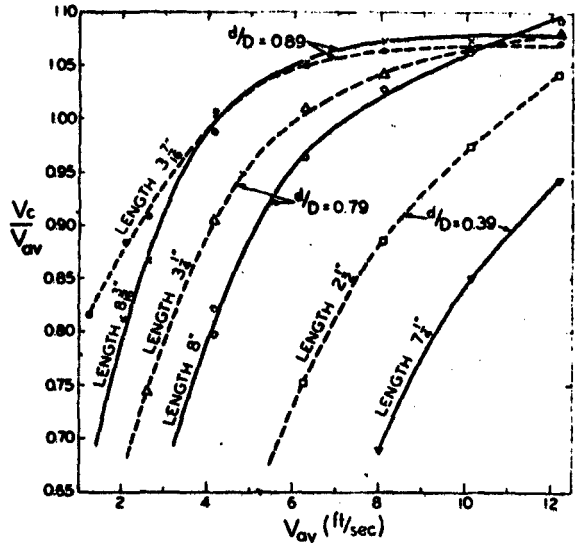

Fig 2.10 from Ellis (ref. 16)

No quantitative measurements of lift off were made and in Chapters 8 and 12 capsule lift will be discussed in detail.

Part 5, by Ellis (reference 17), in the series is not reviewed in detail here since this paper was concerned with spherical capsules and these are not considered practically feasible by the present author. The investigation was mainly concerned with the measurement of the velocities of different diameters of spheres of two densities.

The only observation of relevance to this thesis is a comparison of velocity ratio curves of spheres with those for cylindrical capsules of the same density. Such a comparison shows that the larger diameters of spheres reach constant velocity ratios which are almost the same as those reached by the same diameter of 7 in (178 mm) long cylindrical capsules, but reach them at lower water velocities.

Part 6 in the series by Newton, Redberger and Round (reference 42) was concerned with a "Numerical analysis of some variables determining free flow."

The authors used a numerical analysis approach to investigate the effect of axial displacement of cylindrical capsules with no end effects. Length, deformation of the capsule cross-section (ignoring end effects) and frictional effects between capsule and pipe wall for the capsule in laminar flow, were investigated.

The paper is concerned purely with laminar flow and no experimental observations are presented. Also the analytical results were not verified with experimental data.

The problem involved describing the motion of a capsule in an incompressible fluid flowing laminarly within the pipe.

In mathematical terms the problem was to obtain solutions of the Navier-Stokes and continuity equations assuming an incompressible fluid

of constant viscosity and density, time independence, constant axial pressure gradient and no inertial effects. With these assumptions the Navier-Stokes equation reduces to

$$\mu\Delta^2 V = -(dP/dx) \qquad (2.13)$$

where Δ^2 = the Laplacian operator.

For solution, the above equation was put into a finite difference form corresponding to a mesh system and the equation was solved by standard explicit iterative methods. An appropriate mesh system was found by the use of conformal transformations.

The effect of clearance was to increase the velocity ratio as the capsule approached concentricity. As this velocity ratio increased, the ratio of pressure required to move the capsule compared with the pressure required for tne fluid alone was shown to decrease.

The thicker the layer between capsule and pipe, the more rapidly capsule motion increases.

To obtain a distortion parameter it was assumed that part of the capsule perimeter conformed to its own radius and the remainder to the pipe radius. The distortion was the percentage of the periphery which conformed to the pipe radius.

Up to 15% distortion there was little effect on the pressure gradient. The pressure gradient ratio then increased with distortion. The rate of increase, increased with displacement approximately as the inverse of the thickness of the fluid layer between capsule and pipe.

For consideration of capsule ends and length effects, the analysis was limited to a concentrically flowing capsule. It was assumed that at any point in the flow, the axial pressure gradient is proportional to the velocity at that point.

The results were negative. No significant differences from the

theoretical velocities for infinitely long capsules were obtained regardless of the end shape.

The following two papers in the series, Parts 7 and 8, were concerned with capsule transportation in oil and, as such, are not directly relevant to the present study, although they will be reviewed briefly.

Ellis and Bolt (reference 18) in Part 7 on "An experimental investigation of the transport by two oils of single cylindrical and spherical capsules with density equal to that of the oil," attempt to extend the experimental study of equal density capsules into the laminar regime by the use of rather viscous oils.

Two oils were used; the first (more viscous) being used in the range of pipe Reynolds numbers normally marking laminar pipe flow, and the second enabled the values of the velocity ratio with the more viscous oil to be compared with those for the thinner oil at the same Reynolds numbers. The second oil was also used to extend the flow regime into the turbulent region and comparing the results with those obtained for water at a similar Reynolds number. Reynolds number was defined as $\rho\bar{V}D/\mu$.

Figure 2.11 shows the results of plotting velocity ratio against Reynolds number for the two oils. At low Reynolds numbers (less than 500) the differences between the curves for the "Faxam" and "Mentor" oils are not significant. The most important difference between the curves for the two oils is that the curve trough depths increase with decreasing viscosity. This change in curve trough depth is accentuated at lower diameter ratios. The variations in velocity ratio of the capsules occurs at progressively lower Reynolds numbers as the diameter ratio increases.

With most pipe installations the flow changes from laminar to turbulent in the range of Reynolds numbers from 2000 to 4000.

At Reynolds number of about 2100 an abrupt change takes place and

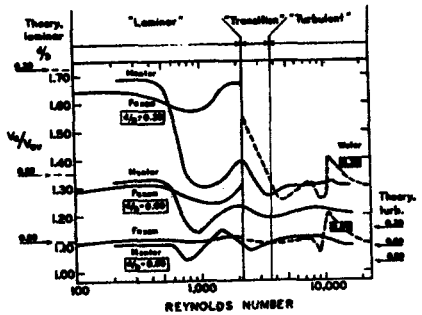

A comparison of the velocity ratios of 7-in. flat-ended cylinders in the three liquids, with diameter ratio as parameter.

Fig. 2.11 from Ellis and Bolt (ref. 18)

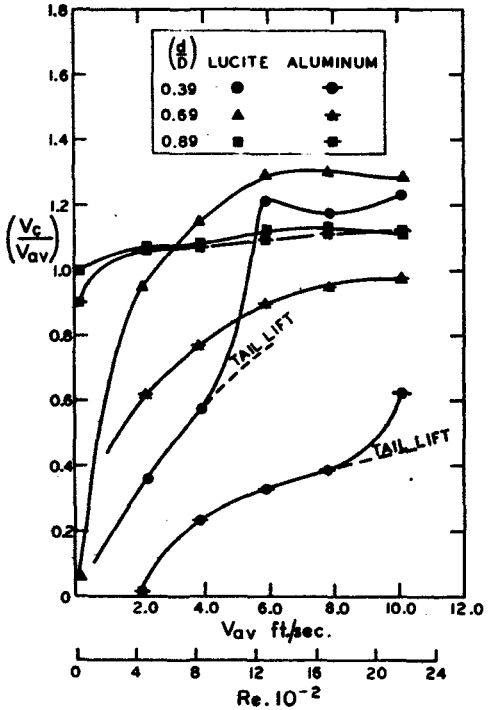

The variation of velocity ratio with average liquid velocity-pipe Reynolds number for flat-ended cylinders, 7-in. long, made of solid lucite and solid aluminum, in Faxam 40: three diameter ratios, 0.39, 0.69 and 0.89.

Fig. 2.12 from Round and Bolt (ref. 58)

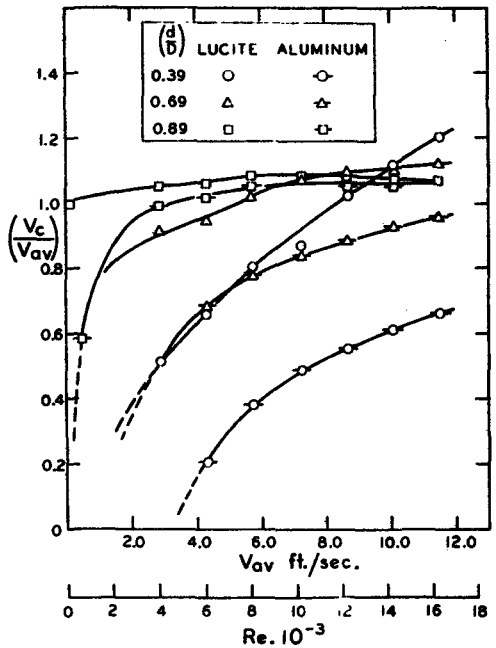

The variation of velocity ratio with average liquid velocity-pipe Reynolds number for flat-ended cylinders, 7-in. long, made of solid lucite and solid aluminum, in Mentor 29: three diameter ratios, 0.39, 0.69 and 0.89.

Fig. 2.13 from Round and Bolt (ref. 58)

note: $V_{av} = \bar{V}$ and $R_e = \rho \bar{V} D/\mu$

eddies in the centre of the pipe grow rapidly (with increasing Reynolds number).

The laminar annulus around the disturbed core dimishes with increasing Reynolds number above 2100 and at about 3500 to 4000 no laminar layer is observable.

The capsules in "Mentor" oil show a dip in velocity ratio curves at these Reynolds numbers. From Figure 2.11 similar curves for water show a sharp peak and then levelling off.

The velocity ratio curves for the three liquids are decreasingly affected as viscosity increases at a given Reynolds number.

It is evident that the velocity ratio generally increases with decrease in capsule diameter. Two lengths of capsules were tested.

At Reynolds numbers less than 2200 capsule length had little effect on velocity ratio of the largest diameter capsules in either oil. Smaller diameter capsules showed an increase of velocity ratio with increase of length at constant diameter and Reynolds number. With smaller capsules still the effect was difficult to determine due to capsule instability. At Reynolds numbers greater than 2100 there was a general increase of velocity ratio with length, the effect becoming more pronounced at increased Reynolds numbers.

The capsules were also tested with ellipsoidal noses. And at Reynolds numbers less than 2200 the ellipsoid nose resulted in a slight increase of the velocity ratio of small diameter capsules. The effects of an ellipsoidal nose were insignificant in turbulent flow.

The most significant feature of the spherical capsules is that they yielded slightly higher velocity ratios than cylinders of the same diameter ratio, but as diameter ratio decreased the velocity ratios of the spheres fell below those of the cylinders at the same Reynolds number.

The most interesting results in this paper is the finding of critical Reynolds numbers at which velocity ratio curves of equal density capsules reach maxima or minima values.

The next paper, Part 8, by Round and Bolt (reference 58) also deals with an oil medium and is entitled "An experimental investigation of the transport in oil of single, denser-than-oil, spherical and cylindrical capsules." This paper was an extension of the work, previously carried out using equal density capsules in two mineral oils, to flow systems in which the capsules were denser than the carrier liquid.

The same equipment and oils were used as in the previous case and the velocity ratio was again the only dependent variable considered.

Figures 2.12 and 2.13 show the variation of velocity ratio with average liquid velocity for the two oils. The data was stated to be unreliable at low liquid velocities. It is apparent that the velocity ratio is greater at a particular average velocity for larger diameter capsules.

It was noted that capsules lift off the bottom earlier in laminar than turbulent flow. All the curves show an increase in velocity ratio as average velocity increases.

At the lowest diameter ratio the effect of tail lift causes a dramatic change in velocity ratio with increasing average liquid velocity. Capsules of three different lengths were studied and it was found, in general, that for a fixed diameter ratio the velocity ratio decreases as L_c/d increases. Exceptions do occur at particular diameter ratios when the capsules go into a state of oscillation.

End configurations were again investigated and ellipsoidal noses were found to have no effect on the highest diameter ratios, but slightly increased velocity ratio at lower diameter ratios.

In general the observations recorded for the water medium do not differ

in principal from those recorded for the oil mediums.

Part 9 by Kruyer, Redberger and Ellis (reference 28) is a theoretical study of capsules in laminar flow concerned with an infinitely long cylinder at varying clearances. It is the first of the series not published in the Canadian Journal of Chemical Engineering and appears to be an alternative approach to that presented in Part 6.

The analysis employs the equation developed by Bentwich, Kelly and Epstein (reference 2) who derived an analytical expression describing laminar flow conditions in the annulus of a pipe with an infinitely long free flowing cylinder.

The equations derived by Bentwich et al are:

$$Q_A = (\pi g D^4/(128\mu))(\Delta P/L)_c\left[(1-\gamma^2)^2 + 2\gamma^2\varepsilon^2 - \{8\gamma\sinh(\alpha+\beta)\}\right.$$
$$\left.\times \{\sum_{n=1}^{\infty} (\coth n(\alpha-\beta))(2(n\varepsilon\sinh\beta-\gamma^2)/(e^{2n\beta}+e^{2n\alpha})+\gamma^2/(e^{2n\alpha}))\}\right] \quad (2.14)$$

where $\alpha = \cosh^{-1}\{(1-\gamma^2-\varepsilon^2)/2\gamma\varepsilon\}$

$\beta = \cosh^{-1}\{(1-\gamma^2+\varepsilon^2)/2\gamma\varepsilon\}$

ε = distance between axis of pipe and cylinder expressed as a fraction of the pipe radius

n = integer

Q_A = flow in the annulus

$\gamma = d/D$

For the cylinder Bentwich et al obtained:

$$Q_c = (\pi g D^4/(128\mu))(dP/L)_c\{4\gamma^3\sinh(\alpha-\beta)\} \quad (2.15)$$

The flow in a free pipe was then equated with $Q_c + Q_A$ to give

$$((\Delta P/L)_c/(\Delta P/L)_w)_{Q=Const} = 1/f(\gamma,\varepsilon)$$

If instead the pressure gradients are equated, then

$$\left[\frac{Q_p}{Q_c+Q_A}\right](\Delta P/L) = \frac{1}{f(\gamma,\varepsilon)}$$

Using these relations, pressure and velocity ratio calculations were compared with previously determined experimental results for a range of diameter ratios from 0,25 to 0,97 and clearances varying from fully eccentric to concentric capsule positions. No attempts were made to measure clearances experimentally.

The results presented for fully laminar flow in a ½in (12,5 mm) pipeline are in good agreement with the theory, but this regime is not applicable in practice. For the 1¼in pipe (32 mm) the experimental results were again for a viscous lubricating oil with laminar flow in the free pipe at all liquid velocities. The experimental points are further removed from the analytical predictions than those of the smaller diameter pipeline.

When oil velocities in the free pipe were turbulent the analytical model of laminar flow both in the annulus and free pipe is no longer valid, and experimental points deviate markedly from the analytical prediction even though laminar flow existed in the annulus.

The theory was thus shown to be valid only for the cases from which it was derived, i.e. laminar flow in both the free pipe and the annulus.

Berkowitz, Brown and Jensen (reference 3) and Brown and Jensen (reference 8), carried out studies on the flow of coal paste slugs in oil. The first paper was concerned with the introduction of the concept. Some experimental results were presented as velocity ratio against average oil velocity.

The slugs were prepared from a water paste of < 48 mesh coal, mixed with sufficient water (70 : 30 coal-water mixture) to form a fairly stiff paste, extruded through a cylindrical chamber and chopped into segments. The mechanical strength was derived from internal particle interlock together with the hydrostatic pressure.

The two papers show that there is a broad conformity between the flow

behaviour of paste slugs and rigid capsules. However, the curves all showed a tremendous amount of scatter.

The paste slugs were found to deform in various ways and the flow behaviour of individual slugs was found to be variable and, thus, residually uncertain.

Ellis and Kruyer (reference 19) in Part 10 discuss "Empirical pressure and velocity correlations for Cylindrical capsules conveyed in pipelines up to 4 inches in diameter." This paper was published at the First International Conference on the Hydraulic Transport of solids in pipes and is the first paper to have emerged, in the series from Alberta, in which pressure losses across capsules in turbulent flow were considered. At the same conference velocity and pressure correlations were proposed by the author of this thesis, and in a later Chapter (Chapter 15) these will be compared with the correlations of Ellis and Kruyer.

Their method was essentially one of correlating capsule pressure gradients with liquid and capsule velocities, and pipe diameter by means of friction factor versus Reynolds number diagrams.

The problem was to determine the characteristic fluid velocity and the relevant dimensions for use in the friction factor and Reynolds number.

The capsule pressure gradient was defined as

$$(\Delta P/L)_c = \left[\Delta P - \frac{L-L_c}{L}\ \frac{\Delta P_f}{L}\right] / L_c \qquad (2.16)$$

where ΔP = total pressure drop

ΔP_f = pressure drop in capsule free pipe

The capsule pressure gradient relates to the section occupied by the capsule only and does not include the liquid pressure gradient in front of and behind the capsule.

There appears to be an error in equation (2.16) and it is rewritten to

conform with present notation as

$$(\Delta H/L)''_c = (\Delta H_m - \Delta h_f(L_p - L_c)/L_p)/L_c \qquad (2.17)$$

This is also the first paper in the series in which capsule velocity was plotted against mean water velocity, and the linear function discovered by the present author and presented at the same conference was confirmed. Previously some of the results given in Part 4 of the series were re-plotted as capsule velocity against mean water velocity by the present author and these are given in Chapter 10.

Ellis and Kruyer found the curves to be non-linear at low capsule velocities. This was not found in the present study and the explanation is probably that at low capsule velocities the capsule does not move steadily along the pipe bottom and may slow down and speed up sporadically on slightly rougher or smoother sections of the pipe.

The first pressure measurements in the series are shown on Figures 2.14 and 2.15 which show the effect of diameter ratio and specific gravity respectively.

These figures, however, do not correspond with those presented in this thesis because of the difference in definition of pressure loss across a capsule. The ΔP_c value of Ellis and Kruyer corresponds with $\Delta H''_c$ in this thesis rather than ΔH_c which was used in preference to $\Delta H''_c$ for reasons given in Chapter 15.

Figure 2.14 shows that diameter ratio has little consistent effect. For some diameters the pressure gradient increases with liquid velocity and decreases with others. This also does not agree with present results and the explanation is probably the comparatively small range of diameter ratios selected by Ellis and Kruyer.

The correlation of Ellis and Kruyer is shown on Figure 2.16. The friction factor is defined as:

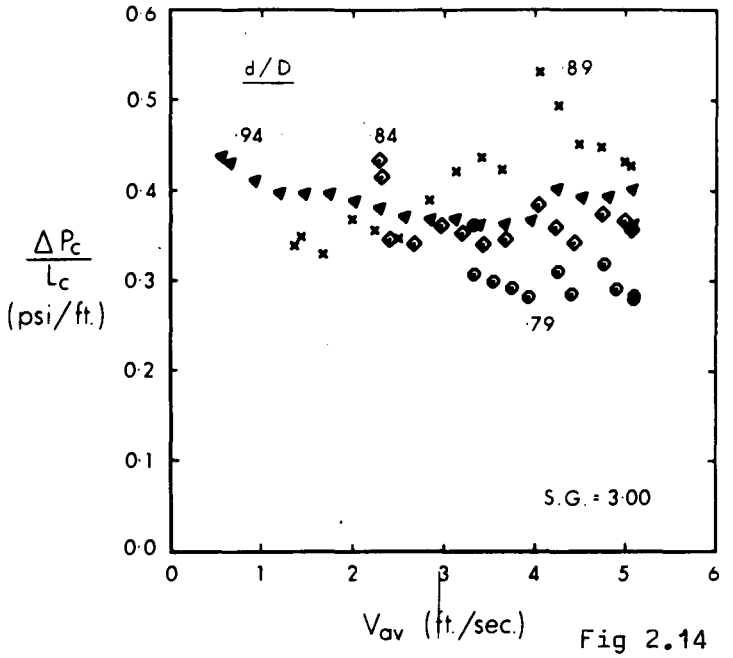

Fig 2.14

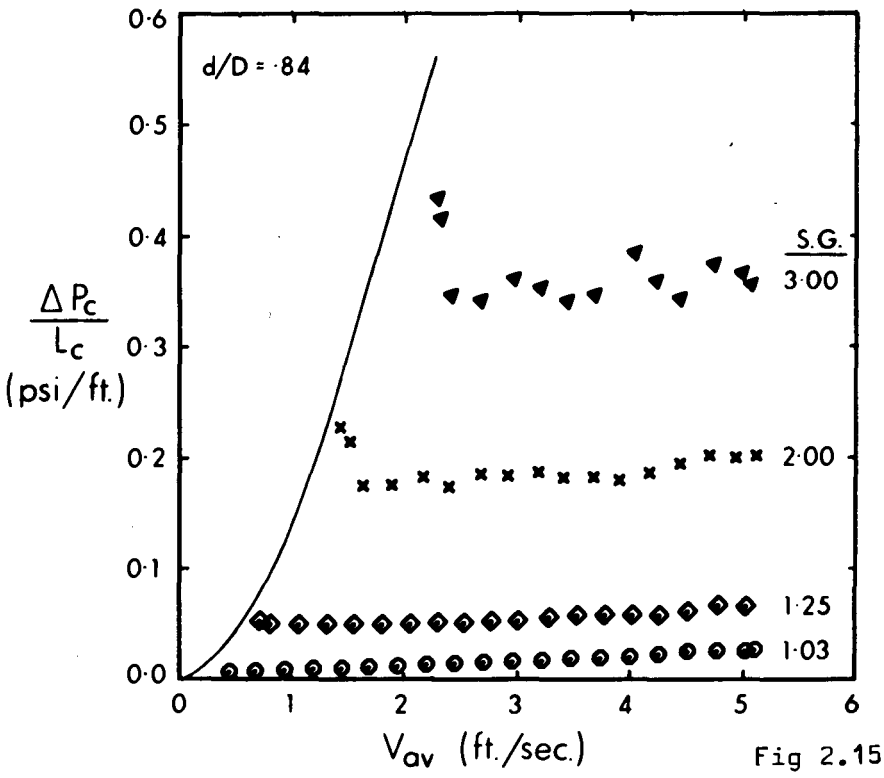

Fig 2.15

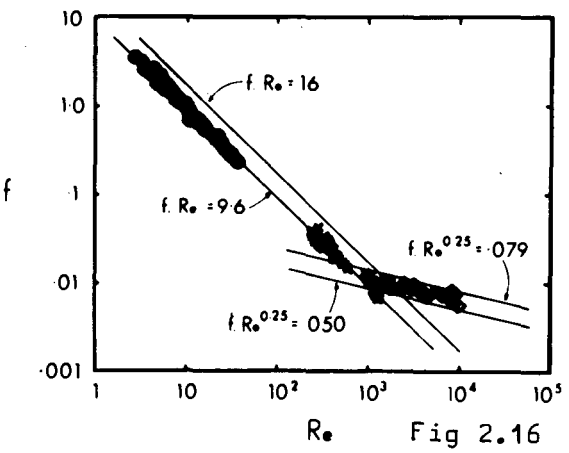

Fig 2.16

From Ellis and Kruyer (ref. 19)

$$f = (\Delta P/L)_c \, g_o(D-d)/(2\rho(\overline{V}_a - AV_c)^2) \qquad (2.18)$$

where g_o is actually introduced because of the system of units used.

The Reynolds number is defined as

$$R_e = (D-d)(\overline{V}_a - AV_c)/\nu \qquad (2.19)$$

The data is apparently correlated on this basis. However, the empirical correlation is only satisfied by choosing specific values of A and in Figure 2.16 A varies from 0,465 to 0,35 for a particular diameter ratio, d/D = 0,9 in a 4,03 in (102 mm) diameter pipe, although the value of A chosen was 0,35.

The correlation of the Alberta team is compared with a present correlation in Chapter 15.

In Part 11 (unpublished at the time of writing) by Kruyer and Ellis (reference 27) on "Friction factors for the eccentric Annulus with a moving core," further explanations for the correlations given in Part 10 are given.

Basically what Kruyer and Ellis have done is to correlate capsule data on friction factor versus Reynolds number diagrams as Ellis and Kruyer did in Part 10. The standard equations (2.18) and (2.19) for f and Reynolds number are again used but in Part 11 they seem to have changed their definition of the equivalent velocity (V_{eq}) and hydraulic mean diameter (D_{eq}) which were given in Part 10 as:

$$V_{eq} = \overline{V}_a - AV_c$$

and

$$D_{eq} = (D-d)/4$$

In Part 11 the equivalent velocity was obtained by substituting a Blasius type relation in the force balance equation for an infinitely long static annulus and putting the equivalent velocity in the form

$$V_{eq_w} = (V_{an} - aV_c) \quad \text{for the wall and}$$

$V_{eq_c} = V_{an} - bV_c$ for the core giving the net equivalent velocity as

$$V_{eq} = \left[\{(V_{an} - aV_c)^{2-n} + \gamma(V_{an} - bV_c)^{2-n}\}/(1-\gamma)\right]^{1/(2-n)} \quad (2.20)$$

where n is an index in the Blasius type equation.

The expressions (2.18) and (2.19) thus now become

$$f = (\Delta P/L)_c \, g_o(D-d)/(2\rho V_{eq}^2) \quad (2.21)$$

and

$$R_{eq} = D_{eq} V_{eq}/\nu \quad (2.22)$$

The equivalent velocity for laminar flow where $n = 1$ (since $f = 16/R_e$) is:

$$V_{eq} = V_{an} - ((a+b\gamma)/(1+\gamma))V_c$$

and the equivalent hydraulic mean diameter becomes

$$D_{eq} = (16/fR_{eq})(D-d)$$

This is in order to make results from eccentric annuli correspond with those for a free pipe.

In turbulent flow $n = 0{,}25$ (since $f \propto 1/R_e^{0,25}$ in the Blasius equation) and the equivalent velocity becomes

$$\overline{V}_{eq} = \{(\overline{V}_{an} - aV_c)^{1,75} + \gamma(\overline{V}_{an} - bV_c)^{1,75}/(1+\gamma)\}^{0,57} \quad (2.23)$$

a and b are given by experiment as $0{,}2$ and $0{,}8$. D_{eq} in turbulent flow is defined, arbitrarily, in the same way as for laminar flow.

The value for V_{eq} given for turbulent flow is used when $R_{eq} > 2000$.

Thus what they have actually done is to try and fit the f versus R_e diagram (with the Blasius equation) using an arbitrary pseudo velocity V_{eq} and an arbitrary hydraulic mean diameter (D_{eq}).

However the use of arbitrarily chosen values of velocity and hydraulic diameter can only be justified if it works, and it will be shown in Chapter 15 that it is not a comprehensive correlation.

For example when correlating capsules of different length, Figure 2.17 shows the experimental points, and for $L_c/d = 6,07$ the scatter about the mean line is 90% above and 58% below. This can hardly be considered a correlation since it only works for $L_c = 48"$.

The constants a and b must have been chosen to fit the long capsules and do not apply to short ones.

The correlation of f versus R_e in Paper 10 and that in Paper 11 appear to be the same although different definitions of V_{eq} and D_{eq} are used.

The final correlation Figure 2.16 is given in both parts 10 and 11 even though different definitions were used for the equivalent velocity.

The empirical correlation of Kruyer and Ellis appears to be essentially for long continuous trains of capsules. At no time, according to the literature, have continuous trains been tested. Either very long capsules of the order of $L_c/d = 48$ have been tested which are in fair agreement with the correlation, or shorter capsules have been tested which do not agree with the correlation. In the paper by Jensen and Bruce (reference 23), which will be reviewed next, and which described experiments in a 4in (101,6 mm) diameter test line, no capsule train fully occupies the section between pressure tappings. One hundred percent linear linefill was obtained by calculation from partial linefill. They state that "Even in ..... sections where measurements could have been made with capsules of ..... trains extending beyond both pressure taps, the trains never represented 100% linefill because of spaces between the individual capsules."

It is the present author's opinion that, for technical reasons, 100% linefill will not prove feasible in practical applications.

Jensen and Bruce (reference 23) in a paper presented at the First

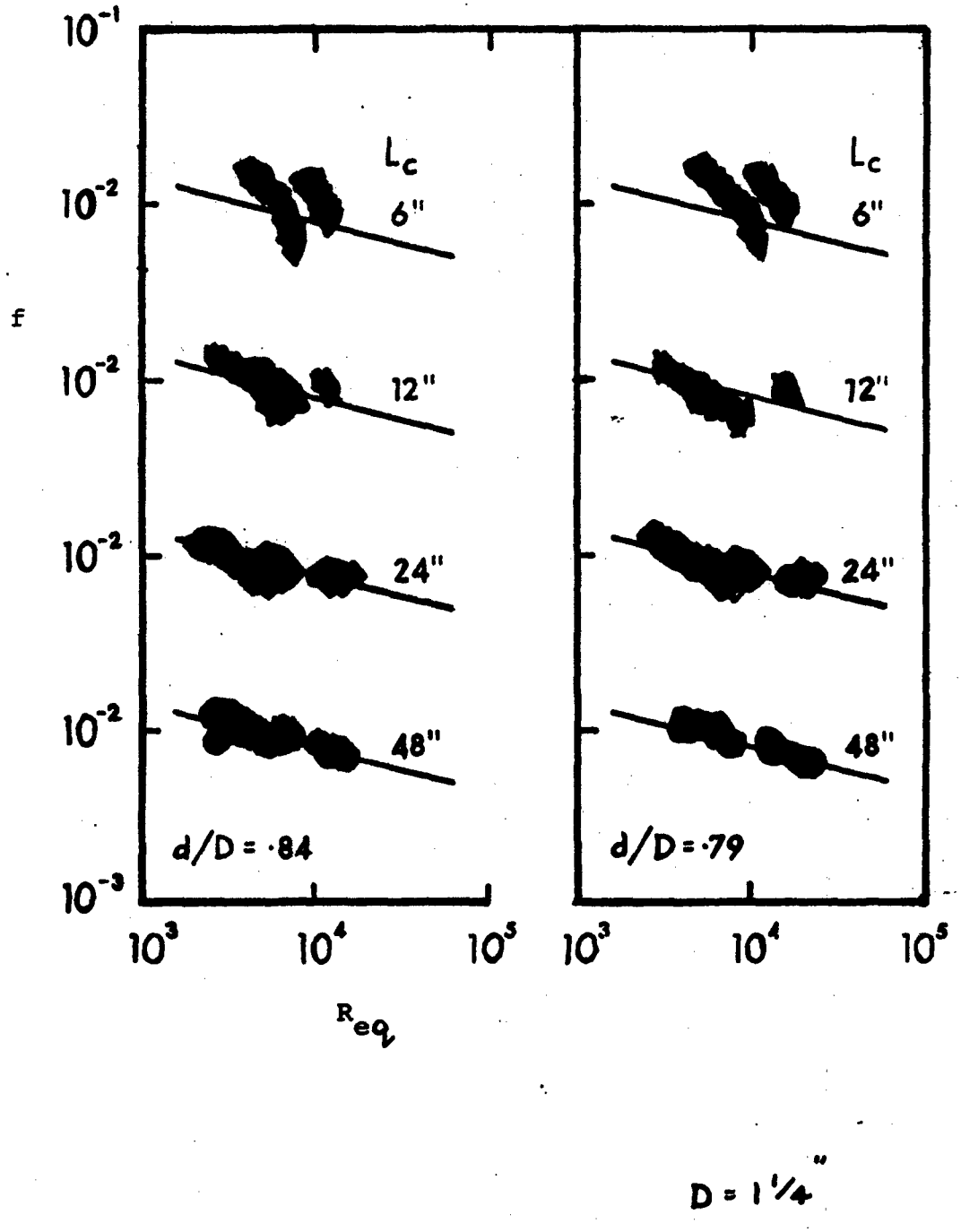

Fig 2.17 from Kruyer and Ellis (ref. 27)

International Conference on the hydraulic transport of solids in pipes reports on tests carried out in a 3900 ft (1200 m) long, 4 in (104 mm) diameter pipeline. The main conclusion of the study is that capsule pipelining is feasible when compared with existing railway tariffs.

The other important point is that this is the first paper to have emerged from the Research Council of Alberta that deals with power requirements. These are represented as horsepower per mile as functions of the average velocity. The presentation of this paper coincided with power requirements calculated by the present author in terms of watts/m.

The expression representing the power requirement per unit length of pipeline divided by the capsule mass flow delivery rate was also presented by the present author at this conference, and Jensen and Bruce introduced the concept in terms of horsepower-hr/ton-mile, but they applied it to spheres only.

The following summarises the main points given in the paper by Jensen and Bruce:

1. Dense capsules travel at capsule velocities which are, in all cases, less than the capsule velocities for less dense capsules, at the same diameter.

2. Increasing the diameter results in higher capsule velocities.

3. Lengthening the capsules yield slightly lower pressure gradients across the capsules.

4. Left to itself a capsule train starting at the point of loading as a continuous string of capsules tends to spread out while travelling through the pipeline.

5. Pressure gradients decreased relative to that of the carrier liquid as viscosity increased.

6. With regard to pressure surges, experiments showed that the presence of capsules attenuates the shock wave amplitude in the pipeline.

7. Little detail was given of the economic study, but capsule pipelining was said to be economically viable.

8. It was also mentioned that a solution to the important and complex question of correlating data to arrive at formulae for predicting hydrodynamics in commercial sizes was not developed.

Hodgson, Kruyer, Roehl, Round and Ellis (reference 22) presented a paper to the Canadian Institute of Mining and Metallurgy which described "A practical projection of Capsule pipelining : Edmonton-Hardisty Trunk-line test."

The test was run in a 109 mile (175,4 km) section of 20 in (508 mm) o.d. pipe. A solitary capsule was used 16 in (406,4 mm) in diameter giving a diameter ratio of 0,83 and 50 in (1270 mm) long (length to diameter ratio = 3,17) filled with crude oil and weighing 514 lbs (mass = 233 kg) giving a capsule density of 1,95 times the density of oil in the pipeline. The velocity of the capsule was measured as was the average oil (the conveying medium) velocity.

The pipeline had welded joints at 40 ft (12,2 m) intervals and was de-waxed and cleaned bi-monthly by the passage of scrapers. Wear on scrapers and batching pigs was found to be negligible.

The tracking method used was the radioisotope, cobalt 60 and detection was achieved by geiger counters. This method was not entirely satisfactory. However, it was possible to hear the capsule in the pipe and it could be detected when contacting the pipe joints. By assuming a 40 ft (12,2 m) spacing between pipe joints it was possible to obtain an indication of capsule velocity. The accuracy of determining capsule velocity was estimated to be $\pm$ 20%.

The pipeline gradient varied somewhat, but the average pipeline gradient was low and the only conclusion drawn was that capsule velocity was slightly higher on downward slopes and higher on upward slopes. No quantitative conclusion could be drawn.

Results of these tests are given in Chapter 10 and will be discussed therein except to point out here that the velocity ratio falls progressively as the pipeline diameter is increased. The reason for this is not discussed in the paper and will be dealt with in Chapter 10.

In general the results of the test indicated no unexpected anomalies and confirm the belief that the method is feasible on a large scale.

CHAPTER 3

TECHNOLOGY

This thesis is primarily devoted to a study of the fluid mechanics of capsule flow. This Chapter is essentially a brief digression into some proposals for overcoming the technological difficulties involved.

This research project can be divided into three broad categories, the scientific, technological and economical aspects.

The bulk of this thesis is concerned with, what can be termed, the scientific study and the primary concern is with the question; what happens? How do the capsules behave in the pipe and what is the effect of the numerous variables involved? Once the scientific questions have been answered, the next question concerns the technology. Only when the scientific and technological questions have been examined can the third aspect be dealt with; the economics, and the question; is it economically feasible? can be examined.

In this Chapter some of the technological problems considered are (1) the preparation of "capsules," (2) the injection of capsules into the pipeline, (3) the recovery of capsules at the outlet end, (4) booster pumps in the line and (5) pipe layout systems.

A certain amount of technological innovation was necessary for the experimental investigation and some suggestions are given in the remainder of this Chapter as to methods of overcoming the technical problems involved.

1. The preparation of capsules

There are various methods of encapsulating the solids to be transported.

1.1 Solid containers

The solid load can be inserted into solid cylindrical containers of metal or plastic. The containers may be re-usable. This type of capsule is particularly useful for conveying substances having a density substantially greater than that of the conveying fluid.

Materials such as iron ore, machine parts or any substance that has to be prevented from contamination by the supporting fluid, can be encapsulated in this manner.

One important advantage of this method is that the bulk density may be controlled by partially filling the container.

Also a multiplicity of commodities may be simultaneously transported in the same pipeline.

1.2 Semi-rigid or flexible containers

These capsules may also be re-usable and could be used for transporting liquid chemicals, such as sulphuric acid or granular solids, such as foodstuffs or fertilisers or liquified or compressed gasses.

1.3 Expendable containers

A disposable film of plastic such as polyethelyne could be used for enclosing the material to be transported and in this case the "packaging" could be discarded by the recipient. This method could also be used for solid waste disposal.

1.4 Casting or sintering

The material could be moulded into cylinders (or spheres) and the cost of encapsulation is eliminated.

Ingots of aluminium or other metals could conceivably be transported in this way.

1.5 Paste slugs

Berkowitz et al (reference 3) proposed a capsule, forming a paste or

slug of the solid to be transported.

A cohesive paste is formed using a binder liquid which is immiscible with the transporting liquid. The paste can be extruded through a circular orifice and chopped into segments of convenient length.

Berkowitz et al carried out experiments with coal paste slugs formed with, 30% by weight, water transported in oil. Another substance amenable to transport by this method is sulphur.

2. Injection

There are various methods of inserting capsules into the pipeline and capsules may be injected under atmospheric pressure or at a high pressure point in the pipeline.

2.1 Injection under positive pressure

The injector used in the present experiments was designed for operation under pressure since the laboratory pipeline was fed from a 15 m elevation constant head tank. Since the injector is part of the experimental apparatus, it will be discussed in Chapter 4.

Figure 3.1 shows a picture of the injector and Figure 4.2 is a drawing of the details. Basically the injector consists of a rotating drum which allows capsules to be injected into the pipeline via an elliptical inlet.

In a prototype situation a double lock valve replaces the lid shown on Figure 4.2. Alternatively, if the pressure is not too high at the injection points, the valves can be dispensed with and the capsules fall under the action of gravity into the injection chamber.

Figure 3.1a shows every second compartment occupied by a capsule (for reasons explained in Chapter 4).

This is a view from the downstream end of the pipe and the elliptical

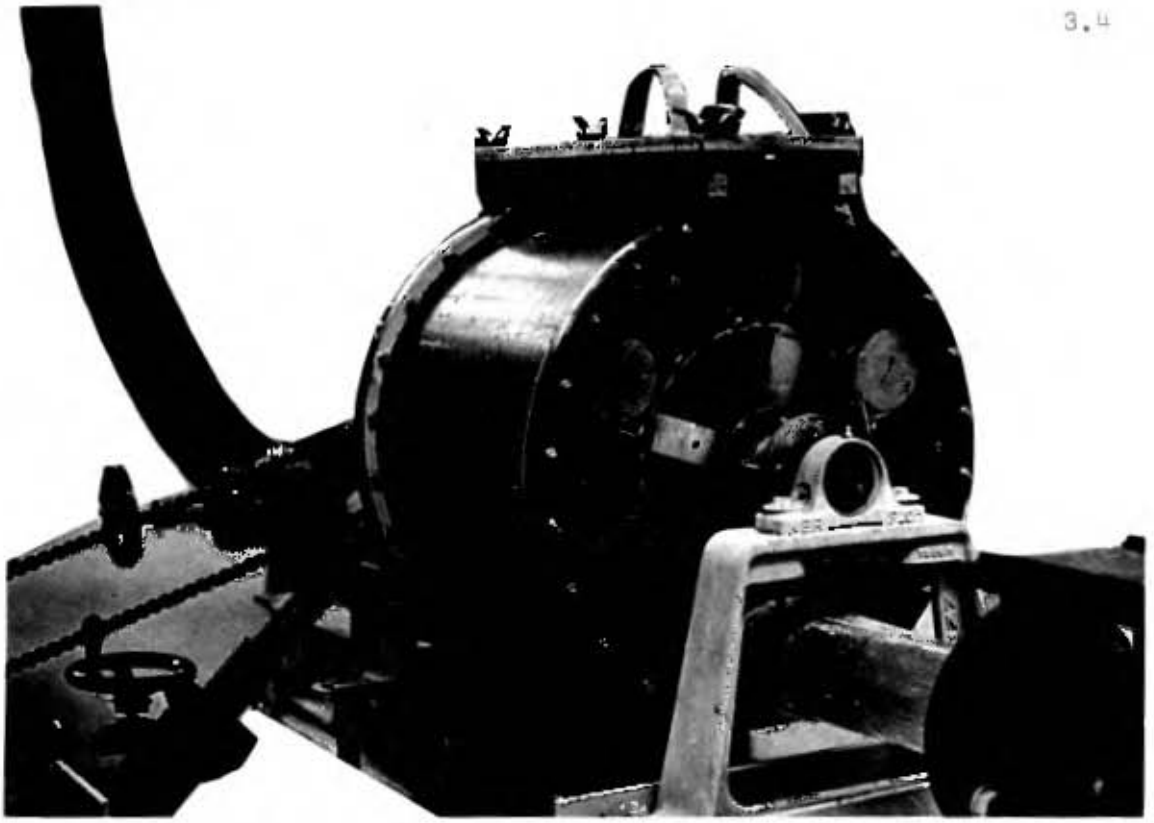

Fig 3.1a View of Injector from Downstream

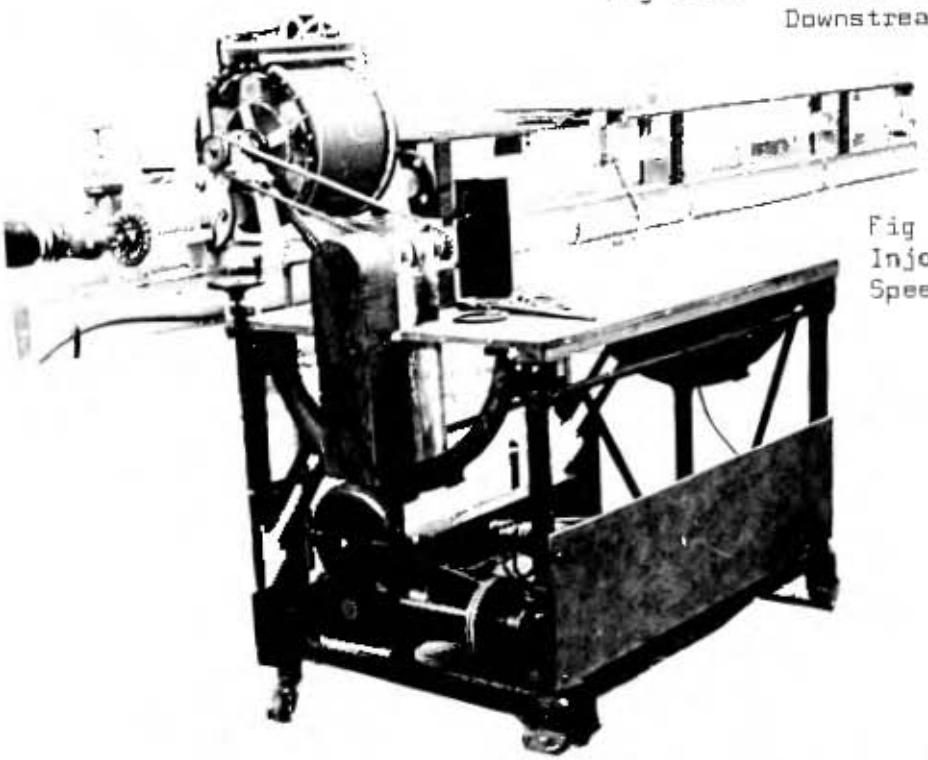

Fig 3.1b View of Injector and Variable Speed Drive-Upstream

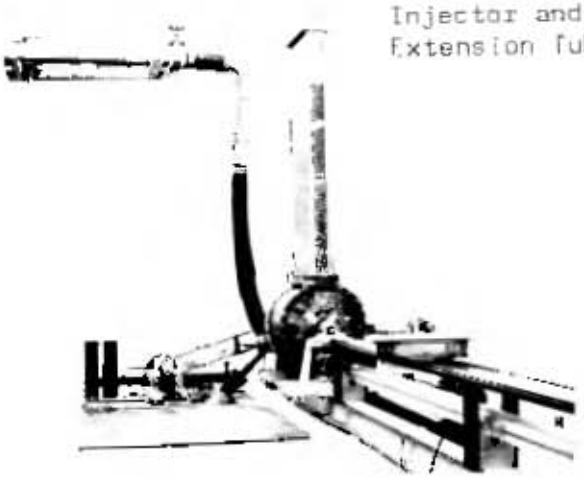

Fig 3.1c View of Injector and Extension Tube

transition zone, to give the capsule time to accelerate into the pipe, is clearly shown.

Figure 3.1b is a view from the upstream end and the variable speed drive for adjusting the injection rate is shown below.

Figure 3.1c shows the extension tube for replacing the lid. The extension tube is continuously fed with capsules, which fall into the injection drum.

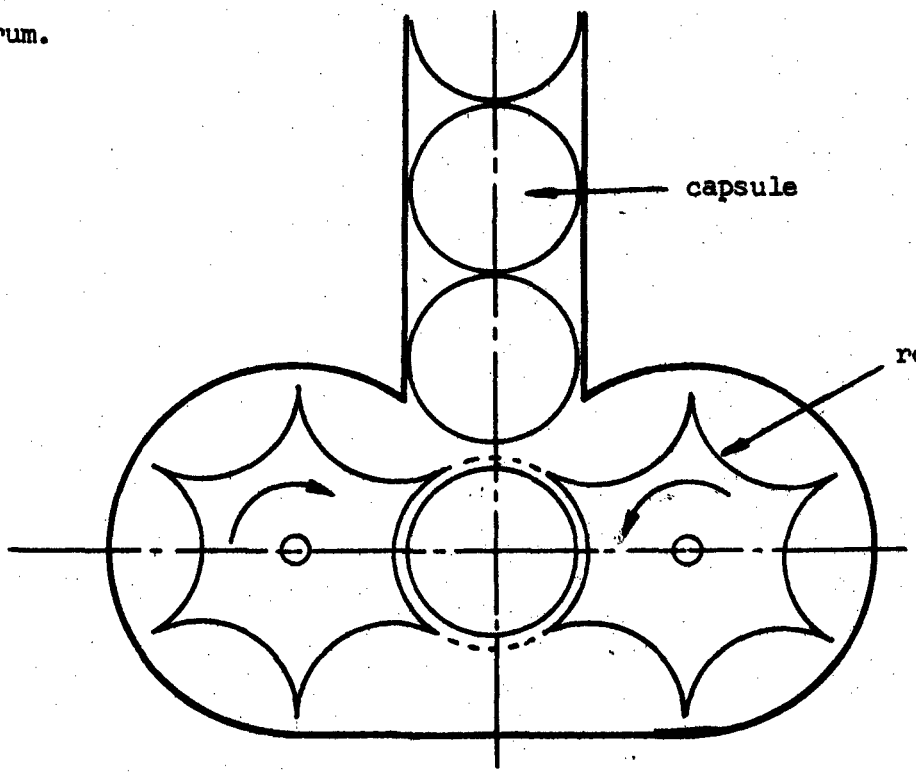

Figure 3.2

Another possible method of injection is shown diagrammatically in Figure 3.2. The capsules are placed in position by counter rotating drums shaped as shown. A stop-start rotary motion allows time for the capsules to accelerate from rest. For both methods of injection, mentioned above, the capsules may have to be spring or weight loaded from above to avoid jamming.

One advantage of injecting under positive pressure is that a conventional pump may be used upstream of the injector. But in a long pipe there may still be booster pumps en route.

2.2 Injection at atmospheric pressure

It is likely that, in a commercial application, the capsules may be inserted at atmospheric pressure.

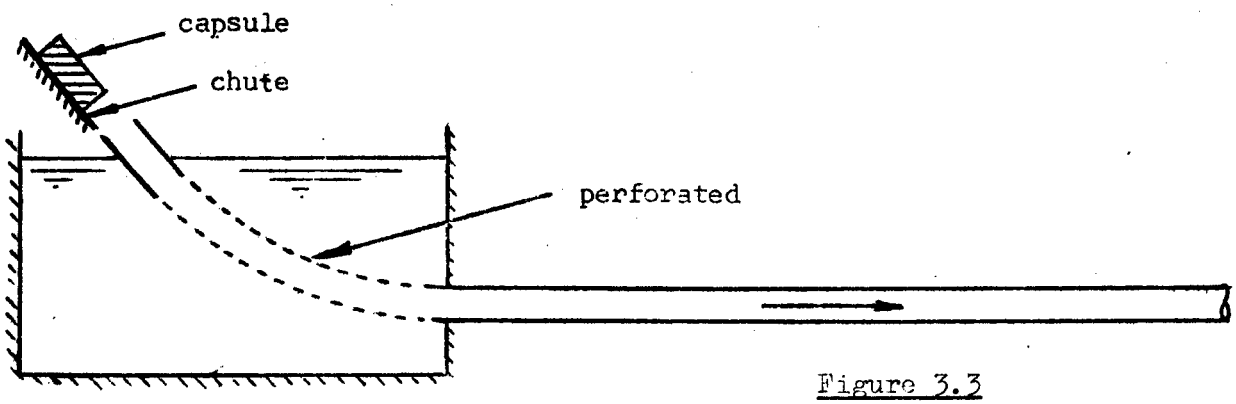

Figure 3.3

Figure 3.3 illustrates a simple system for inserting capsules into the pipeline if there is a booster pump downstream or if a complete gravity system is used.

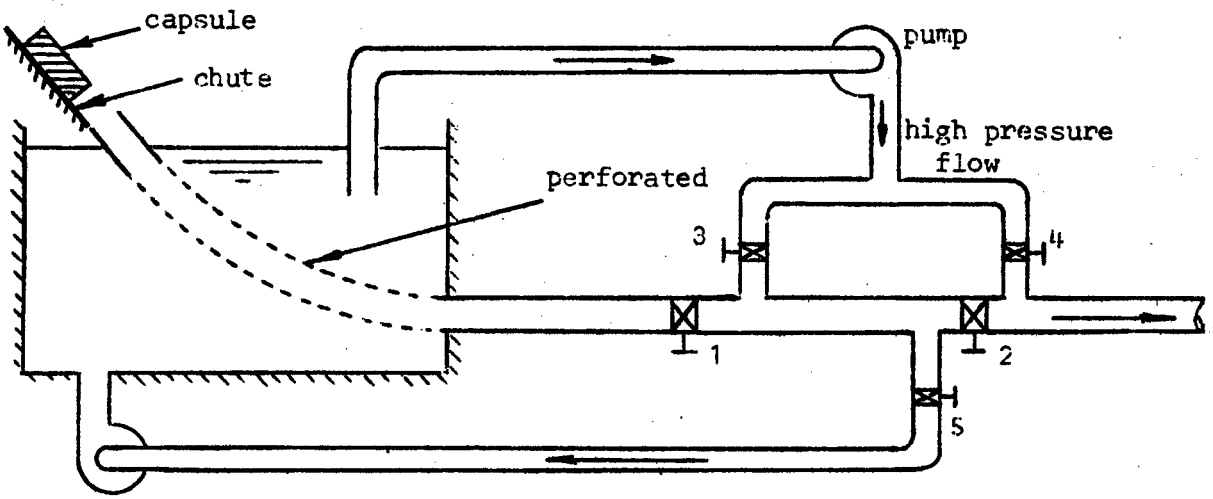

Figure 3.4

Figure 3.4 shows a method of injection at the upstream end of a pipe with an external booster pump.

The high pressure line is bifurcated to feed into the main pipeline upstream and downstream of lock valve No. 2.

To operate the system, valves No. 1, 4 and 5 are open and valves No. 2 and 3 are closed. The recirculation pump is in operation and a capsule is drawn into the lock between valves 1 and 2.

The valves 1; 4 and 5 are now closed and valves 3 and 2 are opened, causing the capsule to be injected into the pipeline.

The opening and closing of the valves to admit successive capsules can be automated so that as a capsule approaches valve No. 1 (the proceeding capsule being ejected from the lock section) a detecting device such as a photo transducer automatically opens valves 1; 4 and 5 and closes valves 2 and 3.

3. Recovery of capsules at the outlet end

This is a simple process compared with separation and recovery of solids transported in suspension.

In the experimental arrangement capsules were simply discharged into a large container with a side weir for discharging the water.

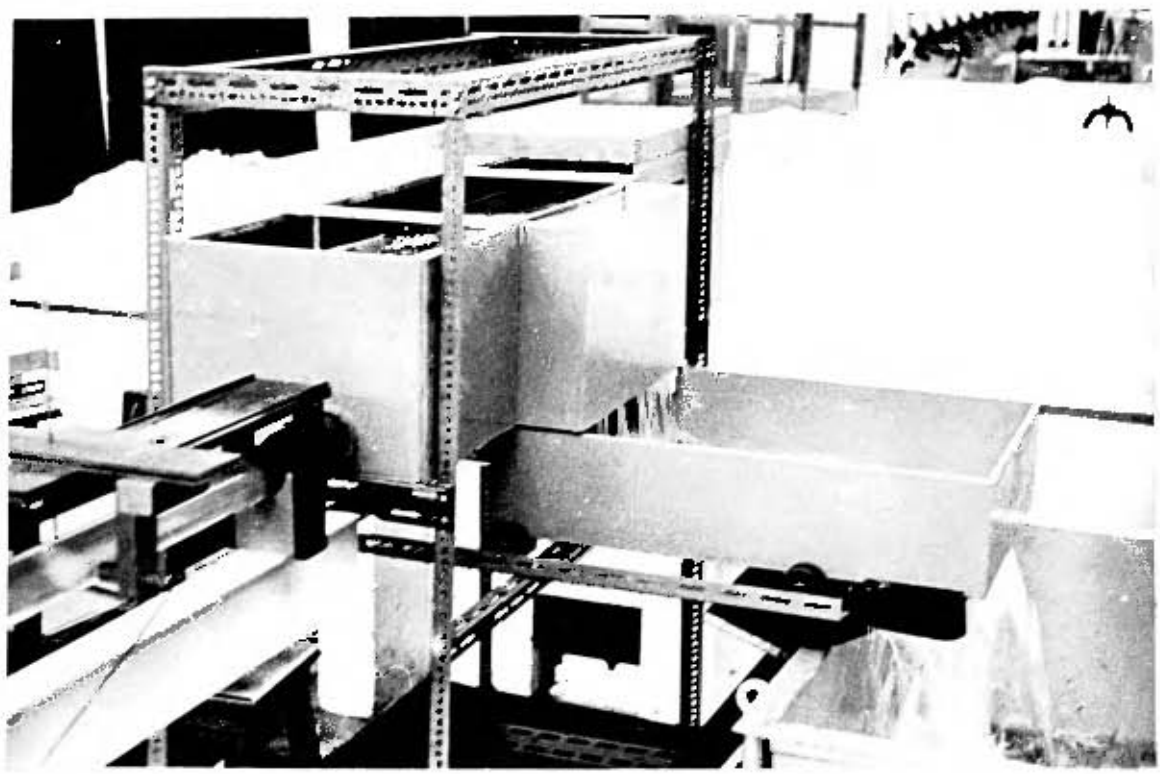

Figure 3.5

Figure 3.5 shows the experimental arrangement. Also shown on this Figure is the sliding drawer used for in situ calibration of the flow

meter. This will be discussed in Chapter 4.

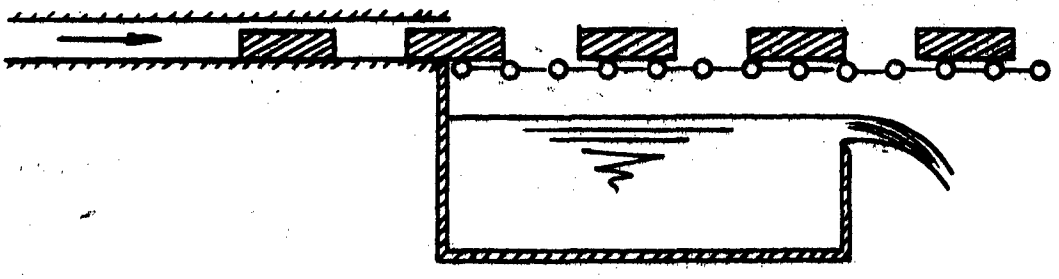

Figure 3.6

Figure 3.6 shows a suitable retrieval method wherein the conveying liquid is discharged into a tank and the capsules are deposited onto a conveyer from which they may be collected.

If it is required to eject certain capsules en route (for example, different commodities in the same line with various destinations) branch lines with some type of valve shunting would have to be incorporated.

The separation and dewatering of load in a fine suspension is a complicated and costly procedure compared with the system shown in Figure 3.6.

4. The pumping of capsules

This aspect of the technology requires the most development.

There are various methods for pumping solid capsule mixtures. And basically they can be divided into two categories.

1. Systems utilising conventional pumps which separate the water and capsule phases by means of lock systems and pump only the water.

2. Pumps which allow the transmission of capsules through and pump both phases.

In the course of the present investigation the former systems were not actually put into operation although many ideas can be expressed on paper.

Two novel pumps in the latter category have been designed and have operated successfully in the University's hydraulics laboratory. These can

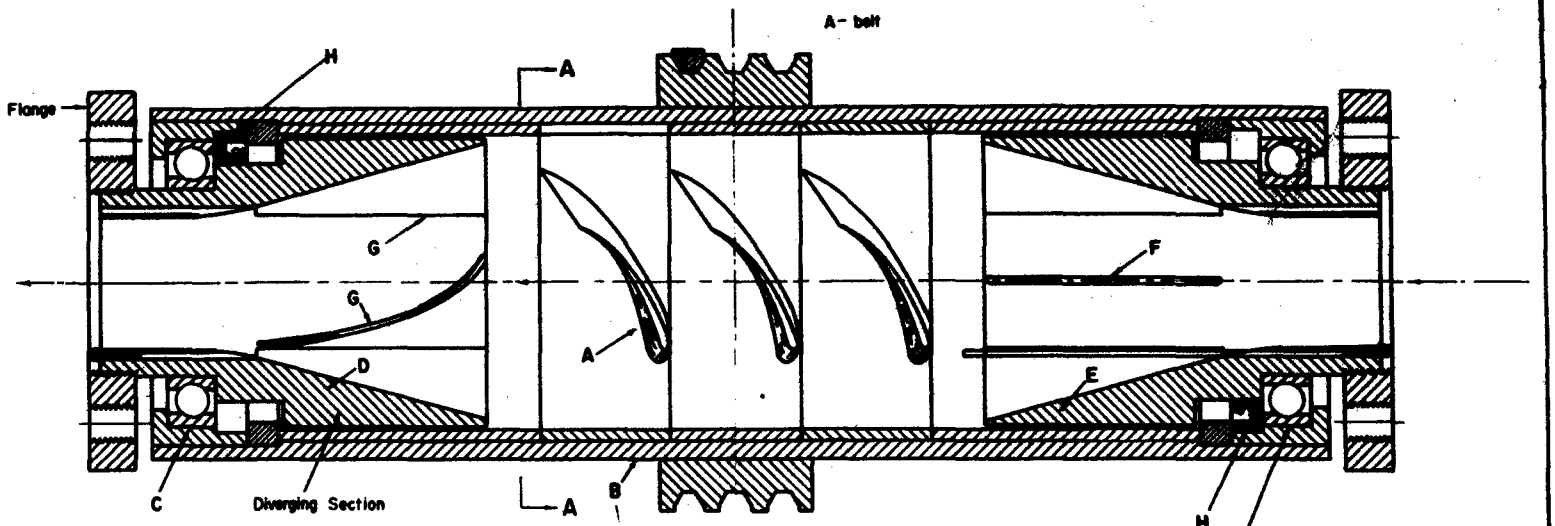

SECTION B-B

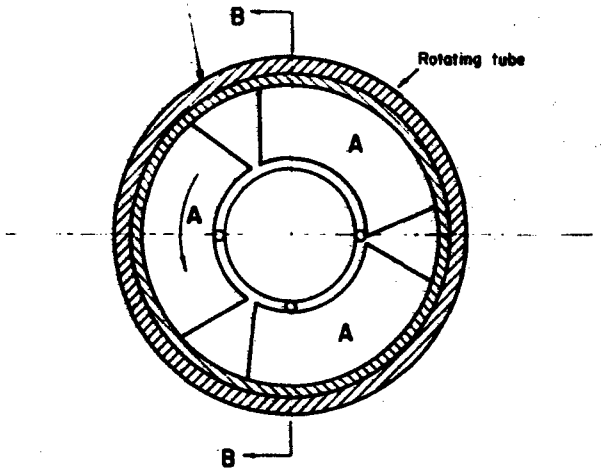

SECTION A - A

ANNULAR AXIAL FLOW PUMP

Designed by J.H. Lazarus 30-4-1988

FIGURE 3.7

be designated the "Annular axial flow" pump and the "annular jet pump."

The annular axial flow pump

Figure 3.7 shows sections through the annular axial flow pump which incorporates curved aerofoil blades (A) attached to the internal perimeter of a rotating tube (B) as shown in section AA. The totating tube is belt driven and mounted on ball bearings (C) which revolve about the fixed gradual expansion (E) and the gradual contraction (D). Straight triangular guide vanes (F) are attached around the perimeter of (E) at inlet and curved guide vanes (G) are attached around the perimeter of the gradual expansion at outlet. High tensile steel rods are connected to the fixed sections (D) and (E) for guiding the capsules. The seals (H) prevent water leakage. After a certain number of teething problems this pump was found to operate successfully. The number of guide rods have to be increased as the diameter of capsules is reduced.

An assemblage of components for the annular axial flow pump is shown on Figure 3.8a with the rotor and rotating tube in the centre, and the contraction and expansion chambers on the left and right. The scale of the rotor and blades is shown on Figure 3.8b.

Experiments were carried out with the curved aerofoils as shown in Figure 3.7 as well as with single and double start helices at various pitch lengths.

The annular jet pump

Figure 3.9 shows a section through the inlet and outlet nozzle of the annular jet pump.

A high head centrifugal pump injects water at a high velocity through the inlet nozzle (A) which mixes with the slower moving water in the capsule laden pipe. The water is withdrawn through the diffuser outlet at (B). The action of the water in the closed circuit acts as a

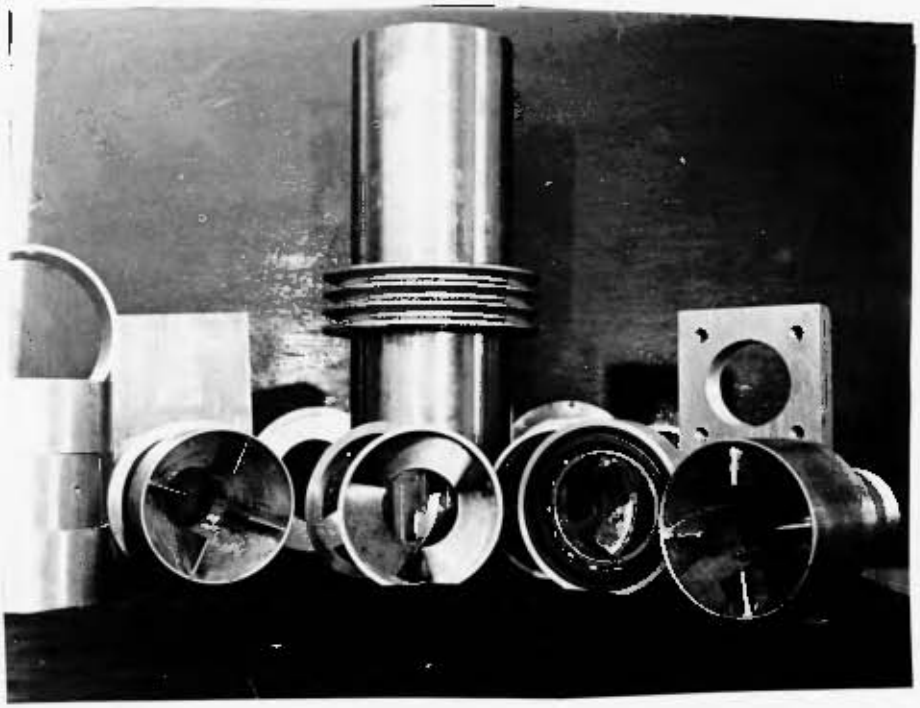

Fig 3.8a Components for Annular axial flow pump

Fig 3.8b View of impellor section and blade

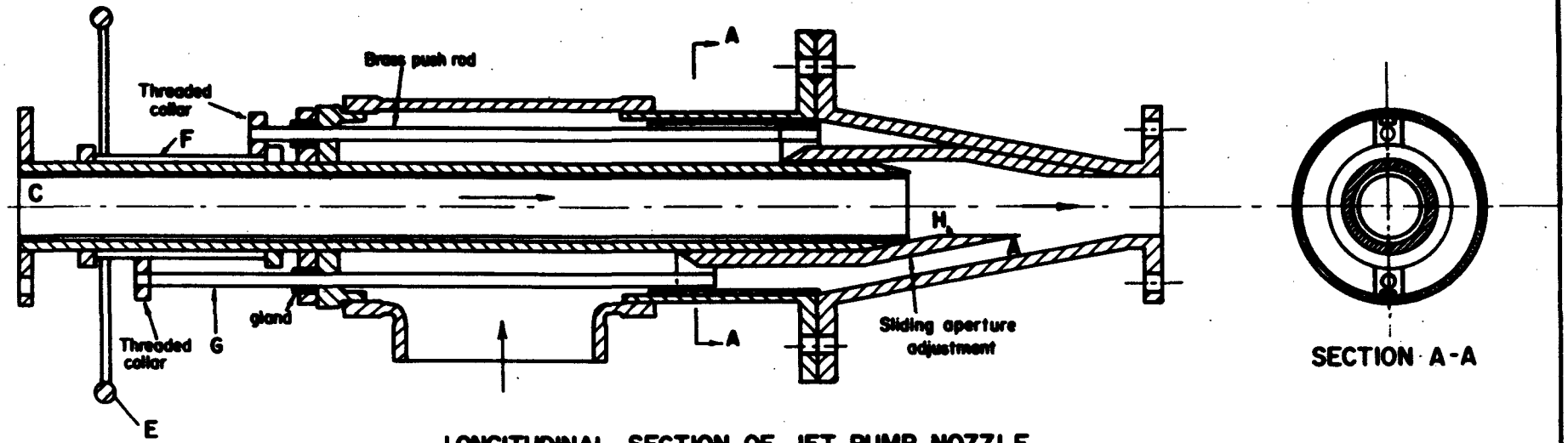

LONGITUDINAL SECTION OF JET PUMP NOZZLE

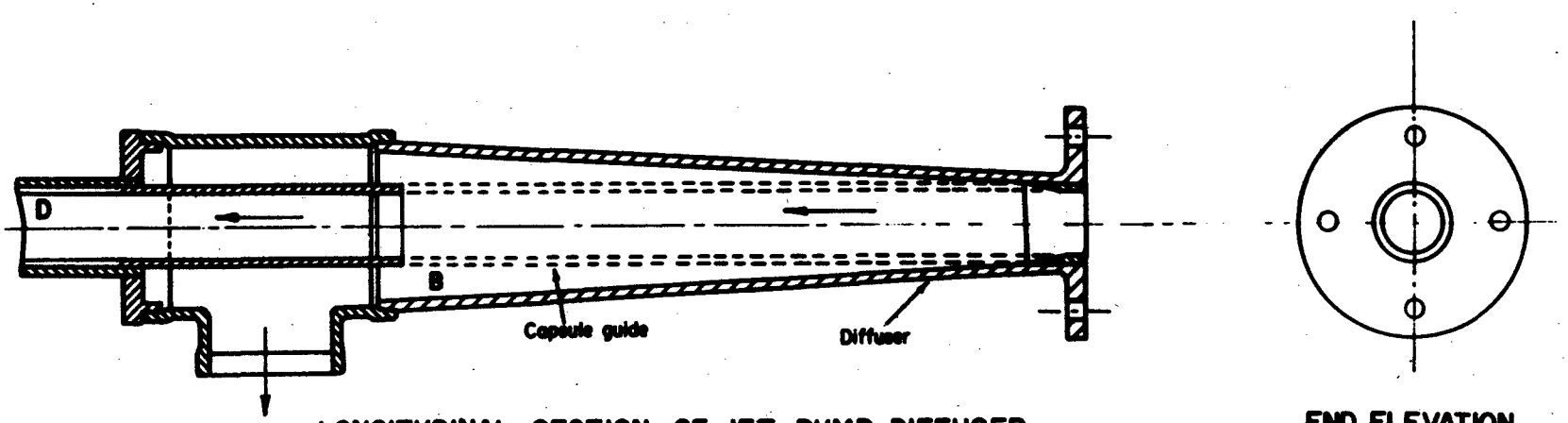

LONGITUDINAL SECTION OF JET PUMP DIFFUSER

ANNULAR JET PUMP (DIAGRAMMATIC)

FIGURE 3.9

transformer increasing the pressure between sections (C) and (D). The inlet nozzle opening is adjustable by means of the handwheel (E) which is attached to the externally threaded sliding sleeve (F). This sleeve is connected via push rods (G) to section (H) for nozzle apperture adjustment. The inlet angle was arbitrarily set at 10°.

This pump was used to drive the closed circuit used for experiments in the 44 mm diameter perspex pipe, and proved successful.

Both of the pumps described above are still in the development stage, and the present author was mainly concerned with the application of technological aspects of the project only to the extent that was needed for the experiments.

5. Pipeline layout system

Pipeline layouts for a capsule transportation systems can be divided up into two categories.

1. Single open circuit
2. Two way circuit

5.1 Single open Circuit

The capsules travel in one direction; being injected at the point of departure and recovered at the destination. Any of the injection techniques mentioned in Section 2 can be employed.

The maximum load factor possible is 100% and any of the packaging processes which are restricted to disposable containers or containers which form part of the load may be utilised.

The system may be gravity fed or have a multiplicity of booster pumps en route.

5.2 Two way Circuit

In this case encapsulation is considered in containers which are re-

turned to the departure end of the pipeline.

There are basically two methods of operation.

5.2.1 A single pipe

In this case the maximum possible load factor is 50% in either direction. The system may be gravity fed in one direction with booster pumps operating in the other direction or incorporate two way pumps.

For the annular axial flow pump with a continuous helical impeller the sense of rotation can be reversed and some method of interchanging the inlet and outlet guide vanes would have to be incorporated in the design.

For the jet pump, either the diffuser can be dispensed with, in which case the outlet nozzle is a replica of the inlet nozzle, and the flow can be in either direction in the boosting circuit. Additional momentum is imparted to the water at outlet. A plurality of pumps with diffusers can be used, some of which are capable of operating in one direction and others in the opposite direction.

This system would become particularly economical if it were desired to transport commodities in both directions, for example, exportable iron ore from an inland region to the coast and imported machine parts from the coast to the inlet region.

If the capsules were to be returned empty they could possibly be made neutrally buoyant by filling them with the conveying liquid. In this case there is an accumulation of liquid at the starting point, for example, the oil pipeline from Durban to Johannesburg could be used for conveying drums (or capsules) of imported oil to an inland region and for transporting an exportable commodity to the coast either in an oil or water medium.

5.2.2 A twin pipe system

A two way circuit with twin pipes could have a maximum possible load

factor of 100%, empty capsules (or neutrally buoyant capsules) or a different commodity being transported in the return pipeline.

Each pipe could have pumps or one of the pipes may be gravity fed.

The cost would not be double that of a single pipeline since a common trench (if required) would be sufficient for both pipes. If the pipes are not tranched the cost of the twin pipe system would naturally be double that of the single pipe.

Another application for such a system would be in the mining industry where the ore is packed into capsules at an injection point at the base of a mine shaft and empty capsules are returned via the downpipe.

P A R T II

EXPERIMENTAL EQUIPMENT

"Pure logical thinking cannot yield us any knowledge of the empirical world, all knowledge of reality starts from experiment and ends in it."

Albert Einstein

CHAPTER 4

APPARATUS FOR EXPERIMENTS

1. The open and closed system

In this chapter two different experimental layout systems are described, these will be designated the "open" and "closed" systems depending on whether the capsules travel intermittently or continuously.

The open system refers to the experimental layout designed for capsule injection at the upstream end and ejection at the downstream end. This involves a device for injecting the capsule and a separate retrieval system remote from the injector.

The closed system implies a recirculating pipe in which the capsules are inserted, rather than injected, at a point in the circuit. They can be removed from the pipeline (after the capsule has completed at least one circuit) at the same point as the insertion.

There are merits and de-merits associated with either system and the two experimental layouts were used for gaining supplementary data. Both systems are novel for experimental investigation of capsule transport systems. The apparatus used by the Research Council of Alberta, in Canada, is essentially an open system (without an injector) consisting of pipes, lock valves, throttle valves and a pump. The capsules were shuttled backwards and forwards without passing through the pump.

The main disadvantage of this system compared with the two incorporated for the present study is that experiments cannot be performed using a succession of capsules.

2. Merits of the two systems

The open system has the following experimental advantages.

2.1 Slope variation is far more conveniently achieved than with the closed system where a change in slope required a complete rearrangement of the circuit.

2.2 The effect of trains of capsules can readily be investigated since the injector was designed to inject discrete capsules at regular intervals.

2.3 It is easier to change pipe materials even of slightly different diameters (within a fairly narrow range unless the injection method is changed) than with the closed system where the pump and bends would have to be altered.

2.4 The open system is easier to construct than the closed circuit since the latter involves a pump and bends which are not required by the former.

2.5 Different capsules can more easily be compared at the same flow rate since the injector is merely loaded with the capsules (of different specific gravity for example), the flow rate is adjusted and the capsules are injected without affecting one another, or the flow rate.

3. Advantages of the closed circuit

3.1 Experiments with the same capsule are easier to repeat than with the open circuit since the capsule remains in the circuit and does not have to be reloaded for each run.

3.2 It is more convenient than the open circuit when investigating trains of capsules just touching. However, the open circuit with the injector is more amenable for studying trains of capsules separated by periodic injection.

3.3 The closed circuit was found to be more convenient for studying capsule transportation in a vertical pipeline since retrieval of both the capsules and the water could more easily be affected.

4. The open circuit

Figure 4.1 shows a diagrammatic layout of the apparatus consisting of the following main components.

4.1 The pipeline: This is shown in the diagram as a 12 m long transparent "Perspex" tube 74 mm internal diameter. The tube was made up of three 4 m long sections carefully flanged without gaskets and no internal projecting edges ensuring a smooth passage for capsules.

An extra 300 mm length of tube at the upstream end was shaped to have an oval inlet, with the major axis of the oval horizontal and perpendicular to the pipe axis, tapering over the 300 mm length to a circular section. The purpose of the oval tapering section will be described below (Section 4.2).

4.2 The Injector: Figure 4.2 shows the injector which consists of a 400 mm diameter P.V.C. pipe 300 mm long with a transparent cover at each end. Glands were built into the end covers through which a shaft passes. The shaft was supported by means of external bearings and a twelve compartment drum was mounted on the shaft. The drum rotated concentrically within the P.V.C. pipe.

The capsules were inserted at the top of the loading device or injection feed box (this is not shown on Figure 4.2 where it is replaced by a lid. However, the injector feed box is shown on Figure 4.1).

As the drum rotated capsules were injected into the pipeline, one at a time. The oval inlet section allowed the capsules enough time to enter the pipe while the particular drum compartment containing the capsule traversed the oval section.

This method of insertion was preferable to the alternative considered, viz a stop-start, jerky motion of the drum allowing twelve stops per rotation, because of the mechanical difficulties involved.

The injector proved capable of injection rates up to 3,9 capsules

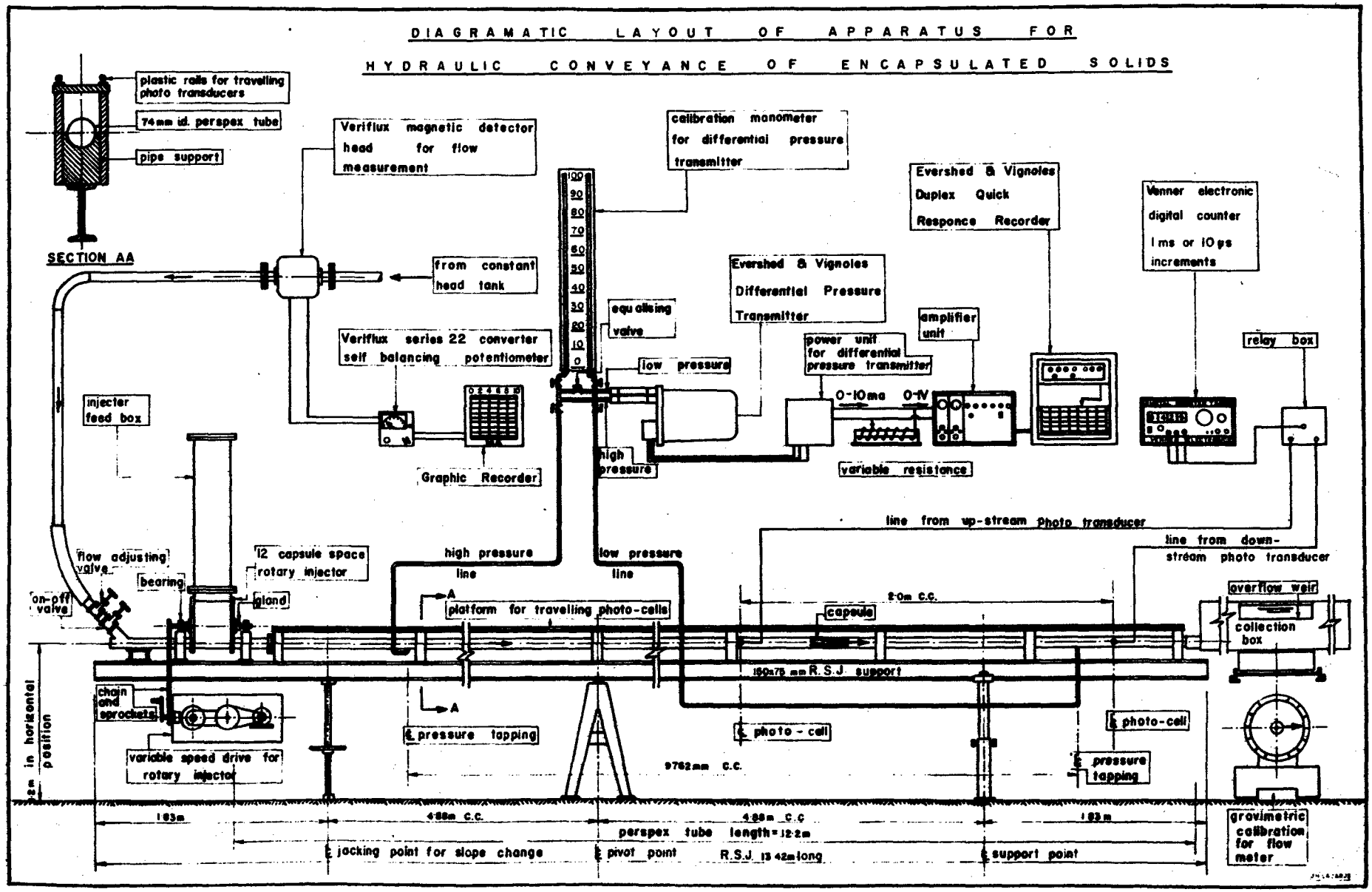
DIAGRAMATIC LAYOUT OF APPARATUS FOR
HYDRAULIC CONVEYANCE OF ENCAPSULATED SOLIDS
plastic rails for travelling photo transducers
74mm id. perspex tube
pipe support
SECTION AA
Veriflux magnetic detector head for flow measurement
calibration manometer for differential pressure transmitter
Eyershed & Vignoles Duplex Quick Responce Recorder
Venner electronic digital counter 1 ms or 10 μs increments
from constant head tank
Eyershed & Vignoles Differential Pressure Transmitter
equalising valve
amplifier unit
relay box
Veriflux series 22 converter self balancing potentiometer
low pressure
power unit for differential pressure transmitter
injecter feed box
0-10ma
0-1V
Graphic Recorder
high pressure
variable resistance
line from up-stream photo transducer
line from down-stream photo transducer
flow adjusting valve
12 capsule space rotary injector
high pressure line
low pressure line
overflow weir
on-off valve
bearing
gland
platform for travelling photo-cells
2·0m c.c.
capsule
collection box
150x75 mm R.S.J. support
chain and sprockets
℄ pressure tapping
℄ photo-cell
℄ photo-cell
variable speed drive for rotary injector
9762mm c.c.
℄ pressure tapping
2m in horizontal position
1·83m
4·88m c.c.
4·88m c.c.
1·83m
perspex tube length = 12·2m
gravimetric calibration for flow meter
℄ jacking point for slope change
℄ pivot point
R.S.J. 13·42m long
℄ support point

FIGURE 4.1

FIGURE 4.2

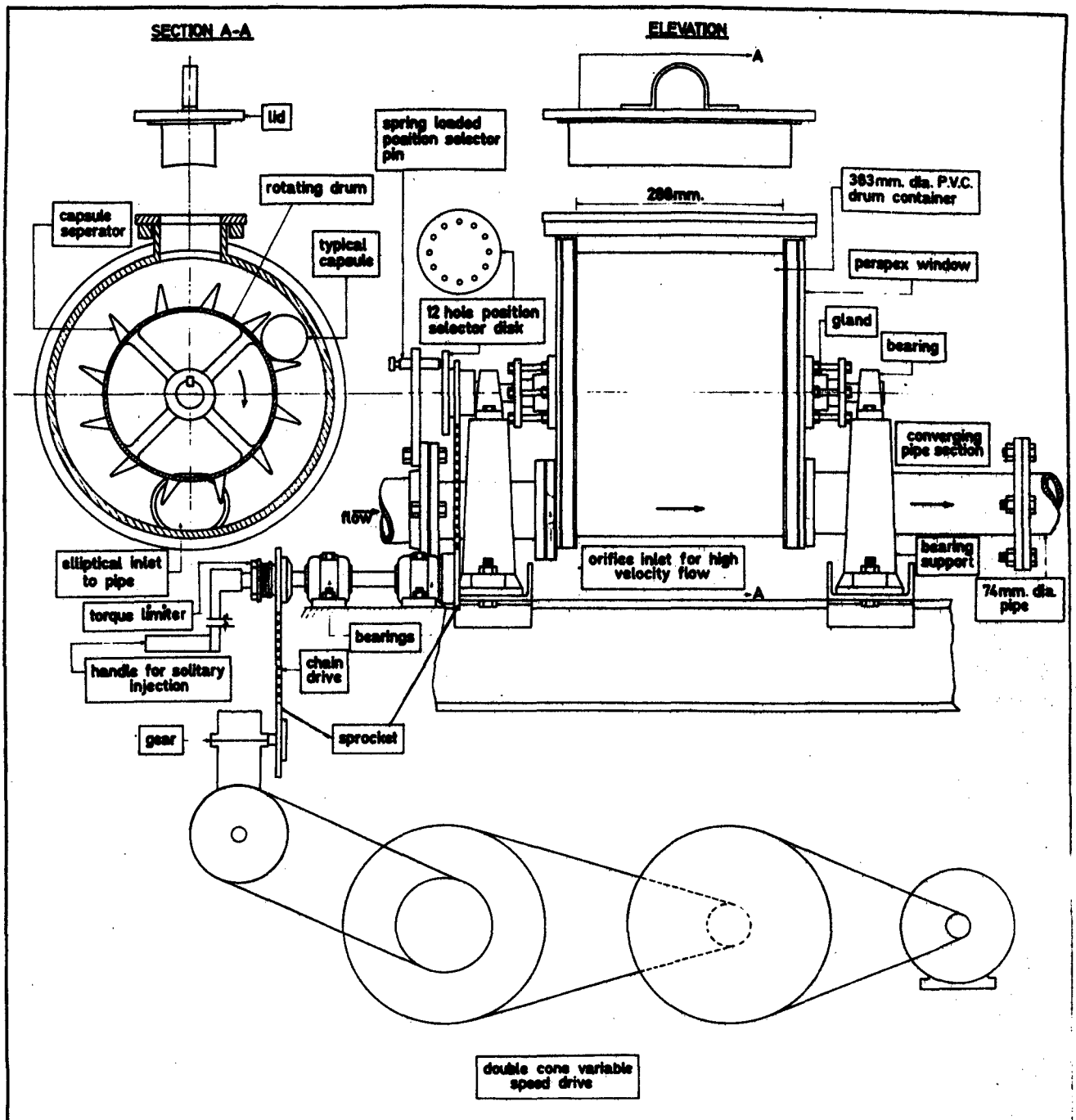

INJECTION DEVICE FOR 12 CAPSULES FOR HYDRAULIC CONVEYANCE OF CAPSULES BY PIPELINE

per second at a capsule velocity of 4 m/s.

The injector feed box was not used during the experiment for two main reasons:

Firstly, it was not entirely successful since it had not been fully developed and, secondly, it would have caused certain errors in flow measurement. These points will be discussed in more detail in the Chapter on measurements.

A specially shaped lid was used, instead of the injection box, which followed the shape of the injection chamber casing.

The injector was driven by a variable speed drive (of the double cone type, salvaged from an old printing machine) for studying successive capsules in trains, or hand operated for the study of individual capsules. Many other systems of injection were considered and these were all rejected in favour of the above.

4.3 The recovery box: This was used for recovering capsules ejected at the pipe outlet and proved to be both simple and effective. The purpose of the recovery box was twofold.

4.3.1 The separation of water from capsules at the downstream end: This was simply achieved by allowing the water to pass over a rectangular side weir covered with wire mesh at the overflow section. The capsules were retained in the box and the water overflow returned to the recirculating system of the hydraulics laboratory.

4.3.2 Minimisation of damage to the capsules: The box was rubber lined throughout and the length (2 metre) was sufficient to ensure deceleration of the capsules preventing collisions with the downstream bulkhead. The width and depth (400 mm × 400 mm) were made reasonably large to reduce chances of inter-capsule collision at emission.

4.4 The support system: The pipeline and injector were supported on a

steel joist (150 mm × 75 mm) pivoted at the centre, with a jacking point for slope change at the upstream end and a further support point at the downstream end.

The recovery box had its own support which could be raised or lowered to suit the slope of the pipeline elevation at the outlet end.

The procedure for slope change will be described in the Chapter on experimental procedure.

The pipeline was supported on the steel joist by means of timber blocks shaped to the pipe soffit and situated approximately 1 metre centre to centre.

A platform was mounted above the entire length of the pipeline and plastic rails on the platform enabled photo transduces to travel axially along the pipe. The cells could be readily positioned along the pipe for capsule acceleration experiments (see Figure 5.3).

4.5 Flow measuring device: The veriflux electro magnetic flowmeter was used.

In the early stages of the investigation an orifice plate with carrier tappings and a double manometer system was employed. The low flow manometer being an inverted U-tube with an enlarged limb using paraffin as the manometer fluid. The high flow manometer was a U-tube with an enlarged limb containing Igema as the manometer fluid. The whole system was calibrated in situ gravimetrically.

The differential pressure type flowmeter was considered unsatisfactory and rejected in favour of the more costly electro-magnetic system for the following reasons:

4.5.1 The manometer response time was not considered sufficiently rapid to detect flow transients that occured due to the presence of capsules in the pipeline if the manometer tube diameters were too small. If the tube

diameters were too large, surging due to the flow transient could mask the transient itself. In addition, the inertia of the manometer fluid had to be overcome, reducing the response time still further.

The duration of the transient could be as low as two seconds and the maximum magnitude was of the order of a few percent of the steady flow in the capsule free pipeline.

4.5.2 The low flow manometer caused considerable difficulties due to gradual diffusion of the water and paraffin causing an indistinct interface and unreliable readings.

4.6 The veriflux electro-magnetic flow-meter has the following components:

4.6.1 Veriflux detector head: The detecting element was inserted in the flowline upstream of the experimental pipeline section (see Figure 4.1).

The accuracy of this meter is unaffected by changes in the viscosity, density, temperature, pressure and flow profile of the metered liquid (according to the manufacturers).

The response time is extremely rapid since the system has virtually no inertia to overcome compared with the differential pressure type meter (particularly when a high specific gravity fluid is used in the manometer). Also, the difficulties mentioned earlier due to manometer tubes were avoided since only electrical connections were made from the detector head. The output follows instantaneously any flow condition taking place within the detector head and if the flow pulsates the output from the head pulsates accordingly.

The instrument is, in fact, so responsive to flow transients that for commercial applications it is recommended to fit a slow response demodulator, giving a three second full scale deflection time. The slow response demodulator was not fitted for the capsule experiments and the full scale deflection time was of the order of 0,3 seconds.

The manufacturers claimed a linear characteristic which improves accuracy over a wide range of flow registration above any form of differential head measurement. They also claim on any given range setting, an accuracy of ± 1% of actual reading down to 1/5th of the maximum flow selected with ± 2% down to 1/10th of this maximum and ± 3% down to 1/15th of this maximum. Bearing in mind that it is possible to select any maximum velocity (on the meter) between 1 m/s and 10 m/s, infinitely variable, it is apparent, from the above, that a total flow range of 1 : 50 can be measured with an accuracy of ± 1% of actual reading by judicious range selection as the flow varies.

The above claims were not, however, justified and the actual accuracy of the flow measurement as a whole (i.e. detector head, convertor and recorder) will be discussed in the chapter on measurements and accuracy.

The unit itself consists of a non-magnetic tube lined with an electrically insulating material. Coil windings are arranged around the tube to provide a homogeneous magnetic field across the bore. As the water flows through the tube and thus through the magnetic field an e.m.f. is induced directly proportional to the rate of flow of the liquid. This e.m.f. passes through electrodes to the converter.

4.6.2 The Veriflux series 2-2 converter: This instrument is designed for use with the veriflux electromagnetic detector head and provides a direct current output which is claimed by the manufacturers to be directly proportional to the mean velocity of flow through the detector. The flow range of the instrument is varied by adjusting switches and a potentiometer at the front of the instrument. The maximum "velocity" can be varied between 1 m/s and 10 m/s and the maximum setting produces a 10 mA output. The actual output is supposed to be linearly proportional to the velocity. The converter is essentially a "self balancing a.c. potentiometer utilising a Hall multiplier connected in series with the

d.c. output of the converter. The voltage derived from the multiplier is accurately proportional to the product of the d.c. output and the flow-meter reference current and, if of the same phase as the flow signal, it is fed back to balance the flow signal from the detector. Quadrature signals are rejected by precise demodulation of the flow signal."

The purpose of the converter is essentially to provide a direct current output which is directly proportional to the mean velocity of flow through the detector head. The converter can be used with any size of detector head.

4.6.3 The graphic recorder: The "Record" graphic recorder accepts the output of the veriflux converter, i.e. 0 - 10 mA.

The chart speed of this recorder can be varied by interchangeable driving gears. A chart speed of 0,85 mm/s was found to be adequate for transient detection. The response time was less than 0,5 seconds for full scale deflection.

The movement is "ultra high torque permanent magnet Moving Coil type characterised by fast response, extreme sensitivity, low consumption, adequate damping and almost complete absence of stray field effects," according to the manufacturers.

4.7 Differential pressure measurement: Pressure was measured using an Evershed and Vignoles differential pressure transmitter (type ER. 355).

Initially attempts were made to measure pressure by means of firstly, open tube piezometers, and secondly, a U-tube manometer with an enlarged limb. However, the pressure transient, due to the presence of the capsule in the line, was required and the difficulties mentioned in the section under flow measurement with an orifice plate and manometer were experienced and, indeed intensified when it came to measuring pressure transients. This is because the transient pressure difference, due to

the capsule, was much higher, expressed as a percentage of the head loss between two tapping points (9,762 m apart) due to friction alone, than the flow transient expressed as a percentage of the steady flow without a capsule in the line.

A change was therefore made to the differential pressure transmitter.

The differential pressure transmitter (Figure 4.3) is designed for measurement and remote indication of differential pressures up to 2,54 m water gauge. The pressure range is infinitely variable from 0 - 500 m to 0 - 2,54 m. The transmission accuracy is claimed to be within ± ½% of full scale deflection.

The differential pressure value is transmitted by direct current in the range 0 - 10 mA proportional to differential pressure over the measuring range.

The four components used in the differential pressure measuring system are:

4.7.1 The transmitter, which measures the differential pressure and establishes a d.c. signal proportional to the pressure difference.

The transmitter operates on a force-balance principle. A measuring element, in this case a twin diaphragm, applies a mechanical force to a beam, proportional to the pressure measured. Figure 4.4 shows a diagrammatic layout illustrating the mechanical principle of the transmitter. The following is a summary from the booklet on the instrument.

"The diaphgram is situated in a horizontal plane between the upper and lower halves of the diaphragm chamber to which the low and high pressures are connected respectively.

The diaphgram is attached to one end of a horizontal primary beam (A) (see Figure 4.4) which is supported by cross-spring pivots outside the pressure chamber.

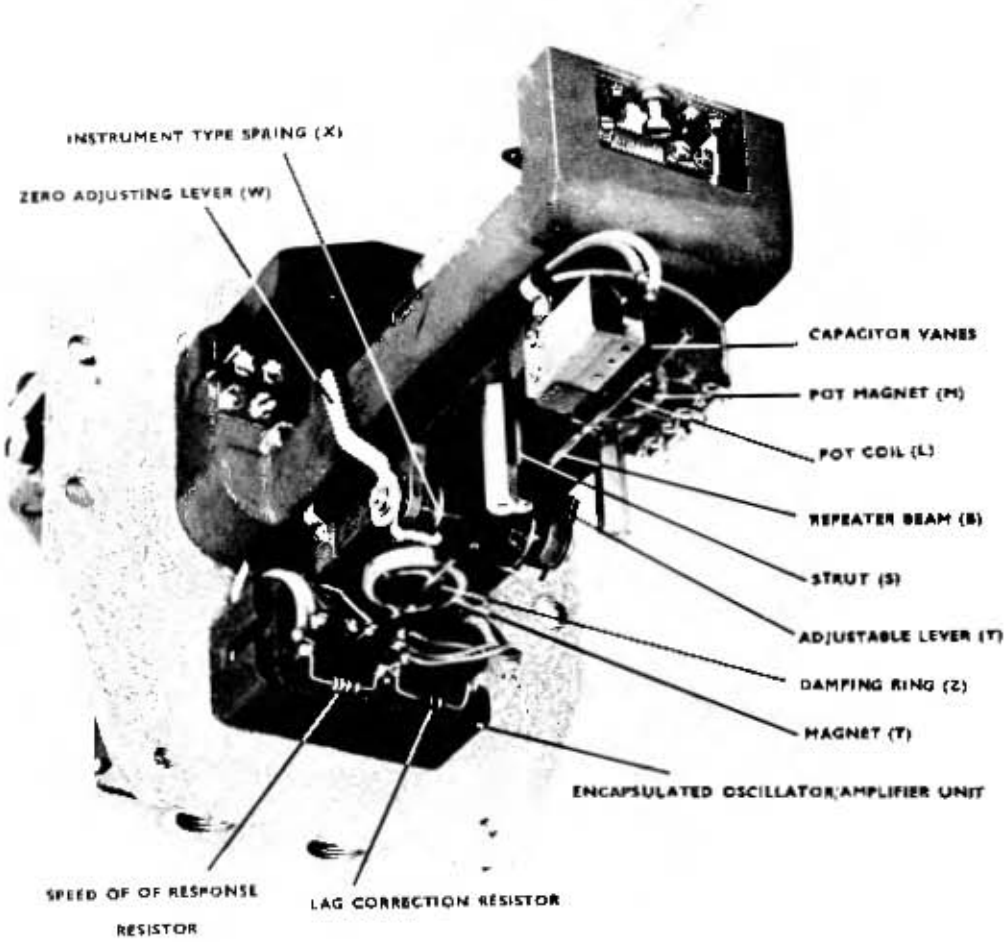
INSTRUMENT TYPE SPRING (X)
ZERO ADJUSTING LEVER (W)
CAPACITOR VANES
POT MAGNET (M)
POT COIL (L)
REPEATER BEAM (B)
STRUT (S)
ADJUSTABLE LEVER (T)
DAMPING RING (Z)
MAGNET (T)
ENCAPSULATED OSCILLATOR/AMPLIFIER UNIT
SPEED OF OF RESPONSE
RESISTOR
LAG CORRECTION RESISTOR

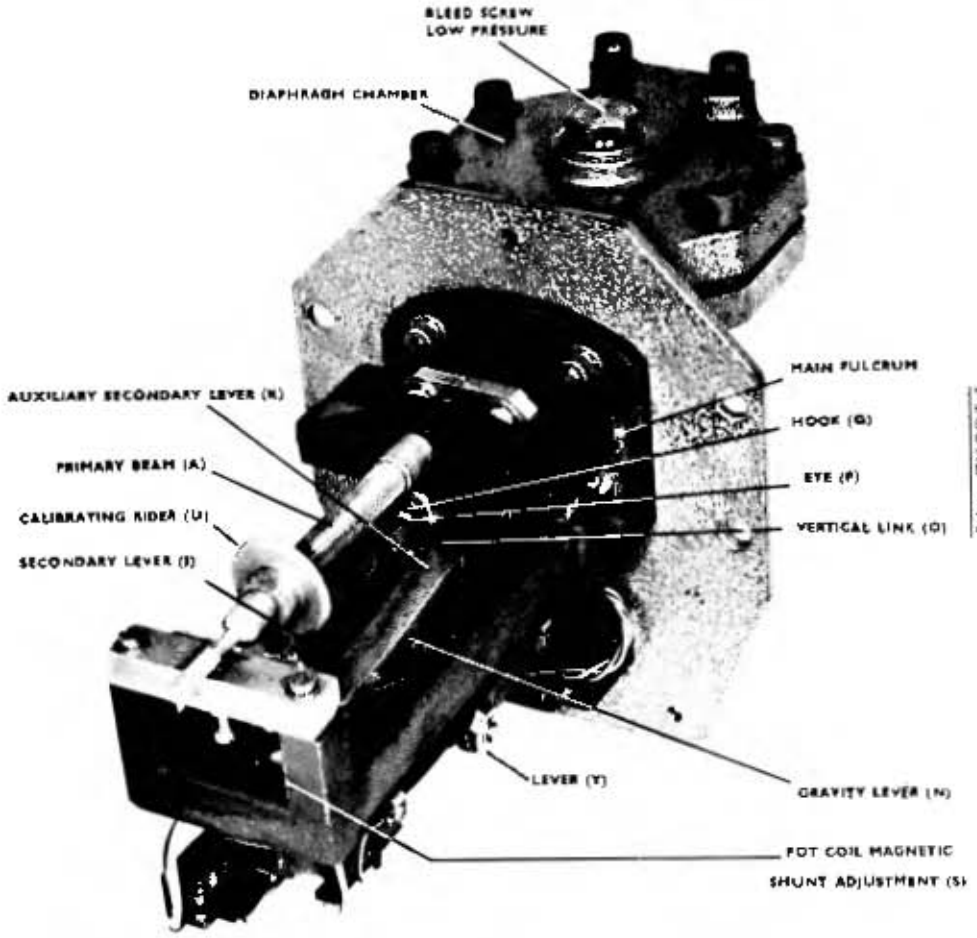
BLEED SCREW
LOW PRESSURE
DIAPHRAGM CHAMBER
MAIN FULCRUM
AUXILIARY SECONDARY LEVER (K)
HOOK (Q)
PRIMARY BEAM (A)
EYE (P)
CALIBRATING RIDER (U)
VERTICAL LINK (O)
SECONDARY LEVER (J)
LEVER (Y)
GRAVITY LEVER (N)
POT COIL MAGNETIC
SHUNT ADJUSTMENT (S)

FIGURE 4.3

FIGURE 4.4

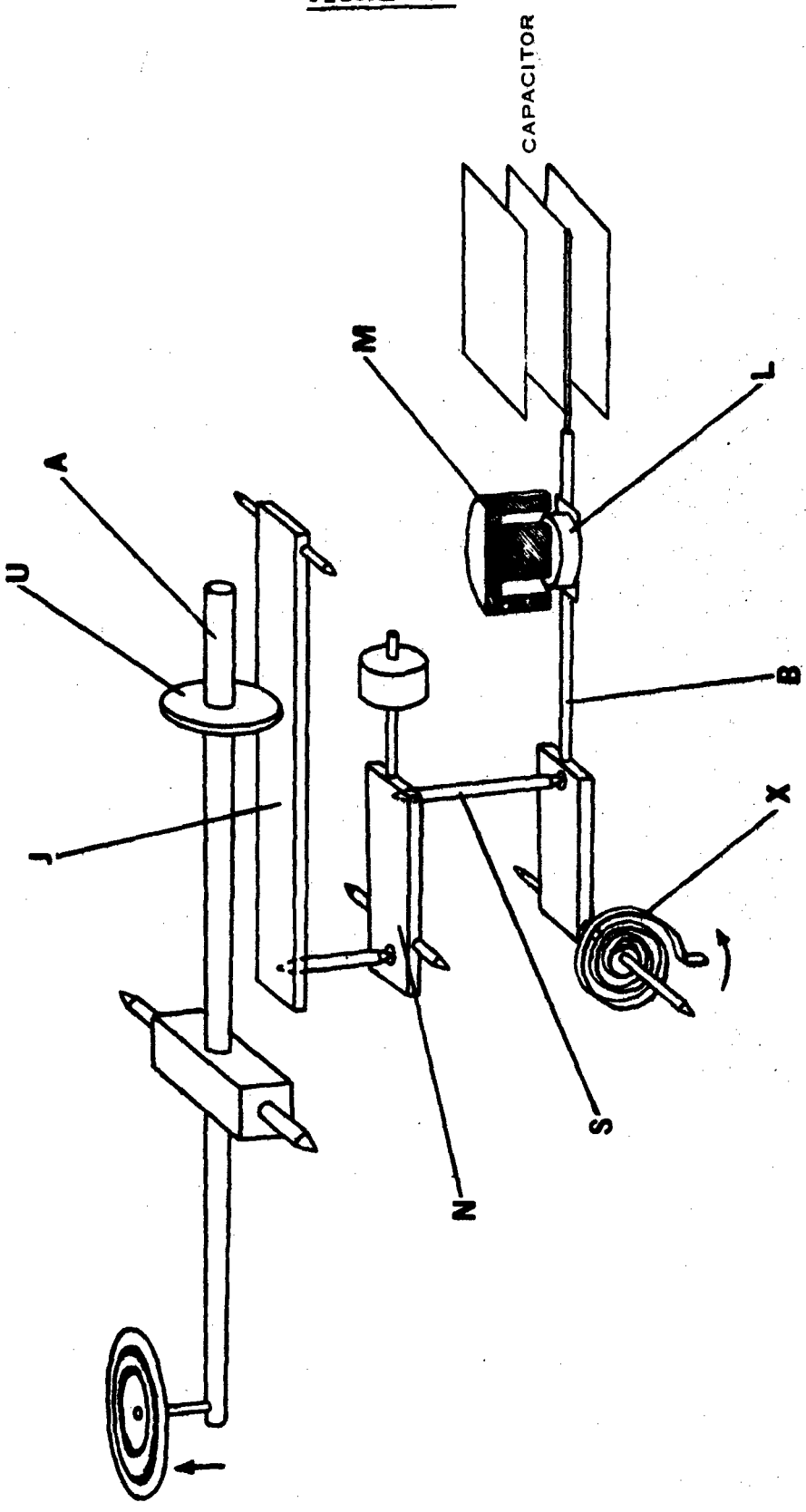

MECHANICAL PRINCIPLE OF THE TRANSMITTER

The primary beam is threaded to permit fine adjustment of the calibrating rider (U) which transmits the diaphgram torque to the secondary beam (J), also supported on cross-spring pivots.

A secondary lever forms part of a compound lever arrangement, the function of which is to protect the pot-coil beam (B) from a forward overload.

The pot-coil beam (B) is horizontally disposed and is supported on pivots and spring loaded jewels near its midpoint. It carries at one end the pot-coil (L) which moves in the gap of a permanent magnet (M). At the other end of the beam a damping ring is fitted which moves in the gap of a second permanent magnet. This serves to damp out insignificant pulsations reaching the diaphragm.

When the pressure across the diaphragm changes, a torque is applied through the lever system to unbalance the beam, causing the central vane of the capacitor, mounted on the end of the beam, to move towards one of the outer vanes. The central vane is connected to the oscillator output of the oscillator/amplifier unit and the outer vanes are connected to a differential rectifier in the same unit. The force produced by the pot-coil current flowing in the field of the permanent magnet exactly balances the force applied from the diaphragm and thus maintains the beam in equilibrium."

4.7.2 A calibration manometer was mounted above the differential pressure transmitter (see Figure 4.1) and the input to the transmitter could be switched to the calibration manometer or alternatively to the pressure tappings from the "Perspex" tube. The calibration manometer was pressurised directly from the hydraulics laboratory water tower so that the transmitter was calibrated in situ using a static pressure differential.

4.7.3 The power unit for the differential pressure transmitter: The

operating current for the pot coil and transmission line was obtained from a series 300 power unit.

The signal output is 0 - 10 mA for full scale deflection of the transmitter. This was converted to a 0 - IV signal by means of a variable resistance (see Figure 4.1). The voltage signal was fed into the recorder.

4.7.4 The recorder: The recorder was an "Evershed and Vignoles Duplex quick response recorder" which has two similar channels, of which only one was used. Each channel is essentially a d.c. recording voltmeter.

The recorder is servo operated, the input being compared with a voltage feed back from a resetting potentiometer actuated by the pen arm. The magnitude of the resetting voltage is determined by the position of the pen. The voltage difference is amplified to drive the pen movement which sets the pen in such a position that the resetting voltage is equal and opposite to the input voltage.

When calibrating, it was the pen recorder itself which was calibrated against a static water pressure differential.

4.8 The timer: The capsule velocity was calculated by measuring its time of travel over a known distance. When the capsule passed the upstream photo-transducer it tripped a relay switch which started the digital counter. The counter was stopped when the capsule passed the downstream photo-transducer.

The counter is a Venner frequency meter type TSA 6634 which has count and timing facilities incorporated. Cold cathode numerical indicators display a four-digit readout. The display time is set to infinity. The timing units are 10 μs increments or 1 ms increments and the 1 ms increments were used thus giving, with a 4 - digit readout, a timing interval up to 9,999 seconds.

When using opaque pipes such as asbestos cement the photo cells were

---

5.2 In order to formulate similarity and scaling criteria it was necessary to have at least one other diameter of pipeline as opposed to

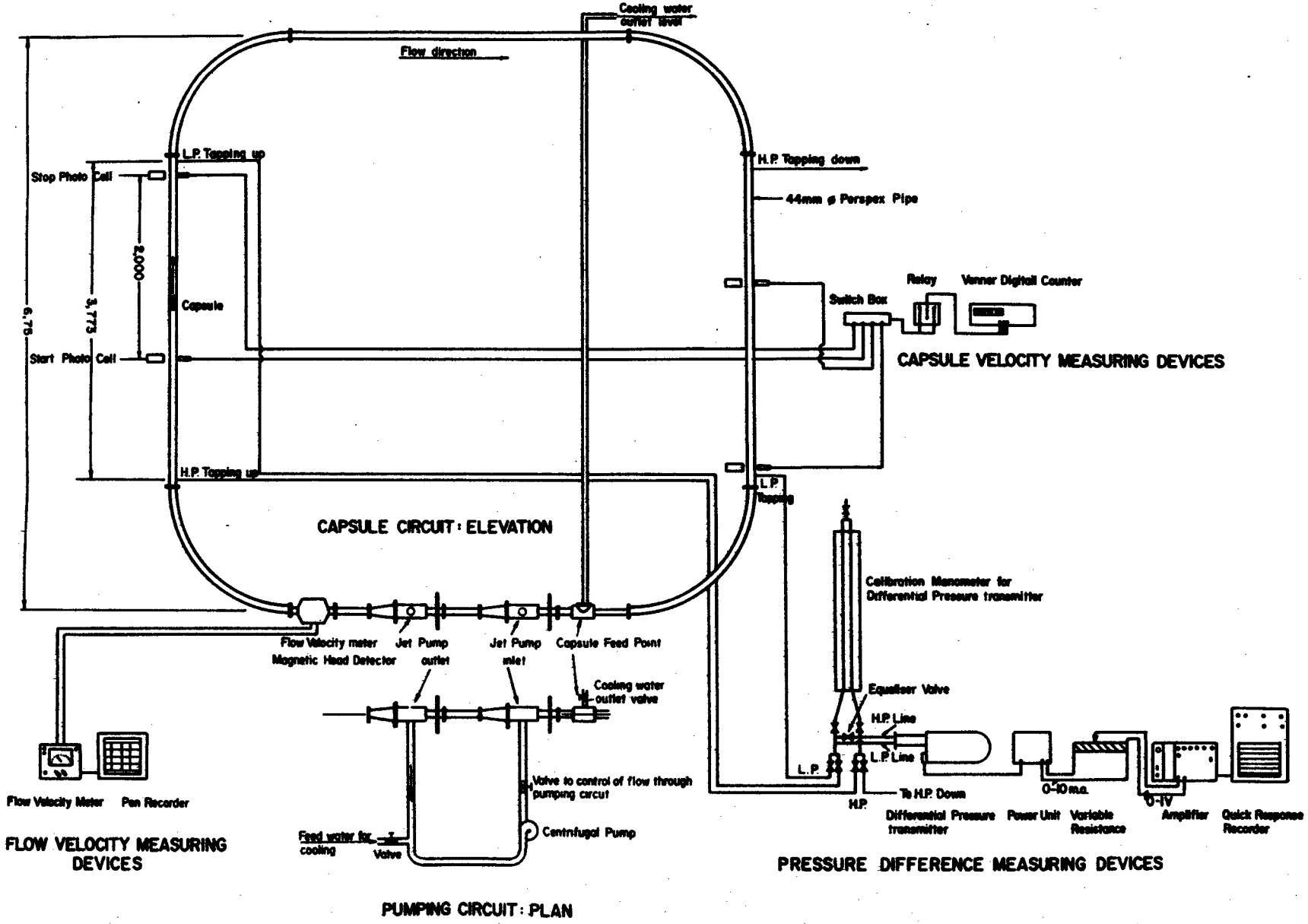

FIGURE 4.5

DIAGRAMMATIC LAYOUT OF APPARATUS FOR STUDYING CAPSULE MOTION IN A VERTICAL PIPELINE.

the original 74 mm diameter open circuit line.

5.3 One aspect of the technology of the investigation was the development of capsule pumps and the closed circuit was an effective means of observing the flow of capsules through an annular jet pump developed for this purpose.

5.4 Many visitors who saw the open circuit expressed doubt as to the effect of bends on the capsule transportation system. The closed circuit supplied qualitative visual evidence of the feasibility of the scheme from this point of view.

5.5 Although the effects of different specific gravities and diameter ratios were determined from open circuit tests, the closed circuit was a convenient tool for observing and verifying these phenomena. It was relatively easy to determine the effect of "catching up," on capsule velocity and excess energy requirements, when several capsules with slightly different characteristics were in the circuit simultaneously.

6. Description of the closed circuit

Figure 4.5 shows the closed circuit with 44 mm diameter plexiglass tube arranged in a vertical plane.

The pipeline is open to the atmosphere upstream of the jet pump system where there is an "insertion trough" for inserting and retrieving the capsules. This feeder trough is simply a 460 mm long section of the 44 mm diameter pipe which was cut to a semi-circular section providing a guide for the capsules and facilitating insertion and removal. The pipe was surrounded by a 200 mm diameter P.V.C. pipe with a raised P.V.C. section to form a reservoir for the capsule insertion trough. At the downstream end of the semi-circular plexiglass tube section a bell mouthed entry eased the capsule into the 44 mm pipeline. This arrangement was satisfactory for the horizontal circuit. However, for

the vertical circuit the insertion box was replaced by a steel container which could be pressurised with a screw-on lid for insertion and removal of capsules. This was necessary because of the difficulty involved in getting the system airtight and ensured that the entire pipeline was above atmospheric pressure.

6.1 The pump: Two pumps were developed during the course of the investigation and they are both described in the Chapter on technology of capsule transportation (Chapter 3).

The two pumps have been designated the "Annular rotary pump" and the "Annular jet pump." The latter was used for the closed circuit, the reason being that flow adjustments could be easily and reliably achieved by means of a valve in the pumping circuit. However, the one disadvantage of the Annular jet pump that would not have occured with the Annular rotary pump was the acceleration of capsules when passing through the pump. However, the acceleration and resultant deceleration only occured over a short length of pipeline and was overcome by making the pipeline long enough and taking all measurements on the opposite side from the pump section.

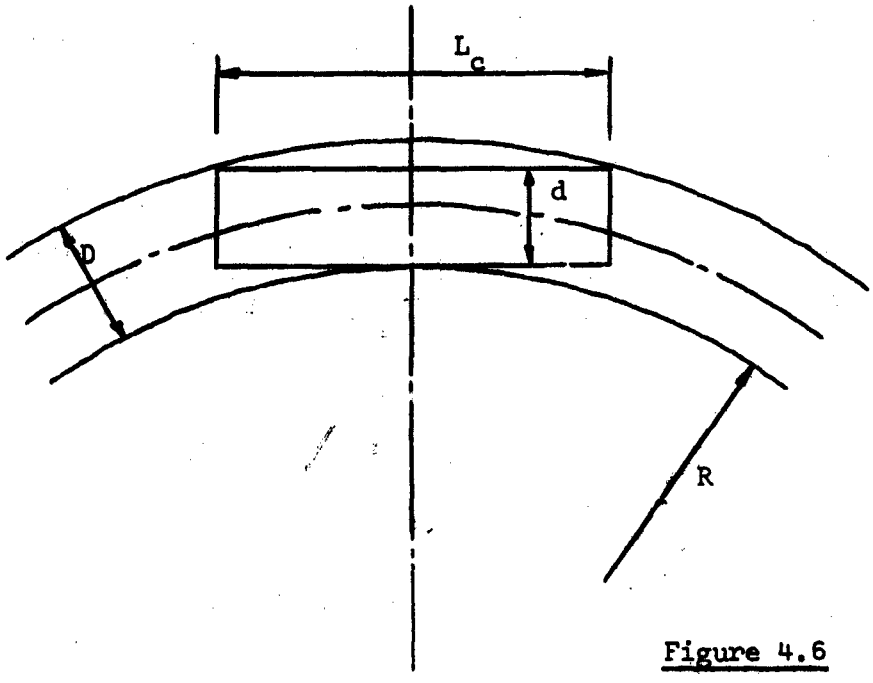

Figure 4.6

6.2 The pipe bends: It can be shown from the geometry of the bend (Figure 4.6) that

$$L_c = 2\sqrt{(D-d)(2R+d+D)} \qquad (4.1)$$

The radius of the bends were 1219,2 mm (4 ft) and this gives a maximum value of L_c = 200,8 mm (for D = 44 mm and d = 40 mm). This is a theoretical value and assumes that the "plexiglass" remains circular when curved to radius R.

The maximum length of single 40 mm diameter capsules used in the experiments was 160 mm (L_c/d = 4,0) and in fact 173 mm long capsules were found to pass round the bends without jamming.

6.3 Flow measurement : Flow measurement posed special problems in the closed circuit since it was imperative that whatever device was used should allow through passage of the capsules.

Initially, one of the bends with pressure tappings drilled in the inside and outside of the bend was used as a bend meter. However, this was not satisfactory due to slow response time and lack of precision.

A magnetic detector head replaced the bend meter and the internal bore of the head was machined to have the same internal diameter as the 44 mm plexiglass tube. The electrodes were made flush with the bore of the head and this allowed easy passage of the capsules through the instrument. By deflecting the water, the flow meter was calibrated in situ.

6.4 Pressure transients and capsule velocity were determined as described in the section on the open circuit.

6.5 Orientation: The closed circuit was oriented horizontally, vertically and on a slope.

The vertical orientation posed special problems since the insertion trough was placed in the lower horizontal limb and since this was at

atmospheric pressure the apparatus had to be less than one atmosphere (10 m) in height to prevent the water from vapourising in the upper limb. It also meant that the whole circuit had to be airtight to prevent de-priming. This proved to be rather difficult to achieve in practice and was overcome as mentioned in Section 6.

The total height of the vertical circuit was in fact 6,75 m with a straight section 4,010 m long. The horizontal dimension was 6,320 m centre to centre. The vertical height was restricted by the laboratory roof.

6.6 Cooling water: One problem to be faced with the closed circuit was cooling. All the energy from the pump was absorbed by the water and it was found that without cooling, the water temperature in the closed circuit rose steadily. In 90 minutes the temperature rose from 20°C to 60°C, at $Q = 2,66\ dm^3/s$, and had still not become stable. This affected the viscosity of the water. In order to alleviate this situation cooling water was fed into the circuit downstream of the jet pump and extracted upstream of the pump.

This resulted in a stable temperature within 8 minutes of starting over the entire range of flow operation. The temperature rose from 21°C to 23°C at a flow of $6,65\ dm^3/s$.

7. Apparatus for static capsule tests

Figure 9.1 shows the apparatus used for static capsule tests.

Pressure tappings were carefully drilled as indicated in the Figure.

The pipeline used was 74 mm diameter perspex. All the pressure tappings in the sides and roof of the tube in the pattern shown in Figure 9.1 were connected to an air over water manometer and were used to determine the hydraulic grade line in the capsule zone.

The flow of water through the test section was measured with the

magnetic detector head upstream and supplemented at low flows by gravimetric measurement.

Capsules were made to 40 mm, 50 mm, 63 mm and 70 mm diameters, each capsule being 880 mm in length. This length to diameter ratio was considerably in excess of that envisaged for practical applications but this was considered necessary to ensure that the inlet, outlet and annular friction losses could be clearly distinguished. The capsules were made of polyvinyl chloride (P.V.C.) tubing and, in the case of fully eccentric static capsule tests, were firmly attached to the pipe wall, eliminating any tendency to lift.

For concentric static capsule tests, vanes shaped to an aerofoil section were used to position the capsules (see Figure 4.7).

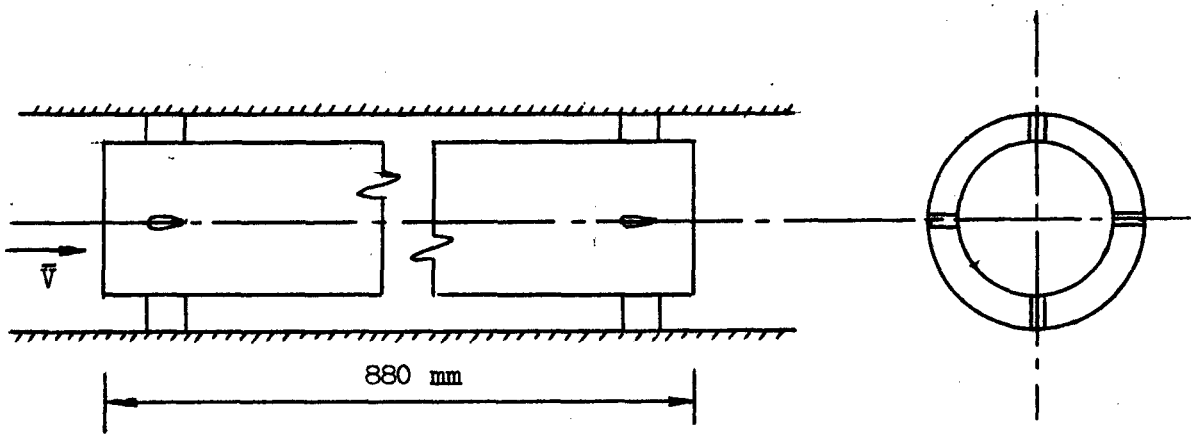

Figure 4.7

8. Other pipelines used

Apart from the 74 mm and 44 mm diameter plexiglass pipes, two other pipes were used.

8.1 The asbestos cement pipe: To test the effect of pipe roughness the 74 mm diameter plexiglass tube was replaced by an undipped asbestos-cement pipe 76 mm diameter. The photo transducers were replaced by magnetic pulse detectors (pulsotronic) which were activated by the metal in the capsules to trip relays and operate the digital counter.

The joints were of the collar type with seal rings. The expansion ring was removed to close the gap between the pipes. The pipeline was

connected to the existing injector with a cast iron flange adapter. Upstream and downstream pressure tappings were required which were turned from brass and fixed in their seatings with epoxy resin.

The alternative method of obtaining a rough pipe surface was to use steel but this is a conducting opaque material and would have prevented the use of both the "pulsotronic" switches and the photo transducers.

8.2 P.V.C. pipe: In order to examine the scaling effect still further a 150 mm diameter pipe made of polyvinyl chloride was connected to the constant head tank supply system.

Since a rather large flow was necessary to give an adequate mean water velocity, care was taken to keep pipeline head losses to a minimum. The maximum flow velocity used was $\overline{V} = 3$ m/s corresponding to a flow of 53 dm^3/s.

The pipe was independently supported along its entire length on a trapezoidal steel section.

For capsule injection an inverted tee was used at the supply point. The end of this extension was threaded and a coupling which could be screwed on and off for insertion of the capsule had a gland fitted, see Figure 4.8.

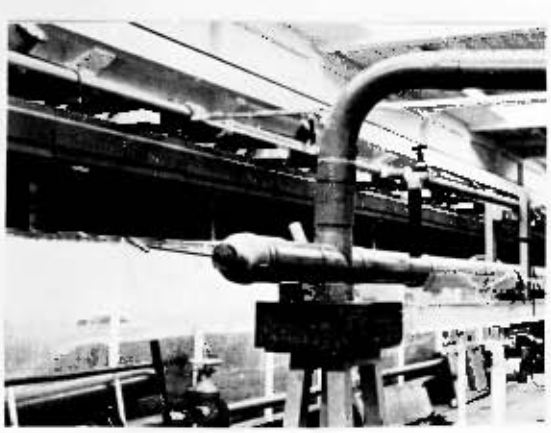

Figure 4.8

A 1 m long brass plunger passing through the gland could be fully withdrawn when setting the flow so that the capsule did not block the flow entry when everything was ready for a test, the plunger could be thrust forward to overcome the initial acceleration and the capsule would then be propelled by the water.

Capsule retrieval was simply achieved in this case by cutting away the upper half of the 150 mm diameter pipe at the end, thus forming an open channel with two side weirs. A plastic spring was placed at the end of the pipe to absorb the capsule energy.

9. Apparatus for measuring capsule clearance

As cylindrical capsules travel along the pipeline they tend to lift off the pipe wall when travelling at high speed.

In order to verify this phenomenon various techniques were employed to determine the clearance between the bottom of the pipe and the capsule. This was a difficult measurement to take since the clearance is small (less than about 1 mm) and only occurs at high velocities.

The final method employed was a differential transformer mounted below the 74 mm diameter perspex pipe (Figure 4.9).

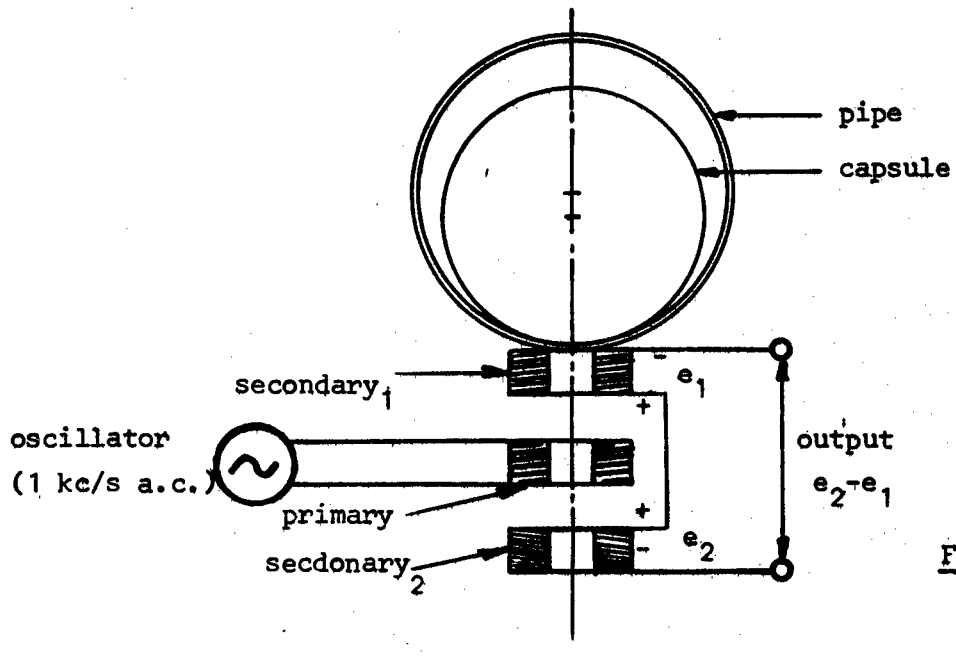

Figure 4.9

The transformer consisted of a central (primary) coil with two other (secondary) coils on either side. The outer coils each had 50 turns and were wound in opposite directions to each other. The number of turns in the central coil was also 50 but this had no significance.

Alternating current was passed into the central primary core and this was converted into flux due to the presence of the outer two coils, forming a magnetic circuit. The induced voltage was zero since the wire on the two outer coils was wound in opposite directions and the resulting induced e.m.f. was equal in magnitude but opposite in direction.

The induced e.m.f. is equal to the rate of change of flux but in the opposite direction

$$\text{e.m.f.} = -d\phi/dt$$

If steel is brought near the secondary coil, the flux is increased due to the low reluctance of the steel

$$\text{flux} = \phi = NI/\mathbb{R}$$

where N = no. of coils

I = excitation current

$\mathbb{R}$ = reluctance

The presence of the steel (in the capsule) increases the flux around the upper secondary coil but hardly affects the flux around the lower secondary coil. This means a larger voltage across the upper secondary coil than the lower. The resultant difference in voltage could then be read from a memory oscilloscope. An oscillator was used to provide current for excitation of the primary coil.

When no capsule was present the system was balanced. The capsule was then placed in the pipeline above the coil and this represented the zero clearance voltage. As the capsule was lifted from the pipe bottom the steel inside the capsule, being at a further distance from the coil, decreased the flux since the non-conducting material between the coil and

the steel (i.e. P.V.C. and perspex) has a relatively high value of reluctance $\mathbb{R}$. The induced voltage was decreased and this new value could be read off the oscilloscope. The system required a calibration curve of voltage versus clearance and the trace on the oscilloscope represented the clearance at every point along the capsule thus giving the orientation (e.g. nose up) of the capsule when travelling in the pipe.

10. Capsules tested

TABLE 4.1

LIST OF CAPSULES TESTED

Capsule No	d (mm)	L_c (mm)	Mass (g)	Volume (cm^3)	L_c/d	S_c	$\frac{d}{D}$ used	Remarks
1	70,2	303	498	1,170	4,32	0,426	0,95	air filled
2	"	"	1243	"	"	1,065	"	water "
3	"	"	2070	"	"	1,77	"	sand "
4	"	"	3072	"	"	2,62	"	brass "
5	"	"	3762	"	"	3,21	"	loose pack steel filled
6	"	"	5666	"	"	4,83	"	lead "
7	63,0	303	473	941	4,82	0,502	0,851	air "
8	"	"	100	"	"	1,064	"	water "
9	"	"	1760	"	"	1,870	"	sand "
10	"	"	2484	"	"	2,640	"	brass "
11	"	"	3089	"	"	3,280	"	steel "
12	"	"	4606	"	"	4,900	"	lead "
13	50,3	303	306	601	6,02	0,51	0,68	air "
14	"	"	651	"	"	1,082	"	water "
15	"	"	1102	"	"	1,835	"	sand "
16	"	"	1496	"	"	2,490	"	brass "
17	"	"	1956	"	"	3,255	"	steel "

Capsule No	d (mm)	L_c (mm)	Mass (g)	Volume (cm^3)	L_c/d	S_c	$\frac{d}{D}$ used	Remarks
18	50,3	303	2978	601	6,02	4,950	0,68	lead filled
19	40,2	303	164	382,5	7,54	0,417	0,543	air "
20	"	"	416	"	"	1,06	"	water "
21	"	"	686	"	"	1,75	"	sand "
22	"	"	964	"	"	2,46	"	brass "
23	"	"	1273	"	"	3,24	"	steel "
24	"	"	1872	"	"	4,77	"	lead "
25	63,0	271,2	361	849	4,32	0,42	0,852	air "
26	"	"	903	"	"	1,06	"	water "
27	"	271,1	1509	"	"	1,77	"	sand "
28	63,0	272,0	2233	846	4,32	2,63	0,852	brass "
29	"	272,0	2730	"	"	3,21	"	steel "
30	"	272,0	4116	"	"	4,84	"	lead "
31	50,3	217,5	182	433	4,32	0,42	0,681	air "
32	"	217,1	458	"	"	1,06	"	water "
33	"	217,7	771	"	"	1,78	"	sand "
34	"	217,7	1124	"	"	2,60	"	brass "
35	"	217,7	1381	"	"	3,19	"	steel "
36	"	217,0	2080	"	"	4,81	"	lead "
37	40,0	173,7	92	218,5	4,32	0,42	0,541	air "
38	"	173,5	233	"	"	1,06	"	water "
39	"	174,0	384	"	"	1,76	"	sand "
40	"	173,5	574	"	"	2,65	"	brass "
41	"	"	700	"	"	3,2	"	steel "
42	"	"	1053	"	"	4,82	"	lead "
7044	70	280	1820	1080	4,0	4,0	0,945	10 No. made
7034	"	210	3240	810	3,0	"	"	"
7024	"	140	2160	540	2,0	"	"	"

Capsule No	d (mm)	L_c (mm)	Mass (g)	Volume (cm^3)	L_c/d	S_c	$\frac{d}{D}$ used	Remarks
7014	70	70	1080	270	1,0	4,0	0,945	10 No. Made
K	25,3	303	410	152	12,0	2,72	0,342	
L	19.4	303	243	90	15,6	2,70	0,262	
M	22,3	303	902	118	13,6	7,8	0,300	
0	13,7	303	302	45	22,1	6,7	0,19	
N	22,4	96	296	38	4,28	7,8	0,800	
6344	63,1	252,4	3150	788	4,0	4,0	0,851	
5044	50,2	200,8	1592	398	4,0	4,0	0,675	
4044	40,0	160,0	807	202	4,0	4,0	0,541	
7044R	70	280	4320	1080	4,0	4,0	0,95	Rough Capsules
6244R	62	252	3045	761	"	"	0,84	"
5044R	50	200	1575	394	"	"	0,68	"
4044R	40	160	807	202	"	"	0,54	"
4024	40,02	80,5	404	101	2,0	4,0	0,91	P.V.C.
4041	40,24	159,0	202	202	3,95	1,00	"	"
4042	40,27	"	403	201	"	2,00	"	"
4043	40,24	"	603	202	"	2,98	"	"
4044	40,29	"	807	202	"	4,00	"	"
4044	40,29	"	805	207	"	4,00	"	"
4044	40,00	158,0	804	198	"	4,06	"	"
4046	40,00	160,0	1207	200	4,0	6,00	"	"
3724	37,55	74,7	327	83	1,98	3,95	0,85	Brass turned
3742	37,31	149,4	325	162	4,0	2,00	"	"
3744	37,31	"	654	"	"	4,05	"	"
3744	37,29	"	660	"	"	4,07	"	"
3746	37,33	"	979	"	"	6,05	"	"
2924	29,71	59,2	161	41	2,0	3,95	0,68	"
2942	29,61	118,3	162	81	4,0	2,00	"	"

Capsule No	d (mm)	L_c (mm)	Mass (g)	Volume (cm^3)	L_c/d	S_c	$\frac{d}{D}$ used	Remarks
3044	30,58	108,5	324	80	3,95	4,07	0,68	brass turned
2944	29,59	118.3	321	81	4,0	4,00	"	"
2946	29,55	118,3	483	81	4,0	5,95	"	"
2324	23,85	48,5	85	21	2,04	3,92	0,54	"
2342	23,89	93,3	86	43	4,0	2,03	"	"
2344	23,86	"	169	43	4,0	3,95	"	"
2344	23,84	95	"	42	4,0	4,00	"	"
2346	23,83	95,3	256	42	4,0	6,05	"	"
4044R	40,0	160,0	802	200	4,00	4,01	0,91	Rough; annular grooves in P.V.C.
3744R	37,5	150,0	652	165	4,10	3,95	0,85	knurled brass
2944R	29,0	119,0	323	78	3,97	4,13	0,66	"
2344R	23,0	95	172	43	4,00	4,05	0,54	"
4088S	40	880			22		0,542	used
5088S	50	"			17.6		0,675	for
6388S	63	"			13,95		0,85	static
7088S	70	"			12,6		0,947	tests
9042	90,0	360,0	4 600	2 300	4,0	2,0	0,600	used
9043	90,0	"	6 900	"	"	3,0	0,600	in
9044	90,0	"	9 200	"	"	4,0	"	150 mm
11042	110,0	440,0	8 320	4 160	"	2,0	0,733	diameter
11043	110,0	"	12 480	"	"	3,0	"	pipe
11044	110,0	"	16 640	"	"	4,0	"	
12542	125,0	500,0	12 340	6 170	"	2,0	0,833	
12543	125,0	"	18 510	"	"	3,0	"	
12544	125,0	"	24 680	"	"	4,0	"	
14042	140,0	560,0	17 200	8 600	"	2,0	0,933	
14043	140,0	560,0	25 800	8 600	"	3,0	"	
4044	140,0	"	34 400	"	"	4,0	"	

Capsule No	d (mm)	L_c (mm)	Mass (g)	Volume (cm^3)	L_c/d	S_c	$\frac{d}{D}$ used	Remarks
5041,10	50,1	225,0	488	443	4,0	1,10	0,676	P.V.C.
5041,51	"	"	670	"	"	1,51	"	with
5042,31	"	"	1 020	"	"	2,31	"	steel
5043,72	"	"	1 650	"	"	3,72	"	inner
6241,11	62,5	250,8	861	770	"	1,11	0,845	lining
6241,44	"	"	1 110	"	"	1,44	"	
6242,35	"	"	1 795	"	"	2,35	"	
6243,62	"	"	2 780	"	"	3,62	"	
6941,11	69,6	280,4	1 188	1 068	"	1,11	0,943	
6941,53	"	"	1 640	"	"	1,53	"	
6942,33	"	"	2 490	"	"	2,33	"	
6943,74	"	"	3 990	"	"	3,74	"	

The capsule characteristics are classified in Table 4.1.

10.1 The first set of capsules numbered 1 to 24 were made of polyvinyl chloride (P.V.C.) plastic tubing in four different diameters, i.e. 70 mm, 63 mm, 50 mm and 40 mm (exact diameters are given in Table 6.1). The length was constant (L_c = 303 mm) throughout. Each set of six capsules had varying specific gravities from 0,426 to 4,95. The tubes were capped at each end and filled with different materials, i.e. air, water, sand, loosely packed brass screws, scrap steel and scrap lead.

10.2 The second set of 24 capsules are numbered 1 to 6 (the same as above) and 25 to 42. There were again four sets of different diameters, each set comprising six similar specific gravities, i.e. 0,426; 1,065; 2,625; 3,22 and 4,84. These capsules were all made dimensionally similar (L_c/d = 4,32) of P.V.C. tube, capped and filled with materials as above.

10.3 The third set had a specific gravity of 4,0, a diameter of 70 mm and an L_c/d ratio of 4,0. There were 10 of these capsules all identical. They were made of P.V.C. tubing with end caps. Steel cylinders were Allen screwed inside each end (see Figure 4.10). Their purpose was to examine concentration effects by varying the injection rate and thus the number of capsules in line at the instant of taking readings.

These capsules were designated 7044, the first two digits denoting the first two digits of the diameter in millimeters, the third digit being the L_c/d ratio and the fourth digit the specific gravity.

10.4 The fourth set of capsules had a specific gravity of 4,0, a diameter of 70 mm and had varying lengths, i.e. L_c/d = 1; 2; 3 and 4. These were numbered 7014; 7024; 7034; and 7044, the digits denoting diameter, L_c/d ratio and specific gravity as above. These capsules were made as the third set (see Figure 4.10). In fact only L_c/d ratios of 1 and 3 were manufactured, L_c/d ratios of 2 and 4 being the combinations of 1 and 3 by joining these capsules with the Allen screws in the end caps.

10.5 The fifth set of capsules was alphabetically designated and were of small diameter not within the range for practical application. These were used to enlarge the range of certain experiments.

10.6 The sixth set was of specific gravity 4,0 and length to diameter ratio 4,0. There were four different diameter ratios. These were numbered 7044; 6344; 5044 and 4044.

10.7 The seventh set were artifically roughened capsules designated 7044R; 6244R; 5044R and 4044R. These were four different diameter capsules all of specific gravity 4,0 and L_c/d ratio 4,0.

These capsules were roughened by turning grooves on the P.V.C. in the lathe. Artificial roughening was also achieved by sieving sand between

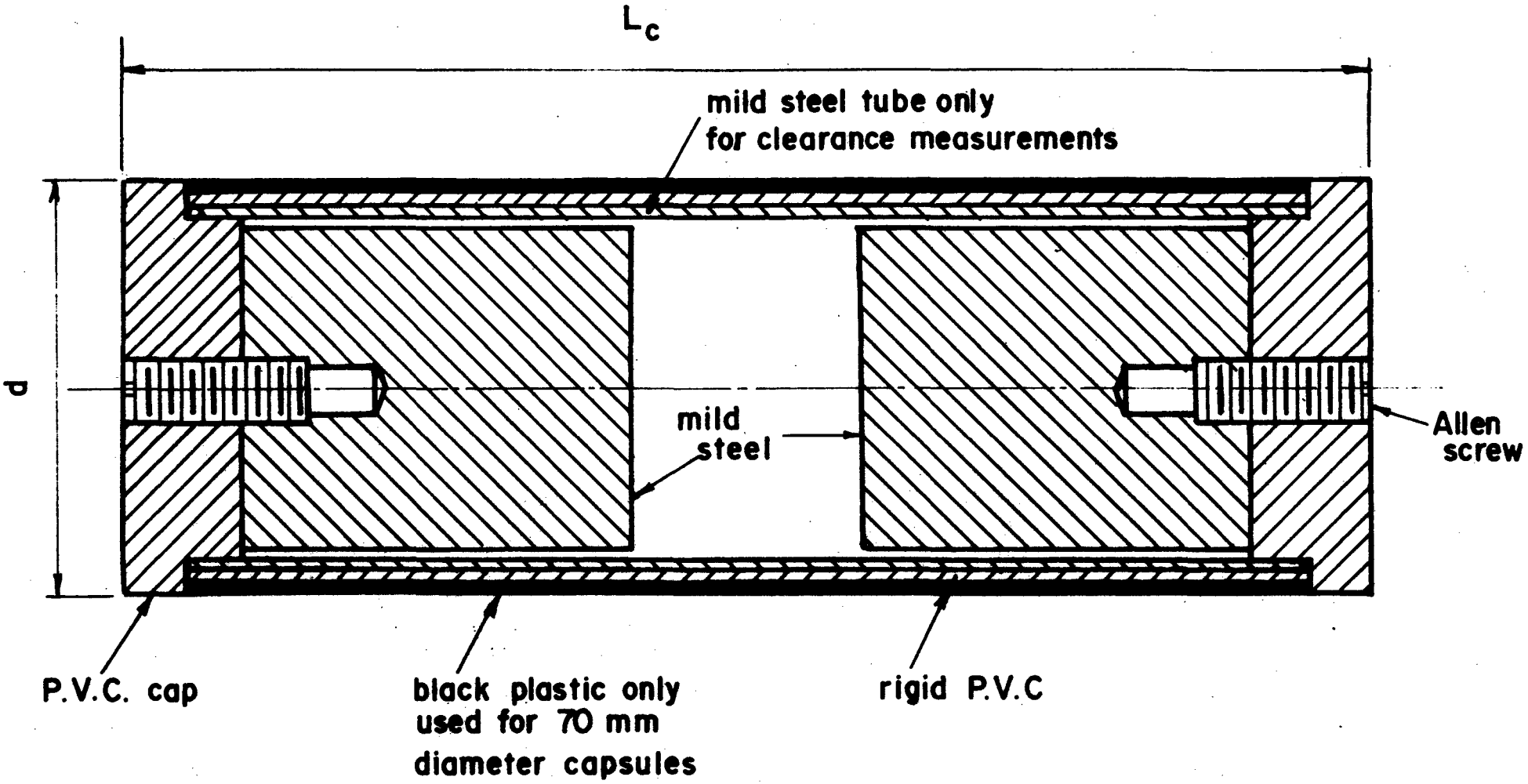

FIG. 4.10

TYPICAL CAPSULE

two sieve sizes and gluing the sand to the outside wall of the capsule. These capsules were not successful from the experimental viewpoint since the readings obtained were far too scattered to be meaningful.

10.8 The eighth set of capsules was 40 mm nominal o.d. and were used mainly in the 44 mm closed circuit line. One capsule had length to diameter ratio of 2,0 and a specific gravity of 4,0. The remainder had L_c/d ratios 4,0 and specific gravities of 1,0; 2,0; 3,0; 4,0 and 6,0. These capsules were used for determining the effect of specific gravity as well as L_c/d ratios.

By combining the appropriate capsules, equivalent capsules in trains could be obtained, e.g. an L_c/d ratio of 14 with a specific gravity of 4,0 could be symthesised using three capsules with L_c/d ratios of 4,0 and one capsule with L_c/d ratio of 2,0. Since low specific gravity capsules travelled faster than high specific gravity capsules, a capsule with $S_c = 6,0$ was placed at the front of the train and one with $S_c = 2,0$ was placed at the tail, thus giving an average specific gravity of 4,0. These capsules were made of P.V.C. tubing with end caps and steel cylinders glued to the end caps.

10.9 The ninth set of capsules was 37 mm nominal o.d. and the same pattern of L_c/d ratio and specific gravity was followed as the eighth set thus allowing combinations of appropriate cpasules to form capsule trains up to $L_c/d = 16$.

10.10 The tenth set of capsules was the same as above except the nominal diameter was 29 mm.

10.11 The eleventh set was as above except the nominal diameter was 23 mm.

The ninth, tenth and eleventh sets were made of brass tubing with the o.d. such as to give the same d/D as was obtained with P.V.C. capsules

in the 74 mm diameter pipeline. The i.d. was bored out to give the capsule the required mass.

T A B L E 4.2

d	S_c	L_c/d	d	S_c	L_c/d	d	S_c	L_c/d	d	S_c	L_c/d
40,2	4,00	2,00	37,55	3,95	1,99	29,71	3,95	2,00	23,85	3,92	2,04
40,00	4,06	3,95	37,31	4,05	4,00	29,59	4,00	4,00	23,84	4,0	4,00
40,00	4,00	7,95	37,32	4,02	8,00	29,58	3,97	8,00	23,86	4,04	8,04
40,08	4,00	9,95	37,37	4,00	10,00	29,62	3,93	10,00	-	-	-
40,03	4,00	11,90	37,31	4,03	12,00	27,58	3,98	12,00	23,85	4,00	12,00
40,08	4,02	15,92	37,31	4,04	16,00	29,83	4,00	15,55	23,85	4,00	16,00

Table 4.2 shows the combinations of capsule trains obtained by combining different capsules in sets, eight, nine, ten and eleven.

10.12 The twelfth set consisted of four capsules 40 mm, 37,5 mm, 29 mm and 23 mm diameter, all with a specific gravity of 4,0 and a length to diameter ratio of 4,0. These capsules were all made of brass and artificially roughened by knurling, except the 44 mm diameter capsule (4044R) which was made of P.V.C. and roughened with grooves cut on the lathe.

10.13 The thirteenth set was used in the 74 mm diameter pipeline for static tests. There were four capsules of different diameters each 880 mm long. The mass and specific gravity are not given for these capsules since they were in all cases held static.

10.14 The fourteenth set of capsules was used in the 150 mm diameter P.V.C. pipe. Three different specific gravity values (S_c = 2,0; 3,0 and 4,0) for each of the four different diameter ratios d/D = 0,600; 0,733; 0,833 and 0,933 were tested. All capsules had a fixed length

to diameter ratio, $L_c/d = 4,0$.

10.15 The fifteenth set of capsules was used for clearance measurement and was steel lined to activate the differential transformer (see Figure 4.10). These capsules were carefully machined internally as well as externally to achieve a constant thickness of steel as well as a constant thickness of P.V.C. around the perimeter.

In all, one hundred and thirteen capsules were tested in a wide variety of situations, i.e. different pipe diameters, materials and slopes, as well as combinations of capsules to form continuous trains and spaced capsules at fixed intervals.

CHAPTER 5

EXPERIMENTAL PROCEDURE

The hydraulics laboratory at the University of Cape Town is in the form of a recirculating system. Water is pumped from a sump, which is connected to a network of floor channels, to a constant head tank, with a bellmouth overflow.

The apparatus for acrrying out experiments on the hydraulic conveyance of capsules was fed from the constant head tank in the open circuit case and recirculating water was used for the closed circuit with cooling water supplied through the laboratory recirculating system.

1. Procedure when using the open circuit

Water entered the system from the constant head tank, passed through the veriflux magnetic detector head, then through the experimental tube section (in most cases 74 mm diameter "perspex") and was discharged over the weir at the downstream end.

The water could, at this stage, be deflected by a diversion system, consisting of a box on rollers, either into the laboratory floor channel or the tank for gravimetric calibration of flow.

The capsules were injected into the pipeline by means of the rotary injector. When passing down the line the additional head due to the presence of the cpasule was measured, with the capsule between the pressure tappings, by means of the differential pressure transmitter and the capsule velocity was calculated, from the measurement of time over a known distance, using the electronic timer.

Before any experiments could be performed the measuring instruments (differential pressure, water flow and timer) had to be calibrated.

2. Calibration of flowmeter

The Veriflux magnetic detector head, converter and recorder were calibrated as a unit, in situ. The unit was calibrated at maximum scale settings of 1; 2; 3 and 4 m/s and at 25%, 50% and 75% of these maximum scale settings. Each reading was repeated several times.

The graph (Figure 5.1) shows the ratio of the mean velocity in the pipe to the velocity through the metre $(\overline{V}/V_m)$ plotted against the velocity through the meter (V_m) for the 74 mm diameter "perspex" tube and a nominal 80 mm diameter meter bore. These are mean data points.

The actual data were plotted to an enlarged vertical scale and above $\overline{V}$ = 0,5 m/s the error in flow measurement is of the order of 1,0%.

Figure 5.2 shows the calibration graph for the 44 mm diameter "plexiglass" tube with the 44 mm diameter meter bore. The error expected in flow measurement is again of the order of 1,0%.

3. Calibration of differential pressure meter

The calibration manometer had one limb connected to the constant head tank and the other open to atmosphere. The former was connected to the high pressure side of the differential pressure transmitter and the latter to the low pressure side. Before each set of tests the pressure transmitter and recorder were calibrated as a unit. Preliminary tests were done to determine the maximum sum of the head loss due to water friction between the tapping points and the transient head due to the presence of the capsule between the points $(\Delta h_f + \Delta H_c)_{max}$. Once this maximum value had been determined the flow was switched off and the high pressure limb of the calibration manometer was pressurised to some value > $(\Delta h_f + \Delta H_c)_{max}$. The output from the power unit for the differential pressure transmitter was adjusted by means of the calibrating rider (U) (Figure 4.4) to give a 10 mA signal on an Avo-meter and 0,0 mA when the pressure in both limbs was atmospheric. The variable resistance was then connected to the

CALIBRATION OF FLOW METERS

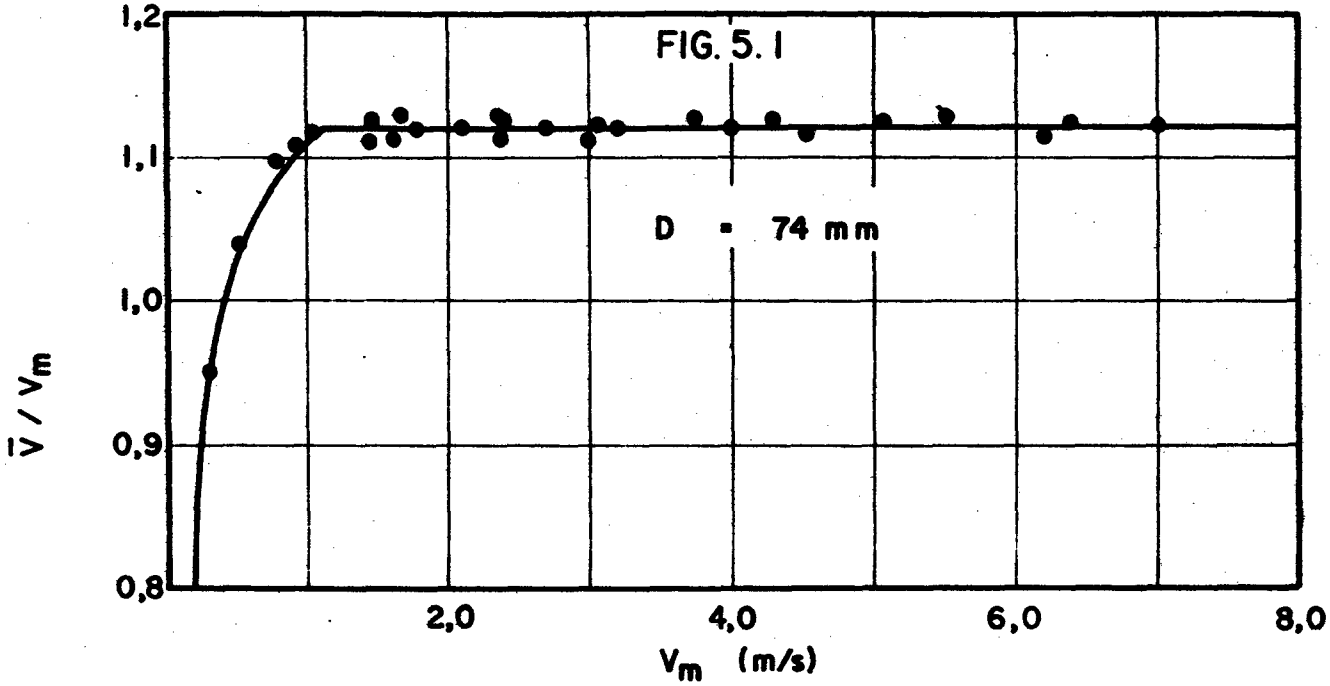

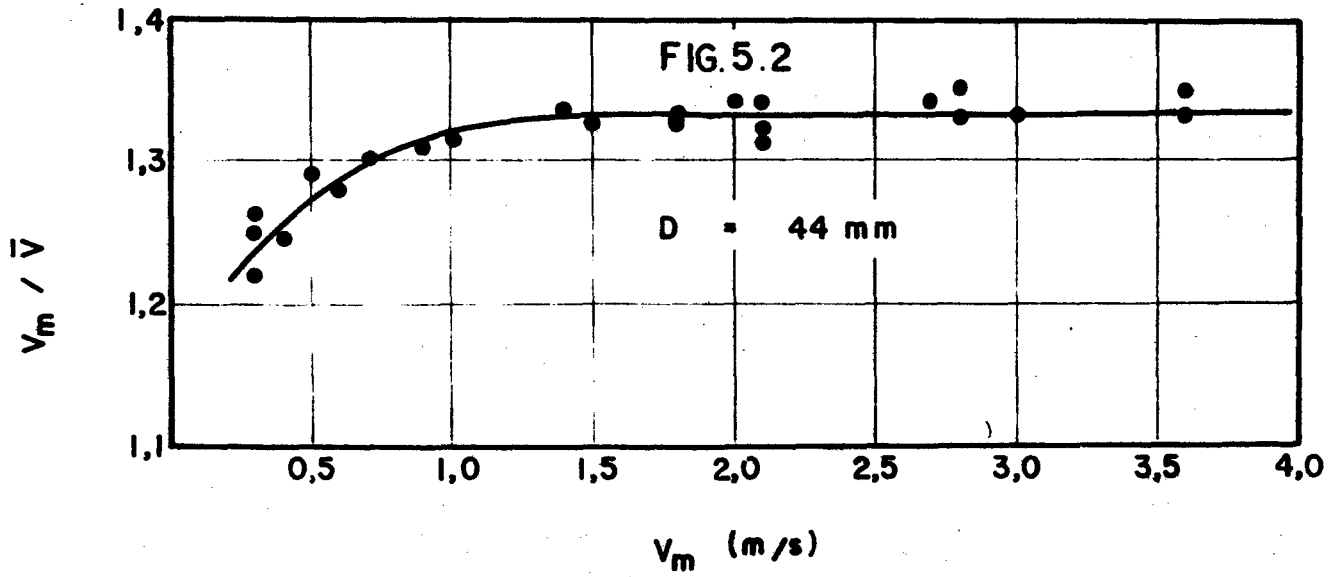

power unit output leads and the recorder was connected to the resistance. The resistance was then adjusted to give full scale deflection on the Duplex quick response recorder with the desired pressure differential (static) on the calibration manometer. Having a 0 to 10 mA signal from the power unit ensured linearity. However, the linear response was checked by setting the calibration manometer at 90%, 80% down to 10% of the maximum and reading the recorder.

This check was usually accurate to less than 1% and repeatability was to within 1%.

After calibration care was taken to ensure that the cocks to the manometer were closed otherwise errors could have resulted from too slow a response time on the transmitter.

4. The digital timer

This was calibrated by simply using a stop watch and allowing the timer to run for several hundred seconds to reduce reaction time error. No difference was found between the stop watch and timer. The timer was assumed to have an indiscernable error.

The errors mentioned above are inherent in the instruments and in Chapter 6 on measurement and errors it will be shown that the experimental errors are more significant than those mentioned above.

5. Levelling the support beam

This was done by taking a level on the perspex tube at the pivot point. The jack at the upstream end was then adjusted to give the same level at the downstream support point as at the pivot point. The support was then clamped in position using the locking screws. The upstream jack was then adjusted to give the same level at the upstream support point and the upstream support point was then clamped in position.

For slope adjustment the same procedure was followed (i.e. setting the downstream support using the upstream jack first and then setting the upstream support) except that the appropriate levels were used at the support points.

6. Procedure for performing a test run in the open circuit

One test run involved the testing of a number of capsules.

After all the instruments had been calibrated and the support beam levelled at the required slope the following procedure was followed.

6.1 The pumps were started ensuring that the constant head tank remained full.

6.2 The instruments were switched on allowing the warming up time required by each instrument (e.g. veriflux converter = 20s, amplifier for Duplex Recorder 15 minutes, etc).

6.3 The injector was preloaded with a maximum of six capsules. As can be seen from Figure 4.2 the injector was designed for twelve capsules.

For the laboratory experiment the capsules could only be fed into the pipeline in batches, i.e. not continuously.

At least one space in the injector had to be left in order not to loose a capsule when opening the flow regulating valve (step 6.4) this meant that, for a set of capsules, the flow conditions (if the drum was consecutively loaded) for the last capsule would differ from the others. In order to prevent this a blank space was left on either side of each capsule in the injector which meant a maximum of six capsules per batch. Thus the first lot of experiments were with batches of six (i.e. six different SG's).

When the magnetic detector head replaced the manometers this re-

quirement could be dispensed with since it was easier to read each flow with a capsule in the line on the pen recorder whereas there had been no time with the manometer.

6.4 The flow regulating valve was opened to the required flow in order to carry out several sets of experiments at the same flow. The other valve was used as an on-off valve (see Figure 4.1).

6.5 The veriflux magnetic flowmeter converter was adjusted to give a reading close of 100% on the chart and this percentage when multiplied by the dial reading (to three decimal places) and the appropriate coefficient (e.g. see graph Figure 5.1) gave the mean flow velocity in the pipeline, i.e. $\bar{V} = V_m \quad p \quad C_o$

where p = % full scale deflection on the recorder

C_o = coefficient for Veriflux meter

V_m = converter velocity reading.

6.6 The friction head lost in the capsule free line was measured on the open tube water manometer (which is the same as the calibration manometer).

6.7 The pressure differential recorder was set to give a reading on the chart as near to zero as possible ensuring that the pen, which oscillated due to the water turbulence, amplitude never reached zero and went off the chart.

6.8 The timer was zeroed.

6.9 The valves to the calibration manometer were closed preventing the manometer from acting as a surge chamber affecting the differential pressure transmitter.

6.10.1 For "single capsule" runs the injector was operated by hand and each capsule was injected into the pipeline separately by rotating the handle and permitting the clutch, connected to the automatic feed, to slip.

6.10.2 For multiple capsule runs the injector drum was fully loaded (i.e. 10 capsules and 2 empty spaces at the bottom). The rotational speed of the rotating drum was set on the variable speed drive and the clutch was engaged. The motor was started and the capsules were injected at a constant injection rate.

6.10.3 For very low flows the above procedure (10.1) was modified since the incipient velocity in the injector casing was lower than in the pipeline due to the larger flow area in the injector.

The capsule was injected at a higher flow than the test flow and while the capsule was still in the first metre of the pipeline the valve was rapidly closed to prevent losing the capsule at the high flow and to trap it in the pipeline just downstream of the enlarged section. The valve could then be opened to the required value. With this mode of injection, at the low flows, the flow could not be preset.

6.10.4 At the threshold velocities the above procedure was followed and the valve was opened gradually until the capsule just moved. This was done in order to obtain information on incipient flows and capsule pressures.

At these low flows, first the manometers and later the Veriflux flow meter were unreliable and the flow was determined gravimetrically. There was plenty of time for flow determination with the capsule in line because the capsule moved so slowly in this case.

6.11 When the capsule passed the first (upstream) pressure tapping point the quick response recorder registered a step up in pressure which was maintained until the capsule passed the downstream pressure tapping.

This step transient had a duration of somewhat less than three seconds for the high velocity capsules (see Chapter 6).

6.12 As soon as the capsule entered the line the graphic recorder registered the step down in the flow (which had a slightly longer duration

than the differential pressure step up) and when the capsule left the line the chart recorded a slight step up back to the capsule free flow.

6.13 The time of travel between the photo transducers was registered in digital form on the counter and this was immediately recorded since the counter tended to pick up spurious digits when not actually counting.

6.14 The capsule was removed from the retrieval box before the next capsule was injected. This precaution prevented succeeding capsules from blocking the pipe outlet and interfering with pressure measurements.

6.15 When the entire batch of capsules was ejected the on-off valve was used to close the flow. The injector was reloaded with the same capsules in the same order and the set repeated at the same flow. This procedure was repeated several times for each flow.

6.16 The water temperature was measured.

7. The closed circuit

The procedure when experimenting with the closed circuit was similar to the above except that tests on a capsule or a train of capsules were carried out over the entire flow range rather than a batch of different capsules being tested at a particular flow. The main differences were:

7.1 Flow was adjusted by regulating the valve in the high flow pumping circuit (see Chapter 4).

7.2 Since the water in the circuit was recirculating, heat tended to accumulate necessitating the supply of cooling water.

8. Procedure for determining the coefficient of friction between capsule and pipe wall.

A 4 m length of "perspex" tube was pivoted about its centre to which point a protractor and pendulum were attached. The pipe was blocked at one end and filled with water. A capsule was placed in the pipe which

was tilted until the capsule just began to slide and the inclination (α) of the pipe relative to the horizontal was measured. The solid to solid friction (μ_f) between the capsule and pipe wall could thus be determined from this simple experiment where

$$\mu_f = \tan \alpha.$$

In the case of large diameter ratios the pipe was not filled with water. Rather the capsule and pipe were thoroughly wetted. This was in order to avoid the dashpot or piston effect.

9. Procedure for determining incipient velocity

The incipient velocity was determined in two ways.

9.1 It will be shown in Chapter 10 that when experimenting with various methods of plotting kinematic results, the graphs of capsule velocity (V_c) plotted against mean water velocity ($\overline{V}$) yielded straight line relations on linear paper. If V_c was plotted as ordinate and $\overline{V}$ as abscissa then the pseudo incipient velocity $\overline{V}_i'$ is given as the point where the $V_c : \overline{V}$ line cuts the abscissa at $V_c = 0$. Pseudo incipient velocities are thus given by extrapolation.

9.2 The second method was the direct method whereby incipient velocities were determined by inserting a capsule in the pipeline and gradually opening the flow regulating valve until the capsule just began to move. This gave the incipient velocity $\overline{V}_i$.

10. Procedure for carrying out acceleration experiments

One of the preliminary experiments was to determine the adequacy of the pipe length used.

The sliding rails above the 74 mm diameter perspex tube were used for rapidly positioning the photocells (see Figure 5.3).

The capsules were timed over a 1,524 m length (originally 5 ft), the

FIGURE 5.3

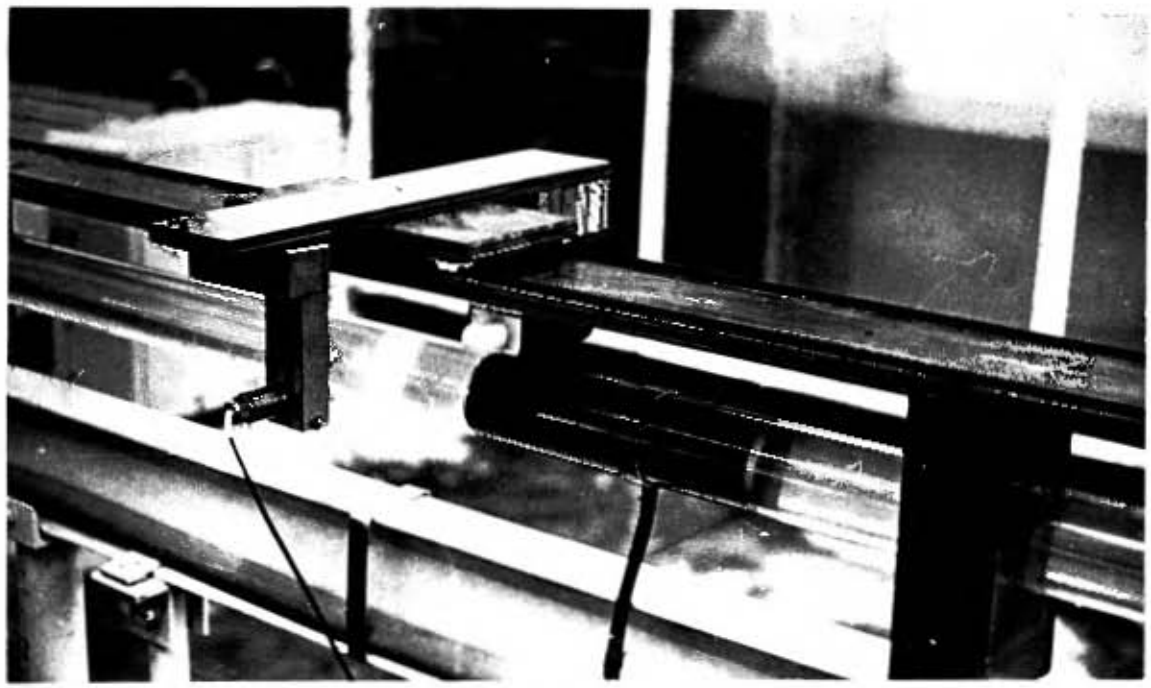

View of 70 mm diameter capsule travelling in 74 mm diameter pipe showing sliding carriage above the pipe for positioning photo cells

photo cells being spaced equally about points 1,524 m; 4,572 m; 7,62 m and 10,668 m from the entrance to the perspex tube.

11. Procedure for clearance measurement

11.1 Calibration of differential transformer

In order to fully utilise the available screen on the memory oscilloscope, the y-scale (mV/cm) was set on a suitable value and the excitation current passing through the coil was adjusted until the amplitude of the signal was exactly 4 cm (i.e. the total height above the centre line of the oscilloscope screen).

For all the tests the y-scale was set at 0,05 mV/cm for the largest capsule tested (i.e. d = 70,0 mm) while for the smaller capsules (d = 63,0 mm and d = 50,0 mm), the scale setting was 0,1 mV/cm. As each capsule contained different amounts of steel for each SG, it was necessary to adjust the excitation each time to ensure a maximum scale deflection of 4 cm. Since four SG values were used for each capsule it appeared as though twelve calibration curves were necessary.

The method of calibration was to fabricate oversized P.V.C. end caps to one end of each capsule. This meant that when the capsule was travelling slowly through the pipe (with no lift), one end had an exact predetermined clearance while the other end was touching the pipe wall. These capsules with the relevant y-scale and current setting were drawn slowly along the inside of the pipe and voltage was read off the oscilloscope. The entire calibration curve from maximum to zero was thus obtained very rapidly.

It was found that the amount of steel in the capsule did not affect the readings (this was probably offset by changing the current for different specific gravity values). Therefore only three calibration curves (for the different diameters) were required.

The calibration curves are shown on Figure 5.4 and are very similar for the two smaller diameters used in spite of the different wall thicknesses of the P.V.C. capsules.

This is again probably due to the initial setting of the excitation current to give full scale deflection on the oscilloscope screen.

11.2 Experimental procedure for clearance measurement

Three capsules of different diameter ratio and a fixed SG were placed in the rotary injector.

The valves were opened to the desired flow and the oscilloscope set to the values determined by previous calibrations.

The Veriflux flow measuring meter and the digital timer were set to the required values. The memory of the oscilloscope was engaged and the injector rotated until the first capsule emerged.

The reading on the oscilloscope was recorded and the flow and digital timer were read.

The oscilloscope flow meter and time were then reset and the same procedure was followed for the remainign two capsules. Approximately twenty readings were taken for each of the twelve capsules.

FIG. 5.4

CLEARANCE OUTPUT CALIBRATION

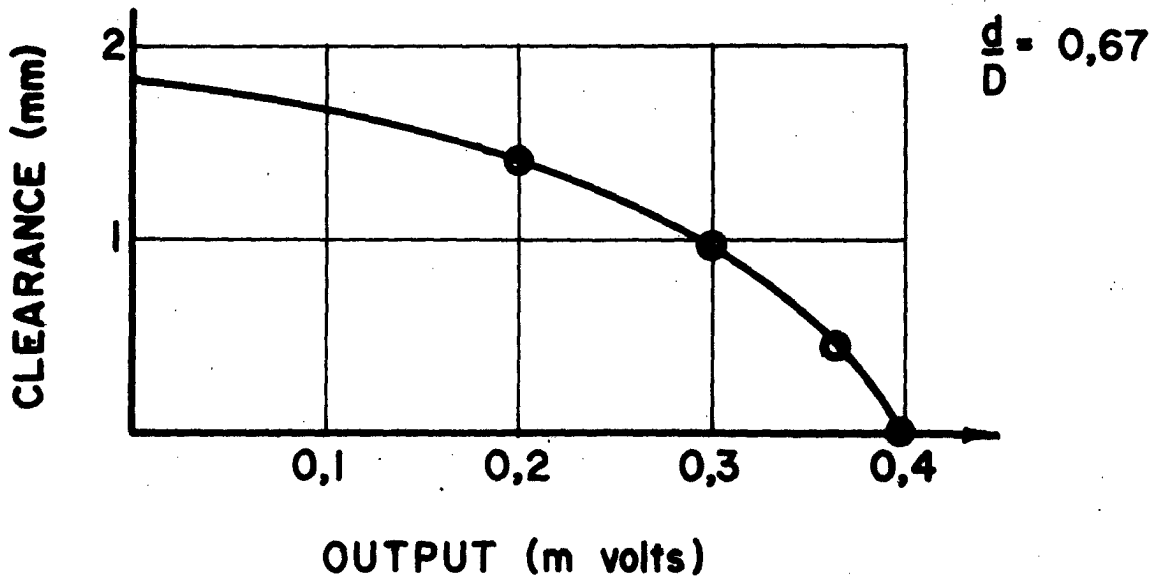

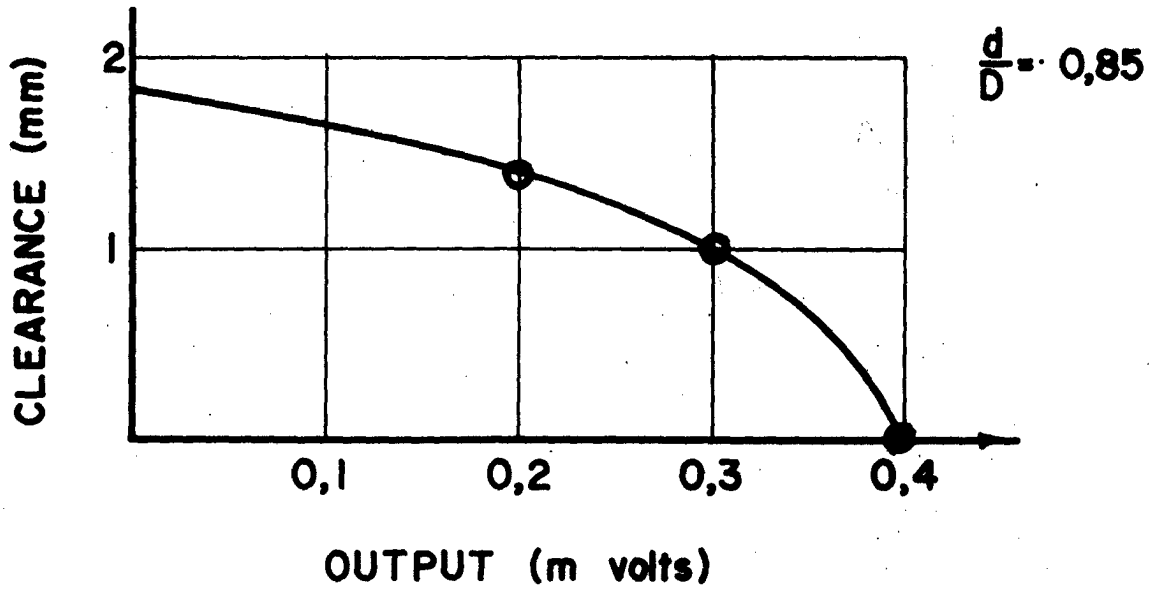

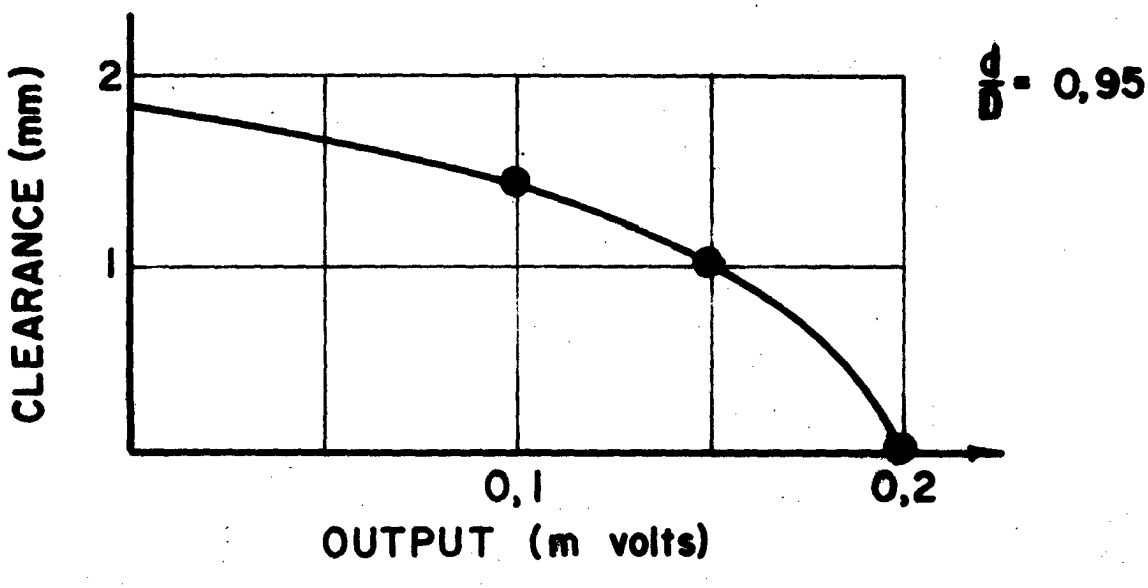

CHAPTER 6

MEASUREMENTS AND ERRORS

The following measurements were taken

1.	Capsule diameter*	(d)
2.	Capsule length*	(L_c)
3.	Capsule specific gravity*	(S_c)
4.	Pipe diameter*	(D)
5.	Pipe slope*	(ϕ)
6.	Fluid density*	(ρ)
7.	Fluid viscosity*	(ν)
8.	Mean flow velocity	($\overline{V}$)
9.	Capsule velocity	(V_c)
10.	Fluid friction head loss	(Δh_f)
11.	Excess head loss due to capsule presence	(ΔH_c)
12.	Incipient velocity	($\overline{V}_i$)
13.	Hydraulic grade line for static capsules	
14.	Fluid temperature	
15.	Clearance between capsule and pipe wall	(C)

*Denotes that these variables were fixed for the duration of an experiment.

Variables 1 and 2 were measured by conventional methods.

The capsule specific gravity is defined as the density of the capsule relative to the density of water and is thus simply the mass (grammes) divided by the volume (cm^3).

The pipe diameter was determined by blocking off the bottom of a vertical section of the pipe and filling with water. From the mass and length of the column of water the mean diameter could be obtained.

The pipe slope was set as explained in the Chapter on experimental procedure, and the slope was checked using a theodolite.

The fluid used for the experiments was, in all cases, water and the density was taken as $1\ Mg/m^3$. This is accurate to 0,2% for the temperature variation encountered in the laboratory water.

The water viscosity was determined from standard viscosity, temperature tables.

1. The mean flow velocity in the pipe

The flow in the open circuit was slightly less when a capsule was in the pipeline than when the line was capsule free.

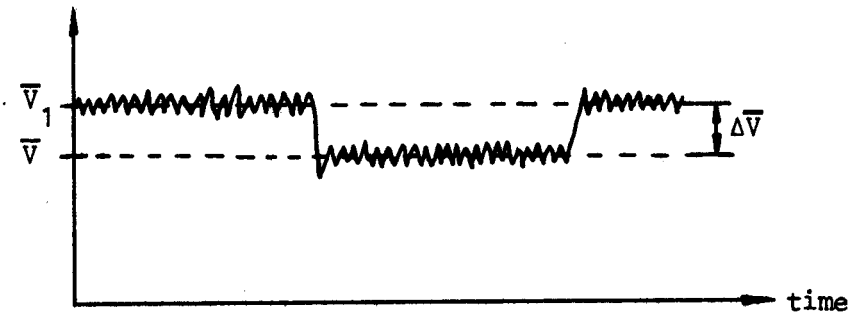

Figure 6.1

Figure 6.1 shows how the mean velocity in the pipeline varies with time. The steady state flow velocity $\overline{V}_1$ is for a capsule free line.

The value $\overline{V}_1$ is the time average velocity and the oscillations are due to turbulence.

There is a transient velocity reduction of $\Delta\overline{V}$ due to the presence of the capsule for the duration of time that the capsule is in the line. A transient function is defined in this context as one that is known to exist over a finite time interval, and is time invarient at all other times. There is a superimposed oscillation due to turbulence at all times. When the capsule is discharged from the pipe there is a step up to the original steady state condition. The duration of the flow transient could be as

short as 3 seconds at the high end of the flow range.

It was thus necessary to have a quick response method of flow recording with very little damping and with the minimum amount of residual oscillation.

Thus the actual flow (capsule in line) had to be read quickly prior to the installation of the recorder and was of the order of 98% of the flow in the capsule free line (this figure depends on the capsule properties, and the percentage is lower at higher diameter ratios and higher values of specific gravity).

The meter was accurate to within $\pm 1\%$ and the flow could be read to $\frac{1}{2}\%$. The flow measurement was accurate to within $\pm 1\frac{1}{2}\%$ above $\overline{V} = 0{,}5$ m/s. Accuracy can be defined as the ratio of the error of the indicated value to the true value. Since there can be no measurement without error, all the instruments have some degree of closeness within which the indications of the instrument approach the true values of the quantities measured.

We are primarily concerned with the accuracy of each system (this includes the detecting element or transducer, the indicating element and the recording element) which can be defined in general terms as the width of the error band, and the percentage of observations falling within the band, e.g. $\pm 5\%$ of full scale for one standard deviation assuming a Gaussian distribution about the calibration line. The actual value of a reading (as opposed to the measured value) can rarely be known, and for the purpose of this Chapter "accuracy" will be defined as, the width of the error band as a percentage of the average value at a typical reading, unless otherwise stated.

2. The Capsule velocity

It was not possible to determine the accuracy of the digital counter and the only two measurements required for capsule velocity were time and the distance apart of the photo magnetic transducers. It is difficult to

see how errors could occur with the measurement of this variable. The repeatability of capsule velocity measurement was impossible to determine since spurious flow changes would have completely overshadowed any differences in capsule velocity measurement under the allegedly same flow conditions. Any non-repeatability of capsule velocity measurement is attributed to slight differences of capsule orientation in the pipeline, or slight irregularities on the capsule or pipe surface.

Since the timer could be read to 1 ms and the fastest time recorded was of the order of 0,5s, the maximum possible error was approximately $\frac{0,001}{0,5} \times 100$, i.e. $\pm \frac{1}{5}\%$.

3. Friction head loss due to the water alone

Open tube water manometers were used for obtaining this value in the capsule free line. The readings were reasonably reliable at low flows. However, at high flows turbulence caused meniscus oscillations and a mean manometer reading had to be taken by eye. This was accurate to within about 2 or 3%.

Turbulent fluctuations were of the order of 100 mm in a head of 600 mm at a velocity $\overline{V} = 2,3$ m/s. The head could vary by approximately $\pm 8\%$. The accuracy was greatly improved by repeated readings.

4. Excess head loss due to presence of capsule in the line

This was the most difficult quantity to measure and the least accurate. The hydraulic grade line transient was measured with the differential pressure transmitter. Figure 6.2 shows friction head lost between two tapping points plotted against time on the abscissa.

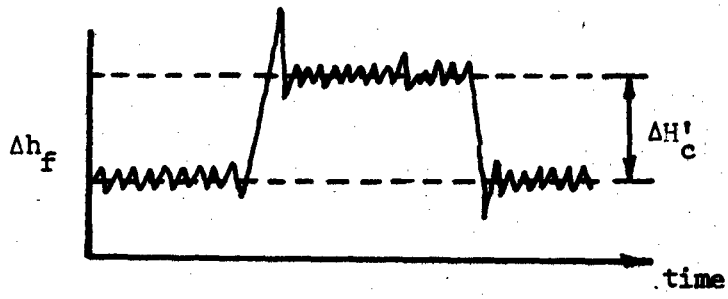

Figure 6.2

The friction head loss Δh_f is the head loss in the pipe due to water alone, and the step transient $(\Delta H'_c)$ is due to the presence of the capsule. The step up represents capsule entry into the zone between the pressure tappings, the upper horizontal section is maintained for the duration of capsule presence between the tappings, and the step down section prepresents capsule emission from the downstream pressure tapping. The dotted lines represent time averaged values.

5. Real hydraulic grade line transient

The excess hydraulic grade line transient, discussed above, is, for the open circuit case, an apparent head increase $(\Delta H'_c)$. The "real" differential head excess due to the capsule (ΔH_c) is greater than $\Delta H'_c$ because of retardation of the water velocity due to the capsule presence.

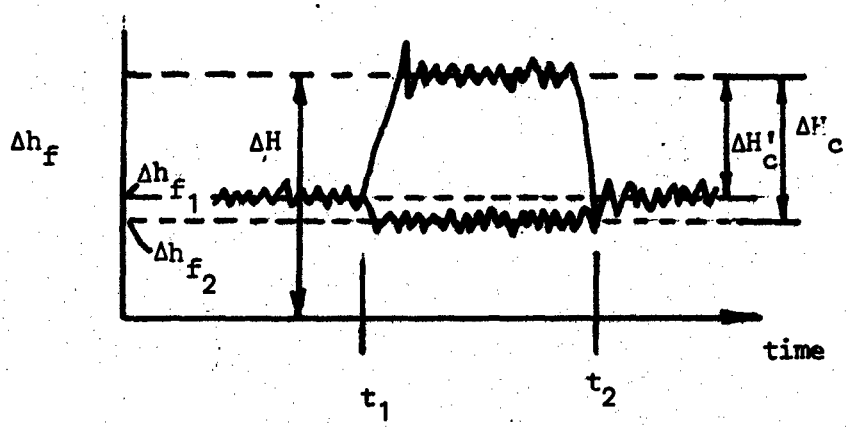

Figure 6.3

Figure 6.3 shows what is meant by "real hydraulic grade line transient" or "real excess head loss across the mobile capsule" where Δh_{f_1} represents the friction head loss for flow Q_1 and Δh_{f_2} represents the friction head loss for flow $Q_2 = Q_1 - \Delta Q$. For the time interval t_1 to t_2 there is a flow reduction due to the "moving valve" effect of the capsule

and consequently a head reduction giving Δh_{f_2}.

The value $\Delta H'_c$ as read from the quick response recorder chart is not correct since the value was essentially obtained from $\Delta H - \Delta h_{f_1}$ where ΔH was the actual reading on the chart.

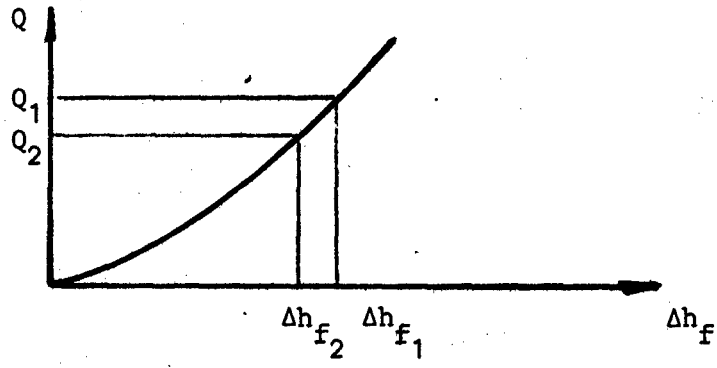

Figure 6.4

Figure 6.4 shows the friction head loss in a capsule free line plotted against flow and the effective reduction in friction head loss, due to the capsule, from Δh_{f_1} to Δh_{f_2} is indicated.

The real hydraulic gradient transient (ΔH_c) is actually $\Delta H - \Delta h_{f_2}$ and since $\Delta H'_c$ is read from the pen recorder chart:

$$\Delta H_c = \Delta H'_c + \Delta h_{f_1} - \Delta h_{f_2} \qquad (6.1)$$

where Δh_{f_1} was obtained from the open tube manometer and the capsule free line, and can be verified on the pen recorder.

The "real" friction head loss due to the water (Δh_{f_2}) could not be read when the capsule was in the line, but was deduced from graphs such as Figure 6.4 using Q_2 which was, of course, read for the capsule in line.

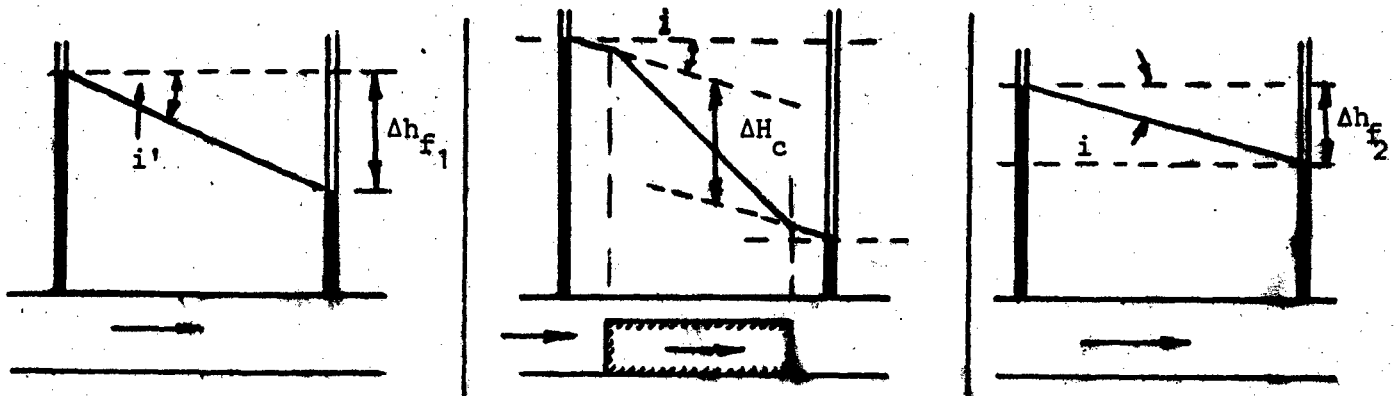

a) Capsule free line before and after capsule in line

b) The hydraulic gradient i is less than i' due to capsule retarding effect

c) Capsule free line for reduced flow (Q_2) i.e. Δh_{f_2} not measured but deduced from $Q : \Delta h_f$ graph

Figure 6.5

The Figure 6.5 above illustrates ΔH_c graphically, $\Delta H'_c$ is not illustrated graphically since $\Delta H'_c$ is merely a reading on the pen recorder chart associated with the hydraulic gradient i' which does not actually occur with the capsule in line.

6. The "real" hydraulic grade line transient due to the capsule assuming friction head loss acts over part of the line not included by the capsule

There is a third way of defining the excess head loss due to the capsule, i.e.

$$\Delta H''_c = \Delta H_c + iL_c \qquad (6.2)$$

Where iL_c is the head loss due to water friction over the length L_c if no capsule were present at a flow Q_2.

The friction head lost due to the water thus only acts over that length of pipe not occupied by capsules. (i.e. $L_p - \sum_1^n L_c$ for n capsules of length L_c.)

$\Delta H''_c > \Delta H_c$ since the friction head loss is now assumed to act over less length of pipeline.

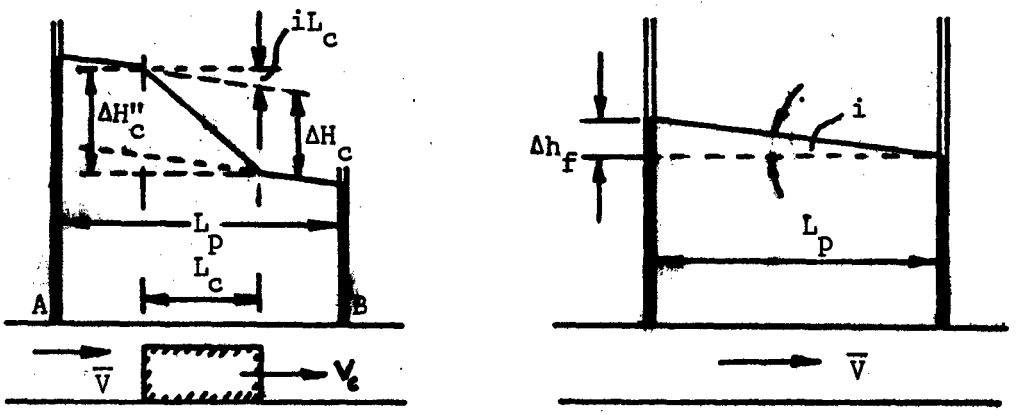

Figure 6.6

Figure 6.6 shows the head loss due to a capsule (3rd definition) travelling between two pressure tappings A and B

$i = \Delta h_f/(L_p)$ = hydraulic gradient in capsule free section of pipe (general)

$i_c = \Delta H''_c/(L_c)$ = hydraulic gradient in vicinity of capsule.

Now $\Delta H = (L_p - L_c)\, i + L_c\, i_c$

$\therefore \quad i_c = \dfrac{\Delta H - (L_p - L_c)\, i}{L_c}$

$\therefore \quad \dfrac{\Delta H''_c}{L_c} = \dfrac{\Delta H - \Delta h_f}{L_c} + \dfrac{\Delta h_f}{L_p}$

The ratio $\Delta H_c/(L_c) : \Delta h_f/L$

1. The first definition of excess head loss due to the capsule is only an apparent loss $(\Delta H'_c)$

2. The second definition gives a value of the ratio thus:

$$\xi = \frac{\Delta H_c}{L_c} \Big/ \frac{\Delta h_f}{L} = \frac{(\Delta H - \Delta h_f)}{L_c} \Big/ \frac{\Delta h_f}{L}$$

where Δh_f friction head lost due to water in capsule free section when capsule in line.

3. The third definition gives:

$$\xi'' = \frac{\Delta H_c''/L_c}{\Delta h_f/(L_p - L_c)} = \left[\frac{(\Delta H - \Delta h_f)}{L_c} + \frac{\Delta h_f}{L_p}\right] \Big/ \frac{\Delta h_f}{(L_p - L_c)}$$

$$\therefore \quad \xi'' = \frac{\Delta H_c}{\Delta h_f}\left(\frac{L_p - L_c}{L_c}\right) + \frac{L_p - L_c}{L_p}$$

and if L_c is small compared with L_p

$$\xi'' = \frac{\Delta H_c}{\Delta h_f}\left(\frac{L_p}{L_c}\right) + 1$$

Basically the definition of excess head loss (ΔH_c) assumes that the friction head loss, due to water, is manifest along the entire length of pipe whereas the excess head loss definition $\Delta H_c''$ assumes that the friction head loss due to water is only manifest in the pipe length excluding the capsule lengths.

The hydraulic grade line transient can be defined as either ΔH_c or $\Delta H_c''$ and the "correct" definition depends on the application of the concept and the expediency of experimental data representation. These points will be discussed in chapter 15.

7. Accuracy of measuring the excess head loss due to the capsule

The accuracy of the quick response pen recorder when deducing the value of ΔH_c varied tremendously. At low flows, large diameter ratios and high specific gravities the accuracy was, in general, greater than for high flows, small diameter ratios and low specific gravities.

The oscillations of the pen recorder were in most instances higher with a capsule present than due to water turbulence alone. This was because of initial rapid transients at capsule entry.

T A B L E 6.1

d/D	S_c	$\overline{V}$	transient fluctuation %	reliability %	repeatability %
0,95	4,84	1,13	~ ± 10	± 3	± 15
"	"	3,2	~ ± 80	± 20	± 20
"	1,77	1,13	~ ± 85	± 28	± 30
"	"	3,2	~ ± 100	± 30	± 40
0,54	4,77	1,13	~ ± 15	± 3	± 15
"	"	3,2	~ ± 40	± 20	± 40
"	1,77	1,13	~ ± 60	± 30	± 30
"	"	3,2	~ ± 150	± 100	± 100

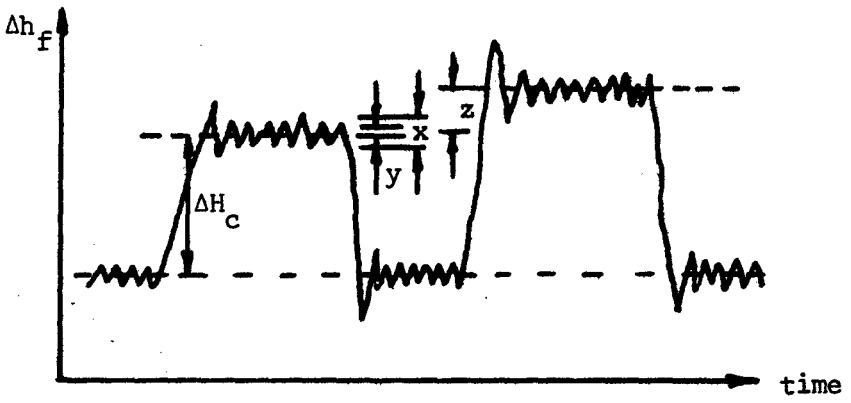

Figure 6.7

transient fluctuation (%) $= \frac{x}{2\Delta H_c} \times 100$

reliability (%) $= \frac{y}{2\Delta H_c} \times 100$

repeatability (%) $= \frac{z}{\Delta H_c} \times 100$

x = extent of oscillation neglecting the initial transient

y = range of certainty for establishing the average value

z = maximum difference between ΔH_c values, the flow conditions and capsule geometry remaining constant.

Table 6.1 gives an idea as to the variation in differential pressure transient fluctuations, reliability of reading the value of ΔH_c and the repeatability.

These concepts as used in this context are defined on Figure 6.7.

For example a high specific gravity capsule (S_c = 4,84) with a large diameter ratio (d/D = 0,95) at a low mean water velocity ($\overline{V}$ = 1,13 m/s) gave on the pen recorder output an initial transient fluctuation of 40% on an excess capsule head loss of 380 mm. The fluctuation died away to ±6½% and the mean value of ΔH_c could be read to an accuracy of ±2,6%. However, the repeatability was of the order of ±15% on successive readings.

For the same capsule at high velocities ($\overline{V}$ = 3,2 m/s) the pressure fluctuation increased to ±80% and the initial transient was difficult to detect since the duration of time during which the capsule was between the pressure tappings reduced from 8,8s at $\overline{V}$ = 1,13 m/s to 3,1s at $\overline{V}$ = 3,2 m/s. The value of ΔH_c at this high velocity could be read to an accuracy of about ±20% and repeatability was also of the order of ±20%.

As the specific gravity of the capsule was reduced the accuracy of measuring ΔH_c decreased. This was because ΔH_c values for low specific gravity capsules were lower than for high specific gravity capsules, and pressure fluctuations were still large.

At a low velocity ($\overline{V}$ = 1,13 m/s), with the same capsule as above, except that the specific gravity was S_c = 1,77 instead of 4,84, the pressure differential fluctuations were of the order of ±85% of the assumed mean value of ΔH_c. The mean position was accurate to within ±28% and repeatability was of the order of ±30%.

Also as diameter ratio decreased the accuracy of excess pressure differential readings decreased,particularly at high velocities.

At low velocities with a diameter ratio of d/D = 0,543 the accuracy of reading excess differential pressure transients was of the order of ±3%

and repeatability of the order of 15% at a specific gravity $S_c = 4,77$. Reducing the specific gravity decreased the accuracy and repeatability percentages.

Also increasing velocity decreased accuracy and repeatability due to higher pressure fluctuations superimposed on a lower value of ΔH_c. At a velocity of $\overline{V} = 3,3$ m/s and a specific gravity of $S_c = 4,77$ the pressure differential fluctuation was of the order of $\pm$ 40% on a ΔH_c value of 63 mm. The accuracy was of the order of 20% and the repeatability 40%.

It would thus appear from these figures that the accuracy of reading the excess head loss due to the capsule presence (ΔH_c) was low. However these values are not as inaccurate as would appear at first sight since many readings were taken for each capsule configuration and velocity, thus giving a statistically valid curve for ΔH_c and hence values which could be assumed to be reasonable. It is difficult to envisage how this situation could be improved upon with presently available devices for differential pressure measurement.

Figure 2.14 shows differential pressure due to capsules (not excess) plotted against velocity, from the paper by Ellis and Kruyer (reference 19), and it can be seen that there is a fair degree of scatter even though the most sophisticated equipment was used (differential pressure transducers and data logging equipment).

The reason for the scatter when measuring the ΔH_c statistic will be discussed in chapter 15.

8. The measurement of clearance

There were many sources of error when measuring the clearance between capsule and pipe wall.

The sensitivity of the system was low. Sensitivity can be defined

as the relation between the movement of the index and the change in the measured quantity producing it.

The repeatability was not very good, and the noise on the oscilloscope reduced the discrimination which is the sensitiveness of the instrument, i.e. the smallest change in the quantity measured which produces a perceptable movement of the index (oscilloscope).

The best way of assessing the overall accuracy is to refer to the graphs of clearance (C) versus capsule velocity (V_c) (Figure 12.2). The term "accuracy" is loosely used here to embrace repeatibility, sensitivity etc. Consider, for example, the error band in Figure 12.2 The accuracy of reading clearance (C) at V_c = 4,0 m/s is of the order ± 30% and the accuracy of reading the mean water velocity at which the capsule first starts to lift is of the order ± 60% at the front of the capsule. In general the accuracy of reading the clearance appears to improve with increase in capsule velocity and diameter ratio, and decreases with SG.

Sources of error

The accuracy of measurements associated with clearance appears poor. However, variables are extremely difficult to measure. A capsule of, say, 240 mm length travelling at, say, 4,0 m/s is only above the differential transformer for 60 ms and although the capsules were carefully machined externally, this did not eliminate the possibility that they were not perfectly cylindrical subsequently or that the P.V.C. walls were not of uniform thickness.

If the above were true the distance from the transformer of the steel in the capsule could vary even when the capsule had the same clearance.

There are other more likely sources of scatter in the readings which are not measuring errors mainly due to the orientation of the capsule at the instant of measuring.

P A R T III

THEORETICAL CONSIDERATIONS

"Nothing will ever be attempted if all possible objections must first be overcome."

Samuel Johnson

CHAPTER 7

THEORETICAL ANALYSIS OF FLOW AROUND CAPSULES

1. Introduction to the Analysis of the Flow of Solid Capsules in a Pipeline

The two-phase flow of capsule water mixtures can be considered as an eleventh order problem in the hydraulics of closed conduits. Figure 7.1 shows various types of closed conduit liquid incompressible flow problems.

Table 7.1 shows the order of difficulty in solving various types of conduit flow situations

TABLE 7.1

Order	Type of Problem
1	Single phase fully developed pipe flow (laminar or turbulent).
2	Concentric stationary core with laminar annular flow.
3	Concentric stationary core with turbulent annular flow.
4	Eccentric annulus with laminar flow.
5	Eccentric annulus with turbulent flow or laminar and turbulent flow in different zones of the cross-section (see Figure 7.3).
6.	Eccentric annulus with end effects (the static capsule case).
7	Concentric annulus with mobile capsule and laminar flow in the annulus.
8	Concentric annulus with mobile core and laminar or turbulent flow in the annulus.

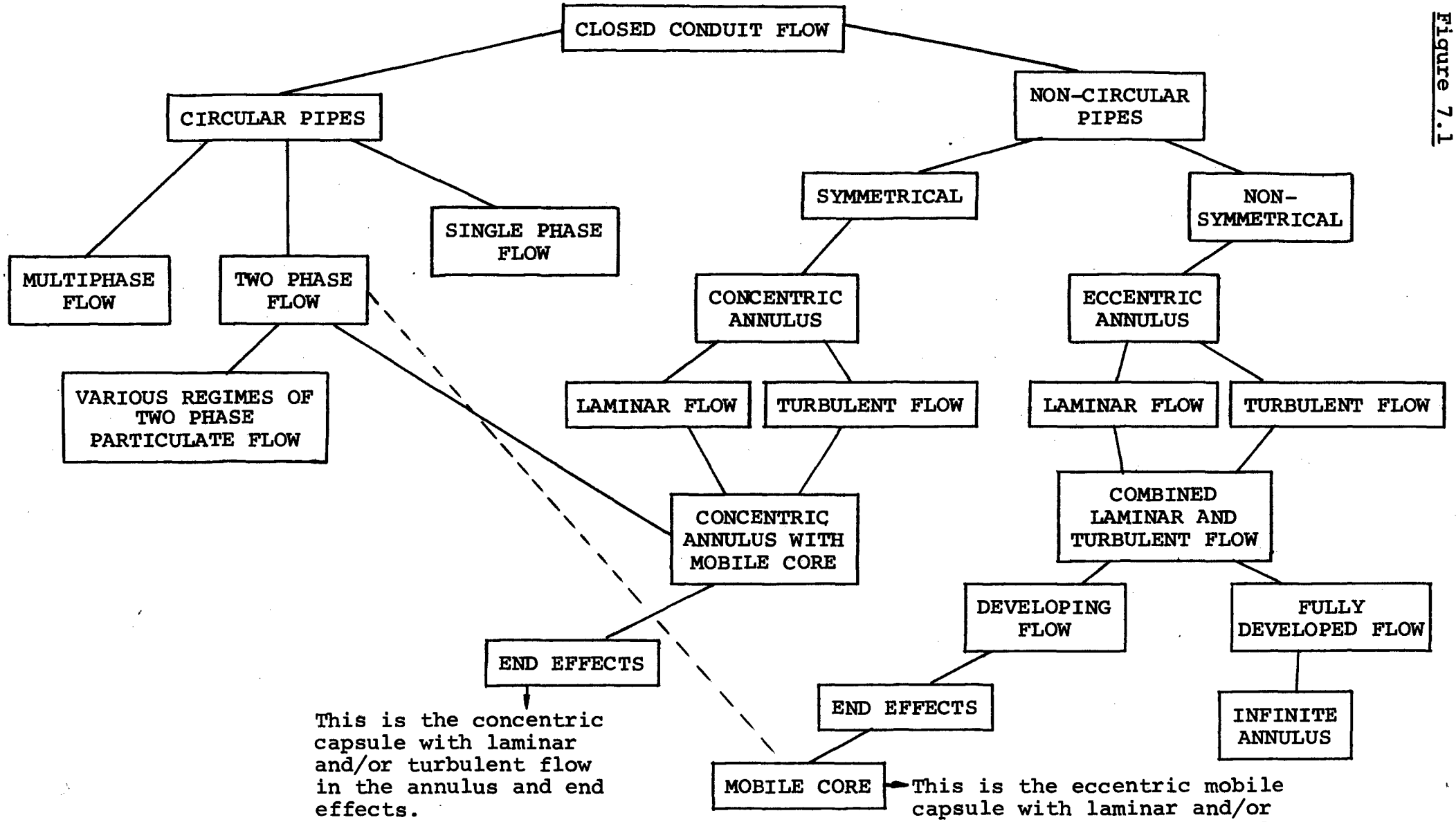
CLOSED CONDUIT FLOW
CIRCULAR PIPES
NON-CIRCULAR PIPES
SINGLE PHASE FLOW
MULTIPHASE FLOW
TWO PHASE FLOW
SYMMETRICAL
NON-SYMMETRICAL
CONCENTRIC ANNULUS
ECCENTRIC ANNULUS
VARIOUS REGIMES OF TWO PHASE PARTICULATE FLOW
LAMINAR FLOW
TURBULENT FLOW
LAMINAR FLOW
TURBULENT FLOW
CONCENTRIC ANNULUS WITH MOBILE CORE
COMBINED LAMINAR AND TURBULENT FLOW
DEVELOPING FLOW
FULLY DEVELOPED FLOW
END EFFECTS
END EFFECTS
INFINITE ANNULUS
MOBILE CORE
This is the concentric capsule with laminar and/or turbulent flow in the annulus and end effects.
This is the eccentric mobile capsule with laminar and/or turbulent flow in the annulus and end effects.

Figure 7.1

9	Eccentric annulus with laminar flow and mobile core.
10	Eccentric annulus with mobile core and laminar or laminar-turbulent flow in the annulus.
11	Eccentric annulus with mobile core and end effects (mobile capsule case).

The first order problem has been extensively studied and is well documented (although not fully understood in the case of turbulent flow compared with laminar flow).

The second order problem can be solved analytically.

The third case has been fairly extensively studied although not nearly to the same extent as turbulent circular pipe flow.

The fourth case has received limited attention (e.g. Caldwell (reference 9), Heyda (reference 20) and Redberger and Charles (reference 49)).

The remaining problems from 5 to 11 have received little or no analytical attention.

An attempt is made in this thesis to solve problem 11, and, in order to do this, a study of previous problems is made and these are used as building blocks for the analysis.

1.1 Statement of the problem

A capsule of specific gravity (Sc) > 1 or $Sc < 1$ always travels eccentrically in a non-vertical pipe.

For all practical cases the flow in the capsule-free pipe is turbulent, whilst the flow in the annulus may be laminar or turbulent or both. In fact the existence of laminar conditions in the small clearances of annuli with capsules at or near unit eccentricity is obligatory.

In the theory that follows the excess head loss across a capsule is defined as the algebraic sum of inlet, outlet and annular head losses.

This definition is applicable whether the capsules are stationary or mobile.

The three components of excess head will be discussed in relation to static capsules. The theory is then extended to the threshold case of incipient capsule motion and further extended to the eccentric mobile capsule case (problem type 11) which will be analysed in two ways; firstly by direct extension of static capsule theory and secondly by the superimposition of pressure and curved Couette flow (explained in Section 19).

In order to appreciate the reason for leading up to problem type 11 in this way, it is necessary to discuss the type of flow which exists in the annulus of a mobile capsule.

1.2 Flow in the annulus of a mobile capsule

One method of dealing with the flow in the annulus of an eccentrically orientated mobile capsule is to consider the flow as being comprised of two separable components, a pressure and a Couette component.

It will be shown (Section 18) that this approach is valid when the flow in the annulus is completely laminar. The assumption is then made that this approach, of adding the two components in the annulus, is valid for turbulent as well as laminar flow.

1.2.1 Pressure flow in the annulus

The flow in the annulus due to a pressure differential ($\Delta P'$) between two sections (1 and 2) in the fully developed flow region will be termed pressure flow (see Figure 7.2).

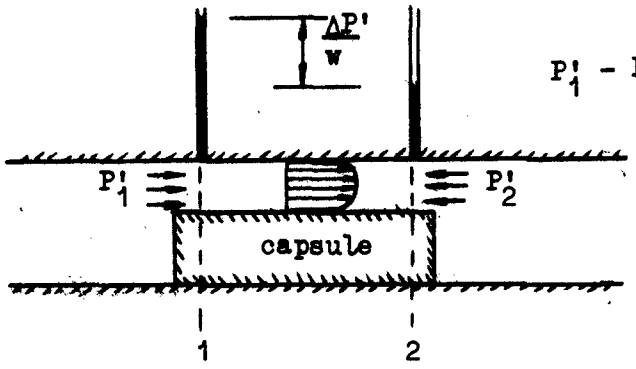

Figure 7.2

1.2.1.1 On a <u>gross</u> basis this flow component may be considered as being either laminar or turbulent (depending on a Reynolds number criterion to be discussed in Section 13).

This approach is similar to that universally accepted for pipe flow where the Reynolds number, which is a function of the mean water velocity, is used as a criterion for laminar or turbulent flow even though in "gross turbulent flow" it is well known that a laminar sub-layer exists.

1.2.1.2 In the case of an eccentric annulus, an alternative approach for the pressure flow component is to consider small, but finite elements of the eccentric annulus, decide whether the flow is laminar or turbulent in each element and, by numerical integration, determine the total pressure flow in the annulus.

The situation, for an eccentric annulus, is more complicated than circular pipe flow or even concentric annular flow. In the latter cases, either laminar or turbulent flows exist along all radii and if the flow is "grossly" turbulent, laminar flow is prevalent only near the walls. In the eccentric annulus case, the flow type changes around the circumference. It is laminar near the point of capsule and pipe contact (for unit eccentricity) and may be laminar or turbulent (with a laminar sub-layer) towards the top of the pipe. (See Figure 7.3)

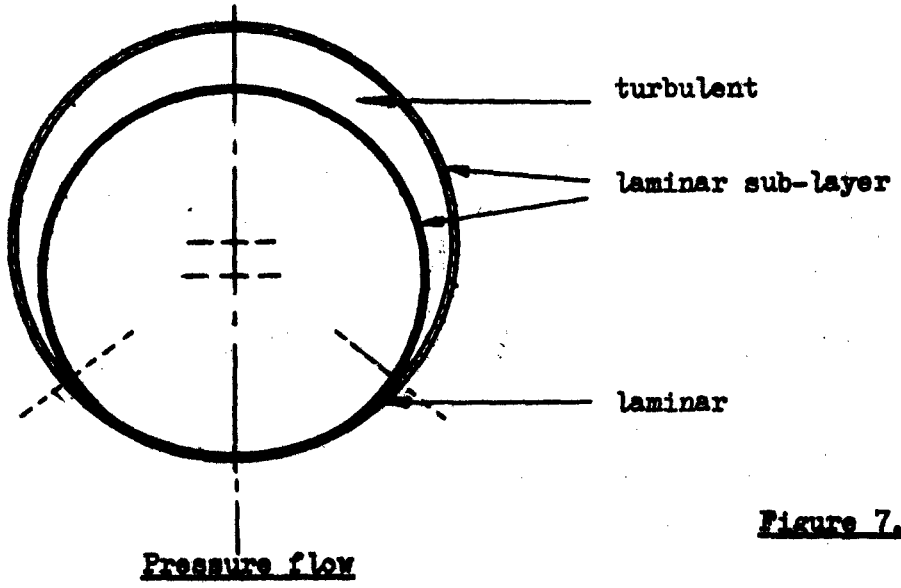

Figure 7.3

The laminar sub-layer does not maintain the same thickness either for the capsule and pipe walls or at different positions around the annulus.

For this method of dealing with pressure flow in the annulus, an understanding of both laminar and turbulent flow in concentric annuli is necessary. These aspects will be dealt with in Sections 6, 8 and 9. The flow in each small element around the circumference can then be considered using a method of quasi-concentric polar co-ordinates as devised in Section 2.

1.2.2 Couette flow in the annulus

The other component of flow is considered, in this context, to be that generated by the motion of the capsule relative to the pipe wall. The theory of laminar and turbulent Couette flow is extended to the curved space comprising the eccentric annulus. Unfortunately, there is no literature available at the present time concerning this type of flow.

The total flow component in the annulus due to capsule motion alone (Couette flow) will be analysed by considering small elements of the eccentric annulus in a manner similar to that used for calculating pressure flow. Quasi-concentric polar co-ordinates are used for evaluating the flow at all positions around the annulus depending on whether the flow is laminar

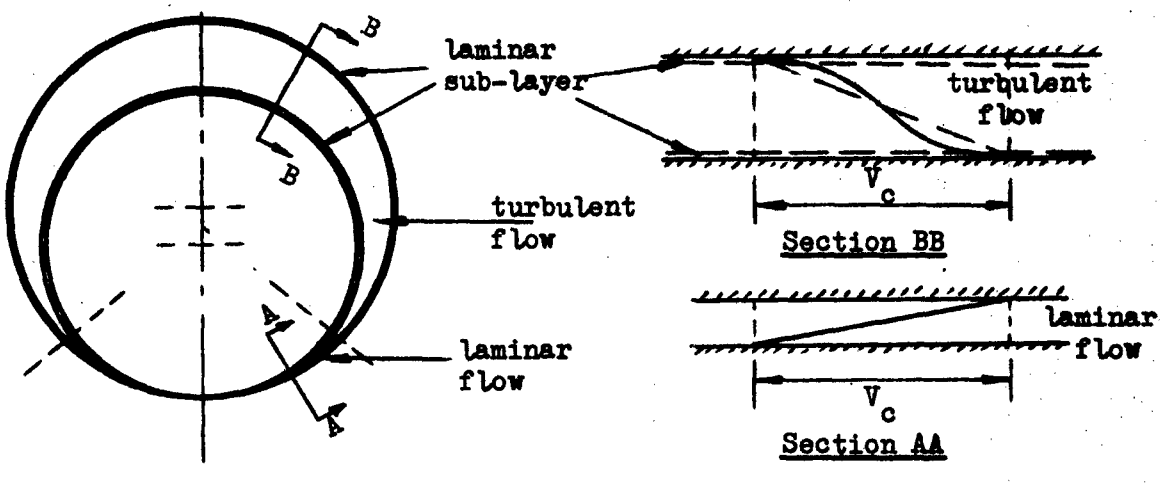

Couette Flow

Figure 7.4

or turbulent. Velocity profiles have to be established to this end.

As in the case of pressure flow, Couette flow in the eccentric annulus can be laminar or turbulent, or both in different zones of the annulus.

In the general case (see Figure 7.4), laminar flow prevails in the small gap near the bottom and turbulent flow, with a laminar sub-layer adjacent to both walls, exists towards the top of the annulus. Couette flow will be discussed in Section 19.

1.3 Layout of the rest of this Chapter

The above brief introduction has been included to indicate the relevance of succeeding subjects which will be discussed in the following order in the remainder of this Chapter.

1.3.1 Geometry of the eccentric annulus.

1.3.2 Static capsules: laminar flow in concentric annulus.
" " " eccentric "
turbulent flow in concentric annulus
" " " eccentric "
end effects.

1.3.3 Incipient motion: energy and momentum
approach.

1.3.4 Mobile capsules: Couette flow component.
continuity equation,
gross method of analysis,
Finite Element method of analysis.

2. Geometry of the eccentric annulus

In order to evaluate the flow through an eccentric annulus (pressure or Couette flow component) it is necessary to locate a point in the annular area, to stipulate a velocity at this point and define an associated area. This involves the geometry of the eccentric annulus. There are basically two approaches;

Firstly: Bi-polar co-ordinates as used by Heyda (reference 20) Caldwell (reference 9) and Redberger and Charles (reference 49).

Secondly: A method devised by the present author which can be designated "quasi-concentric polar co-ordinates".

In order to justify the adoption of the latter geometry a brief discussion follows on the two systems.

2.1 Bi-polar co-ordinates

Bi-polar co-ordinates were used by Caldwell to determine a theory of resistance to streamline (i.e. laminar) flow in a pipe with an eccentric ring section and by Heyda for "A Green's function solution for the case of laminar incompressible flow between non-concentric circular cylinders".

Also Redberger and Charles used bi-polar co-ordinates for solving the laminar flow problem in an eccentric annulus by means of a numerical integration.

All these papers deal only with laminar flow and stationary cores. All are highly analytical and acknowledge mathematicians for help. All three authors integrated the standard Navier Stokes equation.

The bi-polar co-ordinate system is one in which the walls of the pipe and capsule would form the outer and inner boundaries of one family of circles (η) and another family of circles is orthogonal to these (ξ).

If in the x - y plane (Figure 7.5) P is a distance r_1 from the pole O_1 $(-C,0)$, defined by the value of η, and r_2 from the pole O_2 $(+C,0)$ and the angles of the vectors O_1P and O_2P are θ_1 and θ_2 respectively, then P is defined to have the bi-polar co-ordinates (ξ, η).

The curves ξ = constant are a family of circles passing through O_1 and O_2 with centres on the y axis and the curves η = constant, are also a family of circles having centres on the x axis.

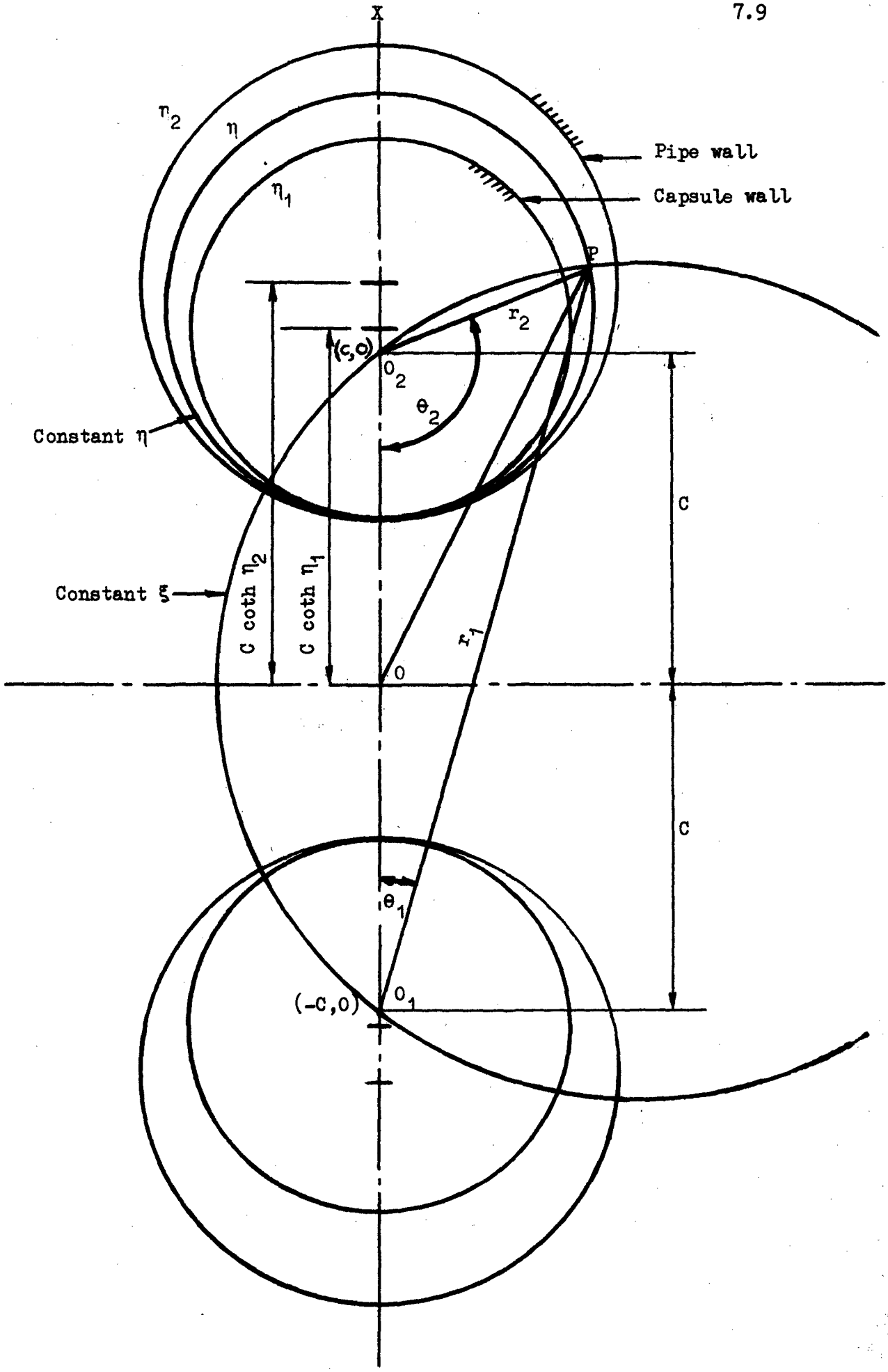

Bi-polar co-ordinates

Figure 7.5

The centres of the η family of circles can easily be located (e.g. C Coth η_1 and C Coth η_2 in Figure 7.5) as can the centres for the ξ curves and Heyda gives equations for evaluating any point P in terms of η and ξ by means of a transformation from the x - y plane.

The above is sufficient to acquaint one with the bi-polar co-ordinate system and the equations for defining points will not be given here since this geometrical system was not used by the present author. Further details are given by Heyda (reference 20).

A discussion of quasi-concentric polar co-ordinates ensues, followed by a comparison of the two systems.

2.2 Quasi-concentric polar co-ordinates

In a concentric annular section any point can be quite simply specified by means of polar co-ordinates and any small section of an eccentric annulus can be considered as pseudo-concentric if the diameter ratio (d/D) is not too small.

The method adopted was to consider the midpoint of the capsule and pipe centres as the zero point of a polar diagram. Any point in the eccentric annulus can thus be specified by means of a quasi-concentric radius (C_r) and an angle (θ).

Figure 7.6(a) shows the eccentric annulus of the 74 mm diameter pipe and 63 mm diameter capsule. The enlargement (Figure 7.6b) shows the angles describing the geometry with the scaled elemental area ΔA shown above (Figure 7.6a).

The distance from O_p or O_c to O is p.

where $$p = \epsilon (r_p - r_c)/2 \qquad (7.1)$$

and ϵ = eccentricity ratio

r_p = pipe radius

r_c = capsule radius.

The angle (θ) is given as

$$\theta = (i - 0{,}5) \frac{\pi}{n}$$

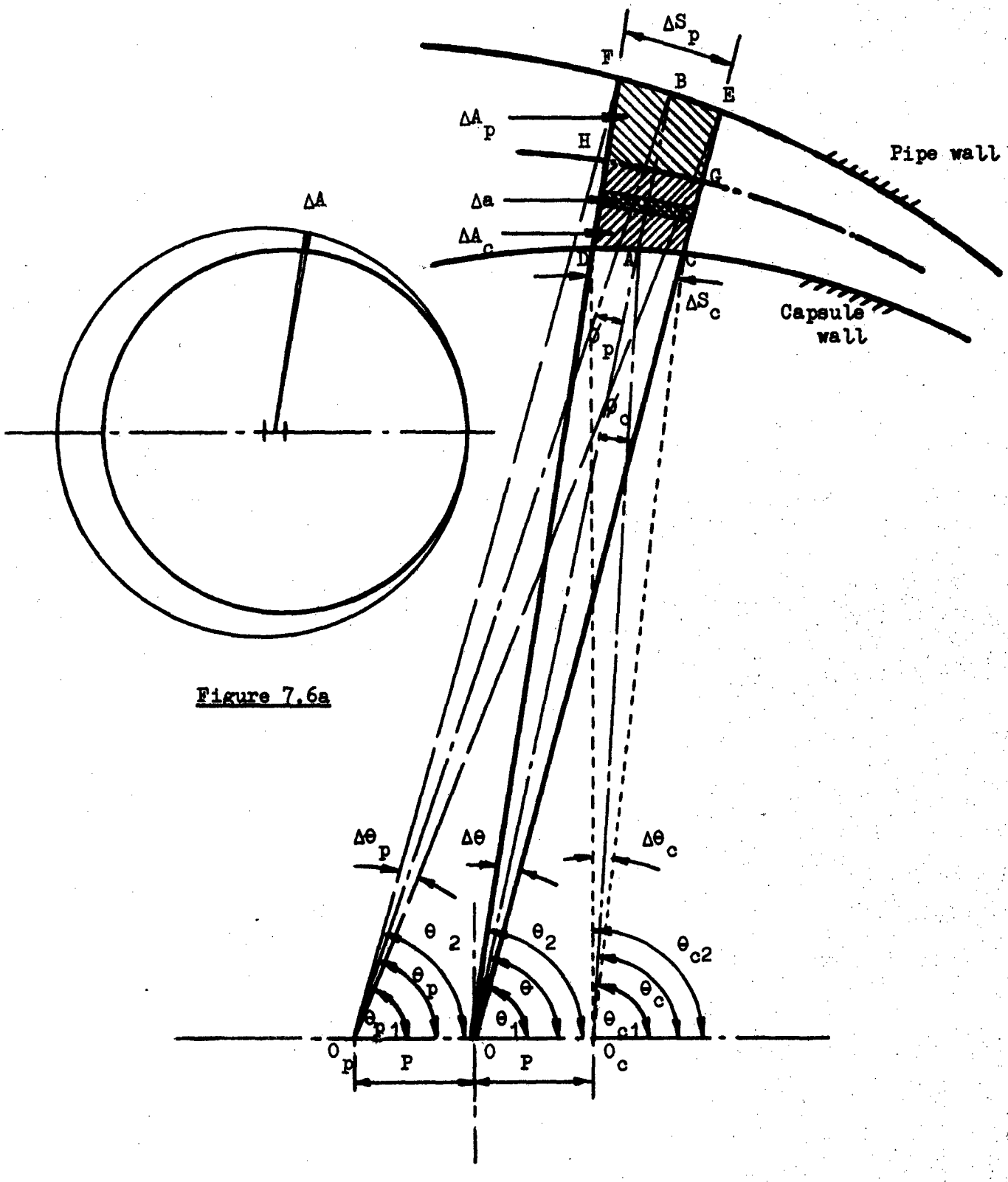

Quasi-concentric polar co-ordinates

Figure 7.6

where n is an integer specifying the number of elements and i is an integer varying from unity to n.

$$\theta_1 = (i - 1)\frac{\pi}{n} \tag{7.2}$$

$$\theta_2 = i\frac{\pi}{n} \tag{7.3}$$

and $\Delta\theta = \theta_1 - \theta_2$

(For $n = 100$; $\Delta\theta \doteq 0{,}0314$ radians $(1{,}8^{o})$

The arc lengths ΔS_c and ΔS_p used for evaluating shear forces on the capsule and pipe wall are given by

$$\Delta S_c = \Delta\theta_c \, r_c \tag{7.4}$$

$$\Delta S_p = \Delta\theta_p \, r_p \tag{7.5}$$

The lengths OC, OA and OD are the quasi-concentric radii for the capsule at θ_1, θ and θ_2 respectively and OE, OB and OF are the corresponding lengths for the pipe.

the quasi-concentric capsule radius (C_{rc}) is given by

$$C_{rc} = \left(\frac{p}{\text{Sin } \phi_c}\right) \text{Sin } \theta_c \tag{7.6}$$

where $\phi_c = \text{Sin}^{-1} \left(\frac{p \text{ Sin } \theta}{r_c}\right)$ (7.7)

and $\theta_c = \phi_c + \theta$ (7.8)

Similarly the quasi-concentric pipe radius (C_{rp}) is given by;

$$C_{rp} = \left(\frac{p}{\text{Sin } \phi_p}\right) \text{Sin } \theta_p \tag{7.9}$$

where $\phi_p = \text{Sin}^{-1} \left(\frac{p \text{ Sin } \theta}{r_p}\right)$ (7.10)

and $\theta_p = \theta - \phi_p$ (7.11)

The clearance between capsule and pipe wall is defined as b and varies as θ varies. The local value being $b_i (i = 1 \ldots\ldots n)$

$$b = C_{rp} - C_{rc} \tag{7.12}$$

or $b_i = C_{rni} - C_{r1i}$

General values of the quasi-concentric radius between C_{rc} (C_{r1i}) and C_{rp} (C_{rni}) are designated C_{rmi} (where both m and i vary from 1 to n) and indicate the exact locality of C_r with respect to angle θ = f(i) and radius = f(m). Thus;

$$C_{rmi} = C_{r1i} + b_i \left(\frac{m}{n}\right) \tag{7.13}$$

The quasi-concentric radius to the midpoint of a sub-elemental area (Δa) is given as $C_{r\ mid}$

and $$C_{r\ mid\ mi} = C_{r1i} + b_i\left(\frac{m - 0.5}{n}\right) \tag{7.14}$$

The elemental area (ΔA) is given by;

$$\Delta A_i = \frac{\Delta\theta_i}{2}\left(C_{rp}^{\ 2} - C_{rc}^{\ 2}\right) \tag{7.15}$$

and the sub-elemental area (Δa) is given by;

$$\Delta a_{mi} = \frac{\Delta\theta_1}{2}\left(C_{rmi}^{\ 2} - C_{r(m-1)i}\right) \tag{7.16}$$

2.3 Comparison of bi-polar co-ordinates with quasi-concentric polar co-ordinates

There are disadvantages and advantages for each system and the latter system was used because the advantages outweigh the disadvantages to some extent.

2.3.1 The bi-polar co-ordinate system has the disadvantage of a curved line joining capsule and pipe surfaces. This implies that clearance values (b) would be slightly higher than in the quasi-concentric annulus case. Since velocity distributions for plane Couette flow are taken along a straight line joining the two surfaces, a straight line in the eccentric annulus is a better approximation. Also, when evaluating the pressure flow component, the straight line is a better approximation to the concentric annulus since radial velocity distributions are used.

2.3.2 The quasi-concentric polar co-ordinate system has the disad-

vantage of radial lines from the centre (0), being oblique to the capsule or pipe surface. The bi-polar co-ordinate system has curved connectors between the capsule and pipe which are perpendicular to the walls. The extent of obliqueness is given by the angle ϕ and this angle is zero at the point of contact between the walls as well as at the position of maximum clearance.

The worst position is at $\theta = \pi/2$ and for $d/D = 0,85$ at this position

$\phi_c = 0,087$ radians $(\div 5^o)$

and $\phi_p = 0,074$ radians $(\div 4^o)$

The curved connectors of the bi-polar co-ordinate system seem to be slightly more serious than the oblique connectors of the quasi-concentric polar co-ordinate system since in the former case it is easy to see that velocity values can be slightly in error whereas it is difficult to visualise the errors caused by oblique connectors.

In both cases the geometrical errors are very slight and decrease as diameter ratio increases and eccentricity decreases.

In the laminar flow case the relation between pressure gradient and annular velocity is determined using both systems. These will be compared in Chapter 13.

3. Static Capsules

3.1 Applicability

At low flows the water velocity is inadequate to supply sufficient forward drag to the capsule to overcome the solid to solid static friction that exists when a capsule has a density other than that of water, in a non-vertical pipe. The capsule remains stationary on the pipe bed or top, depending on whether the density is greater or less than that of water.

In a vertical pipe the capsule can only be static at incipience, if

travelling vertically upwards, and will tend to fall back at velocities less than the incipient velocity.

In an upward sloping pipe, providing the slope is not greater than the angle of static friction between pipe wall and capsule, the capsule will remain static.

If an upward sloping pipe is steep, $(\tan \alpha > \mu_f)$ then the capsule slides back of its own accord and will only remain static if the water velocity is sufficient to provide enough drag to balance the component of capsule weight down the slope and not greater than that required to initiate motion.

The theory of static capsules also applies to downward sloping pipes providing capsule motion cannot be initiated by the combined effect of water drag and capsule weight component down the slope. If the downward sloping pipe has a slope greater than the angle of static friction then a static capsule state cannot exist in this case.

3.2 The object of studying static capsules

3.2.1 The study of capsules at rest (and the limiting threshold case) is amenable to more precise analysis than the moving capsule. The steady state condition permits a relatively conventional type of analysis and experimental investigation.

3.2.2 Once the capsule is moving, at a constant velocity, a quasi-steady state can only be achieved by considering the capsule at rest and the pipe walls moving backwards at capsule speed. This would permit direct measurements of capsule drag if such an experimental rig could be achieved, but the practical difficulties are considerable. It was felt that the data obtained with such a rig could not justify the construction of the apparatus.

3.2.3 A further merit of studying the static capsule is that information is provided for the extreme value, i.e. incipience, which may be viewed as

the limiting value of the mobile capsule case.

3.2.4 One method of analysing the mobile capsule is the superimposition of pressure and Couette flows in the annulus to obtain total annular head losses. The pressure component can be studied via the static capsule. Also, in order to evaluate the inlet and outlet energy losses relative to the mobile capsule, it is necessary first to determine these losses relative to the static capsule.

This is the most important reason for studying static capsules.

3.3 Definition of energy losses for a static capsule

The excess energy loss (ΔH_{cs}) across the static capsule may be subdivided into three parts, the inlet head loss (Δh_i); the outlet head loss (Δh_o); and the excess head loss along the eccentric annular section (Δh_a), excess in the sense of being additional to the frictional head loss which would occur in the same length of pipe in the absence of a capsule. These definitions are illustrated in Figure 7.7. (See also Figure 9.1). The procedure for identifying these losses was to extrapolate the uniformly sloping energy lines upstream and downstream from the capsule to intersect the vertical lines projected from the front and rear faces of the capsule. The uniformly sloping energy line in the annulus was similarly extrapolated and the discrete energy line drops at the capsule faces were regarded as the inlet and outlet losses. The total frictional head loss along the annulus is the sum of the excess annulus loss and the head loss which would occur in a capsule length of unobstructed pipeline.

$$\Delta h_{fa} = \Delta h_a + h_{fc} \qquad (7.17)$$

The following sections will be devoted to a discussion of the three separate components of the excess energy loss across a static capsule, i.e. Δh_{fa}, Δh_i and Δh_o.

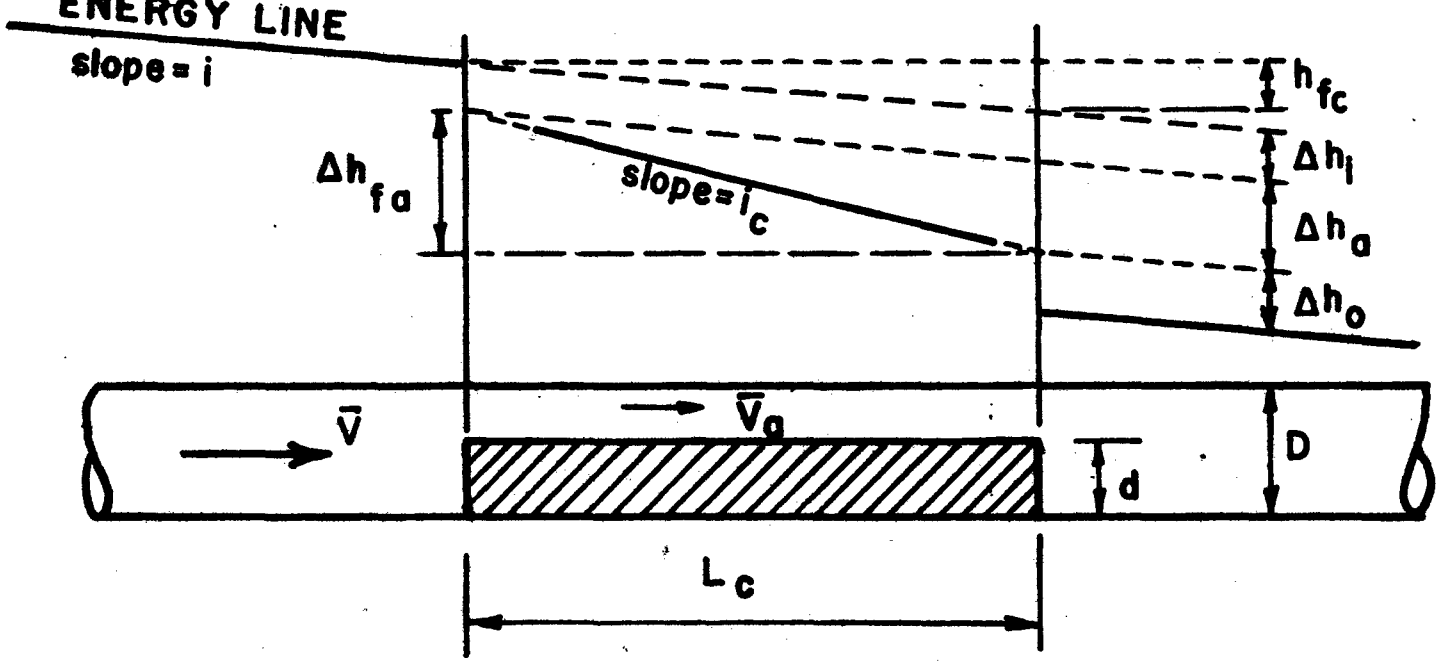

DIAGRAM OF ENERGY LOSSES FOR STATIC CAPSULES

FIG. 7.7

4. Flow in the annulus

The following sections are devoted to analytical and experimental information on the relation between flow and friction loss encountered in the annulus with particular regard to fully eccentric and concentric annular sections.

Flow in annuli will be discussed in the following sequence; applicability to the capsule problem, the general case of annular flow, dimensional analysis, the conventional approach to friction head losses and why this is not applicable to annuli (particularly capsule-pipe annuli) and finally the four cases of laminar and turbulent flow in concentric and eccentric annuli.

4.1 Applicability to the capsule problem

In the static capsule case the eccentric annulus is associated with capsules having densities greater or less than that of water in horizontal or sloping pipes and the concentric annulus is associated with capsules having densities equal to water in the horizontal or sloping pipes and densities other than that of water in vertical pipes.

There are, thus, five cases:

(1) Laminar flow in the concentric annulus.

(2) Turbulent flow in the concentric annulus.

(3) Laminar flow in the eccentric annulus.

(4) Turbulent flow in the eccentric annulus.

(5) Both laminar and turbulent flow in the eccentric annulus.

Consider the general case of annular flow where;

$$\epsilon = \frac{e}{r_p - r_c}$$

where e = eccentricity = $2p$.

and ϵ = eccentricity ratio.

For the fully eccentric annulus $\epsilon = 1{,}0$ and for the fully concentric

annulus $\epsilon = 0$.

4.2 Dimensional analysis

For the general case of pipe flow the friction factor (f) depends on the Reynolds number and relative roughness of the pipe, i.e.;

$$f = f(R_e, \frac{k}{D}) \tag{7.18}$$

It is conventional to define k as the effective roughness height.

For the general case of annular flow one would expect dimensional analysis to yield

$$f = f_1(R_{ea}, \frac{d}{D}, \epsilon, \frac{k_e}{D}, \frac{k_p}{k_c}) \tag{7.19}$$

where R_{ea} = a Reynolds number for the annulus,

k_p = roughness for the pipe

and k_c = roughness for the capsule.

Thus three more parameters are introduced over and above those for the clear pipe flow problem.

For a smooth annulus,

$$f = f_2(R_{ea}, \frac{d}{D}, \epsilon) \tag{7.20}$$

and there are two more parameters than for clear pipe flow.

For a smooth concentric annulus

$$f = f_3(R_{ea}, \frac{d}{D}) \tag{7.21}$$

and in this case there is one additional parameter, compared with circular pipe flow.

4.3 Conventional approach and reasons for inapplicability

The conventional approach to head losses in non-circular conduits (and in the eccentric annulus case the deviation from circularity is considerable) is to use the Darcy equation with f dependent on a Reynolds number defined as

$$R_e = \frac{4\bar{V}R}{\nu} \tag{7.22}$$

Where R is the hydraulic mean radius calculated as the flow area divided by the wetted perimeter which in the case of a capsule or fixed cylindrical core yields $(\frac{D - d}{4})$.

For sections which deviate little from the circle, this approach is probably satisfactory, but for other shapes this approximation may be misleading.

Most of the literature on flow in annuli has attempted to find a representative equivalent velocity and length dimension to satisfy the Darcy equation for pipe flow.

$$f = \frac{\Delta P \times R}{\frac{1}{2}\rho \bar{V}^2 L} \tag{7.23}$$

In most cases the equivalent velocity used is the mean velocity in the annulus $\bar{V} = \bar{V}_a$. Also, most authors have used the hydraulic mean radius as the equivalent length dimension, and many papers (e.g. reference 7, 5, 24, 26 and 46) have been written showing that the <u>form</u> of the Darcy equation is applicable to conduits other than those which are circular in cross-section.

Theoretically, there is no reason to suppose that either the mean annular velocity $(\bar{V}_a)$ or the hydraulic mean radius (R) should represent relevant conditions.

The concept of hydraulic mean radius is associated with uniform longitudinal shear stress distribution round the perimeter of the section, and in cases such as the eccentric annulus, where this assumption is probably erroneous (see Chapter 8) the use of an unmodified hydraulic mean radius lacks justification. In fact, experimental data, when plotted by this method, yielded friction factors up to 15 per cent higher than the smooth pipe correlation.

There are certain other features which can significantly effect the flow in the annulus; the capsule is not always long enough for fully developed flow to occur and the capsule does not automatically maintain its

assumed concentricity or eccentricity.

To summarise;

In the conventional approach, the friction head loss in the annulus is;

$$\Delta h_{fa} = f\, L\, \bar{V}_a^2/2g\, R$$

where $R = (D - d)/4$

and $$\bar{V}_a = Q_a/\left(\frac{\pi(D^2 - d^2)}{4}\right)$$

A force balance yields;

$$\pi(D + d)\bar{\tau}_o = \tfrac{1}{4}\pi(D^2 - d^2)\,\frac{\Delta P}{L}$$

$$\therefore \quad \bar{\tau}_o = (D - d)\,\Delta P/\,4L$$

and $$f = \bar{\tau}_o/\tfrac{1}{2}\,\rho\,\bar{V}_a^2$$

where $\bar{\tau}_o$ = average shear stress on the pipe and capsule walls

5. <u>Shear distribution in concentric annulus due to pressure flow</u>

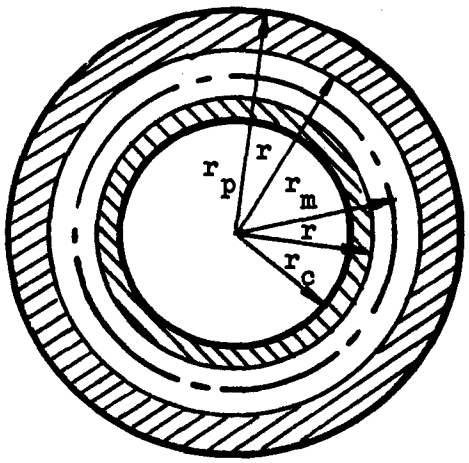

<u>Figure 7.8</u>

Let r_p = pipe radius

r_c = capsule radius

r_m = radius to maximum velocity (or radius to zero shear stress)

τ_o = shear stress at radius r where $r > r_m$

τ_i = shear stress at radius r where $r < r_m$

A force balance on the shaded areas(Figure 7.8) yields):

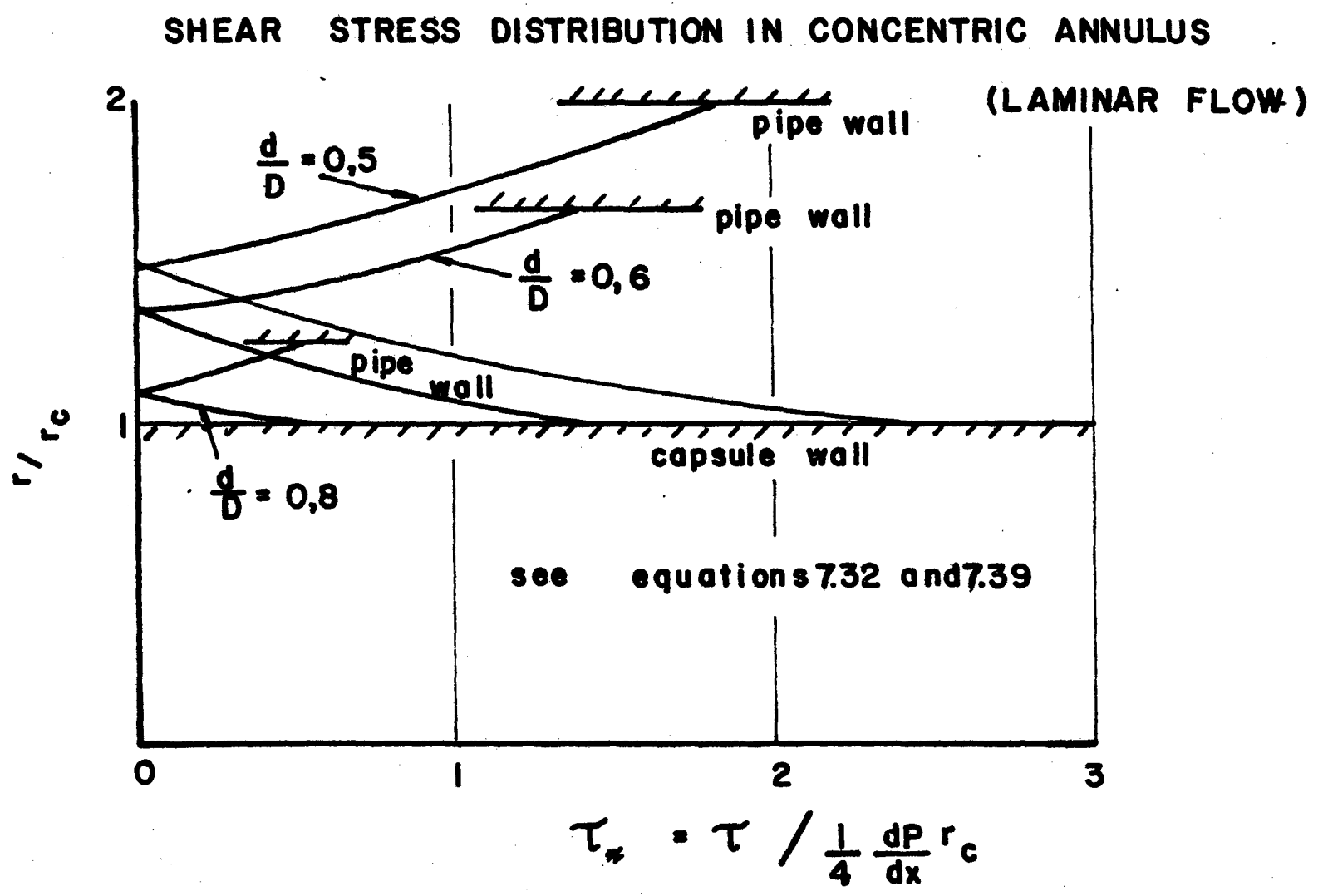
SHEAR STRESS DISTRIBUTION IN CONCENTRIC ANNULUS
(LAMINAR FLOW)
pipe wall
d/D = 0,5
pipe wall
d/D = 0,6
pipe wall
d/D = 0,8
capsule wall
see equations 7.32 and 7.39
r / rc
2
1
0
1
2
3
τ* = τ / 1/4 dP/dx rc

FIG. 7.9

$$\tau_o = \left(\frac{dP}{dx}\right)\left(\frac{r_p^2 - r^2}{2r}\right) + \tau_{pp}\frac{r_p}{r} \qquad (7.24)$$

$$\tau_i = \frac{dP}{dx}\left(\frac{r^2 - r_c^2}{2r}\right) + \tau_{cp}\frac{r_c}{r} \qquad (7.25)$$

τ_{pp} = shear stress on pipe wall due to pressure flow.

τ_{cp} = shear stress on capsule wall due to pressure flow.

The above equations apply to laminar or turbulent flow. Anticipating laminar flow relations (see Section 6) for shear stress on the pipe and capsule walls, it is possible to show the shear stress distribution in an annular section in a non-dimensional form (see Figure 7.9). It is noteworthy that, unlike circular pipe flow, the shear stress distribution is non-linear and the radius where the shear stress reaches a zero value (the maximum velocity radius) does not coincide with the centre of the passage as in pipe flow.

6. Laminar flow in a pipe with a stationary concentric annulus

As has been stated earlier, even though the flow in a capsule-free section of the pipe is probably highly turbulent, it is possible that laminar flow will prevail in the annulus. In fact the existence of laminar conditions, in the small clearances of annuli with capsules at or near unit eccentricity, is obligatory.

6.1 Theory of laminar flow in concentric annulus

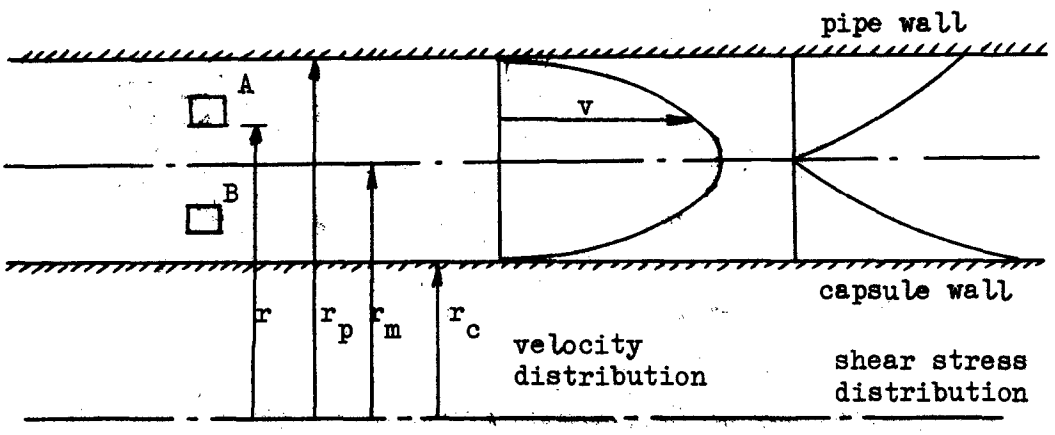

Figure 7.10

Consider the forces acting on an annular element of fluid (A).

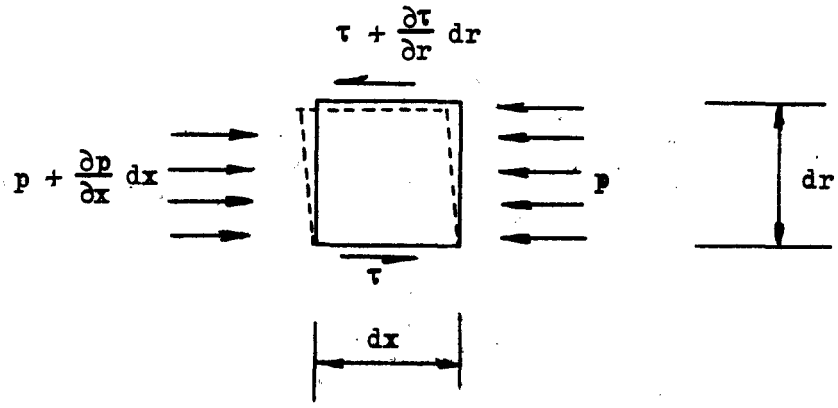

Figure 7.11

Equilibrium in the x direction yields,

$$\frac{\partial p}{\partial x}\, dx\, 2\pi r dr = -\tau\, 2\pi r + (\tau + \frac{\partial \tau}{\partial r} dr)(r + dr)\, 2\pi$$

simplifying; $$\frac{dp}{dx}\, r dr = \frac{d\tau}{dr}\, r dr \qquad (7.26)$$

(neglecting higher than first order terms)

Also $$\tau = -\frac{\mu dv}{dr} \qquad (7.27)$$

The negative sign is inserted because v decreases with increasing r.

$$\therefore \quad \frac{dp}{dx} = -\mu \frac{1}{r} \frac{d}{dr} (r \frac{dv}{dr}) \qquad (7.28)$$

This differential equation is a simple form of Navier Stokes in the x direction only, expressed in cylindrical (polar) co-ordinates.

Integrating gives;

$$r \frac{dv}{dr} = -\frac{1}{2\mu} r^2 \frac{dp}{dx} + A_o$$

$$\therefore \quad dv = -\frac{r}{2\mu} (\frac{dp}{dx})\, dr + \frac{A_o}{r}\, dr$$

Integrating again;

$$v_o = -\frac{r^2}{4\mu} (\frac{dp}{dx}) + A_o \ln r + B_o \qquad (7.29)$$

The subscript "o" is associated with the section of annulus where $r_m < r < r_p$.

The boundary conditions are;

$$v_o = 0 \text{ where } r = r_p \text{ and;}$$

$$\frac{dv}{dr} = 0 \text{ when } r = r_m$$

$$\therefore A_o = \frac{1}{2\mu} r_m^2 \left(\frac{dp}{dx}\right) \tag{7.30}$$

$$\text{and } B_o = \frac{1}{4\mu} \left(\frac{dp}{dx}\right) \left[r_p^2 - 2r_m^2 \ln r_p\right] \tag{7.31}$$

$$\text{since } \tau_o = -\mu \frac{dv}{dr}$$

$$\therefore \tau_o = \frac{r}{2} \frac{dp}{dx} - \frac{1}{2} \frac{r_m^2}{r} \frac{dp}{dx} \tag{7.32}$$

The shear stress at the pipe wall due to laminar flow is;

$$\tau_{pp} = \tfrac{1}{2} \frac{dp}{dx} \left[r_p - \frac{(r_p^2 - r_c^2)}{2r_p \ln\left(\frac{r_p}{r_c}\right)}\right] \tag{7.33}$$

anticipating the formula for radius of maximum velocity equation (7.41).

The first term on the right hand side is the same as for circular pipes and the second term is the effect of annular geometry.

From equations (7.29), (7.30) and (7.31),

$$v_o = \frac{1}{4\mu} \left(\frac{dp}{dx}\right) \left[r_p^2 - r^2 + 2r_m^2 \ln \left(\frac{r}{r_p}\right)\right]$$

Similarly, equilibrium in the x direction of forces acting on the annular element of fluid B yields the following:

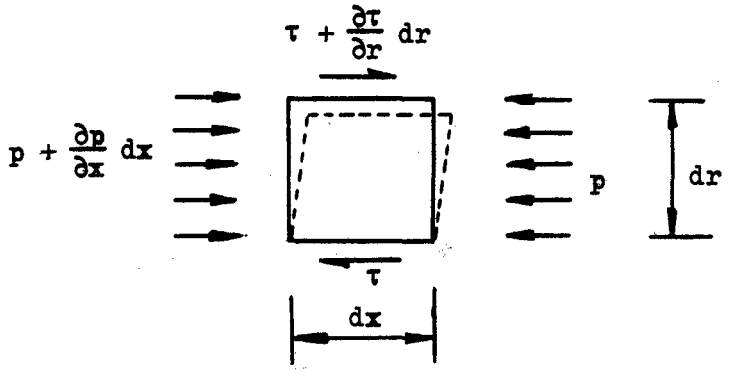

Figure 7.12

Equation (7.26) is now replaced by:

$$-\frac{dp}{dx}\,rdr = \frac{d\tau}{dr}\,rdr \tag{7.34}$$

In this instance $\tau_i = \mu\frac{dv}{dr}$ and

$$-\frac{dp}{dx} = \mu\frac{1}{r}\frac{d}{dr}\left(r\frac{dv}{dr}\right) \tag{7.35}$$

Integrating yields,

$$r\frac{dv}{dr} = -\frac{r^2}{2\mu}\frac{dp}{dx} - A_i$$

Integrating again

$$v_i = -\frac{r^2}{4\mu}\left(\frac{dp}{dx}\right) - A_i \ln r - B_i \tag{7.36}$$

In this instance the boundary conditions are;

$$v_i = 0 \text{ when } r = r_c$$

and $$\frac{dv}{dr} = 0 \text{ when } r = r_m$$

$$\therefore\ A_i = -\frac{1}{2\mu}r_m^2\left(\frac{dp}{dx}\right) \tag{7.37}$$

and $$B_i = \frac{1}{4\mu}\frac{dp}{dx}\left[-r_c^2 + 2r_m^2 \ln r_c\right] \tag{7.38}$$

$$\therefore\ \tau_i = \mu\frac{dv}{dr} = -\frac{r}{2}\frac{dp}{dx} + \frac{r_m^2}{2r}\frac{dp}{dx} \tag{7.39}$$

and $$v_i = \frac{1}{4\mu}\left(\frac{dp}{dx}\right)\left[(r_c^2 - r^2) + 2r_m^2 \ln\left(\frac{r}{r_c}\right)\right] \tag{7.40}$$

The radius of maximum velocity occurs when $v_i = v_o$

$$\text{i.e. } r_c^2 - r_m^2 + 2r_m^2 \ln\left(\frac{r_m}{r_c}\right) = r_p^2 - r_m^2 + 2r_m^2 \ln\left(\frac{r_m}{r_p}\right)$$

$$\therefore\ r_m = \sqrt{\frac{r_p^2 - r_c^2}{2\ln\left(\frac{r_p}{r_c}\right)}} \tag{7.41}$$

The shear stress at the core or capsule wall due to pressure flow is;

$$\tau_{pc} = \tfrac{1}{2}\frac{dp}{dx}\left[-r_c + \frac{r_p^2 - r_c^2}{2r_c \ln\left(\frac{r_p}{r_c}\right)}\right] \tag{7.42}$$

6.2 Rate of flow through the annulus

The expression v_o (or v_i) can be used for determining the rate of flow through the annulus. The answer obtained is the same in both cases.

$$Q_a = 2\pi \int_{r_c}^{r_p} vrdr \tag{7.43}$$

$$= \frac{2\pi}{4\mu}\frac{dp}{dx}\int_{r_c}^{r_p}\left[r_p^2 - r^2 + 2r_m^2 \ln (r/r_p)\right] rdr$$

$$\therefore\ Q_a = \frac{\pi}{2\mu}\left(\frac{dp}{dx}\right)\left[\frac{r_p^2 r^2}{2} - \frac{r^4}{4} + \frac{r_p^2 - r_c^2}{\ln\left(\frac{r_p}{r_c}\right)}\left(\frac{r^2}{2}\left(\ln\frac{r}{r_p} - \tfrac{1}{2}\right)\right)\right]_{r_c}^{r_p}$$

Simplifying gives;

$$Q_a = \frac{\pi}{8\mu}\left(\frac{dp}{dx}\right)(r_p^2 - r_c^2)\left[r_p^2 + r_c^2 - \frac{(r_p^2 - r_c^2)}{\ln(r_p/r_c)}\right] \tag{7.44}$$

$$\therefore\ \bar{V}_{ap} = \frac{1}{8\mu}\left(\frac{dp}{dx}\right)\left[r_p^2 + r_c^2 - \frac{(r_p^2 - r_c^2)}{\ln(r_p/r_c)}\right] \tag{7.45}$$

where $\bar{V}_{ap}$ = mean velocity in the concentric annulus due to laminar pressure flow.

Wiegard and Baker (see ref. 55) show that experimental friction factors obtained from pressure drop measurement indicate only rough agreement with the equation in the higher and middle diameter ratios and at low diameter ratios the data are inconsistent.

Rothfus et al (reference 55) obtained good agreement for a diameter ratio of 0,162. Experimental friction factors approached agreement with theory only at very low Reynolds numbers.

For the large diameter ratios used in capsule transportation, the Navier Stokes equation yields satisfactory results in the laminar flow region.

7. Laminar flow in eccentric annulus

The general case of laminar flow in eccentric annuli has been expressed theoretically by Caldwell (reference 9), Heyda (reference 20) and Redberger and Charles (reference 49) and experimentally by Bourne, Figueiredo and Charles (reference 5). Caldwell noted (from previous experiments) that the hydraulic mean radius, when used as the characteristic length in the Darcy equation, made allowance for geometric form, although in the cases considered, the sections had at least two axes of symmetry.

Caldwell solved the Navier Stokes equation using a transformation to the bi-polar co-ordinate system which characterises the geometry. He emphasised that the hydraulic mean depth as a general and complete representation of the flow section cannot be justified and as a criterion of form may only be applied to doubly symmetric sections. Even this assumption has been shown to be erroneous by later investigators (e.g. Malaika reference 36).

Redberger and Charles (reference 49) solved the equation using a rectangular mesh obtained by transformation from the bi-polar co-ordinate system and a finite difference technique in conjunction with a digital computer to obtain velocity profiles and flow rates as a function of pressure gradient.

Figure 7.13 from Redberger and Charles, shows the ratio of flow between eccentric cylinders to flow between concentric cylinders plotted against the relative displacement $m = 2e/D$ for different d/D ratios. The figure is used as follows:

(1) Calculate the values of diameter ratio and the relative displacement (m).

(2) Evaluate the flow through a concentric annulus.

(3) The flow rate in an eccentric annulus can thus be obtained from the figure and the flow through a concentric annulus.

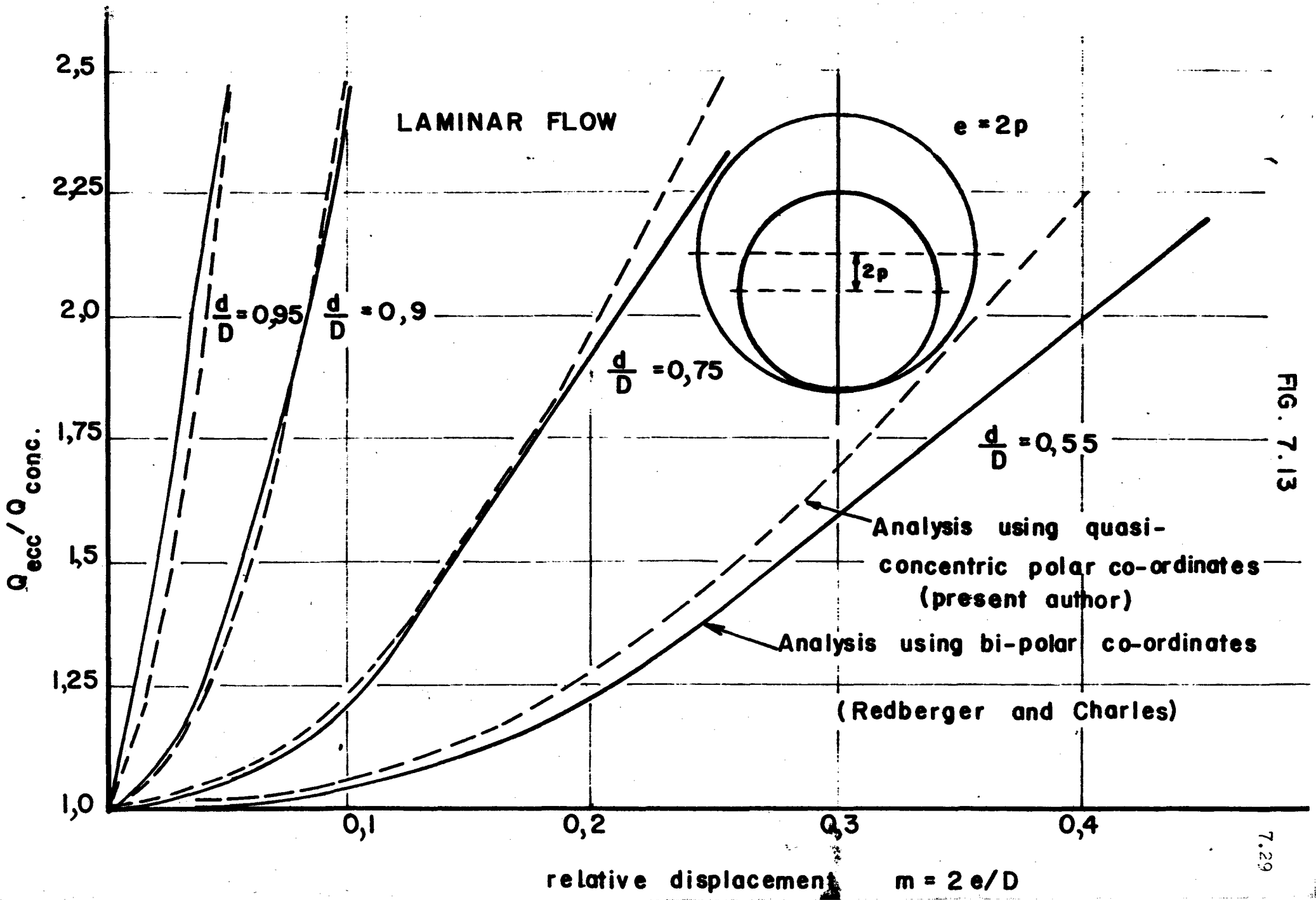
LAMINAR FLOW
e = 2p
2p
d/D = 0,95
d/D = 0,9
d/D = 0,75
d/D = 0,55
Analysis using quasi-concentric polar co-ordinates (present author)
Analysis using bi-polar co-ordinates (Redberger and Charles)
Q ecc / Q conc.
2,5
2,25
2,0
1,75
1,5
1,25
1,0
0,1
0,2
0,3
0,4
relative displacement m = 2 e/D

FIG. 7.13

It can be seen from Figure 7.13 that increased eccentricity increases the flow rate through the annulus, particularly at large diameter ratios. No experimental results were given. The dotted curves will be discussed further in Chapter 13.

An experimental investigation was carried out by Bourne et al and the data is shown plotted on Figure 7.14 as the product of friction

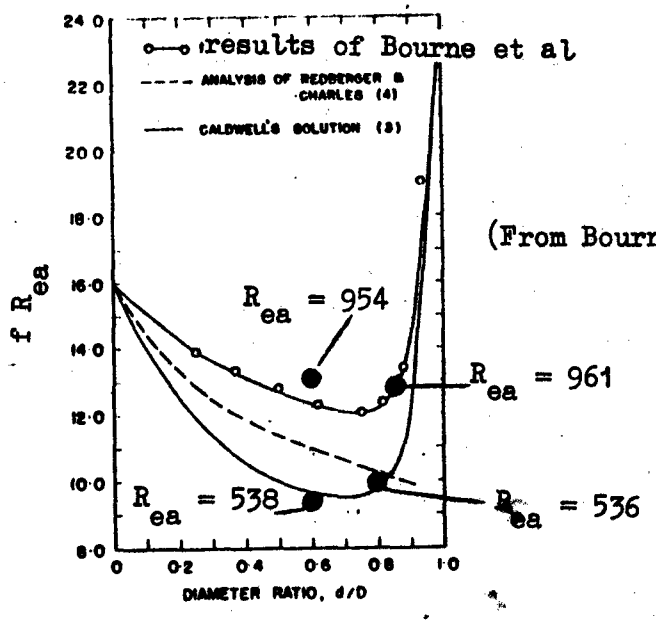

(From Bourne et al (reference 5))

Figure 7.14

factor multiplied by Reynolds number as a function of diameter ratio. Bourne et al accepted the conventional definition of hydraulic mean radius ((D - d)/4 for an annulus) and this gives the impression that the friction factor varies with diameter ratio. Figure 7.14 will be discussed further in Chapter 13.

Note that neither the analytical solutions of Redberger and Charles (numerical) nor that of Caldwell (mathematical) agree with the experimental results. For eccentric annuli, analysis to date does not seem to give correct results, even for laminar flow.

Note that at a diameter ratio of zero the value of $f \times R_{ea}$ product is 16 and the flow geometry approaches that of a clear pipe. At the other extreme of diameter ratio, unity, the product $(f \times R_{ea})$ is 24 and the flow geometry approaches flow between flat plates.

7.1 Analysis of laminar flow in eccentric annulus

An attempt will now be made to analyse laminar flow in the eccentric annulus due to the pressure gradient by incorporating the method of quasi-concentric annuli formulated in Section 2.

The total flow in the annulus is given by;

$$Q_a = \int_{C_{rc}}^{C_{rp}} \int_{0}^{2\pi} v r dr \, d\theta \tag{7.46}$$

where v is the point velocity in laminar flow. However, the mean velocity in a concentric annulus has already been enunciated (equation 7.45) and since quasi-concentric annuli are being untilised, equation (7.46) can be integrated to yield;

$$Q_a = \int_{0}^{2\pi} \bar{V}_{ap}[(C_{rp}^2 - C_{rc}^2)/2] \, d\theta \tag{7.47}$$

$$\therefore \quad Q_a = \sum_{i=1}^{n} \sum_{\theta=0}^{2\pi} [\bar{V}_{api}(C_{rpi}^2 - C_{rci}^2)/2](\Delta\theta) \tag{7.48}$$

where $\bar{V}_{api}$ varies with θ. $\bar{V}_{api}$ is the mean velocity in the quasi-concentric annulus due to pressure flow at a particular location and is given by;

$$\bar{V}_{api} = -\frac{1}{8\mu}\left(\frac{dp}{dx}\right)\left[C_{rpi}^2 + C_{rci}^2 - \frac{(C_{rpi}^2 - C_{rci}^2)}{\ln (C_{rpi}/C_{rci})}\right] \tag{7.49}$$

The analysis will be compared with experimental results in Chapter 13.

8. Turbulent flow in annuli

In the case of turbulent flow in pipes, the absence of an exact theory implies recourse to empirical or semi-empirical approaches. Annular flow which is an even more complex phenomenon is no exception.

Most investigations have been limited to the concentric case.

Turbulent flow in annuli will be discussed from the following points of views; friction factor, radius of maximum velocity, velocity distribution in concentric annuli, experiments in eccentric annuli, velocity profiles in eccentric annuli.

9. Turbulent flow in concentric annuli (Review)

9.1 Friction factor correlation

Early attempts to correlate data for fluid friction in turbulent flow in concentric annuli involved the use of the traditional hydraulic mean radius. Experimental data using the annular hydraulic mean radius instead of the pipe hydraulic mean radius could then be plotted as friction factor versus Reynolds number correlations and compared with the universal diagram for smooth pipes. Experimental data, as mentioned earlier, when plotted by this method yielded friction factors of the order of 15 per cent higher than smooth pipe correlations (in certain instances).

Caldwell (referenoe 9) carried out experiments with concentric and eccentric cores of circular and other cross-sections. He used $\bar{V}_a$ as the characteristic velocity and $(D - d)$ as the hydraulic mean diameter. He later modified the hydraulic mean radius for eccentric flow. This will be mentioned later.

Of the many investigations involving fluid friction in concentric annuli, one of the more successful is probably that due to Rothfus and co-workers. Rothfus, Monrad and Senecal (reference 55) discuss smooth concentric annuli in the first of many papers based on the doctoral thesis by Rothfus entitled "Velocity distribution and fluid friction in concentric annuli".

In this paper, air was the fluid used and it was assumed that a Darcy type equation applied with the hydraulic mean radius $(\frac{D - d}{4})$. Later they used a modified hydraulic mean radius concept. They considered that a portion of the flow area between the maximum velocity contour (shown by their measurements to be the same as the laminar maximum velocity locus) and the outer surface of the annulus was of more concern, for purposes of correlation, than the total flow area.

A force balance on the annulus results in the equation,

$$\tau_{cp}\, r_c + \tau_{pp}\, r_p = \frac{\Delta P}{2L}\,(r_p^2 - r_c^2) \tag{7.50}$$

where τ_{pp} = shear stress on outer wall

and τ_{cp} = shear stress on inner wall

and $$\tau_{pp} = \frac{\Delta P}{2L}\left(\frac{r_p^2 - r_m^2}{r_p}\right) \tag{7.51}$$

$$\tau_{cp} = \frac{\Delta P}{2L}\left(\frac{r_m^2 - r_c^2}{r_c}\right) \tag{7.52}$$

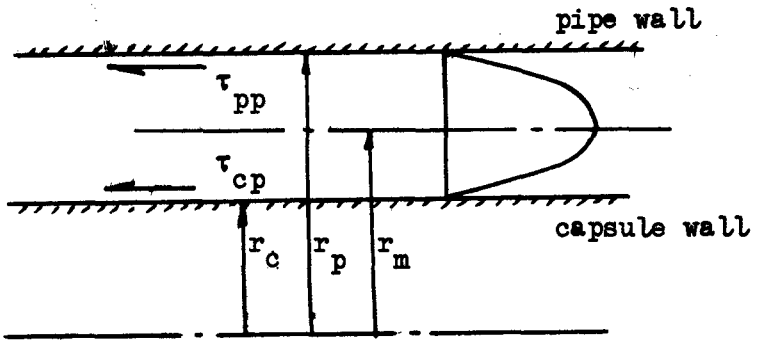

Figure 7.15

The radius of the inner and outer walls as well as the radius of maximum velocity are defined in Figure 7.15 as are the shear stresses at the outer and inner walls (τ_{pp} and τ_{cp}).

The hydraulic mean radius (which can be defined here as R_{rp}) was then taken as

$$R_{rp} = \frac{r_p^2 - r_m^2}{2r_p} \tag{7.53}$$

The friction factor for the outer surface (which can be defined here as f_p) was, by analogy to pipe flow, taken as;

$$f_p = \frac{\tau_{pp}}{\frac{1}{2}\rho \bar{V}_a^2} \tag{7.54}$$

Combining equations (7.51) and (7.54) yields

$$\Delta P = \frac{f_p \rho \bar{V}_a^2 L}{\frac{(r_p^2 - r_m^2)}{r_p}} \tag{7.55}$$

or more familiarily;

$$\Delta h_f = \frac{f_p \bar{V}_a^2 L}{2g R_{rp}} \tag{7.56}$$

The hydraulic mean radius, defined above, was thus used for the Reynolds number;

$$R_{ep} = \frac{D_{ep} \bar{V}_a \rho}{\mu} \tag{7.57}$$

where D_{ep} is an equivalent diameter based on the region of flow outside the radius of maximum velocity.

$$D_{ep} = 2\left(\frac{r_p^2 - r_m^2}{r_p}\right) = 4 R_{rp} \tag{7.58}$$

Similarly by defining a friction factor for the inner surface (which is defined here as f_c)

$$\tau_{cp} = f_c \tfrac{1}{2} \rho \bar{V}_a^2 \tag{7.59}$$

which can be combined with equation (7.52) to give;

$$\Delta P = \frac{f_c \rho \bar{V}_a^2 L}{(r_m^2 - r_c^2)/r_c} 2 \tag{7.60}$$

The equivalent diameter is, in this case;

$$D_{ec} = 2(r_m^2 - r_c^2)/r_c \tag{7.61}$$

Rothfus, Monrad and Senecal (reference 55) found good correlation (using air) between the above method and the conventional Reynolds number versus friction factor curves for plain, clear pipes. In a paper by Walker, Whan and Rothfus (reference 65) experiments were carried out using water. A plot of friction factor (f_p) against Reynolds number (R_{ep}) for annuli

of diameter ratios 0,1653; 0,3312; and 0,4987 agreed well with smooth pipe curves in the laminar and turbulent region for R_{ep} up to 20 000.

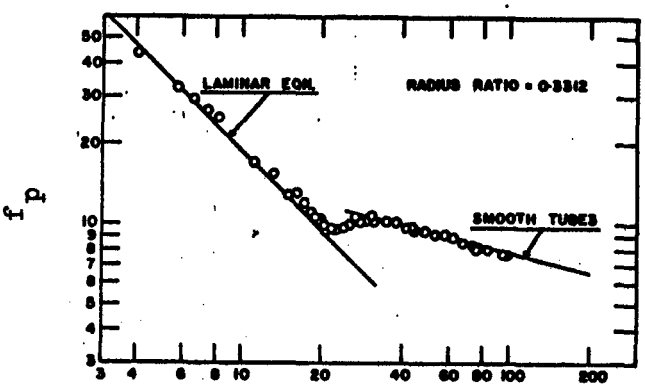

(From Walker et al (reference 65))

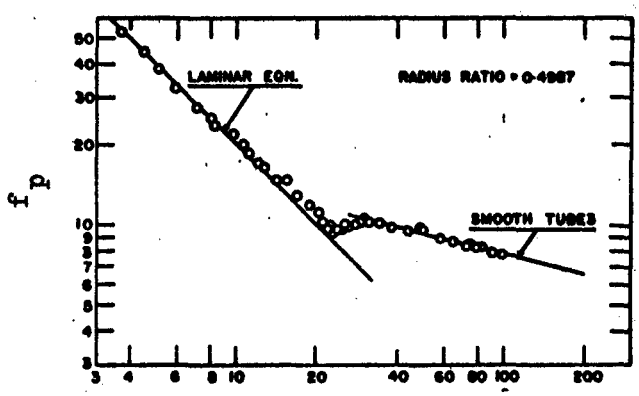

Figure 7.16

The results, using the method outlined above, correlate well using water. However, the maximum diameter ratio used was only about 0,5.

One weakness of the theoretical work of Rothfus and co-workers, is that the friction factor for the inner surface (f_c) is not correlated with R_{ec} with the same degree of success as the outer surface friction factor (f_p) is correlated with R_{ep}.

Meter and Bird (reference 38) used the Prandtl mixing length approach to give a friction factor versus Reynolds number expression for concentric annuli. Flow in circular pipes and parallel plates were given as special cases. They stated that the procedure is substantially more accurate than the hydraulic mean radius procedure and of comparable accuracy to Rothfus et al. Experimental data from sources other than the authors, were used, and although they stated that the method of Rothfus and co-workers is empirical their (Meter and Bird) method is no less empirical, no more accurate and far more complicated and cumbersome.

Ratkowsky (reference 48) redefined the two friction factors of Rothfus and co-workers (i.e. between the radius of maximum velocity and the appropriate wall). The correlation is good for the outer portion of flow but not good for the inner region of flow.

The main difference between the equations of Ratkowsky and those of Rothfus et al is that Ratkowsky used the average velocity from the radius of maximum velocity to the appropriate wall, whereas Rothfus used the mean velocity in the annulus for the calculation of f for both walls.

The momentum transferred from one side of the radius of maximum velocity to the appropriate wall is not influenced by what occurs on the other side of the radius of maximum velocity.

Thus the respective shear stress is related to the average velocity of that region of flow through which momentum is being transferred.

Using the notation already employed we get;

$$\bar{\tau}_{pp} = f'_p \tfrac{1}{2} \rho \bar{V}_p^2 \qquad (7.62)$$

$$\bar{\tau}_{cp} = f'_c \tfrac{1}{2} \rho \bar{V}_c^2 \qquad (7.63)$$

$\bar{V}_p$ = average velocity in the region between the radius of maximum velocity and the outer wall;

$\bar{V}_c$ = average velocity in the region between the radius of maximum velocity and the inner wall.

Ratkowsky tested his hypothesis by analysing the data of other investigators, notably Brighton and Jones (reference 7). The average velocity in each of the two regions of flow was determined from the velocity profiles.

Combining equations (7.51), (7.58) and (7.62) as well as (7.52), (7.61) and (7.63) we get;

$$\frac{\Delta P}{L} = \frac{2 f'_p \rho \bar{V}_p^2}{D_{ep}} \tag{7.64}$$

and $$\frac{\Delta P}{L} = \frac{2 f'_c \rho \bar{V}_c^2}{D_{ec}} \tag{7.65}$$

The Reynolds numbers for each of the two regions of flow are defined as;

$$R'_{ep} = \frac{D_{ep} \bar{V}_p \rho}{\mu} \tag{7.66}$$

$$R'_{ec} = \frac{D_{ec} \bar{V}_c \rho}{\mu} \tag{7.67}$$

Ratkowsky found, by analysing the data of Brighton and Jones, that the friction factor - Reynolds number relation agreed well with the Nikuradse line for turbulent flow in smooth pipes for R'_{ep} up to 3×10^5 from the transition range (for the outer region). For the case of f'_c versus R'_{ec} the agreement is very good for $r_c/r_p > 0{,}6$ but becomes increasingly worse as r_c/r_p decreases.

Ratkowsky explains this by pointing out that the outer velocity profile is in good agreement with smooth pipes. However, the inner profile does not agree with the velocity distribution for smooth pipes and the agreement worsens as r_c/r_p becomes smaller.

One simplified way of looking at the annulus situation is to realize that the outer surface is concave to the flowing fluid (as is the wall of a pipe) and the inner surface is convex. The inner surface (according to Ratkowsky) may not be able to support a boundary layer to the same extent as the outer surface.

Brighton and Jones (reference 7) discuss experiments in concentric annuli with diameter ratios from 0,0625 to 0,562 and with conventional Reynolds numbers from 46 000 to 327 000. They used a 200 mm diameter pipe with the centre pipe supported by struts at three axial positions. Brighton and Jones took some effort to ensure fully turbulent flow at the measuring section by artificially roughening the inside of the outer pipe for 4,5 diameters from the inlet. Fully developed flow was obtained in an entrance length of 34,5 diameters only with the aid of inlet roughness elements and screens. The velocity measurements were taken at four angular locations with a velocity deviation less than 0,5 per cent. Air and water were used and it was found that friction factors using water were 6 to 8 per cent lower than those of Rothfus and 6 to 8 per cent higher than the generally accepted values for smooth pipes. The friction factors for annular flow were 1 to 10 per cent higher than smooth pipe flow values. The friction factors depended only on Reynolds number and were independent of radius ratio (d/D) for $d/D > 0,0625$, for the range of values tested.

Quarmby (reference 46) found results in agreement with Brighton and Jones, i.e. that the friction factor is independent of radius ratio. His results have less scatter and lie closer to Blasius's curve ($f = 0,079\ R_e^{-0,25}$) than Brighton and Jones. The best fit for Quarmby's results gave;

$$f = 0,0844\ R_{ea}^{-0,255} \qquad (7.68)$$

and he concludes that the f versus R_e relation lies between

$$f = 0,087\ R_{ea}^{-0,25}$$

$$\text{and } \frac{1}{\sqrt{f}} = 4 \log (R_{ea}\sqrt{f}) - 0,4$$

for R_{ea} and f defined conventionally. Quarmby used a horizontal rig (73 mm diameter pipe with cores giving diameter ratios from 0,347 down to 0,11)

and a vertical rig (44,6 mm diameter pipe giving diameter ratios from 0,356 to 0,107) and a Reynolds number range from 10 000 to 90 000.

Owen (reference 44) determined head losses in three annular pipes in the Reynolds number range from 4 000 to 700 000.

The annuli tested were;

(i) brass, having an outer diameter $D = 50$ mm and an inner diameter $d = 12$ mm, giving a diameter ratio of 0,405 according to Owen,

(ii) steel, having an outer diameter $D = 150$ mm and a core of $d = 50$ mm giving an actual diameter ratio of 0,392,

(iii) steel, with the same outer diameter but with a core of 75 mm giving an actual diameter ratio of 0,568.

Owen plotted results on a conventional friction factor - Reynolds number diagram using the hydraulic mean radius. He did not consider a modification of hydraulic mean radius.

He shows that the friction factors for annular pipes lie above the curves for circular pipes, and the friction factor at a given Reynolds number increases as the diameter ratio (d/D) increases.

Jonsson and Sparrow (reference 24) found (for concentric annuli) that the friction factor was dependent on diameter ratio and increased as diameter ratio increased. (This is contrary to previous trends in which a radius ratio dependency has been found). However, the effect is very slight.

In 1968, Robertson (reference 52) carried out a literature review of work done to date on concentric annuli and after rejection of some of the data, correlated the remaining data, as shown in Figure 7.17, on the basis of a ratio $(F = \frac{f_{an}}{f_{pipe}})$ of the friction factor in the annulus to that in a pipe.

Some of the reasons for the scatter, particularly for the data of Kratz and Atherton, may be due to inadequate approach lengths. However, it is doubtful whether this can be used as a reason for the scatter in both

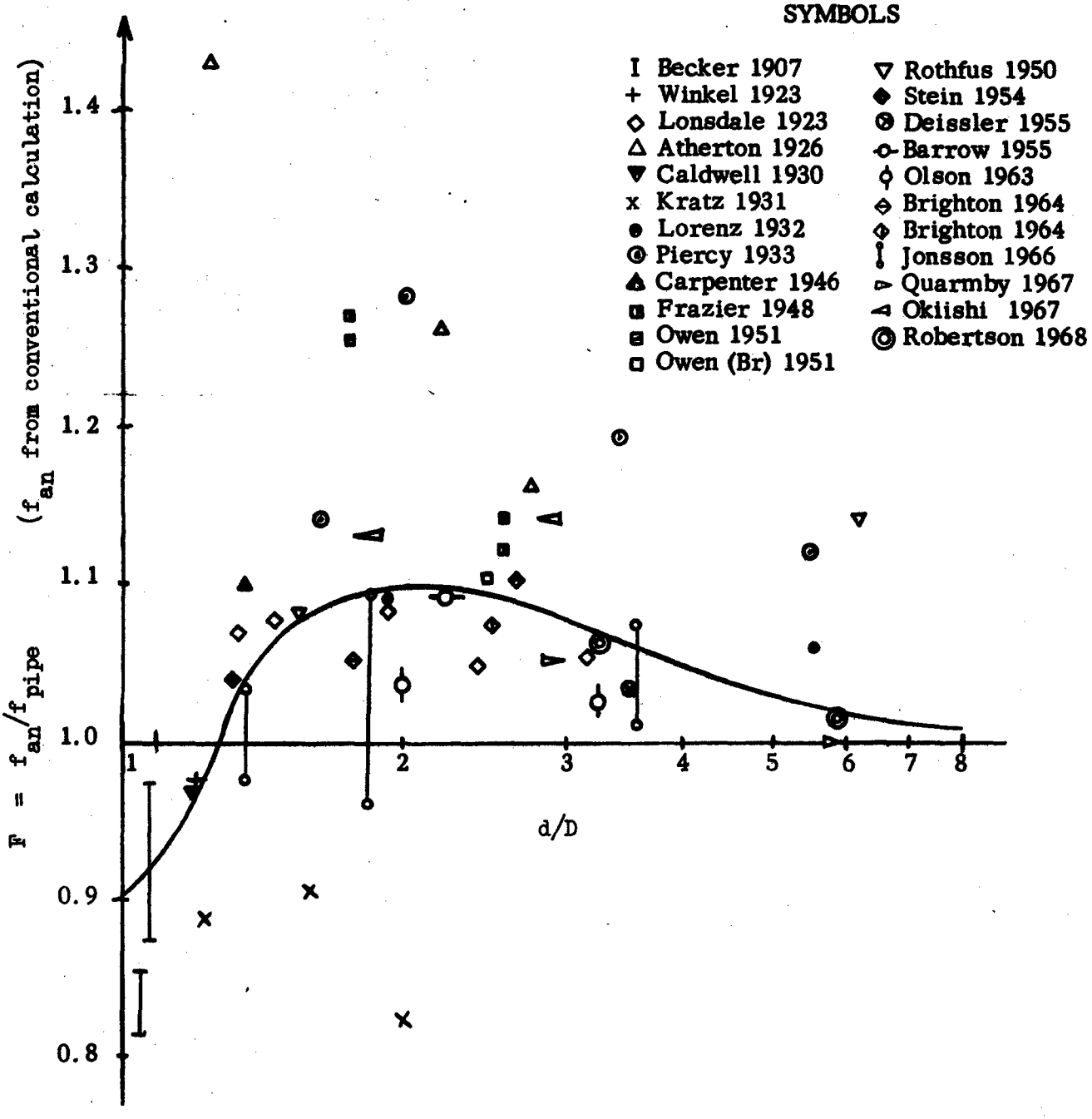

Figure 7.17 Turbulent-Flow Friction Factor for Concentric Annulus as a Function of Diameter Ratio.

From Robertson (reference 52)

cases since Atherton's data are high and Kratz's are low.

Further reasons given for the scatter are the definition of the friction in the reference pipe. Also, the inner core may not be perfectly concentric. The value suggested at $d/D = 1,0$ is based on the friction factor relations for a wide rectangular channel.

$$\frac{1}{\sqrt{4f}} = 2,03 \log\left[\frac{(D - d)\,\overline{V}}{\nu}\sqrt{4f}\right] - 0,47 \qquad (7.69)$$

(See Rouse's elementary Mechanics of Fluids, p 214)
at a Reynolds number of about 7×10^4.

9.2 Radius of maximum velocity

The approach of various authors (Rothfus *et al*, Ratkowsky, etc.) is to evaluate the flow in two separate layers in the annulus, separated by the radius of maximum velocity (r_m). This is an imaginary cylindrical boundary across which there is no turbulent shear interaction.

For concentric annuli, in the laminar case, the location of r_m is well known and can be derived;

$$r_m = \sqrt{\frac{r_p^2 - r_c^2}{2 \log_e(\frac{r_p}{r_c})}} \qquad (7.41)$$

Radial asymmetry is indicated by the above equation and this is also evident in turbulent flow, i.e. the radius of maximum velocity is not midway between r_p and r_c.

From velocity profiles which are flat in the central region, the radius of maximum velocity, in concentric turbulent flow, has proved difficult to determine. There is considerable divergence of opinion as to the location of r_m in turbulent flow.

Rothfus *et al* (reference 55) assumed that the location of (r_m) in turbulent flow was the same as for laminar flow, i.e.

$$r_{mt} = r_{ml} \qquad (7.70)$$

Lorenz (from Quarmby) found $r_{mt} < r_{ml}$ with Reynolds numbers up to 10^6. Mikrjkov (from Quarmby) found with $d/D = 0,543$ and Reynolds numbers between 60 000 and 90 000, for air, that $r_{mt} > r_{ml}$.

Owen with $d/D = 0,575$; 0,405 and 0,392 and Reynolds numbers for water from 4 000 to 70 000, found $r_{mt} < r_{ml}$.

Brighton and Jones found $r_{mt} < r_{ml}$ and the difference increases as diameter ratio decreases but the position of r_{mt} is independent of Reynolds number. The radius of maximum velocity was determined from the curve of velocity gradient which Brighton and Jones claim is more accurate than determining r_m from the velocity distribution curves because of flatness near the maximum velocity.

The fact that r_m is closer to the inner wall reduces the ratio of shear stress at the inner wall to that at the outer wall. The inner wall shear force must balance the pressure force on a smaller annular area as the point of zero shear stress moves towards the inner wall.

Quarmby found that $r_{mt}/r_{ml} < 1,0$ and the divergence from unity is a function of Reynolds number and (d/D) for Reynolds number less than 50 000.

The results of both Quarmby and Brighton and Jones were found to agree well with Leung's equation which is given by equation (7.71).

The position of the radius of maximum velocity relative to r_p as given by Ratkowsky for the data of Knudsen and Katz (reference 26) and for the data of Brighton and Jones is given in Figure 7.18.

Levy (reference 34) determined the radius of maximum velocity analytically using experimental expressions for the eddy diffusivity, substituting in the shear stress expression for turbulent flow in pipes, and equating the velocity distribution for the core wall to that of the outer wall. The analytical solution is shown in Figure 7.19.

Thus the studies of Knudsen and Katz (reference 26) and Rothfus et al (reference 55) indicate that the radius of maximum velocity for Reynolds

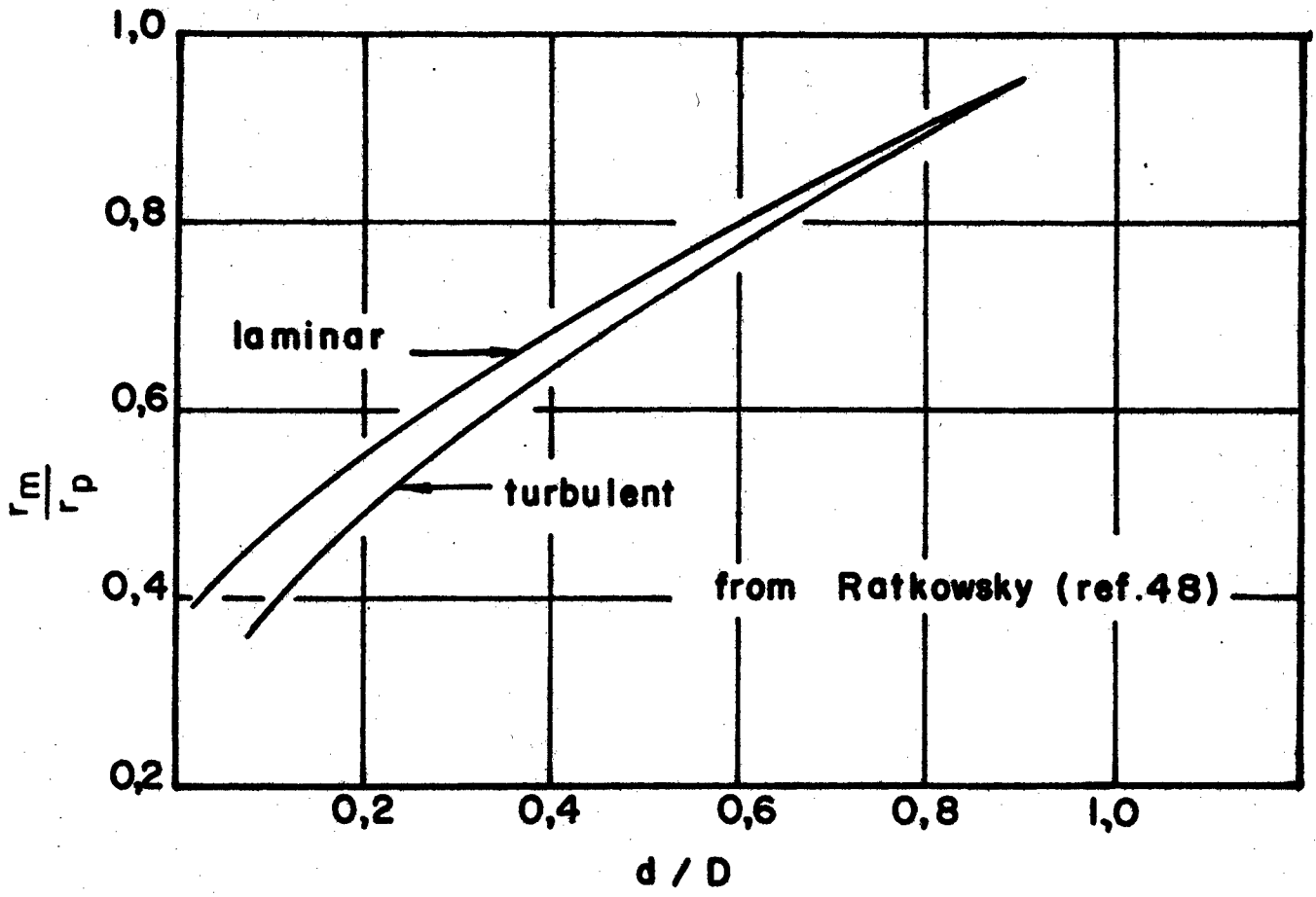

FIG. 7.18

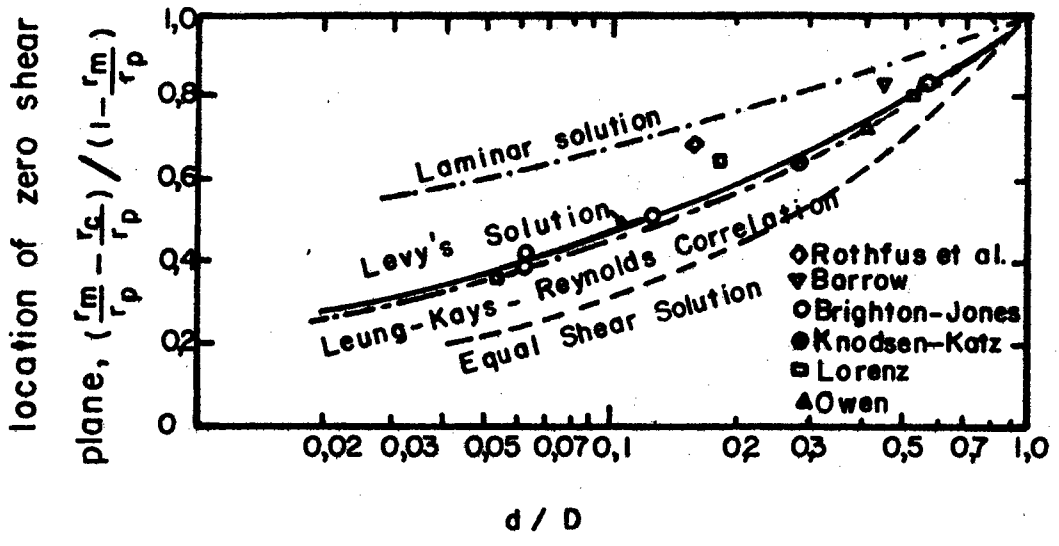

from Levy (ref. 34)

FIG. 7.19

numbers less than 10 000 (based on the conventional hydraulic mean radius) is identical to the radius of maximum velocity for laminar flow and the maximum velocity radius moves slightly towards the inner wall as the Reynolds number increases.

Randhava (reference 47) quotes an expression attributed to Leung et al (unobtainable) which has been found by Randhava to predict available experimental data closer than any other tested expression, i.e.

$$r_{mt} = r_c \left[1 + \left(\frac{d}{D}\right)^{n-1}\right] \Big/ \left[1 + \left(\frac{d}{D}\right)^{n}\right] \qquad (7.71)$$

Compare with Levy's curve on Figure 7.19.

The results of using this expression will be discussed in Chapter 13.

9.3 Radius of Maximum Velocity, eccentric annuli

Wolfe and Clump (reference 66) plotted experimentally determined maximum velocity points together with points predicted from the solution of the Navier Stokes equation for laminar flow. The agreement between experiments and laminar flow analysis is good, but only the one example is given by the authors.

No literature is available on the radius of maximum velocity in eccentric annuli in turbulent flow except for the velocity contours of Jonsson and Sparrow (reference 24).

In Section 14 it will be shown how the radius of maximum velocity can be calculated for the purpose of analysing pressure flow in the annulus.

9.4 Velocity distribution in annuli

Before discussing velocity distributions in annuli a brief review will be given on velocity distribution in pipes.

The following regimes exist in turbulent flow in smooth pipes:

9.4.1 Laminar sub-layer: this layer exists adjacent to the wall and in laminar flow extends to the centre of the pipe - viscous stresses predominate and

$$v^+ = y^+ \qquad \text{i.e.} \quad \frac{v}{v_*} = \frac{yv_*}{\nu} \qquad (7.72)$$

where $y^+ < 5$

9.4.2 Transition zone: the viscous and inertial stresses are comparable. Two alternative equations are;

$$v^+ = -3,05 + 5,0 \ln y^+ \text{ (reference 55)} \qquad (7.73)$$

for $5 < y^+ < 30$

and $$v^+ = 5,75 \log (y^+ - 5,3) + 5,5 \text{ (reference 63)} \qquad (7.74)$$

Squire's (reference 63) equation applies to both the transition region and the outer core.

9.4.3 Fully turbulent flow regime in which inertial stresses predominate: this region extends to the centre of the pipe and can be divided up into the inner core and the outer core. The division is arbitrary and is only made because certain velocity distribution laws apply better to one or other of the regions.

The most common form of velocity distribution law in this region is (Nikuradse)

$$v^+ = 5,5 + 5,75 \log y^+ \qquad (7.75)$$

The form of equation (7.75) can be obtained by integrating von Karman's equation, viz.

$$\sqrt{\tau} = \kappa \sqrt{\rho} \left(\frac{dv}{dy}\right)^2 \left(\frac{d^2v}{dy^2}\right)^{-1} \qquad (7.76)$$

Equation (7.76) is integrated close to the transition layer and the constants are obtained from Nikuradse's experiments.

9.5 Velocity distribution in concentric annuli

The problem is immediately seen to be more complicated than is the case for pipes since two velocity profiles are required instead of one. One profile extends from the pipe wall to the radius of maximum velocity and the other extends from the core wall to the radius of maximum velocity. One wall is convex in relation to the flow and the other is concave. The following experimenters have investigated the problem: Knudsen and Katz;

Rothfus and co-workers; Brighton and Jones; Sparrow, Eckert and Mincowycz (reference 62) (for cylinders longitudinal to the flow); Quarmby, Jonsson and Sparrow, and Randhava.

Knudsen and Katz (reference 26) plotted their own experimentally determined data together with that of Rothfus and co-workers and arrived at;

$$v_p^+ = 6{,}1 \log y_p^+ + 3{,}0 \qquad (y_p^+ > 30) \qquad (7.77)$$

and

$$v_c^+ = 4{,}4 \log y_c^+ + 6{,}2 \qquad (y_c^+ > 40) \qquad (7.78)$$

They admit that few data were available and it is unlikely that these equations are the final correlations.

Rothfus and Monrad (see reference 57) correlated local velocities in pipes and removed the Reynolds number effect by modifying the parameters v^+ and y^+ thus;

$$V^+ = \frac{v}{\sqrt{\frac{\tau_o}{\rho}}} \left(\frac{\bar{V}}{v_{max}}\right)$$

and

$$Y^+ = \frac{y\sqrt{\frac{\tau_o}{\rho}}}{\nu} \left(\frac{v_{max}}{\bar{V}}\right)$$

The use of V^+ and Y^+ breaks down, however, close to the wall. They predicted that V^+ for parallel flat plates equals V^+ for pipes if the clearance between the plates equals the pipe diameter, viz.

$$V_F^+ = V_p^+$$

and

$$Y_F^+ = Y_p^+$$

The Reynolds number for parallel plates is defined as $R_{eF} = \frac{4\, b\, \bar{V}}{\nu}$

Rothfus, Walker and Whan (reference 57) present a method for predicting local velocities in pipes, concentric annuli and parallel plates. Their correlation is independent of radius ratio and Reynolds number. They use the modified parameters of Rothfus, i.e. V^+ and Y^+ and correlate results from

other experiments on the smooth pipe curve for annuli and flat plates.

Figure 7.20a from Brighton and Jones (reference 7) shows v_p^+ plotted against y_p^+ in order to compare mean velocity distribution measurements with the "law of the wall".

The constants established from Nikuradse's pipe flow data in

$$v^+ = A \ln y^+ + B \tag{7.79}$$

are A = 2,5 and B = 5,5 and those established by Clauser according to Brighton and Jones, i.e. 2,44 and 4,9 are shown in Figure 7.20a. The values of v_p^+ are in close agreement with the pipe flow distribution and $v_p^+ = 5,5 + 5,75 \log y_p^+$ is a better fit for the outer profile.

The inner profile (Figure 7.20b) (for $y_c^+ < 40$) is found to agree well with pipe and boundary layer flows. For larger values of y_c^+ the agreement holds for higher radius ratios (d/D = 0,562) with the constants A and B as given by,

$$v^+ = 5,62 \log y^+ + 4,9$$

This equation is in agreement with Sparrow, Eckert and Mincowycz (reference 62).

Figure 7.21 shows the velocity distribution in the velocity defect form for inner and outer profiles. The outer profile agrees well with the constants and functions established by Hinze, viz.

$$\frac{v_{max} - v}{v_*} = 5,62 \log \frac{y}{\delta} + 0.8 + f\left(\frac{y}{\delta}\right) \tag{7.80}$$

where $\delta = r_p - r_m$ or $r_m - r_c$.

Thus the velocity distributions near the outer wall fit the law of the wall for all diameter ratios and for Reynolds numbers higher than 4 600. The results for the inner wall are in agreement with the law of the wall for $d/D > 0,375$.

According to Quarmby (reference 46) the effect of radius ratio on the velocity distribution is less pronounced than the effect of Reynolds number.

For a given radius ratio at low Reynolds number, the Reynolds number

effect on the inner profile is opposite to the effect on the outer profile.

The v_c^+/y_c^+ gradient increases as Reynolds number increases but the v_p^+/y_p^+ gradient decreases as Reynolds number increases.

The radius ratio effect is also opposite for the inner and outer profiles. In the outer profile the Reynolds number effect is reduced as d/D decreases. But for the inner profile the Reynolds number effect is most pronounced for lower values of (d/D). These effects are not particularly noticeable when scrutinising Quarmby's results.

As diameter ratio decreases, the outer profile becomes similar to the velocity profile in a plain pipe, and the inner profile becomes essentially that for longitudinal flow external to a cylinder.

Quarmby concludes that velocity profiles show an involved relation with radius ratio and Reynolds number. The inner profiles, especially, show a strong Reynolds number dependence; for Reynolds number $< 40\,000$ Quarmby gives;

$$v_c^+ = 2{,}27 \log_{10} y_c^+ + 6{,}6 \text{ for } d/D = 0{,}347 \qquad (7.81)$$

$$v_c^+ = 1{,}73 \log_{10} y_c^+ + 9{,}4 \text{ for } d/D = 0{,}1785 \qquad (7.82)$$

$$v_p^+ = 2{,}70 \log_{10} y_p^+ + 3{,}98 \text{ for } d/D = 0{,}347 \qquad (7.83)$$

$$v_p^+ = 2{,}62 \log_{10} y_p^+ + 4{,}6 \text{ for } d/D = 0{,}1785 \qquad (7.84)$$

Levy (reference 34) derived equations for fully developed turbulent flow in an annulus. Empirical expressions for the eddy diffusivity for momentum (ε) were taken from Reichardt, not too close to the wall, and from Deissler, near the wall surface, and substituted in

$$\tau = \rho (\nu + \varepsilon) \frac{dv}{dy} \qquad (7.85)$$

which is the expression for the local shear stress at any radial position in a pipe. Levy then substituted Reichardt's expression, which he postulates applies to the flow regions on both sides of the plane of zero shear for the annular flow, into equation (7.85) and integrates to get the velocity

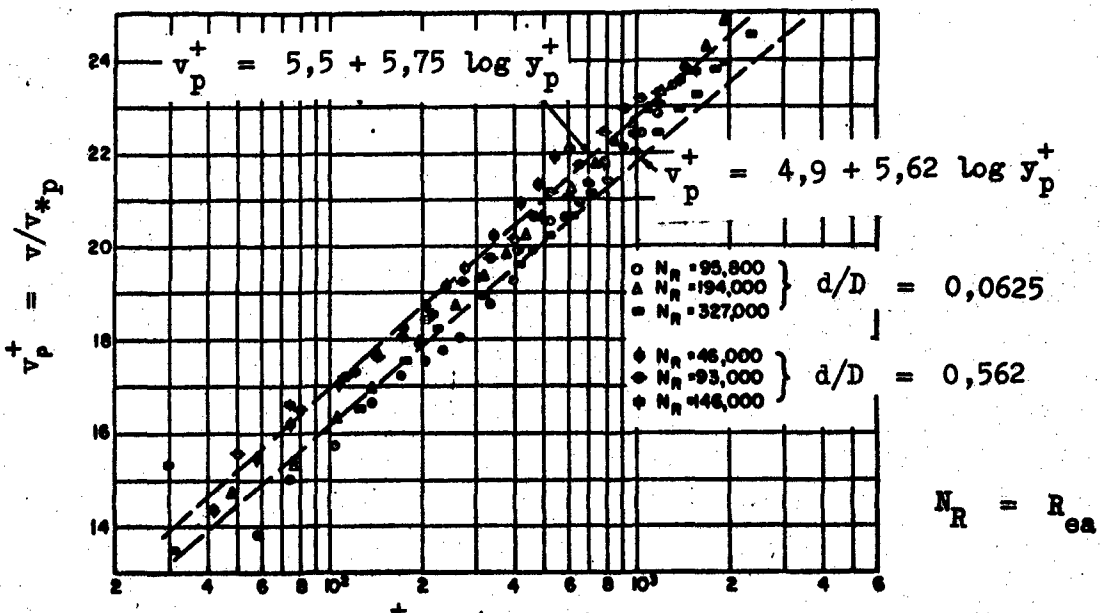

Figure 7.20(a) (From Brighton and Jones (reference 7))

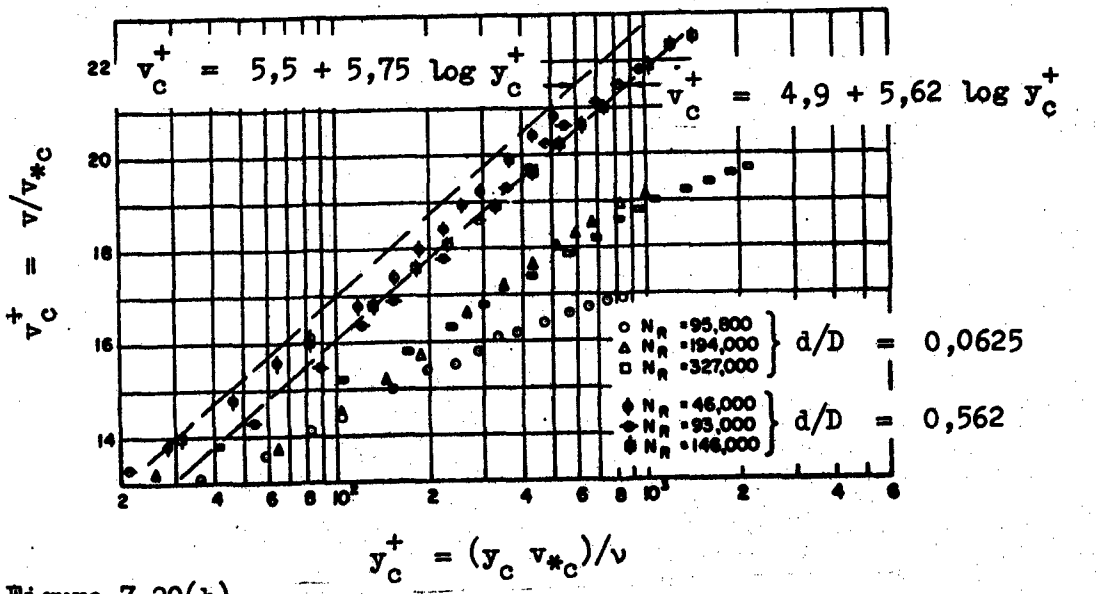

Figure 7.20(b) (From Brighton and Jones (reference 7))

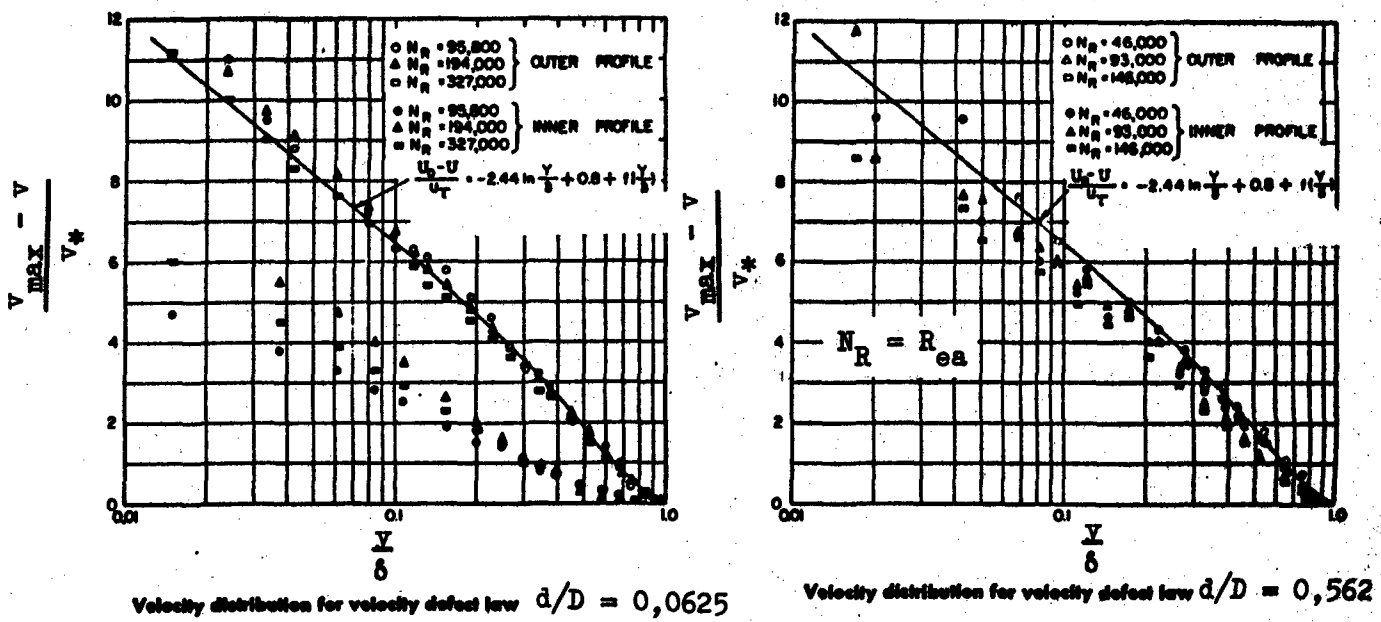

Figure 7.21(a) and (b) (From Brighton and Jones (reference 7))

distribution for the wall and core regions. Unfortunately, Levy's expressions for velocity distribution are rather complicated and unwieldy but he does obtain fairly good agreement with the experimental results of Brighton and Jones.

Jonsson and Sparrow (reference 25) plotted velocity profiles for concentric annuli from d/D = 0,281 to 0,75 for a range of Reynolds numbers. (See Figure 7.22)

The left hand curve is the outer wall profile, correspondingly $\bar{\tau}_{pp}$ is used as the shear stress and y_p is the distance from the outer wall. The right hand curve is for the inner profile and τ_{cp} and y_c are respectively the shear stress on the inner wall and the distance perpendicular to the inner wall.

The lines that appear on the figure are given by;

$$\text{aa} \quad v^+ = 2{,}78 \ln y^+ + 3{,}8 \tag{7.86}$$

$$\text{bb} \quad v^+ = 2{,}56 \ln y^+ + 4{,}9 \tag{7.87}$$

$$\text{cc} \quad v^+ = 2{,}44 \ln y^+ + 4{,}9 \tag{7.88}$$

Line aa corresponds to Nikuradse's corrected data for circular pipes and lines bb and cc are mean lines drawn through the data of Jonsson and Sparrow. The line aa is in good agreement with measured outer profiles. For the inner profile the line falls above the data. Sparrow, Eckert and Minkowycz (reference 62) show that the effect of a convex surface is to produce lower values of v_c^+ at a given y_c^+.

Randhava (reference 47) accepted the conventional logarithmic expression for the outer wall,

$$v_p^+ = A + B \ln y_p^+$$

He shows that an expression for the inner wall is

$$v_c^+ = \frac{B}{\beta} \ln y^+ + A' \tag{7.89}$$

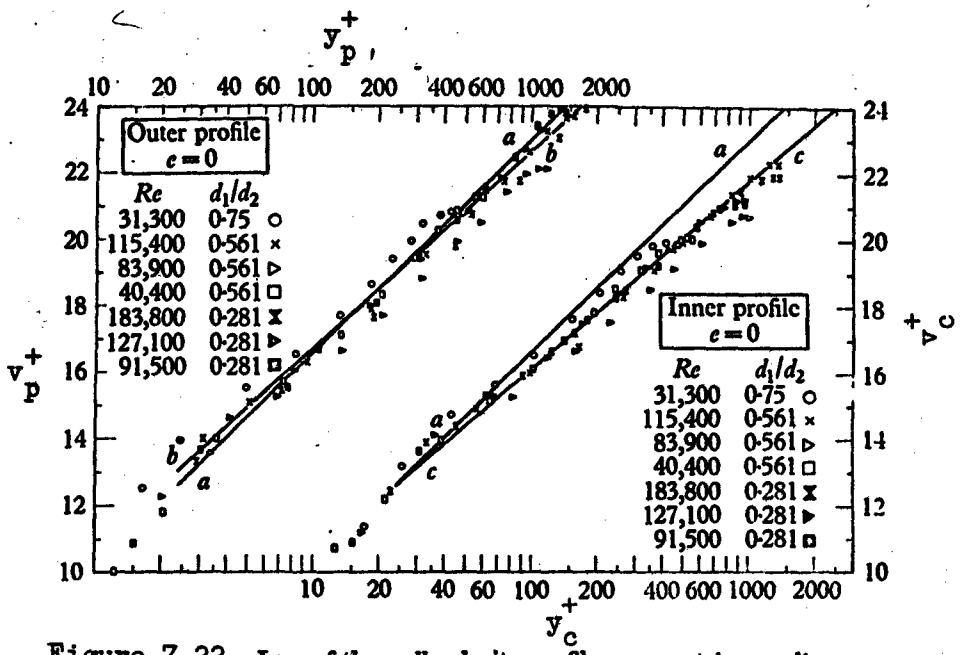

Figure 7.22 Law-of-the-wall velocity profiles, concentric annuli.

(From Jonsson and Sparrow (reference 24))

$$R_e = R_{ea} \qquad \frac{d_1}{d_2} = \frac{d}{D}$$

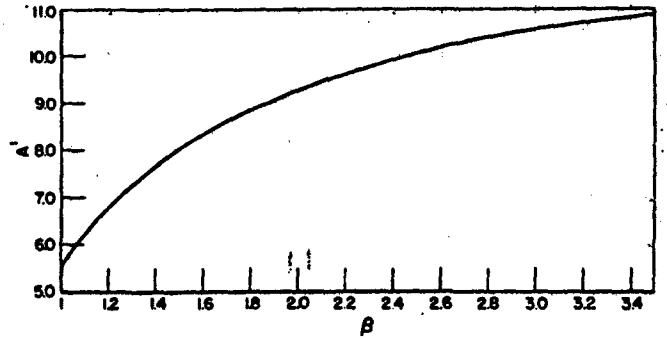

Figure 7.23 Variation of A' with β.

(From Randhava (reference 47))

where $\beta = \left(\frac{v_{*c}}{v_{*p}}\right)^2 = \frac{dv_p^+}{dy_p^+} \Big/ \frac{dv_p^+}{dy_c^+}$

$$= \frac{r_2}{r_1} \frac{r_m^2 - r_c^2}{r_p^2 - r_m^2} \qquad (7.70)$$

and $r_{mt} = r_c \left[\left[1 + \left(\frac{r_p}{r_c}\right)^{1-n}\right] \Big/ \left[1 + \left(\frac{r_c}{r_p}\right)^{n}\right]\right]$ where $n = 0{,}343$ (7.71)

Figure 7.23 shows the variation of A' with β.

Thus according to Randhava both constants vary with d/D.

The most significant velocity distribution equations are summarised in Table 7.2.

TABLE 7.2

$$v_n^+ = A \log_{10} y_n^+ + B$$

$$v_n^+ = \frac{v_n}{v_*}; \qquad y_n^+ = \frac{y_n v_*}{\nu}$$

n = p or c (pipe or capsule subscript)

Source	Inner Profile (Capsule)		Outer Profile (Pipe)		$(\frac{d}{D})_{max}$
	A	B	A	B	
Knudsen and Katz (Reference 26)	4,4 $y^+ > 40$	6,2	6,1 $y^+ > 30$	3,0	
Brighton and Jones (Reference 7)	5,62	4,9	5,75	5,5	0,562
Quarmby (Reference 46)	2,27	6,6	2,7	3,98	0,347
Jonsson and Sparrow (Reference 25)	5,62	4,9	5,9	4,9	0,75
Rothfus, Monrad and Senecal (Reference 55)	5,75	5,5	5,75	5,5	0,65
Randhava (Reference 47)	Analytical		5,75	5,5	

Note that the values for $(d/D)_{max}$ are the maximum diameter ratios used by the various authors. Only Jonsson and Sparrow considered eccentric annuli. The values of A given by Quarmby appear to be in error. Although he stated that all log values were to base 10, it appears as though the A values are associated with Napierian logarithms and should be adjusted to give A values for the inner and outer profiles as 5,23 and 6,22 respectively.

10. Turbulent flow in eccentric annular ducts

The literature on eccentric annuli is far less prolific than on concentric annuli. The laminar case has been described analytically by Caldwell (reference 9) and Redberger and Charles (reference 49) and others. Turbulent flow has been examined by Caldwell, Jonsson and Sparrow (reference 24), Bourne et al (reference 5) and Robertson (reference 52).

Caldwell replaced (D - d) for eccentric annuli by an empirical function of (D - d) and the eccentricity (e). He stated that this had only a limited application. He replaced the hydraulic mean radius by $(A/P)/[1 - 0,38 \frac{e}{A/P}]$. Jonsson and Sparrow carried out an experimental investigation and aimed at determining both the details of the flow field and the pressure drop and friction factor characteristics for turbulent flow in eccentric annular ducts. The eccentricity was varied from zero (concentric) to unit eccentricity (fully eccentric). Contour maps showing lines of constant velocity were constructed. From these, circumferential distributions of the shear stress on the walls, were deduced.

The experiments were conducted with air as the working fluid. Annular ducts having three diameter ratios were employed; d/D = 0,281; 0,561 and 0,750. (D = 104 mm).

The conventional Reynolds number ranged from 18 000 to 180 000. The test section was 6,09 m long and vertical.

Bourne et al (reference 5) carried out experiments in annuli of unit

eccentricity (ε = 1,0) only. The Reynolds number ranged from 200 to 20 000 so that they just overlapped with some results of Jonsson and Sparrow. The test conduit was a 25,5 m diameter, smooth, extruded copper tube, containing smooth metal rods of various diameters ranging from 6,35mm to 23,8mm. The experimental fluid was water.

Robertson (reference 52) reports friction factors in annuli determined in the same 150 mm pipeline used by Owen and Frazier. Considerable care was taken in cleaning out the pipe but Robertson states that the pipe was not smooth. It was found, in fact, that k/D varied from 0,006 to 0,007 with increase in Reynolds number. Only two diameter ratios were tested, i.e. 0,1725 and 0,312.

Some of the results of Robertson were plotted (by the present author) as Bourne suggests, (neither seems to be aware of the other's work) and a large discrepancy is apparent. However, Robertson's results were for rough pipes.

10.1 Friction factor in eccentric annuli

The conventional method (see Section 4.3) of defining friction factors was extended to eccentric annuli by various authors, Jonsson and Sparrow (reference 25), Bourne et al (reference 5).

It will be shown later (Section 11) that the conventional approach (Section 4.3) is over-simplified. Jonsson and Sparrow correlated friction factor information by a power law relationship (see Figure 7.24). The exponent 0,18 is used rather than the conventional 0,25 in the Blasius equation. For a fixed Reynolds number, f decreases as diameter ratio increases. Also, at a fixed diameter ratio and Reynolds number, the friction factor decreases with increasing eccentricity.

Bourne et al (reference 5) presented their results as f versus R_e diagrams using the conventional friction factor and Reynolds number based on the hydraulic mean radius $(\frac{D - d}{4})$. All the results presented in this

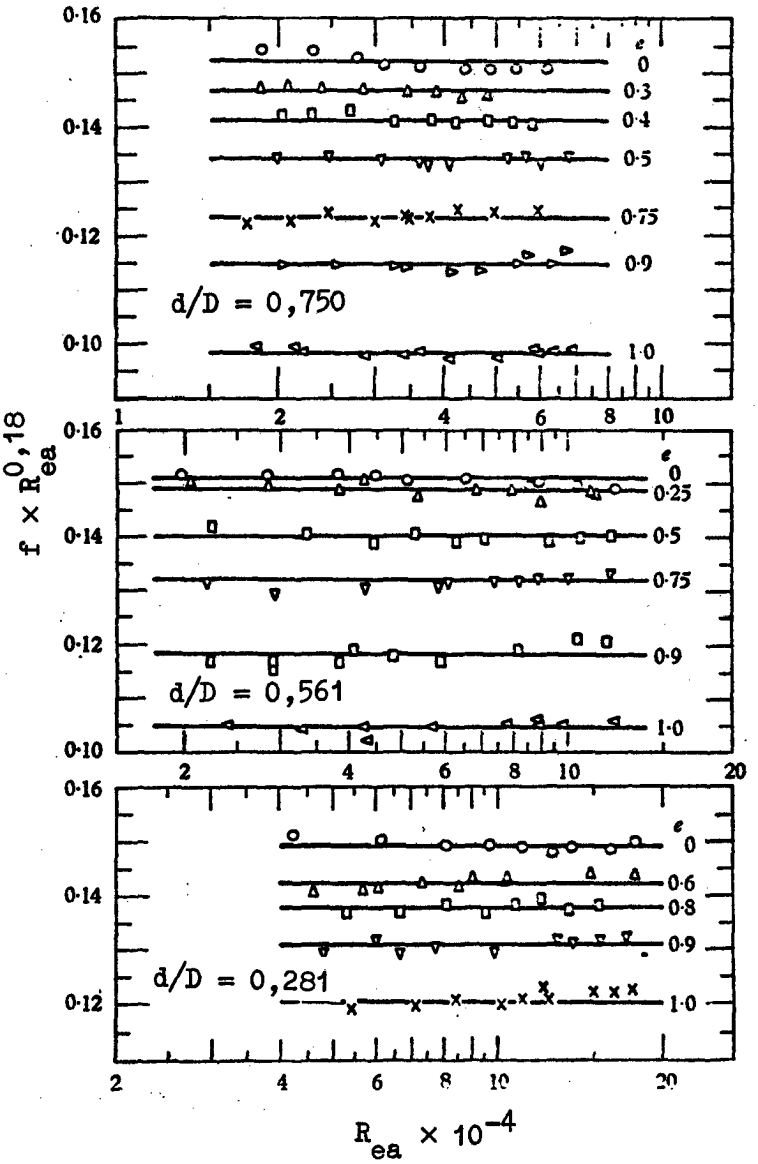

Figure 7.24 (From Jonsson and Sparrow (reference 24))

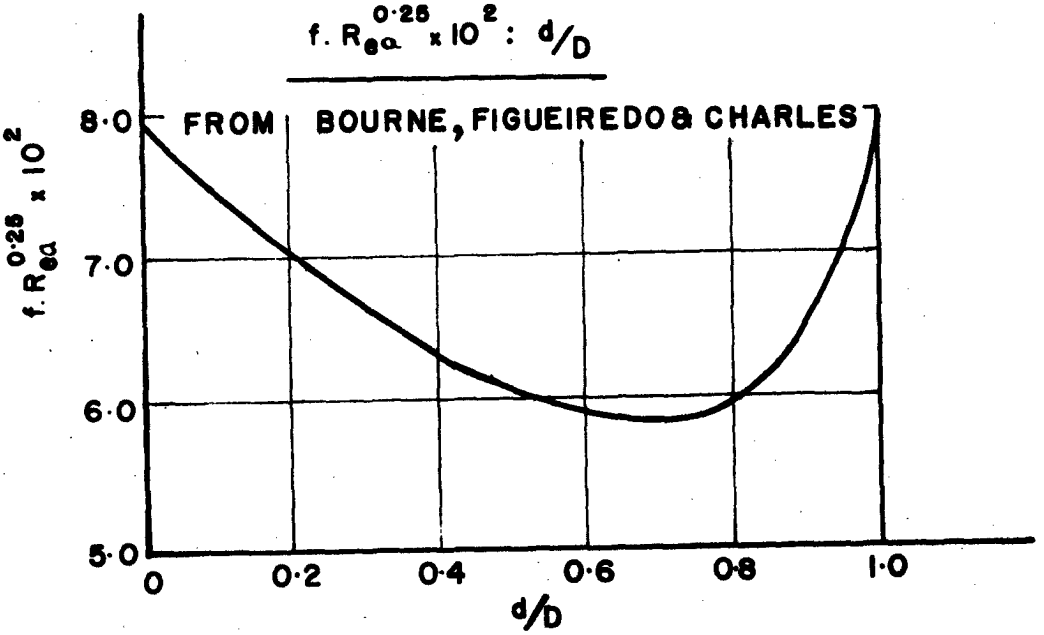

Figure 7.25 (From Bourne et al (reference 5))

way indicate friction factors lying below the smooth pipe curve. Some of their results for turbulent flow are plotted on Figure 7.25 indicating, as in the case of laminar flow, apparent changes in frictional coefficient as diameter ratio is varied.

Figure 7.26 compares results of Bourne et al with those of Jonsson and Sparrow (Reynolds numbers in excess of 18 000). Quite large discrepancies are shown. However, Figure 7.27 compares results of Denton and Dodge with those from Bourne et al and they agree well.

It can be seen from Figure 7.25 that the diameter ratio is an important variable when presenting results in this way and there is a minimum f $R_{ea}^{0,25}$ at d/D = 0,75. This conclusion is due to the conventional use of the hydraulic mean radius by Bourne et al.

10.2 Velocity profiles in eccentric annuli

Jonsson and Sparrow are the only ones to have investigated velocity profiles in eccentric annuli and present contour diagrams constructed from information obtained from velocity traverses. A typical example for unit eccentricity and d/D = 0,75 is shown on Figure 7.28. Each isovel (line of constant velocity) represents a particular value of v/v_{max}. The dotted lines were drawn normal to the isovels. These are defined as gradient lines and in fully developed uni-directional flow, represent lines of zero shear according to Jonsson and Sparrow. Actually they are lines of zero relative shear.

The velocities in the narrow part of the annulus must reduce to nearly zero.

Jonsson and Sparrow also give velocity profiles (see Figure 7.29) for eccentric annuli. The agreement is not as good as for concentric profiles. Data corresponding to a fixed value of θ (θ_1 and θ_2 defined on Figure 7.29) represents a traverse along the normal to the wall at the location θ. It can be seen that for θ from 90° to 120° the experimental points lie sig-

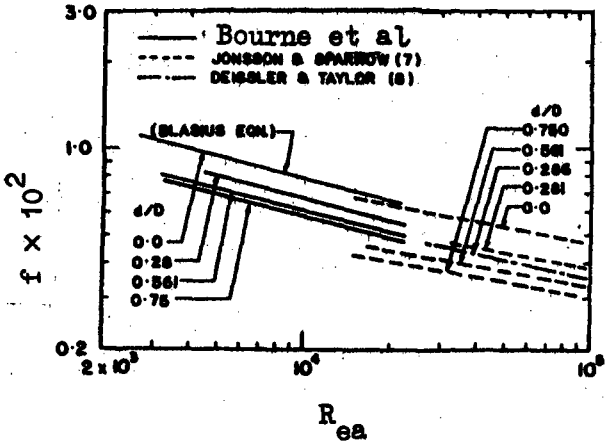

Figure 7.26

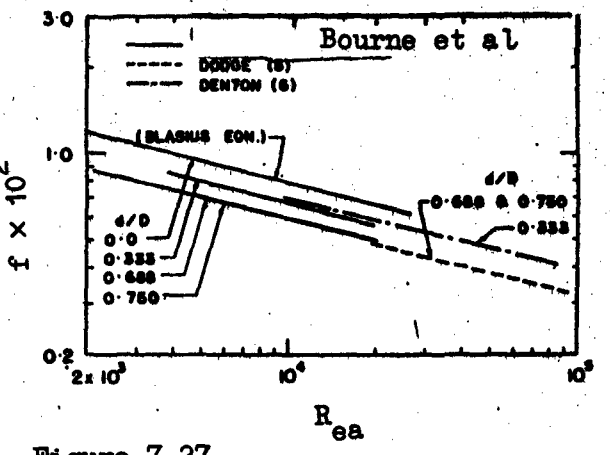

Figure 7.27

(From Bourne et al (reference 5))

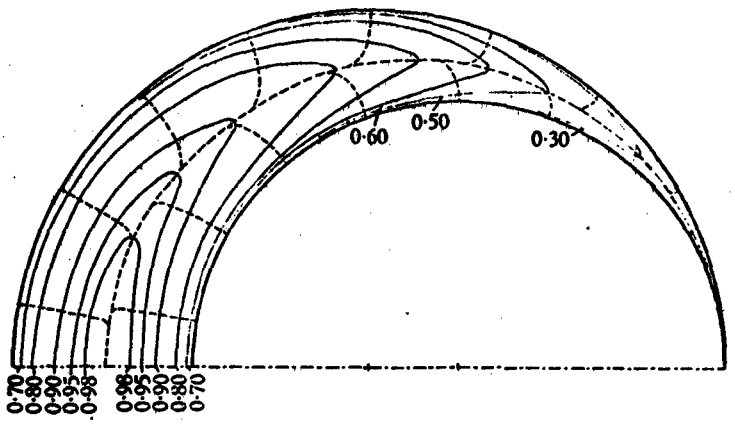

d/D = 0,75 ε = 1,0 R_{ea} = 33 600

Figure 7.28 (From Johnsson and Sparrow (reference 24))

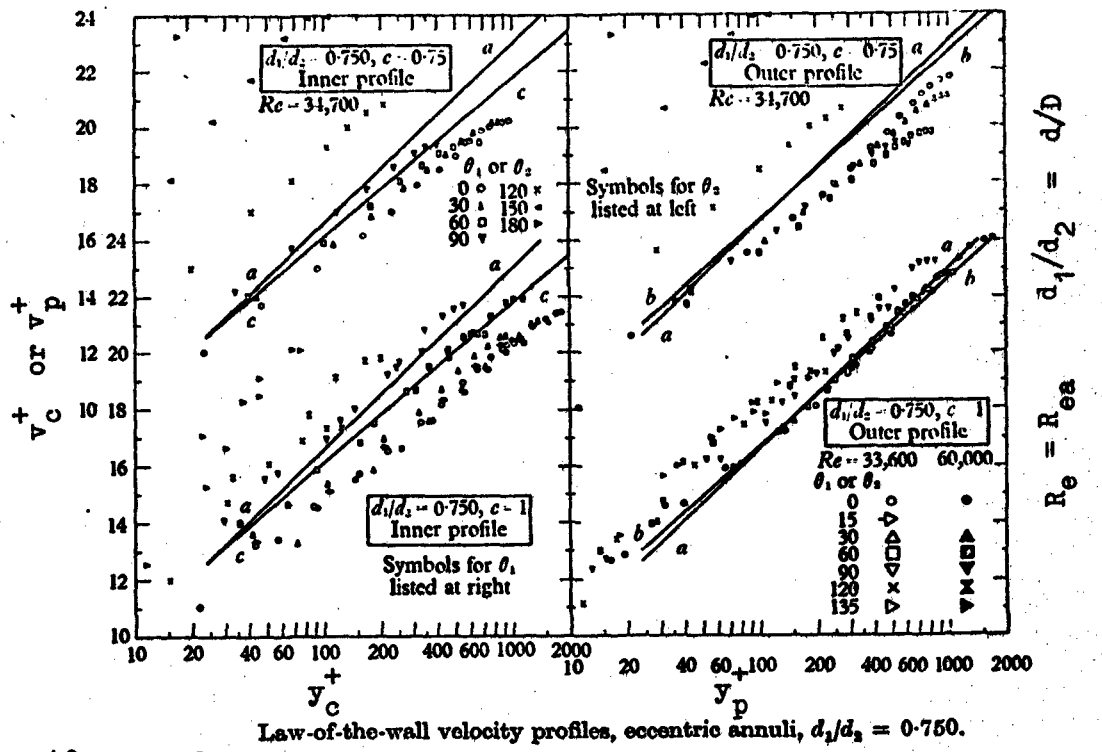

Law-of-the-wall velocity profiles, eccentric annuli, d_1/d_2 = 0·750.

θ_1 or θ_2 = angle around annulus from lowest point.

Figure 7.29 (From Jonsson and Sparrow (reference 24))

nificantly higher than the line given by equation(7.86), both for inner and outer profiles. For smaller diameter ratios there is little similarity between the data and the above equation.

An alternative representation is given as the velocity defect law;

$$\frac{v_{max} - v}{v_*} = -2{,}44 \ln \frac{y}{\Delta} + 0{,}8 + h\left(\frac{y}{\Delta}\right)$$

This is the equation given by Hinze for circular pipes, where $h(y/\Delta)$ is a correction factor and Δ is the distance between the wall and maximum velocity. The equation is superimposed on the data of Jonsson and Sparrow. For a given value of θ, v_{max} is the maximum velocity in a direction normal to the wall at that θ, and Δ is the distance from the wall to the local maximum velocity. The agreement between Hinze's equation and the data is somewhat better than for the "law of the wall". There are significant departures of the data from the "defect law" at larger values of θ and smaller values of y/Δ. The defect law itself has been found not to hold at small distances from the wall, even in pipes. The use of the defect law requires the magnitude and location of the maximum velocity in a direction normal to the wall as well as the local wall shear. Only the latter is needed for the law of the wall.

10.3 Circunferential pressure variation and entrance lengths

Jonsson and Sparrow also found slight circumferential variation of pressure, in the fully developed flow region. However, they did find that hydrodynamic entrance lengths, defined as the distance from the inlet to within 2 per cent of the fully developed pressure gradient value, to be rather large. Jonsson and Sparrow showed that the hydrodynamic entrance length increases as d/D and eccentricity increase.

10.4 Summary

Flow in annuli has been discussed and the following conclusions are drawn.

It is obvious that the conventional approach of the hydraulic mean radius concept cannot be applied to concentric and eccentric annuli, because of shear stress variation.

The standard friction equation assumes that the shear stress equation is constant from point to point around the circumference. If the skin friction stress varies around the perimeter of a conduit, the local friction factor must also change.

The overall friction factor (f) represents the integrated effect of the local values on the pressure drop and may bear a complex relation to the physical situation. Thus, the hydraulic mean radius concept is likely to be successful only where there is uniform shear stress.

Even in the case of a concentric annulus it is obvious that the hydraulic mean radius concept cannot apply. An infinitely thin wire in the centre of a pipe would have no effect on the hydraulic mean radius yet the velocity at the centre would be zero. For a plain pipe the velocity is a maximum at the centre.

11. Present experiments and analysis of flow in the annulus

As has been pointed out previously, the concept of the hydraulic mean radius is associated with uniform shear stress around the perimeter of the section. Even in the case of the concentric annulus, the shear stress on the pipe wall is not equal to the shear stress on the capsule (or core) wall and the conventional approach has been found by many investigators to give results which do not lie on the universal friction factor - Reynolds number graph. In the eccentric annulus case, it is even more apparent that the use of an unmodified hydraulic mean radius lacks justification. The most reliable experiments in the eccentric annulus are probably those of Bourne et al (see Figure 7.25 and 7.27) whose results agreed well with Denton and Dodge. Their (Bourne et al) method of presentation yielded changes in friction factor as diameter ratio varied.

11.1 Empirical approach from present experimental results

The procedure adopted was that in which the Blasius equation is assumed to be valid and a pseudo hydraulic mean radius is used to achieve this conformity. The representative velocity is chosen to be the mean velocity in the annulus $(\bar{v}_a)$.

The present series of tests on static eccentric and concentric annuli were carried out for diameter ratios in the range 0,542 to 0,85.

Assume that Darcy's equation may be written in the form

$$\Delta h_{fa} = \frac{f L_c \bar{v}_a^2}{2g R_p} \qquad (7.91)$$

where Δh_{fa} is defined in Section 3.3 and where R_p is a pseudo hydraulic mean radius or characteristic length dimension and f is a smooth pipe frictional coefficient related to a Reynolds number (R_e) by the Blasius equation.

$$f = \frac{0,079}{R_e^{0,25}} \qquad (7.92)$$

Reynolds number being defined in this context for the annulus as

$$R_e = \frac{4 \bar{v}_a R_p}{\nu} \qquad (7.93)$$

The validation for writing equation (7.91) in terms of the pseudo hydraulic mean radius is given in Chapter 13, Section 3.3.

From equations (7.91), (7.92) and (7.93) we obtain;

$$R_p = \left[\frac{0,079}{\left[\frac{4 \bar{v}_a}{\nu}\right]^{\frac{1}{4}}} \cdot \frac{1}{\frac{\Delta h_{fa}}{L_c} \Big/ \frac{\bar{v}_a^2}{2g}} \right]^{4/5} \qquad (7.94)$$

Experimental results for R_p at different annular velocities and diameter ratios from Figures 9.1 and 9.2, Chapter 9, are plotted against the conventional hydraulic mean radius R (see Figure 9.13, Chapter 9). The effect of velocity is slight and over a working range, a linear correlation for eccentric annuli

$$R_p = 1,25 \, R$$

appears valid.

Figure 9.13 contains results from the experiments of Bourne et al from Figure 7.25 as well as the present results and these are confirmatory.

Inserting the value $R_p = 1,25R$ in Blasius's equation gives;

$$f = \frac{0,316}{[1,25(D - d)\,\tau_a/\nu]^{0,25}} \qquad (7.95)$$

for fully eccentric annular flow.

Combining equation (7.95) with Darcy's equation, gives the following head loss equation;

$$\frac{\Delta h_{fa}}{L_c}\Big/\frac{\tau_a}{2g} = 0,239\Big/\left[\left(\frac{\tau_a}{\nu}\right)^{0,25}(D - d)^{1,25}\right] \qquad (7.96)$$

The graphical verification of this equation is shown on Figure 9.14, Chapter 9.

For concentric annuli the pseudo hydraulic mean radius is taken as

$$R_p = 0,81\ R$$

This is discussed further in Chapter 9.

12. Analytical verification of annular head loss relations

The concentric and eccentric annular flow experiments carried out for this thesis will be compared with other results from the literature in Chapter 13.

In order to find an analytical verification of the pseudo hydraulic mean radius concept, the method of quasi-concentric polar co-ordinates (as formulated in Section 2.2) was applied to pressure flow in the annulus.

A brief outline of pressure flow in the annulus has been given in Section 1.2.1 where it was shown that in the general case the flow in the annulus may be both laminar, in certain zones, and turbulent, in others, see Figure 7.3, Section 1.2.1.2.

Laminar flow in the concentric and eccentric annuli has been discussed in Sections 6 and 7.

In order to analyse the general case, and in the theory described below the concentric and fully eccentric annuli will be treated as special instances of the general case, it is necessary to decide on expressions for the velocity distribution in annular turbulent flow, the radius of maximum velocity in turbulent flow and a Reynolds number criterion for distinguishing between gross laminar and turbulent flow.

12.1 Determination of radius of maximum velocity

As has been pointed out earlier (Section 9.2), the experimental determination of the radius of maximum velocity in turbulent flow (r_{mt}) is very difficult and various results have been given for concentric annuli.

The only literature available on the contour of maximum velocity in eccentric annuli is that of Jonsson and Sparrow (reference 25) and Wolffe and Clump (reference 66).

In the present analysis of the flow in a general eccentric annulus the radius of maximum velocity is determined from the following iterative procedure.

1. Assume for each quasi-concentric slice of annulus a value for the radius of maximum velocity, say equal to the r_m value in laminar flow (r_{ml}).
2. From a force balance on the areas between r_{mt} and the pipe radius (r_p), and the capsule radius (r_c) and r_{mt} respectively, the shear stresses on the capsule and pipe walls can be calculated from assumed values of the pressure gradient.
3. From the capsule and pipe shear stresses the velocity distribution, and hence the velocity at radius r_m can be calculated with respect to each wall, i.e. $v_{max\ c}$ (for the capsule) and $v_{max\ p}$ (for the pipe).

4. If these velocities do not agree, the radius of maximum velocity is altered and the procedure is repeated until $v_{max\ c}$ and $v_{max\ p}$ coincide to within some prescribed limit. For the initial iteration $v_{max\ c}$ and $v_{max\ p}$ are not maximum velocities.

12.2 Determination of velocity distribution

After the radius of maximum velocity has been found, the velocity distribution for each quasi-concentric annular slice can be determined.

After an extensive study of velocity distributions obtained by various investigators, it was decided to consider a three-part velocity distribution law.

Some authors (e.g. Ross, reference 54) consider as many as six different regions, viz., laminar sub-layer, buffer zone, inner turbulent region, blending region and outer turbulent region.

For the eccentric annulus analysis, various velocity distribution laws were fed into the computer programme and the best agreement with present experimental results, when using quasi-concentric polar co-ordinates and the finite element method of analysis, (as described in Section 14) were obtained with the velocity distribution equations of Knudsen and Katz in the core region.

The following equations are chosen:

(1) Laminar sub-layer;

$$v_n^+ = y_n^+ \qquad (\text{for } y_n^+ < 5{,}0) \tag{7.72}$$

(2) Transition zone;

The values for A and B in the transition zones adjacent to the pipe and capsule walls are found by combining the velocity distribution laws in the laminar and core regions (see Appendix II). For example the values of A and B in the transition region adjacent to the pipe wall are given by;

$$A_{Tp} = (A_p \log 30 + B_p - 5)/\log 6 \qquad (7.97a)$$

and $$B_{Tp} = 5 - A_{Tp} \log 5 \qquad (7.97b)$$

The values of A and B in the transition zone adjacent to the capsule wall are similarly calculated (Appendix II).

The extent of the transition zone is given by; $30 > y_n^+ > 5$.

(3) Core region;

Capsule profile $$v_p^+ = 4{,}4 \log_{10} y_p^+ + 6{,}2 \qquad (7.98)$$

Pipe profile $$v_c^+ = 6{,}1 \log_{10} y_c^+ + 3{,}0 \qquad (7.99)$$

$$\text{for } y_n^+ > 30$$

where subscript n = p or c.

The results of the analysis and comparison with experiment is given in Chapter 13.

12.3 Flow in eccentric annulus

The flow can be calculated by considering the flow through each quasi-concentric annular slice.

$$Q_a = \int_{r_m}^{r_p} \int_{o}^{2\pi} v_p \, r\,dr\,d\theta + \int_{r_c}^{r_m} \int_{o}^{2\pi} v_c \, r\,dr\,d\theta \qquad (7.100)$$

where v_p and v_c are the point velocities at the mid-point of sub-slice area $r(dr\ d\theta)$ for the pipe wall and capsule wall velocity distribution respectively.

The integration is carried out both from the pipe and capsule wall to the point where the maximum velocity occurs (r_{mt}) in turbulent flow.

The integrated flow for turbulent pressure flow can then be added to the laminar component, which exists towards the bottom of the eccentric annulus.

13. Reynolds number in annular flow

Since the type of pressure flow existing in various zones of an

eccentric annulus can vary from laminar, where the gap between capsule and pipe wall is small, to turbulent, where the gap is large, it is necessary to establish a criterion for determining the angle θ (see Section 2.2) at which the flow changes from laminar to turbulent.

This transition, in practice, is naturally gradual but for the purposes of analysis is assumed to occur when Reynolds number, in a quasi-concentric annular slice, exceeds a certain value.

From an examination of the literature on concentric annuli, it appears as though the transition from laminar to turbulent flow occurs more gradually (when considering a conventional friction factor versus Reynolds number diagram) than for pipe flow. The critical value of Reynolds number appears to be between 2 000 and 3 000 and it is reasonable to assume a value of 2 400 as for circular pipe flow.

The Reynolds number for a concentric annular section is defined as

$$R_e = \frac{\rho v_{ap}(D - d)}{\mu} \qquad (7.102)$$

For a quasi-concentric annular slice, the Reynolds number can be determined as follows:

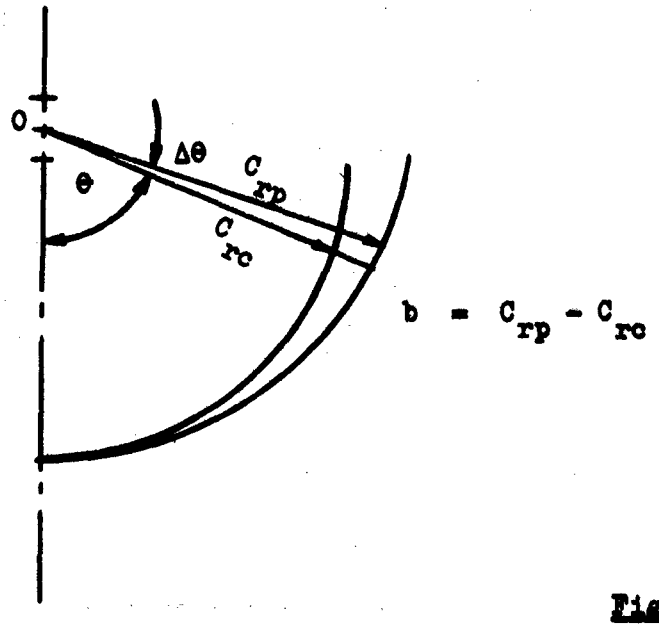

Figure 7.30

Hydraulic mean radius (R_q) = $\frac{\text{area of section}}{\text{wetted perimeter}}$

$$\therefore \quad R_q = \frac{\frac{(C_{rp} + C_{rc})}{2} \Delta\theta \; b}{(C_{rp} + C_{rc}) \Delta\theta} = \frac{b}{2} \qquad (7.101)$$

The Reynolds number for the quasi-concentric annular slice (R_{eq}) is;

$$R_{eq} = \frac{4 R_q v_{ap}}{\nu}$$

$$\therefore \quad R_{eq} = \frac{2 b v_{ap}}{\nu} \qquad (7.102)$$

The Reynolds number for the quasi-concentric annular slice agrees with the concentric annular case since in this instance

$$b = \frac{D - d}{2}$$

for the critical value of R_{eq}, v_{ap} is the mean velocity in the slice for laminar flow.

14. <u>Procedure for analysing turbulent flow in the eccentric annulus</u>

The expressions governing annular flow have been formulated and the analytical procedure for solving the problem can now be described.

(1) The following parameters are chosen:

(a) The pressure gradient ($\Delta P/L$)

(b) The diameter ratio (d/D),

(c) The eccentricity e.

(2) Quasi-concentric section properties are evaluated as described in Section 2.2

(3)

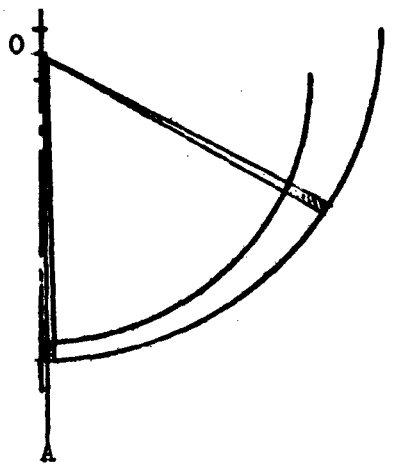

Figure 7.31

Starting from the mid-radius, of the first slice, 0A the velocity in laminar flow is determined from equation (7.45).

(4) The Reynolds number for the section can then be calculated from equation (7.102) and the velocity above.

(5) If the Reynolds number is less than a prescribed value (2 400) the flow can be calculated from

$$\Delta Q = v_{ap} \Delta A \tag{7.103}$$

(6) The shear stress on the pipe and capsule walls can be calculated from $\tau_n = \mu(dv/dy)_n$
where $(dv/dy)_n$ is the velocity gradient at the capsule wall $(dv/dy)_c$ or pipe wall $(dv/dy)_p$.

(7) These shear values can then be checked by a force balance. (This is simply a check built into the computer programme).

$$(\frac{\Delta P}{L}) \Delta A = \tau_{cp} \Delta S_c + \tau_{pp} \Delta S_p \tag{7.104}$$

where ΔS_c = elemental length of capsule perimeter,

ΔS_p = elemental length of pipe perimeter.

(8) If the Reynolds number is greater than 2 400, r_{ml} can be determined from equation (7.41). For a first approximation $r_{mt} = r_{ml}$.

(9)

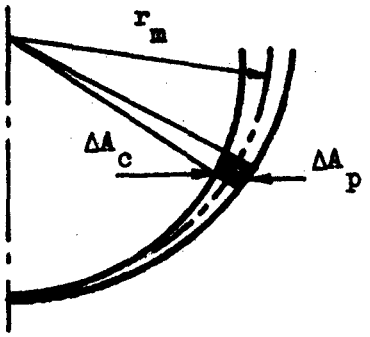

A force balance is applied to the quasi-concentric slice in turbulent flow thus;

$$(\frac{\Delta P}{L}) \Delta A_c = \tau_{cp} \Delta S_c \tag{7.105}$$

and

$$(\frac{\Delta P}{L}) \Delta A_p = \tau_{pp} \Delta S_p \tag{7.106}$$

(10) From equations (7.105) and (7.106)

$$\frac{\tau_{pp}}{\tau_{cp}} = \frac{\Delta A_p}{\Delta A_c}\,\frac{\Delta S_c}{\Delta S_p} = \left[\frac{r_p^2 - r_m^2}{r_m^2 - r_c^2}\right]\frac{r_c}{r_p} \qquad (7.107)$$

and

$$\frac{v^+_{c\ max}}{v^+_{p\ max}} = \frac{v_{c\ max}}{v_{p\ max}}\,\frac{v_{*\ p}}{v_{*\ c}}$$

For

$$v_{c\ max} = v_{p\ max}$$

$$\frac{v^+_{c\ max}}{v^+_{p\ max}} = \frac{v_{*\ p}}{v_{*\ c}} = \sqrt{\frac{\tau_{pp}}{\tau_{cp}}} \qquad (7.108)$$

From equations (7.107), (7.108) and (7.87) and (7.88) or the equivalent velocity distribution equations

$$\sqrt{\frac{r_p^2 - r_m^2}{r_m^2 - r_c^2}\,\frac{r_c}{r_p}} = \frac{4{,}4 \log y_c^+ + 6{,}2}{6{,}1 \log y_p^+ + 3{,}0} \qquad (7.109)$$

at $y = r_m$

where $y_c^+ = \dfrac{v_{*_c}\, y_c}{\nu}$ and $y_p^+ = \dfrac{v_{*_p}\, y_p}{\nu}$

where $v_{*_c} = \sqrt{\dfrac{\tau_{cp}}{\rho}}$

and $v_{*_p} = \sqrt{\dfrac{\tau_{pp}}{\rho}}$

(11) From equation (7.109) the radius of maximum velocity (r_m) can be found by an iterative process.

(12) For each sub-area (Δa) flow can be calculated by considering the velocity profile relative to the pipe and capsule respectively.

(13) The mean velocity in the annulus for pressure flow is then determined from

$$\bar{v}_{ap} = \frac{4}{\pi(D^2 - d^2)}\left[\int_{r_c}^{r_m}\int_{\theta_{LT}}^{2\pi} v_c r\, dr\, d\theta + \int_{r_m}^{r_p}\int_{\theta_{LT}}^{2\pi} v_p r\, dr\, d\theta + \int_{r_c}^{r_p}\int_{o}^{\theta_{LT}} vr\, dr\, d\theta\right] \qquad (7.110)$$

where the first two terms on the right hand side are for turbulent and the third term is for laminar flow. The angle $\theta_{L/T}$ is the angle at which the flow changes from laminar to turbulent.

(14) The gross friction factor and Reynolds number for the eccentric annulus can be determined from

$$f = \left(\frac{\Delta P}{L}\right) \frac{(r_p - r_c)}{\rho \bar{V}_{ap}^2} \qquad (7.111)$$

(15) To check with the pseudo hydraulic mean radius concept, calculate f from Δh_f and R_e from 1,25R.

15. End effects

For an individual capsule of finite length there are end effects contributing to total head loss components, both at the leading face and the tail end of the capsule.

These end effects must be apparent in both the stationary and mobile capsule cases. In both cases the inlet and outlet head losses may be considered as functions of the mean water velocity relative to the capsule.

Experimental coefficients were determined in the former case (for static capsules) and will be extended later to dynamic capsules.

The end effects assume a greater or lesser significance depending on the length of the capsule and compared with annular losses, have a smaller role as length of capsule increases.

15.1 Static capsule - inlet energy loss

The inlet head loss will be discussed in detail in Chapter 9. At this stage it is sufficient to state that non-dimensional values of the inlet head loss are expressed as $\frac{\Delta h_i}{\bar{V}^2/2g}$ and an empirical equation representing the experimental results for the static capsule values is;

$$\frac{\Delta h_i}{\bar{V}^2/2g} = k' \qquad (7.112)$$

In Chapter 9 it will be shown that the value for k' is given by

$$k'_e = 22(d/D)^6 \qquad (7.113)$$

for eccentric annuli.

No simple correlation was found for concentric annuli and a polynomial of degree four was evaluated by computer;

$$k'_c = -28{,}37\left(\frac{d}{D}\right) + 180{,}37\left(\frac{d}{D}\right)^2 - 364{,}60\left(\frac{d}{D}\right)^3 + 244{,}15\left(\frac{d}{D}\right)^4 \qquad (7.114)$$

15.2 Energy losses at outlet

The results of experiments on outlet head losses for static capsules will be dealt with in Chapter 9 where it will be shown that outlet losses can be expressed in the form;

$$\frac{\Delta h_o}{\bar{V}^2/2g} = \left[\frac{1}{1 - \left(\frac{d}{D}\right)^2} - 1\right]^2 \qquad (7.115)$$

An empirical fit to the experimental results yields;

$$\frac{\Delta h_o}{\bar{V}^2/2g} = 0{,}68\left[\frac{1}{1 - \left(\frac{d}{D}\right)^2} - 1\right]^2 \qquad (7.116)$$

for eccentric annuli. For concentric annuli the constant in the above equation becomes 1,15 (see Chapter 9).

The three equations, (7.96), (7.113) and (7.116) are adequate for calculating the excess head loss across a static eccentric capsule in the workable range, viz.,

$$\Delta H_{cs} = \Delta h_{fa} + \Delta h_i + \Delta h_o - h_{fc} \qquad (7.117)$$

The appropriate values can also be used in equation (7.117) for calculating the head loss across a concentric annulus

16. Incipient motion

The following section is concerned with the interaction of the capsule and surrounding flow at incipient capsule motion.

The incipient velocity ($\bar{V}_i$) is defined as the mean water velocity when the capsule is just on the threshold of movement. At this velocity the

total drag on the capsule (form drag and skin friction) just exceeds the solid to solid friction between the capsule and pipe wall, for non-vertical pipes, plus the component of capsule weight down the slope in an upward sloping pipe. It will be shown later that, in general, for a given capsule diameter the incipient velocity increases with increasing capsule length or density and the effect of increasing capsule diameter is to lower the incipient velocity.

The corresponding incipient head loss is defined as the excess head loss across a length of pipeline containing a capsule compared with the same length of capsule-free pipe, both measured at the incipient velocity.

The threshold of capsule movement is studied because it is the limiting condition of the mobile capsule case and a study of incipient conditions yields one extreme point on the excess head loss as a function of mean water velocity curves. The analysis gives the water velocity at which capsules first begin to move and experiments with mobile capsules will be shown to support the equation when extrapolated to zero capsule velocity.

It will be shown in Chapter 10 that the relation between mean water velocity and capsule velocity involves the incipient velocity as one variable.

Flow conditions around static capsules have been shown to be amenable to analysis when supplemented by experimental coefficients and the incipient case indicates a possible form of empirical equation for excess energy loss when the capsules are moving. This will be discussed further in Chapters 14 and 15.

16.1 Momentum and energy principles applied to incipient conditions

Some of this material has already been published with the prior consent of the supervisor (see Lazarus and Kilner reference 31).

Applying the momentum equation to the water in the static capsule case yields (see Figure 7.32)

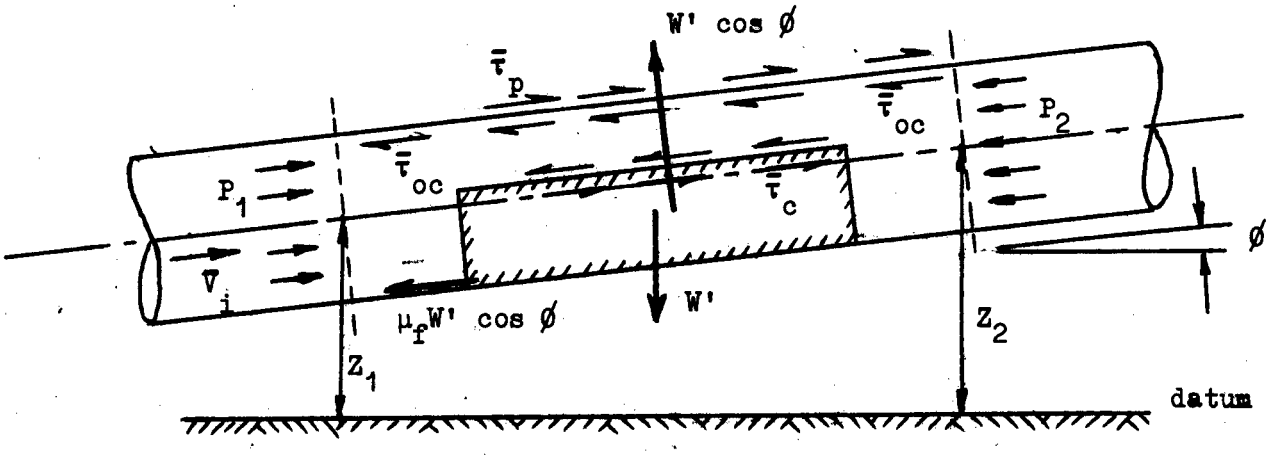

Force diagram for capsule at incipience

Figure 7.32

$$(P_1 - P_2)\frac{\pi D^2}{4} = \bar{\tau}_{oc}\,\pi D(L_1 + L_2) + \bar{\tau}_p\,\pi D L_c + (\bar{\tau}_c\,\pi d L_c + D_f) + w\left[\frac{\pi D^2}{4}(L_1 + L_2 + L_c) - \frac{\pi d^2}{4}L_c\right]\text{Sin}\,\emptyset \qquad (7.118)$$

where $\bar{\tau}_{oc}$ = mean shear stress on the wall of the pipe in the curvilinear flow region just upstream and just downstream of the capsule.

L_1 = length over which curvilinear flow takes place upstream of the capsule.

L_2 = length over which curvilinear flow occurs downstream of the capsule

$\bar{\tau}_p$ = mean wall shear stress on the pipe in the eccentric annular section.

$\bar{\tau}_c$ = mean shear stress on capsule.

D_f = form drag on the capsule.

and the last term on the right hand side

i.e. $w\left[\frac{\pi D^2}{4}(L_1 + L_2 + L_c) - \frac{\pi d^2}{4}L_c\right]\text{Sin}\,\emptyset$ is the component of water weight down the slope in the control volume.

The total forward drag on the capsule is the sum of the skin friction and form drag,

$$D_T = D_f + \bar{\tau}_c \pi d L_c \tag{7.119}$$

Equation (7.118) can be written as,

$$\frac{\pi D^2}{4}[(P_1 - P_2) - w(Z_2 - Z_1)] = \Sigma \text{ wall forces} + D_T - \frac{\pi d^2}{4} w L_c \sin \phi \tag{7.120}$$

where, Σ wall forces $= \bar{\tau}_{oc} \pi D(L_1 + L_2) + \bar{\tau}_p \pi D L_c$

$$\therefore \frac{\pi D^2 w}{4}\left[\left(\frac{P_1}{w} + Z_1\right) - \left(\frac{P_2}{w} + Z_2\right)\right] = \Sigma \text{ wall forces} + D_T - W_b \sin \phi \tag{7.121}$$

where W_b = buoyancy force on capsule.

For equilibrium of the capsule at incipience;

$$D_T = \mu_f W' \cos \phi + W' \sin \phi \tag{7.122}$$

where W' = submerged weight of capsule $= W - W_b$

μ_f = solid to solid static friction factor.

From equations (7.121) and (7.122)

$$\frac{\pi D^2 w}{4}\left[\left(\frac{P_1}{w} + Z_1\right) - \left(\frac{P_2}{w} + Z_2\right)\right] = \Sigma \text{ wall forces} + \mu_f W' \cos \phi + W' \sin \phi \tag{7.123}$$

Applying the energy equation to the sloping pipe;

$$\left(\frac{P_1}{w} + Z_1\right) - \left(\frac{P_2}{w} + Z_2\right) = \Delta h_{fa} + \Delta h_i + \Delta h_o + \frac{4}{Dw} \bar{\tau}_{oc}(L_1 + L_2) \tag{7.124}$$

Combining equations (7.123) and (7.124) to eliminate $\left(\frac{P_1}{w} + Z_1\right) - \left(\frac{P_2}{w} + Z_2\right)$ and inserting the separate Σ wall forces terms, yields

$$\frac{\pi D^2 w}{4}\left[\Delta h_{fa} + \Delta h_i + \Delta h_o - \frac{\bar{\tau}_p 4 L_c}{Dw}\right] = \mu_f W' \cos \phi + W' \sin \phi$$

$$\therefore \frac{\Delta h_{fa} + \Delta h_i + \Delta h_o}{L_c} - \frac{\bar{\tau}_p 4}{wD} = \frac{4}{\pi D^2 w L_c}[\mu_f W' \cos \phi + W' \sin \phi] \tag{7.125}$$

Now for horizontal pipes

$$\frac{\Delta h_{fa} + \Delta h_i + \Delta h_o}{L_c} - \frac{\bar{\tau}_p 4}{wD} = \mu_f \left(\frac{d}{D}\right)^2 |S_c - 1| \tag{7.126}$$

where S_c = specific gravity of the capsule and the term $|S_c - 1|$ indicates that friction may act along the top of the pipe wall where $S_c < 1{,}0$.

The first three terms on the left hand side are given by equations

(7.96), (7.112) and (7.116).

For the wall shear stress on the pipe in the annular section ($\bar{\tau}_p$), the following equation applies:

$$w\Delta h_{fa}\pi\left(\frac{D^2 - d^2}{4}\right) = \bar{\tau}_p\,\pi D L_c + \bar{\tau}_c \pi d L_c \qquad (7.127)$$

For a static capsule and pipe wall having the same frictional shear stress;

$$\bar{\tau}_p = \bar{\tau}_c \qquad (7.128)$$

This is within about 8 per cent for $d/D > 0{,}54$ and improves as $d/D \rightarrow 1$ for unit eccentricity (see Figure 8.13).

$$\therefore \quad \frac{\bar{\tau}_p}{w}\frac{4}{D} = \frac{(D - d)}{D}\,\frac{\Delta h_{fa}}{L_c}$$

$$\therefore \quad \frac{\Delta h_{fa}}{L_c} - \frac{\bar{\tau}_p}{w}\frac{4}{D} = \left(\frac{d}{D}\right)\frac{\Delta h_{fa}}{L_c} \qquad (7.129)$$

Inserting equation (7.129) in equation (7.126) gives;

$$\left(\frac{d}{D}\right)\frac{\Delta h_{fa}}{L_c} + \frac{\Delta h_i}{L_c} + \frac{\Delta h_o}{L_c} = \mu_f\left(\frac{d}{D}\right)^2 \left|S_c - 1\right| \qquad (7.130)$$

and the inherent assumption in this equation is that the mean shear stress value in the eccentric annulus is the same for the capsule and pipe wall.

16.2 Equation for determining the incipient velocity ($\bar{V}_i$)

From equations (7.96) and (7.129) and the relation between $\bar{V}$ and $\bar{V}_a$ for static capsules, viz.

$$\bar{V}_a = \bar{V}/\left[1 - \left(\frac{d}{D}\right)^2\right] \qquad (7.131)$$

we obtain;

$$\Delta h_{fa}\left(\frac{d}{D}\right) = \left(\frac{d}{D}\,L_c\right)\left[\frac{0{,}239\,\bar{V}^{1,75}\,\nu^{0,25}}{2g(D - d)^{1,25}\left[1 - \left(\frac{d}{D}\right)^2\right]^{1,75}}\right] \qquad (7.132)$$

Thus equation (7.126) becomes;

$$C_1\,\bar{V}_i^{1,75} + C_2\,\bar{V}_i^2 - C_3 = 0 \qquad (7.133)$$

where

$$C_1 = \left(\frac{d}{D} L_c\right) \frac{0,239\ \nu^{0,25}}{[1 - (\frac{d}{D})^2]^{1,75}(D - d)^{1,25}\ 2g} \tag{7.134}$$

$$C_2 = \frac{1}{2g}\left[22\ (\frac{d}{D})^6 + 0,68\left[\frac{1}{1 - (\frac{d}{D})^2} - 1\right]^2\right] \tag{7.135}$$

$$C_3 = \mu_f\ L_c(\frac{d}{D})^2\ |S_c - 1| \tag{7.136}$$

Equation (7.133) and (7.117) were solved for $\bar{V}_i$ and ΔH_{cs} on the Univac 1106 computer for $\mu_f = 0,32$ determined experimentally (see Chapter 10) and different values of diameter ratio (d/D), capsule length to diameter ratio (L_c/d) and capsule specific gravity (S_c) as well as different pipe diameters. A comparison with experimental results will be given in Chapter 14.

16.3 Incipient motion in vertical pipes

In vertical pipes the solid to solid friction term falls away and the inlet, outlet and annular head loss terms are modified and not equal to those for fully eccentric capsules.

Equation (7.125) yields, for vertical pipes;

$$\Delta h_{fa} + \Delta h_i + \Delta h_o - \frac{\bar{\tau}_p\ 4L_c}{wD} = (\frac{d}{D})^2\ |S_c - 1|\ L_c \tag{7.137}$$

where

$$\Delta h_{fa} = \frac{0,079\ (\nu)^{0,25}\ L_c\ \bar{V}_i^{1,75}}{2\ \{0,2(D - d)\}^{1,25}(2g)[1 - (\frac{d}{D})^2]^{1.75}} \tag{7.138}$$

$$\Delta h_i = k_c'\ \bar{V}_i^2/2g \tag{7.139}$$

k_c' is given by equation (7.114)

$$\Delta h_o = 1,15\left[\frac{1}{1 - (\frac{d}{D})^2} - 1\right]^2 \frac{\bar{V}_i^2}{2g} \tag{7.140}$$

The equation for excess head loss, equation (7.117), can be inserted in equation (7.137) and the excess head loss in a vertical pipe becomes;

$$(\Delta H_c)'_{is} = \Delta h_a + \Delta h_i + \Delta h_o \tag{7.141}$$

$$= (\frac{d}{D})^2\ |S_c - 1|\ L_c + \frac{\bar{\tau}_p\ 4L_c}{Dw} - h_{fc} \tag{7.142}$$

where $(\Delta Hc)'_{is}$ is the total excess head loss in a non-horizontal pipe.

Even though the first term on the right hand side of the above equation is reflected as a head difference on the differential pressure transmitter (or manometer) it is simply the head due to the submerged weight of the capsule and the fluid head loss is thus $(\Delta H_c)_{is}$ where;

$$(\Delta H_c)_{is} = \frac{\bar{\tau}_p \, 4L_c}{Dw} - h_{fc} \qquad (7.143)$$

From equation (7.129);

$$\frac{\bar{\tau}_p \, 4L_c}{wD} = \Delta h_{fa}(1 - \frac{d}{D})$$

$$\therefore \quad (\Delta H_c)_{is} = \Delta h_{fa}(1 - \frac{d}{D}) - h_{fc}$$

$$= \Delta h_a(1 - \frac{d}{D}) - \frac{d}{D} h_{fc} \qquad (7.144)$$

and $$(\Delta H_c)'_{is} = \Delta h_a(1 - \frac{d}{D}) - \frac{d}{D} h_{fc} + (\frac{d}{D})^2 \left| S_c - 1 \right| L_c \qquad (7.145)$$

From equations (7.141) and (7.145)

$$\Delta h_a + \Delta h_i + \Delta h_o = \Delta h_a(1 - \frac{d}{D}) - \frac{d}{D} h_{fc} + (\frac{d}{D})^2 \left| S_c - 1 \right| L_c$$

$$\therefore \quad \Delta h_i + \Delta h_o = (\frac{d}{D})^2 \left| S_c - 1 \right| L_c - \frac{d}{D}(\Delta h_a + h_{fc})$$

$$\therefore \quad \Delta h_i + \Delta h_o + \frac{d}{D} \Delta h_{fa} = (\frac{d}{D})^2 \left| S_c - 1 \right| L_c \qquad (7.146)$$

And, if equations (7.138), (7.139) and (7.140) as well as (7.131) are inserted in equation (7.146), this equation, together with equation (7.144) yields the incipient velocity and fluid excess head loss for capsules in a vertical pipe.

The solutions of incipient equations for horizontal, vertical and sloping pipelines are discussed in Chapter 14.

17. Mobile capsules

Up to this point the head loss in a pipeline, with a static capsule, has been determined and it has been shown that the excess head loss in the static capsule case consists of three components, i.e.

$$\Delta H_{cs} = \Delta h_a + \Delta h_i + \Delta h_o \qquad (7.117)$$

For investigations of solid to solid friction between the capsule and

pipe wall it has been shown that the limiting case of static capsules, i.e. incipient capsule motion, is also fully determined.

It remains now to extend the analysis to mobile capsules. Laminar flow in the annulus of a mobile capsule water system will first be dealt with in Section 18. In this section it will be proved that the flow in the annulus consists of two superimposable components, a pressure and a Couette component.

In order to extend the analysis yet further to turbulent flow in the eccentric annulus with end effects, in Sections 21 to 25, the Couette component in turbulent flow will first be analysed in Section 19.

18. Laminar flow in a concentric annulus with a moving core

Equation (7.28) which is a form of the Navier Stokes equation in cylindrical co-ordinates can now be applied to the case of laminar flow in the concentric annulus with a moving core.

$$\frac{dP}{dx} = -\frac{\mu}{r}\frac{d}{dr}\left(r\frac{dv}{dr}\right) \qquad (7.28)$$

Integrating twice, as before, yields;

$$\frac{dv}{dr} = -\frac{r}{2\mu}\frac{dP}{dx} + \frac{A}{r}$$

and
$$v = -\frac{1}{4\mu}\left(\frac{dP}{dx}\right) r^2 + A \ln r + B \qquad (7.147)$$

The boundary conditions now become;

$$v = 0 \quad \text{where} \quad r = r_p \quad \text{(pipe radius)}$$

$$v = V_c \quad \text{when} \quad r = r_c \quad \text{(capsule or core radius)}$$

$$B = \frac{1}{4\mu}\frac{dP}{dx} r_p^2 - A \ln r_p$$

and
$$V_c = -\frac{1}{4\mu}\left(\frac{dP}{dx}\right) r_c^2 + A \ln r_c + B$$

$$\therefore \quad A = \frac{1}{4\mu}\left(\frac{dP}{dx}\right)(r_p^2 - r_c^2)/\ln\left(\frac{r_p}{r_c}\right) - V_c/\ln\left(\frac{r_p}{r_c}\right)$$

substituting for A yields;

$$\frac{dv}{dr} = \frac{dP}{dx}\left[-\frac{r}{2\mu} + \frac{1}{4\mu r}\frac{(r_p^2 - r_c^2)}{\ln\left(\frac{r_p}{r_c}\right)}\right] - \frac{V_c}{r}\Big/\ln\left(\frac{r_p}{r_c}\right) \qquad (7.148)$$

note that $\tau = \mu\left(\frac{dv}{dr}\right)$

$$\therefore \quad \tau = \left(\frac{dp}{dx}\right)\left[-\frac{r}{2} + \frac{1}{4r}(r_p^2 - r_c^2)\Big/\ln\left(\frac{r_p}{r_c}\right)\right] - \mu\frac{V_c}{r}\Big/\ln\left(\frac{r_p}{r_c}\right) \qquad (7.149)$$

The first two terms on the right hand side are the same as for concentric annular flow and the third term is the subtracted effect due to capsule motion relative to the pipe.

Equation (7.149) shows that the shear due to pressure flow can be algebraically added to the shear due to Couette flow for laminar flow round concentric capsules. If $dP/dx = 0$ in equation (7.149), then the last term on the right hand side is due to Couette flow.

The shear stress at the capsule wall is;

$$\tau_c = \tfrac{1}{2}\frac{dP}{dx}\left[-r_c + \frac{(r_p^2 - r_c^2)}{2r_c\ln\left(\frac{r_p}{r_c}\right)}\right] - \frac{\mu V_c}{r_c}\Big/\ln\left(\frac{r_p}{r_c}\right) \qquad (7.150)$$

and a similar analysis in the outer zone yields the shear stress at the pipe wall;

$$\tau_p = \tfrac{1}{2}\frac{dP}{dx}\left[r_p - \frac{(r_p^2 - r_c^2)}{2r_p\ln\left(\frac{r_p}{r_c}\right)}\right] + \frac{\mu V_c}{r_p}\Big/\ln\left(\frac{r_p}{r_c}\right) \qquad (7.151)$$

$$\therefore \quad \tau_c = \tau_{cp} + \tau_{cc} \qquad (7.152)$$

$$\text{and} \quad \tau_p = \tau_{pp} + \tau_{pc} \qquad (7.153)$$

where τ_{cp} = shear stress on capsule wall due to pressure flow

τ_{cc} = shear stress on capsule wall due to Couette flow

τ_{pp} = shear stress on pipe wall due to pressure flow

τ_{pc} = shear stress on pipe wall due to Couette flow

Substituting for A and B in equation (7.147) yields;

$$v = \frac{1}{4\mu}\left(\frac{dP}{dx}\right)\left[(r_p^2 - r^2) + (r_p^2 - r_c^2)\ \ln\left(\frac{r}{r_p}\right)/\ln\left(\frac{r_p}{r_c}\right)\right] + V_c\ \ln\left(\frac{r_p}{r}\right)/\ln\left(\frac{r_p}{r_c}\right) \qquad (7.154)$$

If $V_c = 0$, the expression reduces to that for laminar flow in a concentric annulus.

The first two terms on the right hand side of equation (7.154) are those due to pressure flow and occur as long as there is a pressure gradient.

The third term is due to Couette flow and only occurs if $V_c \neq 0$

The total velocity vector at a point in concentric laminar flow with a moving core (or capsule) is thus shown to be composed of a pressure and a Couette component which can be algebraically added together.

Equation (7.154) is a general equation and does not imply that the capsule is travelling under the influence of the pressure gradient.

Equation (7.28) was also integrated by Charles (reference 10) but he did not arrive at the velocity expression given by equation (7.154). Charles obtained the following expression:

$$v = -\frac{1}{4\mu}\left(\frac{dP}{dx}\right)(r_p^2 - r^2) \qquad (7.155)$$

He must have made some assumption not mentioned in his paper since this is not the result of integrating equation (7.28).

It can be shown that equation (7.155) is applicable to a capsule with neutral buoyancy. A long cylindrical capsule in which end effects are ignored is considered to be travelling in a concentric position, relative to the pipe.

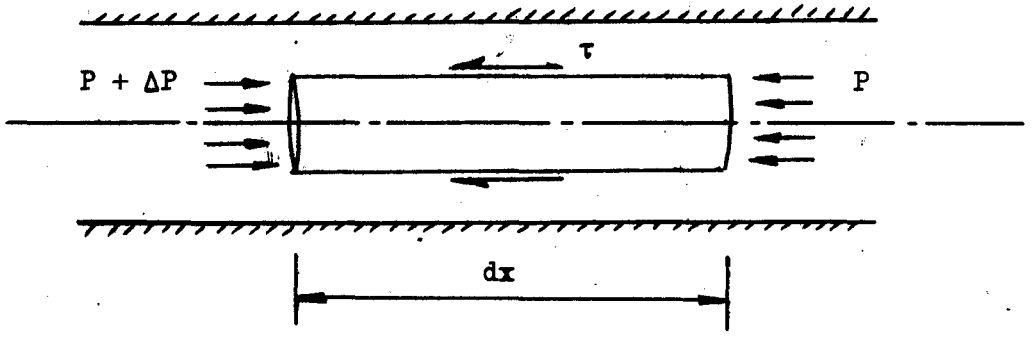

Figure 7.33

Summing forces on the capsule yields;

$$\Delta P\ \pi r^2 = -\mu\ 2\pi r(dx)\ \frac{dv}{dr}$$

$$\therefore \quad \frac{dv}{dr} = -\frac{r}{2\mu}\left(\frac{dP}{dx}\right)$$

Assuming $\left(\frac{dP}{dx}\right)$ = constant and integrating gives;

$$v = -\left(\frac{dP}{dx}\right)\ \frac{r_p^2 - r^2}{4\mu} \qquad (7.155)$$

where $r > r_c$

This is the same equation arrived at by Charles using a more complicated technique and inserting some assumption not mentioned in his paper.

The difference between equation (7.155) and equation (7.154) is that there is an implication inherent in equation (7.155) that the pressure drop along the capsule is balanced by the shear stress on the capsule wall. This is true if the only forces acting on the capsule are the pressure and shear forces along the capsule. The only case when this assumption is applicable is the neutrally buoyant capsule (laminar flow) and the velocity distribution reaches a maximum value at the capsule. (See Figure 7.34a)

In a vertical or sloping pipe equation (7.154) applies, since there is an additional force acting on the capsule, due to the component of capsule weight, and the velocity can reach a maximum in the annulus (see Figure 7.34b).

Equation (7.154) applies to non-neutrally buoyant capsules since there is an additional force due to solid to solid friction and the component of capsule weight. This argument applies to eccentric capsules only and the analysis was for concentric capsules. However, the analysis is extended to cover the eccentric annulus case by means of the quasi-concentric annulus concept. Charles's equation thus has a very limited application and equation (7.154) developed in this section is far more general.

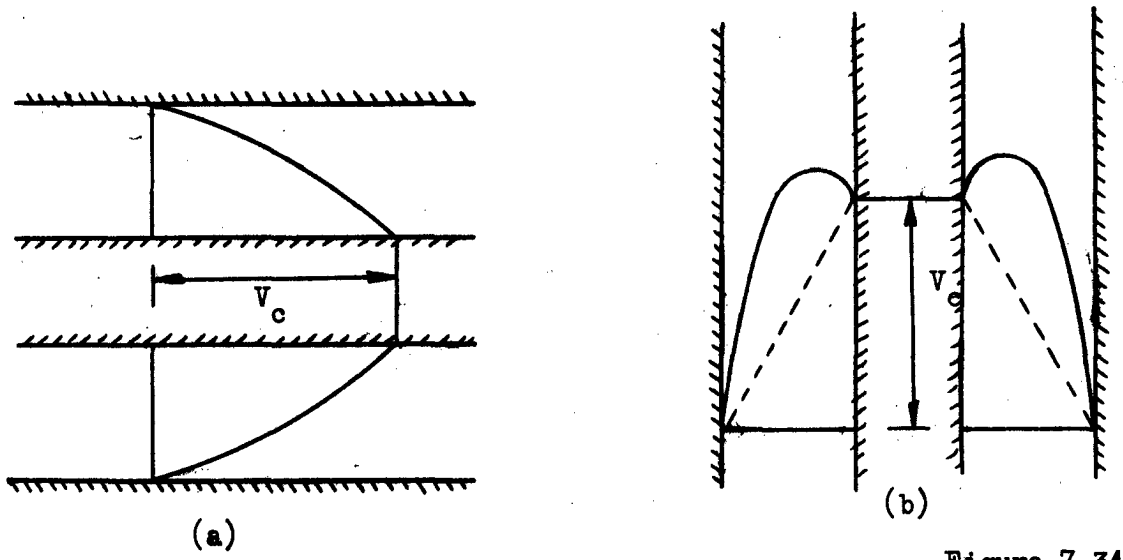

Figure 7.34

18.1 Discharge in the annulus of an infinitely long concentrically orientated capsule (moving at velocity V_c) in laminar flow.

Laminar flow in the annulus (Q_a), can be obtained in the following manner, where the point velocity (v) is from equation (7.154).

$$Q_a = 2\pi \int_{r_c}^{r_p} vr\, dr$$

$$= \frac{2\pi}{4\mu}\left(\frac{dP}{dx}\right) \int_{r_c}^{r_p} \left[(r_p^2 - r^2) + \frac{r_p^2 - r_c^2}{\ln\left(\frac{r_p}{r_c}\right)} \ln\left(\frac{r}{r_p}\right)\right] r\, dr$$

$$+ 2\pi \int_{r_c}^{r_p} V_c \left[\ln\left(\frac{r_p}{r}\right) / \ln\left(\frac{r_p}{r_c}\right)\right] r\, dr$$

Now $$\int \ln\left(\frac{r_p}{r}\right) r\, dr = \frac{r^2}{2} \ln\left(\frac{r_p}{r}\right) - \int \frac{r^2}{2}\left(-\frac{r_p}{r^2}\right)\left(\frac{r}{r_p}\right) dr$$

$$= \frac{r^2}{2} \ln\left(\frac{r_p}{r}\right) + \frac{r^2}{4} = \frac{r^2}{2}\left[\ln \frac{r_p}{r} + \tfrac{1}{2}\right]$$

and $$\int \ln\left(\frac{r}{r_p}\right) r\, dr = \frac{r^2}{2}\left[\ln\left(\frac{r}{r_p}\right) - \tfrac{1}{2}\right]$$

$$\therefore \quad Q_a = -\frac{2\pi}{4\mu}\left(\frac{dP}{dx}\right)\left[\frac{r^4}{4} - \frac{r^2}{2} r_p^2 - \frac{r_p^2 - r_c^2}{\ln\left(\frac{r_p}{r_c}\right)} \left\{\frac{r^2}{2}\left(\ln \frac{r}{r_p} - \tfrac{1}{2}\right)\right\}\right]_{r_c}^{r_p}$$

$$+ 2\pi\left[\frac{V_c}{\ln(\frac{r_p}{r_c})} \frac{r^2}{2}\{\ln(\frac{r_p}{r}) + \tfrac{1}{2}\}\right]_{r_c}^{r_p} \qquad (7.156)$$

Simplifying gives;

$$Q_a = \frac{\pi}{8\mu}(\frac{dP}{dx})(r_p^2 - r_c^2)\left[(r_p^2 + r_c^2) - \frac{(r_p^2 - r_c^2)}{\ln(\frac{r_p}{r_c})}\right] + \pi(r_p^2 - r_c^2)\left[\frac{V_c}{2\ln(\frac{r_p}{r_c})} - \frac{V_c r_c^2}{r_p^2 - r_c^2}\right] \qquad (7.157)$$

$\bar{V}_{am}$ = mean velocity in the annulus of a mobile capsule water system

$$= \frac{Q_a}{\pi(r_p^2 - r_c^2)}$$

$$\therefore \bar{V}_{am} = \frac{1}{8\mu}(\frac{dP}{dx})\left[(r_p^2 + r_c^2) - \frac{(r_p^2 - r_c^2)}{\ln(\frac{r_p}{r_c})}\right] + \left[\frac{V_c}{2\ln(\frac{r_p}{r_c})} - \frac{V_c r_c^2}{(r_p^2 - r_c^2)}\right] \qquad (7.158)$$

Note that the first term on the right hand side is the mean velocity in the annulus due to concentric laminar pressure flow with a fixed core ($\bar{V}_{ap}$) (see equation (7.45)) and the second term is the Couette flow component ($\bar{V}_{ac}$).

$$\therefore \bar{V}_{am} = \bar{V}_{ap} + \bar{V}_{ac} \qquad (7.159)$$

This proves that the mean velocity in the annulus of a mobile concentric capsule with laminar flow in the annulus is composed of pressure and a Couette component.

19. Couette flow

Couette flow can be defined as flow between two parallel walls, one fixed and one moving in its own plane.

The nature of the flow between the plates may be laminar or turbulent and may exist with or without a positive or negative pressure gradient.

Three types of Couette flow can be defined here, depending on the geometry of the walls;

(1) circular Couette flow with the walls curving in the direction of flow, (i.e. the classical viscometer),

(2) plane Couette flow in which one plane surface shears parallel to another,

(3) circular Couette flow in which the walls are curved perpendicular to the flow direction. This type of flow has not been defined or considered previously and can be designated "curved Couette flow" or "cylindrical Couette flow" (e.g. one component of flow in the annulus, which may be eccentric, between a capsule and pipe wall).

19.1 Circular Couette flow occurs between the walls of rotating cylinders and was first investigated by Couette in 1890 (reference 12) in connection with viscometry.

Circular Couette flow with small ratios of clearance to diameter, approach the case of plane Couette flow. However, centrifugal forces are apparent.

19.2 Plane Couette flow

A conceptually simple case, and in laminar flow, one which is used extensively to introduce the ideas of viscosity; plane Couette flow has not been examined experimentally to any great extent. The only references of an experimental nature available, are Reichardt (reference 50), Robertson (reference 51 and reference 53) and Leutheusser and Chu (reference 32).

19.2.1 Literature survey of plane Couette flow

Reichardt used a belt, 800 mm wide, which was suspended between two vertical pulleys of 160 mm diameter (see Figure 7.35a). With oil as the test fluid, laminar flow (evidenced by a linear velocity profile) was obtained at a Reynolds number;

$$R'_e = 600$$

where

$$R'_e = \frac{u_c\, b_1}{\nu} \qquad (7.160)$$

Fig. 7. 35

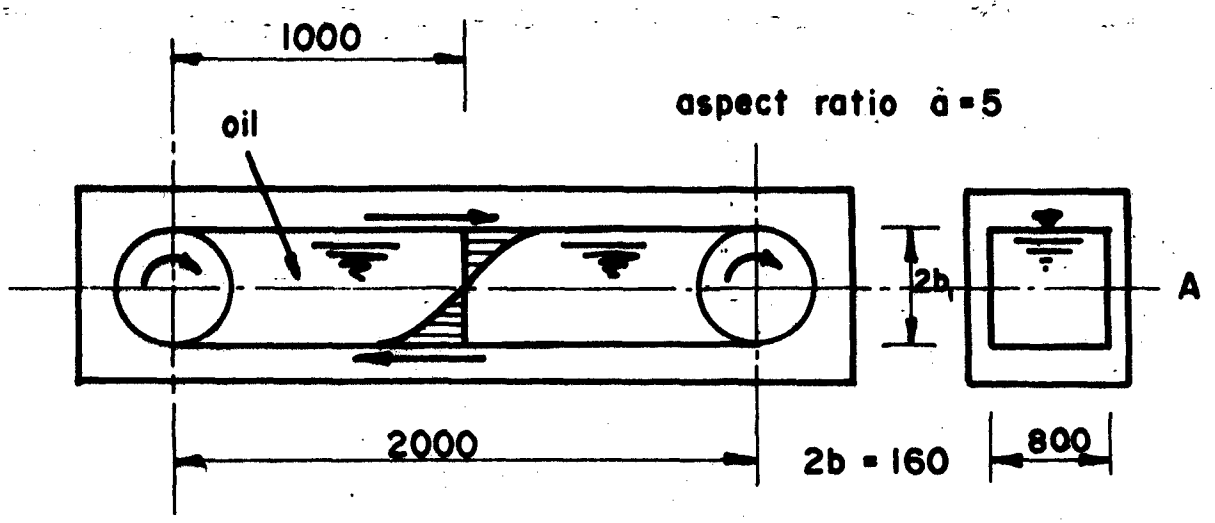

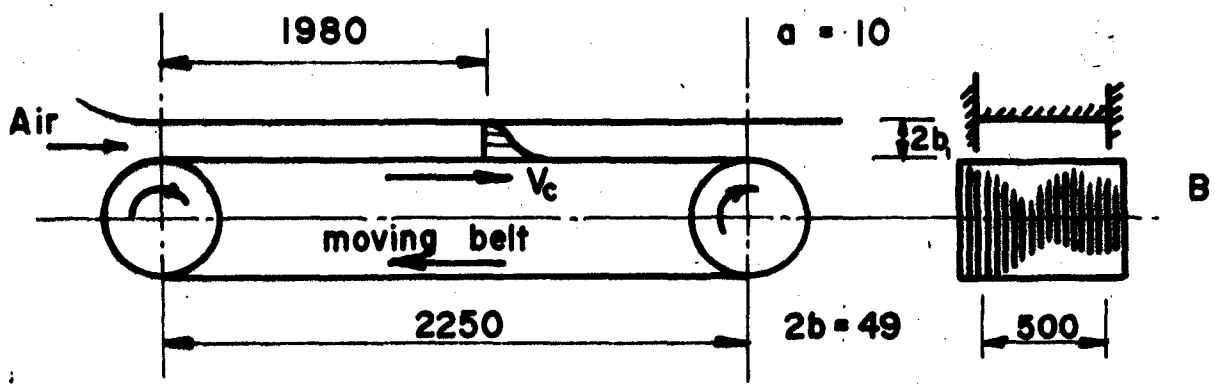

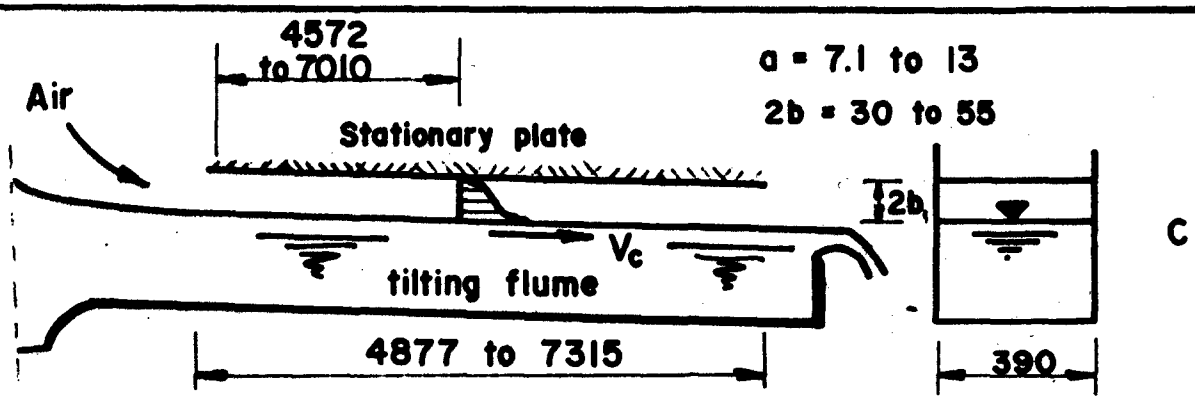

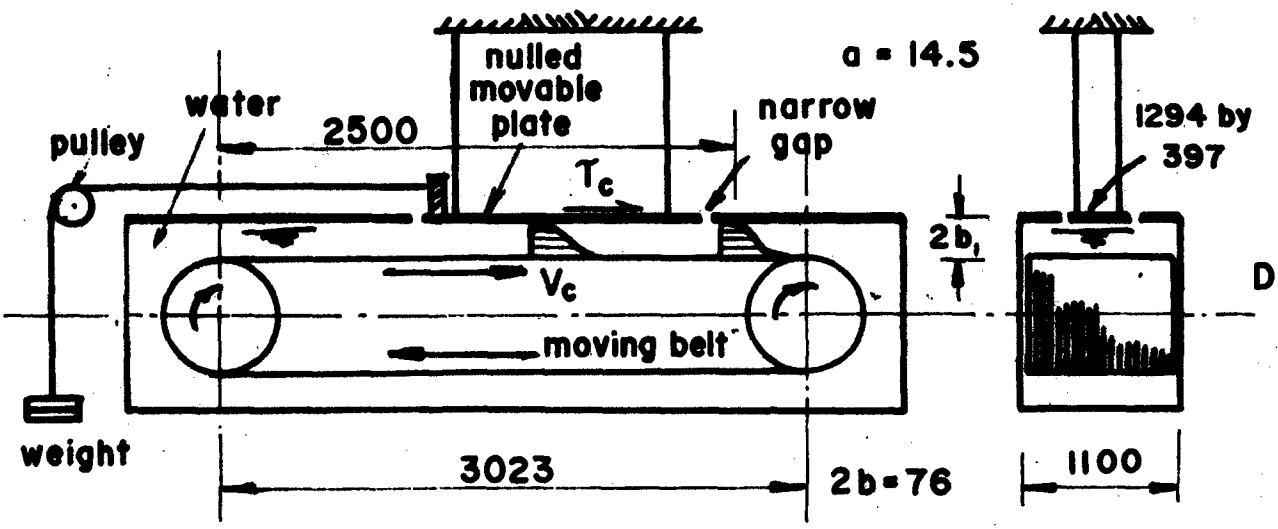

All dimensions in mm.

According to the definition of Reynolds number used in this thesis (see equation 7.102) viz.

$$R_e = \frac{2b\,\bar{V}_a}{\nu} \qquad (7.102)$$

where $b = 2b_1$ and $\bar{V}_a$ = mean velocity between the plates

This corresponds to a Reynolds number $R_e = 4\,R'_e$

$\therefore\ R_e = 2\,400$

This is similar to the criterion for critical Reynolds number in circular pipe flow.

The critical Reynolds number found by Reichardt was about $R'_e = 750$ corresponding to $R_e = 3\,000$.

Figure 7.36 shows the velocity profiles of Reichardt and the relation of Reichardt for turbulent velocity profiles is discussed by Robertson and will be referred to below.

Robertson (reference 51) carried out experiments involving air as the test fluid. Robertson's apparatus consisted of a fixed and moving plane as shown in Figure 7.35b. The belt was 500 mm wide and the pulleys were mounted about 2,250 m apart. The belt was driven at various speeds up to 26 m/s. Velocity profiles were measured using piezometer tubes.

Robertson carried out experiments in the turbulent flow region only at a fixed spacing distance of $2b_1 = 49$ mm. Some experiments were carried out with a fan, set up ahead of the Couette apparatus, which was used to blow enough air down the channel to overcome the extra sidewall friction. This was done in order to overcome the principal defect, from the idealization hoped for, which was that the midpoint velocity was less than half the belt velocity (attributed to the presence of the fixed sidewalls).

Figure 7.37 shows all the results given by Robertson. These are for a range of Reynolds numbers (R'_e) from 5 800 to 15 100, four with the fan and belt (B + F) and two with the belt alone.

since u_c and ρ are constants,

where ΔS_c = surface area of capsule at a particular slice

ΔS_p = surface area of pipe at a particular slice.

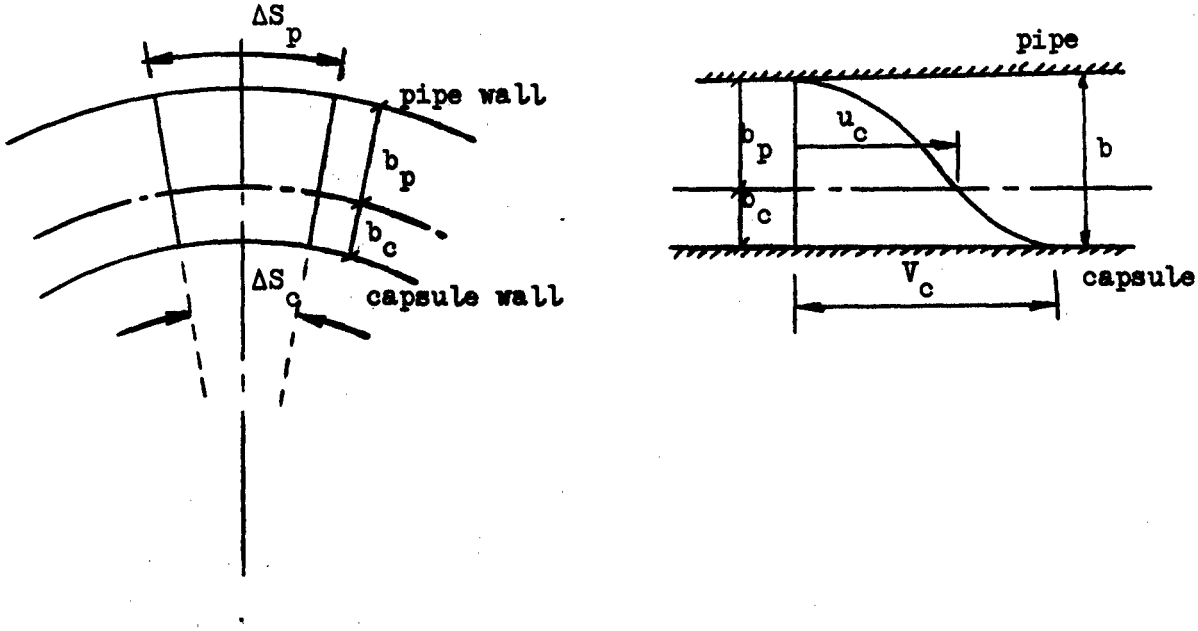

Figure 7.41

The terms used in equation (7.170) are best illustrated in Figure 7.41. It should be emphasised that b_p, b_c and u_c are local values applying at a particular local quasi-concentric annular section.

From equation (7.170)

$$\frac{\log_{10}\left(\frac{b_p u_c}{\nu}\right)}{\log_{10}\left(\frac{b_c u_c}{\nu}\right)} = \sqrt{\frac{\Delta S_p}{\Delta S_c}} = A \qquad (7.171)$$

where A is a constant value, which, according to the method used for subdividing the annulus, varies around the annulus, increasing from the bottom to the top for an eccentrically travelling capsule.

The constant (A) is always greater than unity necessitating $b_p > b_c$.

From equation (7.171);

$$\frac{b_c^A}{b - b_c} = \left(\frac{u_c}{\nu}\right)^{1-A} \qquad (7.172)$$

The only unknown in equation (7.172) is b_c. And b_c can hence be solved at

all points around the annulus by means of the Newton Raphson numerical iterative procedure with equation (7.172) in the form;

$$F(b_c) = b_c^A + \left(\frac{V_c}{2\nu}\right)^{1-A} b_c - \left[\frac{V_c}{2\nu}\right]^{1-A} b = 0 \qquad (7.173)$$

where F denotes function of .....

Figure 7.42 shows an example of the way in which b_c varies from the point where laminar flow ceases to the top of the capsule. The curve shown in this figure was determined by solving equation (7.173)

19.6 Curved Couette flow in an eccentric annular section

As was mentioned previously, the flows in the annulus can be considered as comprising two components, pressure flow and Couette flow. This section is devoted to the Couette flow component and the following points will be briefly discussed; laminar Couette flow, criterion for distinguishing between laminar and turbulent Couette flow and turbulent Couette flow as regards the numerical computation.

19.6.1 Laminar curved Couette flow

In Section 18 it was shown that the average velocity in the annulus due to Couette flow could be expressed as;

$$\bar{V}_{ac} = V_c \left[0{,}5/\ln\left(\frac{r_p}{r_c}\right) - \frac{r_c^2}{r_p^2 - r_c^2} \right]$$

for concentric annuli.

Employing the method of quasi-concentric annuli, the above equation can be replaced by;

$$\bar{V}_{ac} = V_c \left[0{,}5/\ln \frac{C_{rni}}{C_{r1i}} - \frac{(C_{r1i})}{C_{rni}^2 - C_{r1i}^2} \right] \qquad (7.174)$$

Where C_r is the quasi-concentric radius and the subscript (i) denotes the slice under consideration where i varies from 1 to n. The total laminar flow in the annulus due to the Couette component is

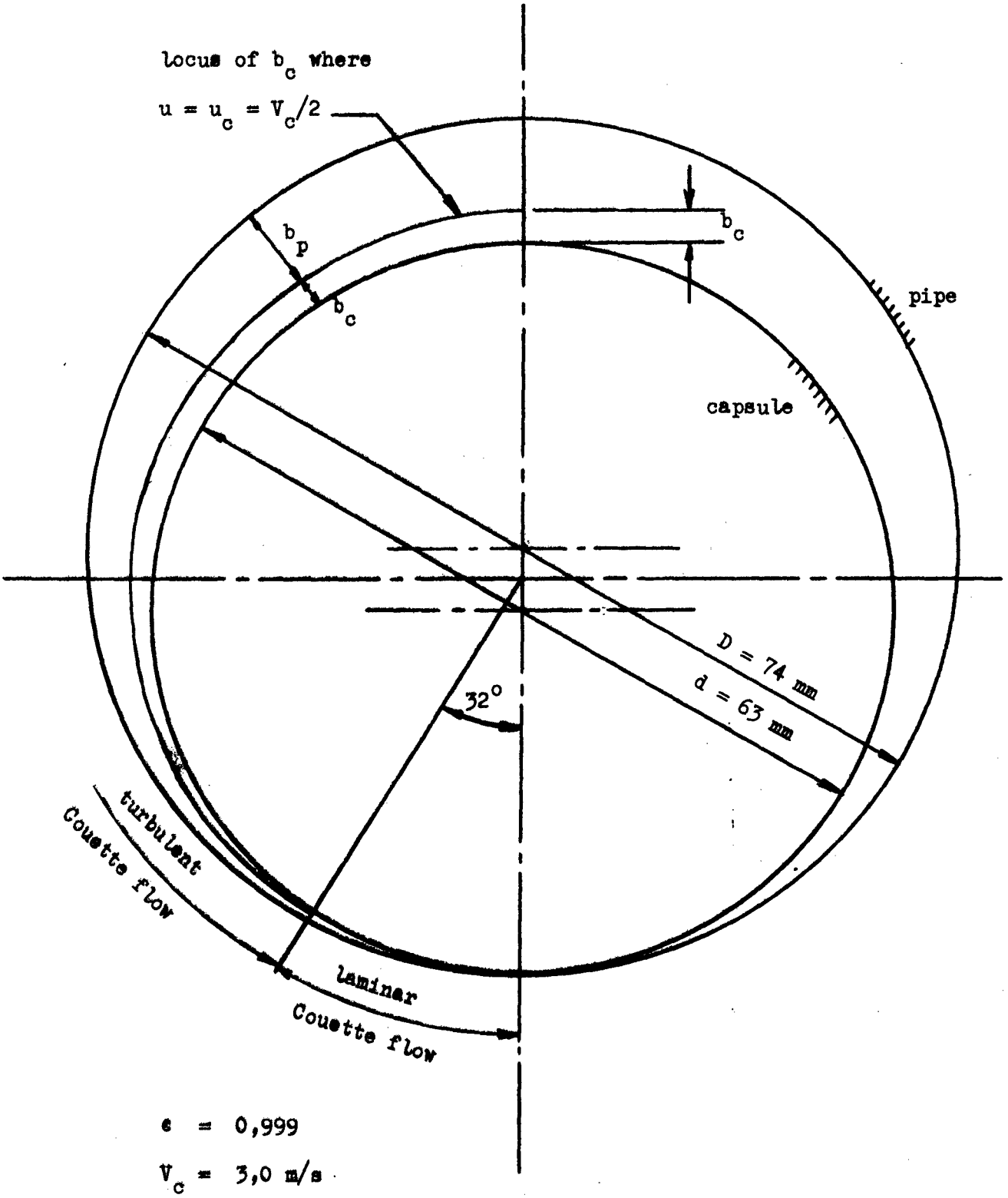

$\epsilon = 0{,}999$

$V_c = 3{,}0$ m/s

$\frac{d}{D} = 0{,}853$

Figure 7.42

$$Q_{ac} = \sum_{i=1}^{LT} V_{ac} \, \Delta A_i \qquad (7.175)$$

LT = value of i at which flow changes from laminar to turbulent. The shear stress on the capsule wall in laminar flow at an angle θ around the perimeter is given by

$$\tau_{cc} = \mu\left(\frac{du}{dr}\right)_c \qquad (7.176)$$

where $$\left(\frac{du}{dr}\right)_c = \frac{V_c}{C_{r1i} \ln\left(\frac{C_{rni}}{C_{r1i}}\right)}$$

For the pipe wall

$$\tau_{cp} = -\mu\left(\frac{du}{dr}\right)_p \qquad (7.177)$$

where $$\left(\frac{du}{dr}\right)_p = -\frac{V_c}{C_{rni} \ln\left(\frac{C_{rni}}{C_{r1i}}\right)}$$

Later on these shear values will be summed together with those for turbulent shear values to find the average values of the Couette shear components.

The criterion for determining the slice at which the flow changes from laminar to turbulent flow was as follows:

$$R_{ec} = \frac{2b \, V_{ac}}{\nu} > 2\,400$$

where R_{ec} = critical Reynolds number

and V_{ac} = laminar Couette flow in an annular slice.

An iterative process was followed to establish the critical Reynolds number prior to the laminar flow calculations.

19.6.2 Turbulent Couette flow in eccentric annulus

After calculating values for laminar flow up to the point where a slice became turbulent, the next step was to find the local value of b_c and b_p, i.e. b_{ci} and b_{pi}.

This was done by solving equation (7.173) as discussed.

Now $R'_{ecc} = \frac{V_c}{2} \frac{b_{ci}}{\nu}$

and $R'_{ecp} = \frac{V_c}{2} \frac{b_{pi}}{\nu}$

and the local values of v_{*_c} and v_{*_p} were found from equations (7.166) and (7.167).

In order to find the flow in the eccentric annulus at each slice in turbulent flow, sub-slices were considered individually and the velocity distribution laws which were found to fit Robertson's plane Couette flow data (equations (7.162), (7.163) and (7.164)) were used in a quasi-concentric slice to find the flow by summing the flows in each sub-slice.

(For D = 74 mm and d/D = 0,85, a typical sub-slice area would be 0,03 mm^2)

To find the total Couette flow, the flows in each sub-slice in turbulent flow and each slice in laminar flow, were summed and divided by the total annular area to give $\bar{V}_{ac}$ (the average velocity component in the annulus due to Couette flow).

The average shear stress on the pipe and capsule wall respectively were found by summing elemental forces around the walls in laminar and turbulent flow and dividing by the appropriate perimeter.

The shear stress in turbulent flow being calculated from

$$\tau_{cc} = \rho v_{*_c}^2$$

and $$\tau_{cp} = \rho v_{*_p}^2$$

where $$v_{*_c} = \frac{V_c}{2} \frac{0,19}{\log R'_{ecc}}$$

and $$u_{*_p} = \frac{V_c}{2} \frac{0,19}{\log R'_{ecp}}$$

The quasi-concentric values of the above being dependent on b_{ci} and b_{pi}.

The results of analysis of curved Couette flow will be discussed in the next section with regard to velocities in the annulus due to curved Couette flow and in Chapter 8 with regard to shear stress and forces on the capsule.

19.7 Results of curved Couette flow analysis

19.7.1 Effect of Capsule Velocity

Figure 7.43 shows typical velocity distributions in curved Couette flow using the equations (7.162), (7.163) and (7.164) for plane Couette flow. These curves are at $\theta = 90^{o}$ where the gap is largest and the diameter ratio (d/D) and eccentricity are kept constant at d/D = 0,85 and $\epsilon = 0,99$ respectively. The only dependent variable is capsule velocity V_c and the effect of this variable on the mean annular Couette flow velocity component ($\bar{V}_{ac}$) as well as wall shear stresses will be dealt with; the former in this Chapter and the latter in the next.

19.7.2 Effect of V_c on velocity in annulus due to Couette flow ($\bar{V}_{ac}$)

The effect of V_c on $\bar{V}_{ac}$ can best be seen on Figure 7.44 where $\bar{V}_{ac}$ is plotted against V_c with diameter ratio as parameter.

The curves are drawn at unit eccentricity but the effect of eccentricity on $\bar{V}_{ac}$ is very slight, as can be seen from Figure 7.45 where the difference between the average annular Couette flow velocity is of the order of 2% (at d/D = 0,85 and V_c = 3 m/s) when the eccentricity is changed from zero to unity. Reverting to Figure 7.44, the most notable feature is the linear relation between $\bar{V}_{ac}$ and $\bar{V}_c$ and Figure 7.46 shows the ratio ($\bar{V}_{ac}/V_c$) as a function of diameter ratio yielding a unique curve regardless of the value of V_c and almost independent of eccentricity (ϵ).

The only other variable which can influence this curve is the absolute value of pipe diameter and since, non-dimensional velocity distribution laws were used, the actual pipe diameter can have no effect as can be seen from Figure 7.47.

Figure 7.46 is thus a unique analytical curve which can be described by the formula;

$$\bar{V}_{ac} = V_c . \text{function } (d/D)$$

FIG. 7.43

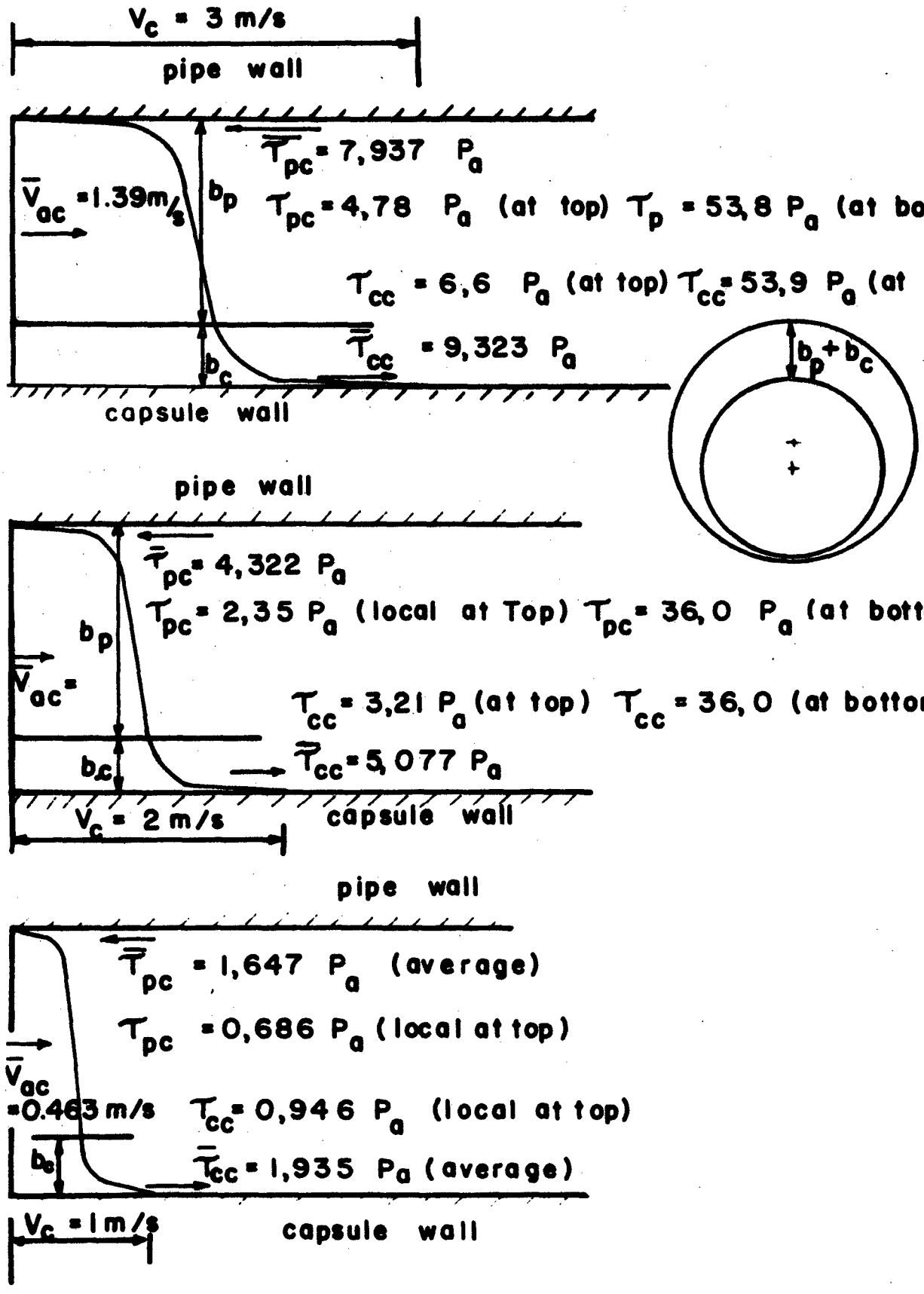

$\epsilon = 0,99 \qquad \frac{d}{D} = 0,85$

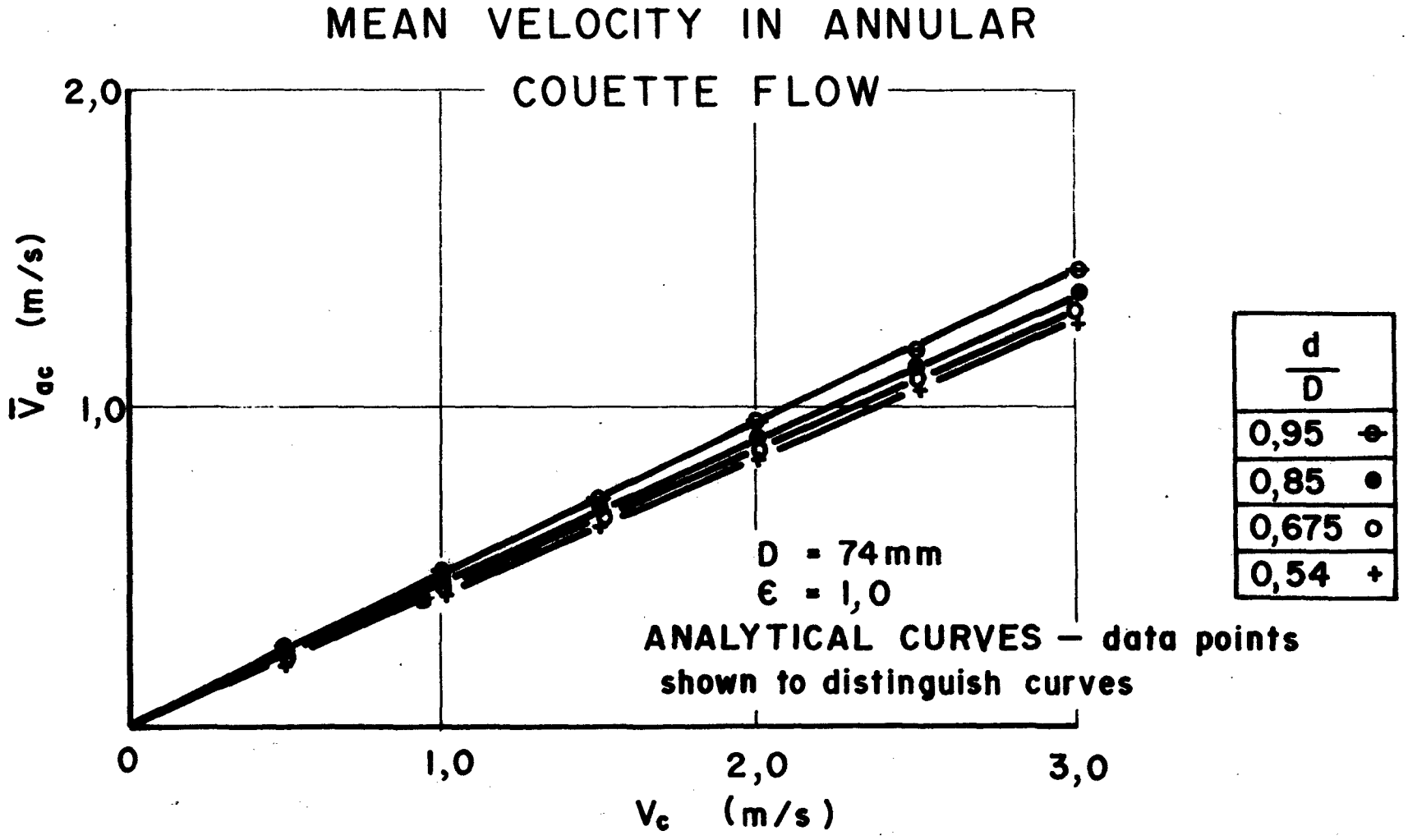
MEAN VELOCITY IN ANNULAR COUETTE FLOW
2,0
1,0
0
1,0
2,0
3,0
$\bar{V}_{ac}$ (m/s)
V_c (m/s)
D = 74mm
ϵ = 1,0
ANALYTICAL CURVES — data points shown to distinguish curves
d/D
0,95
0,85
0,675
0,54

FIG. 7.44

FIG. 7.45

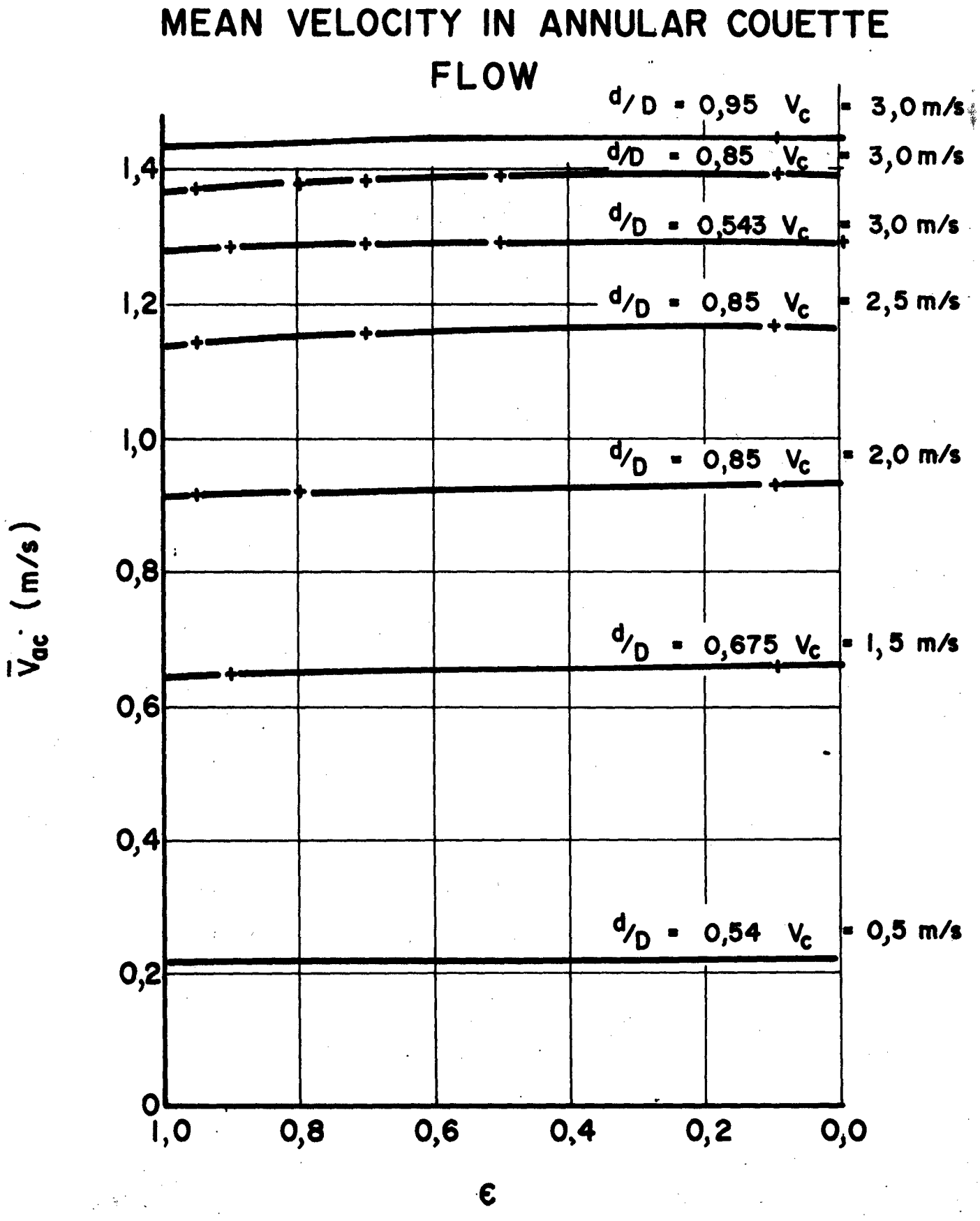
MEAN VELOCITY IN ANNULAR COUETTE FLOW
d/D = 0,95 Vc = 3,0 m/s
d/D = 0,85 Vc = 3,0 m/s
d/D = 0,543 Vc = 3,0 m/s
d/D = 0,85 Vc = 2,5 m/s
d/D = 0,85 Vc = 2,0 m/s
d/D = 0,675 Vc = 1,5 m/s
d/D = 0,54 Vc = 0,5 m/s
1,4
1,2
1,0
0,8
0,6
0,4
0,2
0
1,0
0,8
0,6
0,4
0,2
0,0
ε
Vac (m/s)

FIG. 7.46

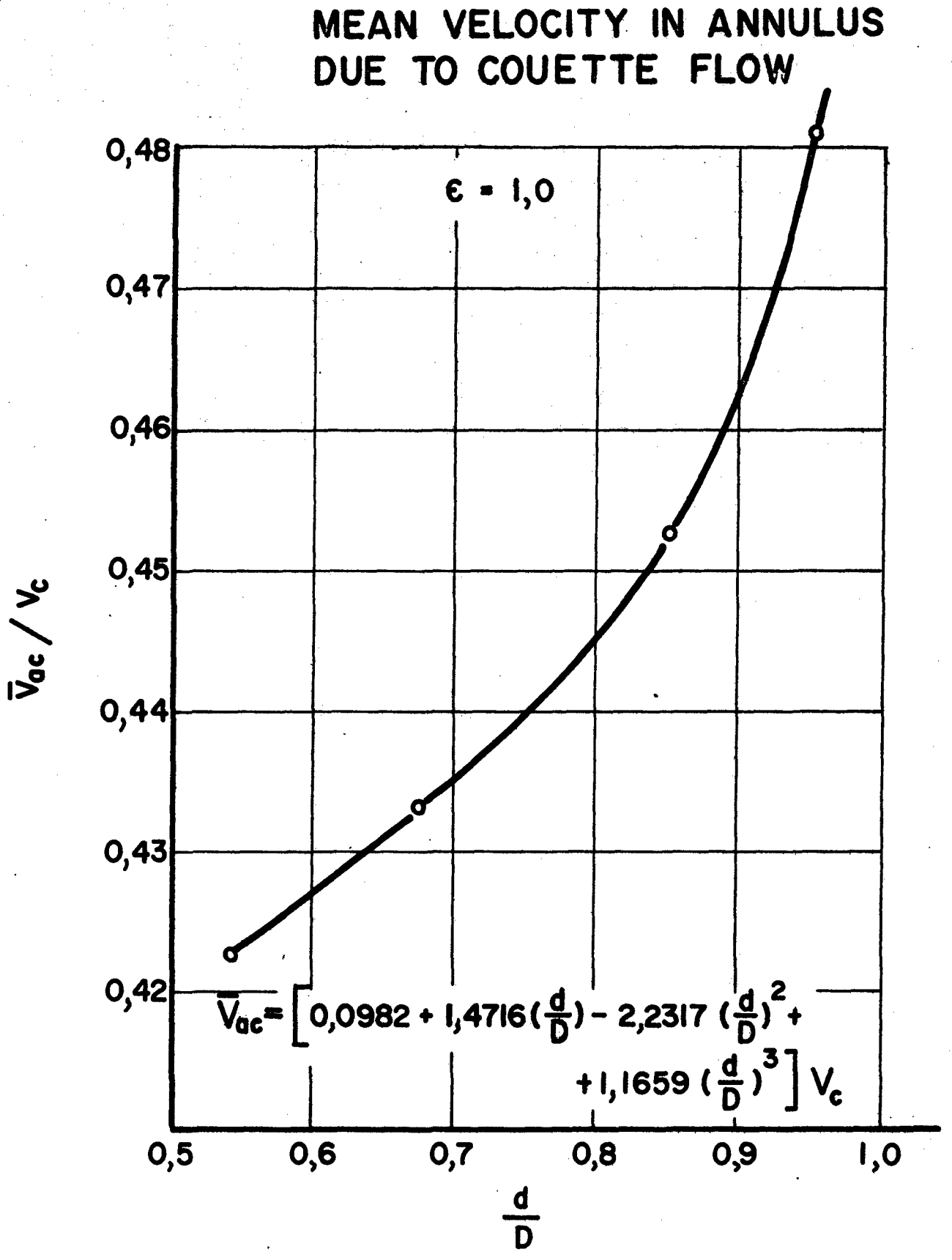
MEAN VELOCITY IN ANNULUS
DUE TO COUETTE FLOW
ε = 1,0
0,48
0,47
0,46
0,45
0,44
0,43
0,42
$\bar{V}_{ac} / V_c$
$\bar{V}_{ac} = \left[0{,}0982 + 1{,}4716\left(\frac{d}{D}\right) - 2{,}2317\left(\frac{d}{D}\right)^2 + 1{,}1659\left(\frac{d}{D}\right)^3\right] V_c$
0,5
0,6
0,7
0,8
0,9
1,0
$\frac{d}{D}$

FIG. 7.47

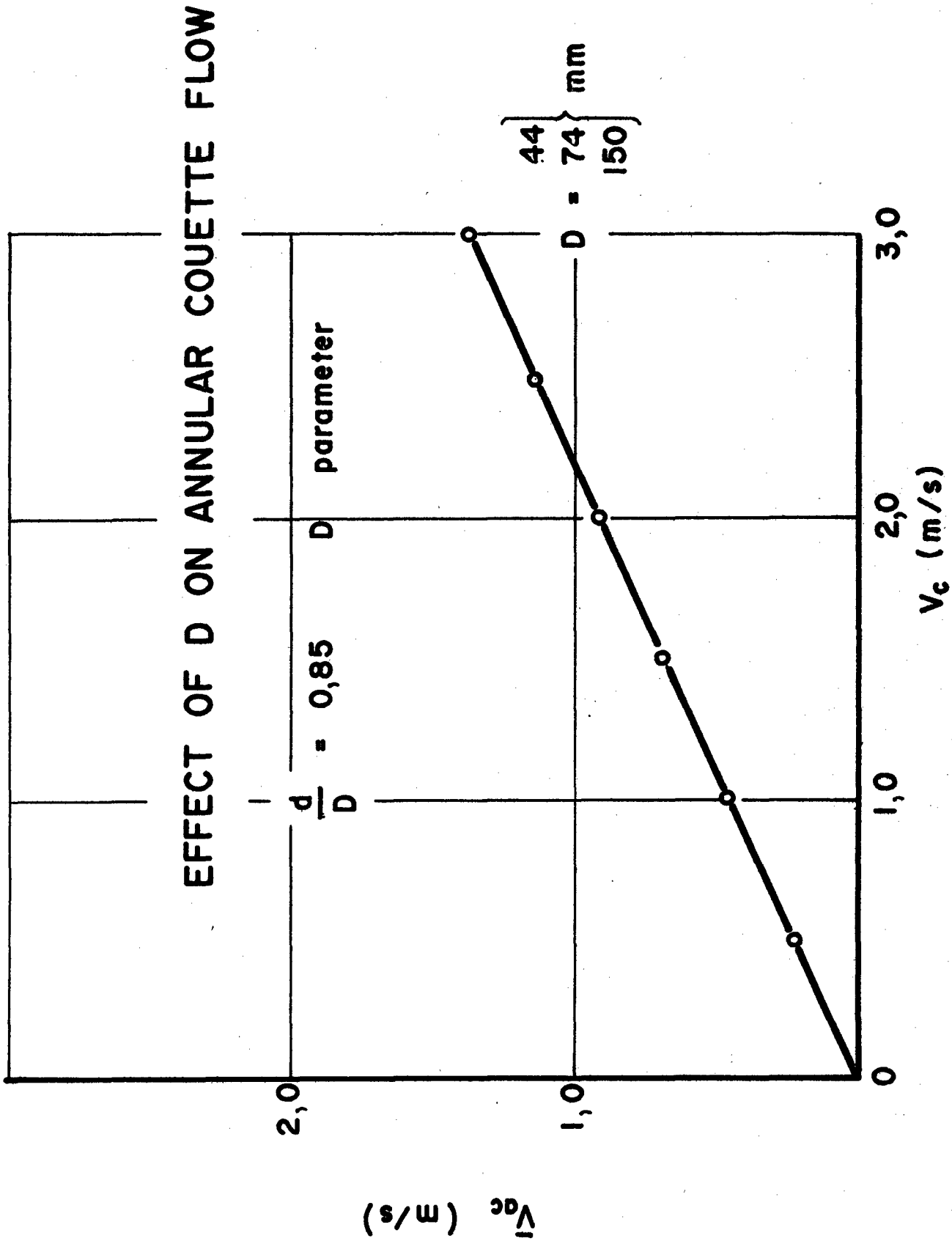
EFFECT OF D ON ANNULAR COUETTE FLOW
d/D = 0,85
D parameter
D = 44 74 150 mm
V_c (m/s)
$\bar{V}_{dc}$ (m/s)
0
1,0
2,0
3,0
1,0
2,0

Unfortunately, no simple expression could be found for this relation and for the purpose of calculation it is expressed as a third degree polynomial thus;

$$\bar{V}_{ac} = V_c[0,0982 + 1,4716(\frac{d}{D}) - 2,2317(\frac{d}{D})^2 + 1,1659(\frac{d}{D})^3] \qquad (7.178)$$

20. Continuity equation for mobile capsule water system

The continuity equation states that the rate of change of the mass of water A B C D E F G H as it moves to A' B' C' D' E' F' G' H', in time (dt) is zero (see Figure 7.48).

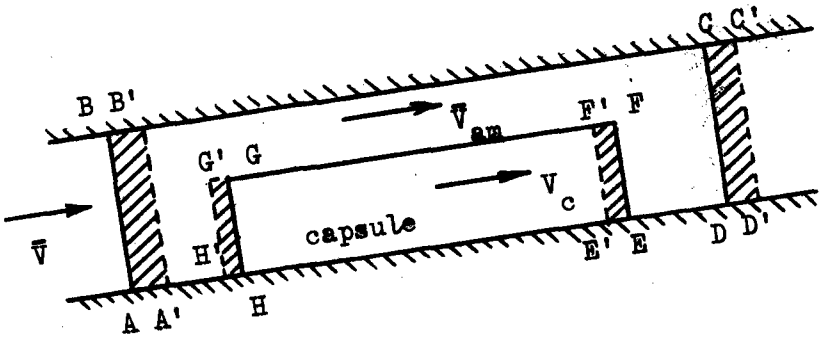

Figure 7.48

Consider the general case of a stationary pipe with a capsule travelling at velocity (V_c). The water velocity in the capsule-free pipe has a velocity ($\bar{V}$) where $V_c < \bar{V}$. The mean velocity in the annulus of the capsule pipe system is $\bar{V}_{am}$.

Superimpose a velocity V_c in the opposite direction to which the capsule is travelling. In this case the capsule remains stationary and the water velocity relative to the capsule is $\overrightarrow{(\bar{V} - V_c)}$, the mean annular velocity relative to the capsule is $\overrightarrow{(\bar{V}_{am} - V_c)}$ and the pipe wall velocity, relative to the capsule is $\overleftarrow{V_c}$.

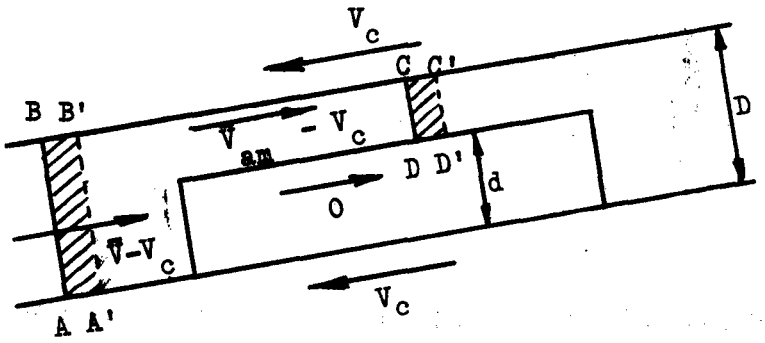

Figure 7.49

Consider the volume of water ABCD moving to position A' B' C' D' in time (dt). The distance BB' is $(\bar{V} - V_c)dt$ and the distance CC' is $(\bar{V}_{am} - V_c)dt$. The volume A' B' C D may be ignored since it is common to both ABCD and A' B' C' D'.

From the definition of the continuity equation, and the fact that the water is considered to be incompressible, the volume A B B' A' = C D D' C'

$$\therefore \quad \frac{\pi D^2}{4}(\bar{V} - V_c)dt = \frac{\pi}{4}(D^2 - d^2)(\bar{V}_{am} - V_c)dt$$

$$\therefore \quad \bar{V}D^2 = \bar{V}_{am}(D^2 - d^2) + V_c d^2$$

$$\therefore \quad \bar{V}_{am} = \frac{\bar{V} - V_c(d/D)^2}{1 - (d/D)^2} \qquad (7.179)$$

Also $$Q = Q_a + Q_c \qquad (7.180)$$

where Q_a = flow in annulus

Q_c = volume flow of capsule.

21. Analysis of general case of mobile capsule water system

Consider the annular section only of a mobile capsule water system.

One way to deal with this system is to superimpose a capsule velocity (V_c) on the whole system in the reverse direction to which the capsule is travelling, as was done when deriving the continuity equation.

However, this approach leads to the pipe wall travelling backwards relative to the capsule and, although this was helpful for the continuity equation, an alternative approach will be used which appears to be more

fruitful. This is to apply a capsule velocity in the reverse direction to the capsule and water only, so that the pipe wall remains stationary and subsequently to superimpose the capsule velocity effect thus;

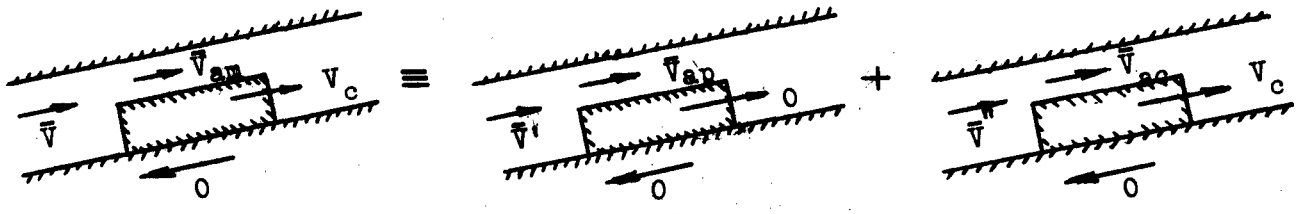

(a) (b) (c)

$$\bar{V}' = \bar{V}_{ap}\left[1 - \left(\frac{d}{D}\right)\right]^2 \qquad \bar{V}'' = \bar{V}_{ac}\left[1 - \left(\frac{d}{D}\right)\right]^2 + V_c\left(\frac{d}{D}\right)^2$$

Figure 7.50

The system shown in Figure 7.50(a) is equivalent to the system shown in Figure 7.50(b) (which can be described as the pressure component) plus the Couette component in Figure 7.50(c) where

$$\bar{V}_{am} = \bar{V}_{ap} + \bar{V}_{ac} \qquad (7.159)$$

where $\bar{V}_{ap}$ = mean velocity in annulus due to pressure component,

$\bar{V}_{ac}$ = mean velocity in annulus due to Couette component.

The continuity and momentum equations can now be applied to the annular portion of system 7.50(b) and 7.50(c) respectively and algebraically added to give the complete system, Figure 7.50(a).

This approach has been shown to be valid for laminar flow, equations (7.150), (7.152), (7.154) and (7.158), and the assumption is made that it is applicable and can be extended to turbulent flow as well.

Note that the flow velocity in the annulus $\neq \bar{V}_{am} - V_c$ as was the case when superimposing V_c on the whole system to get the velocity relative to the capsule.

Now $\bar{V}_{ap} > [\bar{V}_{am} - V_c]$.

21.1 Pressure component

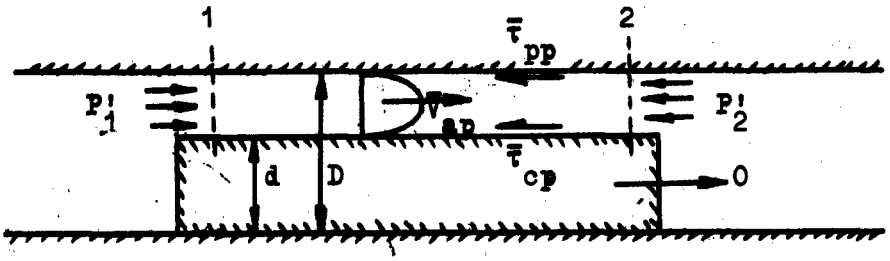

Figure 7.51

The total force equation yields;

$$(P'_1 - P'_2)\left(\frac{D^2 - d^2}{4}\right) = \bar{\tau}_{pp}\, DL_c + \bar{\tau}_{cp}\, dL_c \qquad (7.181)$$

where $\bar{\tau}_{pp}$ = shear stress on water at pipe wall due to pressure flow.

$\bar{\tau}_{cp}$ = shear stress on water at capsule wall due to pressure flow.

The pressure drop between sections 1 and 2 in the annulus has already been defined as $w\,\Delta h_{fa}$. Sections 1 and 2 are just inside the annulus.

$$\therefore \quad \Delta h_{fa} = 4\left(\frac{\bar{\tau}_{pp}\, DL_c + \bar{\tau}_{cp}\, dL_c}{w(D^2 - d^2)}\right) \qquad (7.182)$$

21.2 Couette component

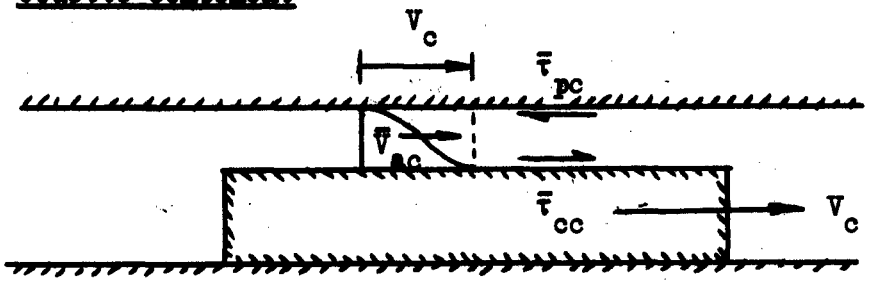

Figure 7.52

The total force equation yields;

$$0 = \bar{\tau}_{pc}\, \pi DL_c - \bar{\tau}_{cc}\, \pi dL_c \qquad (7.183)$$

where $\bar{\tau}_{pc}$ and $\bar{\tau}_{cc}$ are shear stresses at the pipe and capsule wall respectively, due to Couette flow.

Combining equations (7.181) and (7.183),

$$(P_1' - P_2')\left(\frac{D^2 - d^2}{4}\right) = \bar{\tau}_{pp}\, DL_c + \bar{\tau}_{pc}\, DL_c + dL_c(\bar{\tau}_{cp} - \tau_{cc}) \qquad (7.184)$$

$\bar{\tau}_p$ = net shear on water at pipe wall [due to water flow velocity relative to pipe wall $(\bar{V}_{am})$].

$\bar{\tau}_c$ = net shear on water at capsule wall [due to average water velocity relative to capsule wall, i.e. $(\bar{V}_{ap} + \bar{V}_{ac} - V_c)$ or $(\bar{V}_{am} - V_c)$].

$$\bar{\tau}_p = \bar{\tau}_{pp} + \bar{\tau}_{pc} \quad \text{and} \quad \bar{\tau}_c = \bar{\tau}_{cp} + \bar{\tau}_{cc}$$

$$\therefore \Delta h_{fa} = \frac{\bar{\tau}_p\, DL_c + \bar{\tau}_c\, dL_c}{w\left(\frac{D^2 - d^2}{4}\right)} \qquad (7.185)$$

or

$$\Delta h_{fa} = \frac{(\bar{\tau}_{pp} + \bar{\tau}_{pc})DL_c + dL_c(\bar{\tau}_{cp} - \bar{\tau}_{cc})}{w\left(\frac{D^2 - d^2}{4}\right)} \qquad (7.186)$$

There are thus two methods for dealing with the flow in the annulus between the pipe and mobile capsule;

Firstly, from equation (7.185)

$$\Delta h_{fa} = \frac{\bar{\tau}_p\, DL_c + \bar{\tau}_c\, dL_c}{w\left(\frac{D^2 - d^2}{4}\right)}$$

and in this case $\bar{\tau}_p$ and $\bar{\tau}_c$ are the gross average shear stresses on the water at the pipe and capsule walls

where $\bar{\tau}_p$ is assumed to be a function of $\bar{V}_{am}$

and $\bar{\tau}_c$ is assumed to be a function of $(\bar{V}_{am} - V_c)$

Secondly, from equation (7.182),

$$\Delta h_{fa} = \frac{4(\bar{\tau}_{pp}\, DL_c + \bar{\tau}_{cp}\, dL_c)}{w(D^2 - d^2)}$$

since the Couette shear forces $\bar{\tau}_{pc}\, DL_c$ and $\bar{\tau}_{cc}\, dL_c$ are equal and represent force on the pipe and capsule walls due to the motion of the capsule relative to the pipe.

In this case $\bar{\tau}_{pc} = f(\bar{V}_{ac})$ and $\bar{\tau}_{pp} = f(\bar{V}_{ap})$

$\bar{\tau}_{cc} = f(\bar{V}_{ac})$ and $\bar{\tau}_{cp} = f(\bar{V}_{ap})$

Both approaches should be compatible. However, the former method is less precise since gross values were used and the functional relations were more difficult to determine. This will be termed the "gross" method. The latter method is more tedious to apply and a numerical integration technique is used. This appears to be more exact and gives better agreement with experimental results (see Chapter 15). This method will be termed the finite element method since small but finite elements of the annulus are considered in the analysis.

22. Total force equation

Consider a steady state relative to the capsule. The form and skin friction drag on the moving capsule just balance the solid to solid friction force plus the shear resistance due to Couette flow on the capsule.

Applying the total force concept to a steady state water capsule system, we get, when considering the forces acting on the water (see Figure 7.53);

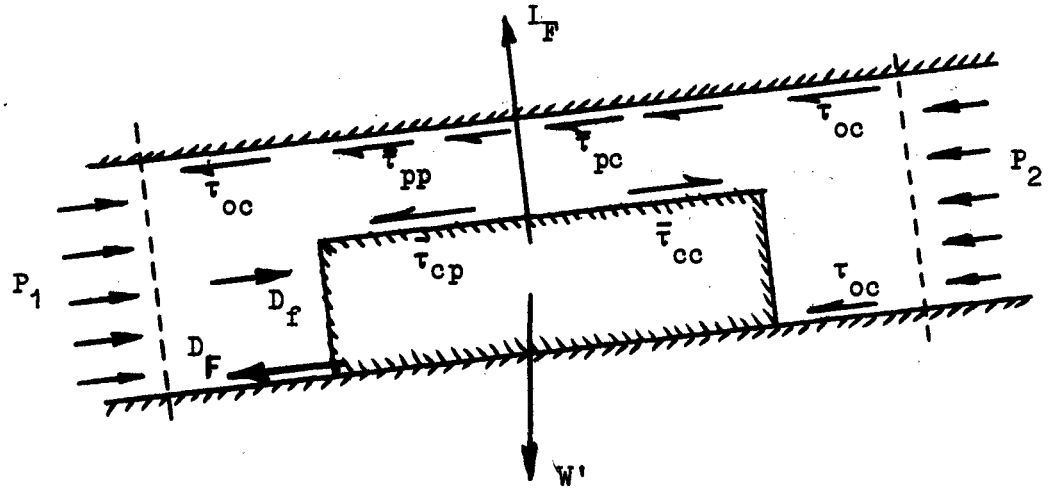

Figure 7.53

$$(P_1 - P_2)\frac{\pi D^2}{4} = \tau_{oc}\,\pi D(L_1 + L_2) + [\bar{\tau}_{pp}\,\pi D L_c + \bar{\tau}_{cp}\,\pi d L_c] + D_f + w\left[\frac{\pi D^2}{4}(L_1 + L_2 + L_c) - \frac{\pi d^2}{4} L_c\right] \sin\phi + [\bar{\tau}_{pc}\,\pi D L_c - \bar{\tau}_{cc}\,\pi d L_c] \quad (7.187)$$

where τ_{oc} = shear stress on wall of pipe in curvilinear flow region upstream and downstream of mobile capsule.

L_1, L_2 = length over which curvilinear flow takes place upstream and downstream of mobile capsule.

D_F = solid friction force on mobile capsule.

D_f = form drag on mobile capsule.

The total drag on the capsule in the direction of flow is the sum of the skin friction drag and the form drag. Thus;

$$D_T = D_f + [\bar{\tau}_{cp}\,\pi d L_c - \bar{\tau}_{cc}\,\pi d L_c] \quad (7.188)$$

For the mobile capsule the total drag is in equilibrium with the solid to solid friction and the component of capsule weight down the slope;

$$\therefore\ D_T = \mu_f(W' \cos\phi - L_F) + W \sin\phi \quad (7.189)$$

Equation (7.187) can be written as

$$\frac{\pi D^2}{4}[P_1 - P_2 - w(z_2 - z_1)] = \Sigma \text{ wall forces} + D_T - \frac{\pi d^2}{4} w L_c \sin\phi$$

where Σ wall forces $= \tau_{oc}\,\pi D(L_1 + L_2) + \bar{\tau}_{pp}\,\pi D L_c + \bar{\tau}_{pc}\,\pi D L_c$

i.e. the wall forces on the water at the pipe wall due to water flow.

$$\therefore\ \frac{w\pi D^2}{4}\left[\left(\frac{P_1}{w} + z_1\right) - \left(\frac{P_2}{w} + z_2\right)\right] = \Sigma \text{ wall forces} + \mu_f(W' \cos\phi - L_F) + W \sin\phi - \frac{\pi d^2}{4} w L_c \sin\phi$$

$$= \Sigma \text{ wall forces} + \mu_f W' \cos\phi - \mu_f L_F + W' \sin\phi \quad (7.190)$$

where L_F = lift force on the capsule

and where $W' = W - \frac{\pi d^2}{4} w L_c = \frac{\pi d^2}{4} w L_c \left| S_c - 1 \right|$

In words, this equation (7.190) states that the total change in force between section 1 and 2 is equal to the sum of the shear forces on the water due to pressure flow at the pipe wall, plus the shear forces on the water at the pipe wall due to Couette flow, plus the solid to solid friction force on the capsule at the pipe wall due to the reduced weight of the capsule (reduced as a result of buoyancy and lift forces), plus the component of capsule weight down the slope.

When applying the energy equation to the mobile capsule pipe system, Bernouilli's equation states that, the total head at section 1 equals the total head at section 2, plus head losses from 1 to 2 (see Figure 7.53). The head loss in the annulus has already been discussed and the other head losses are due to contraction and expansion as the water passes over the leading and trailing faces of the capsule, plus head losses due to curvilinear flow upstream and downstream of the capsule;

$$\left(\frac{P_1}{w} + z_1\right) - \left(\frac{P_2}{w} + z_2\right) = \Delta h_{fa} + \Delta h_i + \Delta h_o + \frac{4}{Dw} \tau_{oc}(L_1 + L_2) \qquad (7.191)$$

This is the same equation as the energy equation for static capsules except that the terms Δh_{fa}, Δh_i and Δh_o are modified as discussed later;

Combining the energy equation (7.191) and total force equation (7.190) yields

$$\frac{w\pi D^2}{4}\left[\Delta h_{fa} + \Delta h_i + \Delta h_o - \frac{4L_c}{wD}(\bar{\tau}_{pp} + \bar{\tau}_{pc})\right] = \mu_f W'(\cos \phi - L_r) + W' \sin \phi$$

$$\therefore \quad D^2\left[\Delta h_{fa} + \Delta h_i + \Delta h_o - \frac{4L_c}{wD}(\bar{\tau}_{pp} + \bar{\tau}_{pc})\right] = d^2 L_c \left| S_c - 1 \right| [\mu_f(\cos \phi - L_r) + \sin \phi] \qquad (7.192)$$

where L_r = lift ratio = L_F/W'

$$\text{i.e. } \frac{\Delta h_{fa} + \Delta h_i + \Delta h_o}{L_c} - \frac{4}{wD}(\bar{\tau}_{pp} + \bar{\tau}_{pc}) = \left(\frac{d}{D}\right)^2 |S_c - 1| \left[\mu_f(\cos \phi - L_r) + \sin \phi\right] \tag{7.193}$$

For horizontal pipes;

$$\frac{\Delta h_{fa} + \Delta h_i + \Delta h_o}{L_c} - \frac{4}{wD}(\bar{\tau}_{pp} + \bar{\tau}_{pc}) = \mu_f\left(\frac{d}{D}\right)^2 |S_c - 1|(1 - L_r) \tag{7.194}$$

The excess head loss across the mobile capsule is;

$$\Delta H_c = \Delta h_{fa} + \Delta h_i + \Delta h_o - h_{fc}$$

$$= \Delta h_a + \Delta h_i + \Delta h_o$$

This excess head loss can be expressed in three ways from equations (7.185), (7.186) and (7.194)

$$\Delta H_c = \frac{\bar{\tau}_p DL_c + \bar{\tau}_c dL_c}{w\frac{(D^2 - d^2)}{4}} + \Delta h_i + \Delta h_o - h_{fc} \tag{7.195}$$

$$\text{or } \Delta H_c = \frac{(\bar{\tau}_{pp} + \bar{\tau}_{pc})DL_c + (\bar{\tau}_{cp} - \bar{\tau}_{cc})dL_c}{w\frac{(D^2 - d^2)}{4}} + \Delta h_i + \Delta h_o - h_{fc} \tag{7.196}$$

$$\text{or } \Delta H_c = \mu_f L_c\left(\frac{d}{D}\right)^2 |S_c - 1|(1 - L_r) + \frac{4L_c}{Dw}(\bar{\tau}_{pp} + \bar{\tau}_{pc}) - h_{fc} \tag{7.197}$$

The three equations above can easily be written for vertical or sloping pipes from equation (7.193).

For vertical pipes (for example) equation (7.195) and (7.196) must be modified by adding in the term $(d/D)^2 |S_c - 1|$ on the right hand side and equation (7.197) is modified by subtracting the first term on the right hand side and adding in the $(d/D)^2 |S_c - 1|$ term.

The values of $\bar{\tau}_{pc}$ and $\bar{\tau}_{pp}$ are also altered to take into account the variation from unit eccentricity. Even in the horizontal pipe $\bar{\tau}_{pc}$ and $\bar{\tau}_{pp}$ are adjusted (in the final computerization) to take into account variation from unit eccentricity when capsule lift occurs.

These three equations, (7.195), (7.196) and (7.197) will now be dealt with separately. Two of them, (7.195) and (7.196) can be used for

determining the total head loss across the capsule analytically.

23. Gross method of determining the total excess head loss across a mobile capsule (Equation 7.195)

In words, equation (7.195) states that the total excess head loss across the capsule (ΔH_c) is the sum of the pressure heads due to energy dissipation in total shear force on the capsule and pipe wall plus the inlet and outlet head losses minus the head loss that would have occurred in a length (L_c) of capsule-free pipe.

Each of the terms on the right hand side of equation (7.195) has to be evaluated for the mobile capsule system.

23.1 Inlet and outlet losses

It has already been shown for static eccentric capsules that;

$$\Delta h_i + \Delta h_o = \left[22\left(\frac{d}{D}\right)^6 + 0{,}68\left[\frac{1}{1-\left(\frac{d}{D}\right)^2} - 1\right]^2\right]\frac{\bar{V}^2}{2g}$$

$$= C_2' \bar{V}^2 \qquad (7.198)$$

where $\bar{V}$ is the mean velocity in the capsule-free pipe relative to the capsule.

Thus if the capsule velocity is V_c then $\bar{V}$ can be replaced by $(\bar{V} - V_c)$ which is still the mean water velocity in the pipe relative to the capsule and;

$$\Delta h_i + \Delta h_o = C_2' (\bar{V} - V_c)^2 \qquad (7.199)$$

If the mobile capsule water system is replaced by the system wherein a backward velocity (V_c) is superimposed, then this approach assumes that the backward pipe wall movement has no effect on the streamline patterns at inlet and outlet ends of the capsule.

The only effect would be to modify the velocity distribution and, since equation (7.198) was determined for a range of average water velocities, it is unlikely that the modification would cause serious error.

Also, it is well known that head loss coefficients for sudden contractions and expansions in circular pipes are not greatly affected by the velocity in the pipes.

23.2 Annular head losses

The next point to consider in the "gross" analysis is the determination of $\bar{\tau}_p$ and $\bar{\tau}_c$ in the first term on the right hand side of equation (7.195).

The terms $\bar{\tau}_p$ and $\bar{\tau}_c$ represent average values of the total (i.e. Couette plus pressure components) shear stress on the pipe and capsule walls respectively.

It is obvious that the local values will vary considerably, particularly in an eccentric annulus with a moving solid capsule. The Couette terms included in $\bar{\tau}_p$ and $\bar{\tau}_c$ are also mean average values for the capsule relative to the pipe.

Conventionally, for pipe flow the shear stress on the wall of the pipe is;

$$\tau = f \tfrac{1}{2}\rho\bar{V}^2$$

and it seems feasible to consider the shear stress, in the annulus, on the pipe wall, as;

$$\bar{\tau}_p = f_{aw} \tfrac{1}{2}\rho\bar{V}_{am}^2 \qquad (7.200)$$

where $\bar{V}_{am}$ is a representative velocity, in the annular region of a mobile capsule, relative to the pipe wall and may be taken as the velocity in the annulus.

f_{aw} = an equivalent friction factor, which satisfies the above equation (7.200) for the annular region, on the pipe wall in the mobile capsule case and for smooth capsules, can be determined from the Blasius type equation.

The shear stress in the annulus on the capsule itself can be taken as;

$$\bar{\tau}_c = f_{ac} \tfrac{1}{2}\rho V_r^2 \qquad (7.201)$$

where V_r = an equivalent velocity in the annular region relative to the capsule $(V_r = \bar{V}_{am} - V_c)$

f_{ac} = an equivalent friction factor for the mobile capsule which satisfies equation (7.201) and can be calculated using a pseudo-hydraulic mean radius and the velocity relative to the capsule.

There are certain assumptions inherent in the above which will be discussed later.

It must be borne in mind that friction factors and velocities are equivalent values causing the above equations to be satisfied.

The above expressions for $\bar{\tau}_p$ and $\bar{\tau}_c$ are not quite correct in the light of previous definitions as can be seen from the following reasoning.

It has already been shown that applying the total force equation to the water in the mobile capsule annulus yields;

$$w\,\Delta h_{fa} = \frac{\bar{\tau}_p\,\pi D L_c + \bar{\tau}_c\,\pi d L_c}{\frac{\pi(D^2 - d^2)}{4}} \qquad (7.202)$$

and Δh_{fa} is composed of two components; the excess head loss and the head loss in a capsule length of capsule-free pipe.

$$\Delta h_{fa} = \Delta h_a + h_{fc} = \frac{f_a\,L_c\,\bar{V}_{am}^2}{2g\,R_p} \qquad (7.203)$$

This equation is valid for static capsules and is assumed to have the same form for mobile capsules.

From equations (7.202) and (7.203) we get;

$$f_a\,\tfrac{1}{2}\frac{\rho\,\bar{V}_{am}^2}{4\,R_p} = \frac{\bar{\tau}_p\,D + \bar{\tau}_c\,d}{(D + d)(D - d)} \qquad (7.204)$$

From the analysis of static capsules

$$R_p = 1{,}25R = 1{,}25\,(\frac{D - d}{4})$$

$$\therefore \quad \frac{f_a \tfrac{1}{2} \rho \bar{V}_{am}^2}{1{,}25(D - d)} = \frac{\bar{\tau}_p D + \bar{\tau}_c d}{(D + d)(D - d)}$$

$$\therefore \quad f_a \tfrac{1}{2} \rho \bar{V}_{am}^2 \frac{(D + d)}{1{,}25} = \bar{\tau}_p D + \bar{\tau}_c d$$

$$\therefore \quad \bar{\tau}_p D + \bar{\tau}_c d = f_a \tfrac{1}{2}\rho \frac{\bar{V}_a^2 D}{1{,}25} + f_a \tfrac{1}{2} \frac{\rho \bar{V}_a^2 d}{1{,}25} \qquad (7.205)$$

Hence it is now assumed that

$$\bar{\tau}_p D = f_{aw} \tfrac{1}{2} \frac{\rho \bar{V}_{am}^2 D}{1{,}25} \qquad (7.206)$$

and

$$\bar{\tau}_c d = f_{ac} \tfrac{1}{2} \frac{\rho V_r^2 d}{1{,}25} \qquad (7.207)$$

This is not to imply that the actual values of $\bar{\tau}_p$ and $\bar{\tau}_c$ can be found from these expressions. These are equivalent values for the shear stresses enabling a solution to be found for equation (7.195).

Thus equations (7.200) and (7.201) are shown to be incorrect in the light of the definition of Δh_a and equations (7.206) and (7.207) apply instead.

Equation (7.195) can now be written as;

$$\Delta H_c = C_2'(\bar{V} - V_c)^2 + \frac{4L_c}{w(D^2 - d^2)} \left[f_{aw} \tfrac{1}{2} \frac{\rho \bar{V}_{am}^2 D}{1{,}25} + f_{ac} \tfrac{1}{2} \frac{\rho V_r^2 d}{1{,}25} \right] - h_{fc} \qquad (7.208)$$

for horizontal pipes,

where $f_{aw} = \dfrac{0{,}079}{(R_{epw})^{0{,}25}}$ (7.209)

and $f_{ac} = \dfrac{0{,}079}{(R_{ecw})^{0{,}25}}$ (7.210)

Let $R_{epw} = \dfrac{\bar{V}_{am} (D - d)\, 1{,}25}{\nu}$ (7.211)

and $R_{ecw} = \dfrac{(\bar{V}_{am} - V_c)(D - d)\, 1{,}25}{\nu}$

24. Method of determining the total drag and lift force on a mobile capsule

Equation (7.197) cannot be utilised for the determination of the total head loss across the capsule since the lift force (L_F) is unknown.

However, the equation can be used for finding the force tending to move the mobile capsule if the total head loss across the capsule is determined.

In words, equation (7.197) may be expressed as follows:-

> The excess pressure drop across the capsule is equal to the pressure loss due to solid to solid friction of the capsule on the pipe wall plus the shear stress on the pipe wall due to pressure and Couette flow minus the pressure drop which would occur in a length (L_c) of capsule-free pipe.

This concept of the total force transmitted to the pipe wall by the water and capsule can be extended to the sloping and vertical pipes as shown in Section 22.

Instead of considering the forces on the pipe wall we can now apply equation (7.197) in order to find the total drag force on the capsule.

If the capsule is not accelerating, the nett force on it must be zero and the nett forward drag is just in balance with the total resisting force. From equations (7.188) and (7.189) we get;

$$D_T = D_f + \left[\bar{\tau}_{cp}\,\pi dL_c - \bar{\tau}_{cc}\,\pi dL_c\right] = \mu_f W'(\cos\phi - L_r) + W\sin\phi \qquad (7.213)$$

which for horizontal pipes reduces to;

$$\overrightarrow{D_f + \bar{\tau}_{cp}\,\pi dL_c} = \overleftarrow{\mu_f W'(1 - L_r) + \bar{\tau}_{cc}\,\pi dL_c} \qquad (7.214)$$

Referring to <u>fluid</u> drag forces, equation (7.214) can be rearranged to give

$$D_{Tf} = D_f + (\bar{\tau}_{cp} - \bar{\tau}_{cc})\,\pi dL_c = \mu_f W'(1 - L_r) \qquad (7.215)$$

and inserting equation (7.194) we get;

$$D_{Tf} = \frac{w\pi D^2}{4}(\Delta H_c + h_{fc}) - (\bar{\tau}_{pp} + \bar{\tau}_{pc})\,\pi DL_c \qquad (7.216)$$

where D_{tf} = total drag force in the direction of capsule motion.

Thus, there are two ways of expressing the <u>fluid</u> drag on the capsule, equations (7.215) and (7.216), and these expressions must be both compatible and equal to the solid to solid retarding force.

The Couette and pressure shear components, on the capsule, in equation (7.215) can be replaced by the gross shear stress on the capsule wall, thus;

$$D_{Tf} = D_f + \bar{\tau}_c \pi d L_c = \mu_f W'(1 - L_r)$$

Also the independent pressure and Couette components on the pipe wall in equation (7.216) can be replaced by the gross value thus;

$$D_T = \Delta H_c - \bar{\tau}_p \pi D L_c + h_{fc} = \mu_f W'(1 - L_r) \qquad (7.217)$$

From equation (7.215) and (7.216)

$$\frac{w\pi D^2}{4} \frac{(\Delta H_c + h_{fc})}{W'} - \frac{(\bar{\tau}_{pp} + \bar{\tau}_{pc}) \pi D L_c}{W'} = \mu_f(1 - L_r) \qquad (7.218)$$

$$\therefore \quad \mu_f(1 - L_r) = \frac{\Delta H_c + h_{fc} - (\bar{\tau}_{pp} + \bar{\tau}_{pc}) \frac{4L_c}{Dw}}{\left(\frac{d}{D}\right)^2 L_c \left| S_c - 1 \right|} \qquad (7.219)$$

The expression on the right hand side of equation (7.219) is the nett fluid force on the capsule causing capsule motion divided by the submerged weight of the capsule.

This expression is, of course, the same as equation (7.197) and since it will be shown that all the terms on the right hand side can be measured or calculated, the equation is useful for the determination of the lift ratio (L_r), if the coefficient of solid to solid friction is known.

If the capsule is lifted completely off the pipe bed, equation (7.219) yields;

$$\Delta H_c''' = (\bar{\tau}_{pp} + \bar{\tau}_{pc}) \frac{4L_c}{Dw} - h_{fc} \qquad (7.220)$$

This equation states that, if there is no physical contact between the capsule and pipe wall, the excess pressure head loss across the capsule is the total shear force on the pipe wall (due to Couette and pressure flow) minus the circular pipe head loss in a capsule-free pipe of length (L_c).

This equation (7.220) is general, and applies to sloping and vertical

pipes if the component of capsule weight is taken into account so that, for vertical pipes;

$$(\Delta H_c)'_s = \left(\frac{d}{D}\right)^2 \left| S_c - 1 \right| L_c + (\bar{\tau}_{pp} + \bar{\tau}_{pc}) \frac{4L_c}{Dw} - h_{fc} \qquad (7.221)$$

which is similar to equation (7.142) except that $\bar{\tau}_p$ for pressure flow is replaced by $(\bar{\tau}_{pp} + \bar{\tau}_{pc})$ for pressure plus Couette flow.

25. Finite element method of analysis

Equation (7.196) provides an alternative (to the "gross" method) analytical procedure for finding the total excess head loss across a mobile capsule (ΔH_c).

The following points have been dealt with:-

1. In Section 1 the type of flow existing in the annulus of a mobile capsule was discussed and it was explained how sections of the annulus (in the eccentric case) can be laminar whilst other sections have turbulent flow.
2. It was also shown in Section 21 that from the analogous case of laminar flow in the mobile capsule annulus, the average velocity for turbulent flow is assumed to consist of two components, the pressure and Couette component,

$$\bar{V}_{am} = \bar{V}_{ap} + \bar{V}_{ac}$$

3. A method for analysing laminar and/or turbulent pressure flow in the annulus of an eccentric capsule has been discussed in Section 14.
4. Finally laminar and/or turbulent Couette flow has been analysed in Section 19.

The finite element method can now be explained.

25.1 Method of analysing the mobile capsule water system by finite elements

Basically, the method is one of integrating the pressure and Couette

flow components using finite elemental areas of annulus.

Starting from given values of mean water velocity $(\bar{V})$, capsule velocity (V_c) and capsule and pipeline geometry, the excess head loss across the capsule can be calculated.

Also, once all the terms on the right hand side of equation (7.219) have been found and the value for solid to solid friction (μ_f) measured, the lift ratio (L_r) can be calculated.

Furthermore, equation (7.220) can then be used for calculating the eccentricity, since $(\bar{\tau}_{pp})$ and $(\bar{\tau}_{pc})$ correspond to particular eccentricity values and all other terms in equation (7.220) are known. The velocity at which the capsule just starts to lift can also be found since the lift ratio is just equal to unity under these conditions.

The above calculations were carried out on the Univac 1106 computer and a detailed description of the programme, together with a listing is given in Appendix II. At this stage, rather than details of the programme, a brief outline of the finite element analytical procedure is given.

25.2 <u>Outline of finite element analysis for mobile capsule water system</u>

1. Given; the capsule characteristics, e.g. capsule diameter (d), pipe diameter (D), capsule length (L_c), specific gravity (S_c) and slope of pipeline. At arbitrarily chosen values of $(\bar{V})$ the excess head loss (ΔH_c) and capsule velocity (V_c) as determined experimentally, are also fed into the computer.

   There are three rounds to the main programme and this will be dealt with in Appendix II in detail. The first round assumes that the experimental value of excess head loss (ΔH_c) is correct and calculates the capsule velocity (V_c). The second round uses the experimental value of (V_c) to find (ΔH_c). The third round uses a semi-empirical value of (V_c) (discussed in Chapter 10) to find (ΔH_c).

2. From equation (7.130) and (7.133) the incipient velocity ($\bar{V}_i$) and incipient excess head loss (ΔH_{ci}) are calculated. The incipient velocity is required later for determining the capsule velocity (V_c) from the semi-empirical method (discussed in Chapter 10). Equation (7.133) is solved by means of the Newton Raphson iteration.
3. By successive approximations a value for (V_c) is found as discussed below, which ensures that the calculated value of (ΔH_c) corresponds to the experimental value. The following calculations are repeated until this is so.
4. The average velocity in the annulus of the mobile capsule water system ($\bar{V}_{am}$) is calculated from equation (7.179).
5. The Couette components of velocity ($\bar{V}_{ac}$) and shear stress due to Couette flow on the capsule and pipe wall ($\bar{\tau}_{cc}$) and ($\bar{\tau}_{cp}$) can next be calculated as follows. A value for the eccentricity (ϵ) of unity is assumed at this stage and this value will also be adjusted by successive approximations.
6. By considering each quasi-concentric annular slice the average velocity in laminar Couette flow can be determined from equation (7.174). The shear stresses on elements of the pipe and capsule walls are calculated from equations (7.176) and (7.177) in laminar Couette flow.
7. The Reynolds number for each slice is tested and the above calculations are terminated at the slice, yielding the critical Reynolds number.
8. If the Couette flow component in the slice under consideration is turbulent, the distance (b_c) from the capsule wall is found where the turbulent Couette velocity component is equal to the value of $V_c/2$ from equation (7.173) and the Newton Raphson iterative procedure.

9. The Reynolds numbers for the flow in the vicinity of capsule and pipe walls are calculated from

$$R'_{ecc} = \frac{V_c\, b_c}{2\nu} \quad \text{and} \quad R'_{ecp} = \frac{V_c\, b_p}{2\nu}$$

10. The shear velocities for capsule and pipe walls for turbulent Couette flow in an elemental area of quasi-concentric annulus are calculated from

$$u_{*p} = \frac{V_c}{2} \frac{0.19}{\log_{10} R'_{ecc}} \quad \text{and} \quad u_{*c} = \frac{V_c}{2} \frac{0.19}{\log_{10} R'_{ecp}}$$

11. Determine the Couette shear stress components on an elemental strip of pipe and capsule wall (ΔS_p and ΔS_c) from

$$\tau_{cc} = \rho\, u_{*c}^2$$

and $$\tau_{pc} = \rho\, u_{*p}^2$$

12. Find the average shear stress due to Couette flow, on the capsule and pipe walls by summing the elemental products of laminar and turbulent shear stresses components from

$$\bar{\tau}_{cc} = \Sigma\, \tau_{cc}\, \Delta S_c / \pi d$$

and $$\bar{\tau}_{pc} = \Sigma\, \tau_{pc}\, \Delta S_p / \pi D$$

13. The average velocity in the annulus due to Couette flow is found as follows:

From the equations for turbulent Couette flow velocity distribution, the flow in each sub-slice of elemental area in the quasi-concentric annulus can be found from

$$\Delta q_{ac} = u\, \Delta a$$

and the Couette flow component in an elemental slice can be found from

$$\Delta Q_{ac} = \Sigma\, \Delta q_{ac}$$

14. Determine the total flow in the annulus due to the Couette component by summing all the elemental flows in laminar and

turbulent flow

$$Q_{ac} = \Sigma \Delta Q_{ac}$$

15. Hence the mean Couette flow velocity in the annulus is determined from

$$\bar{V}_{ac} = Q_{ac}/(\tfrac{\pi}{4}(D^2 - d^2))$$

16. The flow velocity in the annulus due to the pressure flow component can next be obtained by subtraction, i.e.

$$\bar{V}_{ap} = \bar{V}_{am} - \bar{V}_{ac}$$

17. The following elucidates the method for obtaining the relation between the annular head loss due to pressure flow (Δh_{fa}) as a function of $\bar{V}_{ap}$.

In the purely numerical procedure it is necessary to start with the pressure gradient in the annulus $(\Delta P/L)$ and from the finite element method recounted in Section 14, a value for $\bar{V}_{ap}$ can be found. If this value does not agree with $\bar{V}_{ap}$ in step 16, the procedure is repeated until agreement is reached.

This is essentially a lengthy implicit procedure and involves repeating the entire finite element analysis, for pressure flow in the annulus, several times.

Fortunately, a much shorter method was found involving the pseudo-hydraulic mean radius concept discussed in Section 11, for annuli of unit eccentricity. This concept was extended to eccentric annuli in general and when succeeding approximations were done with $\epsilon \neq 1,0$ the empirical relations developed were quite satisfactory. It will be shown later (Chapter 13) that the finite element analysis for pressure flow agrees extremely well with the pseudo-hydraulic mean radius analysis (at any eccentricity) and, hence, with experiment.

The value of Δh_{fa} can thus be calculated from equations (7.94) and (7.96).

18. The finite element analysis for pressure flow is next used for calculating the average shear stress values on the pipe and capsule walls, i.e. $(\bar{\tau}_{pp})$ and $(\bar{\tau}_{cp})$ in pressure flow.

19. The inlet and outlet head losses as functions of $(\bar{V} - V_c)$ are next calculated from equation (7.199).

20. The excess head loss across the mobile capsule is determined from

$$\Delta H_c = \Delta h_{fa} + \Delta h_i + \Delta h_o - h_{fc}$$

21. The total shear stress on the pipe wall due to pressure plus Couette flow is next determined

i.e. $\bar{\tau}_p = (\bar{\tau}_{pp} + \bar{\tau}_{pc})$

22. The excess head across the mobile capsule is next calculated from equation (7.220)

i.e. $\Delta H_c''' = \frac{4L_c}{Dw} (\bar{\tau}_{pp} + \bar{\tau}_{pc}) - h_{fc}$

This value is for the case of no contact between capsule and pipe wall.

23. If the difference between ΔH_c and $\Delta H_c'''$ (i.e. $\Delta_c = \Delta H_c - \Delta H_c'''$) is negative then the capsule has lifted off the pipe bottom. The eccentricity ratio (ϵ) is decreased by a prescribed finite increment and the entire calculation repeated until $\Delta H_c - \Delta H_c''' <$ a small prescribed value, (i.e. when $\Delta H_c \doteq \Delta H_c'''$) the theoretical eccentricity is attained and the first velocity at which this phenomenon occurs corresponds to the velocity at which the capsule first lifts off the pipe bottom.

24. If $\Delta H_c''' < \Delta H_c$ then the capsule does not lift off the pipe bottom and equation (7.219) can be used for calculating the force on the capsule divided by the submerged weight of the capsule as well as the lift ratio (L_r).

25. The whole calculation is repeated three times as discussed in

step 1, and for the first round the experimental value ΔH_c is assumed correct and the capsule velocity (V_c) is evaluated by successive approximations (i.e. the whole calculation is repeated for different V_c values until the calculated ΔH_c is very close to the experimental value of ΔH_c.

The comparison of experimental and analytical results will be discussed in Chapter 15 and any discrepancies must be ascribed to either experimental errors or analytical assumptions. Experimental errors have been dealt with in Chapter 6 and analytical assumptions will be dealt with in Chapter 15.

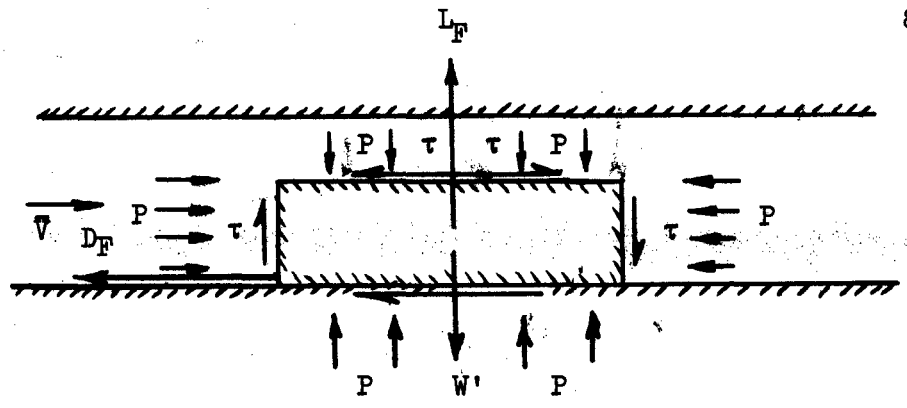

Figure 8.1

1. Normal forces

The normal pressure forces are at right angles to the capsule surface at all points. The pressure forces vary in a longitudinal and circumferential direction in a more complicated manner than shown above.

In general the pressure forces impart a forward drag to the capsule. Any net vertical components of pressure, in a horizontal pipe, would impart a lift to the capsule and possibly a moment about the centre of gravity, although there can be no moment when the capsule is not in contact with the pipe wall.

2. Tangential forces

Shear forces act tangentially to the surface at all points. These tangential forces are, in general, less significant than the normal pressure forces when solid to solid friction is present.

The resultant component of shear forces parallel to the pipe axis may impose a forward or backward drag on the capsule and the perpendicular components will usually cause lift effects and possibly moments.

The flow of water in the annulus gives rise to skin friction which may be divided up into two components; the component due to pressure flow which causes a forward drag skin friction force, and the Couette flow component due to the movement of the capsule relative to the pipe wall, which causes a backward skin friction drag.

The effects of pressure flow stresses and Couette shear stresses

along the capsule vary from point to point around the perimeter and the net effect may be a backward or forward drag force. In most instances of mobile capsules the net effect constitutes a backward drag force.

3. Solid to solid friction forces

The solid to solid wall friction, if it exists, always tends to oppose capsule motion. The coefficient of friction between the capsule and pipe wall is of significance both from the point of view of the dynamics and the kinematics.

The coefficient of friction stems from one of the two basic laws of friction. The friction force is proportional to the load between the surfaces, i.e.

$$\mu_f = \frac{\text{Friction force}}{\text{Load}}$$

The other basic law of friction is that the friction is independent of the area of contact between the solids.

Sometimes quoted as a third law, is the observation by Coulomb (in 1781) who made a clear distinction between static and kinetic (dynamic) friction. He showed that the latter friction could be appreciably lower than the former and the third law is that the kinetic friction is nearly independent of the speed of sliding.

Coulomb considered that the friction might be due to molecular adhesion between the surfaces but rejected this, because, if it were so, the friction should be proportional to the area of contact. He considered the interlocking of the surface asperities caused the friction and represented the work of lifting the load over these asperities.

In fact, his first view is more correct (reference 6) and friction is largely due to adhesion between the surfaces.

3.1 Surface cleanliness

The most important factor affecting the coefficient of friction is surface cleanliness (reference 6).

Even a single molecular layer of grease from the atmosphere or from the fingers may produce a very large change in friction.

3.2 Roughness

A most significant fact is that surface cleanliness is far more important than surface roughness. The latter has only a small effect on the friction.

This is a most important point since corrosion or wear of the capsule or pipeline (if steel) could be expected to have very little effect on the capsule independent variables.

For plastic pipes and capsules, roughening the capsules, providing they are of the same material, would have very little effect. This was verified experimentally and will be discussed in Chapter 11.

3.3 Capsule velocity

The static friction (μ_f) is accepted as being somewhat greater than the kinetic friction (μ_f') but the difference is not usually very great. This is because the basic mechanism is essentially unchanged.

It is conventionally accepted that this is not so since the mechanism of kinetic friction is, for most engineering purposes, different from that for static friction. For example, with increased speed of sliding, frictional heating may cause softening or melting of the surface layers. This is obviously not the case with capsules sliding in a pipeline and, in fact, only occurs at extremely high speeds with metals.

3.4 The mechanism of friction

Even the smoothest of surfaces is rough on an atomic scale. Contact only occurs at the tips of the peaks. Over the rest of the surface there may be large gaps. The gaps are completely separated. The load is thus borne on the tips of the asperities. Over these regions, where intimate contact takes place, the materials become, in effect, a continuous solid.

When the surfaces slide over one another the junctions must be sheared and the force to do this is equal to the frictional resistance. These ideas have been verified experimentally by means of the electron micrograph and these microscopic studies have shown one material adhereing to the other.

If the material to be sheared has a mean shear strength (s) and a real area of contact (a) then according to the two basic laws of friction, the area of contact is proportional to the load and independent of the size or shape of the surface, (see Figure 8.2).

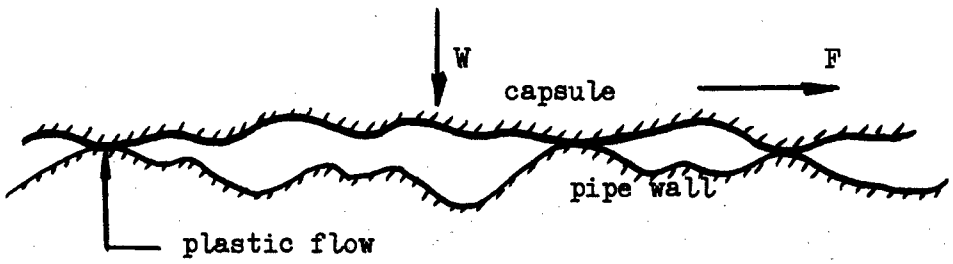

Figure 8.2

The sketch shows plastic deformation at the points of real contact

$$\mu = F/W = as/aP = s/P$$

where P = yield pressure of the material.

Experiments (reference 6) show that (s) is equal to the bulk shear strength of the softer material of a sliding pair.

The materials used for most of the capsule experiments were Polyvinylchloride (P.V.C.) and Polymethylmethacrylate (Perspex) for the pipes. These materials, which are thermoplastics, having long molecular chains and coefficients of friction, when both sliding surfaces are of the same material, of 0,4 to 0,5.

The values are of the same order as those of metals. If a study, of these non-metallic solids, is made of the surface damage produced during sliding (reference 6) it is found that there is marked "adhesion, plucking and transfer of the plastic from one surface to the other".

When sliding on metals (e.g. brass capsule in perspex pipe) there is not only transfer of plastic to the metal but transfer of metal to the plastic.

The mechanism of friction (reference 6) is essentially the same as for metals and the coefficient of friction may again be taken as s/P.

One major difference between the frictional behaviour of these materials and metals is the effect of load. With metals the deformation at the region of contact is directly proportional to load. With plastics the coefficient of friction increases as load is reduced and this effect can be very marked at light loads. This is due to their visco-elastic property so that the contact deformation is not truly plastic.

When a capsule travels down a pipeline, in contact with the pipe, the solid to solid friction is profoundly modified by the presence of the water which acts as a lubricating fluid.

3.5 Fluid lubrication

The moving surfaces are separated by a continuous film of lubricant and resistance to motion arises from the viscosity of the fluid.

It seems likely that surface roughness should have an effect in this case since, if the separating film is comparable with the size of surface asperities, the fluid resistance is supplemented by solid to solid contact.

For hydrodynamic lubrication the distance between the capsule and pipe wall depends on a parameter of the type $\mu.V_c/P$ where p is the pressure between the surfaces. If the capsule velocity (V_c) is low or the pressure high, the separation can become less than the height of the asperities and the surfaces will rub and be separated in places by only a thin layer of water. This is known as boundary lubrication. The conditions for this type of mixed lubrication or semi-hydrodynamic lubrication are satisfied when pressures are high and capsule velocities very low.

The frictional force may be expressed as the sum of two terms: the

force required to shear solid junctions and the force required to shear the lubricant film.

4. Combination of the above forces

The motion of the capsule depends on the interaction and magnitudes of the above forces.

When the capsule is static the pressure forces on the capsule ends plus the skin friction on the capsule surface in the annulus is in balance with the solid to solid friction and the friction coefficient (μ_f) is less than the limiting value.

When the mean water velocity ($\bar{V}$) is greater than the incipient velocity ($\bar{V}_i$), the capsule begins to slide along the pipe bottom. In this case the pressure drag and the skin friction drag cause the motion and are forward acting and must exceed the solid to solid friction force plus the component of capsule weight down the slope (in an upward sloping pipe in the direction of flow), while the capsule is accelerating. And when a steady state is reached all forces are again in balance.

Increasing the velocity still further causes a reversal of the skin friction force on the capsule. This is because the Couette shear force dominates the shear force due to pressure flow. At the same time the solid to solid friction force is decreased and this is due to a reduction in the downward force component on the capsule brought about by lift forces.

Increasing the water velocity yet further causes the capsule to lift off the pipe bottom and the pressure drag (forward) is just in balance with the skin friction drag (backwards) when a steady state is reached.

In this instance the lift force is just in balance with the submerged weight of the capsule.

5. Lift, drag and buoyancy forces

These forces are a result of the normal pressure forces and the

tangential shear forces.

The lift force is caused by the tangential and normal forces with the latter effect dominating. The drag forces are also caused by combinations of normal and tangential forces with the former effect dominating if solid to solid friction is present.

The buoyancy force is defined as that upward force which acts on the submerged capsule at rest. And this value is assumed to be maintained when the capsule is mobile so that lift forces are defined as those vertically upward forces over and above the buoyancy force component.

The above definitions are used because of the difficulty in separating buoyancy and lift forces in the mobile capsule case.

The lift and drag forces will now be discussed separately.

6. Drag forces

The total drag force can be divided up into two components, the form drag and the skin friction drag. The latter can also be divided (somewhat arbitrarily) into skin friction drag due to pressure flow and that due to Couette flow.

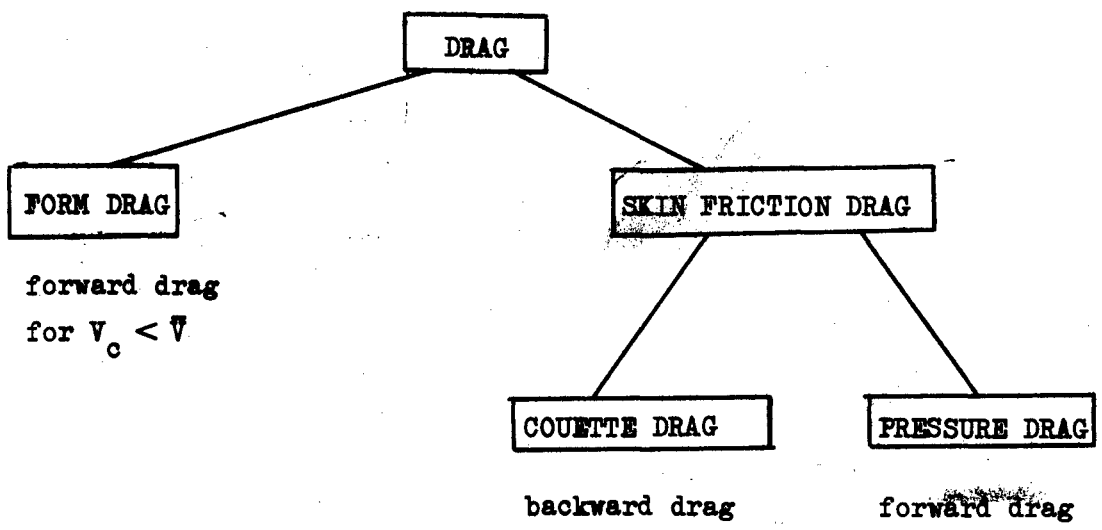

7. Form drag for static capsules

The form drag on the capsule depends on the capsule shape (or form) and for the cylindrical capsules considered, the size (diameter and length) of capsule is the only criterion of form drag at a fixed velocity. It is basically the end effects which give rise to form drag. The form drag is essentially due to the pressure difference acting on the upstream and downstream faces of the capsule.

For a finite capsule the end effects modify the pressure and shear forces acting on the capsule. Separation from the angular upstream face of the capsule, together with expansion downstream of the capsule (causing a wake) give rise to streamline curvature, and these inertial effects influence the form drag, if the water velocity relative to the capsule is positive in the direction of flow.

The form drag (D_f) can be expressed as follows:

$$D_f = f(R_e, \text{form})\, A_c \tfrac{1}{2}\rho(\bar{V} - V_c)^2$$

$$= C_D\, A_c(\rho/2)(\bar{V} - V_c)^2 \qquad (8.1)$$

where $(\bar{V} - V_c)$ is the average water velocity relative to the capsule and A_c is the frontal area of the capsule. $V_c = 0$ for static capsules.

For cylinders in an infinite medium, the value of C_D varies from 1,12 for a circular flat plate $(L_c/d = 0)$ to 0,99 for a cylinder with $L_c/d = 7{,}0$.

The following values are given by Rouse (Fluid Mechanics for Hydraulic Engineers p 228) for Reynolds number $> 10^3$.

C_D	1,12	0,91	0,85	0,87	0,99
L_c/d	0	1	2	4	7

For capsules it is obvious that wall effects will be highly significant, particularly for eccentric capsules, in a closed pipe. And it is likely that these boundaries will modify the form drag markedly.

Only in the most elementary cases can C_D be determined analytically and the study of drag coefficients has remained largely experimental.

For incipient capsules the form drag can be determined from equation (7.119) and

$$D_f = D_T - \bar{\tau}_c \pi d L_c$$

$$= \mu_f W' \cos \phi + W \sin \phi - \bar{\tau}_c \pi d L_c$$

From equation (7.127);

$$\bar{\tau}_c \pi d L_c = w \Delta h_{fa} \pi (D^2 - d^2)/4 - \bar{\tau}_p \pi D L_c$$

For horizontal pipes;

$$D_T = \mu_f W' = \mu_f w \left[\pi d^2/4\right] L_c \left|S_c - 1\right|$$

$$\therefore \quad D_f = \mu_f (\pi d^2/4) w L_c \left|S_c - 1\right| - w \Delta h_{fa} \pi (D^2 - d^2)/4 + \bar{\tau}_p \pi D L_c$$

From equation (7.126);

$$\mu_f (\pi d^2/4) w L_c \left|S_c - 1\right| = (\Delta h_{fa} + \Delta h_i + \Delta h_o - \bar{\tau}_p 4 L_c/wD)(\pi D^2/4) w$$

$$\therefore \quad D_f = (\Delta h_{fa} + \Delta h_i + \Delta h_o)(\pi D^2/4) w - \bar{\tau}_p \pi D L_c - w \Delta h_{fa} \pi (D^2 - d^2)/4 + \bar{\tau}_p \pi D L_c$$

$$= (\pi d^2/4) w \Delta h_{fa} + (\pi D^2/4) w (\Delta h_i + \Delta h_o)$$

$$= A_c w (\Delta h_{fa} + (D/d)^2 (\Delta h_i + \Delta h_o))$$

Now $\Delta h_i + \Delta h_o = 1/2g \{k' + k_o (1/(1 - (d/d)^2) - 1)^2\} \bar{V}^2$

$$= (1/2g) C_2' (\bar{V}^2)$$

$$\therefore \quad D_f = A_c 2\rho g/2 (\Delta h_{fa} + (D/d)^2 (1/2g) C_2' (\bar{V})^2)$$

and $$D_f = C_D A_c \tfrac{1}{2} \rho (\bar{V} - V_c)^2 \qquad (8.2)$$

where $C_D = 2g \Delta h_{fa}/(\bar{V})^2 + (D/d)^2 C_2'$ and $V_c = 0$ for static capsules

$$= f L/[R_p (1 - (d/D)^2)^2] + (D/d)^2 C_2'$$

For all values of diameter ratio d/D the first term on the right hand side is negligible if the capsule is not too long, i.e. $L_c/d < 4,0$

compared with the second term.

$$\therefore \quad C_D = C_2' (D/d)^2$$

and for eccentric annuli the form drag coefficient (C_D) can be written as

$$C_D = \left[22(d/D)^6 + 0{,}68\left[\frac{1}{1 - (d/D)^2} - 1\right]^2\right](D/d)^2 \qquad (8.3)$$

For mobile capsules the form drag is given by equation (8.2) and is a function of $(\bar{V} - V_c)$. Since it is possible for V_c to be greater than $\bar{V}$ the form drag may act backwards although this is not generally so because in the mobile capsule case Δh_{fa} becomes significant. Figure 8.3 shows the value for the form drag coefficient in an infinite medium compared with the coefficient determined for the eccentric annular case of the capsule (the concentric form drag coefficient has a similar pattern).

It is clear that boundary effects are enormous and the boundary proximity causes a high form drag increase at high diameter ratios.

It is easy to see that the form drag coefficient increases with diameter ratio since the pipe wall is closer to the capsule wall for more of the perimeter thus decreasing the skin friction due to pressure flow.

At $d/D = 1{,}0$ the capsule velocity (V_c) must equal the mean water velocity $(\bar{V})$ and all the forward drag becomes form drag. It becomes meaningless to speak of a drag coefficient in such a situation and the drag coefficient tends towards infinity.

8. Skin friction drag due to Couette flow

Due to capsule motion the additional component of flow in the annulus is designated Couette flow and the shear force on the capsule wall is a backward drag which always opposes capsule motion.

There can be no flow relative to the capsule at the surface of the capsule itself and the same applies to the pipe wall.

In this section it will be shown how the Couette shear stress is distributed around the capsule and the effect of capsule velocity, eccentricity,

FIG. 8.3

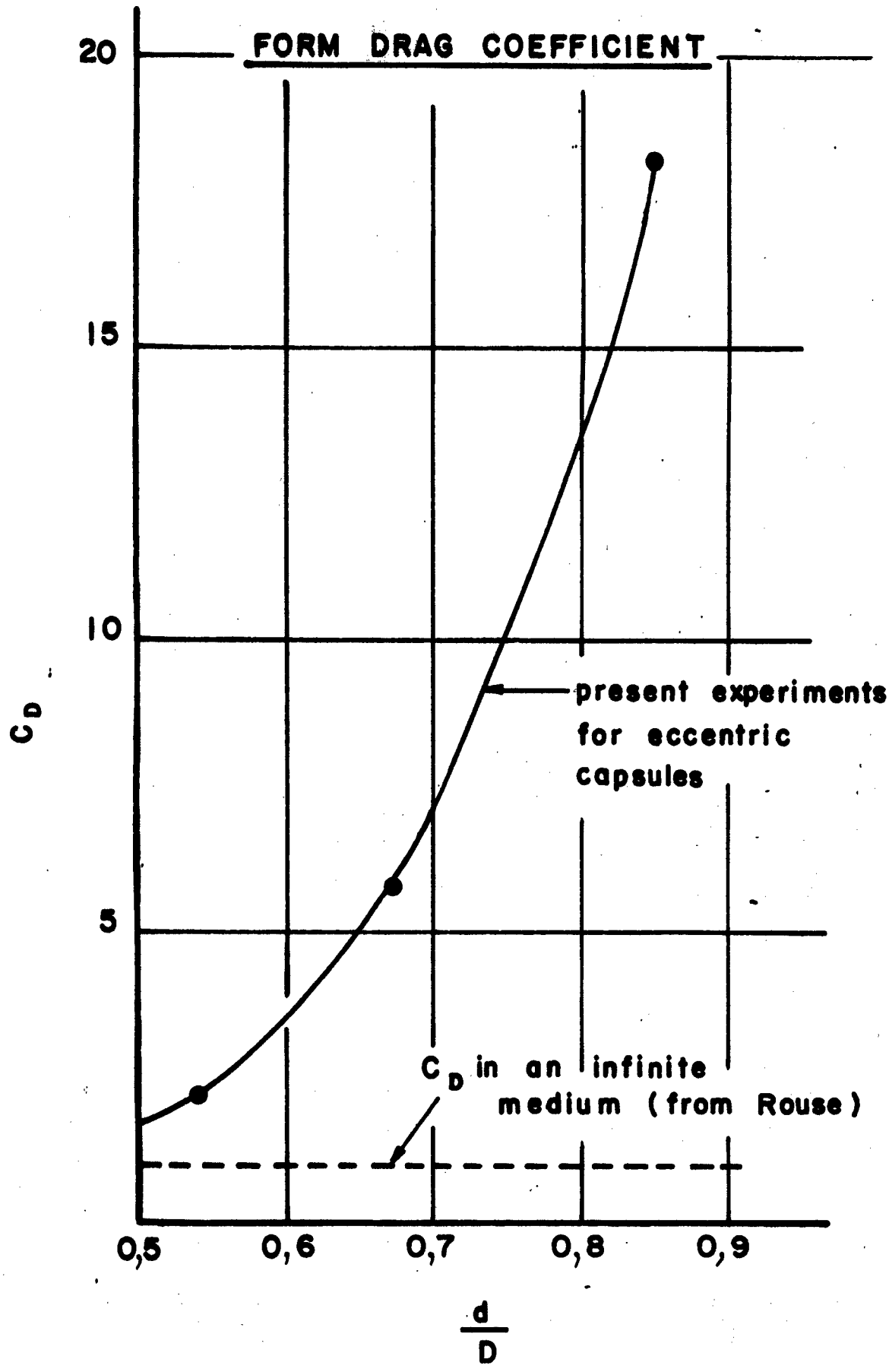
FORM DRAG COEFFICIENT
20
15
10
5
C_D
present experiments for eccentric capsules
C_D in an infinite medium (from Rouse)
0,5
0,6
0,7
0,8
0,9
$\frac{d}{D}$

diameter ratio and pipe diameter on the shear stress due to Couette flow will be dealt with.

8.1 Effect of capsule velocity on Couette shear stress

Figure 7.43 shows velocity distributed curves for annular, curved (cylindrical) Couette flow as well as shear stresses on the water due to the motion of the capsule relative to the pipe wall.

Consider the top velocity profile (i.e. V_c = 3 m/s) the average shear stress on the pipe wall due to Couette flow is $\bar{\tau}_{pc}$ = 7,937 Pa. This is for a variation from top to bottom of τ_{pc} = 4,78 Pa to 53,8 Pa, roughly 11 to 1. Similarly the average shear stress on the capsule due to Couette flow is slightly greater.

$$\bar{\tau}_{cc} = 9{,}323 \text{ Pa}$$

with a variation of τ_{cc} = 53,9 Pa at the bottom to τ_{cc} = 6,6 Pa at the top. roughly 8 : 1.

Thus, the shear stress (due to Couette flow) on the capsule wall is greater than that on the pipe wall (according to the diameter ratio d/D) and the ratio shear stress at the bottom to shear stress at the top is greater for the pipe wall than the capsule wall. This is obvious since the shear stress at the bottom, where the pipe and capsule walls are parallel, must be identical for both walls.

Note that the contour of $u = V_c/2$ is much closer to the capsule than the pipe wall.

Figure 8.4 shows how the shear stress, due to Couette flow, is distributed around the capsule perimeter with capsule velocity (V_c) as parameter at a fixed eccentricity (ϵ = 0,99) and diameter ratio (d/D = 0,85). These curves are derived from the finite element analysis for Couette flow using quasi-concentric polar co-ordinates.

The shear stress is highest where the gap (G = 55 μm) is smallest, at the bottom, in laminar flow, and the value of τ_{cc} decreases rapidly

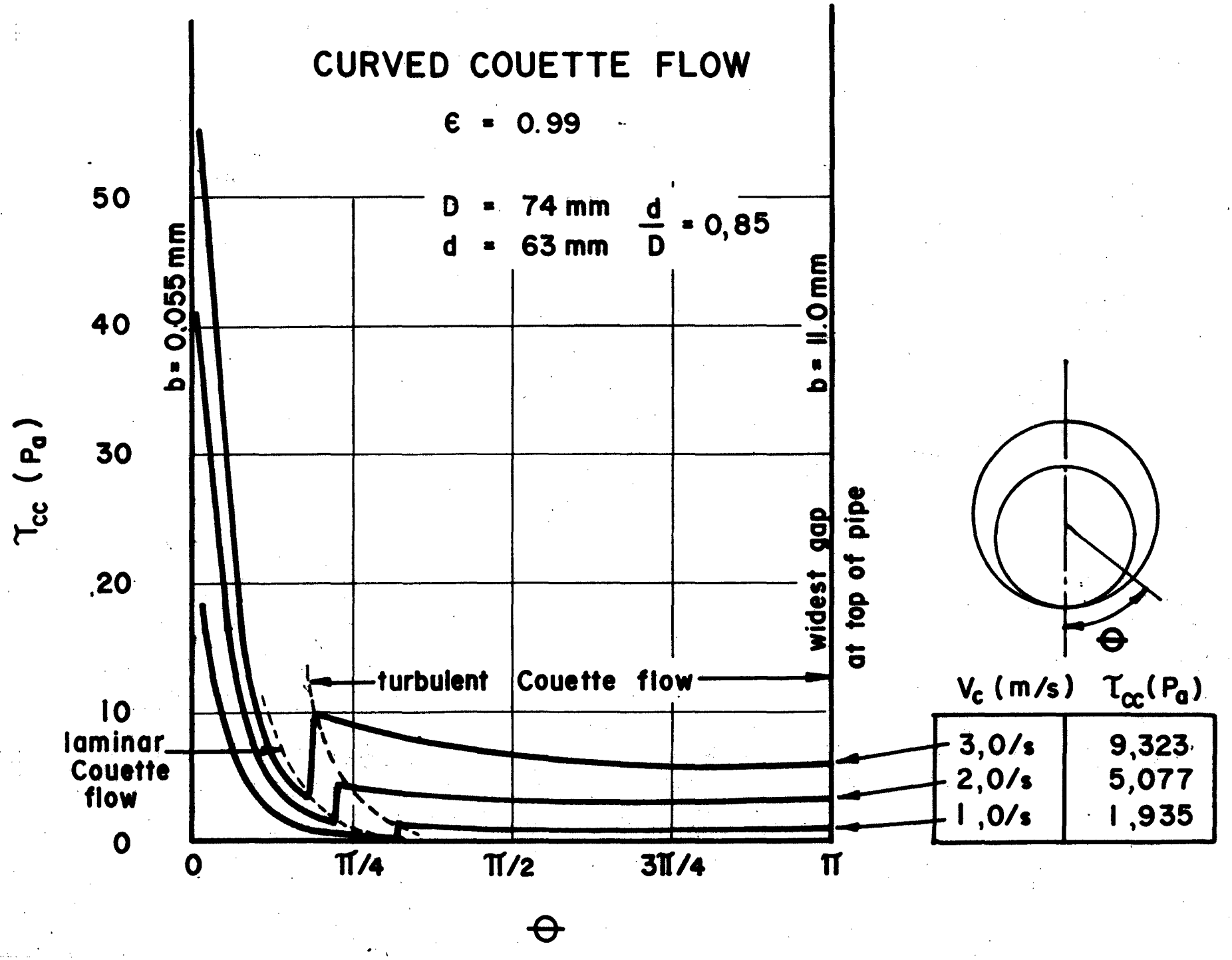
CURVED COUETTE FLOW
ϵ = 0.99
D = 74 mm
d = 63 mm
d/D = 0,85
b = 0,055 mm
b = 11,0 mm
widest gap at top of pipe
turbulent Couette flow
laminar Couette flow
τcc (Pa)
50
40
30
20
10
0
0
π/4
π/2
3π/4
π
ϕ
Vc (m/s)
τcc (Pa)
3,0/s
9,323
2,0/s
5,077
1,0/s
1,935

FIG. 8.4

until $\theta \doteq \pi/4$ when the Couette flow becomes turbulent with a sudden increase in shear stress and then a gradual decrease until $\theta = \pi$ where the gap is widest at the top of the pipe. The Couette flow component becomes turbulent at decreasing angles around the perimeter (θ) as the capsule velocity increases and the transition occurs over a wider shear stress range (τ_{cc}).

It should not be assumed that the pattern of change from laminar to turbulent Couette flow is correct when pressure flow is superimposed, and it must be emphasised that these curves are essentially analytical. Cylindrical curved Couette flow is not discussed in the literature and no experimental results are available.

8.2 Effect of eccentricity on Couette shear distribution around capsules

The curves shown on Figure 8.4 are for one eccentricity. The effect of eccentricity is considerable, as would be expected, and at unit eccentricity the shear stress tends to infinity at the point of contact between capsule and pipe wall (since $dv/dr \rightarrow \infty$).

Figure 8.5 shows the effect of eccentricity (ε) on the shear stress variation. As the eccentricity decreases from 1,0 to 0,95 there is a 400 : 1 ratio of shear stress on the capsule wall at $\theta = 0{,}01\pi$ (at the bottom).

At low eccentricities $(\varepsilon < 0{,}8)$ the eccentricity does not have a great influence on the angle at which the flow change from laminar to turbulent, and (at $V_c = 3$ m/s) the flow is turbulent around the entire annulus. Whereas, at higher eccentricity values $(\varepsilon > 0{,}8)$ the flow becomes turbulent at ever increasing values of θ as the eccentricity increases towards unity.

8.3 Effect of eccentricity on average Couette shear on capsules

Figure 8.6 shows the average value of shear stress on the capsule due

FIG. 8.5

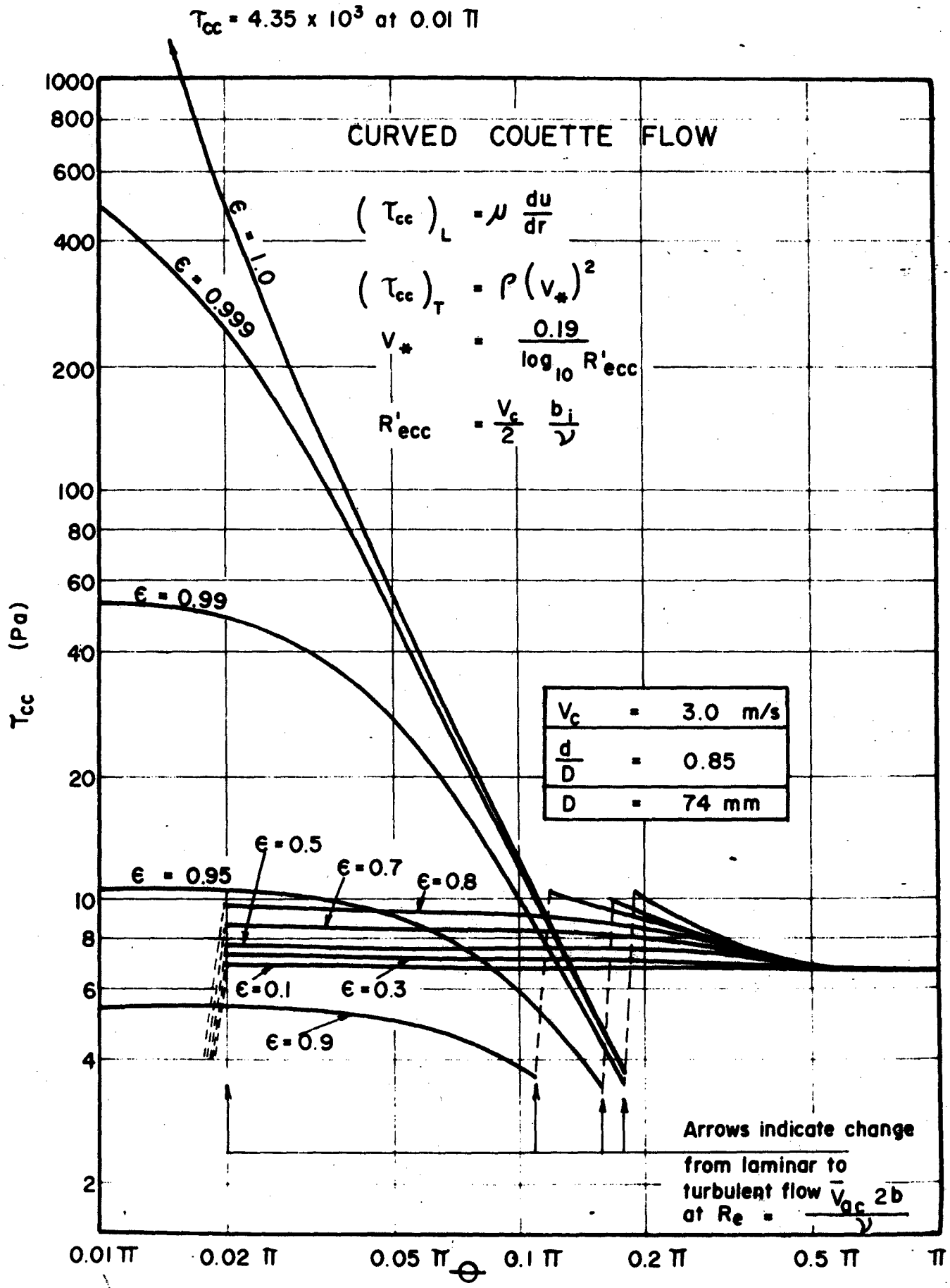
$\tau_{cc} = 4.35 \times 10^3$ at 0.01 π
CURVED COUETTE FLOW
$(\tau_{cc})_L = \mu \frac{du}{dr}$
$(\tau_{cc})_T = \rho (V_*)^2$
$V_* = \frac{0.19}{\log_{10} R'_{ecc}}$
$R'_{ecc} = \frac{V_c}{2} \frac{b_i}{\nu}$
ε = 1.0
ε = 0.999
ε = 0.99
ε = 0.95
ε = 0.5
ε = 0.7
ε = 0.8
ε = 0.1
ε = 0.3
ε = 0.9
V_c = 3.0 m/s
$\frac{d}{D}$ = 0.85
D = 74 mm
Arrows indicate change from laminar to turbulent flow at $R_e = \frac{\bar{V}_{ac} 2b}{\nu}$
τ_{cc} (Pa)
1000
800
600
400
200
100
80
60
40
20
10
8
6
4
2
0.01 π
0.02 π
0.05 π
0.1 π
0.2 π
0.5 π
π
θ

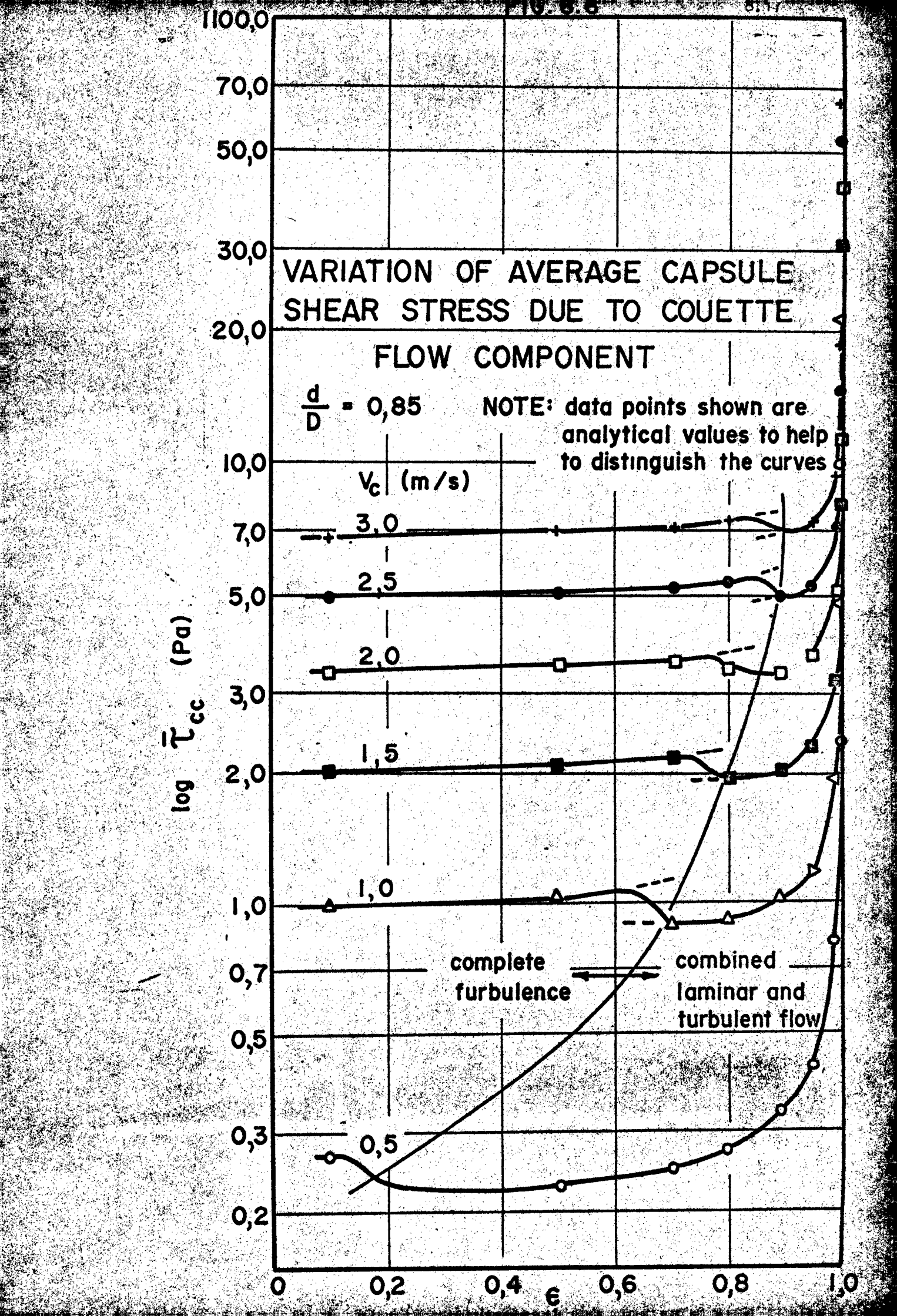
VARIATION OF AVERAGE CAPSULE SHEAR STRESS DUE TO COUETTE FLOW COMPONENT
d/D = 0,85
NOTE: data points shown are analytical values to help to distinguish the curves
Vc (m/s)
3,0
2,5
2,0
1,5
1,0
0,5
complete furbulence
combined laminar and turbulent flow
log τcc (Pa)
ε
1100,0
70,0
50,0
30,0
20,0
10,0
7,0
5,0
3,0
2,0
1,0
0,7
0,5
0,3
0,2
0
0,2
0,4
0,6
0,8
1,0

to Couette flow ($\bar{\tau}_{cc}$) as a function of eccentricity ratio (ϵ) with capsule velocity as parameter. There is a slight discontinuity in the average shear stress values ($\bar{\tau}_{cc}$). This occurs when the flow changes from complete turbulence to combined laminar and turbulent flow.

Combined laminar and turbulent flow occurs at lower eccentricities as the capsule velocity is decreased. This is because complete turbulence is maintained at higher eccentricities as capsule velocity (and hence $\bar{V}_{ac}$) increases.

At a particular capsule velocity the average Couette shear stress on the capsule ($\bar{\tau}_{cc}$) increases very slightly with eccentricity increase, until complete turbulence is no longer evident. In the combined laminar and turbulent region the average shear stress increase with eccentricity, is more rapid (particularly at high capsule velocities) and becomes asymptotic to the abscissa value of unit eccentricity. This is due to high local values of τ_{cc} near the bottom in laminar flow where dv/dy for Couette flow becomes infinite when the capsule touches the pipe wall.

Similar curves are obtained for the average shear stress, due to Couette flow, on the pipe wall.

8.4 The effect of diameter ratio on Couette shear stress distribution around capsules

Figure 8.7 shows τ_{cc} as a function of θ for varying capsule diameters in a pipe of fixed diameter ($D = 74$ mm) at a constant capsule velocity ($V_c = 3$ m/s) and eccentricity ($\epsilon = 0{,}999$).

The graph is symmetrical about the vertical axis of pipe and capsule at an abscissa value of π.

Considering a particular capsule diameter, the shear stress around the perimeter, due to Couette flow, decreases rapidly until the flow becomes turbulent, at which angle there is a discontinuity. For the second largest capsule shown ($d = 63$ mm) there is an approximately 100 : 1 decrease in

FIG. 8.7

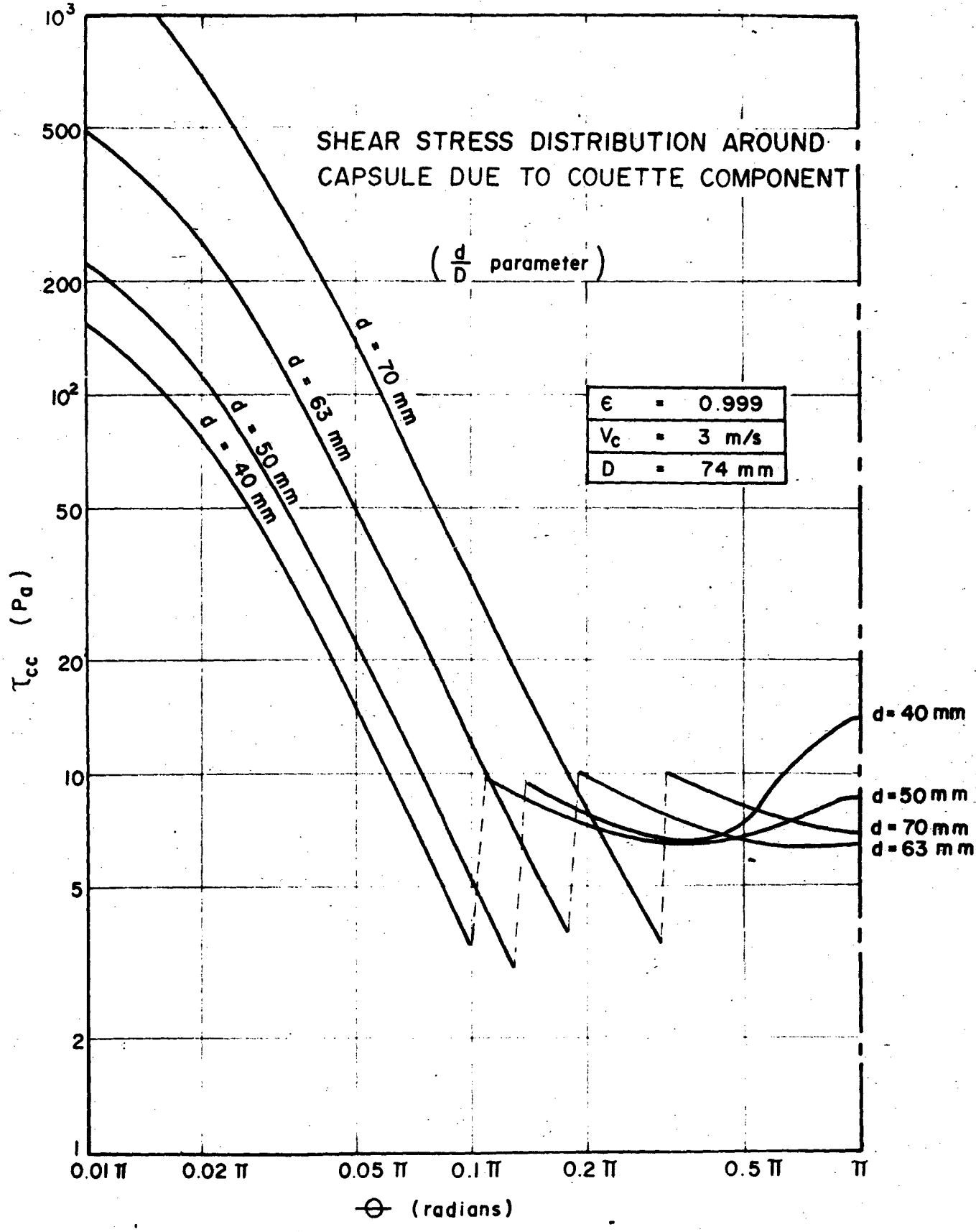
SHEAR STRESS DISTRIBUTION AROUND CAPSULE DUE TO COUETTE COMPONENT
(d/D parameter)
ε = 0.999
Vc = 3 m/s
D = 74 mm
d = 70 mm
d = 63 mm
d = 50 mm
d = 40 mm
d = 40 mm
d = 50 mm
d = 70 mm
d = 63 mm
τcc (Pa)
10³
500
200
10²
50
20
10
5
2
1
0.01 π
0.02 π
0.05 π
0.1 π
0.2 π
0.5 π
π
θ (radians)

shear stress from the bottom of the capsule to the angle $(\theta = 0,18\pi)$ when the flow ceases to be laminar. This ratio decreases considerably with diameter ratio, because the surfaces of capsule and pipe wall are less parallel at the point of closest contact, as diameter ratio decreases. Laminar flow is maintained to a greater extent around the capsule as diameter ratio increases. This is because the distance between capsule and pipe wall is less at a greater angle around the perimeter. Proceeding around the capsule perimeter in the turbulent regime, the shear stress decreases initially and then begins to rise again, the minimum value in the turbulent regime occurring at an ever increasing angle as diameter ratio increases. This is because the local shear stress value is a function of the local value of the shear velocity squared, which is in turn a function of the inverse of R'_{ecc}.

$$\therefore \qquad \tau_{cc} \propto 1/b_c^2$$

Figure 8.8 serves to illustrate the way in which b_c and b (whose local values are b_{ci} and b_i) vary with angle (θ). The value of b_{ci} is shown in polar co-ordinates in the top figure and the lower figure is an expanded view of the perimeter showing local values of b and b_c for two different diameter ratios (i.e. $d/D = 0,85$; and $d/D = 0,54$).

For the large diameter ratio $(d/D = 0,85)$ the value of b_c increases with angle increase up to π radians, about which axis the figure is symmetrical. In the case of the smaller diameter ratio, the Couette flow force balance yields a value of b_c which increases up to approximately $0,35\pi$ radians and then decreases. Reverting to Figure 8.7 it can be seen that the minimum value of τ_{cc} occurs at about $0,35\pi$ radians.

Since, $b_{pi} = b_i - b_{ci}$ and for both diameter ratios given in Figure 8.8, b_p increases with θ, it can be expected that the shear stress distribution around the pipe wall in Couette flow, would not show a minimum shear stress value in the turbulent regime. This is verified on Figure 8.9 which shows

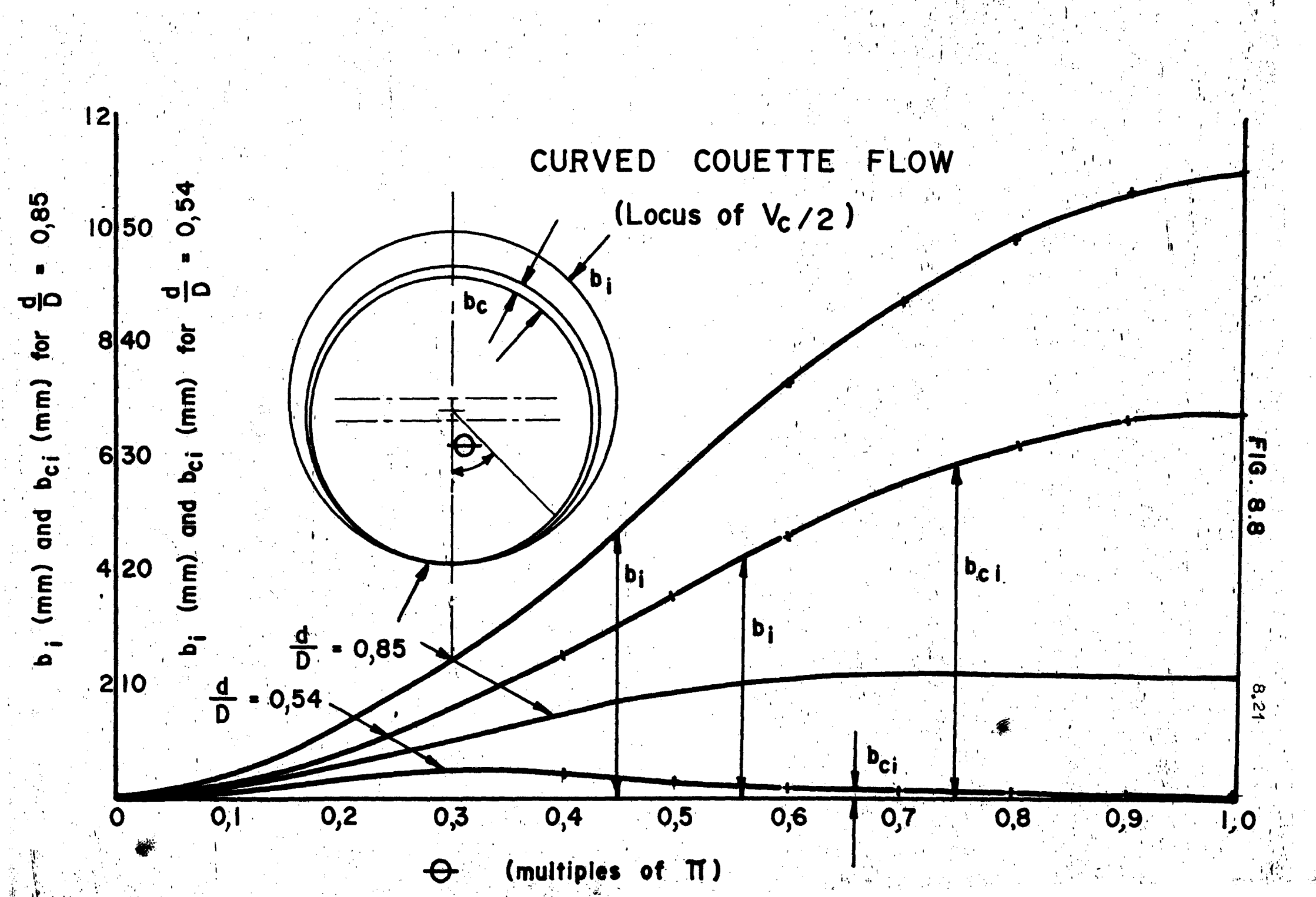
CURVED COUETTE FLOW
(Locus of $V_c/2$)
b_i (mm) and b_{ci} (mm) for $\frac{d}{D}$ = 0,85
b_i (mm) and b_{ci} (mm) for $\frac{d}{D}$ = 0,54
b_i
b_c
θ
$\frac{d}{D}$ = 0,85
$\frac{d}{D}$ = 0,54
b_i
b_i
b_{ci}
b_{ci}
12
10
8
6
4
2
50
40
30
20
10
0
0,1
0,2
0,3
0,4
0,5
0,6
0,7
0,8
0,9
1,0
θ (multiples of π)
FIG. 8.8
8.21

FIG. 8.9

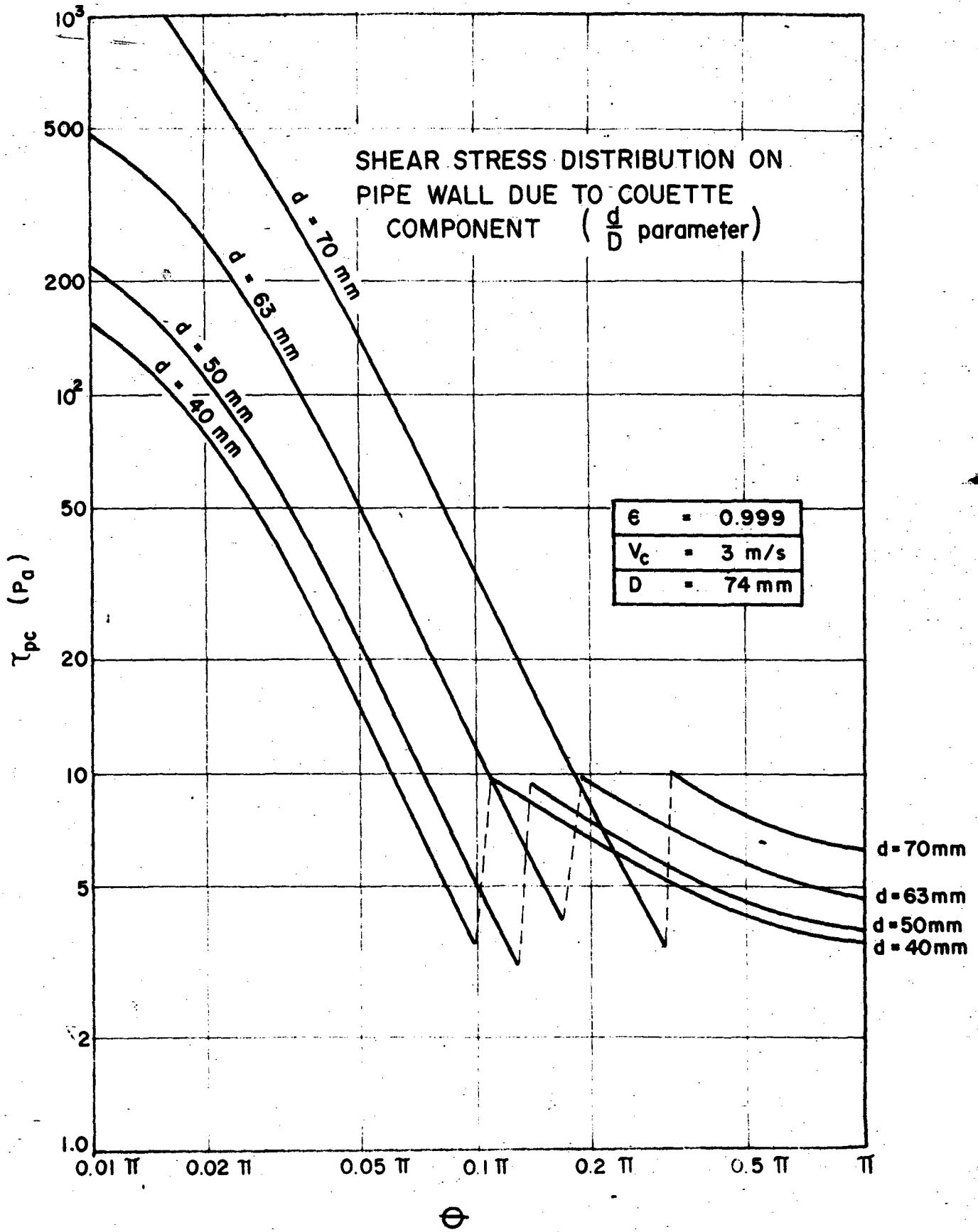
SHEAR STRESS DISTRIBUTION ON PIPE WALL DUE TO COUETTE COMPONENT (d/D parameter)
d = 70 mm
d = 63 mm
d = 50 mm
d = 40 mm
ε = 0.999
Vc = 3 m/s
D = 74 mm
τpc (Pa)
θ
0.01 π
0.02 π
0.05 π
0.1 π
0.2 π
0.5 π
π
d=70mm
d=63mm
d=50mm
d=40mm

an ever decreasing shear stress on the pipe wall around the perimeter except for the discontinuity between laminar and turbulent flow.

8.5 Effect of diameter ratio on the average shear stress on pipe and capsule wall

Figure 8.10 shows average shear stresses ($\bar{\tau}_{cc}$ and $\bar{\tau}_{pc}$) as functions of diameter ratio keeping eccentricity ($\epsilon = 0{,}999$), capsule velocity ($V_c = 3$ m/s) and pipe diameter ($D = 74$ mm) constant.

As has been shown previously, the average Couette shear stress on the capsule $\bar{\tau}_{cc}$ is invariably higher than that on the pipe wall, and both values increase with diameter ratio tending towards an infinite asymptote at unit diameter ratio (in which case $\epsilon = 0$).

8.6 Effect of pipe diameter on average Couette shear

Figure 8.11 shows the average Couette shear stress on the capsule ($\bar{\tau}_{cc}$) plotted against pipe diameter. A typical diameter ratio ($d/D = 0{,}85$) is shown and other diameter ratios yield similar curves. Three eccentricity values are given and a range of capsule velocities are represented.

The most significant feature of this graph is the increase of average capsule Couette shear stress as pipe diameter is decreased.

A particular value of $\bar{\tau}_{cc}$ corresponds to a higher velocity in a larger pipe. The pipe diameter giving a $\bar{\tau}_{cc}$ value of (say) 8,0 Pa at $V_c = 2{,}5$ m/s is $D = 57$ mm and the same Couette shear stress would be generated on a capsule in a larger pipe diameter ($D = 103$ mm) at $V_c = 3{,}0$ m/s keeping the diameter ratio and eccentricity constant.

This corresponds to circular pipe flow where wall shear stress is less in larger diameter pipes at a constant mean water velocity since

$$\tau = f \tfrac{1}{2} \rho \bar{V}^2$$

and f decreases with increasing pipe diameter (in smooth pipes).

A further point to note in connection with figure 8.11 is that increase in capsule shear stress, due to Couette flow, with pipe diameter reduction,

FIG. 8.10

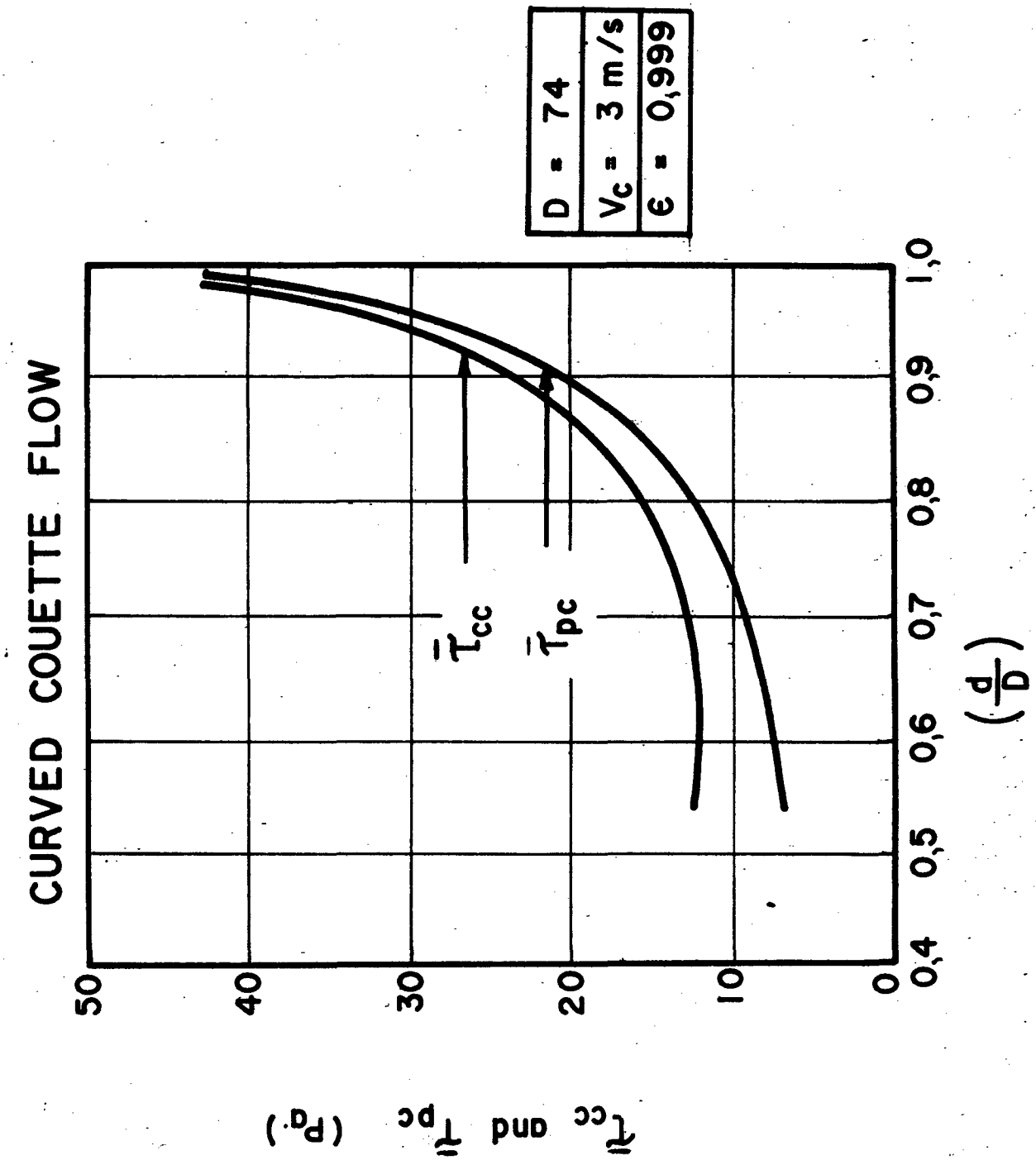
D = 74
Vc = 3 m/s
ε = 0,999
CURVED COUETTE FLOW
$\bar{\tau}_{cc}$
$\bar{\tau}_{pc}$
50
40
30
20
10
0
0,4
0,5
0,6
0,7
0,8
0,9
1,0
$\left(\frac{d}{D}\right)$
$\bar{\tau}_{cc}$ and $\bar{\tau}_{pc}$ (Pa)

FIG. 8.11

CURVED COUETTE FLOW

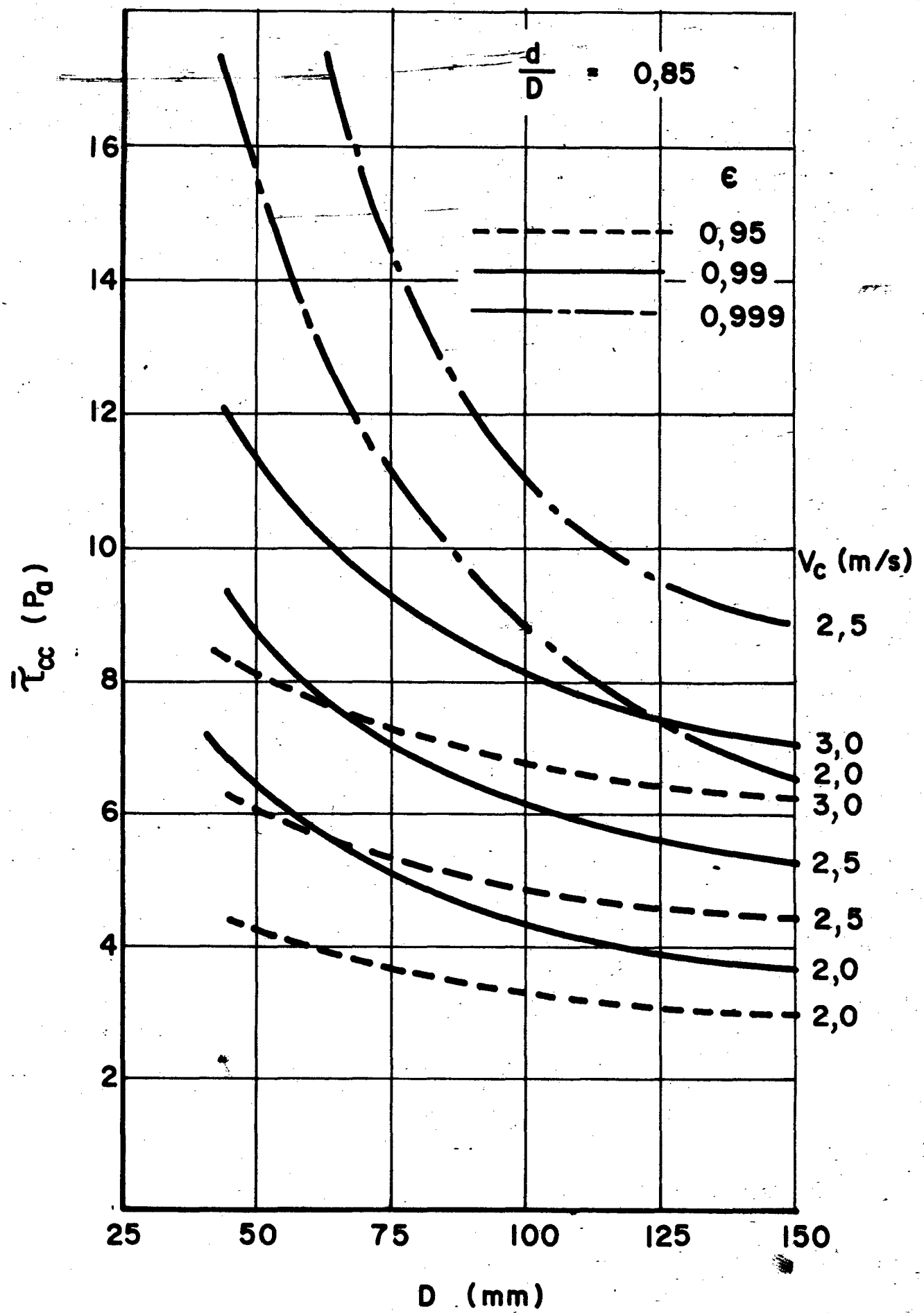

at a constant capsule velocity, is accentuated as eccentricity increases.

For example, reducing the pipe diameter by half, from $D = 150$ mm to 75 mm, at $V_c = 2,5$ m/s causes a 17,8 % increase in the value of $\bar{\tau}_{cc}$ at $\epsilon = 0,95$. Whereas, the same diameter reduction at the same capsule velocity and an eccentricity of $\epsilon = 0,999$, results in a 62 % increase in the value of $\bar{\tau}_{cc}$.

A third point to note is that absolute changes in $\bar{\tau}_{cc}$ with pipe diameter decrease, are similar at different capsule velocities.

To sum up: Of most significance is the tremendous effect that eccentricity has on the shear stress due to Couette flow and hence the backward drag on the capsule. This is mainly due to the large stresses at the bottom in the laminar flow region. The other noteworthy features are the effects of diameter ratio, capsule velocity and pipe diameter, all of which, when increasing, cause an increased backward shear on the capsule wall.

9. Skin friction drag due to pressure flow

The shear on the capsule wall due to pressure flow always imposes a forward drag and would appear to be a function of the capsule surface area $(d^2 L_c)$ as well as the average water velocity relative to the capsule. However, the excess head loss across the capsule is also a function of the pipe surface area in the capsule zone as well as the water velocity relative to the capsule in this zone.

These were the assumptions for the gross method of analysis. For the finite element method, the excess head loss was assumed to be a function of the pressure flow velocity in the annulus $(\bar{V}_{ap})$.

9.1 Effect of pressure flow velocity component $(\bar{V}_{ap})$

Two components of flow velocity were assumed in the annulus, i.e. the pressure component $(\bar{V}_{ap})$ and the Couette component $(\bar{V}_{ac})$. It is assumed in the finite element analysis that the latter is unaccompanied by pressure

drop so that the skin friction drag (forward) on the capsule due to the pressure flow component is a function of $\bar{V}_{ap}$.

Figure 8.12 shows the drag force (forward) on the capsule as well as the pipe wall, as determined from the finite element analysis for pressure flow only (using the velocity distribution laws mentioned in Appendix II). The curves show how the forward drag increases with $\bar{V}_{ap}$ and this is expected.

These curves were also plotted on logarithmic paper and the force on the capsule, due to pressure flow $\bar{F}_{cp}$, is related to $\bar{V}_{ap}$ via a power law;

$$\bar{F}_c = f(\bar{V}_{ap}^{1,73})$$

Two sets of curves are shown on Figure 8.12 for different diameter ratios and it is clear that as diameter ratio is decreased the ratio of force on the capsule to force on the pipe is increased.

The shear force on the pipe and capsule wall due to pressure flow is generally higher for increasingly higher diameter ratios.

The effect of diameter ratio on the pipe to capsule force ratio can best be seen on Figure 8.13, which is mainly for concentric annuli and shows that the rapidity of increase in the force ratio with decreasing d/D is much greater for eccentric than for concentric annuli.

Figure 8.13 is obtained from equations (7.51) and (7.52) using the radius of maximum velocity from equation (7.41) for the concentric laminar case and Randhava's equation, (7.71) (from Leung) for turbulent flow. It is clear from this Figure (8.13) that the ratio $\bar{\tau}_{pp}/\bar{\tau}_{cp}$ is less for laminar than for turbulent flow.

There is experimental evidence that the ratio $\bar{\tau}_{pp}/\bar{\tau}_{cp}$ as given by making use of Randhava's equation, may be too low.

The solid point (at $d/D = 0,476$) was obtained by direct measurement of the force on the pipe wall (reference 33).

Briefly, this was done by fixing the core in position and suspending

PRESSURE FORCE AT CAPSULE AND PIPE WALL

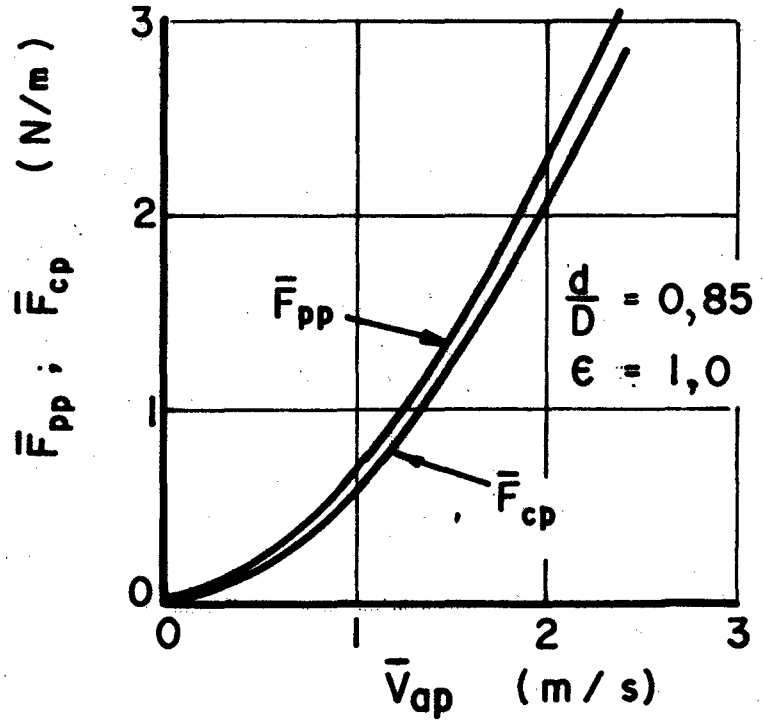

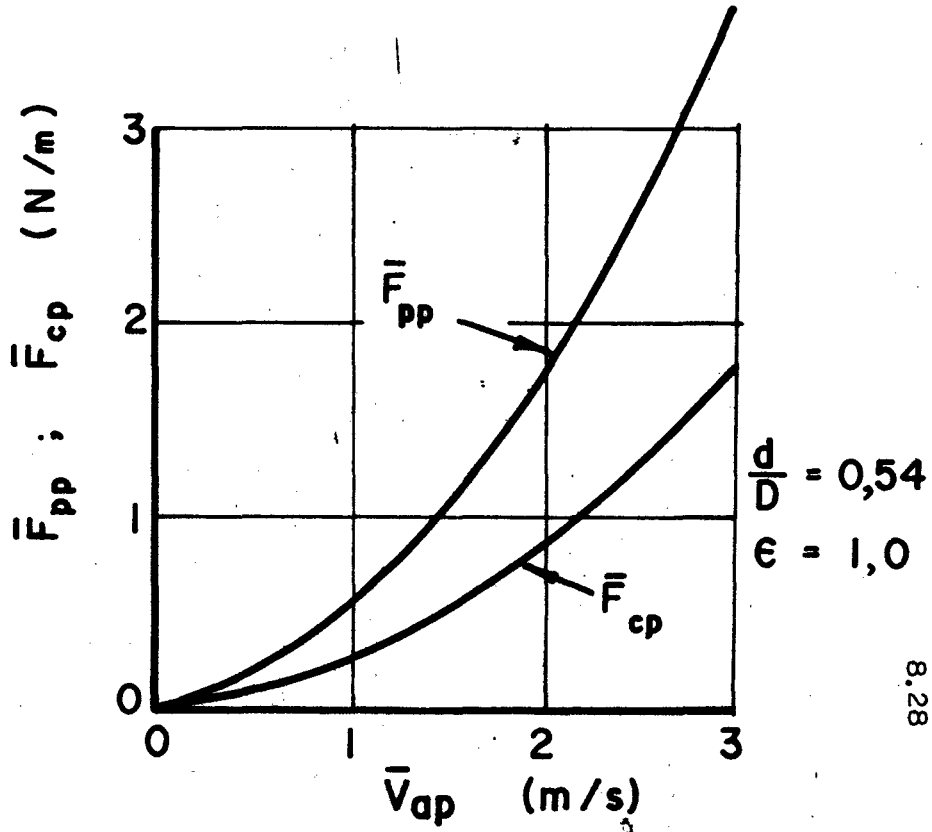

FIG. 8.12

FIG. 8.13

FORCE AND SHEAR STRESS RATIO DUE TO PRESSURE FLOW IN CONCENTRIC ANNULUS

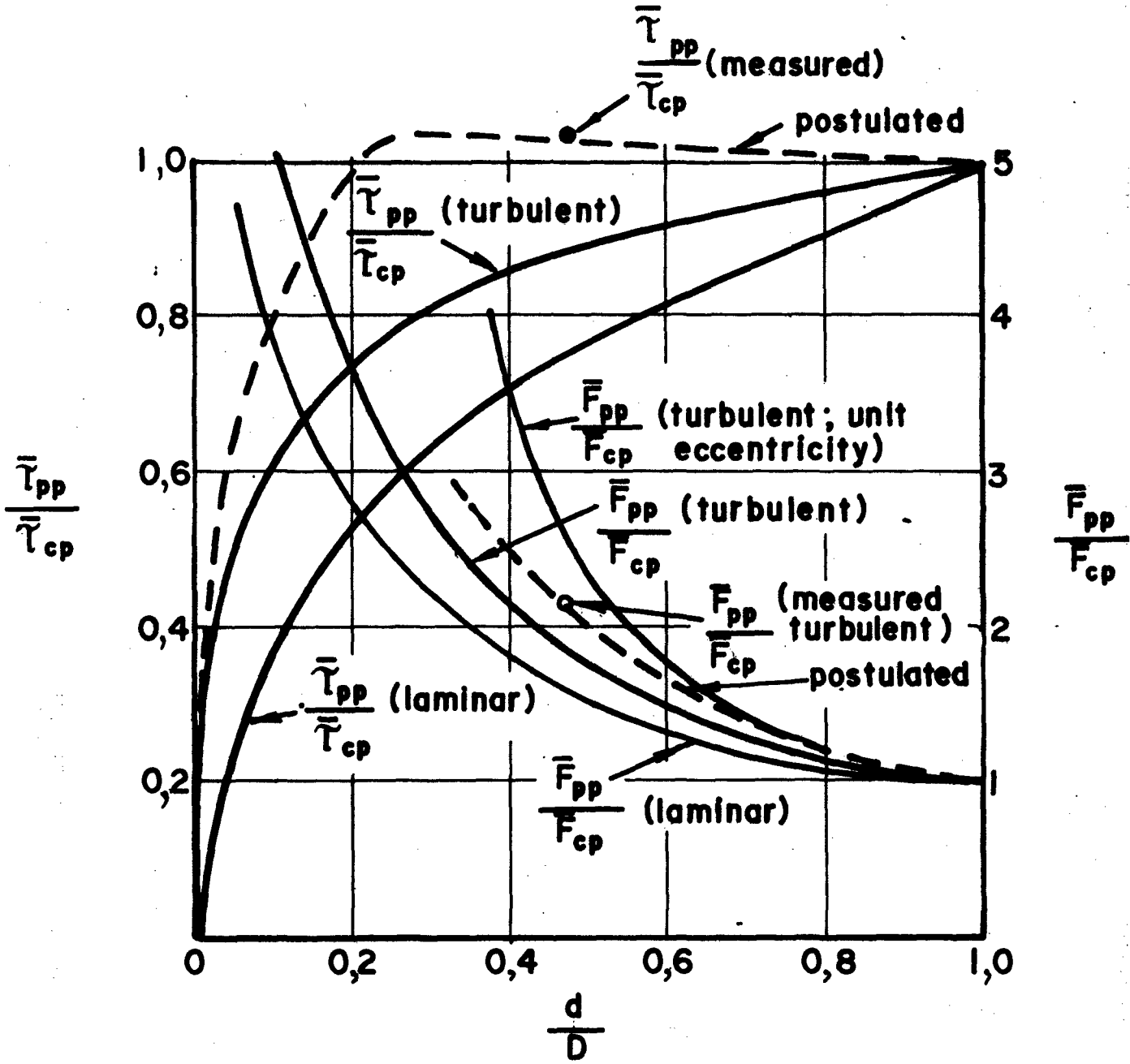

the pipe on a weight balance so that the force reduction, due to upward flow of water in the annulus, could be determined directly.

By measuring the pressure drop, it was possible to obtain the total force on the pipe and core from the force balance equation. The measured force on the pipe could then be subtracted from the total force to get the force on the core. It can be seen from the graph that the measured force ratio ($\bar{F}_{pp}/\bar{F}_{cp}$) (due to pressure flow) is about 14 % higher than that calculated when using Randhava's equation. From the postulated dotted curves it is apparent that as diameter ratio increases the discrepancy decreases and is of the order of 11 % at $d/D = 0,85$.

For comparison, the force ratio, force on pipe : force on capsule, is also shown. This curve was obtained from the finite element analysis using quasi-concentric polar co-ordinates and the velocity distribution of Knudsen and Katz. This is shown for turbulent flow and unit eccentricity.

Figure 8.14 shows, for the same diameter ratio ($d/D = 0,851$) at a fixed eccentricity of unity, how the pressure shear stress varies around the capsule perimeter, with the velocity due to pressure flow in the annulus ($\bar{V}_{ap}$) as parameter. The most significant features are, firstly, the substantial circumferential variation with the largest shear occurring at the widest gap and, secondly, the increase in shear stress with velocity which occurs all the way round the circumference.

The change from laminar to turbulent flow always occurs a fair way around the circumference and even at the highest velocity, 23 % of the circumference is in laminar pressure flow. This value increases to 30 % as the velocity is reduced to $\bar{V}_{ap} = 1,18$ m/s. A 55 % velocity reduction causes a 30 % increase in the amount of circumference in laminar flow. The circumferential variation of shear stress is in direct conflict with the shear stresses imposed by Couette flow and the effects of this will be discussed in Section 10.

SHEAR STRESS DISTRIBUTION ON CAPSULE WALL DUE TO PRESSURE FLOW

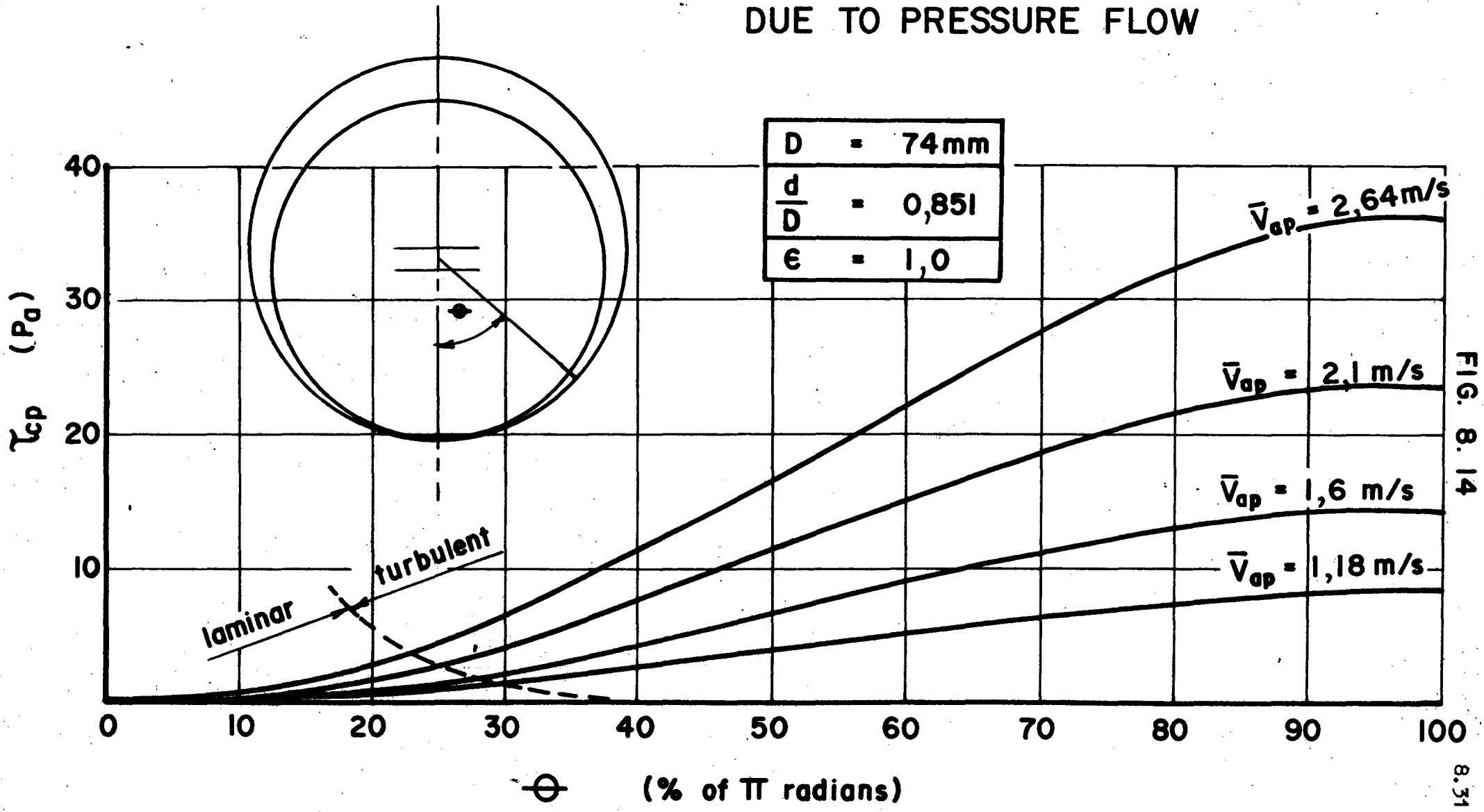

FIG. 8.14

9.2 Effect of eccentricity on pressure shear (τ_{cp}) around capsule

Figure 8.15 shows the effect of eccentricity on the circumferential shear stress distribution. This effect is substantial, the shear stress, at zero eccentricity, being uniformly distributed around the capsule and the variation from uniformity increasing steadily as eccentricity increases towards unity. Note that the shear stress has the same value quarter way round the circumference, regardless of the eccentricity.

The top insert curve shows how the shear force on the capsule due to pressure flow decreases with eccentricity. The effect of eccentricity is slight giving a total (pressure flow) shear force reduction of only about 7 % as eccentricity ratio (ϵ) is increased from zero to unity.

The numerical analysis for results given on Figure 8.15 was carried out for a constant annular head loss ($\Delta h_{fa}/L_c = 0.25$) and this meant that the velocity in the annulus ($\bar{V}_{ap}$) changed slightly for different eccentricities. Figure 8.15 (top insert) shows that the effect of increasing the eccentricity is to cause a slight increase in the velocity ($\bar{V}_{ap}$) and this effect is partially responsible for the slight reduction in the force on the capsule wall. Nonetheless, it is clear that eccentricity does not greatly affect the average pressure force on the capsule as opposed to the Couette shear where eccentricity exerts a tremendous effect. The combined effect is discussed in Section 10.

Figure 8.15 also shows how eccentricity increase causes the capsule laminar region to fall away at eccentricities other than unity. The dotted curve indicates change from laminar to turbulent flow and only the curve for $\epsilon = 1$ is affected.

Figure 8.16 shows how the forward pressure drag on both capsule and pipe wall is affected by eccentricity and the slight decrease in capsule drag, due to pressure flow, is accompanied by an increase in drag at the pipe wall as eccentricity ratio (ϵ) increases.

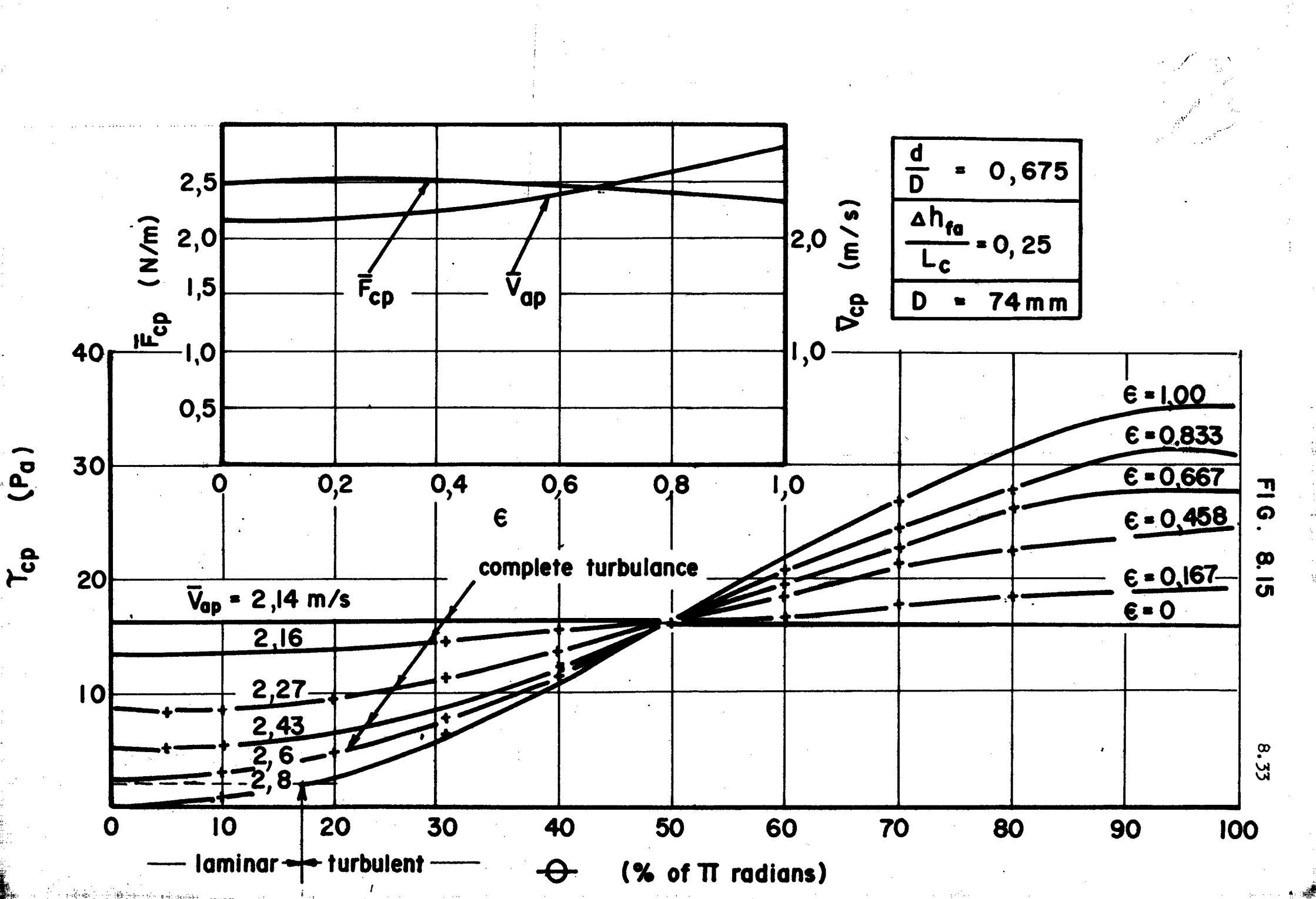
$\frac{d}{D}$ = 0,675
$\frac{\Delta h_{fa}}{L_c}$ = 0,25
D = 74 mm
$\bar{F}_{cp}$ (N/m)
$\bar{V}_{cp}$ (m/s)
$\bar{F}_{cp}$
$\bar{V}_{ap}$
2,5
2,0
1,5
1,0
0,5
0
0,2
0,4
0,6
0,8
1,0
ϵ
τ_{cp} (Pa)
40
30
20
10
0
10
20
30
40
50
60
70
80
90
100
ϵ = 1,00
ϵ = 0,833
ϵ = 0,667
ϵ = 0,458
ϵ = 0,167
ϵ = 0
complete turbulance
$\bar{V}_{ap}$ = 2,14 m/s
2,16
2,27
2,43
2,6
2,8
laminar
turbulent
(% of π radians)

FIG. 8.15

FIG. 8.16

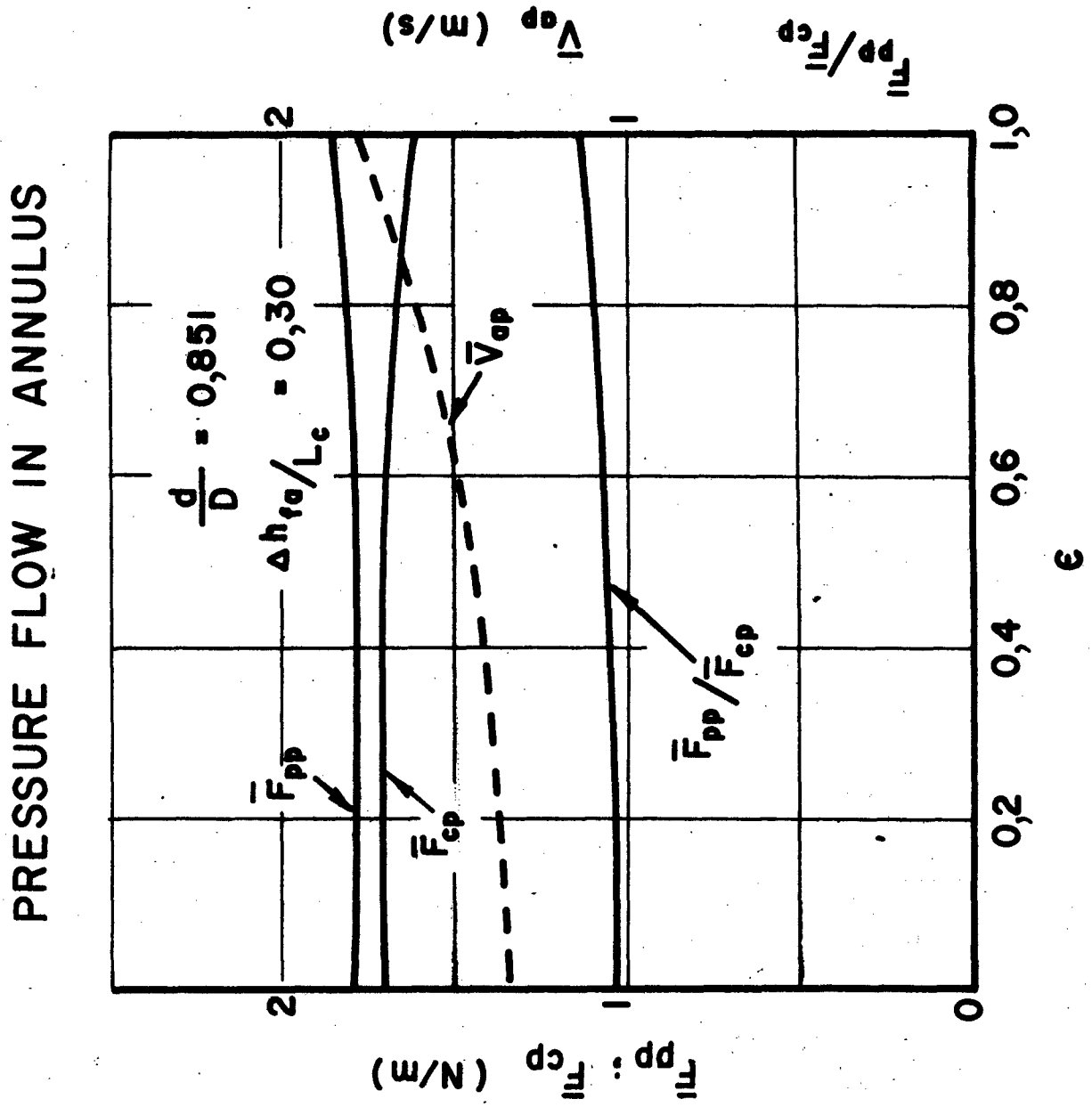
PRESSURE FLOW IN ANNULUS
d/D = 0,851
Δh_fa/L_c = 0,30
V̄_ap
F̄_pp
F̄_cp
F̄_pp/F̄_cp
V_ap (m/s)
F_pp ; F_cp (N/m)
ε
0
0,2
0,4
0,6
0,8
1,0
2
1
2
1

This means that the ratio of pressure drag on the pipe wall to pressure drag on the capsule wall $(\bar{F}_{pp}/\bar{F}_{cp})$ increases with ϵ as shown on the lower part of the figure.

9.3 Effect of diameter ratio on shear stress distribution and average forward drag on the capsule due to pressure flow

Figure 8.17 shows how the capsule shear stress distribution increases around the circumference with diameter ratio (d/D) as parameter for a fixed value of annular head loss $(\Delta h_{fa}/L_c = 0,25)$. There is a substantial increase of shear stress at all points around the circumference as diameter ratio decreases. At the same time, less of the annulus has laminar flow, so that, for a diameter ratio $(d/D = 0,95)$, almost half of the annulus per metre length is in the laminar regime, whilst, for $(d/D = 0,543)$ only about 15 % of the annulus is laminar.

The effect of diameter ratio on the total drag force is shown in the top of the diagram (Figure 8.17) and the shear stress distribution increase with diameter ratio decrease is manifest as an increase in the average force on the capsule. Although the effect of diameter ratio does tend to drop off below $d/D = 0,6$. Also shown on the diagram for constant ϵ and $\Delta h_{fa}/L_c$ is the way in which the pressure flow velocity component increases as d/D is reduced.

This result is expected since there is less obstruction to the flow with decreasing diameter ratio.

9.4 Effect of pipe diameter on capsule force due to pressure flow

Figure 8.18 indicates how the force on the capsule due to pressure flow varies as the value of $\bar{V}_{ap}$ increases with pipe diameter (D) as parameter. The increase in $\bar{F}_{cp}$ with $\bar{V}_{ap}$ is expected (see Figure 8.12) and at a fixed velocity the pipe diameter (D) has the effect of accentuating the pressure flow force on the capsule. Approximately doubling the diameter (D) from 74 mm to 150 mm increases the force on the capsule by about 75 % (at

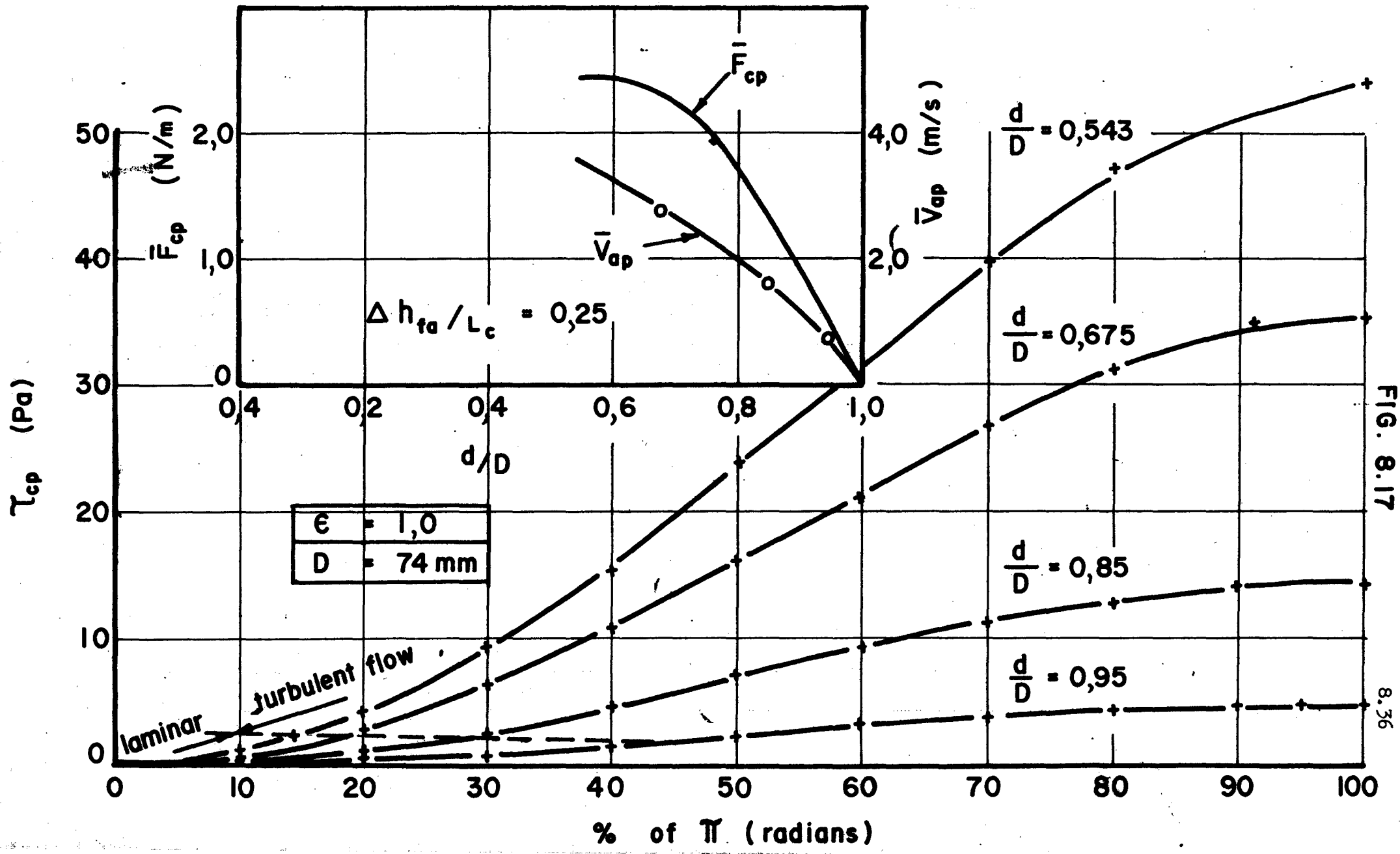
$\bar{F}_{cp}$
$\bar{V}_{ap}$
$\Delta h_{fa} / L_c = 0,25$
$\bar{F}_{cp}$ (N/m)
$\bar{V}_{ap}$ (m/s)
τ_{cp} (Pa)
d/D
ϵ = 1,0
D = 74 mm
$\frac{d}{D} = 0,543$
$\frac{d}{D} = 0,675$
$\frac{d}{D} = 0,85$
$\frac{d}{D} = 0,95$
laminar
turbulent flow
% of π (radians)
0
10
20
30
40
50
60
70
80
90
100
0,4
0,2
0,4
0,6
0,8
1,0
2,0
1,0
4,0
2,0

FIG. 8.17

8.36

FIG. 8.18

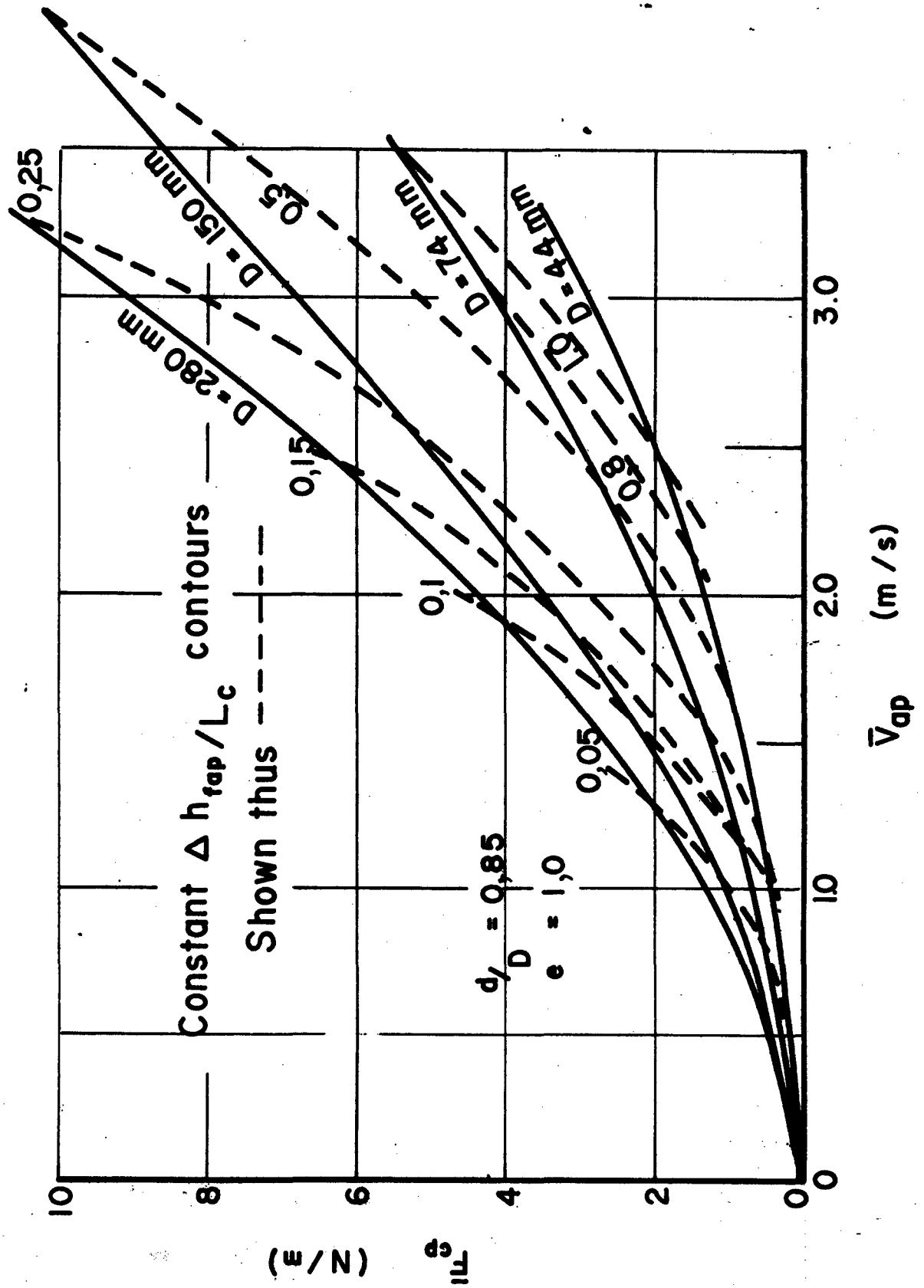
Constant Δ h_tap/L_c contours
Shown thus
d/D = 0,85
e = 1,0
D = 280 mm
D = 150 mm
D = 74 mm
D = 44 mm
0,25
0,15
0,1
0,05
0,3
0,8
0,5
0
2
4
6
8
10
0
10
2.0
3.0
(N/m)
(m/s)

$\bar{V}_{ap}$ = 2 m/s). The dashed curves are constant pressure gradient contours $(\Delta h_{fa}/L_c)$ and for the above pipe diameter increase there is a considerable reduction on the hydraulic gradient, a fixed hydraulic gradient corresponding to a much lower velocity $(\bar{V}_{ap})$ as pipe diameter is decreased.

The diameter ratio and eccentricity ratio are held constant (d/D = 0,85 and ϵ = 1,0).

10. Interaction of total drag forces on capsule

This section deals with the part played by each component of the drag on mobile capsules.

Equation (7.217) can be written as follows:

$$\frac{w\pi d^2}{4} L_c |S_c - 1| \mu_f (1 - L_r) = (\Delta H_c + h_{fc}) \frac{\pi D^2}{4} w - \pi D L_c (\bar{\tau}_{pp} + \bar{\tau}_{pc}) \tag{8.4}$$

and from equation (7.182)

$$\bar{\tau}_{pp} \pi D L_c = w \Delta h_{fa} \frac{\pi(D^2 - d^2)}{4} - \bar{\tau}_{cp} \pi d L_c \tag{8.5}$$

Substituting equation (8.5) in equation (8.4) gives:

$$wA_c L_c |S_c - 1| \mu_f (1 - L_r) = (\Delta h_{fa} + \Delta h_i + \Delta h_o) \frac{\pi D^2}{4} w - w \Delta h_{fa} \frac{\pi(D^2 - d^2)}{4} + \bar{\tau}_{cp} \pi d L_c - \bar{\tau}_{pc} \pi D L_c \tag{8.6}$$

Adding the shear force on the capsule due to Couette flow $(\bar{\tau}_{cc} \pi d L_c)$ to both sides and simplifying yields;

$$A_c w(\Delta h_{fa} + (D/d)^2(\Delta h_i + \Delta h_o)) - wA_c L_c |S_c - 1| \mu_f (1 - L_r) + \bar{\tau}_{cp} \pi d L_c - \bar{\tau}_{cc} \pi d L_c = 0 \tag{8.7}$$

Equation (8.7) can be written as

$$D_f - D_F + D_{sfp} - D_{sfc} = 0 \tag{8.8}$$

where $\vec{D}_f = w(\Delta h_{fa} + (D/d)^2(\Delta h_i + \Delta h_o))$ (8.9)

= form drag (forward)

$$\overleftarrow{D}_F = A_c w L_c |S_c - 1| \mu_f (1 - L_r) \quad (8.10)$$

= solid to solid frictional force (backward).

$$\overrightarrow{D}_{sfp} = \bar{\tau}_{cp} \pi d L_c \quad (8.11)$$

= skin friction drag due to pressure flow in annulus (forward).

$$\overleftarrow{D}_{sfc} = \bar{\tau}_{cc} \pi d L_c \quad (8.12)$$

= skin friction drag due to Couette flow in the annulus (backward).

$$\overrightarrow{D}_{sf} = D_{sfp} - D_{sfc} \quad (8.13)$$

= total skin friction drag on the capsule (forward).

Note that in most instances $D_{sfc} > D_{sfp}$ so that D_{sf} actually acts backwards on the capsule.

If there is no contact between capsule and pipe wall, then

$$D_f = D_{sf} = D_{sfc} - D_{sfp} \quad (8.14)$$

Figures 8.19 and 8.20 show the various drag forces acting on a capsule of $d/D = 0,85$ in a horizontal pipe, $D = 74$ mm diameter.

In the case of Figure 8.19 the SG is 4,0 and for the capsule represented in Figure 8.20, SG = 1,87. It will be shown later (see Chapter 12) that the former capsule is not likely to lift off the pipe bottom in the velocity region tested, whereas, the latter is.

10.1 Form drag

Referring first to the form drag; Figure 8.19 shows that for the heavy capsule, the form drag (D_f) drops steadily with capsule velocity and this is to be expected since D_f is a function of Δh_i and Δh_o, both of which depend on the velocity defect $(\bar{V} - V_c)$ and this quantity reduces as the capsule speeds up relative to the mean water velocity.

The form drag tends to level off at high velocities and in figure 8.20 it is apparent that the form drag of the lighter capsule starts to increase when the capsule velocity (V_c) is greater than about 2 m/s. This is attributed to the increased contribution of Δh_{fa} as the pressure

FIG. 8.19

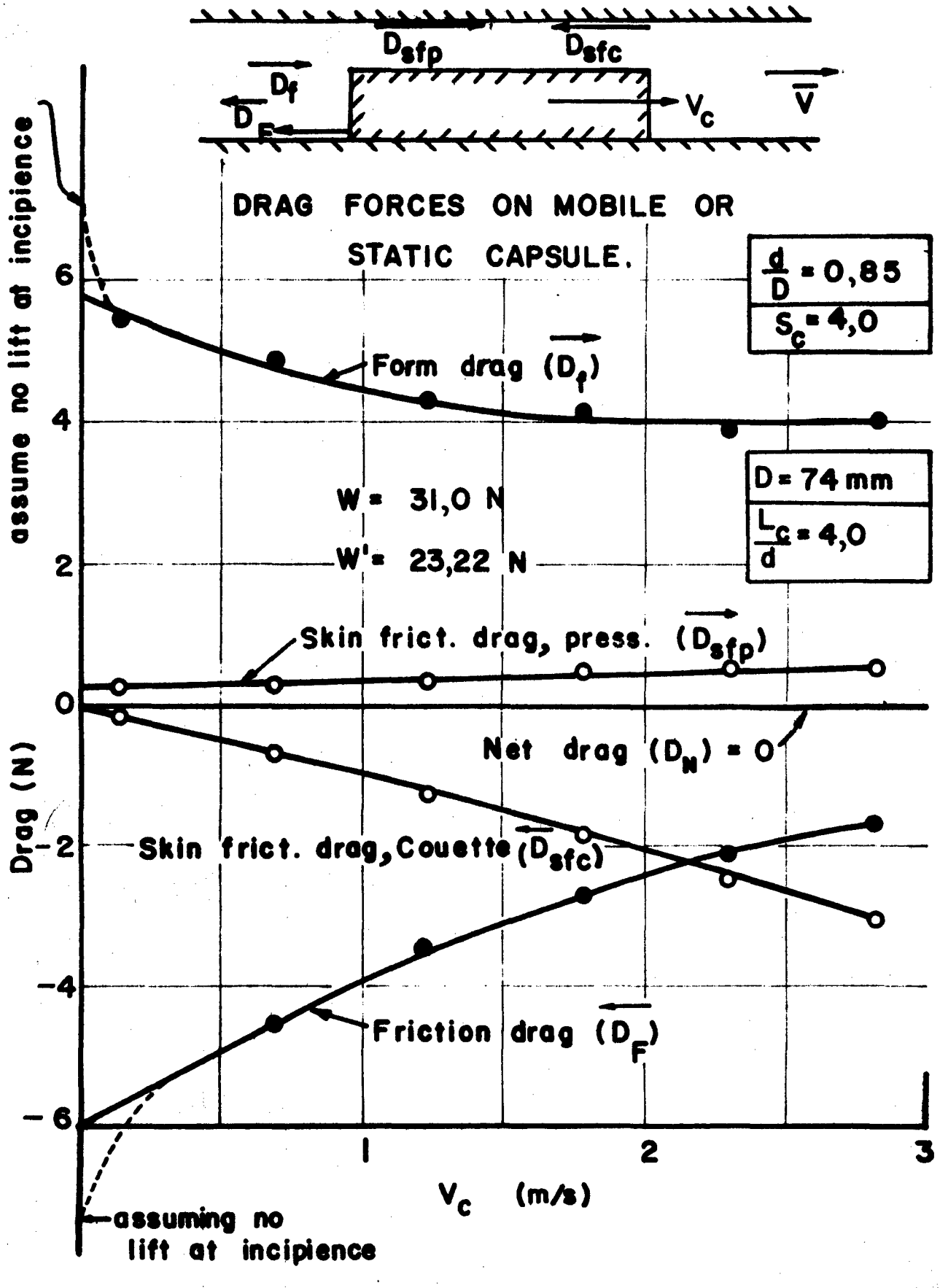
D_{sfp}
D_{sfc}
D_f
D_F
V_c
$\overline{V}$
DRAG FORCES ON MOBILE OR STATIC CAPSULE.
$\frac{d}{D} = 0,85$
$S_c = 4,0$
Form drag (D_f)
D = 74 mm
$\frac{L_c}{d} = 4,0$
W = 31,0 N
W' = 23,22 N
Skin frict. drag, press. (D_{sfp})
Net drag (D_N) = 0
Skin frict. drag, Couette (D_{sfc})
Friction drag (D_F)
assume no lift at incipience
Drag (N)
6
4
2
0
-2
-4
-6
1
2
3
V_c (m/s)
assuming no lift at incipience

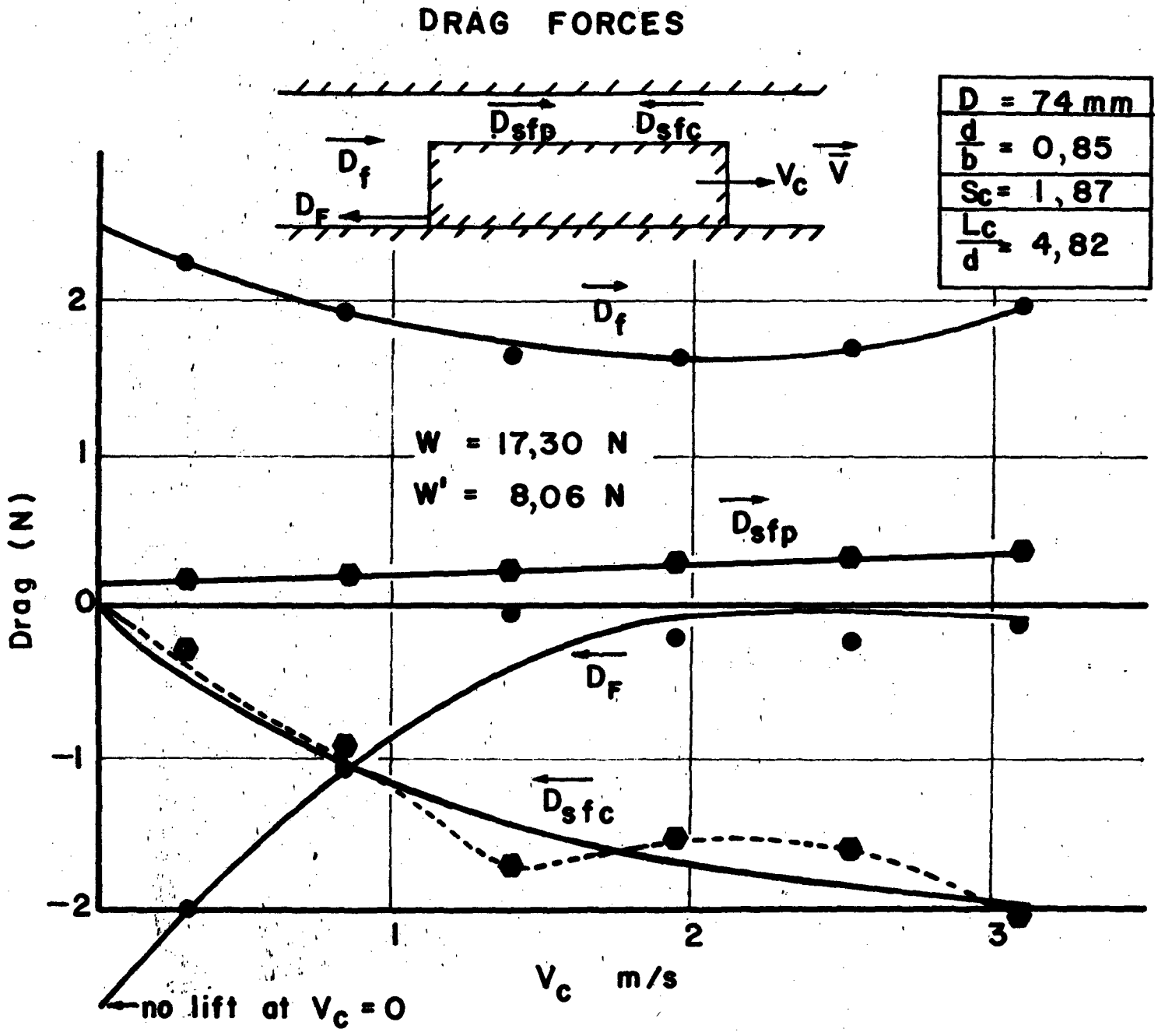
DRAG FORCES
D = 74 mm
d/b = 0,85
Sc = 1,87
Lc/d = 4,82
Dsfp
Dsfc
Df
DF
Vc
V
W = 17,30 N
W' = 8,06 N
Drag (N)
2
1
0
-1
-2
1
2
3
Vc m/s
no lift at Vc = 0

FIG. 8.20

flow in the annulus increases. Figure 8.21 shows the influence of average water velocity $(\bar{V})$ on the capsule velocity (V_c), the velocity in the annulus due to pressure flow $(\bar{V}_{ap})$, the velocity in the annulus due to Couette flow $(\bar{V}_{ac})$ and the average velocity in the annulus $(\bar{V}_{am})$ for the two capsules under consideration. It is clear that even though the pressure flow in the annulus $(\bar{V}_{ap})$ is generally less for the lighter than the heavier capsule, the form drag rises in the former and not the latter case because the percentage contribution of Δh_{fa} to the form drag is greater for the lighter capsule. This is because the capsule velocity (V_c) is greater for the lighter capsule, thus reducing the Δh_i and Δh_o contributions to the form drag.

10.2 Net skin friction drag

It is clear from Figure 8.19 that as capsule velocity increased the skin friction drag due to pressure flow $(\overrightarrow{D}_{sfp})$ and Couette flow $(\overleftarrow{D}_{sfc})$ both increase correspondingly but they act in opposite directions.

The value of D_{sfp} is almost invariably dominated by D_{sfc} so that the net skin friction drag acts backwards.

Figure 8.22 shows the average values of the skin friction drag due to the two components of flow, on both the pipe and capsule walls. For the pipe wall the components are additive and for the capsule wall subtractive, i.e. $\overleftarrow{\bar{\tau}}_c = \overleftarrow{\bar{\tau}}_{cc} - \overrightarrow{\bar{\tau}}_{cp}$.

Figure 8.23 shows the total average shear stress on the pipe and capsule walls. The shear stress on the pipe wall $(\bar{\tau}_p)$ increases, whereas the shear stress on the capsule wall $(\bar{\tau}_c)$ increases while the capsule is stationary, but as soon as the capsule starts to move (the incipient velocity $\bar{V}_i$ is indicated on the diagram) a reversal of the shear stress on the capsule wall occurs and the value of $\bar{\tau}_c$ then increases monotonically in a backward direction, retarding capsule motion.

Reverting to Figure 8.20 for the lighter capsule at the same diameter

FIG. 8.21

na. 6344			
D = 74 mm	$\frac{d}{D}$ = 0,851	$L_c/_d$ = 4,0	S_c = 4,0

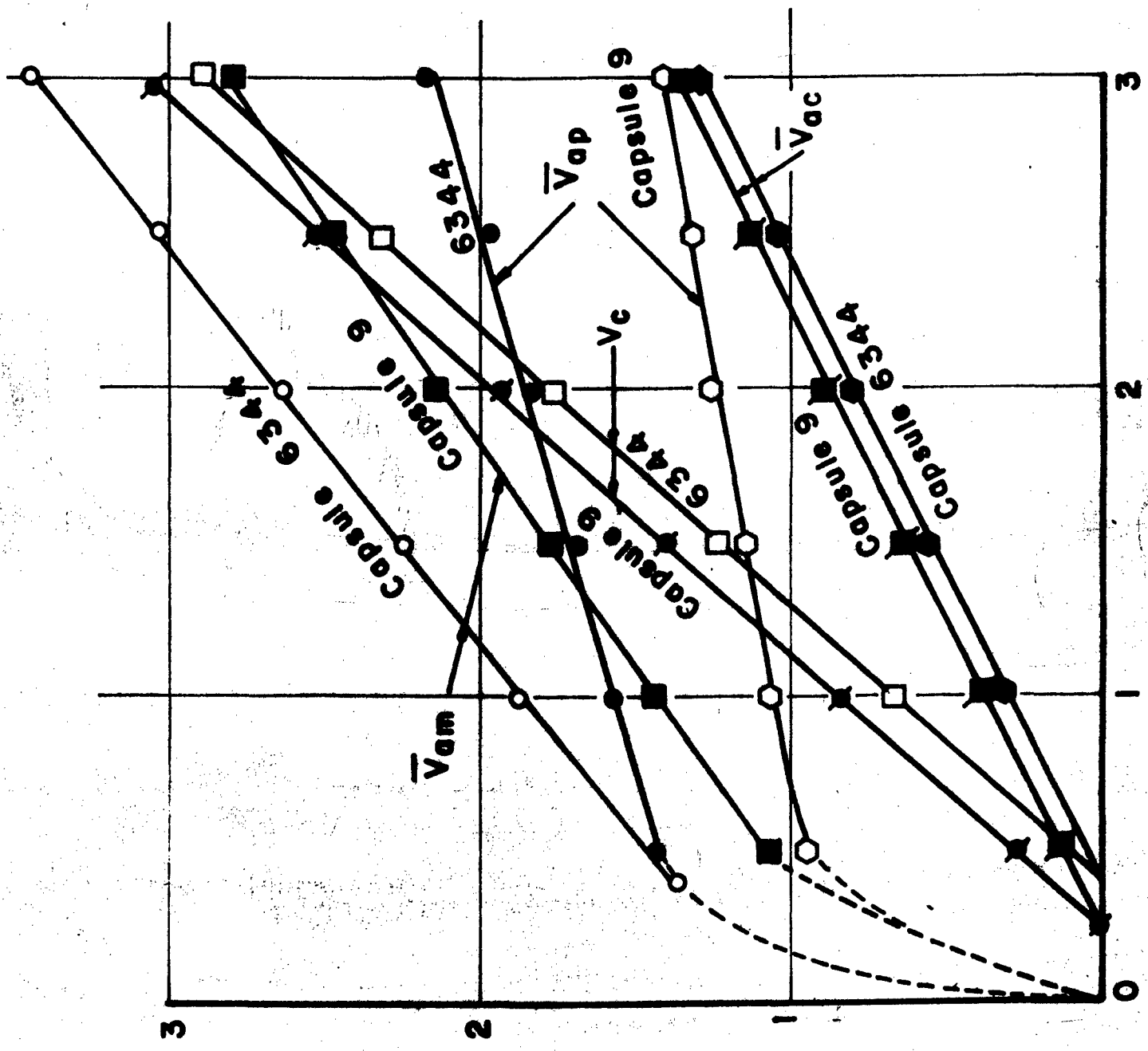

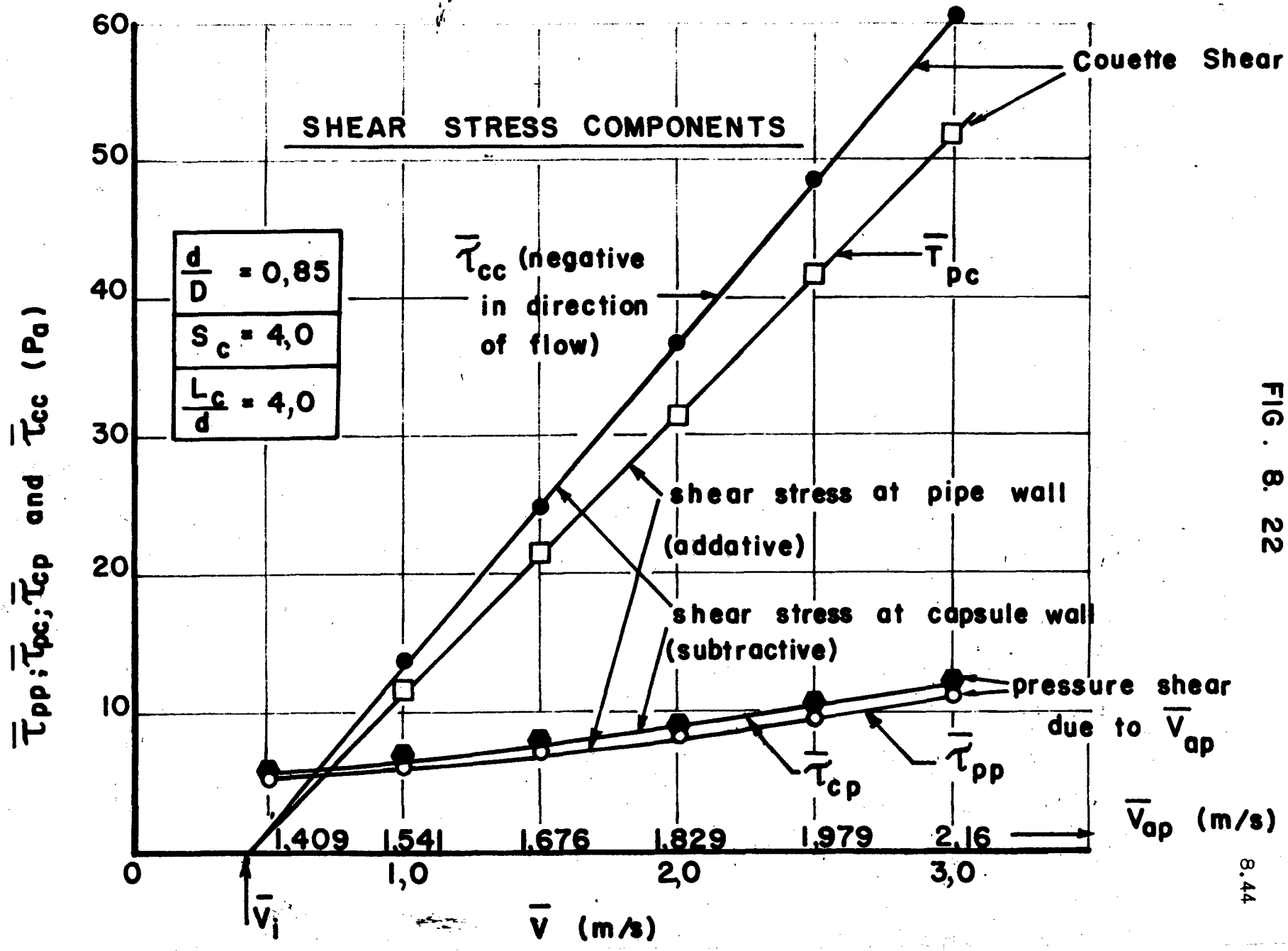
SHEAR STRESS COMPONENTS
$\frac{d}{D}$ = 0,85
S_c = 4,0
$\frac{L_c}{d}$ = 4,0
$\bar{\tau}_{cc}$ (negative in direction of flow)
Couette Shear
$\bar{T}_{pc}$
shear stress at pipe wall (addative)
shear stress at capsule wall (subtractive)
pressure shear due to $\bar{V}_{ap}$
$\bar{\tau}_{cp}$
$\bar{\tau}_{pp}$
$\bar{\tau}_{pp}$; $\bar{\tau}_{pc}$; $\bar{\tau}_{cp}$ and $\bar{\tau}_{cc}$ (Pa)
60
50
40
30
20
10
0
1,409
1,541
1,676
1,829
1,979
2,16
$\bar{V}_{ap}$ (m/s)
1,0
2,0
3,0
$\bar{V}_i$
$\bar{V}$ (m/s)

FIG. 8. 22

FIG. 8.23

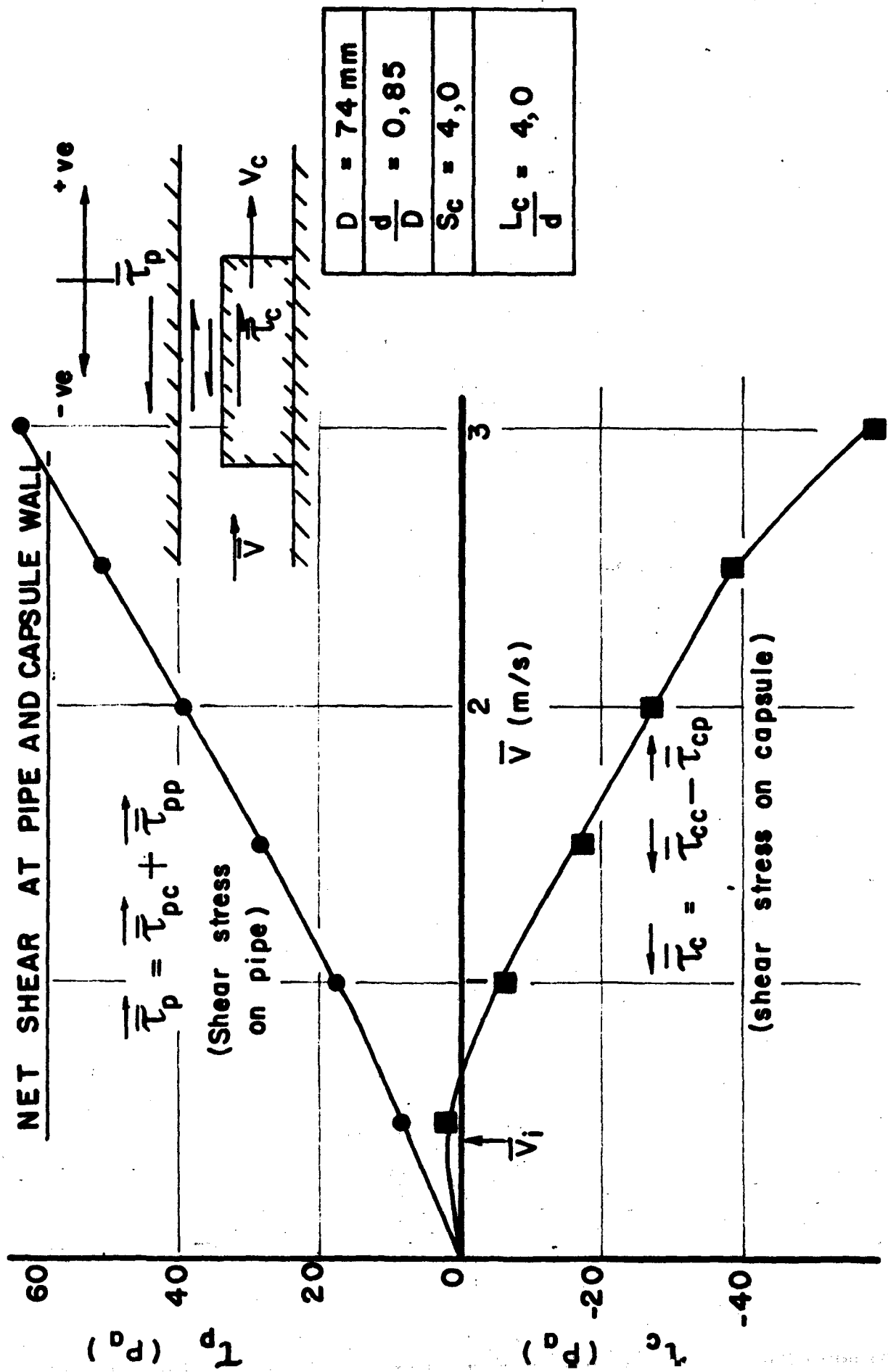
D = 74 mm
d/D = 0,85
Sc = 4,0
Lc/d = 4,0
+ve
-ve
Vc
V
NET SHEAR AT PIPE AND CAPSULE WALL
(Shear stress on pipe)
(shear stress on capsule)
V (m/s)
Vi
60
40
20
0
-20
-40
1
2
3

ratio, the dotted curve for the skin friction drag due to Couette flow indicates a decreasing drag as capsule velocity increases up to about 1,5 m/s at which state a reversal occurs until about 2,0 m/s and then the value of $\overleftarrow{D}_{sfc}$ continues to decrease. This pattern is reflected as a net shear stress on the capsule seen on Figure 8.24, where the abscissa is now $\bar{V}$.

Tracing the net shear stress curve on the capsule from $\bar{V} = 0$ to $\bar{V} = 3$ m/s the following phenomena are noted:

The value of $\bar{\tau}_c$ first increases until the Couette shear $(\overleftarrow{\bar{\tau}}_{cc})$ exceeds the pressure shear $(\overrightarrow{\bar{\tau}}_{cp})$ and a reversal occurs at incipience as for the heavier capsule. The shear stress $(\bar{\tau}_c)$ then becomes increasingly dominated by the Couette component $(\bar{\tau}_{cc})$ as $\bar{V}$ increases, and at about 1,3 m/s the net shear reverses again and starts to increase, and the reason is that, at this point, the capsule starts to lift and the Couette shear decreases at both the pipe and capsule walls due to an eccentricity reduction (see Figure 8.6). The way in which the separate pressure and Couette components influence $\bar{\tau}_c$ and $\bar{\tau}_p$ can be seen on Figure 8.25. According to the analysis from which these curves were derived, equation (7.220) becomes operative as soon as the excess head loss across the capsule $\Delta H_c'''$ calculated from equation (7.220) exceeds the measured value of ΔH_c and the eccentricity is adjusted to give the values of $\bar{\tau}_{pp}$ and $\bar{\tau}_{pc}$ to satisfy equation (7.220). This explains the reduction of $\bar{\tau}_{pc}$ and $\bar{\tau}_{cc}$.

The calculation does not take into account any of the other lift forces (which are discussed in Section 11), and so the eccentricity remains very close to unity in the calculation, and as capsule velocity increases further the shear stresses due to Couette flow continue to increase. This accounts for the reversal of shear stress that occurs at about 2,3 m/s.

The above reasoning can be employed in a similar way to explain the shear reversals that appear to occur on the pipe wall due to Couette flow.

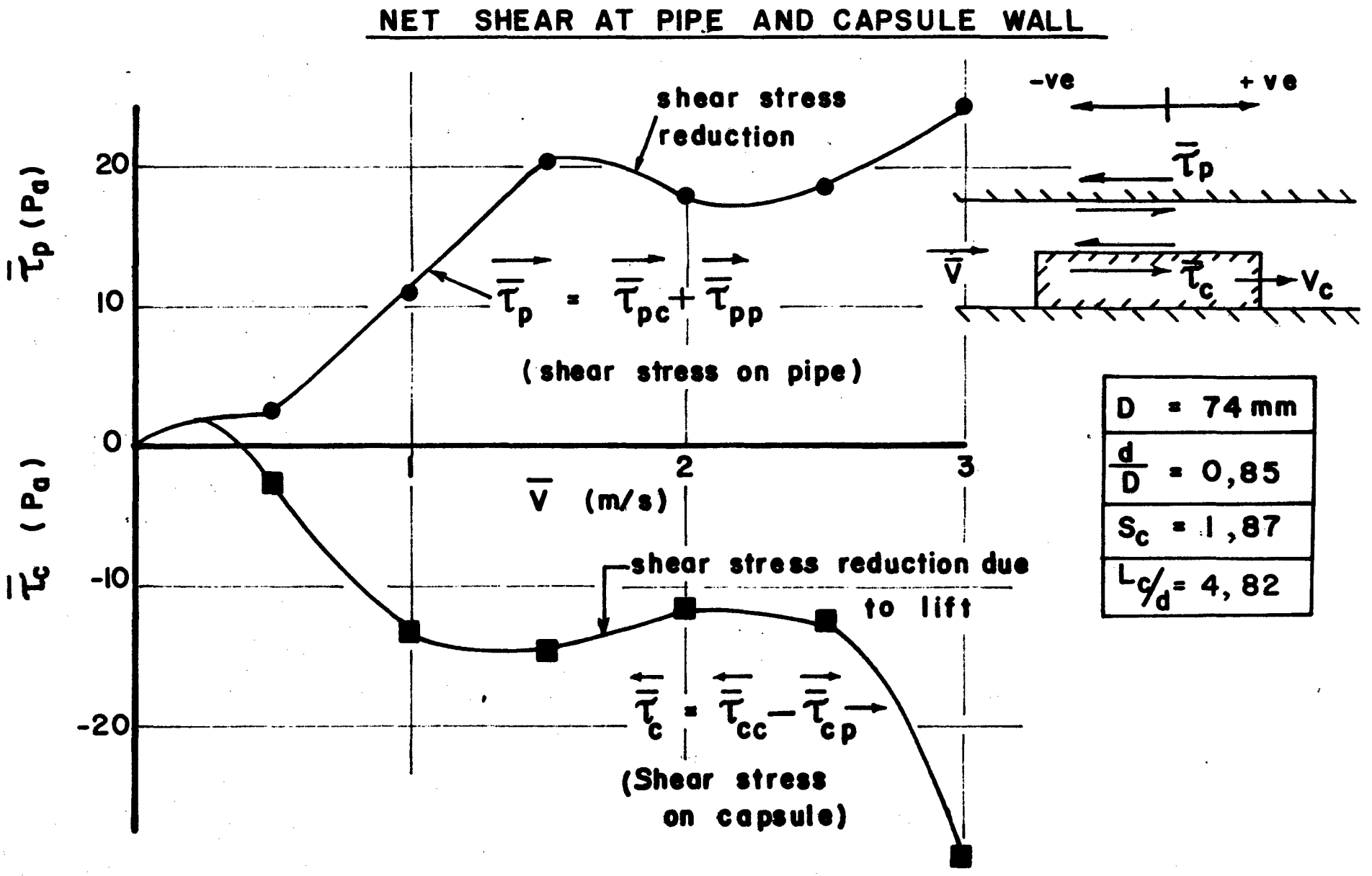
NET SHEAR AT PIPE AND CAPSULE WALL
shear stress reduction
-ve
+ve
$\bar{\tau}_p$
$\bar{V}$
$\bar{\tau}_c$
V_c
$\bar{\tau}_p = \bar{\tau}_{pc} + \bar{\tau}_{pp}$
(shear stress on pipe)
$\bar{\tau}_p$ (Pa)
$\bar{\tau}_c$ (Pa)
20
10
0
-10
-20
1
2
3
$\bar{V}$ (m/s)
shear stress reduction due to lift
$\bar{\tau}_c = \bar{\tau}_{cc} - \bar{\tau}_{cp}$
(Shear stress on capsule)
D = 74 mm
$\frac{d}{D}$ = 0,85
S_c = 1,87
L_c/d = 4,82

FIG. 8.24

FIG. 8.25

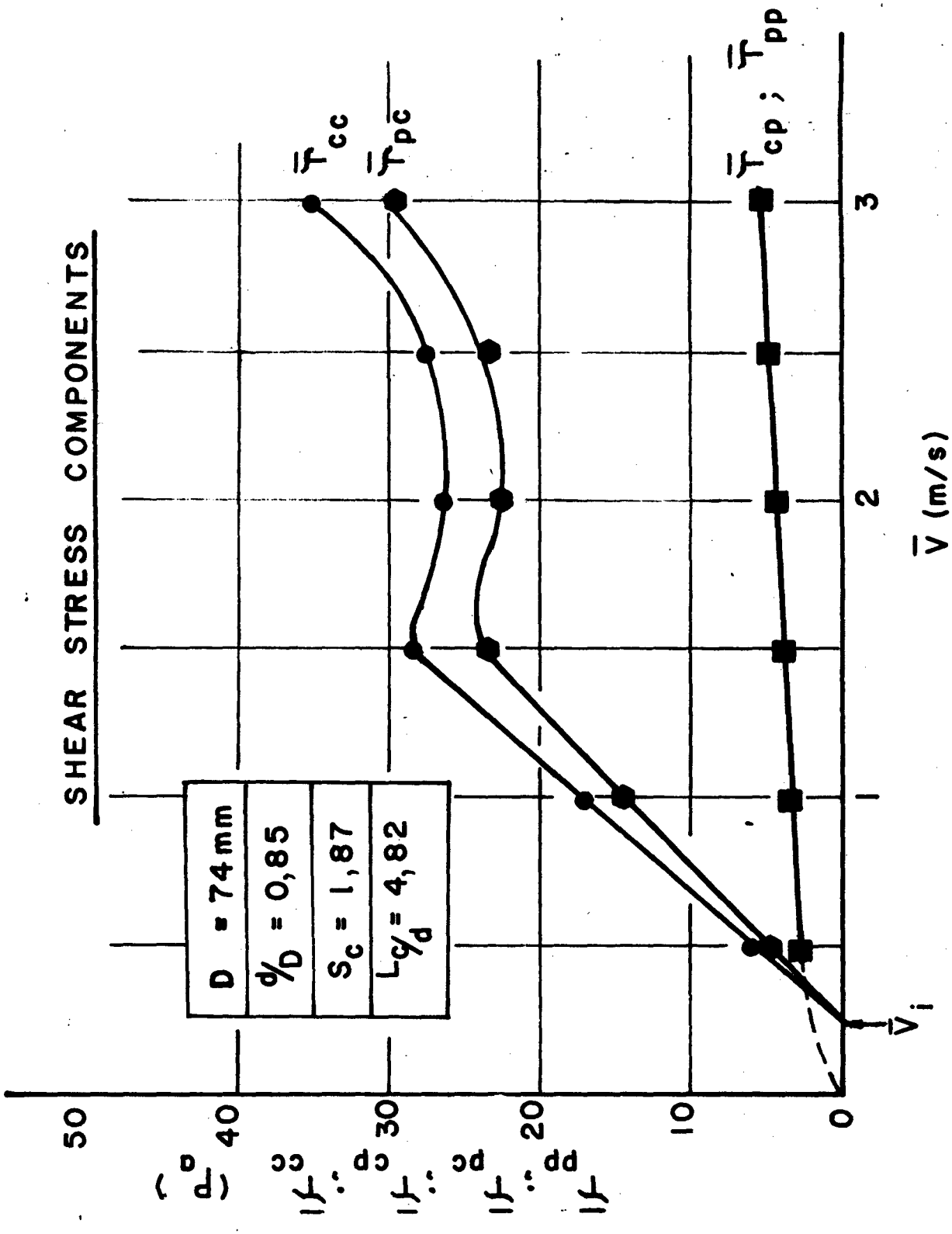
SHEAR STRESS COMPONENTS
$\bar{\tau}_{cc}$
$\bar{\tau}_{pc}$
$\bar{\tau}_{cp}$; $\bar{\tau}_{pp}$
D = 74 mm
ϕ/D = 0,85
S_c = 1,87
L_c/d = 4,82
$\bar{\tau}_{pp}$; $\bar{\tau}_{pc}$; $\bar{\tau}_{cp}$; $\bar{\tau}_{cc}$ (N/m^2)
50
40
30
20
10
0
1
2
3
$\bar{V}_i$
$\bar{V}$ (m/s)

These patterns indicated on Figure 8.24 are not necessarily correct in practice, since the eccentricity continues to decrease after $\bar{V} = 2$ m/s (see Chapter 12).

10.3 Distribution of net shear stress on capsule

Although the average shear stress on the capsule $(\bar{\tau}_c)$ gives rise to a backward drag, the actual values of shear stress (τ_c) around the perimeter may act either way.

Figure 8.26 shows the distribution around the capsule of the pressure and Couette components of shear for the two capsules considered. The mean water velocity is $\bar{V} = 2$ m/s for the heavy capsule and $\bar{V} = 3$ m/s for the lighter one. In order to obtain the net shear stress distribution around the capsule, the Couette component is subtracted from the pressure component as shown on Figure 8.27 for the heavy capsule and on Figure 8.28 for the light one.

It is of interest to note that the two curves associated with the heavy capsule on Figure 8.26 show a change over from laminar to turbulent flow between $\theta = 25$ % and 26 % of π and Figure 8.27 shows that for $\theta < 20$ % to 30 % of π the shear stress on the capsule (τ_c) acts backwards and around the rest of the perimeter τ_c acts forwards.

Thus, for most of the perimeter τ_c acts forwards and the flow is turbulent. Nonetheless, the net average shear stress on the capsule $(\bar{\tau}_c)$ is backwards and the shear on less than 20 % of the perimeter in laminar flow completely dominates the forward component (i.e. $\bar{\tau}_{cc} = 36{,}581$ and $\bar{\tau}_{cp} = 8{,}754$) or the Couette component (backwards) is much greater than the pressure shear component (forwards).

A quick glance at Figure 8.27 is thus misleading since the Couette shear (τ_{cc}) is concentrated mainly at the bottom of the pipe where the gap approaches zero (and $dv/dy \to \infty$) generating a Couette shear which tends to infinity at the point of contact.

FIG. 8.26

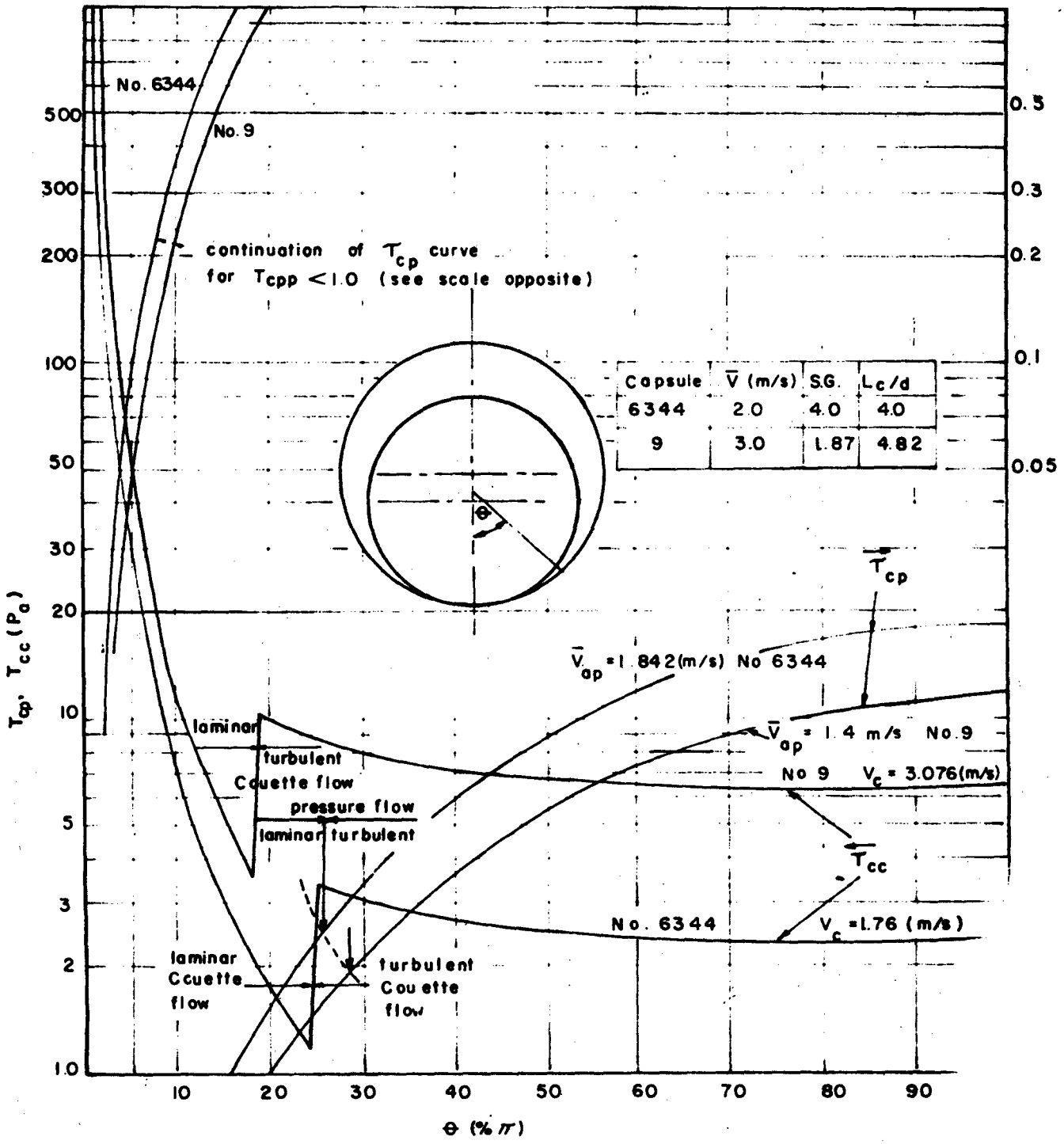
No. 6344
No. 9
continuation of τ_{cp} curve for $T_{cpp} < 1.0$ (see scale opposite)
Capsule | $\bar{V}$ (m/s) | S.G. | L_c/d
6344 | 2.0 | 4.0 | 4.0
9 | 3.0 | 1.87 | 4.82
θ
$\bar{\tau}_{cp}$
$\bar{V}_{ap}$ = 1.842(m/s) No 6344
$\bar{V}_{ap}$ = 1.4 m/s No. 9
No 9 V_c = 3.076(m/s)
$\bar{\tau}_{cc}$
No. 6344 V_c = 1.76 (m/s)
laminar
turbulent
Couette flow
pressure flow
laminar turbulent
laminar Ccuette flow
turbulent Couette flow
T_{cp}, T_{cc} (P_a)
θ (% π)
500
300
200
100
50
30
20
10
5
3
2
1.0
0.5
0.3
0.2
0.1
0.05
10
20
30
40
50
60
70
80
90

FIG. 8.27

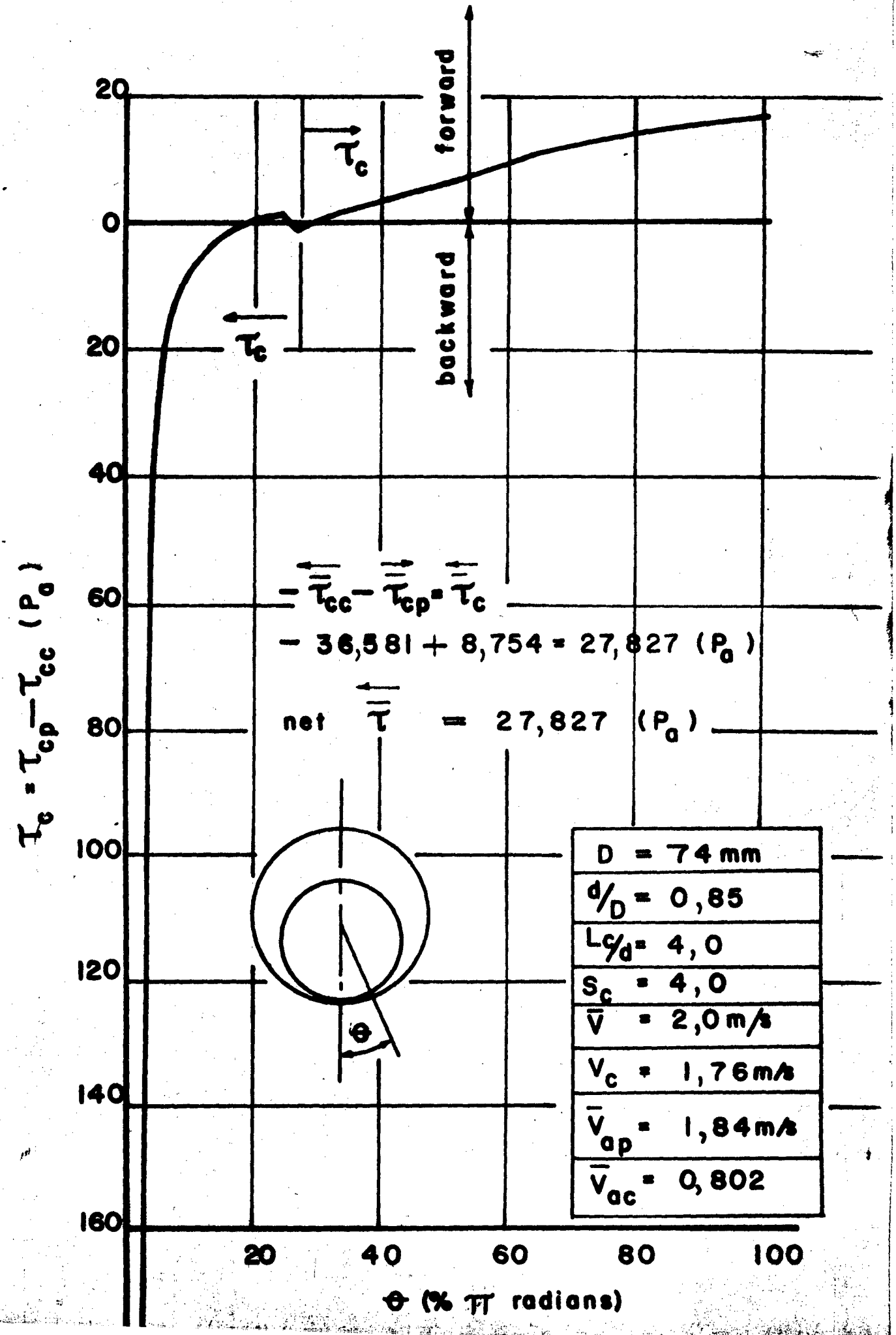
forward
backward
τ_c
τ_c
$-\bar{\tau}_{cc} - \bar{\tau}_{cp} = \bar{\tau}_c$
$-36{,}581 + 8{,}754 = 27{,}827\ (P_a)$
net $\bar{\tau} = 27{,}827\ (P_a)$
θ
D = 74 mm
d/D = 0,85
Lc/d = 4,0
S_c = 4,0
$\bar{V}$ = 2,0 m/s
V_c = 1,76 m/s
$\bar{V}_{ap}$ = 1,84 m/s
$\bar{V}_{ac}$ = 0,802
$\tau_c = \tau_{cp} - \tau_{cc}\ (P_a)$
20
0
20
40
60
80
100
120
140
160
20
40
60
80
100
θ (% π radians)

FIG. 8.28

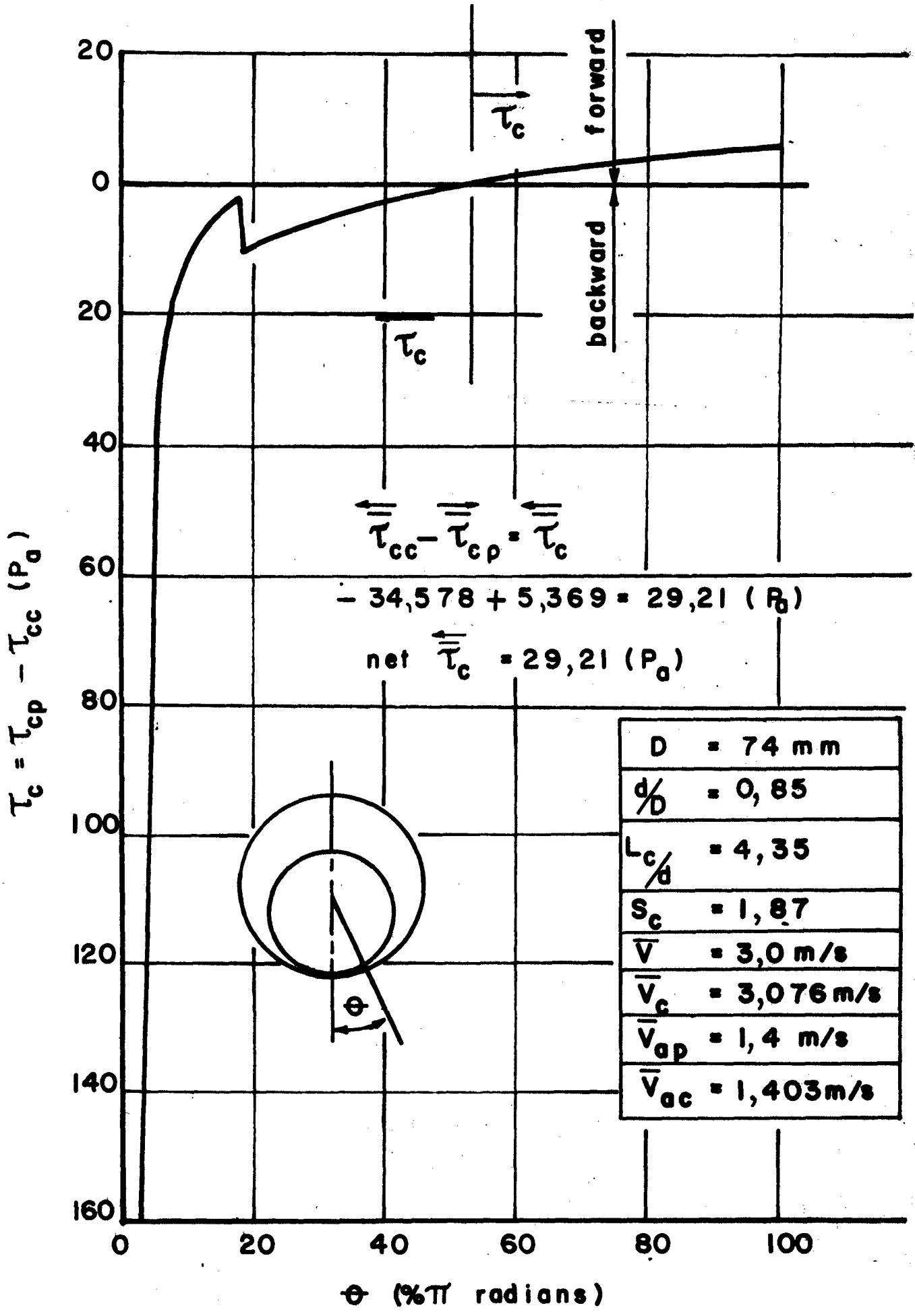
20
0
20
40
60
80
100
120
140
160
0
20
40
60
80
100
τ_c
forward
backward
τ_c
$\overleftarrow{\tau}_{cc} - \overrightarrow{\tau}_{cp} = \overleftarrow{\tau}_c$
− 34,578 + 5,369 = 29,21 (P_a)
net $\overleftarrow{\tau}_c$ = 29,21 (P_a)
$\tau_c = \tau_{cp} - \tau_{cc}$ (P_a)
θ
θ (%π radians)
D = 74 mm
$\frac{d}{D}$ = 0,85
$\frac{L_c}{d}$ = 4,35
S_c = 1,87
$\bar{V}$ = 3,0 m/s
$\bar{V}_c$ = 3,076 m/s
$\bar{V}_{ap}$ = 1,4 m/s
$\bar{V}_{ac}$ = 1,403 m/s

Figure 8.28 is the composite diagram derived from the curves on Figure 8.26 for the lighter capsule. Change over from laminar to turbulent flow in this case occurs at $\theta = 0,18\pi$ for the Couette component and $0,28\pi$ for the pressure component.

This is clearly impossible in practice since the fluid cannot be both laminar and turbulent at the same point, and this is a source of error in the theory, which is merely an analytical technique for dealing with the problem. This point will be dealt with further in Chapter 15.

Figure 8.28 shows a discontinuity in the curve at about $\theta = 0,18\pi$ and this is due to the discontinuity in the Couette component when changing from laminar to turbulent flow. In this case, about half of the perimeter is subject to backward shear $(\theta < 0,53\pi)$ and the flow may be laminar or turbulent. The forward component is completely turbulent and, in this case (the lighter capsule at a higher velocity), the backward shear is even more dominating than in the previous case.

10.4 Velocity distribution in annulus

Figures 8.29 and 8.30 show velocity distributions for the two capsules ($SG = 4,0$ at $\bar{V} = 2$ m/s and $SG = 1,87$ at $\bar{V} = 3$ m/s). The top half of the diagrams show longitudinal velocity distribution at the top and bottom of the capsule (view A and view B), and the bottom half of the diagrams shows velocity distributions around the perimeter. In both cases the pressure and Couette components are shown dotted and the summation is shown in full.

In Figure 8.29, the top diagram shows that dv/dy (at the capsule wall) is such as to give a forward shear at the top of the capsule $(\theta = \pi)$ and when proceeding around the perimeter from the top dv/dy gradually decreases and becomes zero at about $\theta = 0,28\pi$. As θ decreases yet further dv/dy changes direction, increasing in a negative sense and becoming infinite at $\theta = 0$ (for zero clearance). The velocity

FIG. 8.29

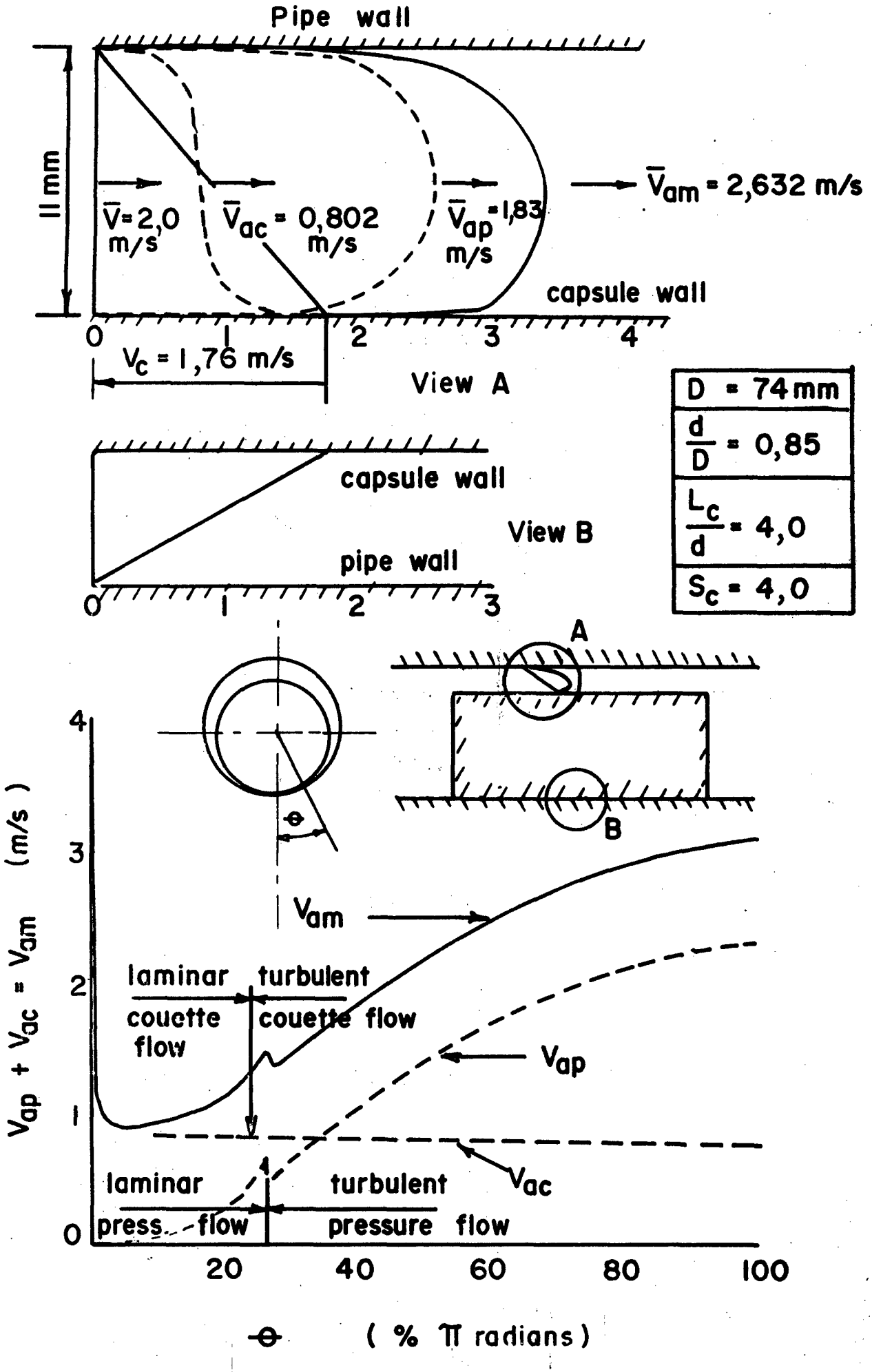
Pipe wall
11 mm
$\bar{V}$=2,0 m/s
$\bar{V}_{ac}$ = 0,802 m/s
$\bar{V}_{ap}$=1,83 m/s
$\bar{V}_{am}$ = 2,632 m/s
capsule wall
0
2
3
4
V_c = 1,76 m/s
View A
capsule wall
View B
pipe wall
0
1
2
3
D = 74 mm
$\frac{d}{D}$ = 0,85
$\frac{L_c}{d}$ = 4,0
S_c = 4,0
A
B
θ
4
3
2
1
0
$V_{ap} + V_{ac} = V_{am}$ (m/s)
V_{am}
laminar couette flow
turbulent couette flow
V_{ap}
V_{ac}
laminar press. flow
turbulent pressure flow
20
40
60
80
100
θ (% π radians)

FIG. 8.30

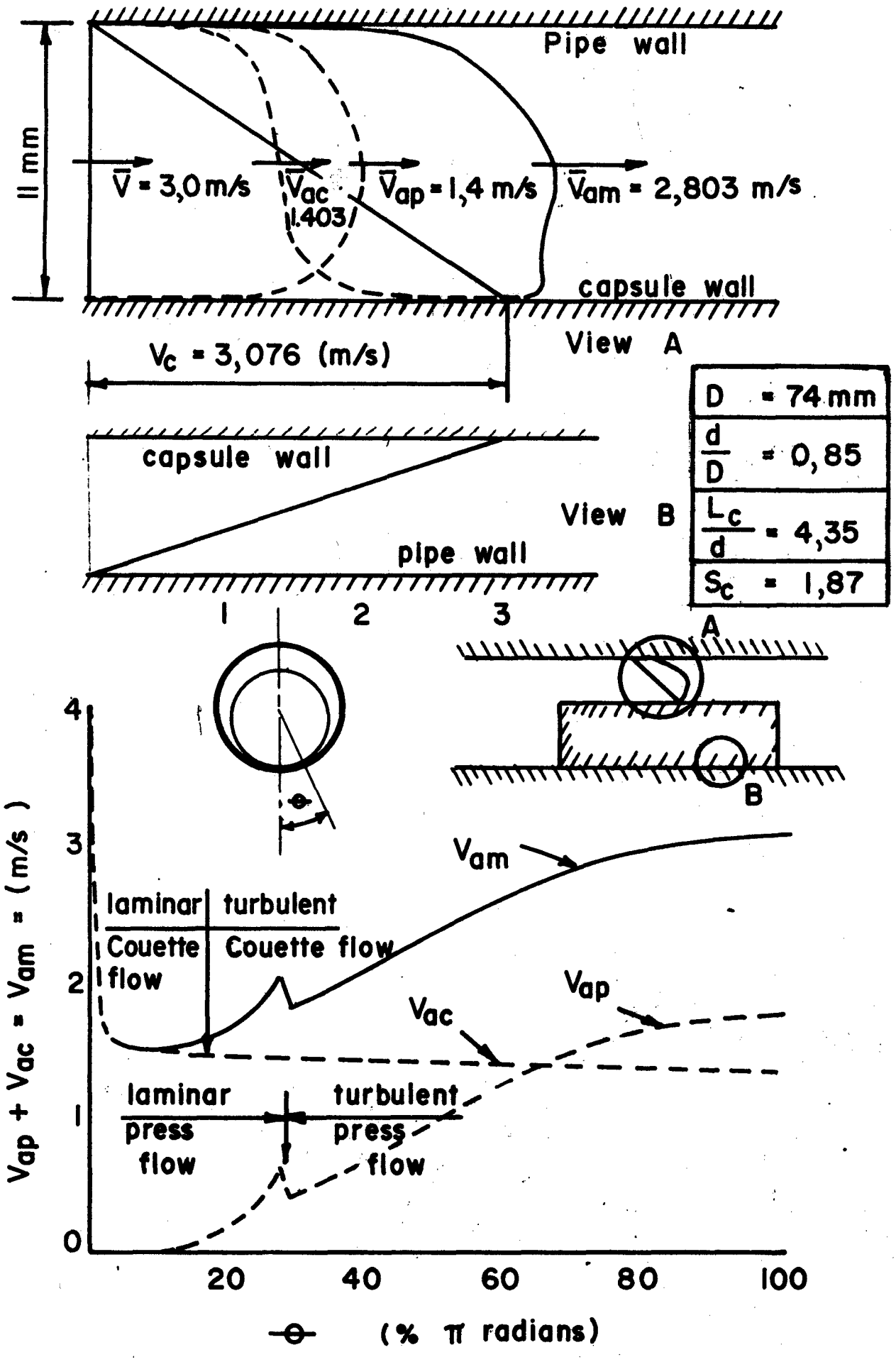
Pipe wall
11 mm
$\bar{V}$ = 3,0 m/s
$\bar{V}_{ac}$
1.403/
$\bar{V}_{ap}$ = 1,4 m/s
$\bar{V}_{am}$ = 2,803 m/s
capsule wall
View A
V_c = 3,076 (m/s)
capsule wall
View B
pipe wall
1
2
3
D = 74 mm
$\frac{d}{D}$ = 0,85
$\frac{L_c}{d}$ = 4,35
S_c = 1,87
A
B
θ
$V_{ap} + V_{ac} = V_{am}$ = (m/s)
V_{am}
laminar Couette flow
turbulent Couette flow
V_{ap}
V_{ac}
laminar press flow
turbulent press flow
0
1
2
3
4
20
40
60
80
100
θ (% π radians)

distribution at the bottom (view B) is also shown and this is the distribution for zero pressure gradient and laminar flow which is applicable since the pressure flow tends to zero at the point of contact.

Considering the lower half of Figure 8.29, it is clear that the Couette component of flow decreases as θ increases; extremely rapidly below $\theta = 0{,}6\pi$ and then very gradually. The Couette flow is almost constant around most of the annulus. The pressure flow increases steadily with θ (Jonsson and Sparrow (reference 25) found similar results experimentally, see Figure 7.28) except for the slight discontinuity at about $0{,}26\pi$ where the flow changes from laminar to turbulent. There is no discontinuity when the Couette component of flow changes from laminar to turbulent.

The composite flow distribution around the annulus thus decreases below $\theta \doteq 0{,}06\pi$ and then rises steadily (except for the transition discontinuity) until $\theta = \pi$.

Figure 8.30 shows similar distributions to those given in Figure 8.29, except that at the top (view A) the velocity gradient at the capsule wall is less steep resulting in a lower shear stress at this point ($\tau_c = 5{,}5$ Pa) as opposed to 16 Pa for the heavier capsule). Since this capsule travels faster than the heavier one, less of the flow velocity component in the annulus is due to pressure flow (i.e. $\bar{V}_{ap}$ is reduced by about 24 %). This alters the shape of the velocity distribution because the Couette component has a greater influence. As the capsule SG is further decreased the net velocity distribution approaches the shape of the Couette component of velocity distribution, causing a reversal of dv/dy at the capsule wall.

At the bottom (view B) the velocity gradient is also less than for the heavier capsule (the diagram is deceptive because the magnification is less than in Figure 8.29 owing to clearance at the bottom. In Figure 8.29 the gap between capsule and pipe wall approaches zero at the bottom, whereas it is finite on Figure 8.30).

The velocity distribution around the perimeter (lower half of Figure 8.30) is similar to that shown on Figure 8.29 even though both the mean water velocity ($\bar{V}$) and the capsule velocity (V_c) are less in the latter case. This is because the pressure flow component is so much less for the lighter capsule, giving roughly the same mean annular velocity ($\bar{V}_{am}$) in both cases.

10.5 Friction drag

Reverting to Figure 8.19, it is clear that the friction drag increases as capsule velocity is decreased, and this is ascribed to an intensification of the lift force as the capsule speeds up.

In Figure 8.20 for the lighter capsule, the friction drag decreases to zero at about $V_c \doteq 2$ m/s and in this case the capsule lifts completely off the pipe bottom.

Figure 8.31 shows the lift force (L_F) for the two capsules considered, and the value of L_F for the lighter one (submerged weight $W' = 8{,}0$ N) approaches 8,0 N indicating zero vertical forces and, consequently, lift.

As an aside:
This figure indicates zero lift at incipience for the light capsule and a positive lift for the heavier one.

It is clear that lift at incipience is a function of the incipient velocity ($\bar{V}_i$) and this velocity is higher for the heavier capsule (i.e. $\bar{V}_i = 0{,}429$ m/s as opposed to $\bar{V}_i = 0{,}242$ m/s for the light capsule).

It is also certain that any positive water velocity will induce a lift force whether the capsule is stationary or not. These points will be dealt with in the section on lift forces, (see Section 11).

10.6 Relative values of the drag forces

It is evident from Figures 8.19 and 8.20 that both form drag (D_f) and solid friction drag (D_F) are predominant at low capsule velocities

FIG. 8.31

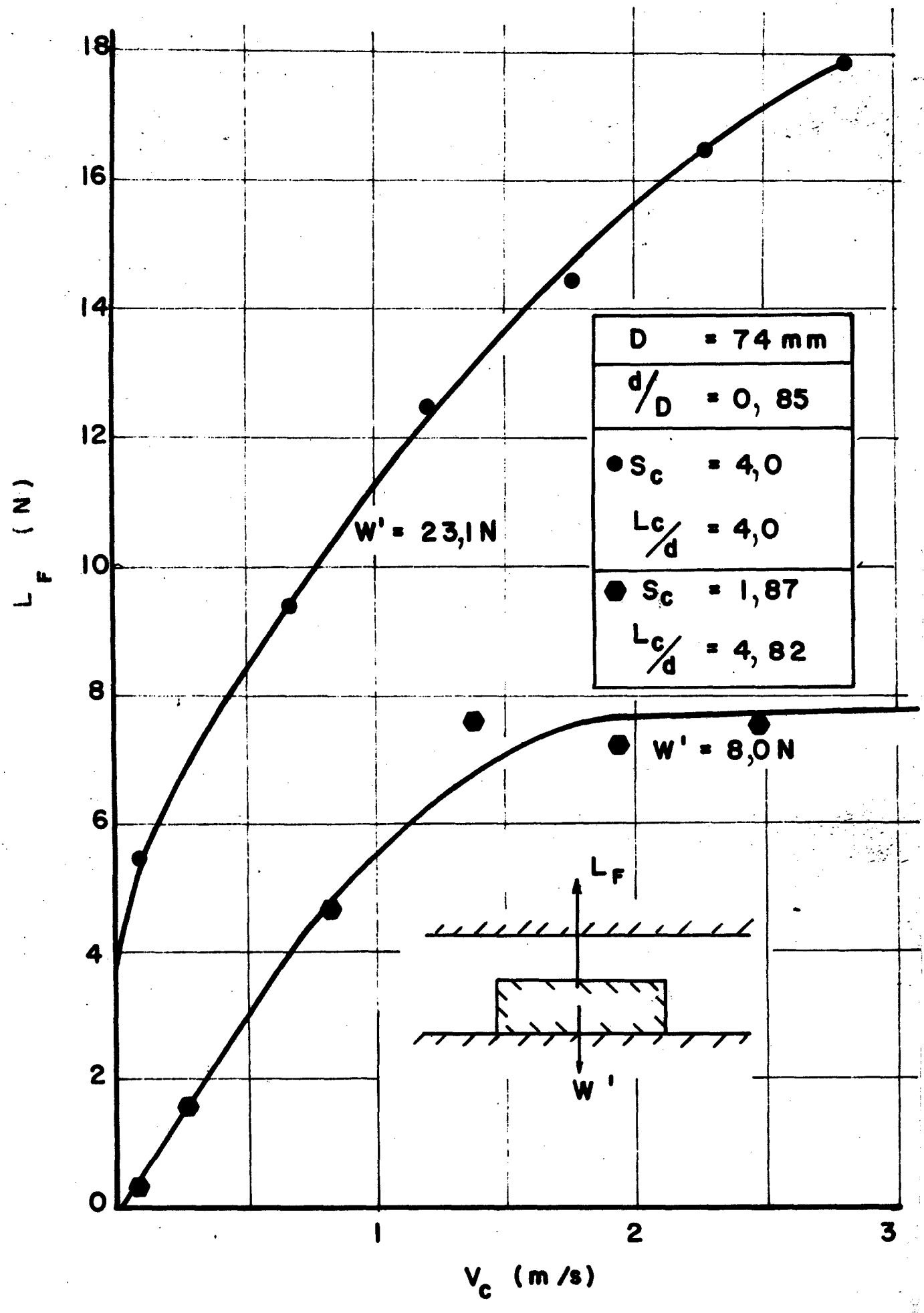
18
16
14
12
10
8
6
4
2
0
1
2
3
L_F (N)
V_c (m/s)
D = 74 mm
d/D = 0, 85
● S_c = 4,0
L_c/d = 4,0
⬢ S_c = 1,87
L_c/d = 4, 82
W' = 23,1 N
W' = 8,0 N
L_F
W'

and the skin friction drag (D_{sf}) only becomes appreciable as V_c increases.

At higher velocities it is the form drag and skin friction drag due to Couette flow that have an increasing influence. In all cases the skin friction drag due to pressure flow plays the least significant rôle.

10.6.1 Backward drag

The lighter the capsule of the same geometry the sooner the solid friction drag decreases, to be replaced by skin friction drag due to Couette flow as the main retarding force.

The solid friction drag (D_F) is less than the skin friction drag due to Couette flow at capsule velocities (V_c) greater than 0,8 m/s for a capsule of $d/D = 0,85$ and SG = 1,87 (see Figure 8.20). Increasing the SG to 4,0 raises the value of V_c where $\overleftarrow{D}_{sfc} > \overleftarrow{D}_F$ to about 2,6 m/s. The ratio $D_{sfc} : D_F$ increases with capsule velocity increase, tending to infinity when the capsule to wall clearance becomes finite. This ratio increases more rapidly as SG is decreased and less rapidly as diameter ratio is decreases, (see Figure 8.32).

The absolute value of D_F as well as D_{sfc} is less at lower than higher diameter ratios because the submerged weight and surface area of the lower diameter (dimensionally similar) capsule is less.

10.6.2 Forward drag

For both SG's (1,87 and 4,0) at $d/D = 0,85$, the form drag $(\overrightarrow{D_f})$ due to pressure differential on the end faces of the capsule, is of the order 10 times greater than the forward skin friction drag due to pressure flow $(\overrightarrow{D_{sfp}})$. Although the ratio (D_f/D_{sfp}) decreases as capsule velocity increases. For $d/D = 8.5$ and SG = 4,0 the ratio D_f/D_{sfp} decreases from 13,6 (at $\overline{V}$ = 1,0 m/s and V_c = 0,677 m/s) to 7,0 (at $\overline{V}$ = 3,0 m/s and V_c = 2,828 m/s). For $d/D = 0,85$ and SG = 1,87 the ratio D_f/D_{sfp}

FIG. 8.32

EFFECT OF DIAMETER RATIO.

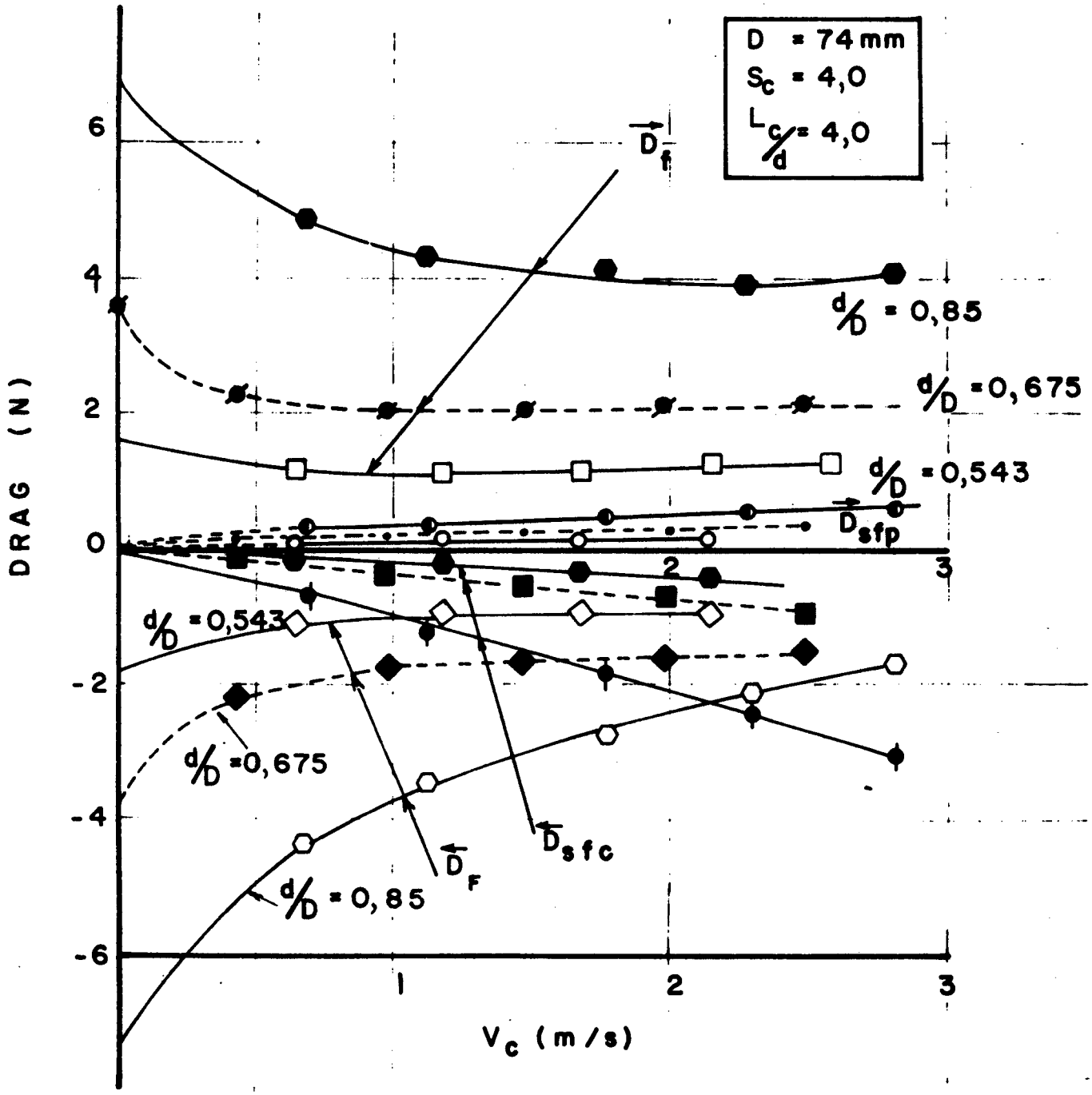

decreases from 14,0 (at $\bar{V}$ = 0,5 m/s) to 9,8 (at $\bar{V}$ = 1,0 m/s) and 6,55 (at $\bar{V}$ = 3,0 m/s). The ratio (D_f/D_{sfp}) also decreases with velocity increase at other diameter ratios and the decrease is slightly accentuated as diameter ratio is reduced, (e.g. d/D = 0,541 and SG = 4,0) the ratio (D_f/D_{sfp}) decreases from 13,0 at $\bar{V}$ = 1,5 m/s to 6,0 at $\bar{V}$ = 3,0 m/s.

The absolute values of the form and skin friction drag due to pressure flow are also less at reduced diameter ratios and this balances the backward drag components, (see Figure 8.32).

10.7 Effect of length to diameter ratio on drag force components

Figure 8.33 shows that the effect of increasing the length to diameter ratio is to increase all four drag components at a particular capsule velocity (V_c). The dotted curve shows that the solid friction drag is greater than the backward skin friction drag due to Couette flow at slightly decreasing velocities as length to diameter ratio is reduced.

At a capsule velocity of 1,0 m/s, increasing the length of the capsule sixfold (from $L_c/d = 2$ to $L_c/d = 12$) causes the form drag to be increased roughly sixfold, and these factors remain roughly constant over the range tested.

The differences in solid friction drag, for different capsule lengths, gradually decreases as capsule velocity increases and the capsules tend to lift.

Since skin friction drag due to Couette and pressure flow depends on the surface area of a capsule, increasing the length causes the skin friction drag, in both directions, to increase. The absolute values of skin friction drag differences for increasing capsule length are accentuated as capsule velocity is increased.

11. Lift forces on capsules

The lift force on a capsule is defined as the net force acting

FIG. 8.33

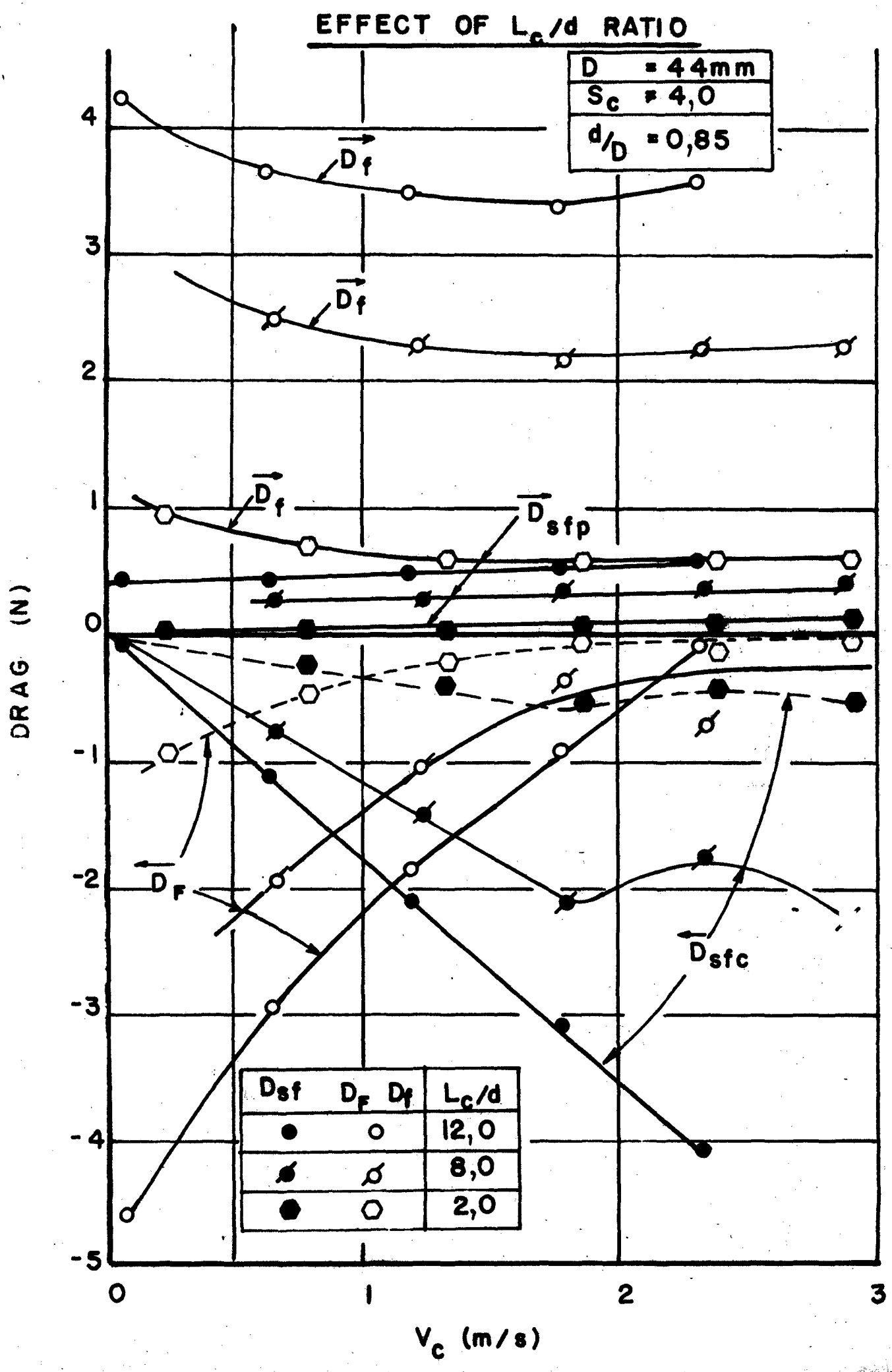
EFFECT OF L_c/d RATIO
D = 44mm
S_c = 4,0
d/D = 0,85
$\overrightarrow{D_f}$
$\overrightarrow{D_f}$
$\overrightarrow{D_f}$
$\overrightarrow{D_{sfp}}$
$\overleftarrow{D_F}$
$\overleftarrow{D_{sfc}}$
D_{sf} D_F D_f L_c/d
12,0
8,0
2,0
DRAG (N)
V_c (m/s)
4
3
2
1
0
-1
-2
-3
-4
-5
0
1
2
3

perpendicular to the flow direction (in a horizontal pipe) over and above the buoyancy force on a static capsule.

Five regimes of orientation are considered.

1. The capsule is in complete contact with the pipe wall (i.e. the static capsule and the capsule at incipient velocity).
2. Semi-hydrodynamic lubrication exists; where solid to solid friction (at the asperities of the surfaces) and fluid friction due to shearing of the fluid film are both present and no lift occurs. There is a slight elastic expansion of the capsule and a reduced reaction.
3. Microscopic lift occurs; where there is a nominal amount of solid to solid contact but where clearance between the capsule and pipe wall would be invisible to the naked eye. Liquid shear is the dominating shear force present. There is a slight upward tilt at the nose of the capsule.
4. Macroscopic lift is apparent; where only at the rear of the capsule is in contact with the pipe wall and liquid shear predominates.
5. Free travel with the capsule completely suspended ($L_F > W'$).

The theory of incipient capsule motion assumed no lift and it will be seen in Chapter 14 that there is good agreement between theory and experiment at incipience. The lift forces for static and incipient capsules are insignificant compared with the submerged weight of the capsule. It is only when the capsules are mobile and moving at fairly high velocities (of the order of 2 to 3 m/s) that lift forces become appreciably large.

The device of dividing the flow around the capsule into two components (i.e. the Couette and the pressure flow component) is convenient for explaining the mechanism of lift. Lift forces, generated by pressure flow through the annulus, will be dealt with and this will be followed

by secondary lift effects and lift due to the Couette component of flow.

The following sections will now be dealt with:

(1) Stream lines around a static capsule.

(2) Primary lift due to pressure flow and streamline curvature in the annulus.

(3) Secondary lift due to end effects.

(4) Secondary lift due to secondary flow.

(5) Lift due to Couette component of flow.

(6) Combined effect of pressure and Couette flow.

11.1 Streamline patterns around static capsules

In the static capsule tests, small particles of solid material in the water, as well as small air bubbles, were observed, in order to build up an idea of the streamline pattern.

Figure 8.34 is a composite diagram combining these observations with conjecture.

At the leading edge of the capsule separation occurs more towards the top and vortices are generated by the water flowing through the annulus. The amount of separation is likely to increase with diameter ratio and mean water velocity. At very large diameter ratios the separation is inhibited by the proximity of the pipe.

A vortex also occurs at the bottom of the upstream face, due to the zone of stagnation, and this vortex is likely to diminish as soon as the path of least resistance (see section 11.2.1) of the water is through the annulus.

The vortex is in the shape of a partial toroid extending around the lower fraction of the upstream edge of the capsule. At the downstream face of the capsule, the water leaving the annulus generates a large weak vortex as shown on Figure 8.34, and it is likely that this vortex, shown only in a vertical plane, exists in other planes as well, dying out

FIG. 8.34

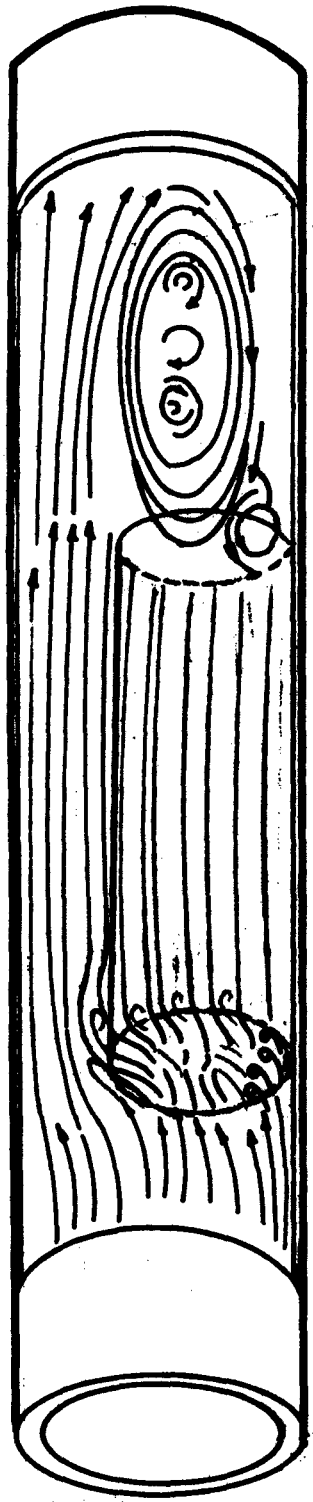

towards the bottom of the crescent where the jet velocity is likely to be less. A smaller reversed vortex occurs in front of the capsule near the bottom of the pipe to maintain continuity.

The forces generated by the postulated streamline patterns are upward on the back face of the capsule and may be either way on the front face although they are more likely to be upward.

It is extremely difficult to draw the streamline pattern for the mobile case. For slow moving capsules $(V_c << \bar{V})$ the streamlines are likely to be similar to those shown for the static capsule.

For rapidly moving capsules $(V_c > \bar{V})$ the streamlines relative to the capsule would (in certain regions, where the water velocity is less than the capsule velocity) approximate the static capsule pattern in reverse.

11.2 Mechanism of lift

11.2.1 Primary lift due to streamline curvature

Consider the line of streamlines in a vertical plane in the centre of the pipe upstream of the capsule where $V_c << \bar{V}$.

The streamline of maximum velocity in the centre of the pipe, if the capsule were concentric, would tend to disperse evenly around the perimeter of the capsule. In the case of a fully eccentric capsule the vertical components of this streamline can only pass over the top of the capsule since there is no space between the bottom of the capsule and the pipe wall.

By the principle of least resistance (Leonardo da Vinci stated that "processes in nature occur on the shortest path"), the other components of this central streamline would tend to pass through the crescent annulus formed by the space between the capsule and pipe wall, more towards the top where the gap is widest than towards the bottom. The reason for this being that the velocity must be zero at the capsule and pipe wall and tend

towards a maximum between the two walls. Consequently, there is least restriction to flow where the walls are further apart.

Streamlines in a vertical plane, close to the bottom of the pipe, can only be forced upwards to pass through the annulus. Those in the vertical plane at the top of the pipe need not change their path to follow the line of least resistance.

Next, consider streamlines in a horizontal plane at the pipe centre line. Those nearer the centre of the pipe can only pass over the top of the capsule. Those, nearer the pipewall, can only curve upwards since the annular space increases towards the top.

All other streamline planes can be considered in a like manner and it can be reasoned that the preferred orientation is always towards the largest distance between the pipe and capsule surfaces.

An alternative visualisation to that above, i.e. planes of streamlines passing through the centre of the pipe, is to imagine coaxial circles in the capsule-free section of the pipe; the diameter of each circle differing by a small finite amount. The outermost circles of streamlines are in a zone of low velocity due to pipe wall proximity.

As the neighbourhood of the capsule is approached the topmost streamlines can continue unretarded, whereas the ones near the bottom can only be diverted upwards. A ring of high velocity streamlines near the centre of the pipe would have to curve around the capsule when encountering the upstream face of the capsule and, for an eccentric capsule, it is clear that the diversion must be eccentric. Again, by the principle of least resistance, the ring of streamlines must assume a preferred orientation where wall proximity offers least resistance.

The above reasoning makes it easier to visualize streamline patterns passing around the capsule. It is clear that all the streamlines originate from a region of hydrostatic pressure distribution since streamlines are parallel upstream of the capsule.

If the obstructing capsule gives a modified orientation of streamlines, with higher velocities along the top of the capsule, the pressure there must be less according to Bernouilli's equation, causing a net lift force on the capsule. The pressure distribution is not hydrostatic and the streamlines are not parallel.

From the velocity contours of Jonsson and Sparrow (see Figure 7.28) for a stationary eccentric annulus, it is clear that the velocity diminishes where the angular space diminishes and this is to be expected, as discussed earlier.

However, Jonsson and Sparrow did measured pressure distributions around the eccentric annulus and found a slight pressure reduction towards the top of the annulus which diminishes as entrance length increases with a substantially larger difference as eccentricity increases.

It must be remembered that they considered fully developed steady flow and end effects were not taken into account. The effect of a finite capsule is to introduce the streamline curvature already mentioned and this causes a pressure reduction at the top of the annulus not found in the fully developed steady flow examined by Jonsson and Sparrow.

Streamlines, travelling around the top of the capsule, would also have greater energy losses due to entrance effects than those near the bottom and this also diminishes the pressure at the top of the capsule.

If the capsule velocity exceeds the mean water velocity and the flow in the annulus is generally backwards (i.e. $V_c > \bar{V}_{am}$) relative to the capsule, then the situation would be similar to that described above, but in reverse.

11.2.2 Lift due to end effects

Assume that the capsule velocity is less than the mean water velocity. In the capsule-free zone, one co-axial circle of streamlines must have the same velocity as the capsule. Inside this circle of streamlines the

water velocity is faster and outside the circle slower than the capsule velocity.

There is, thus, a movement of water around the rear face of the capsule, into the deficient areas, similar to the static capsule case.

This outward movement of water passes around the periphery of the capsule near the top and causes a zone of streamline curvature near the bottom of the upstream face, and breakaway near the top.

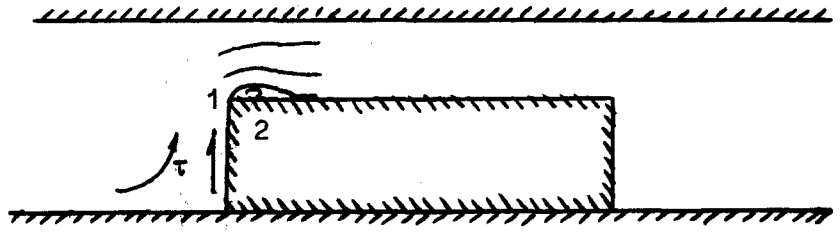

Figure 8.35

At the leading edge of the capsule there are two methods of inducing lift.

1. Streamline curvature upstream of the capsule causes a vertical shear on the upstream face which can only act upwards, (Figure 8.35 (1)).
2. Breakaway from the upstream surface of the capsule caused by streamlines travelling vertically upwards over the capsule, which separate from the edge. This causes an eddy, semi-toroidal in shape, which forms around the upper edge of the capsule (Figure 8.35 (2)).

In the case of an eccentric annulus this effect must be more pronounced at the widest part of the crescent annulus. This induces a low pressure region just above the capsule at the leading edge. What is meant by the leading edge of a capsule? If the water is moving generally

relative to the capsule, in the direction of capsule flow ($\bar{V} > V_c$) the leading edge is at the rear end. But if $V_c > \bar{V}$ the water generally moves from nose to tail and the nose end is the leading edge.

The end effects described above could, thus, result in either a nose up or tail up orientation. This will be discussed further in Chapter 12.

The front end is also subjected to lift forces. The vortex shown on Figure 8.34 at the front of the capsule gives rise to back flow which rises to meet the annulus stream in front of the capsule nose, and as it rises an upward shear is produced. The small vortex in front of the capsule at the bottom gives rise to a slight downward component.

Since the vortex in front of the capsule is likely to be weak, any vertical lift generated by this mechanism will be slight.

11.2.3 Lift due to secondary flow

It is difficult to separate this lift component from that due to primary streamline curvature. Nonetheless, secondary flow does exist and is likely to generate a secondary lift effect. Secondary flow is defined as components of flow other than axial and those due to primary streamline curvature.

There are two sources of secondary flow.

1. As a result of the streamline pattern described earlier, it is mandatory for circumferential velocity components to exist in addition to axial components.
2. In addition it is well known that secondary flows exist in all straight pipes of non-circular cross-section.

11.2.3.1 Secondary flows as a result of overall streamline curvature:

In the case of a capsule, which is laterally concentric and vertically eccentric, secondary flow components occur, which may be circumferentially symmetrical, (Figure 8.36).

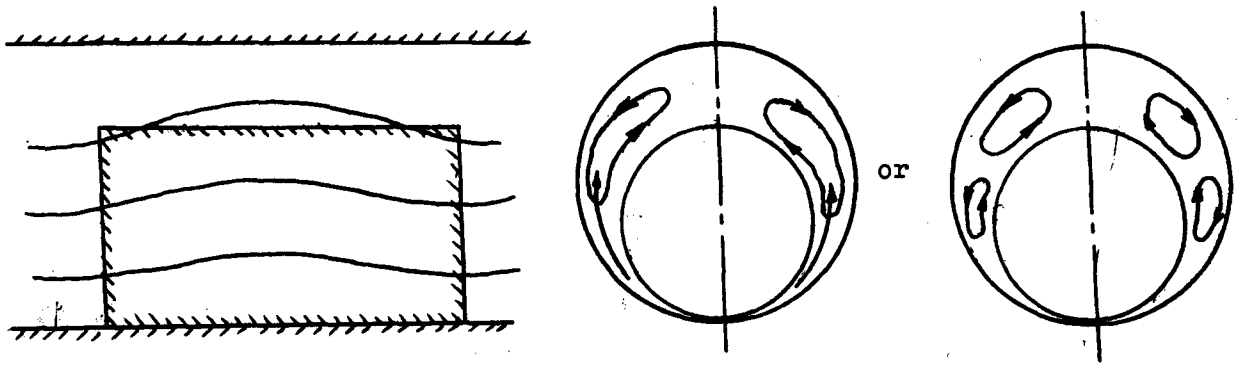

Figure 8.36

For relatively short capsules, the upward spiralling component could predominate since the downward component may only occur after the water has left the immediate vicinity of the capsule.

Even for longer capsules there could be a predominantly upward component, since the spiralling cycle would start off with an upward component and, unless the capsule were the exact length for a complete period to occur, there would still only be out-of-balance upward velocity components in the vicinity of the capsule.

If the capsule tends to lift by rolling up the side wall and adopting a laterally eccentric orientation periodically, the water, as in the case of a vertically eccentric capsule, tends to flow towards the widest part of the annular gap at the top. In the case of an obliquely eccentric capsule, the water tends to flow towards the widest gap, between capsule and pipe wall, which is not at the top. As the capsule rolls periodically up each side of the inside pipe wall, further secondary circumferential flows are generated. The evidence for this is an observed periodic spiralling of the capsule as it travels along, which is superimposed on the longitudinal motion.

These circumferential velocity components give rise to vertical shear components around the circumference, which could induce lift.

11.2.3.2 Secondary flows due to infinitely long non-circular cross-section

The secondary flows described above are further augmented by secondary flows generated in the triangular sections at the bottom of the pipe.

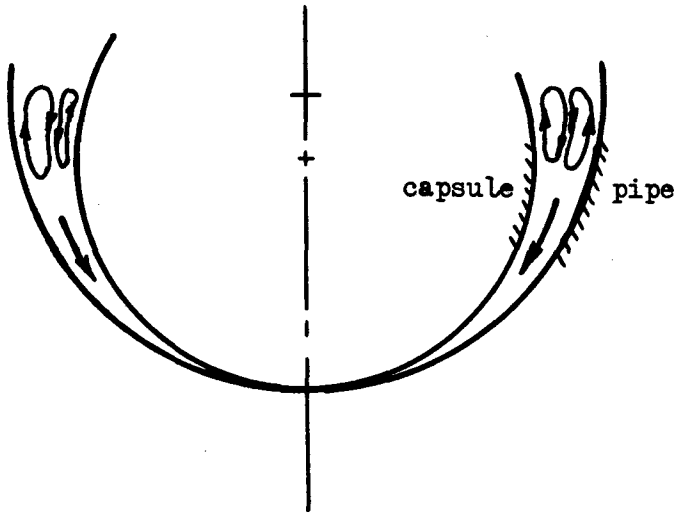

Figure 8.37

The water flows towards the bottom corners of the curved triangles along the bisectrix of the angles and then outwards in both directions. Momentum is transported from the centre to the corners and high velocities, as shown in Figure 8.37, are generated.

11.2.4 Lift due to Couette flow (Lift due to lubricating film)

It will be shown in Chapter 12 that the capsules generally travel in a nose up position. This means that the capsule slides on a wedge of water which thickens towards the front of the capsule. The velocity of the water is zero at both the capsule and pipe walls. Relative to the capsule the velocity must change from zero to V_c at the pipe wall. According to Figure 7.28, the pressure flow component of velocity ($\bar{V}_{ap}$) is negligible in the narrow region near the bottom where the capsule wall approaches the pipe wall.

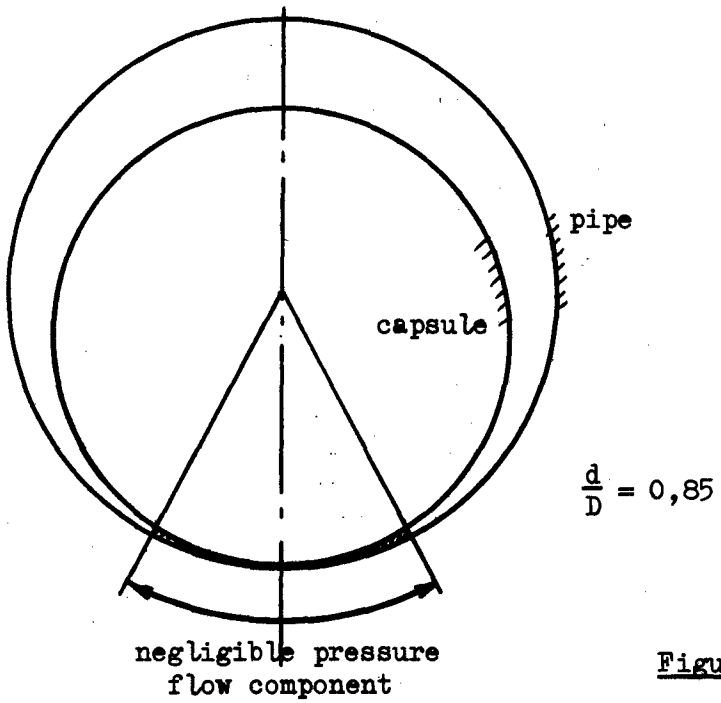

Figure 8.38

In a capsule water system, where the capsule has lifted, the flow, in the region shown shaded in Figure 8.38, is, virtually, entirely due to the Couette flow component and is similar to that found between parts of a machine in relative motion (such as a slipper and guide) where one solid face is sliding on a fixed face with a thin layer of fluid preventing contact. It can be seen on Figure 8.5 that the flow conditions are laminar for Couette flow up to an angle (θ) of about $0,16\pi$ for $\epsilon > 0,95$ at a capsule velocity (V_c) of 3 m/s for a fairly large diameter ratio $(d/D = 0,85)$.

It will be shown in Chapter 12 that, depending on the SG of the capsule, the above conditions represent a larger clearance (C) than actually occurs, i.e. $\epsilon > 0,95$ means that the gap $C < 0,825$ mm and for $SG = 3,7$ the maximum clearance (C) is less than 0,7 mm so that laminar flow certainly occurs for a total included angle of at least $0,32\pi$ when the capsule just lifts.

11.2.4.1 Viscous lift between plane surfaces

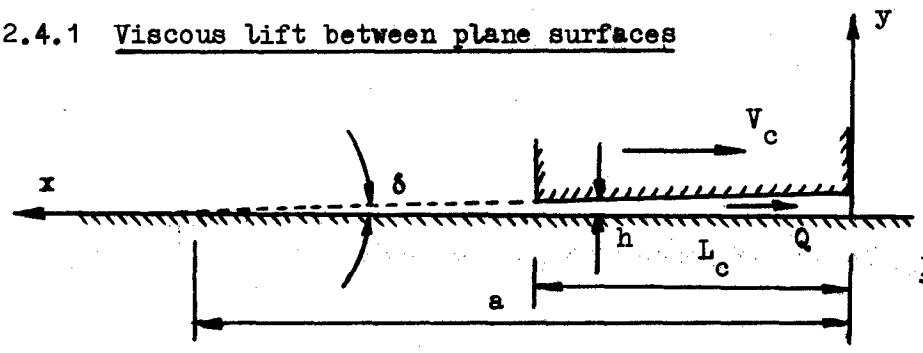

Figure 8.39

The standard equation for pressure drop in the x direction (e.g. Prandtl reference 45) is

$$dP/dx = \frac{12\mu}{h^3}\left[\frac{V_c h}{2} - Q\right] \qquad (8.15)$$

where Q = flow between two flat plates a distance h apart.

This equation is quite simply derived by integrating the basic equation for laminar flow between two flat plates ($dP/dx = \mu\, d^2V/dx^2$) twice, inserting the appropriate boundary conditions and integrating a third time to find Q (the Couette flow between the plates).

If the surfaces are parallel, h = constant and integrating equation (8.15) yields

$$P = \frac{12\mu}{h^3}\left[\frac{V_c h}{2} - Q\right] x + \text{const.} \qquad (8.16)$$

If the pressure is the same at each end (e.g. $P = 0$) then const. = 0 and $\left[V_c h/2 - Q\right] = 0$ (from equation (8.16)) and $dP/dx = 0$. This means that no vertical load can be supported. If a load is supported, the pressure must rise with x and decrease again at $x = L_c$, i.e. dP/dx must be a variable and from equation (8.15) h must be a function of x. Therefore, the surfaces must be inclined to each other.

From Figure 8.39 it can be seen that

$$h = (a - x)\delta$$

and it is easy to show (Prandtl reference 45) that

$$P_m = \frac{\mu V_c L_c^2}{h_m^2 (2a - L_c)} \qquad (8.17)$$

where P_m = mean pressure supporting the load

h_m = mean thickness of fluid film (mean gap between capsule and pipe wall).

The following shows how clearance due to the lubricating film can be calculated for a capsule travelling at $V_c = 4$ m/s assuming that the flow in the laminar Couette region is similar to flow between flat plates.

Consider a capsule of diameter ratio $d/D = 0{,}85$; length to diameter

ratio, $L_c/d = 4,0$ and $SG = 3,62$ in a 74 mm diameter pipe. The total submerged weight is $W' = 19,4$ N (i.e. including buoyancy forces). If the lubricating effect is assumed to act only in the region of laminar flow, see figure 8.38, then the bearing area is 0,007 m^2 and the average pressure is $P_m \doteq 2,77$ kPa.

By inserting the above values in equation (8.17) it can be shown that the front clearance is 0,3 mm with the back clearance 0,1 m. From Figure 12.5 it is seen that these clearance values correspond to a measured capsule velocity of about 2,2 m/s.

The elementary calculation above thus gives a capsule velocity (V_c) of about twice that measured, for an average clearance of 0,2 mm. This is explained below.

It is not surprising that the clearance given by the lubricating film analysis is an underestimation of the measured value since there are other factors contributing to capsule lift as mentioned earlier. Even that part of the lift component, due to the lubricating effect alone, is likely to be in error because assumptions made in deriving equation (8.17) are not complied with in the capsule case. The main assumptions are as follows:-

1. The analysis assumes plane surfaces which are parallel to each other at right angles to the motion. The curvature of the capsule and pipe walls as well as the non-parallel nature of the surfaces are both sources of deviation from the idealised theory. Although the former is less of a source of error than the latter.
2. The surfaces are also assumed to be of infinite extent, normal to the direction of motion, which means that no transverse components of flow are considered. It is evident that, in a capsule of finite length, the water is squeezed out of the narrowest section and passes around the capsule perimeter towards the back of the capsule. Although this escape of water is likely to reduce the pressure

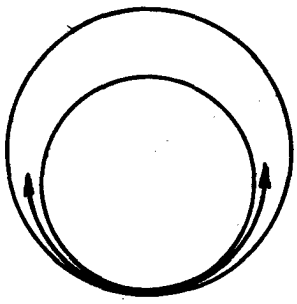

in the lubricating layer, it does give rise to secondary flow which induces capsule lift due to shear around the perimeter as discussed in Section 11. The secondary lift effect is probably less significant than the lubricating film effect and the reduction in the latter is not likely to be compensated by the former.

3. Viscous forces are the only ones taken into account in the theory. However, an upward component of pressure in the turbulent region, below the centre of the capsule, is also induced by a similar mechanism to the laminar effect at the bottom. This effect is far less significant than the viscous lubricating film below the capsule for three reasons: firstly, the clearance between the capsule and pipe wall increases around the perimeter from the bottom: secondly, the pressure forces causing lift must be at right angles to the capsule and the vertical components decrease steadily, becoming zero at the capsule centre-line, and thirdly, there is an opposing effect which is manifest in the turbulent region above the centre-line of the capsule. The pressure distribution around the capsule due to the lubricating effect is shown qualitatively in Figure 8.40

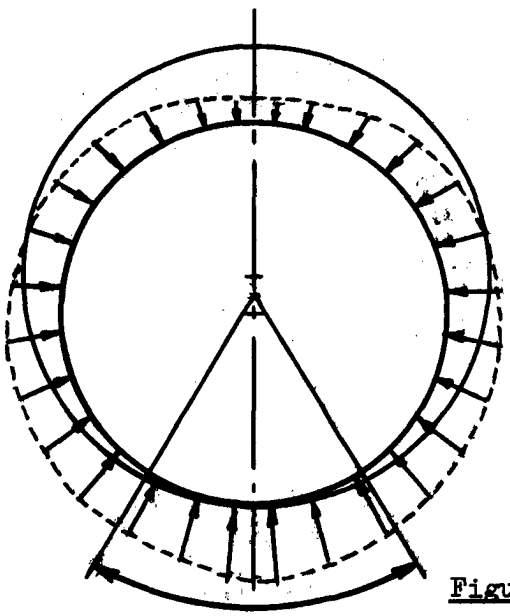

Figure 8.40
laminar Couette flow

Note that if the downward force due to the submerged capsule weight is kept constant and lift effects, other than that due to viscous lubricating film, are ignored, then;

$$h_m^2 \, (2a - L_c) \propto V_c$$

Also if $(2a - L_c)$ is assumed constant;

$$h_m \propto \sqrt{V_c} \qquad (8.18)$$

Increasing capsule velocity (V_c) from 4 to 6 m/s causes an h_m rise from 0,6 to 0,73 mm from equation (8.18). At the same time Couette flow, relative to the capsule, decreases at the bottom because the capsule rises into a lower velocity field (relative to the capsule), and a higher velocity field at the top of the capsule. The capsule lift is thus restricted as capsule velocity increases.

11.2.5 Lift due to combined effect of pressure and Couette flow

The pressure flow component causes a high velocity field, relative to the capsule, at the top where the gap is largest, and this causes a circulation pattern around the capsule.

Couette flow causes a backward flow relative to the capsule, and this reversed velocity further amplifies the circulation pattern around the capsule (Figure 8.41).

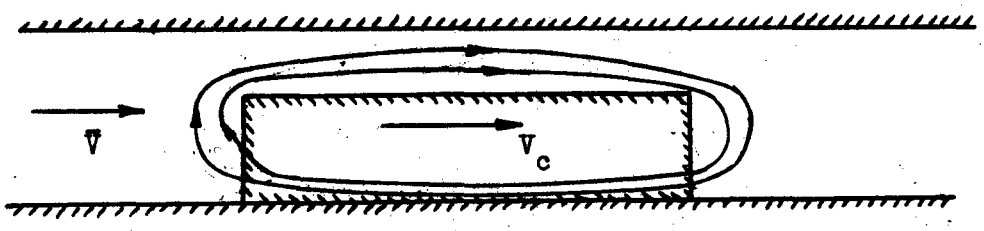

Figure 8.41

When the capsule lifts in a nose-up orientation the circulation is increased towards the centre of the capsule (Figure 8.42).

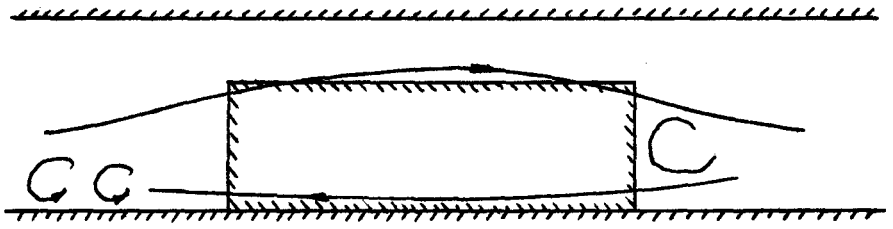

Figure 8.42

In order to balance the circulation around the capsule, vortices are cast off at the trailing edge initially.

These cast off vortices are in the same direction as those described earlier for static capsules, which create upward shears on the back face of the capsule.

11.3 Calculation of lift ratio neglecting secondary flow and lubricating film effects

The lift ratio is defined as the lift force divided by the submerged weight of the capsule.

$$L_r = L_F/W'$$

The value for $\mu_f(1 - L_r)$ can be obtained from equation (7.219) and Figure 8.43 shows how this parameter, which represents the total excess force acting across the capsule zone, minus the force due to skin friction on the pipe wall, changes with $\bar{V}$ and diameter ratio as parameter. As $\bar{V}$ increases $\mu_f(1 - L_r)$ decreases regardless of diameter ratio, but at a greater rate as diameter ratio increases. This is because the excess head loss across the capsule increases with corresponding increase in the subtractive shear on the pipe wall as velocity increases. This leads to the representation of L_r as a function of $\bar{V}$, also shown in the diagram (Figure 8.43). The lift, and hence the value of L_r, must be zero at $\bar{V} = 0$ and increases in the manner shown, the higher diameter ratio capsules

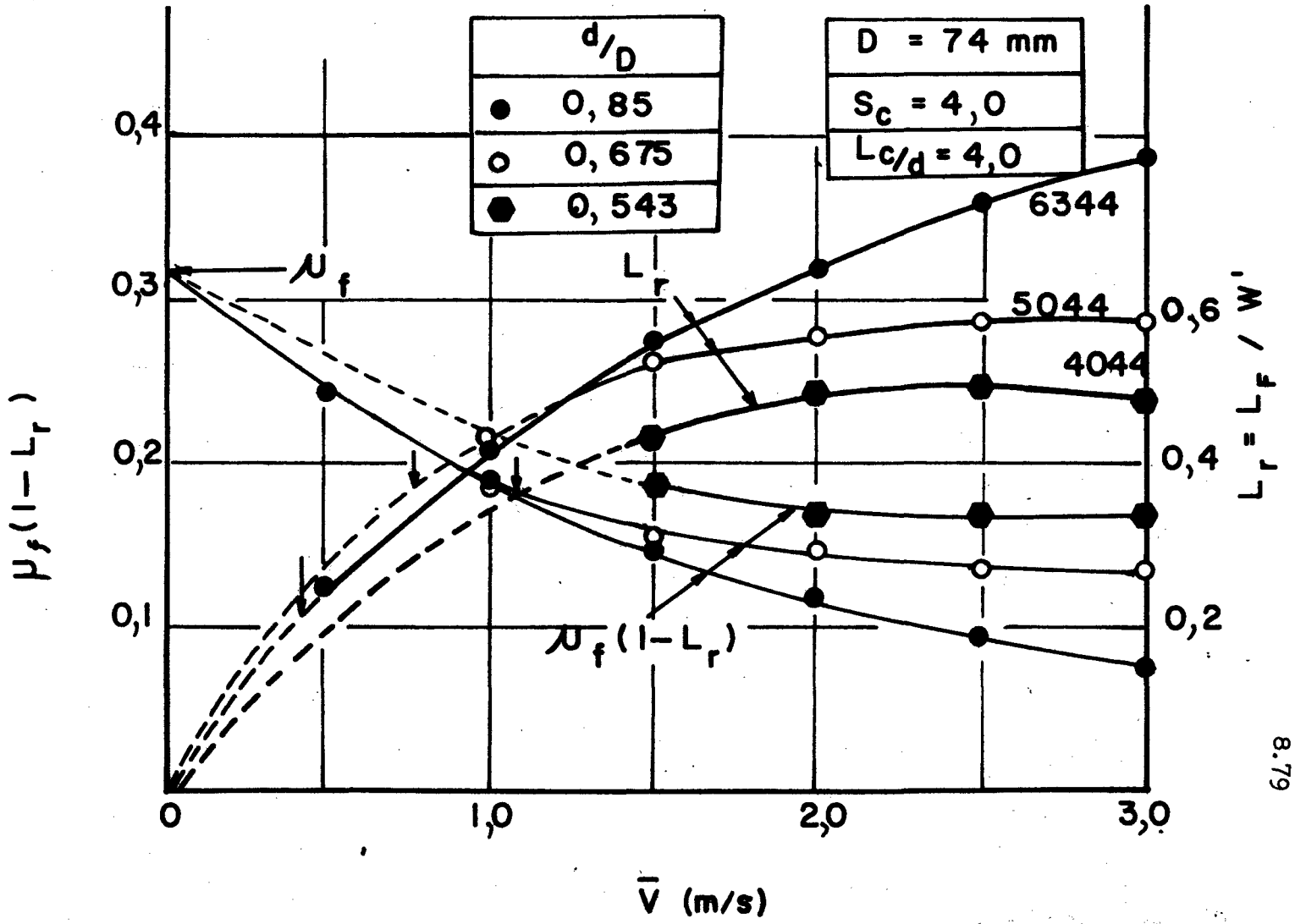
d/D
0,85
0,675
0,543
D = 74 mm
Sc = 4,0
Lc/d = 4,0
6344
5044
4044
μ_f
L_r
$\mu_f(1-L_r)$
0,4
0,3
0,2
0,1
0
1,0
2,0
3,0
0,6
0,4
0,2
$\mu_f(1-L_r)$
$L_r = L_f / W$
$\bar{V}$ (m/s)

FIG. 8.43

attaining a greater lift force per unit submerged weight. And it will be shown in Chapter 12 that increasing the diameter ratio (up to $d/D \doteq 0,95$) causes incipient lift at progressively lower velocities.

Figure 8.44 shows the lift ratio as a function of capsule velocity with diameter ratio as parameter. The dotted curves indicate zero lift at $V_c = 0$. This is incompatible with the previous figure. On Figure 8.43 the arrows indicate incipient velocity and the lift ratio values at these points can be transferred to Figure 8.44 showing, by means of the full lines, positive values of L_r at $V_c = 0$. This reveals one erroneous assumption in the theory, i.e. zero lift at incipience.

Figure 8.45 shows the value of L_r as a function of capsule velocity for different density capsules, and it is clear that the lift ratio must increase as the submerged weight of the capsule increases.

It would appear that the lightest capsule (SG = 1,87) approaches a unit value of L_r at $V_c \doteq 2$ m/s and if the theory were correct this would be the incipient lift velocity.

However, it will be shown in Chapter 12 that incipient lift actually occurs at a much lower velocity (for this capsule at about 1,6 m/s).

The primary purpose of the theory described in Chapter 7 was not to calculate lift forces on capsules. This was merely a side issue, the main one being to calculate energy losses across capsules. It will be shown in Chapter 15 to what extent this was successful.

The theory does not take into account lift forces due to lubricating film effect, and secondary flows (probably the main causes of lift). The foregoing three figures serve more to indicate trends than an accurate estimation of lift forces.

12. Modes of travel of capsule

As has been stated earlier, the sum of all forces on a non-accelerating capsule must be zero and the forces act in such a way as to maintain the

FIG. 8.44

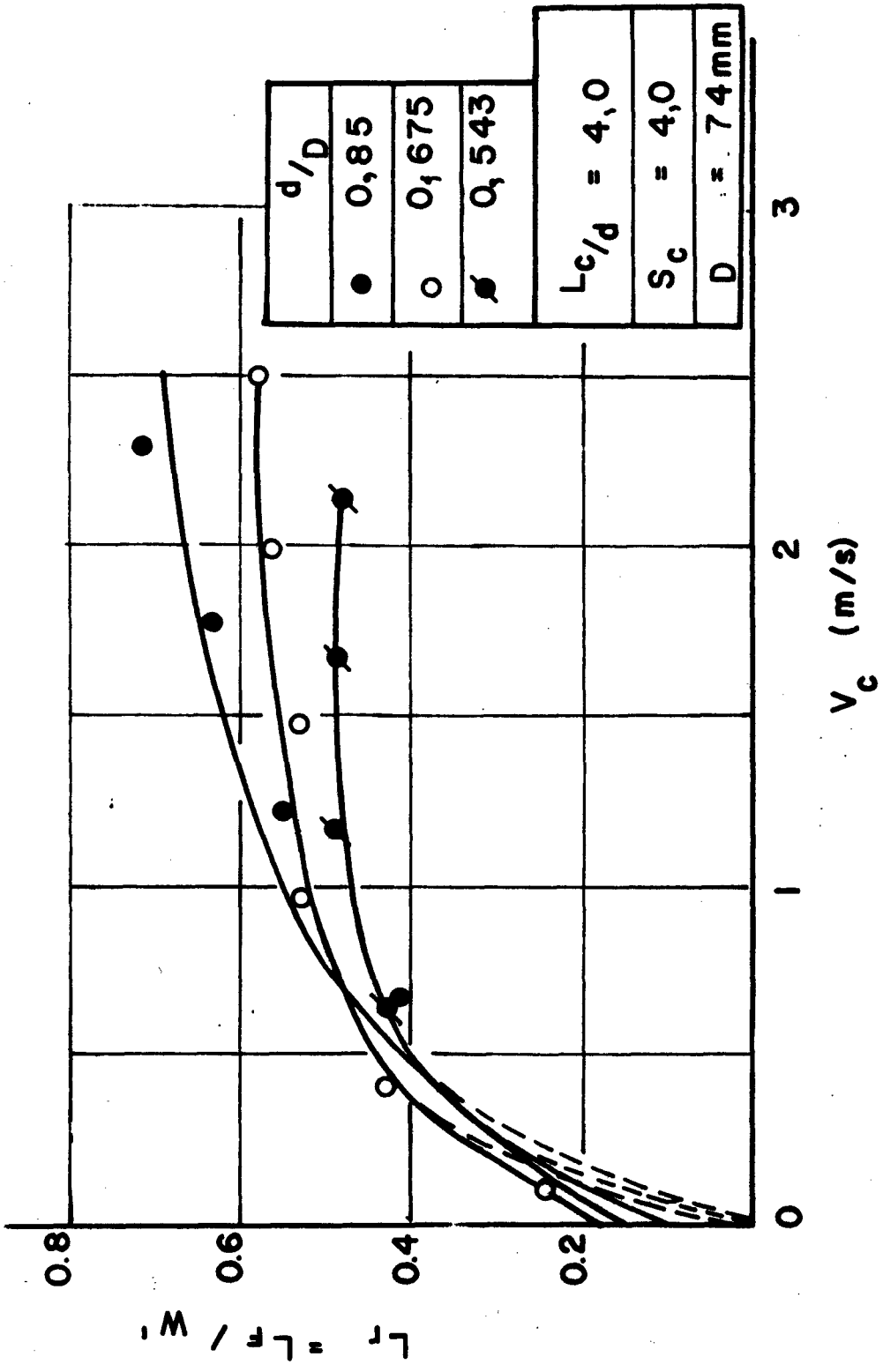

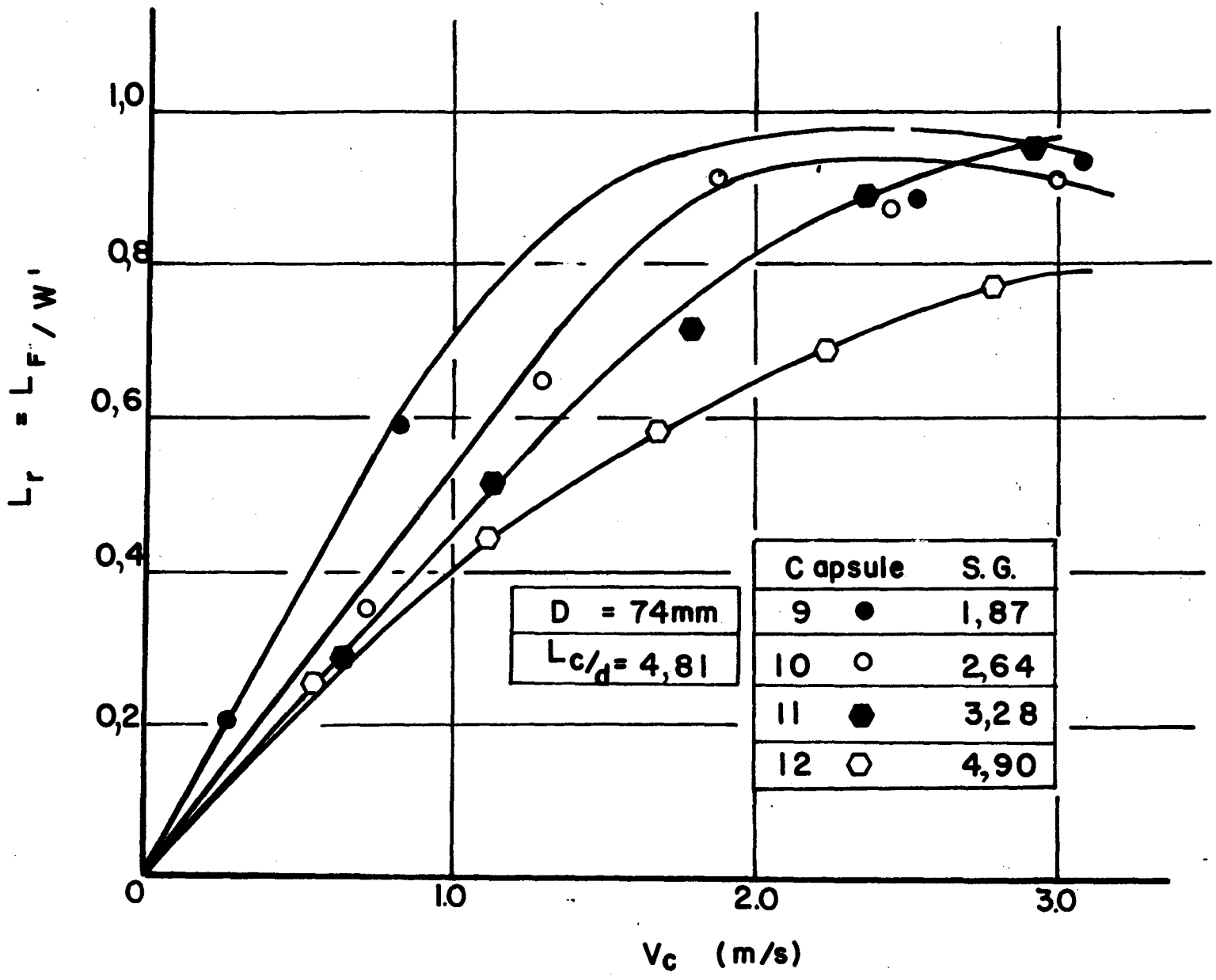
1,0
0,8
0,6
0,4
0,2
0
1.0
2.0
3.0
$L_r = L_{F'} / W'$
V_c (m/s)
D = 74mm
$L_{c/d}$ = 4,81
Capsule S.G.
9 ● 1,87
10 ○ 2,64
11 ⬢ 3,28
12 ⬡ 4,90

FIG. 8.45

capsule in equilibrium.

Restricting the following to horizontal pipes, the capsules have been observed to travel basically in one of three ways; that is, in contact with the pipe bottom (or top), completely suspended, or travelling nose-up with the rear end trailing along the pipe bottom (or vice versa for SG < 1). This is a vast oversimplification of the basic modes of travel and the above patterns may be modified to include; combinations of the above three modes (i.e. adopting different positions intermittently), rolling up the side of the pipe wall, yawing (axis of capsule not parallel to pipe axis in plan) pitching (intermittent nose-up and horizontal) and rotating about their own axis in the direction of flow.

12.1 Capsule and pipe wall in contact

When travelling in contact with the pipe bottom, the skin friction drag plus the solid to solid friction drag is in balance with the form drag in a direction parallel to the main flow, and the lift and buoyancy forces are in balance with the weight of the capsule in a perpendicular direction to the main flow.

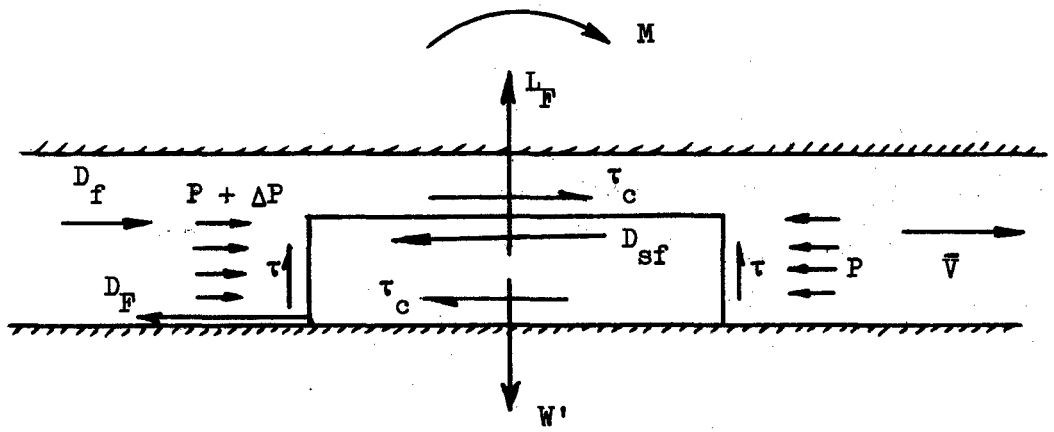

Figure 8.46

Any moments acting on the capsule (due to the fluid) merely have the effect of distributing the reaction on the pipe bottom.

In this instance, there is likely to be a clockwise moment due to fluid forces. This is because the skin friction drag, due to pressure flow, acts forward and more towards the top of the capsule (see Figure 8.17). Whereas the Couette shear acts backwards and more towards the bottom of the capsule (see Figure 8.7 for example).

An additional factor causing a clockwise moment is the flow around the upstream face of the capsule, which causes a low pressure region at the top of the rear face and a shear stress vertically upwards on the rear face (see Section 11.2.2).

This clockwise moment is not sufficient to cause macroscopic capsule lift since the capsule only lifts at mean water velocities of the order of capsule velocity (see Chapter 12).

12.2 Travelling free

When travelling free of the pipe bottom, the form drag is in balance with skin friction drag in a direction parallel to the main flow. And the lift forces are in balance with the submerged weight of the capsule.

In this case no moments can be transmitted to the pipe wall. The capsule adopts a particular orientation resulting in a net zero moment.

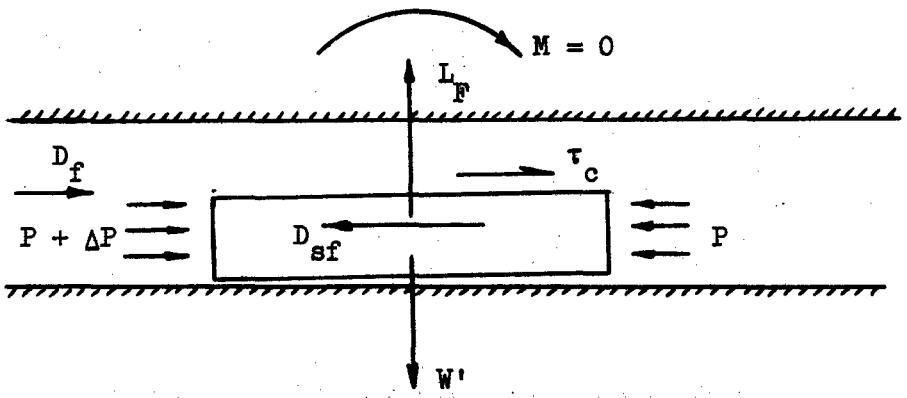

Figure 8.47

Consider the case where $V_c \geq \bar{V}$. There is a co-axial circle of streamlines similar to that described previously (for $V_c < \bar{V}$) wherein

the capsule velocity is less than the local water velocity and outside of which the water velocity is less than the capsule velocity.

In this case consider the front of the capsule. The capsule overtakes the water outside the circle and the fluid inside must move upwards and outwards into the deficient zone at the front of the capsule.

This is best visualised by considering a stationary capsule with the pipe wall moving backward at a velocity (V_c), and the water moving forwards at a velocity $(v - V_c)$ at any point in the capsule-free pipeline section (see Figure 8.48).

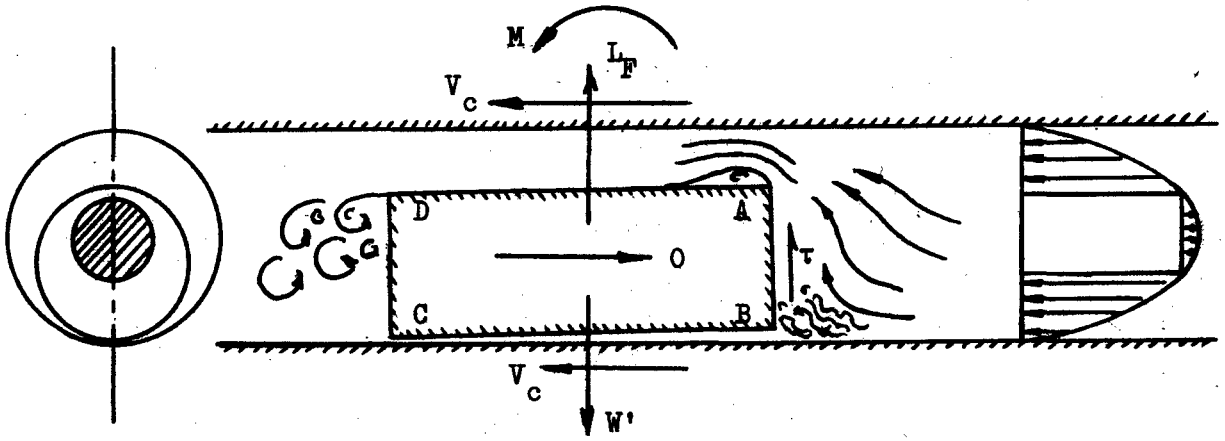

Figure 8.48

Assume that the capsule does not lift in this situation. All the streamlines curve up towards the top of the crescent annulus, and the velocity in the region A is higher than at the bottom in region B. There is a stagnation zone on the front face towards the bottom causing an anticlockwise moment about the point C.

This moment is further amplified by the shear due to flow over the capsule surface, and low pressure due to breakaway behind A as well as at D.

As the velocity of water relative to the capsule increases the moment increases and a velocity is reached when the anticlockwise moment is sufficient to overcome the clockwise moment about C due to the

submerged weight of the capsule.

As soon as lift occurs, the water is able to flow around the capsule towards the bottom in the region of B. Although there is likely to be a great deal of turbulence near B.

The water, well upstream of the capsule (on the right hand side of the relative motion diagram, Figure 8.48) originates from a hydrostatic pressure region, and flows around the capsule in a restricted area towards the top, causing a lower pressure than in the capsule-free zone, since there is relatively little energy loss for these upper streamlines.

The water from the stagnation zone B, where the pressure is higher than in the capsule-free section of the pipe, is now able to flow under the capsule at an even higher velocity.

However, the water passing around the bottom of the capsule has incurred a greater energy loss travelling from the hydrostatic pressure distribution region than that which passes around the top, even though the velocity under the capsule is greater than above. This is because it has passed through the highly turbulent high pressure zone at B.

As the capsule tends to lift even more, the flow around the capsule tends to become more symmetrical, since the capsule eccentricity decreases. This causes less energy loss for streamlines passing around the underside of the capsule since flow conditions are not so restricted at B, and the pressure decreases at B thus pulling the capsule down into an equilibrium position.

Any further increase in velocity around the capsule causes a pressure reduction around the upper and lower sections of the capsule, which tend to be less different as the clearance at the bottom decreases.

In addition to the above, once the capsule has lifted substantially, the lubricating film pressure, along the underside of the capsule, becomes significant and the resultant force acts behind the middle.

If the inclination of the capsule is increased due to the anti-clockwise moment, the point of application of the lubricating film pressure moves further back causing a clockwise moment and tending to stabilise the capsule at different velocities. At equilibrium the net moment on the capsule is zero.

PART IV

EXPERIMENTAL RESULTS AND DISCUSSION

"Physics is said to be an empirical science based upon observation and experiment."

Bertrand Russell

CHAPTER 9

HEAD LOSSES ACROSS STATIC CAPSULES

The apparatus used for static capsule tests was described in Chapter 4 and is shown diagrammatically in Figure 9.1.

The applicability of the static capsule investigation was dealt with in Chapter 7, Section 3.1, and the object of studying static capsules was given in Chapter 7, Section 3.2. Definitions of energy losses for static capsules are shown diagrammatically on Figure 7.7, and discussed in Chapter 7, Section 3.3

Experimental results of static capsule tests will now be dealt with in the following sequence; hydraulic grade lines for eccentric and concentric capsules, energy losses at inlet and outlet for eccentric and concentric capsules, and finally annular losses.

1. Hydraulic Grade lines and energy lines

Figures 9.1 and 9.2 show hydraulic grade lines and energy lines for static capsules orientated eccentrically. Three different velocities at each of three diameter ratios are shown, and for each curve pressure heads were measured at positions indicated on Figure 9.1. A notable feature of these curves is the sharp dip in the hydraulic grade line at the inlet.

Figures 9.3 to 9.5 show hydraulic grade lines and energy lines for static capsules concentrically orientated, and the curves are slightly different from those for eccentric capsules. At inlet, there is no sharp dip in the hydraulic grade line. Whereas at outlet, a slight dip is apparent.

This is difficult to explain, and will be discussed further in the next section.

2. Inlet head losses for static capsules

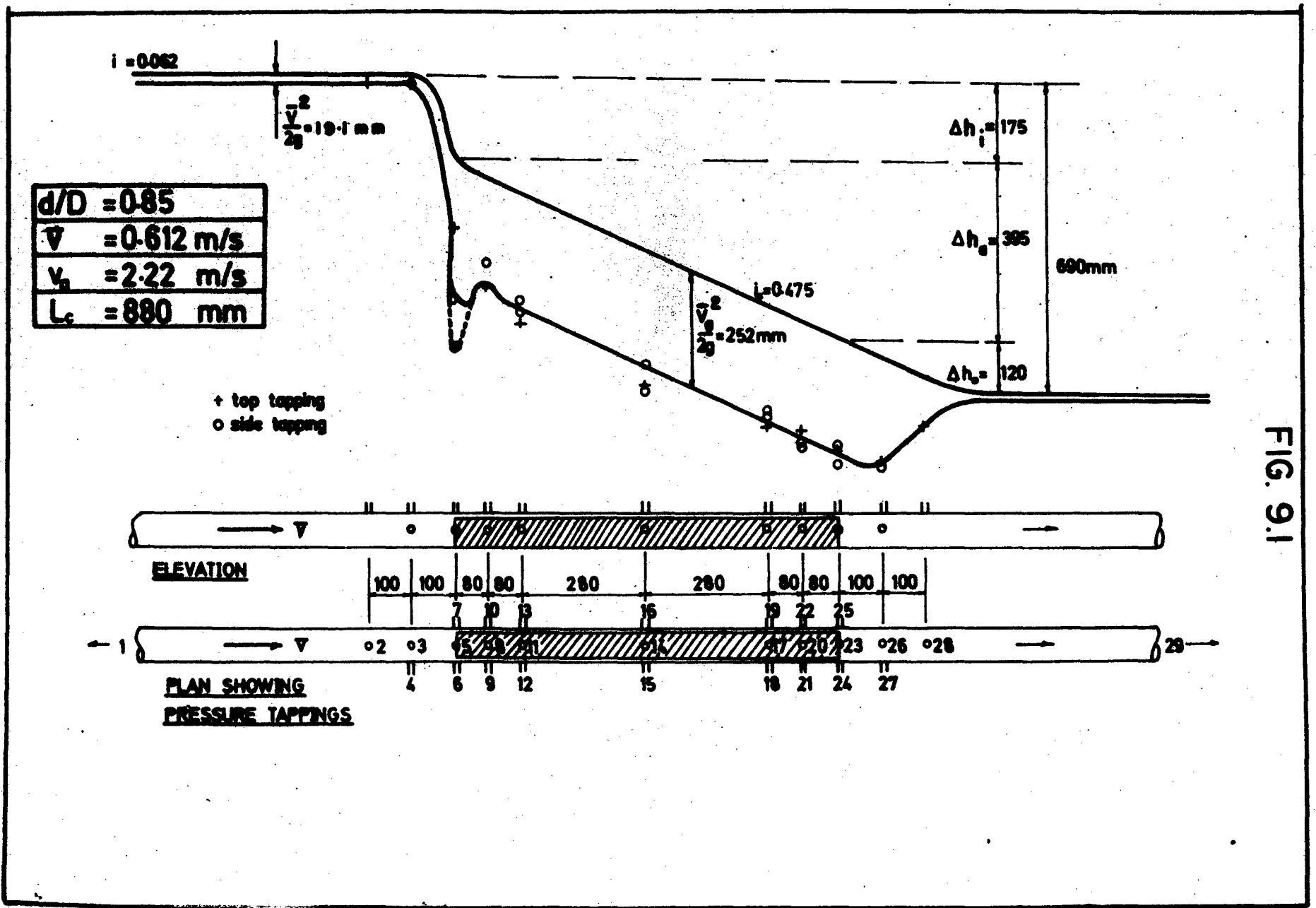
i = 0.062
$\frac{\bar{V}^2}{2g}$ = 19·1 mm
d/D = 0·85
$\bar{V}$ = 0·612 m/s
V_n = 2·22 m/s
L_c = 880 mm
Δh_i = 175
Δh_e = 395
690mm
i = 0·475
$\frac{\bar{V}^2}{2g}$ = 252mm
Δh_o = 120
+ top tapping
o side tapping
ELEVATION
PLAN SHOWING
PRESSURE TAPPINGS
100 100 80 80 280 280 80 80 100 100
1 2 3 4 5 6 7 8 9 10 11 12 13 14 15 16 17 18 19 20 21 22 23 24 25 26 27 28 29

FIG. 9.1

Fig. 9.2

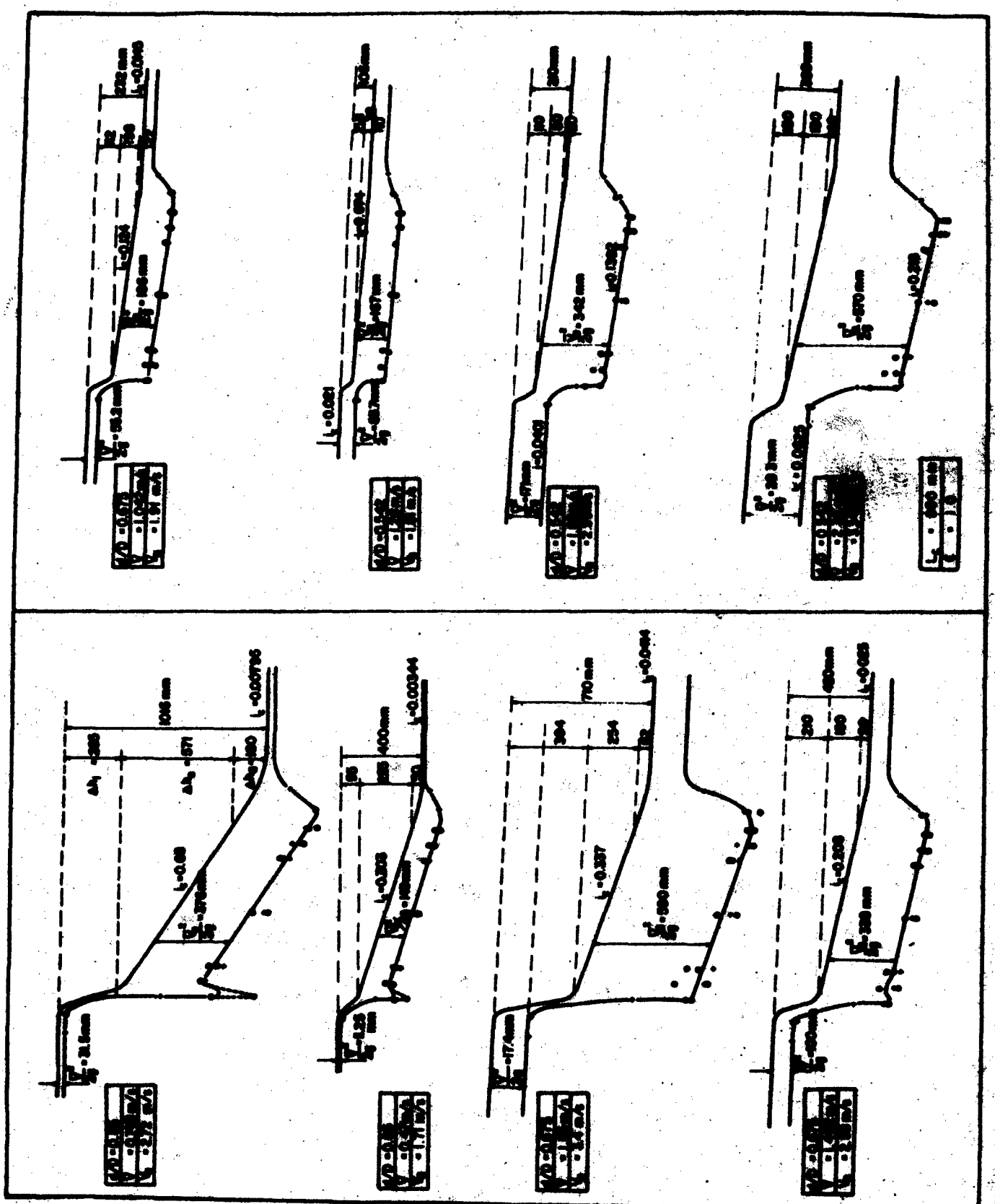

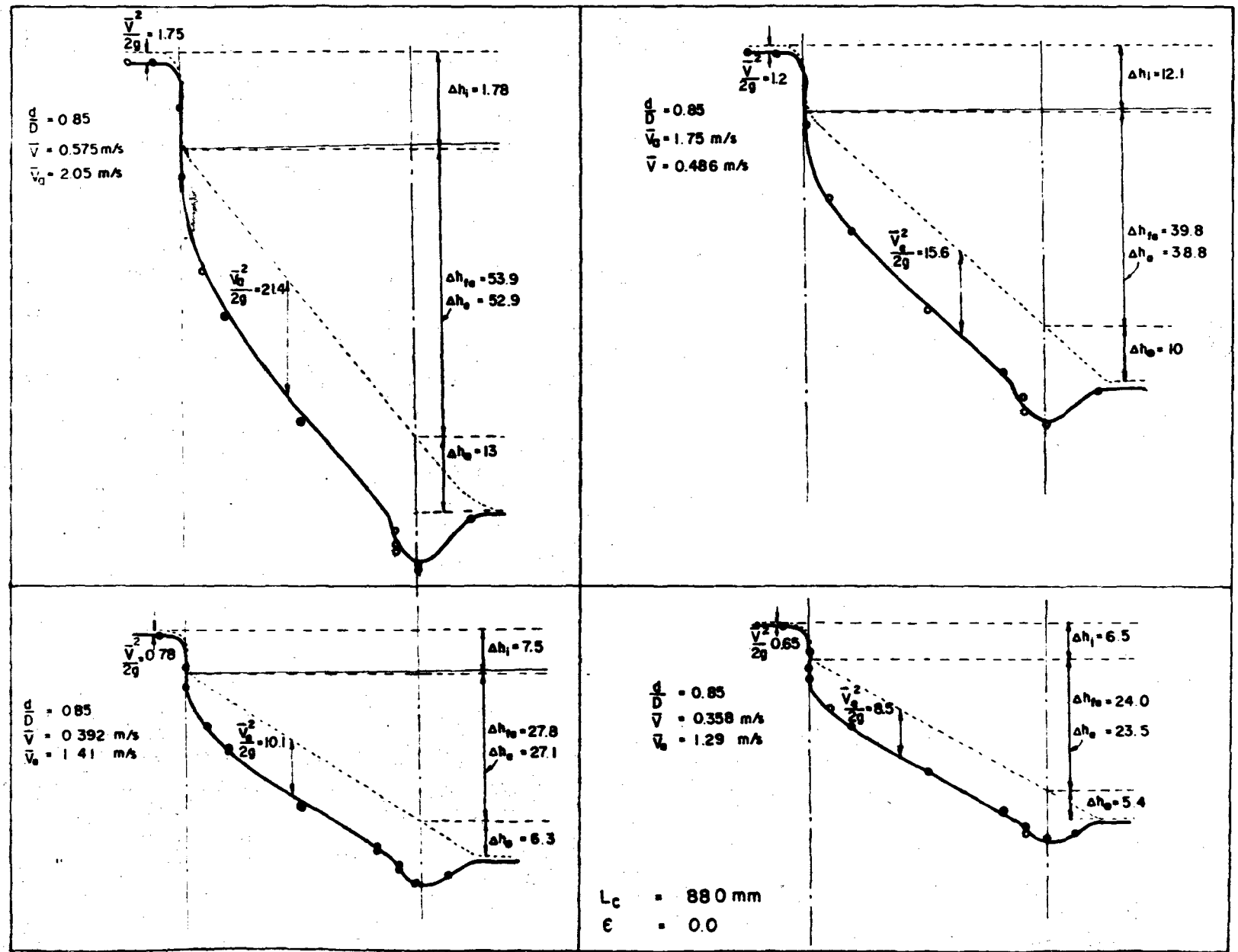
$\frac{\bar{V}^2}{2g}$ = 1.75
$\frac{d}{D}$ = 0.85
$\bar{V}$ = 0.575 m/s
$\bar{V}_o$ = 2.05 m/s
Δh_i = 1.78
$\frac{\bar{V}_o^2}{2g}$ = 21.4
Δh_{fe} = 53.9
Δh_e = 52.9
Δh_o = 13
$\frac{\bar{V}^2}{2g}$ = 1.2
$\frac{d}{D}$ = 0.85
$\bar{V}_o$ = 1.75 m/s
$\bar{V}$ = 0.486 m/s
Δh_i = 12.1
$\frac{\bar{V}_o^2}{2g}$ = 15.6
Δh_{fe} = 39.8
Δh_e = 38.8
Δh_o = 10
$\frac{\bar{V}^2}{2g}$ = 0.78
$\frac{d}{D}$ = 0.85
$\bar{V}$ = 0.392 m/s
$\bar{V}_o$ = 1.41 m/s
Δh_i = 7.5
$\frac{\bar{V}_o^2}{2g}$ = 10.1
Δh_{fe} = 27.8
Δh_e = 27.1
Δh_o = 6.3
$\frac{\bar{V}^2}{2g}$ = 0.65
$\frac{d}{D}$ = 0.85
$\bar{V}$ = 0.358 m/s
$\bar{V}_o$ = 1.29 m/s
Δh_i = 6.5
$\frac{\bar{V}_o^2}{2g}$ = 8.5
Δh_{fe} = 24.0
Δh_e = 23.5
Δh_o = 5.4
L_c = 88.0 mm
ϵ = 0.0

FIG 4.3

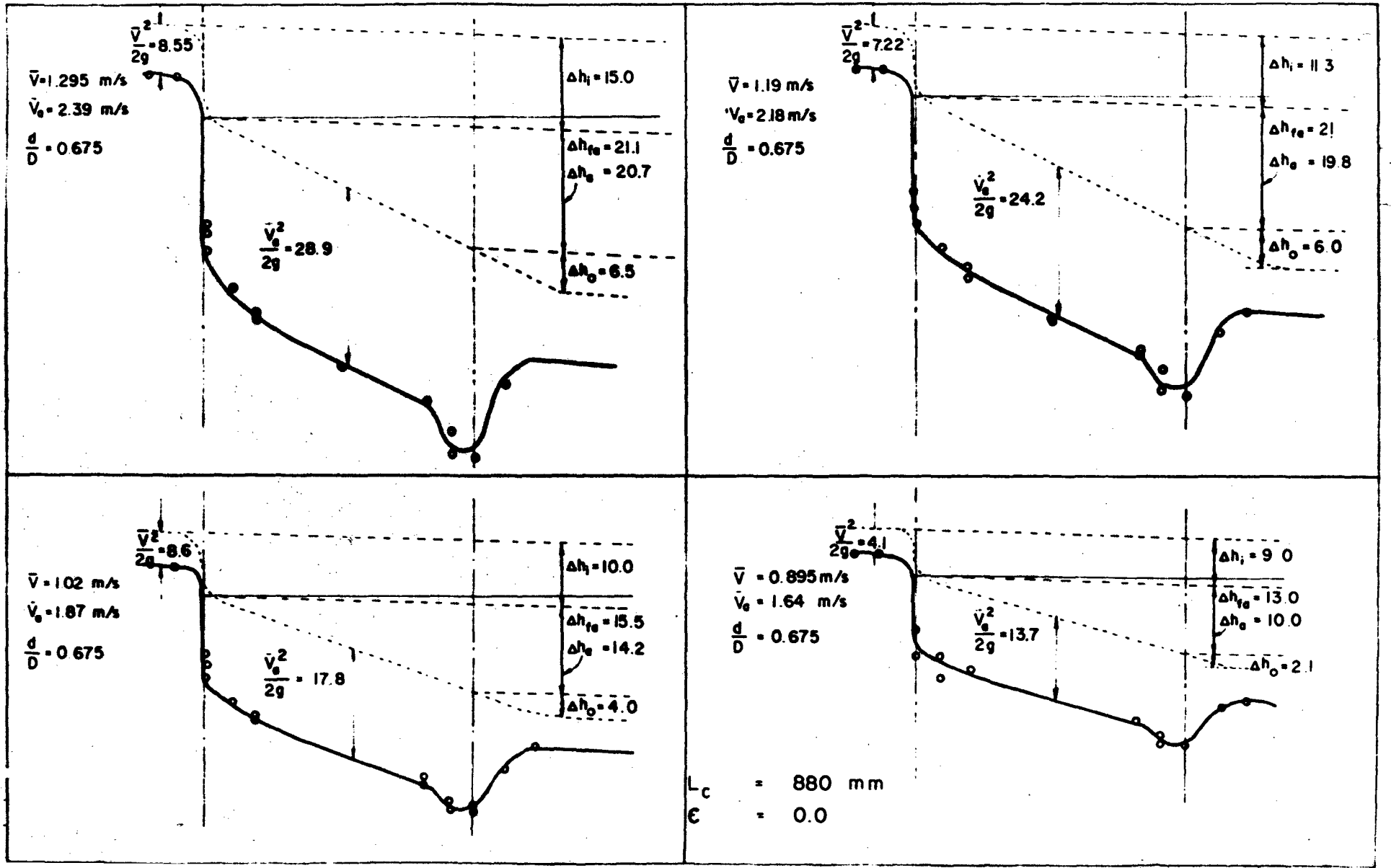
$\frac{\bar{V}^2}{2g}$ = 8.55
$\bar{V}$ = 1.295 m/s
$\bar{V}_e$ = 2.39 m/s
$\frac{d}{D}$ = 0.675
Δh_i = 15.0
Δh_{fe} = 21.1
Δh_e = 20.7
$\frac{V_e^2}{2g}$ = 28.9
Δh_o = 6.5
$\frac{\bar{V}^2}{2g}$ = 7.22
$\bar{V}$ = 1.19 m/s
$\bar{V}_e$ = 2.18 m/s
$\frac{d}{D}$ = 0.675
Δh_i = 11 3
Δh_{fe} = 21
Δh_e = 19.8
$\frac{V_e^2}{2g}$ = 24.2
Δh_o = 6.0
$\frac{\bar{V}^2}{2g}$ = 8.6
$\bar{V}$ = 1.02 m/s
$\bar{V}_e$ = 1.87 m/s
$\frac{d}{D}$ = 0.675
Δh_i = 10.0
Δh_{fe} = 15.5
Δh_e = 14.2
$\frac{V_e^2}{2g}$ = 17.8
Δh_o = 4.0
$\frac{\bar{V}^2}{2g}$ = 4.1
$\bar{V}$ = 0.895 m/s
$\bar{V}_e$ = 1.64 m/s
$\frac{d}{D}$ = 0.675
Δh_i = 9 0
Δh_{fe} = 13.0
Δh_e = 10.0
$\frac{V_e^2}{2g}$ = 13.7
Δh_o = 2.1
L_c = 880 mm
ϵ = 0.0

FIG 9.4

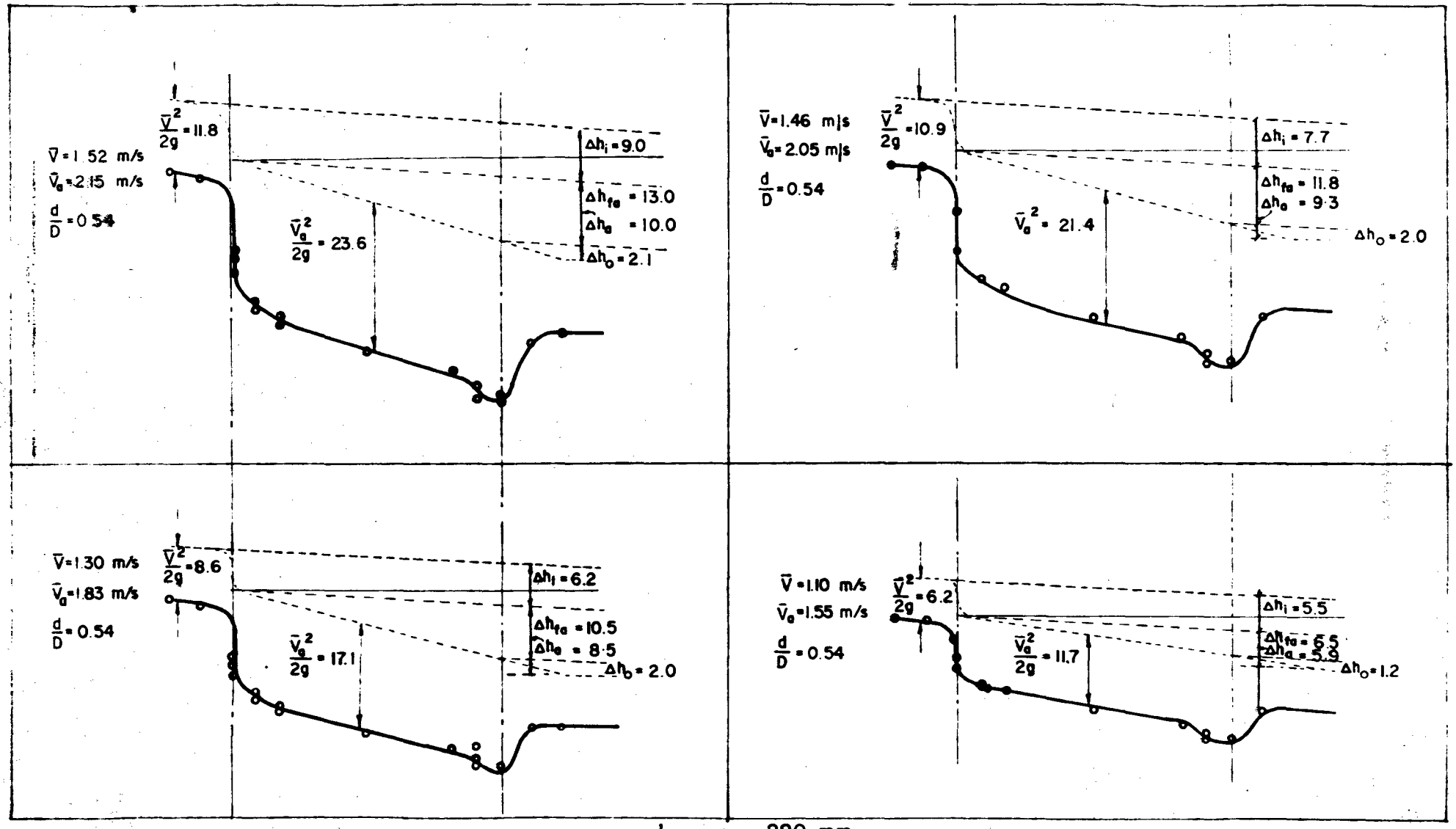

L_c = 880 mm

ϵ = 0.0

FIG. 9.5

The inlet head loss for static capsules is a case where flow converges from the circular pipe flow condition to the annulus condition. As such, no information could be found in the existing literature.

The concentric and fully eccentric positions are extremes of the general situation and are, basically, the only two cases of concern for static capsules, in the present context.

It can clearly be seen from Figures 9.1 and 9.2 that, for eccentric annuli, there is a sharp local drop at the inlet due to the increased velocity in the restricted area of flow just downstream of the inlet face. this is due to contraction and re-expansion of the streamlines which are asymmetrical in the case of the eccentric annulus. Consider a streamline almost parallel to the upstream face at right angles to the axis of the pipe. This streamline cannot turn through a right-angle and must cause a contracted area just downstream of the leading edge. In the eccentric annulus case, the contraction is asymmetrical around the perimeter of the capsule, with a maximum contraction at the top and zero contraction at the bottom of the capsule. Furthermore, the contraction of the stream only takes place along the capsule side of the annulus, whereas, along the pipe wall, no contraction occurs.

Boundary layer growth along the capsule starts after the leading edge. However, for the pipe wall, the boundary layer exists before contraction. The laminar sub-layers for the capsule and pipe are, in all probability, not of constant thickness circumferentially, in the eccentric case, due to the variation in velocity around the perimeter of the annulus. The pipe and capsule laminar sub-layers approach each other towards the bottom of the pipe, in this case, and must merge with one another before this point.

The energy loss is, in fact, largely due to the expansion downstream from the vena contracta. Eddies are generated and energy is lost keeping

them in rotation.

The above indicates that the velocity distribution, just upstream and downstream of the inlet section, is extremely complicated.

The non-dimensional value of the inlet head loss in conventionally expressed as $\Delta h_i/(\bar{V}^2/2g)$ and if this value is plotted against d/D an empirical equation representing the experimental results for the static capsule values is

$$\Delta h_i/(\bar{V}^2/2g) = k' \qquad (7.112)$$

This is shown in Figure 9.6 for the different flows and diameter ratios. And for eccentric annuli;

$$k'_e = 22(d/D)^6 \qquad (7.113)$$

It has already been pointed out that the sudden dip at inlet is suppressed for concentric capsules. One possible explanation is that the pressure tappings are at the top and sides of the pipe (i.e. tappings 5; 6 and 7, Figure 9.1). And it is only in the case of the largest diameter ratio (d/D = 0,85) that one side tapping is mainly responsible for the pressure dip (Figures 9.1 and 9.2). For the eccentric capsule there is probably less contraction just downstream of the inlet face, at the same velocity, since the flow is evenly distributed around the perimeter. Another possible reason for the low pressure in the eccentric case is the secondary streamline curvature towards the top of the crescent annulus (as described in Chapter 8) at inlet.

Note that inlet and outlet head losses are somewhat unconventionally defined in Chapter 7, Section 3.3. Conventionally, the head loss is defined as existing between sections upstream and downstream of the contraction where the streamlines are parallel. Note also that the diagrams are essentially for wall streamlines, there are no pressure tappings on the capsule.

Figure 9.7 shows the inlet head loss for concentric annuli as a function of the mean water velocity $(\bar{V})$ and Figure 9.8 shows the non-dimensional presentation.

FIG. 9.6

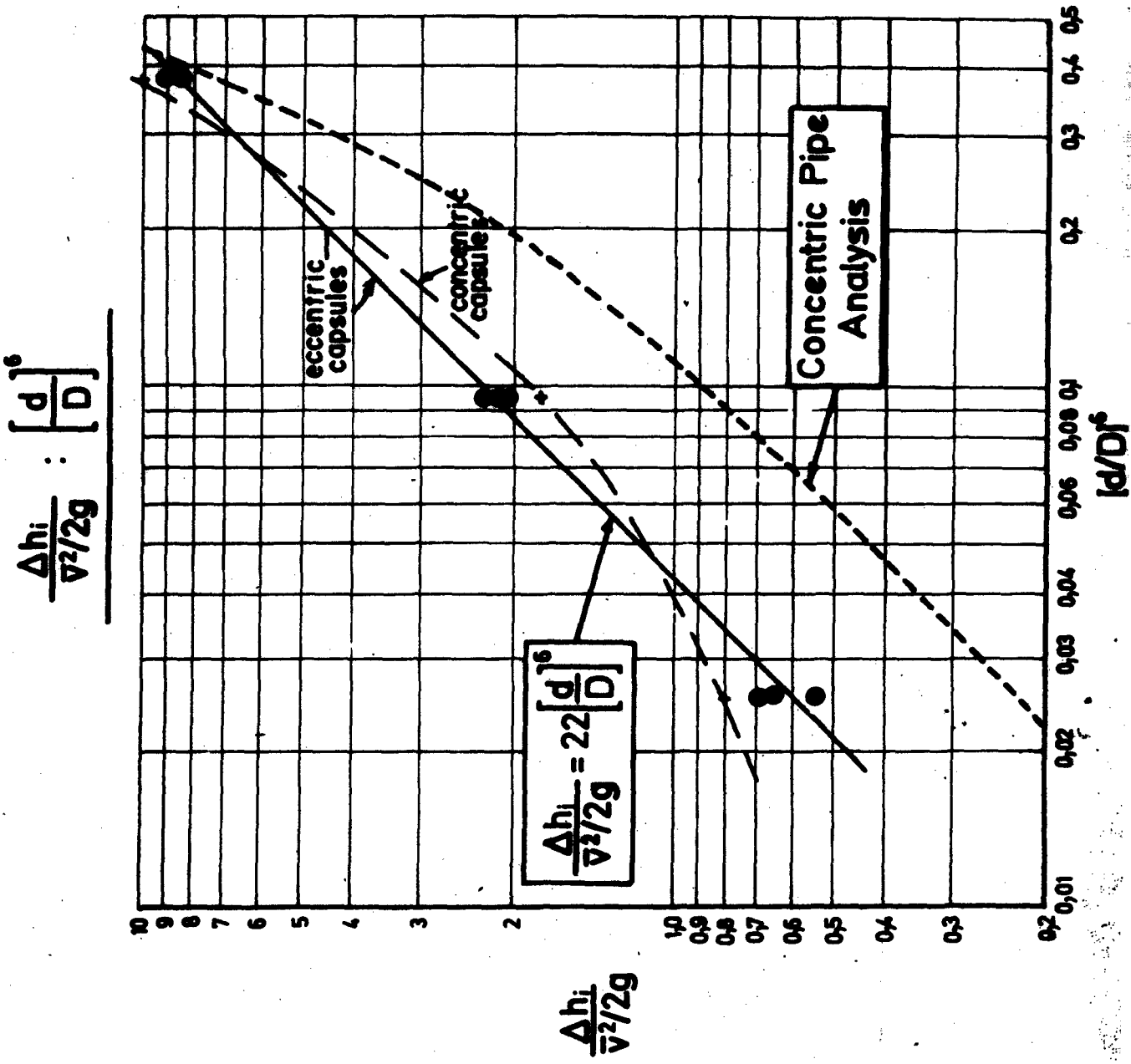
$\frac{\Delta h_i}{\bar{v}^2/2g} : \left[\frac{d}{D}\right]^6$
eccentric capsules
concentric capsules
Concentric Pipe Analysis
$\frac{\Delta h_i}{\bar{v}^2/2g} = 22\left[\frac{d}{D}\right]^6$
$\frac{\Delta h_i}{\bar{v}^2/2g}$
$[d/D]^6$

FIG. 9.7

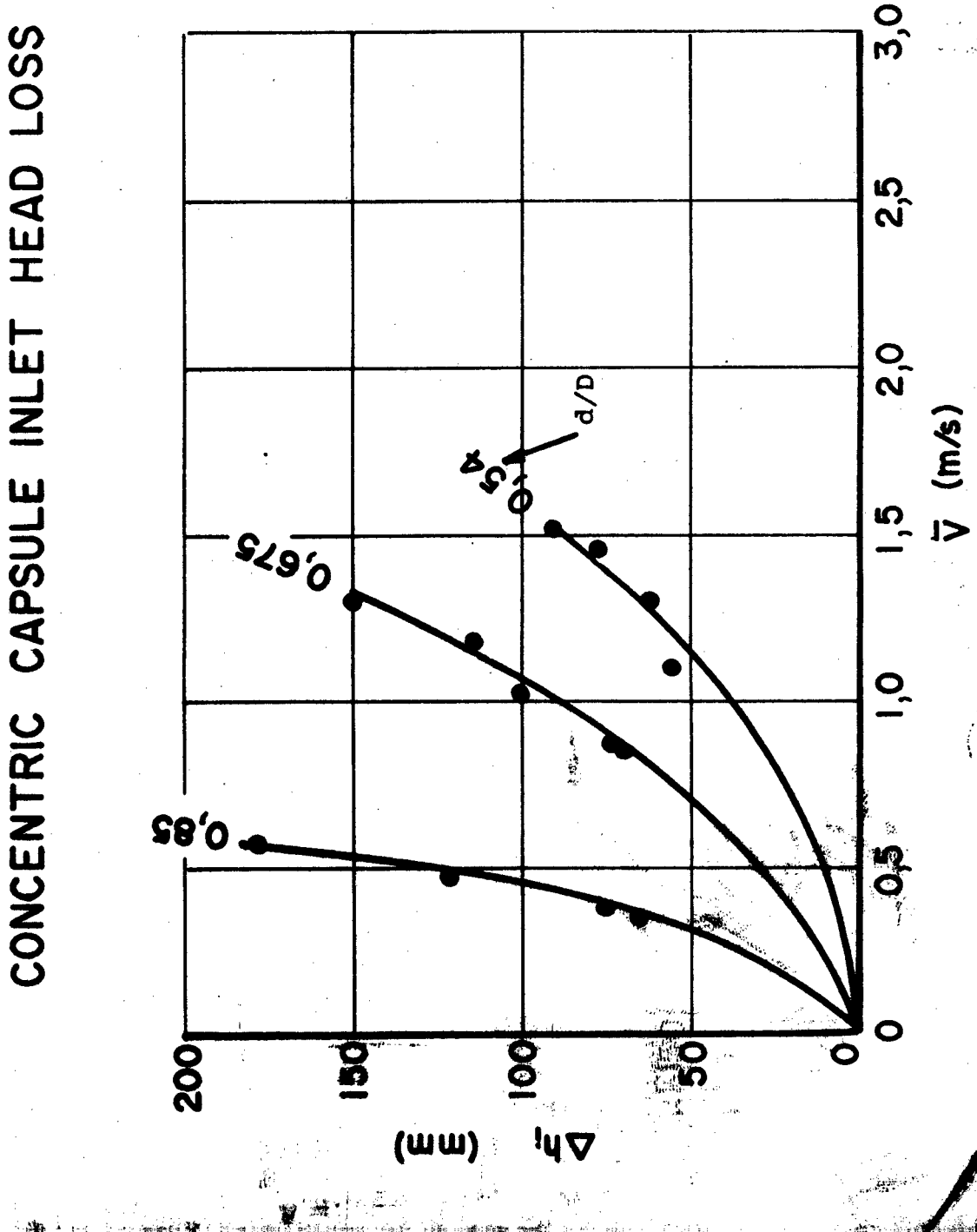
CONCENTRIC CAPSULE INLET HEAD LOSS
Δhi (mm)
200
150
100
50
0
0,5
1,0
1,5
2,0
2,5
3,0
V̄ (m/s)
d/D
0,85
0,675
0,54
0,1

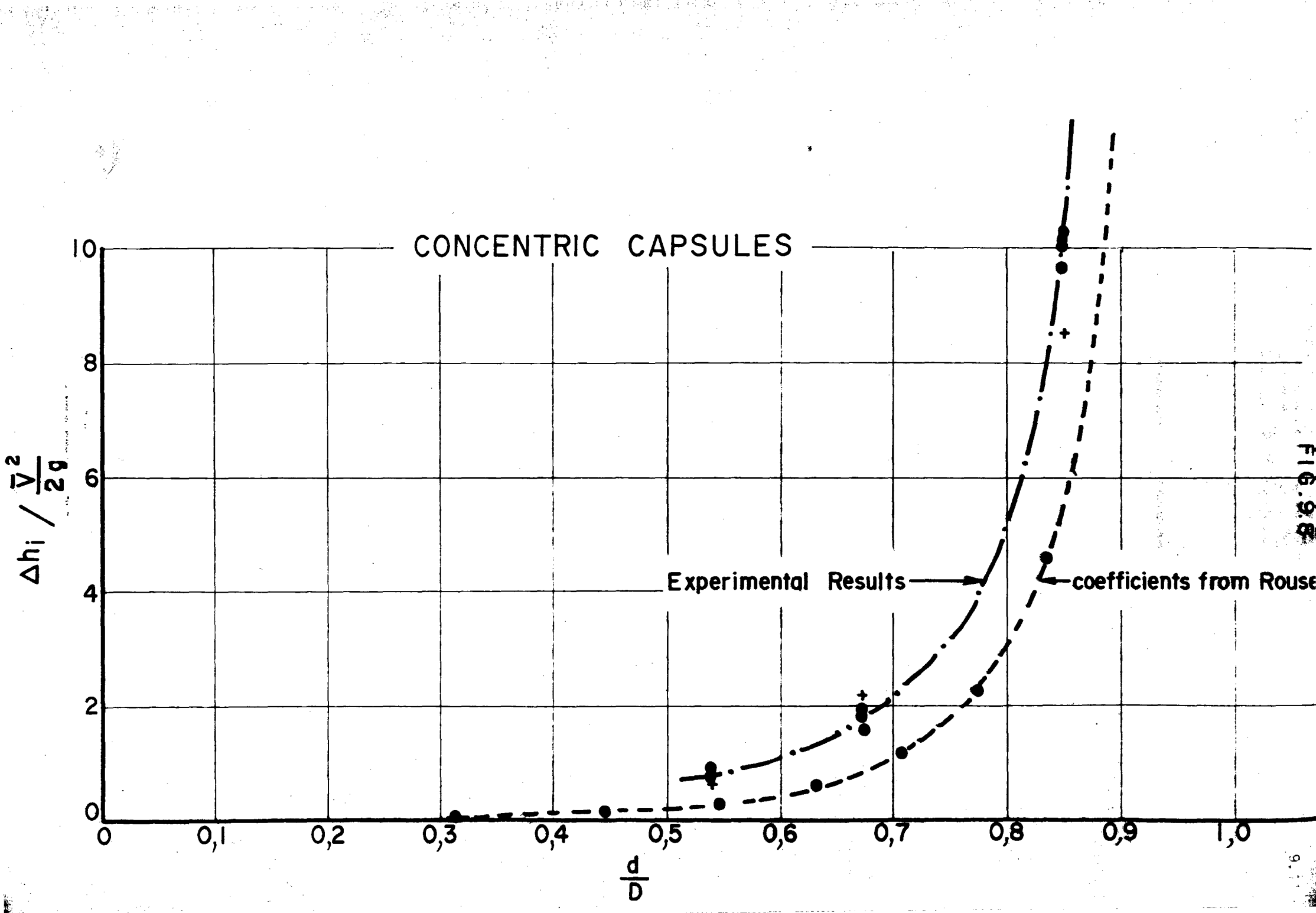
CONCENTRIC CAPSULES
Experimental Results
coefficients from Rouse
$\Delta h_i / \frac{\bar{V}^2}{2g}$
$\frac{d}{D}$
0
2
4
6
8
10
0
0,1
0,2
0,3
0,4
0,5
0,6
0,7
0,8
0,9
1,0

FIG. 9.8

The dotted curves on Figures 9.6 and 9.8 will be discussed in Chapter 13.

Unfortunately, no simple correlation was found for concentric annuli as opposed to eccentric capsules. And a polynomial of degree four was found by computer analysis for the concentric inlet head loss coefficient,

i.e. $k'_c = -28{,}37(d/D) + 180{,}73(d/D)^2 - 364{,}60(d/D)^3 + 244{,}15(d/D)^4$ (7.114)

(The concentric results for inlet head loss are superimposed as a broken line on Figure 9.6.)

3. Outlet energy loss for static capsules

Referring to the hydraulic gradients (Figures 9.1 to 9.5) it can be seen that, at the outlet, the changes in hydraulic grade line are not so pronounced as at the inlet. In this case, the flow diverges from the annulus condition to circular pipe flow and large eddies may be formed, downstream of the capsule, which dissipate energy.

The reasons for the energy losses being less pronounced than at the inlet section are:

3.1 At the outlet, some kinetic energy is converted to pressure energy and this dispersion takes place in an unconfined area (compared with the contraction at inlet).

3.2 The pattern of rapid contraction followed by confined expansion at inlet leads to greater pressure changes than the relatively unconfined expansion at the outlet end.

3.3 The streamlines at the outlet end, although initially asymmetrical, in the eccentric annulus case, expand into a region which is symmetrical.

3.4 The velocity distribution in the annulus at outlet is not affected, in the case of the eccentric annulus, by asymmetrical contraction as at the inlet.

3.5 The boundary layer in the annulus (concentric or eccentric) is probably fully developed both along the capsule and pipe wall.

From the foregoing it seems hopeful that the expansion loss as used for concentric pipes may prove more fruitful in the capsule case than is the case at the inlet (see Chapter 13).

The expansion loss for concentric pipes is normally taken as the square of the velocity difference divided by 2g. Applying this concept to the capsule problem leads to a head loss of

$$\Delta h_o/(\overline{V}^2/2g) = (1/(1-(d/D)^2) - 1)^2 \qquad (7.115)$$

This equation is plotted together with the results from the eccentric capsule experiments in Figure 9.9, where it may be seen that the trend of both sets of results is similar, but the capsule outlet head losses are less than those indicated by the concentric theory for the capsule case. An empirical fit to the experimental results yields the equation

$$\Delta h_o/(\overline{V}^2/2g) = k_o(1/(1-(d/D)^2) - 1)^2$$

And for the eccentric annulus the outlet head loss coefficient (k_{oe}) is given by:

$$k_{oe} = 0,68 \qquad (9.1)$$

Typical Δh_o versus $\overline{V}$ curves for the concentric annulus are shown on Figure 9.10. And these values when plotted non-dimensionally on Figure 9.9 yield the outlet head loss coefficient for concentric capsules (k_{oc});

$$k_{oc} = 1,15 \qquad (9.2)$$

The outlet head loss coefficient for concentric capsules is thus 15% higher than the sudden expansion loss derived from the conventional pipe formula. And in the case of the eccentric annulus the coefficient is 32% lower.

An explanation for the above phenomenon is attempted in Chapter 13.

FIG. 9.9

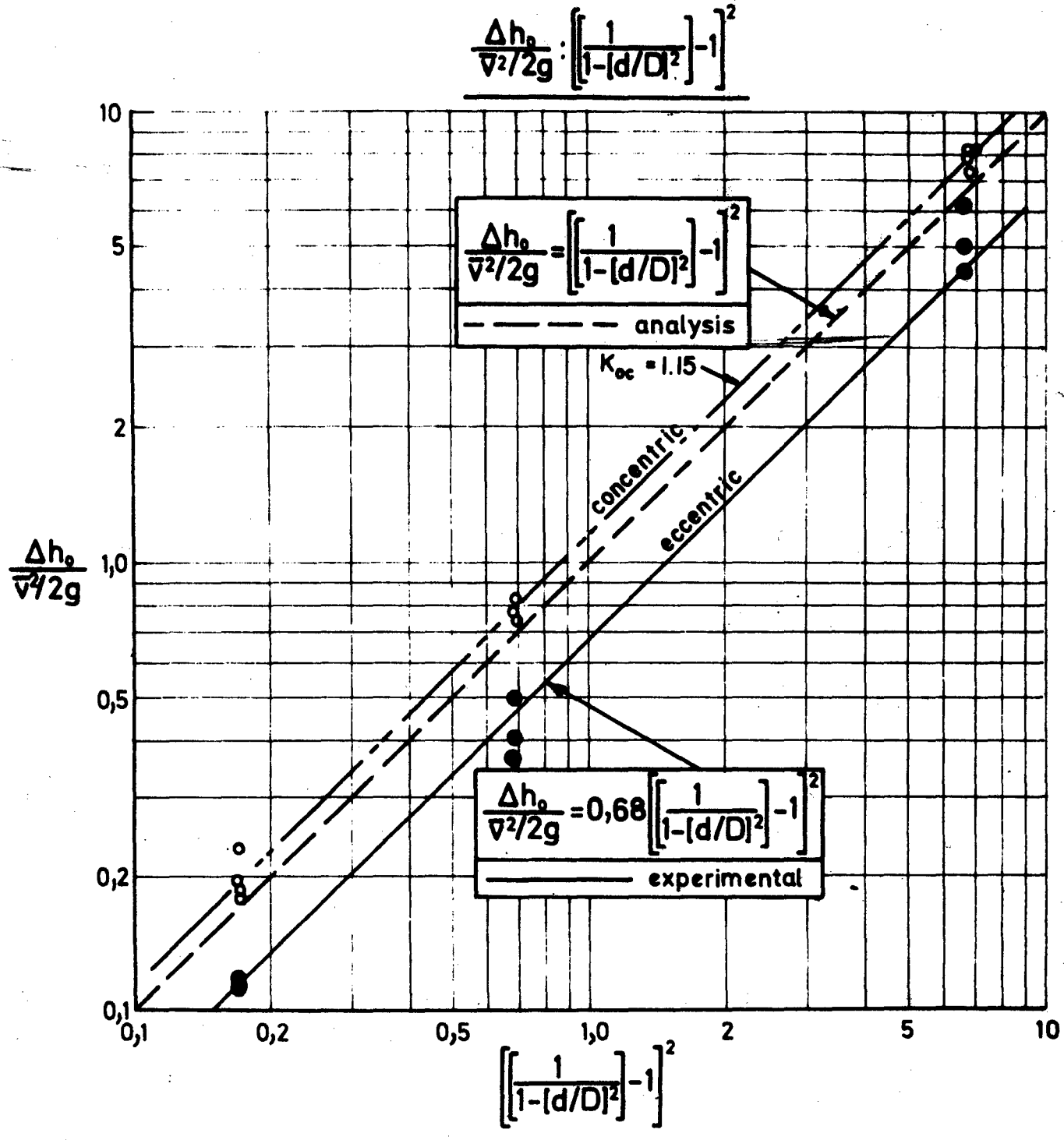
$\frac{\Delta h_o}{\bar{v}^2/2g} : \left[\left[\frac{1}{1-[d/D]^2}\right]-1\right]^2$
$\frac{\Delta h_o}{\bar{v}^2/2g} = \left[\left[\frac{1}{1-[d/D]^2}\right]-1\right]^2$
analysis
$K_{oc} = 1.15$
concentric
eccentric
$\frac{\Delta h_o}{\bar{v}^2/2g} = 0{,}68\left[\left[\frac{1}{1-[d/D]^2}\right]-1\right]^2$
experimental
$\frac{\Delta h_o}{\bar{v}^2/2g}$
10
5
2
1,0
0,5
0,2
0,1
0,1
0,2
0,5
1,0
2
5
10
$\left[\left[\frac{1}{1-[d/D]^2}\right]-1\right]^2$

FIG. 9.10

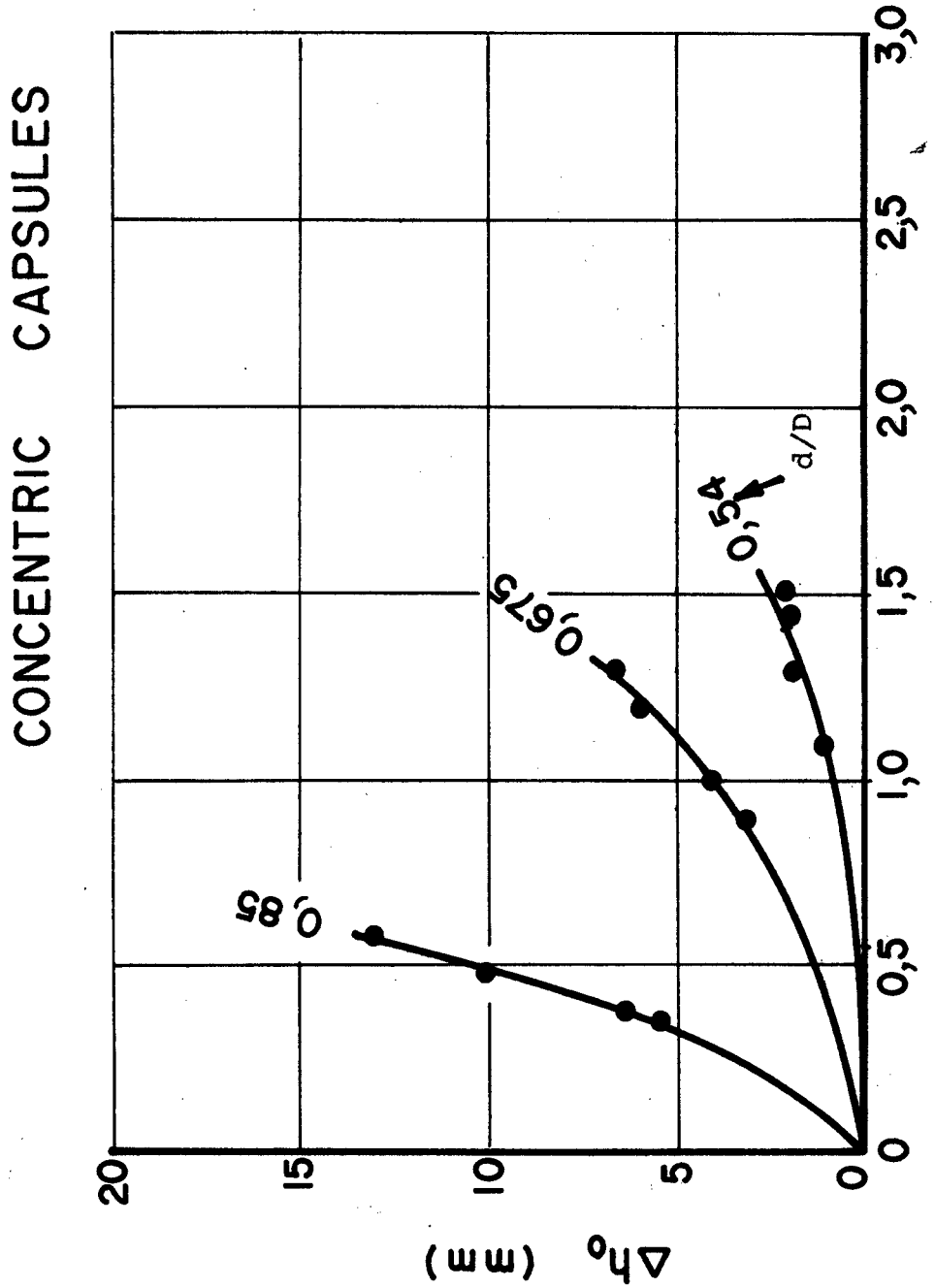
CONCENTRIC CAPSULES
Δh₀ (mm)
0
5
10
15
20
0
0,5
1,0
1,5
2,0
2,5
3,0
V̄ m/s
d/D
0,54
0,675
0,85

4. Annular losses for static capsules

The empirical method of analysing annular friction head losses was described in Chapter 7, Section 11.1. The Blasius equation was assumed valid and the mean velocity in the annulus $\overline{V}_a$ was chosen as the representative velocity. A pseudo hydraulic mean radius was introduced to render the Blasius equation applicable.

The definition of annular head loss given in Chapter 7, Section 3.3 is unconventional. Frictional head losses in pipes are defined for fully developed flow. Whereas, the hydraulic gradient in the capsule annulus is given by the best straight line through the points representing pressure along the annulus, (e.g. see Figure 9.1), and the flow is not fully developed.

By substituting the hydraulic gradient $(\Delta h_{fa}/L_c)$ in equation (7.94) the pseudo hydraulic mean radius (R_p) is obtained.

Figure 9.11 shows the annular head loss (Δh_{fa}) determined from the concentric capsule hydraulic grade lines on Figures 9.3 to 9.5 as a function of the mean water velocity $(\overline{V})$. The velocities are converted to mean annular velocities via;

$$\overline{V}_a = \overline{V}/(1-(d/D)^2)$$

And inserting these experimentally determined values in equation (7.94), Figure 9.12 is obtained. Over the experimental range a linear correlation is valid and

$$R_p = 0{,}95R \qquad (9.3)$$

for concentric annuli. The dotted curves on Figure 9.12 will be discussed further in Chapter 13.

Substituting the values from Figures 9.1 and 9.2, for eccentric annuli, in equation (7.94) yields Figure 9.13.

Superimposed on this Figure are the present analytical results as well as experimental results of Bourne et al (discussed further in Chapter 13).

FIG. 9.11

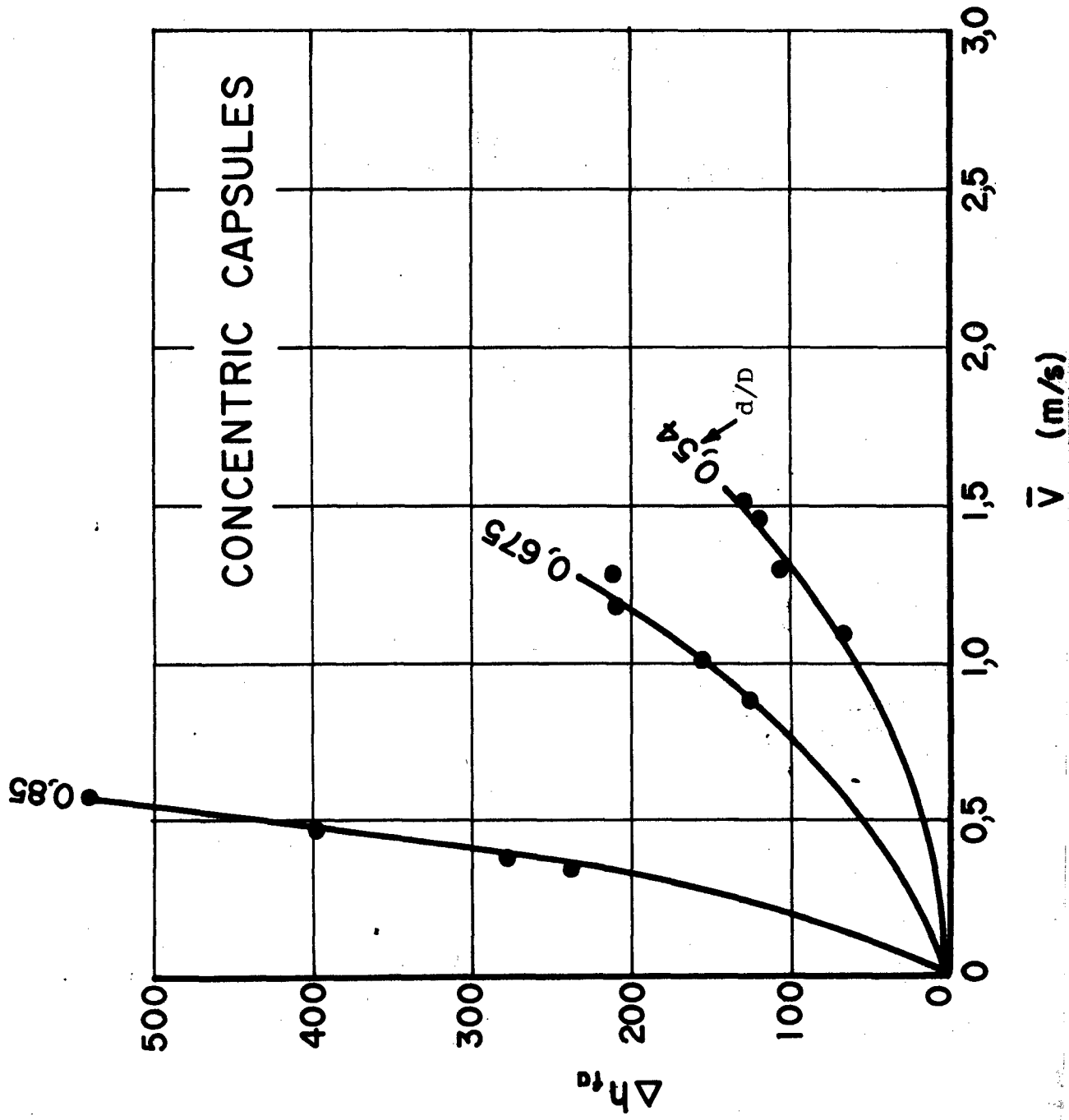
CONCENTRIC CAPSULES
0,85
0,675
0,5
d/D
500
400
300
200
100
0
0
0,5
1,0
1,5
2,0
2,5
3,0
Δh_{fa}
$\bar{V}$ (m/s)

FIG. 9.12

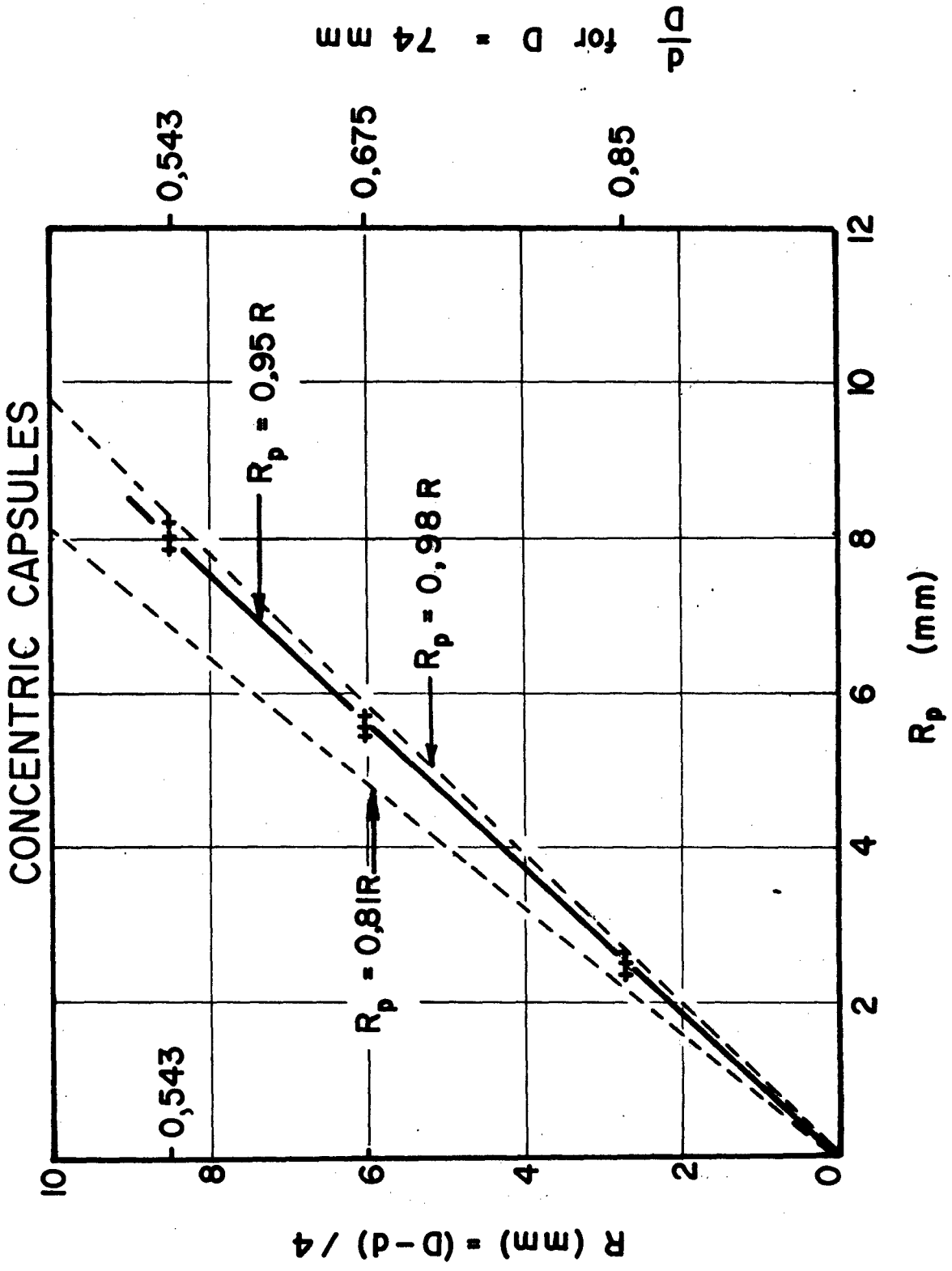
CONCENTRIC CAPSULES
R_p = 0,95 R
R_p = 0,98 R
R_p = 0,81R
0,543
0,675
0,85
0,543
d/d for D = 74 mm
R (mm) = (D−d) / 4
R_p (mm)
0
2
4
6
8
10
12

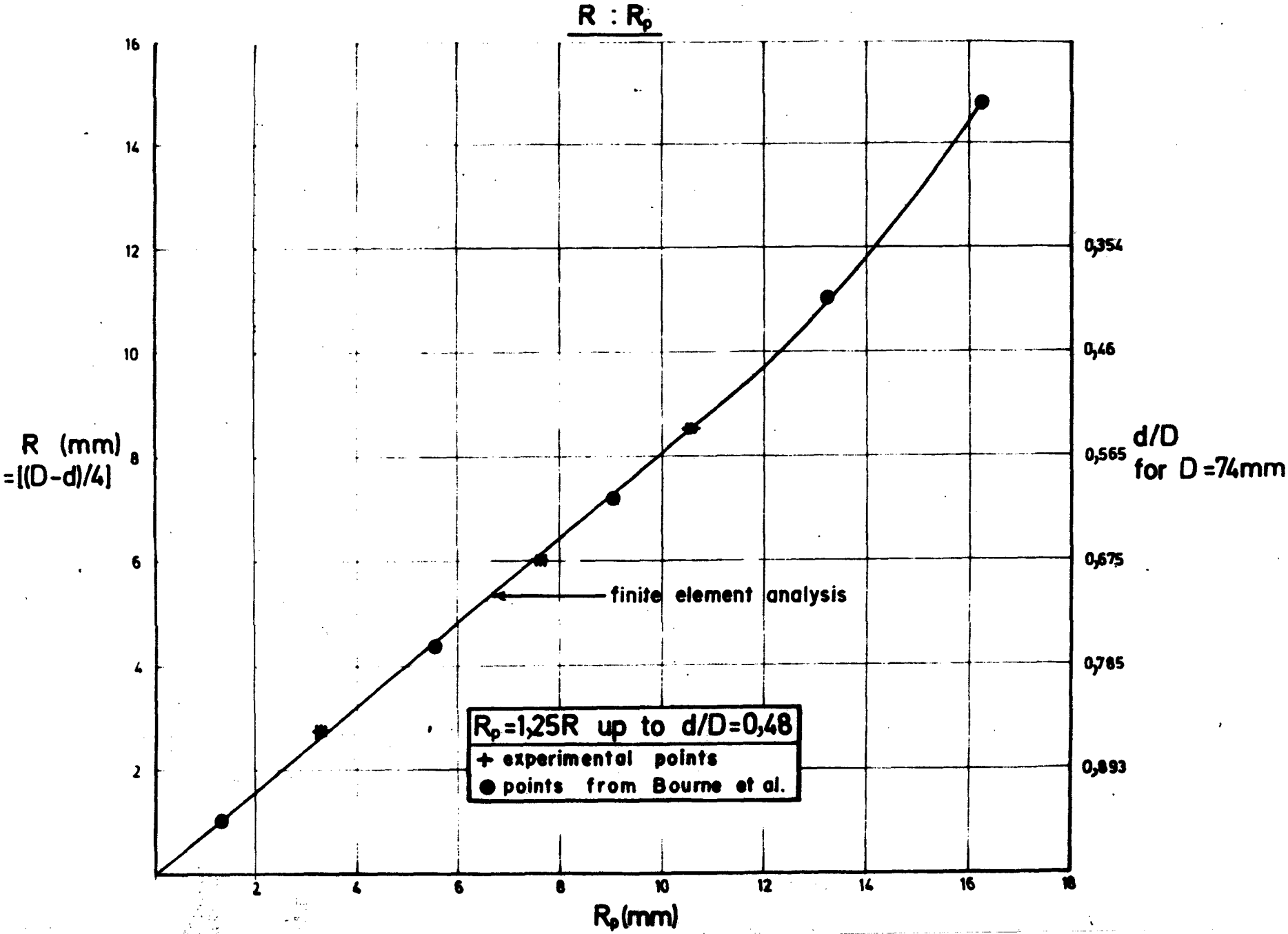
R : Rp
R (mm) =[(D-d)/4]
Rp (mm)
d/D for D=74mm
finite element analysis
Rp=1,25R up to d/D=0,48
+ experimental points
● points from Bourne et al.
0,354
0,46
0,565
0,675
0,785
0,893

FIG. 9. 13

Inserting the value of R_p for eccentric annuli in Blasius's equation gives equation (7.95) for the friction factor in the annulus ($\varepsilon = 1$). And the graphical verification of equation (7.95) when combined with Darcy's equation is given on Figure 9.14. A similar operation is performed for concentric annuli using the appropriate pseudo hydraulic mean radius.

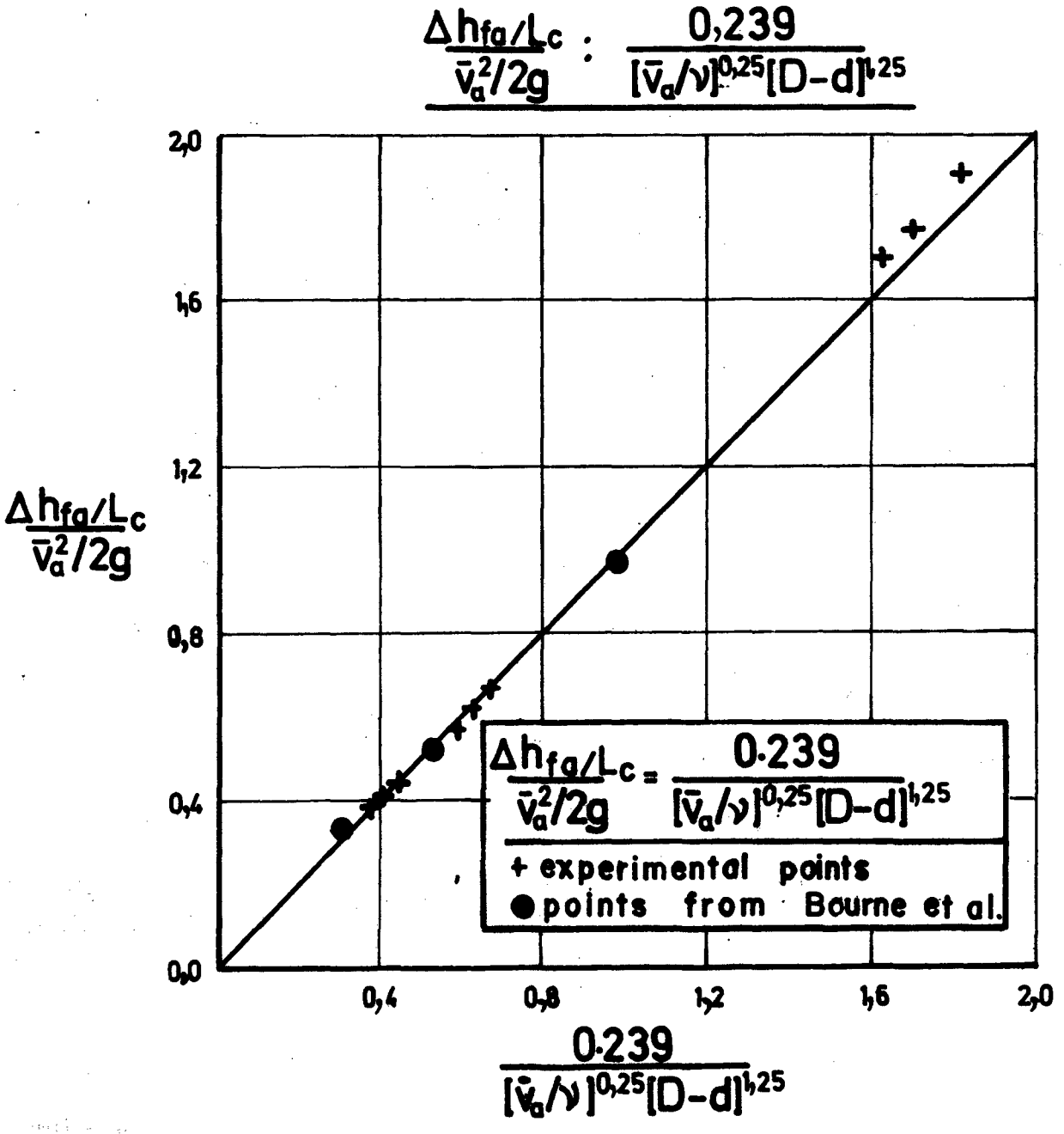
$\frac{\Delta h_{fa}/L_c}{\bar{v}_a^2/2g} : \frac{0,239}{[\bar{v}_a/\nu]^{0,25}[D-d]^{1,25}}$
$\frac{\Delta h_{fa}/L_c}{\bar{v}_a^2/2g}$
2,0
1,6
1,2
0,8
0,4
0,0
0,4
0,8
1,2
1,6
2,0
$\frac{\Delta h_{fa}/L_c}{\bar{v}_a^2/2g} = \frac{0.239}{[\bar{v}_a/\nu]^{0,25}[D-d]^{1,25}}$
+ experimental points
● points from Bourne et al.
$\frac{0.239}{[\bar{v}_a/\nu]^{0,25}[D-d]^{1,25}}$

FIG. 9.14

CHAPTER 10

CAPSULE KINEMATICS

1. The kinematics of mobile capsules

The meaning of the term kinematics in the following context is restricted to that part of the mechanics of capsule motion which deals with quantities derivable from units of space and time.

Although the various forces (pressure, shear, gravitational and solid friction) are the causes responsible for moving the capsules, the kinematics is concerned solely with the effects of the motion on the displacement and time relations of velocity and acceleration.

To describe the motion of a capsule, a fixed co-ordinate system must be established and the capsule velocity (V_c) will be taken to mean the displacement of the capsule per unit time relative to the pipeline. To a stationary observer (relative to the pipeline) the flow of solitary capsules will thus represent an unsteady condition with time. A steady state can only be achieved when the observer is stationary relative to the capsule (in which case $V_c = 0$).

An accelerating capsule represents a higher order unsteady state and care was taken to ensure that all experimental data were statistics of non-accelerating capsules (that is, a steady state relative to the capsule).

The rest of this Chapter will be devoted to the effect of the numerous variables involved on the capsule kinematics, preceeded by a brief discussion on the acceleration tests.

2. Acceleration

The purpose of carrying out these tests was to determine the adequacy of the experimental pipeline length rather than an actual study of the

behaviour of an accelerating capsule. The essential objective was to establish whether the pipelines were long enough to achieve a constant capsule velocity at the section where this statistic was measured.

Capsules of specific gravity 0,39; 1,05; 1,77; 3,2 and 4,8 were used for acceleration tests in the 74 mm diameter pipeline at a diameter ratio d/D = 0,95 at $\overline{V}$ = 3,04 m/s; $\overline{V}$ = 1,265 m/s and $\overline{V}$ = 0,792 m/s and capsules of specific gravity 1,05; 1,71; 3,2 and 4,8 were tested in the 74 mm diameter pipeline at a diameter ratio d/D = 0,542 at $\overline{V}$ = 3,03 m/s and 1,68 m/s.

Figures 10.1, 10.2, 10.3, 10.4 and 10.5 show capsule velocity as ordinate plotted against the distance travelled from the inlet of the pipe for the different specific gravities, capsule velocities and diameter ratios. The acceleration tests involved about 600 experiments. However, the only variables requiring measurement were the photo cell position, the capsule velocity and mean water velocity, rendering the experiments comparatively quick and simple to perform.

The acceleration tests were carried out in the 74 mm diameter pipeline only. It is obvious that when starting from rest the capsule must accelerate at least part of its way when travelling through the pipe. The 44 mm diameter line was a closed circuit. Accelerations were simply due to bend decelerations and were thus slight compared with the 74 mm diameter pipe. The experience gained in operating the large pipe enabled the design lengths of the 44 mm diameter pipe to be determined with confidence.

The results on Figure 10.1 indicate that for a diameter ratio (d/D) = 0,948 and a mean water velocity of 3,04 m/s the heaviest capsule which has the most inertia requires the longest acceleration length. Although, at 1,52 m from the pipe entrance, the velocity is within 2% of what appears to be the steady velocity at 10,66 m from the

FIGURE 10.1

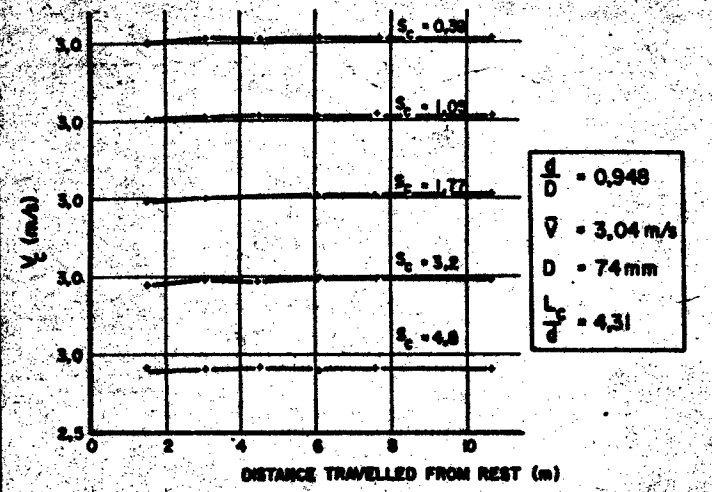

ACCELERATION CURVES

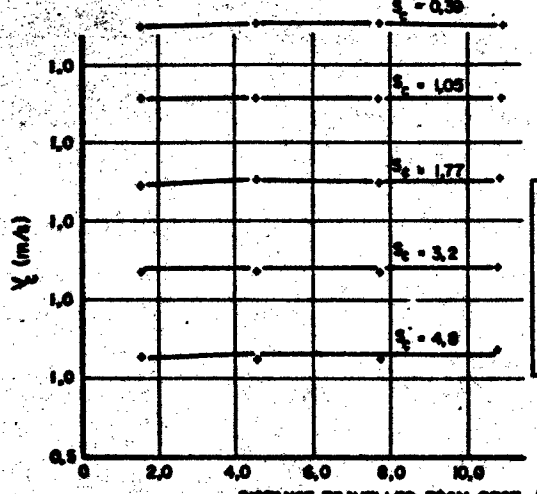

FIGURE 10.2

FIGURE 10.3

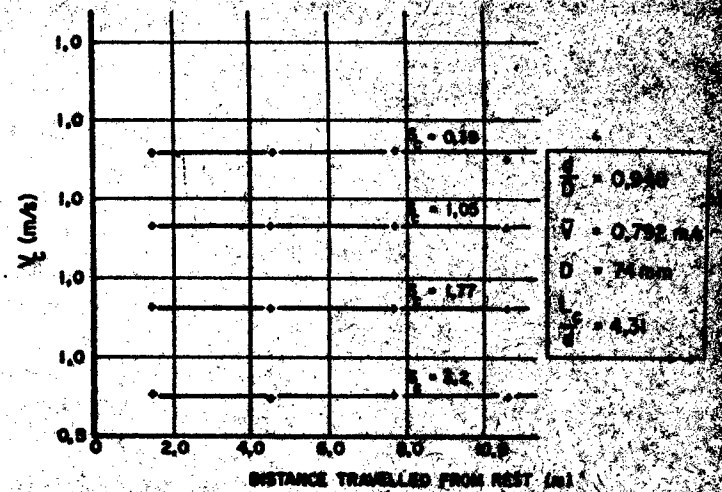

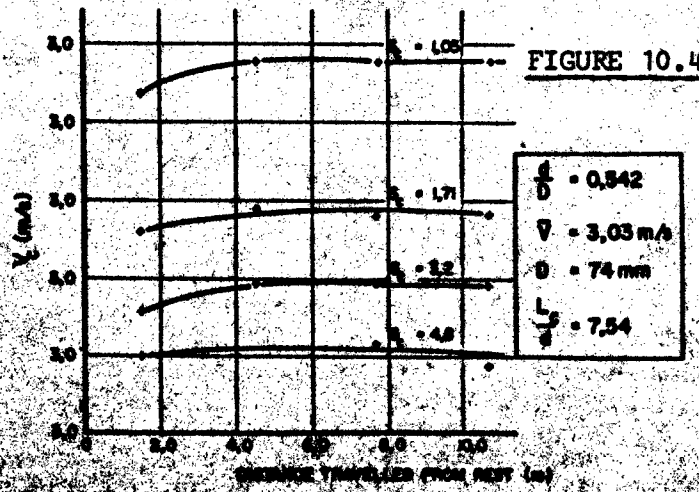

FIGURE 10.4

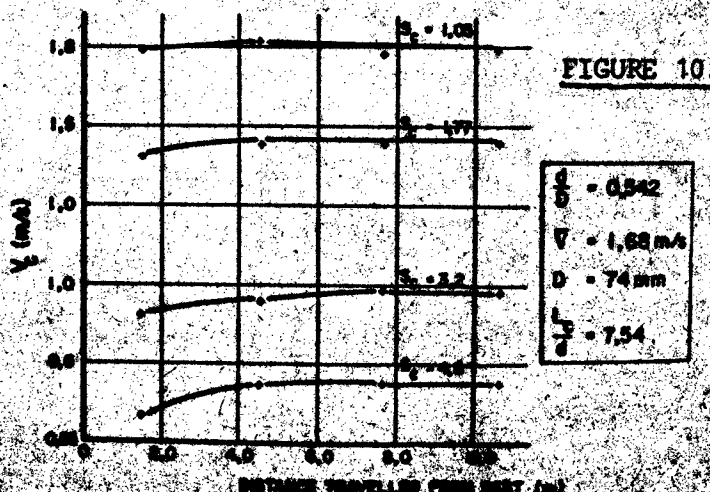

FIGURE 10.5

entrance.

It is clear from Figures 10.2 and 10.3 that at lower mean water velocities the pipeline length is more than adequate for the higher diameter ratios. The following two Figures (Figures 10.4 and 10.5) indicate that at a lower diameter ratio (d/D) = 0,542 the highest specific gravity capsule (S_c) = 4,8 again requires the longest acceleration length.

These results were considered sufficient to prove that the length of pipeline was adequate as far as steady capsule velocities in the test section, about 10 m from the pipe entrance, were concerned.

3. Dimensional Analysis

Dimensional analysis is a useful tool where experimental data are available and the variables enter the problem in too complex a manner for more detailed analysis. The variables involved in the phenomenon are known while the relation between them is not.

Such is the case with pure water flow in a pipe where there are far fewer variables than in the capsule problems. The analysis of concentric annular flow with a stationary core (see Chapter 7) indicates the degree of complexity introduced by even one more variable. For a number of variables the complexity increases manyfold, and an analytical solution becomes impossible. Resort can then be made to dimensional analysis to indicate a form of grouping of variables.

We are concerned with the capsule velocity (V_c) and the influence thereon due to the following variables.

$\overline{V}$ = mean water flow velocity
d = capsule diameter
D = pipe diameter
ρ_c = density of capsule
ρ = density of vehicle (fluid)
L_c = capsule length

μ_f = coefficient of solid to solid friction between capsule and pipe wall
k = roughness size (mean) of pipe
k_c = roughness size (mean) of capsule
ϕ = slope of pipeline
μ = viscosity of fluid

If the capsule velocity (V_c) is made a function of the above variables, it can be shown by dimensional analysis that;

$$V_c/\overline{V} = f\left(\frac{d}{D}, \frac{\rho_c}{\rho}, \frac{L_c}{d}, \mu_f, \frac{k}{d}, \frac{k_c}{d}, \frac{\rho\overline{V}D}{\mu}, \phi\right) \qquad (10.1)$$

This equation indicates that the velocity ratio ($V_c/\overline{V}$) can be plotted against the Reynolds number ($\rho\overline{V}D/\mu$) while holding the other parameters constant. The above equation is, of course, only one solution and others could be given. It is useful for showing the effect of the variables on the velocity ratio.

For a constant pipe diameter (D) and fluid kinematic viscosity (ν), the velocity ratio can simply be plotted against the mean velocity ($\overline{V}$).

It will be shown later that this form of plot is not the best from the point of view of grouping variables. However, the velocity ratio ($V_c/\overline{V}$) is shown plotted against $\overline{V}$ on Figures 10.6 to 10.9 for the following reasons. Firstly, these Figures were drawn out before it was realised that a better, less obvious, form of presentation would be found later and secondly, as was mentioned before, this form of plot is useful for discussing the effect of variables.

4. Velocity ratio

Figures 10.6 to 10.9 show the velocity ratio plotted against the mean water velocity for the 74 mm diameter pipeline on a horizontal slope. Capsules numbered 1 to 24 were used in these experiments comprising four diameter ratios of six specific gravities each. Each graph is for a particular diameter ratio and fixed capsule geometry but varying specific gravity.

FIG. 10.6

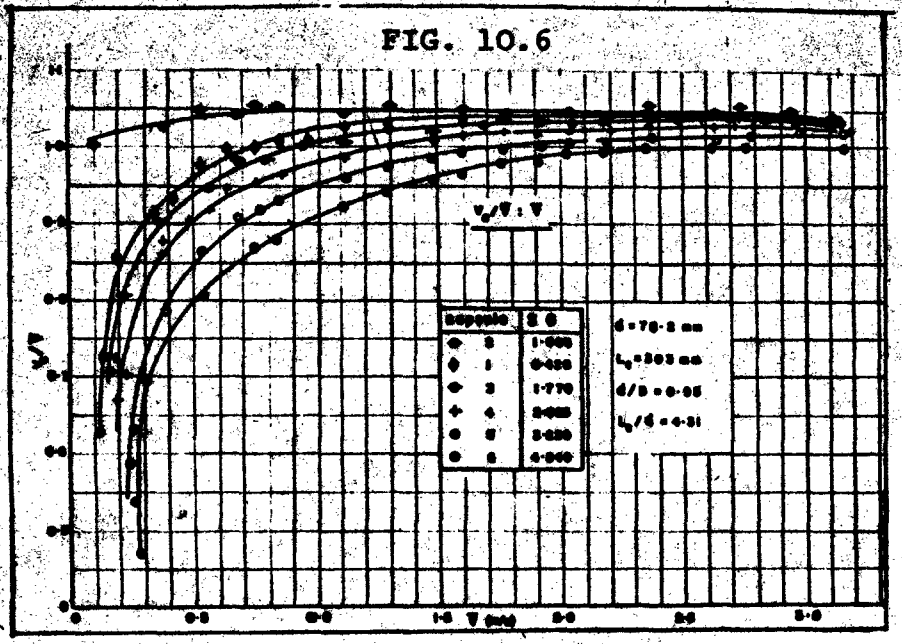

FIG. 10.7

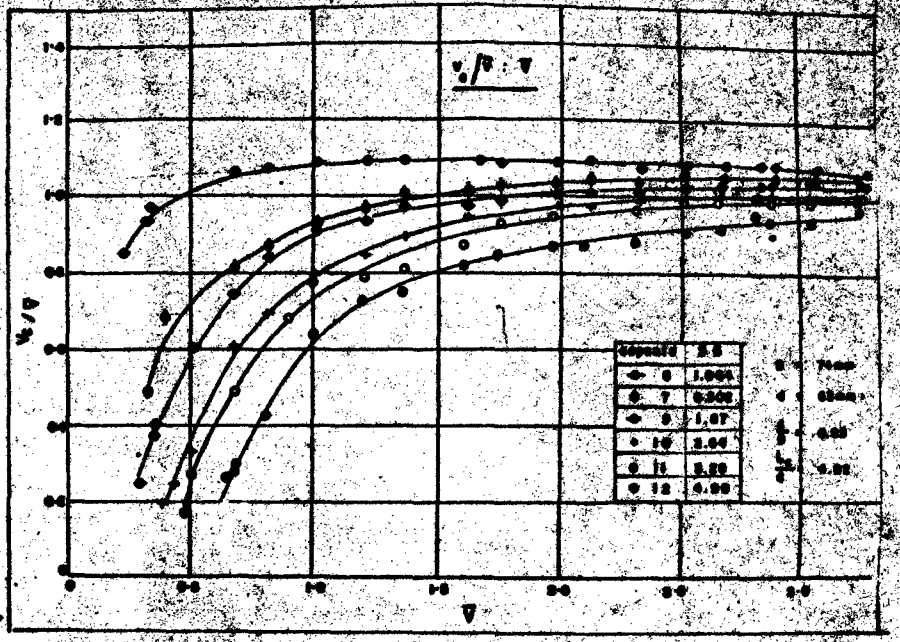

FIG. 10.8

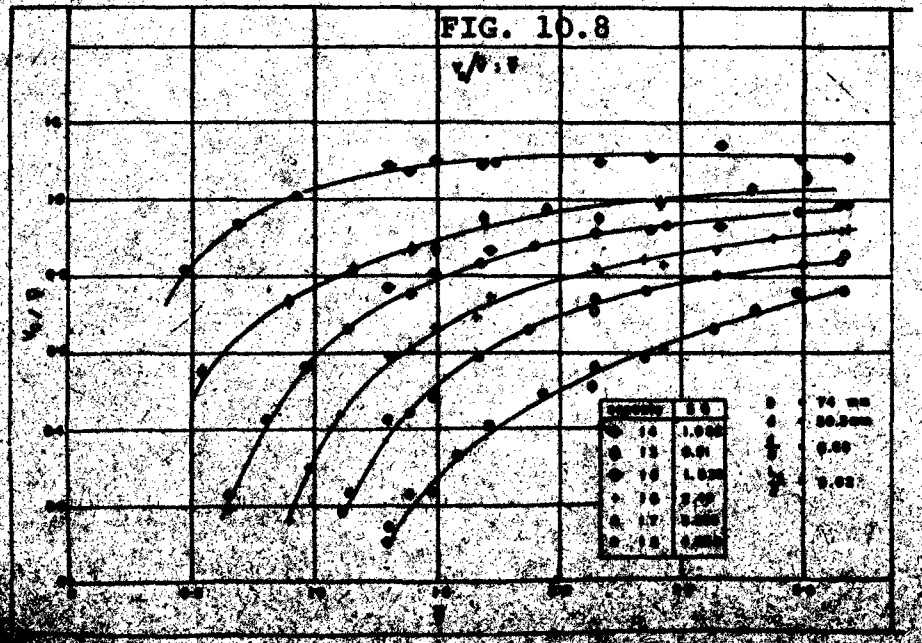

FIG. 10.9

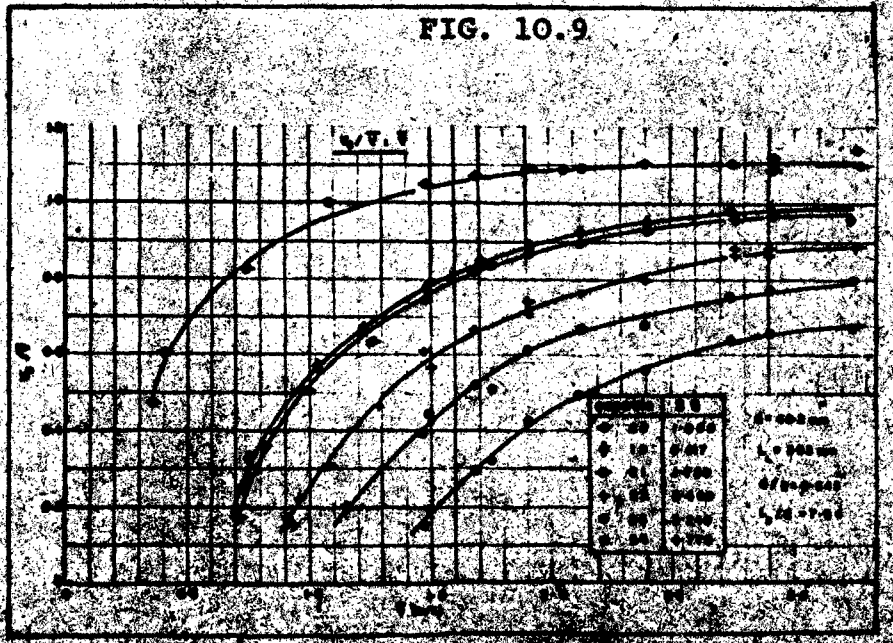

As the mean velocity of the water increases the velocity ratio increases, rapidly at first, but at a steadily decreasing rate until the ratio becomes constant. (The constancy is only achieved for $d/D = 0,95$ and neutrally buoyant capsules at other d/D ratios.)

However, it will be seen in Chapter 12 that increasing the mean water velocity further would yield a constant velocity ratio for all the capsules tested.

This characteristic trend is found for all diameter ratios, length to diameter ratios, specific gravities and slopes.

For the largest diameter ratio ($d/D = 0,95$), see Figure 10.6, the constant velocity ratio is reached and is at least unity (for the heaviest capsule) and the lesser specific gravity capsules have velocity ratios which are greater than unity once the velocity ratio has become constant.

The neutrally buoyant cpasule has a velocity which is consistently greater than the mean water velocity.

Figure 10.6 also indicates that as the specific gravity of the capsule increases the velocity ratio becomes unity at increasingly higher mean water velocities.

This appears to indicate that solid to solid friction, between the capsule and pipe wall, has less effect as the capsule speeds up and as the specific gravity of the capsule decreases.

If the velocity ratio reaches a constant value any change in the mean water velocity ($\bar{V}$) produces a corresponding change of capsule velocity. The capsule is thus subject to the same influences as a mass of water particles, neglecting internal shear. This seems to imply that solid to solid friction has become inoperative when $V_c/\bar{V}$ reaches a constant. (For further discussion see Chapter 12.)

Figure 10.8 (for d/D = 0,68) shows that only the neutrally buoyant capsule attains a state where $V_c/\overline{V}$ is a constant. The capsules of specific gravity other than unity do not attain velocity ratio values that are constant except in the case of the largest diameter ratio (d/D = 0,95).

To sum up: The effect of increasing the mean water velocity is to increase the velocity ratio in all cases. In some cases, a constant velocity ratio is reached and this occurs sooner as the diameter ratio increases and the specific gravity (relative to water) decreases. It seems likely that lower diameter ratio capsules will also reach a constant velocity ratio if the mean water velocity were sufficiently high.

5. The specific gravity effect on the capsule velocity

The solid to solid friction between the capsule and pipe wall depends on the relative density (or specific gravity) of the capsule, other capsule properties remaining constant. In the zone where solid to solid friction predominates (at lower velocities) the heavier capsules require a higher incipient velocity and thus commence to travel at higher water velocities and also continue to have capsule velocities less than for lower specific gravities.

However, in the zone where solid to solid friction is assumed to be inoperative (i.e. where the velocity ratio is a constant) the heavier capsules do not appear to travel much slower than the lighter capsules and this fact adds support to the hypothesis of capsule lift.

It will be shown in Chapter 12 that the heavier capsules travel in a lower velocity field even after lift off.

The capsules numbered one and three (Figure 10.6), although of differing specific gravities, 0,426 and 1,77, have submerged specific gravities that are close, i.e. 0,574 and 0,77 and it is clear that the velocity ratio curve for these two capsules is similarly close.

This pattern is consistent at other diameter ratios, for example, capsules numbered 19 and 21 at diameter ratio 0,543 have submerged specific gravities of 0,583 and 0.75 and the velocity ratio curves are again close (see Figure 10.9).

This indicates that the submerged density ratio $((\rho_c-\rho)/\rho = S_c-1)$ is a more significant variable than the density ratio and this parameter was adopted instead of the specific gravity.

A further conclusion is that it makes no difference whether the solid to solid friction is between the top of the capsule and the pipe or between the bottom of the capsule and the pipe.

Thus capsules of submerged specific gravities of zero will experience no solid to solid friction and should travel concentrically along the pipe axis. Also, these capsule velocities should be greater than the mean water velocity.

Since the mean water velocity can be computed by sampling the entire velocity distribution it takes into account the low velocities near the wall. A small diameter capsule travelling concentrically will thus sample the highest velocity region.

Thus capsules whose specific gravities approach unity should increasingly travel at higher velocities and for these capsules, as the diameter ratio decreases, the capsule velocity should increase. The opposite is true for capsules of significantly high specific gravity.

This trend is illustrated on Figure 10.10 which is a plot of diameter ratio (d/D) against velocity ratio $(V_c/\overline{V})$, once the velocity ratio has become constant, for neutrally buoyant capsules.

A further noteworthy characteristic of neutrally buoyant capsules is that the velocity ratio is independent of the mean water velocity over a wide range. This is true for all diameter ratios and the effect would be

NEUTRALLY BOUYANT CAPSULES

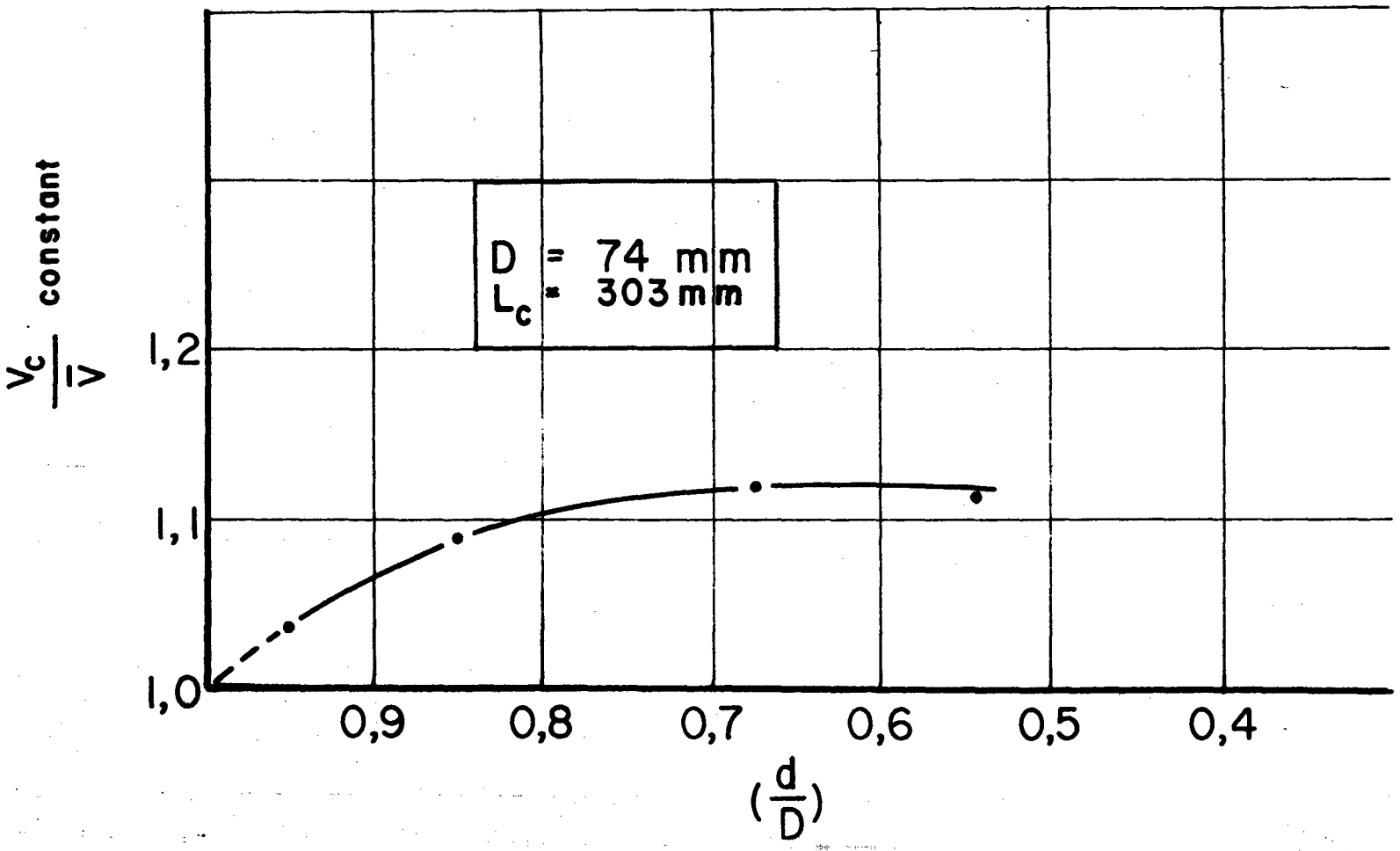

FIG. 10.10

even more apparent if the specific gravities were exactly unity.

The approximately neutrally buoyant capsule (no. 2, specific gravity = 1,065) of diameter ratio 0.95 has a velocity ratio independent of the mean water velocity from 0,9 m/s upwards. At lower diameter ratios, the velocity ratio seems to be independent of the mean water velocity at higher mean water velocities, e.g. about 2,5 m/s for diameter ratio 0,543 (see Figure 10.9). No significance is attached to this trend since the specific gravities were not exactly unity, and for submerged specific gravities greater than unity this pattern is expected as will be discussed in Section 7.

The effect of submerged specific gravity on the velocity ratio is far more apparent as the diameter ratio decreases. In fact, for a diameter ratio of 0.95, the velocity ratio difference between the capsules (Figure 10.6) due to the effect of specific gravity is only 0.235 (i.e. 0,8 to 1,035) for a specific gravity ratio of 4,84 to 1,065. This is at the mean water velocity where the effect is most apparent, viz. 0,5 m/s. Compare this with the 0,543 diameter ratio capsules (Figure 10.9). At the velocity where the effect is most noticeable (viz. 1,5 m/s), the difference in velocity ratio is 0.85 for a submerged specific gravity ratio of 4,77 : 1,06.

Thus for the two diameter ratios 0.95 and 0,543, the change in velocity ratio for the latter is 3,62 times that of the former for a specific gravity ratio of 4,5 to 1.

Figure 10.11 shows velocity ratio ($V_c/\overline{V}$) plotted against the submerged specific gravity (S_c-1) and the variation of the latter is seen to have a far more significant effect on $V_c/\overline{V}$ as the diameter ratio decreases. Or, the greater the diameter ratio, the less the effect on $V_c/\overline{V}$ for changes in specific gravity.

FIG. 10. 11

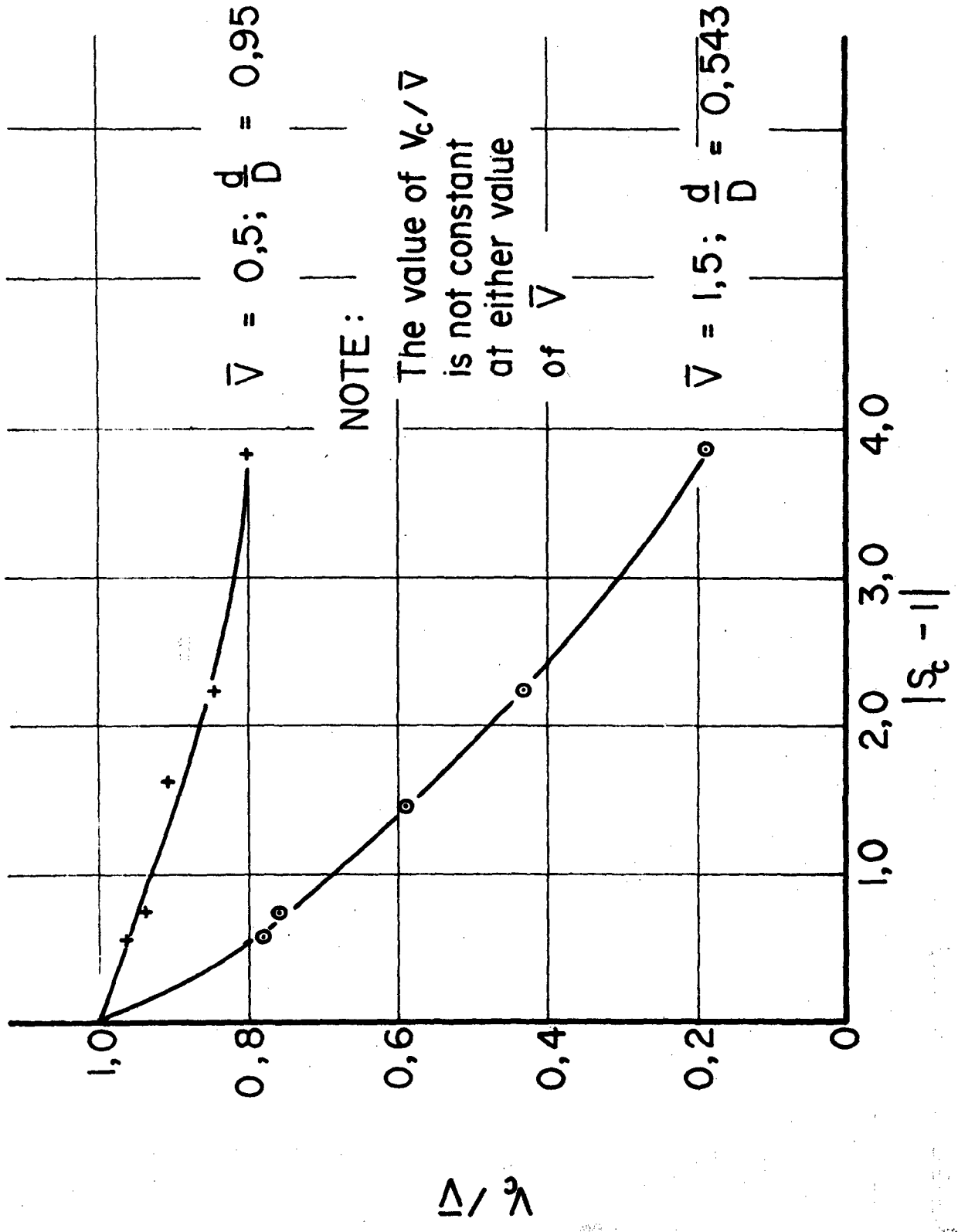
$\bar{V}$ = 0,5; $\frac{d}{D}$ = 0,95
NOTE:
The value of $V_c/\bar{V}$ is not constant at either value of $\bar{V}$
$\bar{V}$ = 1,5; $\frac{d}{D}$ = 0,543
1,0
0,8
0,6
0,4
0,2
0
1,0
2,0
3,0
4,0
$|S_c - 1|$
Δ / λ

6. Kinematic correlation

Since the curves on Figures 10.6 to 10.9 for different specific gravities and diameter ratios seem to form families of curves when plotted in this way it is possible that some form of non-dimensional grouping can be found. This was done in three steps.

6.1 The first step was to attempt the bringing together of all the curves representing the velocity ratio against mean water velocity for different specific gravities.

In Chapter 15 it will be shown that $\overline{V}/\sqrt{gD|S_c-1|}$ is a significant parameter for representing the dynamic effects on a non-dimensional empirical basis. This has a similar form to the Froude number for open channel flow with the inclusion of the submerged specific gravity (or density ratio) term and can be designated the "densometric pipe Froude number based on the mean water velocity."

This is not meant to imply that the parameter is a Froude number (which is usually restricted to open channel flow) but rather that the form is similar, thus;

$$F_{rdm} = \overline{V}/\sqrt{gD|S_c-1|}$$

F_{rdm} is first of all plotted against velocity ratio (see Figures 10.12 to 10.15).

Figure 10.16 is a summary of Figures 10.17, 10.18, 10.19 and 10.20 which represents the same form of non-dimensional plot as discussed above. However these data points are for a sloping pipe from Figures 10.36 to 10.39 (which will be discussed later) and indications are that the method is applicable to different density capsules on sloping as well as a horizontal pipe.

To test the applicability of this method of correlation yet further, data from Ellis (reference 16) is represented as shown on Figures 10.21

Figure 10.12

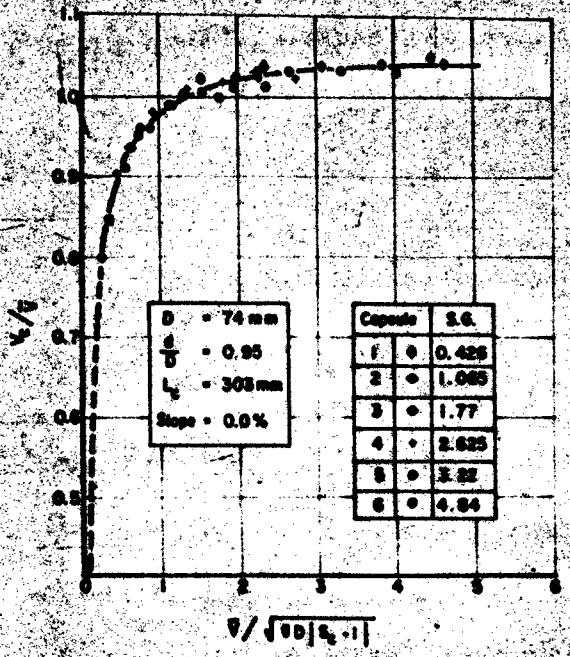

Figure 10.13

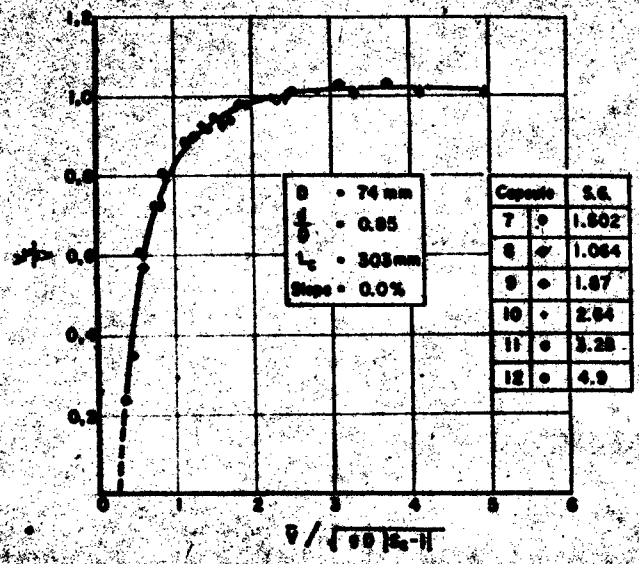

Figure 10.14

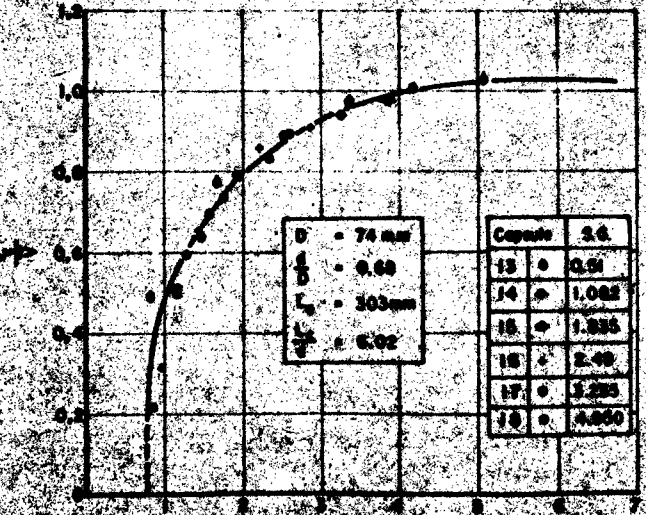

Figure 10.15

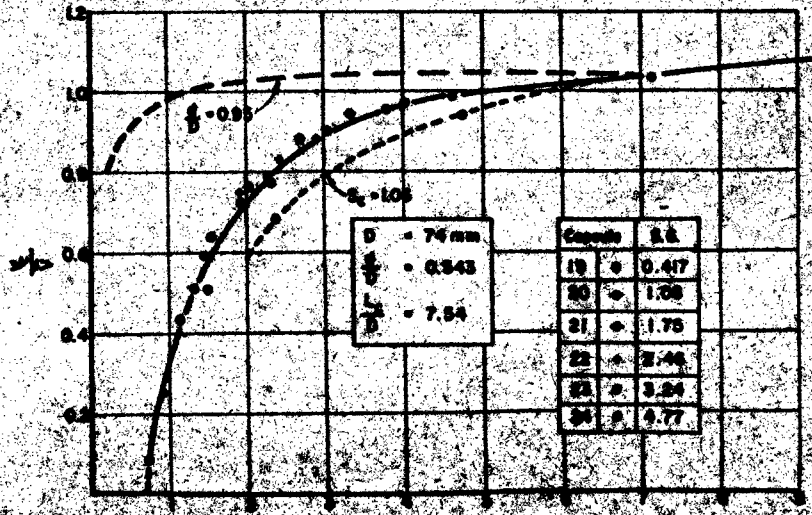

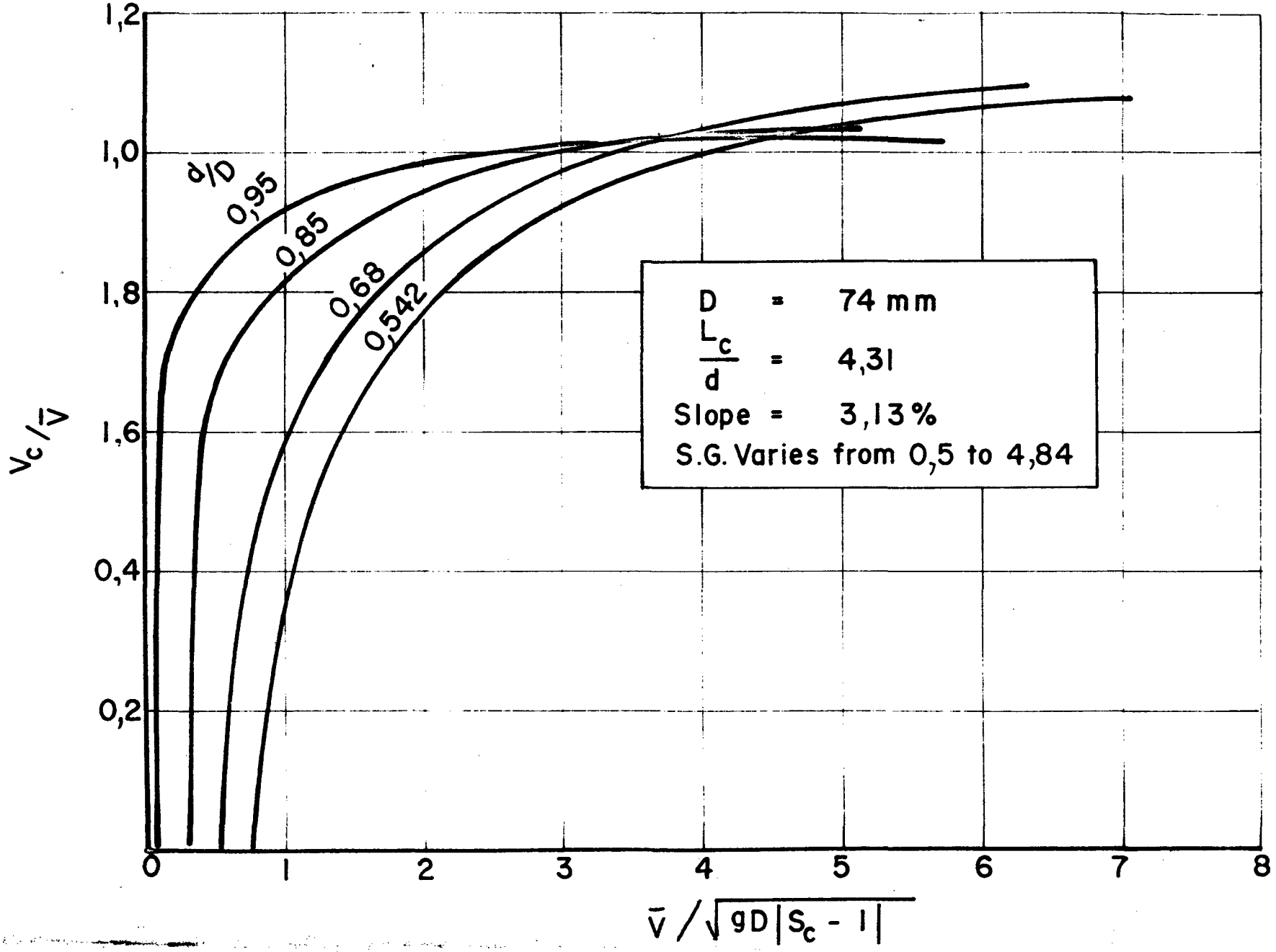
1,2
1,0
1,8
1,6
0,4
0,2
0
1
2
3
4
5
6
7
8
d/D
0,95
0,85
0,68
0,542
D = 74 mm
Lc/d = 4,31
Slope = 3,13%
S.G. Varies from 0,5 to 4,84
Vc/V̄
V̄ / √gD|Sc - 1|

FIG. 10.16

Figure 10.17

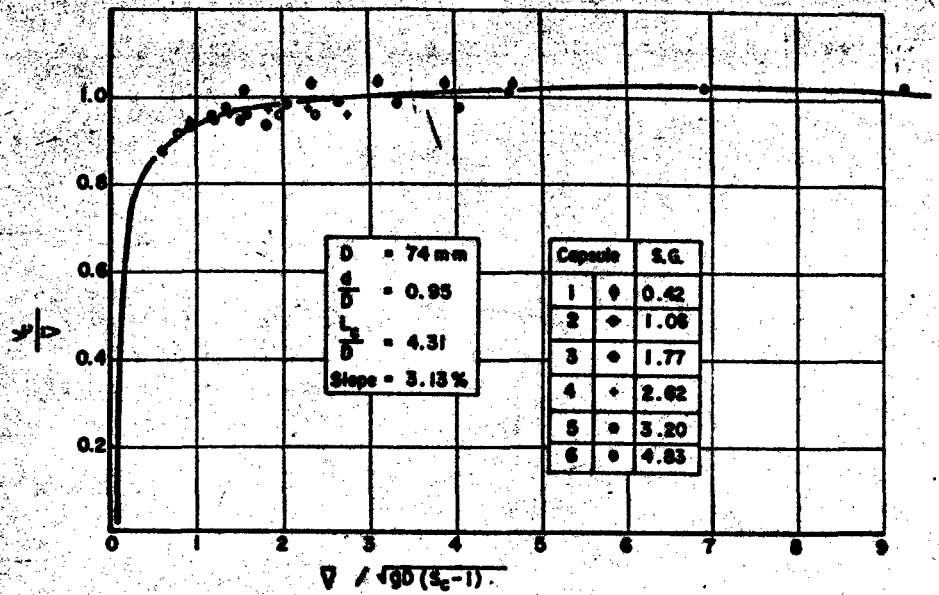

Figure 10.18

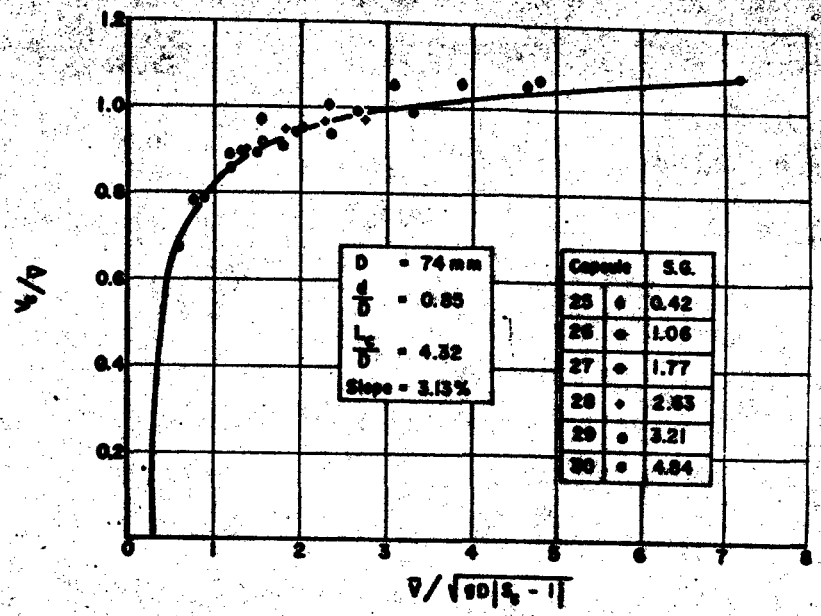

Figure 10.19

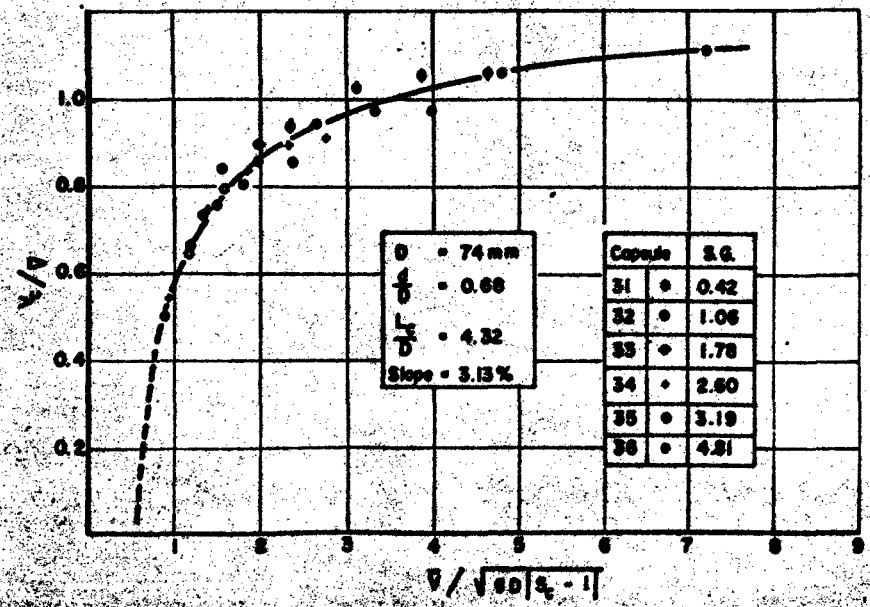

Figure 10.20

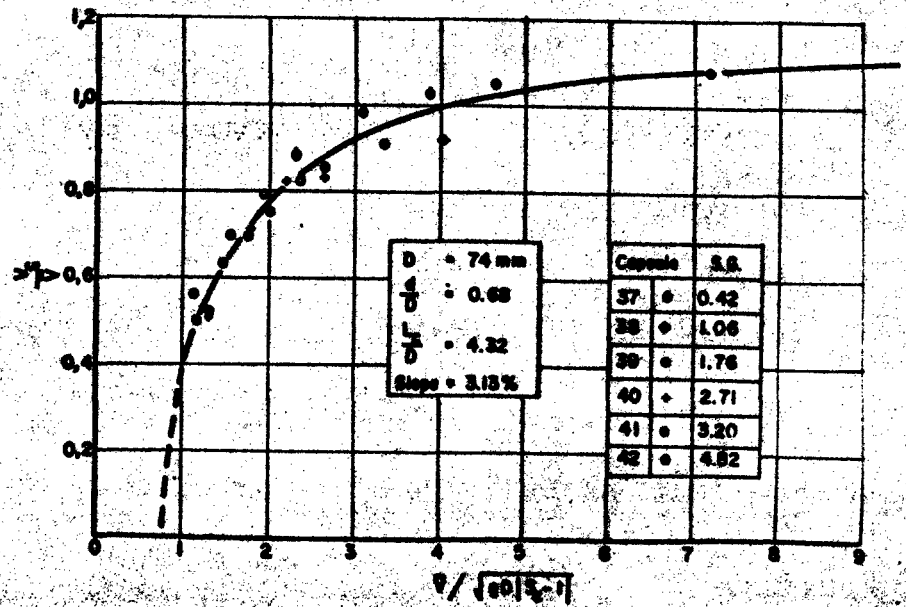

and 10.22 for a $1\frac{1}{4}$ in. (32 mm) diameter pipeline. Two length to diameter ratios (L_c/d) and capsule to pipe diameter ratios (d/D) are shown, and the correlation absorbs a wide range of capsule densities.

These results (Figures 10.12 to 10.22) are all promising since a wide range of specific gravities is accounted for with little scatter of data even when the pipe diameter and slope vary.

6.2 The second step was to plot capsule velocity against mean water velocity.

All the results on Figures 10.6 to 10.9 were re-plotted on the basis of capsule velocity versus mean water velocity and, surprisingly, these yielded linear relations even though the capsules were finite in length (thus end effects are evident) and were orientated eccentrically.

Dimensionally similar capsules of constant length to diameter ratio $L_c/d = 4{,}0$ and specific gravity $S_c = 4{,}0$ are shown with capsule velocity plotted against mean water velocity to illustrate the linearity on Figures 10.23 to 10.26. These figures are summarised on Figure 10.26.

These experiments were carried out in the 74 mm diameter pipeline using dimensionally similar capsules of constant specific gravity once it was realised that the specific gravity effect could be absorbed by plotting as mentioned above.

6.3 The third step was a combination of the first two steps and involved plotting the densometric Froude number for the pipe based on the capsule velocity (F_{rdc}) where; $F_{rdc} = V_c/\sqrt{gD|S_c-1|}$ against the densometric Froude number for the pipe based on the mean water velocity; $F_{rdm} = \overline{V}/\sqrt{gD|S_c-1|}$. This step evolved since step 1 achieved the effect of combining different specific gravity capsules, whereas step 2 yielded a linear relation.

This form of presentation proved to be successful. Figures 10.27 to

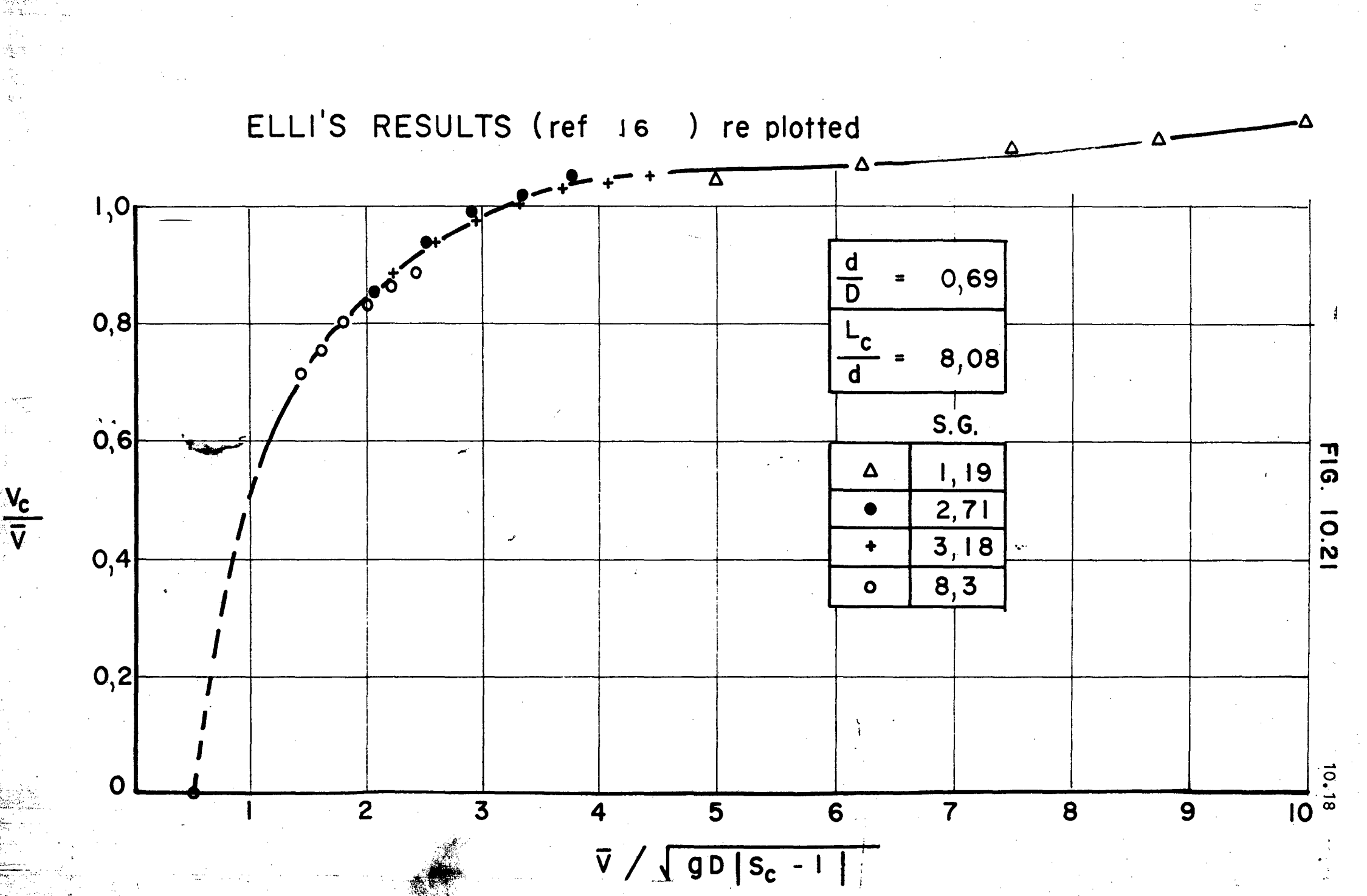

FIG. 10.21

10.18

FIG. 10.22

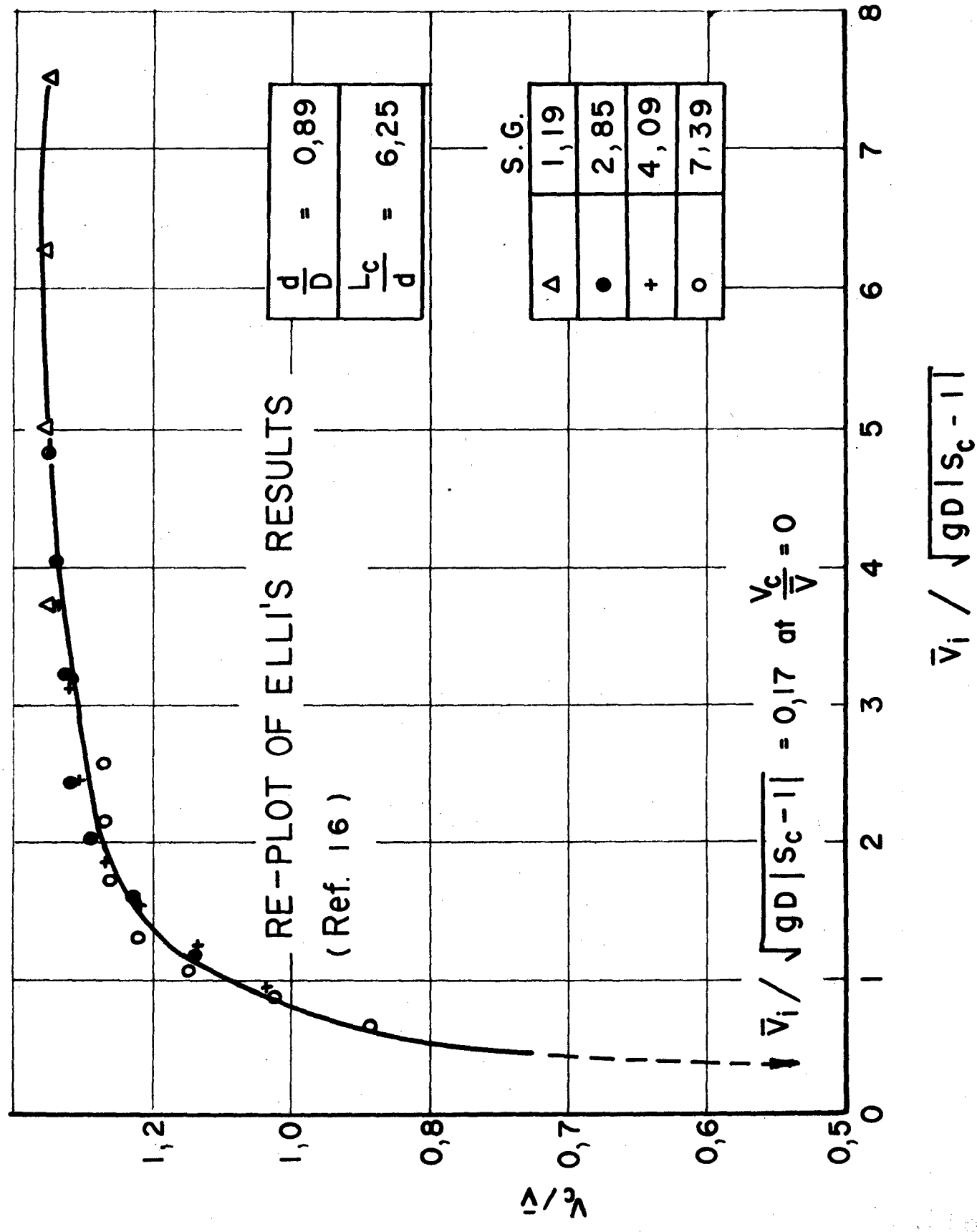
RE-PLOT OF ELLI'S RESULTS
(Ref. 16)
d/D = 0,89
Lc/d = 6,25
S.G.
1,19
2,85
4,09
7,39
Δ
●
+
o
$\bar{V}_i / \sqrt{gD|S_c-1|} = 0,17$ at $\frac{V_c}{\bar{V}} = 0$
$\bar{V}_i / \sqrt{gD|S_c-1|}$
$\bar{V}_i / \sqrt{gD|S_c-1|}$
0
1
2
3
4
5
6
7
8
0,5
0,6
0,7
0,8
1,0
1,2

Figure 10.23

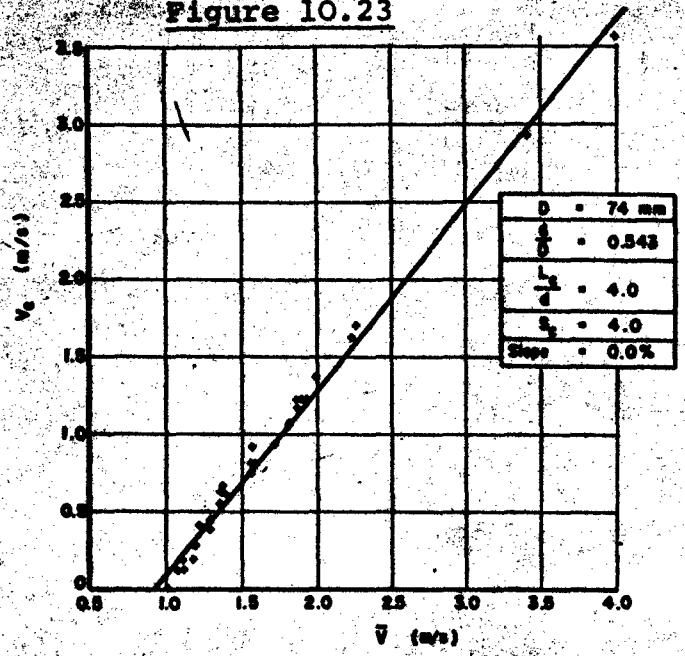

Figure 10.24

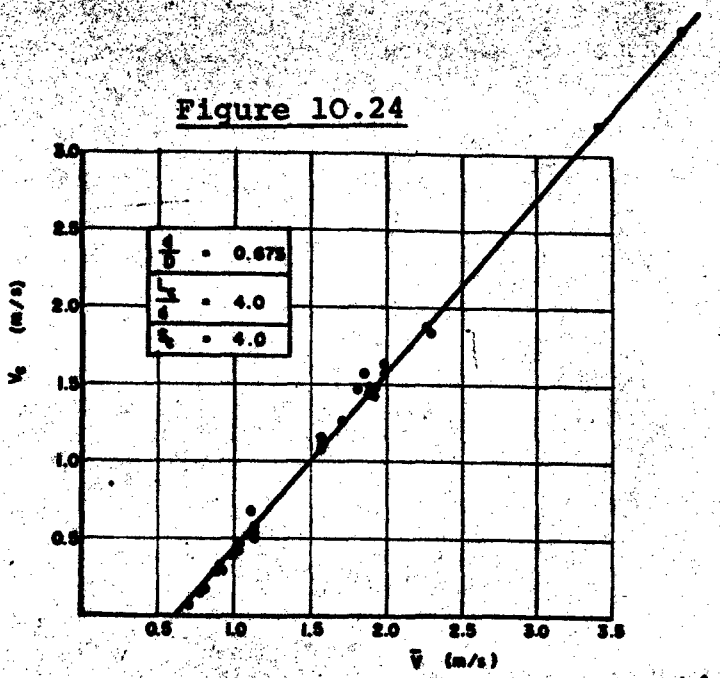

Figure 10.25

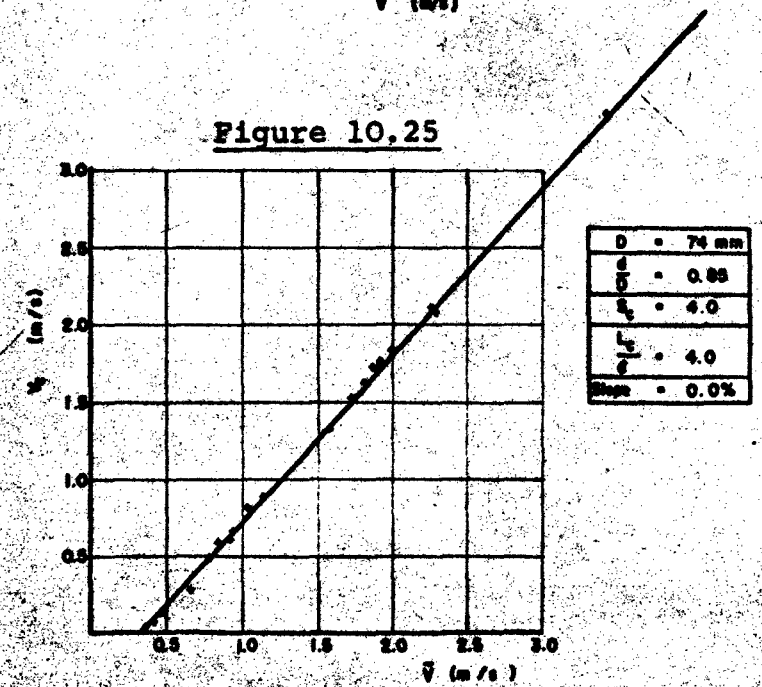

Figure 10.26

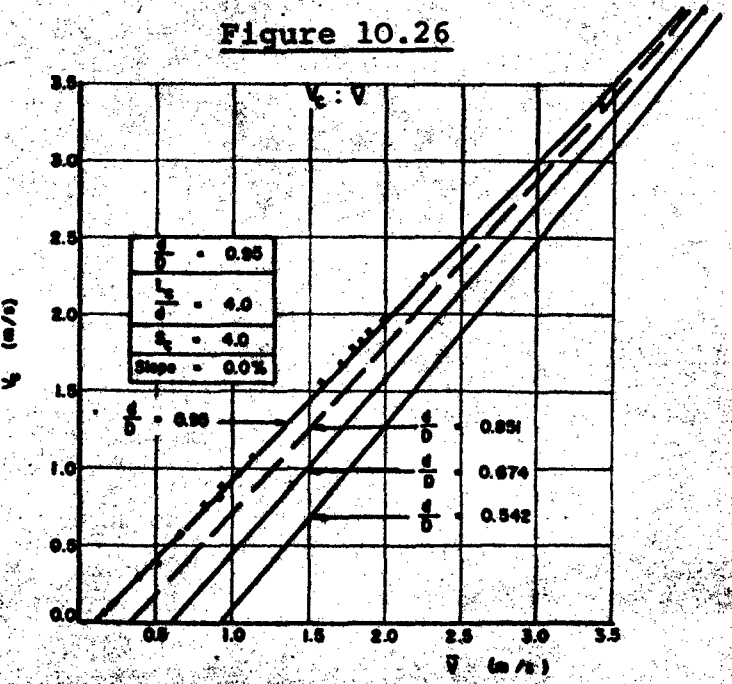

10.30 show $V_c/\sqrt{gD|S_c-1|}$ plotted as ordinate against $\overline{V}/\sqrt{gd|S_c-1|}$ as abscissa and a linear relation is obtained for a capsule of fixed geometry but variable specific gravity.

Figure 10.30 shows the kinematic results plotted in this way for a diameter ratio of 0,85 and superimposed on the same curve are results of Hodgson and co-workers (reference 22). Their original readings are shown on Figure 10.31 which is a plot of $V_c/\overline{V}$ against $\overline{V}$ ($V_{av} = \overline{V}$, where V_{av} is in ft/s). Figure 10.32 shows the velocity ratio as a function of F_{rdm} for the results (which are re-plotted from Figure 10.31) and Figure 10.33 shows the non-dimensional kinematic re-plot of the three pipe diameters. The scatter is not great even though there is a 16 : 1 ratio of pipe diameter presented on Figure 10.33. The remarkable result (shown on Figure 10.30) is found that for various pipe diameters the linear relation is still applicable when plotting in the way suggested. This indicates that the results for different values of the pipe diameter and different specific gravity values can be accommodated on the same curve.

The results of Hodgson et al lie slightly above the results of the present experiments. Their length to diameter ratio of $L_c/d = 3,17$ is less than the length to diameter ratio $L_c/d = 4,82$ of the present results and it is clear from the results given in Chapter 14 on incipient motion that a lower L_c/d value gives a lower value of the pipe densometric Froude number at incipience ($\overline{V}_i/\sqrt{gD|S_c-1|}$) and hence it is to be expected that the points for the shorter length to diameter ratio will lie above the present experimental data.

In order to determine the capsule velocity at a particular mean water velocity two quantities are required; the slope of the line (m) and the mean incipient water velocity. Thus the equation to the straight lines such as those on Figures 10.27 to 10.30 can be obtained. The general form for the equation for determining the capsule velocity (V_c) from the mean

FIG. 10.27

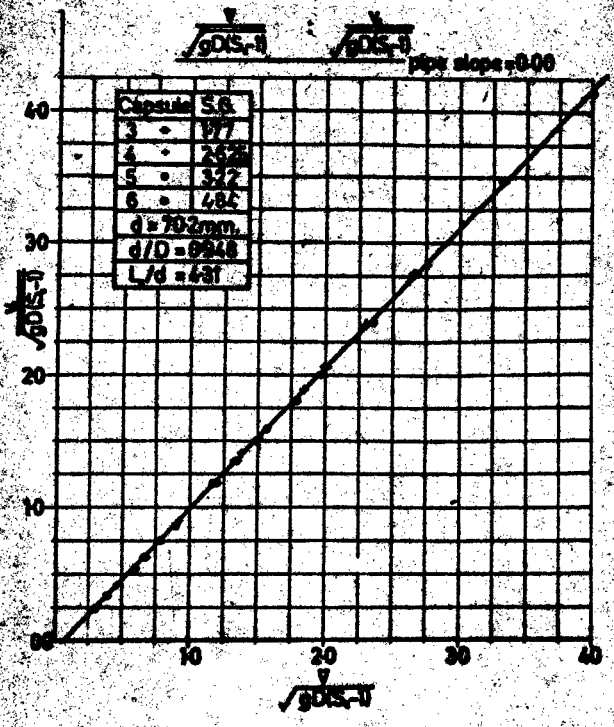

FIG. 10.28

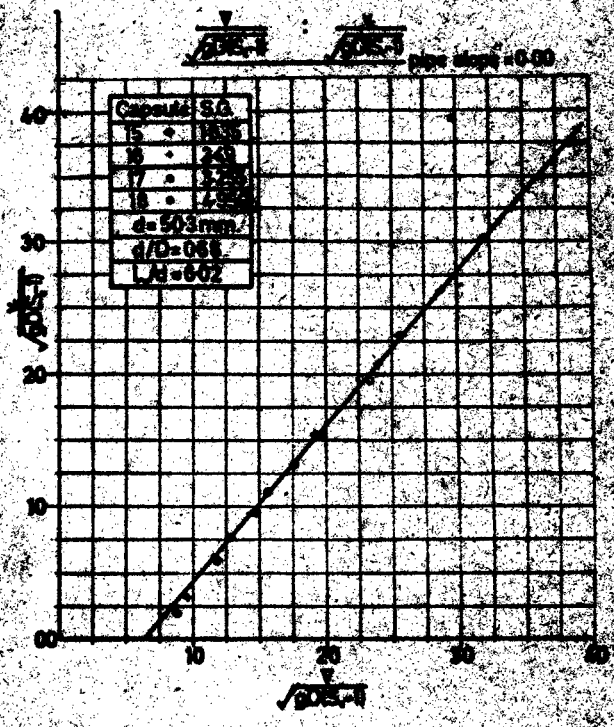

FIG. 10.29

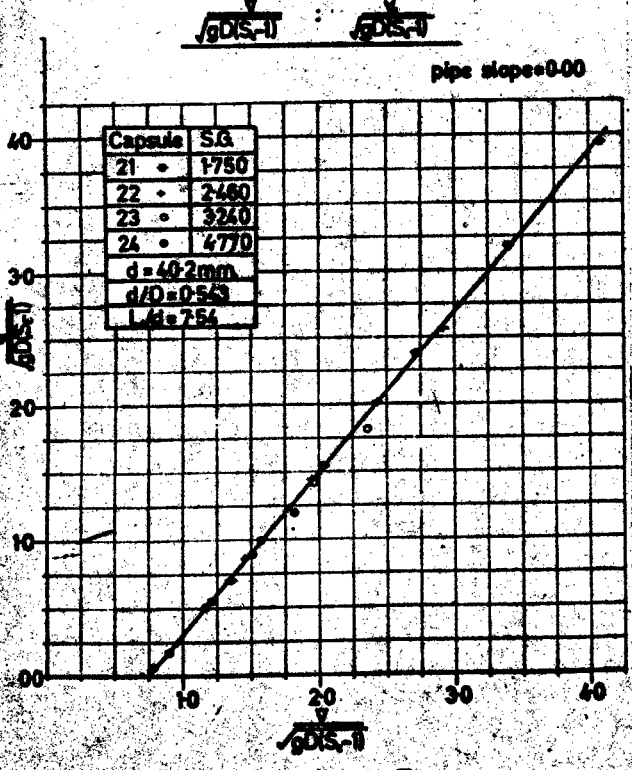

FIG. 10.30

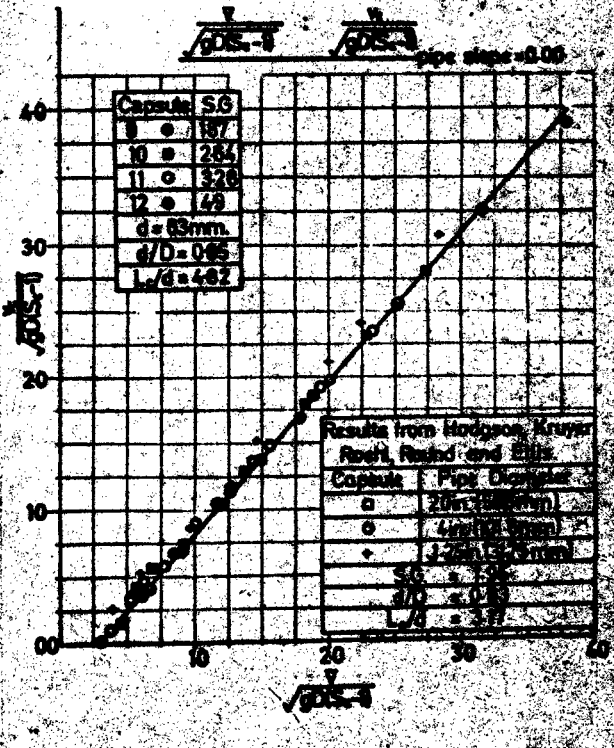

FIG. 10.31

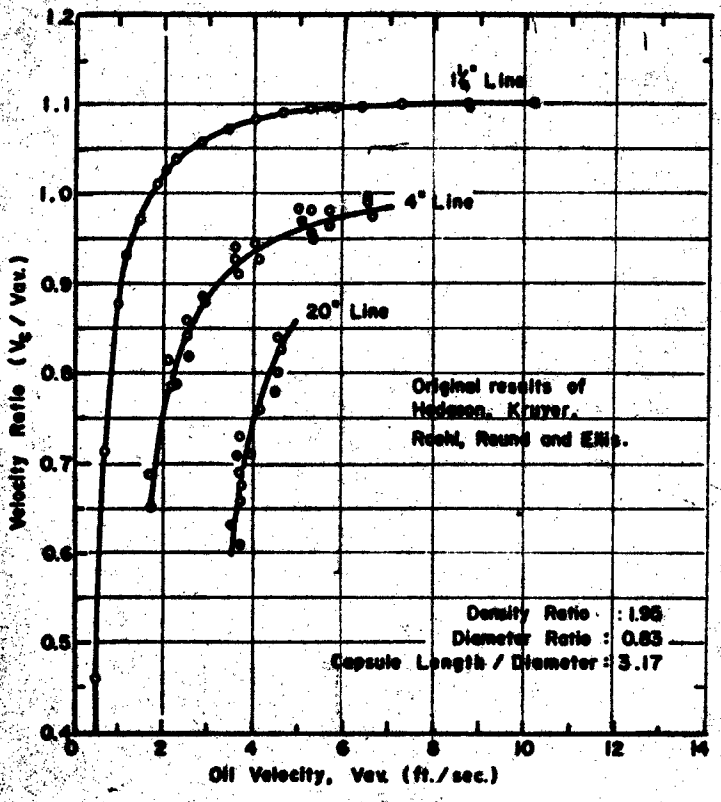

FIG. 10.32

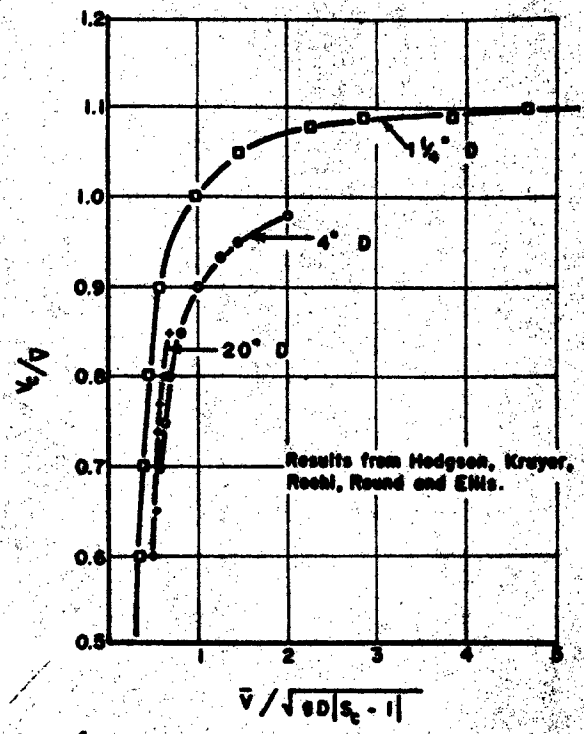

FIG. 10.33

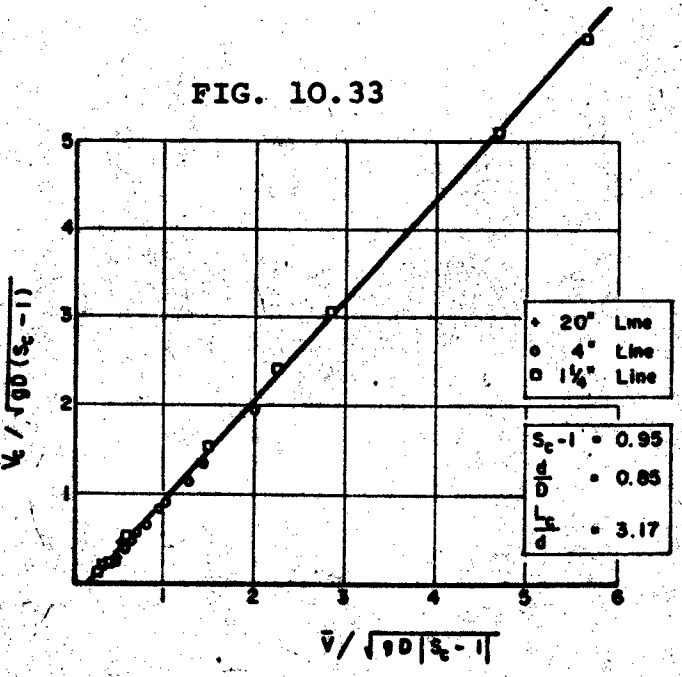

Results from Hodgson, Kruyer, Roehl Round and Ellis.

water velocity $(\overline{V})$ is;

$$V_c = m(\overline{V} - \overline{V}_i)$$

The slope of the line (m) will be discussed later and it will be seen that it lies in the range 1,0 to 1,2 and m decreases with increase in diameter ratio.

The effect of pipe diameter on capsule kinematics will also be dealt with in more detail later in this Chapter.

7. The effect of diameter ratio

As the diameter ratio decreases, all other variables remaining constant, the velocity ratio decreases for the range of capsules considered practicable.

Figure 10.34 shows the diameter ratio plotted against the velocity ratio for three different mean water velocities for capsules of the same specific gravity (S_c = 4,0) and length to diameter ratio (L_c/d = 4,0).

This Figure shows the diameter ratio decreasing as the velocity ratio decreases for a particular value of $\overline{V}$ and this effect is accentuated at low water flows. At a diameter ratio of unity the capsule velocity becomes equal to the mean water velocity irrespective of the value of the latter. This "piston" effect could not be otherwise.

Figure 10.35 is a graph showing velocity ratio $(V_c/\overline{V})$ as a function of diameter ratio for dimensionally similar capsules with submerged density ratio (S_c-1) as parameter at a constant mean water velocity of 2,0 m/s. This family of curves is obtained from results of Figures 10.36, 10.37, 10.38 and 10.39 in an upward sloping pipe and the slope aspect will be discussed later in this Chapter.

The heavier capsules (Figure 10.35) display an almost linear relation and as the submerged density drops a curve develops at higher diameter

FIG. 10.34

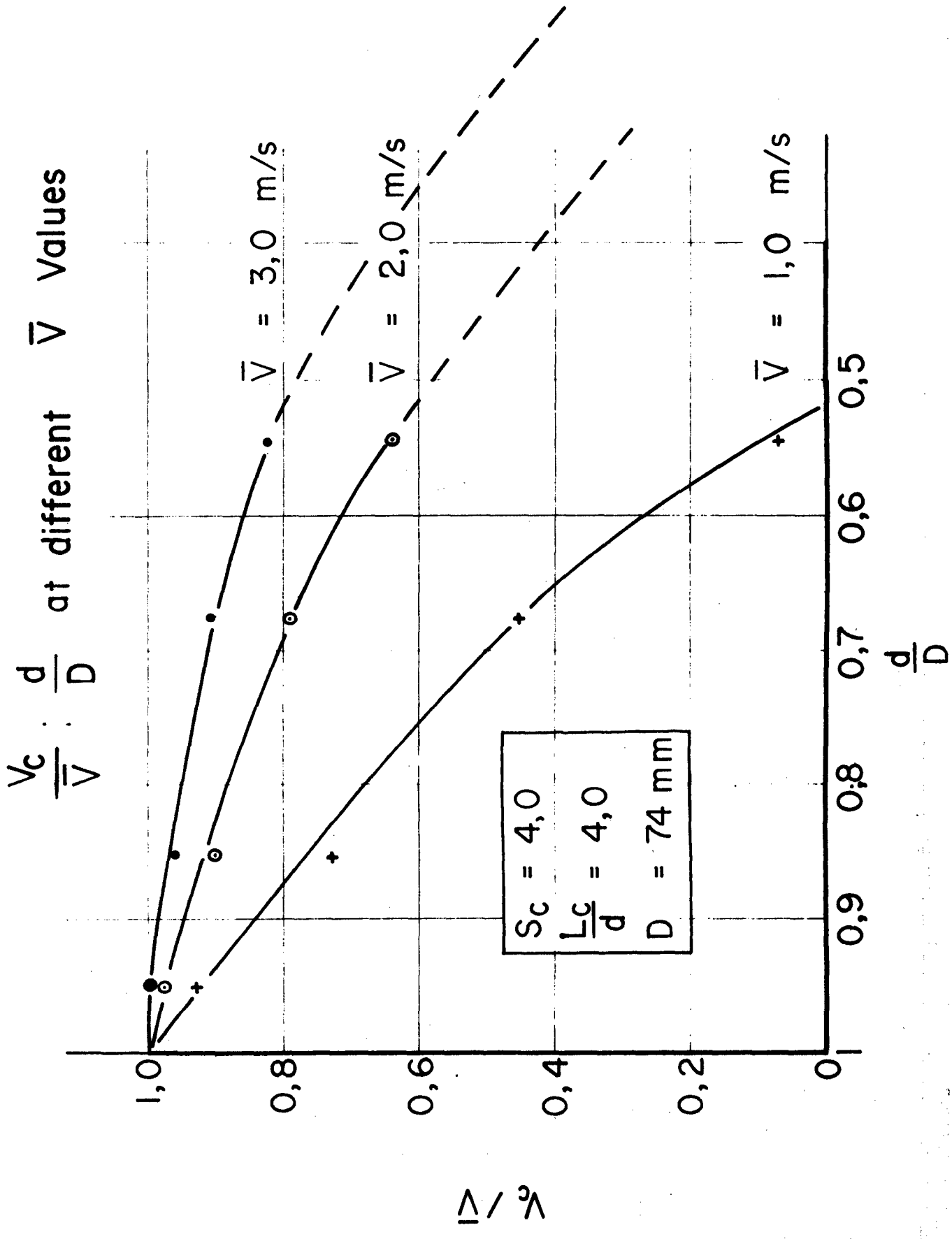
$\frac{V_c}{\bar{V}}$: $\frac{d}{D}$ at different $\bar{V}$ Values
$\bar{V}$ = 3,0 m/s
$\bar{V}$ = 2,0 m/s
$\bar{V}$ = 1,0 m/s
S_c = 4,0
$\frac{L_c}{d}$ = 4,0
D = 74 mm
$V_c / \bar{V}$
$\frac{d}{D}$
1,0
0,8
0,6
0,4
0,2
0
0,5
0,6
0,7
0,8
0,9
1

FIGURE 10.35

$\frac{d}{D}$ vs $\frac{V_c}{\bar{V}}$ for different SG's at const. $\frac{L_c}{d}$ and $\bar{V}$ = 2,0 m/s

10.26

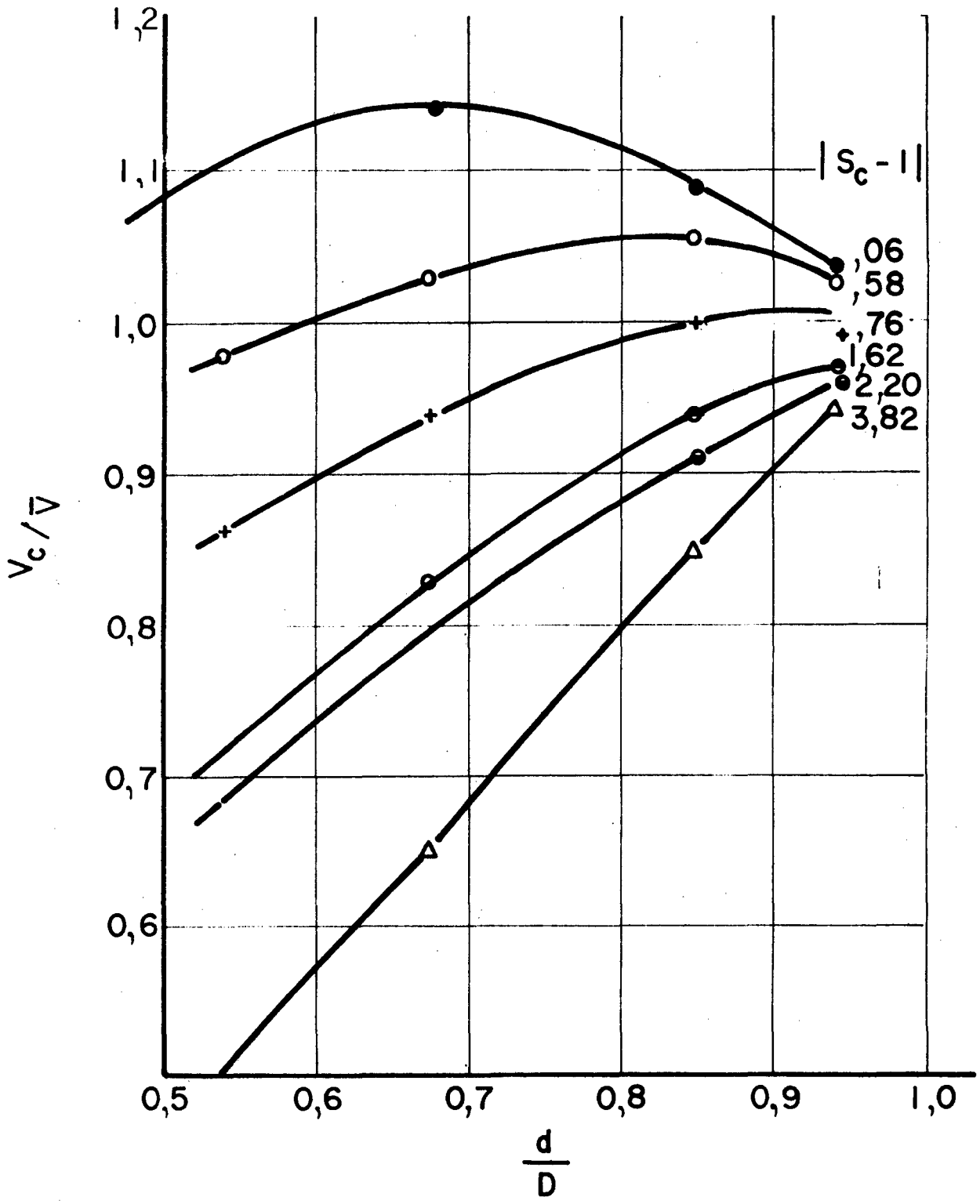

Figure 10.36

D	= 74 mm
$\frac{d}{D}$	= 0.95
$\frac{L_c}{d}$	= 4.32
Slope	= 3.13%

Capsule		SG
1	●	0.426
2	+	1.065
3	■	1.77
4	△	2.625
5	o	3.22
6	□	4.84

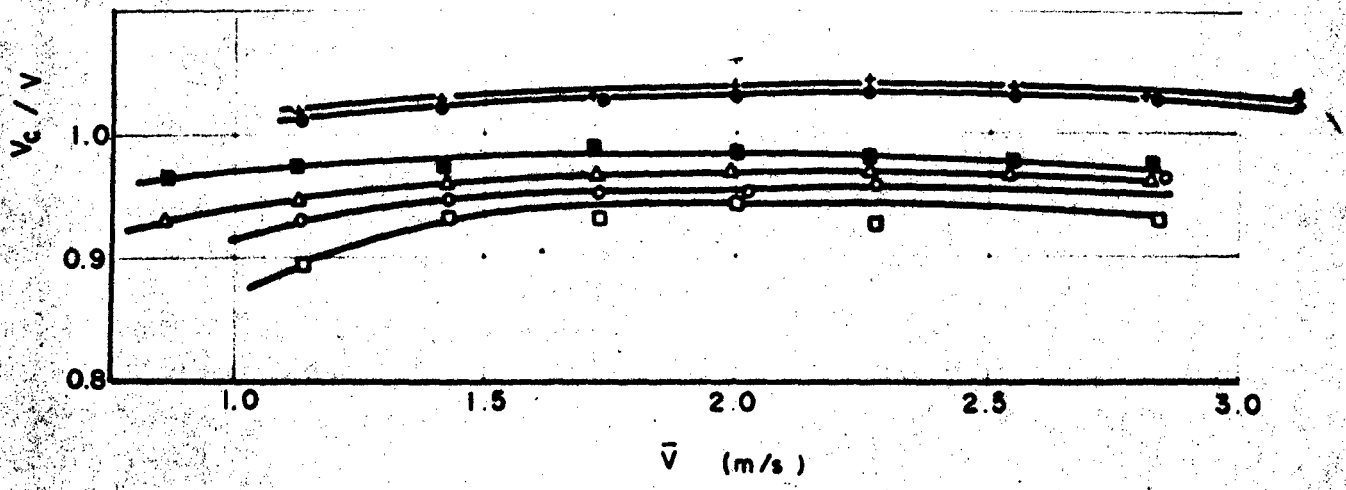

Figure 10.37

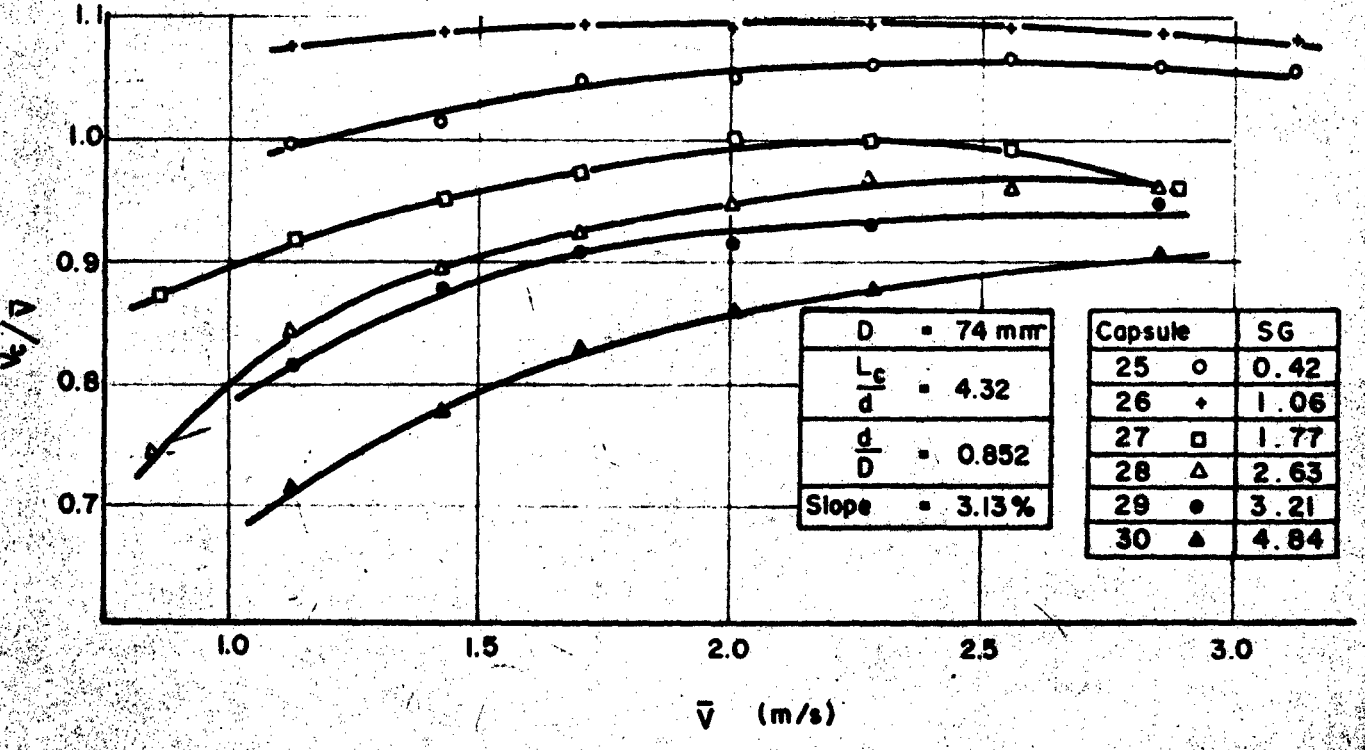

FIG. 10.38

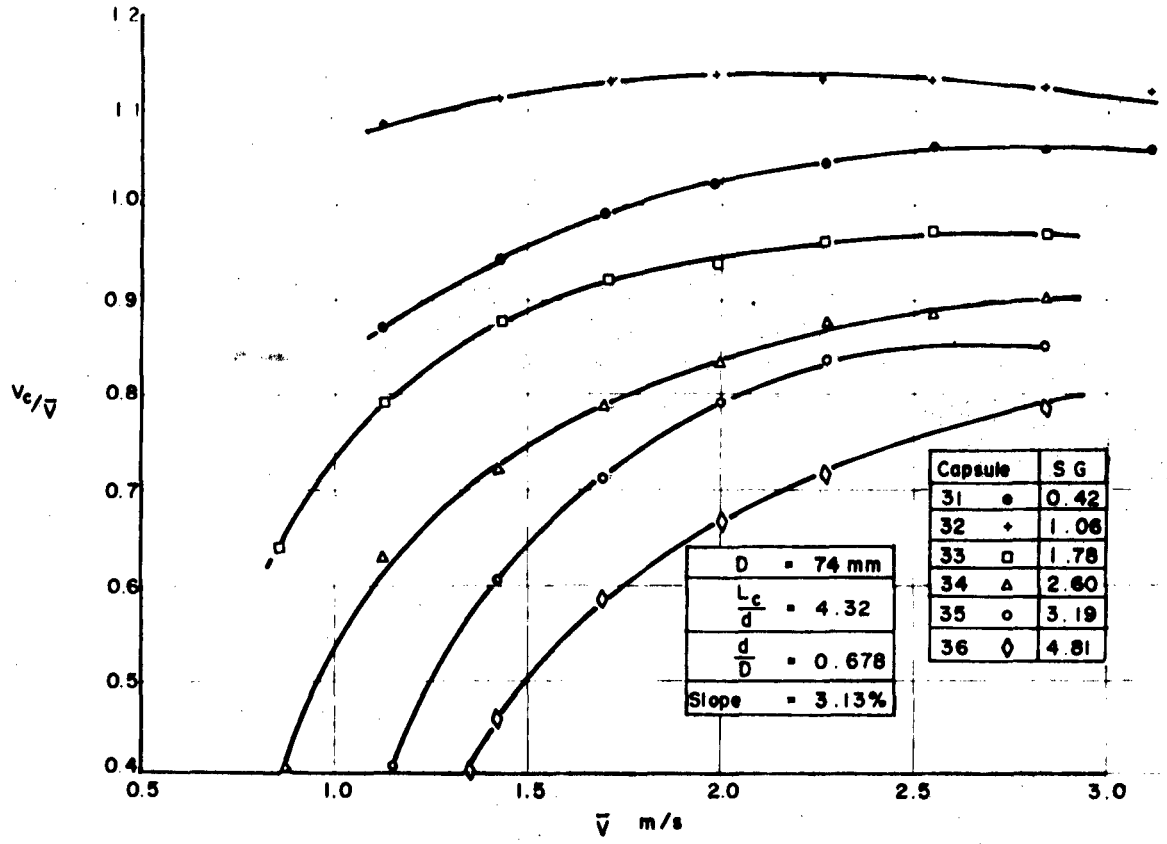

FIG. 10.39

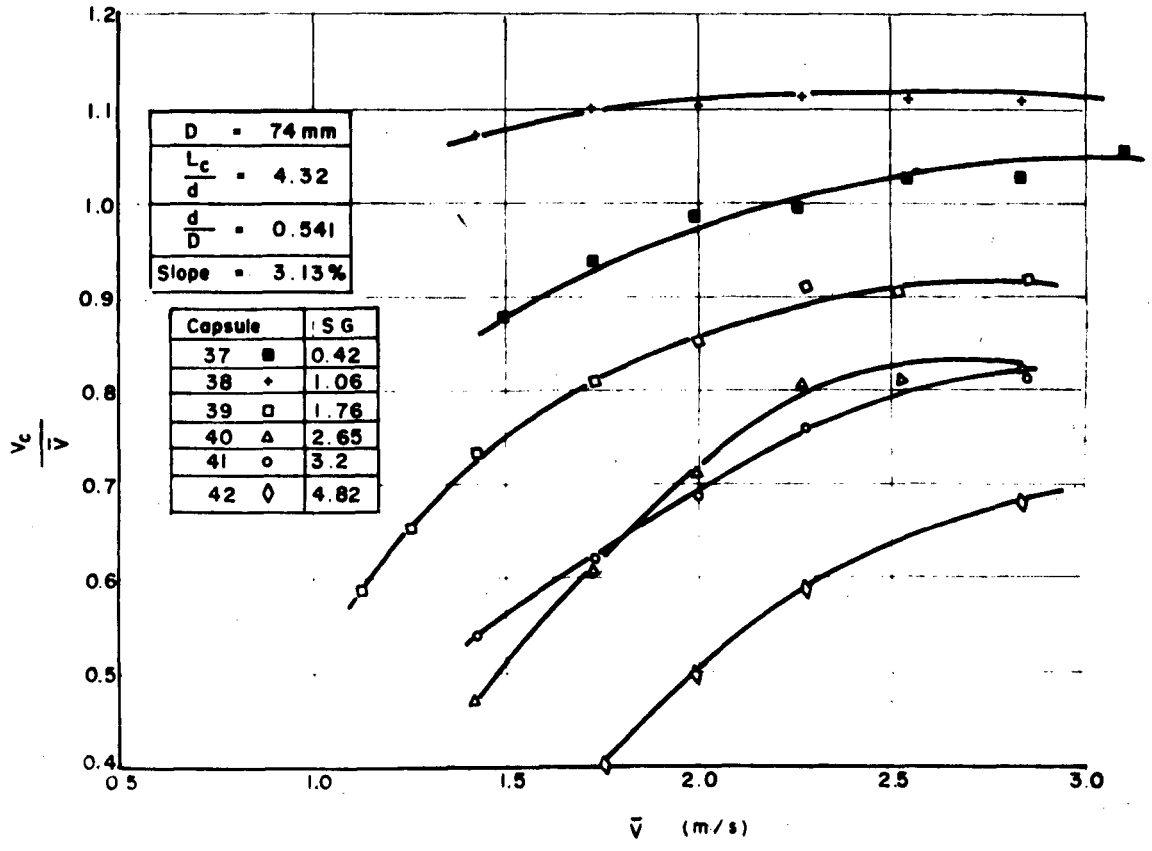

ratios and a maximum value of velocity ratio occurs at decreasing diameter ratios as the value of (S_c-1) decreases.

The extreme value of $V_c/\overline{V} = 1,23$ should occur with a neutrally buoyant capsule at a diameter ratio of zero (where $V_{max} = 1,23\ \overline{V}$ in turbulent flow).

Note that as the diameter ratio tends to unity the velocity ratio of all the specific gravity capsules should tend to 1,0.

As the diameter ratio decreases, for a specific water velocity and capsules of $SG \neq 1$, a value will eventually be reached at which $V_c/\overline{V} = 0$ and the capsule remains stationary. From Figure 10.34 this point is reasonably clear at 1 m/s and occurs at a diameter ratio $d/D = 0,52$. At higher mean water velocities the value for which $V_c = 0$ occurs at a much lower diameter ratio and, indeed, for the range of capsule diameter ratios tested at 3 m/s, for example (Figure 10.34) a capsule of specific gravity 4,0 and length to diameter ratio 4,0 will always be above the threshold velocity no matter what the diameter ratio. If lower diameter ratio capsules had been tested the $\overline{V} = 3$ m/s curve would eventually reach a zero velocity ratio value. In fact this is true for any velocity since the smaller the diameter ratio the higher the incipient velocity. The limit is reached with $d/D = 0$ in which case the capsule velocity would be zero since the water velocity at the pipe wall is zero, no matter what the mean water velocity is.

The reason for the decrease of capsule velocity (V_c), at a particular mean water velocity $(\overline{V})$, with diameter ratio at low water velocities (Figure 10.34) is that the smaller diameter capsules present less frontal area to the flow and hence are subjected to less form drag forces.

Secondly, smaller diameter capsules occupy lower velocity regions than larger capsules and would also travel more slowly for this reason.

A third factor is that the annular velocity, relative to the capsule

($\overline{V}_{am}$), increases at a greater rate with $\overline{V}$ constant as diameter ratio increases. This is particularly evident if V_c for the small diameter ratio capsules is less than for the large, since

$$\overline{V}_{am} = \frac{\overline{V} - V_c \left(\frac{d}{D}\right)^2}{1 - \left(\frac{d}{D}\right)^2}$$

This causes a higher pressure drop along the capsule and consequently a greater shear stress along the capsule tending to increase the capsule velocity.

On the other hand the solid to solid friction between capsule and pipe wall is proportional to the cube of the capsule diameter (for a constant length to diameter ratio and specific gravity) and this increased friction tends to decrease capsule velocity at a fixed mean water velocity. However, there seems to be a paradox, since the solid to solid friction increase tends to cause a higher annular velocity which increases the pressure drop along the capsule because the annular velocity relative to the capsule increases as the capsule velocity decreases.

The effects described above (i.e. orientation, form drag and increased shear along the capsule) cause higher capsule velocities. Whereas the increased solid to solid friction causes decreased capsule velocity but increased shear on the capsule. The net result of these effects is that capsule velocity increases as diameter ratio increases. The situation described above is reversed at very high mean water velocities. That is, the lower diameter ratios eventually reach a velocity in excess of the high diameter ratios at high mean water velocities.

From Figure 10.40 (or 10.26) (the difference between these Figures will be made clear later on in the Chapter in Section 12), which is a plot of capsule velocity against mean water velocity for length to diameter ratio and specific gravity both equal to 4,0, it is clear that the different dia-

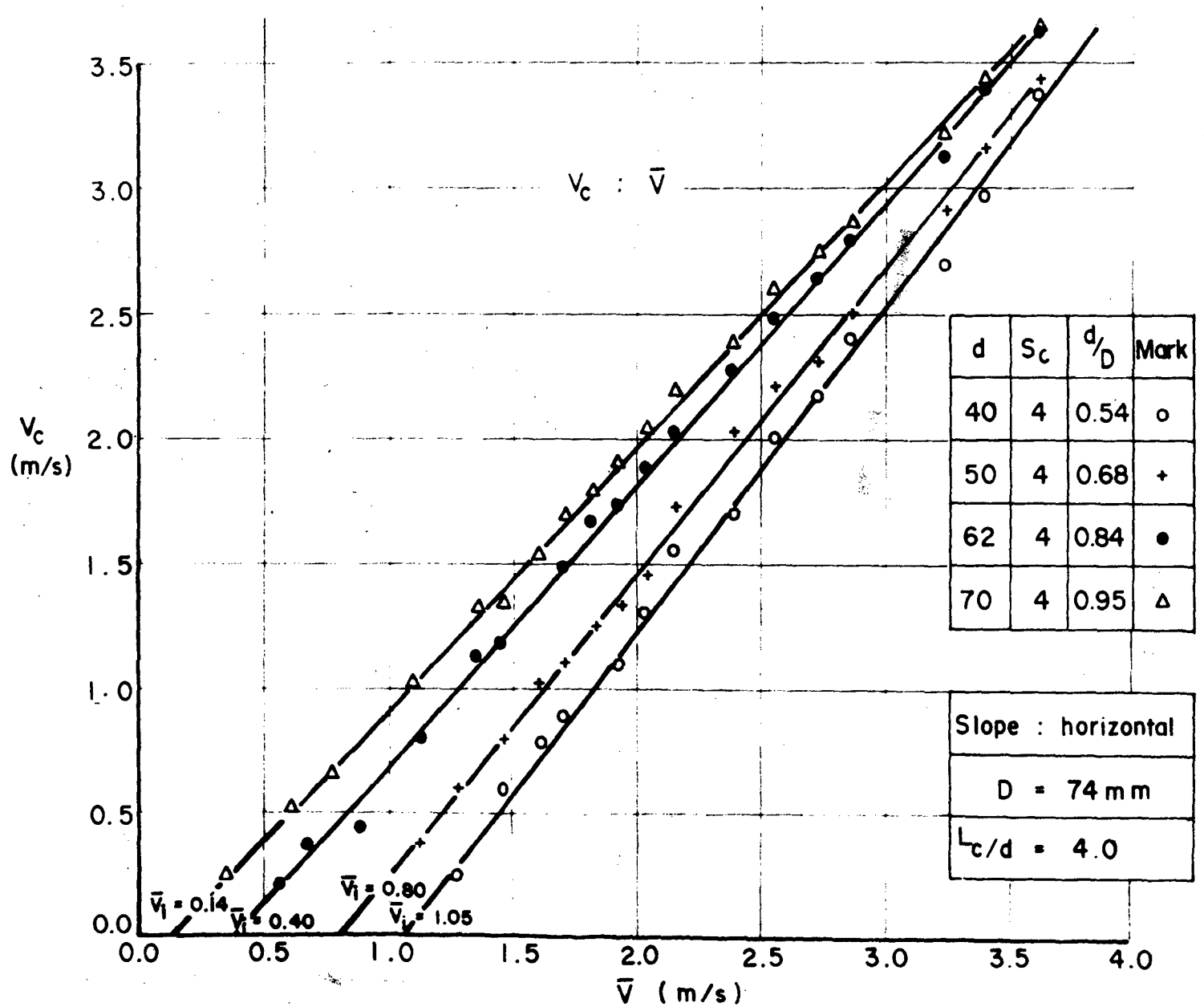
$V_c : \bar{V}$
V_c (m/s)
$\bar{V}$ (m/s)
0.0
0.5
1.0
1.5
2.0
2.5
3.0
3.5
4.0
$\bar{V}_i$ = 0.14
$\bar{V}_i$ = 0.40
$\bar{V}_i$ = 0.80
$\bar{V}_i$ = 1.05
d | S_c | d/D | Mark
40 | 4 | 0.54 | o
50 | 4 | 0.68 | +
62 | 4 | 0.84 | ●
70 | 4 | 0.95 | △
Slope : horizontal
D = 74 mm
L_c/d = 4.0

FIG. 10.40

FIG. 10.41

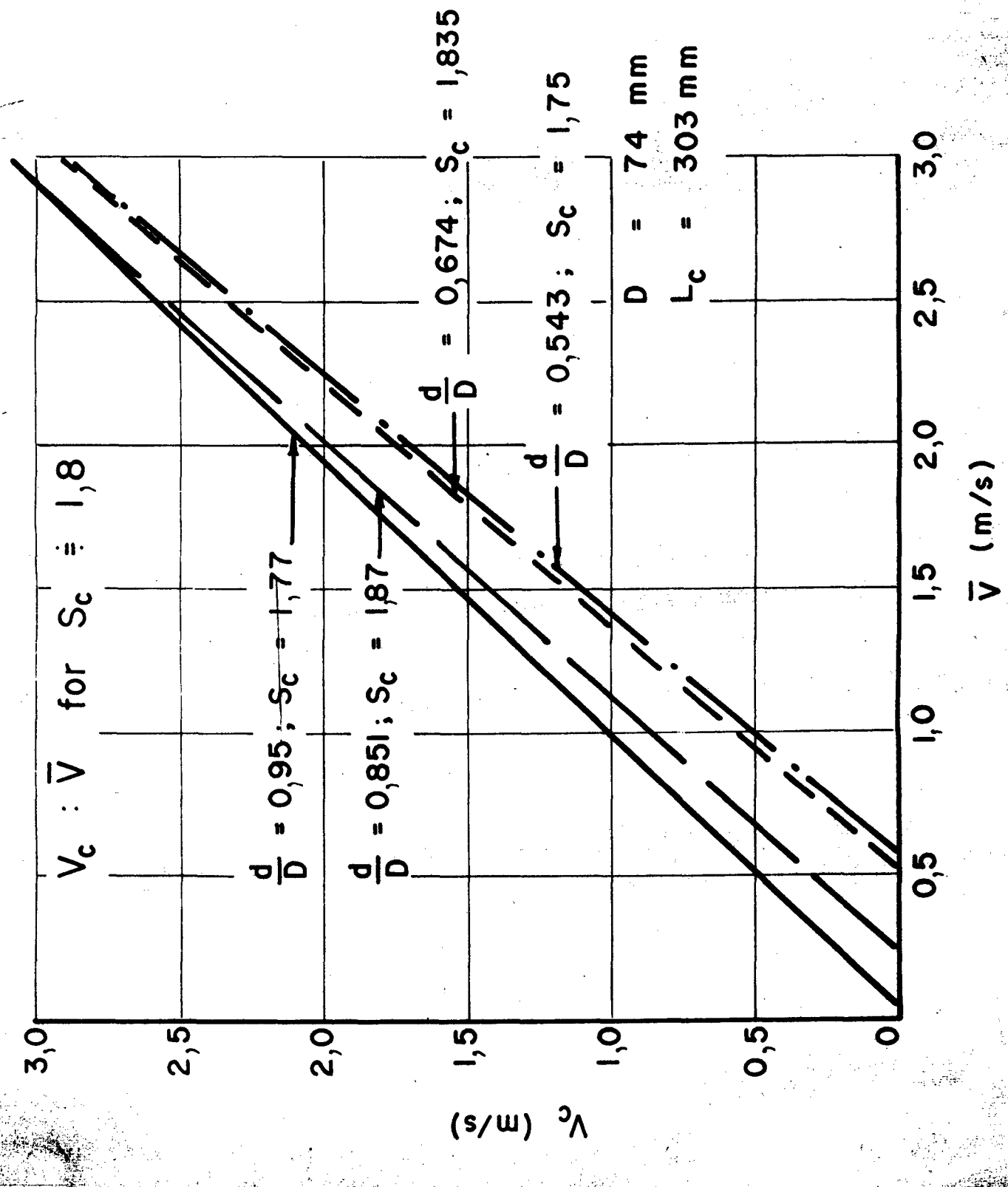
V_c : $\bar{V}$ for S_c = 1,8
$\frac{d}{D}$ = 0,95 ; S_c = 1,77
$\frac{d}{D}$ = 0,851 ; S_c = 1,87
$\frac{d}{D}$ = 0,674 ; S_c = 1,835
$\frac{d}{D}$ = 0,543 ; S_c = 1,75
D = 74 mm
L_c = 303 mm
V_c (m/s)
$\bar{V}$ (m/s)
0
0,5
1,0
1,5
2,0
2,5
3,0

meter ratio lines will eventually cross and the smaller diameter ratio capsules will overtake the larger ones. This trend is more pronounced with lower density capsules (see Figure 10.41) as this plot, of velocity ratio against mean water velocity at specific gravities of about 1,8 shows.

One explanation for this trend is that the smaller diameter ratio capsules are being lifted appreciably off the pipe bottom and entering the higher velocity zone, in the velocity distribution, near the centre of the pipe. This situation can be compared with the neutrally buoyant capsules mentioned earlier.

This point will be dealt with in more detail later.

The curves of capsule velocity plotted against mean water velocity can be brought into coincidence for varying specific gravities as described in the previous section. The curves can also be made coincident for different diameter ratios by horizontally shifting and simultaneously rotating so that in the formula;

$$V_c/\sqrt{gD|S_c-1|} = m(\overline{V}/\sqrt{gD|S_c-1|} - \overline{V}_i/\sqrt{gD|S_c-1|}) \qquad (10.2)$$

the shift is represented by $\overline{V}_i/\sqrt{gD|S_c-1|}$ and the rotation by m.

The incipient velocity ($\overline{V}_i$) has been determined experimentally and analytically (in Chapters 7 and 14) and it has been shown that incipient velocity can be represented by equation (7.133).

The value of m will be discussed later in this Chapter (Section 12).

8. The effect of length to diameter ratio (L_c/d) on the capsule velocity (V_c)

Figures 10.42 to 10.50 show capsule velocity plotted against mean water velocity for the capsules in the 44 mm diameter pipeline at four different diameter ratios, six different length to diameter ratios and a specific gravity held constant at 4,0.

Figure 10.42

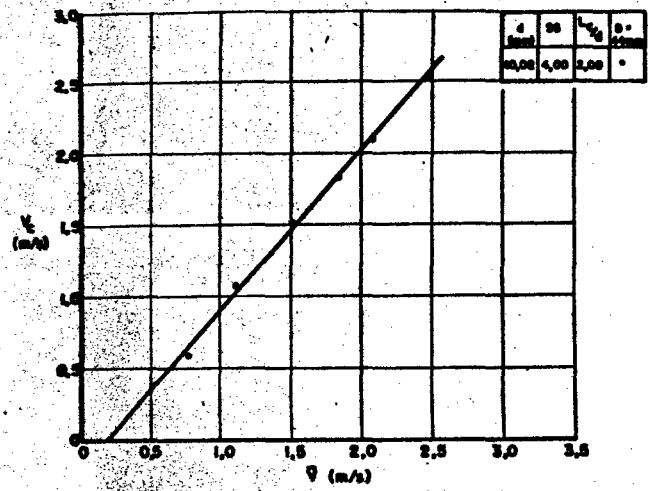

Figure 10.43

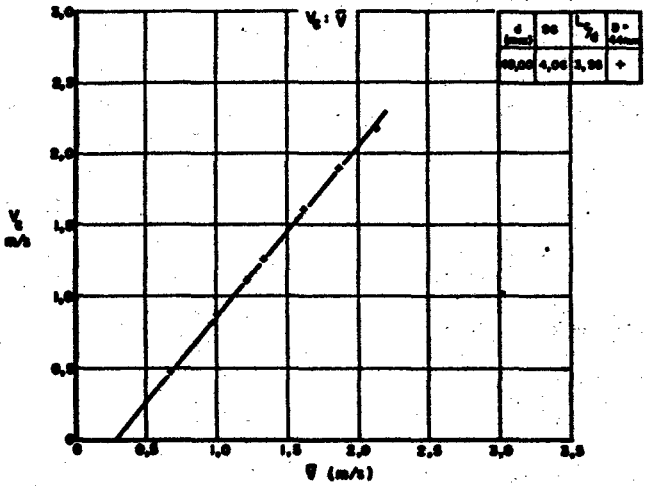

Figure 10.44

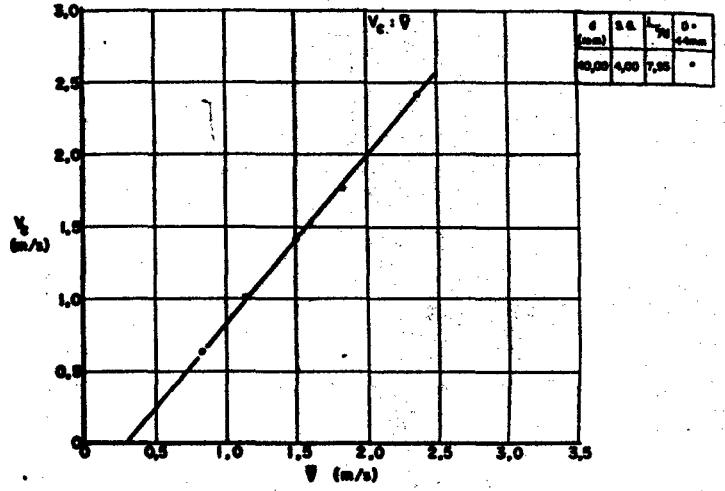

Figure 10.45

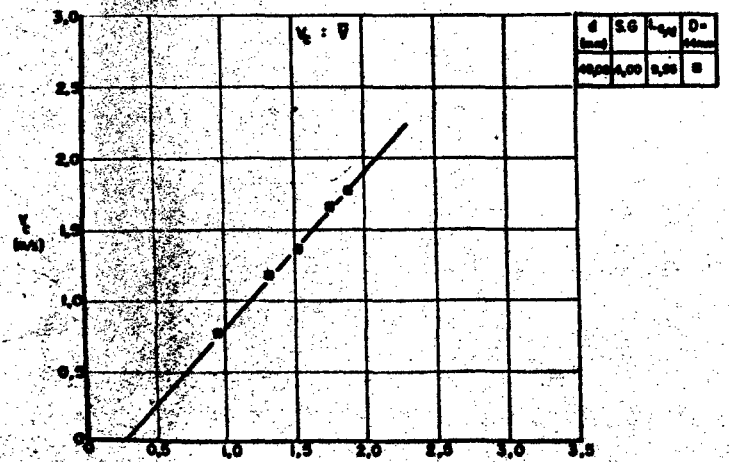

Figure 10.46

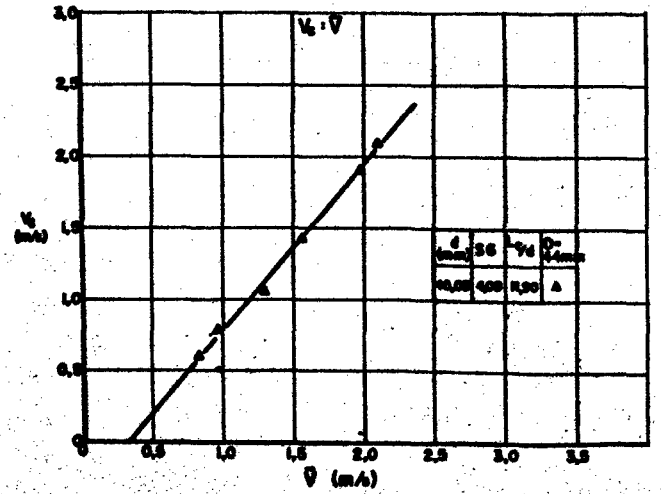

Figure 10.47

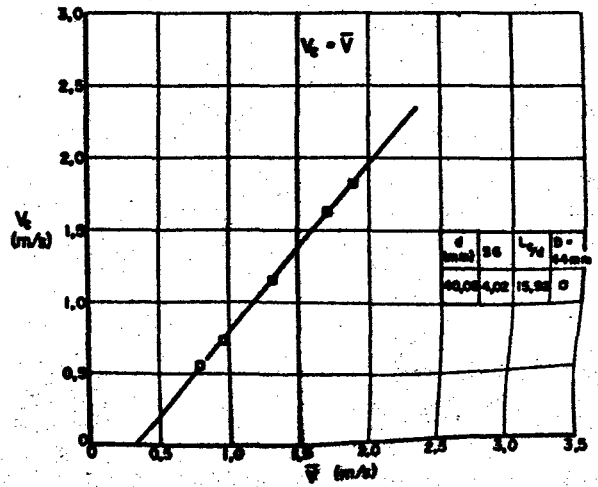

FIG. 10.48

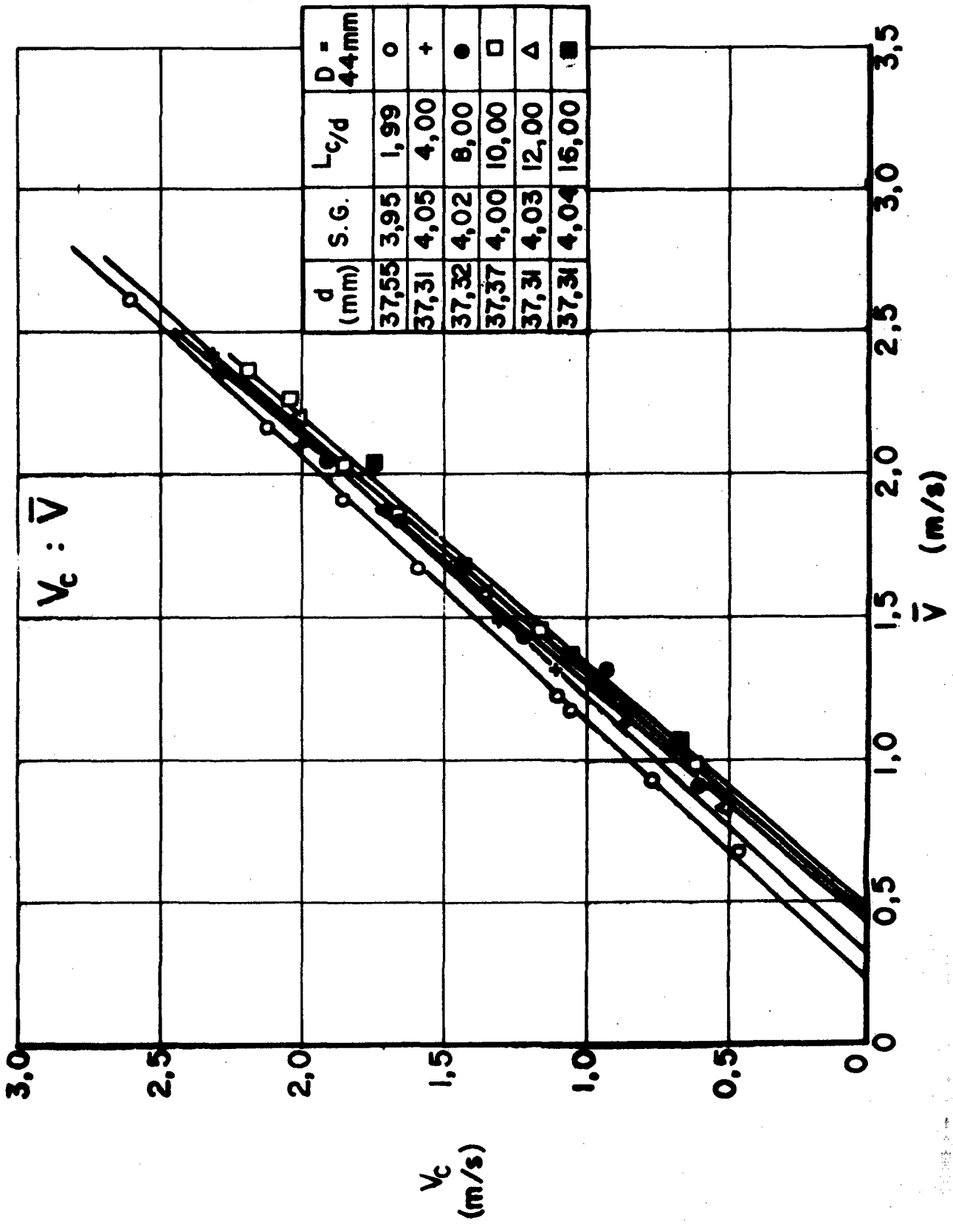
$V_c : \bar{V}$
D = 44mm
L_c/d
S.G.
d (mm)
o 1,99 3,95 37,55
+ 4,00 4,05 37,31
● 8,00 4,02 37,32
□ 10,00 4,00 37,37
Δ 12,00 4,03 37,31
■ 16,00 4,04 37,34
V_c (m/s)
$\bar{V}$ (m/s)
0
0,5
1,0
1,5
2,0
2,5
3,0
3,5

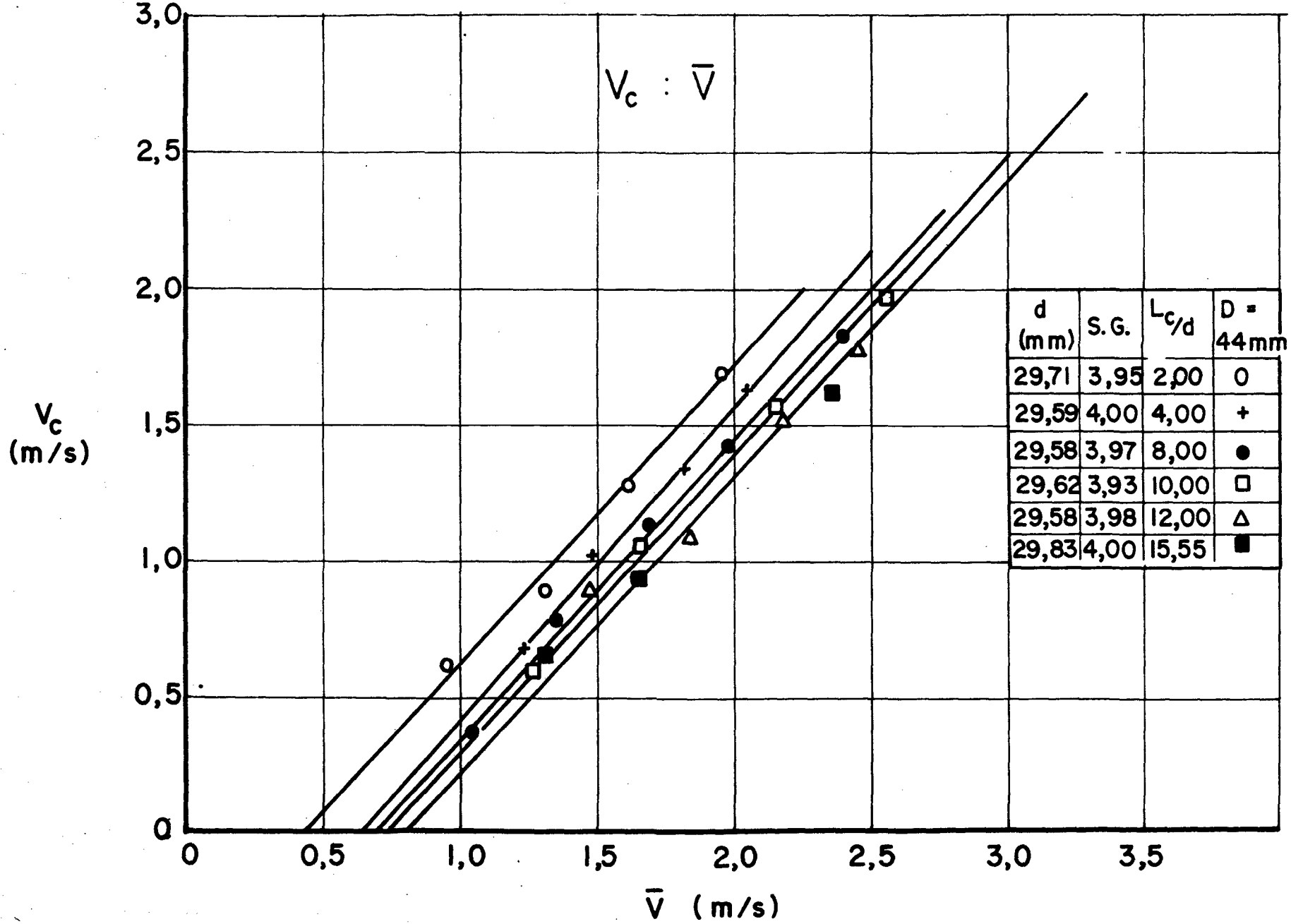
$V_c : \bar{V}$
V_c (m/s)
$\bar{V}$ (m/s)
0
0,5
1,0
1,5
2,0
2,5
3,0
3,5
d (mm) | S.G. | L_c/d | D = 44mm
29,71 | 3,95 | 2,00 | o
29,59 | 4,00 | 4,00 | +
29,58 | 3,97 | 8,00 | ●
29,62 | 3,93 | 10,00 | □
29,58 | 3,98 | 12,00 | △
29,83 | 4,00 | 15,55 | ■

FIG. 10.49

FIG. 10.50

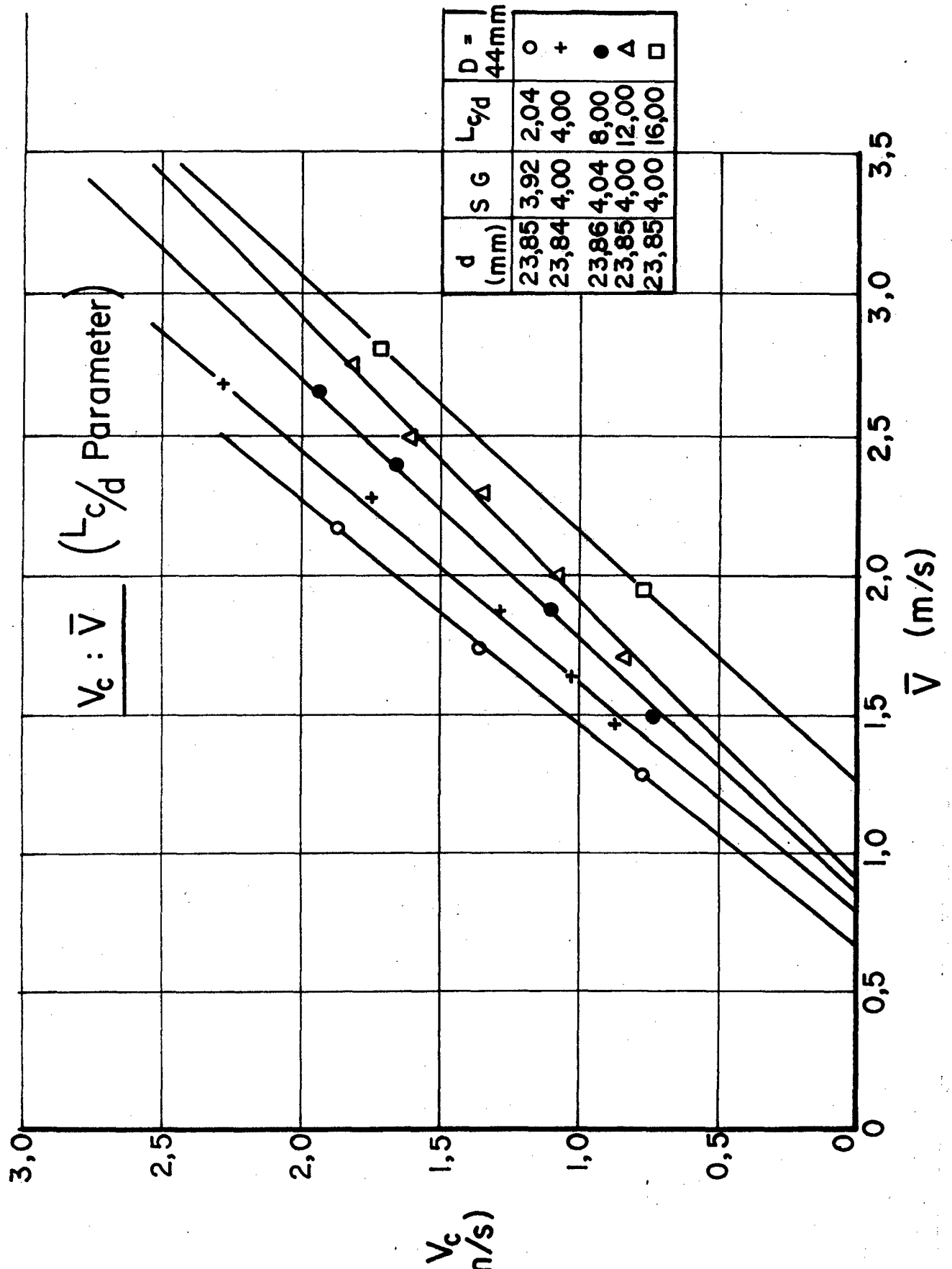
$V_c : \bar{V}$ (L_c/d Parameter)
V_c (m/s)
$\bar{V}$ (m/s)
0
0,5
1,0
1,5
2,0
2,5
3,0
3,5
d (mm) | S G | $L_{c/d}$ | D = 44mm
23,85 | 3,92 | 2,04 | o
23,84 | 4,00 | 4,00 | +
23,86 | 4,04 | 8,00 | ●
23,85 | 4,00 | 12,00 | Δ
23,85 | 4,00 | 16,00 | □

The variable length to diameter ratio was conveniently studied by using trains of capsules as was mentioned in Chapter 5. The capsules were machined brass cylinders carefully weighted to give the desired mass and turned to give the same diameter ratios as those used in the 74 mm diameter pipeline, with the exception of the largest capsule having a diameter ratio $d/D = 0,91$ as opposed to 0,95 in the large pipe. The alteration of diameter ratio in this case was to facilitate the negotiation of bends.

It can be seen that at a particular diameter ratio the various length to diameter ratio curves result in parallel straight lines. This means that the value of the line slope (m) in equation (10.2) remains constant and the abscissa shift $\overline{V}_i/\sqrt{gD|S_c-1|}$ takes length to diameter ratio into account completely.

Figure 10.51 shows $\overline{V}_i/\sqrt{gD|S_c-1|}$ plotted against d/D for these results in the 44 mm diameter pipeline for different L_c/d ratios and the solid curves represent superimposed analytical results. The analysis was determined using equation (7.133) and a coefficient of solid to solid friction (μ_f) of 0,32 was determined from 74 mm diameter pipeline tests. The agreement is good in spite of the fact that all the capsules were made of brass (except for the $d/D = 0,91$ capsules).

Since all the kinematic results obtained can be correlated by means of the capsule velocity and mean water velocity densometric Froude numbers as well as an abscissa shift of $\overline{V}_i/\sqrt{gD|S_c-1|}$, it appears as though the line slope (m) is independent of length to diameter ratio in the range tested. The most notable effects of length to diameter ratio (L_c/d) variation are:

1. As L_c/d decreases the capsule velocity increases at a particular mean water velocity. This occurs at all diameter ratios (see Figure 10.52).

2. However, Figure 10.48 of V_c against $\overline{V}$ for $d/D = 0,85$ appears to indicate that the situation tends to reverse at high mean water velocities.

Figure 10.51

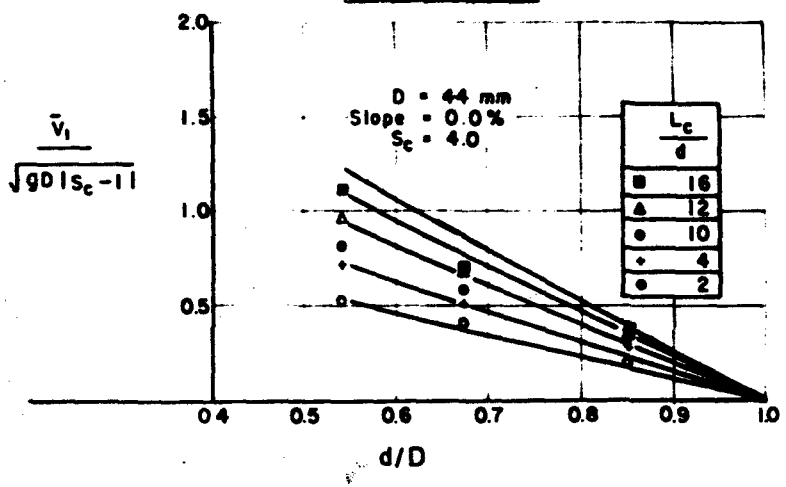

Figure 10.52

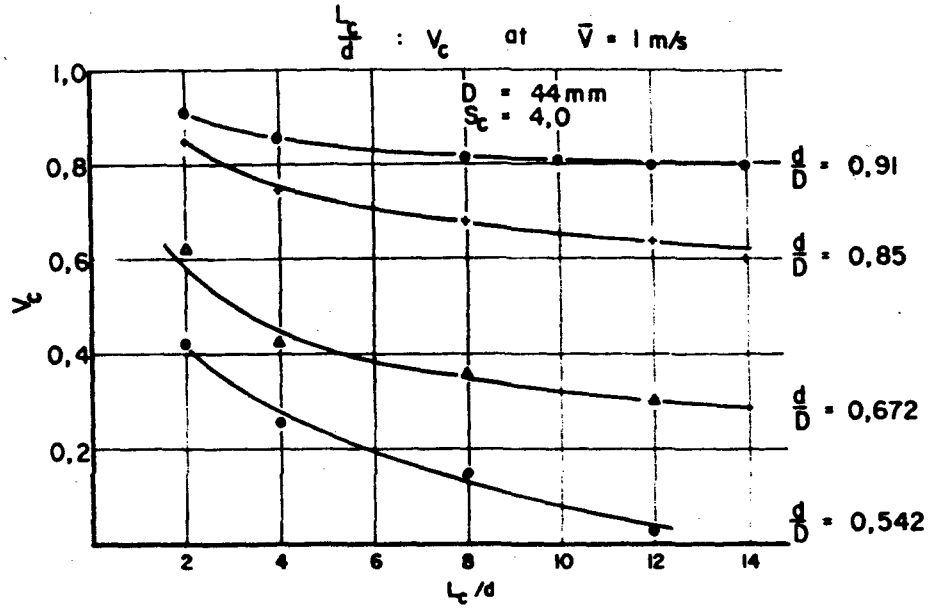

Figure 10.53

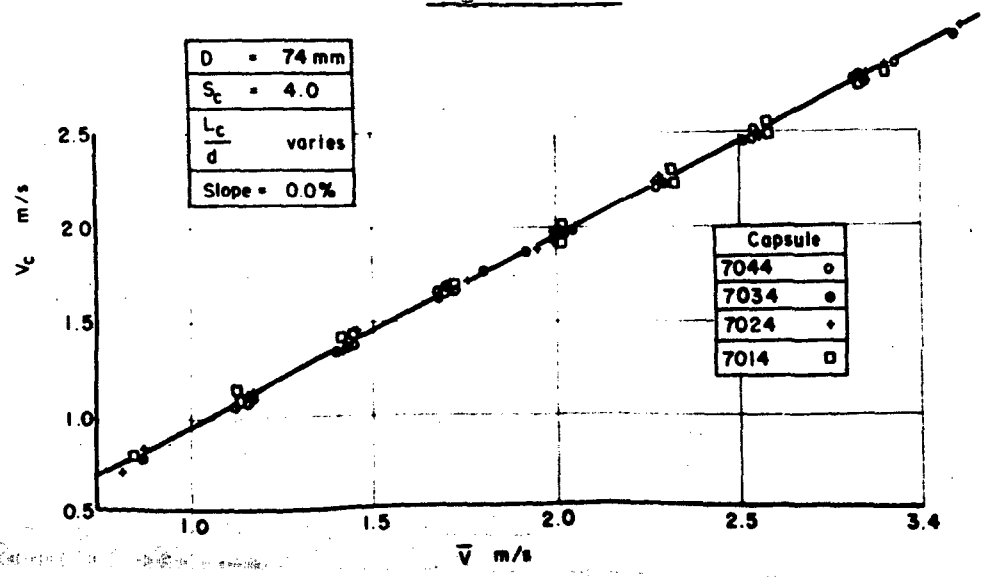

Figure 10.54

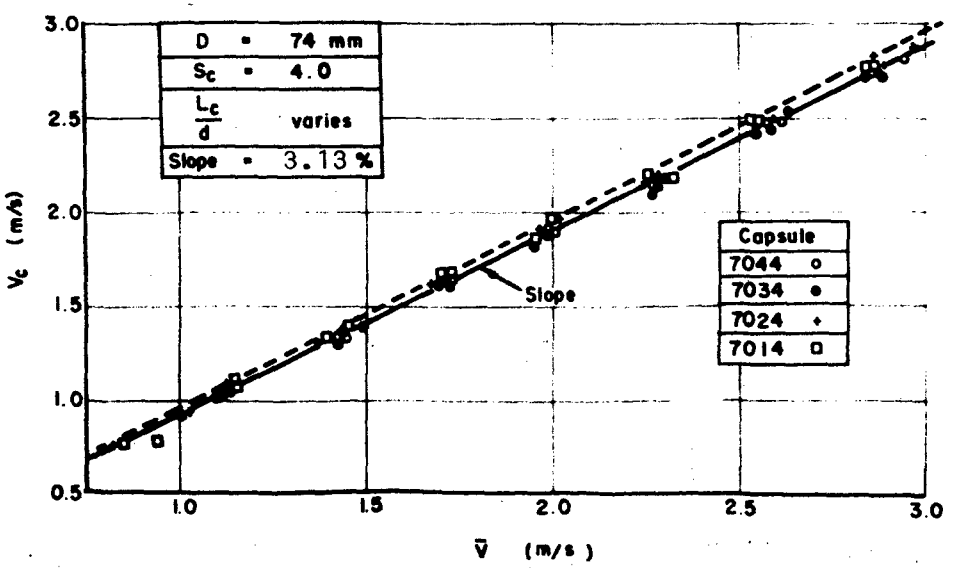

3. The effect of L_c/d variation diminishes as the diameter increases and is not detectable at high diameter ratio as can be seen from the curve for $d/D = 0,91$ on Figure 10.52. Figures 10.53 and 10.54 show V_c against $\overline{V}$ curves for capsules of length to diameter ratio varying from 1,0 to 4,0 in a horizontal and gently upward sloping pipeline (slope = 3,13%) and in these ranges the length to diameter ratio effect is eliminated. These were, unfortunately, preliminary tests which gave an initially wrong impression as to the effect of length to diameter ratio.

The above points can be explained thus: A decrease in the length to diameter ratio (all other variables being equal) implies a reduced capsule weight and hence reduced solid to solid friction. A greater drag is necessary to induce the capsule to reach the same velocity if the capsule length is increased, because of the greater solid to solid friction, and this implies increased mean water velocity for the same capsule velocity.

On the other hand, the longer the capsule, the greater the surface area. This has the effect of increasing form drag as well as skin friction drag due to pressure flow. And if the capsule tends to lift at high velocities the solid friction force is diminished.

When the capsule actually lifts the solid friction force disappears and the backward acting shear due to Couette flow decreases due to eccentricity reduction.

This explains the reversal trend mentioned earlier at high water velocities, i.e. the increased forward drag and decreased backward drag on a high (L_c/d) capsule tends to give it an advantage over lower (L_c/d) ratio capsules. This is an added argument for lift at high water velocities.

Far greater velocities would have been needed to clinch the argument at the high specific gravity $(S_c = 4,0)$ used in the experiments. This was

experimentally impossible in the closed circuit.

Figure 10.52 of L_c/d against V_c at $\overline{V}$ = 1 m/s shows the trends described above for low mean water velocities and represents a way of showing up the length effect for different diameter ratios.

9. The effect of pipeline slope on capsule velocity

The slope of the pipeline will be described as positive when sloping upwards in the direction of flow and negatively designated when sloping downwards in the direction of flow.

Initially, experiments were done on a rather mild slope variation (3,13%) with the large diameter capsules (d/D = 0,95) and slope did not appear to have much effect; see Figures 10.53 and 10.54. In the course of the following discussion the reason for this will become clear as trends are determined over a wide range of pipe slopes and using different diameter ratios.

Figures 10.40 and 10.55 to 10.57 show capsule velocity plotted against mean water velocity for the 74 mm diameter pipeline ranging in slope from 30.8% to -5,4%. Each set of graphs represents a different slope. Figures 10.58 to 10.61 show for each characteristic capsule (i.e. constant d/D, L_c/d and S_c) the capsule velocity plotted against mean water velocity for different slopes. These graphs were obtained from Figures 10.55 to 10.57 and data points are omitted.

9.1 The following noteworthy features were observed and will be discussed afterwards:

9.1.1 On all slopes the large diameter capsules travel faster, at the same mean water velocity, than the small diameter capsules. This is apparent when comparing the $V_c : \overline{V}$ graphs for each slope at varying diameter ratios (Figures 10.40 and 10.55 to 10.57).

9.1.2 Also from these graphs it is clear that the greater the slope of

Figure 10.40

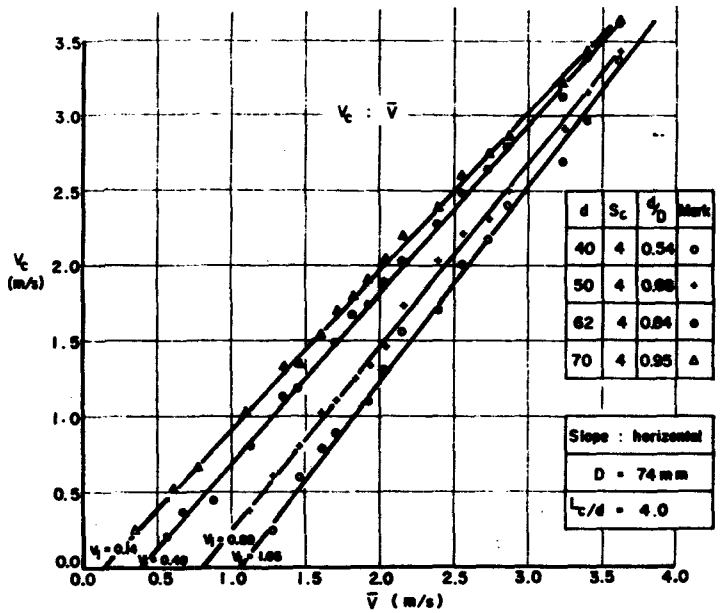

Figure 10.55

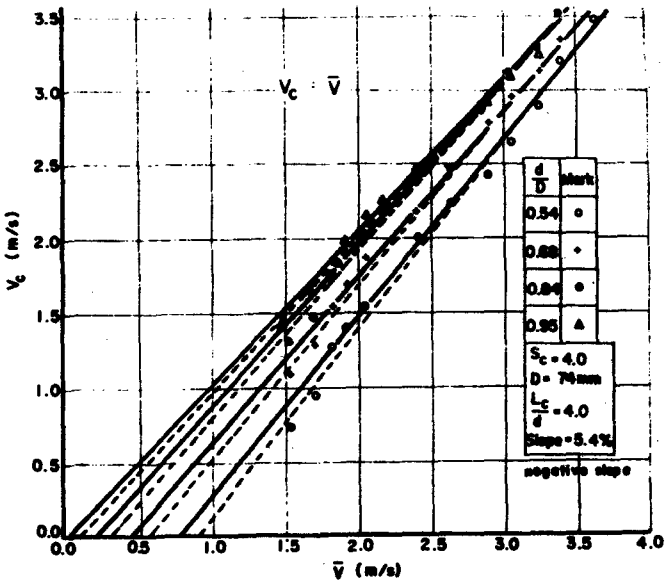

Figure 10.56

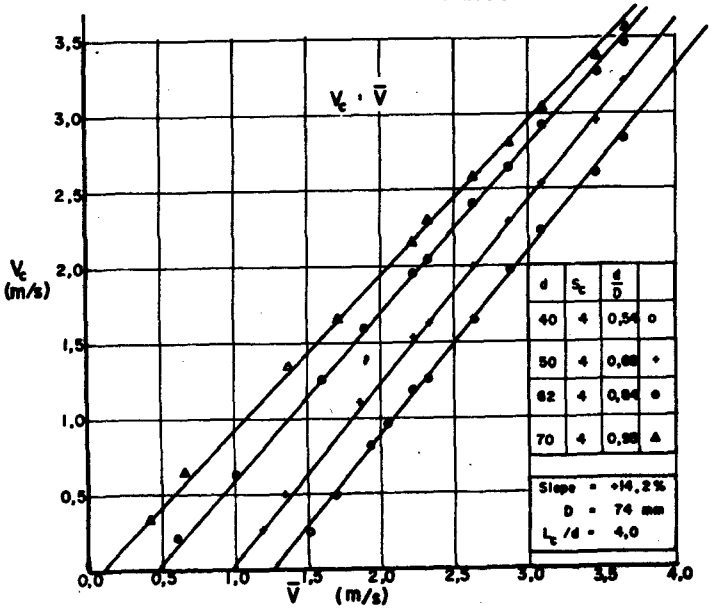

Figure 10.57

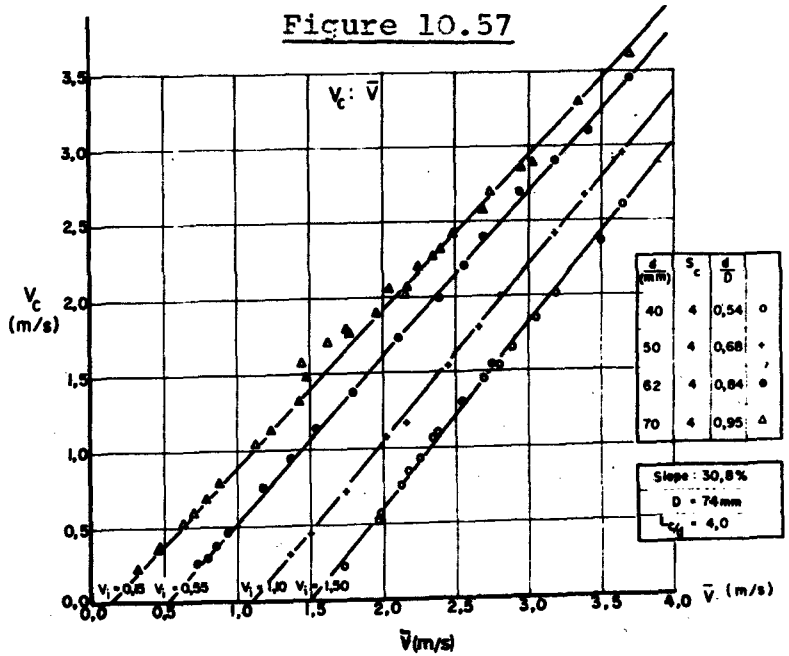

FIGURE 10.58

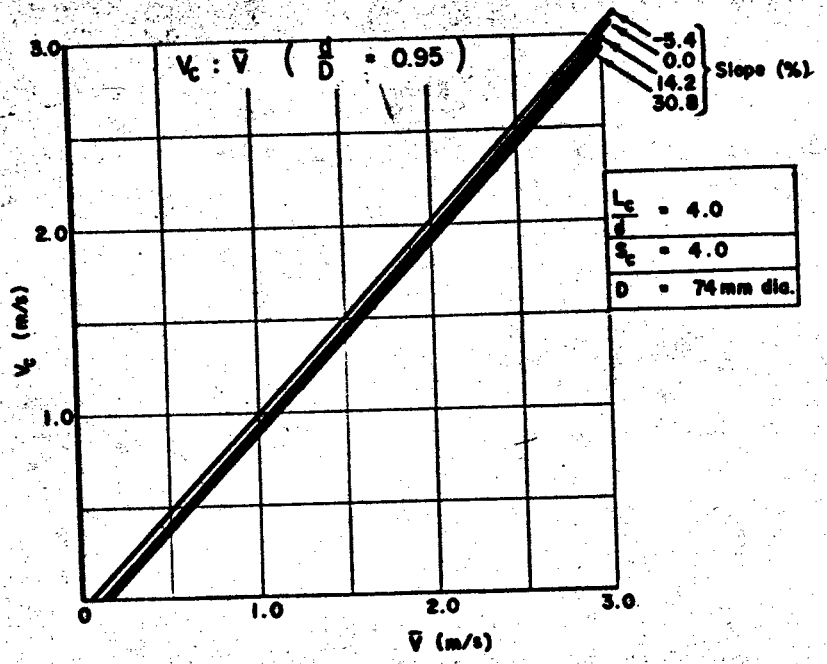

FIGURE 10.59

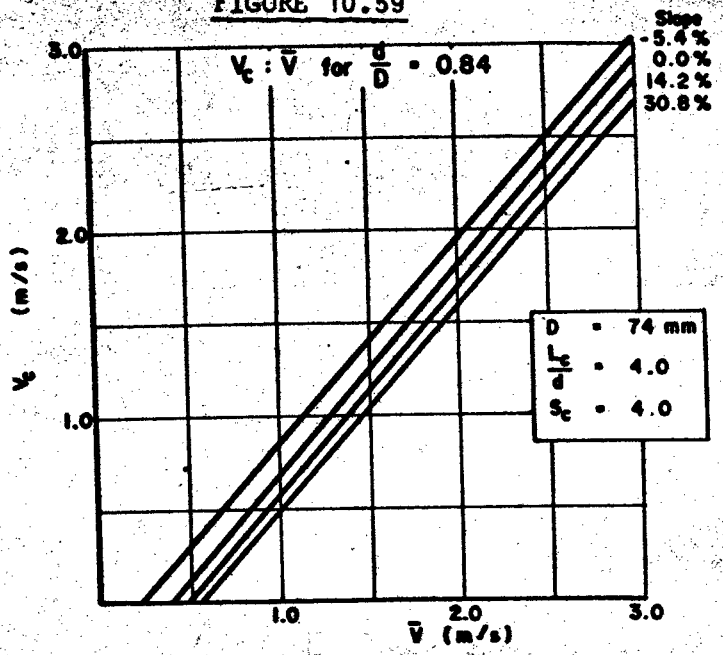

FIGURE 10.60

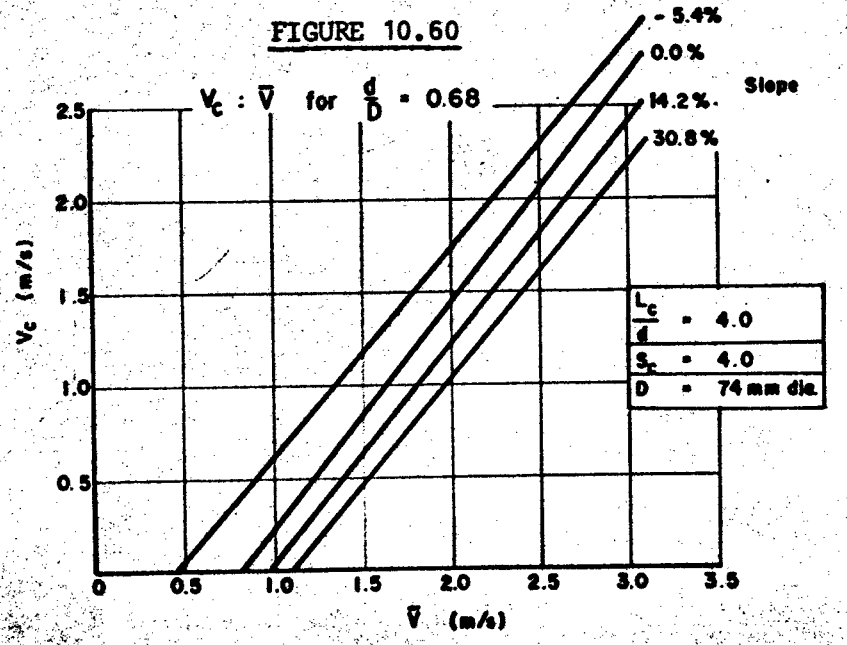

FIGURE 10,61

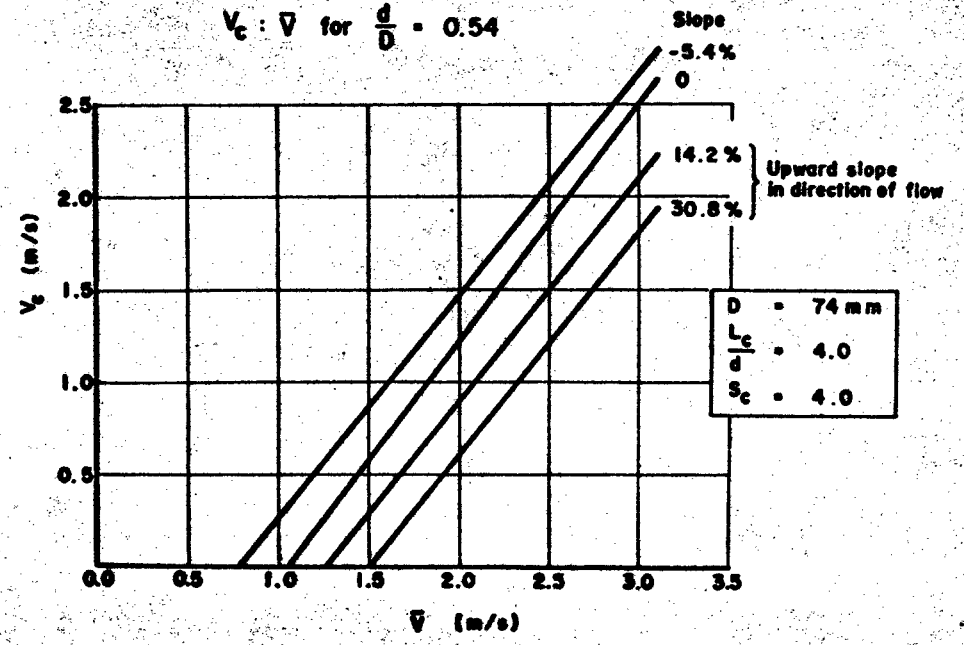

the pipeline, the greater the difference in capsule velocity at a particular mean water velocity as the diameter ratio varies. This can also be seen on Figure 10.62 of graphs of V_c against slope.

9.1.3 The trend tends towards reversal at high mean water velocities and it is clear that there is a tendency for the small diameter ratio capsules to catch up with the larger diameter ratios as the mean water velocity increases. This is illustrated by the cross plot on Figure 10.63.

9.1.4 The greater the slope the higher the mean water velocity at which the above reversal phenomenon occurs. At steeper pipeline slopes the small capsules will only overtake the large ones at extremely high velocities if at all. And at very steep slopes the large diameter capsules always travel faster than the small diameter ones just as at very steep negative slopes the small capsules will always travel faster than the large ones. It is hypothesised that these phenomena only occur at positive or negative slopes greater than the angle of static friction between the capsule and pipe wall. The capsules considered are of SG = 4,0.

9.1.5 From the graphs of $V_c : \overline{V}$ for different slopes at particular diameter ratios (Figures 10.58 to 10.61), it is obvious that as the diameter ratio increases the effect of slope is minimised. This is apparent from the plot of d/D against V_c shown on Figure 10.63.

9.1.6 It is also clear from Figures 10.58 to 10.61 that the linear relation of capsule velocity as a function of mean water velocity, is parallel at different slopes as long as the diameter ratio is held constant.

This point implies that an abscissa shift will account for slope variation as was the case for length to diameter variation. Also, support is added to the argument that the slope of the $V_c : \overline{V}$ line is dependent solely on the diameter ratio.

9.2 Explanation of the foregoing

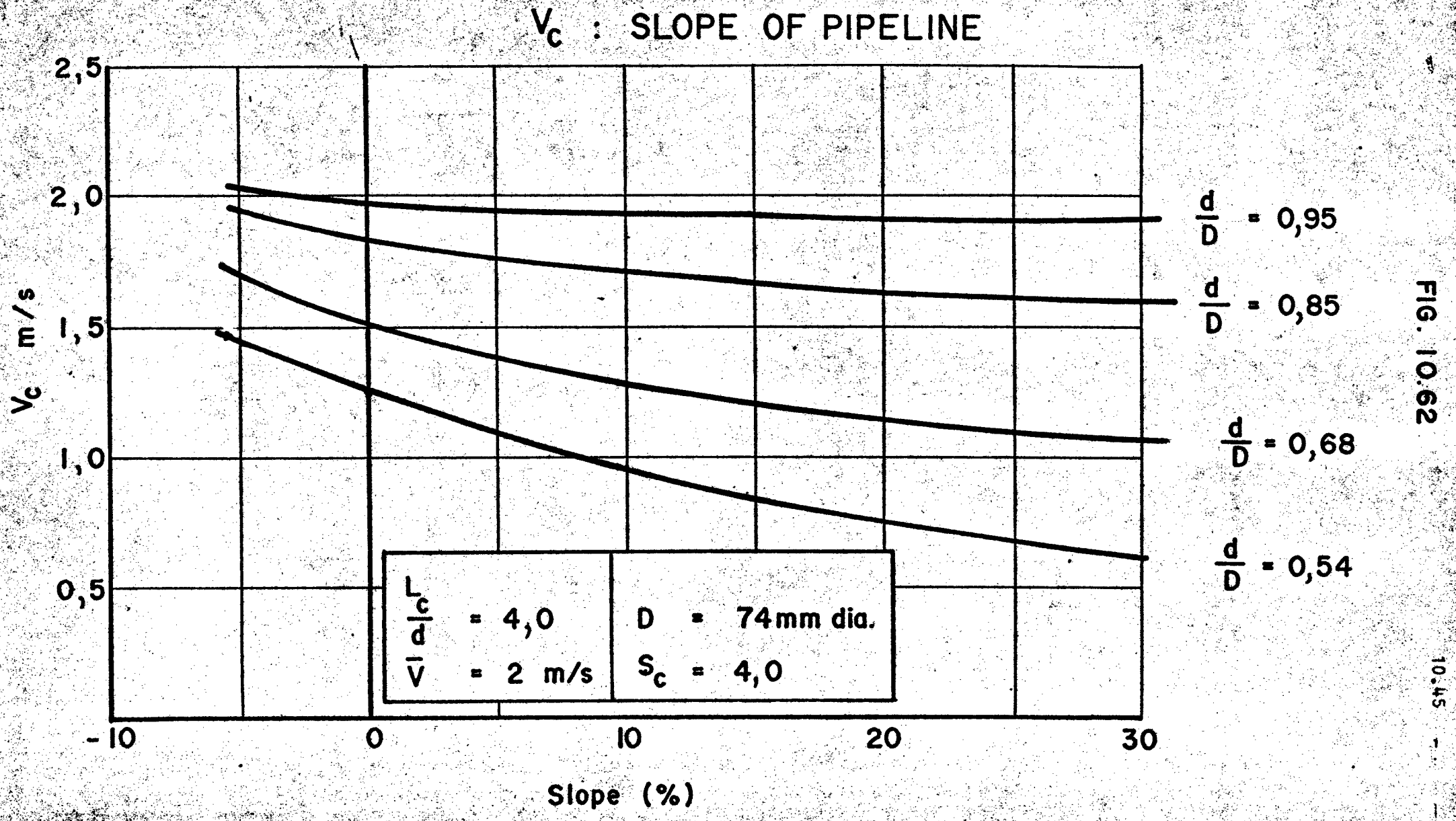
V_c : SLOPE OF PIPELINE
2,5
2,0
1,5
1,0
0,5
V_c m/s
-10
0
10
20
30
Slope (%)
$\frac{L_c}{d}$ = 4,0
$\bar{V}$ = 2 m/s
D = 74mm dia.
S_c = 4,0
$\frac{d}{D}$ = 0,95
$\frac{d}{D}$ = 0,85
$\frac{d}{D}$ = 0,68
$\frac{d}{D}$ = 0,54

FIG. 10.62

FIG, 10.63

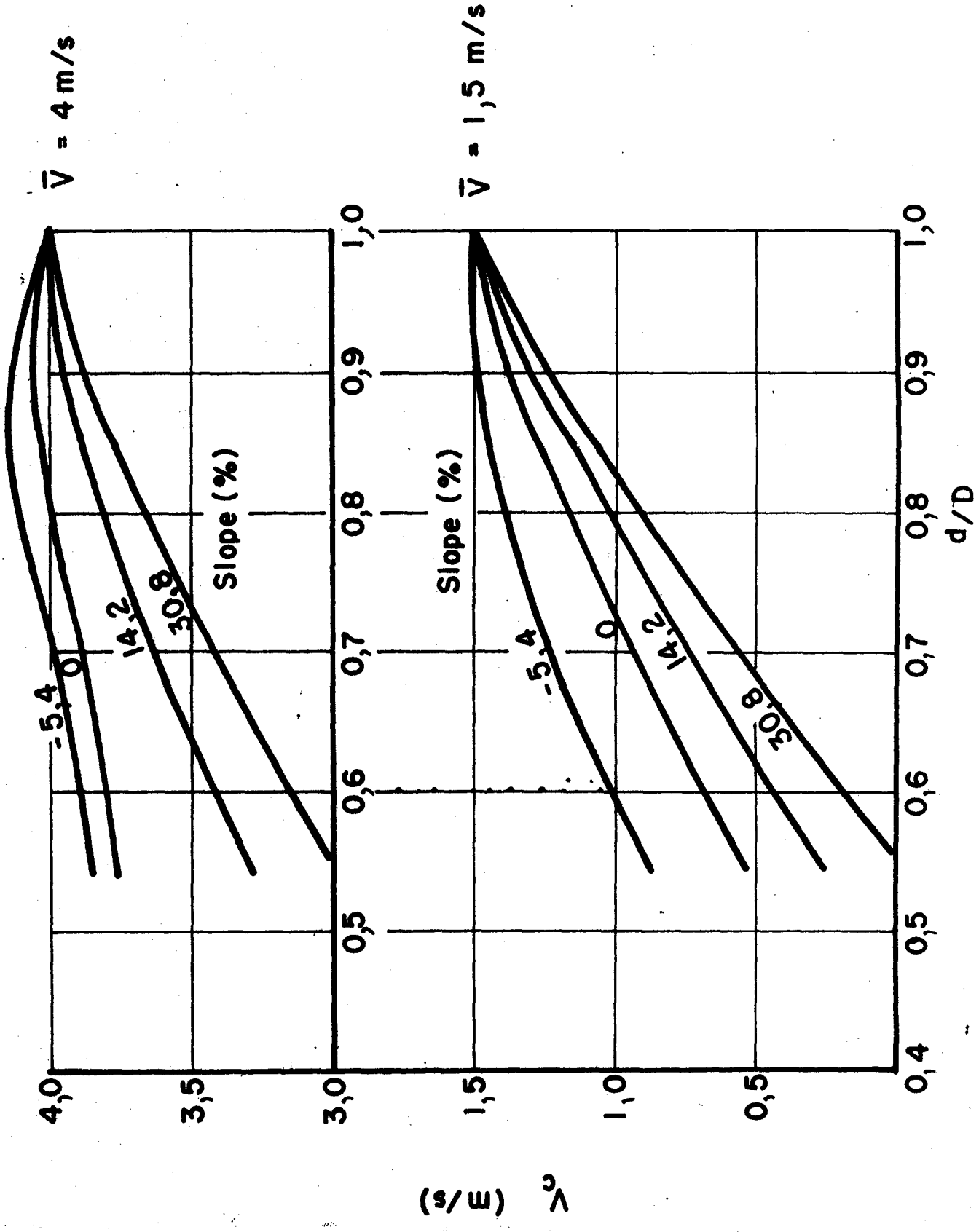
$\bar{V}$ = 4 m/s
$\bar{V}$ = 1,5 m/s
Slope (%)
-5,4
0
14,2
30,8
d/D
V_c (m/s)
4,0
3,5
3,0
1,5
1,0
0,5
0,4
0,5
0,6
0,7
0,8
0,9
1,0

The large diameter capsules tend to travel faster than small diameter capsules at low velocities since there is a greater water drag on the large capsules due to greater frontal and surface area. If the small diameter capsules tend to lift as they speed up, the combined effect of moving towards the high velocity zone in the centre of the pipe as well as the reduced solid to solid friction, causes the tendency of the small diameter capsules to overtake the larger ones.

Slope reduction causes a greater velocity increase for the small capsules than the large capsules as mean water velocity is increased. Consequently, the large diameter capsules decrease speed at a reduced rate as slope is increased. This is due to the dash pot effect as well as reduced solid friction forces as slope is increased due to a reduction in the pipe wall to capsule reaction force. It is easily seen in the extreme case of the vertical pipe when there is very little slip of large capsules relative to the water and an increasing amount of slip as diameter ratio decreases. Thus, in the extreme slope conditions, viz. vertically up and vertically down, the large capsules travel consistently faster in the former case and the small capsules travel consistently faster in the latter case (for $SG > 1,0$).

The above explains why small capsules overtake large capsules at increasingly higher water velocities and the phenomenon is more pronounced as a pipe slope decreases, not occurring at steep positive slopes and occurring consistently at steep negative slopes (for the range of velocities tested).

In the equation for capsule velocity (V_c) as a function of mean water velocity and other variables, the incipient velocity is an important variable and non-dimensional incipient velocity is plotted against diameter ratio on Figure 10.64 with slope as parameter. The incipient velocity is significantly dependent on slope at low diameter ratios. But the dependence

FIG . 10.64

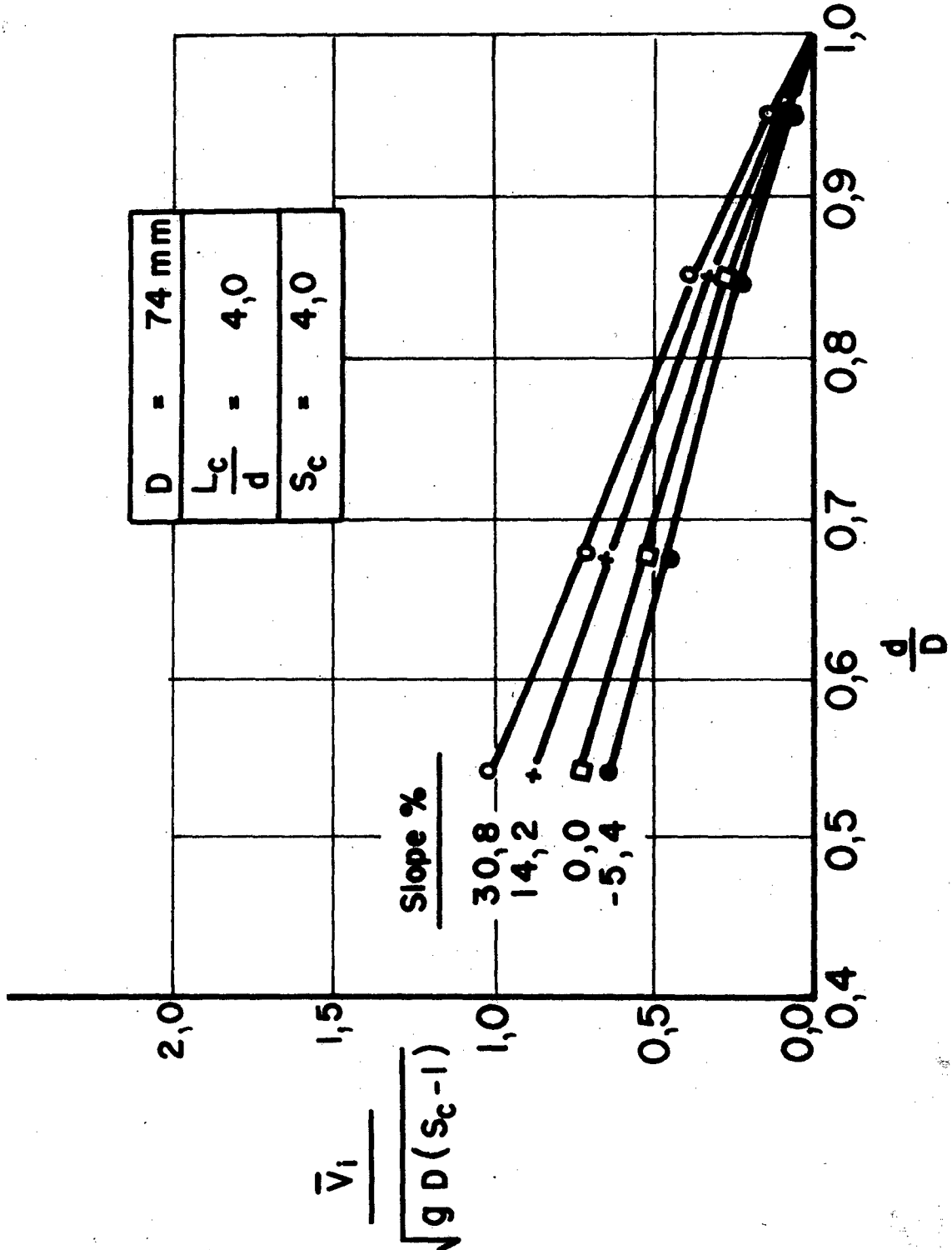
D = 74 mm
Lc/d = 4,0
Sc = 4,0
Slope %
30,8
14,2
0,0
-5,4
V̄i / √(g D (Sc-1))
d/D
2,0
1,5
1,0
0,5
0,0
0,4
0,5
0,6
0,7
0,8
0,9
1,0

decreases as diameter ratio increases. Initial tests carried out on a 3,13% slope with the large diameter capsules thus failed to reveal significant slope effects and it is clear from Figure 10.64 together with Figure 10.58 why this is so.

9.3 Kinematics of capsule flow in a vertical pipe

The relation between capsule velocity and mean water velocity is easier to deal with for vertical pipes rather than horizontal or sloping ones. The settling or slip velocity can be determined from equation (7.146) for incipient velocity of capsule flow in a vertical pipe. Thereafter any increase in mean water velocity results in a corresponding increase in the capsule velocity (see Figure 10.65).

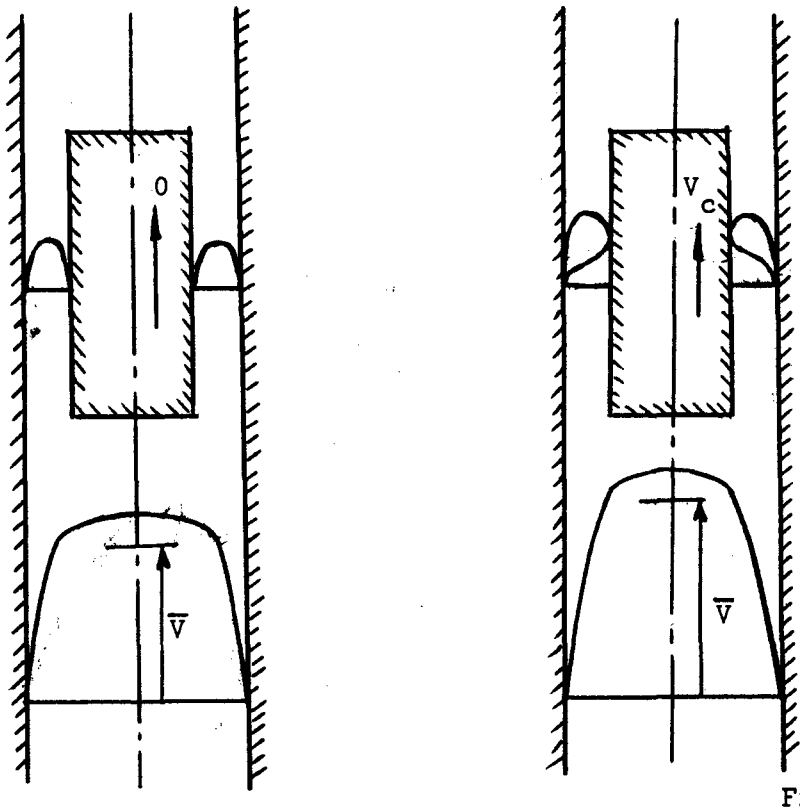

Figure 10.65

Assume that the capsule is neutrally buoyant and concentrically orientated so that the slip velocity is zero, i.e. $\overline{V}_i = 0$. The capsule moves with the water and its velocity corresponds to the velocity of the streamline field in which it is situated. For $d/D \to 0$ the capsule moves at a velocity corresponding to the central streamline, i.e. $V_c \to V_{max} \doteqdot 1{,}22\ \overline{V}$.

For $d/D \to 1$, $V_c \to \bar{V}$. For practical diameter ratios the neutrally buoyant capsule velocity (V_c) is between unity and 1,22.

The two situations, i.e. incipient velocity analysis and concentric neutral buoyancy analysis can be superimposed to obtain an analytical version of $\bar{V}$ versus V_c relation. The former has been dealt with and the latter can be considered by using equation (2.8) derived by Charles (reference 10) for turbulent flow in the annulus.

Unfortunately Charle's equation ignores the existence of a laminar sublayer at the capsule wall and assumes that the capsules are infinitely long and neutrally buoyant. Although his theory is not satisfactory for calculating capsule velocities, it can be used for determining the average velocity of the water field occupied by the capsule. This gives the slope of the $V_c : \bar{V}$ curves. And the analysis for incipient velocity gives the abscissa shift and these two devices, when combined, yield an analytical version of $\bar{V}$ versus V_c for finite capsule flow in vertical pipes.

Figures 10.66 to 10.69 show experimentally determined curves for two diameter ratios, three SG's and five length to diameter ratios. Also shown on the curves are the slopes of the $\bar{V} : V_c$ lines as determined from equation (2.8). The comparison between theory and experimentally determined incipient velocities for vertical pipes will be dealt with in Chapter 14.

Figures 10.66 and 10.68 (for two different diameter ratios) show capsule velocity as a function of mean water velocity with SG as parameter, and, as expected, decreasing the SG yields a higher capsule velocity at a constant value of $\bar{V}$.

The abscissa shift is achieved by means of the incipient velocity calculation and the slope is determined as described above.

Figures 10.67 and 10.69 show the effect of length to diameter ratio

FIGURE 10.66

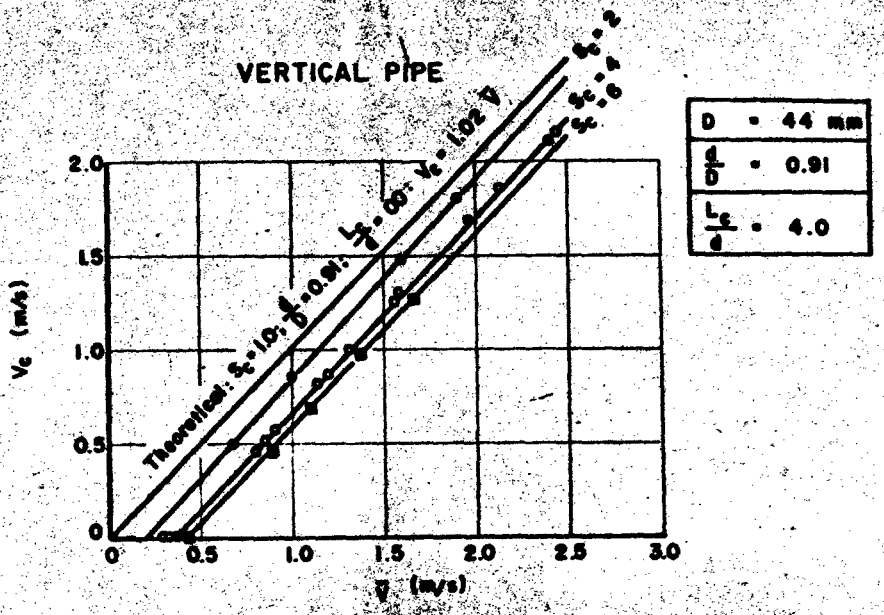

FIGURE 10.67

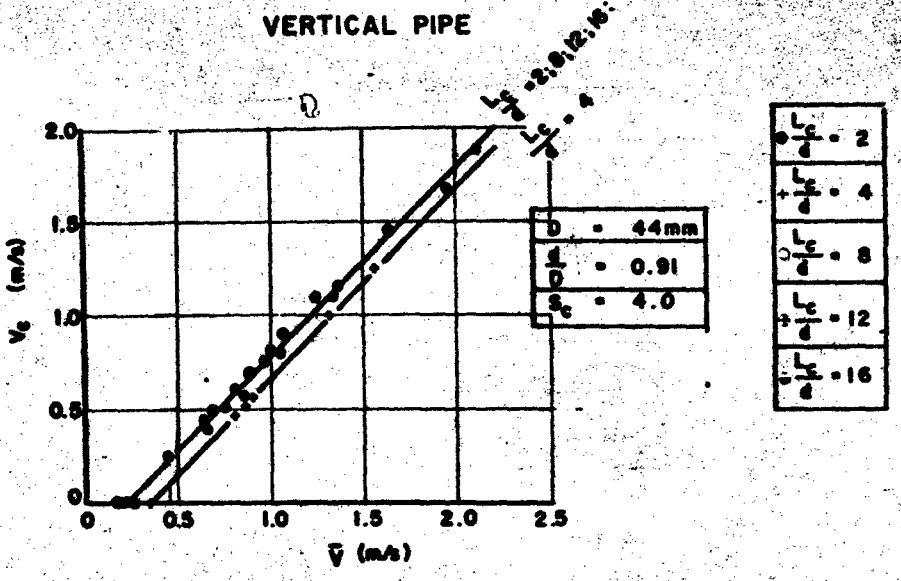

FIGURE 10.68

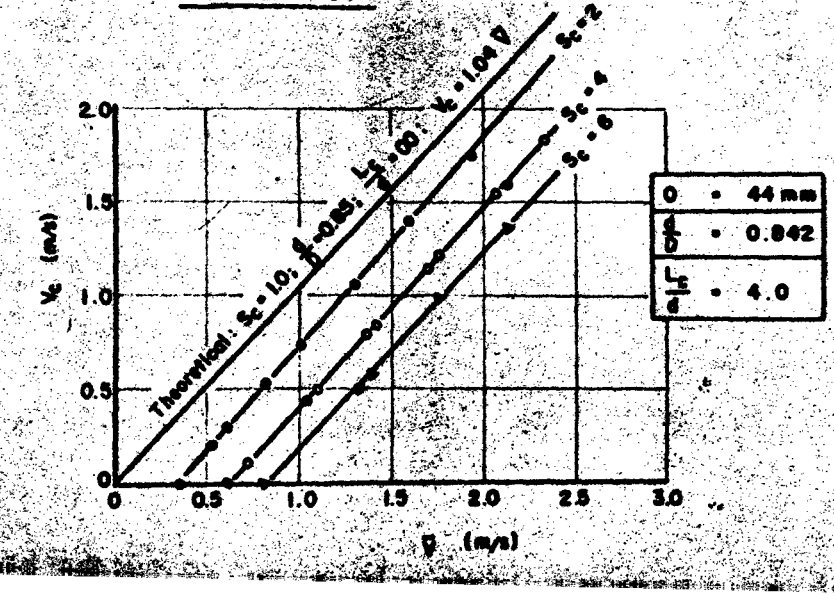

FIGURE 10.69

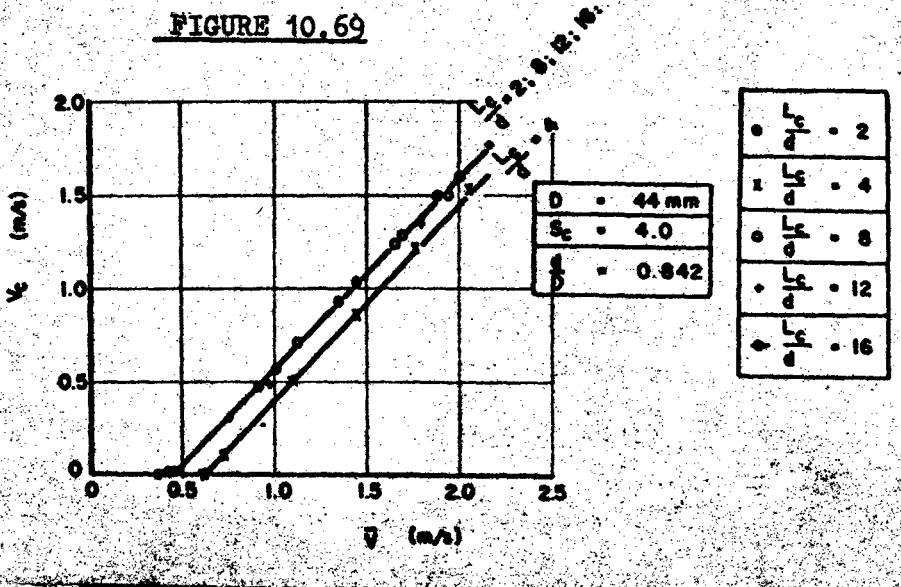

(L_c/d) and in both cases the $L_c/d = 4,0$ curves are below those for the other L_c/d values, i.e. $L_c/d = 2; 8; 12$ and 16 which are coincident. This does not agree with the theoretical determination of incipient velocity (see Chapter 14) which should cause an increase in mean water velocity at a fixed capsule velocity as L_c/d increases.

One reason for the discrepancy is that the analysis (for $\overline{V}_i$) was based on concentricity. Whereas the shortest capsule ($L_c/d = 2$) was, more often than not, skewed across the pipeline with its axis not parallel to the pipe axis (see Figure 11.60b).

A reason for the discrepancy for the train of capsules ($L_c/d > 4$) is that to achieve the train (of $SG = 4$) a lighter capsule was placed at the bottom and a heavier one at the top (thus for $L_c/d = 16$ the sequence from bottom to top was $S_c = 2; 4; 4; 6$).

With these four capsules not being concentric (see Figure 11.61a), the equations for inlet, outlet and annular head losses could be considerably modified when compared with those used for concentric capsule analysis to compute the incipient velocity.

10. The effect of roughness (μ_f)

The coefficient of solid to solid static friction (μ_f) is defined as the ratio of the force required to just move a capsule in a horizontal pipe to the component of capsule weight downwards, the capsule and pipe wall both being wet.

The experimental procedure for determinig μ_f was to find the slope (α) of the appropriate pipe down which the capsule just begins to slide; in which case

$$\mu_f = \tan \alpha$$

Smooth and rough capsules were tested in the 74 mm and 44 mm diameter pipelines.

A 76 mm diameter asbestos cement pipe was also used with smooth and rough capsules.

Experiments were conducted to determine the coefficient of solid to solid static friction and the following values were obtained.

pipeline diameter	μ_f	
perspex 74 mm	0,32	smooth PVC
perspex 44 mm	0,32	smooth } brass rough }
	0,39	smooth } PVC rough }
Asbestos 76 mm	0,44	capsule 7044 R
	0,411	capsule 6244 R
	0,393	capsule 4044 R

The above values were repeatable to within about 15%.

Figures 10.70 to 10.73 show capsule velocity plotted against mean water velocity for rough capsules in the 44 mm diameter pipeline. The curves for smooth capsules are superimposed and in general the rough capsules have a slightly higher capsule velocity at the same mean water velocity than the smooth capsules, although it is difficult to draw firm conclusions. The reason for this will be explained later in this section.

Figure 10.74 shows the non-dimensional incipient plot (for smooth and rough capsules in the 44 mm diameter pipeline) and it is clear that nothing definite can be concluded showing that roughening the capsules in this way has little effect on the incipient velocity.

The 74 mm diameter perspex pipeline was then used for experiments with rough capsules in order to (try and) exaggerate the effects slightly and Figure 10.75 shows the capsule velocity against mean water velocity for

FIGURE 10.70

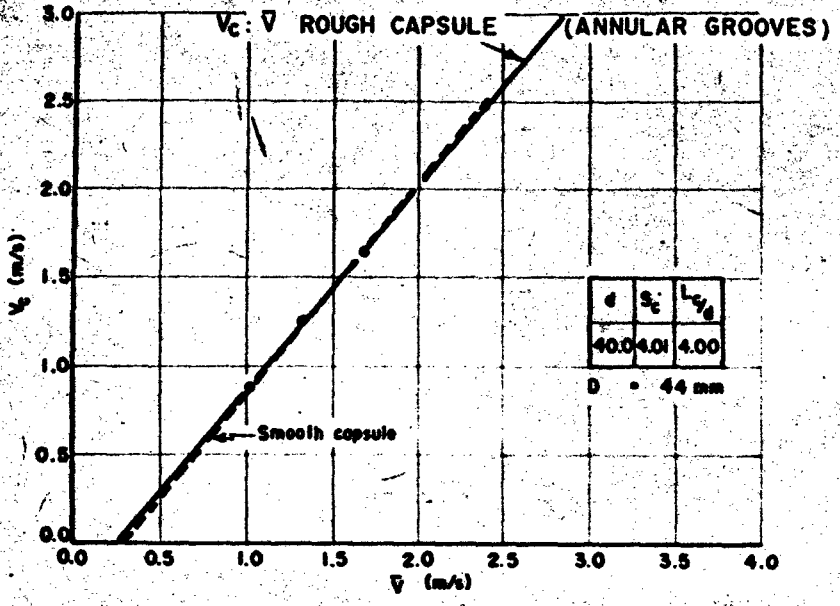

FIGURE 10.71

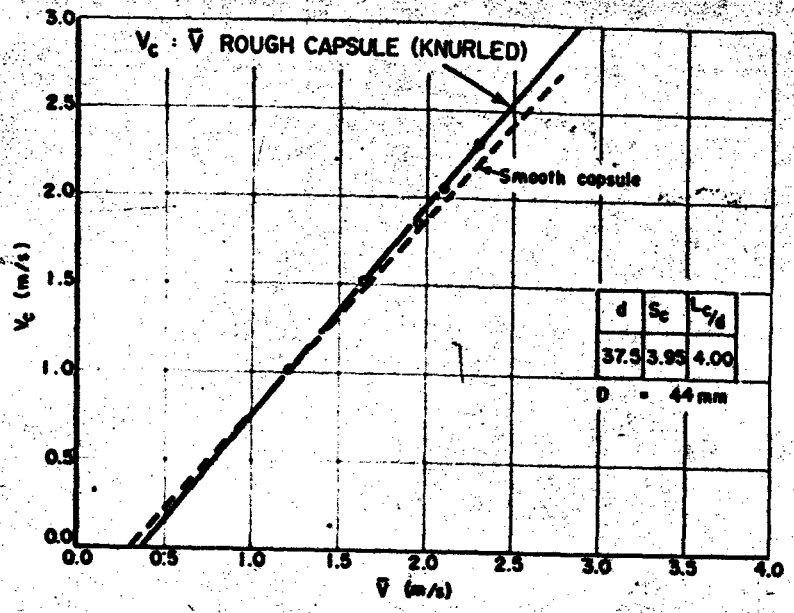

FIGURE 10.72

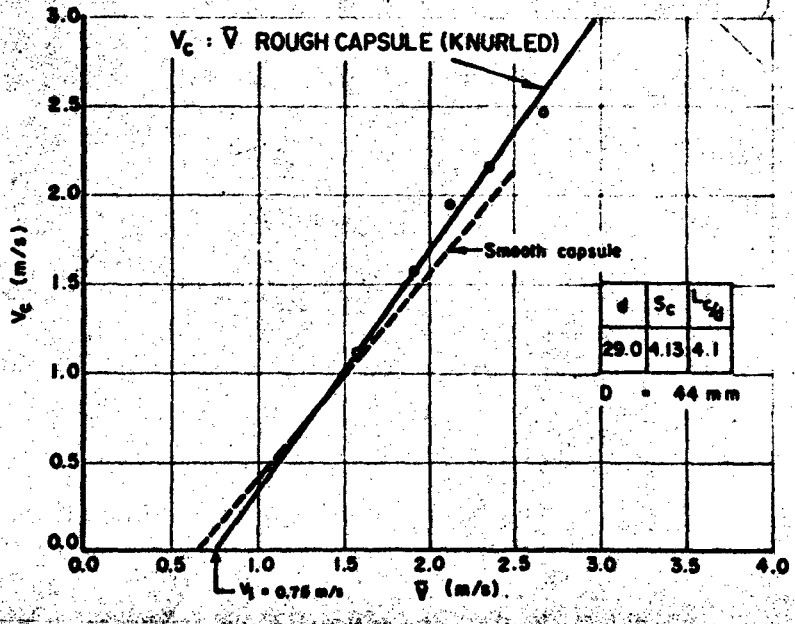

FIGURE 10.73

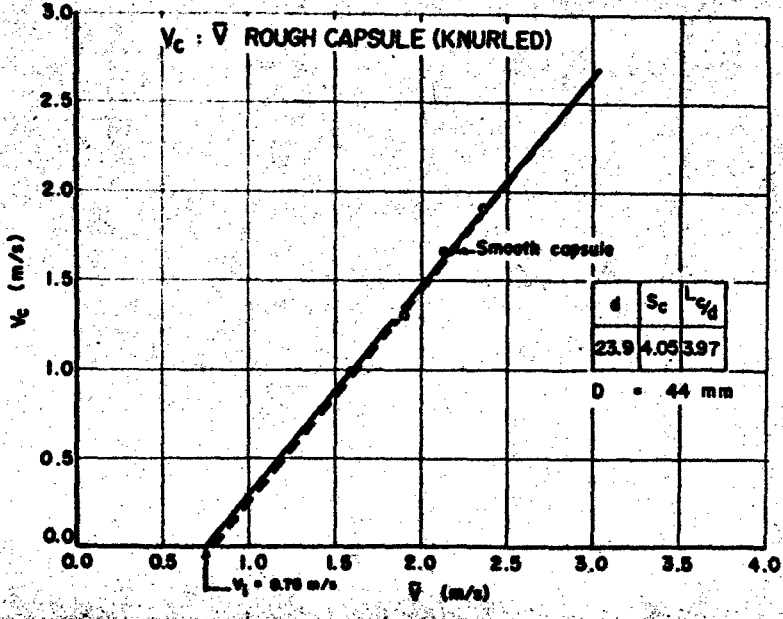

FIGURE 10.74

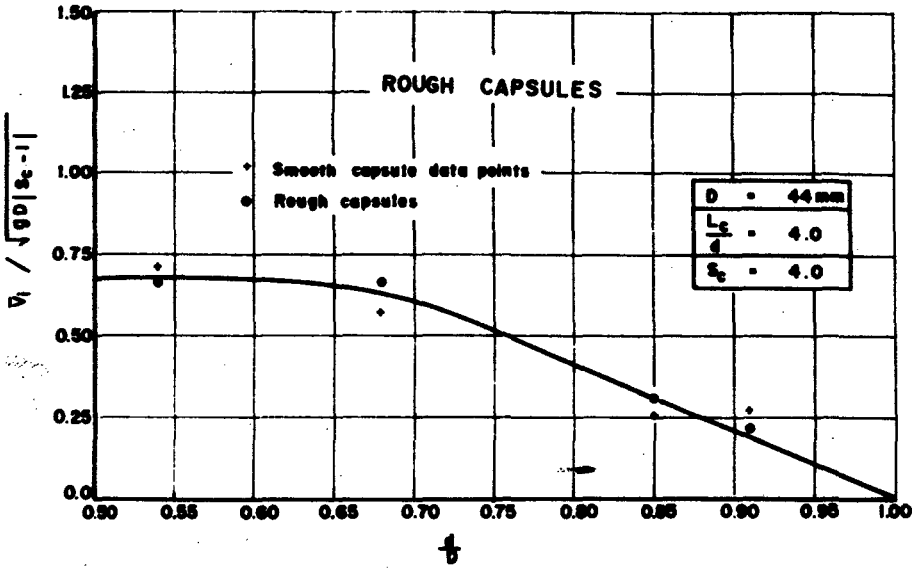

FIGURE 10.75

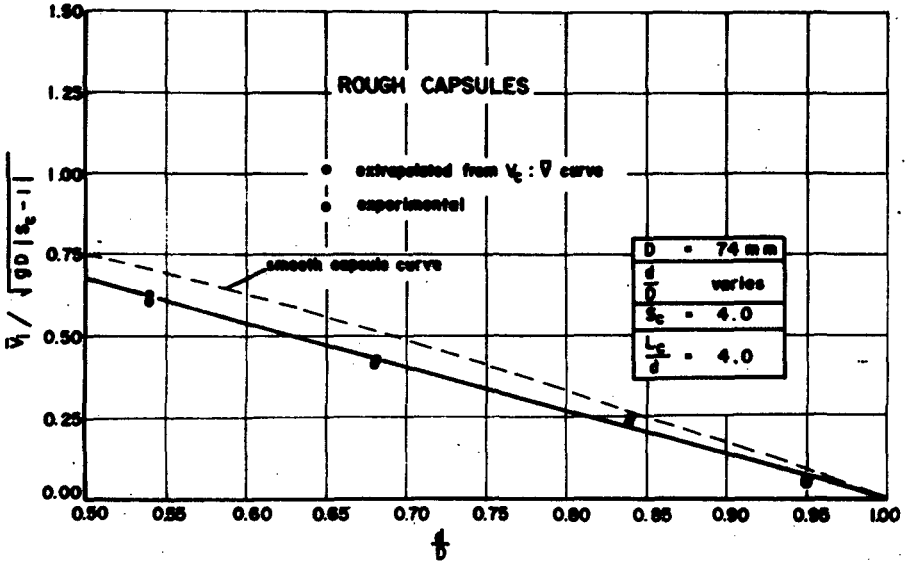

FIGURE 10.77

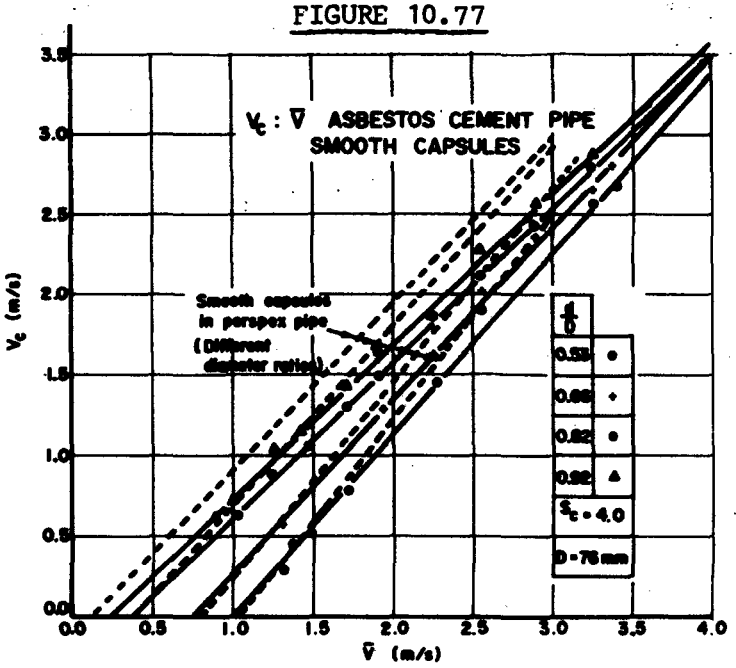

FIGURE 10.78

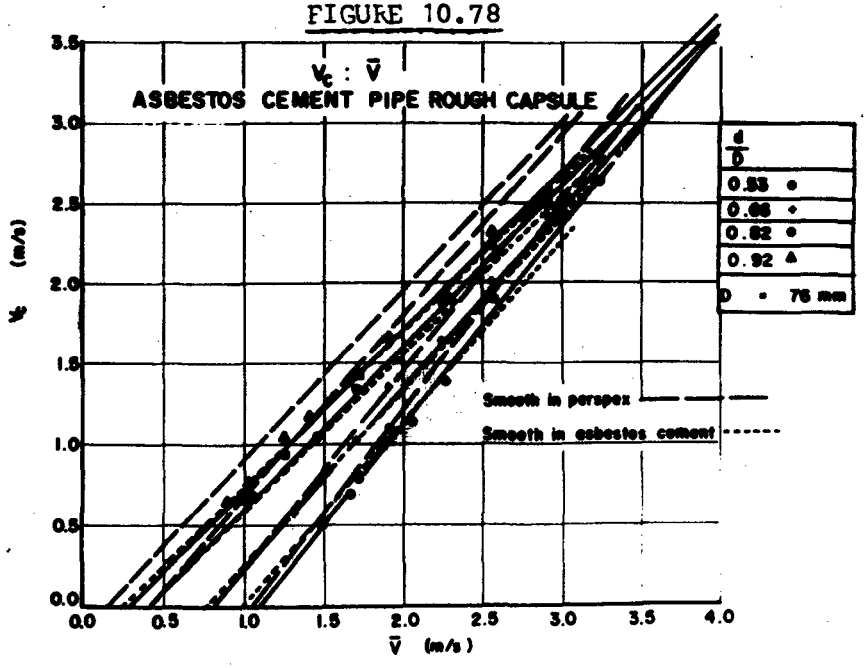

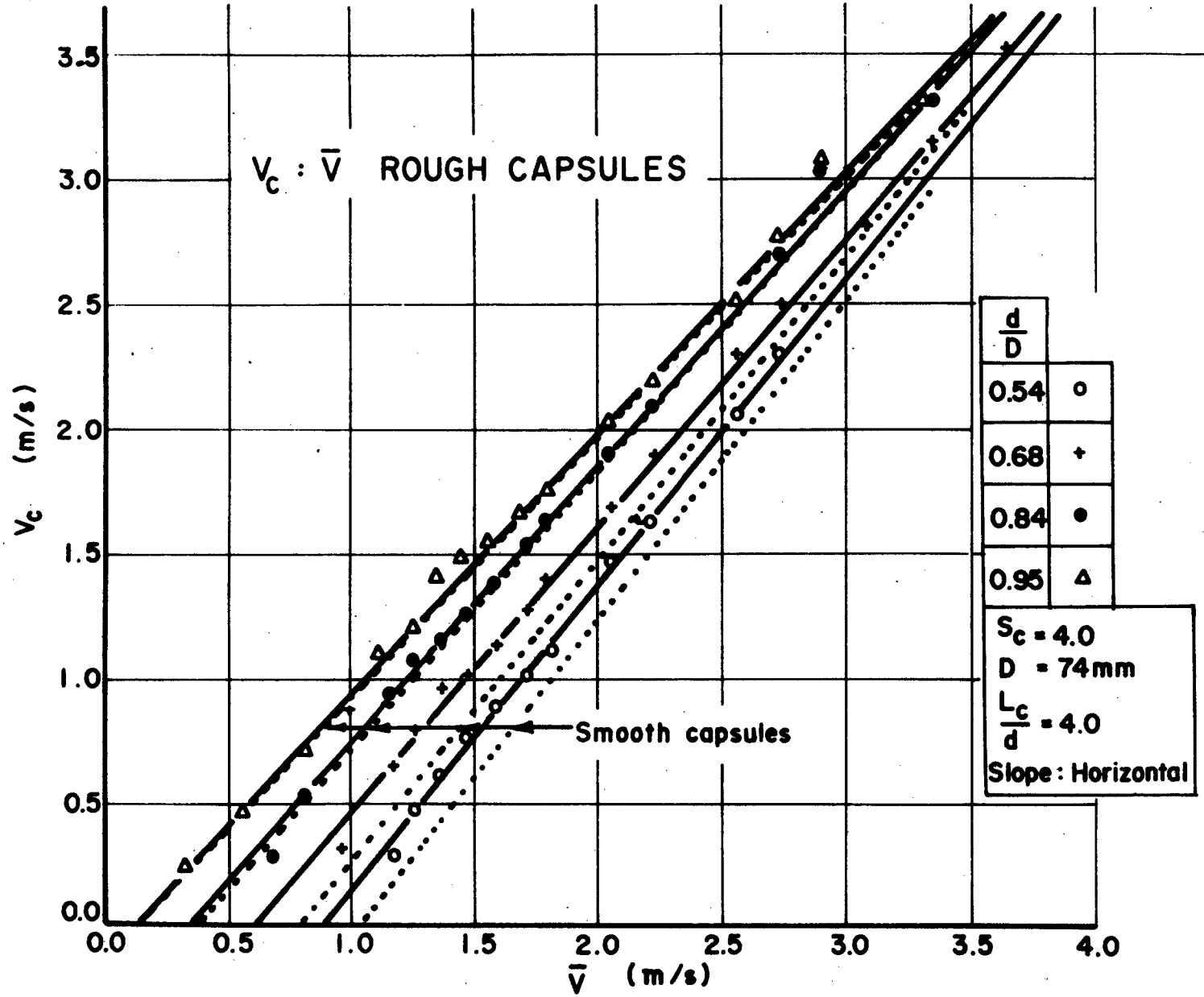
$V_c : \bar{V}$ ROUGH CAPSULES
V_c (m/s)
$\bar{V}$ (m/s)
0.0
0.5
1.0
1.5
2.0
2.5
3.0
3.5
4.0
Smooth capsules
d/D
0.54 o
0.68 +
0.84 ●
0.95 Δ
S_c = 4.0
D = 74mm
L_c/d = 4.0
Slope : Horizontal

FIG. 10.75

the four different diameter ratio rough capsules. The dotted lines represent smooth capsules and it is clear from this diagram that the rough capsules travel faster than the smooth capsules in all cases.

This, apparently startling, conclusion will be discussed later in this section. It is apparent from Figure 10.76 that incipient velocities are higher for smooth than rough capsules and from Figure 10.75 that the $V_c : \overline{V}$ line slope (m) is independent of roughness. Although, this independency is not born out by the tests in the 44 mm diameter pipe.

An asbestos cement pipe was utilised in an attempt to exaggerate effects yet further in a rough pipe. As Photo cells could not be used for measuring capsule velocities in a non-transparent pipe, Pulsotronic solid state proximity switches were substituted. These are electro-magnetic devices and a non-conducting pipe material is obligatory. The only types of piping material readily available in this sort of size and satisfying the above requirements is asbestos cement and P.V.C. The former was chosen because of its greater roughness.

Figure 10.77 shows capsule velocity plotted as abscissa against mean water velocity for smooth capsules in the asbestos cement pipe. And superimposed on these curves are those for smooth capsules in the perspex pipe.

The capsules in the perspex pipe appear to travel faster than those in the asbestos cement pipe. However, the incipient velocities are very much the same with a tendency towards higher incipient velocities for the capsules in the perspex pipe at low diameter ratios.

A similar tendency is found by examining Figure 10.78 where capsule velocity is plotted against mean water velocity for rough capsules in the asbestos cement pipe. The dotted lines represent smooth capsules in the asbestos cement pipe and the dashed lines are for smooth capsules in the perspex pipe.

The above phenomena can be accounted for as follows:

The comparison of smooth and rough capsules in the 44 mm diameter perspex pipeline must be considered in the light of the following factors.

Firstly, the solid to solid static friction factors for rough capsules in the smooth pipe showed little difference from smooth capsule friction factors. If anything, the latter values of μ_f were slightly higher than the former. Secondly, the skin friction drag on the rough capsules is obviously higher than on smooth ones. Even though this may be a small percentage of the total forward drag (depending on capsule length), it is enough to account for the higher capsule velocities experienced by the rough capsules. Figure 10.75 shows this effect repeated for the 74 mm diameter pipeline and the effect mentioned above is exaggerated on the larger scale. The higher incipient velocities for the smooth capsules which are shown on Figure 10.76 are also explained by the above reasoning.

If form drag is the dominant fluid force for a static capsule then incipient velocities should be higher for a rougher capsule due to a greater solid to solid friction force. This effect is balanced because skin friction drag is greater for rough than smooth capsules causing incipient velocity to be less for smoother capsules.

The observations made on the comparison of smooth capsules in the asbestos cement pipe with smooth capsules in the perspex pipe are not very conclusive. It does seem as though the smooth pipe capsules overtake the rough pipe capsules. However, the difference is not great when cognisance is taken of the fact that the dotted lines on Figure 10.77 are for diameter ratios that are higher than the solid lines, since the asbestos cement pipe diameter is greater than the diameter of the perspex pipe and it has been shown that capsule velocity is dominantly affected by diameter ratio.

The observations made on the rough capsules in the asbestos cement pipe (Figure 10.78) reaffirm that even for a situation where the static friction factor is significantly higher than for smooth capsules on smooth pipes, the rough capsules in the asbestos cement pipe do travel, in general, faster than the smooth capsules although there does appear to be a slight reversal of this tendency at low mean water velocities.

It appears from the above that regularly roughened capsules do not have a great influence on capsule velocity even when in an asbestos cement pipe, which has a different texture from the perspex pipe. The roughness experiments were limited in scope and since the effects appear to be small the effect of roughness may only be established with artificially roughened pipes on a large scale. This would be warranted only if a pilot scale test becomes necessary.

11. The effect of capsule spacing

Ten capsules all dimensionally similar numbered 7034 with d = 70 mm; S_c = 4,0 and L_c/d = 3,0 were used in the 74 mm diameter perspex line. The injector was loaded with all ten capsules and for each flow the injector was operated at different rotational speeds; increasing until the injector jammed. A stop watch was started when the first capsule passed a convenient point and stopped as the tenth capsule passed the same point. The capsule spacing could thus be calculated from this statistic together with the capsule velocity (V_c).

The injection rate I in capsules per second is related to the spacing length between capsule centres (L_s) thus;

$$I = V_c/L_s \qquad (10.3)$$

The linear concentration (C_L) or length of pipe occupied by capsules as a fraction of the whole pipe is

$$C_L = L_c/L_s \qquad (10.4)$$

The numerical concentration (C_N) is the number of capsules as a fraction of 1 metre

$$C_N = I/V_c = 1/L_s \qquad (10.5)$$

Figure 10.79 shows the linear concentration (C_L) plotted against capsule velocity (V_c) with $\overline{V}$ as parameter. The capsules tested had a length to diameter ratio of $L_c/d = 3,0$ and the concentrations on the extreme right represent maximum injection rates achievable without jamming the injector, at the highest injection rate of $I \doteqdot 3,15$ capsules/s.

The capsule velocity appears to be slightly lower than for the lowest injection rate (represented by a solitary capsule in the line). The difference is comparatively small, of the order of 6%, but fairly consistent although the difference occurs mainly at the highest velocities which are, incidentally, the most unreliable. The linear concentration appears to have less effect on V_c as velocity ($\overline{V}$) decreases.

The range of velocity change with concentration can be seen from Figure 10.80 where the two extreme linear concentration values of 5% and 20% are shown, without data points. It appears as though concentration increase causes lower capsule velocities at higher water velocities.

Figure 10.81, which shows the velocity ratio plotted against the mean water velocity in the pipe indicates that the scatter at a particular concentration is, in fact, no more than that due to the concentration effect. Thus for concentrations of the order of magnitude shown on Figures 10.79 and 10.81 the concentration has little effect on the capsule velocity at a particular mean water velocity.

In order to obtain further readings with spaced capsules the 40 mm diameter capsules were tested in the 44 mm diameter pipe. In all cases the specific gravity values were $S_c = 4,0$ and capsules were of length to diameter ratio of $L_c/d = 4,0$.

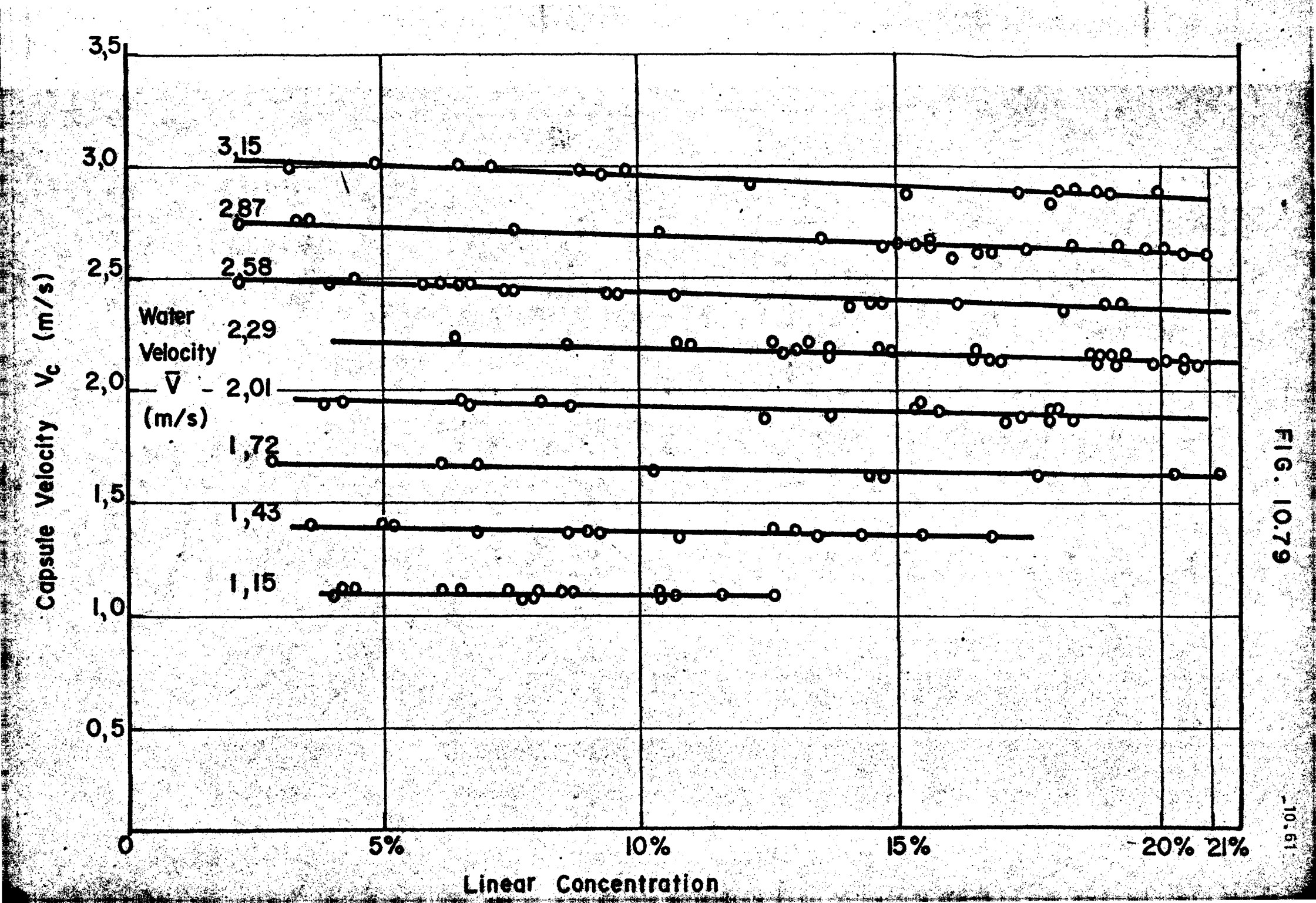
3,5
3,0
2,5
2,0
1,5
1,0
0,5
0
5%
10%
15%
20%
21%
Capsule Velocity V_c (m/s)
Linear Concentration
Water Velocity $\bar{V}$ (m/s)
3,15
2,87
2,58
2,29
2,01
1,72
1,43
1,15

FIG. 10.79

FIG. 10. 80

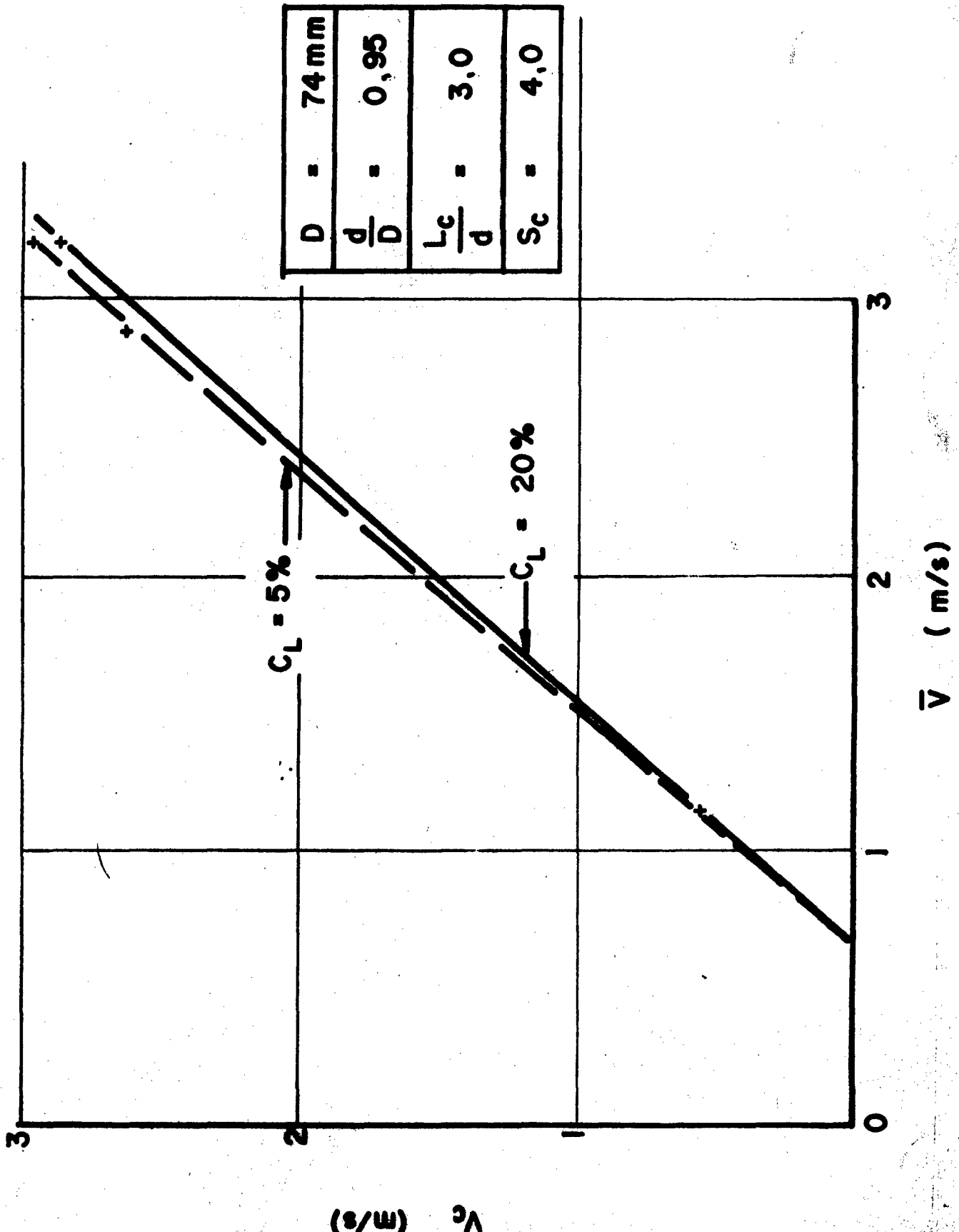

FIG. 10. 81

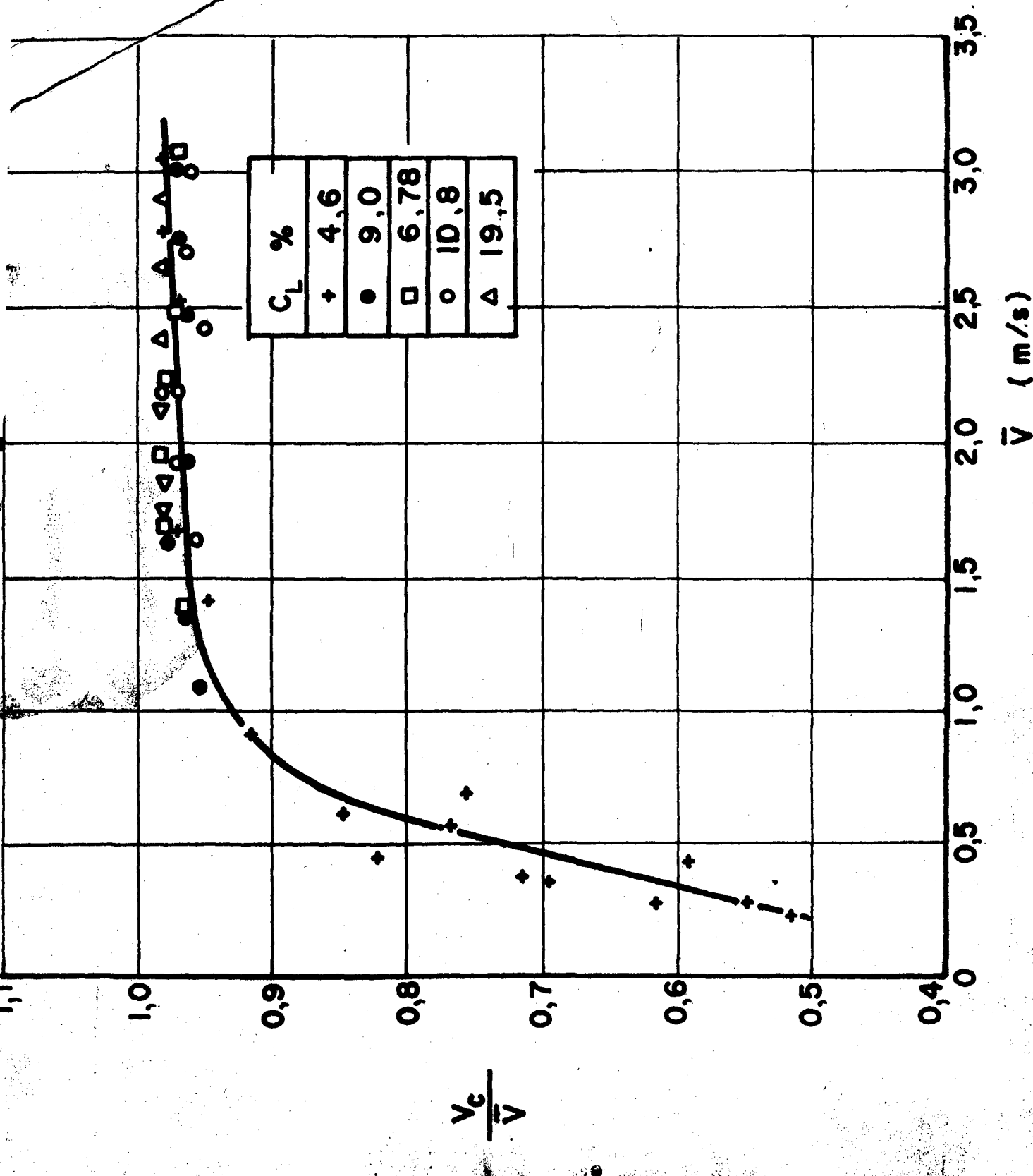
C_L %
+ 4,6
● 9,0
□ 6,78
○ 10,8
△ 19,5
$\bar{V}$ (m/s)
3,5
3,0
2,5
2,0
1,5
1,0
0,5
0
1,1
1,0
0,9
0,8
0,7
0,6
0,5
0,4
$\frac{V_c}{\bar{V}}$

Figures 10.82 to 10.84 show 2; 3 and 4 capsules spaced a capsule length apart by means of a wire spacer.

In order to maintain the centre to centre spacing as constant and to ensure that the average specific gravity was a constant value; the leading capsule had a specific gravity of five and the trailing capsule had a value of 3,0.

Since lower specific gravity capsules have been shown to travel faster this ensured that the spacing length was kept constant.

Figure 10.82 shows two capsules of S_c = 3,0 and 5,0 spaced a capsule length apart giving a linear concentration C_L = 50%.

The dashed and dotted lines respectively are for L_c/d = 8 (i.e. the total length equivalent of the spaced capsules) and L_c/d = 4,0 (the length equivalent of a single capsule).

There is not a great deal of difference between the values for capsule velocity at a particular mean water velocity for the single capsule and the two spaced capsules. Although the single capsule values are closer to those of the spaced capsule than the capsule of the same equivalent length, depending on the velocity.

All three graphs (Figures 10.82, 10.83 and 10.84) display the same characteristics, the kinematic values of one capsule being closer to the spaced capsules than the longer capsule of equivalent length, within the range of velocities tested.

Also, in all cases the spaced capsules travel faster than the single capsules. However, the discrepancy reduces at higher capsule velocities.

These results were unexpected but are comparatively easily explained and are reasonable in view of the explanation.

It has already been shown that longer capsules travel slower than

Figure 10.82

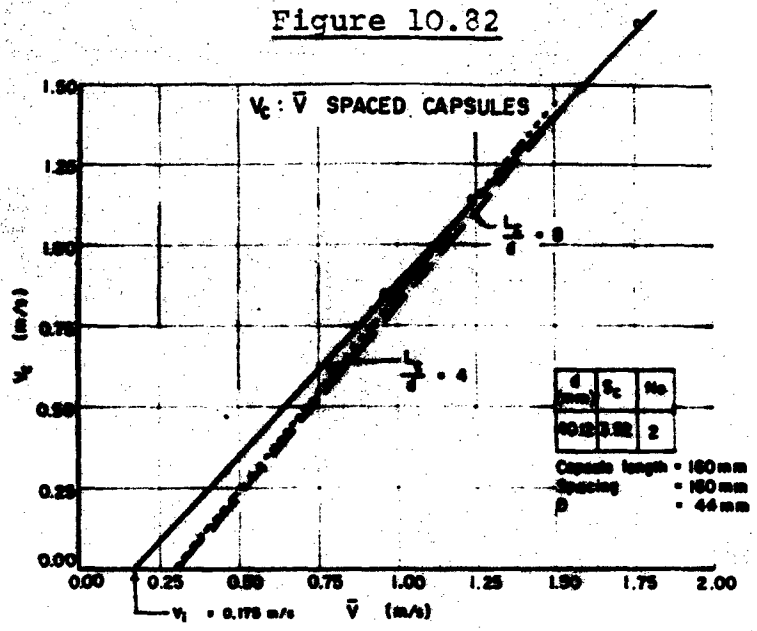

Figure 10.83

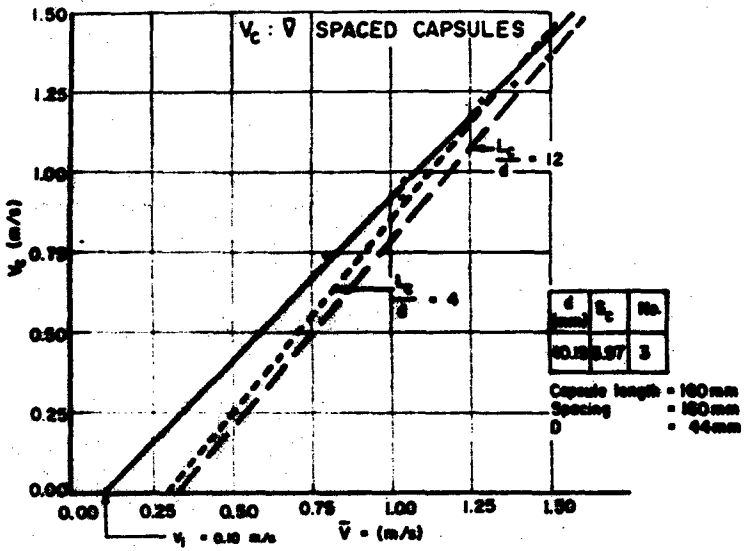

Figure 10.84

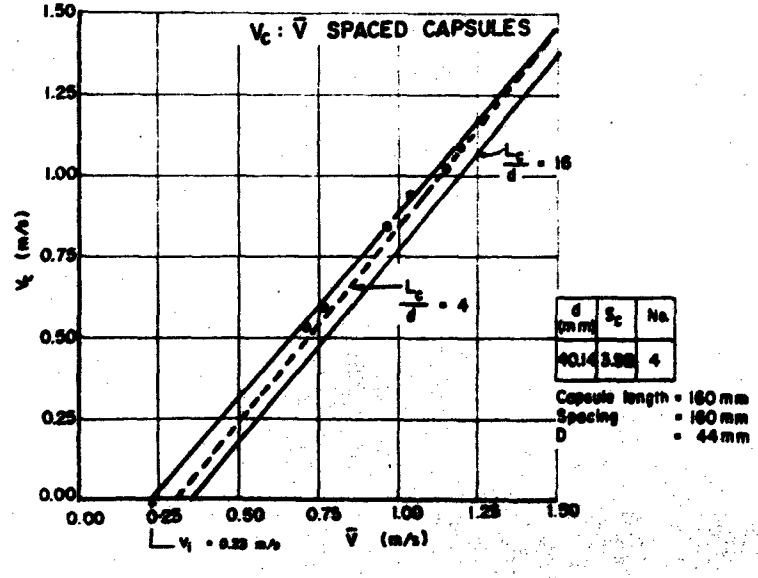

Figure 10.85

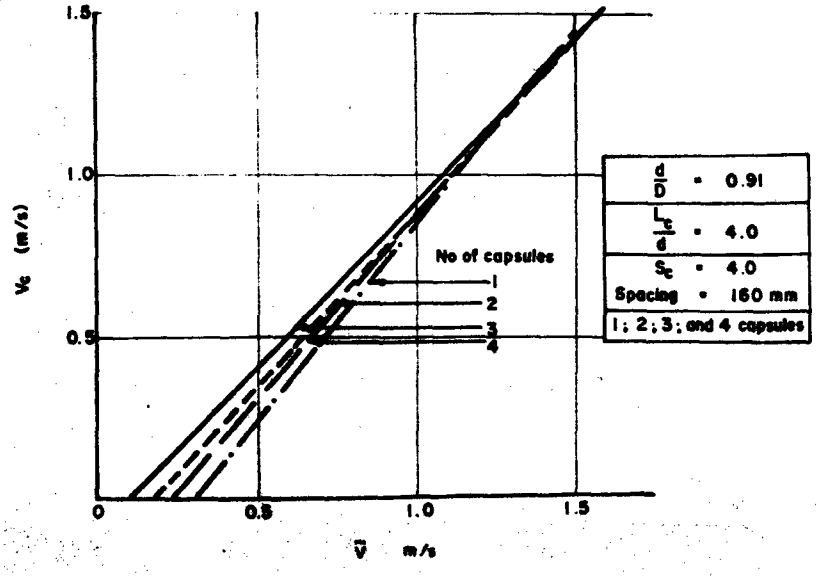

short ones with a reversal of this trend at high mean water velocities. It has also been shown that rough capsules have higher mean water velocities than smooth capsules, and these two phenomena have been explained.

The spaced capsules have a greater form drag exerted on them than capsules of the same equivalent total length and the skin friction drag is effectively the same as for unspaced capsules. The form drag is greater because, for the same length, there is more projected face area.

It is thus obvious that spaced capsules will travel faster than solitary ones of the same length, and this has been experimentally verified. The spacing acts as a macroscopic type of "roughness."

A further point is that there is a reversal of the above trend at higher velocities (i.e. the solitary capsules catch up with the spaced capsules, see Figure 10.85). This may be ascribed to the effect of lift. As the capsules tend to lift off the bottom of the pipe the solid friction drag effect on the capsules decrease. And capsule velocity increases since the capsules are influenced by the local velocity field and are not restrained by solid to solid friction. Thus, the mean velocity in the region of the capsule, relative to the capsule, tends to zero and the drag effect is reduced. An added effect is Couette shear and this will be discussed below.

At the lower concentrations used in the 74 mm diameter pipeline it was shown that at high velocities the trains of spaced capsules actually travelled slightly slower, if anything, than the solitary capsules. This implies that at these concentrations and large diameter ratios the solitary capsule would not only catch up with the spaced capsules but gradually overtake them, not in the same pipe of course. This could be explained in terms of Couette flow which gives rise to a retarding skin friction force and depends on the velocity of the capsule (V_c), the capsule longitudinal surface area, which in turn depends on the total length of capsule surface

($n \times L_c$) where n is the number of capsules) and the capsule diameter (d). All three variables (V_c, ($n \times L_c$) and d) when increasing induce an increased Couette shear. And for large diameter ratio capsules at high velocities the Couette shear retardation overcomes the "roughness" effect of spaced capsules giving rise to forward drag.

The above explains why these solitary capsules actually overtake the trains of spaced capsules.

To sum up: The effect of capsule spacing has little effect on the capsule velocity. Although for closely spaced capsules (C_L = 50%) at low velocities the solitary capsule travels slightly slower and for more sparsely spaced capsules (C_L < 20%) and larger diameter ratios the solitary capsules travel slightly faster than spaced capsules.

Within engineering accuracy the kinematic effect of a multitude of capsules compared with solitary capsules can be discounted at concentrations of the order of those mentioned above.

12. The slope of the $V_c : \overline{V}$ line (m)

It has been shown in the previous discussion that the parameter (m) is largely independent of all the variables in equation (10.1) except for diameter ratio (d/D).

Figure 10.86 shows m plotted against d/D for a wide range of capsules including some values derived from results by Ellis (reference 16) who plotted velocity ratio against mean water velocity and these curves are re-plotted as capsule velocity (V_c) against mean water velocity ($\overline{V}$) on Figures 10.87 and 10.88.

Experiments were carried out using small diameter steel and aluminum capsules to try and extend the range of this curve yet further and line slopes (m) from these curves, Figure 10.89, are also shown on Figure 10.86. The broken curve at the top is the mean through the diamond marks,

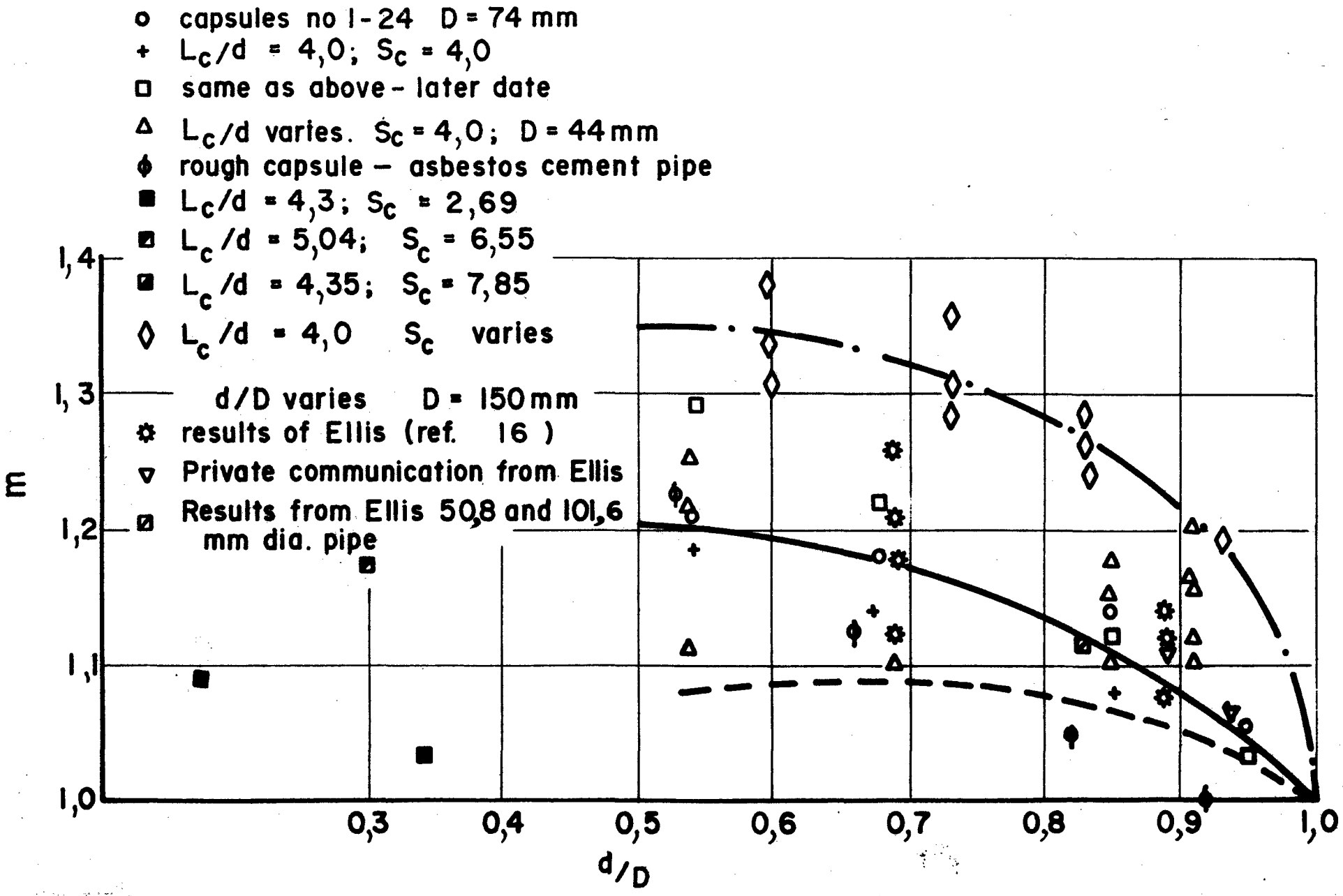

FIG. 10.86

10.68

FIG. 10.87

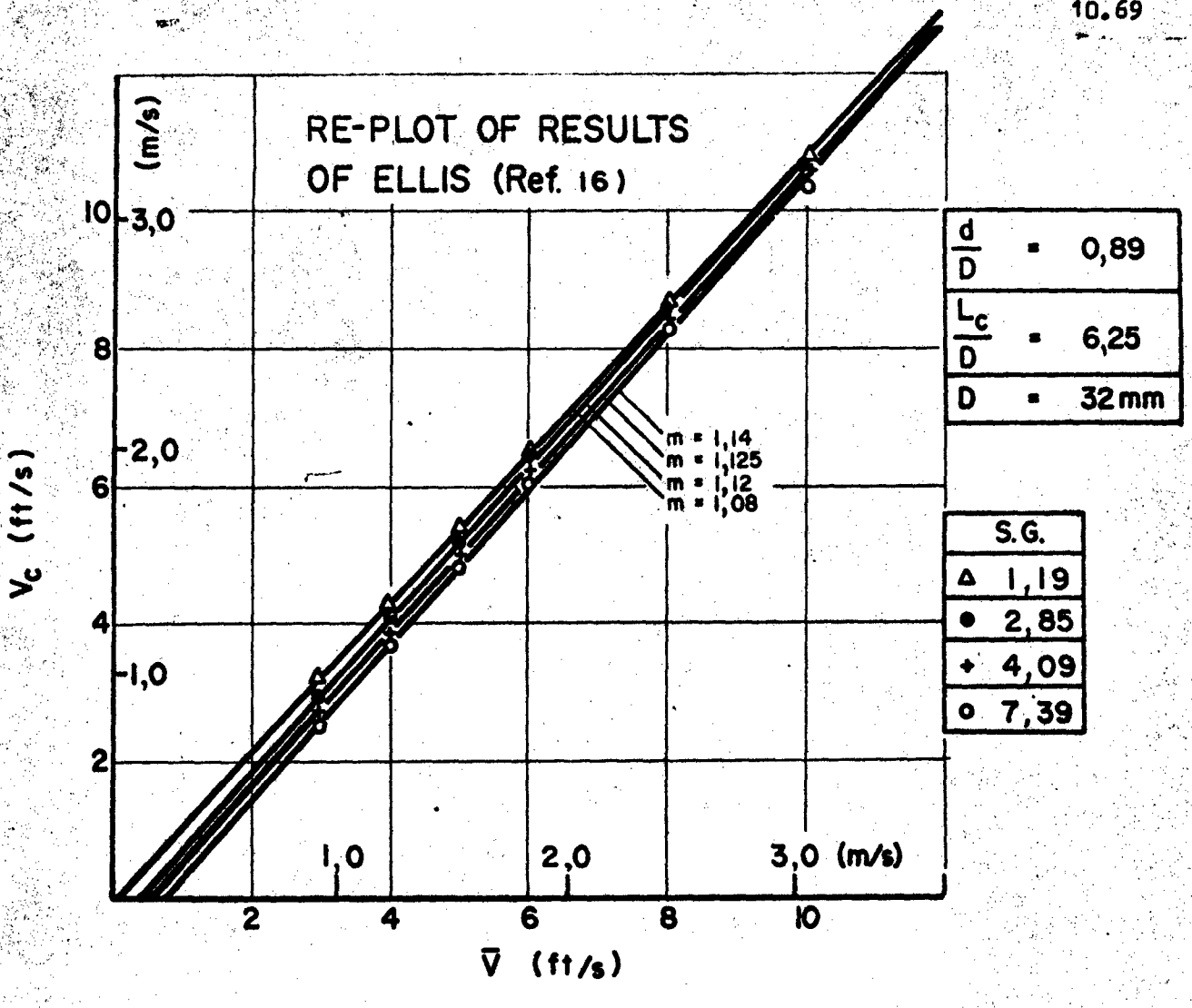

FIG. 10.88

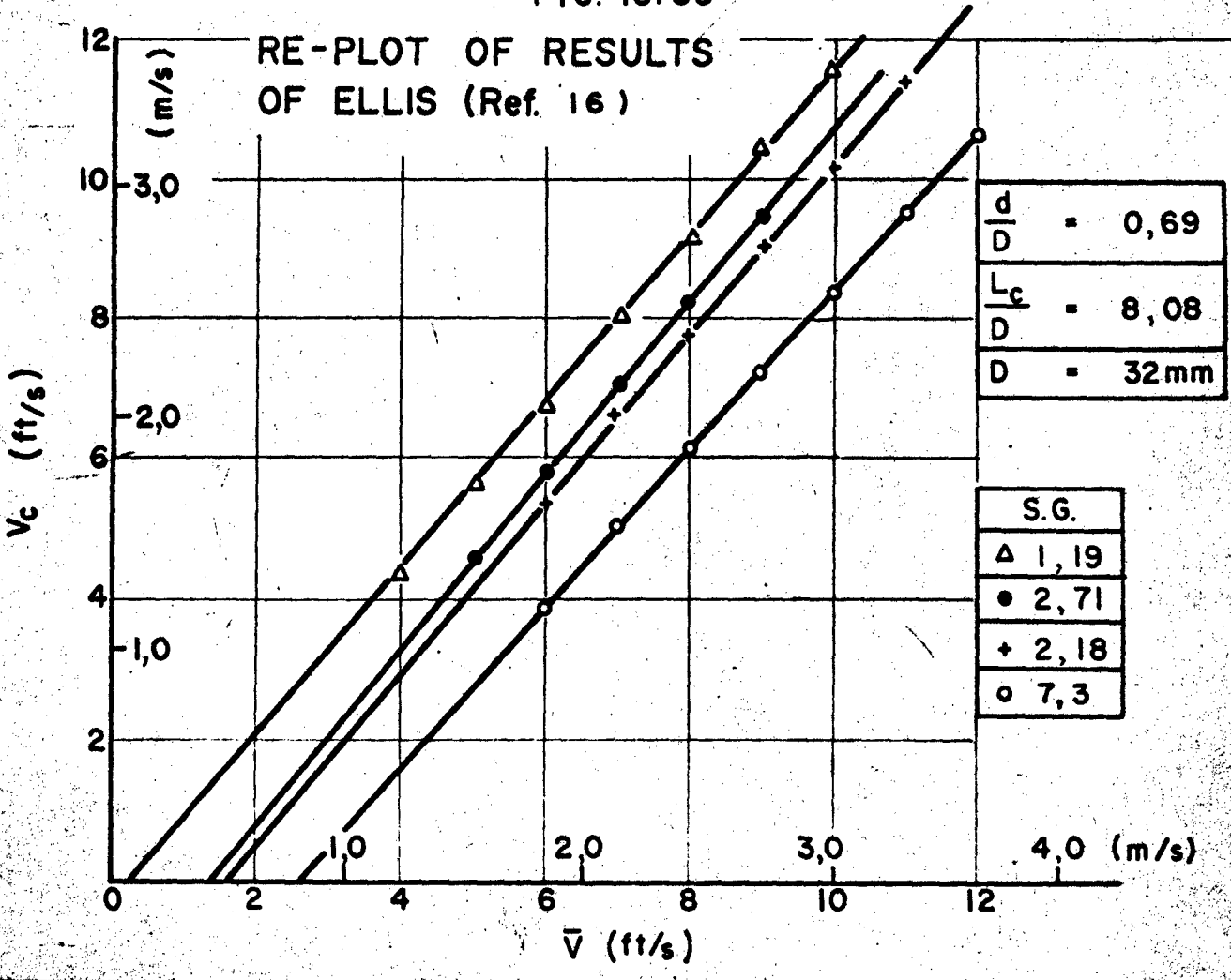

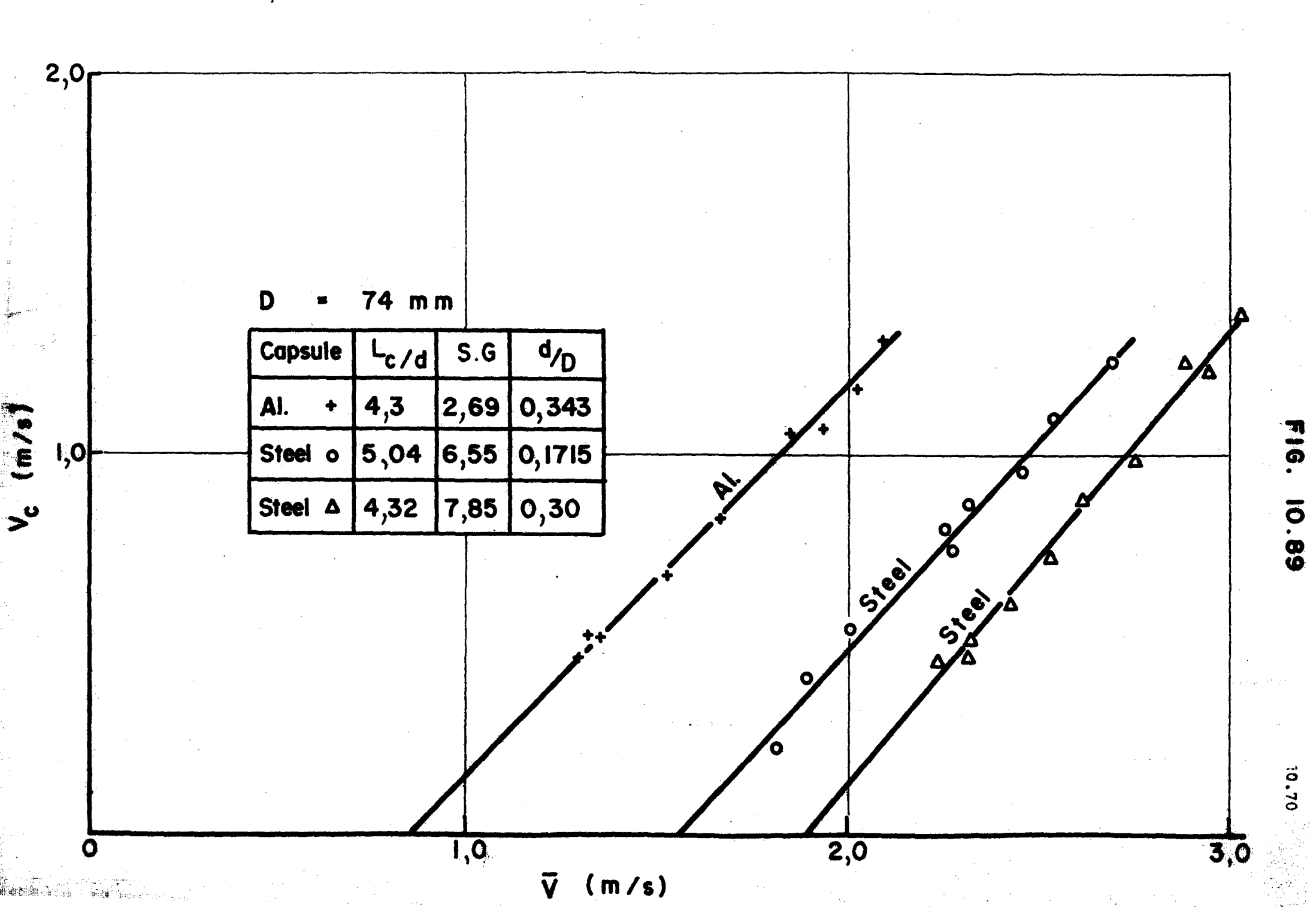

FIG. 10.89

10.70

and these points represent the results from the 150 mm diameter P.V.C. pipe over a range of diameter ratios and densities with a higher solid to solid friction coefficient, see Figures 10.90 to 10.93. Unfortunately, the slope of the V_c to $\overline{V}$ line is not easy to determine since a range of possible values of m can satisfy the same data points depending on how the line is drawn.

Figure 10.94 shows the extent of repeatability of the m parameter. These two sets of results are for the same capsules in the 74 mm diameter pipeline. The upper curve represents data points from experiments carried out about nine months after the data for the lower curve was obtained, (see Figures 10.26 and 10.40). Although the method of plotting, by suppressing the zero, exaggerates the error, the greatest error is still of the order of 4% from the mean position on Figure 10.94. The scatter about the mean position on Figure 10.86 is of the order of 7,5%.

The curve on Figure 10.86 was replotted as $y = 1,2 - m$ on the ordinate and $x = d/D - 0,5$ on the abscissa on log - log paper and the resulting equation is;

$$m = 1,2 - 0,8\,(d/D - 0,5)^2 \qquad (10.6)$$

$$\text{or} \quad m = 1 + 0,8\,(d/D) - 0,8\,(d/D)^2$$

It can be seen from the range of experimental data (i.e. d/D varies from about 0,2 to 0,95) that m ranges from 1,0 to 1,2 and increases as d/D decreases down to a value of $d/D = 0,5$. The line slope (m) must naturally be fixed at unity for the "piston" case of $d/D = 1,0$.

It has been pointed out that the determination of capsule velocity is dependent on two parameters; the incipient velocity which can be determined analytically as discussed in Chapter 7, and depends on a number of other variables (equation (7.133)) and the slope of the $V_c : \overline{V}$ line which can be determined empirically from equation (10.6).

FIGURE 10.90

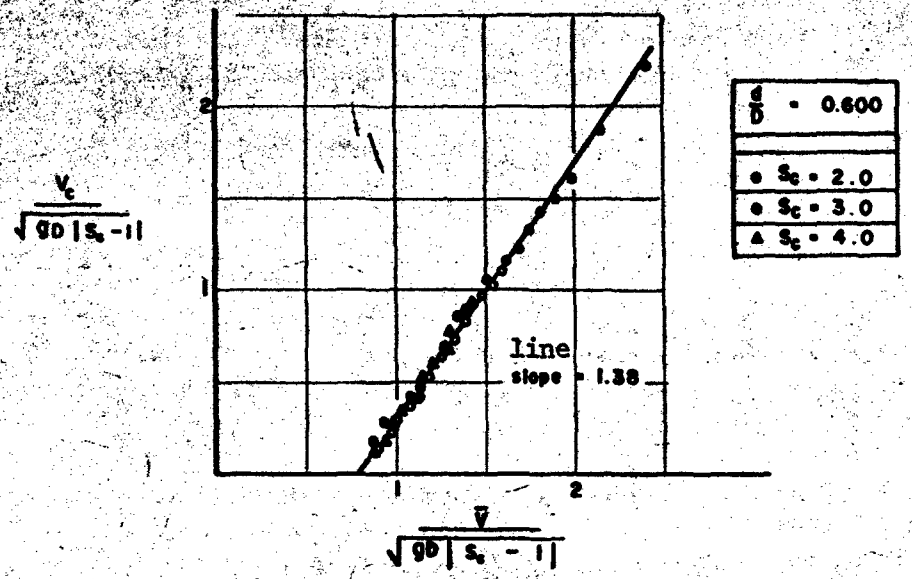

FIGURE 10.91

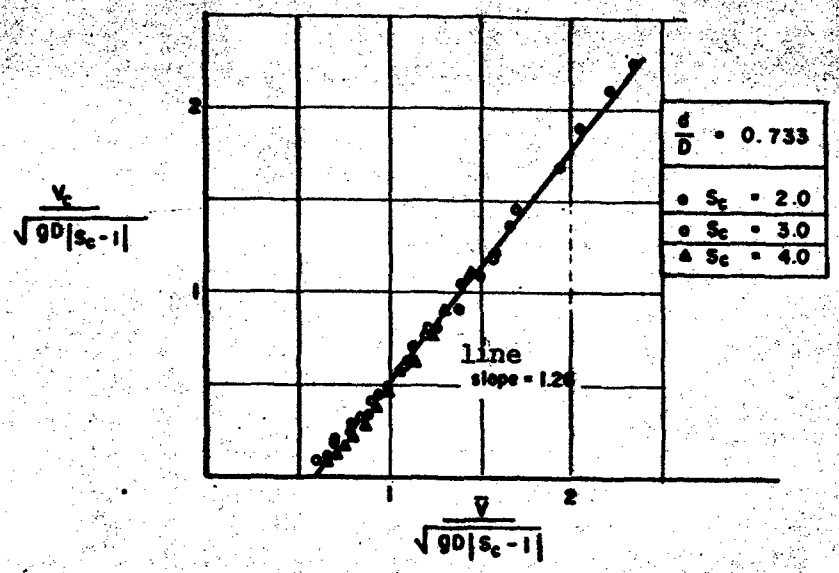

D = 150 mm

FIGURE 10.92

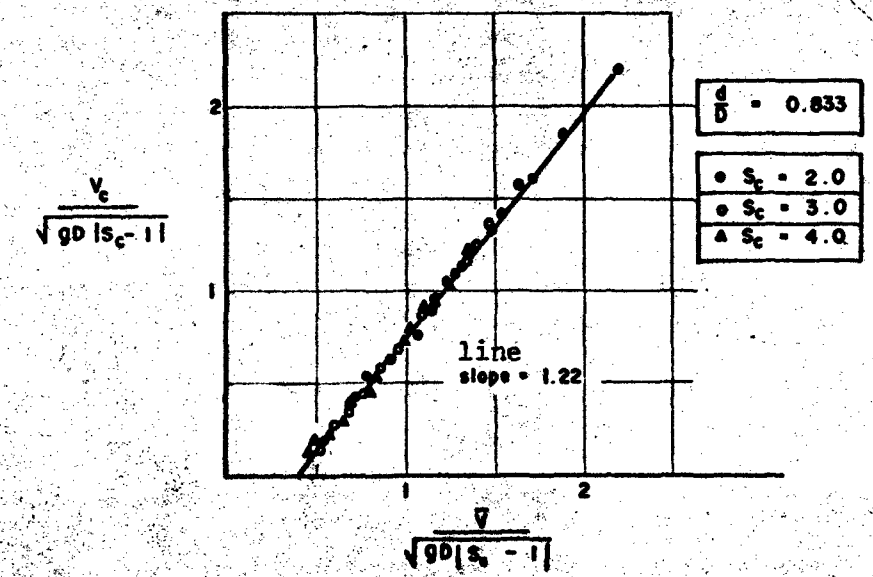

FIGURE 10.93

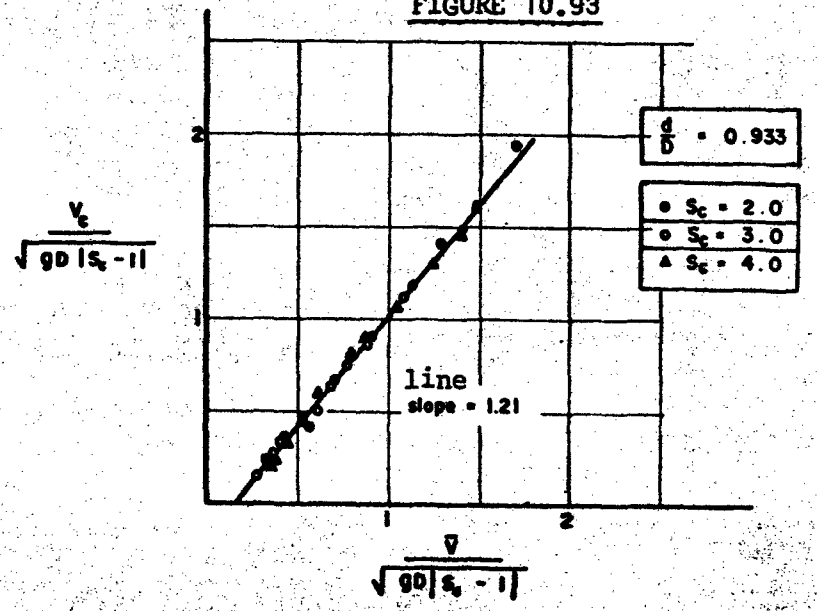

FIG. 10.94

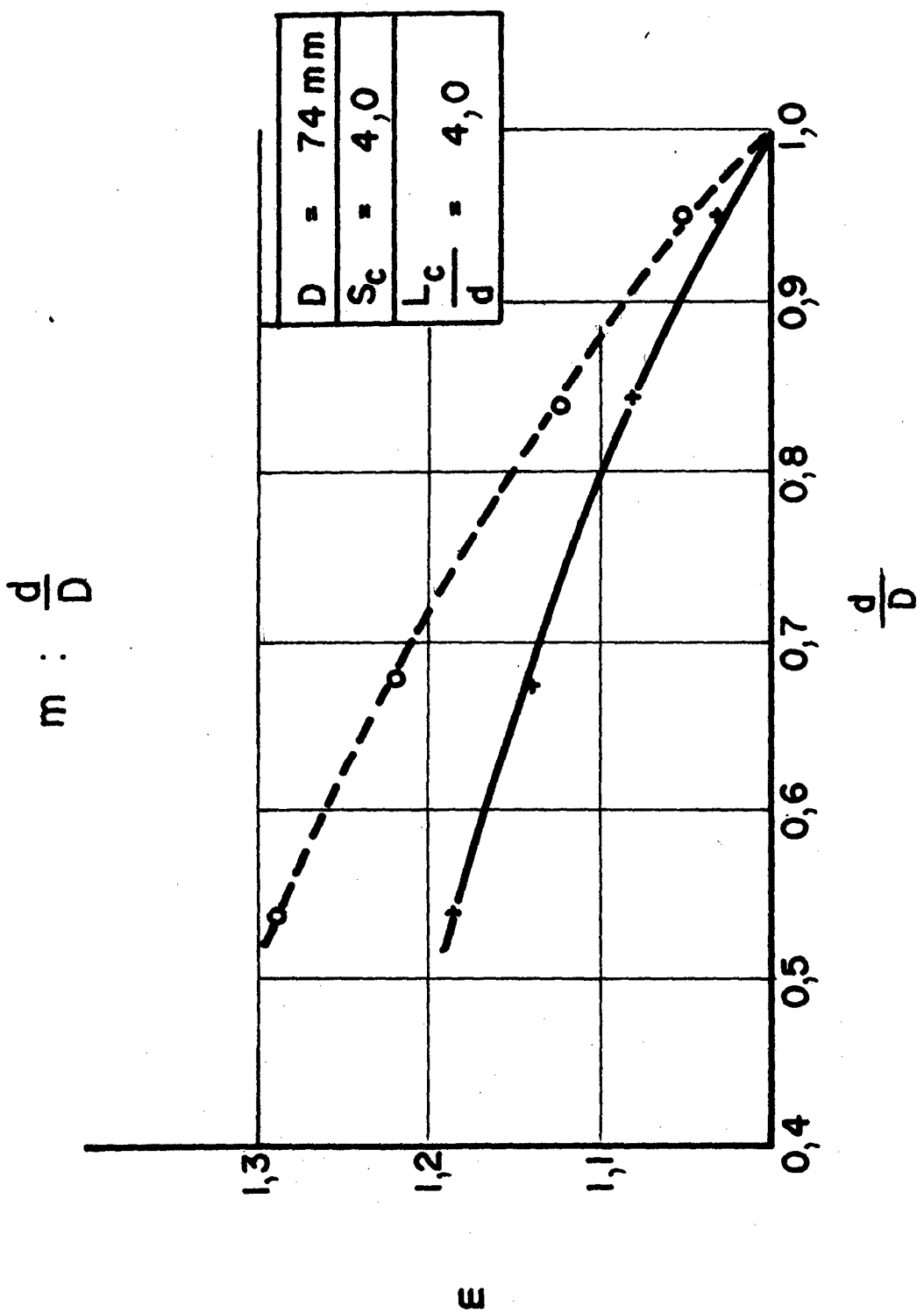

A satisfactory analytical explanation has been given for $\overline{V}_i$ and a somewhat more qualitative explanation follows for the shape of the m versus d/D curve.

Figure 10.95 shows the velocity distribution in a 74 mm diameter smooth pipe as determined from the non-dimensional parameters available in many textbooks on fluid mechanics (e.g. Schlichting p. 505). Superimposed on the pipe cross-section is a capsule cross-section. By considering finite concentric pipe areas over which the velocity was assumed constant and equal to the mean value in the narrow concentric annuli, the net mean velocity over the area occupied by the capsule could be computed. This procedure was repeated for three other capsule areas and at other velocity distributions represented by different Reynolds numbers.

The mean velocity over a capsule area was then plotted against the mean velocity for the pipe and straight lines through the origin were obtained. For a d/D ratio of unity it is obvious that the slope of the line is unity.

The results of the above analysis are given on Figure 10.96 as m_* plotted on the ordinate against d/D on the abscissa. m_* represents the ratio of the local mean velocity acting at the capsule frontal surface $(\overline{V}_L)$ to the mean velocity in the pipe $(\overline{V})$. Also shown on this graph is the empirical relation given by equation (10.6) and it is clear that the shape of the curves are similar showing that the mean velocity in the region of the capsule (if the capsule were not present) is similar to the capsule velocity itself.

It is interesting to note that the (m) values given by the capsules are higher than those given by $(\overline{V}_L)$. This does not mean that $V_c > \overline{V}_L$ since the capsules have an incipient velocity. However, it is clear that capsules which do not travel in a fully eccentric orientation but are lifted more towards the centre of the pipe will travel in a mean water

FIG. 10.95

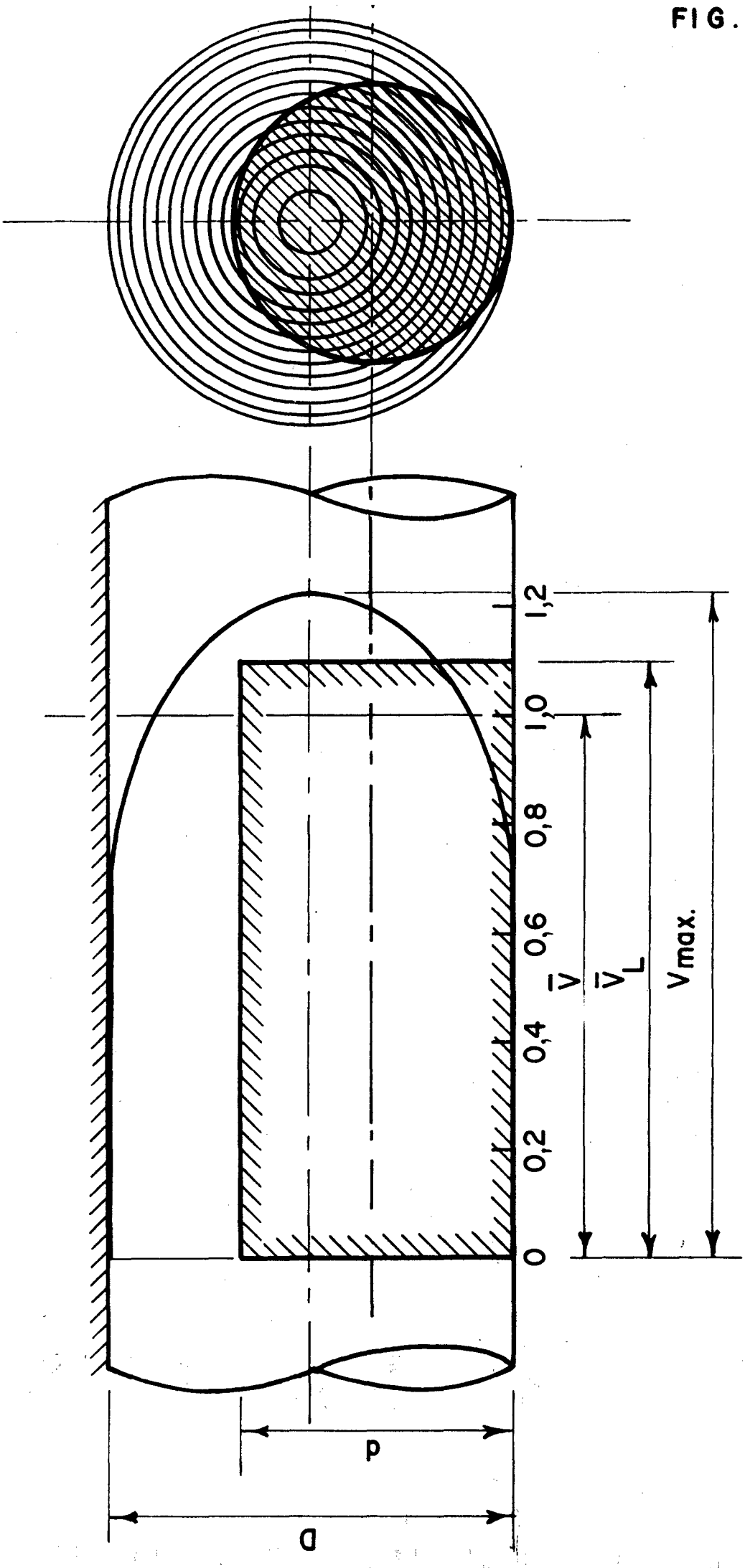

FIG. 10.96

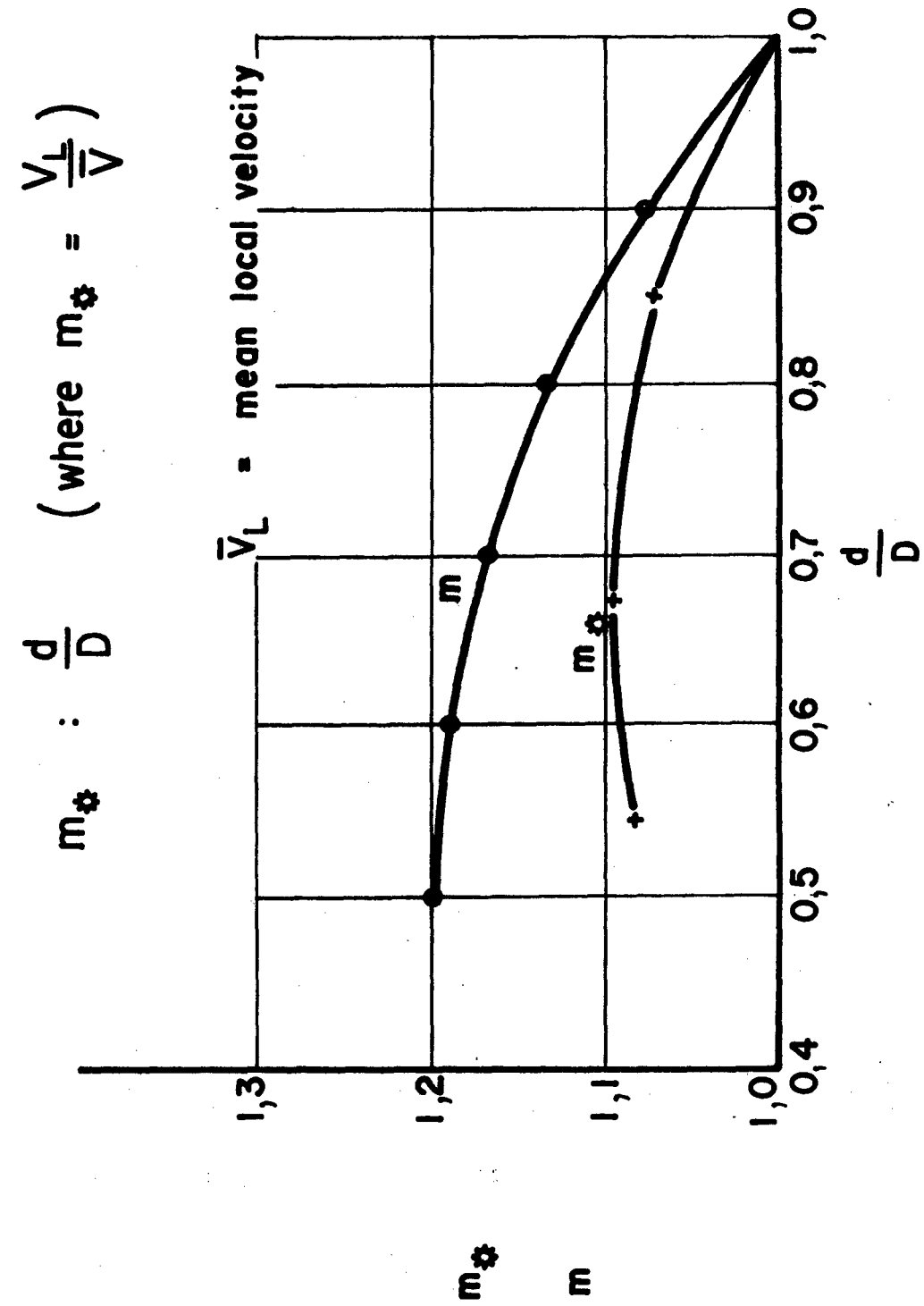
$m_* : \frac{d}{D}$ (where $m_* = \frac{V_L}{\bar{V}}$)
$\bar{V}_L$ = mean local velocity
m
m_*
1,3
1,2
1,1
1,0
0,4
0,5
0,6
0,7
0,8
0,9
1,0
$\frac{d}{D}$
m_* m

velocity zone which is higher than the value of $\overline{V}_L$ and it is possible to determine the degree of capsule eccentricity (or the clearance between the capsule and pipe wall) for m to equal m_*. Unfortunately this computation cannot be assumed to give the capsule clearance because of internal water shear which does not occur in a capsule occupied zone as well as secondary lift effects.

Basically the problem is to find an explanation for the fact that the lower the diameter ratio of the capsules the higher the slope of the V_c versus $\overline{V}$ lines in the range considered.

Since the incipient velocities increase as diameter ratio decreases, the above implies that at high velocities the low diameter ratio capsules overtake the large diameter ratio capsules. In other words the lower incipient velocities for the smaller capsules in addition to higher m values must cause smaller capsules to travel slower than larger ones at low mean water velocities and faster than larger ones at high mean water velocities.

The effects of diameter ratio on capsule velocity at different mean water velocities have been discussed in Section 7.

The following is an attempt to explain the shape of the m versus d/D curve by referring to the forces acting on capsules.

12.1 The forward drag on the capsule is a function of the velocity relative to the capsule, as well as the pressure flow component of velocity in the annulus. It is obvious that a change in velocity relative to the capsule will tend to accelerate the larger capsules more than the smaller ones due to larger surface area and frontal projected area. And both $(\overline{V} - V_c)$ as well as $\overline{V}_{ap}$ increase more for larger capsules.

12.2 The solid to solid friction is a function of the solid friction factor (μ_f) and the submerged weight minus the lift force. The net

effect of the forces perpendicular to the axial flow direction before the capsule flows free, is that the larger capsule will have a greater solid to solid friction force since the submerged weight more than offsets the increased lift of a larger capsule. This effect would be to speed up the small capsule more than the large for the same $\overline{V}$ increase.

12.3 The effect of frictional forces slowing down the larger diameter ratio capsules as described above (12.2), is reflected back as an increased forward drag on the large capsules contributing to the forward drag as discussed above (12.1).

12.4 The effect of lift is to cause the smaller d/D capsules to be carried to a higher velocity region than the larger d/D capsules even for the same amount of lift. This fact becomes clear from Figure 10.95 since larger diameter ratios are affected more by the low velocity region near the top perimeter of the pipe.

Thus, in this case it is likely that small velocity changes would accelerate the small d/D capsules more than larger diameter ratio capsules which also have more mass.

12.5 The Couette shear stress causes a retarding force on the capsule due to the fact that around the perimeter of the capsule the velocity is zero and around the pipe perimeter the velocity is also zero. This would probably retard a large d/D capsule more at the same mean water velocity since the surface area is larger and the flow velocity component due to Couette flow ($\overline{V}_{ac}$) is also slightly larger. Thus effects of $\overline{V}$ change would in cases 12.1 and 12.3 cause the large capsule to speed up in preference to the small one, whereas effects 12.2, 12.4 and 12.5 would cause the large capsule to be retarded more. The net effect must be that the latter three effects dominate the former two effects at high velocities.

13. <u>Effect of pipe diameter</u>

Extensive experiments have been carried out in the 44 mm, 74 mm and 150 mm diameter pipes and a few results are available in a range of pipelines (reference 22) as shown on Figure 10.31.

In the paper by Hodgson et al (reference 22) it was stated that "velocity ratio falls progressively as the pipeline diameter is increased; e.g. at an oil velocity of 4 ft/s (1,22 m/s) the velocity ratio varies approximately inversely as the 1/8th root of the pipe diameter." This can be seen on Figure 10.31.

The data from Figure 10.31 has been re-plotted on a capsule velocity versus mean water velocity basis in metric units as shown on Figure 10.97.

Included in this Figure are results from the 74 mm pipeline determined by the present author for the capsule No. 9, which has the closest characteristics to those given by Hodgson et al as well as results from the 150 mm pipe which are geometrically closest.

Figure 10.98 shows reproduced results of dimensionally similar capsules in the 74 mm and 44 mm pipelines.

Both these curves (Figures 10.97 and 10.98) indicate that dimensionally similar capsules travel faster in smaller diameter pipelines at the same mean water velocity.

Figure 10.98 also shows that as diameter ratio is decreased the discrepency, between capsule velocities in the large, compared with the small, diameter pipes, increases at a fixed mean water velocity.

The above can be explained as follows:

The submerged weight of the capsules is less in the smaller diameter pipelines since the capsules are themselves correspondingly smaller and of the same density. Thus for the same solid to solid friction factor, (μ_f) the net friction force opposing the fluid drag is less with the smaller capsules . This point will be discussed in more detail in Chapter 11.

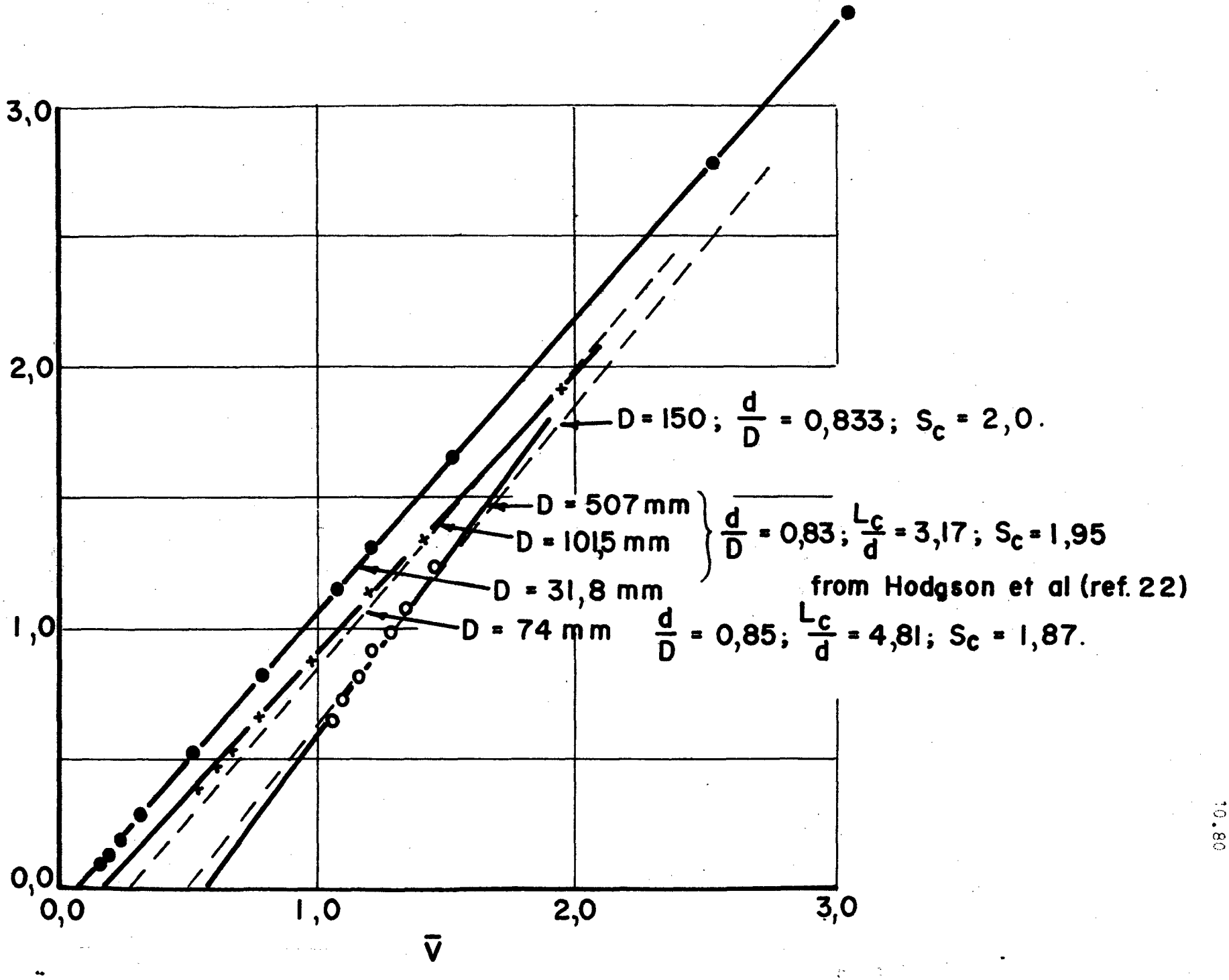

FIG. 10.97

08.10.

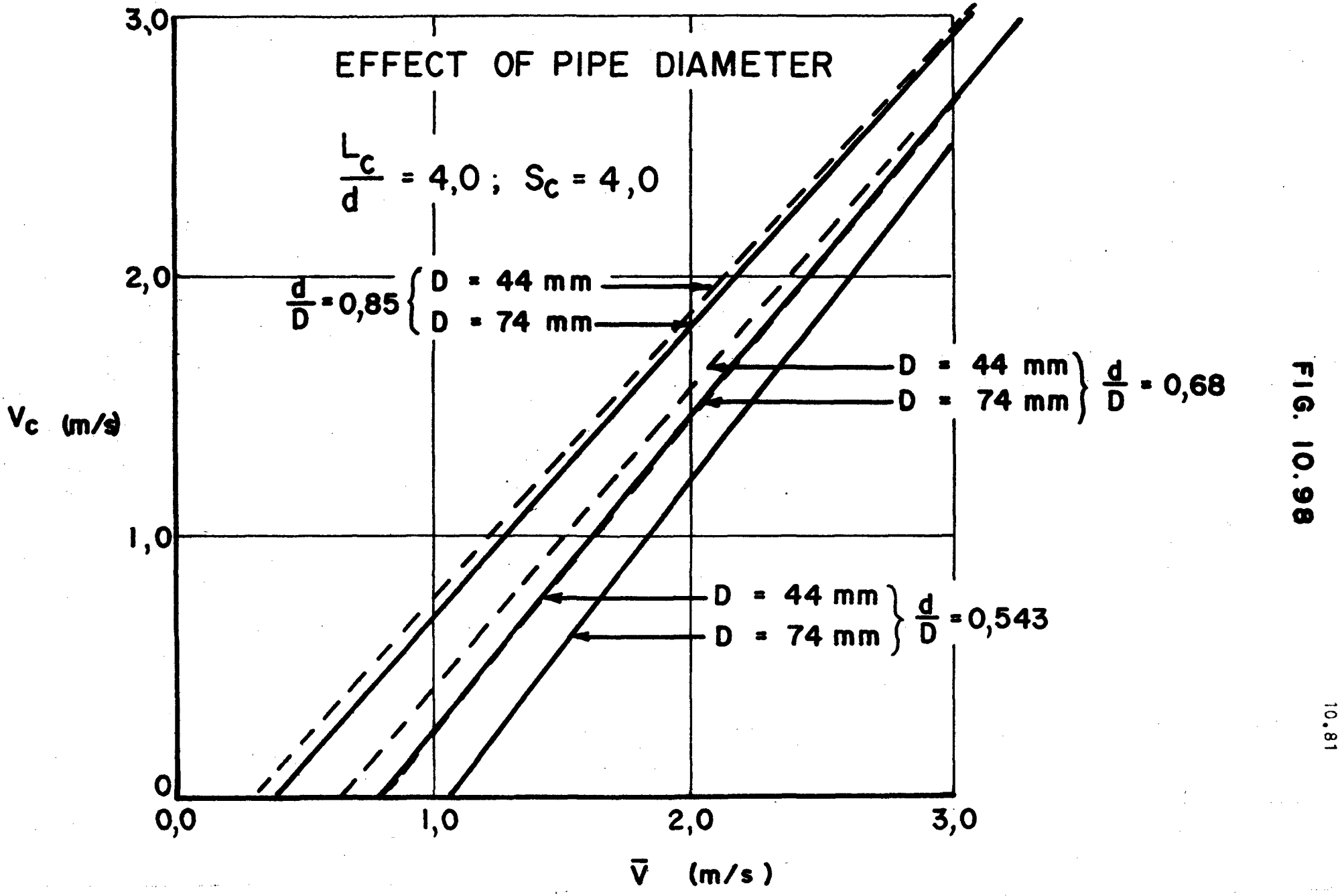
EFFECT OF PIPE DIAMETER
$\frac{L_c}{d}$ = 4,0 ; S_c = 4,0
$\frac{d}{D}$ = 0,85
D = 44 mm
D = 74 mm
D = 44 mm
D = 74 mm
$\frac{d}{D}$ = 0,68
D = 44 mm
D = 74 mm
$\frac{d}{D}$ = 0,543
V_c (m/s)
$\bar{V}$ (m/s)
0
1,0
2,0
3,0
0,0
1,0
2,0
3,0

FIG. 10.98

The slopes of the lines on Figures 10.97 and 10.98 are close to parallel except for the 507 mm and 150 mm pipes. This can be attributed to the internal nature of the pipe surfaces.

In the 507 mm diameter pipe there were welded joints every 12,2 m (see Chapter 2) and also the accuracy of determining capsule velocity was estimated to be of the order of only ± 20%. The 150 mm pipe was also rougher than the rest having a coefficient of static friction with P.V.C. capsules of $\mu_f = 0,38$.

All the curves represented on Figure 10.97 (and Figure 10.31) have successfully been made coincident by the non-dimensional form of presentation discussed earlier in this Chapter and illustrated on Figure 10.30, which includes the results of other capsules of different densities.

Thus, for dimensionally similar capsules of the same density in different pipe diameters, dividing both the capsule velocity and mean water velocity by the square root to the pipe diameter proves to be a successful method of correlation.

This is best shown on Figure 10.99 where two co-ordinate points are selected from the D = 31,8 mm pipe and the D = 507 mm pipe at extreme ends of the mean velocity range shown on Figure 10.97, viz at $\overline{V}$ = 1,0 m/s and $\overline{V}$ = 1,5 m/s for the latter diameter (507 mm) and $\overline{V}$ = 0,5 m/s and 2,0 m/s for the former (31,8 mm) pipeline. These four points lie on a single line as can be seen from Figure 10.99.

On the same diagram (Figure 10.99) selected points at extreme ends of the velocity range for D = 44 and 150 mm are also shown on the same straight line of $V_c/\sqrt{D}$ versus $\overline{V}/\sqrt{D}$.

FIG. 10.99

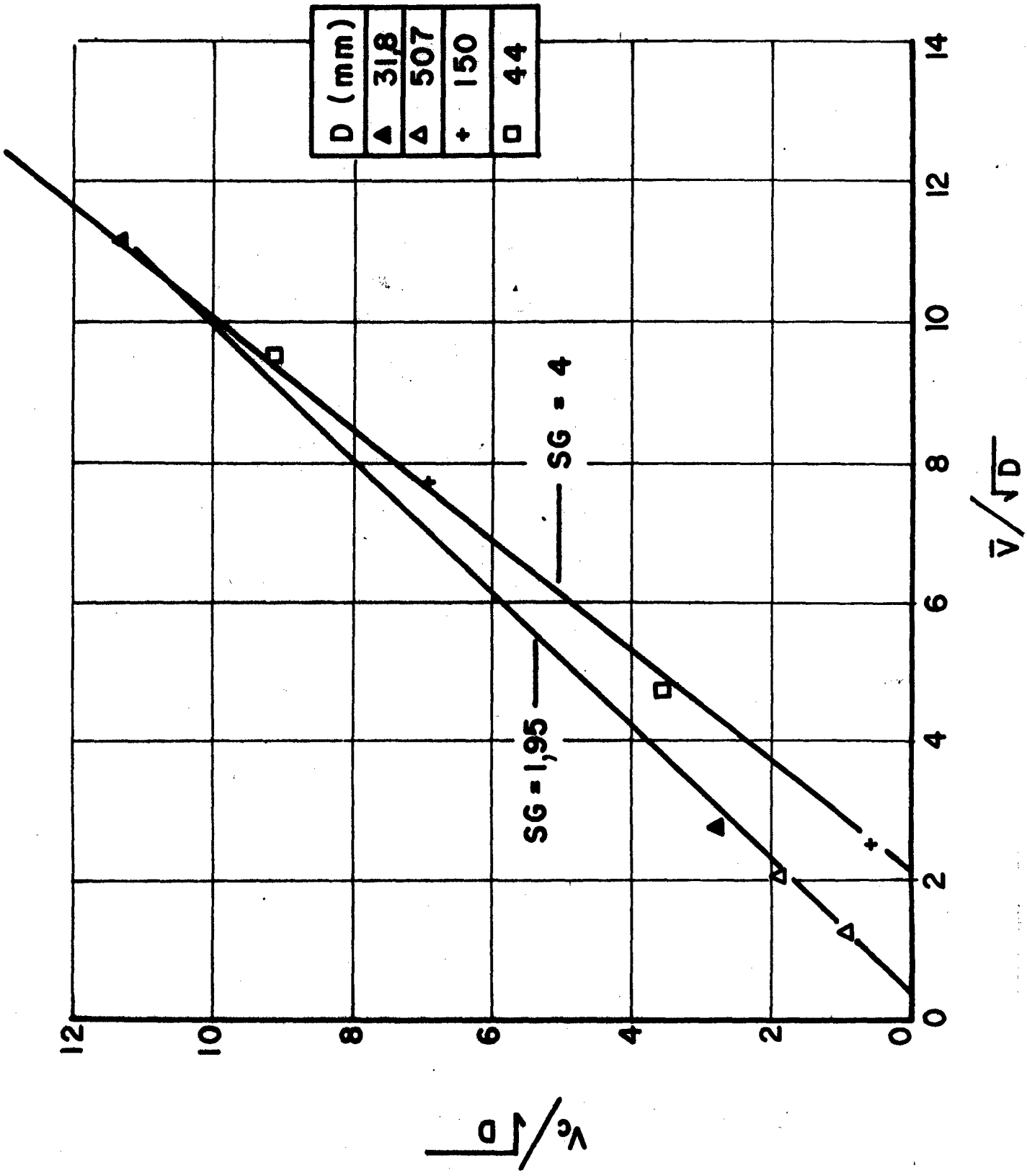

CHAPTER 11

ENERGY DISSIPATION ACROSS MOBILE CAPSULES

In this Chapter results of experimentally determined head losses across mobile capsules will be discussed. The forces acting on static and mobile capsules have been dealt with in Chapter 8, and these forces are reflected as energy losses across the capsule. The excess head loss across a capsule (ΔH_c) has been defined earlier as the head loss over and above that due to friction head loss in a capsule free section of the pipe.

Figures 11.1 to 11.4 show typical excess energy losses for the capsules numbered 1 to 24 with different specific gravity capsules superimposed for the same diameter ratio.

The results of energy loss experiments will be discussed in terms of the effect of independent variables on the excess head drop across capsules.

The variables considered are:

1. The mean water velocity ($\overline{V}$)
2. The specific gravity of the capsule (S_c)
3. The diameter ratio (d/D)
4. The length to diameter ratio (L_c/d)
5. The slope of the pipeline (ϕ)
6. The roughness of the capsule and pipe
7. The effect of capsule centre to centre spacing (L_s)
8. The pipeline diameter (D)

1. The effect of mean water velocity

The most significant trend is that the value of the excess energy loss (ΔH_c) in all cases drops off with increasing values of the mean water velocity ($\overline{V}$). The decrease is most noticeable at high capsule densities for a constant diameter ratio. This is clear from curves such as those

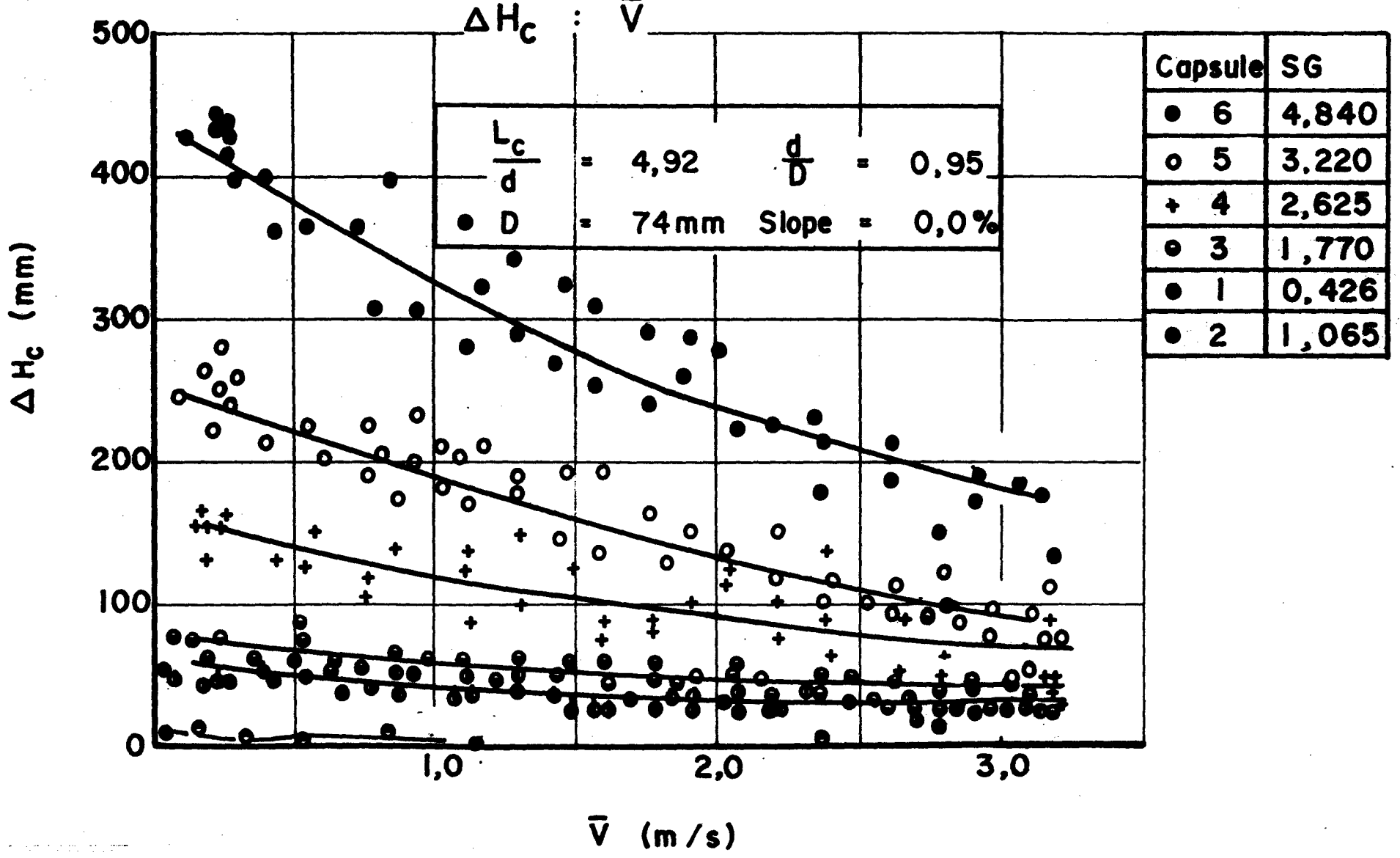
ΔHc : V̄
500
400
300
200
100
0
ΔHc (mm)
Lc/d = 4,92
d/D = 0,95
D = 74mm
Slope = 0,0%
Capsule | SG
6 | 4,840
5 | 3,220
4 | 2,625
3 | 1,770
1 | 0,426
2 | 1,065
1,0
2,0
3,0
V̄ (m/s)

FIG. II.1

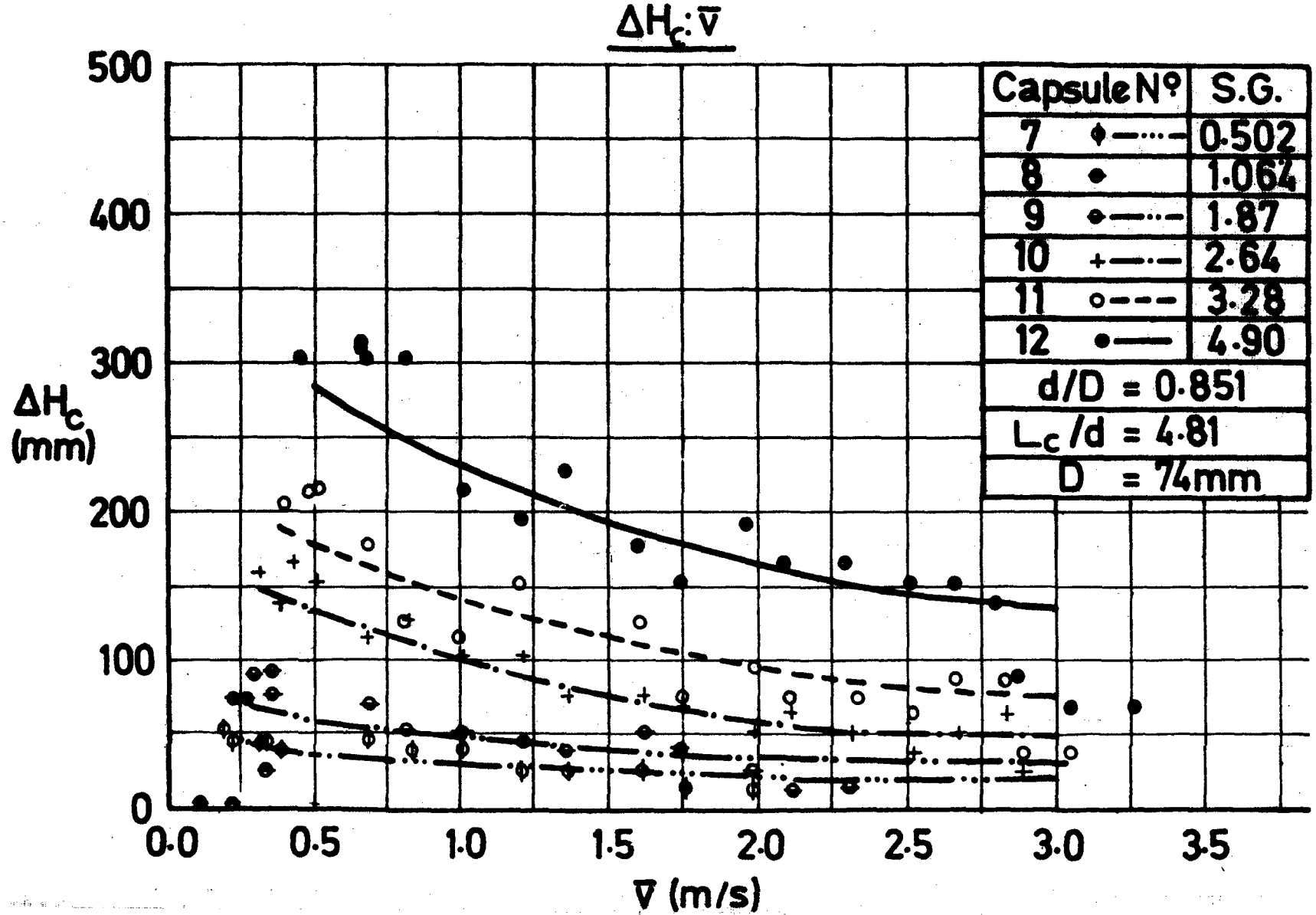
ΔHc : V̄
ΔHc (mm)
V̄ (m/s)
0
100
200
300
400
500
0.0
0.5
1.0
1.5
2.0
2.5
3.0
3.5
Capsule Nº
S.G.
7
0.502
8
1.064
9
1.87
10
2.64
11
3.28
12
4.90
d/D = 0.851
Lc/d = 4.81
D = 74mm

FIG. II.2

$\Delta H_c : \bar{V}$

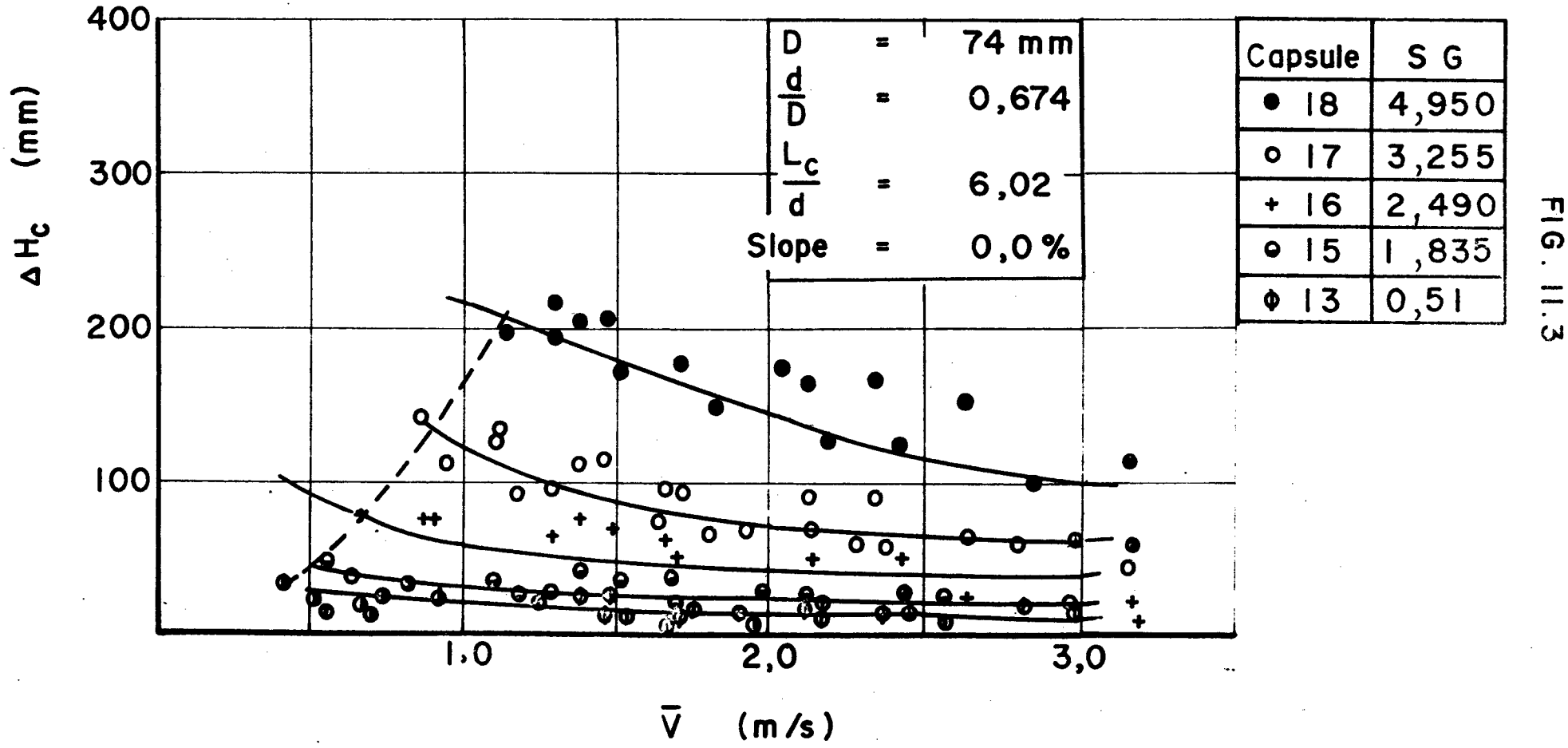

FIG. II.3

$\Delta H_c : \bar{V}$

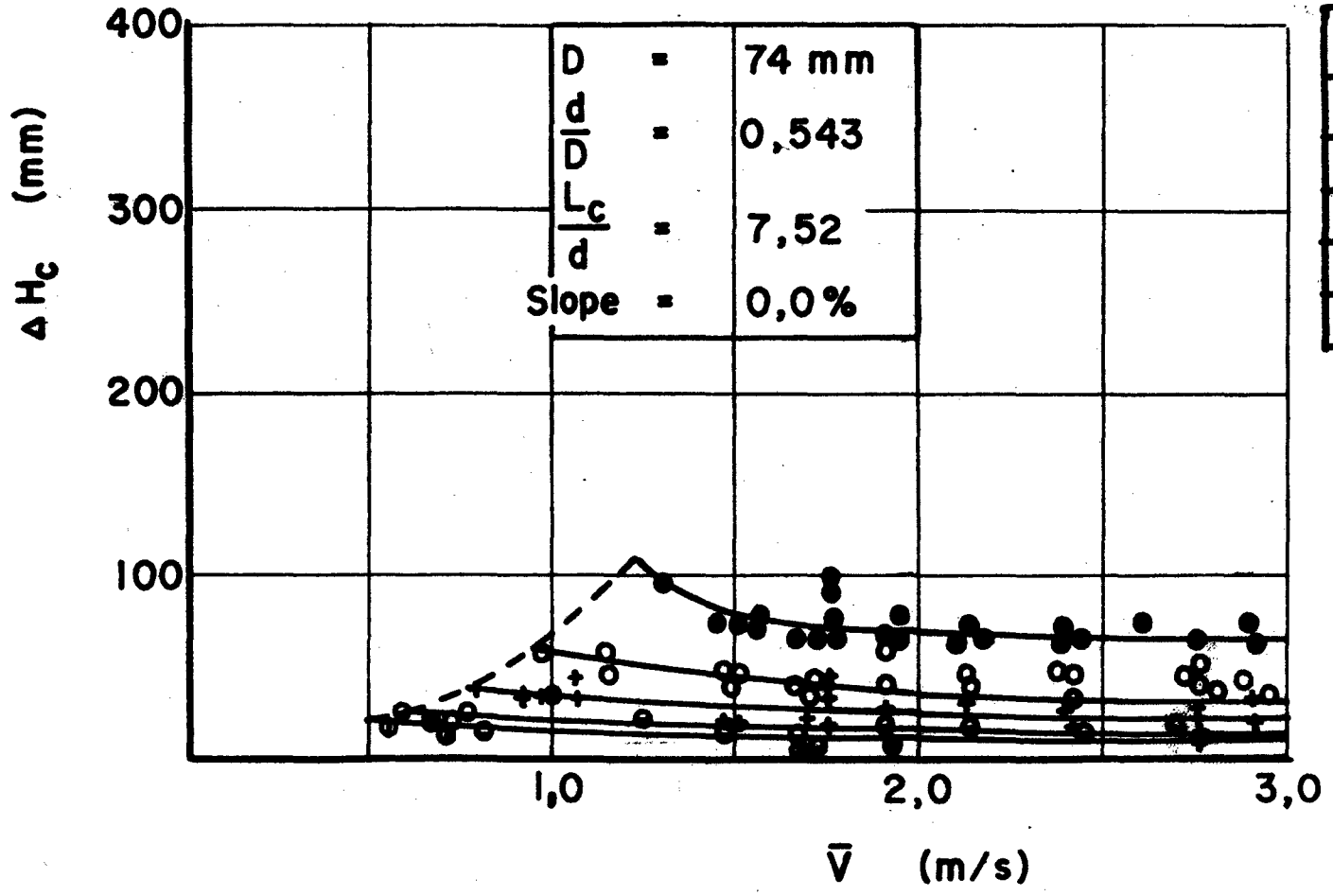

CAPSULE	S.G.
⊙ 24	4,77
o 23	3,24
+ 22	2,46
● 21	1,75
◆ 19	0,417

FIG. II.4

on Figure 11.1 where the curve for $S_c = 4,84$ drops off more rapidly than the lower specific gravity curves. Figure 11.5 shows ΔH_c plotted against the density ratio S_c at $\overline{V}$=0,5 m/s and 3 m/s for the capsules of diameter ratio d/D = 0,851. The 0,5 m/s velocity produces a much greater rise in the excess head loss as the specific gravity (or density ratio) of the capsule increases, than the 3,0 m/s velocity.

The above observations can be ascribed to the following:

1.1 At zero and low capsules velocities the excess head loss across the capsule depends on the solid to solid friction force between the capsule and pipe, and this force is a function of the submerged capsule weight. If the capsule does not lift one would expect the curves (such as those on Figure 11.1) to remain virtually parallel. If the capsules tend to lift off the bottom of the pipe the solid to solid friction force decreases and the density of the capsule has less effect on the value of ΔH_c.

1.2 In Chapter 10 it was shown that the capsule velocities of high density capsules approach those of low density capsules as the mean water velocity increases, (see for example Figure 10.7). The excess head loss across a mobile capsule (ΔH_c) has been shown to be a function of the mean velocity of the water relative to the capsule ($\overline{V} - V_c$), as well as the velocity due to pressure flow of water in the annulus ($\overline{V}_{ap}$) or, alternatively the velocity relative to the capsule (V_r).

These velocities decrease as the velocity ratio increases towards unity. Consequently, the excess head loss decreases.

2. <u>The effect of specific gravity</u>

The following effects are discernable.

2.1 As specific gravity increases, the excess energy dissipated at a particular mean water velocity and capsule geometry increases. This is clear from Figures 11.1 to 11.4.

$\Delta H_c : S_c$

FIG. 11.5

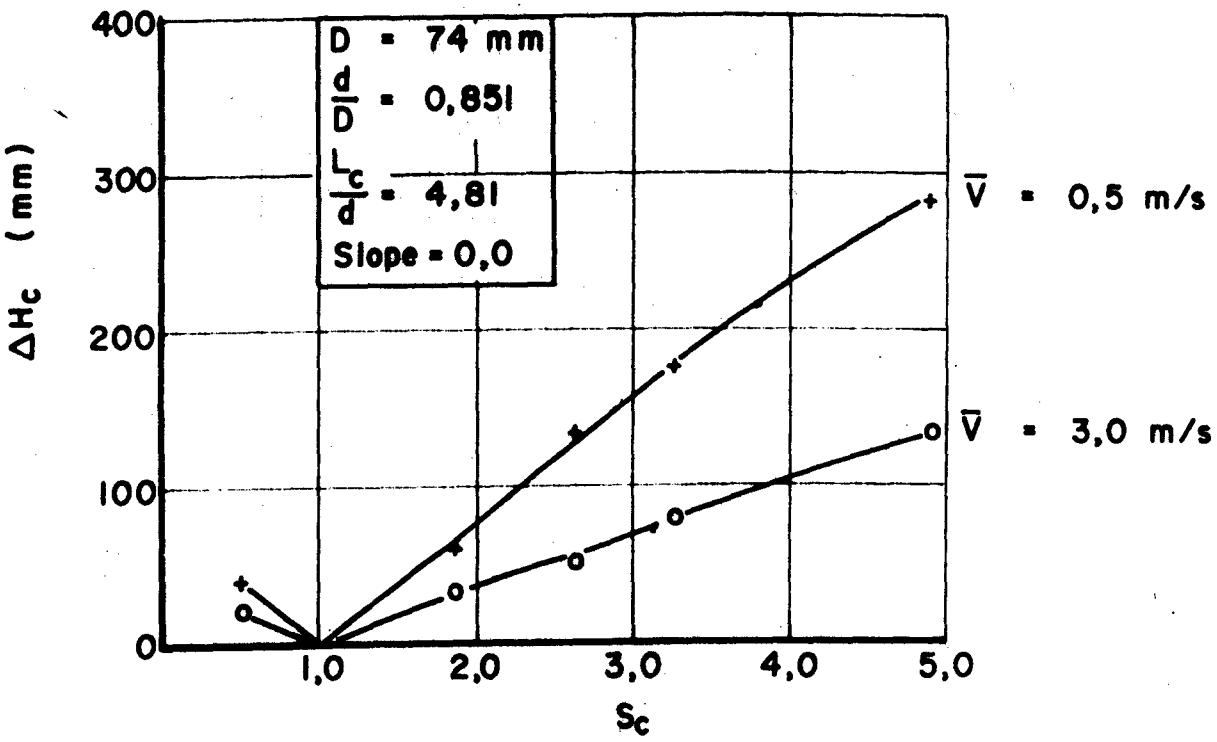

FIG. 11.6

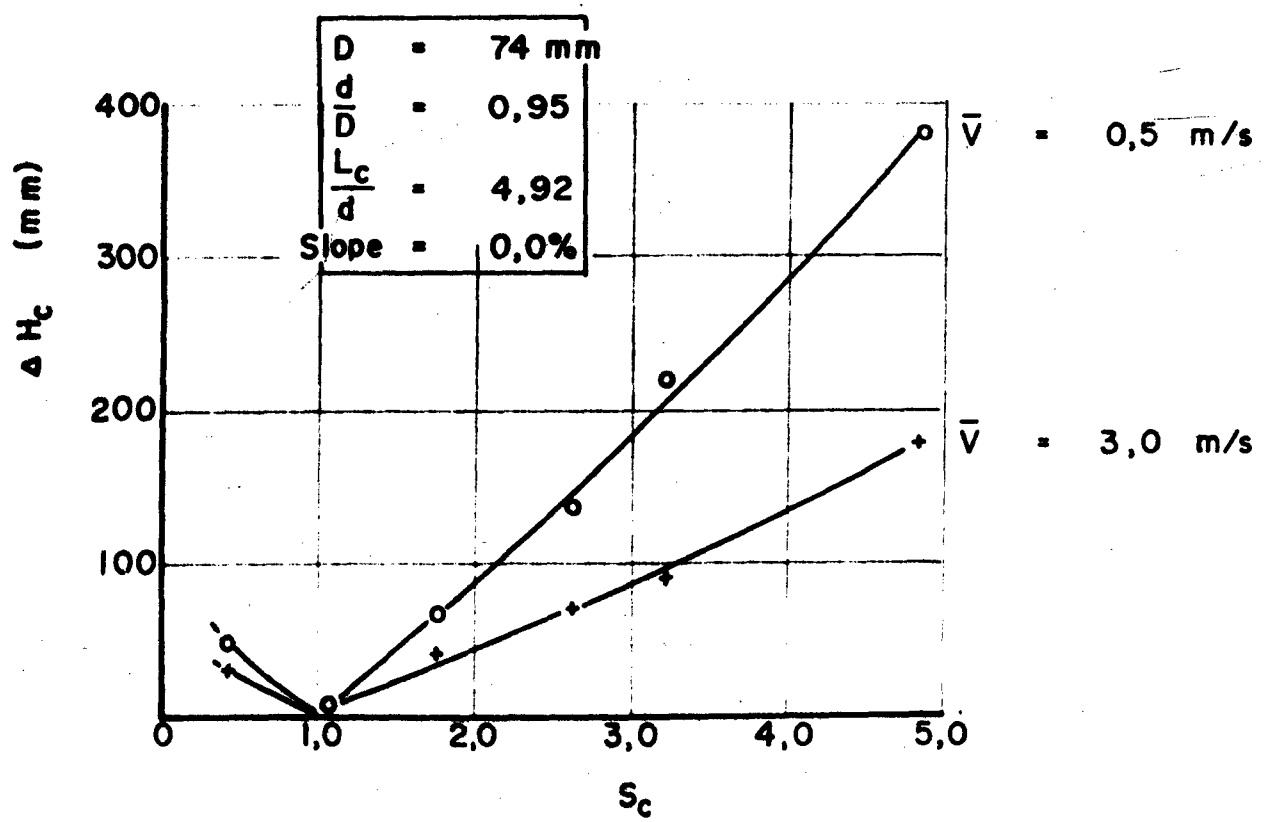

2.2 As was pointed out in the last section, the effect of specific gravity increase on ΔH_c is magnified at low velocities.

2.3 Figures 11.1 to 11.4 also illustrate that as diameter ratio decreases the difference, between excess energy losses for high and low specific gravity capsules, also decreases. That is, the family of curves are progressively closer together from Figures 11.1 through to 11.4

2.4 The modular value of the submerged specific gravity $|S_c-1|$ is a more significant factor than the specific gravity itself. Thus, the effect is the same, for capsules orientated eccentrically, if the friction (for example) acts along the top of the pipe wall where $S_c < 1,0$. This is clearly seen on Figure 11.1 where capsules of specific gravity 0,426 and 1,77 have $\Delta H_c : \overline{V}$ curves which are close and greater than $S_c = 1,065$.

Figures 11.5 and 11.6 illustrate the above observations for $d/D = 0,85$ and 0,95. These two Figures are also effective in showing the more rapid increase of ΔH_c with specific gravity as mean water velocity is decreased.

3. <u>The effect of diameter ratio</u>

Figure 11.7 shows the results of dimensionally similar capsules of $S_c = 4,0$ and $L_c/d = 4,0$. The dotted curves will be discussed below.

Figures 11.8, 11.9, 11.10 and 11.11 show the results for the same four diameter ratios and same geometrically similar capsules.

These experiments were carried out about nine months earlier than those depicted on Figure 11.7. Far more data points were actually determined in the case of the results given on Figures 11.8 to 11.11, and actual data points are shown on these Figures in order to give an idea of the scatter involved. The mean curves from Figures 11.8 to 11.11 are summarised without data points on Figure 11.12, and are shown dotted on Figure 11.7, where only average values of data points, determined for the latter experiment, are shown. An idea as to the difficulty of establishing these

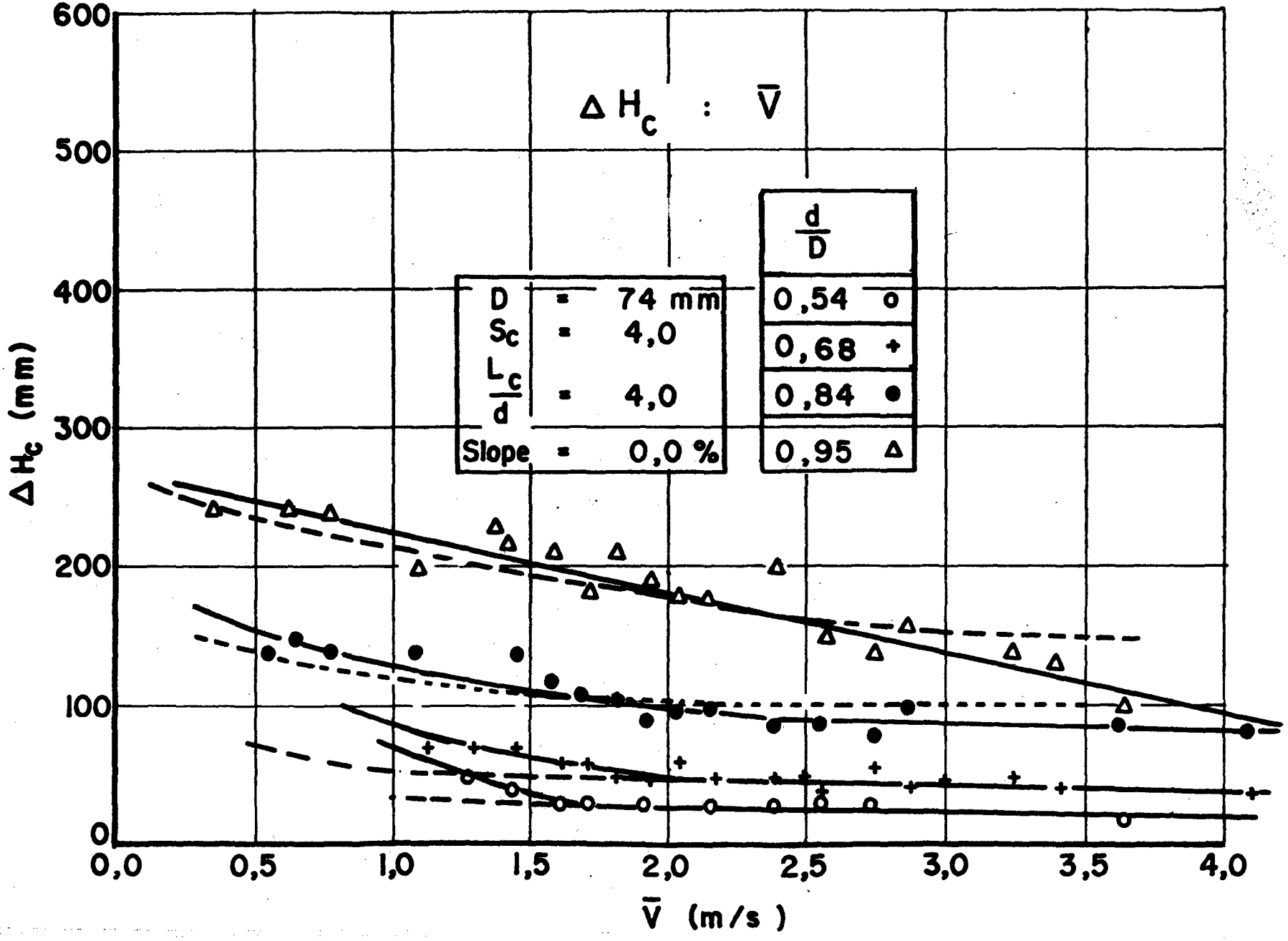
ΔHc : V̄
D = 74 mm
Sc = 4,0
Lc/d = 4,0
Slope = 0,0 %
d/D
0,54 o
0,68 +
0,84 •
0,95 Δ
ΔHc (mm)
V̄ (m/s)
0
100
200
300
400
500
600
0,0
0,5
1,0
1,5
2,0
2,5
3,0
3,5
4,0

FIG. II.7

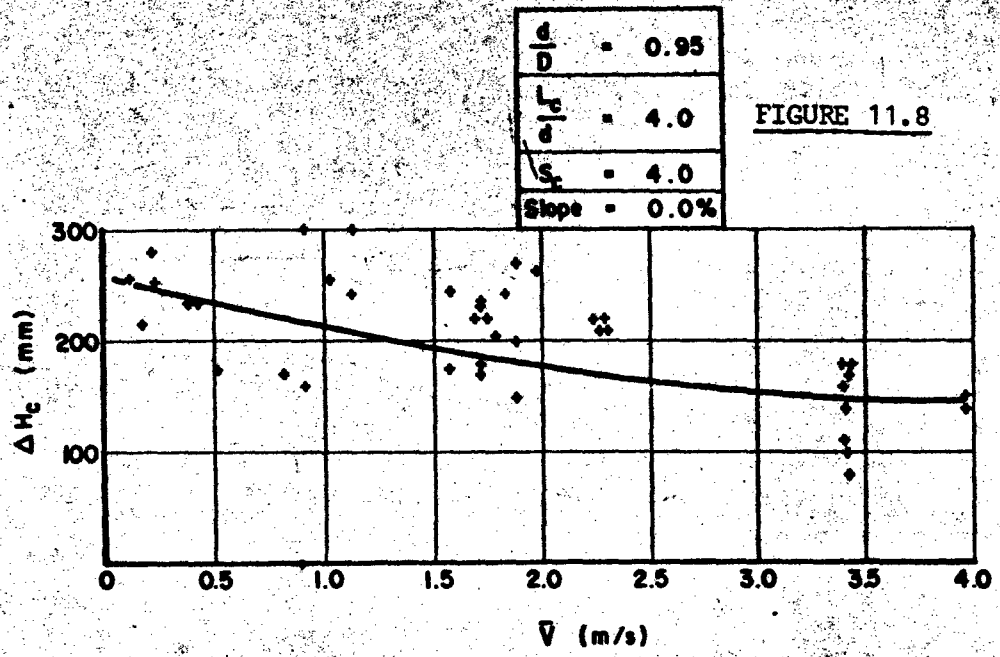

FIGURE 11.8

FIGURE 11.9

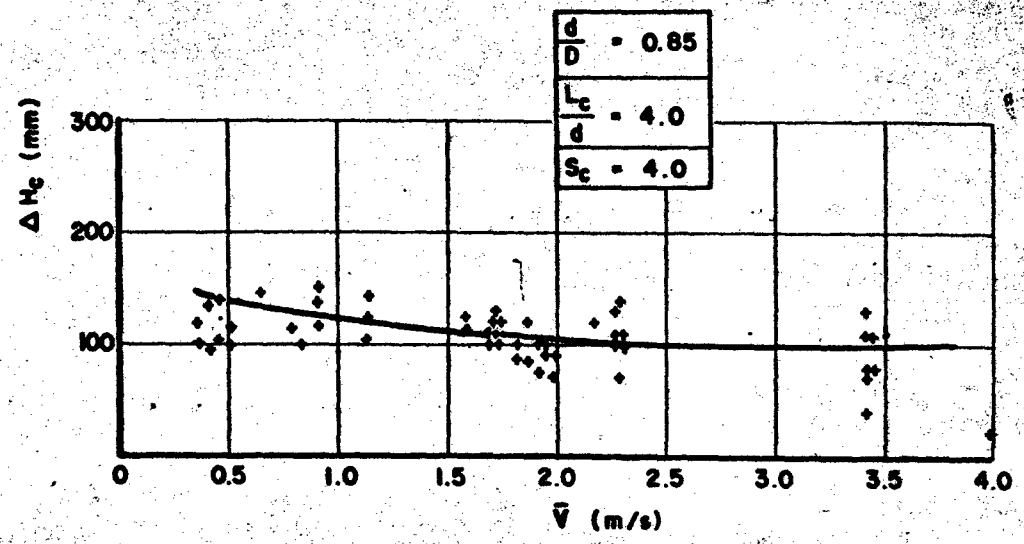

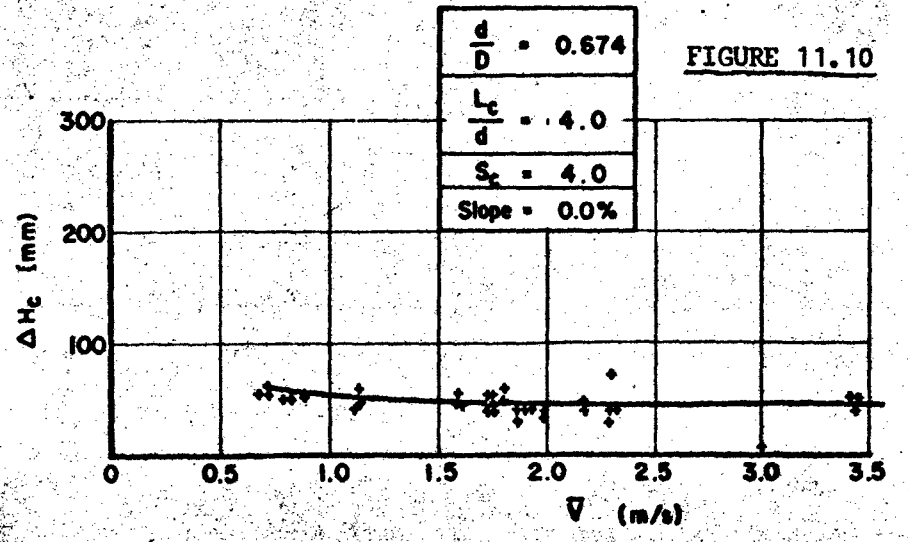

FIGURE 11.10

FIGURE 11.11

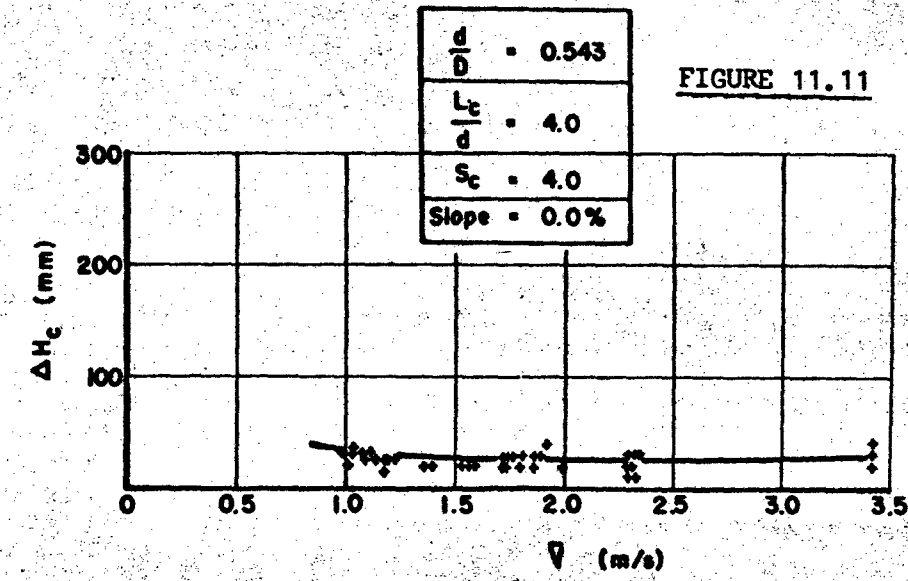

$\Delta H_c : \bar{V}$

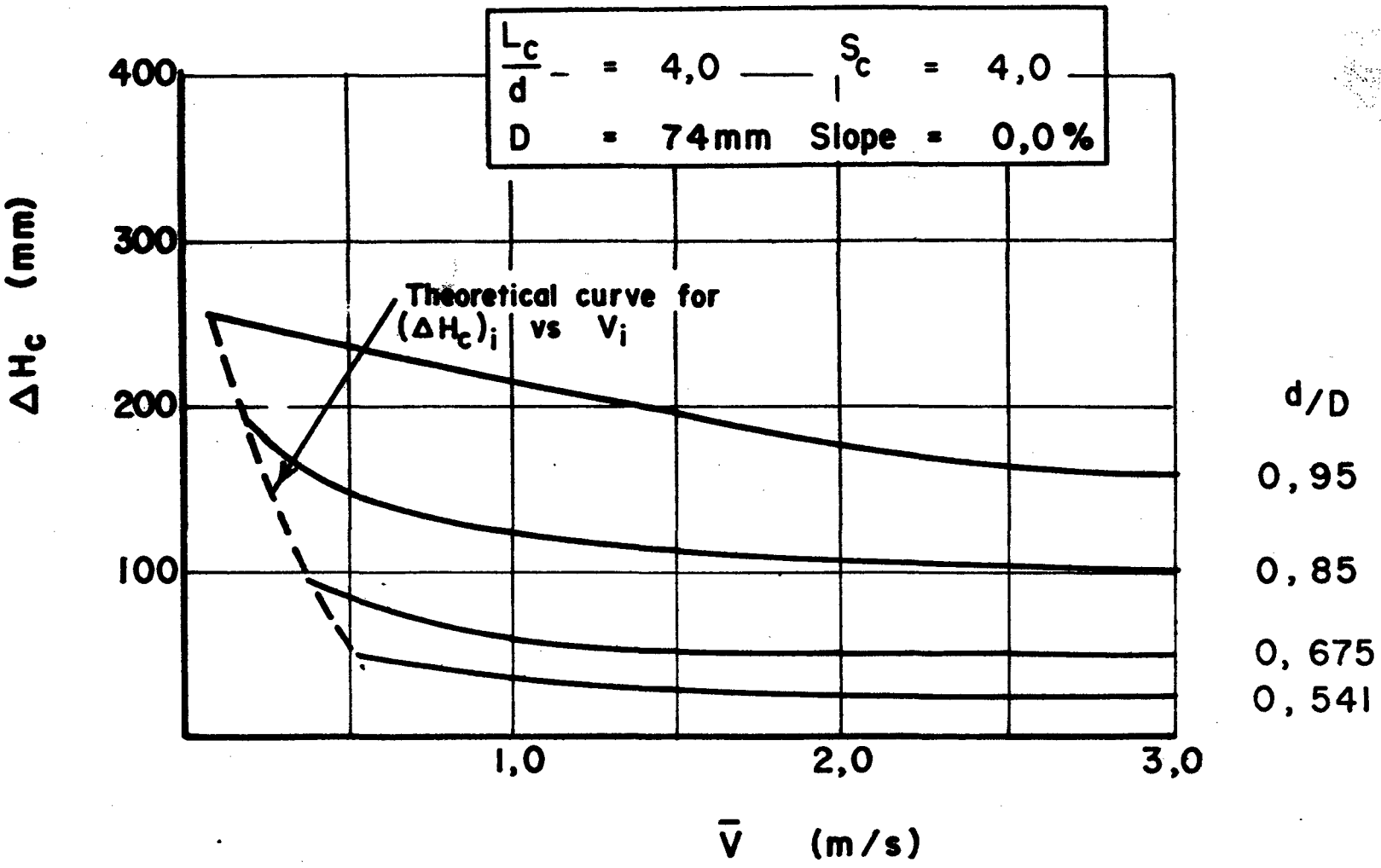

FIG. 11.12

curves with any degree of certitude is emphasised by the above comparison.

The curves alluded to above have been dealt with in some detail since they are taken as examples in other Chapters (e.g. Chapter 8, Chapter 15 and Chapter 16).

The following are the most significant features noted in connection with diameter ratio:

1. It is clear that as d/D increases the excess energy loss (ΔH_c) also increases.
2. The increase of ΔH_c with diameter ratio is greater for low velocities than for high velocities.
3. Figure 11.13 shows the capsule specific gravity (S_c) plotted against the excess energy loss (ΔH_c) for different diameter ratios at $\overline{V}$ = 1 m/s and it is apparent that the rate of increase of ΔH_c with S_c increases at higher diameter ratios.
   This point is amplified further when considering Figure 11.14 which is a plot of excess hydraulic head loss across the capsule as a function of diameter ratio at different submerged density ratios. This composite plot is taken from Fgiures 11.41 to 11.44, which will be referred to later and represents values at a fixed mean water velocity of $\overline{V}$ = 2 m/s.
   It is clear that for all the relative densities shown, the excess head loss increases progressively for increasing diameter ratios.
4. For diameter ratios $d/D > 0,85$ the increase referred to above becomes rather sharp, see Figure 11.14, and this sharp increase occurs at lower values of diameter ratio (d/D) for higher values of the submerged relative density (S_c-1).
5. The increase of ΔH_c with diameter ratio is slightly intensified at high capsule densities.

The reasons for the above observations are as follows:

FIG. 11.13

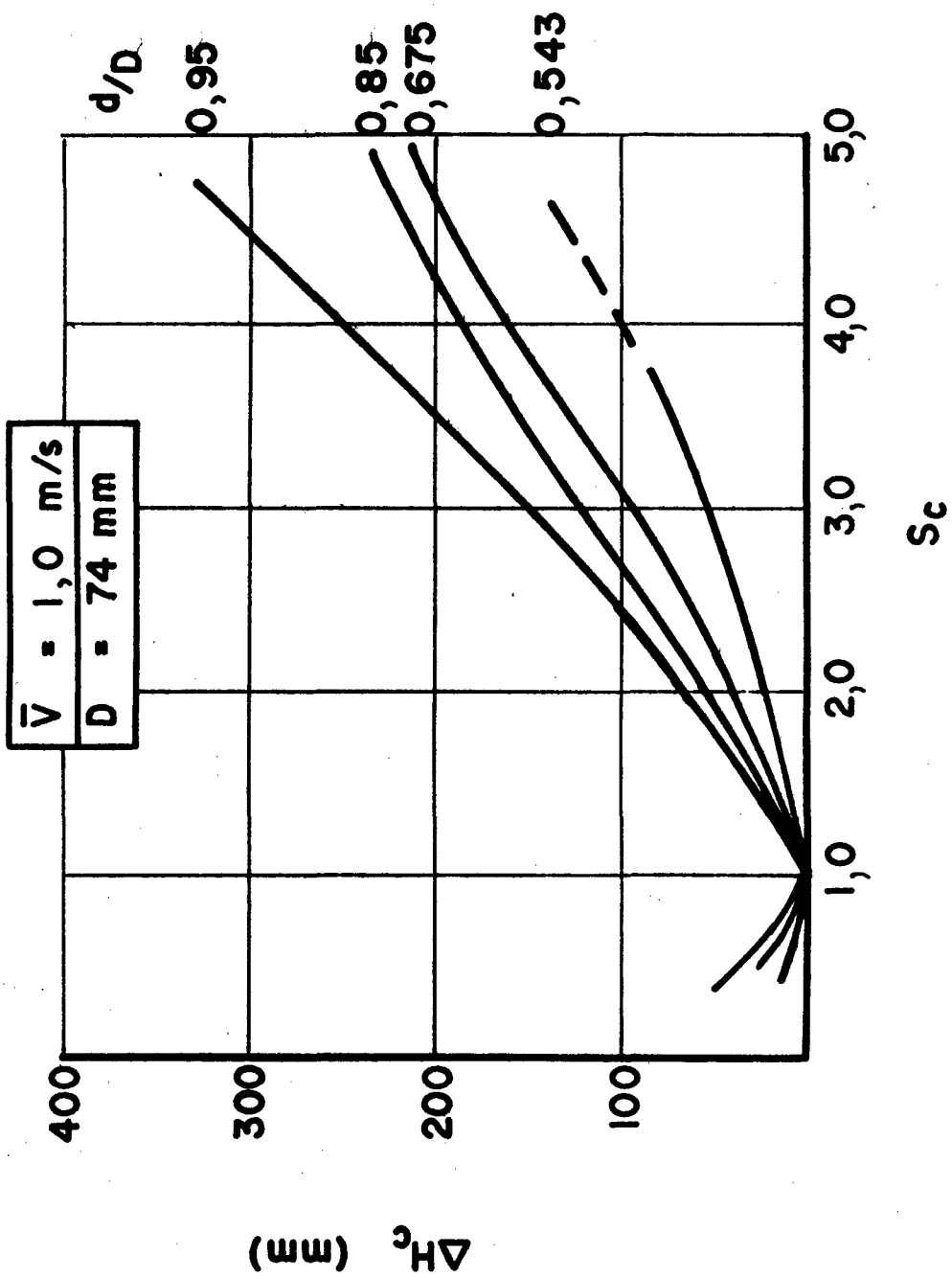
d/D
0,95
0,85
0,675
0,543
$\bar{V}$ = 1,0 m/s
D = 74 mm
400
300
200
100
1,0
2,0
3,0
4,0
5,0
Sc
ΔH_c (mm)

FIG. 11. 14

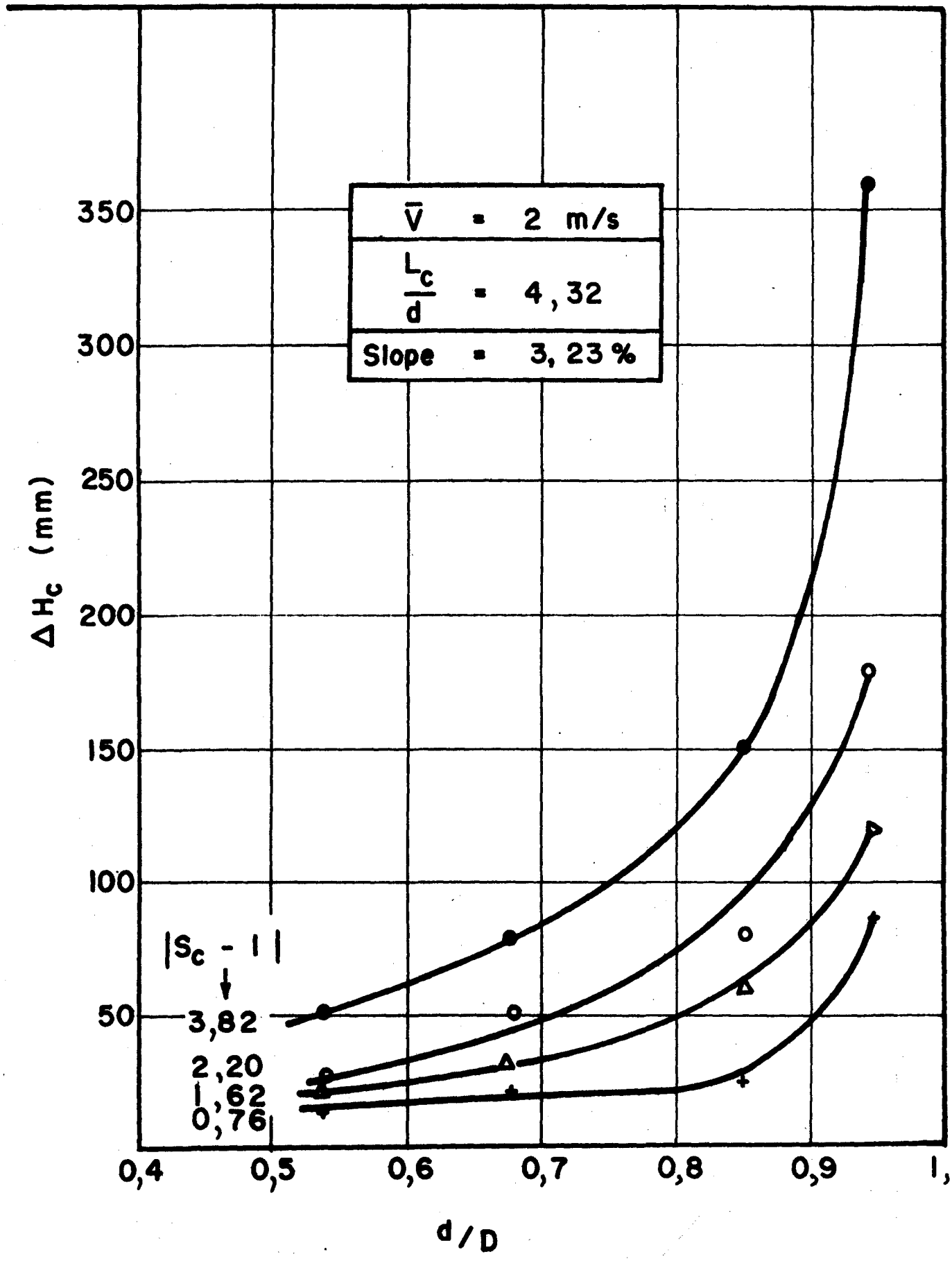
$\bar{V}$ = 2 m/s
$\frac{L_c}{d}$ = 4,32
Slope = 3,23 %
350
300
250
200
150
100
50
ΔH_c (mm)
$|S_c - 1|$
3,82
2,20
1,62
0,76
0,4
0,5
0,6
0,7
0,8
0,9
1,0
d/D

The form drag has been shown to be dependent on the frontal surface area of the capsule, which is dependent on the capsule diameter.

The skin friction drag depends on the surface area of the capsule which is again related to the diameter of the capsule.

For equal density geometrically similar capsules, the retarding solid to solid friction force is proportional to the capsule diameter cubed. Thus, excess head loss is greater for larger diameter ratios if solid to solid friction exists. The form and skin friction drags are also functions of the mean water velocity, and the mean annular water velocity relative to the capsule, as has been discussed. In Chapter 10 it was shown that, all other factors being equal, the larger diameter capsules travelled appreciably faster than those smaller and this discrepancy reduces at higher velocities.

Thus, the mean water velocity, relative to the capsule, is less for large diameters, and the form drag should be reduced for large capsules in so far as form drag is a function of the mean relative velocity. It is, thus, obvious that the frontal area effect dominates the velocity effect as a cause of increased ΔH_c. Although the second observation above, viz, the increase in excess head for large, compared with, small diameter capsules being greater for low than high velocities, is likely to be due to the velocity effect, which has in turn been attributed to capsule lift, (i.e. lift at high velocities causes smaller capsules to approach the velocities of larger ones as velocity increases).

Conversely, the velocity relative to the capsule in the annulus may be greater or smaller for large rather than small diameter ratios. So again the skin friction drag is dominated by the diameter and length (or surface area) of the capsule rather than the relative velocity.

The Couette flow component always imposes retardation and the larger

the diameter the greater the retardation, and the higher the value of ΔH_c.

4. The effect of capsule length

In order to determine the effect of length to diameter ratio, capsules of diameter ratio $d/D = 0,95$ and L_c/d ratio of 1,0; 2,0; 3,0; and 4,0 were utilised in the 74 mm diameter pipeline and trains of capsules ranging from $L_c/d = 2,0$ to $L_c/d = 16,0$ were tested at the four diameter ratios $d/D = 0,91$; 0,85; 0,675 and 0,54 in the 44 mm diameter pipe. These later results are represented as $\Delta H_c : \overline{V}$ curves as shown on Figures 11.15 to 11.18.

Figure 11.15 indicates that as the mean water velocity $(\overline{V})$ increases the value of ΔH_c decreases and the decrease appears to be most apparent at $L_c/d = 16,0$. All the other curves are reasonably parallel and Figures 11.15 to 11.18 show a consistent decrease of ΔH_c irrespective of the length to diameter ratio. The curves tend to flatten slightly as L_c/d decreases.

It must be born in mind that excess energy losses are by far the most unreliable measurements in this experiment, due to the superimposed turbulence as manifest on the rapid response pen recorder chart from the differential pressure transducer. It is difficult to attach any particular significance to the L_c/d ratio of 16,0 curve on Figure 11.15 as being the only curve which does not follow the pattern indicated by the other diameter ratios and length to diameter ratios. However, Figure 11.19 shows that the ratio excess head loss to capsule length $(\Delta H_c/L_c)$ plotted against the mean water velocity, absorbs the length effect fairly satisfactorily, even for $L_c/d = 16,0$. With $L_c/d = 10$ and 12 being slightly above the mean curve and $L_c/d = 2$ and 4 being slightly below. It appears as though there is a fair amount of scatter, but this effect is magnified by the scale of the graph. For example, one cm of differential

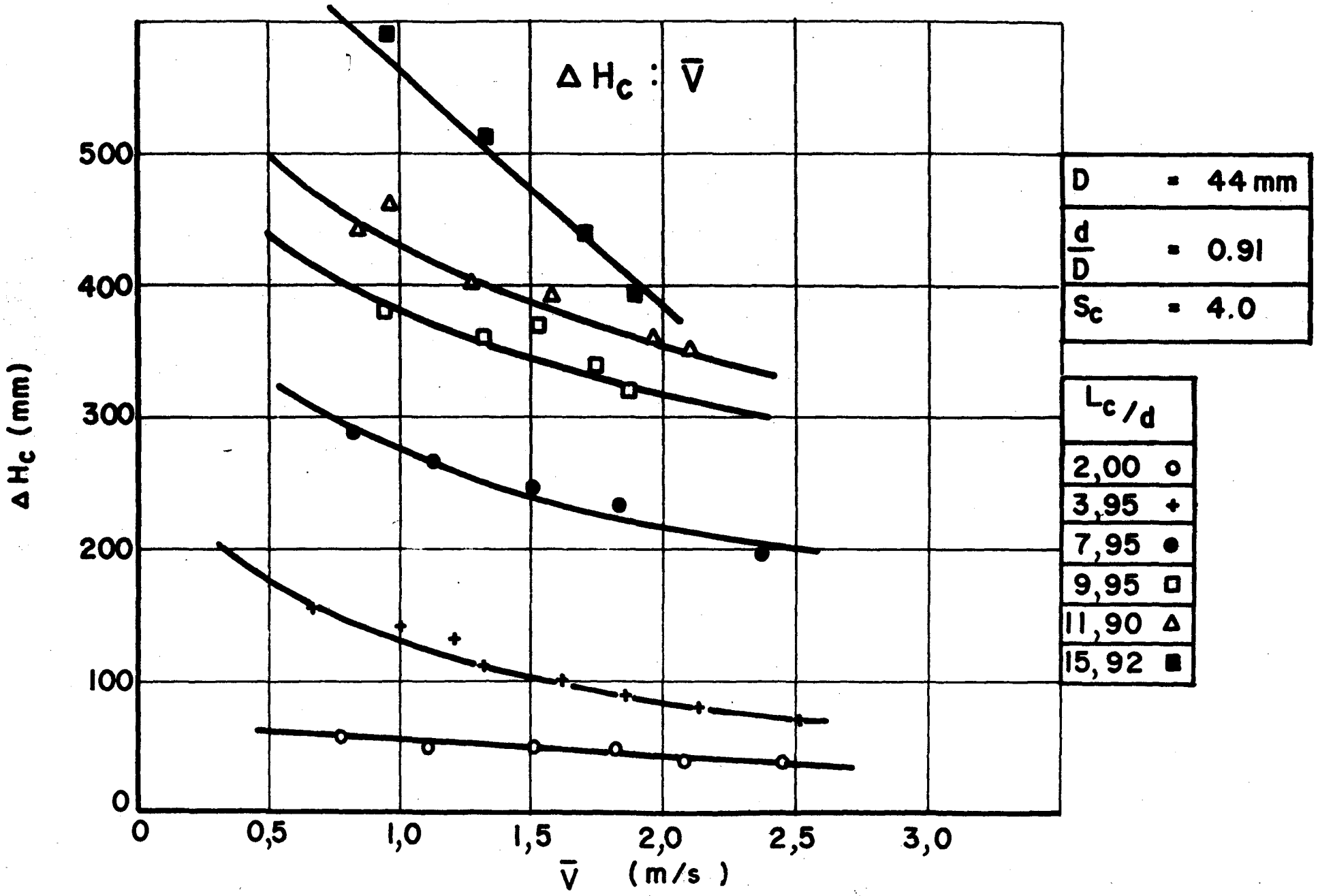
ΔHc : V̄
ΔHc (mm)
500
400
300
200
100
0
0
0,5
1,0
1,5
2,0
2,5
3,0
V̄ (m/s)
D = 44 mm
d/D = 0.91
Sc = 4.0
Lc/d
2,00 o
3,95 +
7,95 ●
9,95 □
11,90 △
15,92 ■

FIG. II.15

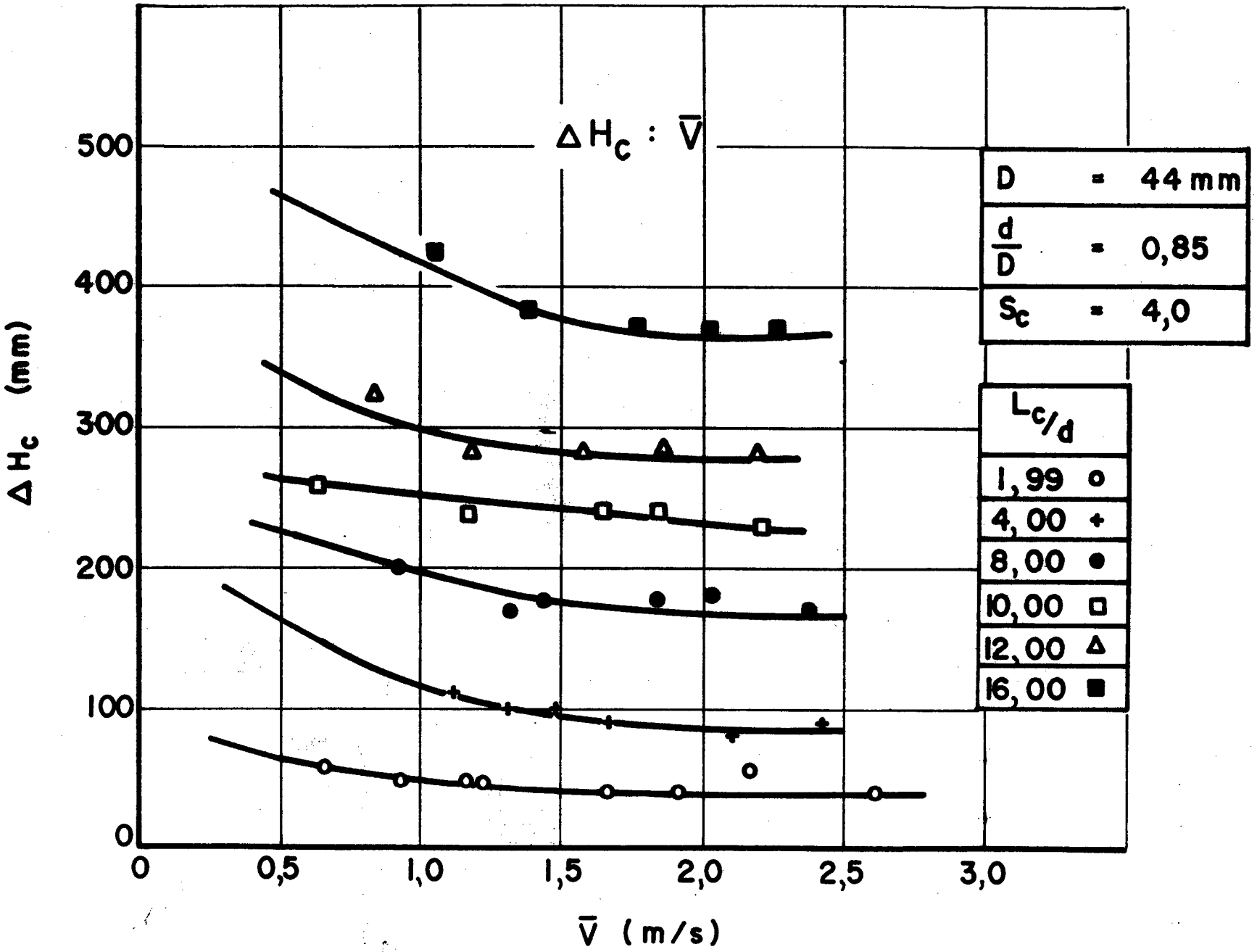
ΔHc : V̄
ΔHc (mm)
500
400
300
200
100
0
0
0,5
1,0
1,5
2,0
2,5
3,0
V̄ (m/s)
D = 44 mm
d/D = 0,85
Sc = 4,0
Lc/d
1,99
4,00
8,00
10,00
12,00
16,00

FIG. II.16

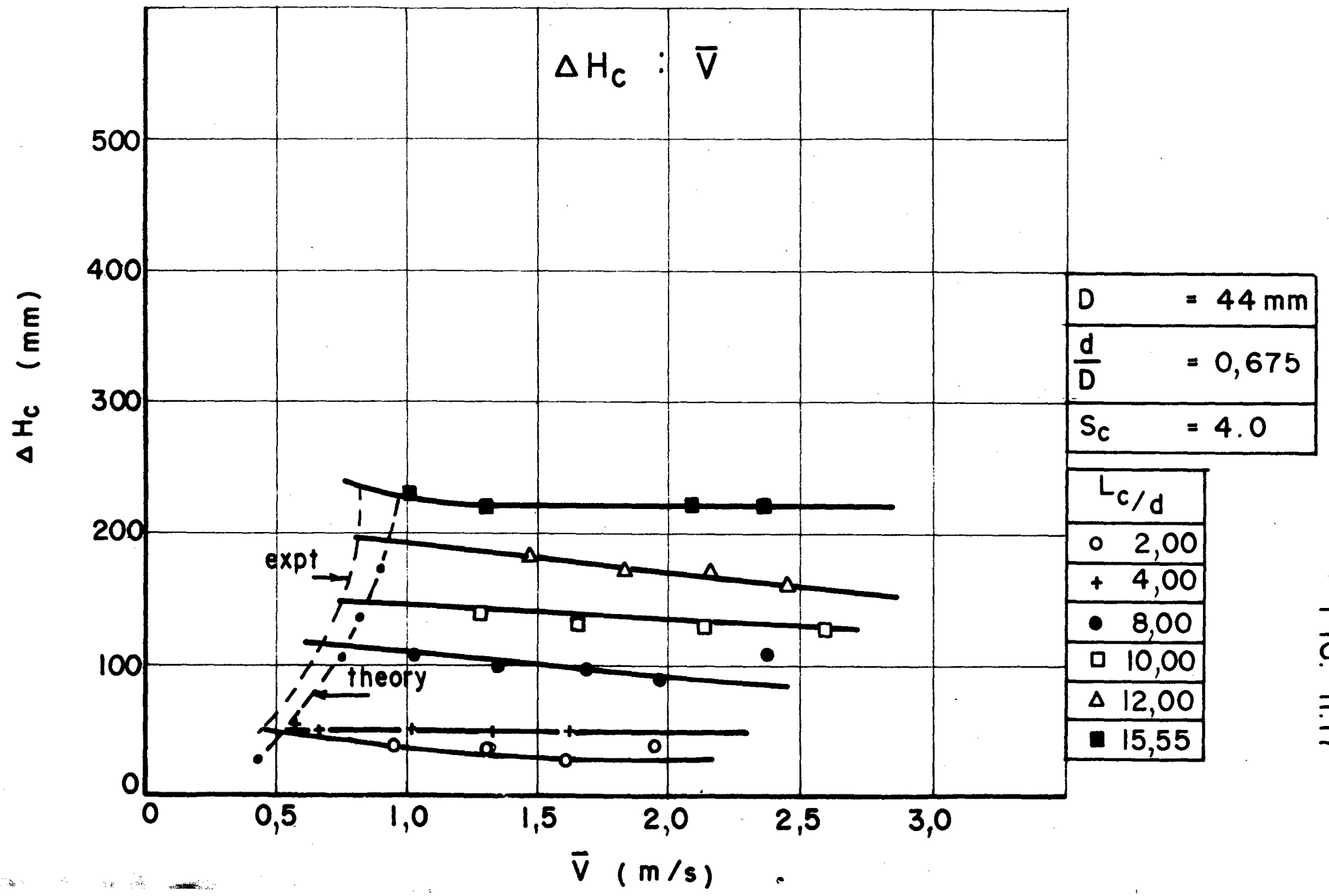
ΔHc : V̄
500
400
300
200
100
0
ΔHc (mm)
0
0,5
1,0
1,5
2,0
2,5
3,0
V̄ (m/s)
expt
theory
D = 44 mm
d/D = 0,675
Sc = 4.0
Lc/d
o 2,00
+ 4,00
● 8,00
□ 10,00
△ 12,00
■ 15,55

FIG. 11.17

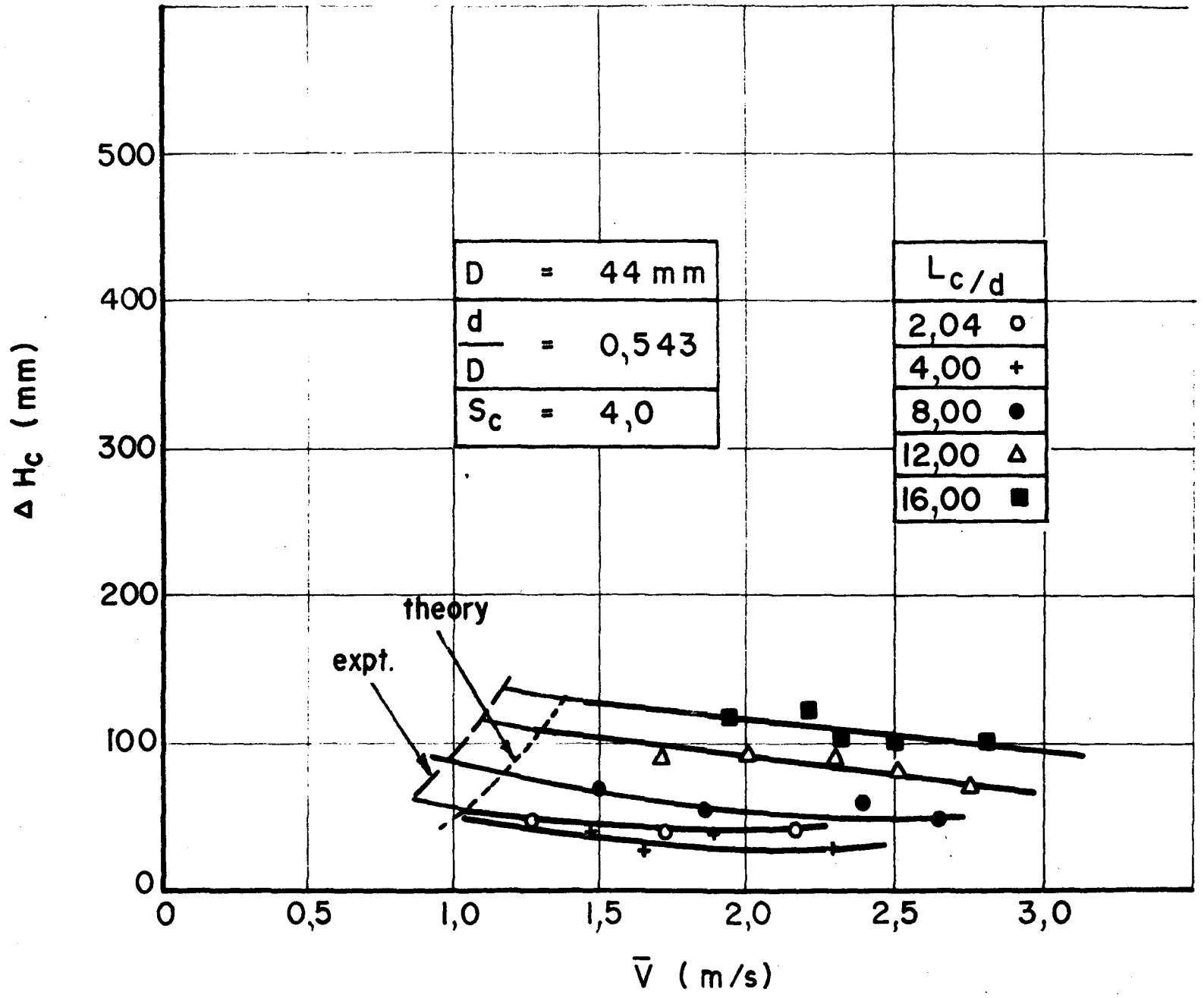
D = 44 mm
d/D = 0,543
Sc = 4,0
Lc/d
2,04 o
4,00 +
8,00 ●
12,00 △
16,00 ■
theory
expt.
Δ Hc (mm)
V̄ (m/s)
0
100
200
300
400
500
0,5
1,0
1,5
2,0
2,5
3,0

FIG. II.18

FIG. II.19

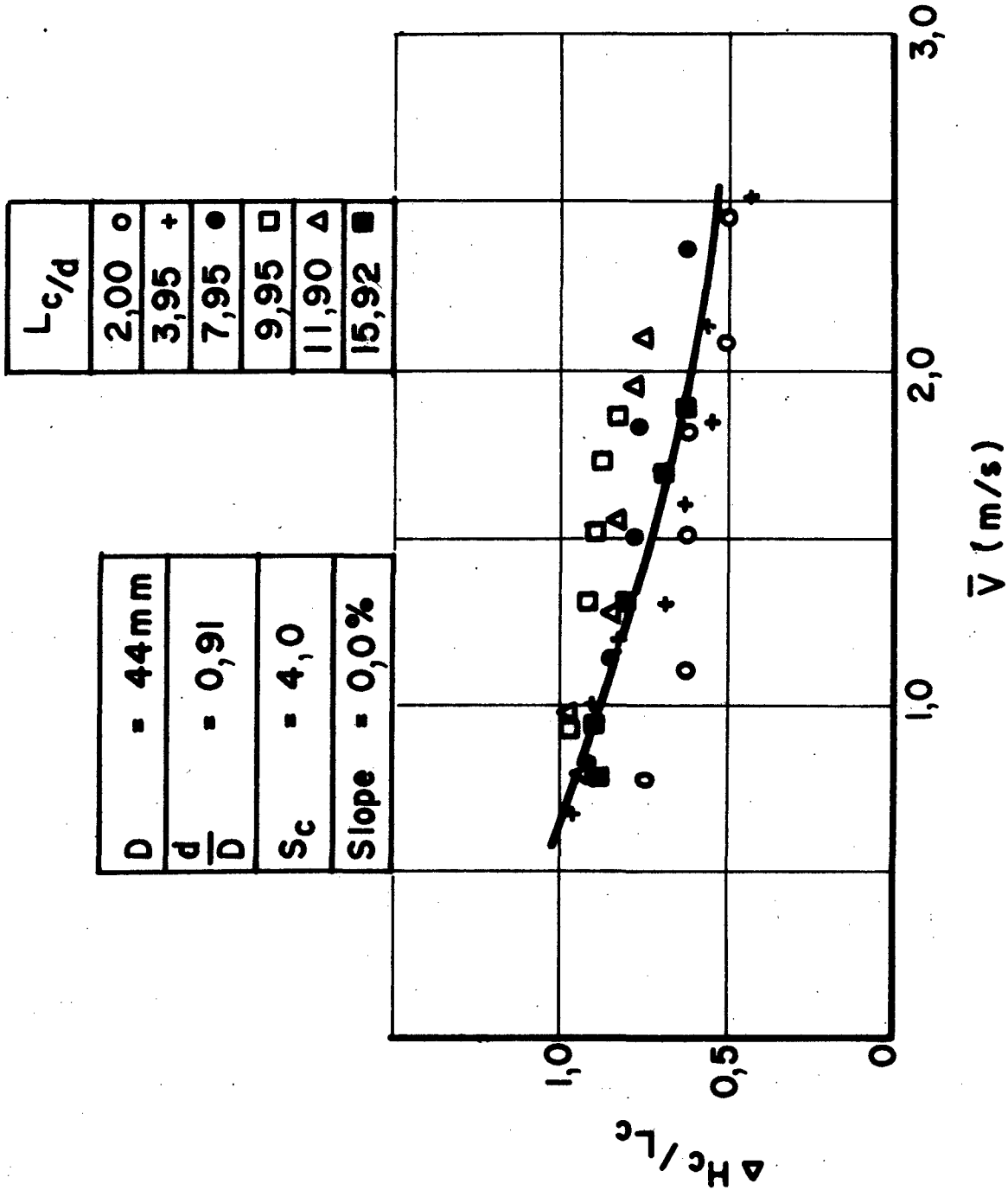
$L_{c/d}$
2,00 o
3,95 +
7,95 ●
9,95 □
11,90 △
15,92 ■
D = 44mm
$\frac{d}{D}$ = 0,91
S_c = 4,0
Slope = 0,0%
$\Delta H_c / L_c$
1,0
0,5
0
1,0
2,0
3,0
$\bar{V}$ (m/s)

pressure head of water is represented by 1,3 mm on the pen recorder chart, and due to turbulence this can represent the extent of experimental error. For $L_c/d = 2,0$, represented by open circles on the graph, a change of $\Delta H_c/L_c$ from 0,5 to 0,624, i.e. a 25% change in $\Delta H_c/L_c$ would only be equivalent to a 1,0 cm change of ΔH_c and 1,3 mm change on the chart, and this is hardly detectable when superimposed on the fluctuation of ΔH_c.

A scatter from the mean curve of $\Delta H_c/L_c = 0,182$ for the $L_c/d = 10$ result at $\overline{V} = 1,74$ m/s appears to be a 27% variation. Again, in terms of ΔH_c this is a 7,0 cm difference which on the pen recorder chart scale is 0,91 cm; in this case of the same order of magnitude as the turbulence fluctuation.

This technique of plotting (viz $\Delta H_c/L_c$ versus $\overline{V}$) is more successful in embracing the L_c/d effect with the other diameter ratios, see Figures 11.20, 11.21 and 11.22. The only exception is the ratio $L_c/d = 2,0$ at $d/D = 0,543$ (Figure 11.22).

However, if reference is made back to Figure 11.18, it can again be seen that the error is considerably magnified by the scale of plotting particularly at the low values of ΔH_c and L_c/d.

A summary of Figures 11.19 to 11.22 is shown on Figure 11.23 without data points.

As a preliminary investigation, capsules of $d/D = 0,95$ and $L_c/d = 1,0$; 2,0; 3,0 and 4,0 were tested in the 74 mm diameter perspex line and excess head losses (ΔH_c) are shown plotted against $\overline{V}$ in a horizontal pipe on Figures 11.24 to 11.27.

Average values of data points are shown summarised for these figures on Figure 11.28 and total head loss values on Figure 11.29 (this will be referred to later).

FIG. 11.20

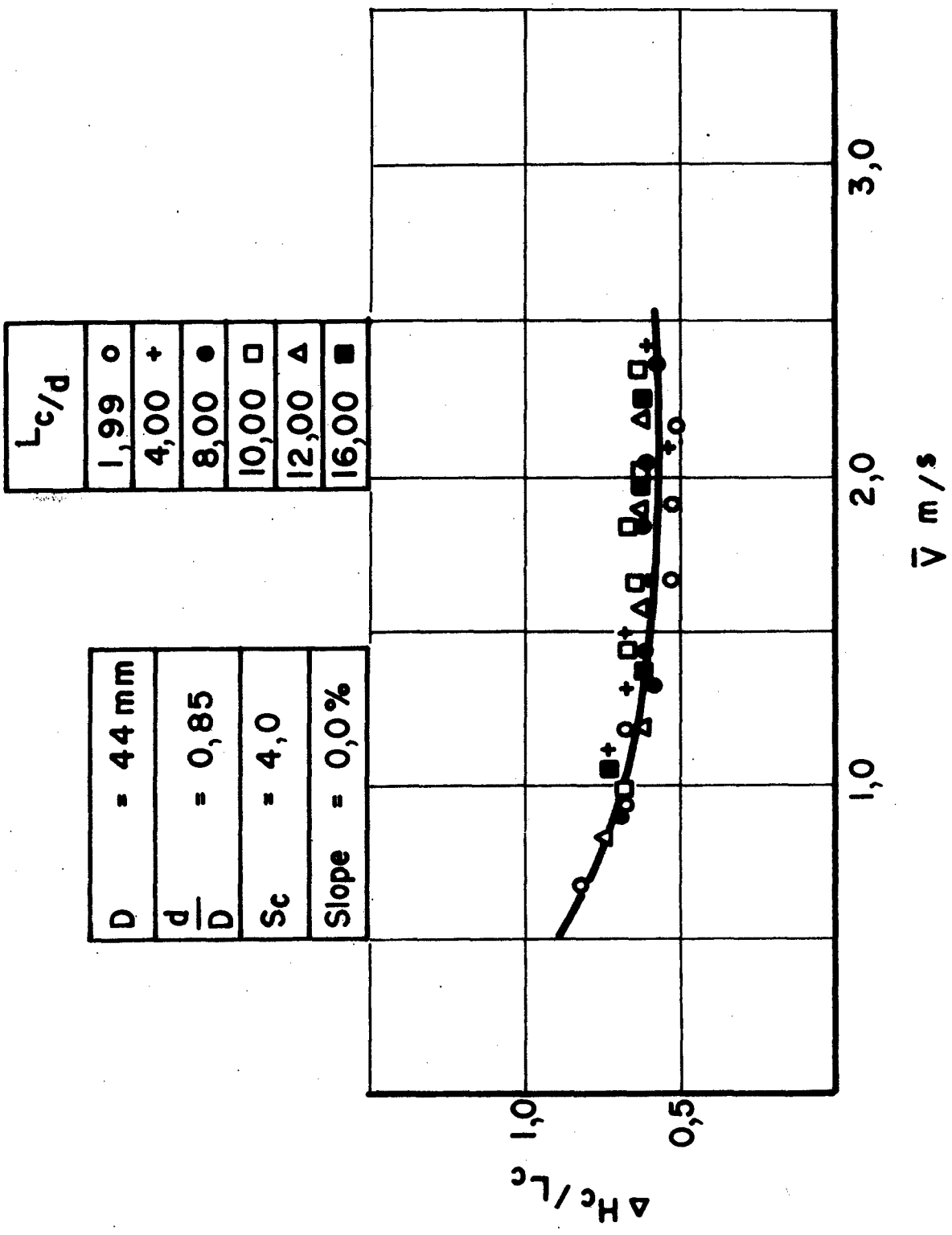
$L_{c/d}$
1,99 o
4,00 +
8,00 ●
10,00 □
12,00 △
16,00 ■
D = 44 mm
d/D = 0,85
Sc = 4,0
Slope = 0,0%
$\Delta H_c / L_c$
1,0
0,5
1,0
2,0
3,0
$\bar{V}$ m/s

FIG . II.21

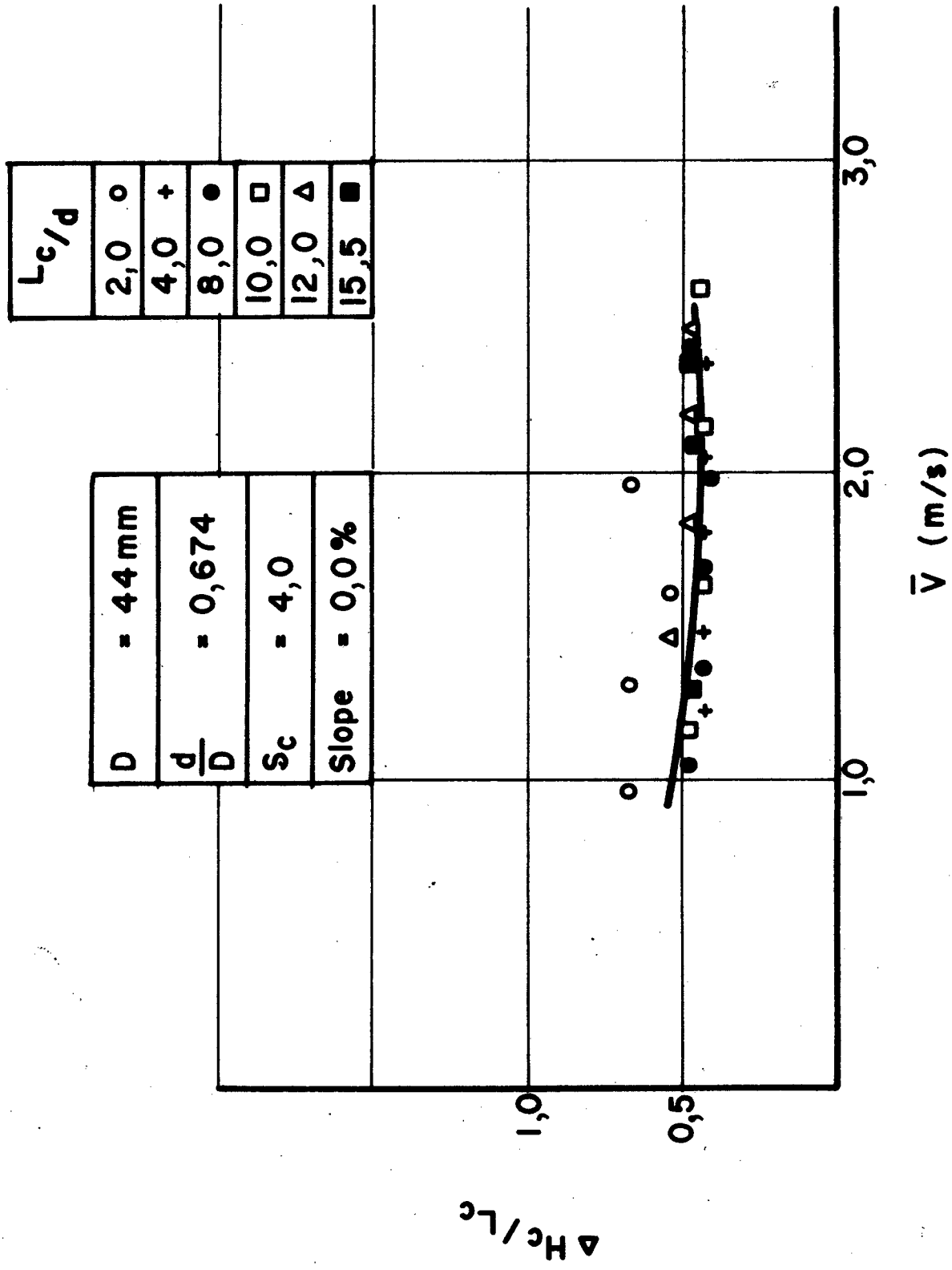
Lc/d
2,0 o
4,0 +
8,0 ●
10,0 □
12,0 △
15,5 ■
D = 44 mm
d/D = 0,674
Sc = 4,0
Slope = 0,0%
ΔHc/Lc
1,0
0,5
1,0
2,0
3,0
V̄ (m/s)

FIG. II.22

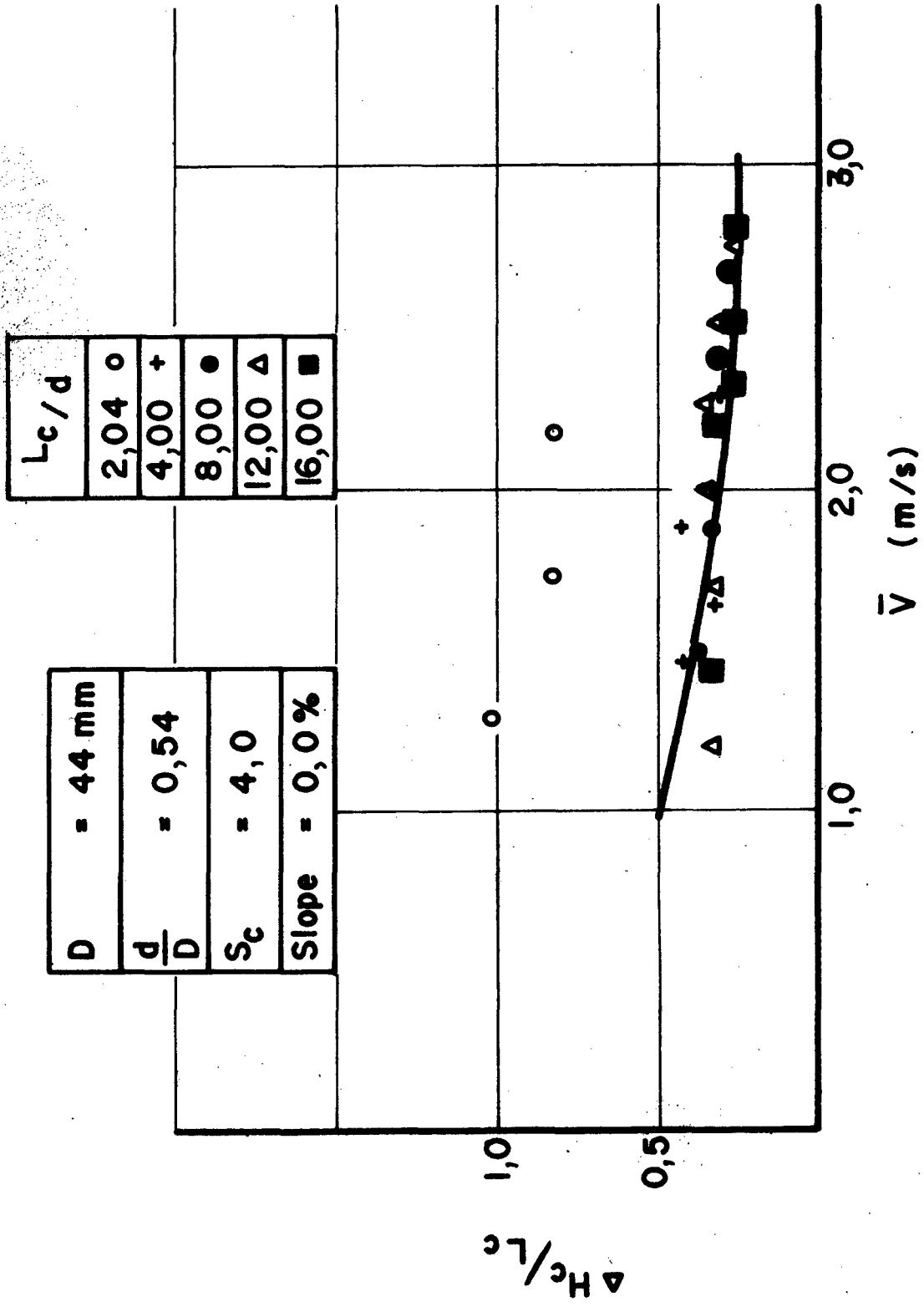
Lc / d
2,04 o
4,00 +
8,00 ●
12,00 Δ
16,00 ■
D = 44 mm
d/D = 0,54
Sc = 4,0
Slope = 0,0%
1,0
0,5
1,0
2,0
3,0
V̄ (m/s)
ΔHc/Lc

FIG. 11.23

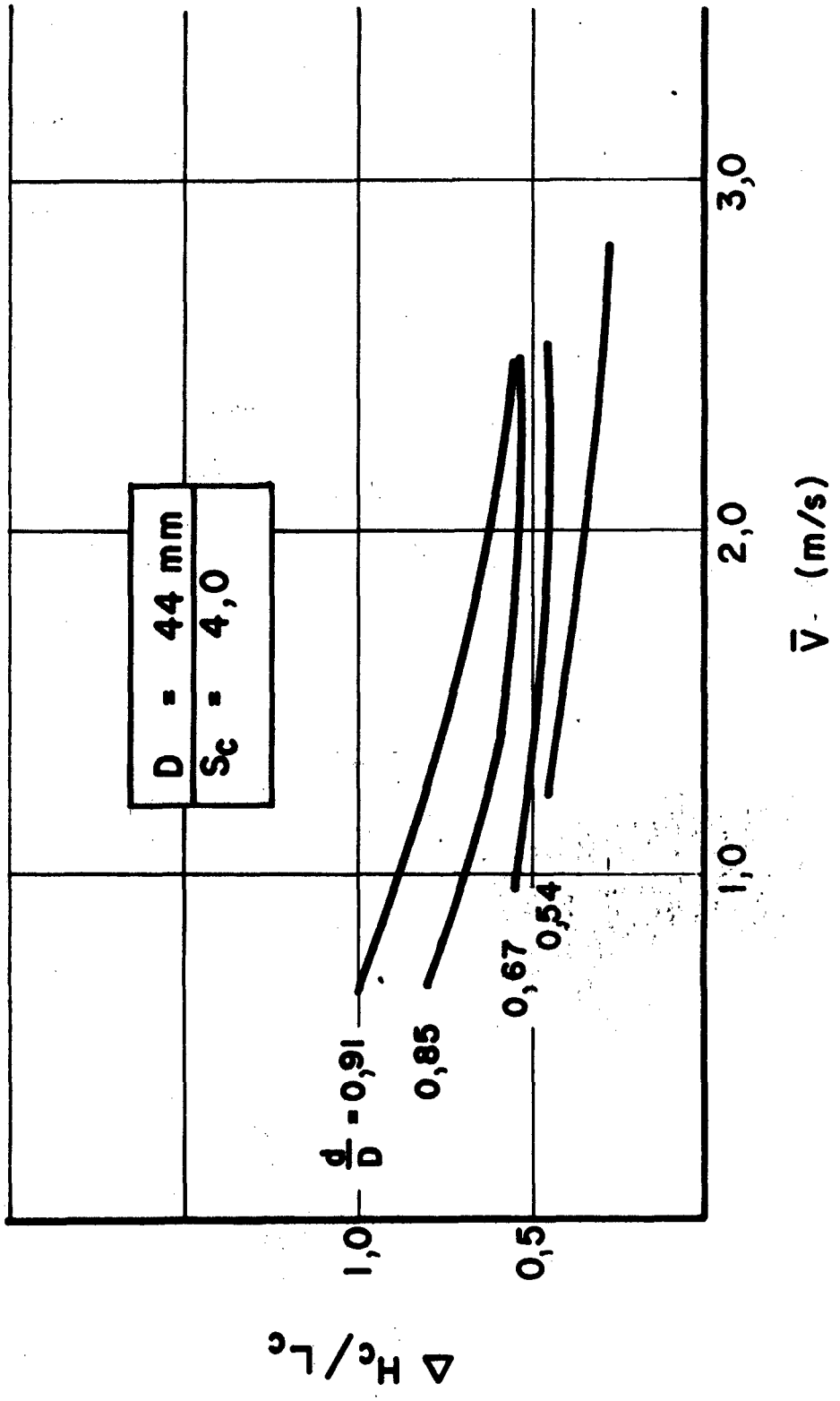

Figure 11.24

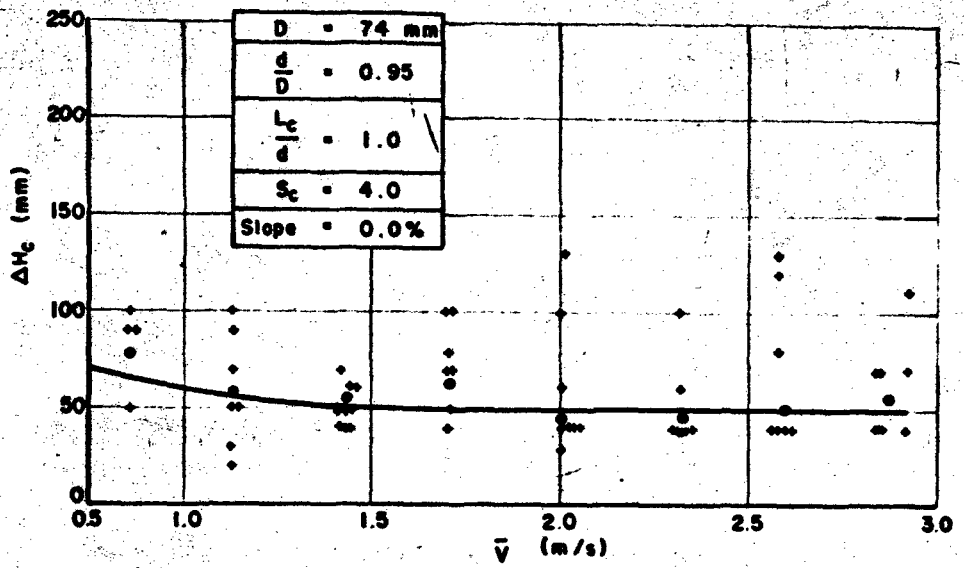

Figure 11.25

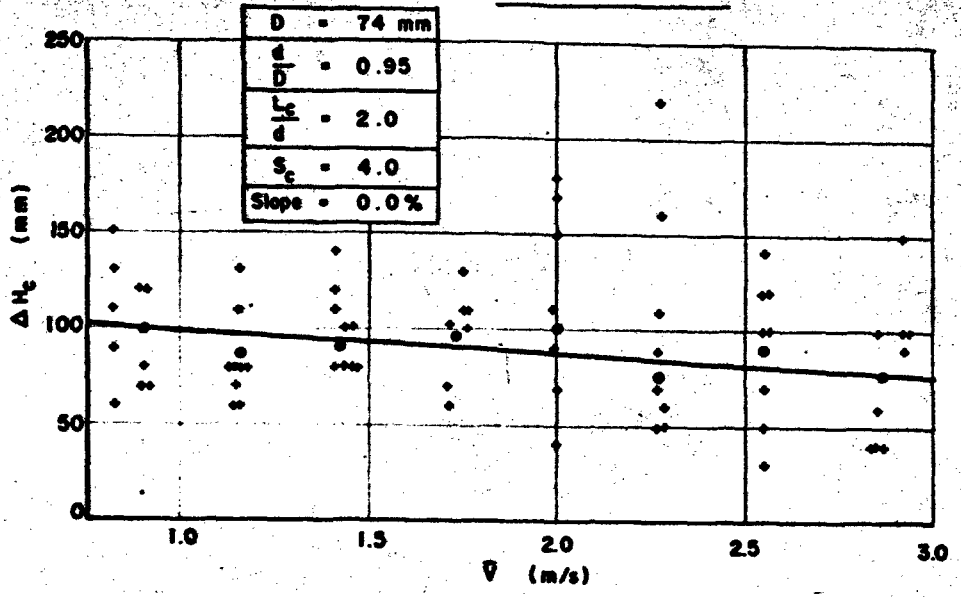

Figure 11.26

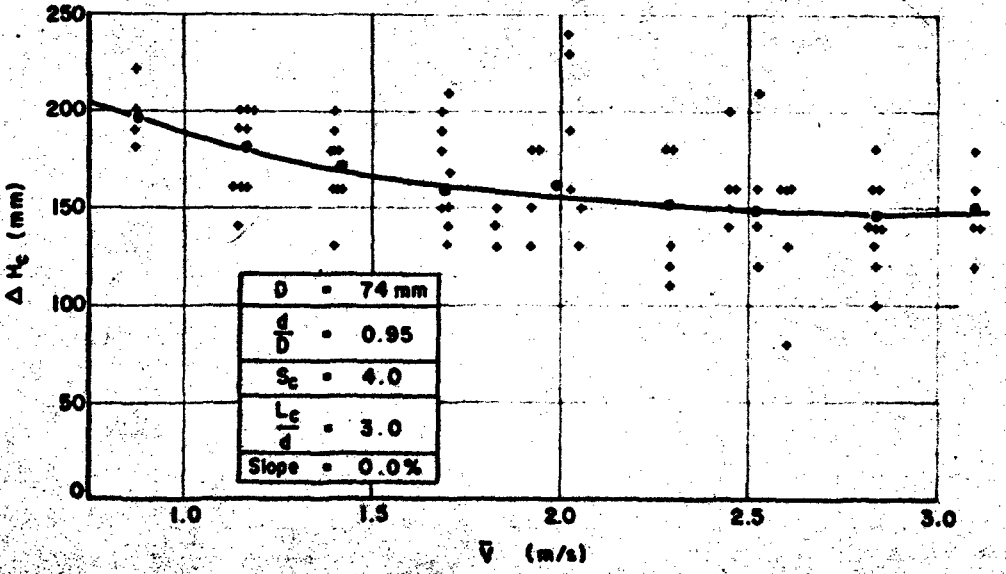

Figure 11.27

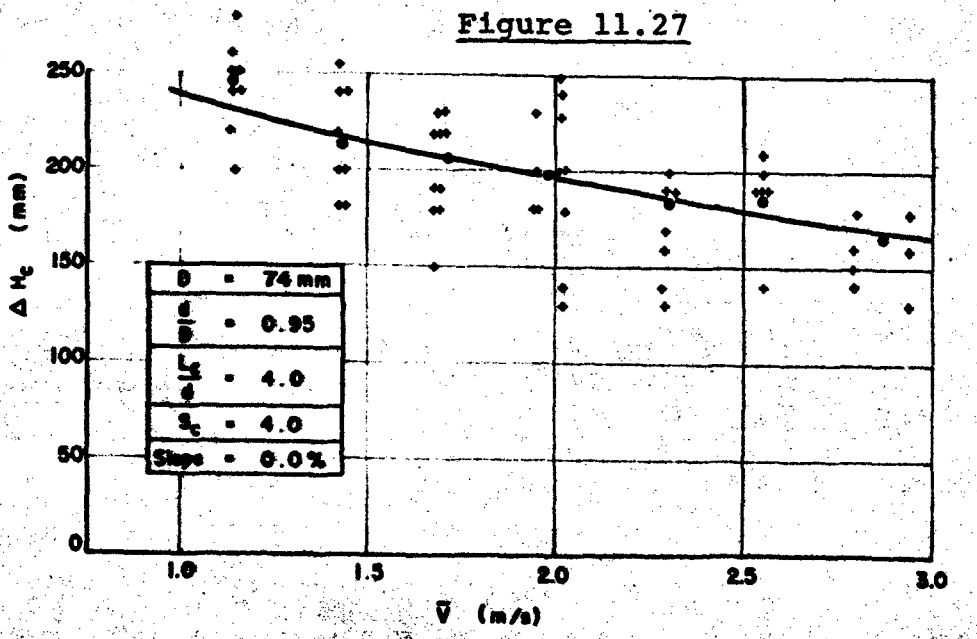

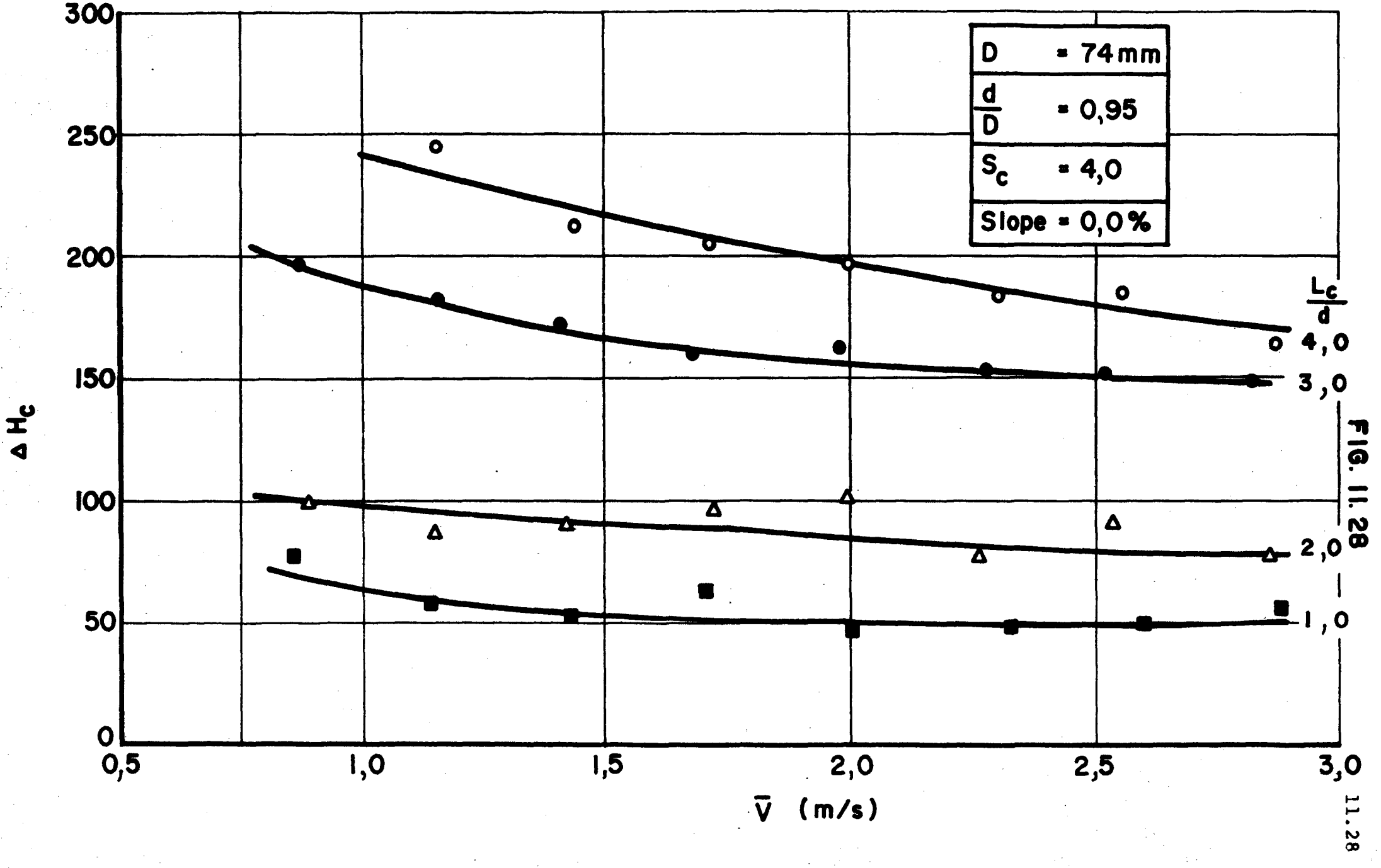

FIG. 11.28

11.28

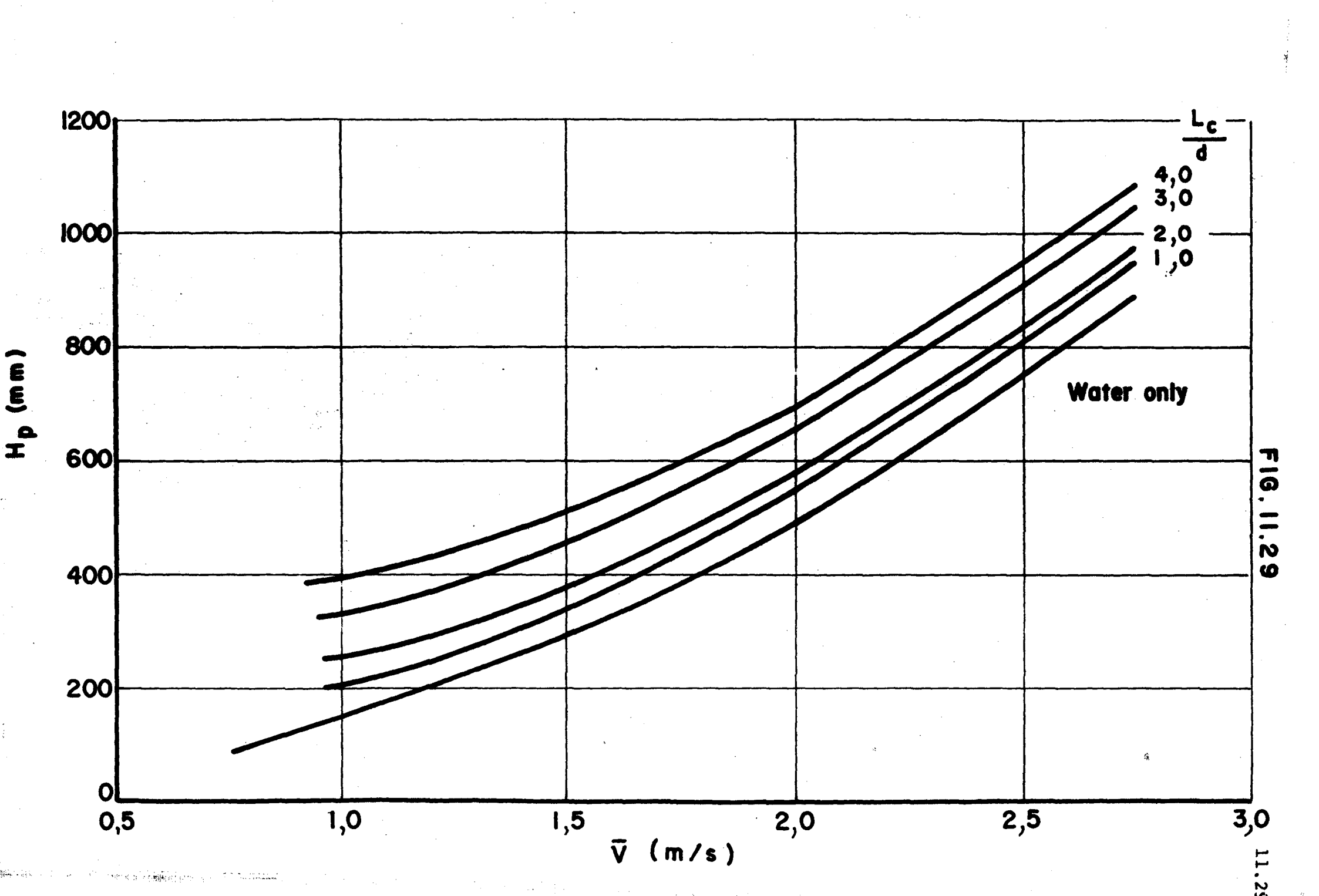
1200
1000
800
600
400
200
0
H_p (mm)
L_c / d
4,0
3,0
2,0
1,0
Water only
0,5
1,0
1,5
2,0
2,5
3,0
$\bar{V}$ (m/s)

FIG. II.29

Also, in anticipation of the next section, Figures 11.30 to 11.33 are shown for an upward sloping pipe (slope = 3,13%) and these results are summarised on Figure 11.34 where $(\Delta H_c)'_s$ is plotted against $\bar{V}$ for average values of data points only. The meaning of $(\Delta H_c)'_s$ is discussed in the next section. Figure 11.35 shows the total head for these capsules in the mildly upward sloping pipeline.

The technique of plotting the ratio $\Delta H_c/L_c$ has absorbed the length effect for the trains of capsules in the 44 mm diameter pipe. Can the method be extended to these capsules of larger diameter ratio (d/D = 0,95) and differing (L_c/d) ratios? Figures 11.36 and 11.37 validate this method of taking L_c/d into account in this case.

The successful absorption of the length effect by the above non-dimensional device of ordinate plotting can be ascribed to the fact that the force required to propel a capsule of a particular diameter and SG at a rixed velocity along the pipe, must be resisted by the solid friction force plus the Couette force, both of which are proportional to the capsule length.

If the capsule lifts, the retarding force is due to Couette shear and is proportional to the length of capsule.

Therefore, whether the capsule lifts or not, the forces required are proportional to the length of capsule.

5. The effect of pipe slope

Equation (7.193) can be written as;

$$(\Delta H_c)'_s = (4L_c/wD)\bar{\tau}_p + L_c(d/D)^2|S_c-1|(\mu_f(\cos\phi-L_r) + \sin\phi) - h_{fc} \quad (11.1)$$

Where $(\Delta H_c)'_s$ replaces ΔH_c as the total excess head drop across the capsule on a slope and includes the effect of energy dissipation as well as elevational head, and takes into account the shear stress in the

Figure 11.30

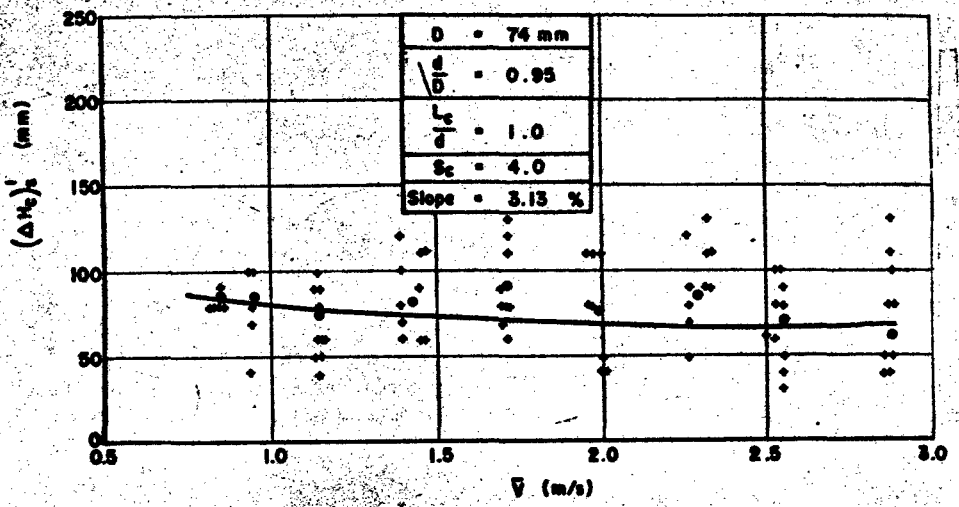

Figure 11.31

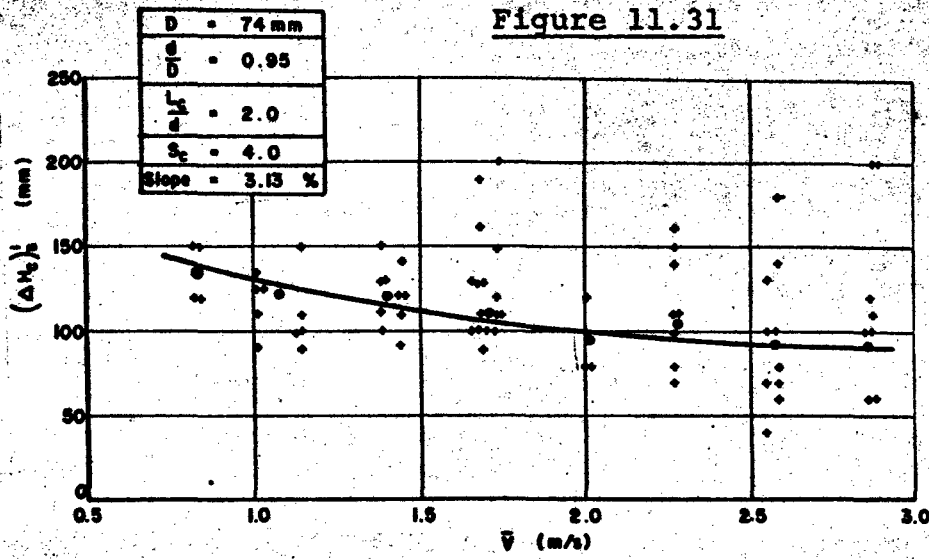

Figure 11.32

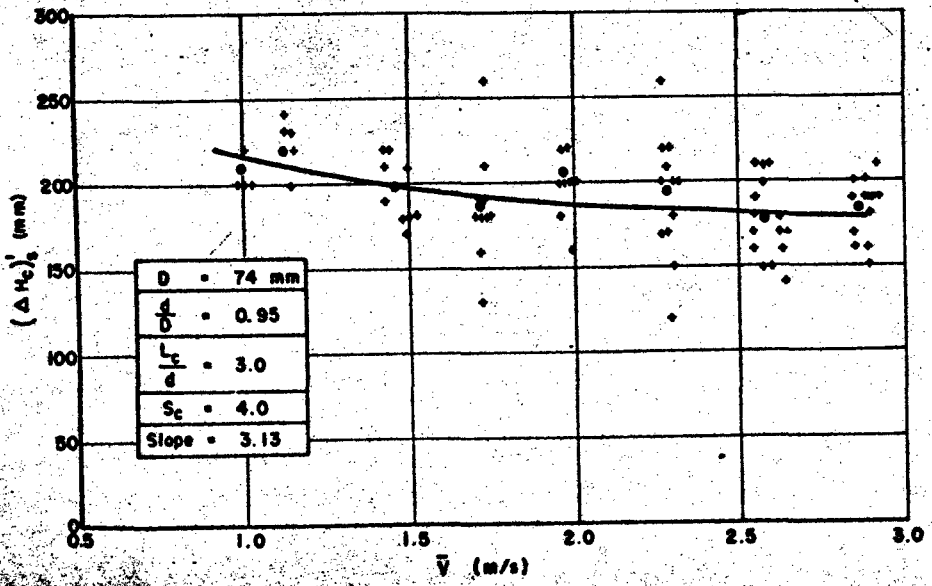

Figure 11.33

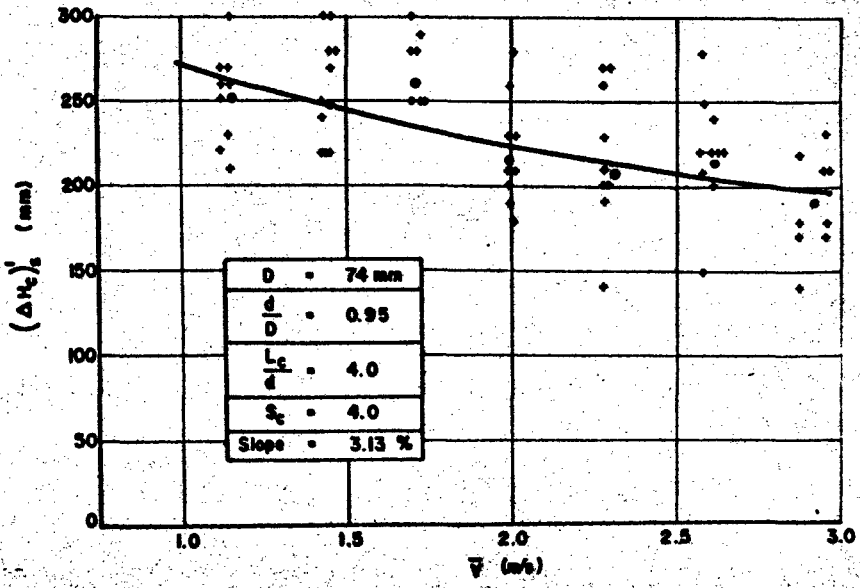

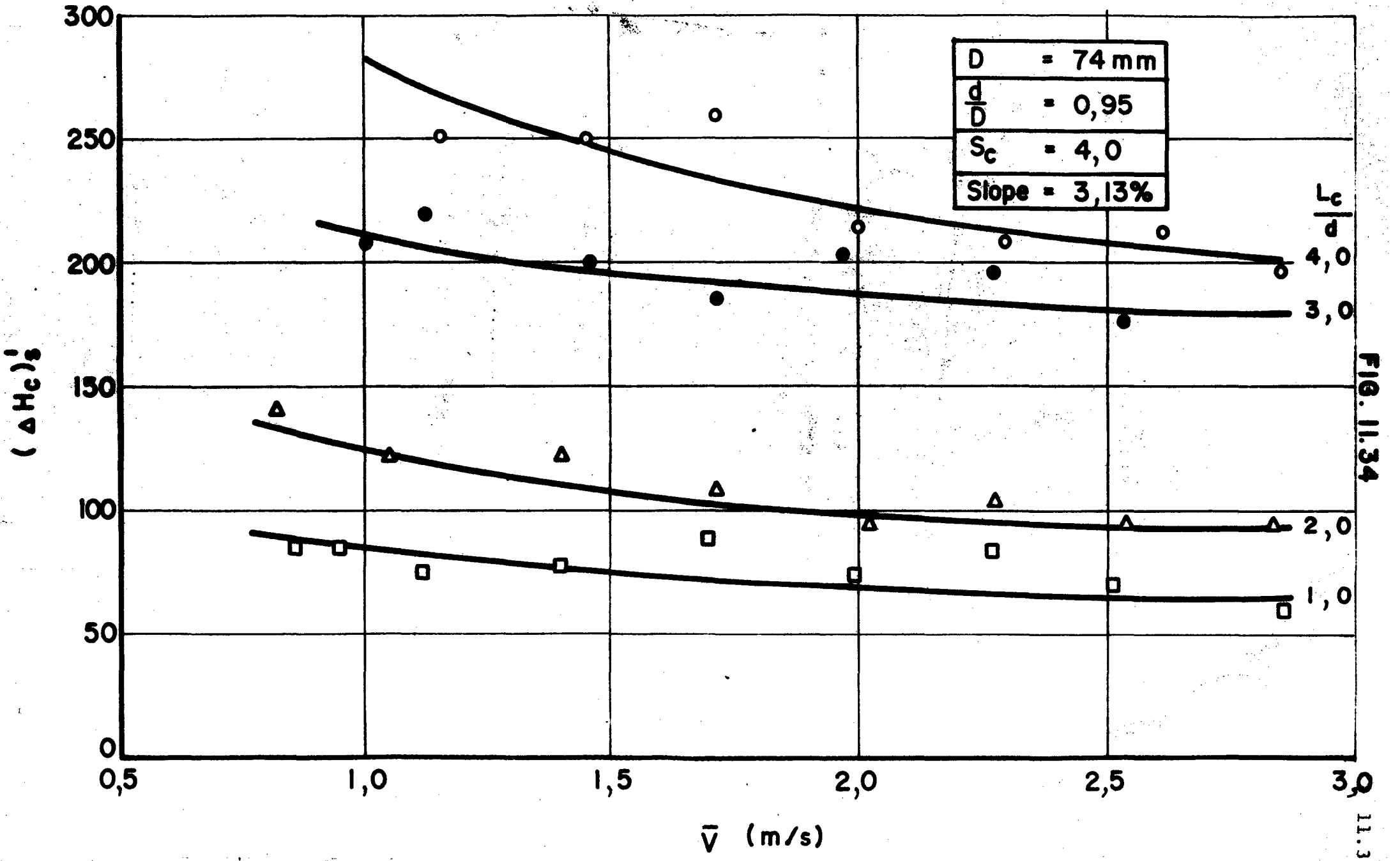

FIG. II.34

11.32

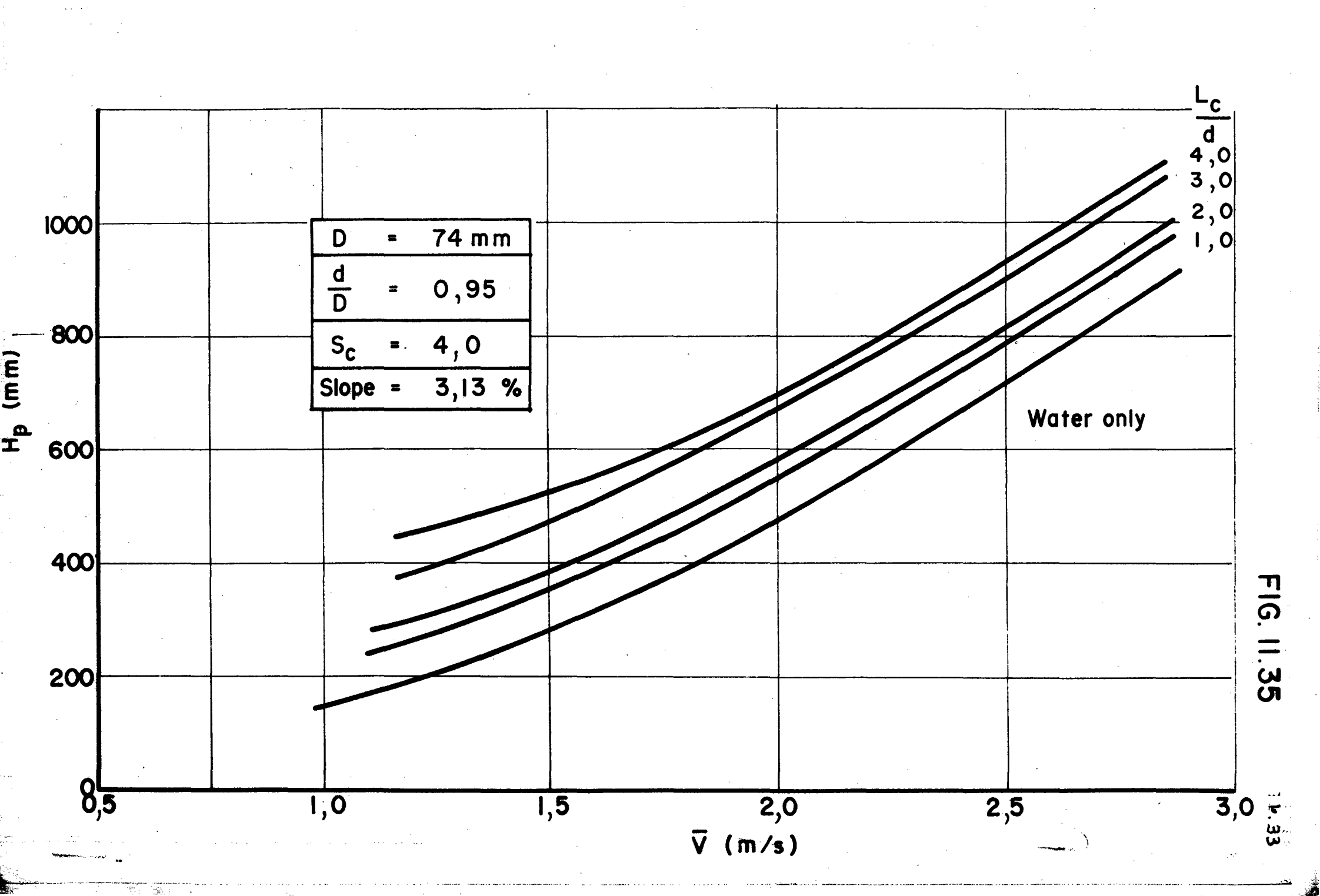
D = 74 mm
d/D = 0,95
Sc = 4,0
Slope = 3,13 %
Lc/d
4,0
3,0
2,0
1,0
Water only
Hp (mm)
0
200
400
600
800
1000
0,5
1,0
1,5
2,0
2,5
3,0
V̄ (m/s)

FIG. II.35

FIG. 11.36

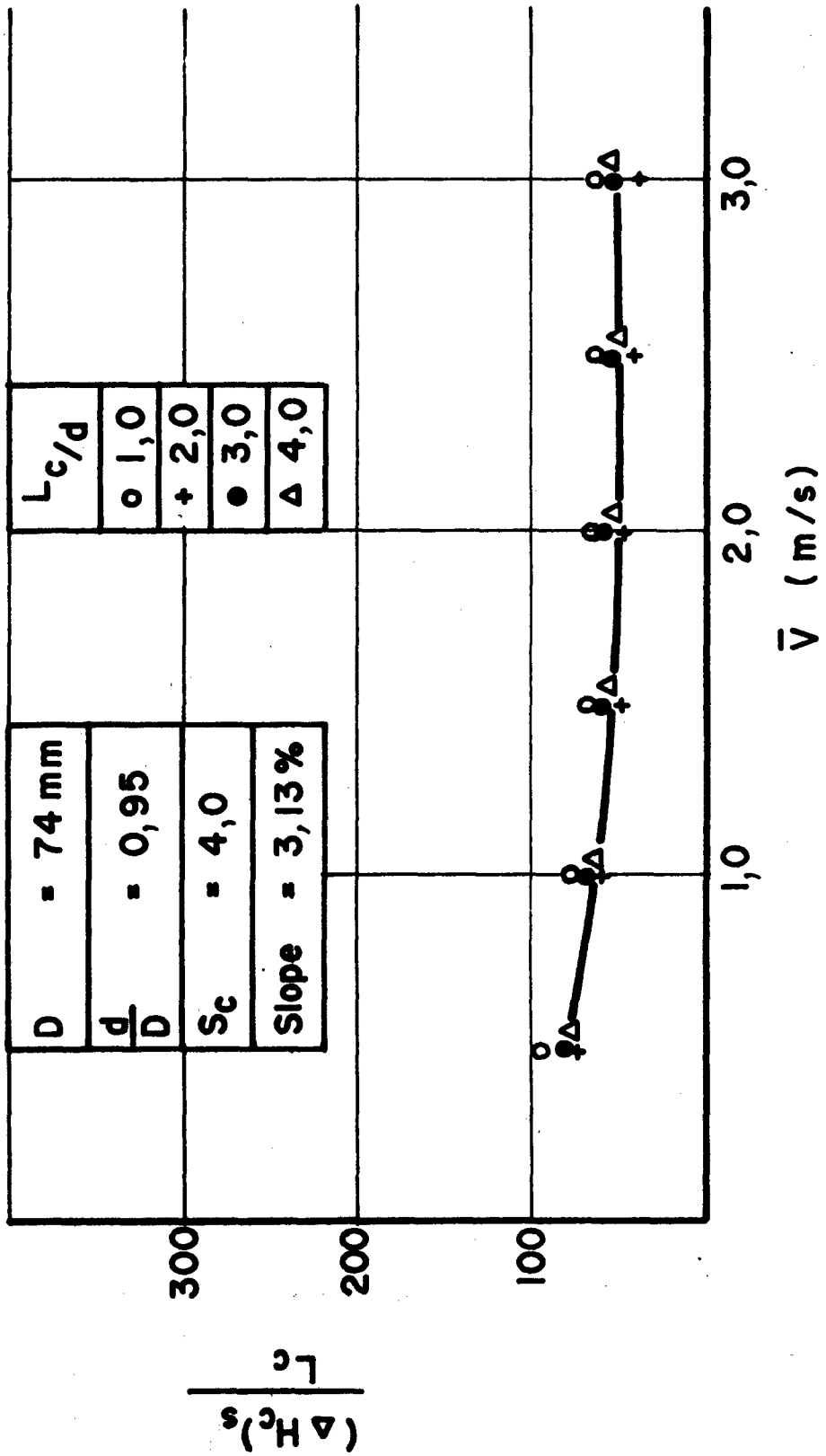
D = 74 mm
d/D = 0,95
Sc = 4,0
Slope = 3,13%
Lc/d
o 1,0
+ 2,0
● 3,0
Δ 4,0
300
200
100
1,0
2,0
3,0
V̄ (m/s)
(ΔHc)s / Lc

FIG. 11.37

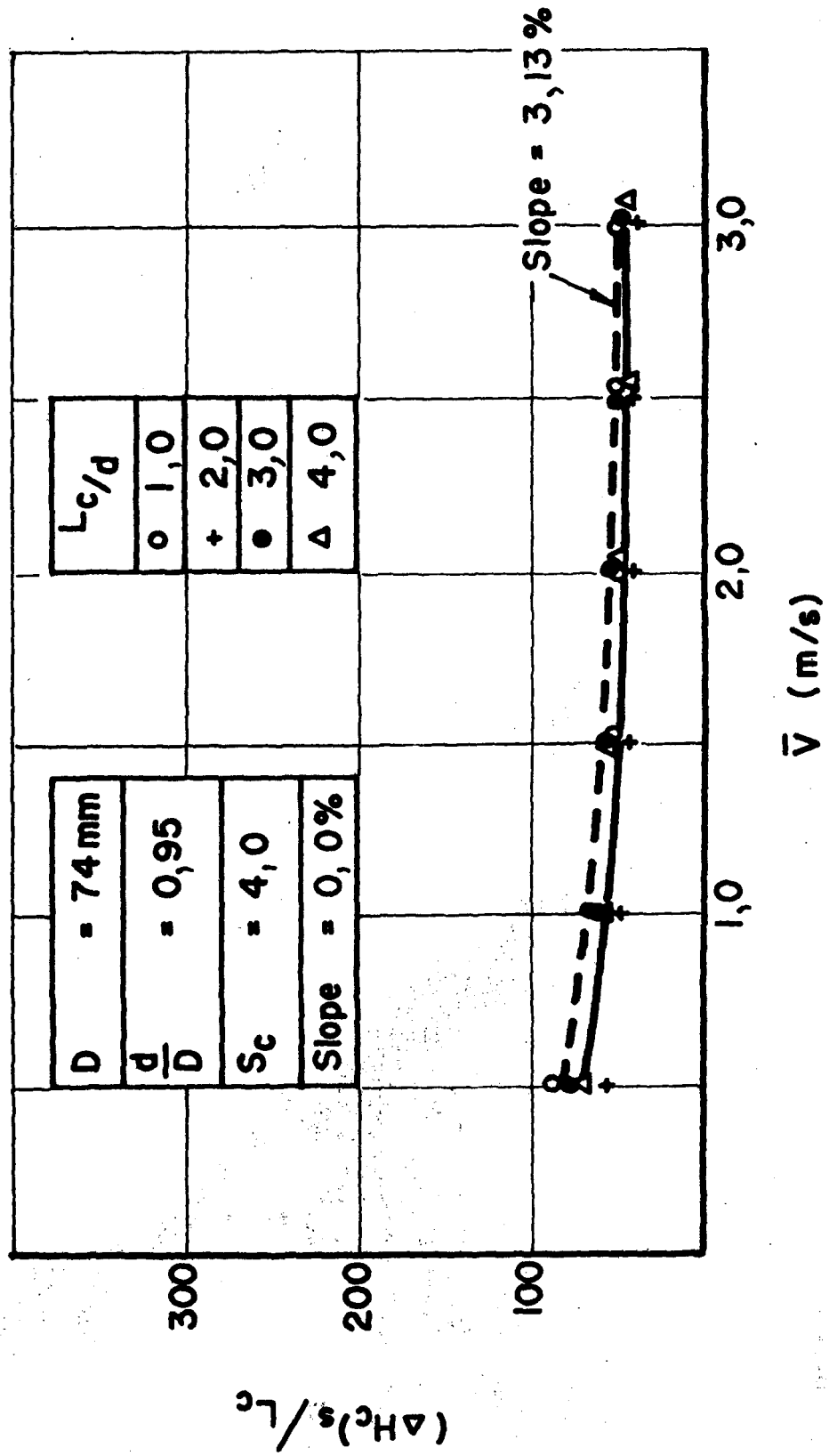
Slope = 3,13 %
$L_{c/d}$
o 1,0
+ 2,0
• 3,0
Δ 4,0
D = 74 mm
d/D = 0,95
S_c = 4,0
Slope = 0,0%
300
200
100
1,0
2,0
3,0
$\bar{V}$ (m/s)
$(\Delta H_c)_s / L_c$

curvilinear flow region upstream and downstream of the capsule (see equation (7.19)). Equation 11.1 can be written as;

$$(\Delta H_c)'_s = (\Delta H_c)_s + (d/D)^2 |S_c - 1| L_c \sin \phi \qquad (11.2)$$

where $(\Delta H_c)_s$ = net excess head loss across the capsule on the slope

i.e. $(\Delta H_c)_s = \mu_f L_c (d/D)^2 |S_c - 1| (\cos \phi - L_r) + (4L_c/Dw)\overline{\tau}_p - h_{fc}$ (11.3)

If the slope of the pipe is relatively small then

$$(\Delta H_c)_s \doteqdot \Delta H_c$$

The first term on the right hand side of equation (11.3) is only about 13% lower than for horizontal pipes if the slope is as much as 30^o, and 4,9% lower if the slope is 30,8% (i.e. 18^o).

It will be shown later in this section that the presentation of $(\Delta H_c)_s$ as opposed to $(\Delta H_c)'_s$ is a useful method of correlating excess energy in sloping pipes. First the experimental results are presented as obtained (i.e. $(\Delta H_c)'_s$ versus $\overline{V}$)

Figures 11.38, 11.39 and 11.40 show the experimental results of total excess head loss measured across the capsule. These results were determined on four slopes ranging from -5,4% to +30,8% in the 74 mm diameter perspex pipe. Four diameter ratios were used and each graph represents data points for each of the four diameters on a particular slope.

Figures 11.41 to 11.44 show summaries of dimensionally similar capsules of different specific gravities and different diameter ratios on the +3,13% slope. Figure 11.36 summarises the results for four different length to diameter ratios for the d/D = 0,95 capsules on the 3,13% slope.

Thus a wide range of slopes were considered (from ϕ =-5,3% to ϕ = 30,8%) for different diameter ratios. Different specific gravities and length to diameter ratios were considered on one slope.

5.1 The following are the most prominent effects of slope on the excess head loss.

FIG. 11.38

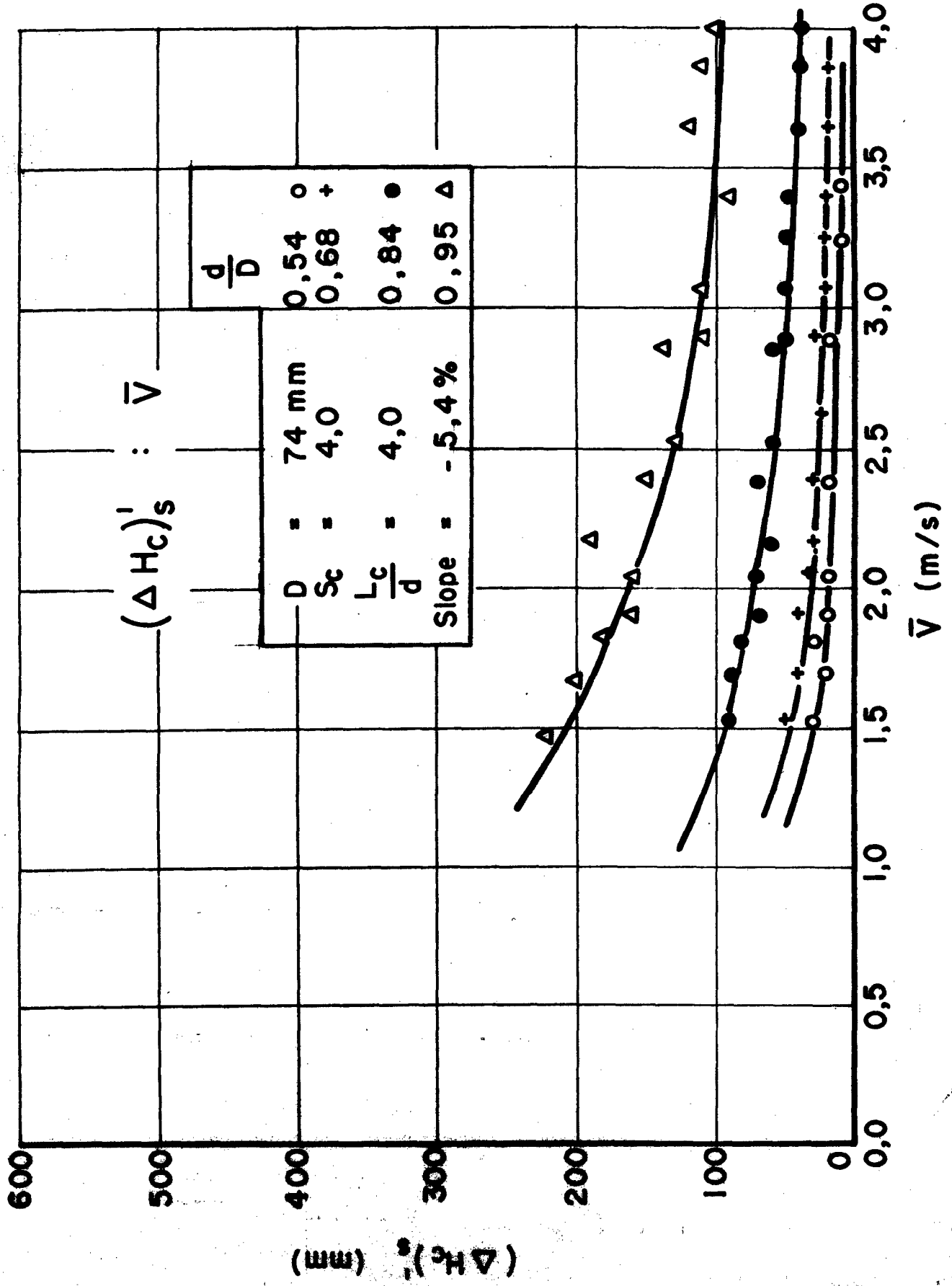
$(\Delta H_c)'_s$: $\bar{V}$
D = 74 mm
Sc = 4,0
$\frac{L_c}{d}$ = 4,0
Slope = -5,4 %
$\frac{d}{D}$
0,54 o
0,68 +
0,84 ●
0,95 Δ
$(\Delta H_c)'_s$ (mm)
$\bar{V}$ (m/s)
600
500
400
300
200
100
0
0,0
0,5
1,0
1,5
2,0
2,5
3,0
3,5
4,0

FIG. II. 39

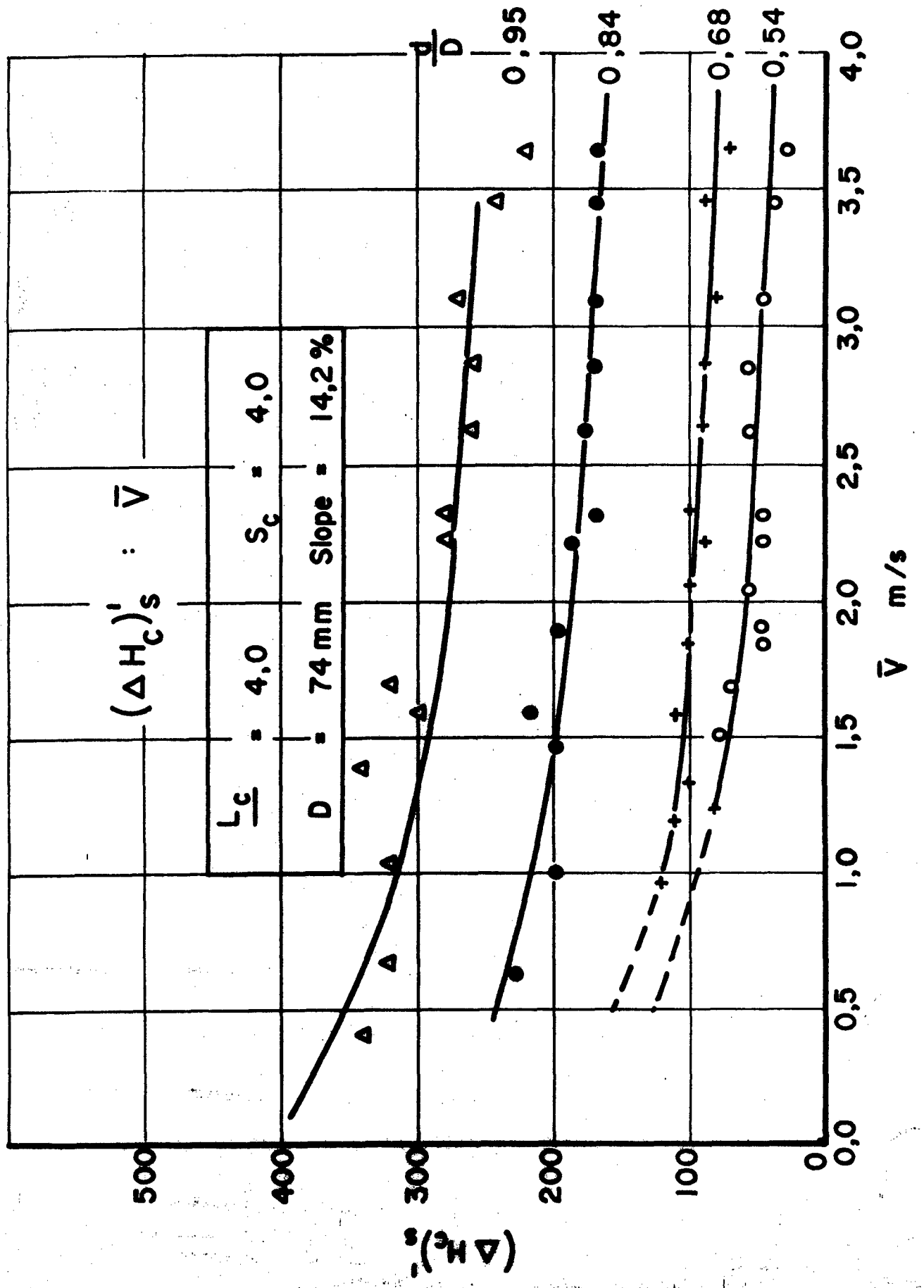
$(\Delta H_c)'_s : \bar{V}$
L_c = 4,0
D = 74 mm
S_c = 4,0
Slope = 14,2 %
d/D
0,95
0,84
0,68
0,54
$(\Delta H_c)'_s$
$\bar{V}$ m/s
0
100
200
300
400
500
0,0
0,5
1,0
1,5
2,0
2,5
3,0
3,5
4,0

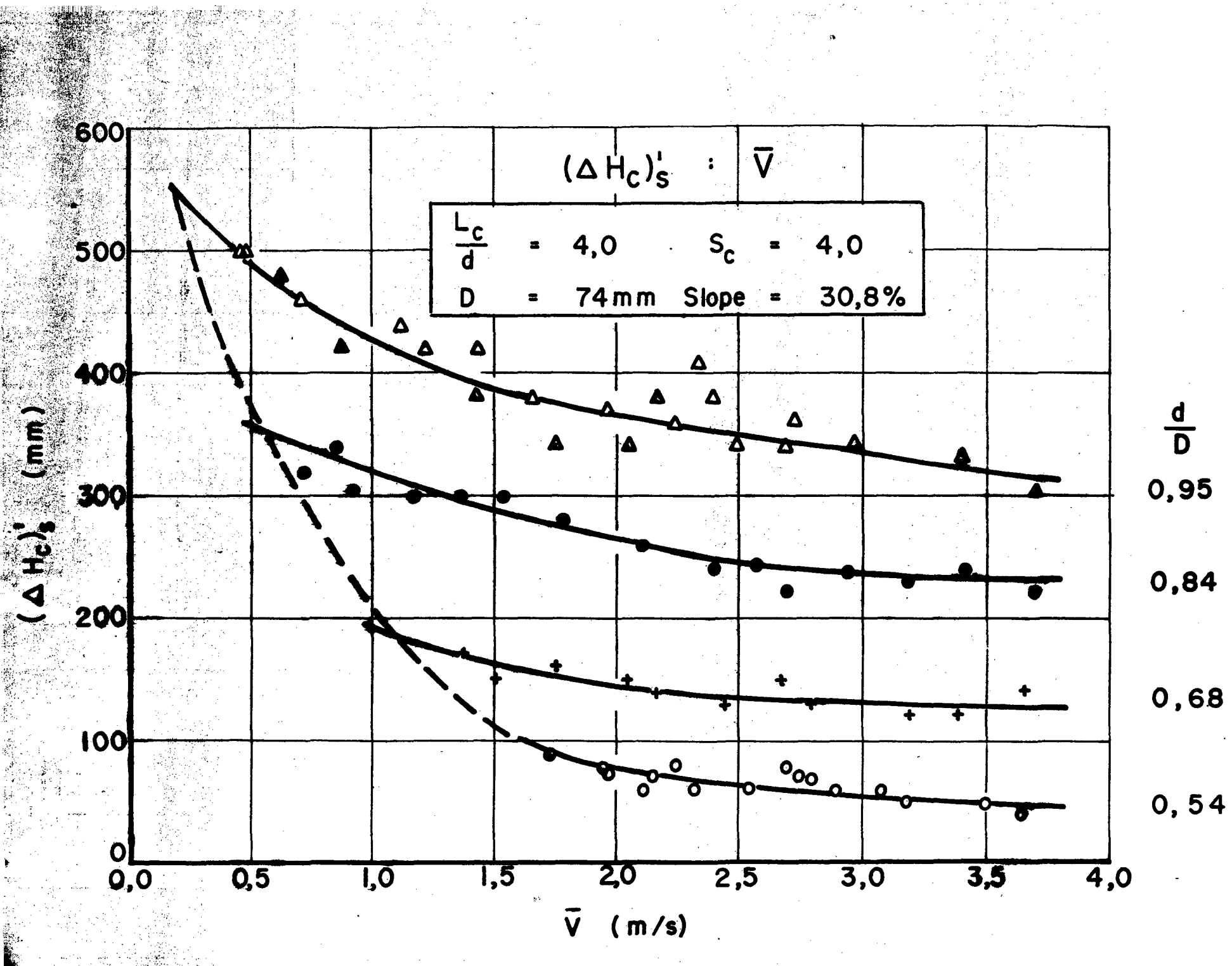
$(\Delta H_c)'_s$: $\bar{V}$
$\frac{L_c}{d}$ = 4,0 S_c = 4,0
D = 74mm Slope = 30,8%
$(\Delta H_c)'_s$ (mm)
$\bar{V}$ (m/s)
0
100
200
300
400
500
600
0,0
0,5
1,0
1,5
2,0
2,5
3,0
3,5
4,0
$\frac{d}{D}$
0,95
0,84
0,68
0,54

FIG. II.40

Figure 11.41

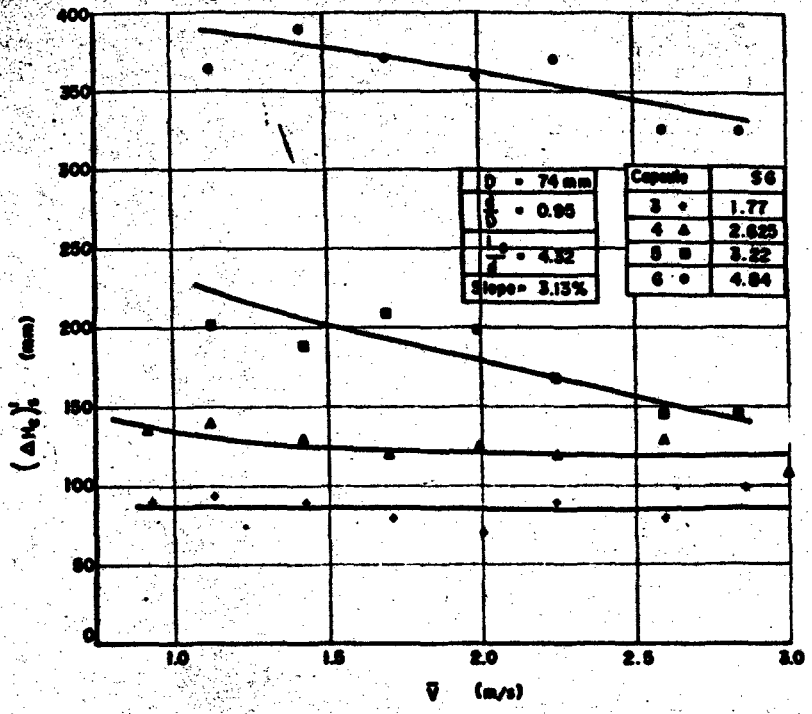

Figure 11.42

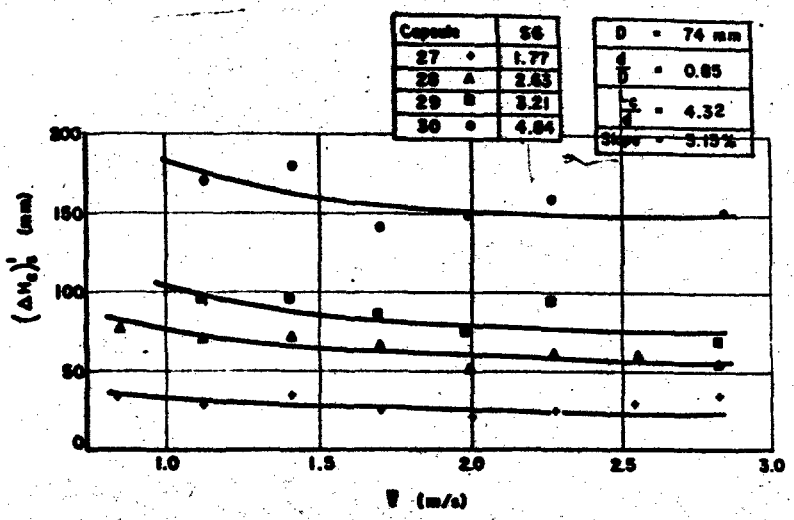

Figure 11.43

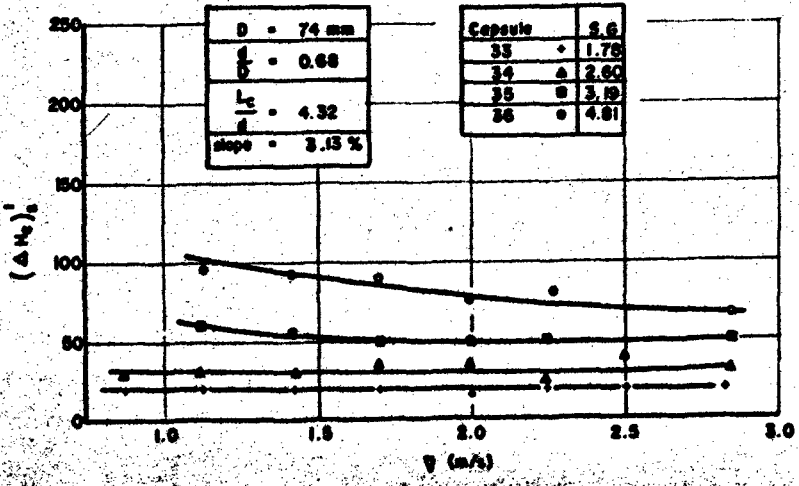

Figure 11.44

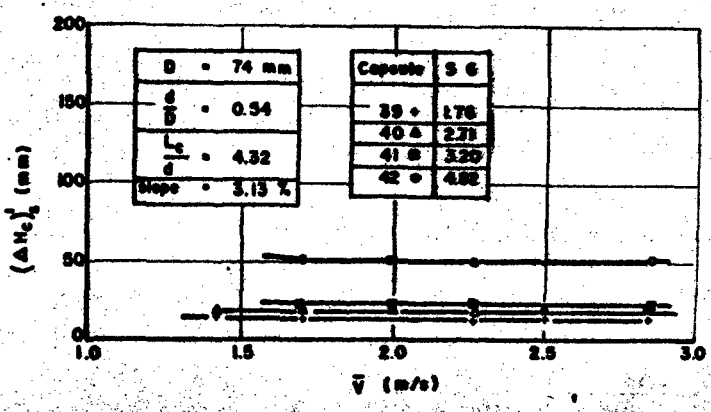

5.1.1 In all cases the value of $(\Delta H_c)'_s$ decreases with mean water velocity increase.

5.1.2 The rate of decrease of $(\Delta H_c)'_s$ with velocity increase is diminished as slope increases (e.g. increasing $\bar{V}$ from 1,5 to 3 m/s causes about 50% reduction in $(\Delta H_c)'_s$ at -5,4% slope, and only about 15% reduction at 30,8% slope at $d/D = 0,945$.

5.1.3 As diameter ratio is increased $(\Delta H_c)'_s$ increases at a fixed mean water velocity, and the increase becomes more prominent as slope increases. That is, the curves are further apart as slope increases from -5,4% to 30,8% (see Figures 11.38, 11.12, 11.39 and 11.40).

To illustrate this phenomenon $(\Delta H_c)'_s$ is plotted against diameter ratio on Figure 11.45 for a fixed mean water velocity $\bar{V} = 1,5$ m/s and the absolute ordinate between curves increases as diameter ratio increases, i.e. the difference between $(\Delta H_c)'_s$ for -5,4% slope and 30,8% slope is 80 mm at $d/D = 0,543$ and 183 mm at $d/D = 0,95$. Increasing the slope has more effect on $(\Delta H_c)'_s$ as d/D increases. Although the percentage change in $(\Delta H_c)'_s$ when increasing diameter ratio from 0,543 to 0,95 is less (i.e. $(\Delta H_c)'_s$ for a 30,8% slope is 3,55 times larger at $d/D = 0,95$ than $d/D = 0,543$, whereas at -5,4% slope $(\Delta H_c)'_s$ is 6,94 times larger at $d/D = 0,95$ compared with $d/D = 0,543$.

Figure 11.46 shows slope plotted against $(\Delta H_c)'_s$ for different diameter ratios, and the effect mentioned above is shown up more clearly although as d/D is increased to 0,95 the rate of increase of $(\Delta H_c)'_s$ is no more than for $d/D = 0,84$.

Before an explanation for the above effect is given, the graphs of $(\Delta H_c)_s$ against $\bar{V}$ will be discussed as these have a bearing on the explanation. Remember that $(\Delta H_c)_s$ is defined as

$$(\Delta H_c)_s = (\Delta H_c)'_s - (d/D)^2 \, L_c \sin \phi \, |S_c - 1|$$

$(\Delta H_c)'_s$: $\frac{d}{D}$

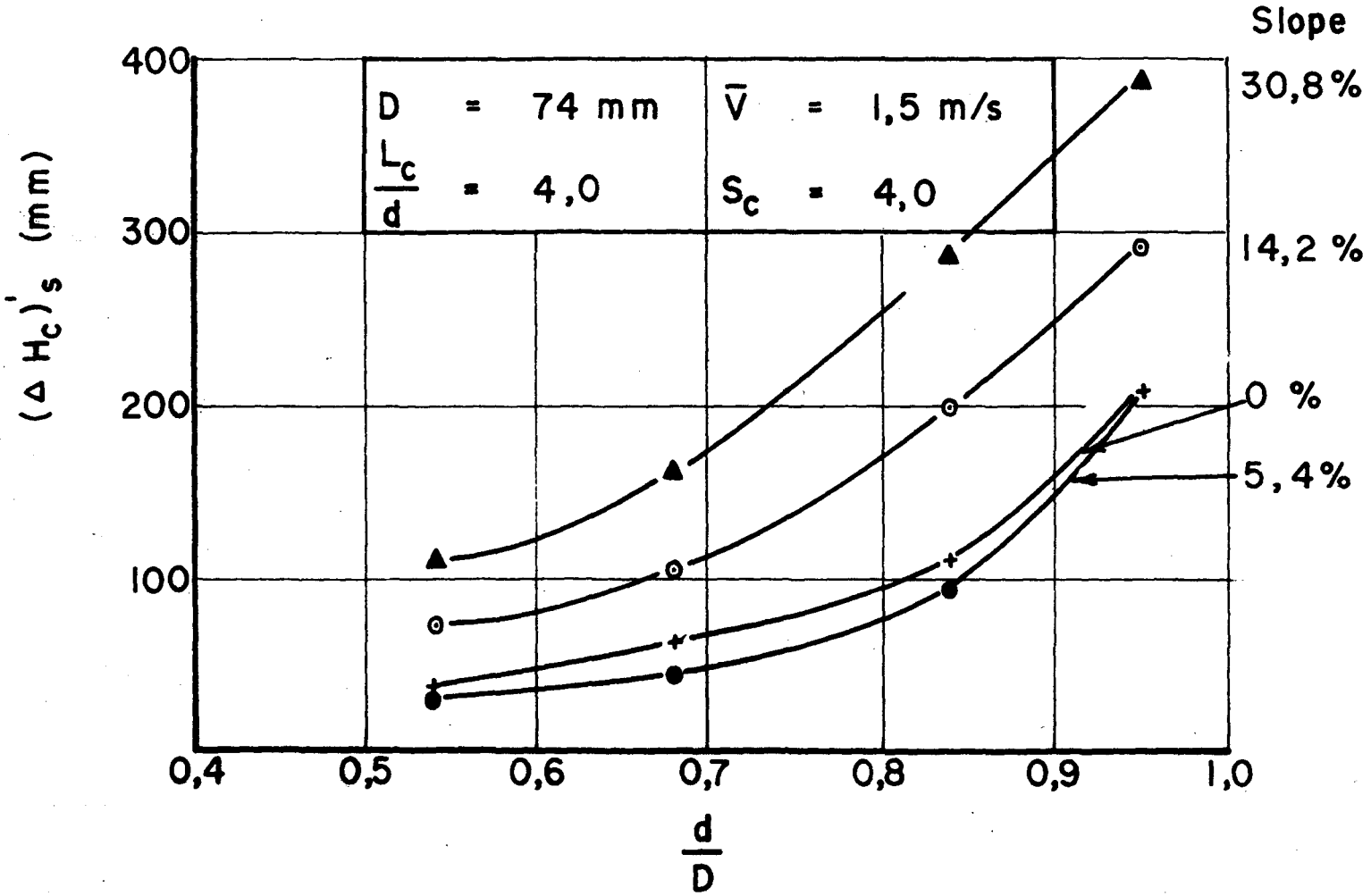

FIG. II.45

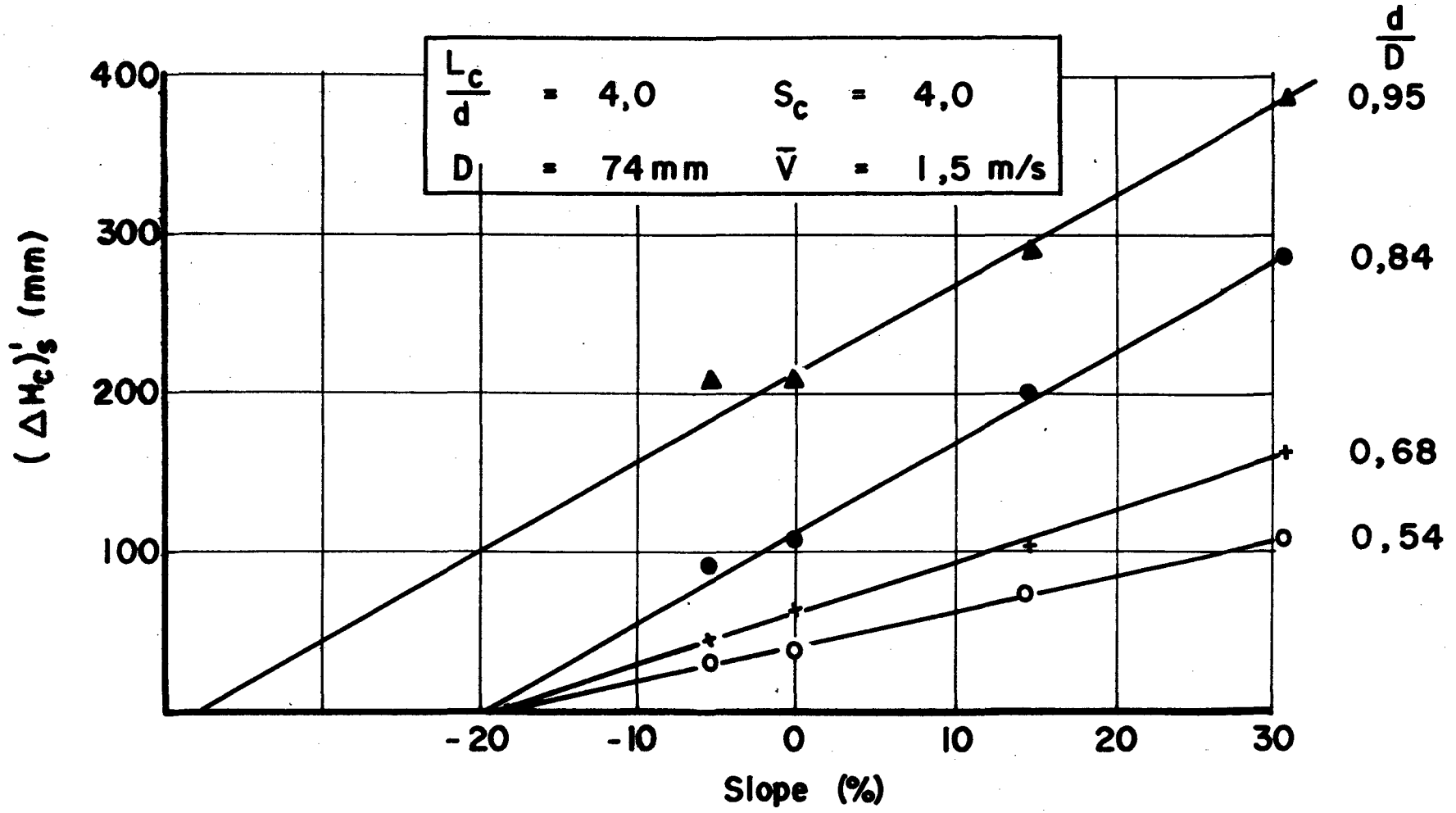
$\frac{L_c}{d}$ = 4,0 S_c = 4,0
D = 74mm $\bar{V}$ = 1,5 m/s
$\frac{d}{D}$
0,95
0,84
0,68
0,54
400
300
200
100
$(\Delta H_c)'_s$ (mm)
-20
-10
0
10
20
30
Slope (%)

FIG. II.46

Figures 11.47, 11.48 and 11.49 are graphs of $(\Delta H_c)_s$ against $\overline{V}$ for the slopes -5,4%; 14,2% and 30,8%, the horizontal slope is not represented since $\sin \phi = 0$. These graphs have the same shape as all the excess head loss versus mean water velocity curves. Figure 11.50 shows $(\Delta H_c)_s$ plotted against the diameter ratio with slope as parameter and this method of plotting is successful in bringing the curves for different slopes together.

If this curve is compared with Figure 11.45 the effect of subtracting out the $(d/D)^2 L_c \sin \phi |S_c - 1|$ term is clearly discernible.

Likewise, when plotting slope against $(\Delta H_c)_s$ with diameter ratio as parameter on Figure 11.51, the nearly horizontal lines testify to the elimination of the slope effect by this plotting method.

The specific instances mentioned above for $\overline{V} = 1{,}5$ m/s are completely generalised on Figures 11.52, 11.53, 11.54 and 11.55, which show $(\Delta H_c)_s$ against $\overline{V}$ for different slopes and each diameter ratio.

The effects of slope alluded to earlier can be ascribed to the capsule weight down the slope. The effect of correlating excess head loss at different slopes by subtracting the $(d/D)^2 L_c \sin \phi |S_c - 1|$ term and the favourable agreement as regards $(\Delta H_c)_s$ (evidenced by lack of scatter) on Figures 11.52 to 11.55 lends support to the fact that solid friction plays a small role at high velocities where there is somewhat less absolute scatter. The only case where excessive scatter is evidenced is on Figure 11.55 where the $(\Delta H_c)_s$ values at the largest slope shows some divergence from the mean line at zero slope.

According to the theory given in Chapter 7, the excess head loss should increase as slope increases because V_c decreases.

$$\text{i.e.} \quad \Delta H_c = \Delta h_i + \Delta h_o + \Delta h_{fa} - h_{fc} \tag{7.195}$$

$$\text{and} \quad \Delta h_i + \Delta h_o = f(\overline{V} - V_c)^2$$

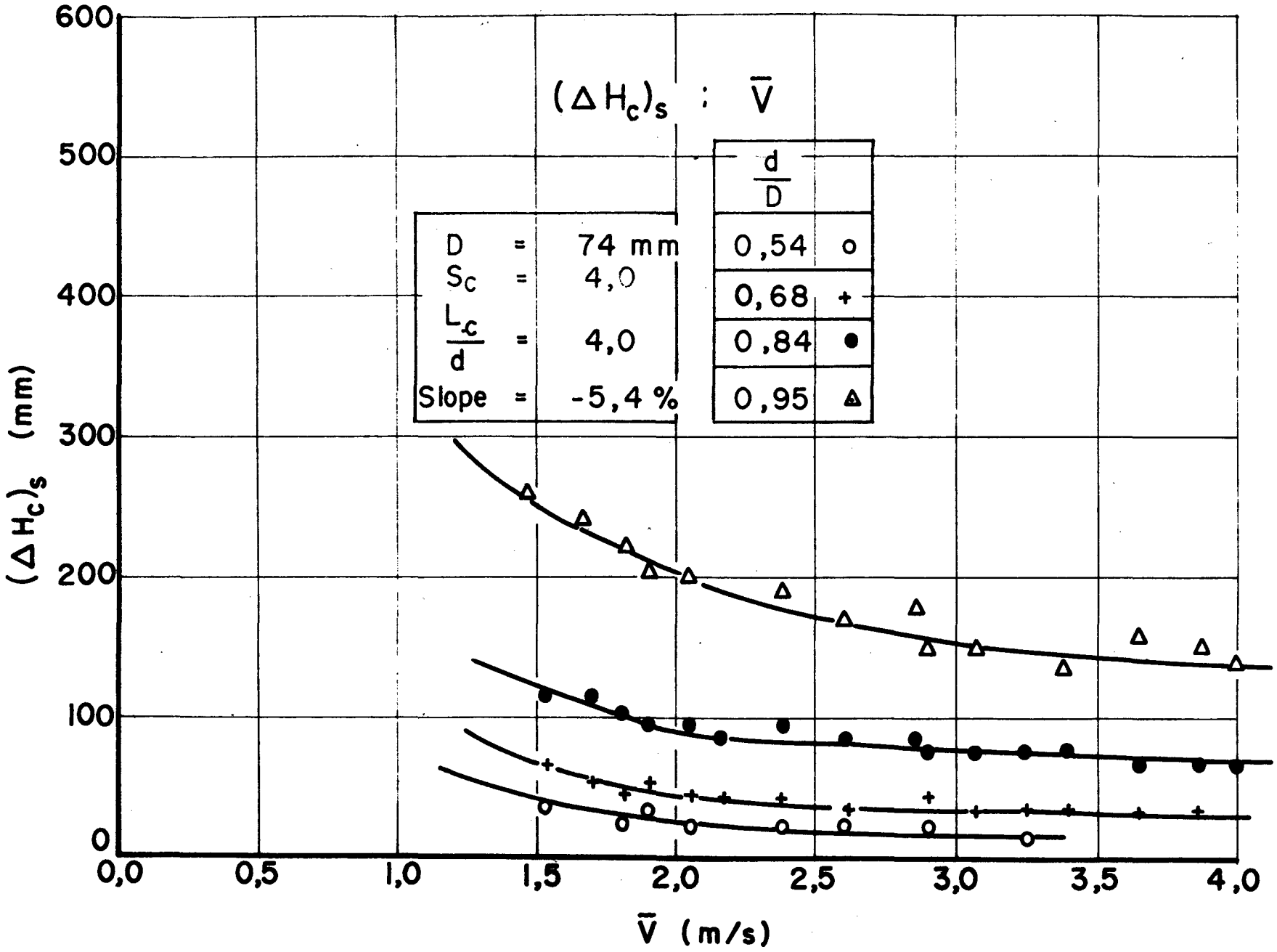
$(\Delta H_c)_s$: $\bar{V}$
D = 74 mm
S_c = 4,0
$\frac{L_c}{d}$ = 4,0
Slope = -5,4 %
d/D
0,54 o
0,68 +
0,84 ●
0,95 △
$(\Delta H_c)_s$ (mm)
600
500
400
300
200
100
0
0,0
0,5
1,0
1,5
2,0
2,5
3,0
3,5
4,0
$\bar{V}$ (m/s)

FIG. 11.47

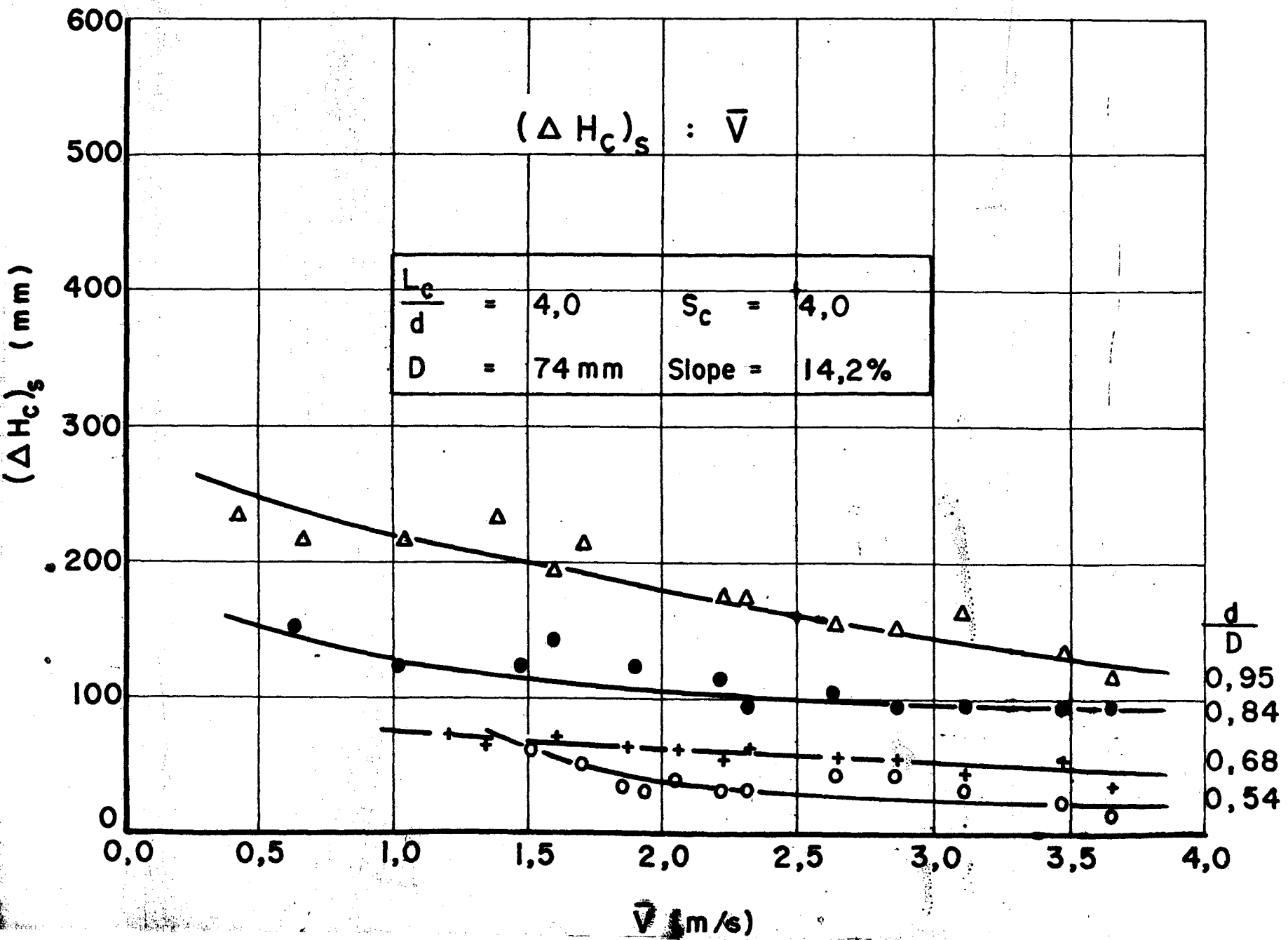
$(\Delta H_c)_s : \bar{V}$
$\frac{L_e}{d}$ = 4,0
S_c = 4,0
D = 74 mm
Slope = 14,2%
$(\Delta H_c)_s$ (mm)
$\bar{V}$ (m/s)
600
500
400
300
200
100
0
0,0
0,5
1,0
1,5
2,0
2,5
3,0
3,5
4,0
$\frac{d}{D}$
0,95
0,84
0,68
0,54

FIG. II.48

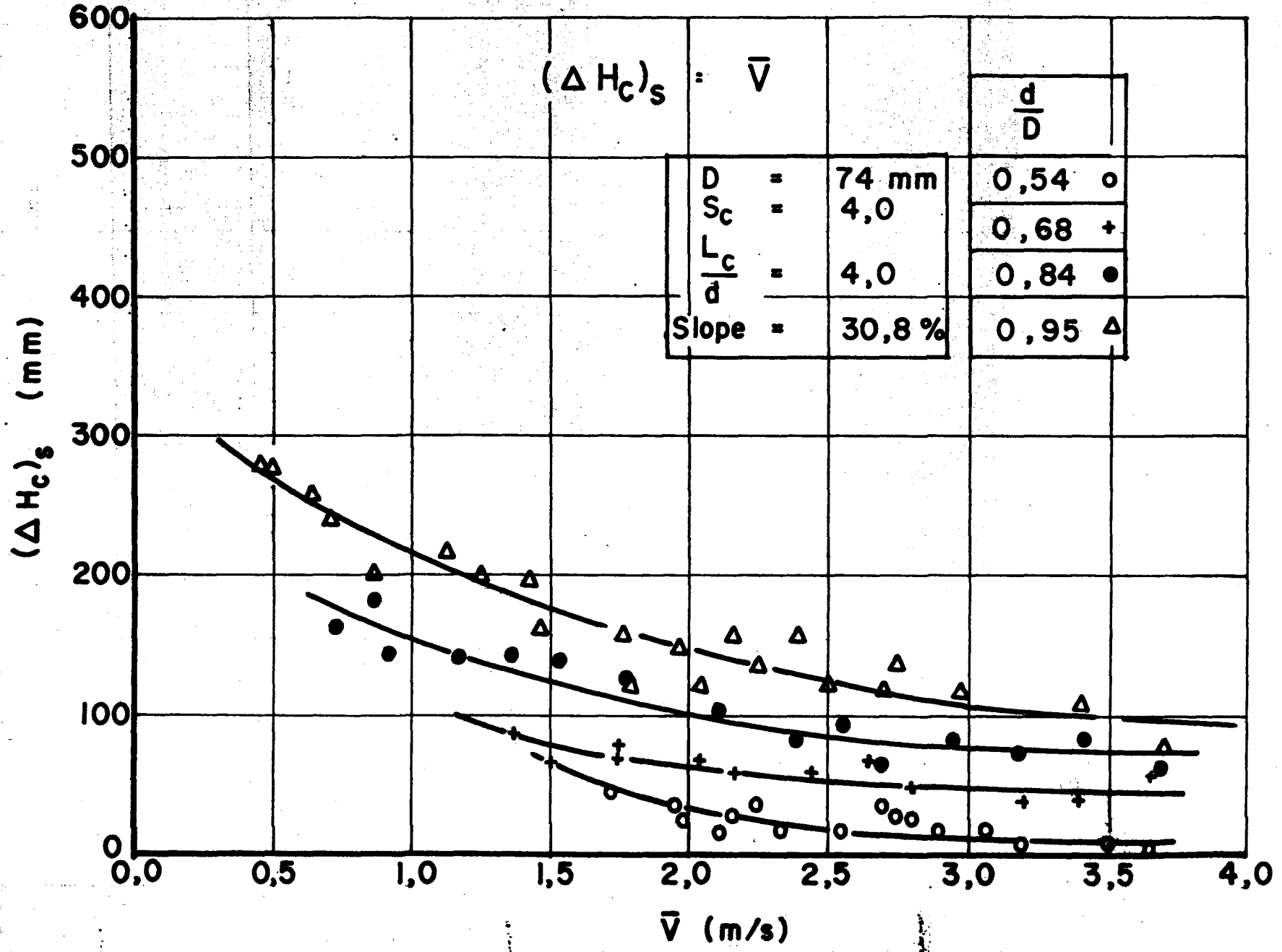
$(\Delta H_c)_s$: $\bar{V}$
D = 74 mm
S_c = 4,0
$\frac{L_c}{d}$ = 4,0
Slope = 30,8 %
d/D
0,54 o
0,68 +
0,84 ●
0,95 △
$(\Delta H_c)_s$ (mm)
$\bar{V}$ (m/s)
600
500
400
300
200
100
0
0,0
0,5
1,0
1,5
2,0
2,5
3,0
3,5
4,0

FIG. II.49

FIG. II.50

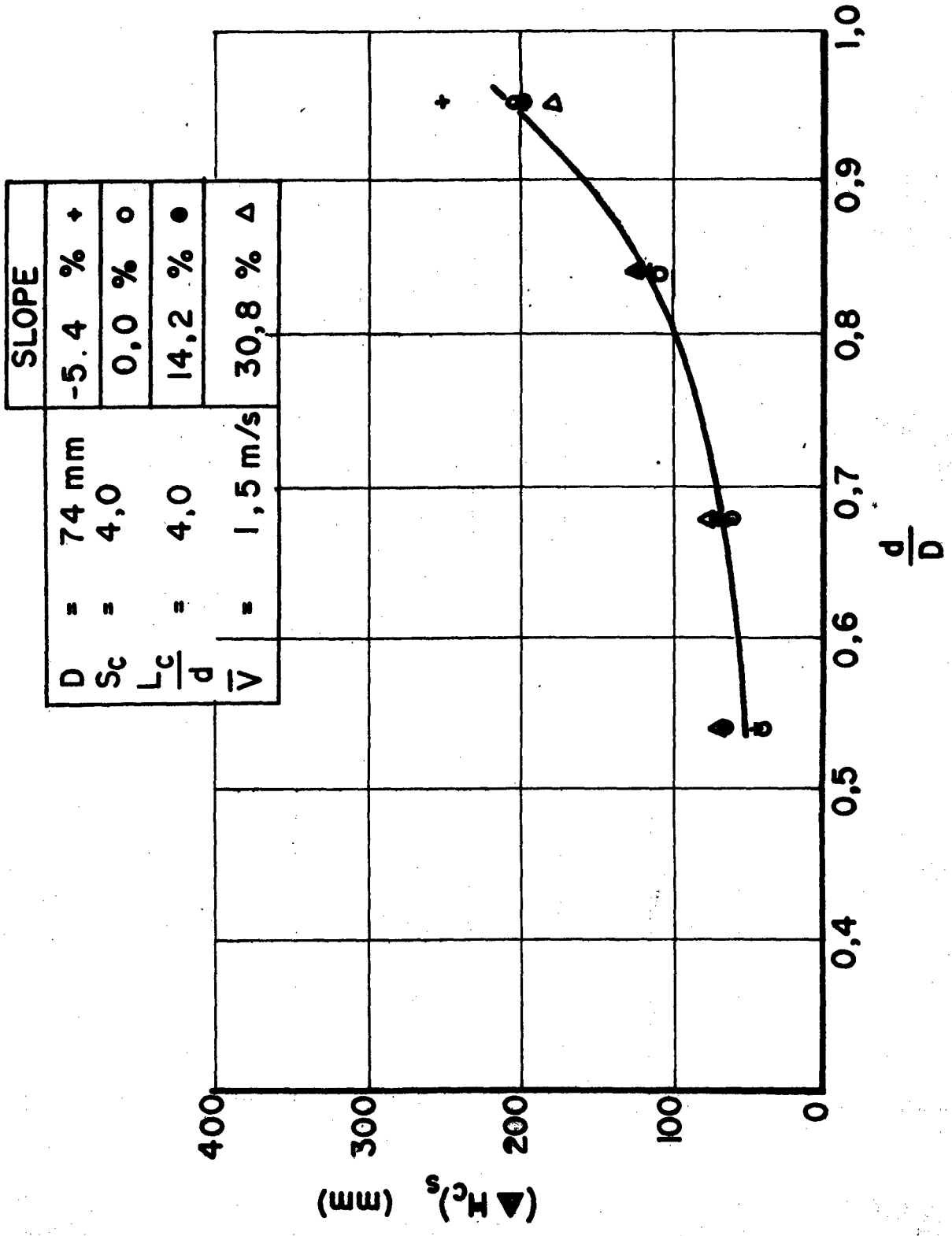
SLOPE
-5.4 % +
0,0 % o
14,2 % •
30,8 % Δ
D = 74 mm
Sc = 4,0
Lc/d = 4,0
V = 1,5 m/s
(Δ Hc)s (mm)
400
300
200
100
0
0,4
0,5
0,6
0,7
0,8
0,9
1,0
d/D

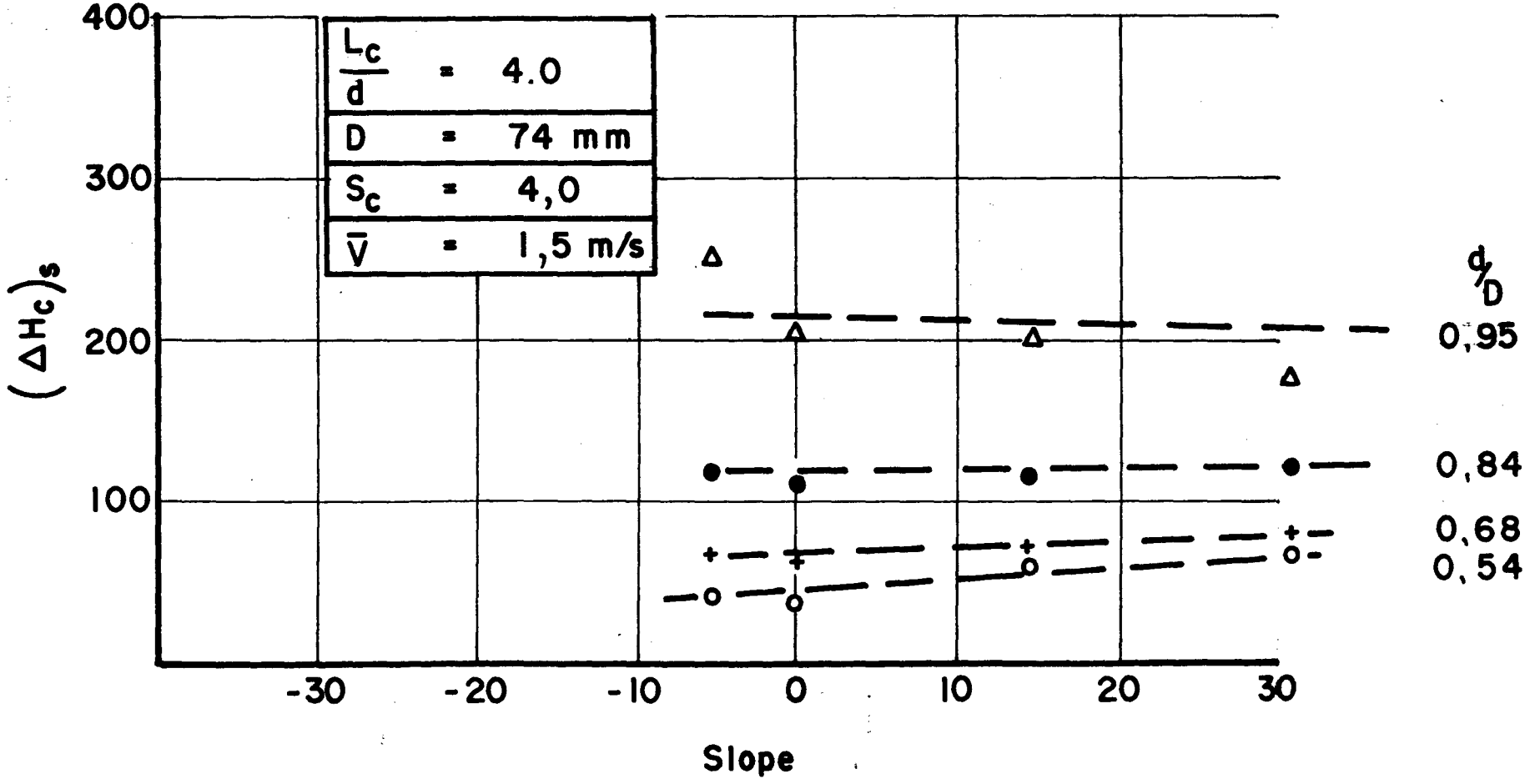
400
300
200
100
$(\Delta H_c)_s$
$\frac{L_c}{d}$ = 4.0
D = 74 mm
S_c = 4,0
$\bar{V}$ = 1,5 m/s
$\frac{d}{D}$
0,95
0,84
0,68
0,54
-30
-20
-10
0
10
20
30
Slope

FIG. II.51

$\therefore$ inlet and outlet losses increase as V_c decreases.

Also $\Delta h_{fa} = f(\overline{V}_{ap})$

and $$\overline{V}_{ap} = \frac{\overline{V} - V_c(d/D)^2}{1 - (d/D)^2} - \overline{V}_{ac} \qquad (11.4)$$

where $\overline{V}_{ac} = f(V_c)$

$\therefore$ as V_c decreases Δh_{fa} increases.

Therefore the three excess head loss terms on the right hand side of equation (7.195) increases as V_c decreases.

Alternatively, from equation (11.3), the first term on the right hand side is decreased as slope increases (although the effect of $\cos \phi$ is slight for the maximum slope tested, i.e. 30,8%). The reduction in the first term on the right hand side of equation (11.3) due to the slope effect is accompanied by an increase in the second term on the right hand side (i.e. $\overline{\tau}_p = \overline{\tau}_{pp} + \overline{\tau}_{cp}$).

The pressure component of $\overline{\tau}_p$ increases as a result of reduced capsule velocity and the Couette component decreases.

For equation (11.3) to give compatible results with equation (7.195) the increase in $\overline{\tau}_{pp}$ must dominate the decrease (due to the effect of $\cos \phi$ and $\overline{\tau}_{cp}$).

The above theories both indicate that $(\Delta H_c)_s$ should be greater than (ΔH_c). However it is clear from Figures 11.52 to 11.55 that this is not verified experimentally. Three reasons are proposed for the discrepancy between theory and experiment.

1. The lift ratio (L_r) is greater as slope increases (in the extreme case of a vertical pipe there is no solid to solid friction at any velocity and $(\Delta H_c)_s$ is very low as can be seen in Section 5.2). Thus the first term on the right hand side of equation (11.4) is

further reduced due to slope (over and above the cos ϕ affect).

2. As a result of capsules lifting at lower velocities as slope increases the shear stress at the pipe wall $(\overline{\tau}_p)$ is also less than would be expected from the theory at unit eccentricity.
3. The scatter due to turbulence when reading the value of (ΔH_c) or $(\Delta H_c)'_s$ on the pen recorder completely masks the slight affects alluded to above.

Figure 11.36 of $((\Delta H_c)_s/L_c)$ against $\overline{V}$, for capsules of diameter ratio 0.95 in the 74 mm diameter pipeline for varying length to diameter ratios, verifies the efficacy of accommodating slope variation, for the zero and 3,13% slopes, as regards the excess head loss, by means of the subtractive term.

Methods have thus been given for absorbing the L_c/d and slope variables in a satisfactory manner.

5.2 Vertical pipes

Experiments were carried out in the 44 mm diameter pipe in a vertical orientation and some values for the total energy loss across mobile capsules moving upwards, are given on Figures 11.56 to 11.59.

A range of diameter ratios, length to diameter ratio and capsule densities were tested.

The total excess head loss $(\Delta H_c)'_s$ includes the excess energy dissipated due to the presence of the capsule as well as the energy required to lift the submerged weight of the capsule $((d/D)^2|S_c-1|L_c)$.

This expression is shown as a series of horizontal lines on the diagrams. The values of $(\Delta H_c)_s = (\Delta H_c)'_s - (d/D)^2|S_c-1|L_c$ were also plotted but because the total excess head, $(\Delta H_c)'_s$ was in most instances of the same order of magnitude as $(d/D)^2|S_c-1|L_c$ the evaluation of $(\Delta H_c)_s$ was deemed to be unreliable. This was due to the subtraction of similar large

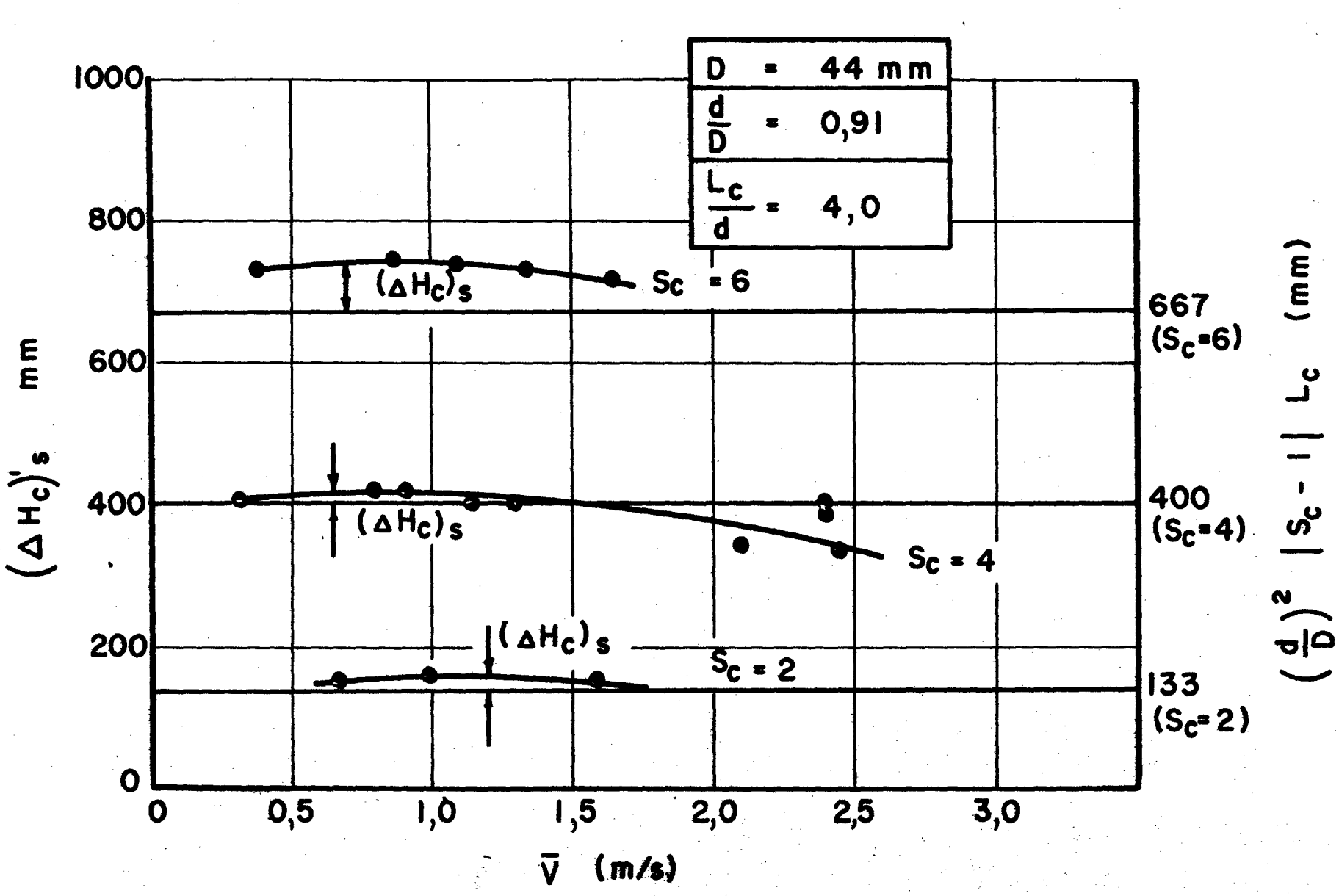
VERTICAL PIPE
D = 44 mm
d/D = 0,91
Lc/d = 4,0
Sc = 6
Sc = 4
Sc = 2
(ΔHc)s
667 (Sc=6)
400 (Sc=4)
133 (Sc=2)
(ΔHc)'s mm
V̄ (m/s)
0
0,5
1,0
1,5
2,0
2,5
3,0
200
400
600
800
1000
(d/D)² |Sc - 1| Lc (mm)

FIG. 11.56

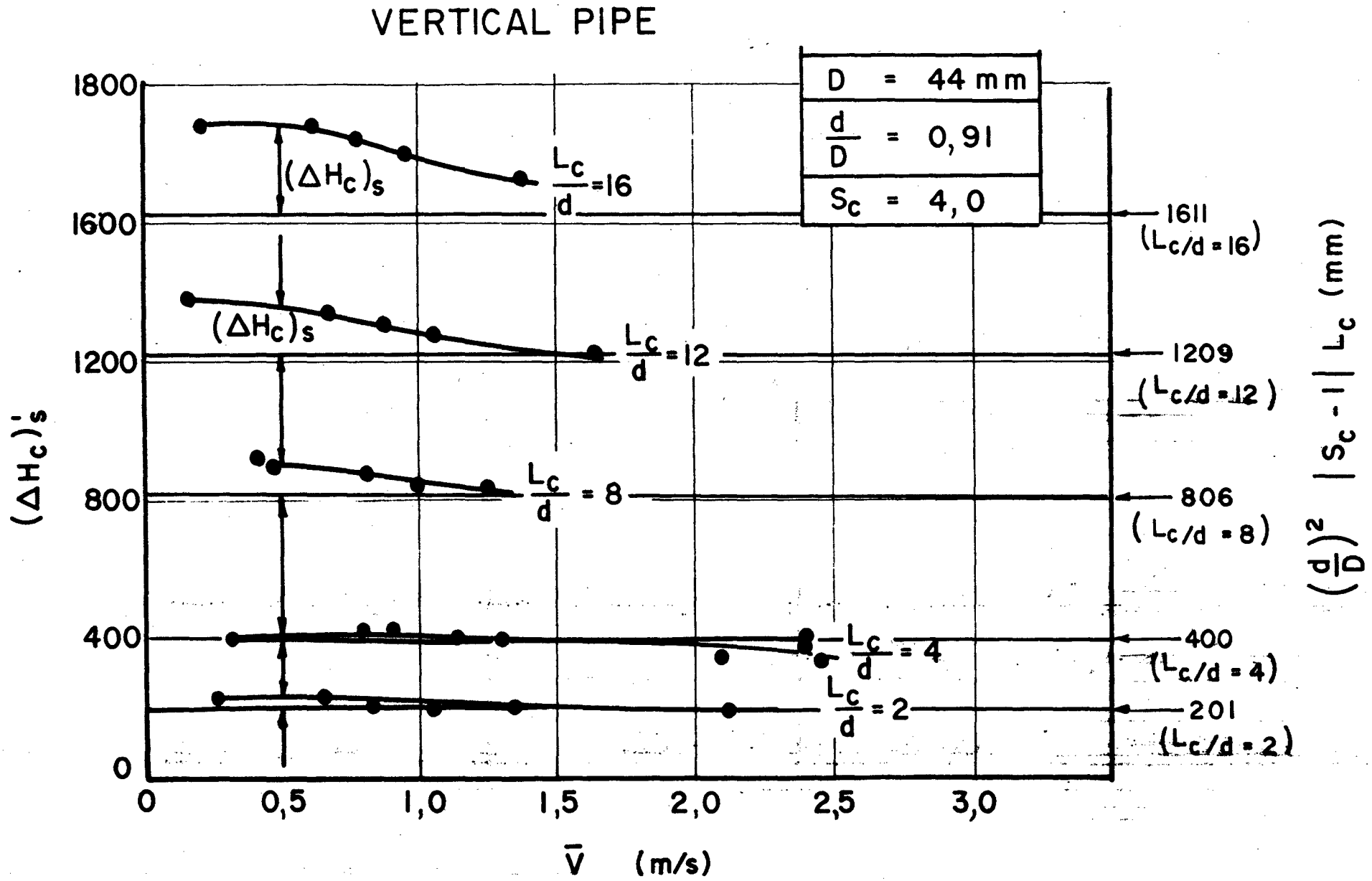
VERTICAL PIPE
D = 44 mm
d/D = 0,91
Sc = 4,0
(ΔHc)'s
(ΔHc)s
Lc/d = 16
Lc/d = 12
Lc/d = 8
Lc/d = 4
Lc/d = 2
1611 (Lc/d = 16)
1209 (Lc/d = 12)
806 (Lc/d = 8)
400 (Lc/d = 4)
201 (Lc/d = 2)
(d/D)² |Sc - 1| Lc (mm)
1800
1600
1200
800
400
0
0
0,5
1,0
1,5
2,0
2,5
3,0
V̄ (m/s)

FIG. 11.57

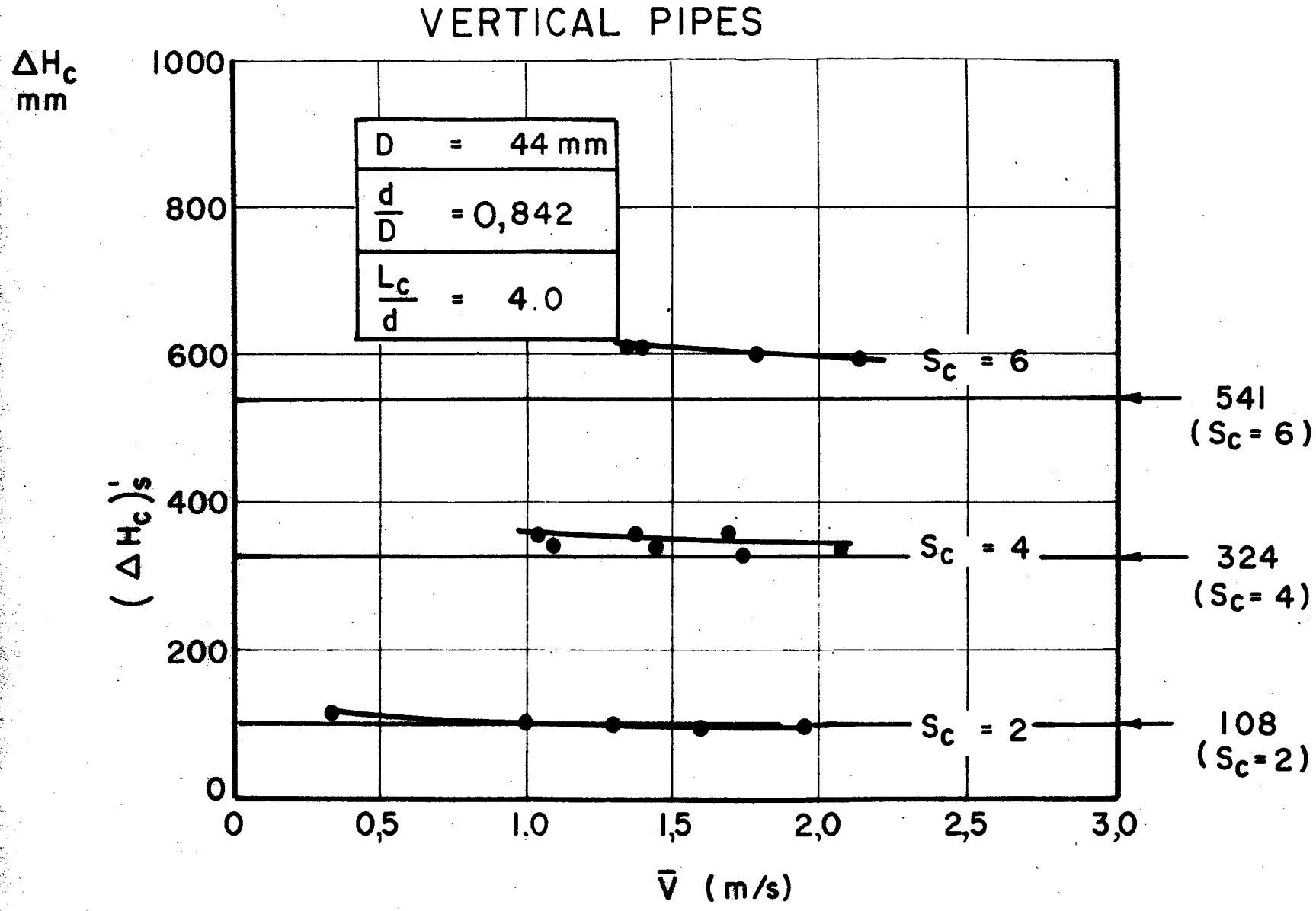

$$\left(\frac{d}{D}\right)^2 \left|S_c - 1\right| L_c \text{ (mm)}$$

FIG. 11.58

FIG. 11.59

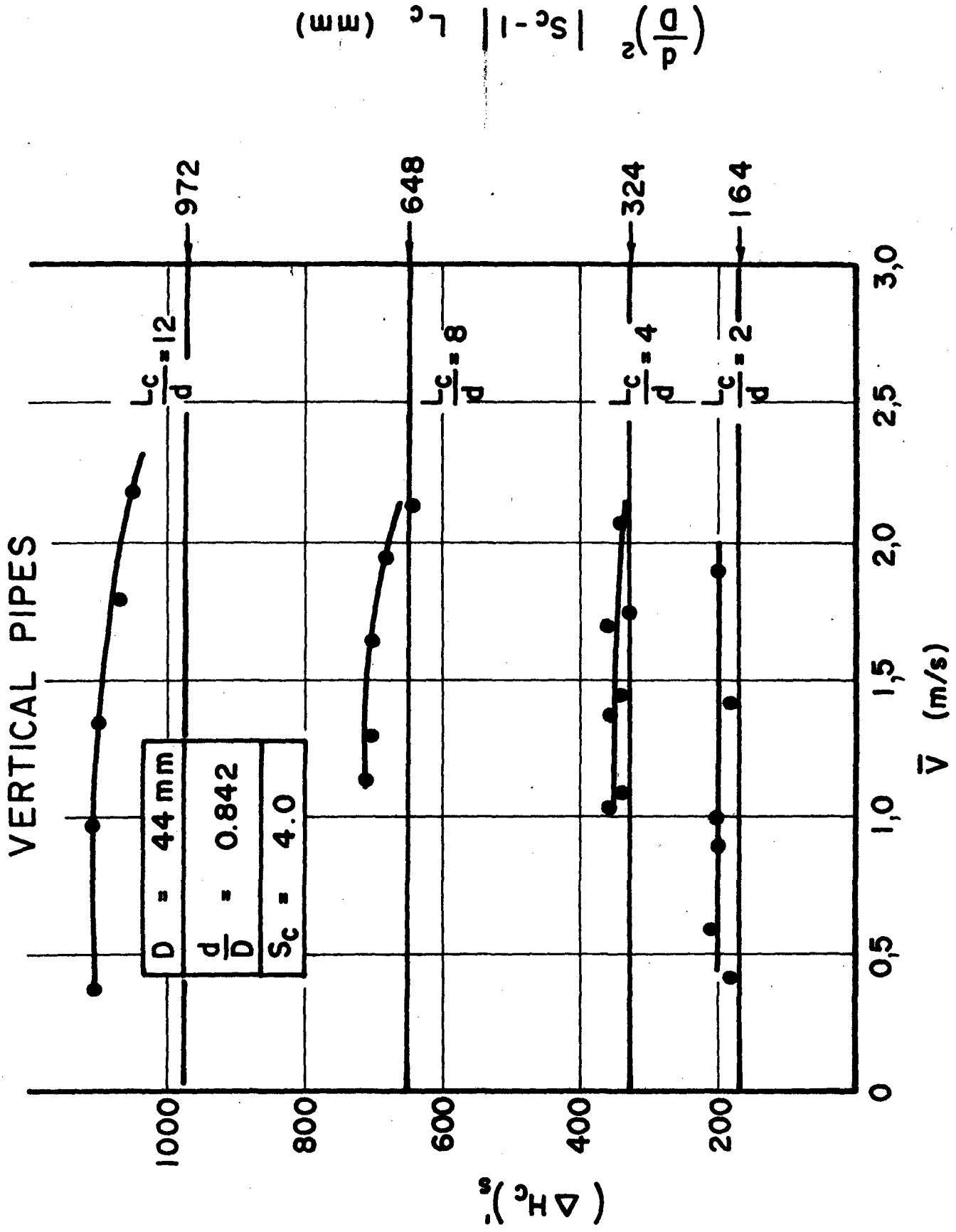
VERTICAL PIPES
D = 44 mm
d/D = 0.842
Sc = 4.0
Lc/d = 12
Lc/d = 8
Lc/d = 4
Lc/d = 2
972
648
324
164
1000
800
600
400
200
0
0,5
1,0
1,5
2,0
2,5
3,0
V̄ (m/s)
(ΔHc)'s
(d/D)² |Sc-1| Lc (mm)

quantities. In some cases even negative values of $(\Delta H_c)_s$ were indicated, (see Figure 11.56 S_c = 4,0). This is clearly impossible. It was only at very high values of SG (i.e. S_c = 6,0) or L_c/d (e.g. $L_c/d > 8$) that positive $(\Delta H_c)_s$ values were easily discernible.

The excess head loss in a vertical pipe arises due to shear on the pipe wall over and above the shear in capsule free flow. This shear can be considered as having two components, i.e. pressure flow and Couette flow. The latter is much less for concentric than for eccentric annuli, and this accounts for net excess head losses $(\Delta H_c)_s$ being very much lower than for horizontal pipes. Another reason being the lack of any solid to solid friction in this case.

Experiments were also carried out for vertically downward flow, and in this case the total excess energy loss was negative (for $S_c > 1$), the capsules moving faster than the mean water velocity, depending on capsule density and diameter ratio. Decreasing diameter ratio and increasing density causes capsules to travel appreciably faster than the mean water velocity.

To revert to the capsules travelling vertically upwards, it was observed that the short solitary capsules (L_c/d = 2 and L_c/d = 4) did not travel concentrically in the pipe.

Nutation was observed at incipience, and when travelling the capsules would often migrate towards the pipe wall or have their axis at an angle to the pipe axis, (see Figures 60a and b).

The trains of capsules ($L_c/d > 4$) did not travel with their axis aligned and this was particularly prevalent at low diameter ratios. (See Figures 61a and b.) These are reasons for causing the readings to be somewhat unreliable and inducing additional energy losses at high L_c/d values. Misalignment would effectively increase the roughness of a train of capsules.

FIG 11.60a

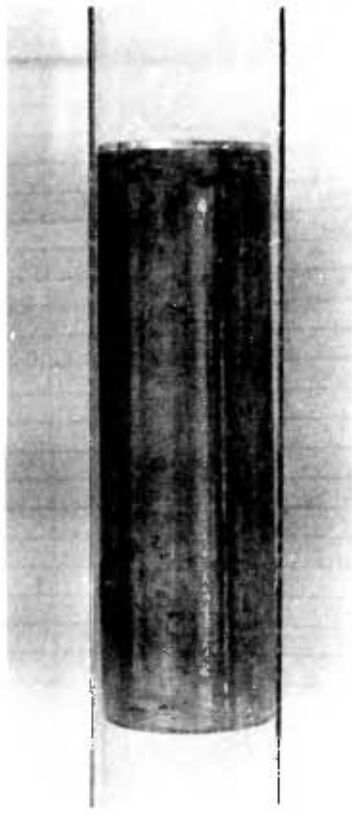

d = 37 mm

D = 44 mm

L_c/d = 4,0

S_c = 4,0

FIG 11.60b

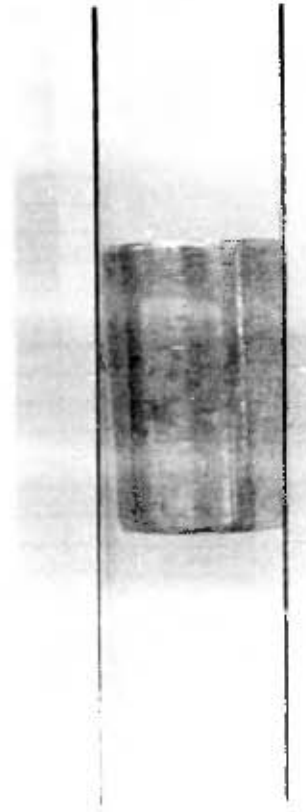

d = 37 mm

D = 44 mm

L_c/d = 2

S_c = 4,0

FIG 11.61a

d = 29 mm

D = 44 mm

L_c/d = 16

S_c = 4,0

FIG 11.61b

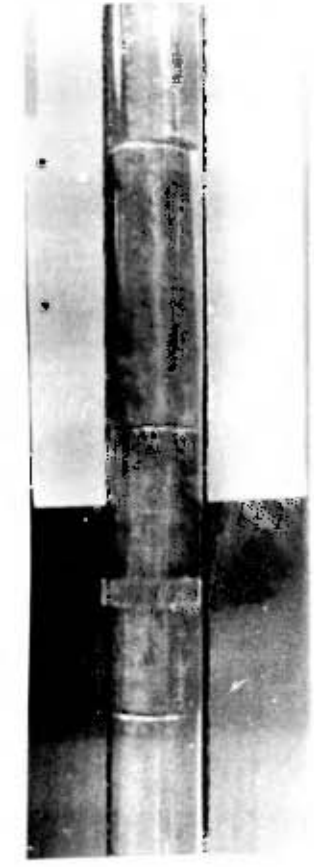

d = 37 mm

D = 44 mm

L_c/d = 16

S_c = 4,0

6. The effect of capsule roughness

Three of the pipelines were used for this set of experiments. Figure 11.62 shows a comparison of rough and smooth capsules in the 44 mm diameter horizontal pipeline.

The largest capsule $d/D = 0,91$ was roughened by means of annular grooves in P.V.C. The other three diameter ratios $d/D = 0,85$; $0,66$ and $0,54$ were roughened by means of knurled brass.

None of these capsules displayed any significant ΔH_c difference due to capsule roughness.

Up to $d/D = 0,85$ the smooth capsules have a higher excess head loss. Whereas for the largest diameter ratio the rough capsule has an excess head loss which is increasingly higher as the mean velocity increases.

It should be noted that in all cases the mean data points for the $d/D = 0,91$ capsule show capsule velocities that are lower than the mean water velocities (see Chapter 10) and observation indicated turbulence vortices preceeding the capsules.

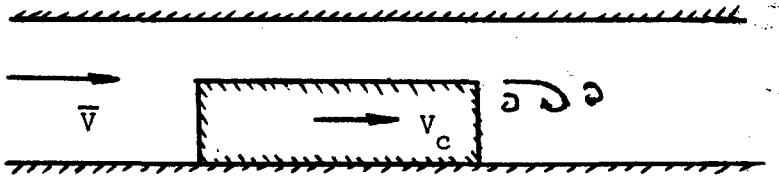

This appears to have contributed to the excess head loss by increasing the energy dissipated at the nose of the capsule.

The knurled brass capsules were observed to revolve about their own axis periodically. This spin in addition to the capsule roughness does not seem to have made much difference to the excess head loss. It should always be born in mind that each data point represents the mean of a number of readings.

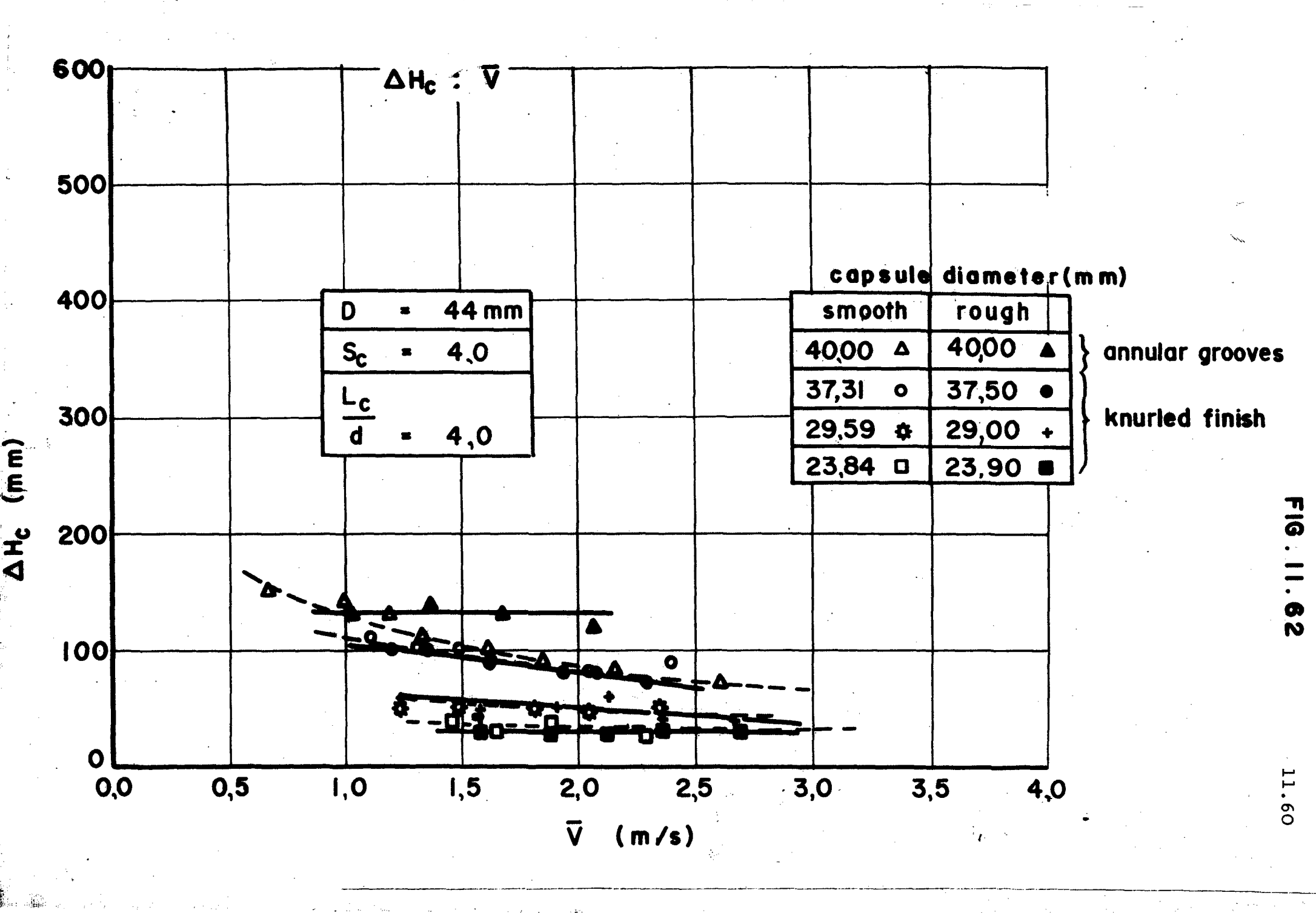

FIG. II.62

11.60

Further experiments were carried out in the 74 mm perspex line on a horizontal slope. The capsules were again artifically roughened in the lathe (i.e. capsules numbered 7044R; 6244R; 5044R and 4044R).

Figure 11.63 shows ΔH_c for rough and smooth capsules plotted against the mean velocity and in all cases the excess head loss values are greater for the smooth capsules.

It should be remembered that Figure 10.75 showed rough capsule velocities higher than smooth capsule velocities.

The following explains how head losses for smooth can be greater than for rough capsules.

The head loss across a mobile capsule has been shown to depend on the form drag which is a function of $(\overline{V} - V_c)^2$ and, if for the same value of $\overline{V}$ the capsule velocity is higher for rough than smooth capsules, one would expect to find a greater form drag in the case of the smooth capsules.

The form drag depends to some extent on the annular head loss due to pressure flow which is a function of the surface roughness of the capsule and pipe walls as well as the water velocity in the annulus due to pressure flow $(\overline{V}_{ap})$ where;

$$\overline{V}_{ap} = (\overline{V} - (d/D)^2 V_c)/(1-(d/D)^2) - \overline{V}_{ac} \qquad (11.4)$$

For a high, as compared with a low, capsule velocity the first term on the right hand side of the above equation is reduced and the second term $(\overline{V}_{ac})$ is increased, at the same mean water velocity, thus rendering $\overline{V}_{ap}$ less for higher capsule velocities.

The other component of forward drag is due to the shear on the capsule wall and this also depends on $\overline{V}_{ap}$ and the capsule roughness.

It is conceivable that the excess head loss, which is related to the forward drag force on the capsule, is less for rough than smooth capsules, if the capsule velocity is greater for the former case at the same mean

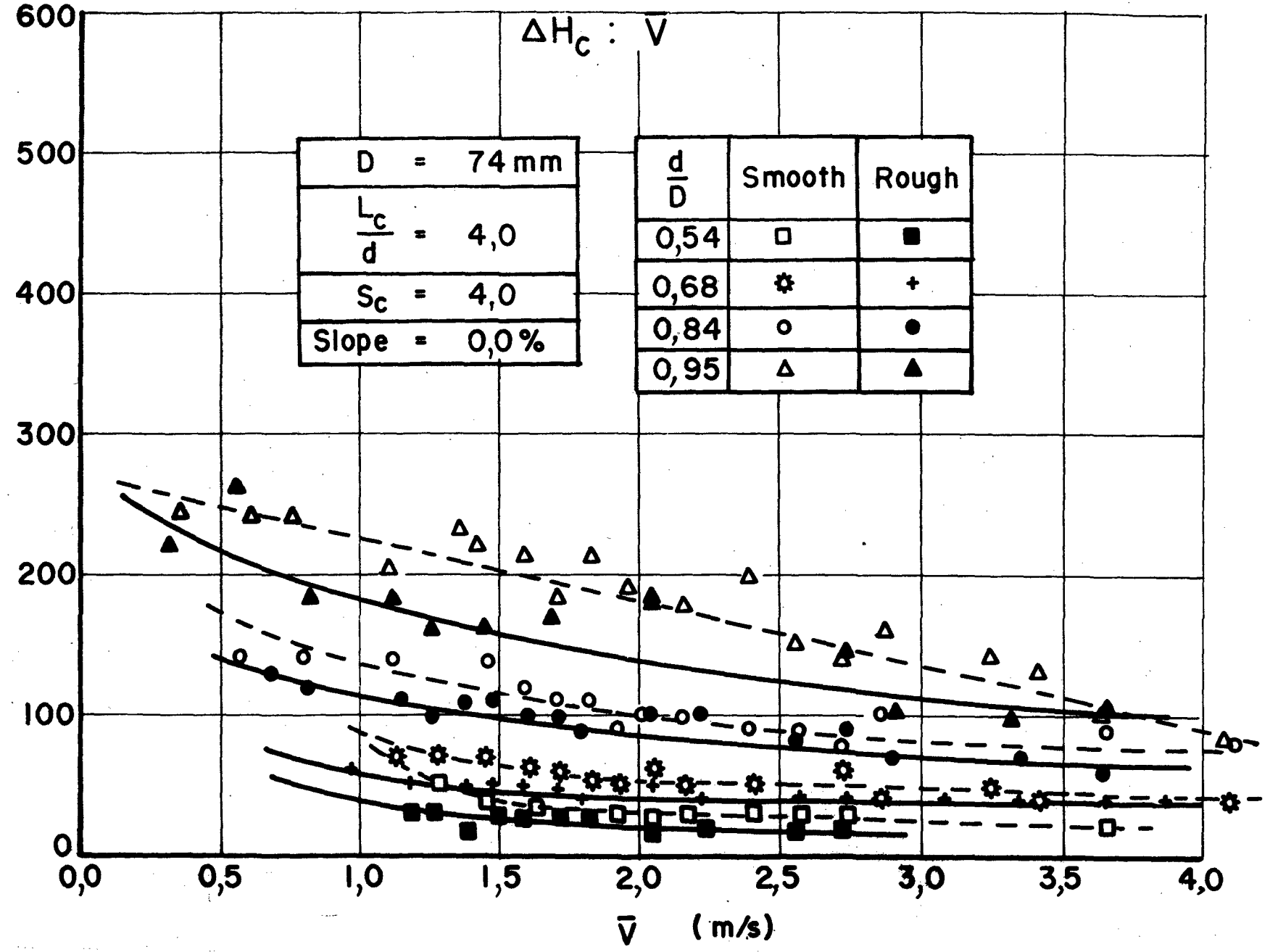
ΔHc : V̄
D = 74 mm
Lc/d = 4,0
Sc = 4,0
Slope = 0,0%
d/D | Smooth | Rough
0,54
0,68
0,84
0,95
ΔHc (mm)
600
500
400
300
200
100
0
0,0
0,5
1,0
1,5
2,0
2,5
3,0
3,5
4,0
V̄ (m/s)

FIG. II.63

water velocity. The losses due to forward form and skin friction drag, which depend on relative velocity terms squared, predominate the increase due to capsule roughness.

The same argument as that given above applies to the gross method of analysis wherein the shear on the capsule depends on ~~the relative velocity~~ $(V_r)^2$ ~~squared.~~ Since V_r is less for higher values of V_c.

Perhaps one would have instinctively thought that rough capsules travel slower than smooth capsules, and that the excess head losses are greater for rough than smooth capsules. This is not so. The explanation given above, together with the realisation that roughness is not a highly significant criterion as regards solid to solid friction factors, shows why it is not so.

It is likely that at very high velocities, when the capsule lifts, the rough capsules would have a greater excess head loss than the smooth. This is hypothesised since the forward drag on the capsule, which is largely a function of frontal area (as described above) would not change in form, whereas the backward drag becomes entirely due to Couette shear which, being a fluid friction, is an unique function of capsule velocity and capsule roughness. This implies a more significant retarding force, as roughness and capsule velocity are increased, than when much of the backward drag is solid friction. And this in turn means that a greater forward drag is required. This trend is illustrated on Figure 11.63 for $d/D = 0,95$ at very high velocities.

In order to exaggerate the surface roughness effects, the asbestos cement pipe was utilised for experiments with dimensionally similar smooth and rough capsules. The results of smooth and rough capsules are shown superimposed on the basis of ΔH_c against mean velocity curves on Figure 11.64, and it is clear that a slightly rougher pipe, whether the capsules themselves are smooth or rough, makes little difference. The explanation

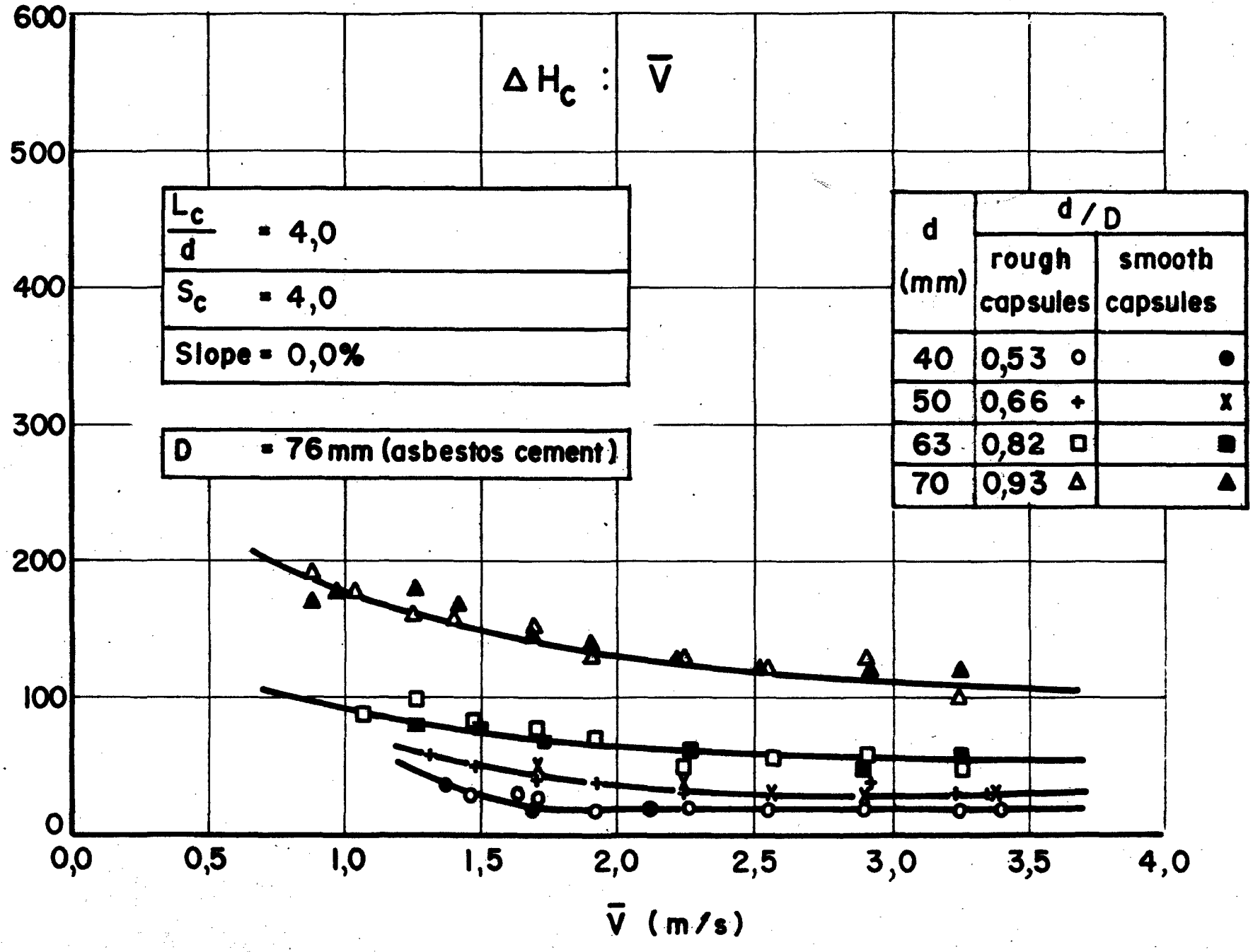

FIG. II.64

II.64

is that there are so many conflicting effects present simultaneously, tending to give higher excess head losses for rough capsules, and others tending to give higher excess head losses for smooth capsules, as discussed above. The various effects tend to cancel out.

In this case, the solid friction force between two rough surfaces is such as to slow the rough capsules down slightly, compared with smooth capsules, so that the increased forward drag forces, for rough as opposed to smooth capsules, are compensated. As can be seen from Figure 10.78, the rough and smooth capsules in the asbestos cement pipe do not travel at appreciably different velocities.

Figure 11.65 shows excess head losses for smooth capsules in the asbestos cement as well as the perspex pipe. For the two larger capsules the energy dissipation in the perspex pipe was greater. The trend was not so significant for the smaller capsules. Unfortunately, the diameter ratios were slightly different and the excess head loss is significantly dependent on diameter ratio, particularly at high (d/D) values. This tends to mask the effect of pipe roughness change on smooth capsules. It is apparent, however, that the pipe roughness does not have a great effect on ΔH_c since the capsule of diameter ratio d/D = 0,92 in the asbestos cement pipe has excess head losses between those of d/D = 0,84 and 0,95 in the perspex pipe.

7. The effect of capsule spacing

As described in Chapter 10, basically two sets of experiments were performed; the first set by injecting capsules numbered 7034, successively, at different mean water velocities, into the 74 mm diameter pipeline, and the second set by using spacers and working at a constant linear spacing concentration (C_L) of 50% with different numbers of capsules at varying mean water velocities.

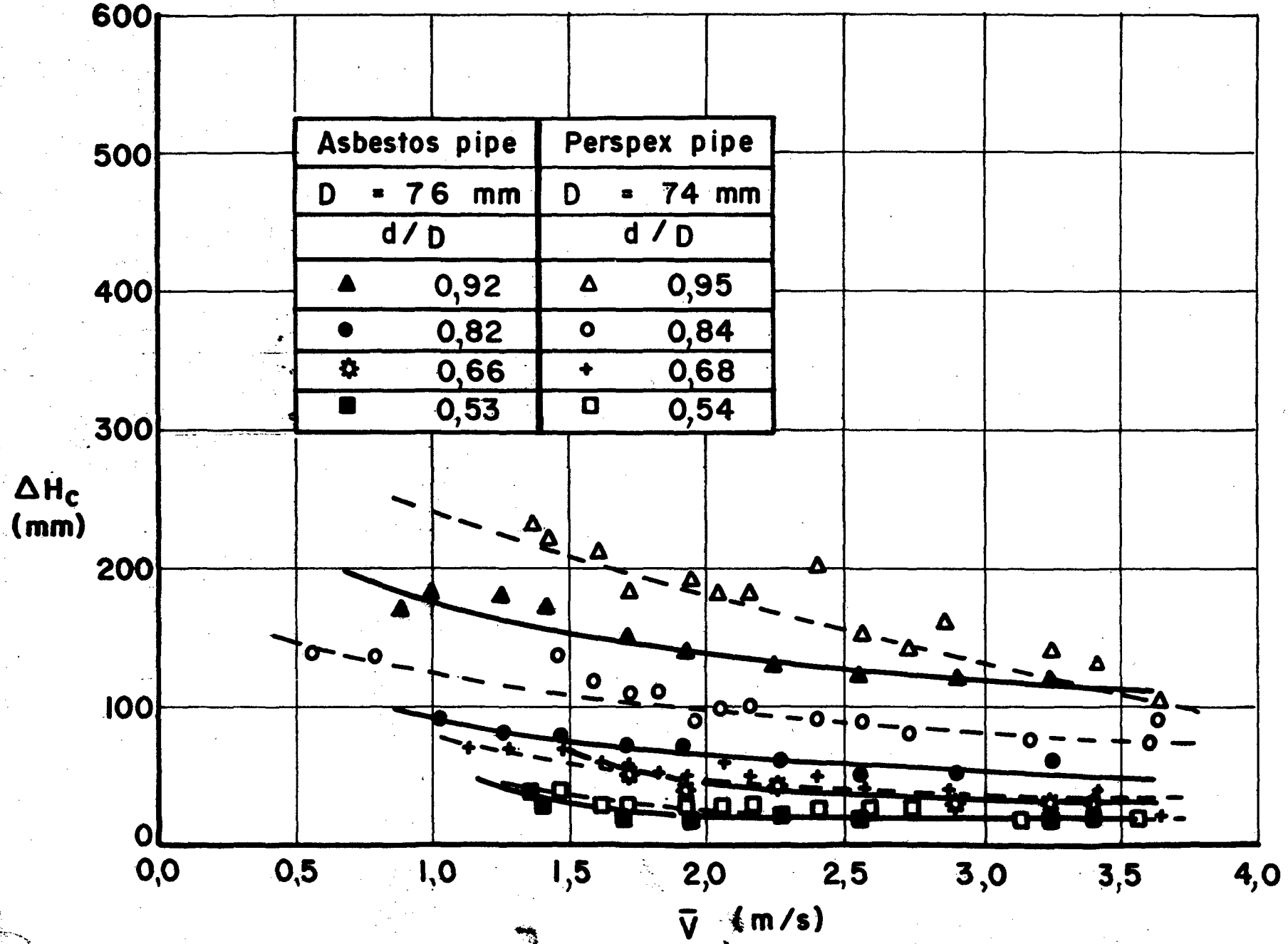

FIG. II. 65

11.66

Figure 11.66 shows the total head loss between pressure tappings (9762 mm apart) for various numbers of capsules in the line, each data point representing a mean of many others. The linear concentration is shown in brackets.

Figure 11.67 shows the excess head loss across mobile capsules per capsule, from Figure 11.66, plotted against the linear spacing with mean water velocity as parameter. It is evident that a succession of capsules has virtually no effect on the head loss at mean water velocities of 1,0 and 2,0 m/s. But at a high velocity (3 m/s) the excess head loss does appear to increase slightly with capsule concentration.

This result should not be taken too seriously since the movement of the injector at this high injector speed generated pressure waves down the pipe, which could have interfered with differential pressure measurement.

Figure 11.68 depicts results determined in the 44 mm diameter pipe with different numbers of capsules separated by spacers.

These results are superimposed on the curve for excess head losses across a solitary capsule at the bottom of Figure 11.68. The ordinate represents excess head losses across the capsules per capsule, and it can be seen that successive capsules give excess head losses per capsule that lie on either side of the curve for a single capsule.

Reference is made back to Figures 10.82 to 10.85, and the discussion thereon. It was shown that at low velocities spaced capsules travelled faster than solitary capsules, with an indication of a reversal of this trend at high mean water velocities. It has also been shown that excess head losses are generally higher at low capsule velocities. This is because solid to solid friction is more prominent at low capsule velocities and drag forces on the capsules are higher due to higher velocities relative to the capsule.

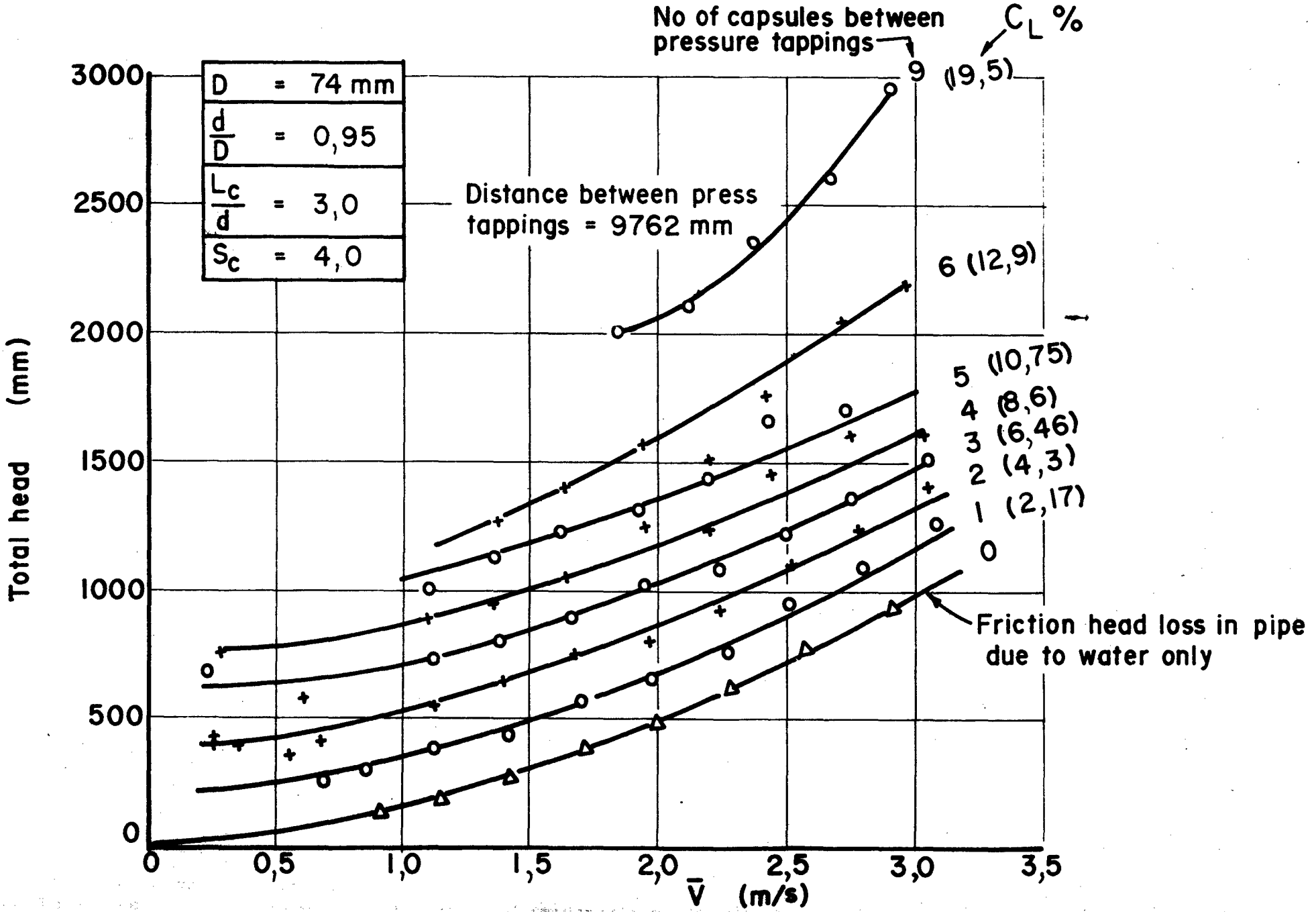

FIG. II. 66

II.68

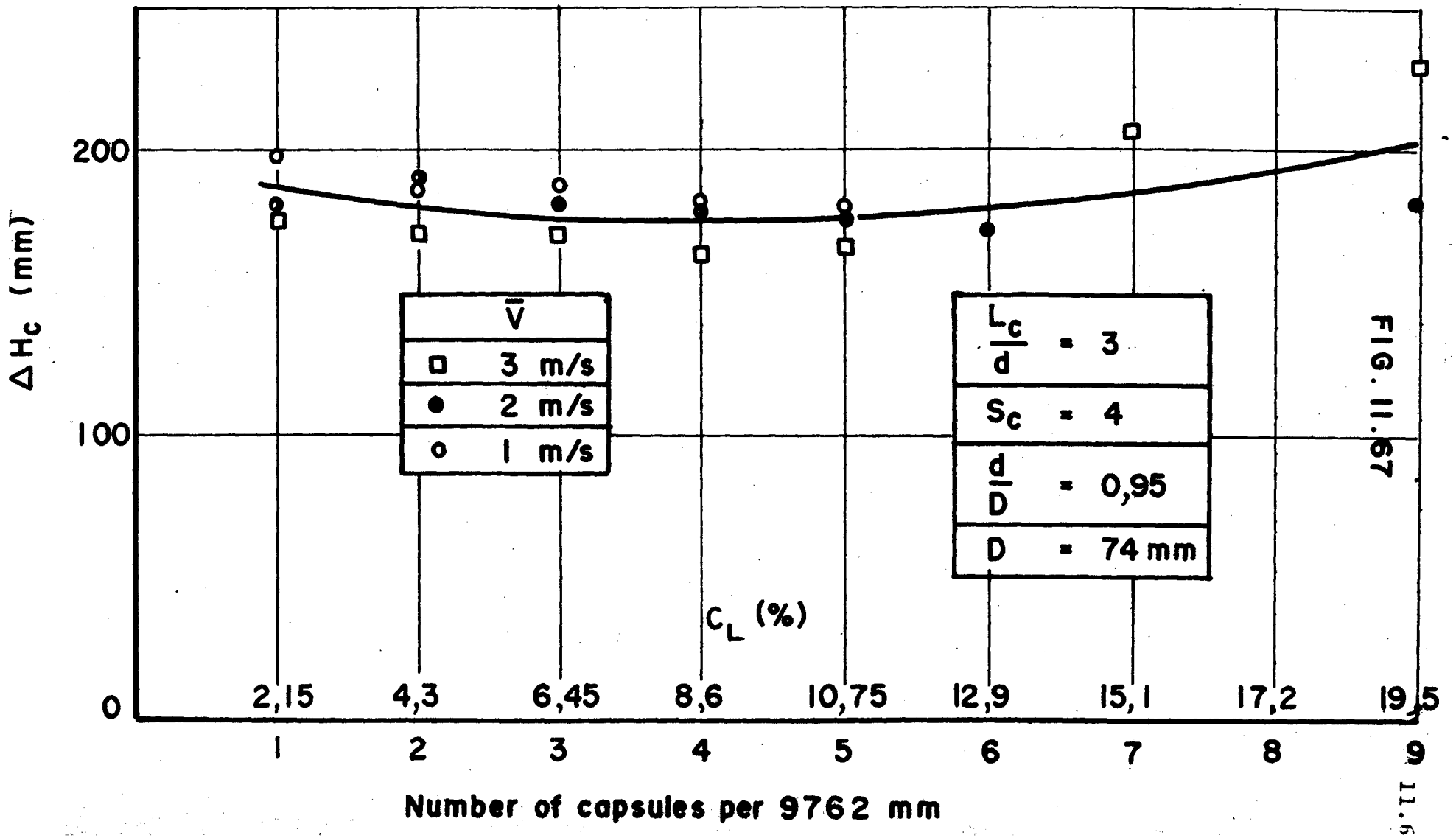

FIG. 11.67

11.69

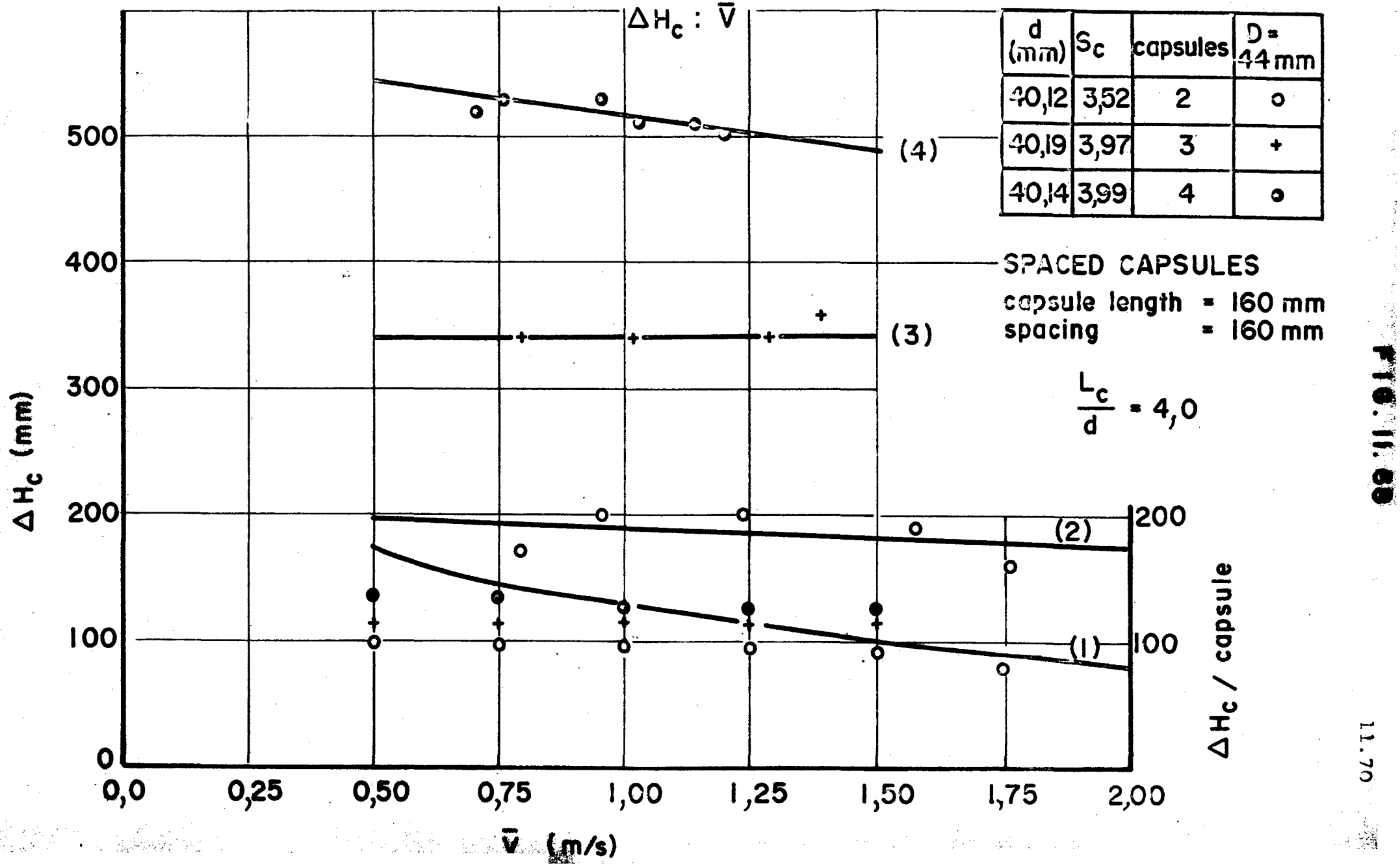
ΔHc : V̄
d (mm) | Sc | capsules | D = 44 mm
40,12 | 3,52 | 2 | o
40,19 | 3,97 | 3 | +
40,14 | 3,99 | 4 | o
SPACED CAPSULES
capsule length = 160 mm
spacing = 160 mm
Lc / d = 4,0
(4)
(3)
(2)
(1)
ΔHc (mm)
ΔHc / capsule
V̄ (m/s)
0
100
200
300
400
500
0,0
0,25
0,50
0,75
1,00
1,25
1,50
1,75
2,00

Thus, it would be expected that at low velocities, where the solitary capsule velocity is lower than the trains of spaced capsules, the excess head loss would be higher for solitary capsules, with a reversal of this trend as velocity increases. From Figure 11.68 it is seen that, indeed, this is so. With points for excess head loss across the capsule per capsule for multiple capsules lying below the solitary capsule curve at low velocities, and tending generally, to lie above the solitary capsule curve at higher velocities.

A further reason, for the excess head loss per capsule, for a train of capsules at low velocities, lying below that for a solitary capsule, is that the head loss is composed of inlet, outlet and annular components.

The inlet and outlet head losses are not able to develop fully because of the proximity of preceeding and succeeding capsules. At higher velocities the inlet and outlet head losses become less significant because the velocity relative to the capsules $(\overline{V} - V_c)$ decreases.

The work on trains of capsules is by no means conclusive but it intended to indicate trends. This has been done above, and it appears as though trains of capsules do not have an appreciable effect on excess head losses.

8. Effect of pipeline diameter on ΔH_c

Figure 11.69 shows excess head loss as a function of mean water velocity for different diameter ratio capsules used in the 150 mm, 74 mm and 44 mm pipelines.

In general, the capsules in the larger diameter pipe have a greater excess head loss than the smaller diameter pipe and this difference decreases as diameter ratio decreases.

In fact the lowest diameter ratio displays a reversal of the above mentioned trend. This may be due to experimental error. It has been mentioned earlier that as the diameter ratio decreases the reliability of

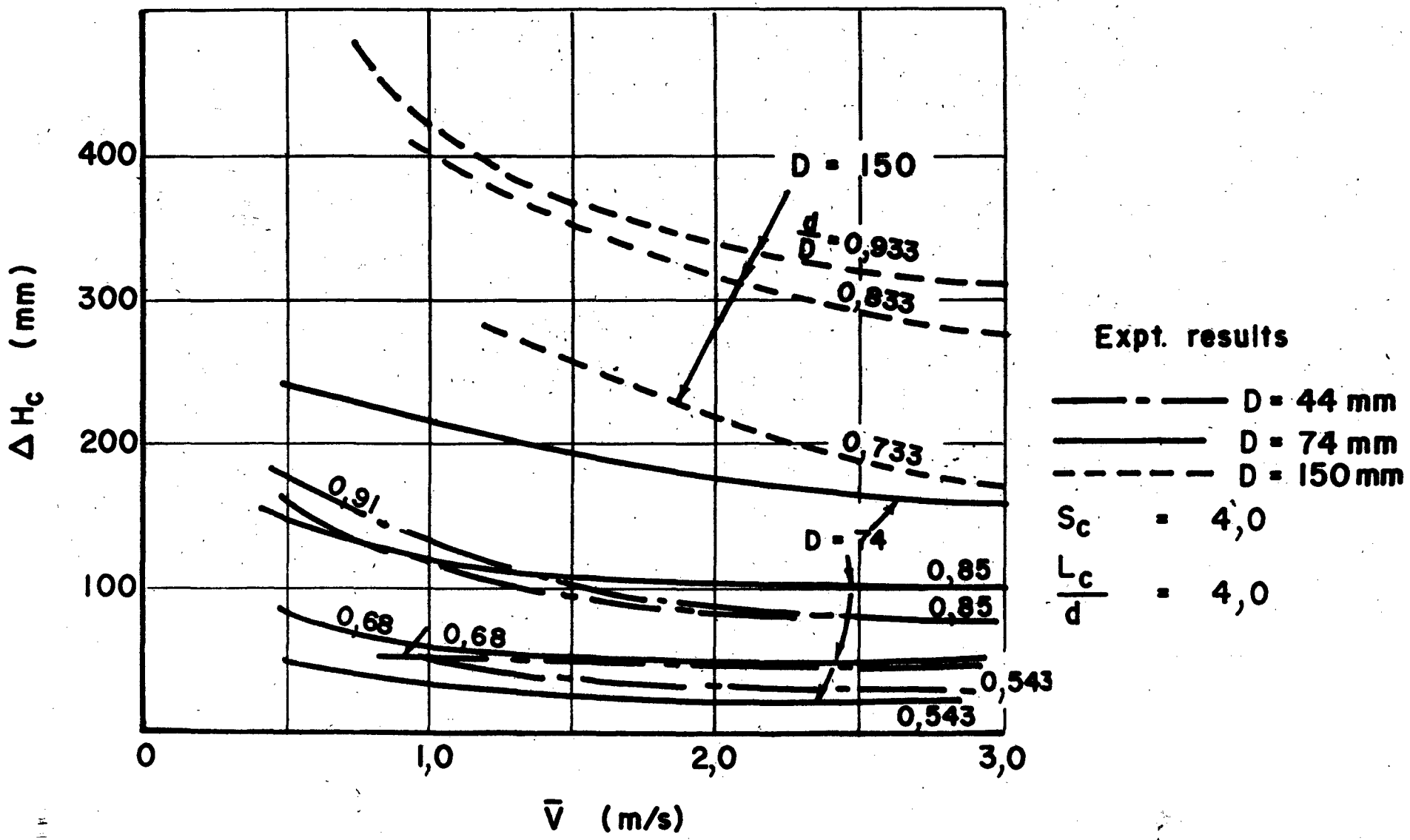

FIG. 11.69

11.72

excess head loss reading decreases since the scale of fluid turbulence as manifest on the quick response recorder from the differential pressure transmitter is commensurate with the scale of excess head losses.

Figure 11.70 is a plot of theoretically determined excess head losses derived from the empirical formula discussed in Chapter 15, and the trend of large diameter pipes having greater excess head losses is apparent. Again the discrepancy decreases as diameter ratio decreases.

The reasons for the above trends are discussed below:

Even though the capsules are dimensionally similar it is obvious that in the large diameter pipeline the capsules themselves are physically larger both as regards diameter and length. Since the densities are the same, for all the capsules discussed, those in the larger pipeline are considerably heavier.

There is thus a greater solid to solid friction force between capsule and pipewall in the case of the larger pipeline as well as an increased frontal area and surface area of capsule giving larger form drag and skin friction drag at the same velocity.

It has been shown in Chapter 10 that dimensionally similar capsules travel faster in a smaller diameter pipeline at the same mean water velocity.

Thus, the mean water velocity relative to the capsule is greater for the larger pipeline than the smaller pipeline. This applies to the mean velocity in the annulus relative to the capsule as well, and since the net drag forces on the capsule are functions of these velocities, this is an added reason for greater excess head losses in larger diameter pipelines.

At small diameter ratios, the ratio of ΔH_c values in large , compared with small diameter pipes, is of the same order as the larger diameter ratios. But the absolute values of ΔH_c show less difference for different pipe diameters as diameter ratio decreases.

FIG. II.70

11.74

The excess head loss for dimensionally similar capsules at the same mean water velocity increases as pipe diameter increases. This is, of course, the opposite type of energy loss to mean water velocity relation that exists in capsule free pipes.

CHAPTER 12

CAPSULE TO WALL CLEARANCE

This Chapter deals firstly with the a priori evidence of lift. As a result of the evidence, experiments were carried out in order to verify that the capsules did, in fact, lift off the pipe bottom. The results of these experiments, which supply a posteriori proof of lift, are also given in this Chapter.

1. A priori evidence of lift

1.1 In the Chapter on kinematics (Chapter 10) it was shown that the velocity ratio $(V_c/\overline{V})$ tends to a constant value as the mean water velocity increases. That is, the capsule catches up with the water and in certain instances the capsule velocity (V_c) exceeds that of the mean water velocity (this phenomenon becomes increasingly prevalent as diameter ratio increases and as specific gravity decreases). In order that the capsules may "gain" on the mean water speed it is likely that the solid to solid friction is reduced and that the capsules are elevated into a region of higher velocity. Both of the above reasons for the increase and ultimate levelling off of the velocity ratio $(V_c/\overline{V})$ can only occur if the capsule tends to lift, in some way, off the pipe bottom.

1.2 In Chapter 11 it was shown that velocity increase caused a steady reduction in the excess head loss (ΔH_c) in all cases. Since the excess head loss decreases as the lift coefficient increases, and as the net shear on the water at the pipe wall decreases (both of which occur as the eccentricity decreases) it is evident that capsule lift helps to explain the reduction in ΔH_c as mean water velocity increases (see Chapter 11).

1.3 For dimensionally similar capsules of different densities it was shown (see Figures 10.6 to 10.9) that the effect of appreciably different capsule densities, on the velocity ratio, is minimised as velocity $(\overline{V})$

increases. That is, heavier capsules tend to "catch up" with lighter ones at higher mean water velocities. This can be explained by a decrease in solid to solid friction brought about by a decrease in the effective weight of capsules on the pipe bottom. This decrease results in the tendency of capsules to lift at high velocities.

1.4 The decrease in excess head loss (ΔH_c) with velocity increase is most noticeable at high densities. This can be attributed to lift, which diminishes the effect of capsule density difference.

1.5 Dimensionally similar small diameter capsules were found to travel slower than larger ones at relatively low velocities, but exhibited a tendency to overtake the larger ones at relatively higher velocities, (see Figure 10.34). This is attributed to the smaller diameter capsules being lifted off the pipe bottom, thus decreasing solid to solid friction and at the same time entering a zone of higher velocity.

1.6 The effect of increasing the length of capsules of the same diameter and density is to cause them to travel slower, relative to the mean water velocity, yet at higher velocities the larger capsules overtake the shorter ones.

This is again attributed to lift since the solid to solid friction force is proportional to length and as the capsules lift, the solid friction force diminishes and the longer capsules speed up due to increased drag as a result of pressure flow in the annulus. Also the retarding effect of skin friction due to Couette shear is reduced as eccentricity decreases below unity.

1.7 The Couette flow component of shear stress on the capsule always imposes a retarding effect and this effect is magnified at increasing capsule velocities and decreased as lift occurs (see Chapter 8).

All the phenomena noted above imply that the reduction in solid to

solid friction due to lift, plus the reduction in Couette shear also due to lift (decreased eccentricity) more than offsets the increased retardation force due to Couette flow if the capsule does not lift.

1.8 A stethoscope was attached to the 74 mm diameter pipe and it was possible to detect a shrill scraping sound as capsules travelled along the pipe at low velocities. As capsule velocities were increased, the sound gradually disappeared. It was not possible to determine the exact threshold velocity at which the change over from touching to non-touching occured since, firstly, this was a gradual process and secondly the detection method was somewhat subjective.

2. Friction factor

Note that some of the above observations (1 to 6 above) could partially be ascribed to a reduction of the friction factor (μ_f). However, it is unlikely that kinetic friction would be effected by capsule velocity to the extent necessary to cause the phenomena, particularly in the range of velocities considered in the experiments (see Chapter 8, Section 3).

3. Four regimes of lift

Four regimes of lift are hypothesized.

The first stage being on a microscopic scale and having the effect of reducing the submerged weight of the capsule on the pipe bottom. It is hypothesized that a slight elastic expansion of the capsule is accompanied by a reduced reaction on the pipe bottom.

This regime can be defined as ranging from the position when the full submerged weight of the capsule is just not taken on the pipe, and the fluid resistance is supplemented by solid to solid contact (semi hydrodynamic lubrication. See Chapter 8, Section 3.5) to the position when the peaks of the asperities on the capsule and pipe just loose contact except at the back.

The second stage is microscopic upward tilt at the front of the capsule. The capsule is separated from the pipe by a film of water and is in contact only at the rear.

The third stage is on a macroscopic scale and the clearance should become visible with the naked eye. However, the curvature of the pipe and the refraction of light when passing through water, perspex and air, make it difficult to see lift on a small scale by eye. The capsule is still in contact with the pipe at the back and tilts upwards when travelling.

The fourth stage is free travel with the capsule completely free of pipe contact.

For the first three stages $L_F < W'$ and for the last stage $L_F > W'$.

It was possible to detect lift of the lower density capsules visually, and the capsules in general lifted nose-up first, although in certain instances, tail-up. Whether the nose or rear lifts off first will be discussed further later in the Chapter, although the sensitivity of capsule orientation to the exact position of the centre of gravity is probably pronounced.

4. Results of experiments on capsule lift

Initially, the purpose of these experiments was merely to affirm the existence of lift. However, with the apparatus described in Chapter 4, it was possible to obtain, to a limited accuracy, some qualitative data.

Reference is made to the apparatus involved, which has already been described (Chapter 4, Section 9).

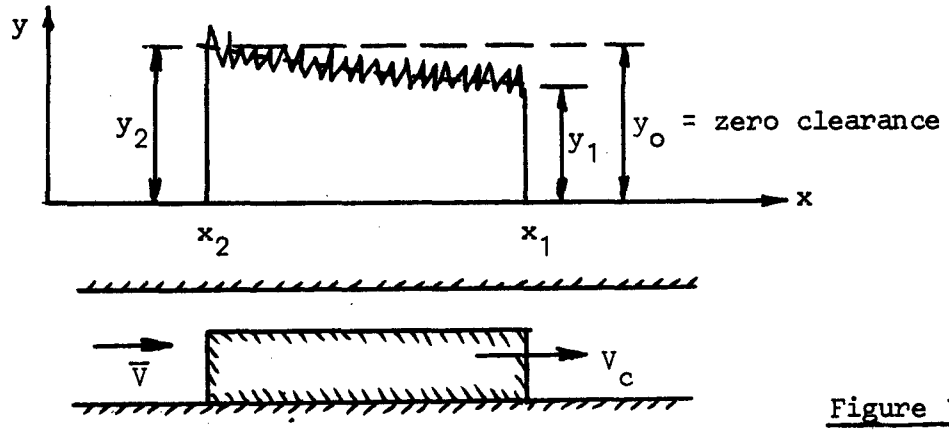

Figure 12.1

Typically, the output on the oscillioscope was of the form indicated on Figure 12.1. The nose clearance is represented in terms of the y-scale amplitude (y_1) at x_1 and the rear in terms of the y-scale amplitude (y_2) at x_2. These readings (cm) were converted to the output signal (millivolts) by means of the y-scale value selected (mV/cm). The actual clearance was then read of the relevant clearance versus output calibration curves (see Chapter 6). The clearance between the bottom of the capsule (C) is shown as a function of the capsule velocity (V_c) on Figures 12.2 to 12.5.

Despite the large amount of scatter indicated, general trends are apparent.

In all cases some degree of clearance is indicated. The amount of clearance varies according to the size, specific gravity and capsule velocity.

4.1 Effect of capsule velocity

At low velocities there is no detectable clearance between capsule and pipe wall. As the velocity increases the nose of the capsule generally lifts first and at a still higher velocity the rear commences to lift.

The front clearance is at all times higher than the back clearance (except as visually observed for very short ($L_c/d < 2$) light capsules) thereby showing that the capsule travels at an angle with a wedge of water between capsule bottom and pipe wall in a nose-up position (see Chapter 8).

As the velocity is still further increased the clearance becomes

Figure 12.2

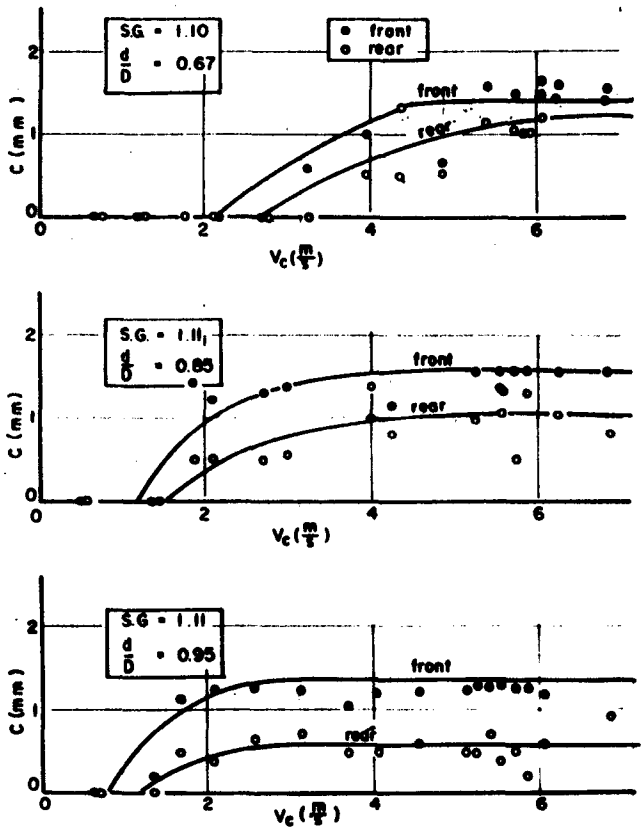

Figure 12.3

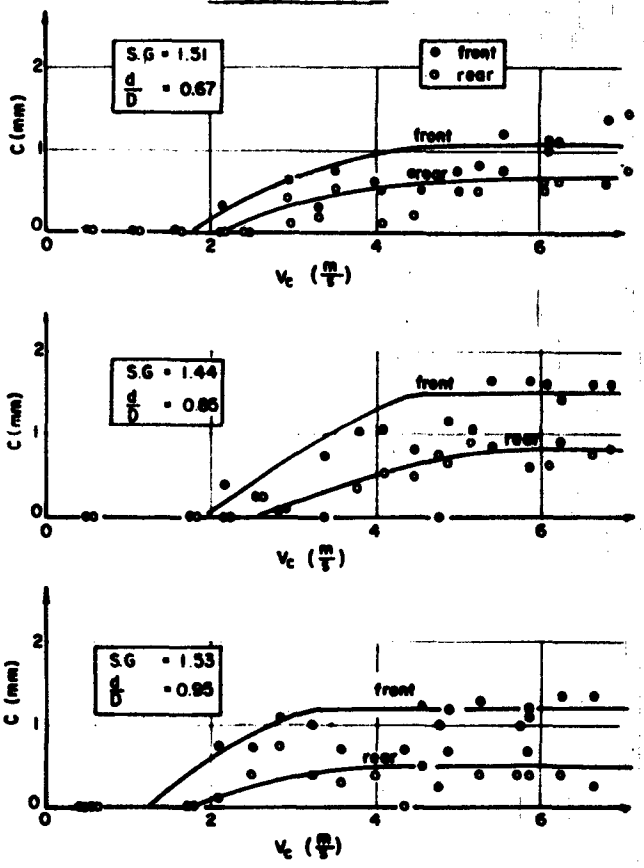

Figure 12.4

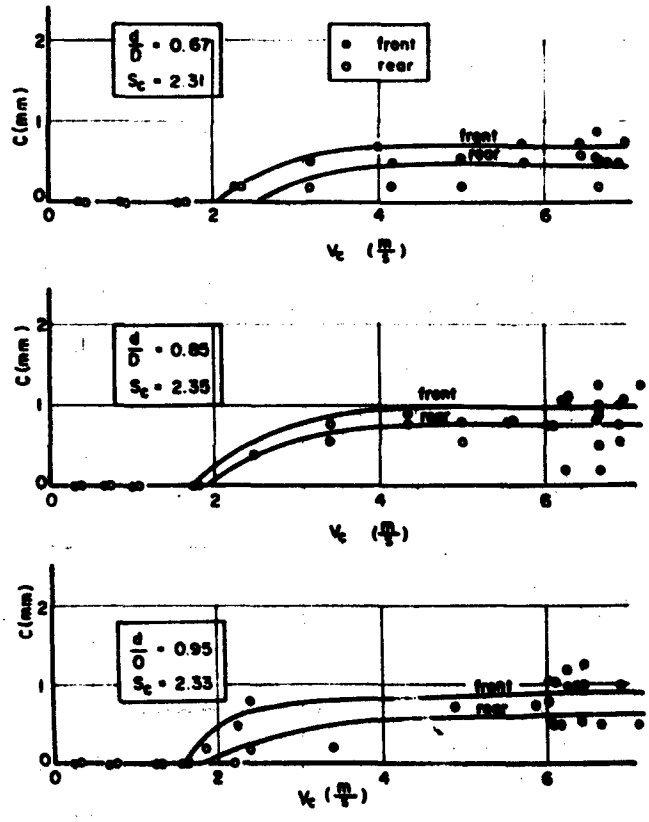

Figure 12.5

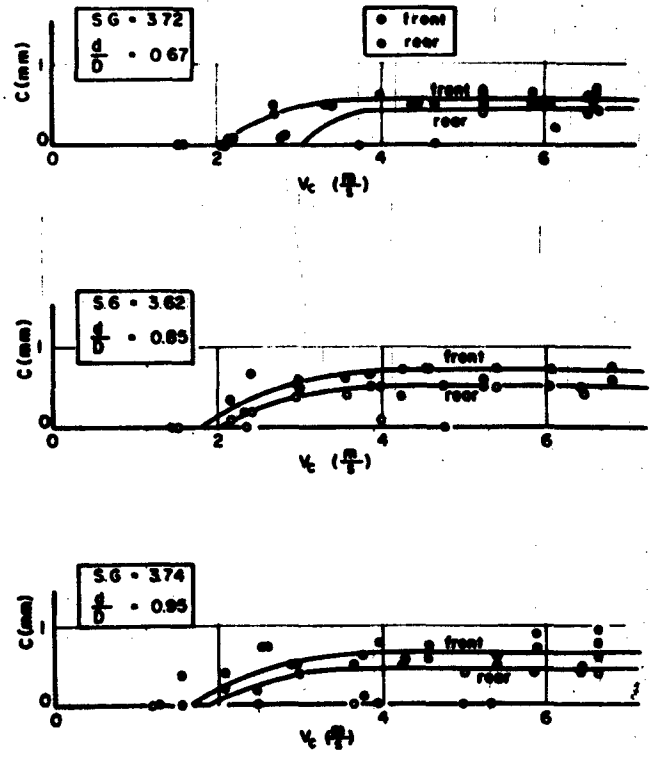

constant and this constant clearance is maintained at further velocity increases. For the capsules tested the constant clearance varied between 0,4 and 1,6 mm. The constant maximum clearance (at the front of the capsule) is designated C^*. In general, the capsule velocity at which $C = C^*$ is higher as diameter ratio decreases and the value of C^* increases as SG decreases.

From the clearance (C) versus capsule velocity (V_c) curves it is clear that the capsules start to lift at the nose and rear at different velocities, and the capsule velocity at which lift first commences is designated (V_{cil}), (i.e. capsule velocity for incipient lift).

Although there is a large amount of scatter, it appears as though the nose always starts to lift at a lower velocity (V_c) than the rear.

Note that in these experiments capsule velocities were generally considerably higher than those envisaged for practical application, and outside the range of V_c values for previous tests. It was anticipated that the lift phenomena would detectably occur at relatively high velocities, and this turned out to be correct.

The mechanism of lift has been dealt with in Chapter 8, Section 11.2, and the shape of the curves (Figures 12.2 to 12.5) can be understood when referring to Chapter 8, Section 12.2. It was explained how the capsule reaches an equilibrium position regardless of velocity increase, and this is verified in the experiments. This will be dealt with further (see Section 4.4).

Two dependent variables are considered in the discussion, i.e. maximum clearance (C^*) and capsule velocity for incipient lift (V_{cil}). The effect of dimensionally similar capsules of different diameter ratio and SG on the two dependent variables will not be considered.

4.2 Incipient capsule velocity for lift (V_{cil})

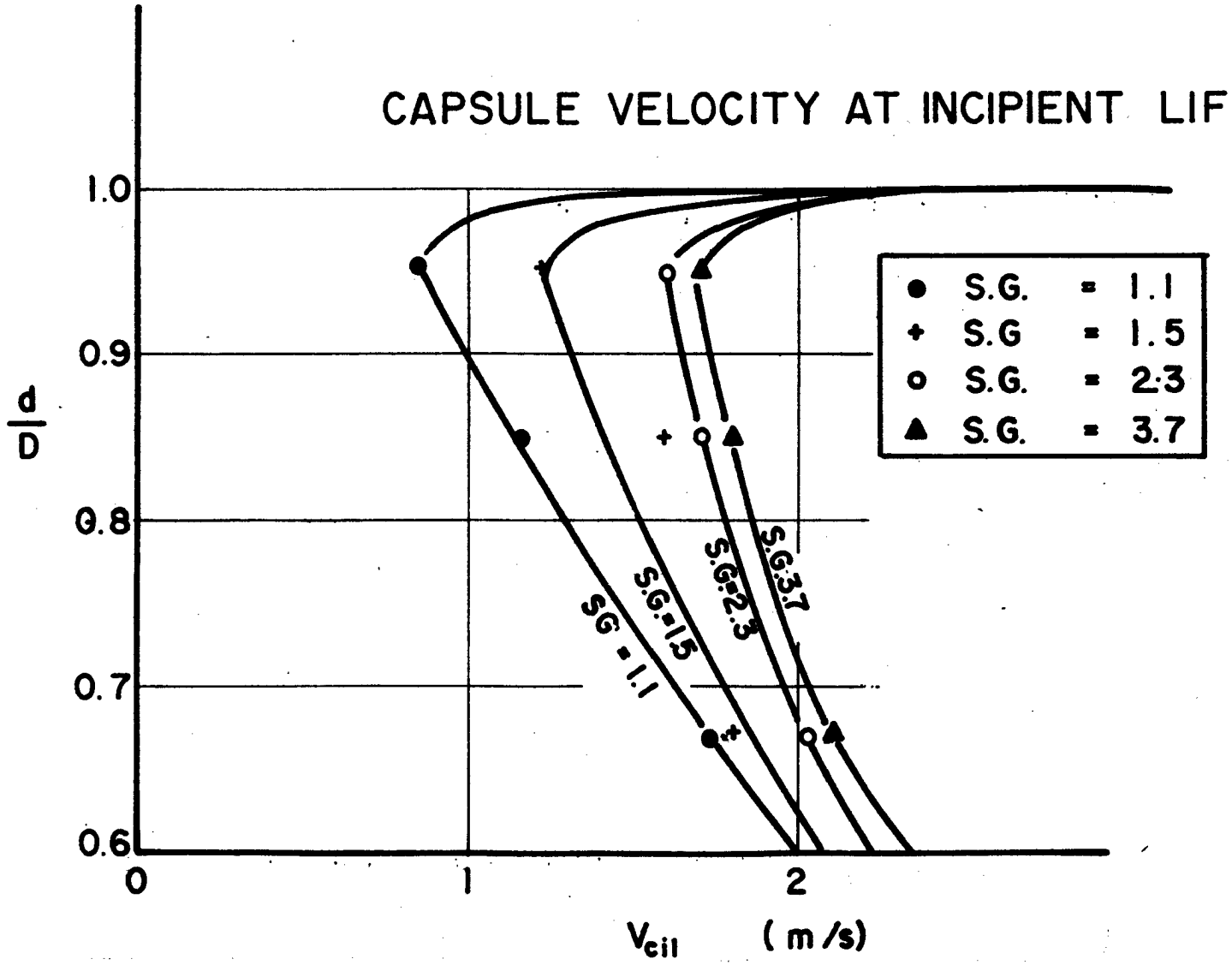
CAPSULE VELOCITY AT INCIPIENT LIFT
1.0
0.9
0.8
0.7
0.6
d/D
0
1
2
V_{cil} (m/s)
S.G. = 1.1
S.G = 1.5
S.G. = 2.3
S.G. = 3.7
SG = 1.1
S.G.=1.5
S.G.=2.3
S.G.3.7

FIG. 12.6

Figure 12.6 shows the capsule velocity for incipient lift plotted against diameter ratio with SG parameter.

There can be no clearance when diameter ratio is unity. The value of $V_{ci\ell}$ tends to infinity and approaches the unit value of diameter ratio asymptotically. At the other end of the diameter ratio scale, as d/D approaches zero, the capsule velocity required for lift off also tends to be high.

There appears to be a minimum lift off velocity which occurs at d/D = 0,95 and as diameter ratio decreases below d/D = 0,95 or increases above d/D = 0,95 the value of $V_{ci\ell}$ increases.

Since there are only three points (representing three diameter ratios) on each of the curves, the value d/D = 0,95 is an approximate estimate.

There appears to be no discernable SG effect on the diameter ratio at which the minimum value of incipient lift off velocity occurs. It appears as though the value remains constant at d/D = 0,95 regardless of the capsule density.

The curves indicate that for a particular diameter ratio the capsule velocity for incipient lift increases as SG increases, and the effect of SG becomes increasingly evident as diameter ratio approaches d/D = 0,95. Figure 12.7 shows capsule velocity at incipient lift ($V_{ci\ell}$) as a function of SG. When SG is equal to unity the submerged weight of the capsule is zero, and the capsule travels concentrically thus giving $V_{ci\ell} \rightarrow 0$ as $SG \rightarrow 1$.

Another trend indicated by the curves is that as SG increases the value of $V_{ci\ell}$ increases, but above an SG value of about 4,0 any further density increase would not require a higher capsule velocity for lift off. It must be remembered that a higher mean water velocity corresponds to the same capsule velocity as SG increases. A plot of

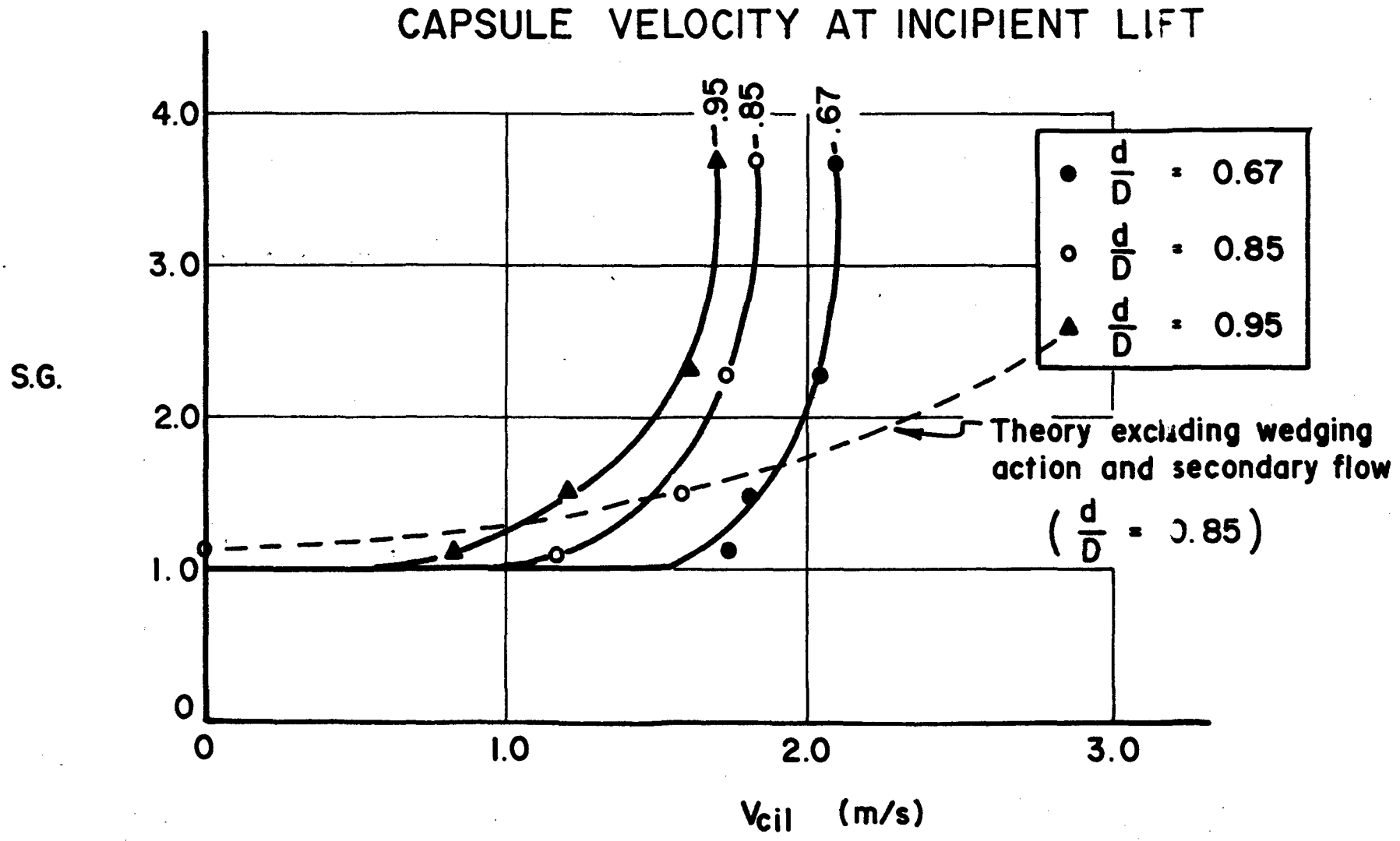
CAPSULE VELOCITY AT INCIPIENT LIFT
S.G.
4.0
3.0
2.0
1.0
0
0
1.0
2.0
3.0
V_{cil} (m/s)
.95
.85
.67
$\frac{d}{D}$ = 0.67
$\frac{d}{D}$ = 0.85
$\frac{d}{D}$ = 0.95
Theory excluding wedging action and secondary flow
($\frac{d}{D}$ = 0.85)

FIG. 12.7

$\overline{V}$ corresponding to the relevant value of $V_{ci\ell}$ shows a steady increase in $\overline{V}$ for incipient lift as SG increases.

It is nonetheless, unlikely that the curves indicated by the four points (Figure 12.7) are valid since local water velocities relative to the capsule in a backward direction decrease as SG increases, although it will be shown (Section 4.3) that the maximum lift attained is less for heavier than lighter capsules.

The dotted curve on Figure 12.7 shows calculated values for $V_{ci\ell}$ (for $d/D = 0,85$) based on the analysis described in Chapter 7 when equation (7.220) first becomes valid.

The dotted curve generally gives $V_{ci\ell}$ values which are too high (particularly at high SG's). This is easily explained, since the theory is primarily for calculating energy losses across mobile capsules and none of the secondary flow or lubricating effects have been included.

It is reasonable to expect that existing theory would not be applicable to this situation since even comparatively simple shapes in an infinite medium require experimentally determined lift coefficients.

4.3 Maximum clearance

Figure 12.8 shows maximum clearance (C^*) as a function of SG with diameter ratio as parameter.

These curves indicate that, for a fixed diameter ratio, the maximum clearance (C^*) achieved by a capsule decreases as SG increases.

The curves tend to level, implying that further SG increases would result in the capsules rising to the same position. The mean water velocity to achieve this position would be greater. It appears from Figures 12.2 to 12.5 that as diameter ratio increases at a fixed SG the minimum capsule velocity required for initiating maximum clearance (C^*) is lessened and as SG increases at a fixed diameter ratio the minimum

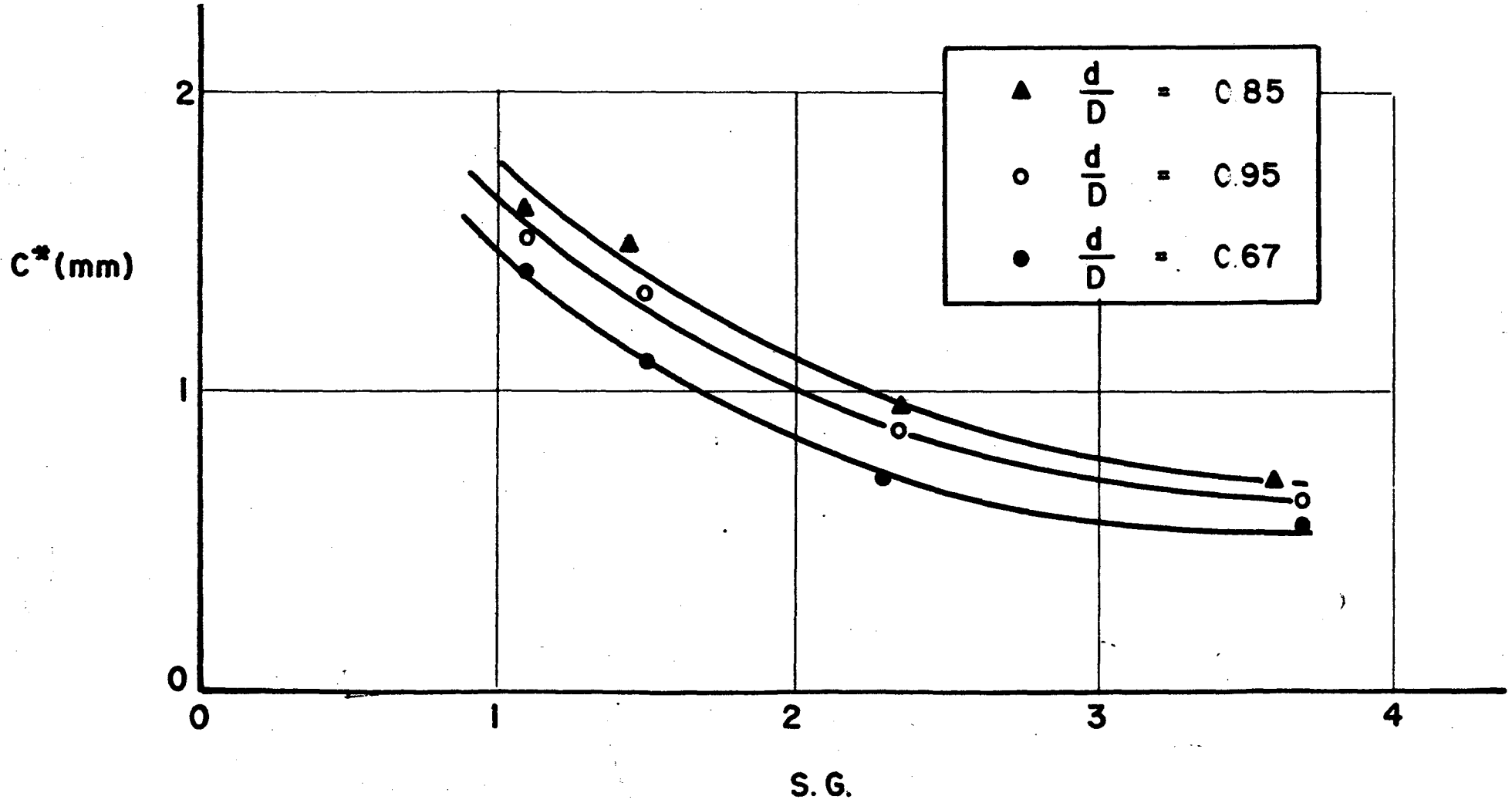

FIG. 12.8

capsule velocity as well as the minimum mean water velocity, required for maximum clearance, must increase.

At a fixed SG decreasing the diameter ratio below 0,85 and increasing above 0,85 yields decreasing values for the maximum clearance attained.

This trend is more clearly shown on Figure 12.9.

Figure 12.9 shows maximum constant clearance (C^*) as a function of diameter ratio with SG as parameter. At both ends of the diameter ratio scale (i.e. zero and unity) the clearance must be zero. This is obvious at $d/D = 1,0$ and as $d/D \to 0$, capsules of $SG > 1,0$ would tend to remain at the pipe wall where the local water velocity is zero. For a particular diameter ratio the clearance increases with SG decrease.

For each SG there is a particular diameter ratio at which the maximum constant clearance (C^*) reaches a maximum value (C^*max). The locus of maximum clearance (C^*max) is shown on the graph and passes through zero at $d/D = 1,0$.

As SG decreases the maximum clearance (C^*max) occurs at ever decreasing diameter ratio, and at $SG = 1,0$ the clearance for a diameter ratio $d/D = 0$ would theoretically be $\frac{1}{2}D$.

It is easy to see that the curves on Figure 12.9 must have the shape shown if lift occurs. But the questions that spring to mind are; firstly, why does the diameter ratio at which maximum clearance occurs decrease as SG decreases? And secondly, why does the maximum clearance generally occur in the region $d/D = 0,85$?

In answer to the first question, three facts must be emphasised for a constant mean water velocity and capsule geometry. Firstly, the lower the SG of the capsule, the faster it travels. Secondly, decreasing diameter ratio decreases capsule velocity, and thirdly, lighter capsules lift at lower velocities than heavier ones.

FIG. 12.9

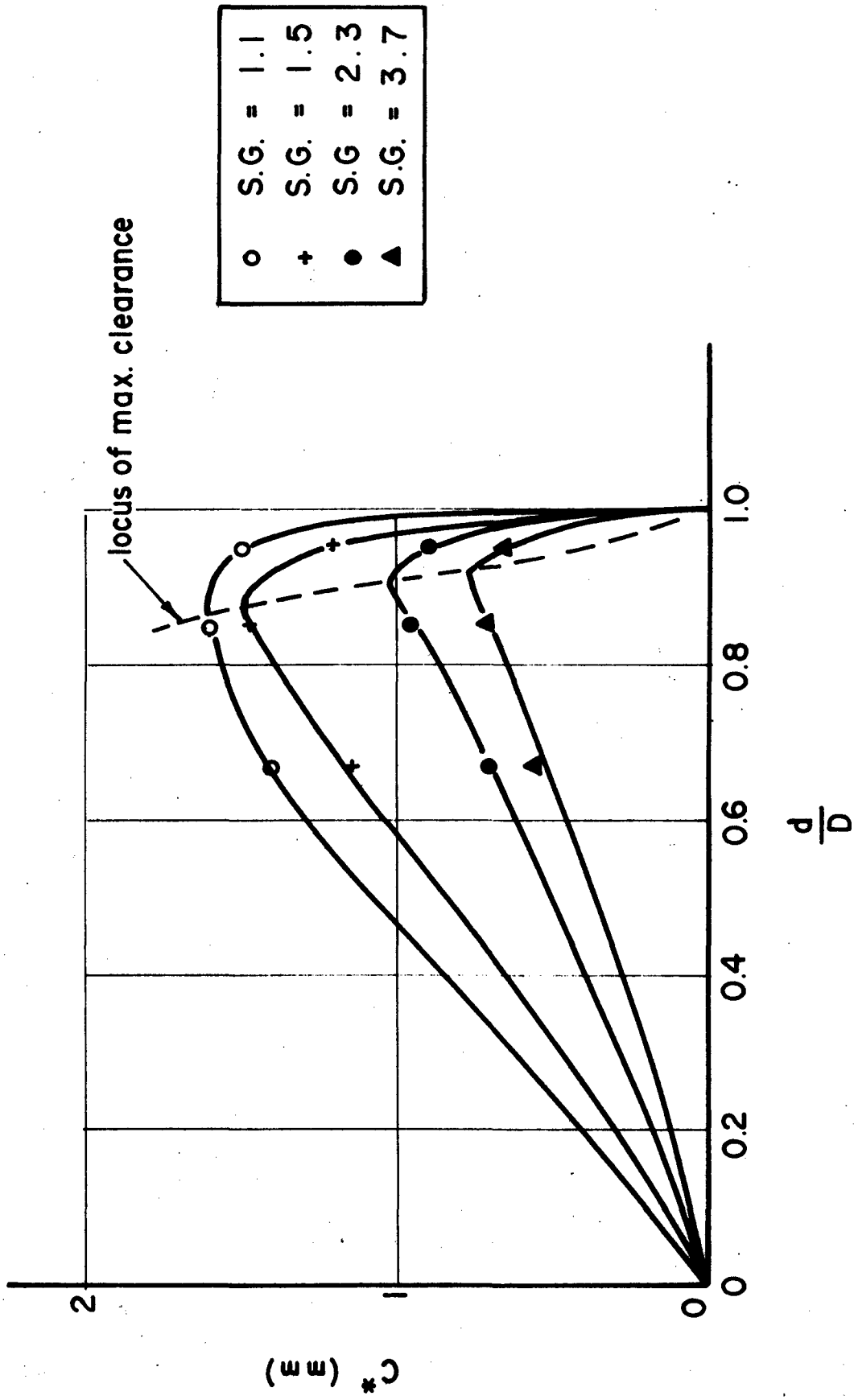
o S.G. = 1.1
+ S.G. = 1.5
● S.G = 2.3
▲ S.G. = 3.7
locus of max. clearance
C* (mm)
2
1
0
0
0.2
0.4
0.6
0.8
1.0
d/D

Since it is the local water velocities relative to the capsule that induce lift, it is plausible that decreasing $\overline{V}$, d/D and SG appropriately results in water velocities, at salient points around the capsule, which cause maximum lift on the smaller diameter ratio capsules at lower SG's. The second question, as to maximum lift occurrence at roughly the same diameter ratio, can be explained as follows:

If the capsule lifts and the diameter ratio is large (say $d/D > 0,9$), then the mechanisms inducing lift, which rely on the proximity of the pipe to the underside of the capsule, become effective at the top due to the proximity of the pipe at the upper side of the capsule. If the capsule is relatively small (say $d/D < 0,85$), and at the same time somewhat lighter than the larger diameter ratio capsule, then the mechanism preventing further lift, i.e. reduction of the lubricating film pressure due to increasing clearance, causes the maximum lift to occur at about the same diameter ratio.

It can thus be seen qualitatively that lighter capsules can reach maximum clearance at roughly the same diameter ratio as heavier capsules in the range tested. Although increasing SG does cause maximum lift to occur at higher diameter ratios.

4.4 Relation of velocity ratio to clearance

Figures 12.10, 12.11 and 12.12 show the velocity ratio as a function of mean water velocity for three diameter ratios and four specific gravities.

The mean water velocities ($\overline{V}$), corresponding to capsule velocities, at which lift is initiated (V_{cil}) as well as at which the back of the capsule just starts to lift, and the maximum clearance first becomes apparent, are also shown on these diagrams as dashed curves.

As the nose of the capsule first starts to lift, the rapid increase of

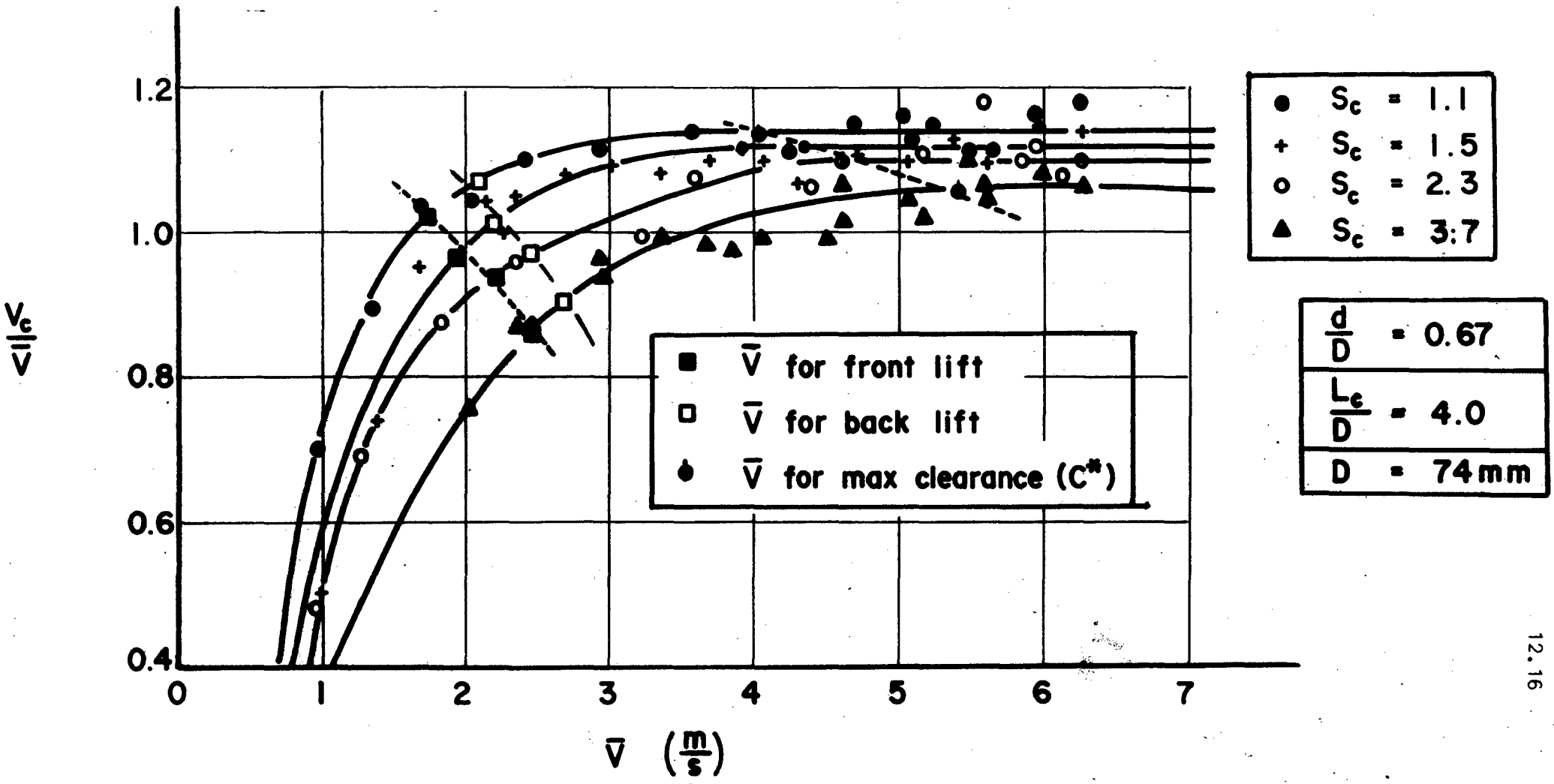
1.2
1.0
0.8
0.6
0.4
0
1
2
3
4
5
6
7
$\frac{V_c}{V}$
$\bar{V}$ $(\frac{m}{s})$
S_c = 1.1
S_c = 1.5
S_c = 2.3
S_c = 3.7
$\bar{V}$ for front lift
$\bar{V}$ for back lift
$\bar{V}$ for max clearance (C^*)
$\frac{d}{D}$ = 0.67
$\frac{L_c}{D}$ = 4.0
D = 74mm

FIG. 12.10

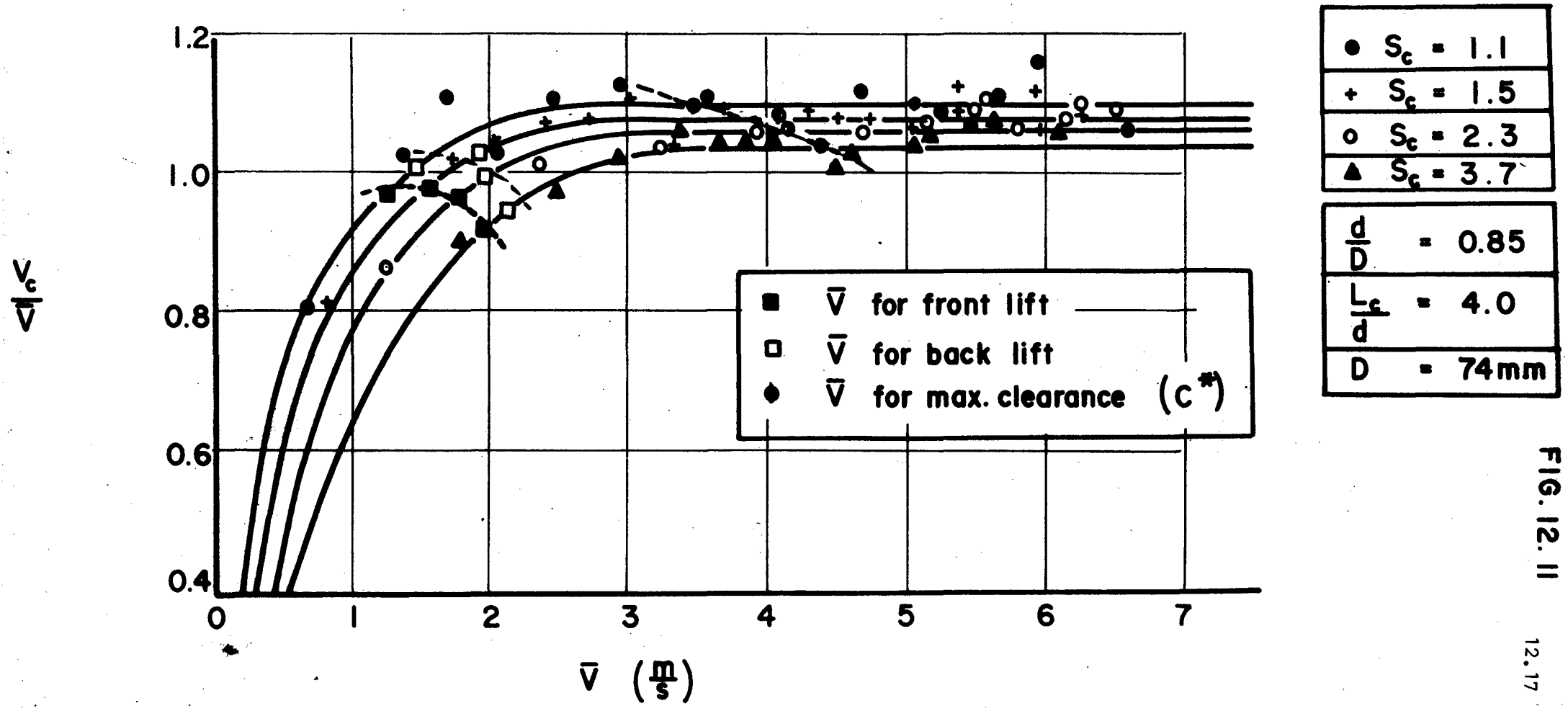
1.2
1.0
0.8
0.6
0.4
0
1
2
3
4
5
6
7
$\frac{V_c}{\bar{V}}$
$\bar{V}$ $(\frac{m}{s})$
$\bar{V}$ for front lift
$\bar{V}$ for back lift
$\bar{V}$ for max. clearance (C^*)
S_c = 1.1
S_c = 1.5
S_c = 2.3
S_c = 3.7
$\frac{d}{D}$ = 0.85
$\frac{L_c}{d}$ = 4.0
D = 74mm

FIG. 12. 11

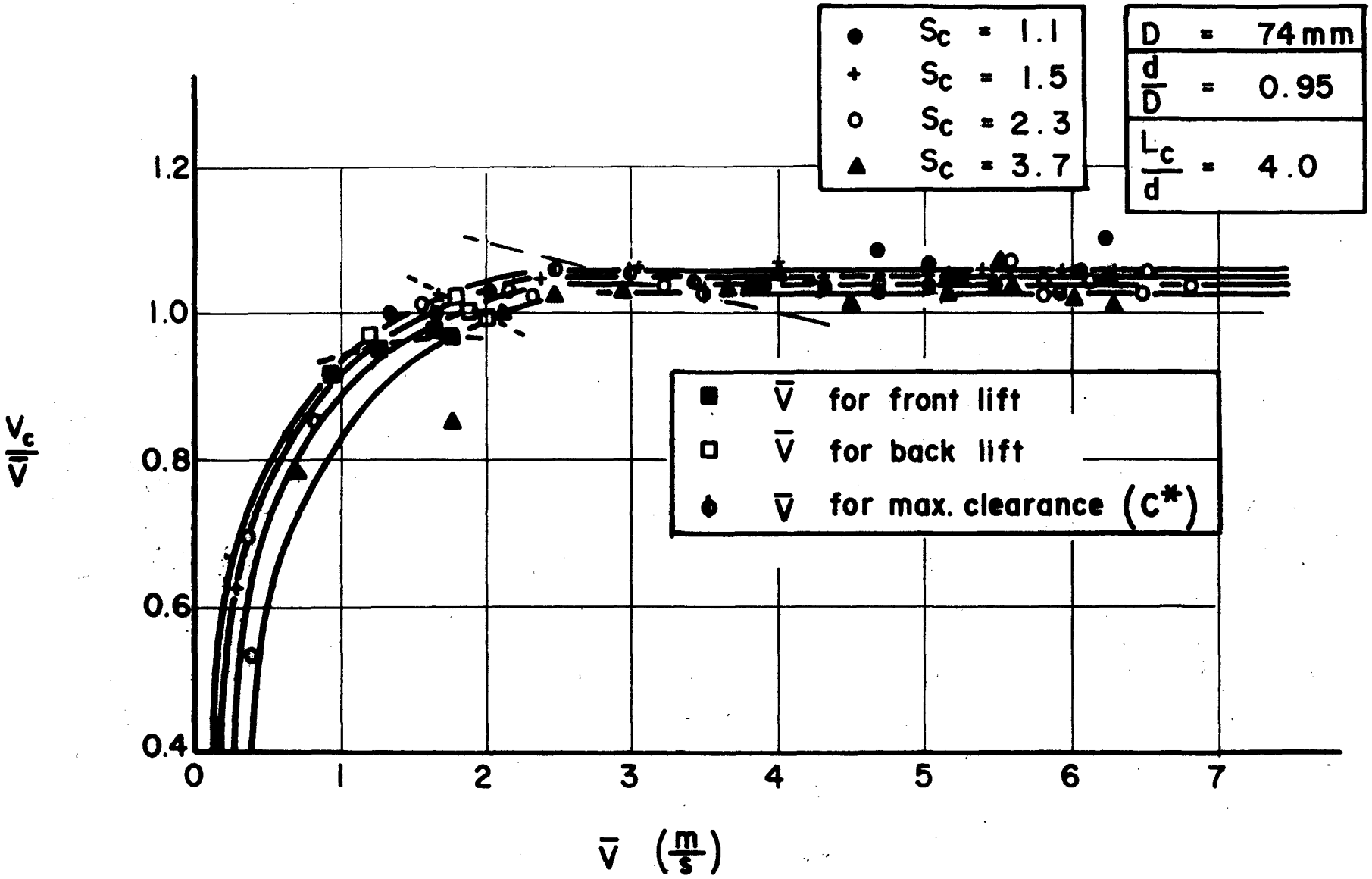
S_c = 1.1
S_c = 1.5
S_c = 2.3
S_c = 3.7
D = 74mm
$\frac{d}{D}$ = 0.95
$\frac{L_c}{d}$ = 4.0
$\bar{V}$ for front lift
$\bar{V}$ for back lift
$\bar{V}$ for max. clearance (C^*)
$\frac{V_c}{\bar{V}}$
$\bar{V}$ $(\frac{m}{s})$
1.2
1.0
0.8
0.6
0.4
0
1
2
3
4
5
6
7

FIG. 12.12

the velocity ratio $(V_c/\overline{V})$ tends to drop off and the capsule velocity tends to increase relative to the mean water velocity less rapidly. This continues as the rear lifts. Finally, when the capsule has achieved maximum lift the capsule velocity reaches a constant multiple of the mean water velocity.

At the position on the velocity ratio $(V_c/\overline{V})$ versus mean water velocity $(\overline{V})$ curve where incipient lift occurs at the front of the capsule, the submerged weight of the capsule (W') is greater than the lift force (L_F). As soon as the rear of the capsule lifts $L_F = W'$ and any further increase in velocity momentarily increases the lift force. This causes the capsule to rise to a position where local velocities are such as to reinstate stability, i.e. $L_F = W'$ at an increased clearance.

This process continues until the velocity ratio becomes constant. And on all three graphs (Figures 12.10, 12.11 and 12.12) the capsule velocity (V_c) is greater than the mean water velocity $(\overline{V})$, i.e. $V_c = C'\overline{V}$ where $C' > 1,0$. Any further increase in velocity will not cause an increased lift force since the velocity relative to the capsule remains a constant value of $\overline{V}$, i.e. $\overline{V} - V_c = \overline{V}(1-C')$. Since $C' > 1,0$, the mean velocity in the pipe relative to the capsule is in a backward direction.

In the capsule free pipe, further increase of velocity will not alter the velocity distribution at these high Reynolds numbers, and $\overline{V}$ can be replaced by the local water velocity corresponding to V_c or the local water velocities responsible for lift. The capsule thus moves with the water surrounding it and no further lift is generated.

PART V

COMPARISON OF EXPERIMENTAL AND ANALYTICAL RESULTS

"There is no more common error than to assume that, because prolonged and accurate mathematical calculations have been made, the application of the result to some fact of nature is absolutely certain."

A.N. Whitehead

CHAPTER 13

COMPARISON OF EXPERIMENTAL AND ANALYTICAL RESULTS FOR STATIC CAPSULES

The bulk of this Chapter is devoted to a comparison of results, derived from the finite element analysis, with experimental values, for pressure flow in the annulus.

The other two components of energy loss across a static capsule (inlet and outlet losses) will be briefly discussed in relation to conventional sudden contraction and sudden expansion losses in circular pipes.

1. Comparison of experimental inlet head losses with sudden contraction losses for conventional concentric pipes

The energy losses at entry to the capsule annulus are due to sudden contractions and, as such, may be compared with the more elementary cases of contractions involving concentric circular tubes. Rouse (reference 59) gives values of head loss coefficients for sudden contractions for various area ratios, as given below, for the concentric pipe case:

TABLE 13.1

(A_2/A_1)	00	0,1	0,2	0,3	0,4	0,5	0,6	0,7	0,8	0,9	1,0
K	0,5	0,48	0,45	0,41	0,36	0,29	0,21	0,13	0,07	0,01	0

These K values are to be used in the equation

$$\Delta h_i = K\, V_2^2/(2g) \qquad (13.1)$$

where V_2 is the velocity in the smaller pipe, equivalent in the capsule case to the annular velocity. If the head loss is referred to the velocity in the larger pipe, the K values given by Rouse have to be divided by the area ratio squared. For an annular area the ratio is related to the diameter ratio by the equation

$$d/D = \sqrt{1 - A_2/(A_1)} \qquad (13.2)$$

With these changes Rouse's values may be re-presented for the capsule case as follows:

TABLE 13.2

d/D	1	0,948	0,894	0,837	0,775	0,707	0,632	0,548	0,447	0,315	0
k'	∞	48	11,2	4,55	2,25	1,16	0,582	0,265	0,109	0,012	0

where

$$\Delta h_i = k' \bar{V}^2/(2g) \qquad (13.3)$$

These values are shown on Figure 9.6 and may be compared with values obtained in the present experiments. In Chapter 9, Section 2, the pattern of streamlines at the inlet face of a static capsule was discussed and it was pointed out how the velocity distribution just upstream and downstream of the inlet section is complicated by the capsule geometry, particularly in the eccentric capsule case.

It is clear that there are appreciable differences between the two sets of values on Figure 9.6, i.e. for the eccentric annulus and concentric pipe analysis.

Figure 9.8 shows a comparison between the experimentally determined coefficients for concentric annuli and those for concentric pipe analysis as given by Rouse (see Table 13.2).

It is clear that the shape of the curves is similar in the concentric capsule case (Figure 9.8) and this is probably because in both cases the streamline patterns are similar (see Figure 13.1).

However, the head loss coefficients are consistently higher for the concentric annulus than the concentric pipe.

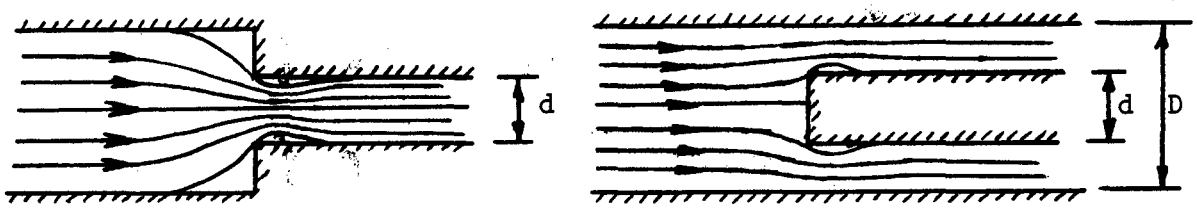

(a) Concentric pipe (b) Concentric annulus

Figure 13.1

From Figure 13.1 it is clear that the contraction takes place around a convex perimeter in the concentric annulus case as opposed to a concentric concave perimeter in the case of circular pipes (Figure 13.1(a)). Case (a) leads to a general contraction of streamlines and it is well known that less energy is dissipated in such a system than when streamlines expand in a diverging conduit as in case (b). However, most of the energy is expended in eddy formation between the section of maximum streamline contraction (at the vena contracta) and a region downstream where the streamlines are parallel. There is a larger region where eddy generation takes place in case (b) than in case (a), (i.e. separation occurs around a convex edge in case (b)).

From Figure 9.6, it can be seen that the eccentric annular inlet head losses are also greater than for concentric pipe analysis. And the curves are dissimilar. This is due to the eccentric nature of the annulus. The percentage discrepancy decreases as diameter ratio increases, both tending towards an asymptotic value of infinity as diameter ratio approaches unity.

One further point is that the head loss for concentric pipe analysis is somewhat differently defined from the head loss of a concentric or eccentric annular inlet section (see Chapter 7, Section 3.3).

2. Comparison of experimental outlet losses with sudden expansion losses in concentric pipes

It has already been shown, in Chapter 9, Section 3, that energy losses

at the outlet are not so pronounced as at the inlet and reasons for this phenomenon were given.

Furthermore, it was pointed out that the coefficient in equation (7.117) is 15% higher than unity for concentric capsule outlet losses and 32% lower for eccentric capsules. The relevant curves are shown in Figure 9.9.

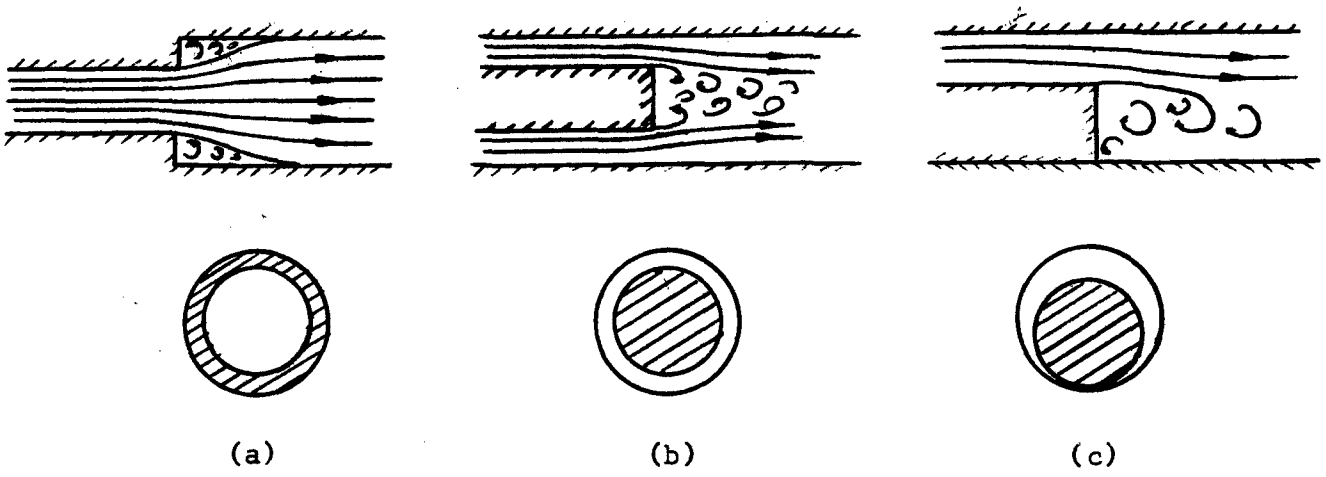

Figure 13.2

Figure 13.2 shows streamline patterns for (a) a sudden expansion in a concentric pipe, (b) the outlet of a concentrically orientated capsule and (c) the eccentric capsule.

In Figure 13.2 eddies are generated from the section where the sudden expansion occurs until the section where streamlines are again parallel. In case (a) the zone of eddy formation extends around the inside of the larger pipe. This pipe wall has an inhibiting effect, suppressing eddy generation and decreasing energy dissipation when compared with case (b). In this case there is no wall to suppress the eddies which are shed peripherally, It is likely that vortices from opposing sides of the capsule face encourage one another. This accentuates the disturbance, which is free of any inhibiting wall effects, yielding a larger head loss coefficient than in case (a).

The next problem is to explain why the head loss coefficient is about 32% less for case (c) compared with case (a). The size of the

generated vortices is probably larger than in the two previous cases and the strength of eddies are also weaker. They can only be generated around the top part of the crescent annulus since the annular velocity, towards the underside of the capsule is very low.

Furthermore, the eddies are generated asymmetrically and the accentuating effect, of opposing eddies, is largely eliminated. And thirdly, the suppressing action of the wall is apparent around the lower part of the pipe.

These three factors cause the energy dissipation to be less than for case (b) and, indeed considerably less than for case (a).

3. Comparison of analytical and experimental results - pressure flow in the annulus of static capsules

This section offers support to the finite element analysis using quasi-concentric polar co-ordinates, as described in Chapter 7, for analysing pressure flow in the annulus.

Experimental and analytical results are compared for turbulent flow in the concentric annulus and laminar and turbulent flow in the eccentric annulus.

3.1 Concentric annuli

Many experimenters have shown that accepted velocity distribution laws, for circular pipe flow, show good agreement with experimentally determined velocity profiles in the outer wall region. However, the turbulent velocity profiles for the inner region are not well established.

In the main, investigators have accepted the conventional form of the velocity distribution law for both walls, although there is no *a priori* reason why the logarithmic laws derived for pipe flow should also apply to other geometries.

The velocity distribution for circular pipe flow was derived by

integrating von Karman's stress law for turbulent flow in a pipe where shear stress is proportional to radius.

The main difference between the shear stress distribution in circular pipes and annuli is that in the former it is linear whereas in the latter it is not. (See Figure 7.9).

However, the logarithmic velocity distribution law (or "law of the wall") was obtained, for circular pipes, by integrating von Karman's equation near the transition layer and assuming that the shear stress is constant and equal to its wall value. This agrees with the integration of Prandtl's equation (making the same assumption).

There is thus no reason to suppose that the form of the velocity distribution law deviates greatly from the law for circular pipes when the shear stress deviates slightly from linearity, as in the case of the annulus. Anyway, the shear stress was assumed constant to obtain the logarithmic law for circular pipes.

The only rule that can be applicable in this case is that of expediency, i.e. which law agrees best with experiment. The same criterion was ultimately applied to circular pipe flow.

Many attempts were made in the course of this investigation to analyse the problem of the concentric annulus using various velocity distribution laws; for example - Knudsen and Katz (reference 26), Brighton and Jones (reference 7) and Randhava (reference 47). Good agreement with most of the experimental data was obtained using Randhava's method, which was outlined in Chapter 7, Section 7.5, equations (7.71) and (7.89) to (7.90).

Figure 13.3 shows a friction factor Reynolds number diagram, using the conventional definitions, for concentric annuli. The analytical results were determined using the Univac 1106 computer and Randhava's velocity distribution as well as the velocity laws of Knudsen and Katz. Experi-

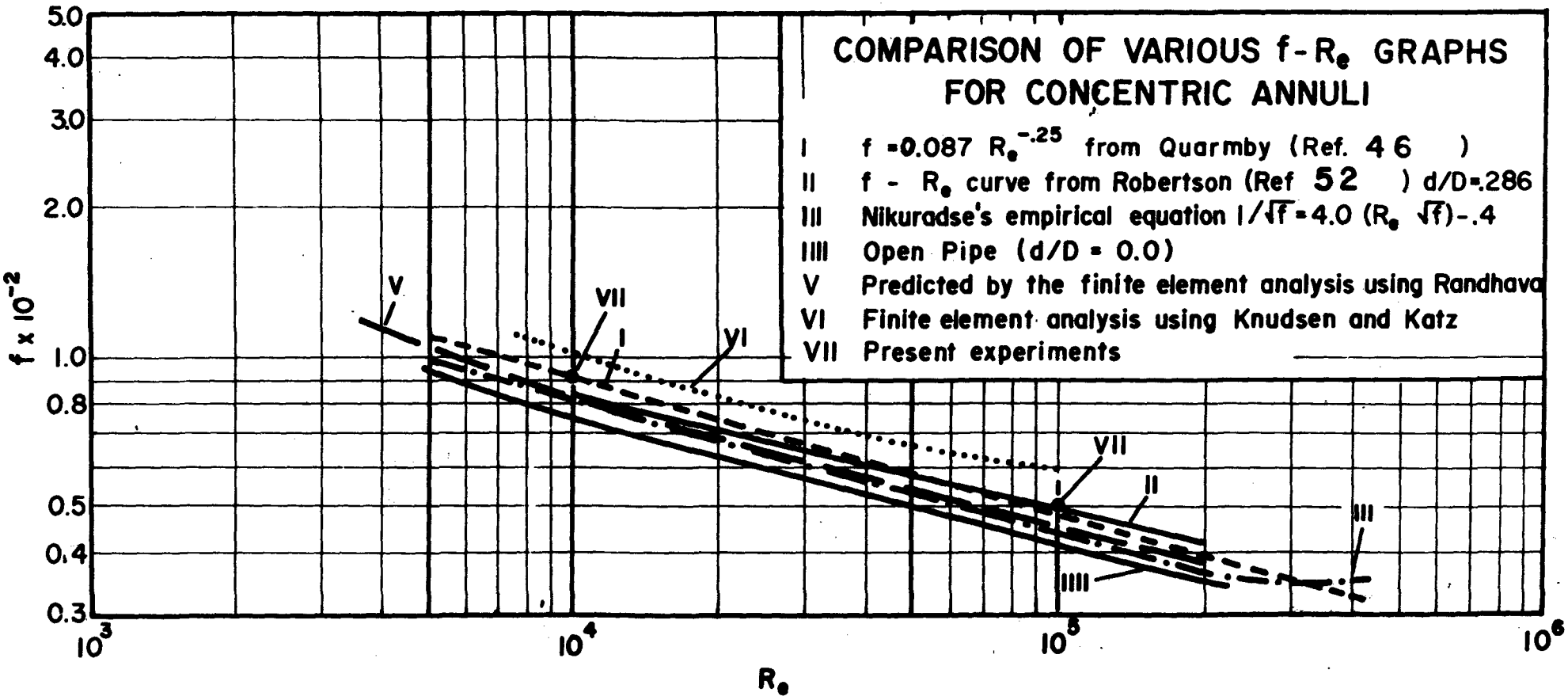
COMPARISON OF VARIOUS f-R_e GRAPHS FOR CONCENTRIC ANNULI
I $f = 0.087\ R_e^{-.25}$ from Quarmby (Ref. 46)
II f - R_e curve from Robertson (Ref 52) d/D=.286
III Nikuradse's empirical equation $1/\sqrt{f} = 4.0\ (R_e\sqrt{f}) - .4$
IIII Open Pipe (d/D = 0.0)
V Predicted by the finite element analysis using Randhava
VI Finite element analysis using Knudsen and Katz
VII Present experiments
$f \times 10^{-2}$
5.0
4.0
3.0
2.0
1.0
0.8
0.5
0.4
0.3
10^3
10^4
10^5
10^6
R_e
V
VII
I
VI
VII
I
II
III
IIII

FIG. 13.3

mental results from three sources are also shown in the Figure, viz. Quarmby (reference 46), Robertson (reference 52) and Levy (reference 33).

Nikaradse's empirical equation is also shown, as is the circular pipe curve.

Randhava's A and B values used in the velocity distribution laws are dependent on the diameter ratio (d/D) and the computer program takes this into account, each quasi-concentric annulus having a different d/D value and hence different A and B values.

It is clear that most of the experimental results shown, lie between the two analytical curves (using velocity distributions of Randhava and Knudsen and Katz). The latter being too high and the former, if anything somewhat low.

3.2 Eccentric annuli- complete laminar flow

A computer program was written for solving equations (7.48) and (7.49) (i.e. flow versus pressure gradient in the laminar regime with diameter ratio and eccentricity as parameter). This program was subsequently absorbed into the general program for calculating turbulent or laminar flow in annuli of varying eccentricities. The entire program eventually formed two sub-routines containing three other internal sub-routines of the main program for calculating excess head losses across mobile capsules (see Appendix II).

The method of quasi-concentric polar co-ordinates was used and in this instance (i.e. laminar flow in the eccentric annulus) other results (of Redberger and Charles (reference 49)) are available for comparison with the bi-polar co-ordinate system.

Figure 7.13 shows the results of eccentric annulus analysis for laminar flow. The full lines representing the analysis of Redberger and Charles using the bi-polar co-ordinate system and the dotted curves representing

the results of the present author's quasi-concentric annuli.

At the higher diameter ratios, above $d/D = 0,75$ the two methods agree well.

As d/D decreases the quasi concentric method gives ever increasing values for the flow ratio compared with the bi-polar co-ordinate system and the divergence increases as eccentricity increases.

Figure 7.14 shows results of the experimental investigation of Bourne et al (reference 5) and the analytical solutions of Caldwell and Redberger and Charles as well as the present author (i.e. three different analytical techniques). Conventional values of friction factor and Reynolds number are used.

The solid circles are points calculated using the quasi-concentric annulus method at different Reynolds numbers.

Herein lies the key to the discrepancy between Caldwell's and Redberger and Charles's analytical solution as compared with the experiments of Bourne et al, which they stated was "too large for experimental error and difficult to explain at the present time."

The explanation is that Bourne et al described the transition regime as occurring between a Reynolds number of 1000 and 3000. In the light of the present analysis this seems unlikely because at $d/D = 0,96$; the lower point given by the present analysis occurs at a Reynolds number of $R_e = 538$ (see Figure 7.14) and this agrees with Caldwell's solution. This is also the highest Reynolds number at which the flow was completely laminar in the eccentric annulus according to the present results from the quasi-concentric annulus theory. The upper point at $d/D = 0,6$ is actually given by the theory for mainly turbulent flow in the annulus (to be discussed in Section 3.3) and this point is even higher than the supposedly laminar curve of Bourne et al. In this case the Reynolds

number is 954 which is lower than the critical value given by Bourne et al. The discrepancy between the experimental and analytical results is thus, probably, due to the experimental values not being in the completely laminar regime.

Another example (see Figure 7.14) is the point given at d/D = 0,85 (R_e = 961). Here the Reynolds number is adjusted so that the point lies on Bourne's experimental curve. But in the analysis the flow was not laminar throughout. The lower solid point at d/D = 0,8 was determined for the highest Reynolds number (R_e = 536) at which the entire flow was laminar and agrees well with the other theories.

The Reynolds number criterion used by the present author was discussed in Chapter 7, Section 13.

It is thus apparent that the discrepancy noted by Bourne et al between their experiments and the analysis of Caldwell, Redberger and Charles, as well as the present author, (using different techniques) is due to the definition of Reynolds number. The experiments of Bourne et al were unlikely to have been carried out in the completely laminar regime.

3.3 Eccentric annuli turbulent flow

In Section 10.1 of Chapter 7, it was concluded that for fully eccentric annuli, the only reliable experimental results were those of Bourne et al (reference 5).

The empirical approach of the present author was discussed in Section 11.1, Chapter 7, as a result of analysing static capsules and Figure 9.13 shows very good agreement between the experiments of Bourne et al and those of the present author when using the pseudo-hydraulic mean radius concept.

Of all the velocity distribution laws those of Knudsen and Katz, when integrated numerically, for quasi-concentric annuli, showed the best agree-

FIG. 13.4

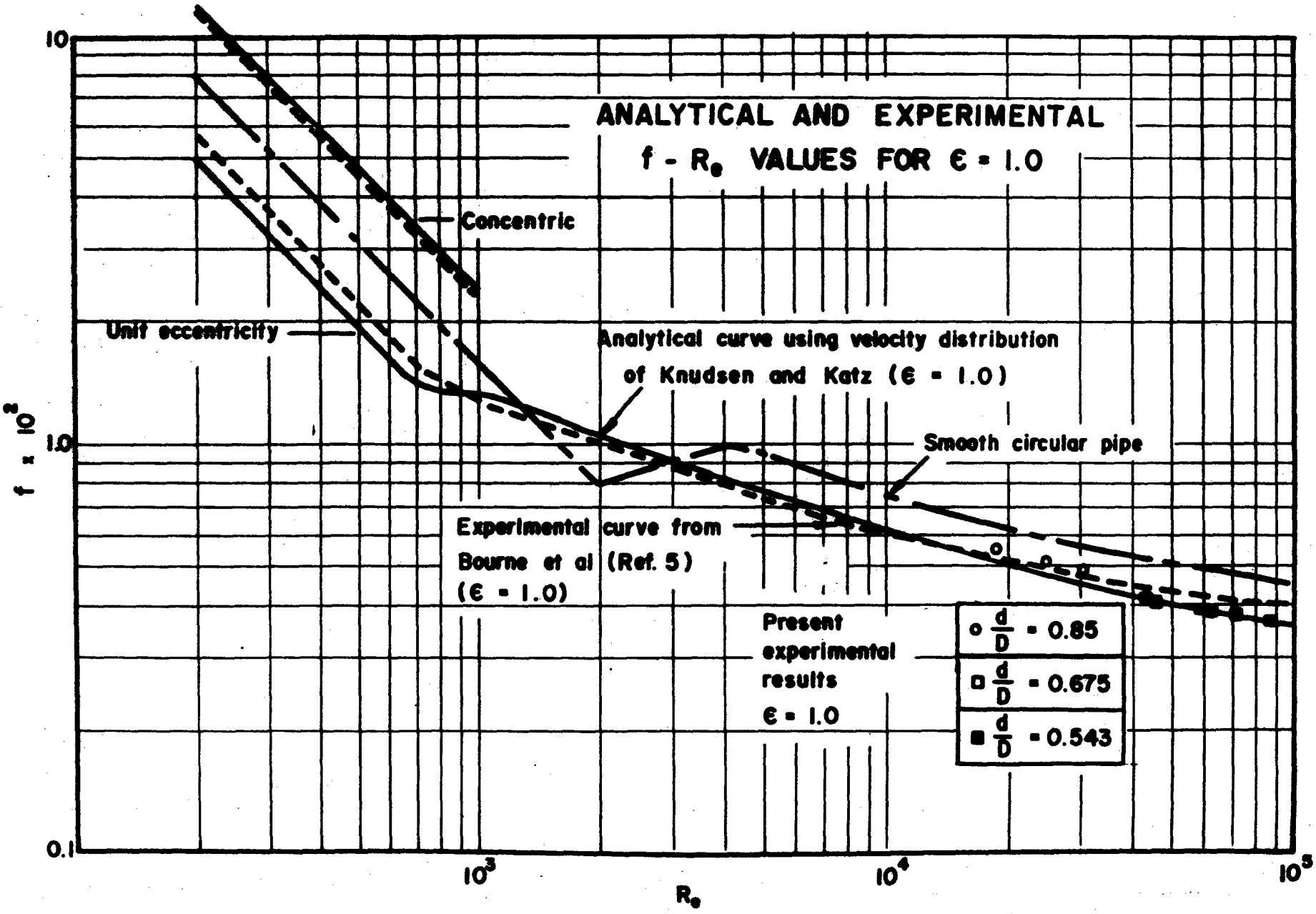
ANALYTICAL AND EXPERIMENTAL
f - Re VALUES FOR ϵ = 1.0
Concentric
Unit eccentricity
Analytical curve using velocity distribution of Knudsen and Katz (ϵ = 1.0)
Smooth circular pipe
Experimental curve from Bourne et al (Ref. 5) (ϵ = 1.0)
Present experimental results ϵ = 1.0
o d/D = 0.85
□ d/D = 0.675
■ d/D = 0.543
f x 10²
10
1.0
0.1
10³
10⁴
10⁵
Re

ment with experiments. Figure 13.4 shows experimental results of Bourne et al as well as the present experimental results, together with curves obtained by computer analysis and the correlation is extremely good (particularly around R_e = 10 000) when cognisance if taken of the assumptions inherent in the analysis (discussed in Chapter 15).

Figures 13.5 and 13.6 show results of the computer analysis for varying eccentricities at two diameter ratios. Unfortunately there are no published results (other than concentric or fully eccentric) with which to compare these curves, neither analytical nor experimental. The exception being those of Jonsson and Sparrow which, in the case of annuli of unit eccentricity, disagree considerably with the results of Bourne et al, Dodge (reference Bourne et al), Denton (reference Bourne et al) and the present author. The two diameter ratios yield f versus R_e curves which are virtually identical (except for the higher Reynolds number range) so that varying diameter ratio within a range applicable to capsule experiments, has little effect on the f versus R_e relation.

This has been verified further in Section 11.1, Chapter 7 (for annuli of unit eccentricity) where it was shown that the ratio R_p/R is constant.

The empirical approach of the pseudo hydraulic mean radius has been discussed in Chapter 7, Section 11.1, and a value of R_p/R = 1,25 was obtained for annuli of unit eccentricity. Figure 13.7 shows the ratio Z where $Z = R_p/R$ for various eccentricities at a diameter ratio d/D = 0,851. The velocity profiles of Knudsen and Katz as well as those of Randhava are used for the analysis.

Knudsen and Katz's velocity distribution being chosen because analysis using their equations yielded the best agreement with the fully eccentric case and Randhava's profiles yielded good agreement in the concentric case.

Reference is now made to the curves in Figure 9.12 where the curve

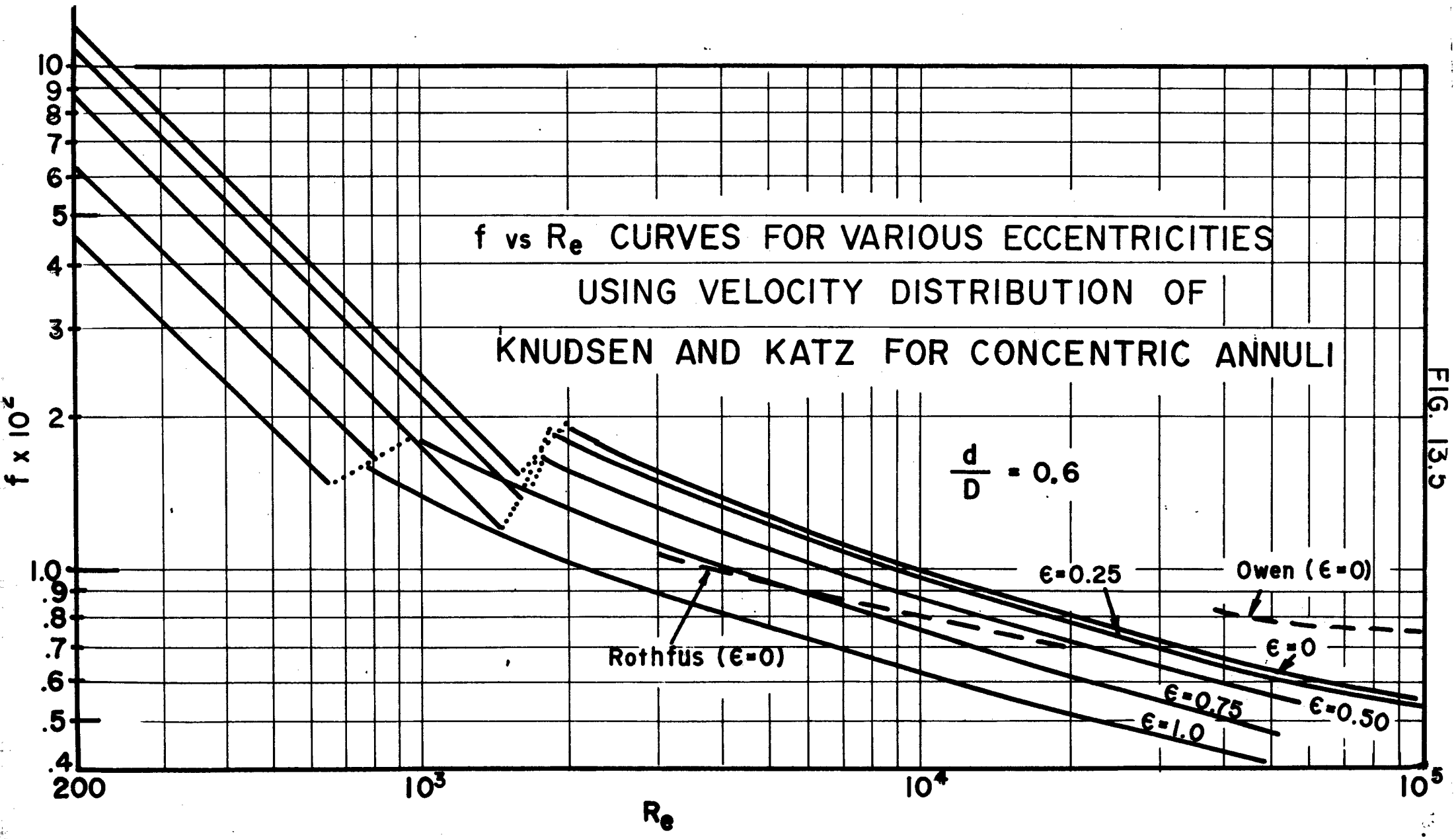
f vs R_e CURVES FOR VARIOUS ECCENTRICITIES
USING VELOCITY DISTRIBUTION OF
KNUDSEN AND KATZ FOR CONCENTRIC ANNULI
$\frac{d}{D} = 0.6$
f x 10^2
R_e
200
10^3
10^4
10^5
10
9
8
7
6
5
4
3
2
1.0
.9
.8
.7
.6
.5
.4
Rothfus (ε=0)
ε=0.25
Owen (ε=0)
ε=0
ε=0.75
ε=0.50
ε=1.0

FIG. 13.5

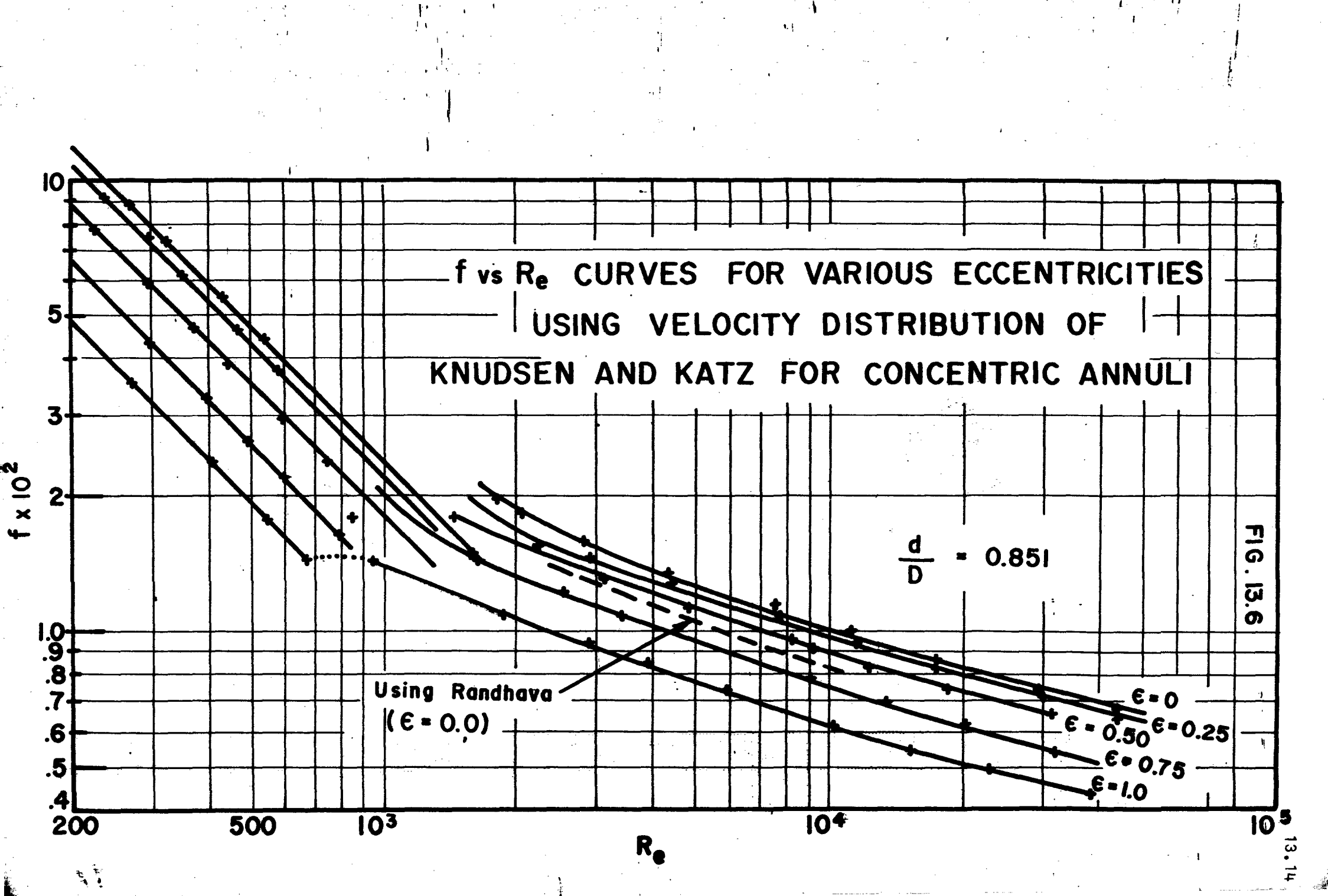
f vs Re CURVES FOR VARIOUS ECCENTRICITIES
USING VELOCITY DISTRIBUTION OF
KNUDSEN AND KATZ FOR CONCENTRIC ANNULI
d/D = 0.851
Using Randhava
(ε = 0.0)
ε = 0
ε = 0.25
ε = 0.50
ε = 0.75
ε = 1.0
f x 10²
Re
10
5
3
2
1.0
.9
.8
.7
.6
.5
.4
200
500
10³
10⁴
10⁵

FIG. 13.6

FINITE ELEMENT METHOD FOR PRESSURE FLOW IN ANNULUS USING QUASI-CONCENTRIC POLAR CO-ORDINATE.

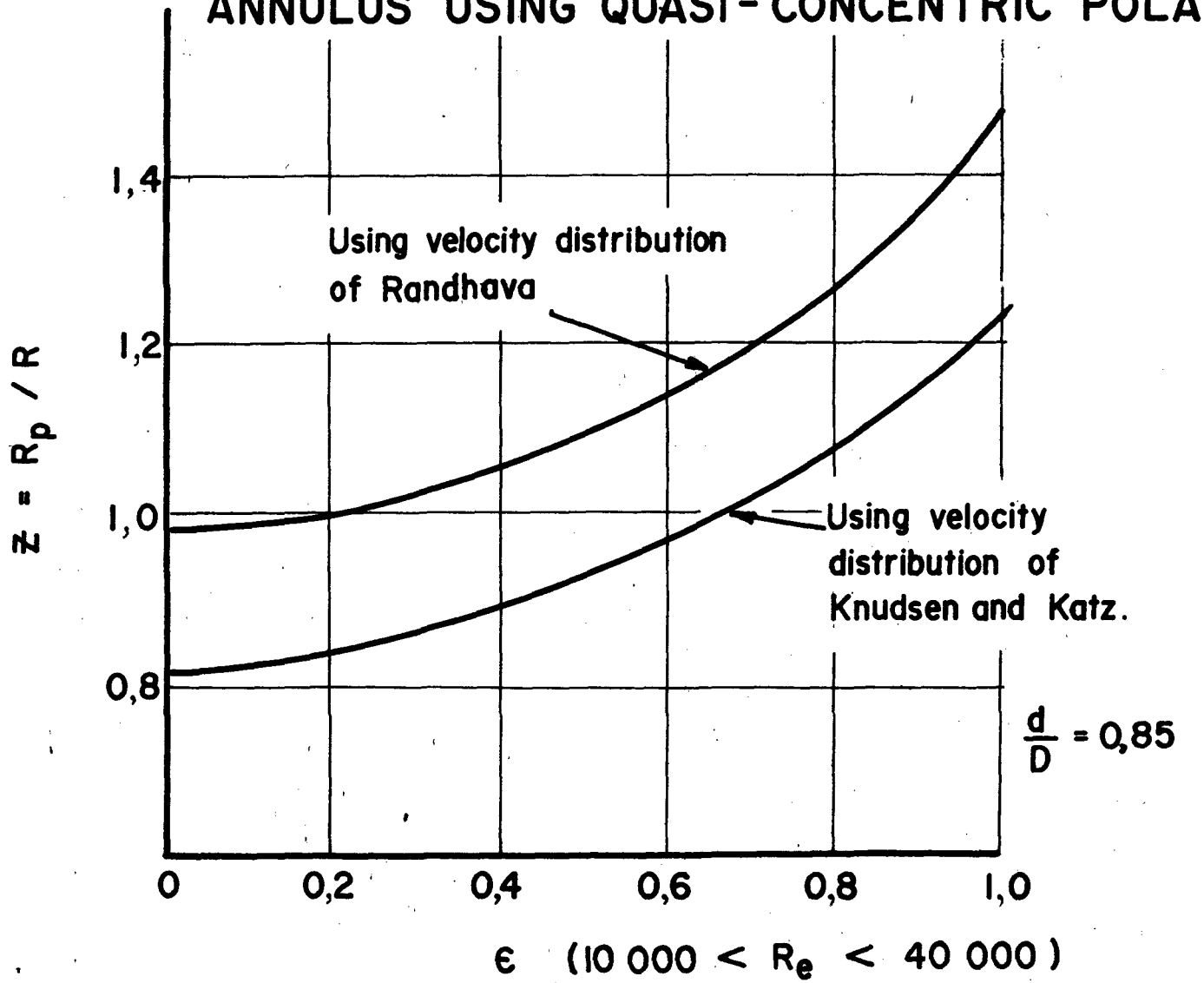

FIG. 13.7

(R_p = 0,98R) is an analytical one based on Randhava's method of velocity distribution and R_p = 0,81R is analytical based on substituting Knudsen and Katz's velocity distribution laws in the quasi-concentric annulus method.

Many velocity profiles were tried in the hope of finding universal equations for all eccentricities. However, this did not prove possible.

For the quasi-concentric method of analysing head loss, equations in eccentric annuli, the force balance equations for each slice is from (7.105) and (7.106).

$$(\Delta P/L)\ (\Delta A_c + \Delta A_p) = \tau_{cp}\ \Delta S_c + \tau_{pp}\ \Delta S_p$$

The total force balance is thus

$$(\Delta P/L)\left[\Sigma(\Delta A_c + \Delta A_p)\right] = (\Delta P/L)\pi(D^2-d^2)/4 = \Sigma\tau_{cp}\Delta S_c + \Sigma\tau_{pp}\Delta S_p$$

The conventional form of the force balance equation for uniform shear on both capsule and pipe surfaces is

$$(\Delta P/L)\pi(D^2-d^2)/4 = \pi(d+D)\overline{\tau}_o$$

and $\overline{\tau}_o = (\Sigma\tau_{cp}\ \Delta S_c + \Sigma\tau_{pp}\ \Delta S_p)/\pi(d+D)$

where $\overline{\tau}_o$ = average shear stress on pipe and capsule surface.

The friction factor is conventionally defined as

$$f = \overline{\tau}_o/(\tfrac{1}{2}\rho\overline{V}_{ap}^2)$$

assuming that the relevant velocity is the average for the section $(\overline{V}_{ap})$

$$\therefore \quad f = \frac{\Sigma\ \tau_{cp}\ \Delta S_c + \Sigma\ \tau_{pp}\ \Delta S_p}{\pi(d+D)\tfrac{1}{2}\rho\ \overline{V}_{ap}^2}$$

$$\therefore \quad f = \frac{\alpha\ \overline{\tau}_o d + \beta\ \overline{\tau}_o D}{\pi(d+D)\tfrac{1}{2}\rho\ \overline{V}_{ap}^2} \qquad (13.4)$$

$$\text{where} \quad \alpha = \frac{\Sigma\ \tau_{cp}\ \Delta S_c}{\overline{\tau}_o d} = \frac{\overline{\tau}_{cp}}{\overline{\tau}_o} \qquad (13.5a)$$

$$\text{and} \qquad \beta = \frac{\Sigma\, \tau_{pp}\, \Delta S_p}{\bar{\tau}_o D} = \frac{\bar{\tau}_{pp}}{\bar{\tau}_o} \qquad (13.5b)$$

where $\bar{\tau}_{pp}$ and $\bar{\tau}_{cp}$ are average values. And α and β are constants which take into account the variation of shear stress due to pressure flow in the annulus around the capsule and pipe perimeter. α and β may vary, with capsule eccentricity and diameter ratio as well as with Reynolds number.

In the pseudo hydraulic mean radius method

$$R_p = ZR$$

And Z takes into account the difference in shear on capsule and pipe walls respectively, i.e. α and β variation, as well as the shear stress variation.

The average values of Z are shown on Figure 13.7. These values are calculated for a range of diameter ratios and Reynolds numbers and Table 13.3 shows how R_p/R varies with eccentricity and diameter ratio assuming that the velocity distribution laws of Knudsen and Katz are valid. (See Figure 13.4). R_p is calculated from equation (7.94).

3.4 Comparison of conventional friction factor and hydraulic mean radius with pseudo values

It has already been shown that the experimental results of Bourne et al as depicted in Figure 7.25 agrees with present experimental values for the eccentric annulus (see Figure 9.13).

If equations (7.91, (7.92) and (7.93) are rewritten with subscript (p) (for the friction factor and Reynolds number terms) denoting the pseudo condition then from equation (7.91)

$$\Delta h_{fa} = \frac{(f)_p\, L_c\, \bar{V}_a^2}{2g\, R_p} = \frac{f\, L_c\, \bar{V}_a^2}{2g\, R} \quad \text{(where } f = \text{conventional friction factor)}$$

$$\therefore \quad (f)_p = Z\, f$$

According to equation (7.93)

TABLE 13.3

D	d/D	$\Delta h_{fa}/L$	$\bar{V}_{ap}$	R	$\varepsilon = 1,0$ R_p	z	f	R_e	$100fR_e^{0,25}$
0,074	0,851	0,200	1,408	0,00275	0,00339	1,234	0,0054	15488	6.02
0,074	0,851	0,300	1,778	0,00275	0,00340	1,237	0,0051	19554	6,03
0,074	0,851	0,400	2,095	0,00275	0,00340	1,237	0,0049	23046	6,04
0,074	0,674	0,02	0,665	0,00603	0,00749	1,243	0,0053	16020	5,96
0,074	0,674	0,100	1,667	0,00603	0,00749	1,243	0,0042	40182	5,95
0,074	0,674	0,050	1,124	0,00603	0,00751	1,247	0,0047	27099	6,03
0,074	0,674	0,200	2,477	0,00603	0,00748	1,242	0,0039	59686	6,10
0,074	0,541	0,005	0,386	0,00849	0,01059	1,248	0,0056	13083	5,99
0,074	0,541	0,010	0,576	0,00849	0,1066	1,256	0,0050	19639	5,91
0,074	0,541	0,020	0,856	0,00849	0,01068	1,258	0,0045	29064	5,88
0,074	0,541	0,100	2,142	0,00849	0,01064	1,254	0,0036	72713	5,91
0,074	0,541	0,200	3,164	0,00849	0,01054	1,242	0,0033	107370	5,97
0,074	0,951	5,000	4,010	0,00091	0,00112	1,229	0,0055	14597	6,05
0,074	0,951	10,000	5,970	0,00091	0,00112	1,233	0,0050	21732	6,07
2,000	0,813	0,004	0,361	0,00935	0,01153	1,233	0,0056	13487	6,03
2,000	0,813	0,000004	0,036	0,09350	0,11528	1,233	0,0056	13487	6,03
2,000	0,813	0,000010	0,061	0,09350	0,11578	1,238	0,0049	22838	6,02
2,000	0,813	0,000020	0,091	0,09350	0,11556	1,236	0,0045	33892	6,11
0,200	0,750	0,002	0,300	0,0125	0,01547	1,238	0,0055	14973	6,08
0,200	0,750	0,005	0,507	0,0125	0,01553	1,242	0,0048	25337	6,06
	ε			d/D = 0,851; D = 0,2					
	0,00	0,005	0,256	0,00745	0,00597	0,801	0,0111	7628	10,37
	0,00	0,010	0,385	0,00745	0,00607	0,815	0,0099	11474	10,25
	0,25	0,002	0,150	0,00745	0,00590	0,792	0,0129	4481	10,55
	0,25	0,005	0,261	0,00745	0,00613	0,823	0,0107	7776	10,05
	0,25	0,010	0,396	0,00745	0,00630	0,846	0,0093	11787	9,69
	0,25	0,020	0,595	0,00745	0,00642	0,862	0,0082	17743	9,46
	0,25	0,050	1,013	0,00745	0,00649	0,870	0,0071	30173	9,36
	0,50	0,010	0,420	0,00745	0,00686	0,921	0,0083	12523	8,78
	0,50	0,020	0,630	0,00745	0,00694	0,931	0,0074	18758	8,66
	0,50	0,050	1,066	0,00745	0,00697	0,935	0,0064	31759	8,54
	0,75	0,010	0,461	0,00745	0,00781	1,049	0,0069	13740	7,47
	0,75	0,020	0,688	0,00745	0,00786	1,056	0,0062	20512	7,42
	0,75	0,050	1,160	0,00745	0,00784	1,053	0,0054	34565	7,36
	1,00	0,010	0,518	0,00745	0,00920	1,234	0,0054	15436	6,02
	1,00	0,020	0,771	0,00745	0,00921	1,237	0,0049	22968	6,03
	1,00	0,050	1,297	0,00745	0,00917	1,231	0,0043	38658	6,03

$$(R_e)_p = \frac{4\,\bar{V}_a\,R_p}{\nu} = Z\left(\frac{4\,\bar{V}_a\,R}{\nu}\right)$$

According to equation (7.92)

$$(f)_p = 0{,}079/(R_e)_p^{0{,}25}$$

$$\therefore \quad Zf = 0{,}079/(ZR_e)^{0{,}25}$$

$$\therefore \quad f = 0{,}079/Z^{1{,}25}\,R_e^{0{,}25}$$

For $Z = 1{,}25$

$$f\,R_e^{0{,}25} = 0{,}079/(1{,}25)^{1{,}25}$$

$$= 5{,}98 \times 10^{-2} \qquad (13.6)$$

Figure 7.25 shows that for $0{,}55 < d/D < 0{,}8$ the value of $f\,R_e^{0{,}25}$ from Bourne et al is of the above order of magnitude (equation (13.6)).

However, the implication inherent in Figure 7.25 is that $Z \to 1{,}0$ as $d/D \to 1{,}0$ and as $d/D \to 0{,}0$. The results of Bourne et al are only given up to $d/D \doteqdot 0{,}87$ and the portion of the curve on Figure 7.25 for $d/D > 0{,}87$ is conjecture.

It is mentioned by Bourne et al that Dodge actually did experiments up to $d/D = 0{,}975$ and concluded that with d/D from 0,688 to 0,975, the diameter ratio was not an important parameter.

It is likely that the dependence of friction factor on the diameter ratio is not so pronounced as indicated by Bourne et al.

To conclude, the quasi concentric polar co-ordinate method of analysing flow in annuli has been shown to agree with the present experiments as well as those carried out by others.

The theoretical analysis is also in good agreement with the empirical formulation using the pseudo-hydraulic mean radius.

CHAPTER 14

COMPARISON OF EXPERIMENTAL AND ANALYTICAL RESULTS FOR INCIPIENT CAPSULE MOTION

In this Chapter analytical and experimental results of incipient capsule studies are discussed.

There are three sections:

1. The effect of length to diameter ratio (L_c/d) and diameter ratio (d/D)
2. The effect of specific gravity of the capsules (S_c) as well as the effect of pipe diameter (D).
3. The effect of pipeline slope (ϕ)

In each of the three sections the relevant parameters are discussed; firstly, in terms of excess incipient head loss $(\Delta H_c)_i$ to mean incipient water velocity $(\overline{V}_i)$ relations, Figures 14.1, 14.6 and 14.13; secondly, in terms of correlating representations showing how the analytical results can be generalised and thirdly; in terms of experimental results showing to what extent the analytical correlations are justified.

The equation for excess energy loss across a static capsule at incipience can be written in the following form, from equation (7.125)

$$(\Delta H_c)'_{is} = \mu_f (d/D)^2 |S_c - 1| \cos\phi + (d/D)^2 (S_c - 1) \sin\phi + \frac{\overline{\tau}_p}{w} \frac{4}{D} - \frac{h_{fc}}{L_c}$$

In a horizontal pipe this reduces to (from equation (7.126));

$$(\Delta H_c)_i/(L_c) = \mu_f (d/D)^2 |S_c - 1| + \frac{\overline{\tau}_p}{wD} 4 - \frac{h_{fc}}{L_c}$$

$$= (\Delta h_i + \Delta h_o + \Delta h_{fa} - h_{fc})/(L_c)$$

The equation for incipient velocity $\overline{V}_i$ has been shown to be:

$$C_1 \overline{V}_i^{1,75} + C_2 \overline{V}_i^2 - C_3 = 0 \qquad (7.133)$$

where $C_3 = \mu_f L_c (d/D)^2 |S_c - 1| \cos \phi + (d/D)^2 |S_c - 1| \sin \phi$

for the general case of sloping pipes, and this term again reduces appropriately for horizontal pipes.

For the incipient case, once a value of μ_f has been determined and the independent variables have been selected, a purely analytical solution is now available and, with the aid of a computer, the above equations can be solved. The solutions, although carried out on a digital computer, are conveniently presented graphically and these results will now be discussed.

1. Effect of length and diameter ratio

Figure 14.1 shows the incipient excess head loss plotted as a function of the mean water velocity (for a constant SG) with length to diameter ratio and diameter ratio as parameter. At $d/D = 0,91$, increase in L_c/d causes a large increase in $(\Delta H_c)_i$ with very little velocity increase. The excess energy is thus virtually independent of the velocity but highly dependent on the length to diameter ratio.

As the diameter ratio is decreased the velocity becomes an increasingly significant variable and at $d/D = 0,543$, large changes in velocity are required for relatively smaller excess energy changes. On the other hand, the length to diameter ratio has a decreasing influence as diameter ratio is diminished and less excess head is required to overcome the threshold velocity, for increasing values of L_c/d, than when the diameter ratio is large.

The reason for the "collapse" of the grid towards the right of the figure is that, since these are all constant density capsules ($S_c = 4,0$), decreasing diameter ratio has the effect of decreasing the net weight of a capsule. Decreasing the length to diameter ratio has the same effect. Since the excess head loss required for the initiation of motion is

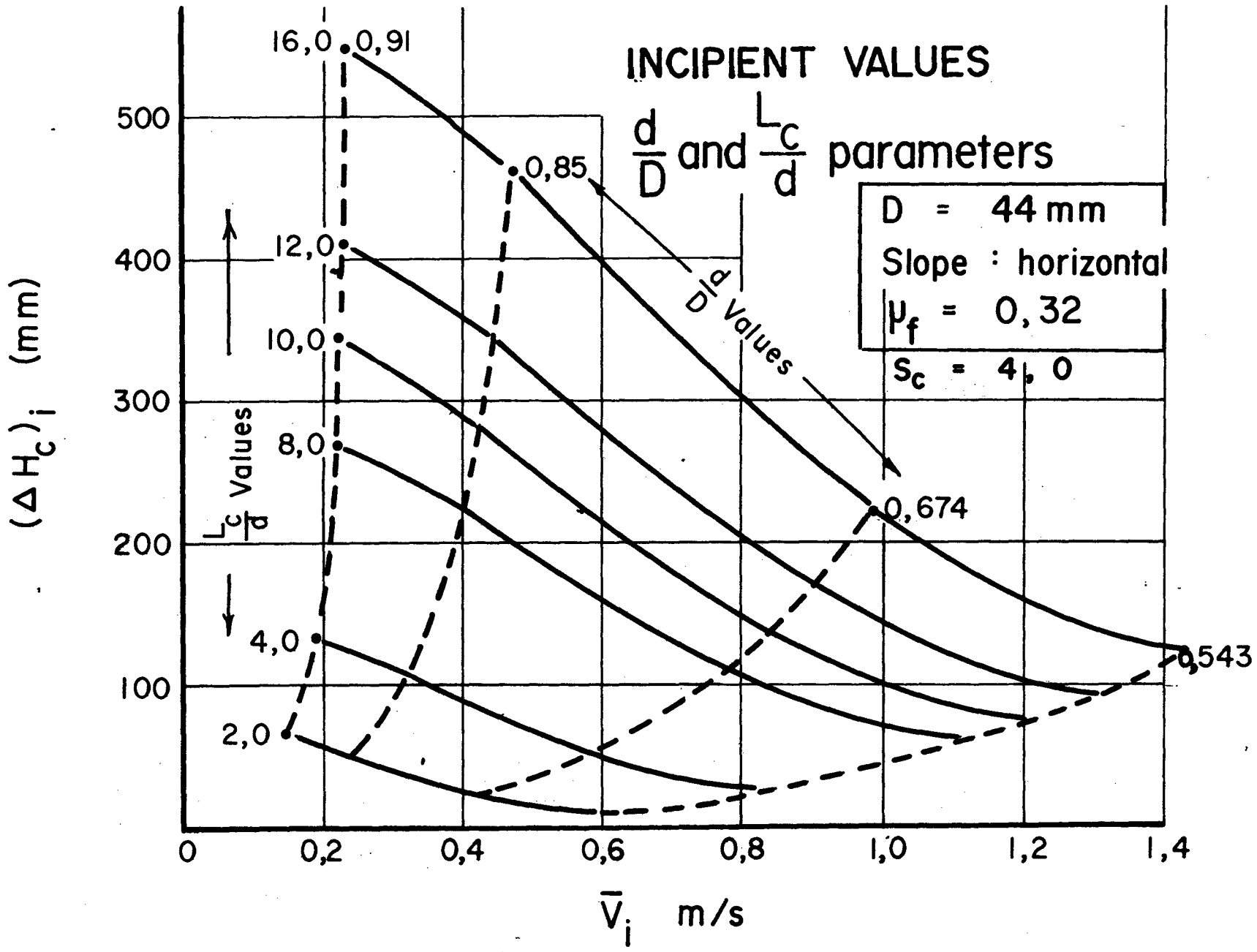
INCIPIENT VALUES
d/D and Lc/d parameters
D = 44 mm
Slope : horizontal
μf = 0,32
Sc = 4,0
D/d Values
Lc/d Values
16,0
12,0
10,0
8,0
4,0
2,0
0,91
0,85
0,674
0,543
500
400
300
200
100
0
0,2
0,4
0,6
0,8
1,0
1,2
1,4
(ΔHc)i (mm)
V̄i m/s

FIG. 14.1

intimately related to the net weight of the capsule, decreasing either diameter or length means a reduction in $(\Delta H_c)_i$.

The reason for small capsules requiring increasingly greater incipient velocities as L_c/d increases, compared with large d/D ratios is that the forward drag components have less frontal and surface areas to act on in the case of the small capsule (bearing in mind that the capsules are dimensionally similar).

The curves in Figure 14.1 are very useful for interpolating $(\Delta H_c)_i$ and $\overline{V}_i$ values for selected combinations of diameter and length to diameter ratio. However, these curves only apply to a horizontal pipeline of diameter $D = 44$ mm and capsules of $S_c = 4{,}0$.

1.1 Correlation

In order to determine a simple equation for the curves on Figure 14.1 as well as to increase their generality a more concise method of presentation is necessary. This applies to both the curves themselves and the complicated equations they represent.

One method of presenting the information shown on Figure 14.1 is the graph shown on Figure 14.2, which successfully correlates the information on a Γ_i to χ_i plot. There is no scatter to speak of and the equation to Figure 14.1 is thus:(The parameters Γ and χ will be discussed in Chapter 15).

$$\Gamma_i = 35/\chi_i^{1,71} \qquad (14.1)$$

1.2 Experimental incipient velocity at different L_c/d ratios

Figure 10.51, which shows the non-dimensional incipient velocity as a function of diameter ratio, indicates the extent to which the analytical curves discussed above are in agreement with experimental results. Length to diameter ratio is shown here as parameter and when cognisance is taken of the difficulty in establishing the incipient velocity the agreement between analysis and observation is reasonable. Also, the agreement

FIG. 14.2

CORRELATION FOR INCIPIENT CONDITIONS

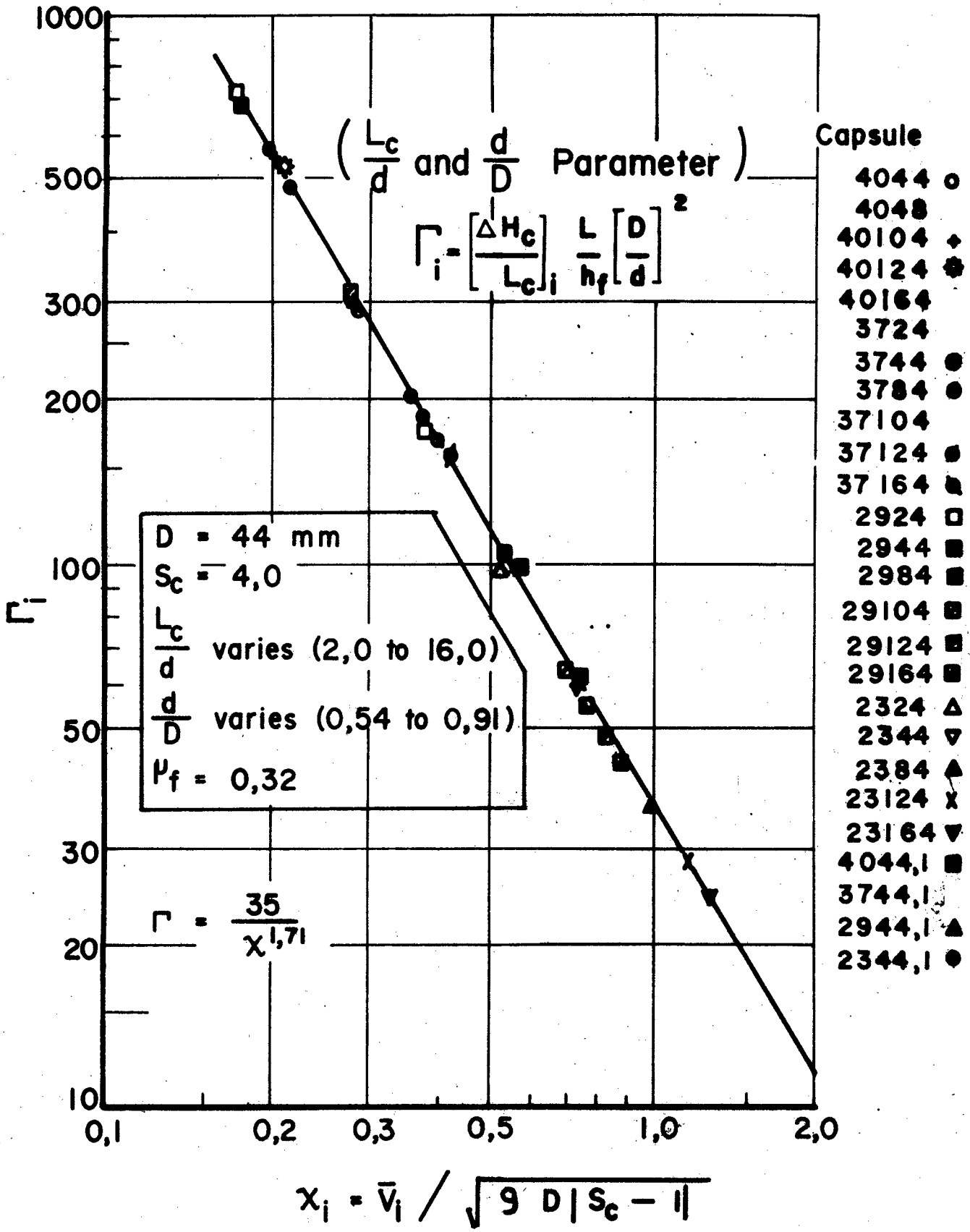

appears to improve as length to diameter ratio decreases.

Increasing length or decreasing diameter both have the expected effect of increasing incipient velocity.

The former effect is due to the greater skin friction shear which is proportional to capsule length and the latter effect is due to the reduced frontal area exposed to the incipient pressure differential across the static capsule as diameter is decreased.

1.3 Experimental incipient excess head loss at different L_c/d ratios

Figure 14.3 verifies the agreement between experimentally determined incipient velocities (in the 74 mm diameter pipeline) and theoretical results. The dashed curve represents values obtained from static capsule tests at incipience. Values of $\overline{V}_i/\sqrt{gD|S_c-1|}$ have been plotted against diameter ratio (d/D) with capsule length to diameter ratio (L_c/d) as parameter.

Figure 14.4, which shows ΔH_{ci} as a function of diameter ratio for length to diameter ratio as parameter, indicates the extent to which experimental values agree with the analysis and, in this case, agreement appears to improve as length increases.

The dotted curves on Figures 15.15, 11.17 and 11.18 represent loci of incipient excess energy losses superimposed on the ΔH_c to $\overline{V}$ curves. The dashed lines are experimentally observed results and when these figures are considered in conjunction with Figure 14.4, which represents the superimposed experimental results in the range for which the analysis is applicable, it can be seen that the analysis is in fair agreement with the experiments in the 44 mm diameter pipe.

Three main effects are observable.

1.3.1 Incipient excess head loss increases as length to diameter ratio increases, for two reasons; firstly, the submerged weight of the capsule

FIG. 14.3

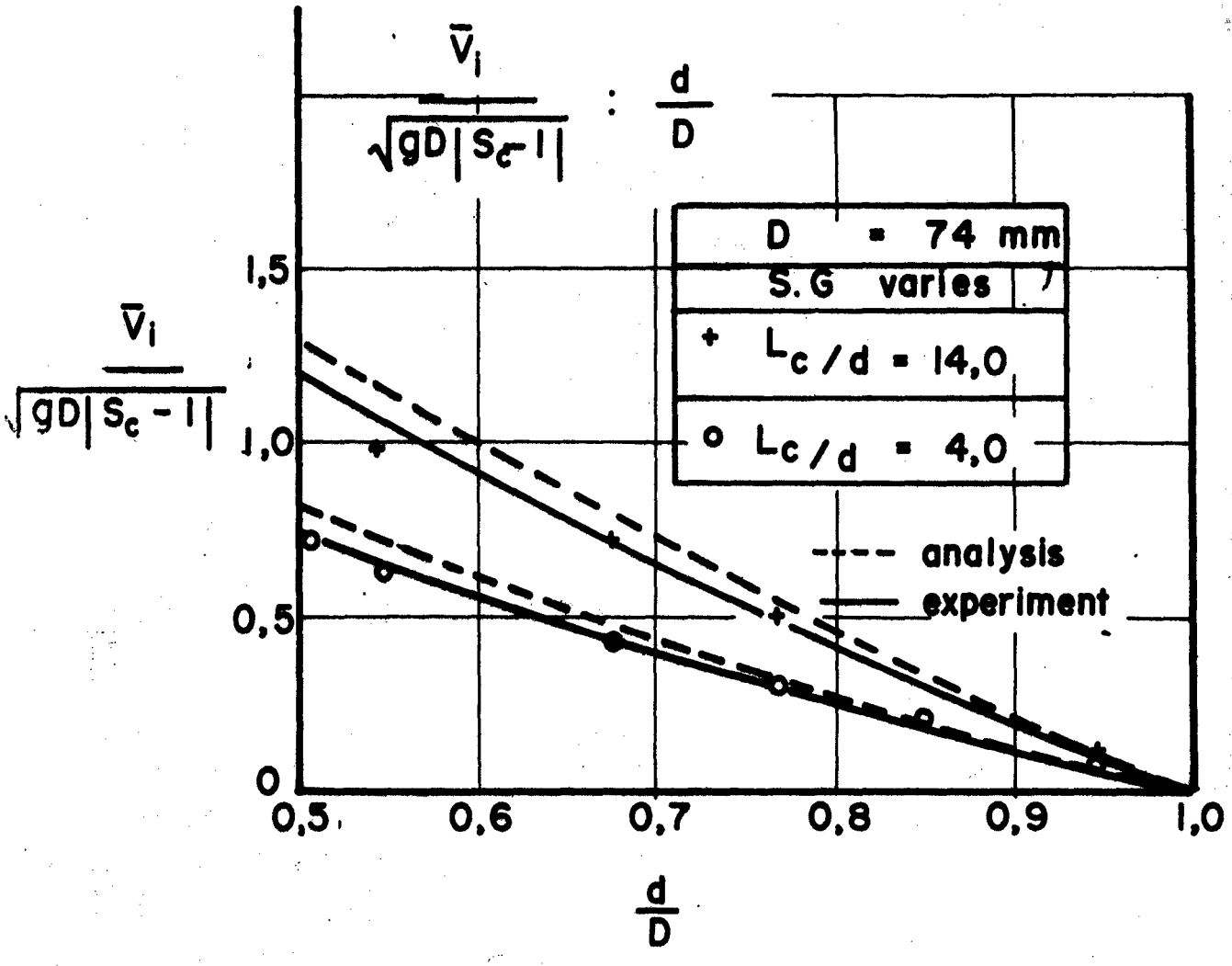
$\frac{\bar{V}_i}{\sqrt{gD|S_c-1|}}$: $\frac{d}{D}$
D = 74 mm
S.G varies
+ L_c/d = 14,0
o L_c/d = 4,0
---- analysis
—— experiment
$\frac{\bar{V}_i}{\sqrt{gD|S_c-1|}}$
1,5
1,0
0,5
0
0,5
0,6
0,7
0,8
0,9
1,0
$\frac{d}{D}$

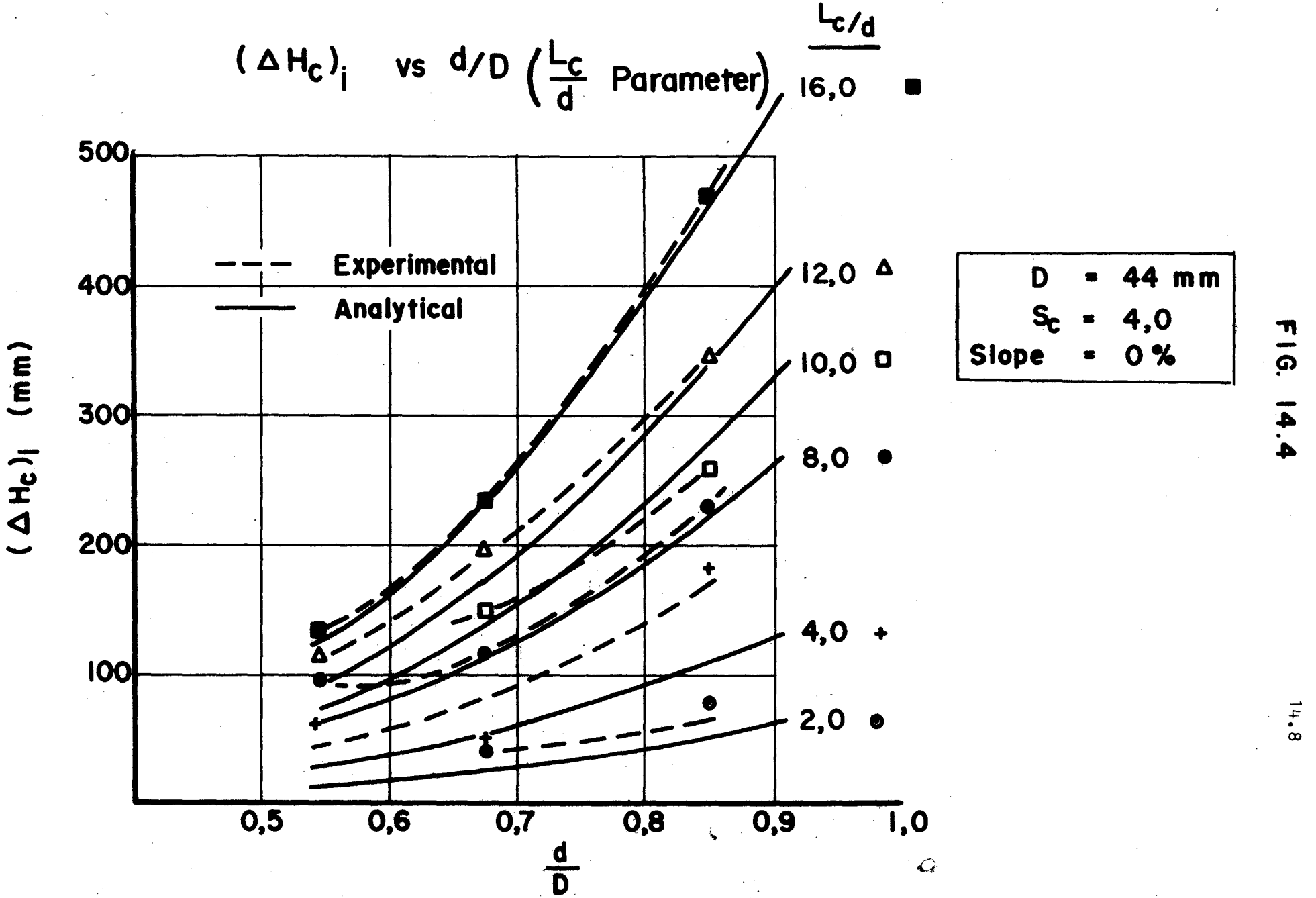
$(\Delta H_c)_i$ vs d/D ($\frac{L_c}{d}$ Parameter)
$\frac{L_c/d}{}$
16,0
12,0
10,0
8,0
4,0
2,0
Experimental
Analytical
D = 44 mm
S_c = 4,0
Slope = 0 %
$(\Delta H_c)_i$ (mm)
500
400
300
200
100
0,5
0,6
0,7
0,8
0,9
1,0
$\frac{d}{D}$

FIG. 14.4

is directly dependent on length at a fixed specific gravity thus imposing a greater solid to solid friction force and secondly, the surface skin friction shear or annular head loss is also dependent on length.

1.3.2 The value of $(\Delta H_c)_i$ also increases as diameter ratio increases for the above two reasons plus the fact that inlet and outlet losses, which are contributary causes of form drag, increase with increasing diameter ratio.

1.3.3 Figure 14.5 shows that the ratio incipient excess head loss $(\Delta H_c)_i$ to the L_c/d ratio or effectively the $(\Delta H_c)_i/L_c$ ratio, since the diameter ratio is plotted as abscissa, yields a single curve, indicating that $(\Delta H_c)_i$ is proportional to capsule length which, for the fixed density capsules depicted, means that $(\Delta H_c)_i$ is proportional to the capsule weight.

2. Effect of capsule density

Figure 14.6 shows an analytical representation of $(\Delta H_c)_i$ as a function of $\bar{V}_i$, with specific gravity (S_c) and diameter ratio (d/D) as parameters.

The analysis was carried out for capsules 1 to 24 and the actual values of S_c for these capsules are shown at the nodes.

It is clear that the increase in $(\Delta H_c)_i$ is highly dependent on specific gravity at high diameter ratios. Whilst the velocity dependence is relatively slight, in terms of absolute velocities, although the ratio, of incipient velocity at diameter ratio $d/D = 0,95$ for an increase of specific gravity from $S_c = 1,065$ to $S_c = 4,84$, is of the same order of magnitude as the ratio of velocity $(\bar{V}_i)$ from $S_c = 1,06$ to $4,77$ at diameter ratio $d/D = 0,543$. Also, as diameter ratio decreases the absolute velocity affect (for initiation of motion at increasing SG values) is magnified. It requires a larger velocity change to initiate capsule motion although the increase of excess head loss required is not so pronounced,

FIG. 14.5

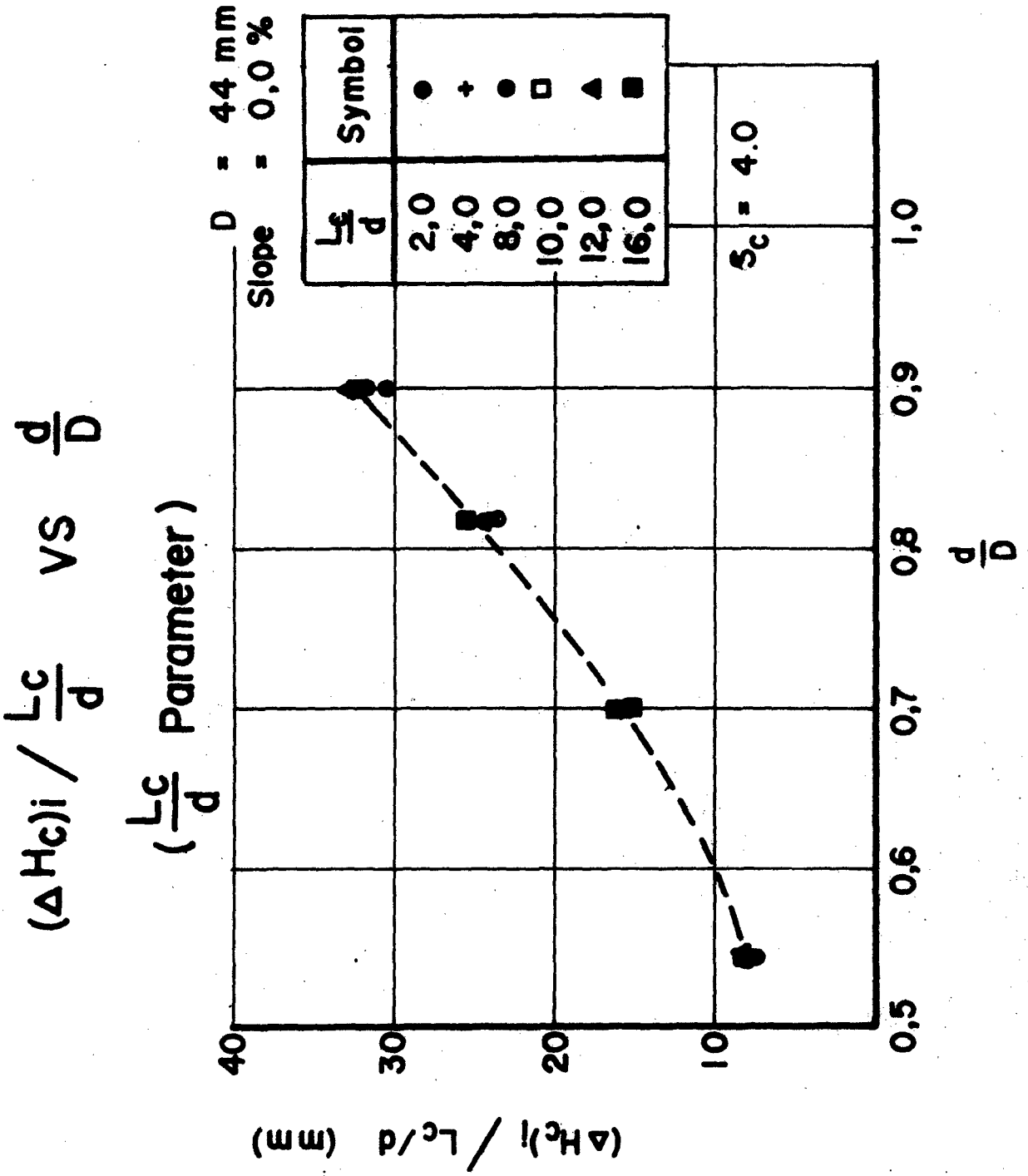
(ΔHc)i / Lc/d VS d/D
(Lc/d Parameter)
D = 44 mm
Slope = 0,0 %
Lc/d
Symbol
2,0
4,0
8,0
10,0
12,0
16,0
Sc = 4.0
(ΔHc)i / Lc/d (mm)
40
30
20
10
0,5
0,6
0,7
0,8
0,9
1,0
d/D

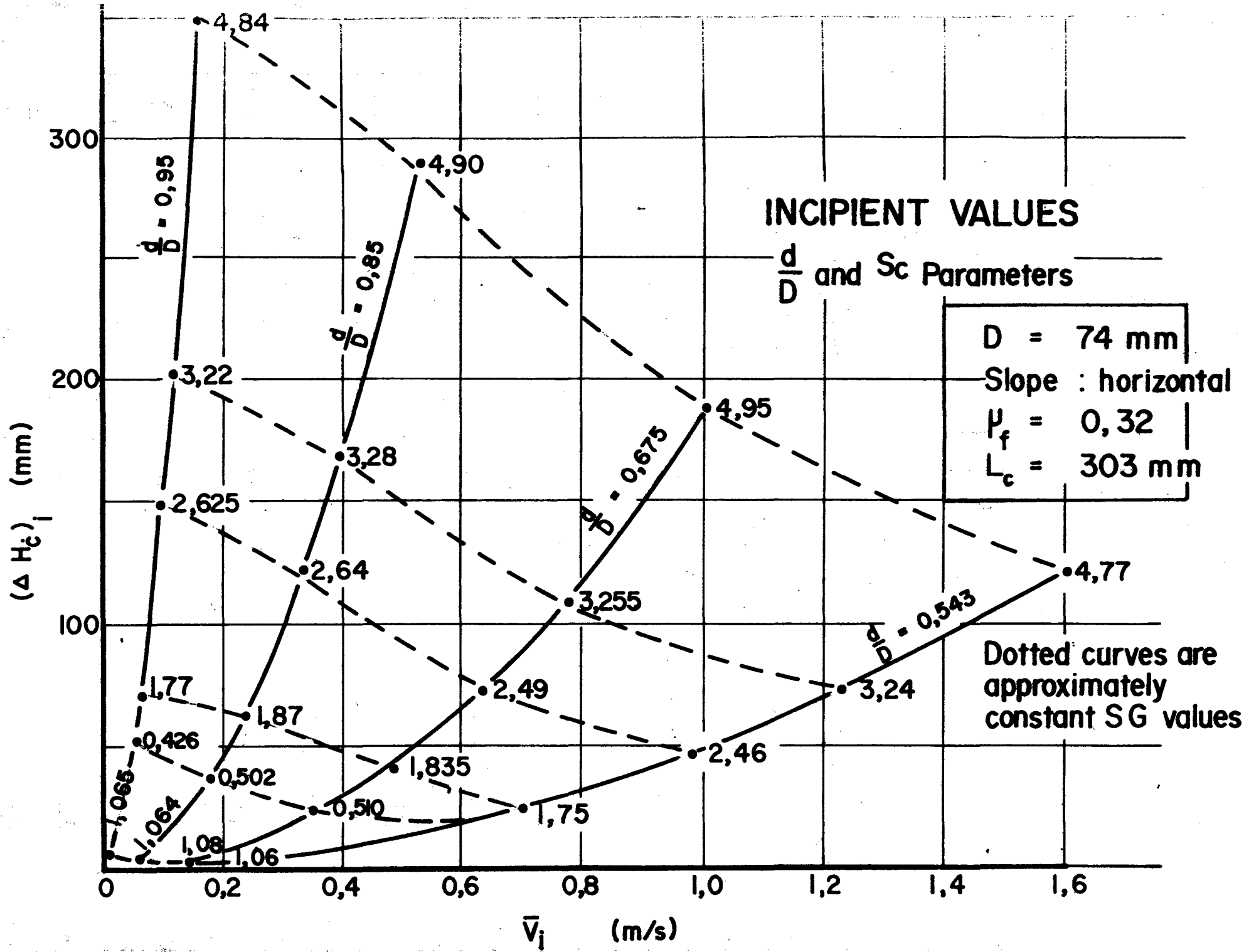
INCIPIENT VALUES
d/D and Sc Parameters
D = 74 mm
Slope : horizontal
μf = 0,32
Lc = 303 mm
Dotted curves are approximately constant S G values
d/D = 0,95
d/D = 0,85
d/D = 0,675
d/D = 0,543
4,84
4,90
4,95
4,77
3,22
3,28
3,255
3,24
2,625
2,64
2,49
2,46
1,77
1,87
1,835
1,75
0,426
0,502
0,510
1,08
1,06
1,065
1,064
300
200
100
0
0,2
0,4
0,6
0,8
1,0
1,2
1,4
1,6
(Δ Hc)i (mm)
V̄i (m/s)

FIG. 14.6

and there is a correspondingly decreasing dependence on specific gravity.

An explanation for the above is that at large diameter ratios an increase in specific gravity results in a greater backward drag force than the same specific gravity increase at small diameter ratios.

Figure 14.6 has the same general shape as Figure 14.1 and in both cases the net submerged weight of the capsule increases towards the top of the graph although the effect is less pronounced towards the right. Hence the right hand side "collapse" is evident in both figures.

Note that on Figure 14.6 the submerged specific gravity $|S_c-1|$ is obviously the relevant parameter since both specific gravities of $\sim$0,5 and $\sim$1,8 are above the capsules which are slightly above neutral buoyancy.

2.1 Correlation

In order to generalise the information on Figure 14.6, the successful implementation of the plotting device indicated for generalising Figure 14.1 is shown on Figure 14.7. Different values of specific gravity are shown on this Figure compared with the values given on Figure 14.3. But this does not matter since both Figure 14.6 and Figure 14.7 represent the results of analysis. What is significant, is that a wide range of specific gravities and length to diameter ratios can be represented by a Γ_i versus χ_i plot with virtually no scatter. The equation in this case is

$$\Gamma_i = 33/\chi_i^{1,86} \qquad (14.2)$$

The exponent differs slightly from that of equation (14.1) but the pipe friction head loss equations are different in the two cases, being

$\Delta h_f/L = 0,014\ \overline{V}^{1,84}$ for the 74 mm diameter pipe and;

$\Delta h_f/L = 0,025\ \overline{V}^{1,75}$ for the 44 mm diameter pipe (see Appendix I)

2.2 Experimental incipient values at different capsule densities

FIG. 14.7

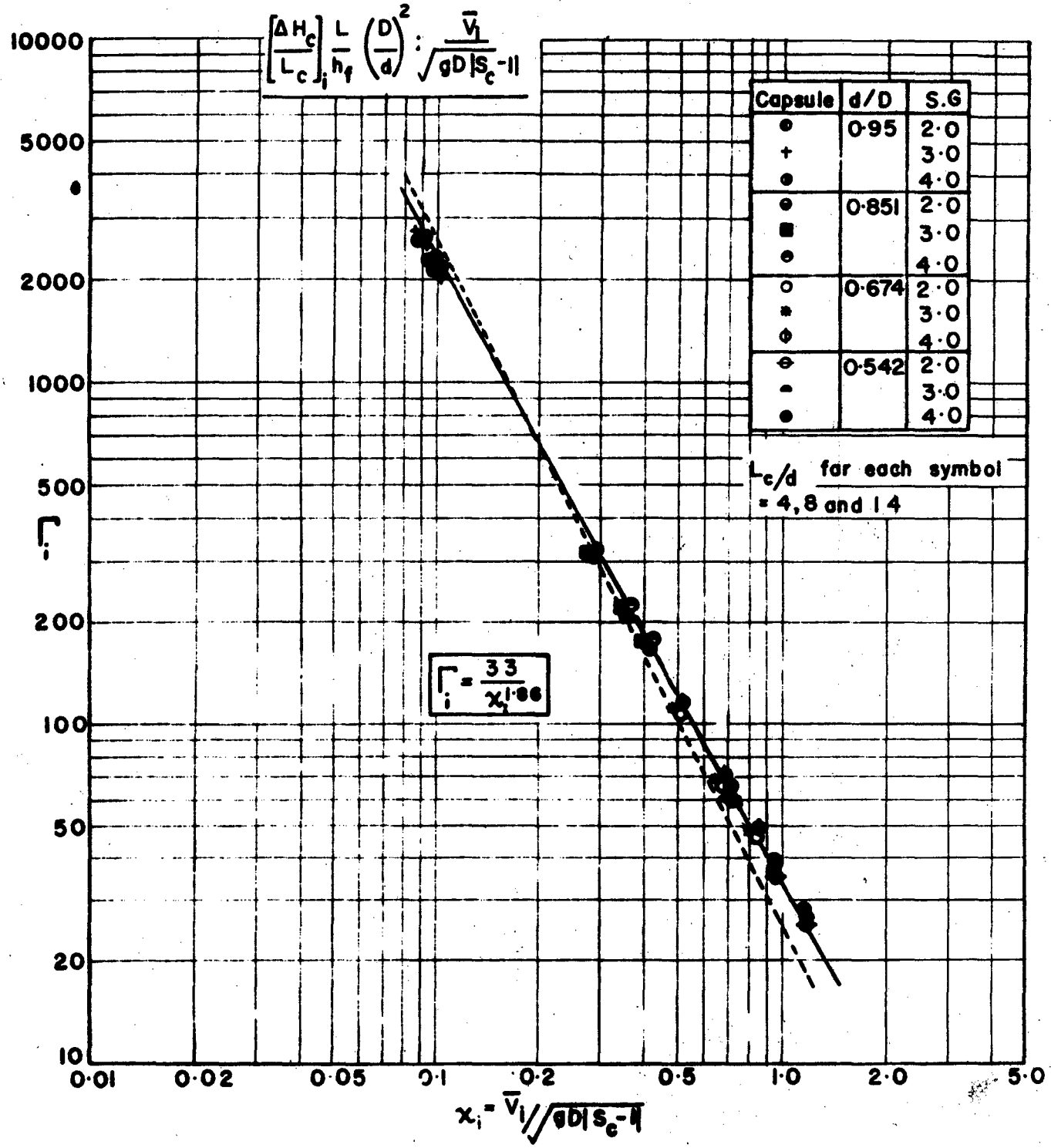
$\left[\frac{\Delta H_c}{L_c}\right]_i \frac{L}{h_f}\left(\frac{D}{d}\right)^2 : \frac{\bar{V}_l}{\sqrt{gD\,|S_c-1|}}$
10000
5000
2000
1000
500
200
100
50
20
10
Γ_i
$\Gamma_i = \frac{33}{x_i^{1\cdot86}}$
0·01
0·02
0·05
0·1
0·2
0·5
1·0
2·0
5·0
$x_i = \bar{V}_l / \sqrt{gD\,|S_c-1|}$
Capsule | d/D | S.G
0·95 | 2·0 | 3·0 | 4·0
0·851 | 2·0 | 3·0 | 4·0
0·674 | 2·0 | 3·0 | 4·0
0·542 | 2·0 | 3·0 | 4·0
L_c/d for each symbol = 4, 8 and 14

Figure 14.8 shows the non-dimensional incipient velocity as a function of diameter ratio. This curve covers a range of experimental values of diameter ratios and specific gravities (capsules numbered 1 to 24). The curve is determined analytically as described earlier and the experimental results are abscissa intercepts from Figures 10.27 to 10.30. There is excellent agreement between analytical and experimental values especially when one considers the difficulties encountered in determining the incipient velocity experimentally.

Figure 14.9 shows a similar graph to that given in Figure 14.8. In this case the pipe diameter is approximately doubled (D = 150 mm). Experimental values are slightly higher than analytical results. One reason for this is the difficulty experienced in determining the incipient velocity in an opaque pipe. The mean water velocity versus capsule velocity curves were extrapolated to give $V_c = 0$. This does not really explain why all the experimental points are high. The joints in this pipe were more prominent than in the case of the 74 mm perspex pipe and this could cause capsule velocities to be slightly lower than for a smooth jointed pipe. This results in a value of $\overline{V}_i$ which may be too high.

Also shown in Figure 14.9 are curves from Figure 14.8 and it is evident that pipe diameter is successfully absorbed in the correlation (see also Figure 10.30).

Three capsule densities are represented by the data and analytical points in Figure 14.9 and they are coincident.

Figure 14.10 shows the excess head loss across incipient capsules as a function of diameter ratio, the dotted curves representing experimental results and the full curves representing analytical results.

The agreement is good, decreasing towards high diameter ratios. However, the analysis is only applicable up to $d/D = 0,85$ (remember, static

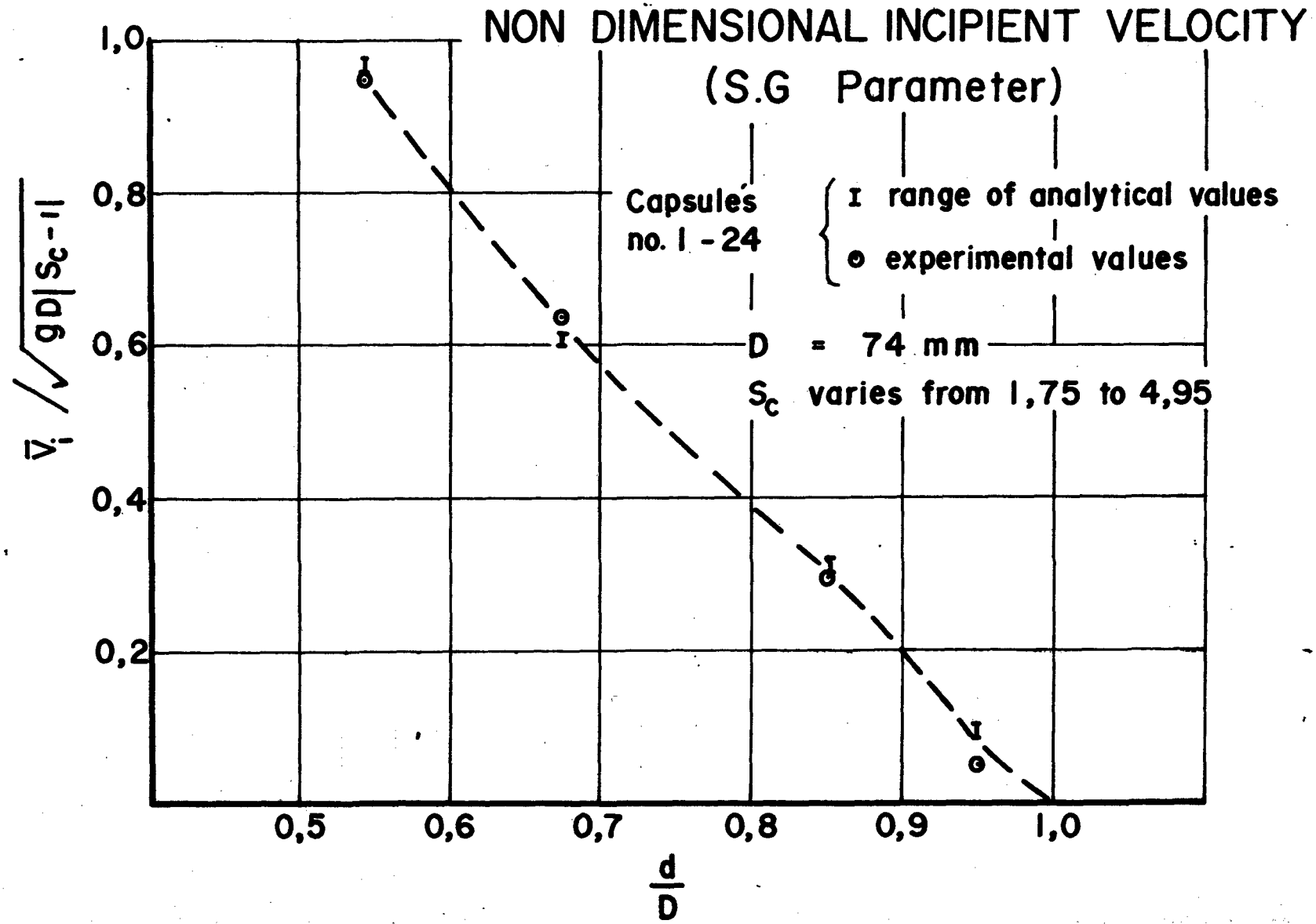
NON DIMENSIONAL INCIPIENT VELOCITY
(S.G Parameter)
Capsules
no. 1 - 24
I range of analytical values
o experimental values
D = 74 mm
S_c varies from 1,75 to 4,95
$\bar{V}_i / \sqrt{g D |S_c - 1|}$
1,0
0,8
0,6
0,4
0,2
0,5
0,6
0,7
0,8
0,9
1,0
$\frac{d}{D}$

FIG. 14.8

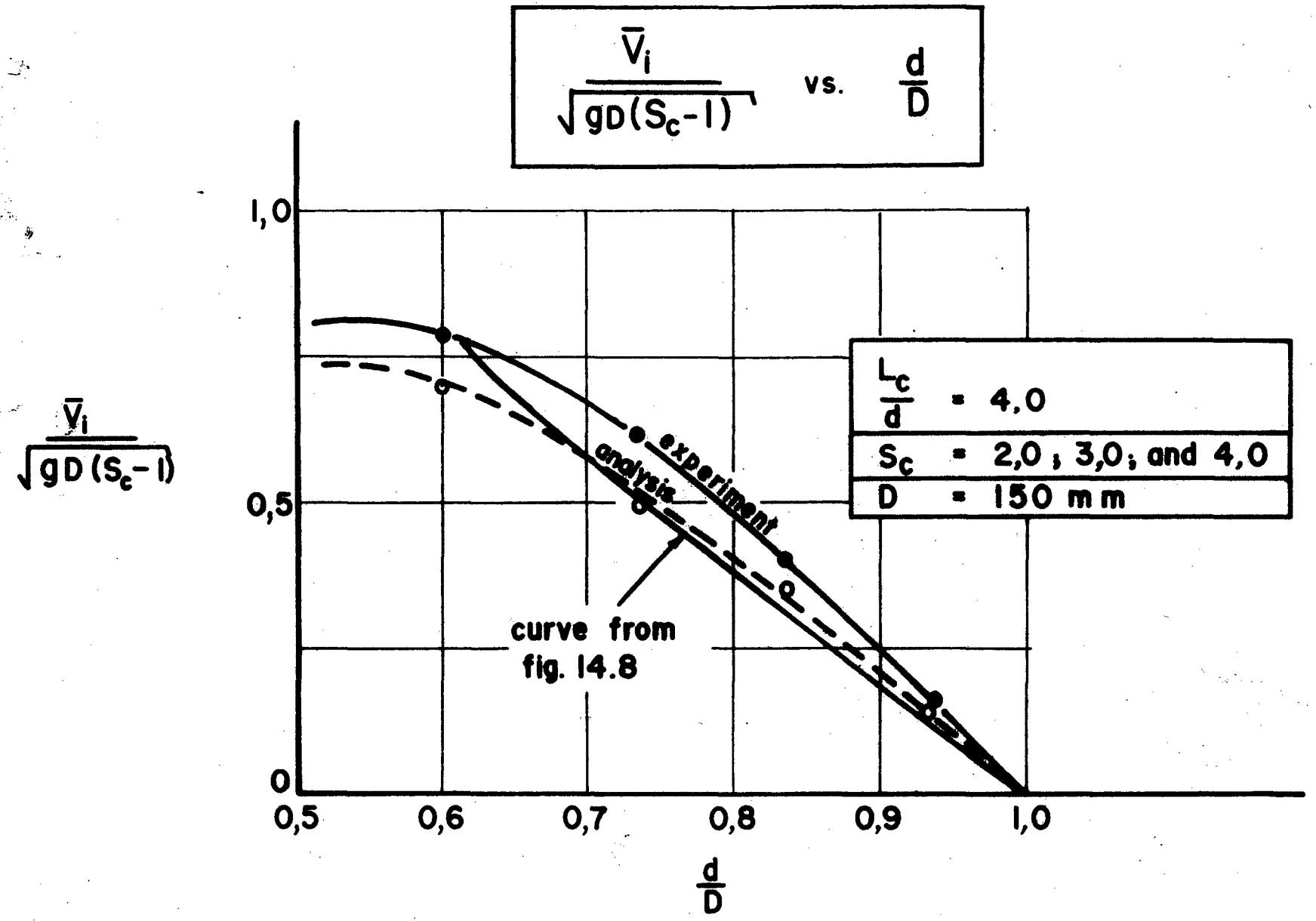
$\frac{\bar{V}_i}{\sqrt{gD(S_c-1)}}$ vs. $\frac{d}{D}$
$\frac{\bar{V}_i}{\sqrt{gD(S_c-1)}}$
1,0
0,5
0
0,5
0,6
0,7
0,8
0,9
1,0
$\frac{d}{D}$
$\frac{L_c}{d}$ = 4,0
S_c = 2,0 ; 3,0; and 4,0
D = 150 mm
experiment
analysis
curve from fig. 14.8

FIG. 14. 9

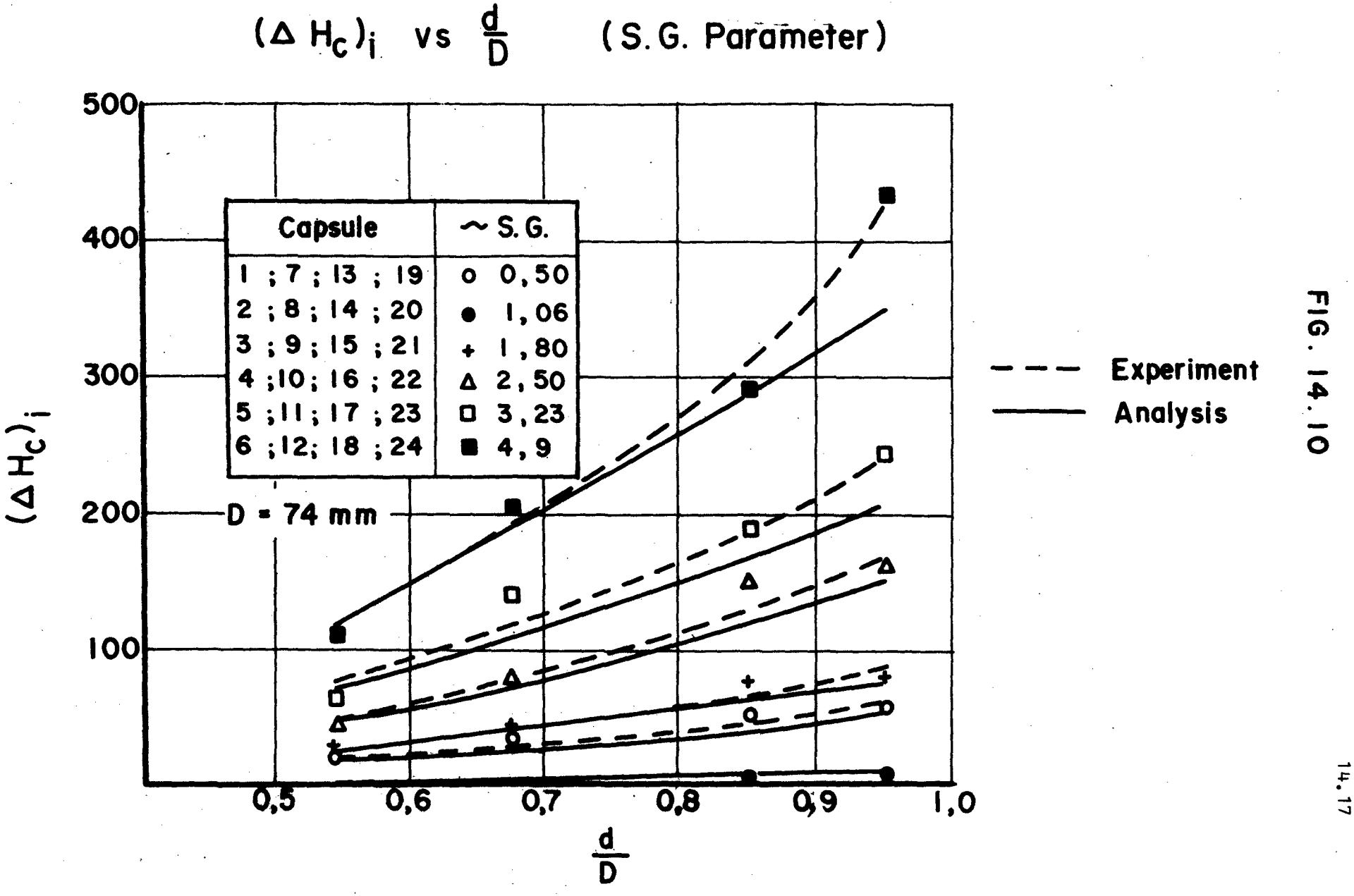
$(\Delta H_c)_i$ vs $\frac{d}{D}$ (S.G. Parameter)
500
400
300
200
100
$(\Delta H_c)_i$
Capsule
~ S.G.
1 ; 7 ; 13 ; 19
o 0,50
2 ; 8 ; 14 ; 20
● 1,06
3 ; 9 ; 15 ; 21
+ 1,80
4 ;10; 16 ; 22
Δ 2,50
5 ;11; 17 ; 23
□ 3,23
6 ;12; 18 ; 24
■ 4,9
D = 74 mm
0,5
0,6
0,7
0,8
0,9
1,0
$\frac{d}{D}$
Experiment
Analysis

FIG. 14.10

capsule tests were carried out with capsule diameter ratios ranging from d/D = 0,54 to 0,85).

Figure 14.11 shows a graph similar to that in Figure 14.10. In this case the pipe diameter is doubled (D = 150 mm) and experimental results can be directly compared with analysis. The same sort of pattern emerges as for the 74 mm pipe and the agreement is extremely good for a range of diameter ratios and capsule densities.

Figure 14.12 shows the non-dimensional correlation for experimental results obtained in the 150 mm diameter pipe. This curve can be compared with the analytical curve in Figure 14.7 in the 74 mm diameter pipe. The correlation is, in this case, excellent and the resulting equation is similar to equation (14.2), except that the constant is slightly higher;

$$\text{i.e.} \quad \Gamma_i = 38/\chi_i^{1,86} \qquad (14.3)$$

One reason for the constant in equation (14.3) being higher than in equation (14.2) is that the non-dimensional incipient velocity curve, obtained experimentally, is higher than the analytical curve in Figure 14.9.

3. Effect of pipeline slope

Figure 14.13 shows the excess head loss across capsules at incipience $(\Delta H_c)'_{is}$ as a function of mean water velocity with slope and daimeter ratio as parameters. Once again the dominating effect is shown to be diameter ratio.

The steepest sloping pipe (ϕ = 30,8%) yields the steepest $(\Delta H_c)'_{is}$ to $\overline{V}_i$ curve and as diameter ratio is increased the rise in the value of $(\Delta H_c)'_{is}$ required to cause capsule motion is more pronounced than for the more mildly sloping pipes.

As pipe slope is increased at a particular diameter ratio a greater value of the excess head loss is required and at a higher mean water velocity. Although the head loss effect is far more pronounced as diameter

CHAPTER 15

COMPARISON OF ANALYTICAL AND EXPERIMENTAL RESULTS FOR MOBILE CAPSULES

In this Chapter the outcome of computer calculations based on the analytical procedure described in Chapter 7 are compared with experimental results for mobile capsules.

An empirical equation, for embracing the independent variables to yield the excess energy loss, is also proposed.

Figures 15.1 to 15.4 (capsules 9; 10; 11 and 12) show experimental results as mean curves through the data points as full lines.

1. Definitions of terms used

The results of "empirical m" analysis and "experimental m" analysis are shown as dashed (------) and broken lines (—— - ——) respectively, and the results of the "gross" analysis is shown thus (—— - - ——). Where "m" is the slope of the relevant V_c versus $\overline{V}$ line.

1.1 "Empirical m" analysis (finite element analysis)

In order to calculate the value of the excess head loss across a mobile capsule (ΔH_c) it is necessary to know the capsule characteristics (such as diameter ratio, length to diameter ratio and SG) as well as the mean water velocity, pipeline slope, and capsule velocity.

The mean water velocity has been arbitrarily chosen (e.g. $\overline{V}$ = 0,5; 1,0; 1,5; 2,0; 2,5; and 3,0 m/s) and the capsule velocity can then be determined either by measurement or using the semi-empirical formula worked out in Chapter 10, viz;

$$V_c = m(\overline{V} - \overline{V}_i)$$

An empirical relation has been given for obtaining the slope (m) (equation (10.6)) and $\overline{V}_i$ can be calculated as shown in Chapter 7.

FIG. 15.1

$\Delta H_c : V$

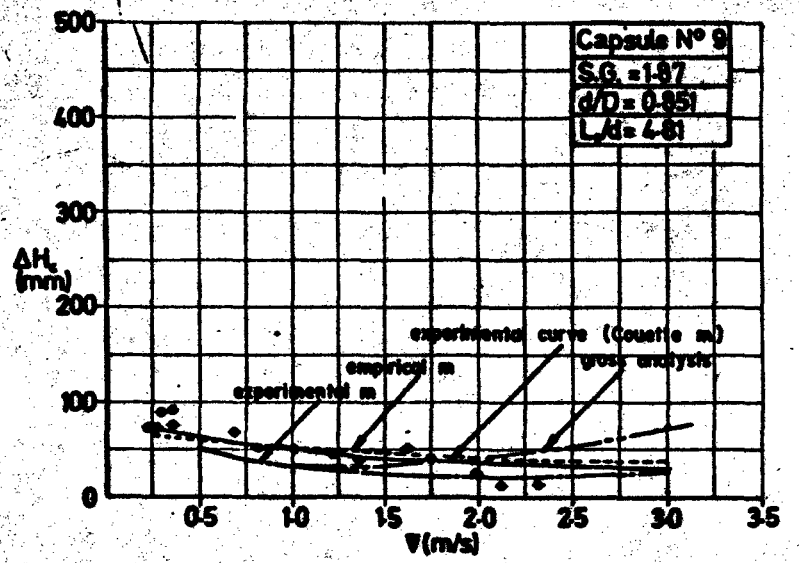

FIG. 15.2

$\Delta H_c : V$

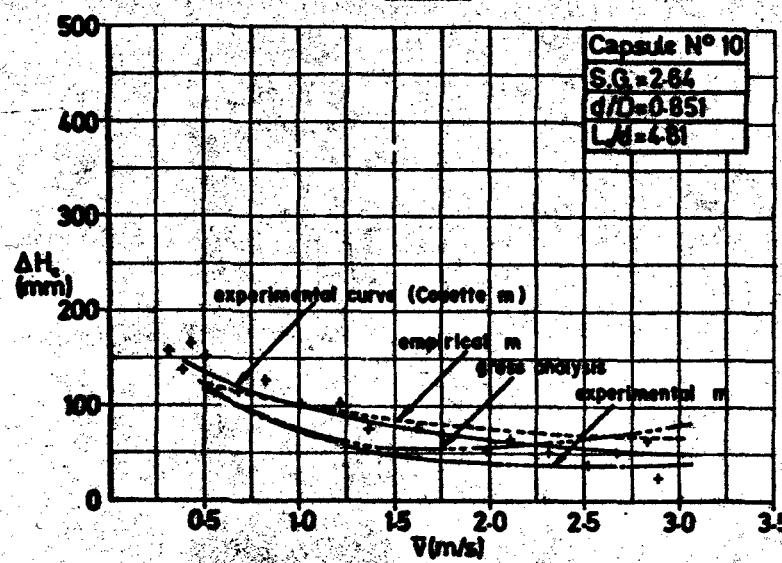

FIG. 15.3

$\Delta H_c : V$

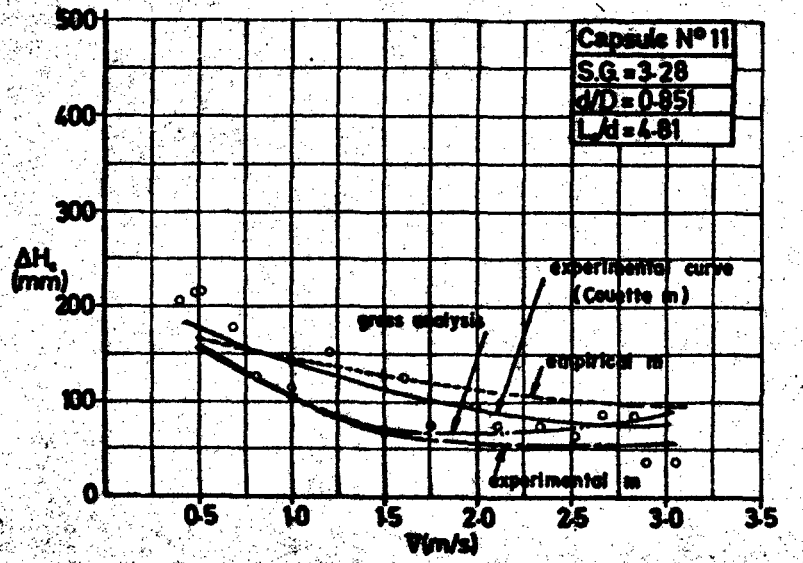

FIG. 15.4

$\Delta H_c : V$

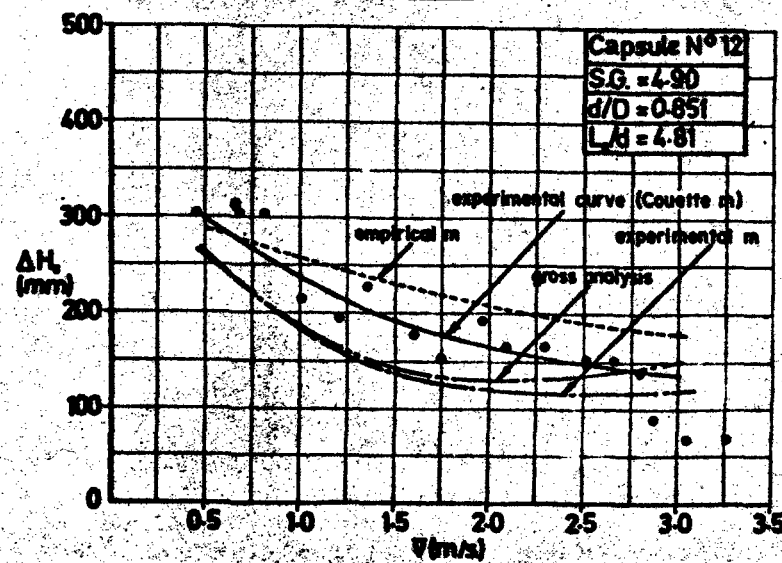

If, in the finite element analysis, m has been obtained from the empirical formula then the calculation has been designated "empirical m".

1.2 "Experimental m" analysis (finite element)

If a measured value of capsule velocity in injected into the computer program then the effective value of "m" used is an experimental one and in this case the calculation has been designated "experimental m". An analytical value is found for excess head loss (ΔH_c) .

1.3 "Couette m" analysis (finite element)

If the measured value of excess head loss (ΔH_c) is used in the finite element analysis then the resultant calculation to find the capsule velocity has been designated "Couette m". This is not a good designation, but has been retained since it was used in the computer analysis.

1.4 Gross analysis

As discussed in Chapter 7, a gross method has also been evolved for calculating (ΔH_c) given $\overline{V}$ and V_c or for calculating (V_c) given ΔH_c and $\overline{V}$.

All the above analytical procedures have been dealt with in Chapter 7 and the computer formulation is given in detail in Appendix II.

The effect on the analytical results of capsule variables, which were investigated experimentally, will be discussed in the following sections.

2. The effect of capsule velocity (V_c) on ΔH_c

The most significant observations is that small errors in calculating or measuring capsule velocity (V_c) have very large effects on the calculated value of (ΔH_c).

However, small errors in V_c can represent large errors in the values of ($\overline{V} - V_c$) and considerable errors in $\overline{V}_{ap}$. It will be shown later in

$\Delta H_c : \bar{V}$

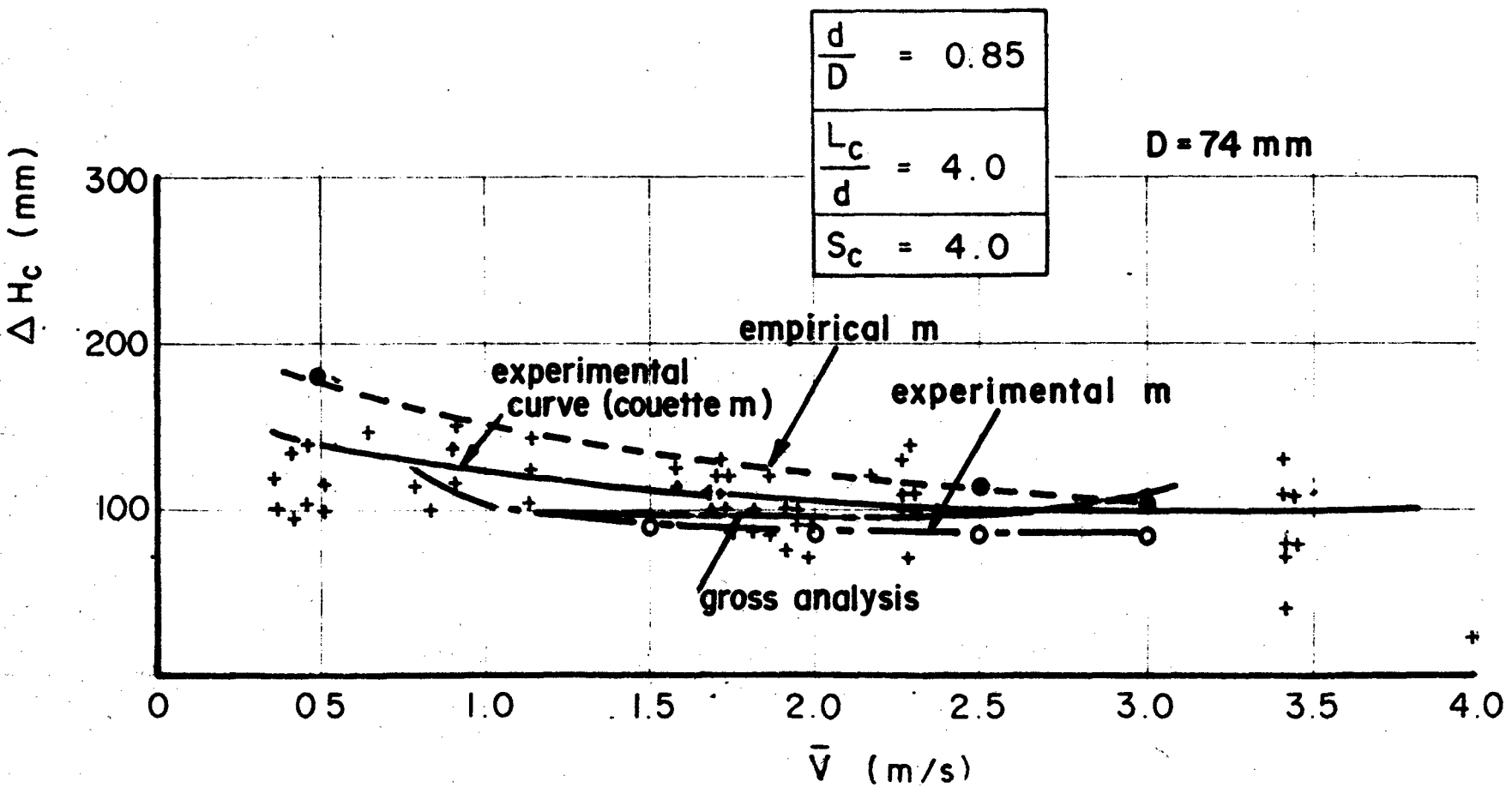

FIG. 15.5

this Chapter how ΔH_c varies with the above velocities.

Consider Figure 15.5 (for example). The "empirical m" analysis (making use of empirical values of V_c for obtaining ΔH_c) yields a curve which lies somewhat above the mean experimental curve, although the entire curve is within the range of experimental scatter. The "experimental m" curve (making use of experimental values of capsule velocity to obtain ΔH_c), lies below the mean experimental curve, again well within the spread of data points.

The only difference between these curves (both obtained from the finite element analysis using quasi-concentric polar co-ordinates) is that the capsule velocity (V_c) for the computation is different.

Figure 15.6 shows (for the same capsule depicted on Figure 15.5) capsule velocity as a function of mean water velocity.

The experimental and empirical values are given as well as those from the "Couette m" analysis (analytical values of V_c obtained from experimental values of ΔH_c).

Consider a mean water velocity of 1,5 m/s (on Figure 15.5). The "experimental m" analysis gives ΔH_c values which are 23,8% lower than the mean experimental curve, and the experimental value of capsule velocity (V_c) (Figure 15.6) is 4,0% higher than the value of V_c determined from the "Couette m" analysis. An error of 4,0% in the measurement of V_c causes a 23,8% error in ΔH_c calculation.

The "empirical m" analysis at $\overline{V}$ = 1,5 m/s (Figure 15.5) gives a ΔH_c value which is 23,5% high, for an empirically calculated value of V_c which is 3,43% low.

The "gross analysis" yields a ΔH_c value at $\overline{V}$ = 1,5 m/s (Figure 15.5) which is 18,2% lower than the mean experimental value, for an experimental value of V_c. If V_c is adjusted to give ΔH_c in exact

FIG. 15.6

15.6

3.0
2.0
1.0
0
1.0
2.0
3.0
V_c (m/s)
$\bar{V}$ (m/s)
$\frac{d}{D}$ = 0.85
S_c = 4.0
$\frac{L_c}{d}$ = 4.0
D = 74 mm
empirical m
couette m
experimental m
gross analysis

agreement with the experimental value, then V_c is 3,94% lower than the measured value, for the "gross" analysis.

Thus, whichever of the methods of analysis (proposed in this thesis) is used, agreement is extremely good if V_c is calculated from a measured value of ΔH_c. But the calculation of ΔH_c from a measured value of V_c is dependent on the exact value of V_c. An explanation for the above will be given later in this Chapter.

In the discussion that follows, on the comparison of experimental and analytical results, the cases where agreement is poorest will be discussed first.

2.1 Effect of SG

Figures 15.1 to 15.4 show similar curves depicting the various analyses and, in terms of absolute values, theories applied to the lower SG capsules give better agreement with experiment.

The worst agreement, in terms of absolute ΔH_c values, occurs at 1,5 m/s (see Figure 15.4) for the capsule of SG = 4,90.

However, in terms of percentage errors in the calculation, Table 15.1 (on the following page) shows that the error is greatest when calculating ΔH_c for the lightest capsule.

In all cases the analytical values of ΔH_c are best determined using the empirically derived value of capsule velocity.

It should be noted that the data points in Figures 15.1 to 15.4 are all mean values and the analytical curves lie within the spread of experimental data. This fact will be more clearly seen when discussing the comparison of experimental and analytical curves in the next section where all data points are shown.

The calculation of capsule velocity from a measured value of ΔH_c ("Couette m" analysis) or an empirical determination of V_c or the

calculation of V_c from the gross analysis and measured value of ΔH_c all give good results yielding curves similar to those on Figure 15.6. The percentage errors at $\overline{V}$ = 1,5 m/s are shown in Table 15.1, this being the mean water velocity where most deviation occurs.

T A B L E 15.1

		% error at $\overline{V}$ = 1,5 m/s					
d/D	SG	Calculation of ΔH_c			Calculation of V_c		
		expt m	emp m	gross m	Couette m	emp m	gross m
0,85	1,87	50	7,7	25,0	5,45	5,7	4,76
	2,64	46	14,1	55,2	6,50	7,9	6,91
	3,28	44	12,1	34,5	7,35	8,3	7,50
	4,9	31	24,1	49,0	6,62	11,5	6,60

2.2 Effect of diameter ratio

Figures 15.5, 15.7 and 15.8 show the three analytical curves (determined by different methods) compared with the experimental curves at three diameter ratios. In all three figures the two extreme analytical curves are within the spread of experimental data.

For the smallest diameter ratio (d/D = 0,543; Figure 15.7) the analytical curve using empirical values of capsule velocity (V_c) are slightly higher than the mean ΔH_c curve at mean water velocities less than $\overline{V}$ = 2,5 m/s. The analytical ΔH_c values determined from experimental values of V_c ("experimental m" analysis) are coincident with the mean experimental curve below $\overline{V}$ values of 2,0 m/s. The "gross analysis" curve coincides with the "experimental m" analysis curve.

In Figure 15.8 the pattern is similar with "empirical m" and "experimental m" analytical curves crossing the mean experimental ΔH_c curve at $\overline{V}$ values of 2,3 m/s and 1,0 m/s respectively.

ΔH_c : $\bar{V}$ Zero slope

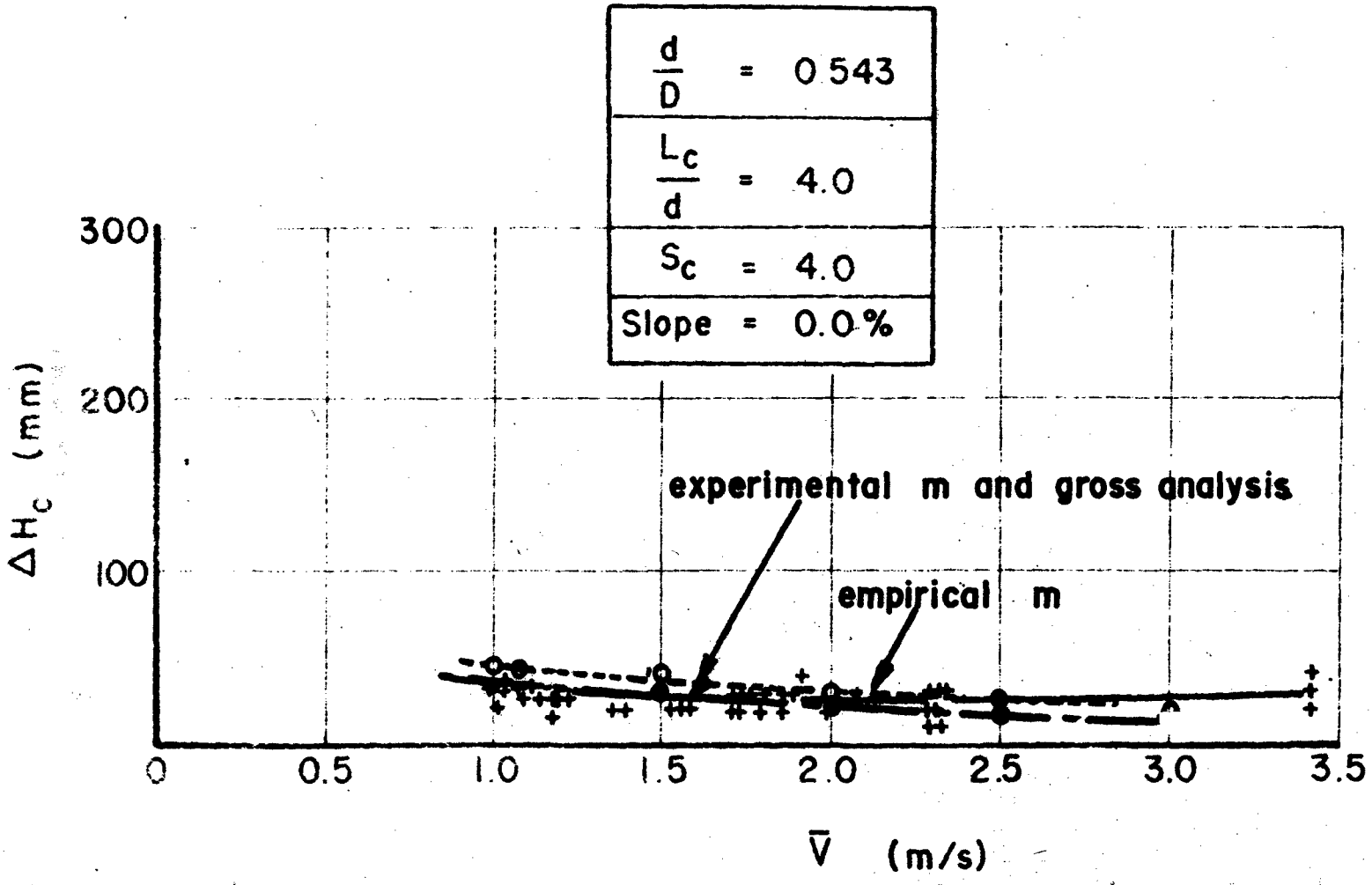

FIG. 15.7

FIG. 15.8

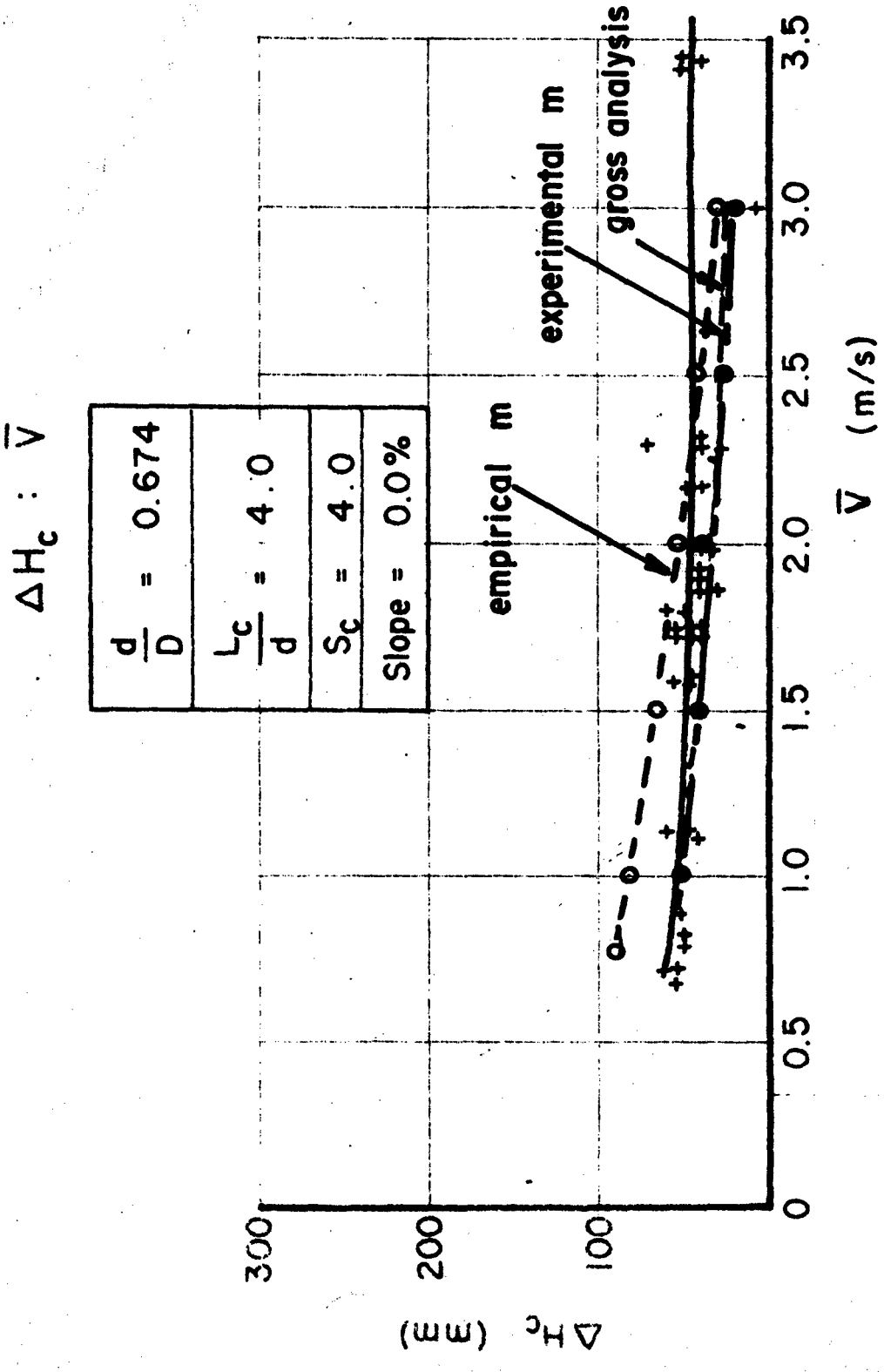
ΔHc : V̄
d/D = 0.674
Lc/d = 4.0
Sc = 4.0
Slope = 0.0%
empirical m
experimental m
gross analysis
ΔHc (mm)
300
200
100
0
0.5
1.0
1.5
2.0
2.5
3.0
3.5
V̄ (m/s)

3. Predicted analytical values of ΔH_c for D = 150 mm for a range of diameter ratios and capsule densities

Before carrying out experiments in the larger diameter pipe (D = 150 mm) an attempt was made to predict excess head loss from the finite element analysis using the empirically determined values of V_c.

Figure 15.9 shows analytically determined values of ΔH_c and $(\Delta H_c)_i$ as a function of mean water velocity for three specific gravities at d/D = 0,60. In terms of the absolute value of ΔH_c the agreement between analysis and experiment diminishes as SG increases. However, the correlation is reasonable. The agreement for capsules of SG = 2,0 and 3,0 is extremely good, the analytical values lying within the range of experimental data.

For the heaviest capsule (S_c = 4,0) the correlation between analysis and experiment deteriorates as velocity increases. This is explained as follows:

The incipient velocity as calculated from the empirical equation in Chapter 10 is somewhat low (see Figure 15.9) and this has a bearing on the empirical determination of capsule velocity since

$$V_c = m(\overline{V} - \overline{V}_i)$$

This fact alone renders the capsule velocity too high. However, the slope of the $V_c : \overline{V}$ line (m) was found to be larger (see Figure 10.86) than the value of m obtained from the empirical equation (in Chapter 10) used for deriving V_c, i.e.

$$m = 1,2 - 0,8\ (d/D - 0,5)^2 \qquad (10.6)$$

The net result is an empirical capsule velocity which is slightly too low (4,16% too low) (see Figure 15.12) and this yields an analytical result for ΔH_c which is 36% too high. This is the worst agreement. Figure 15.10 shows excess head loss (ΔH_c) as a function of mean water velocity in the 150 mm diameter pipe for d/D = 0,733 and three SG values.

FIG. 15.9

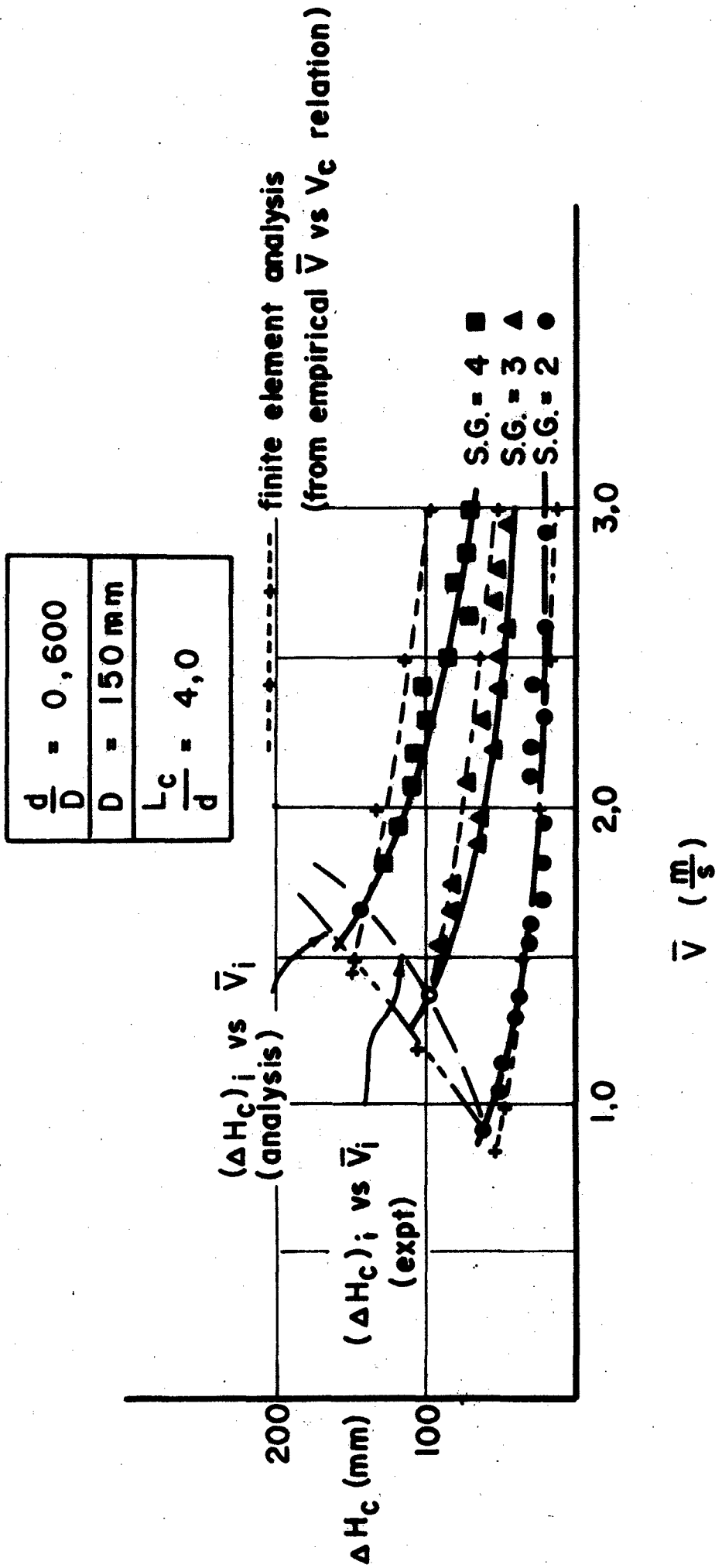
$\frac{d}{D}$ = 0,600
D = 150 mm
$\frac{L_c}{d}$ = 4,0
finite element analysis
(from empirical $\bar{V}$ vs V_c relation)
S.G. = 4
S.G. = 3
S.G. = 2
$(\Delta H_c)_i$ vs $\bar{V}_i$ (analysis)
$(\Delta H_c)_i$ vs $\bar{V}_i$ (expt)
ΔH_c (mm)
200
100
1,0
2,0
3,0
$\bar{V}$ $(\frac{m}{s})$

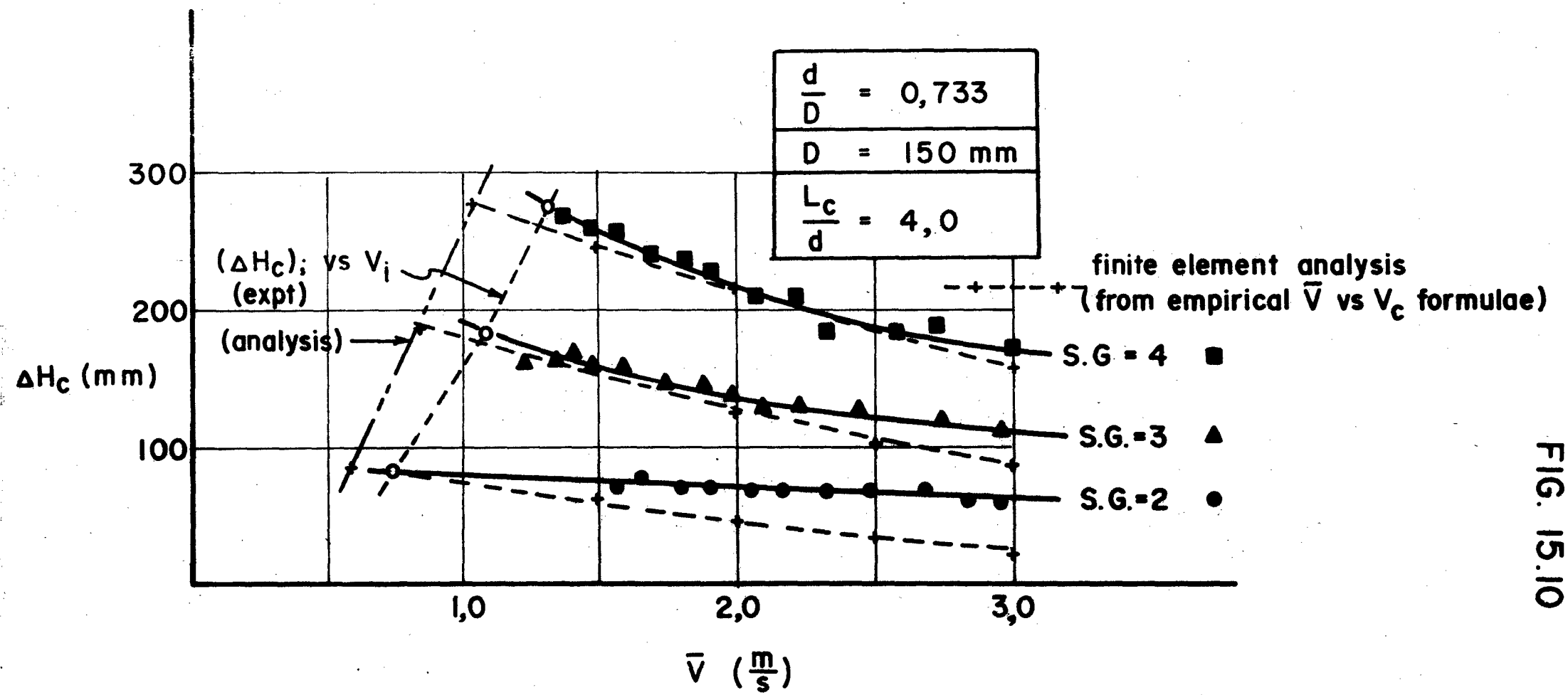
H_c vs. $\bar{V}$
$\frac{d}{D}$ = 0,733
D = 150 mm
$\frac{L_c}{d}$ = 4,0
300
200
100
ΔH_c (mm)
$(\Delta H_c)_i$ vs V_i
(expt)
(analysis)
finite element analysis
(from empirical $\bar{V}$ vs V_c formulae)
S.G = 4
S.G.=3
S.G.=2
1,0
2,0
3,0
$\bar{V}$ $(\frac{m}{s})$

FIG. 15.10

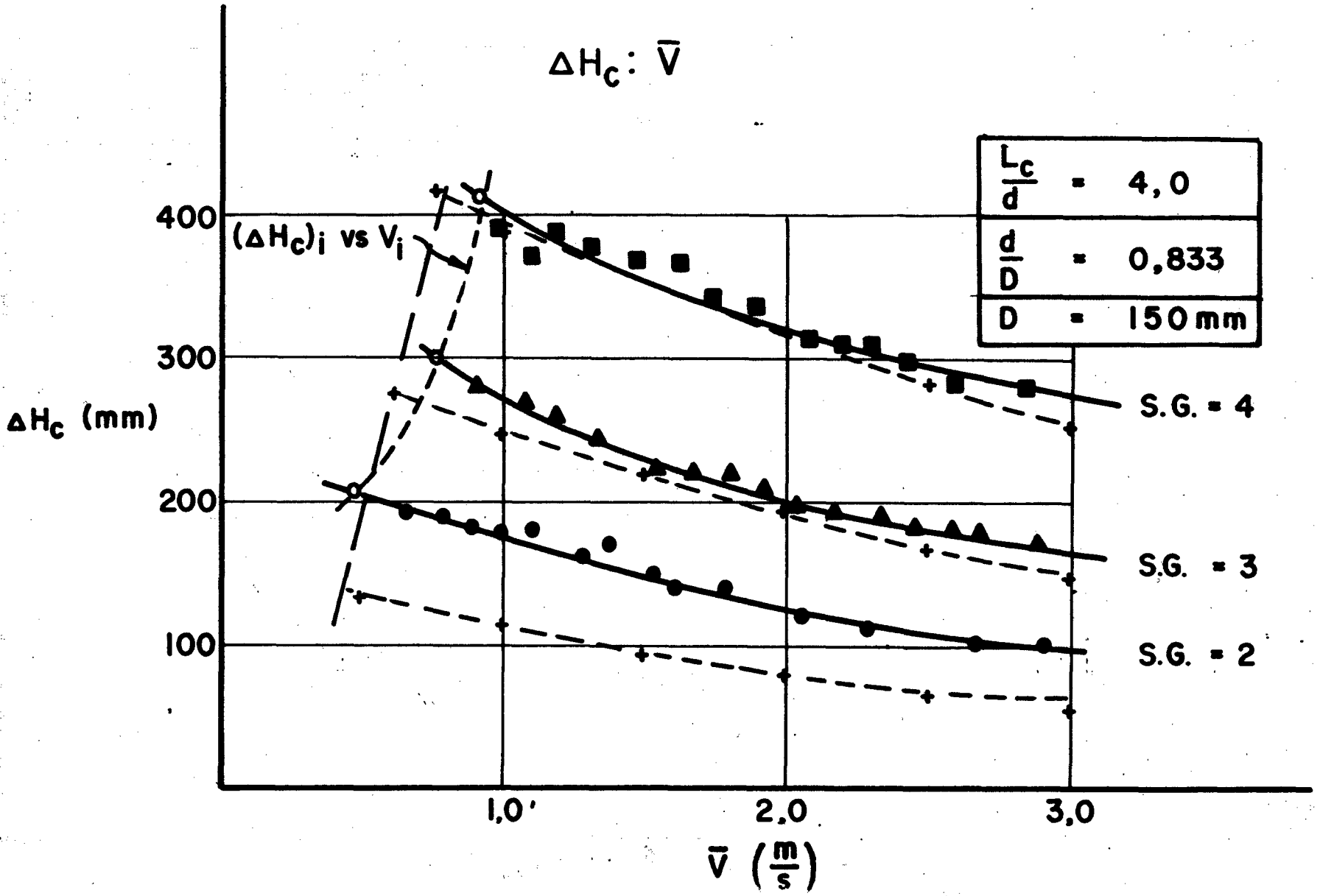
ΔHc : V̄
(ΔHc)i vs Vi
Lc/d = 4,0
d/D = 0,833
D = 150 mm
S.G. = 4
S.G. = 3
S.G. = 2
ΔHc (mm)
400
300
200
100
1,0
2,0
3,0
V̄ (m/s)

FIG. 15.11

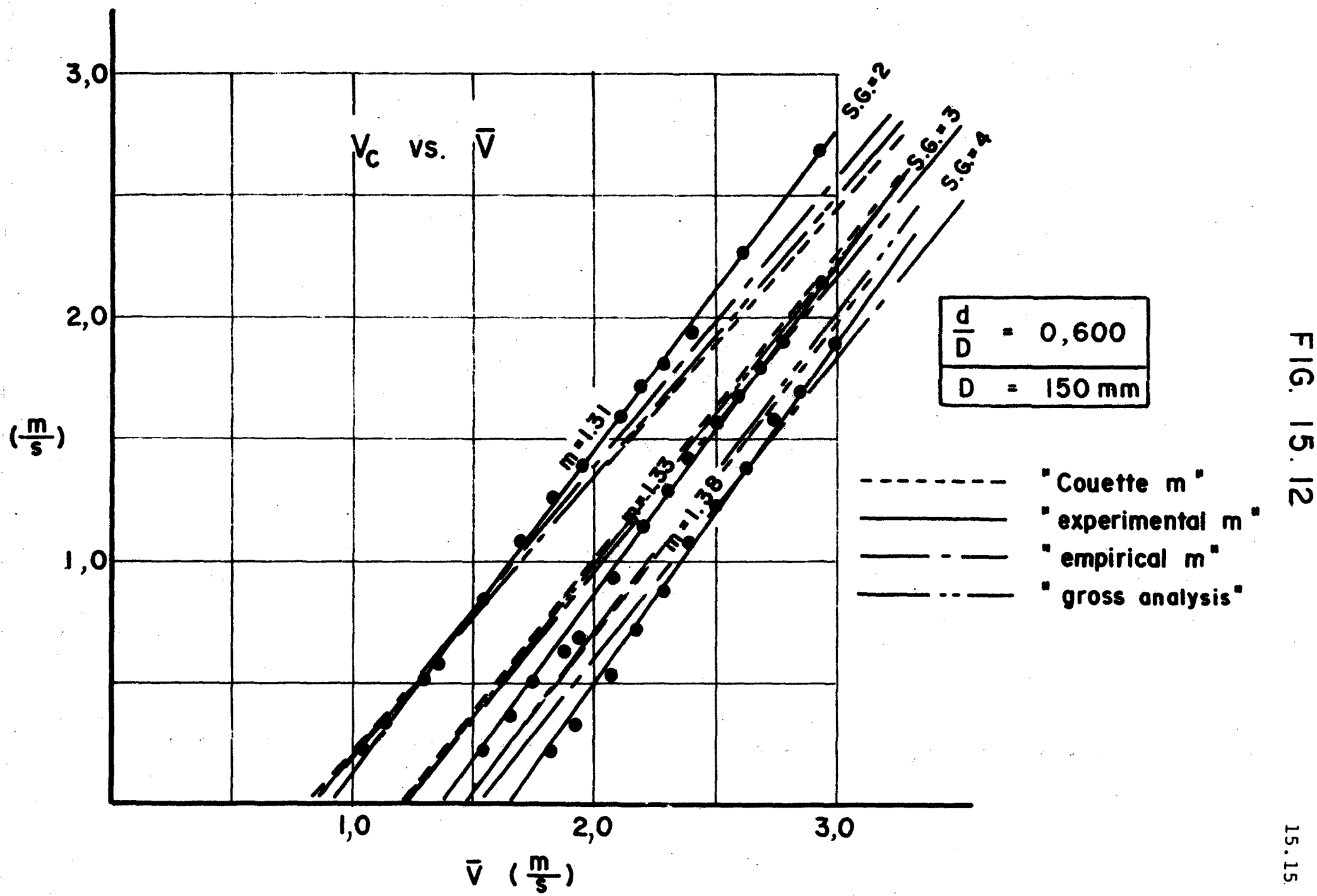
V_c vs. $\bar{V}$
3,0
2,0
1,0
$(\frac{m}{s})$
1,0
2,0
3,0
$\bar{V}$ $(\frac{m}{s})$
S.G.=2
S.G.=3
S.G.=4
m=1.31
m=1.33
m=1.38
$\frac{d}{D}$ = 0,600
D = 150 mm
"Couette m"
"experimental m"
"empirical m"
"gross analysis"

FIG. 15.12

In all cases the agreement between analysis and experiment is satisfactory except for the lowest SG (S_c = 2,0).

Also, agreement improves with decreasing velocity as in the case of the last capsules. In this case, however, and in the following case (Figure 15.11) the degree of correlation deteriorates with the lowest SG. The worst case occurring at 3 m/s (see Figures 15.10 and 15.11) where the capsule velocity has to be 8% lower in the case of d/D = 0,733 (S_c = 2) (see Figure 15.13) and 5% lower in the case of d/D = 0,733 (S_c = 2) (see Figure 15.14) to achieve an exact correlation between analysis and theory.

Note: Due to the high degree of turbulence manifest on the pen recorder at high velocities the measurement of ΔH_c at a mean water velocity of 3,0 m/s is extremely difficult.

In general, agreement with experiment is good, considering assumptions in the theory, difficulty of measuring ΔH_c at high velocities due to superimposed spurious turbulence effects and the scatter of experimental data.

The details of experimentally determined capsule velocities compared with empirical and analytical values (i.e. "Couette m" calculating V_c from measured ΔH_c values) are shown on Figures 15.12, 15.13 and 15.14. In all cases the slope of $V_c : \overline{V}$ lines (experimental) are steeper than the empirical and analytical ("Couette m") values. The latter two slopes are virtually parallel in most cases.

The discrepancy between the dotted lines (on Figures 15.12, 15.13 and 15.14) and "empirical m" lines represent the amount by which V_c has to be changed to make the experimental values of ΔH_c coincident with the analytical values (on Figures 15.9, 15.10 and 15.11). In general where the above velocity discrepancy is largest, there is a resulting discrep-

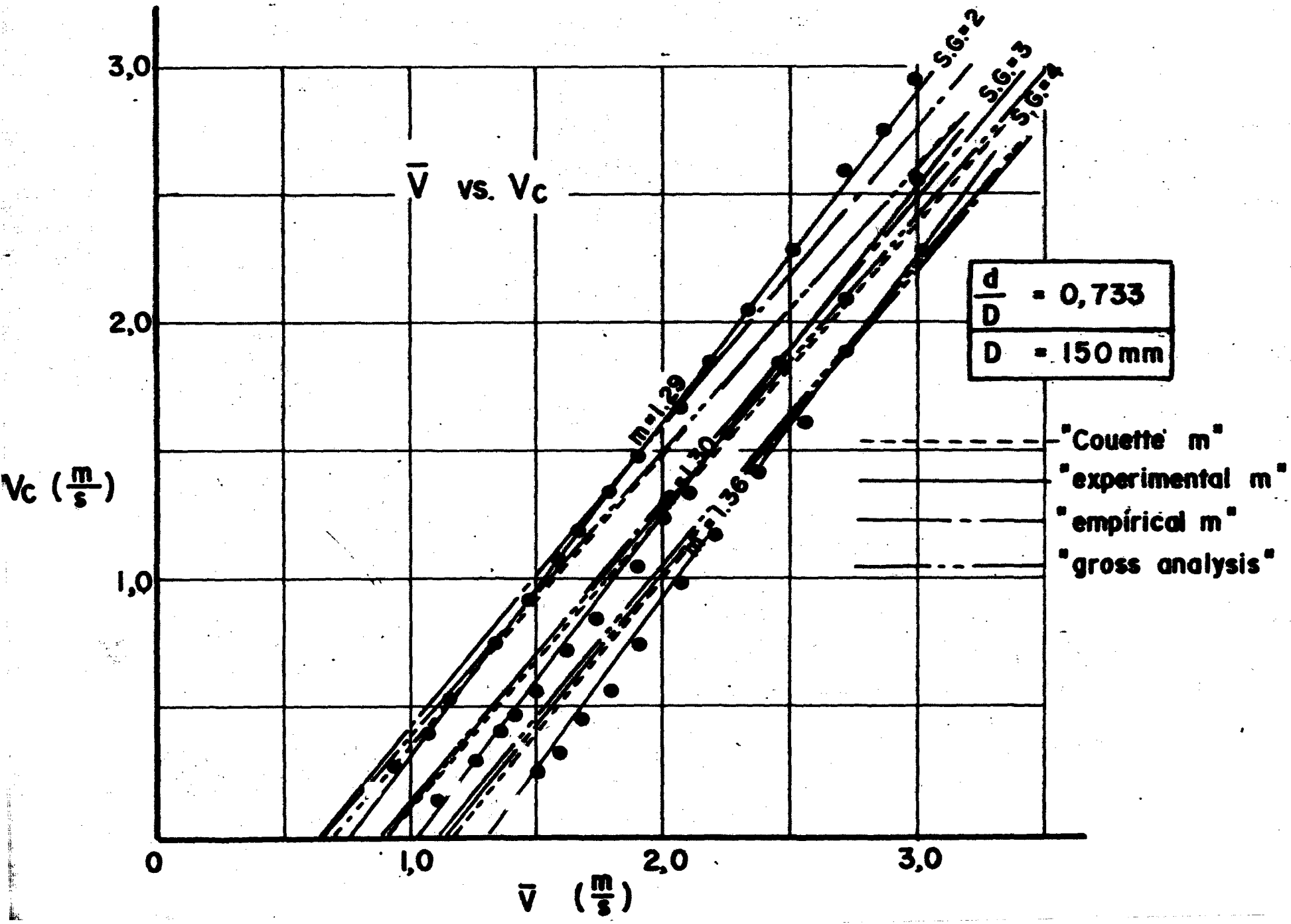
$\bar{V}$ vs. V_c
S.G.=2
S.G.=3
S.G.=4
m=1.29
m=1.30
m=1.36
$\frac{d}{D}$ = 0,733
D = 150 mm
"Couette' m"
"experimental m"
"empirical m"
"gross analysis"
V_c ($\frac{m}{s}$)
$\bar{V}$ ($\frac{m}{s}$)
0
1,0
2,0
3,0

FIG. 15.13

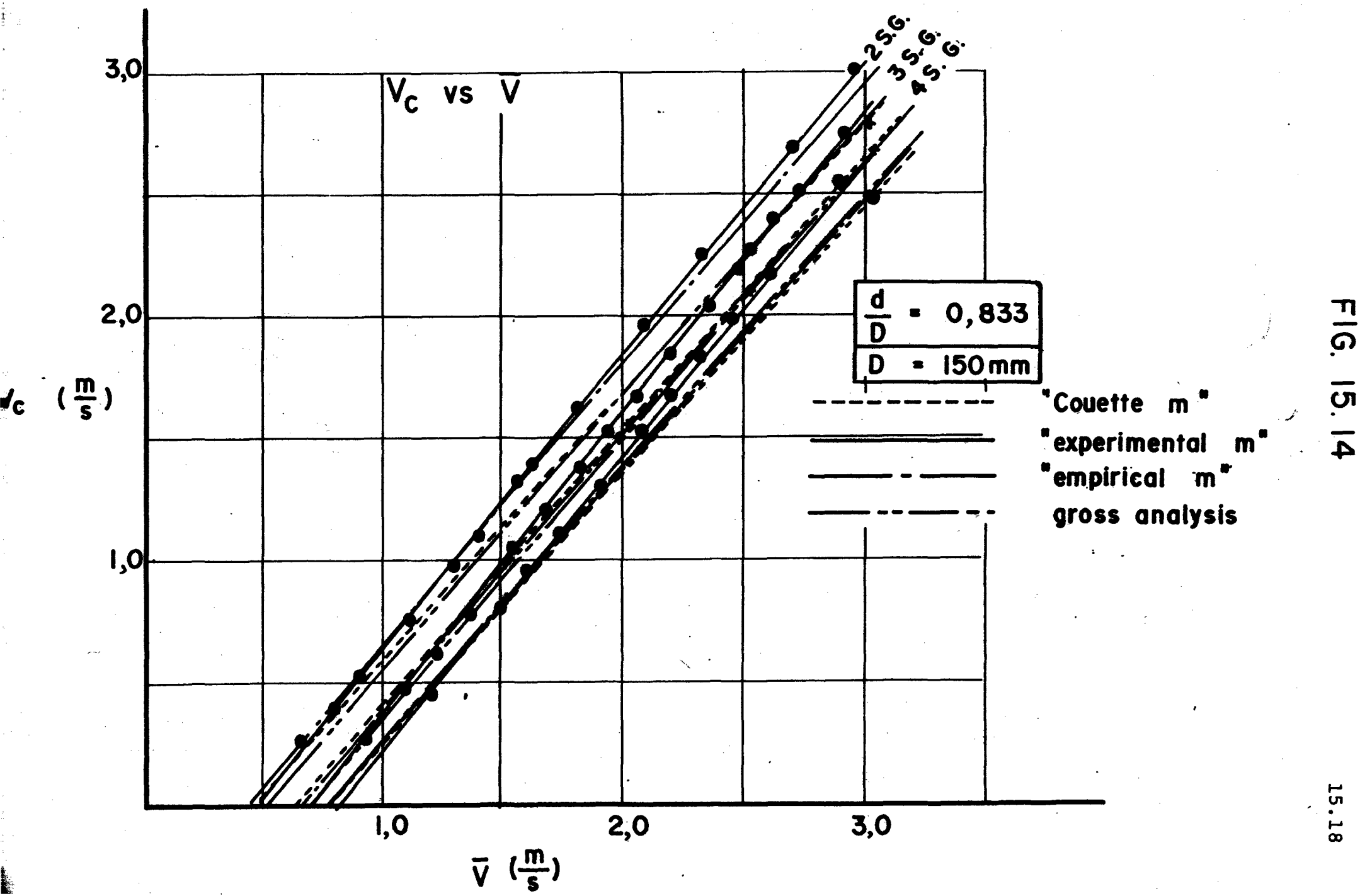
V_c vs $\bar{V}$
2S.G.
3S.G.
4S.G.
$\frac{d}{D}$ = 0,833
D = 150mm
"Couette m"
"experimental m"
"empirical m"
gross analysis
3,0
2,0
1,0
V_c $(\frac{m}{s})$
1,0
2,0
3,0
$\bar{V}$ $(\frac{m}{s})$

FIG. 15.14

ancy between analytical and experimental values of ΔH_c. The discrepancy is accentuated for low density capsules except in the case of the smallest diameter ratio ($d/D = 0,60$). This will be explained in Section 7.

The values of ΔH_c were also calculated analytically from the "gross method". It was found that for the 150 mm diameter pipe agreement although fair, decreases considerably as SG increases, and the gross theory was found to be less universally applicable than the finite element method. Nonetheless, values of V_c, when calculated to yield ΔH_c values in agreement with experiment, differ by only a few percent from measured values of V_c. The results of these calculations are shown on Figures 15.12, 15.13 and 15.14 (V_c calculated from "gross analysis").

4. Effect of L_c/d ratio

Figure 15.15 shows mean experimental curves duplicated from Figure 11.16. Superimposed are analytical curves using the finite element technique ("empirical m" analysis).

For the longest train of capsules ($L_c/d = 16$) the analytical results of ΔH_c (calculated from empirical capsule velocities) are about 12,3% high. Generally the discrepancy decreases down to $L_c/d = 8$ and then the analytical curves are low although still in fairly good agreement and within the range of experimental scatter (not shown on the graph).

Figure 15.16 shows experimentally determined $V_c : \overline{V}$ curves from Figure 10.48 and superimposed are capsule velocities from the "empirical m" analysis (i.e. corresponding to the dotted curves on Figure 15.15) as well as capsule velocities determined from the "Couette m" analysis (i.e. corresponding to the solid experimentally determined curves on Figure 15.15).

It is clear that the "empirical m" curve lies below the experimental values at high L_c/d ratios, gradually becoming closer as L_c/d is

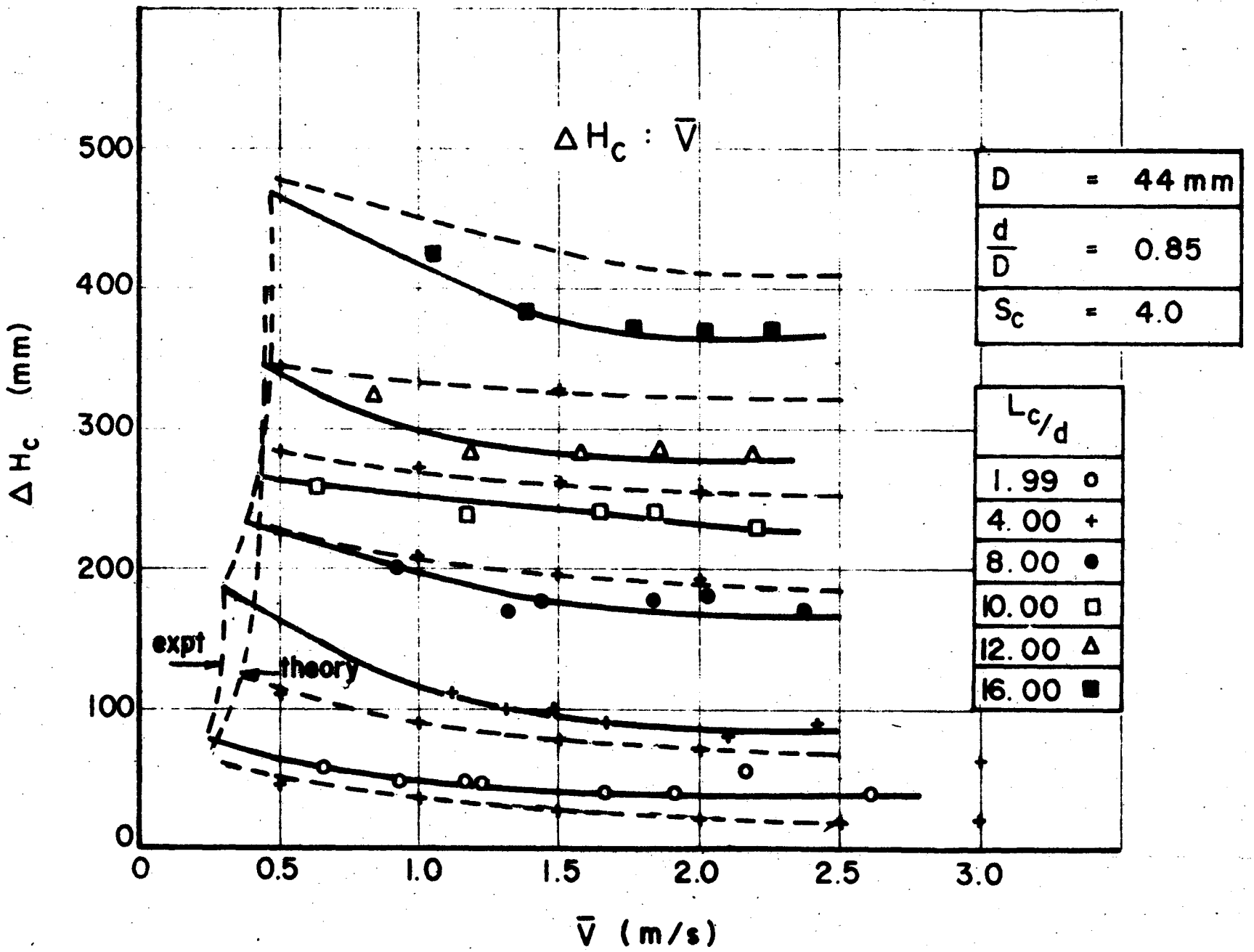
$\Delta H_c : \bar{V}$
ΔH_c (mm)
$\bar{V}$ (m/s)
0
100
200
300
400
500
0
0.5
1.0
1.5
2.0
2.5
3.0
expt
theory
D = 44 mm
d/D = 0.85
S_c = 4.0
L_c/d
1.99 o
4.00 +
8.00 ●
10.00 □
12.00 △
16.00 ■

FIG. 15.15

FIG. 15.16

D = 44 mm S_c = 4.0

$\frac{d}{D}$ = 0,85 Slope = 0,0 %

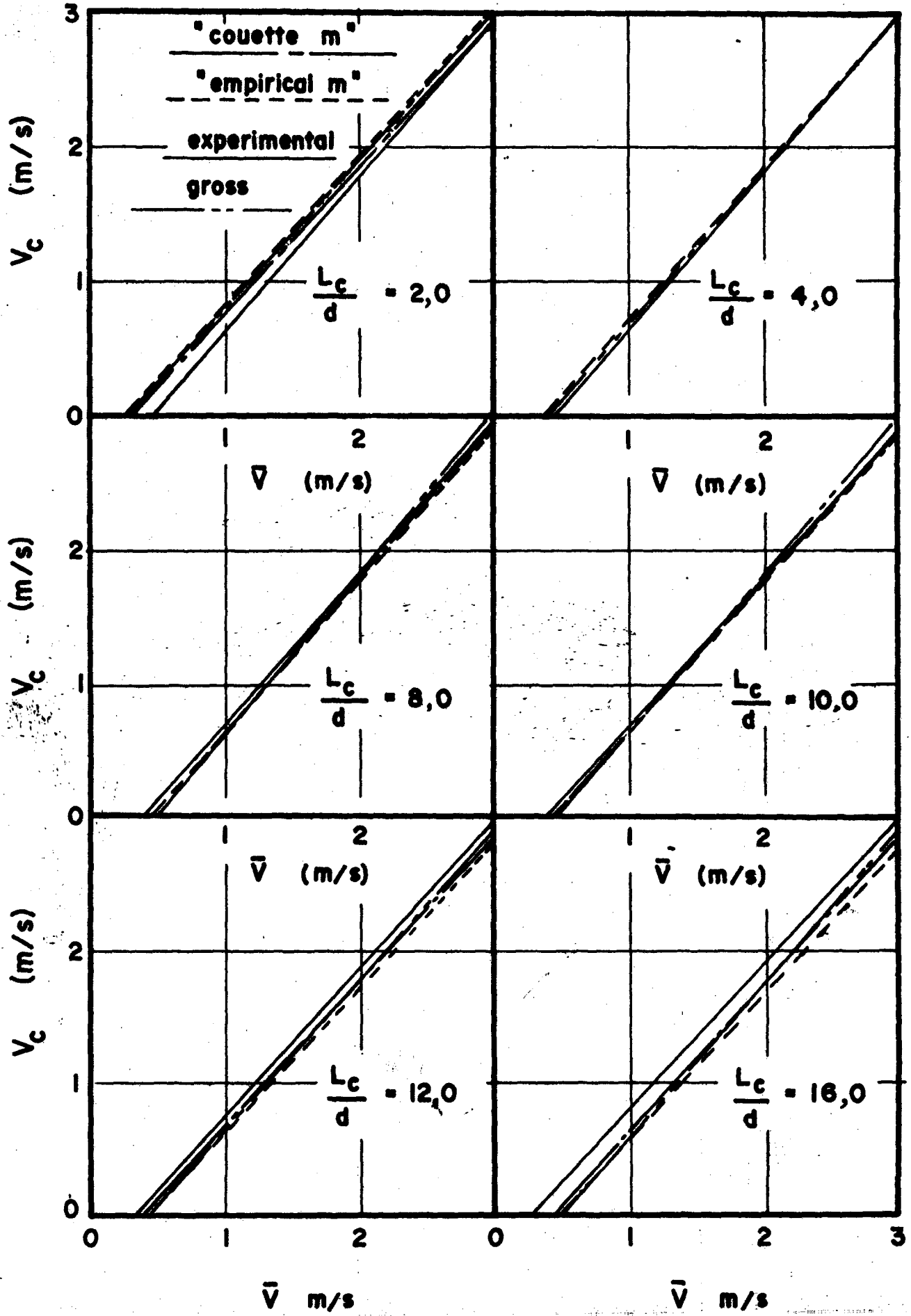

reduced, until at $L_c/d = 4,0$ and $2,0$ the empirical value of V_c is above the experimental value.

As can clearly be seen on Figure 15.16 the V_c discrepancies are extremely small compared with the errors generated on Figure 15.15 (i.e. up to about 12%) when calculating ΔH_c.

As with the different SG and d/D capsules discussed earlier, the gross analysis was also attempted for the capsules shown on Figure 15.15, and except for the lower L_c/d ratio capsules (L_c/d 8,0) the agreement was not as satisfactory as the finite element "empirical m" analysis.

The capsule velocity versus mean water velocity curves shown on Figure 15.16 include those analytical results derived from the "gross analysis" (i.e. calculated capsule velocities to ensure that experimental ΔH_c values are obtained). In no instance is the error more than a few percent. But the curves do have a slightly different slope from experimental and other analytical curves.

It is, thus, concluded that the gross method, besides being analytically less precise than the finite element method, yields less satisfactory results particularly for high L_c/d capsules.

5. The individual components of excess head loss: gross analysis

The results of the gross analysis are shown on Figures 15.5 and 15.6 and the gross analysis using experimental values of V_c has been shown to give slightly better agreement with the experimental ΔH_c curve than the finite element analysis using experimental values of V_c and slightly worse than when using empirical values of V_c. The analytical value of $\Delta H_c = 92,4$ mm lying 18.25% lower than the mean experimental curve at $\overline{V} = 1,5$ m/s (see Figure 15.5), V_c needing to be 3,94% higher for the curves to coincide. In this case the excess head loss has four components.

Δh_i, Δh_o, Δh_{shp} and Δh_{shc} where

$$\Delta h_{shp} = \frac{\bar{\tau}_p D 4 L_c}{w(D-d)^2}$$

$$\Delta h_{shc} = \frac{\bar{\tau}_c d 4 L_c}{w(D-d)^2}$$

The values of $\bar{\tau}_p$ and $\bar{\tau}_c$ are different from those obtained using the finite element analysis

$\bar{\tau}_p$ is a function of $\bar{V}_{am}$

and $\bar{\tau}_c$ is a function of $V_r = \bar{V}_{am} - V_c$

The foundations of this analytical procedure are less secure than for the finite element analysis. The reason being that average shear stress on the pipe wall is assumed to be a function of the average water velocity in the annulus relative to the pipe wall, and the average shear stress on the capsule is assumed to act forwards and is a function of the average velocity in the annulus relative to the capsule wall. We know from the finite element analysis that the average shear stress on the capsule actually acts backwards, retarding capsule motion.

Although the gross method of analysis is altogether oversimplified and cruder than the finite element analysis, because of the assumptions inherent in the analysis, it does yield results of almost comparable accuracy with the finite element analysis using empirical values of capsule velocity, but only in certain cases. It is, of course, very much simpler to use than the finite element of analysis.

Figure 15.17 shows the role played by the four components of ΔH_c to give the experimental curve on Figure 15.5 using the gross method of analysis. This results in capsule velocities which are slightly lower than those determined experimentally (see Figure 15.6).

The details of why small changes in V_c make such large changes in

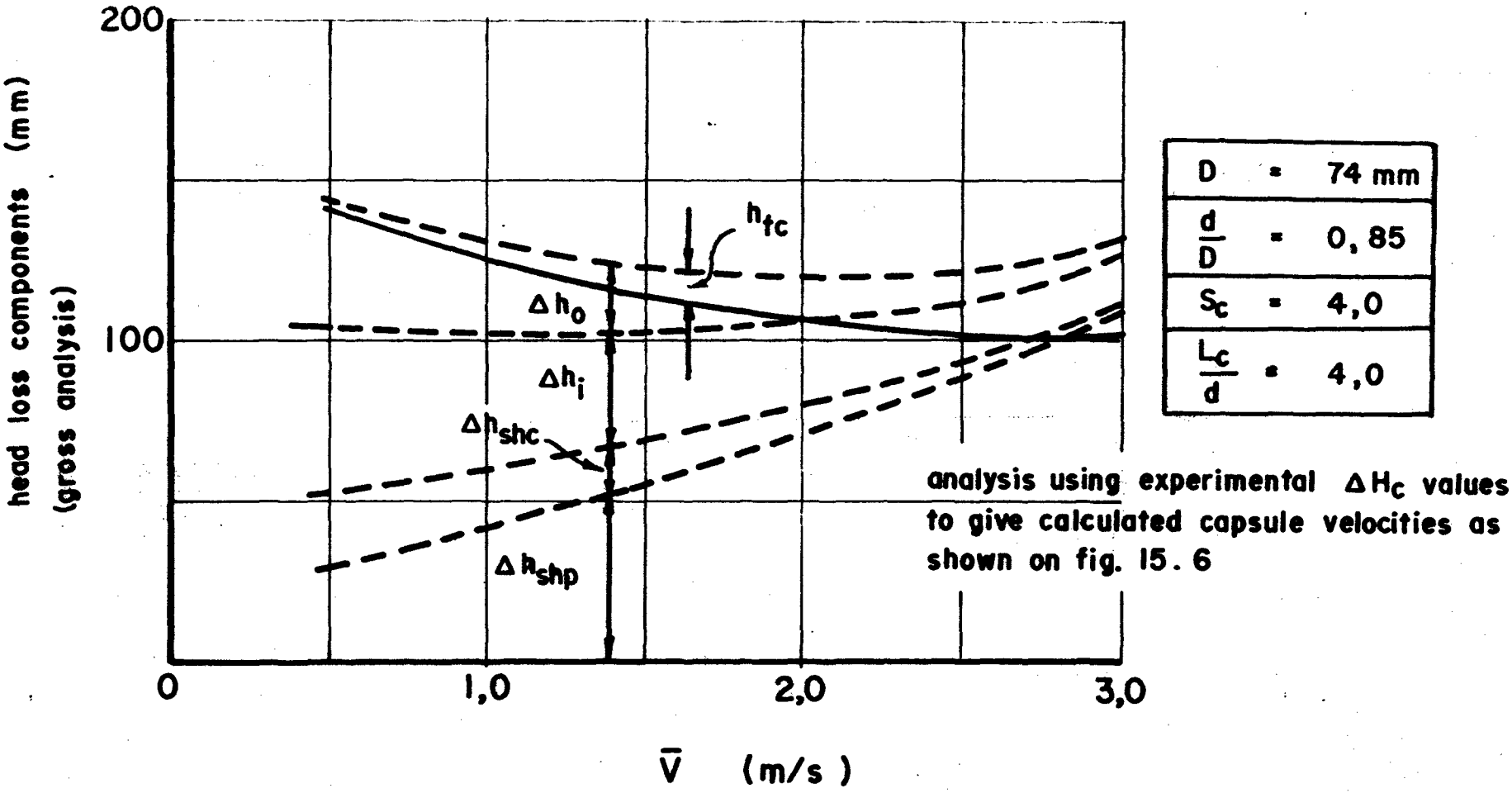
200
100
0
1,0
2,0
3,0
head loss components (mm)
(gross analysis)
$\bar{V}$ (m/s)
h_{fc}
Δh_o
Δh_i
Δh_{shc}
Δh_{shp}
D = 74 mm
$\frac{d}{D}$ = 0,85
S_c = 4,0
$\frac{\Gamma_c}{d}$ = 4,0
analysis using experimental ΔH_c values to give calculated capsule velocities as shown on fig. 15.6

FIG. 15.17

ΔH_c are largely due to inlet and outlet losses and will be discussed in the next section. However, the values of Δh_{shp} and Δh_{shc} do play a considerable part since

$$\Delta h_{shp} = \text{function } (f_{aw} \overline{V}_{am}^2)$$

$$= \text{function } (\overline{V}_{am}^{1,75})$$

and $$\Delta h_{shc} = \text{function } (f_{ac} \times V_r^2)$$

$$= \text{function } (V_r^{1,25})$$

where $$\overline{V}_{am} = \frac{\overline{V} - V_c(d/D)^2}{1 - (d/D)^2}$$

and $$V_r = \overline{V}_{am} - V_c$$

Thus, Δh_{shp} and Δh_{shc} can be represented as functions of $\overline{V}_{am}$ and V_r respectively, see Figure 15.18, and it can be shown how small changes in capsule velocity are reflected as large changes in ΔH_c. Note that, generally, as the mean water velocity increases the value of $\overline{V}_{am}$ increases and the value of V_r decreases.

This is not dealt with in detail here since the gross method is not as precise a tool as the finite element method for calculating ΔH_c. The way in which small changes in capsule velocity affect large variations in the individual components of ΔH_c is rather dealt with for the finite element analysis.

6. The individual components of excess head loss (in the finite element analysis)

Small errors in the calculation (or measurement) of V_c, have a large effect on ΔH_c. This is explained below by considering the separate components of ΔH_c.

Consider Figure 15.5 and the experimental values of ΔH_c which lead to the "Couette m" values of capsule velocity shown on Figure 15.6.

FIG. 15.18

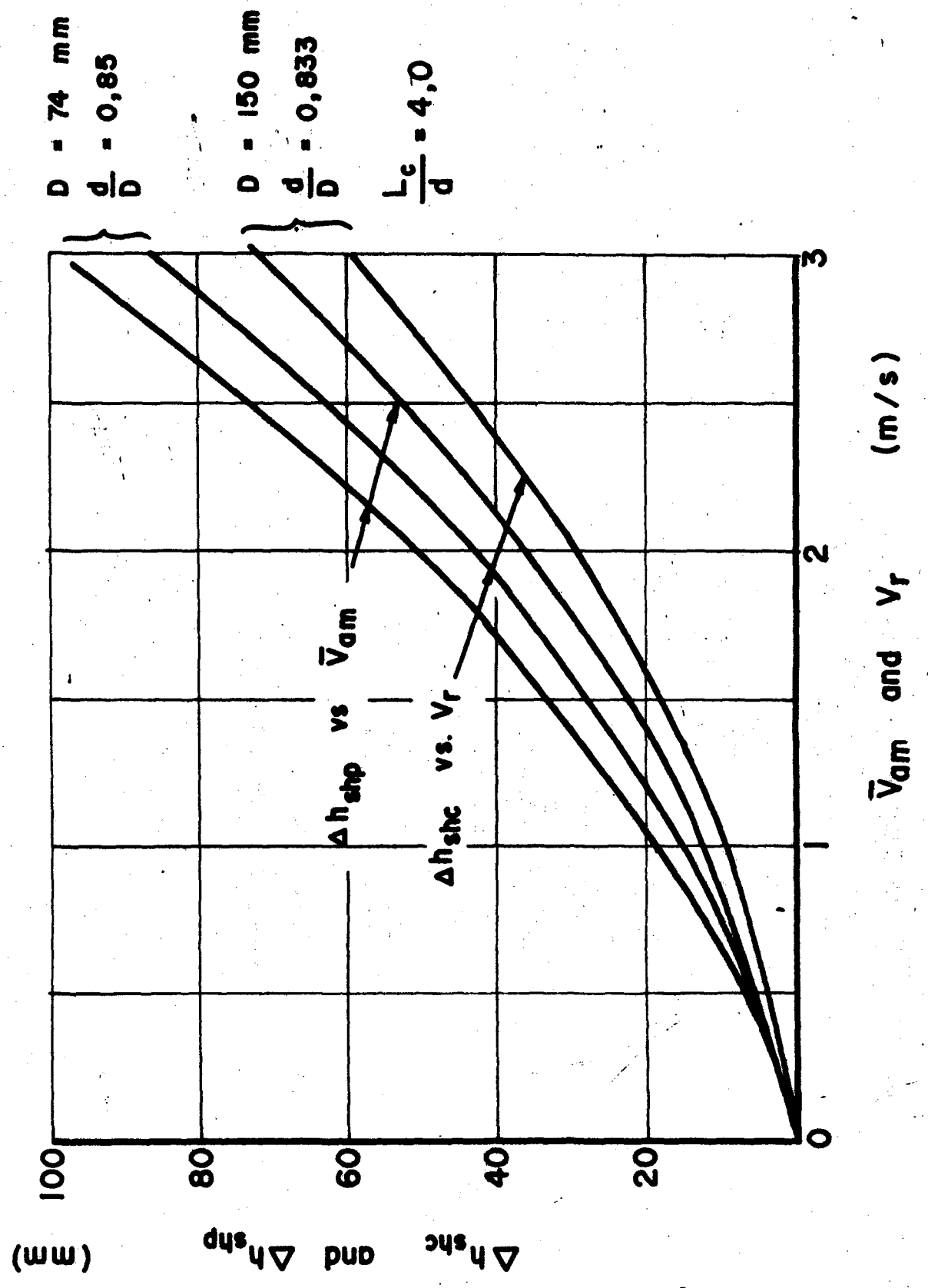
D = 74 mm
d/D = 0,85
D = 150 mm
d/D = 0,833
L_c/d = 4,0
Δh_{shp} vs $\bar{V}_{am}$
Δh_{shc} vs. V_r
Δh_{shc} and Δh_{shp} (mm)
100
80
60
40
20
0
1
2
3
$\bar{V}_{am}$ and V_r (m/s)

It has already been pointed out (Section 2) that if V_c were 3,43% higher the "empirical m" analysis would yield ΔH_c values (determined by the finite element analysis) which coincide with experimental values. In other words the "empirical m" calculation for V_c is 3,43% lower than the "Couette m" analysis.

Figure 15.19 shows the three separate components of ΔH_c, i.e. Δh_i; Δh_o and $\Delta h_a = \Delta h_{fa} - h_{fc}$. At $\overline{V}$ = 1,5 m/s (for example) Δh_i is 29,3% of ΔH_c, Δh_o is 16.7% of ΔH_c and Δh_a is 54,0% of ΔH_c.

As the mean water velocity ($\overline{V}$) decreases, the influence of Δh_{fa} (and h_{fc}) diminish whilst the influence of Δh_i and Δh_o is accentuated. These effects are clearly shown on Figure 15.20, which also shows the individual components of ΔH_c calculated from empirical and experimental capsule velocities. The difference between the individual components (i.e. Δh_{fa}, Δh_i and Δh_o) as calculated from "Couette m" analysis and "empirical m" analysis is due to a 3,43% difference in the value of V_c (at $\overline{V}$ = 1,5 m/s). The component h_{fc} has not been shown on Figure 15.20 because the discussion is essentially concerned with the way in which small changes in V_c affect large changes in ΔH_c and h_{fc} is not affected by V_c.

Figures 15.21 and 15.22 show Δh_{fa}, which is a function of $\overline{V}_{ap}$, and Δh_i and Δh_o, which are functions of $(\overline{V} - V_c)$. For the "Couette m" analysis at $\overline{V}$ = 1,5 m/s; V_c = 1,221 m/s whilst the empirical value of V_c = 1,179 m/s and the experimentally measured value of V_c = 2,27 m/s.

Each of the three components on Figures 15.21 and 15.22 can now be discussed separately:

6.1 Inlet head loss (Δh_i)

For the "Couette m" analysis $(\overline{V} - V_c)$ = 0,279 m/s yielding Δh_i = 33,5 mm. Changing V_c by -3,43% alters the value of $(\overline{V} - V_c)$

FIG. 15.19

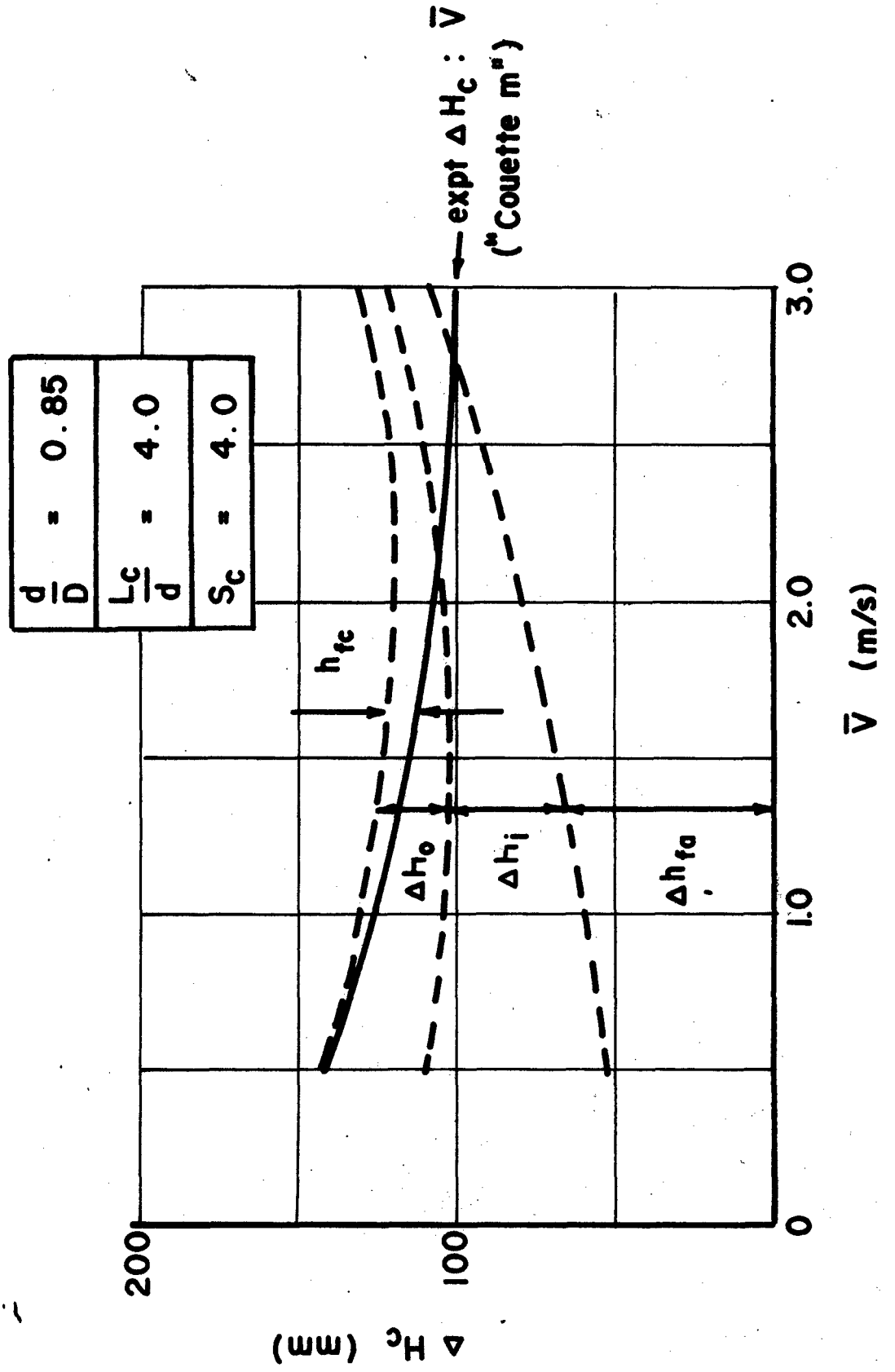
expt ΔHc : V̄
("Couette m")
d/D = 0.85
Lc/d = 4.0
Sc = 4.0
hfc
Δho
Δhi
Δhfo
200
100
0
1.0
2.0
3.0
V̄ (m/s)
Δ Hc (mm)

FIG. 15.20

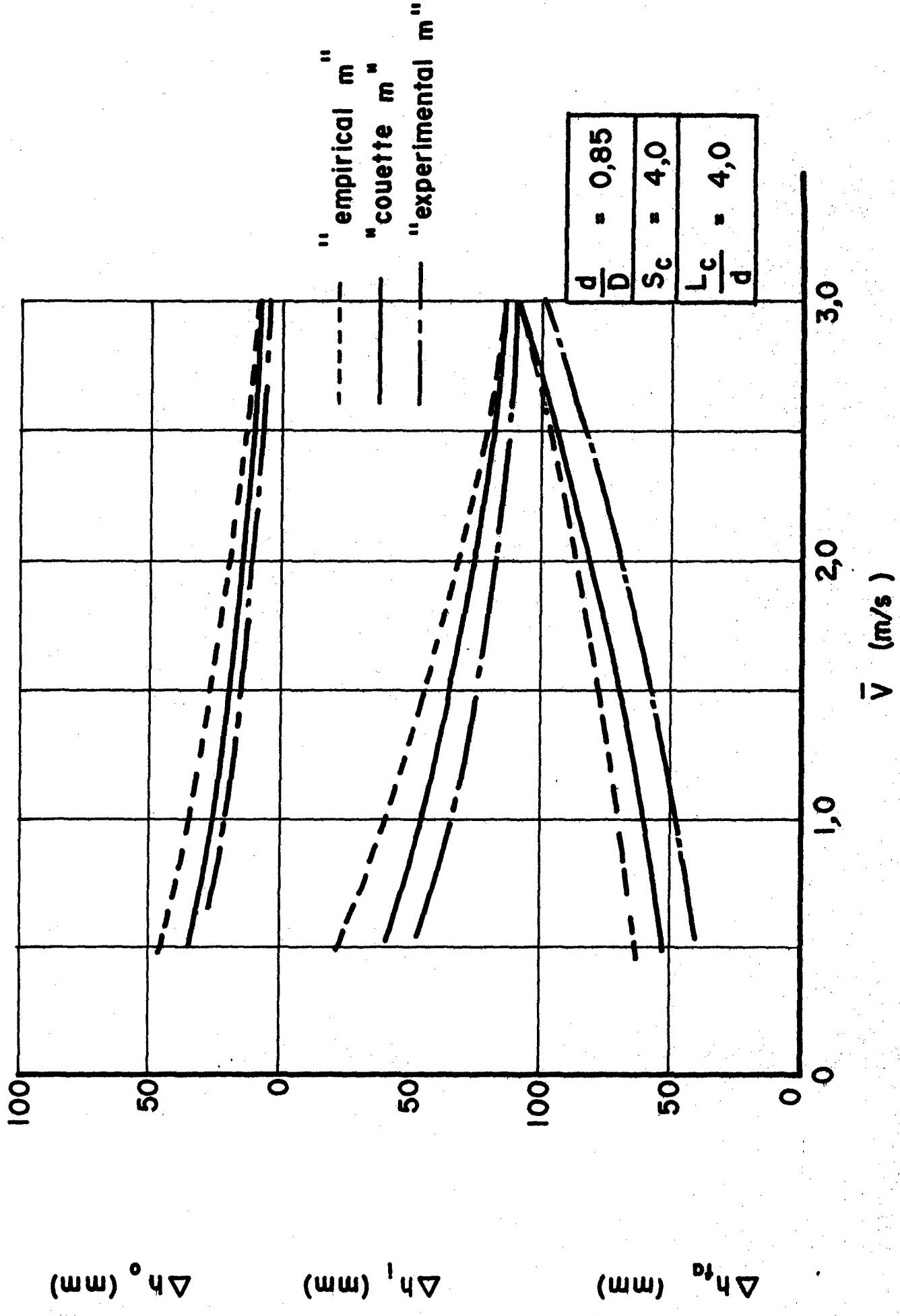
"empirical m"
"couette m"
"experimental m"
d/D = 0,85
Sc = 4,0
Lc/d = 4,0
100
50
0
50
100
50
0
0
1,0
2,0
3,0
V̄ (m/s)
Δh_fa (mm)
Δh_i (mm)
Δh_o (mm)

FIG. 15.21

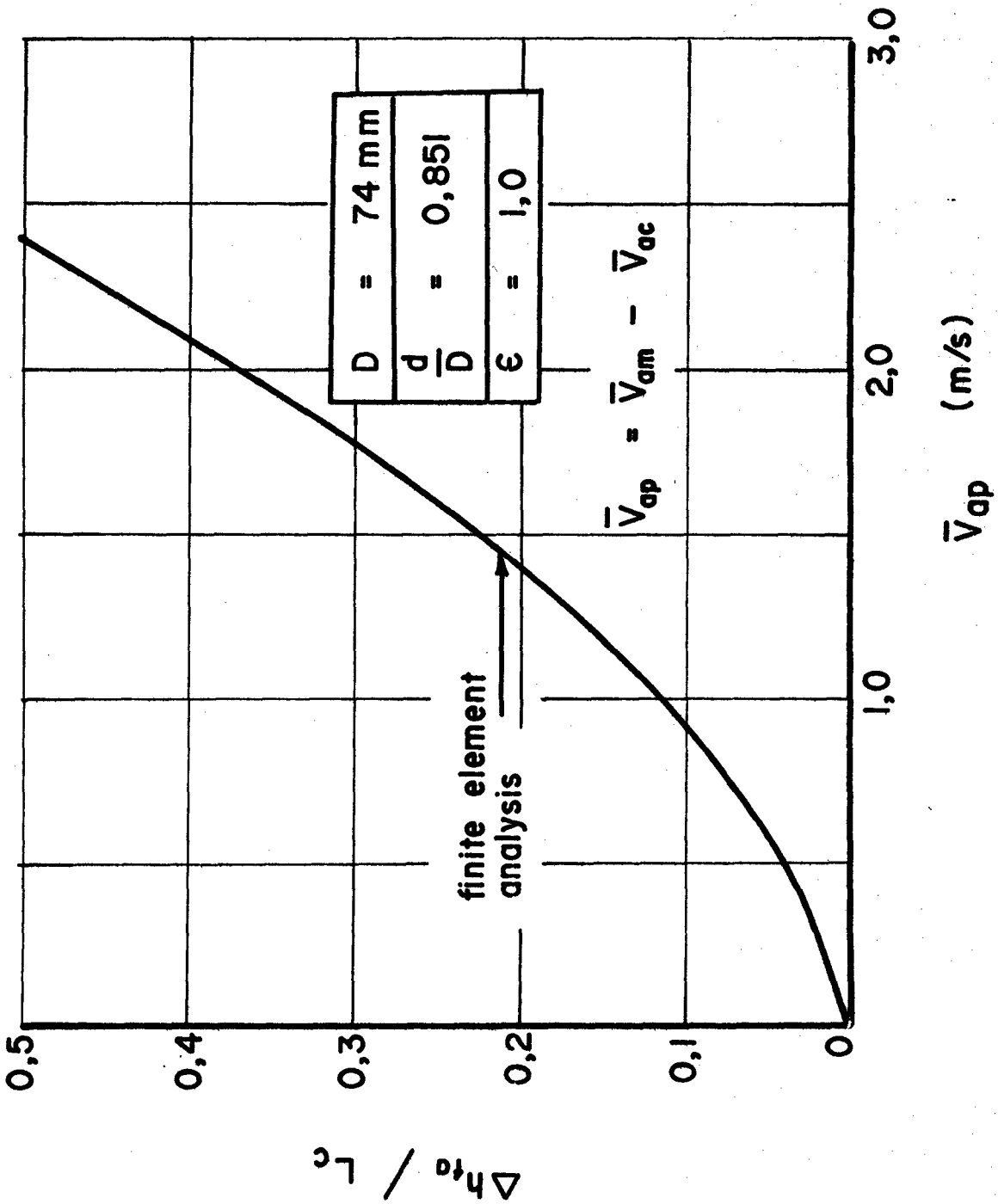
D = 74 mm
d/D = 0,851
ε = 1,0
$\bar{V}_{ap} = \bar{V}_{am} - \bar{V}_{ac}$
finite element analysis
0
0,1
0,2
0,3
0,4
0,5
1,0
2,0
3,0
$\bar{V}_{ap}$ (m/s)
$\Delta h_{fa} / L_c$

FIG. 15.22

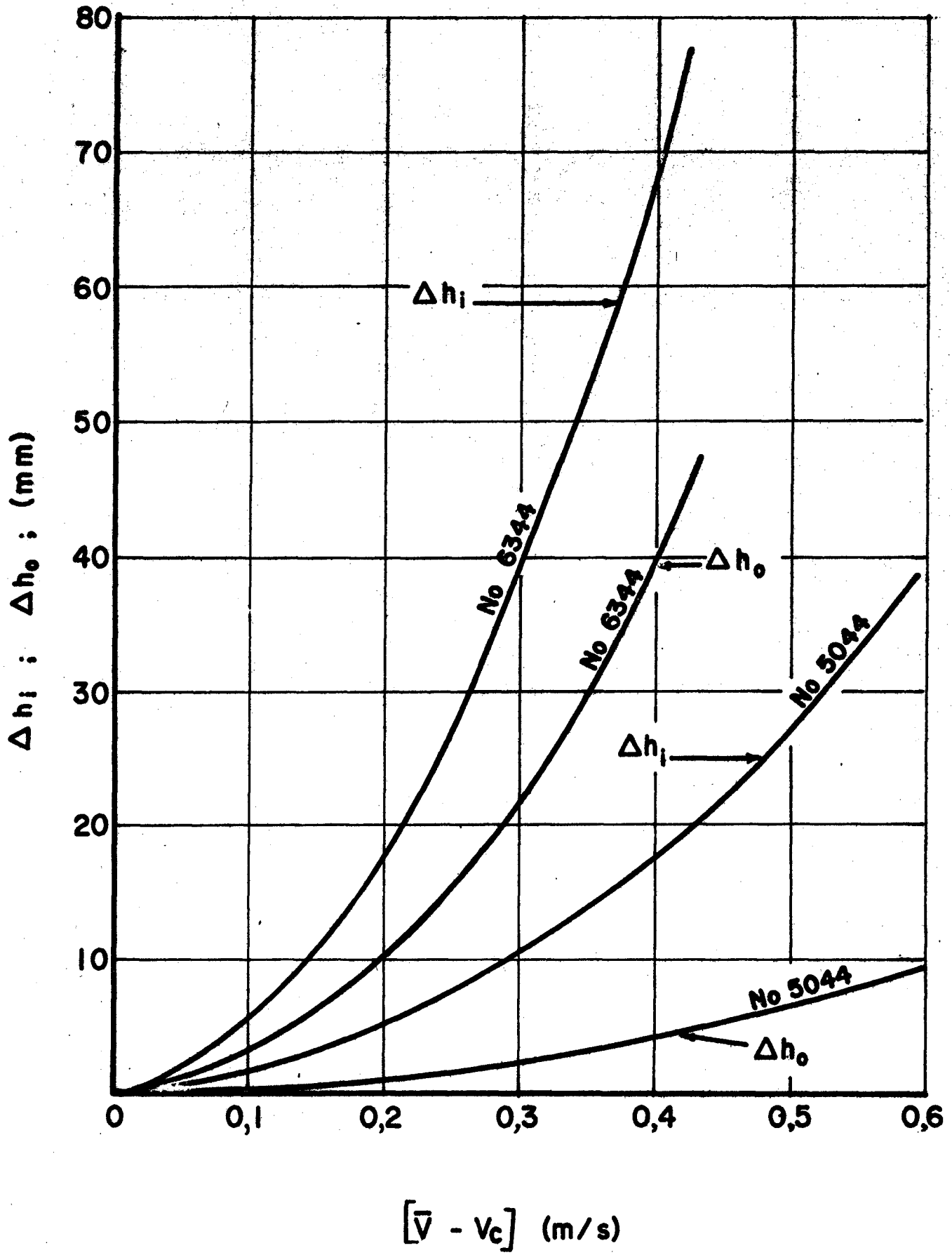
80
70
60
50
40
30
20
10
0
0,1
0,2
0,3
0,4
0,5
0,6
Δhi ; Δho : (mm)
[V̄ - Vc] (m/s)
Δhi
Δho
No 6344
No 6344
No 5044
Δhi
No 5044
Δho

to 0,321 m/s (i.e. a 15% increase) and this gives Δh_i = 44,5 mm; approximately a 30% increase.

6.2 Outlet head loss (Δh_o)

The same (-3,34%) reduction of V_c to yield the empirical value of V_c causes Δh_o to increase from 19,1 mm to 25,4 mm, somewhat more than a 30% increase (33%).

Since both Δh_i and Δh_o are, in fact, functions of $(\overline{V} - V_c)^2$, a 15% error in calculating or measuring the difference $(\overline{V} - V_c)$ should yield a 30% error in Δh_i and Δh_o.

6.3 Annular head loss (Δh_{fa})

The pressure flow component of velocity ($\overline{V}_{ap}$) is a function of V_c thus,

$$\overline{V}_{ap} = \overline{V}_{am} - \overline{V}_{ac}$$

$$= \frac{\overline{V} - V_c(d/D)^2}{1 - (d/D)^2} - f(V_c)$$

and for the situation under consideration $\overline{V}_{ac}$ = 0,454 V_c (see equation (7.178)). This relation is obtained from the finite element analysis.

It is clear from the equation above that the alteration of -3,43% in the value of V_c causes an increase of 7,88% in the value of $\overline{V}_{ap}$, i.e. from $\overline{V}_{ap}$ = 1,676 m/s to $\overline{V}_{ap}$ = 1,808, and this results in an increase in the value of Δh_{fa}, determined from the finite element analysis for pressure flow, from 69,2 mm to 78,9 mm (i.e. +14%).

The changes in the three components of ΔH_c can be seen graphically on Figures 15.21 and 15.22 and are summarised in Table 15.2

T A B L E 15.2

$\overline{V}$ = 1,5 m/s; d/D = 0,85; S_c = 4,0; L_c/d = 4,0			
Analysis	"Couette m"	"empirical m"	"experimental m"
V_c(m/s)	1,221	1,179	1,270
$\Delta V_c/V_c$(%)	-3,43%	+4,0%	
$(\overline{V}-V_c)$(m/s)	0,279	0,321	0,230
$\Delta(\overline{V}-V_c)/(\overline{V}-V_c)$(%)	+15%	-17,5%	
Δh_i	33,5	44,5	22,8
$\Delta(\Delta h_i)/\Delta h_i$	+30%	32%	
Δh_o	19,1	25,4	13,0
$\Delta(\Delta h_o)/\Delta h_o$	+33%	32%	
Δh_{fa}	69,2	78,9	58,7
$\Delta(\Delta h_{fa})/\Delta h_{fa}$	+14%	15,2%	
ΔH_c	114,4	141,3	87,1
$\Delta(\Delta H_c)/\Delta H_c$	+23,5%	-23,8%	

At $\overline{V}$ = 1,5 m/s the values of Δh_i and Δh_o, although less than that of Δh_{fa}, increase by about twice as much as Δh_{fa} for the 3,43% change in the value of V_c.

7. Assumption inherent in the analysis

Although the analytical theories, using the finite element analysis and quasi concentric polar co-ordinates, are in reasonable agreement with experiment there are certain instances, particularly low density capsules, where agreement is not so satisfactory.

There are basically two reasons for discrepancies between analytically derived results and experimental data. The first is due to experimental error, the sources of which have been discussed in Chapter 6. The

second reason for discrepancy is the various assumptions in the mathematical model which has been used to describe the phenomenon. These assumptions will be discussed below.

7.1 Geometry

The geometry of the eccentric annulus was rendered amenable to analysis by assuming that small slices of the annulus were concentric. An alternative geometry, bi-polar co-ordinates, involved curved slices and it was felt (see Chapter 7, Section 2.3) that this geometry had no advantages over the quasi-concentric polar co-ordinates. If slices are made small enough this should not constitute a serious source of error.

The half annulus was divided up into one hundred slices for all the analyses. Computer runs with fewer slices were tried and even as few as fifty slices made little difference to the results. Each slice (in turbulent flow) was divided into one hundred segments and the geometry of a quasi-concentric slice distorts each sub-slice slightly. This is also not considered to be a serious source of error.

The method of quasi-concentric polar co-ordinates was validated by analysing turbulent pressure flow in the eccentric annulus, and comparing with experimental results (Chapter 13) and by analysing laminar pressure flow and comparing with different analyses.

7.2 Results of plane Couette flow used in curved Couette flow

Experimentally determined velocity profiles and shear stress values in plane Couette flow were assumed to apply to curved Couette flow. This assumption is associated with the quasi-concentric annular slices and it would be extremely difficult to carry out experiments in curved Couette flow on a large enough scale to determine shear stresses and velocity profiles.

7.3 Static friction coefficient (μ_f) equal to kinetic friction coefficient

This assumption affects the evaluation of forces acting on the capsule (discussed in Chapter 8), and seems reasonable for the relatively low velocities involved (see discussion on friction in Chapter 8).

7.4 No lift at incipience

The incipient velocity is required for calculating the semi-empirical value of capsule velocity, and although the lift force at incipience may be slight, compared with the submerged weight of a capsule, it nonetheless exists.

7.5 The addition of velocity and shear stress components due to Couette and pressure flow in the annulus

The algebraic sum of two components of flow, i.e. pressure flow when the capsule is fixed, and Couette flow due to the motion of the capsule relative to the pipe wall has been shown to be valid in laminar flow (in Chapter 7). The shear at any point on the capsule pipe wall is the algebraic sum of the Couette and pressure components. This statement has also been validated in Chapter 7 for concentric laminar flow.

The assumption is that the addition of velocity and shear components, due to pressure and Couette flow, is valid in turbulent flow as well as laminar flow.

7.6 Energy dissipation at inlet and outlet of a static capsule applies in the mobile capsule case

The inlet and outlet head loss coefficients were determined experimentally, with static capsules, as functions of $(\overline{V})$, which is the mean velocity of the water relative to the capsule. The assumption is that the same inlet and outlet head loss coefficients apply if the capsule is mobile and the head losses are made functions of the velocity relative to the capsule $(\overline{V} - V_c)$. This is equivalent to the superposition of a velocity (V_c), in the reverse direction, on the whole system.

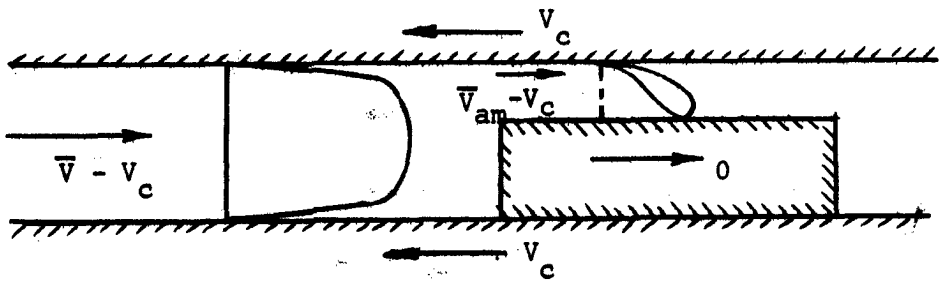

Figure 15.23

The assumption that Δh_i and Δh_o are functions of $(\overline{V} - V_c)$ and that the same head loss coefficients apply, implies that the backward wall movement of the pipe does not affect the shape of the velocity distribution. This assumption is valid in the pipe. Velocity distributions are, however, distorted in the annulus. The only justification for the assumption is the ultimate agreement between analytical and experimental results.

7.7 Lines of neutral shear occur along quasi-concentric radii

This is true for concentric annuli. However, for eccentric annuli the dotted neutral shear lines or zero relative shear lines (see Figure 7.28) are not straight lines along radii, although towards the top of the annulus the assumption becomes increasingly valid. Towards the bottom of the annulus Jonsson and Sparrow have shown curved neutral shear lines.

The direction of curve is such that quasi-concentric radii approach the curved neutral shear lines, on Figure 7.28, more closely than bi-polar co-ordinates, which curve in the opposite sense to the curvature of the neutral shear lines.

7.8 Change from laminar to turbulent flow may occur at a different position around the annulus for pressure and Couette flow

The Reynolds number criterion could imply change from laminar to turbulent flow for one of the components before the other. This gives a zone which is laminar for one component and turbulent for the other, which is obviously impossible, although the zone was found to extend over

only a small angle (θ).

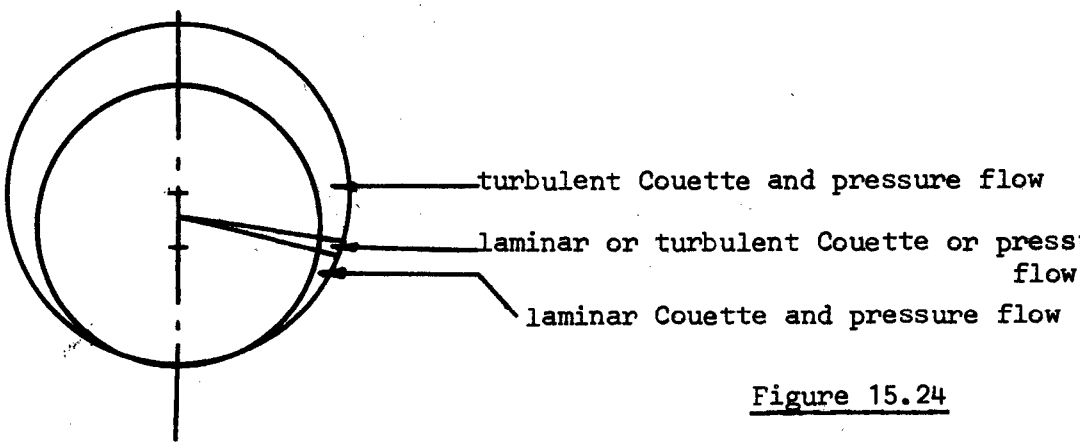

Figure 15.24

It is possible that the transition zone may occur over a wider range of Reynolds numbers for combined pressure and Couette flow than for each of the individual components separately.

7.9 Reynolds number criterion

The change from laminar to turbulent flow was assumed to occur at a specific Reynolds number for laminar flow. It is well known (in circular pipes) that the transition region occurs over a range of Reynolds numbers.

The Reynolds number, for pressure flow, at which the flow becomes turbulent in a quasi-concentric annular slice was assumed to correspond to the critical Reynolds number at which flow ceases to be laminar in a concentric annulus.

The Reynolds number for Couette flow, at which flow becomes turbulent in a quasi-concentric annular slice, was assumed to correspond to the Reynolds number at which flow ceases to be laminar in plane Couette flow.

7.10 Force on capsule wall equals force on pipe wall for Couette flow component

The assumption that the curved Couette flow component is unassociated with any pressure drop in the annulus (in circular Couette flow there cannot be any pressure gradient) implies (as was shown in Chapter 7 by applying the total force concept) that the shear force on capsule and

pipe wall must be equal.

This leads to the (valid) assumption that the pressure gradient in the annulus is entirely attributed to the pressure flow component.

7.11 Shear stress on capsule wall equals the shear stress on the pipe wall in pressure flow

This assumption was made in the incipient capsule analysis and is not quite valid (see Figure 8.13 Chapter 8) for concentric annuli. Although for large diameter ratios the errors are not large. This point has been dealt with in Chapters 7 and 8.

7.12 Velocity profiles in concentric annuli assumed to apply to quasi-concentric annuli

The velocity profiles established by Knudsen and Katz for pressure flow in concentric annuli were used in the finite element analysis for eccentric annuli. The validation of this assumption is the agreement with experimental results (see Chapter 13). The force balance equation for pressure flow in the annulus led to the determination of shear on pipe and capsule walls.

For concentric annuli the ratio of these average values are not in full accord with measured values (as discussed above). The errors involved are not likely to be large.

7.13 Fully developed flow assumed in the annulus

Both for pressure and Couette components of flow in the annulus, it was assumed that fully developed flow existed for the total length of a capsule. This is obviously not valid. However, for pressure flow, the pseudo hydraulic mean radius concept determined experimentally for static capsules was found to agree well with the finite element analysis, and experimental values embraced the developing regions towards the ends of the capsule.

The developing regions for pressure flow in the annulus as

well as the developing zones for inlet and outlet losses in the capsule free pipe, and the annulus, were all absorbed into the values for inlet, outlet and annular losses.

Therefore, the only effective assumption in this case is that Couette flow, and shear stresses due to Couette flow, are constant along the length of a capsule.

7.14 Capsule axis parallel to pipe axis

The analysis implies that a constant annular section is maintained along the length of a capsule, and that the capsule always remains with its prescribed eccentricity.

As is shown (in Chapter 12) the capsules lift at increasingly higher velocities and at decreasing densities.

It is important to note that agreement between experimental and analytical results deteriorates as density decreases and generally towards high velocities.

When capsules lift, pitch or yaw, the analytical model is distorted.

7.15 No account taken of wedging action

Perhaps one of the most serious defects in the analysis is that forces are apparent, which have not been included in the analysis, when macroscopic lift occurs.

This situation is fully discussed in Chapter 8. An important force, inducing lift, is the lubricating film under a capsule. This affect is closely associated with the assumption mentioned (in 7.14 above) that capsule axes are parallel with the pipe and maintain their prescribed eccentricity.

Not only are there small geometrical modifications (mentioned in (7.14 above) but additional forces are brought into the picture.

7.16 No account taken of primary streamline curvature and secondary flow

It is shown in Chapter 12 that capsules do, indeed, lift. It is also shown in Chapter 8 that lift cannot occur if secondary flow and the lubricating film effect is absent. Although streamline curvature and secondary flow were not taken into account, as such, the static capsule tests on inlet, outlet and annular losses implicitly include these effects in the pressure flow component.

Secondary effects due to the Couette component of flow as well as due to the combination of Couette and pressure flow are not considered.

7.17 Irregularities and distortion

Any deviation from capsule or pipe circularity as well as any surface irregularities were not considered.

8. Empirical correlation of excess energy loss

The analysis using finite elements is extremely complex and requires a large computer for solution.

The gross analysis is a lot simpler although more empirical and less precise.

colloquial

These theories lead to a better understanding of the mechanics of flow around capsules and yield reasonable correlations with experimental data.

The next objective is to find a theory which yields even better results and which does not require enormous computer facilities. This is done empirically in this section. And correlations are found which are entirely satisfactory for design purposes, being simple to understand and use.

The empirical relation was arrived at somewhat intuitively by the author. Nonetheless, an attempt is made to give it a rational explanation.

It has already been shown (in Chapter 10) how all the variables can be accounted for with a kinematic correlation involving non-dimensional capsule and mean water velocity parameters.

The objective here is to correlate, for design purposes, excess energy losses across mobile capsules embracing all the variables.

The usual starting point for establishing non-dimensional parameters from experimental data where a large number of independent variables are involved, is dimensional analysis, and one such analysis has already been given for kinematic results.

The dependent variable in this case is the excess energy (or head) loss across the capsule. Thus,

$$\Delta H_c = f(\overline{V}, \frac{\Delta h_f}{L}, \rho_c, \rho, g, L_c, d, D, \phi, \mu_f) \qquad (15.1)$$

where $\Delta h_f/L$ = hydraulic gradient in capsule free pipe.

It has already been stated that a large number of variables increases the complexity of the problem manyfold. It has also been shown that the capsule length (L_c) was successfully absorbed by plotting the excess head loss to capsule length ratio $(\Delta H_c/L_c)$ against $\overline{V}$ and that slope can be accounted for by means of a subtractive term thus;

$$(\Delta H_c)_s = (\Delta H_c)'_s - (d/D)^2 L_c \sin \phi |S_c - 1|$$

A further aid for establishing the grouping of variables is that the submerged density ratio has proved more useful than the capsule density itself thus;

$$\frac{\rho_c - \rho}{\rho} = |S_c - 1|$$

The use of the absolute form of $|S_c - 1|$ has also been explained.

Equation (15.1) can thus be written as;

$$\Delta H_c/L_c = f_1(\Delta h_f/L, |S_c - 1|, d/D, L_c/d$$

$$\overline{V}/\sqrt{gD}, \rho\overline{V}D/\mu, \mu_f) \qquad (15.2)$$

Both the pipe "Froude number" and Reynolds number terms can have either the pipe or capsule diameter and the pipe or capsule velocity variables included.

There are many ways of grouping the parameters in equation (15.2) and by trying various groupings it was found that the non-dimensional parameters Γ and χ yielded most satisfactory results;

where $$\Gamma = \frac{\Delta H_c}{L_c} \frac{L}{\Delta h_f} \left[\frac{D}{d}\right]^2 \qquad (15.3)$$

and $$\chi = \overline{V}/\sqrt{gD|S_c - 1|} \qquad (15.4)$$

These parameters are similar to those used for correlating excess head loss at incipient capsule motion.

Equation (15.2) can be written as;

$$\Gamma = \chi\ f_2\ (\mu_f,\ \rho\overline{V}D/\mu,\ L_c/d) \qquad (15.5)$$

Figure 15.25 shows Γ on the ordinate plotted against χ on the abscissa (on logarithmic paper) for $d/D = 0{,}95$ and a range of specific gravity capsules. A large number of data points are represented.

The different specific gravities are successfully correlated by this method.

Figure 15.26 shows the same data plotted on an arithmetic scale to give an idea of the absolute scatter which in this case is minimal.

Figures 15.27 and 15.28 show that neither plotting ΔH_c against χ nor Γ against $\overline{V}$ successfully copes with the submerged density effect.

Since a wide range of capsule and pipe velocities are successfully incorporated into Figure 15.25, as well as a range of specific gravities, equation (15.5) can be written as

$$\Gamma = \chi\ f_3\ (L_c/d,\ \mu_f) \qquad (15.6)$$

The Reynolds number term is dropped since the viscosity of the fluid was held constant.

FIG.15.25

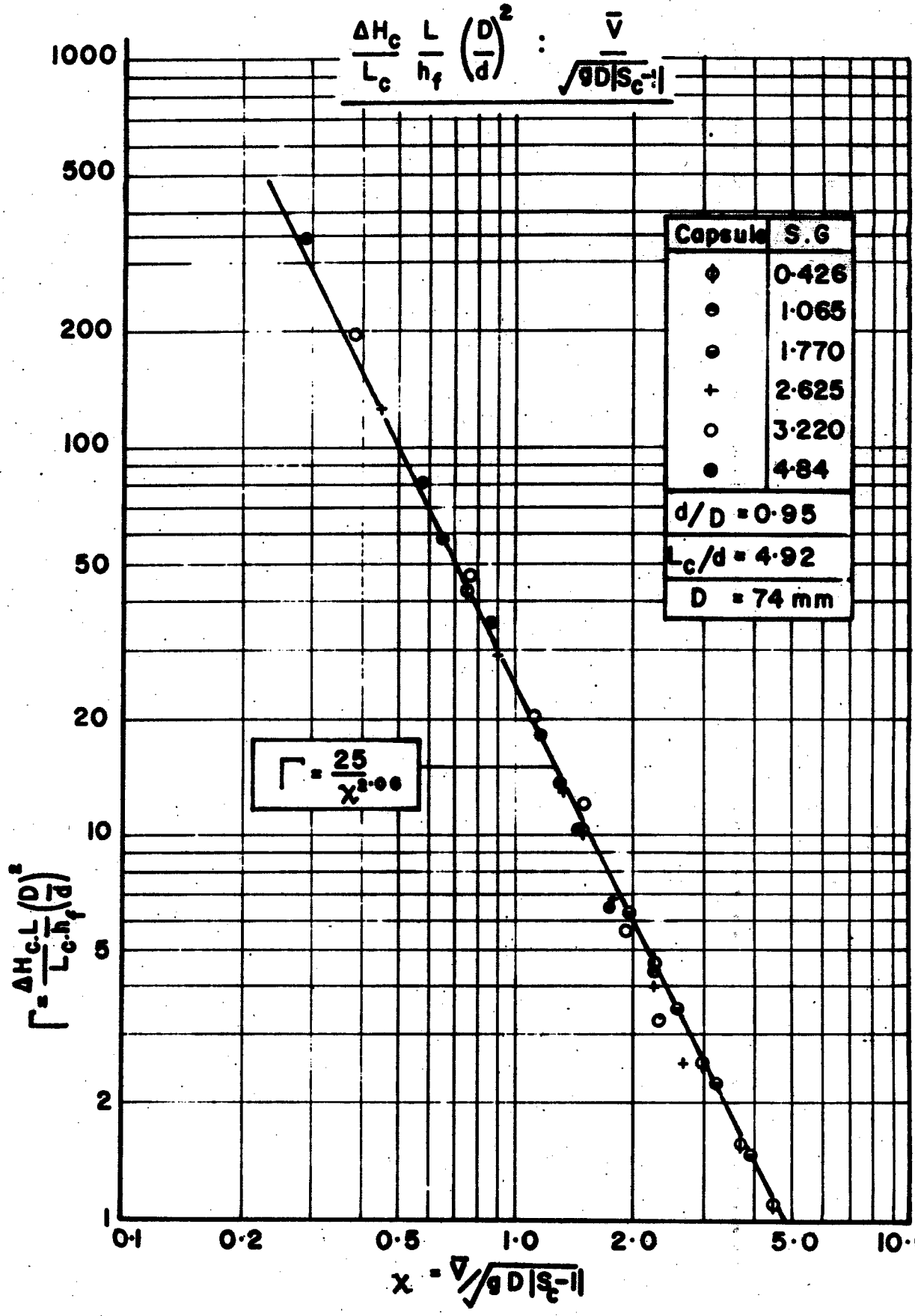
$\frac{\Delta H_c}{L_c}\frac{L}{h_f}\left(\frac{D}{d}\right)^2 : \frac{\bar{V}}{\sqrt{gD|S_c-1|}}$
1000
500
200
100
50
20
10
5
2
1
0·1
0·2
0·5
1·0
2·0
5·0
10·0
$\Gamma = \frac{\Delta H_c L}{L_c h_f}\left(\frac{D}{d}\right)^2$
$\chi = \frac{\bar{V}}{\sqrt{gD|S_c-1|}}$
$\Gamma = \frac{25}{\chi^{1\cdot06}}$
Capsule | S.G
Φ 0·426
1·065
1·770
+ 2·625
○ 3·220
● 4·84
d/D = 0·95
L_c/d = 4·92
D = 74 mm

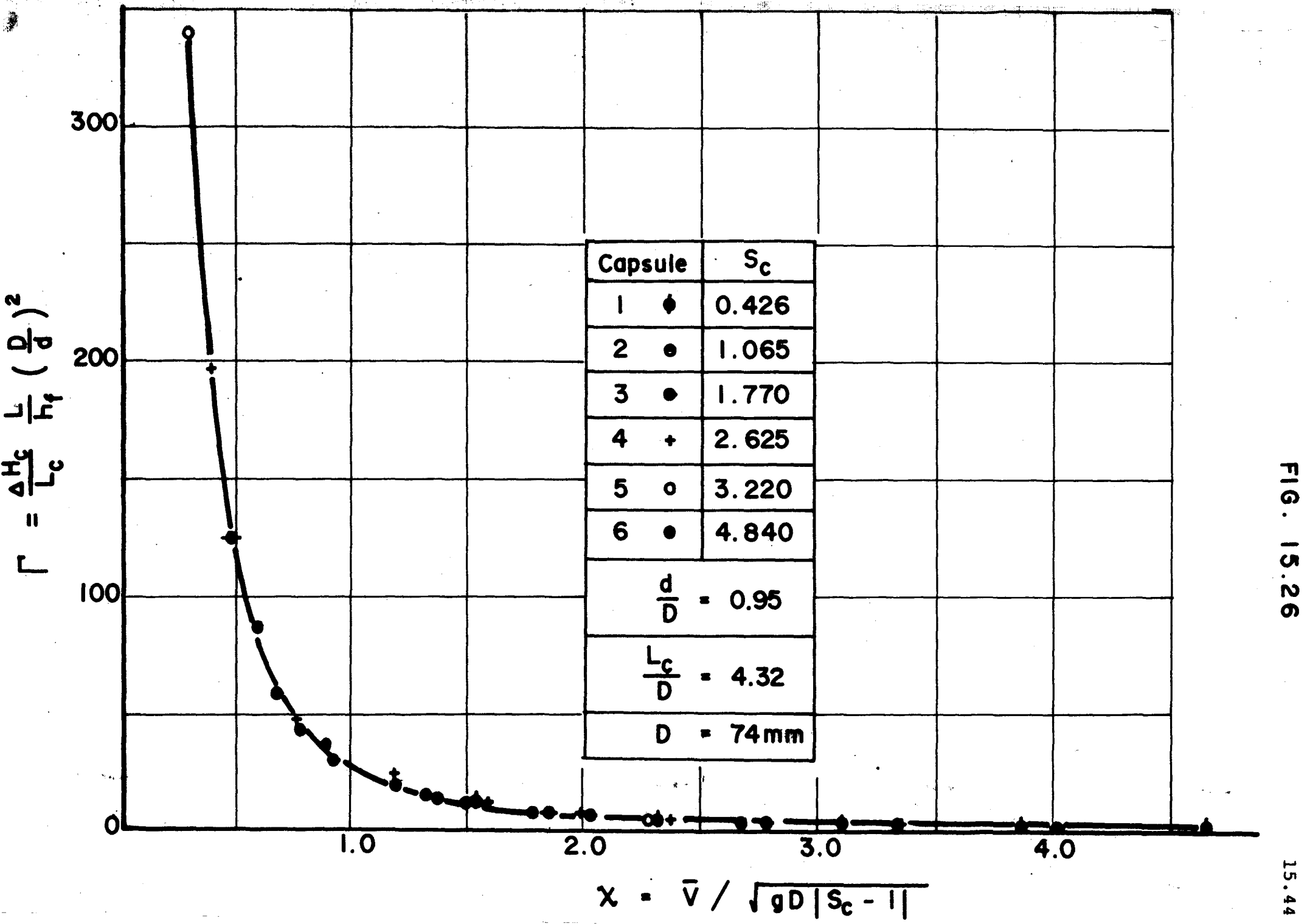
$\Gamma = \frac{\Delta H_c}{L_c} \frac{L}{H_f} \left(\frac{D}{d}\right)^2$
300
200
100
0
1.0
2.0
3.0
4.0
$\chi = \bar{V} / \sqrt{gD\,|S_c - 1|}$
Capsule
S_c
1 0.426
2 1.065
3 1.770
4 2.625
5 3.220
6 4.840
$\frac{d}{D} = 0.95$
$\frac{L_c}{D} = 4.32$
D = 74mm

FIG. 15.26

FIG. 15.27

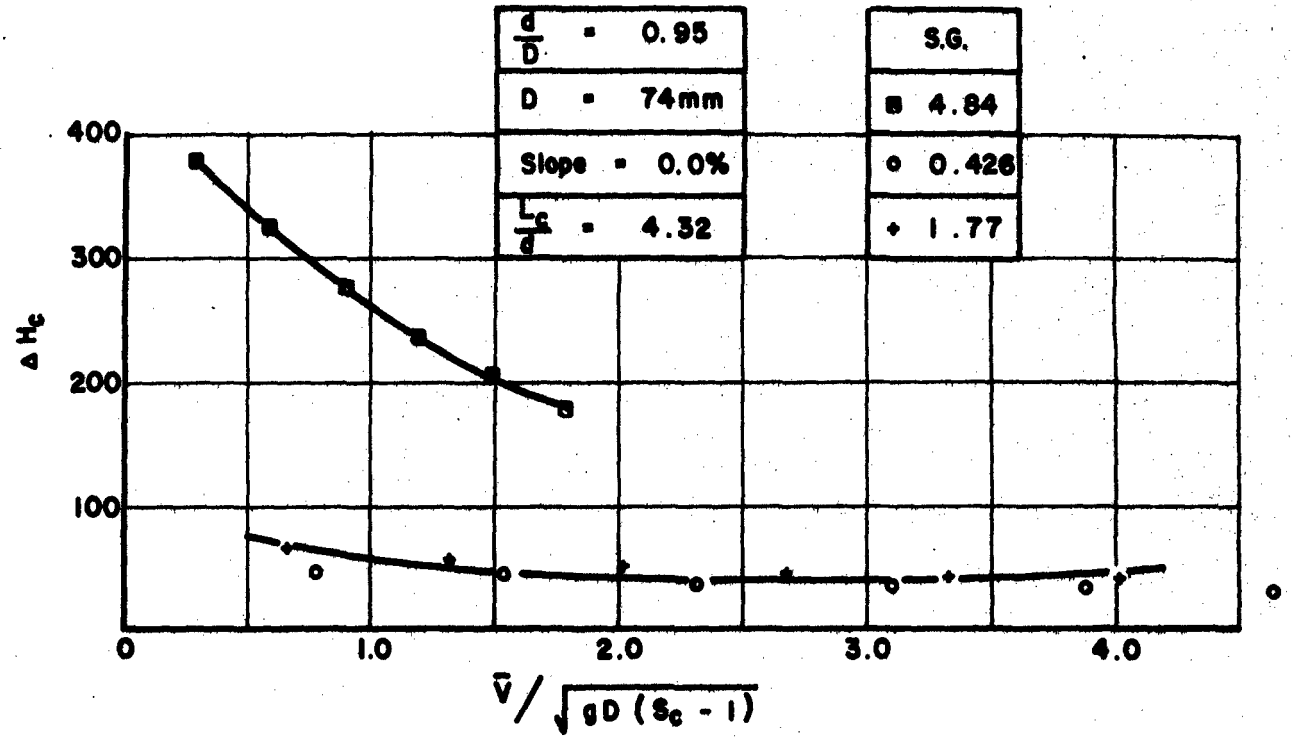

FIG. 15.28

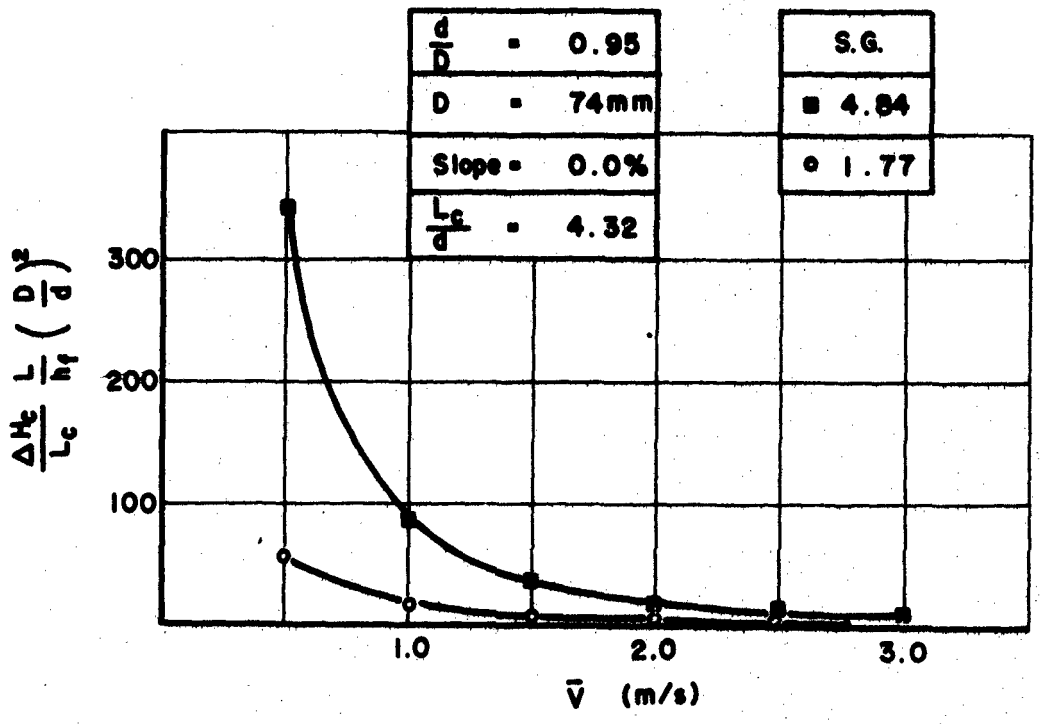

Figures 15.29, 15.30 and 15.31 show Γ plotted against χ on logarithmic paper for the other diameter ratios. The scatter is slight thus justifying the correlation. There does, however, appear to be a slight diameter ratio effect, and this is emphasised with the dimensionally similar capsules of $L_c/d = 4{,}0$ and constant specific gravity $S_c = 4{,}0$ shown plotted on Figures 15.32 to 15.35. These figures show up the linear logarithmic relation very clearly and are summarised in Figure 15.36, which emphasises the diameter effect. Figure 15.56, which is a composite plot of 15.25, 15.29, 15.30 and 15.31 does not display the diameter effect to the same extent. See page 15.69

In order to verify the successful absorption of the length to diameter ratio as well as to test the correlation at a different pipe diameter, dynamic results as given on Figures 11.15 to 11.17 were replotted as Γ versus χ graphs and Figures 15.37, 15.38 and 15.39 depict these results. The equation to all the results given this far is;

$$\Gamma = K/\chi^q \qquad (15.7)$$

The linear relation is still apparent, but the constant and index in equation (15.7) again indicate a diameter effect.

Figure 15.40 shows a composite diagram embracing four diameter ratios, and three SG's in the 150 mm idameter pipe.

Some of the results have already been published by Lazarus and Kilner (reference 31), and in a private communication from Ellis commenting favourably on the correlation presented, it was shown that data from a 1¼ inch (32 mm) diameter line agreed well with the correlations. Unfortunately, the author is not permitted to publish the experimental graphical plots since the correspondence was confidential, but results are summarised in Table 15.3 including the Canadian work.

FIG. 15.29

$\frac{\Delta H_L}{L_c h_f}\left[\frac{D}{d}\right]^2 : \frac{V}{\sqrt{gDIS_c - 1}}$

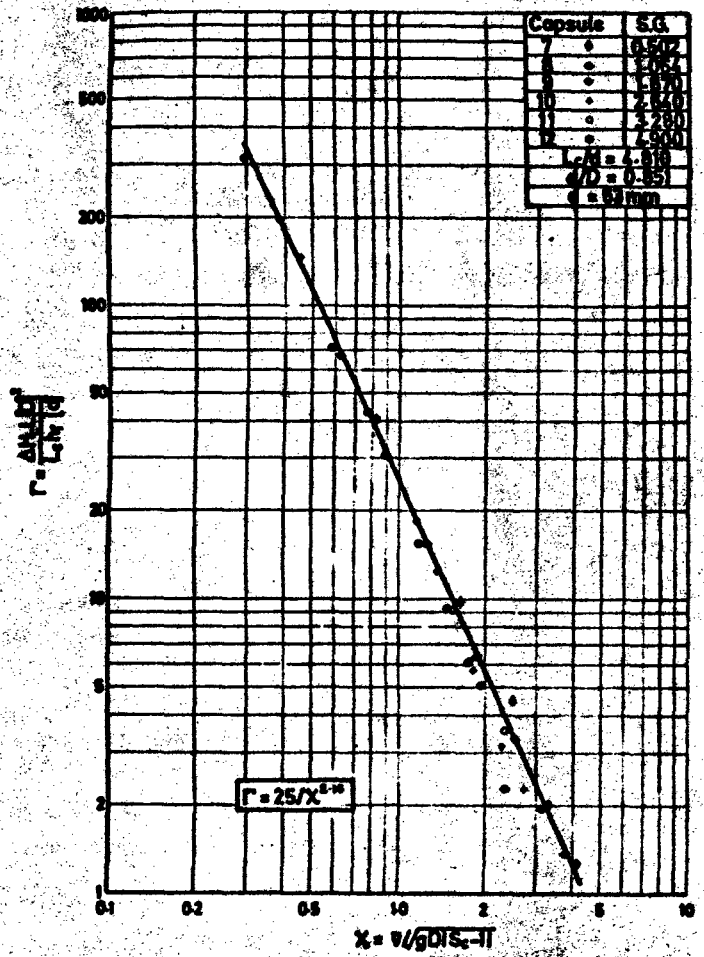

FIG. 15.30

$\frac{\Delta H_L}{L_c h_f}\left[\frac{D}{d}\right]^2 : \frac{V}{\sqrt{gDIS_c - 1}}$

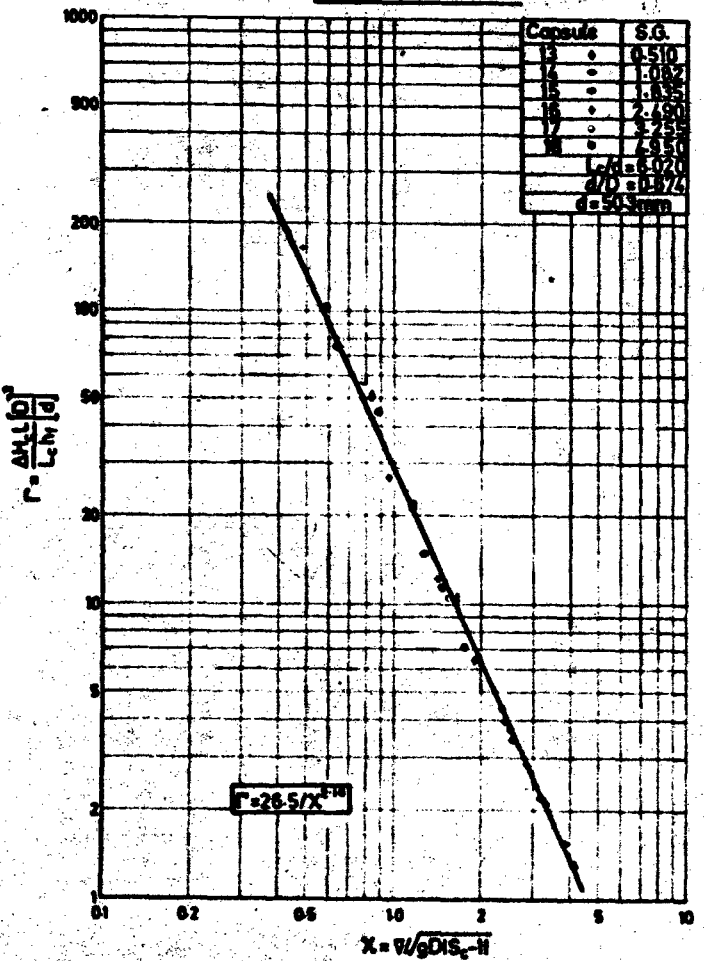

FIG. 15.31

$\frac{\Delta H_L}{L_c h_f}\left[\frac{D}{d}\right]^2 : \frac{V}{\sqrt{gDIS_c - 1}}$

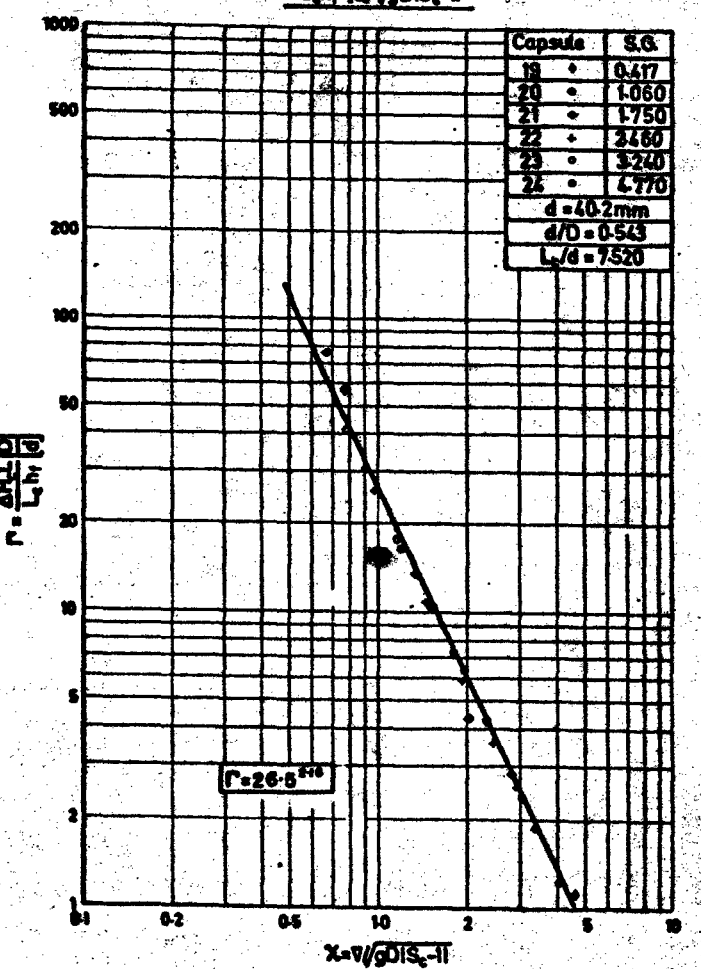

FIG. 15.32

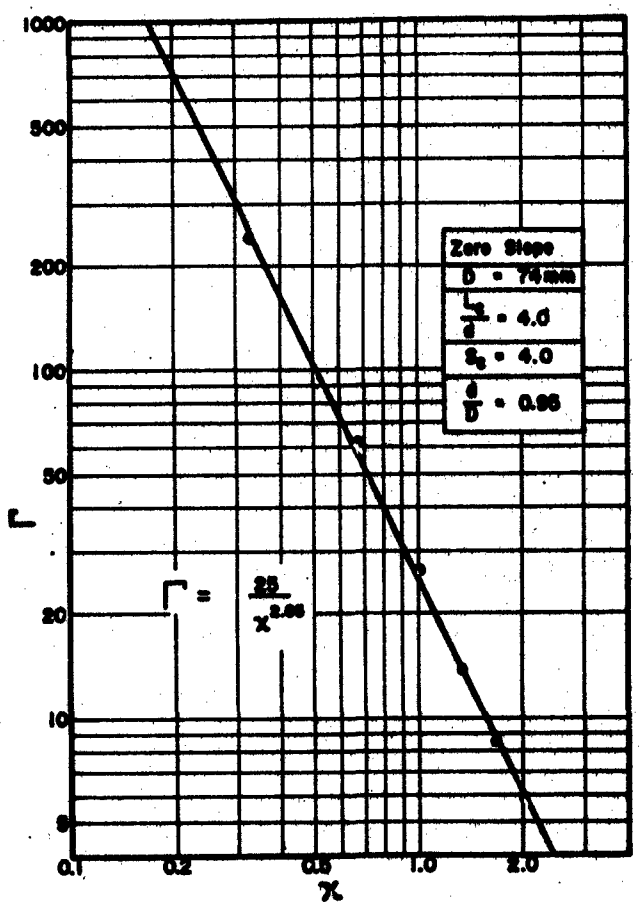

FIG. 15.33

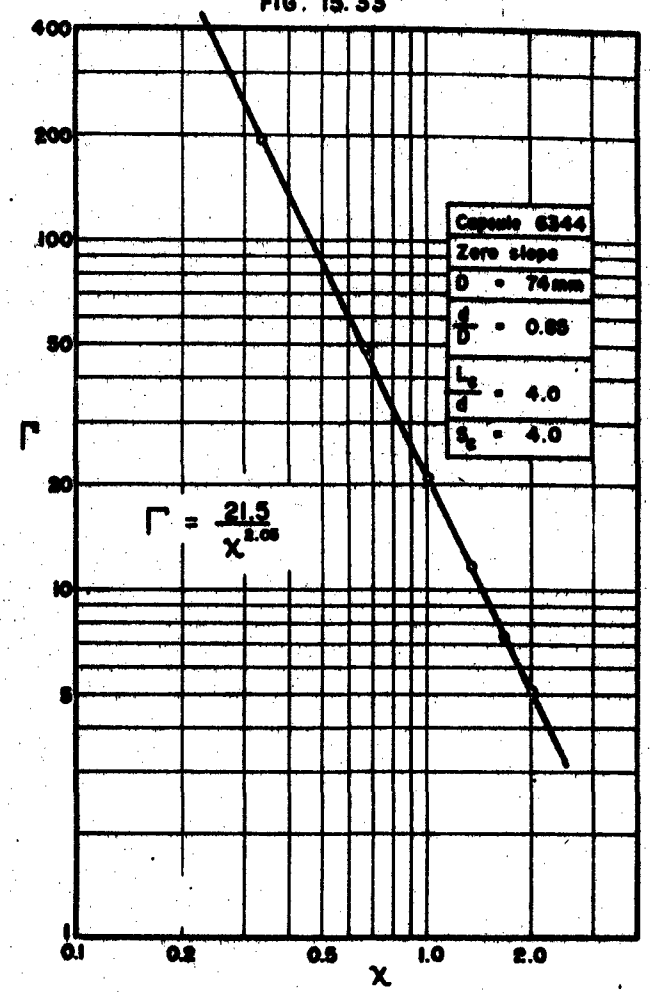

FIG 15.34

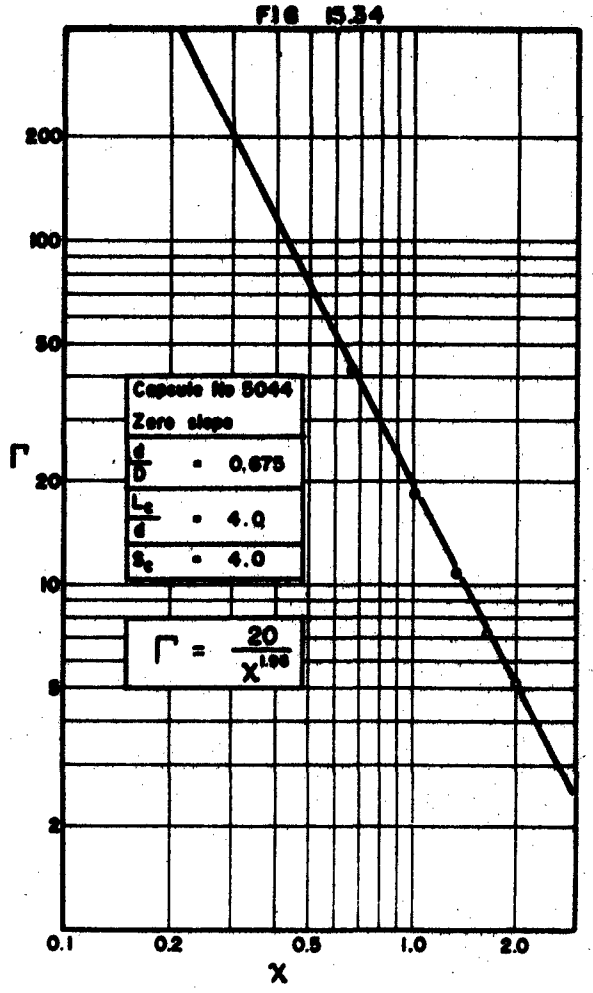

FIG. 15.35

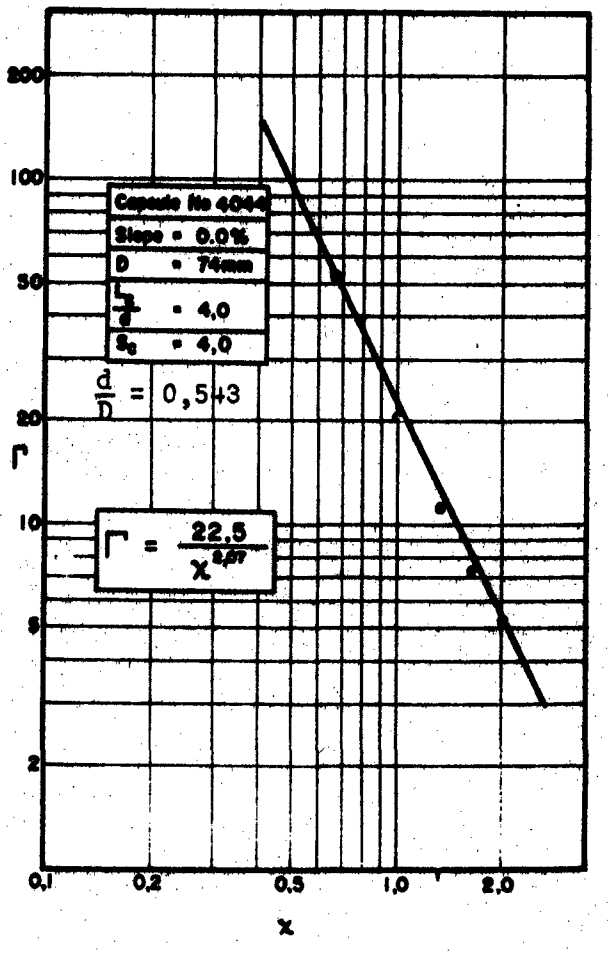

FIG. 15.36

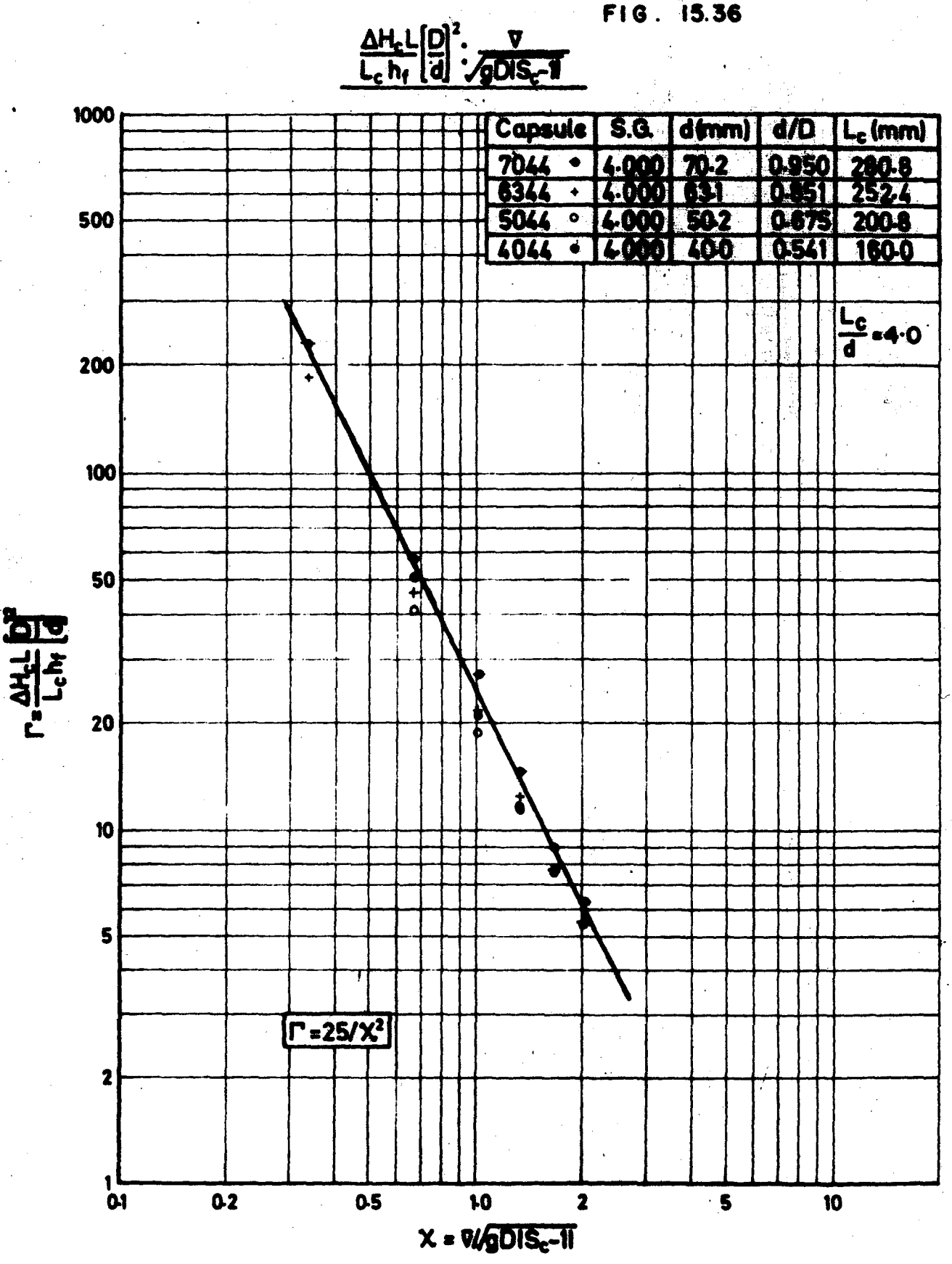
$\frac{\Delta H_c L}{L_c h_f}\left[\frac{D}{d}\right]^2 : \frac{v}{\sqrt{gDIS_c - 1}}$
Capsule | S.G. | d(mm) | d/D | L_c (mm)
7044 • | 4.000 | 70.2 | 0.950 | 280.8
6344 + | 4.000 | 63.1 | 0.851 | 252.4
5044 ○ | 4.000 | 50.2 | 0.675 | 200.8
4044 • | 4.000 | 40.0 | 0.541 | 160.0
$\frac{L_c}{d} = 4.0$
$\Gamma = \frac{\Delta H_c L}{L_c h_f}\left[\frac{D}{d}\right]^2$
$\Gamma = 25/X^2$
$X = v/\sqrt{gDIS_c - 1}$
1000
500
200
100
50
20
10
5
2
1
0.1
0.2
0.5
1.0
2
5
10

FIG. 15.37

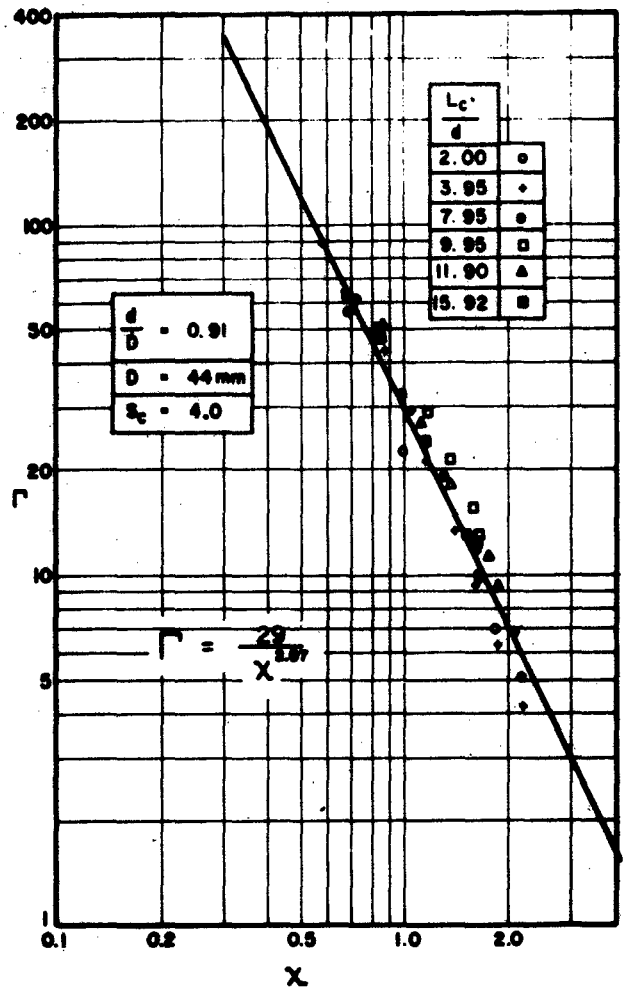

FIG. 15.38

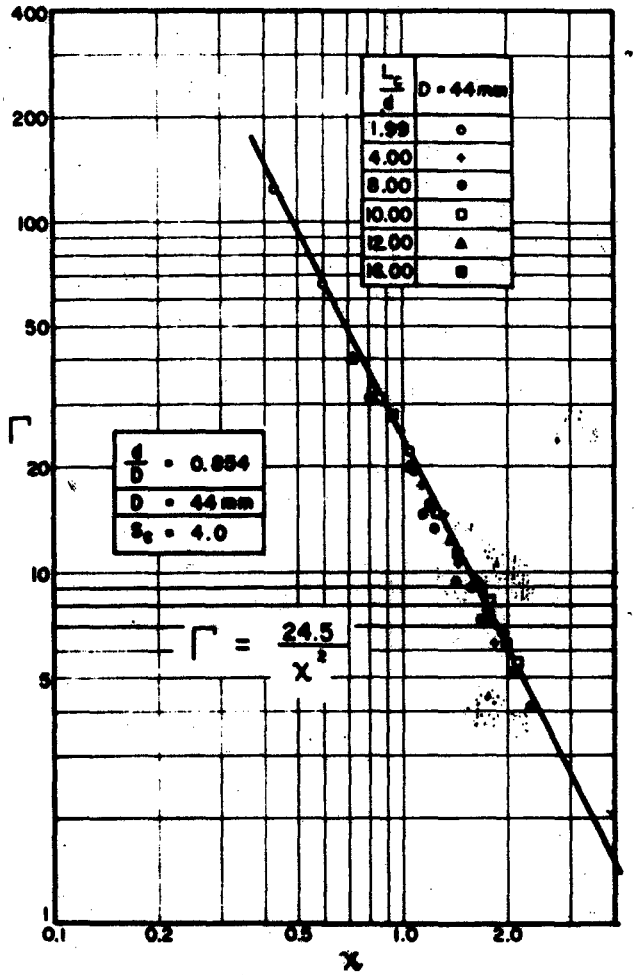

FIG. 15.39

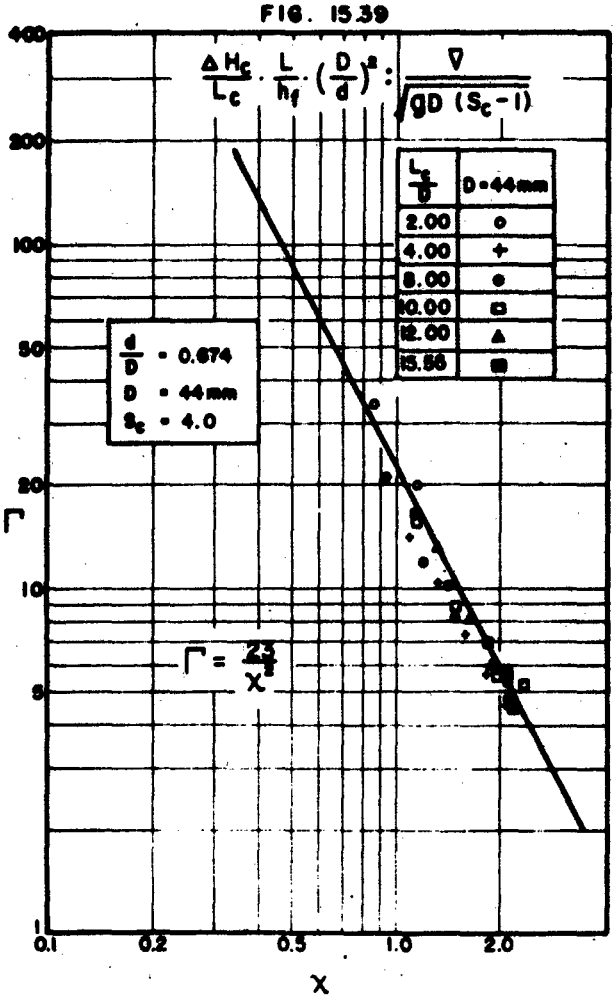

FIG. 15.40

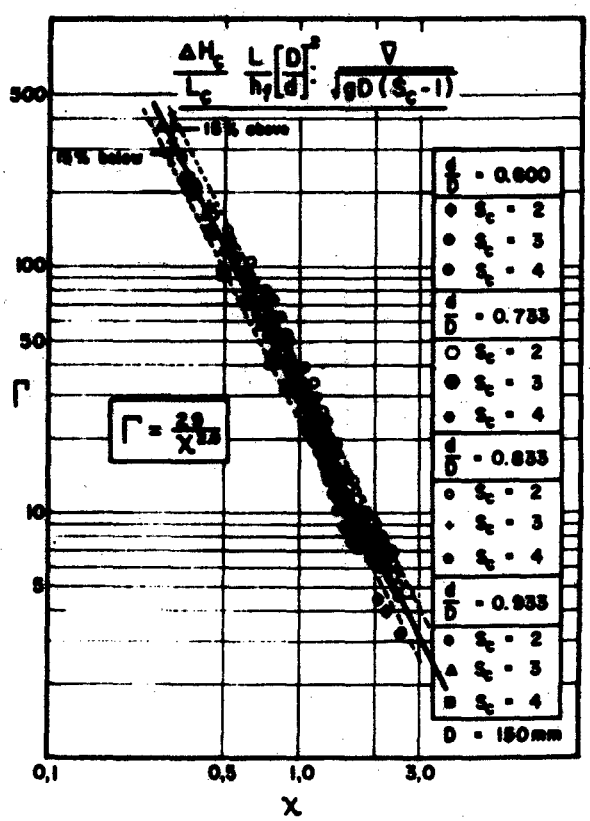

T A B L E 15.3

D (mm)	d/D	K	q	
74	0,95	25	2,06	
	0,85	25	2,16	range of $S_c + L_c/d$
	0,675	26,5	2,16	values
	0,543	26,5	2,16	
74	0,95	25	2,05	
	0,85	21,5	2,05	$S_c = 4,0$
	0,675	20	1,96	$L_c/d = 4,0$
	0,543	22,5	2,07	
44	0,91	29	2,07	range of L_c/d values
	0,854	24,5	2,0	
	0,674	23	2,0	
150	varies	29	2,0	S_c = 2, 3 and 4
32	0,94	25,12	2,01	Results from Ellis
	0,89	32,8	2,0	
74	0,95	24	2,1	$S_c = 4,0$ $L_c/d = 4,0$
	0,85	22,5	2,14	
	0,675	22,5	2,0	Slope varies from -5,4%
	0,543	23,5	2,25	to 30,8%

Figure 15.41 shows the ordinate intercept K plotted against diameter ratio and if a mean value of K = 25 is chosen the scatter is of the order of 20%, the main deviation from the arbitrarily chosen K = 25 is below this value at low diameter ratios and slightly above at high diameter ratios.

The Canadian results were only given for two diameter ratios d/D = 0,89 and d/D = 0,94, and in both cases S_c = 2,00 and 1,25. The capsules

$K = \Gamma \chi^2$

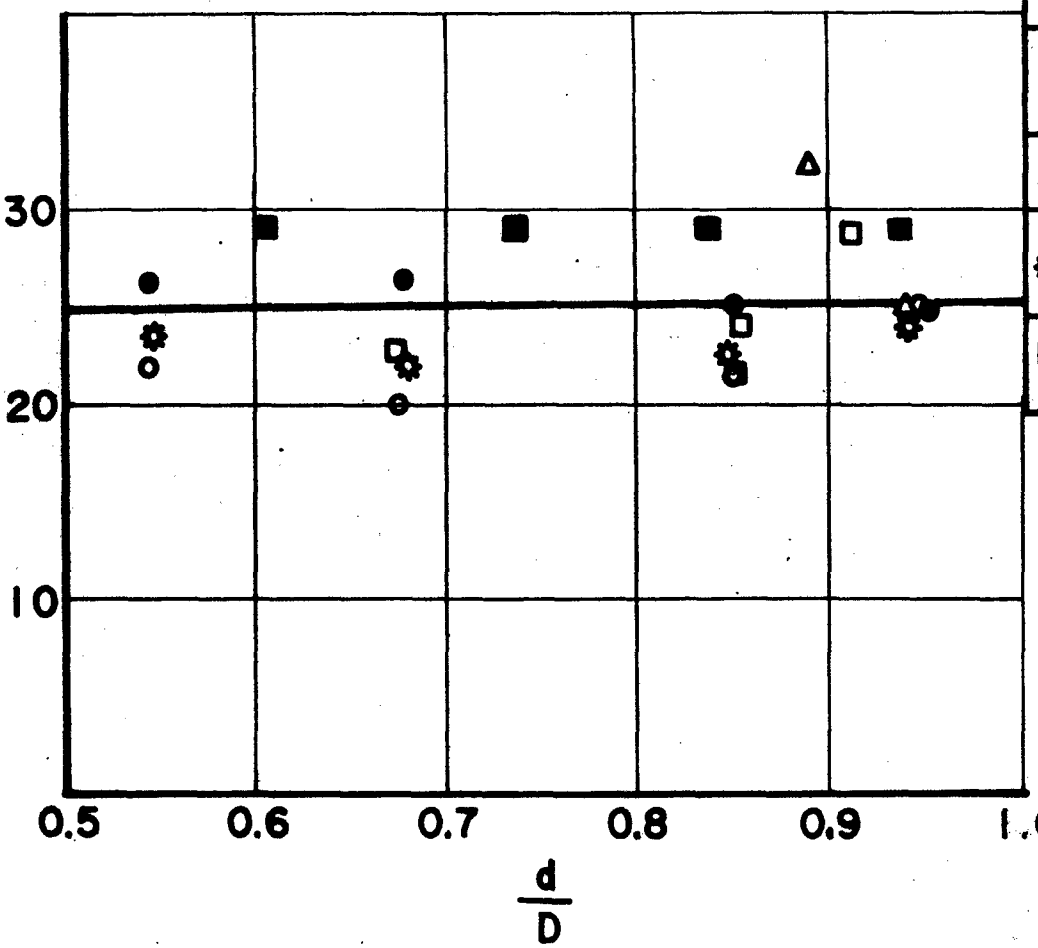

Pipe diameter (D)		
●	74 mm	range of SG $\frac{d}{D}$
○	74 mm	diamensionally similar
□	44 mm	range of $\frac{L_c}{d}$ and $\frac{d}{D}$
△	32 mm	(from Ellis)
✡	74 mm	range of SG $\frac{d}{D}$ and slope
■	150 mm	range of SG^s and $\frac{d}{D}$

FIG. 15.41

were also tested with the capsules run tail first. This is presumably because their experimental apparatus involved a type of shuttling arrangement. On Γ versus χ logarithmic plots, linearity was obtained for a wide range of mean water velocities, although there did appear to be slight orientation and density effects as well as diameter effects. However, different capsule materials were used for the different density capsules, and it is possible that this was the cause of non-dimensional excess head differences, rather than the density, since different capsule surfaces in the same pipe could have different values of μ_f.

Ellis's interpretation of the difference in pressure drop for the same specific gravity capsules when run tail first is that small differences in the position of the centre of gravity or small geometrical differences, perhaps due to the direction of polishing, could have an effect.

The pressure gradient was found to be extremely sensitive to variations in capsule or liquid velocity. Very small differences in capsule velocity (V_c) at the same mean water velocity led to large differences in ΔH_c. Figure 15.40 for results obtained in the 150 mm diameter pipe gives a K value of 29. The coefficient of solid friction for this pipe was $\mu_f = 0{,}38$ as opposed to 0,32 for the 74 mm perspex pipe.

It was shown in Chapter 14 that this had the effect of increasing the excess head loss at incipience $(\Delta H_c)_i$. This is a possible explanation for the high value of K. Equation (15.6) can thus be written as $\Gamma = \chi\, f_4\,(\mu_f)$; and the effect of μ_f is small.

8.1 Other methods of non-dimensional plotting

In order to find a non-dimensional correlation many groupings were investigated subsequent to the plot of Γ against χ.

Abscissa parameters

Because of the diameter ratio effect apparent on Figure 15.36, it could

be argued that the parameter $\chi = \overline{V}/\sqrt{gd|S_c-1|}$ is not necessarily the best one as far as the abscissa is concerned.

The relevant velocity is not necessarily represented by the mean water velocity, and any of the following velocities could arguably be used instead, viz; the capsule velocity (V_c), the mean velocity (relative to the pipe) in the annulus ($\overline{V}_{am}$), the mean velocity relative to the capsule in the annulus (V_r), the mean velocity relative to the capsule in the pipe ($\overline{V} - V_c$), and the local mean velocity acting over the capsule frontal area ($\overline{V}_L$).

The relevant length dimension in the χ-parameter may also conceivably be the capsule or the pipe diameter.

The ten combinations of the above velocities and diameters were all plotted against the Γ-parameter on log-log paper, and it was found that they all gave inferior correlations to the χ-parameter involving $\overline{V}$ and D. One notable exception was the parameter χ_L where;

$$\chi_L = \overline{V}_L/\sqrt{gD|S_c-1|} \qquad (15.8)$$

where $\overline{V}_L$ has been defined as the average local velocity over the capsule frontal area.

Figure 15.42 shows χ_L plotted against Γ, and there is less scatter than in the case of Figure 15.36 for the same capsules.

The method used for obtaining $\overline{V}_L$ was described (Chapter 10) and it is a more complex mean velocity than the mean water velocity in the pipe.

There are basically two criteria when searching for a correlation. Firstly, the correlation should give good agreement with experimental data and secondly, it should not be too complicated.

As regards the first criterion. Although in the case cited, (Figure 15.42) χ_L appears to be superior to χ, this was not consistently

FIG. 15.42

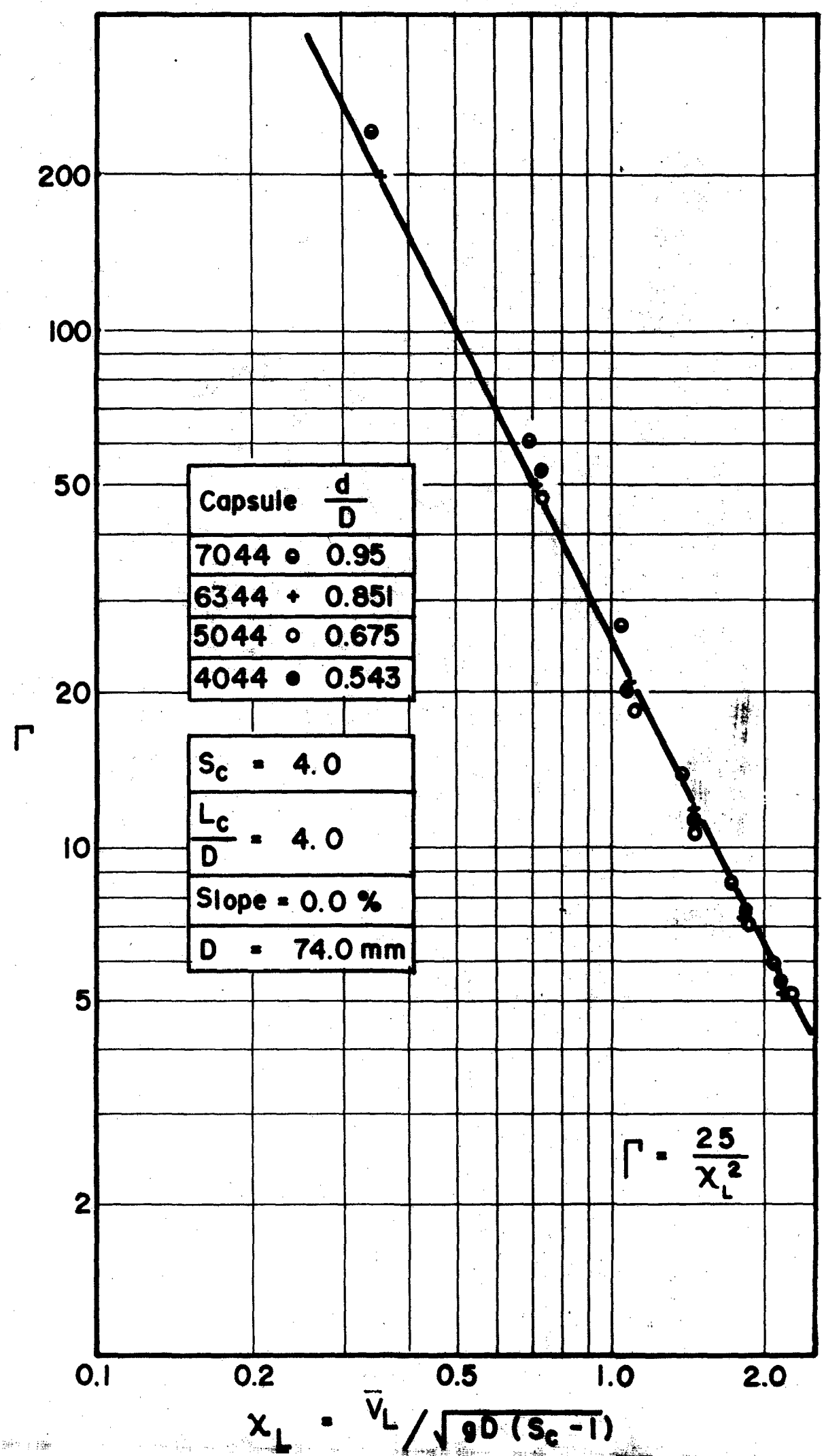
Capsule d/D
7044 • 0.95
6344 + 0.851
5044 ○ 0.675
4044 ● 0.543
S_c = 4.0
L_c/D = 4.0
Slope = 0.0 %
D = 74.0 mm
$\Gamma = 25/X_L^2$
Γ
200
100
50
20
10
5
2
0.1
0.2
0.5
1.0
2.0
$X_L = \bar{V}_L / \sqrt{gD(S_c - 1)}$

apparent and the variability of the original experimental data does not justify the adoption of χ_L. As regards the second criterion χ is obviously superior to χ_L.

Ordinate Parameters

The ordinate parameter could also be considered in relation to the excess head loss assuming the friction head loss acts only over the length of pipeline not included by the capsule ($\Delta H''_c$ defined in Chapter 6).

In this case the ratio of excess hydraulic gradient due to the capsule to that of the capsule free section of pipe is;

$$\xi'' = \{\Delta H_c/\Delta h_f(L_p/L_c) + 1\}$$

The ordinate parameter can be defined as;

$\Gamma'' = (D/d)^2\ \xi''$ and this parameter is plotted against χ on Figure 15.43 for a wide range of capsules. The scatter is more extensive than when using the Γ-parameter.

There is another disadvantage to this presentation. For ΔH_c values that are very small, or zero, a positive lower limit is placed on Γ'' for a fixed diameter ratio. In the case of diameter ratio $d/D = 0{,}543$ the minimum value of Γ'' is $3{,}388$, and this tends to cause horizontal spread of Γ'' values at low ΔH_c values and varying mean water velocities.

This seems to imply that Γ'' could be plotted against a χ parameter with capsule velocity as the relevant parameter.

However, this also proved unsuccessful using the two criteria mentioned earlier.

8.2 Ratio of forces acting on the capsule

8.2.1 Empirical force ratio (R_i)

Once the values of K and q in equation (15.7) are established as

FIG. 15.43

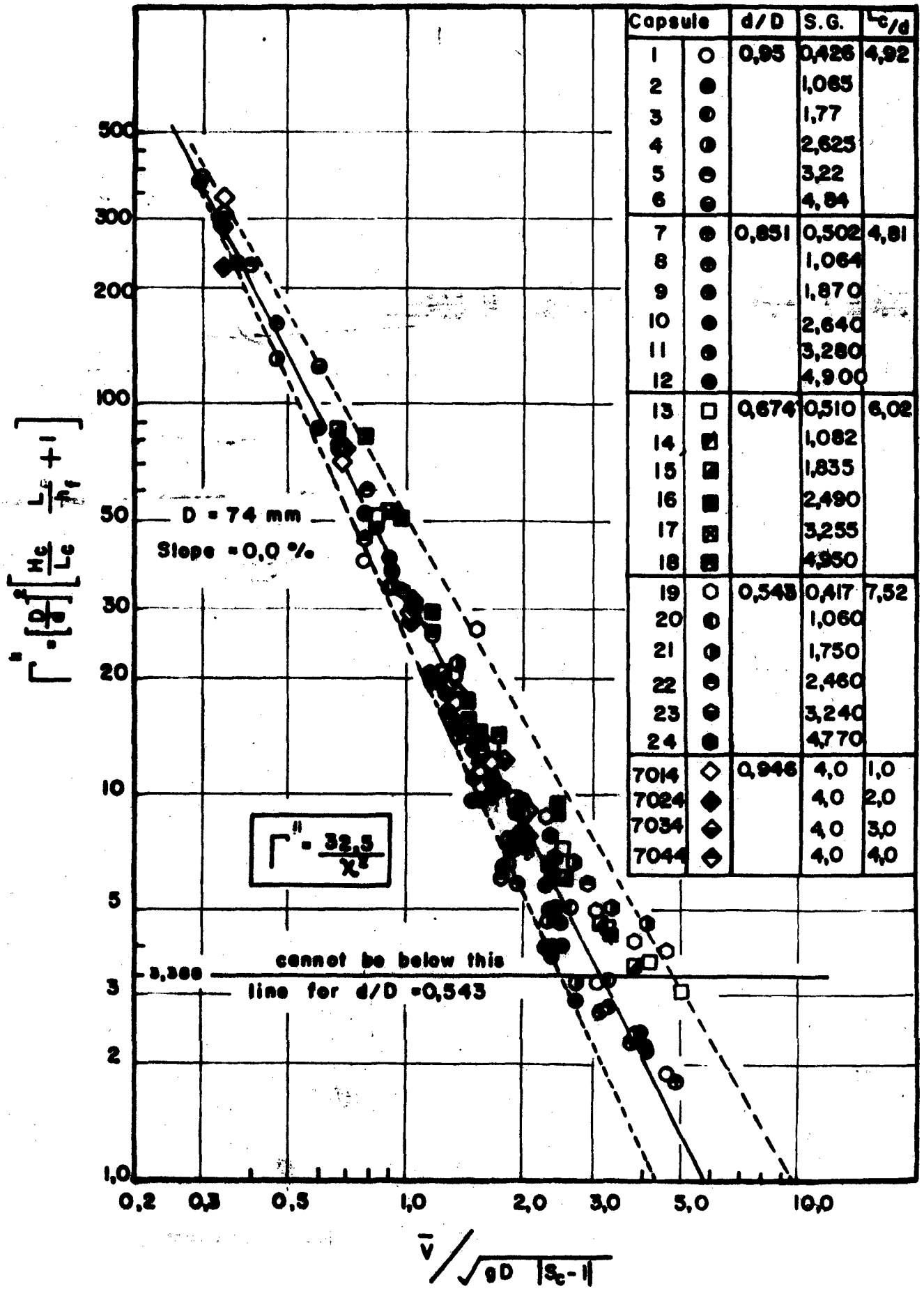
Capsule
d/D
S.G.
L_c/d
1 0,95 0,426 4,92
2 1,065
3 1,77
4 2,625
5 3,22
6 4,84
7 0,851 0,502 4,81
8 1,064
9 1,870
10 2,640
11 3,280
12 4,900
13 0,674 0,510 6,02
14 1,082
15 1,835
16 2,490
17 3,255
18 4,950
19 0,543 0,417 7,52
20 1,060
21 1,750
22 2,460
23 3,240
24 4,770
7014 0,946 4,0 1,0
7024 4,0 2,0
7034 4,0 3,0
7044 4,0 4,0
D = 74 mm
Slope = 0,0 %
$\Gamma'' = \frac{32,5}{\chi^2}$
cannot be below this line for d/D = 0,543
3,300
$\Gamma = \frac{D^2}{d^2}\left[\frac{H_c}{L_c}\right]\left[\frac{L_c}{H_c}+1\right]$
$\bar{v}/\sqrt{gD\,|S_c-1|}$
500
300
200
100
50
30
20
10
5
3
2
1,0
0,2
0,3
0,5
1,0
2,0
3,0
5,0
10,0

K = 25 and q = 2,0 then;

$$\frac{\Delta H_c}{L_c}\ \frac{L}{h_f}\ (D/d)^2 = 25\ gD|S_c-1|/\overline{V}^2 \qquad (15.9)$$

Combining equation (15.9) with the Darcy Weisbach equation;

$$h_f/L = 4\ f\ \overline{V}^2/2gD$$

yields;

$$\frac{\Delta H_c}{L_c(d/D)^2|S_c-1|} = 50f \qquad (15.10)$$

multiplying the numerator and denominator of the left hand side of equation (15.10) by $\frac{w\pi}{4}$ yields;

$$\frac{\Delta F_c}{W'} = 2fK \qquad (15.11)$$

where $\Delta F_c = \frac{w\pi D^2}{4}\ \Delta H_c$

The parameter $R_i = \Delta F_c/W'$ is the ratio of the excess force acting across the capsule water system (ΔF_c) to the submerged weight of the capsule (W'),

and $$R_i = 50\ f \qquad (15.11)$$

8.2.2 Analytical force ratio for the capsule water mixture (R_m)

From equation (7.219);

$$\frac{\Delta H_c}{L_c(d/D)^2|S_c-1|} = \mu_f(1-L_r) + (\frac{4\overline{\tau}_p}{wD} - \frac{h_{fc}}{L_c})/\{(d/D)^2|S_c-1|\} \qquad (15.12)$$

and $$R_m = \mu_f(1-L_r) + (\frac{4\overline{\tau}_p}{wD} - \frac{h_{fc}}{L_c})/\{(d/D)^2|S_c-1|\} \qquad (15.13)$$

8.2.3 The ratio of forward force on the capsule to the submerged weight of the capsule (R_o)

The forward force on the capsule has two components; the form drag and the skin friction drag due to pressure flow.

$$\therefore \quad R_c = \vec{D}_{Tf}/W' = (\vec{D}_f + \vec{D}_{sfp})/W'$$

$$= \frac{\{(\Delta h_i + \Delta h_o)(D/d)^2 + \Delta h_{fa}\}A_c w + \bar{\tau}_{cp}\,\pi d L_c}{A_c w |S_c - 1| L_c}$$

$$= \frac{w A_c L_c |S_c - 1| \mu_f (1 - L_r) + \bar{\tau}_{cc}\,\pi d L_c}{A_c w |S_c - 1| L_c}$$

$$\therefore \quad R_c = \mu_f (1 - L_r) + \frac{\bar{\tau}_{cc}\,4d}{D^2 w} / \{(d/D)^2 |S_c - 1|\} \qquad (15.14)$$

These three non-dimensional parameters (R_i, R_m and R_c) are plotted against the mean water velocity in the pipe (which is proportional to the Reynolds number of the pipe if D and ν are constant).

Figure 15.44 shows that the empirical correlation represented by the value $R_i = 50f$ is in close agreement with the ratio of forward drag on the capsule to the submerged weight of the capsule (R_c) and also with the ratio of force acting across the capsule water system to the submerged weight of the capsule (R_m).

The discrepancy does not vary by much more than 10% at different ratios.

The values for $\bar{\tau}_p$ and $\bar{\tau}_{cc}$ in equations (15.13) and (15.14) were computer calculated from the quasi-concentric polar co-ordinate finite element method.

An interesting feature of these graphs is that the value of the empirical force ratio ($R_i = 50f$) and the analytical force ratios stabilise at a value of about 0,2 for $\bar{V}$ 2 m/s. This value is obviously not a constant over a wide range of Reynolds numbers and is only exact at $f = 0{,}004$ (for R_i).

Figure 15.45 shows that the agreement holds over a wide range of SG's (except for $S_c = 1{,}87$ at $\bar{V} = 3$ m/s).

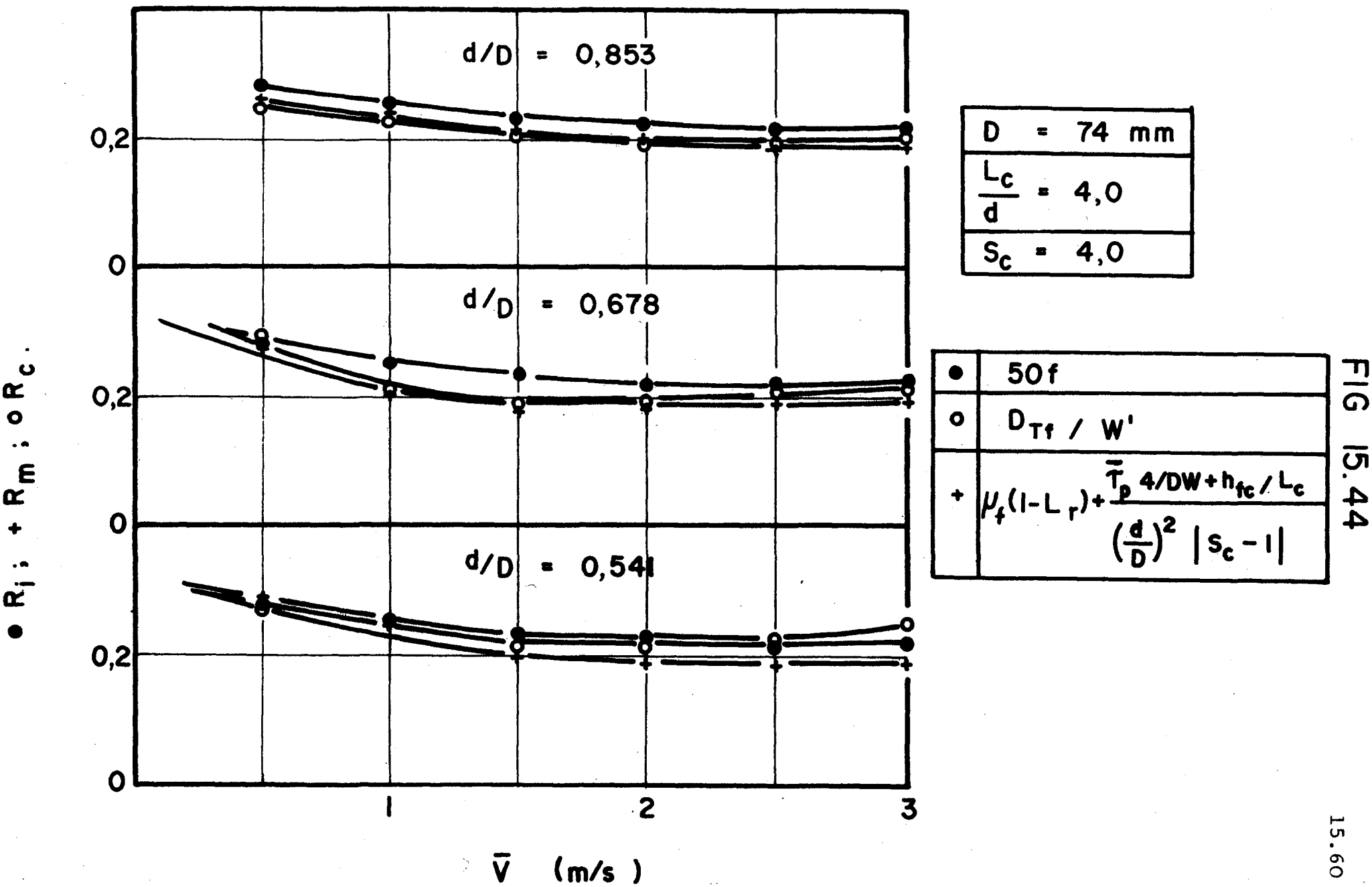
d/D = 0,853
d/D = 0,678
d/D = 0,541
0,2
0
0,2
0
0,2
0
1
2
3
$\bar{V}$ (m/s)
• R_j ; + R_m ; o R_c .
D = 74 mm
$\frac{L_c}{d}$ = 4,0
S_c = 4,0
• 50f
o D_{Tf} / W'
+ $\mu_f(1-L_r)+\frac{\bar{\tau}_p\, 4/DW+h_{fc}/L_c}{\left(\frac{d}{D}\right)^2 |S_c-1|}$

FIG 15.44

FIG. 15.45

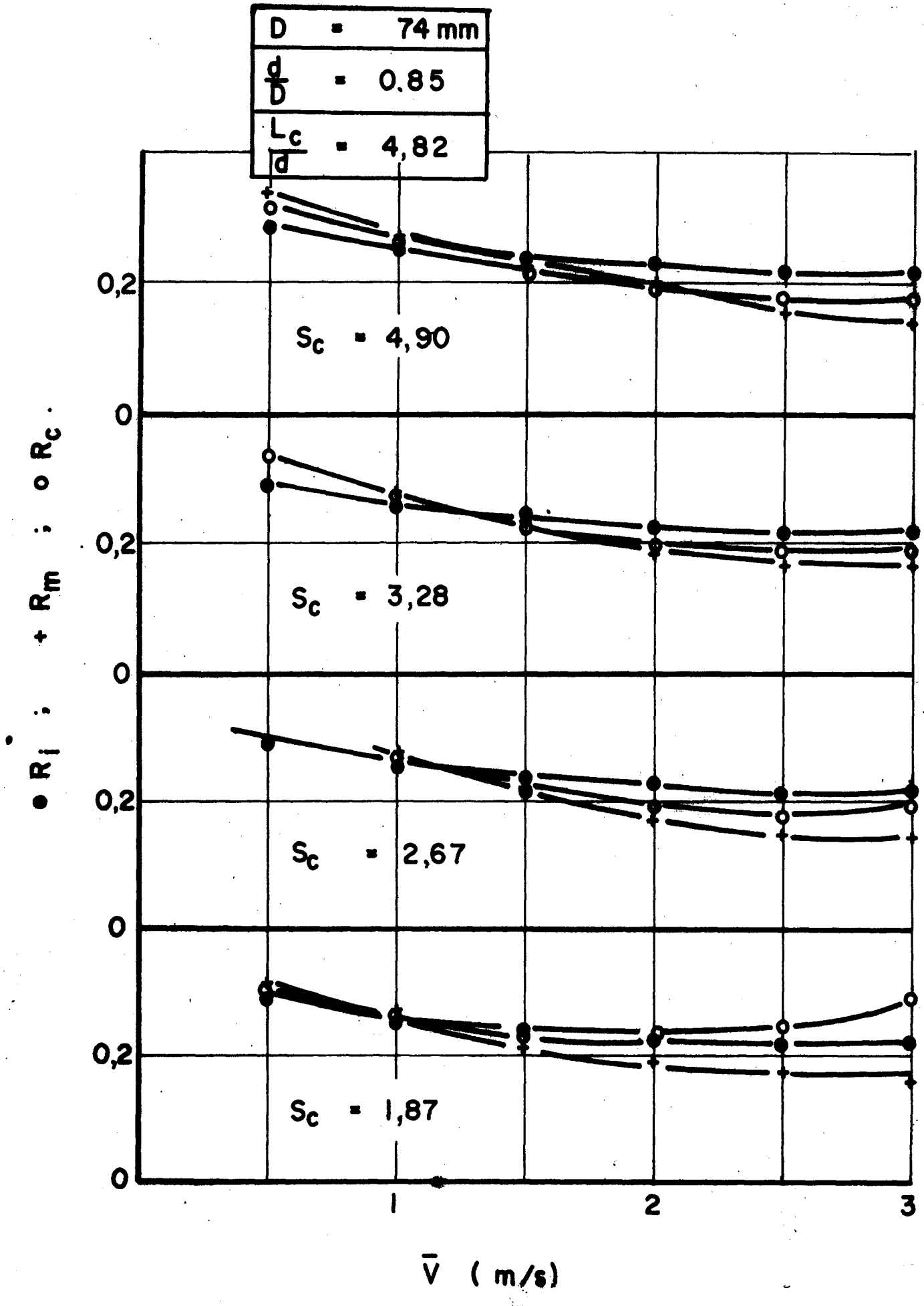
D = 74 mm
d/D = 0,85
Lc/d = 4,82
Sc = 4,90
Sc = 3,28
Sc = 2,67
Sc = 1,87
0,2
0
1
2
3
● Ri ; + Rm ; o Rc .
V̄ (m/s)

8.3 Correlation to include the pipeline slope

Figures 15.46, 15.47, 15.48 and 15.49 are log-log plots of the dimensionally similar capsules 4044; 5044; 6344 and 7044 on slopes ranging from -5,4% to +30,8%. Each slope and capsule diameter is represented by curves which can be formulated by straight line equations on a log-log plot of the form

$$(\Gamma)'_s = K/\chi^q$$

For each of the four diameter ratios, the curves are parallel for the positive slopes, but there is a great deal of scatter between the curves for different slopes, although, the data from individual capsules exhibit very little scatter. The maximum deviation from linearity occurs with the only negative slope (-5,4%).

In order to bring these curves together the device mentioned earlier was employed, viz, the subtractive term; $\lambda = (d/D)^2 L_c \sin\phi|S_c-1|$, i.e. $(\Delta H_c)_s = (\Delta H_c)'_s - \lambda$.

Figure 15.50 shows $(\Gamma)_s$ where

$$(\Gamma)_s = [(\Delta H_c)_s/L_c](L/\Delta h_f)(D/d)^2$$

plotted against χ for $d/D = 0,95$ and different slopes.

It is clear that the subtractive term successfully incorporates the excess head loss across the capsule on slope.

The solid line represents a mean through the points shown on the graph whereas the dotted line is for the zero slope.

Figure 15.51 for $d/D = 0,85$ also shows relatively little scatter.

However, at the lower diameter ratios shown plotted on Figures 15.52 and 15.53 there is more scatter.

The greatest scatter on Figures 15.50 to 15.53 occurs for the lowest diameter ratio: $d/D = 0,54$ at the highest velocity, between slopes

FIG. 15.46

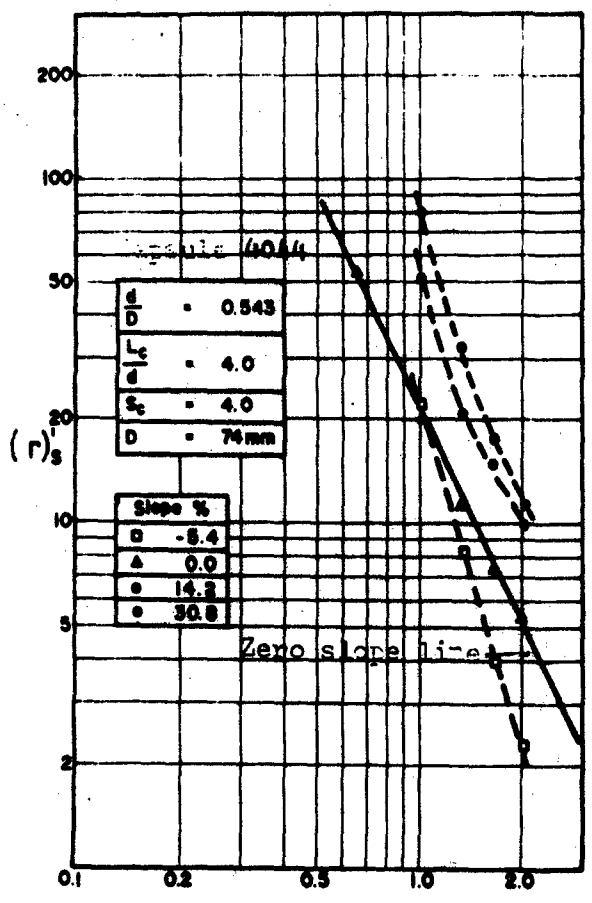

FIG. 15.47

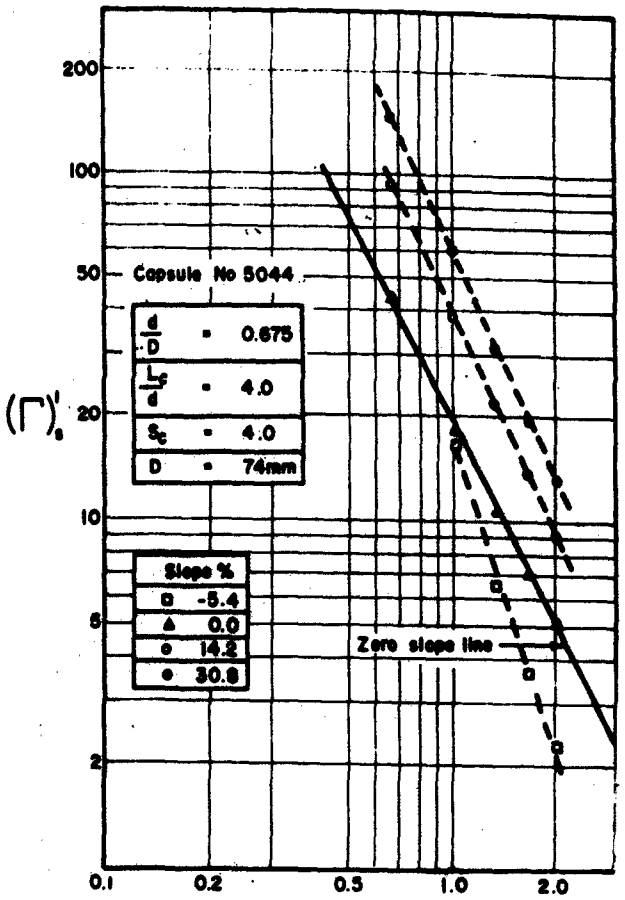

$X = \bar{v} / \sqrt{gD\,(S_c - 1)}$

FIG. 15.48

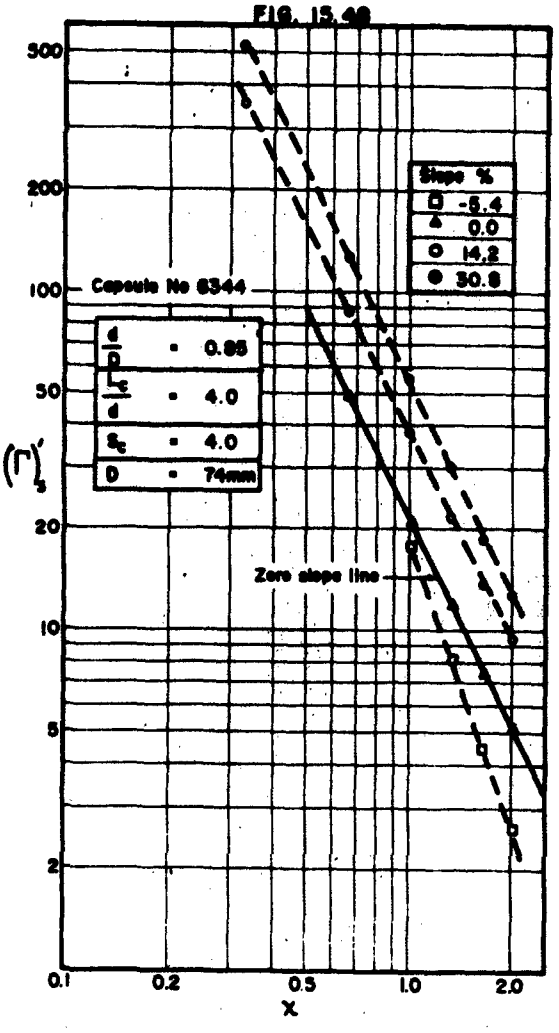

FIG. 15.49

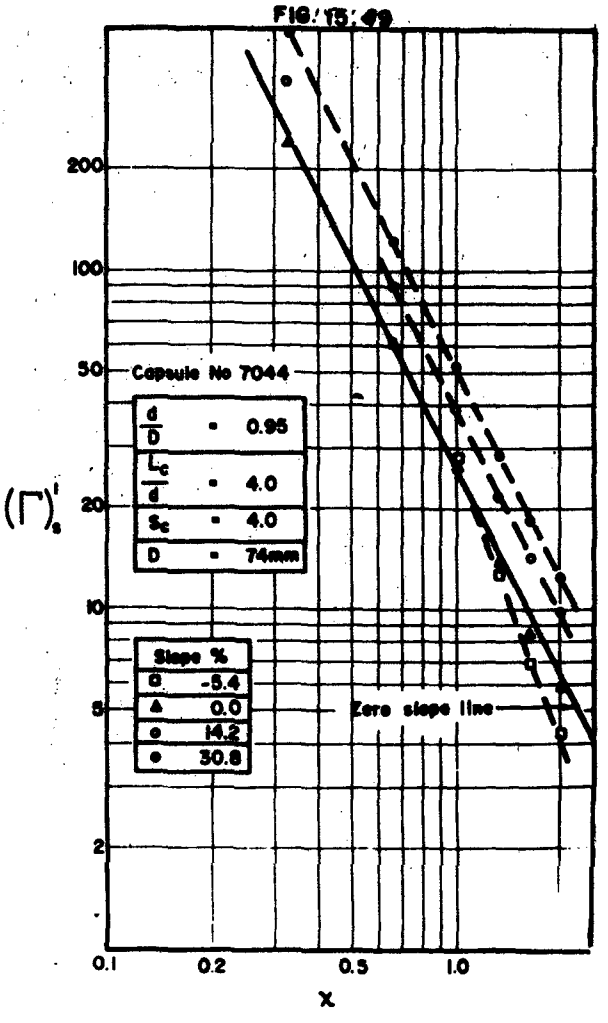

FIG. 15.50

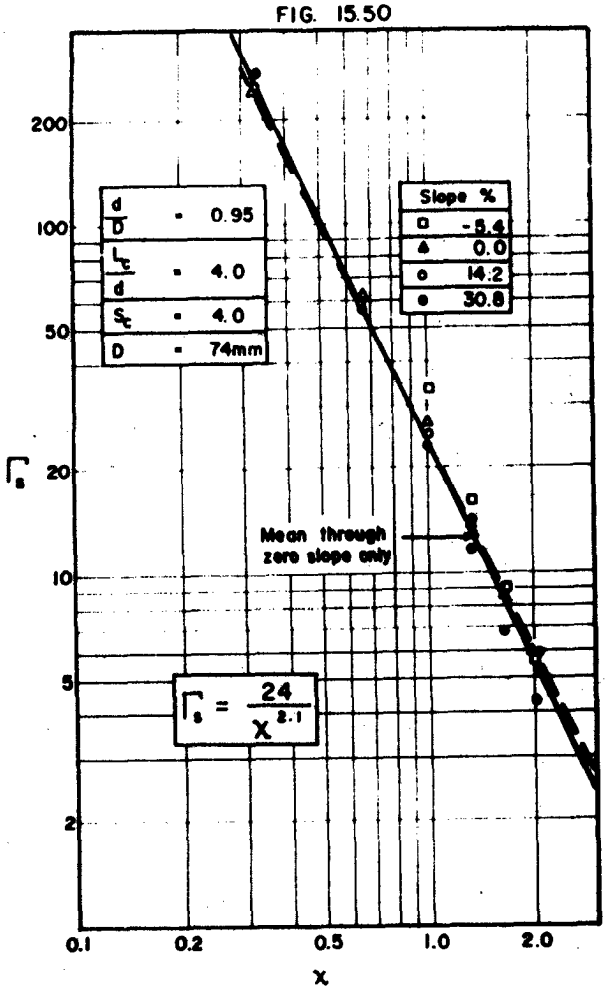

FIG. 15.51

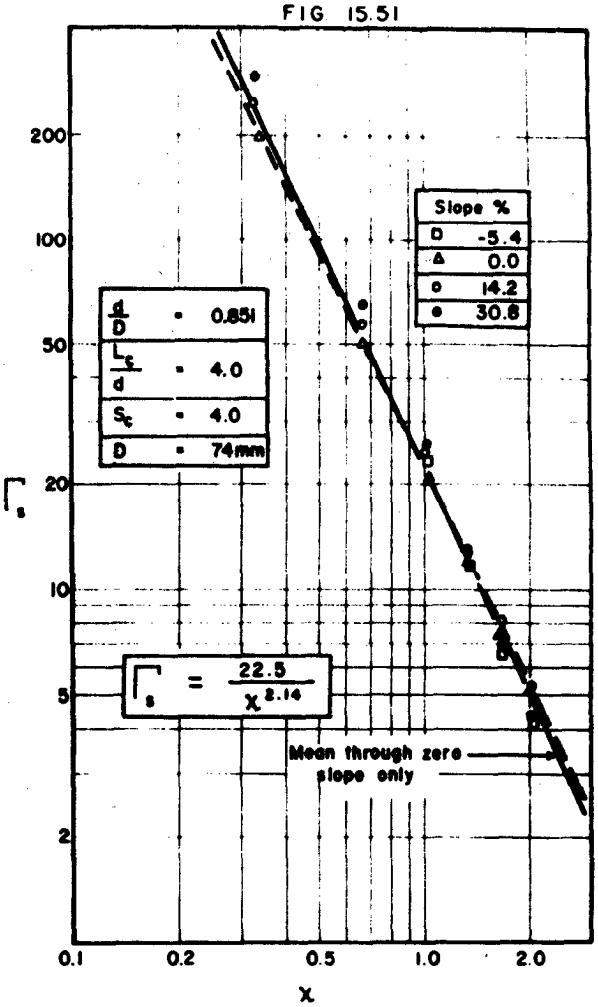

FIG. 15.52

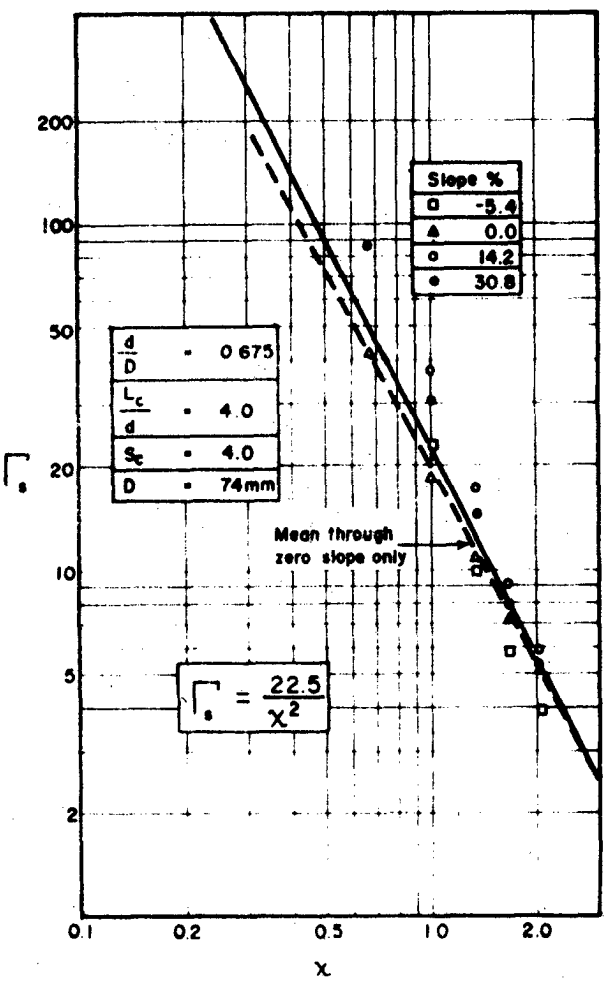

FIG. 15.53

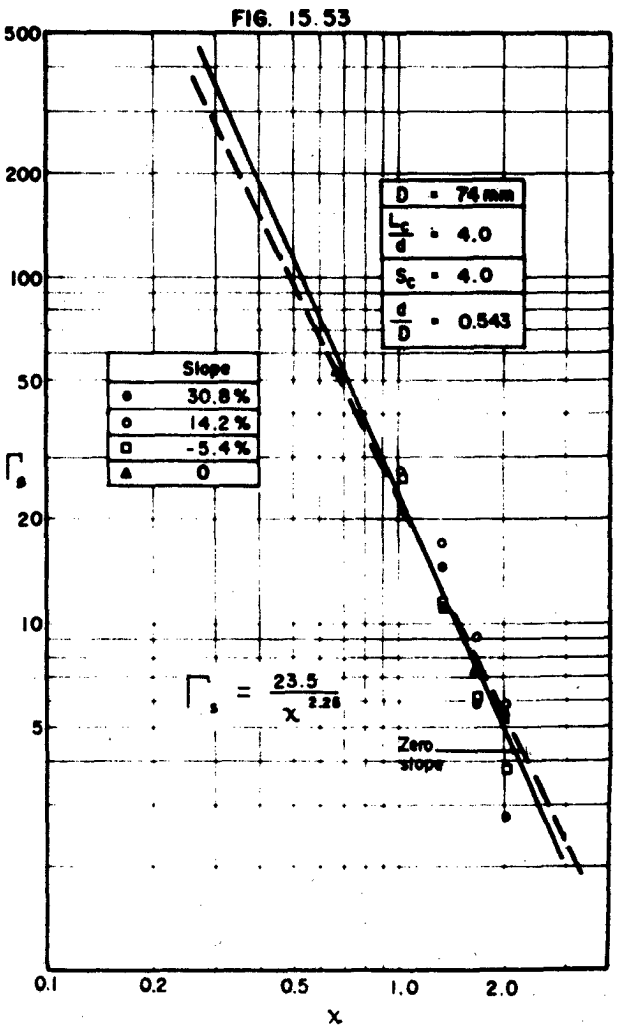

30,8% and 14.2%. The difference in values of $(\Gamma)_s$ being represented in the following Table.

T A B L E 15.4

Slope (%)	30,8	14,2	mean
$(\Gamma)_s$	2,77	5,92	5,0
error from mean	2,23	0,92	
% error	44,6	18,4	
$(d/D)^2 \lvert S_c - 1 \rvert L_c \sin \phi$	40,6 mm	19,5 mm	
$(\Delta H_c)'_s$	55 mm	49 mm	

A closer look at the 44,6% error represented by the deviation at 30,8% slope from the mean line at $\chi = 2{,}03$ reveals that $(\Delta H_c)'_s$ can vary by as much as 16% (the variation from the mean is even less). This is well within the variation of $(\Delta H_c)'_s$ due to turbulent fluctuation as registered on the pen recorder chart.

In order to reduce the 44,6% error to zero, for example, the value of $(\Delta H_c)'_s$ would have to be about 66 mm instead of 55 mm and if reference is made to Figure 11.40 it is obvious that it is quite possible for this to be so. In other words, a 16% error in $(\Delta H_c)'_s$ represents a 44,6% error in $(\Gamma)_s$. On the pen recorder chart, for differential pressure, it has already been shown that 10 mm differential pressure represents a 1,3 mm pen movement which at this high velocity is well within the range of turbulence fluctuation. Thus, the scatter manifest on Figure 15.53 is by no means excessive.

Figure 15.54 shows $(\Gamma)_s$ (i.e. with the submerged weight component subtracted out) plotted against pipeline slope for a particular mean water velocity of 1,5 m/s representing a χ value of 1,01. Since the value K in the equation $(\Gamma)_s = K/\chi^q$ is taken at a χ value of unity, the

$$\bar{V} = 1{,}5 \quad m/s\,; \quad \frac{\bar{V}}{\sqrt{gD\,|s-1|}} = 1{,}01$$

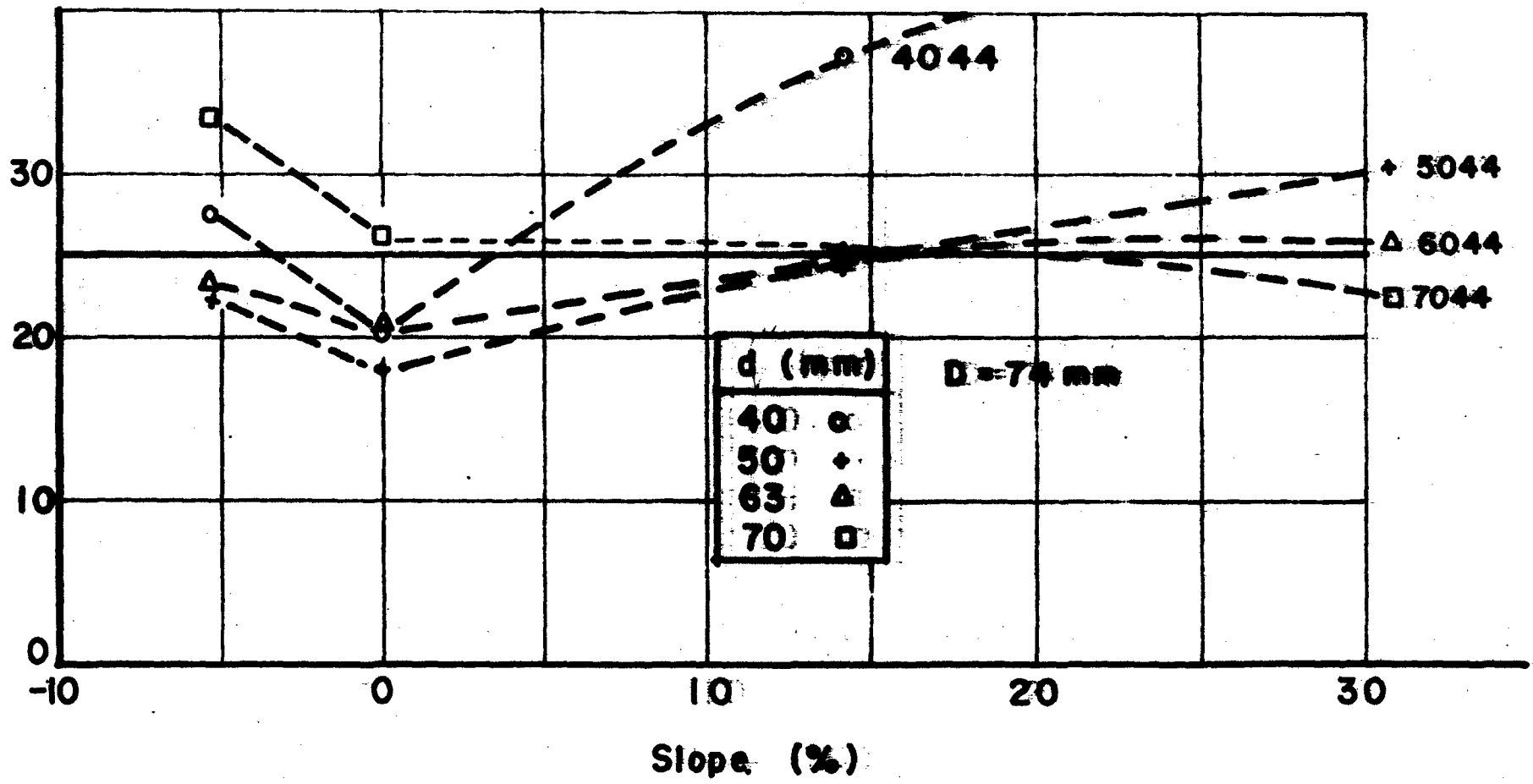

FIG. 15.54

values of $(\Gamma)_s$ shown on this figure are very nearly K values.

If a mean K value is taken as 25,0, as for the horizontal pipe case, it can be seen that the scatter from a pipe slope of -5,4% to 90,8% is no more than for the horizontal pipe (compare Figure 15.41).

The only extreme value being the smallest diameter ratio d/D = 0,543 at 14,2% slope. Again the scale of Figure 15.54 magnifies the errors as discussed above, and the scatter is not as serious as it appears.

The variation of the index (q) for sloping pipes, can best be seen by comparing the solid, lines for sloping pipes, and the dotted lines, for horizontal pipes, on Figures 15.50 to 15.53, and q has the values given in Table 15.3.

8.4 Percentage of data differing by more than 15% from the correlation line for different pipe diameters

The correlation given herein effectively embraces a wide range of capsule to pipe diameter ratios, pipe diameters and slopes for a large variation of mean water velocities and capsule velocities, and enables the excess head loss across capsules to be estimated to an accuracy within about ± 15%. Consider Figures 15.40, 15.55 and 15.56, i.e. a large number of data points for three pipe diameters (44 mm, 74 mm and 150 mm).

Figure 15,40 for D = 150 mm shows parallel lines representing a 15% deviation above and below the log normal line; 7,5% of the data points deviate by more than 15% above the line represented by the equation for calculating the dependent non-dimensional parameter Γ from χ, and 6,6% of the data points are below the lower 15% deviation from the log normal distribution.

The percentage of data points outside a 15% deviation above and below the log normal distribution is indicated in the Table below.

FIG. 15.55

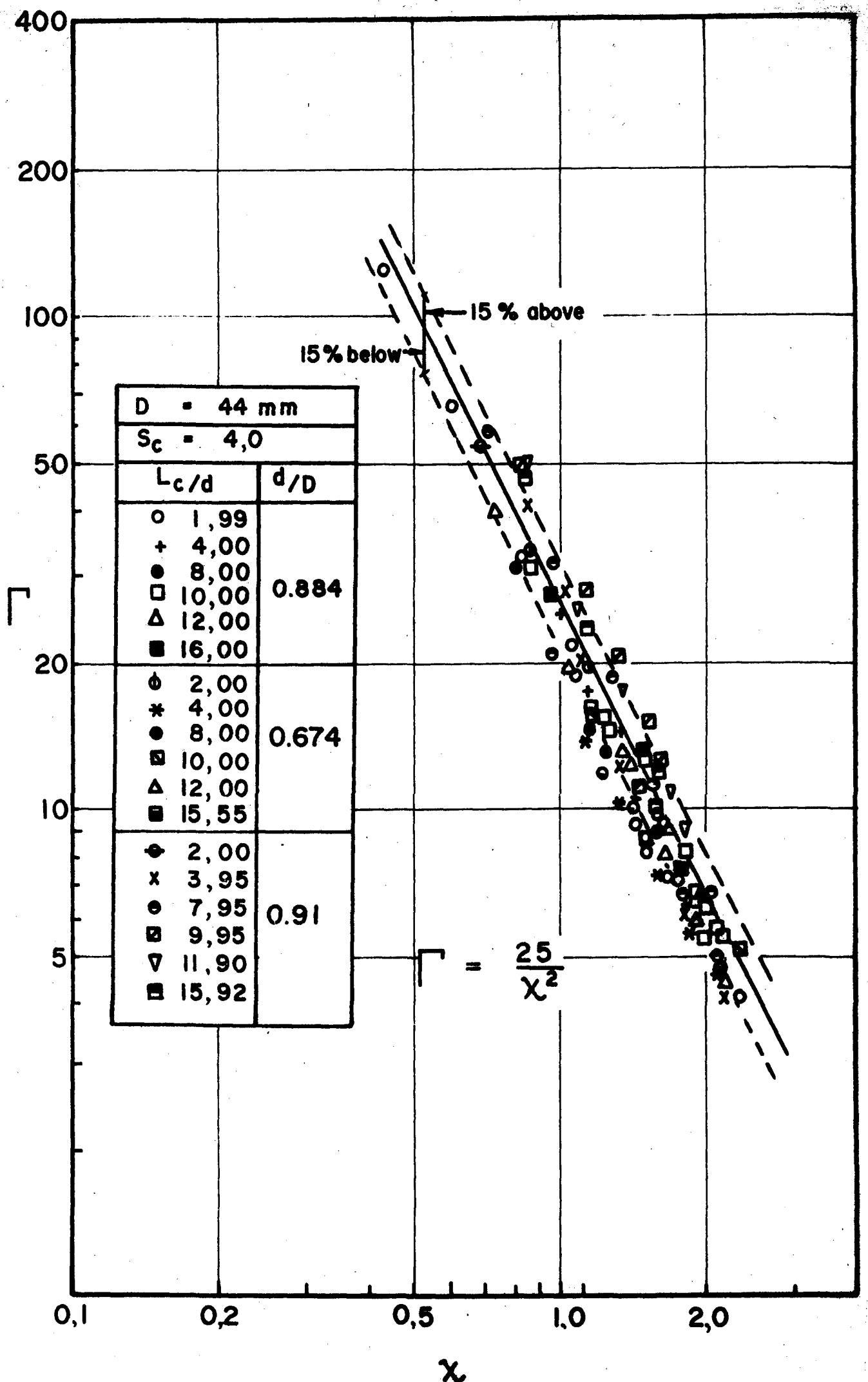
400
200
100
50
20
10
5
0,1
0,2
0,5
1,0
2,0
χ
Γ
15 % above
15 % below
Γ = 25/χ²
D = 44 mm
Sc = 4,0
Lc/d
d/D
1,99
4,00
8,00
10,00
12,00
16,00
0.884
2,00
4,00
8,00
10,00
12,00
15,55
0.674
2,00
3,95
7,95
9,95
11,90
15,92
0.91

FIG. 15.56

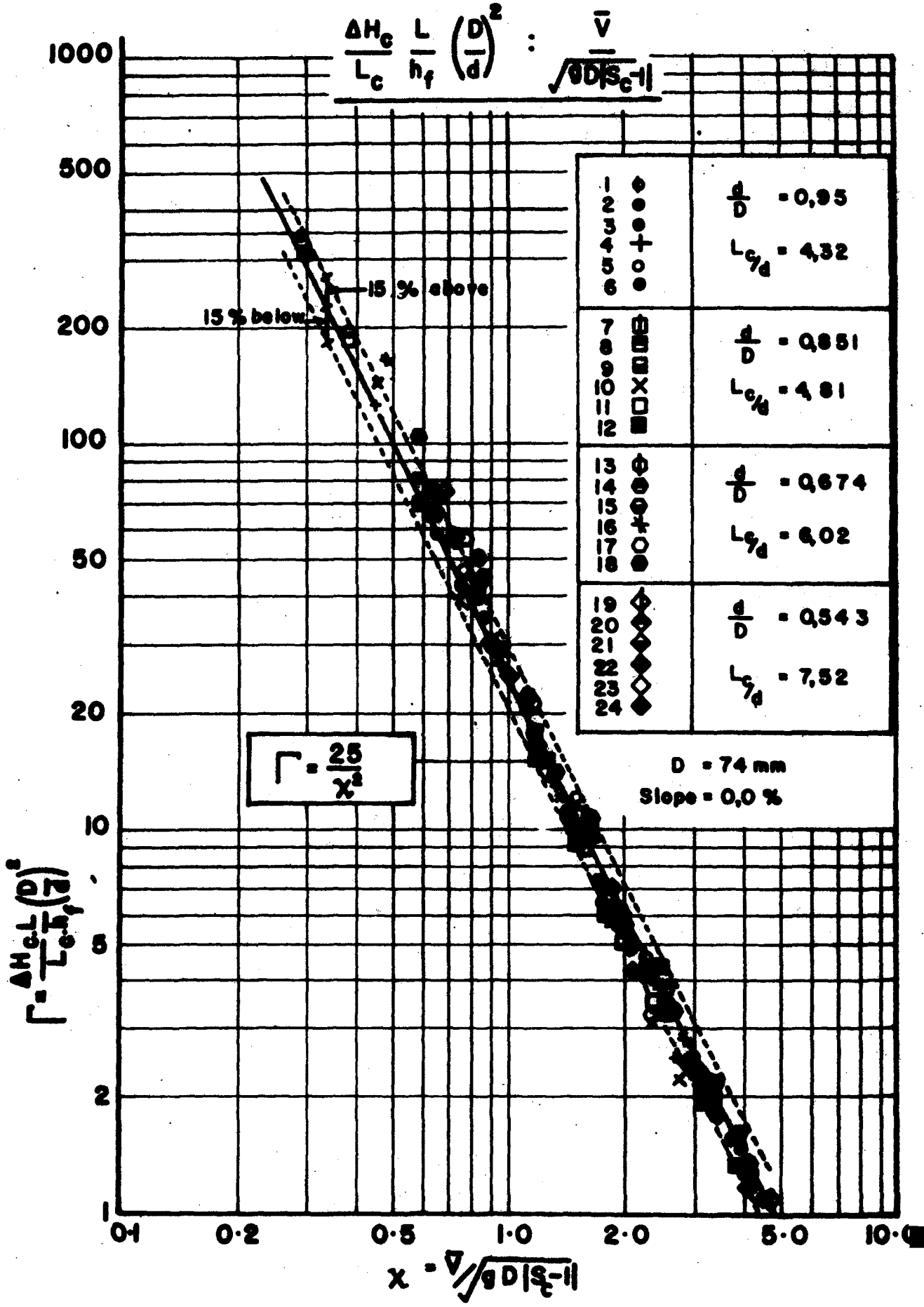
$\frac{\Delta H_c}{L_c}\frac{L}{h_f}\left(\frac{D}{d}\right)^2 : \frac{\bar{V}}{\sqrt{gD\left|S_c-1\right|}}$
1000
500
200
100
50
20
10
5
2
1
0·1
0·2
0·5
1·0
2·0
5·0
10·0
15 % above
15 % below
1 2 3 4 5 6 ◆ ● ● + o ●
$\frac{d}{D}$ = 0,95
L_c/d = 4,32
7 8 9 10 11 12 ⊞ ■ ■ X □ ■
$\frac{d}{D}$ = 0,851
L_c/d = 4,81
13 14 15 16 17 18 Φ ● ● + ○ ●
$\frac{d}{D}$ = 0,674
L_c/d = 6,02
19 20 21 22 23 24 ◆ ◆ ◆ ◆ ◇ ◆
$\frac{d}{D}$ = 0,543
L_c/d = 7,52
$\Gamma = \frac{25}{x^2}$
D = 74 mm
Slope = 0,0 %
$\Gamma = \frac{\Delta H_c L}{L_c h_f}\left(\frac{D}{d}\right)^2$
$x = \bar{V}/\sqrt{gD\left|S_c-1\right|}$

T A B L E 15.5

Pipe diameter (D) mm	150	74	44
% of data points more than 15% above the log-normal distribution	7,5%	4,6%	5,8%
% of data points more than 15% below the log-normal distribution	6,6%	5,3%	12%

8.5 Comparison with the correlation of Ellis and Kruyer (reference 19)

Figure 2.16 represents the correlation presented at Hydrotransport I (1970) by Ellis and Kruyer (reference 19). It has already been mentioned that capsule excess head losses in a 32 mm diameter laboratory pipeline as determined by Ellis (private correspondence), have successfully been correlated by the method presented by the present author.

Figure 15.57 shows the friction factor (f) versus Reynolds number (R_e) diagram as defined by Ellis and Kruyer (see Chapter 2).

All of the data represented on Figures 15.25, 15.29, 15.30 and 15.31 was re-processed on the computer to give friction factor and Reynolds number parameters defined by Ellis and Kruyer. The data points are shown on Figure 15.57 covering a range of mean water velocities from 0,5 m/s to 3,0 m/s as on Figure 15.56. There is a tremendous amount of scatter and if the mean curve is taken as

$$f\, R_e^{0,25} = 0,0645$$

the variation of (f) values extends from 600% above the mean to over 60% below the mean. In fact, most of the data lies outside the limits of the correlation given on Figure 2.16 as $f\, R_e^{0,25} = 0,05$ to 0,079.

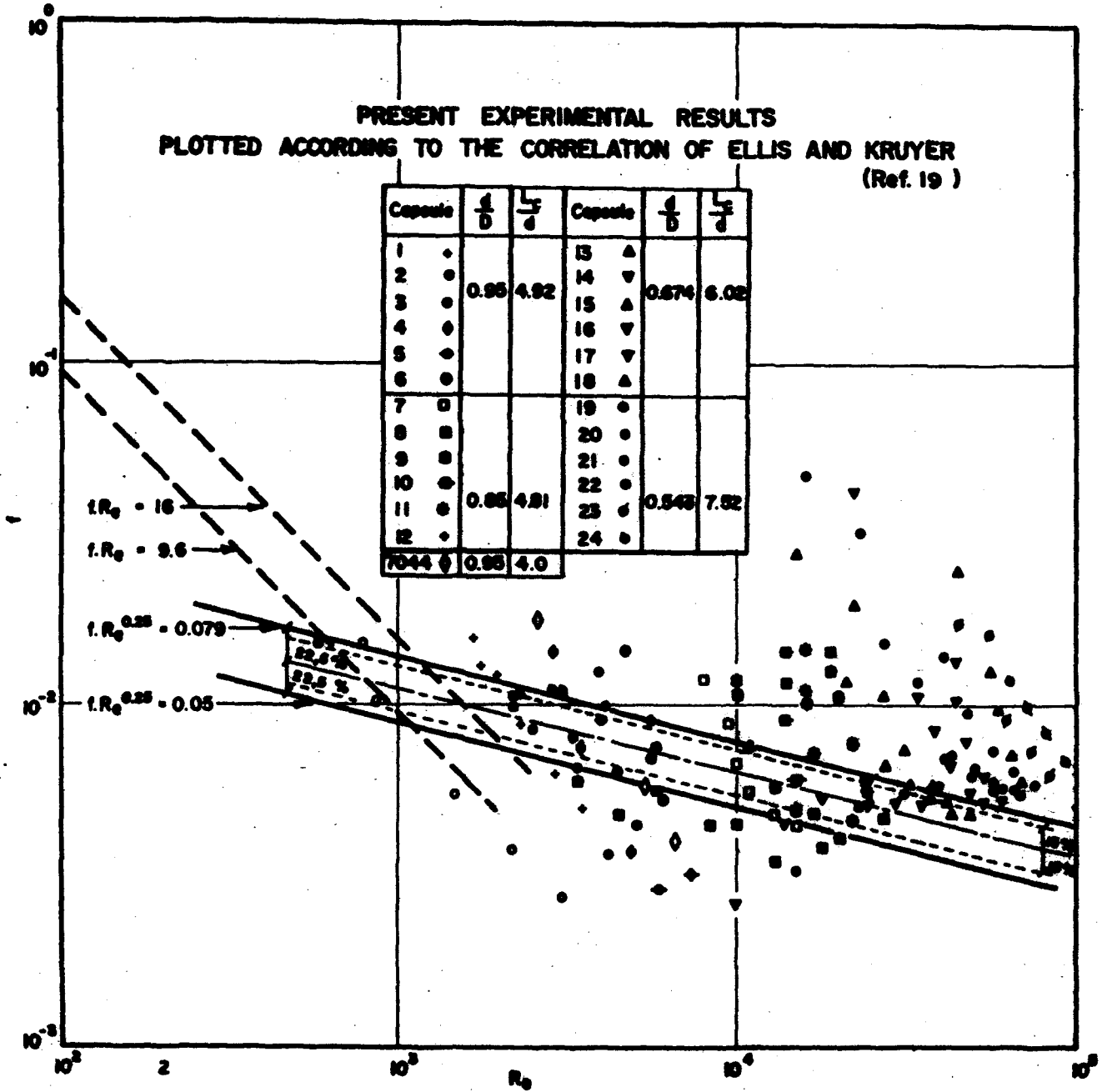
PRESENT EXPERIMENTAL RESULTS
PLOTTED ACCORDING TO THE CORRELATION OF ELLIS AND KRUYER
(Ref. 19)
Capsule
d/D
L/d
0.674
6.02
0.543
7.52
f.R_e = 16
f.R_e = 9.6
f.R_e^0.55 = 0.079
f.R_e^0.55 = 0.05
R_e

FIG. 15.57

These limits extend 22,5% above and below the mean curve $f R_e^{0,25} = 0,065$ and 60% of the data deviate by more than 22,5% above the mean curve, and 19% of the data deviate by more than 22.5% below the mean curve. If the 15% limits (shown dotted) are considered as in the case of the present correlation then 67.5% of data points differ by more than 15% above the log normal curve and 22% by more than 15% below the log normal curve.

Comparing the extreme deviations of data on the log plot (Figure 15.57) (reference 19) with extreme values on Figures 15.40, 15.55 and 15.56, it is clear that those points outside the arbitrary 15% limits are far more widely scattered in the former case. The same data were used for the graphs on Figures 15.56 and 15.57.

The experimental points given by Kruyer and Ellis (Figure 2.17) show a variation of 90% above and 58% below the mean for experimental data for capsules of $L_c/d = 6,07$.

As has already been pointed out (Chapter 2) the correlation only applies to very long capsules, of the order of $L_c/d > 40$.

Note that, not only does the correlation of Ellis and Kruyer give far greater scatter, than the one presented by the present author, but the equation from which it is derived (see Chapter 2) is far more complicated. Also the total head loss is evaluated as opposed to the excess head loss. Capsule lengths have to be subtracted from the total pipeline length for calculating the friction head loss in a capsule free section of the pipe.

P A R T VI

POWER CONSIDERATIONS

"The discovery that solid-water mixtures with a solids content up to 70% in weight cause less pipe friction loss, expressed in feet of mixture, than clear water, is the most important discovery in hydraulics in the last one hundred years."

A.J. Stepanoff

CHAPTER 16

POWER REQUIREMENTS

1. Definitions

In this Chapter power requirements for transporting trains of capsules are considered.

The power required, or utilised, is defined as the total power requirement of the system and is equal to the pumping power.

The power dissipated is defined as that due to energy dissipation and consists of two components, the excess power and the water power.

The water power is that which is required to overcome friction in a capsule free pipeline at velocity $(\overline{V})$, and the excess power is due to the additional energy dissipation across capsules.

Thus, the total power requirement consists of elevational power required to raise capsules, water power and excess power.

These definitions will first be dealt with in more detail and then the effect of the independent variables on the power will be discussed.

There are basically two problems involved: (1) The power requirement per unit length of pipeline to maintain a steady flow of capsules and (2) The power required for starting a capsule laden pipe from rest should the pipeline be temporarily shut down.

Figure 16.1 shows the power required per unit length (P/L) as a function of the mean water velocity $(\overline{V})$ in the pipeline for capsule number 12 ($d/D = 0,85$; $L_c/d = 4,81$ and $S_c = 4,90$) with mass flow delivery rate (θ) as parameter. The lowest curve, i.e. "water only" is the power dissipated for a capsule mass flow delivery rate of zero.

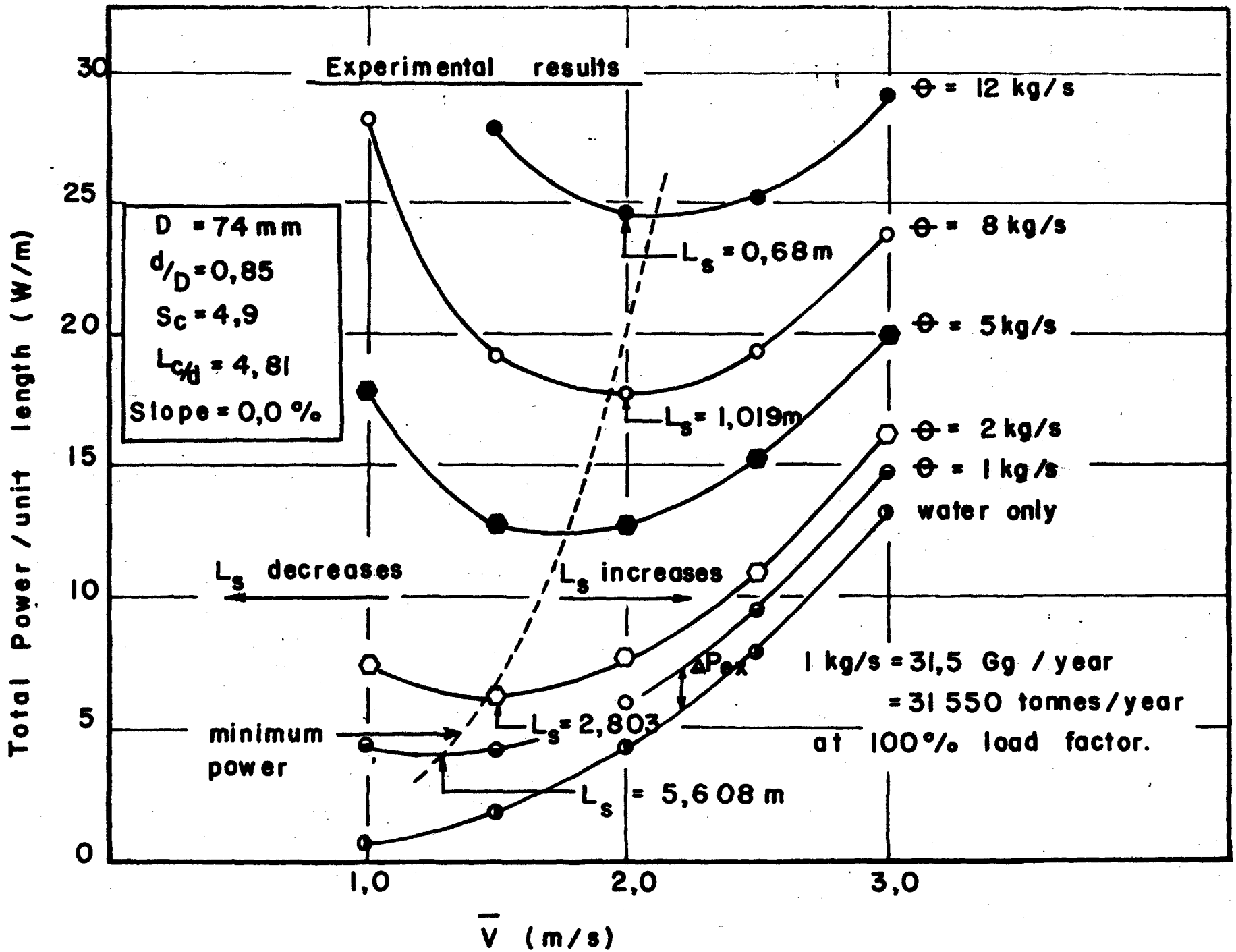
Experimental results
D = 74 mm
d/D = 0,85
Sc = 4,9
Lc/d = 4,81
Slope = 0,0 %
Θ = 12 kg/s
Θ = 8 kg/s
Θ = 5 kg/s
Θ = 2 kg/s
Θ = 1 kg/s
water only
Ls = 0,68 m
Ls = 1,019 m
Ls = 2,803
Ls = 5,608 m
Ls decreases
Ls increases
minimum power
ΔPex
1 kg/s = 31,5 Gg / year
= 31 550 tonnes/year
at 100 % load factor.
Total Power / unit length (W/m)
V̄ (m/s)
0
5
10
15
20
25
30
1,0
2,0
3,0

FIG. 16.1

This curve represents the power dissipated by water friction alone in a capsule free pipeline.

The power utilised per unit length (i.e. due to dissipation and elevation gain) is:

$$P_T/L = wQ_w\Delta H_p/L_s \qquad (16.1)$$

$$= \frac{w\pi D^2}{4}\ \overline{V}\left[\frac{(\Delta H_c)_s}{L_s} + (d/D)^2\ \frac{L_c}{L_s}|S_c-1|\sin\phi + \Delta h_f/L_s + \sin\phi\right] \qquad (16.2)$$

However the total power <u>dissipated</u> per unit length is:

$$P/L = \frac{w\pi D^2}{4}\ \overline{V}\left[\frac{(\Delta H_c)_s}{L_s} + \frac{2f\overline{V}^2}{gD}\right] \qquad (16.3)$$

$P = P_T$ for a horizontal pipe

where $(\Delta H_c)_s$ = excess energy dissipation due to capsule

$= \Delta H_c$ when $\phi = 0$.

Note that the power <u>dissipated</u> on the slope is different from that which is dissipated when the pipeline is horizontal due to the effect of centre to centre capsule spacing length (L_s) which is a function of the capsule velocity (V_c). Thus, for the same capsule mass delivery rate the capsule spacing is less on the slope (see Section 7).

<u>Water only</u>

The "water only" curve for a horizontal pipe is represented by:

$$\left(\frac{P}{L}\right)_w = w\,\overline{V}\,\frac{\pi D^2}{4}\ \frac{2f\overline{V}^2}{gD} \propto \overline{V}^3\,Df \qquad (16.4)$$

from Blasius $f \propto (\overline{V}D)^{-0,25}$

$$\therefore \qquad (P/L)_w \propto \overline{V}^{2,75} \times D^{0,75}$$

and for a particular pipe diameter

$$(P/L)_w \propto \overline{V}^{2,75} \qquad (16,5)$$

Excess Power (experimental)

The excess power dissipated over and above the water power per unit length of pipeline, is:

$$\Delta P_{ex}/L = wQ\ (\Delta H_c/L_s) \qquad (16.6)$$

$$= \frac{w\pi D^2}{4}\ \overline{V}\left[\frac{(\Delta H_c)'_s}{L_s} - (d/D)^2(L_c/L_s)|S_c-1|\sin\phi\right] \qquad (16.7)$$

and for horizontal pipes

$$\Delta P_{ex} = (w\pi D^2/4)\ \overline{V}(\Delta H_c/L_s)$$

Experimental values of excess power can be obtained from the above equation.

It is now clear how all the terms in Figure 16.1 were obtained.

2. Effect of mean water velocity on power

For a particular mass flow delivery rate the total power dissipated per unit length decreases to a minimum value and then increases with increasing velocity values, approaching the "water only" curve.

Figure 16.2 shows the power per unit length separated into the two components of excess power (ΔP_{ex}) and water power.

The water power per unit length increases approximately as the mean water velocity to the power 2,75 for smooth pipes and this exponent is increased to 3,0 for fully turbulent flow in rough pipes.

At the same time the excess power due to the capsule presence decreases as a function of mean water velocity to the power 0,75 and the reciprocal of the capsule velocity. The later observation is described below:

It has previously been shown (Chapter 15) that

$$\Delta H_c/L_c = 25(2f)(d/D)^2|S_c-1|$$

Inserting the Blasius equation for smooth pipes yields

$$\Delta H_c = \frac{(0,079\times25\times2)}{(\overline{V}D/\nu)^{0,25}}\ L_c\ (d/D)^2|S_c-1|$$

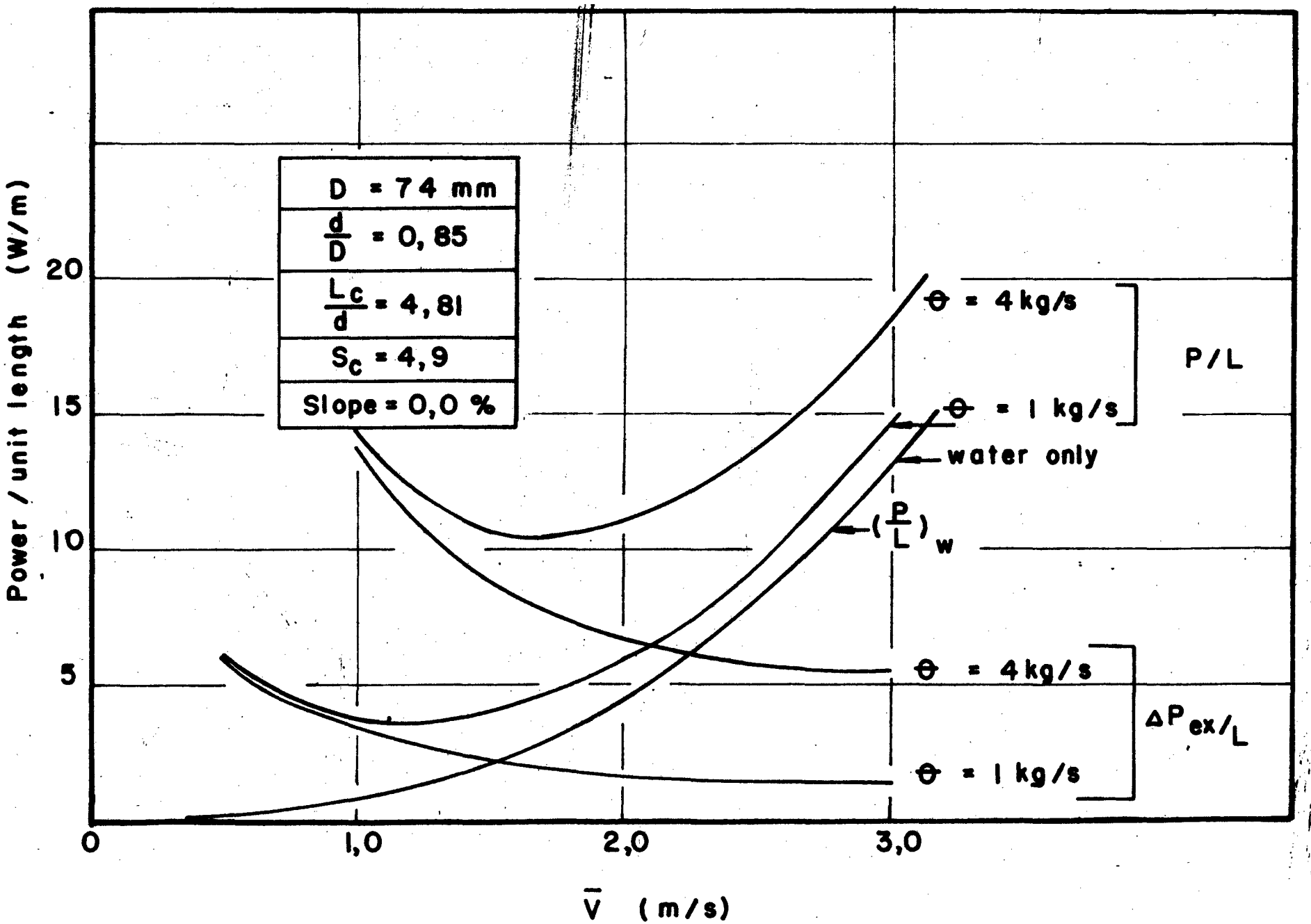
D = 74 mm
d/D = 0,85
Lc/d = 4,81
Sc = 4,9
Slope = 0,0 %
Power / unit length (W/m)
20
15
10
5
0
1,0
2,0
3,0
V̄ (m/s)
θ = 4 kg/s
θ = 1 kg/s
water only
(P/L)w
P/L
θ = 4 kg/s
θ = 1 kg/s
ΔPex/L

FIG. 16.2

Inserting this value for ΔH_c in equation (16.6) for excess power gives:

$$\Delta P_{ex}/L = (\tfrac{\pi}{4} \times 50 \times 0{,}079)\ w\ \overline{V}^{0,75}(\nu/D)^{0,25}(L_c/L_s)\ d^2|S_c-1|$$

For a capsule mass flow delivery rate (θ) of unity (kg/s) the centre to centre capsule spacing is given by:

$$L_s = M_c\ V_c \tag{16.8}$$

where M_c = capsule mass (kg)

$$\therefore \quad \Delta P_{ex}/L = 38{,}8 \left[\frac{|S_c-1|}{S_c^2}\ \frac{\overline{V}^{0,75}}{V_c}\right](\nu/D)^{0,25}$$

$$\therefore \quad \Delta P_{ex}/L \propto \frac{|S_c-1|}{S_c^2}\ \frac{\overline{V}^{0,75}}{V_c D^{0,25}} \tag{16.9}$$

and $V_c = m(\overline{V} - V_i)$

$$\therefore \quad \Delta P_{ex}/L \propto \frac{|S_c-1|}{S_c^2}\ \left|\frac{\overline{V}^{0,75}}{m(\overline{V}-\overline{V}_i)}\right|\ 1/D^{0,25}$$

For a particular capsule geometry and density in a pipe of fixed slope and diameter:

$$\Delta P_{ex}/L \propto \overline{V}^{0,75}/(\overline{V} - \text{const}) \tag{16.10}$$

As $\overline{V}$ increases the numerator decreases and the denominator increases. Thus, the excess power per unit length decreases with increasing velocity.

The combination of increasing water power and decreasing excess power due to capsules, must yield minimum power values as shown on Figure 16.1.

These minimum values will be discussed later.

3. Effect of θ and L_s

As would be expected, the power dissipated per unit length at a particular value of the mean water velocity increases with increasing capsule mass flow delivery rate (θ). Figure 16.3 shows that this increase is linear with the rate of increase of power per unit length decreasing with

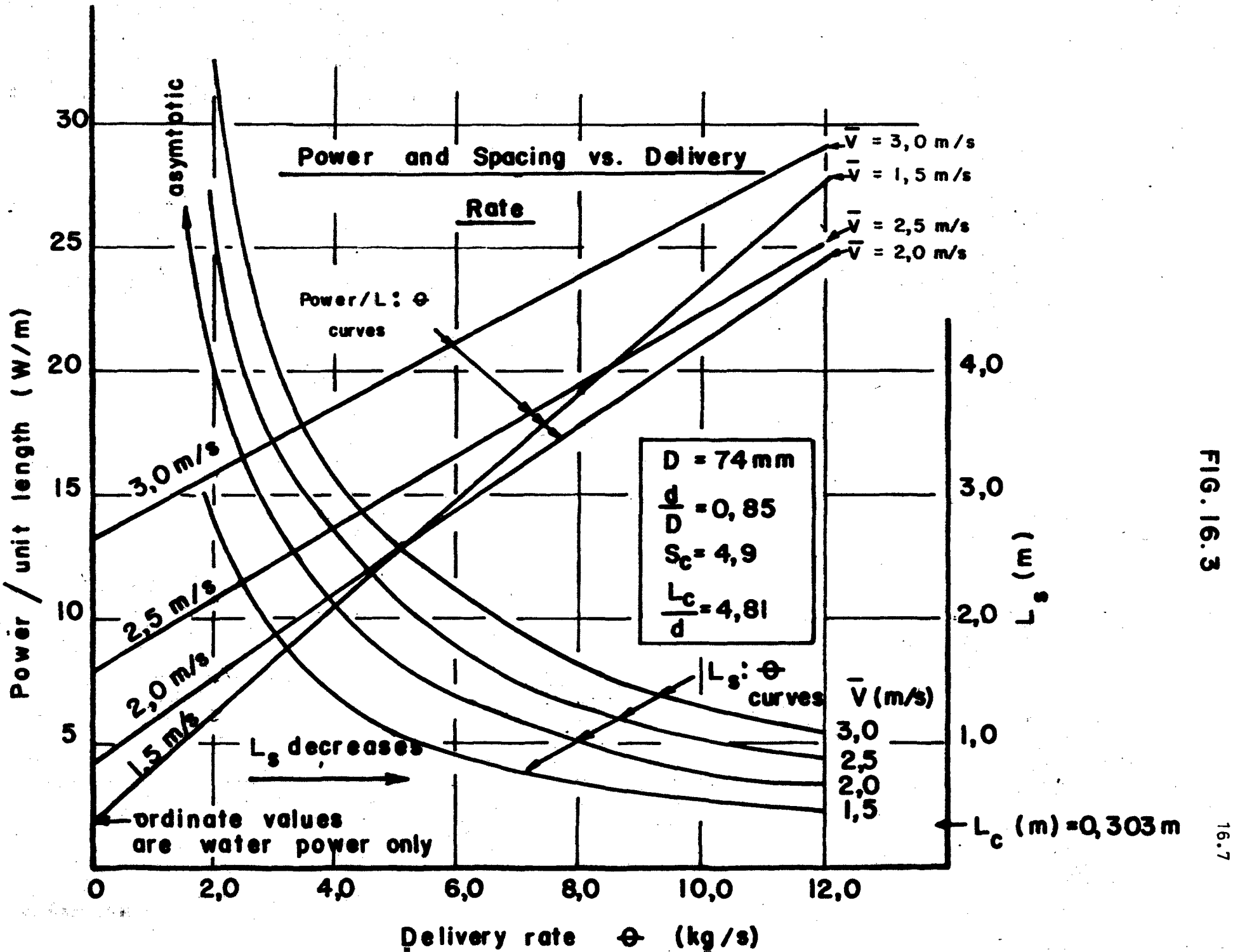
Power and Spacing vs. Delivery Rate
asymtptic
$\bar{V}$ = 3,0 m/s
$\bar{V}$ = 1,5 m/s
$\bar{V}$ = 2,5 m/s
$\bar{V}$ = 2,0 m/s
Power/L: Θ curves
3,0 m/s
2,5 m/s
2,0 m/s
1,5 m/s
D = 74 mm
d/D = 0,85
S_c = 4,9
L_c/d = 4,81
L_s: Θ curves
$\bar{V}$ (m/s)
3,0
2,5
2,0
1,5
L_s decreases
ordinate values are water power only
L_c (m) = 0,303 m
Power / unit length (W/m)
L_s (m)
Delivery rate Θ (kg/s)
0
2,0
4,0
6,0
8,0
10,0
12,0
5
10
15
20
25
30
1,0
2,0
3,0
4,0

FIG. 16.3

velocity.

As the delivery rate increases the spacing length between capsules naturally decreases as can be seen from Figure 16.1. So that at θ = 1 kg/s (i.e. θ = 31,55 Gg p.a. = 31 550 tonnes p.a. at 100% load factor) the spacing between capsules (L_c = 303 mm) is L_s = 5,608 m, for minimum power, and if the delivery rate is increased to θ = 12 kg/s (378 000 tonnes p.a.), the spacing length decreases to L_s = 0,68 m, implying a higher injection rate. The mean velocity has been increased from $\overline{V}$ = 1,25 to 2,0 m/s for a 12 to 1 ratio of capsule mass delivery rate whereas the power increase per unit length is from 4,0 W/m to 24,6 W/m; a ratio of approximately 6 to 1. Thus a ratio of 6 : 1 power increase gives about a 12 : 1 capsule mass flow delivery rate increase.

Figure 16.3 also shows how the spacing length (L_s) between capsules has to decrease for increasing delivery rates. The right hand side ordinate representing spacing length with the capsule length (L_c) shown near the bottom.

It is clear that for $\theta \to 0$ the spacing length $\to \infty$ and the curve is asymptotic to the ordinate on the left hand side. And as the capsule mass flow delivery rate increases a point will eventually be reached when $L_s < L_c$ which is physically impossible.

4. Effect of diameter ratio

Perhaps the most interesting aspect of the power dissipated is the effect of diameter ratio, since this answers the question: What is the most economical diameter ratio at which to operate from the viewpoint of minimum energy dissipation?

Figure 16.4 shows power per unit length of pipeline as a function of mean water velocity for various diameter ratio capsules all of the same

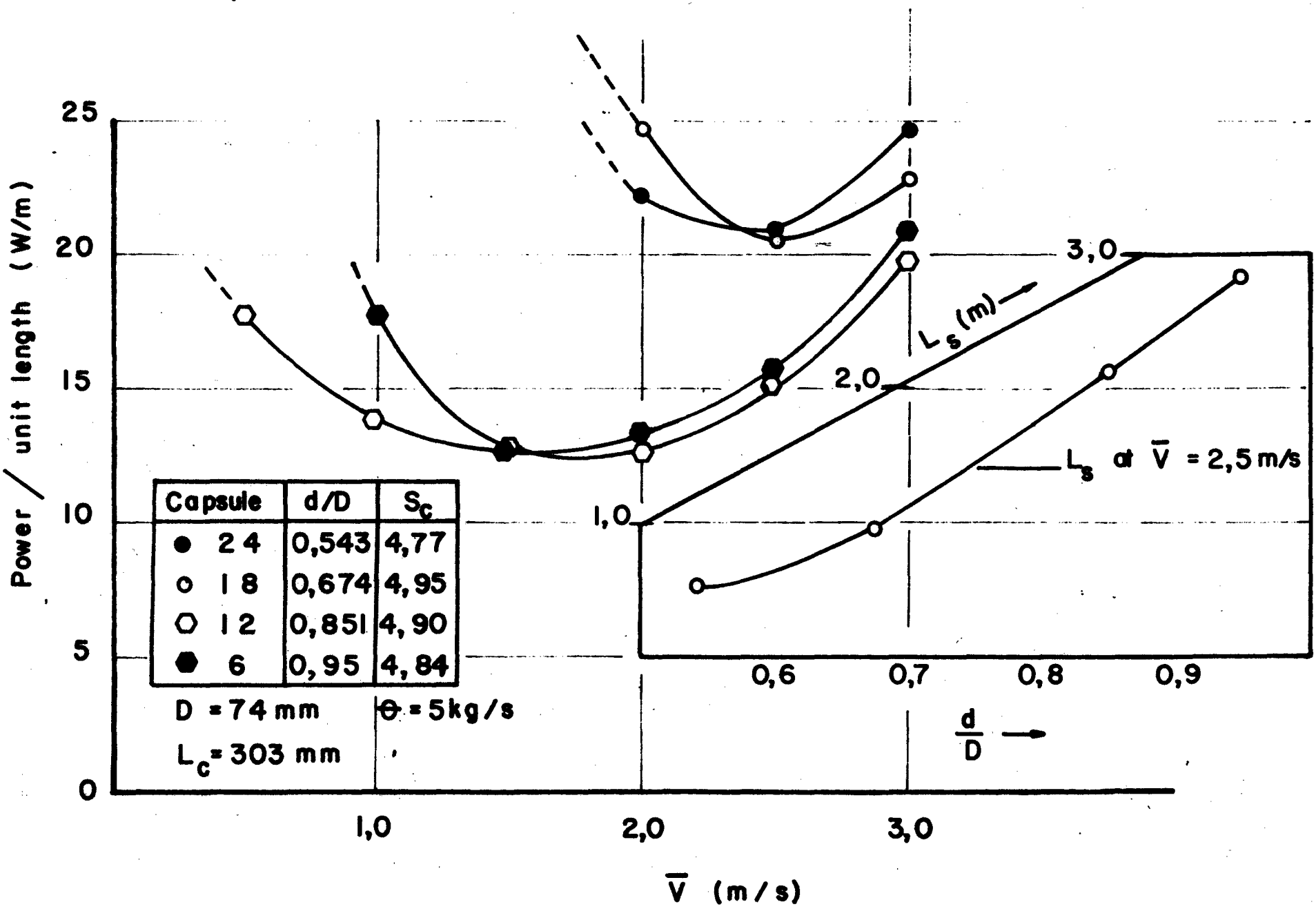
Power / unit length (W/m)
25
20
15
10
5
0
1,0
2,0
3,0
$\bar{V}$ (m/s)
Capsule | d/D | S_c
● 24 | 0,543 | 4,77
○ 18 | 0,674 | 4,95
⬡ 12 | 0,851 | 4,90
⬢ 6 | 0,95 | 4,84
D = 74 mm
L_c = 303 mm
$\dot{m}$ = 5 kg/s
L_s (m)
3,0
2,0
1,0
L_s at $\bar{V}$ = 2,5 m/s
0,6
0,7
0,8
0,9
$\frac{d}{D}$

FIG. 16.4

length (L_c = 303 mm) and of roughly the same density.

The larger diameter ratios are considerably more economical to transport than the smaller ones although there is little to choose between capsules 6 and 12 (d/D) = 0,95 and 0,851 respectively). However, capsule no. 12 requires less material if containerisation is considered, capsule no. 6 (d/D = 0,95) requires fewer capsules.

The capsule spacing as a function of diameter ratio is shown on the right of the diagram, and this curve indicates the rate at which distance between capsules increases as diameter ratio increases. Figure 16.5 is a similar diagram except that in this case dimensionally similar capsules were used (L_c/d = 4,0 and S_c = 4,0).

For a constant delivery rate (θ = 5 kg/s) it is clear that minimum power dissipation per unit length occurs at $\overline{V}$ = 1,5 m/s and the diameter ratio is again d/D = 0,85. In this case (as before) more capsules are required for d/D = 0,851 than for d/D = 0,950, and the spacing length (L_s) as well as the capsule velocity (V_c) is greater for the larger capsule. On the other hand the capsules themselves are longer.

The power dissipation per unit length for the smaller pipeline tested (D = 44 mm) shows the same trend (see Figure 16.6). That is, the power requirement increases with diameter ratio decrease. Note that the dotted sections of the curves represent an impossible situation since $L_s < L_c$. The way in which linear spacing (C_L) and volumetric concentration (C_V) decreases as spacing length and diameter ratio increase, is shown on the diagram in the top right hand corner. The linear concentration is defined as:

$$C_L = L_c/L_s$$

and the transport (or spatial) volumetric concentration (in the pipe) is defined as:

FIG. 16.5

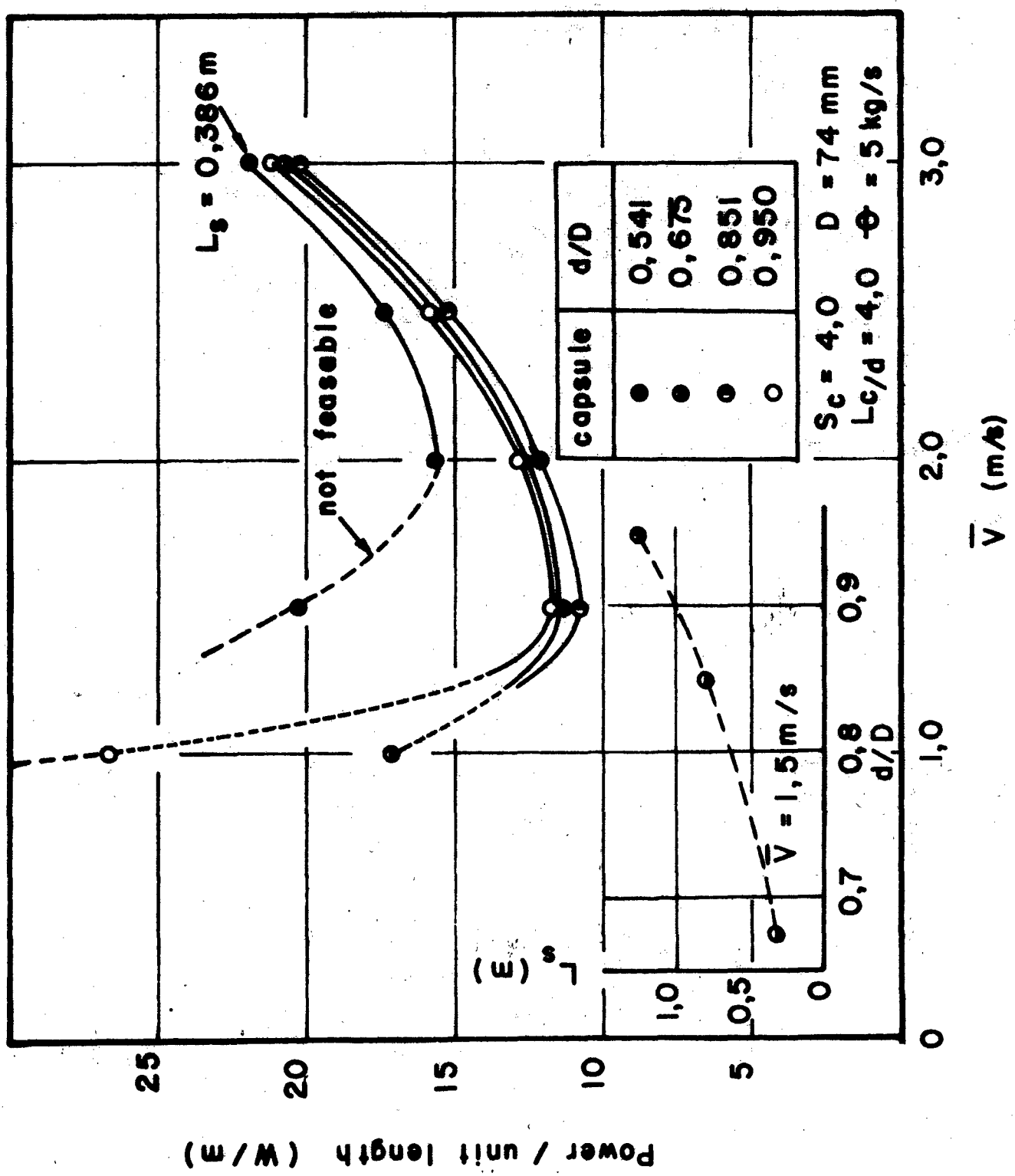
Power / unit length (W/m)
25
20
15
10
5
0
1,0
2,0
3,0
$\bar{V}$ (m/s)
L_s = 0,386 m
not feasable
S_c = 4,0 D = 74 mm
$L_{c/d}$ = 4,0 Φ = 5 kg/s
capsule
d/D
0,541
0,675
0,851
0,950
L_s (m)
$\bar{V}$ = 1,5 m/s
0
0,5
1,0
0,7
0,8
0,9
d/D

FIG. 16.6

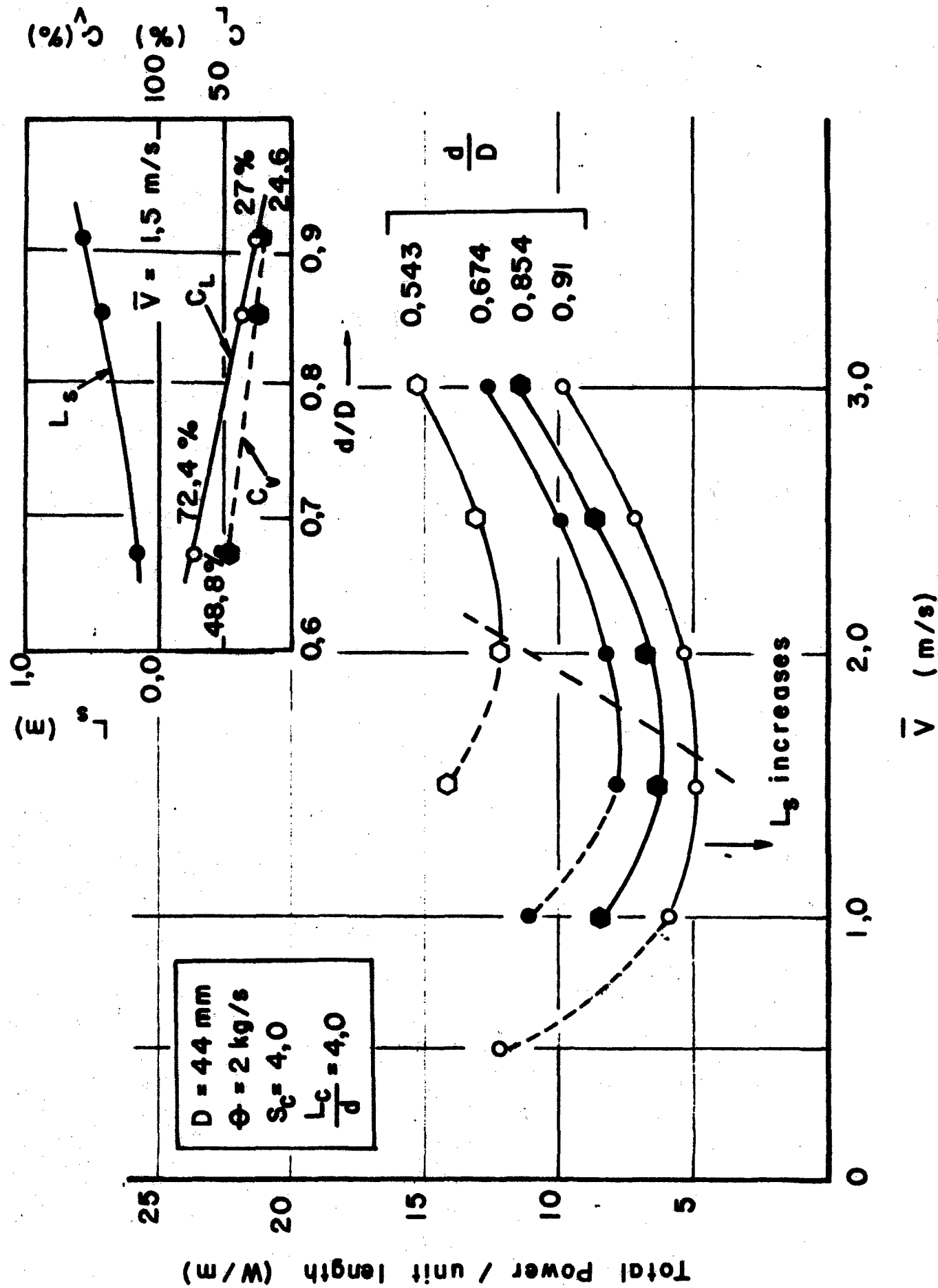
Total Power / unit length (W/m)
25
20
15
10
5
0
1,0
2,0
3,0
$\bar{V}$ (m/s)
L_s increases
d/D
0,543
0,674
0,854
0,91
$\frac{d}{D}$
D = 44 mm
Φ = 2 kg/s
S_c = 4,0
$\frac{L_c}{d}$ = 4,0
L_s (m)
1,0
0,0
0,6
0,7
0,8
0,9
$\bar{V}$ = 1,5 m/s
C_L
C_V
72,4 %
48,8%
27%
24,6
100 (%)
50
C_L
$\hat{C}$ (%)

$$C_{vt} = \frac{L_c}{L_s} (d/D)^2 \qquad (16.11)$$

At $\overline{V}$ = 1,5 m/s the spacing length (L_s) increases from 163 mm for d/D = 0,543 and L_c = 118 mm to 585 mm for d/D = 0,91 and L_c = 158 mm. At the same time linear concentration (C_L) decreases from 72,4% to 27% and volumetric concentration from 48,8% to 24,6%.

Thus Figure 16.6 indicates that diameter ratio of 0,91 (the highest used for negotiating bends) requires the least power per unit length for a load of θ = 2 kg/s and the concentration (i.e. the number of capsules per unit length) is also lower for the largest diameter ratio.

The conclusion that can be drawn from experimental results presented in this way is that for minimum power the diameter ratio should be as large as is feasible for negotiating bends. The reasons for this are:

(1) the larger the capsule diameter (all other factors being equal) the greater the capsule velocity.
(2) The larger capsules have a greater carrying capacity.
(3) Even though the large capsules dissipate more excess energy, this adverse effect is not sufficient to overcome the above two advantages.

5. Effect of capsule density

The question here is; which capsule transportation system requires less power, many sparsely packed capsules or a few densely packed capsules?

It will be shown that the lower specific gravity capsules have the advantage, powerwise, over the heavier capsules.

Figure 16.7 shows power per unit length as a function of mean water velocity with capsule specific gravity as parameter at a constant value of diameter ratio, d/D = 0,85.

This figure indicates that the power requirement drops continuously with reduction in specific gravity. However, there is, naturally, a

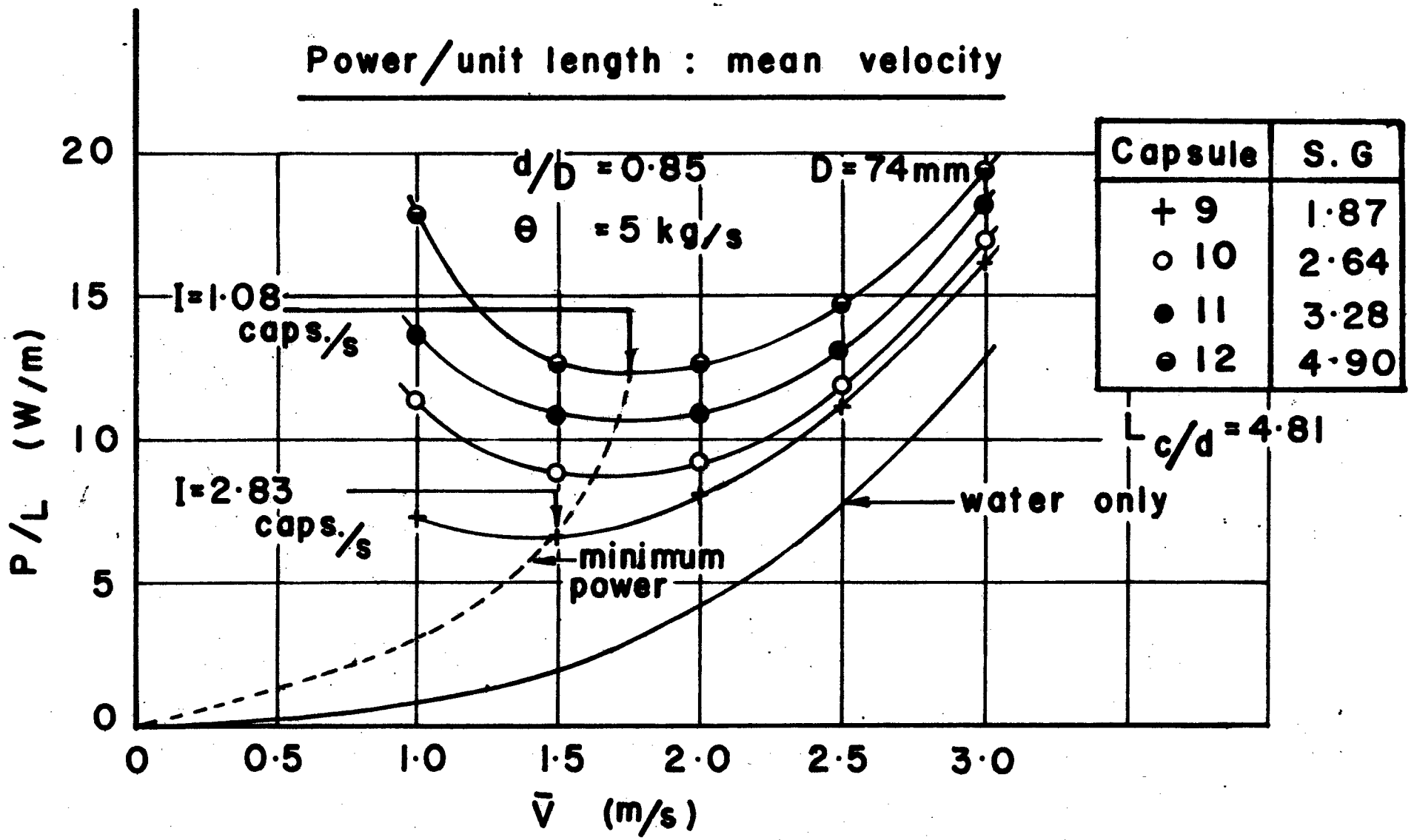
Power/unit length : mean velocity
d/D = 0·85
θ = 5 kg/s
D = 74mm
I = 1·08 caps./s
I = 2·83 caps./s
minimum power
water only
L c/d = 4·81
Capsule
S.G
+ 9
1·87
○ 10
2·64
● 11
3·28
● 12
4·90
P/L (W/m)
V̄ (m/s)
0
5
10
15
20
0·5
1·0
1·5
2·0
2·5
3·0

FIG. 16.7

corresponding increase in the required injection rate since L_s decreases and a practical limit is reached when successive capsules are in contact. Even before this situation is achieved the number of containers, or capsules, stored in the pipeline may be considered excessive.

For example with a capsule specific gravity of 1,87 and θ = 5 kg/s, a minimum power requirement is achieved at a water velocity of 1,5 m/s. For this condition the required injection rate is I = 2,83 capsules per second and the linear concentration (C_L) = 58,3% (nearly 60% of the pipeline length is occupied by capsules). This gives a volumetric concentration (C_{vt}) = 42%.

Even though sparsely packed capsules lead to a reduced power demand it is obvious that less capsules are required at, say, capsule specific gravity (S_c) = 4,9. In this case the injection rate is only 1,08 capsules/s and linear linefill is reduced to about C_L = 43% although the mean water velocity should be slightly higher for the minimum power requirement.

In the extreme case of capsule specific gravity (S_c) = 1,0, the power requirements for a capsule transportation system are coincident with the "water only" curve and the only excess power in this case, for the system, is that due to capsule injection. At a mean water velocity of 1,5 m/s and a delivery rate (θ) = 5 kg/s, the injection rate (I) now becomes 4,52 capsules/s, with a linear concentration (C_L) of 91%.

More capsules are required in this case because less material can be packed into the same volume. However, since the capsule velocity is in this case slightly higher than the mean water velocity, the delivery rate is somewhat increased.

To sum up; the effect of capsule specific gravity is to reduce the power requirement as specific gravity is decreased. Conversely, more

capsules are required and an economic analysis to determine the optimum specific gravity can only be carried out if the cost of manufacturing and handling each capsule is compared with the reduction in power due to the lighter capsules.

Note that it is not always possible to vary capsule specific gravity over a wide range so that this variable may be fixed for design purposes.

6. Effect of capsule length

Figure 16.8 shows total power per unit length of pipeline as a function of mean water velocity with capsule length to diameter ratio as parameter for a constant capsule mass delivery rate of $(\theta) = 5$ kg/s. For this diameter ratio, $(d/D) = 0{,}91$, the minimum power per unit length is at a mean velocity $(\overline{V}) = 2$ m/s.

The length to diameter ratio yielding the minimum power appears to be $L_c/d = 4{,}0$. This can be more clearly seen on Figure 16.9, which shows the minimum power per unit length (at $\overline{V} = 2$ m/s) as a function of length to diameter ratio (L_c/d).

It is likely that this curve is not of much significance and if the power per unit length at $\overline{V} = 2{,}0$ m/s is calculated from the empirical formulation, the dotted line which passes through the solid circles is obtained, and in this case the power per unit length of pipeline is not affected by the length of capsule.

This fact is verified in Figure 16.10 for the diameter ratio $(d/D) = 0{,}853$ with all other parameters unchanged. Figure 16.10 is an experimental plot whereas the solid circle points on Figure 16.9 are empirical.

It can be concluded that the power per length of pipeline is unaffected by the capsule length for a constant delivery rate.

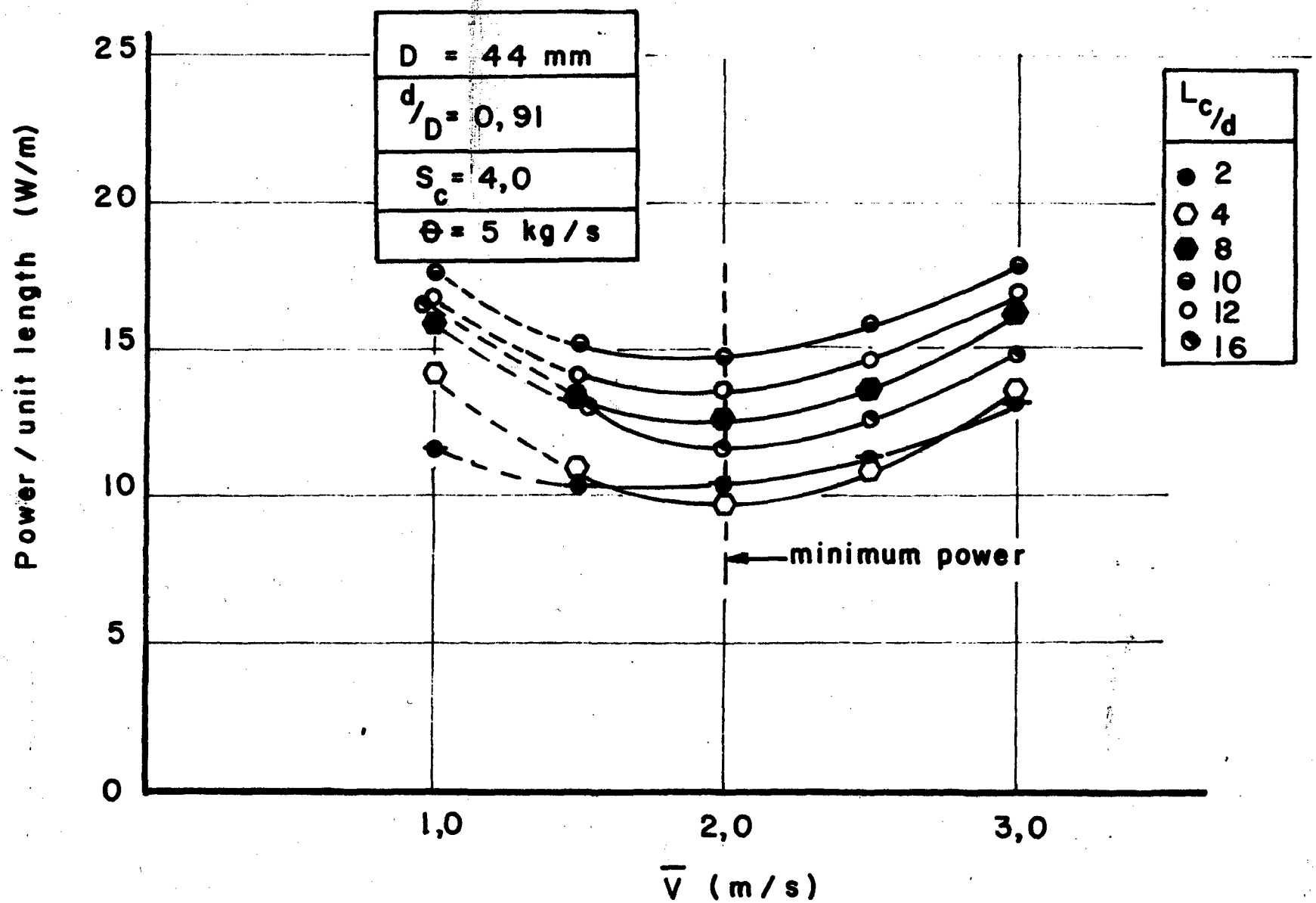
D = 44 mm
d/D = 0,91
Sc = 4,0
Θ = 5 kg/s
Lc/d
2
4
8
10
12
16
minimum power
Power / unit length (W/m)
25
20
15
10
5
0
1,0
2,0
3,0
V̄ (m/s)

FIG. 16.8

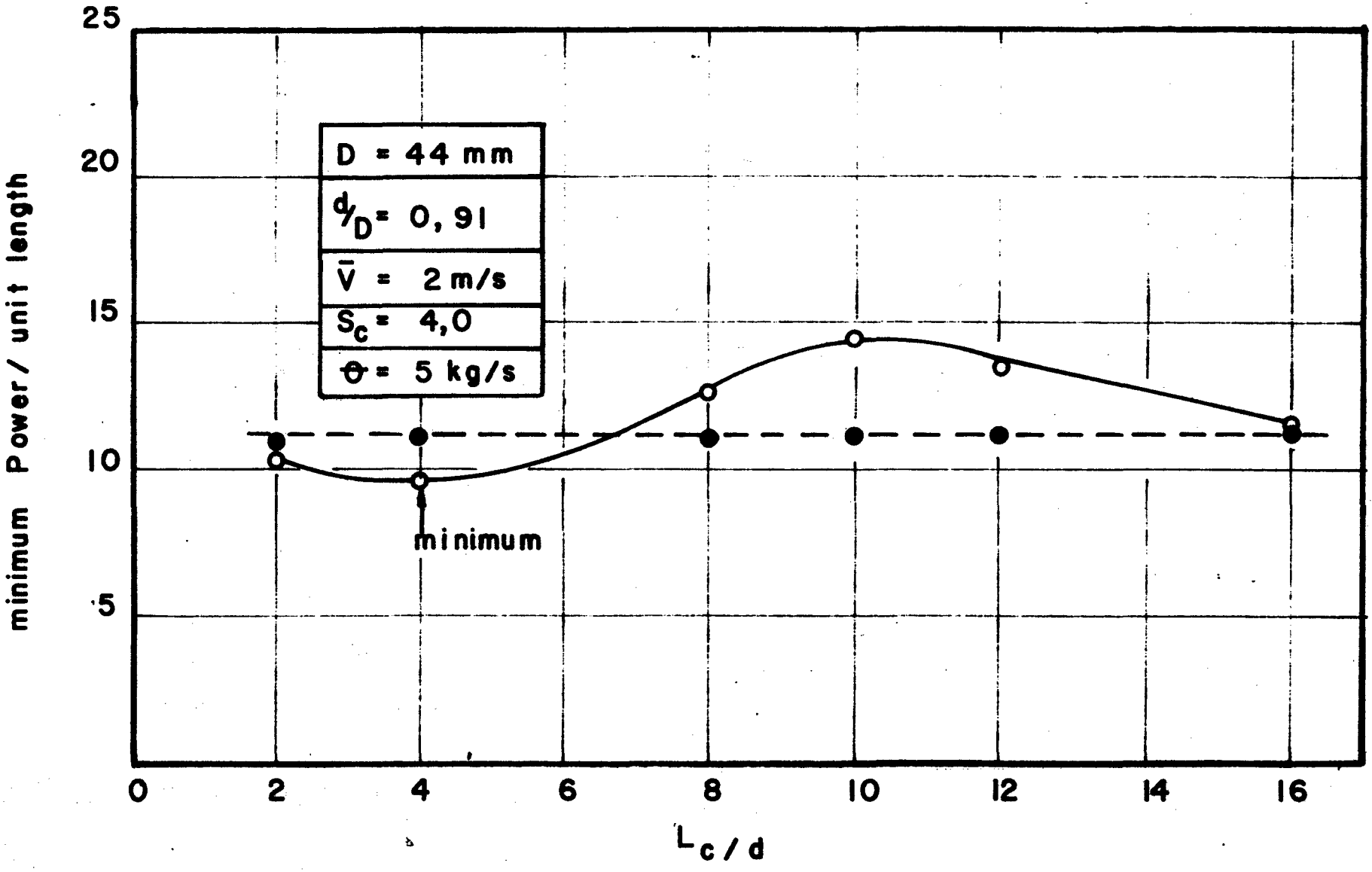
minimum Power / unit length
25
20
15
10
5
0
2
4
6
8
10
12
14
16
L_c / d
D = 44 mm
d/D = 0,91
$\bar{V}$ = 2 m/s
S_c = 4,0
θ = 5 kg/s
minimum

FIG. 16.9

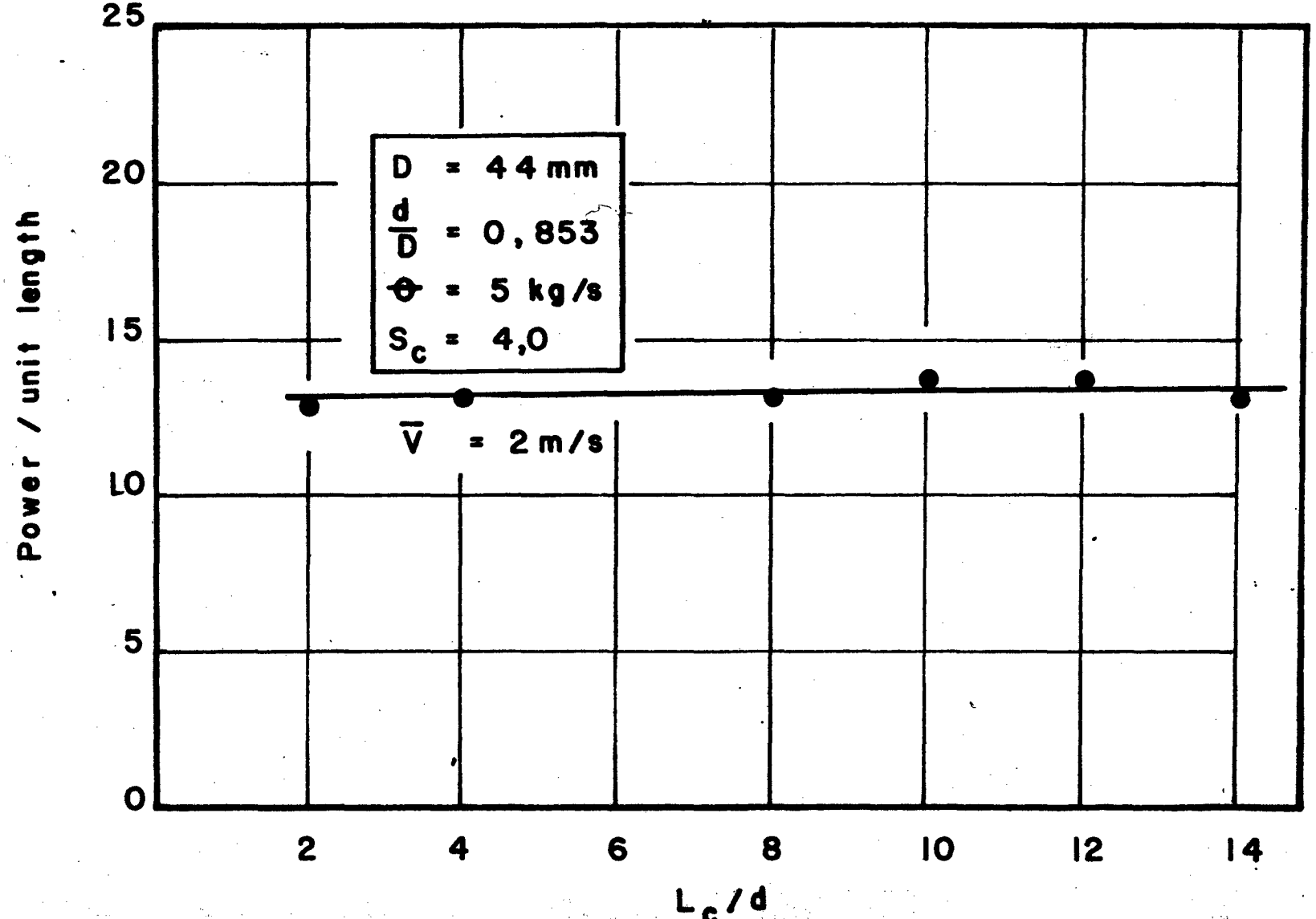
25
20
15
10
5
0
Power / unit length
D = 44 mm
d/D = 0,853
Φ = 5 kg/s
Sc = 4,0
V̄ = 2 m/s
2
4
6
8
10
12
14
Lc/d

FIG. 16.10

The only advantage to be gained from using longer capsules is that the spacing length can be increased and thus the injection rate decreased, whilst the linear concentration naturally remains constant for a specific delivery rate (see Figure 16.11). The saving here is that fewer capsule ends are needed, but the decreased injection rate must be offset against the difficulty of handling longer capsules.

7. Effect of slope

The main effect of having to transport capsules up a slope is the increase in the total power requirement due to potential energy as slope increases, but this power is required for any transportation system. There is, also, an increase in the excess dissipative power on the slope and this is due to decreasing capsule velocity on the slope for a constant delivery rate.

Figures 16.12 and 16.13 show total power utilised per unit length, (i.e. potential plus dissipated power) per capsule mass delivery rate of 1 kg/s for fixed geometries as the mean water velocity varies, with pipeline slope as parameter.

For the two diameter ratios shown, a pattern is evident which is repeated for other capsule geometries. The solid lines are experimental results and the dotted lines are theoretical results, where the excess head loss $(\Delta H_c)_s$ is obtained from the empirical relation

$$\Gamma = 25/\chi^2$$

These curves show that the total power utilised generally increases with velocity although for the lower slopes there appears to be a minimum power (i.e. slopes 0,0 and -5,4%) and the manner in which the lines curve indicate that there is a tendency towards a minimum total power value at higher slopes.

It is also to be expected that as slope increases the total power

FIG. 16. 11

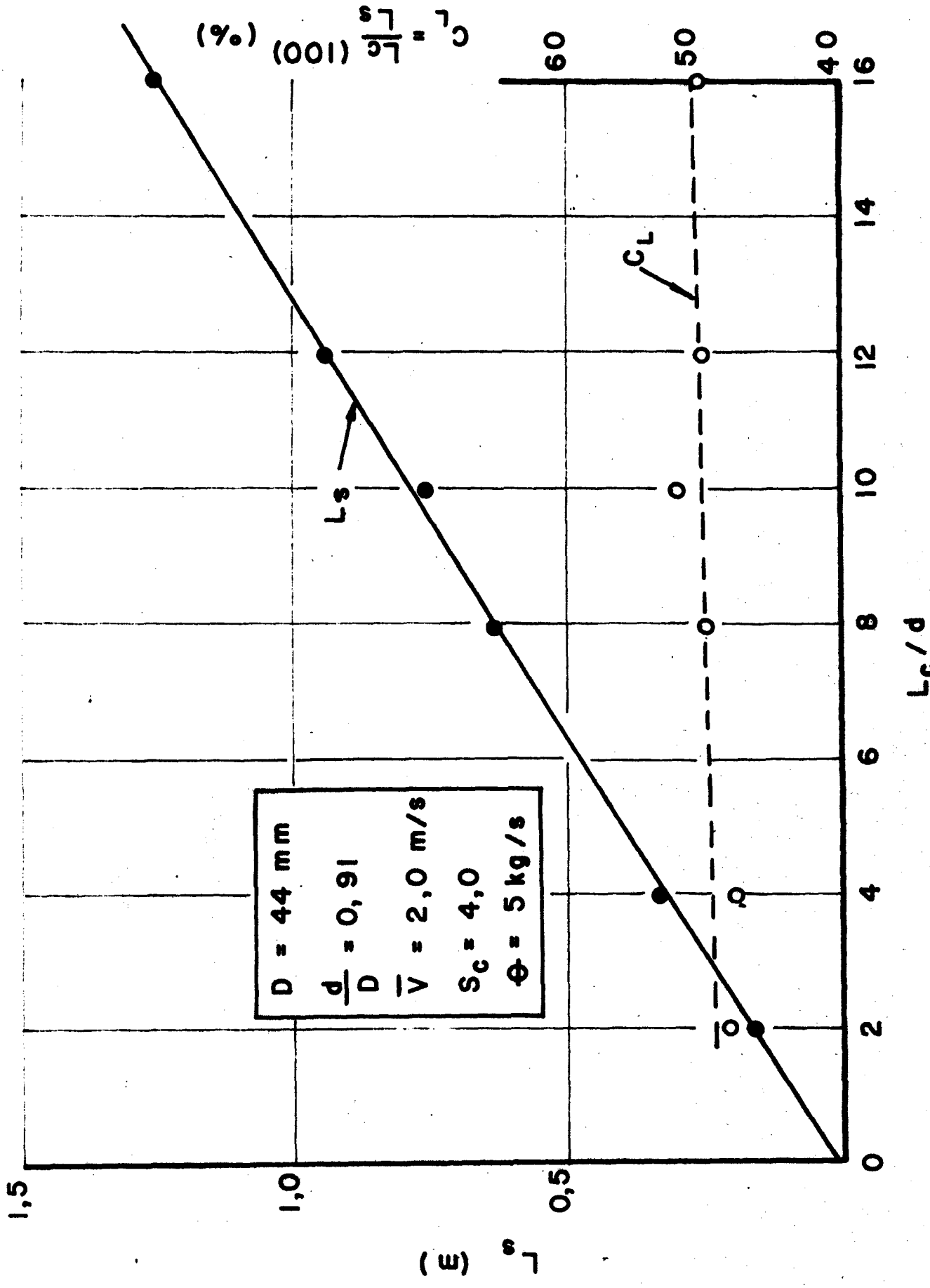
$C_L = \frac{L_c}{L_s}$ (%) (001)
60
50
40
16
14
12
10
8
6
4
2
0
L_c / d
C_L
L_s
D = 44 mm
$\frac{d}{D}$ = 0,91
V = 2,0 m/s
S_c = 4,0
Φ = 5 kg/s
1,5
1,0
0,5
L_s (m)

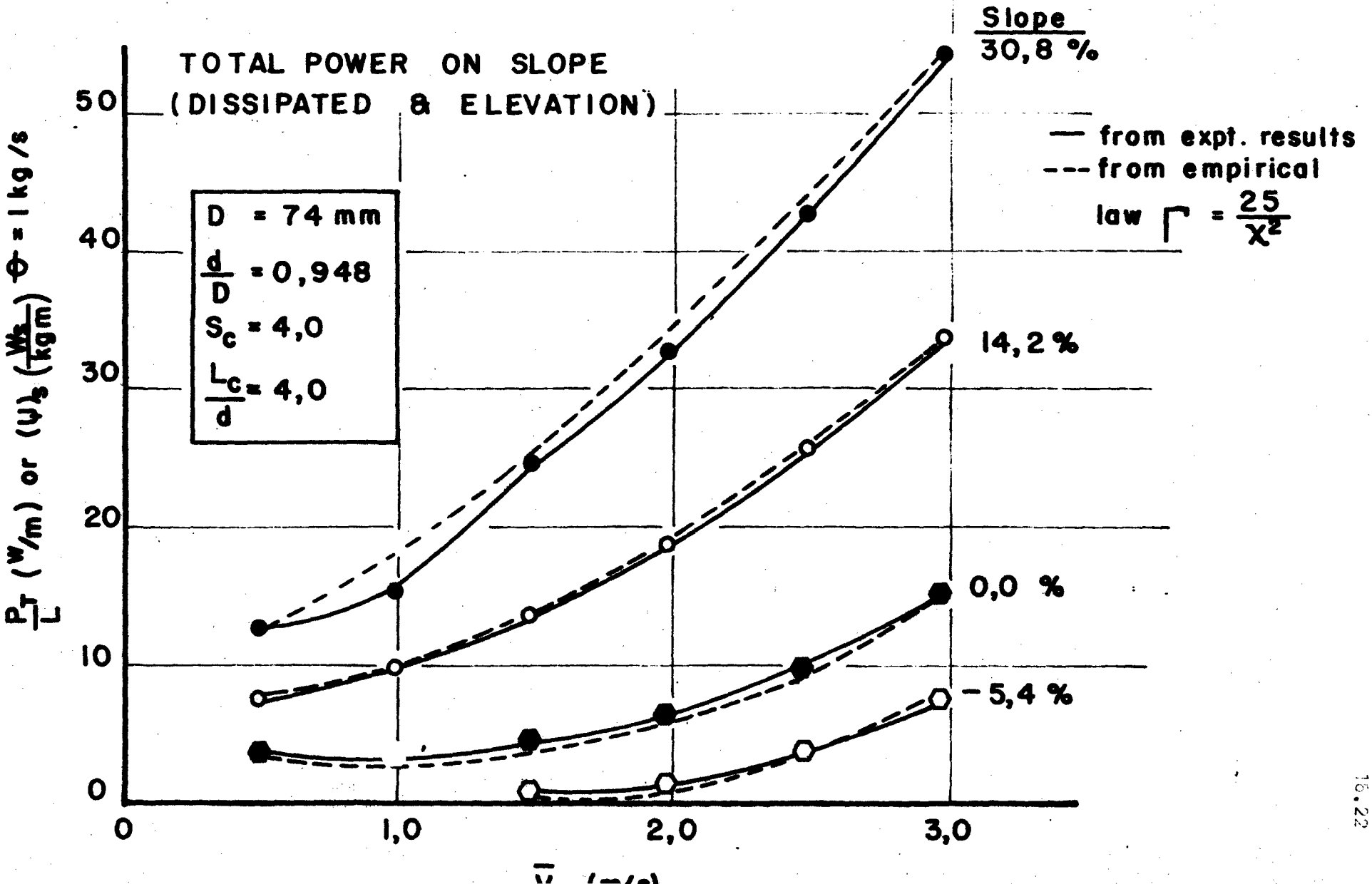
TOTAL POWER ON SLOPE
(DISSIPATED & ELEVATION)
D = 74 mm
d/D = 0,948
Sc = 4,0
Lc/d = 4,0
Slope
30,8 %
14,2 %
0,0 %
-5,4 %
— from expt. results
--- from empirical
law Γ = 25/X²
P_T/L (W/m) or (ψ)_s (Wk/kgm) Φ = 1 kg/s
0
10
20
30
40
50
0
1,0
2,0
3,0

FIG. 16.12

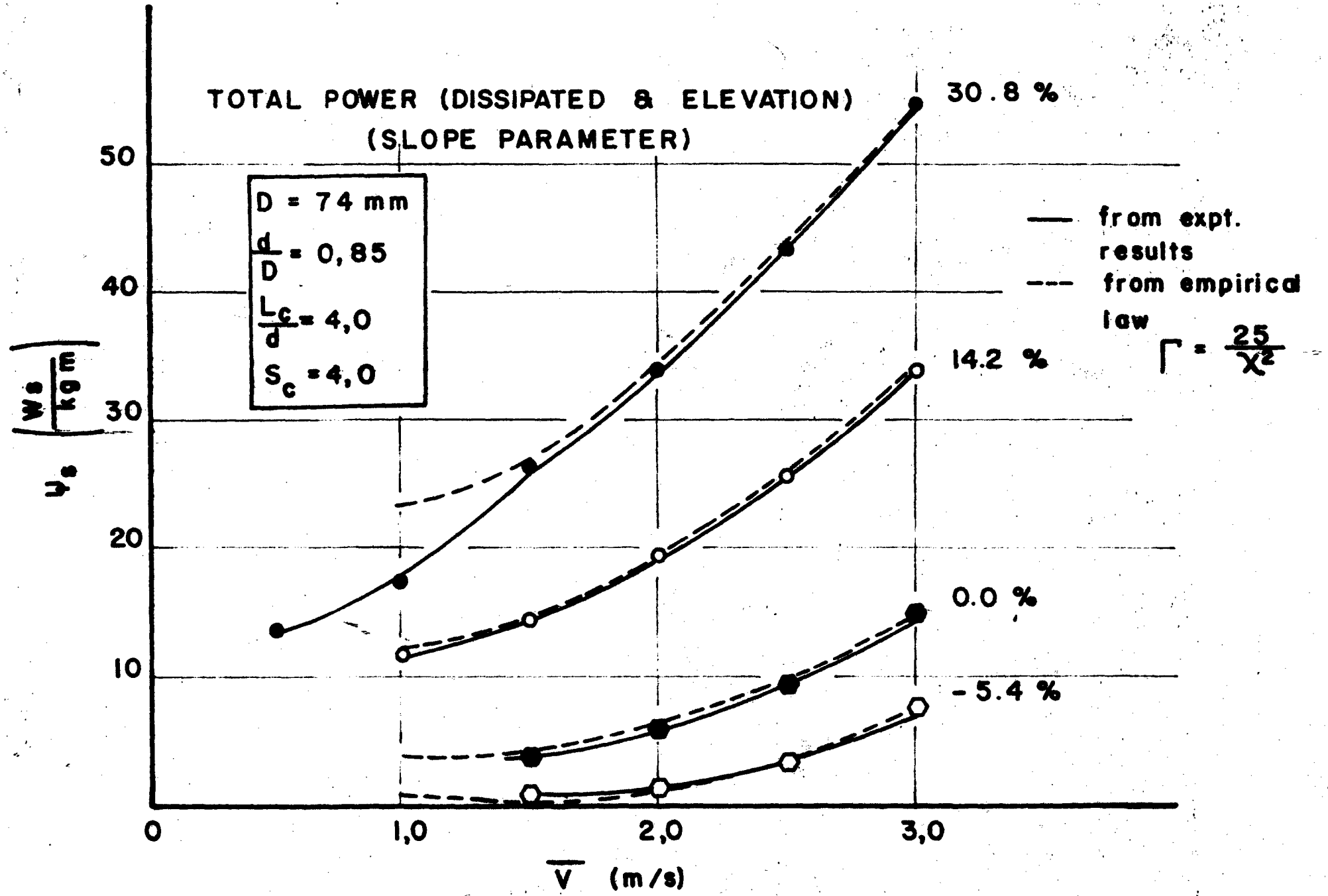

FIG. 16. 13

16.23

increases at all velocities.

7.1 Dissipated power

Figures 16.12 and 16.13 include elevational and dissipative power for the capsule and water, and a clearer picture of power demand for capsules on the slope can be obtained if the excess power due to the presence of the capsule alone is considered.

Subtracting from the ordinate values shown on graphs such as 16.12 and 16.13, the values for capsule elevational power plus water elevational and dissipative power yields graphs such as those given on Figure 16.14 to 16.17. In Figures 16.14, 16.15 and 16.16 (each for a different diameter ratio) it is seen that the excess ψ values increase steadily with mean water velocity. This is to be expected and was explained (see Section 1). ψ is defined as the power per unit length of pipe divided by the mass flow delivery rate and has the dimensions m/s^2.

Also on these graphs (Figures 16.14 to 16.17) it is apparent that as the slope increases from -5,4% to 30,8% the value of ψ_{ex} increases and the rate of increase becomes more rapid at low diameter ratios. This is the case for all diameter ratios as is apparent from the representative diameter ratios of $d/D = 0,946$; 0,84 and 0,675 given on Figures 16.14 to 16.16.

The reason for this phenomenon can be seen from equation (16.7) which can be simplified to:

$$\Delta P_{ex} \propto 1/L_s \, (C_1 - C_2 \sin \phi) \qquad (16.12)$$

where C_1 and C_2 are constants if the capsule geometry, excess head loss and delivery rate are kept constant.

As the slope increases the capsule velocity decreases for a constant mean water velocity. Therefore the centre to centre spacing length (L_s) must decrease to maintain the same delivery rate,

FIG. 16.14

EFFECT OF SLOPE ON ψ_{ex}

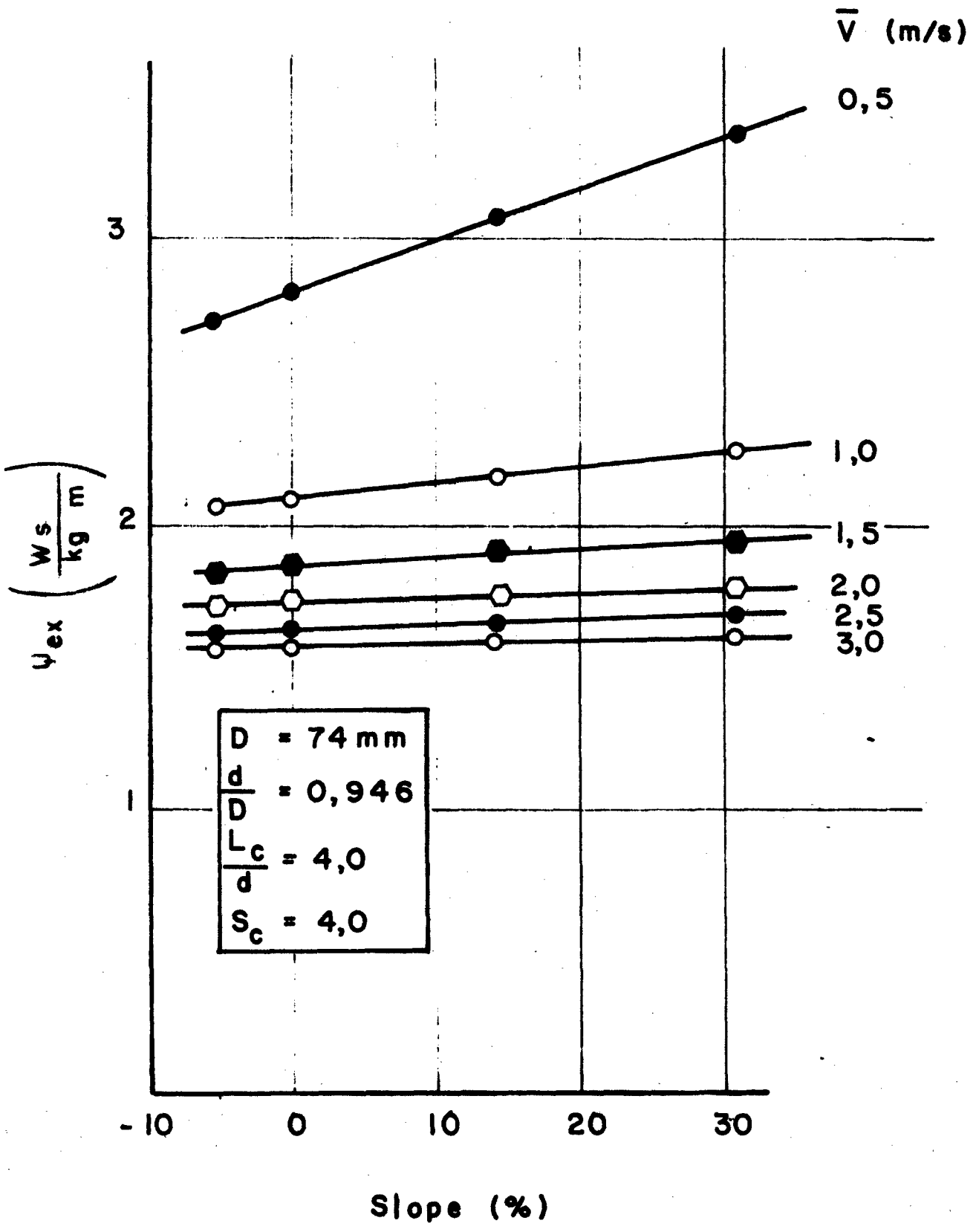

FIG. 16. 15

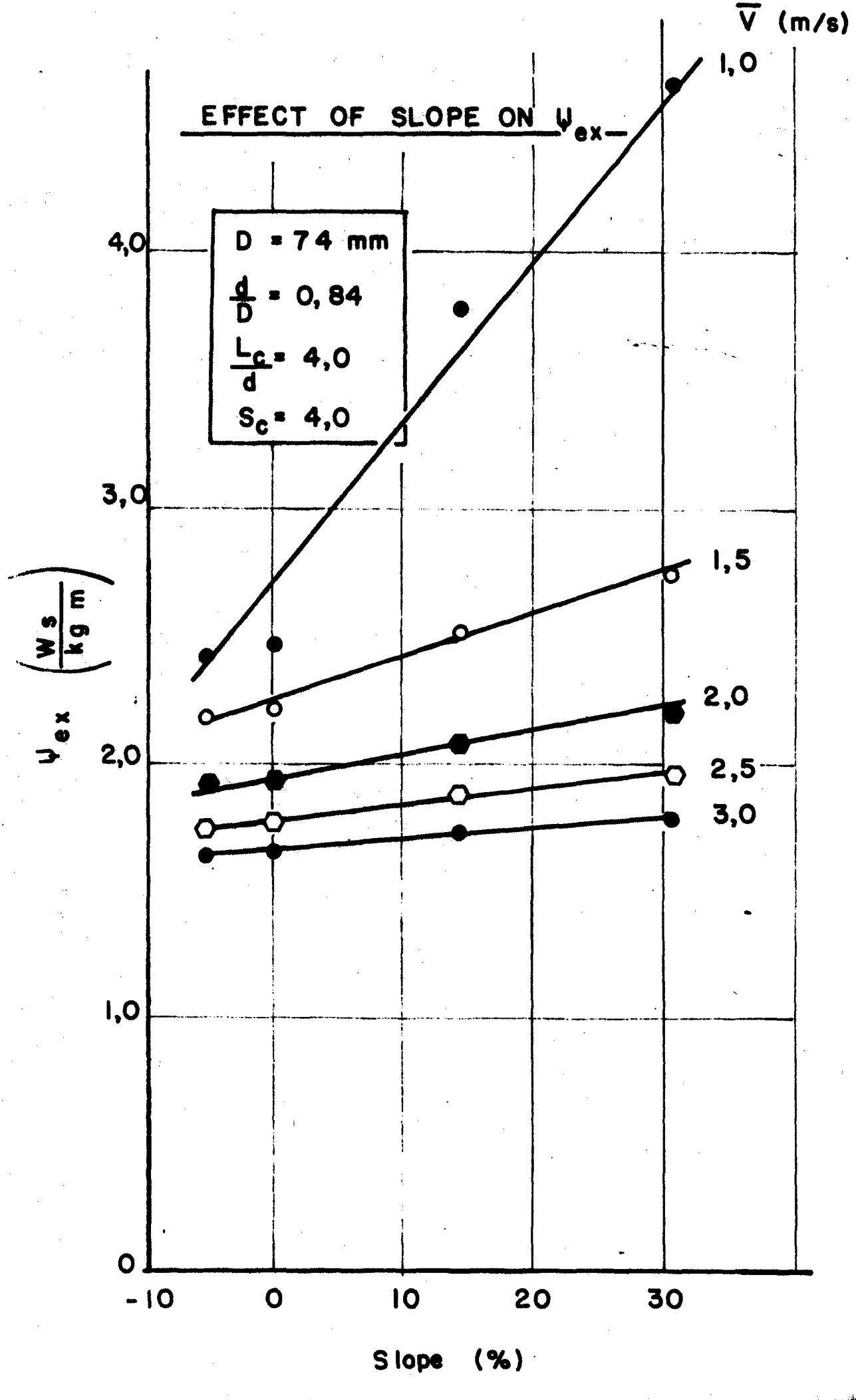
EFFECT OF SLOPE ON ψ_{ex}
D = 74 mm
d/D = 0,84
Lc/d = 4,0
Sc = 4,0
$\overline{V}$ (m/s)
1,0
1,5
2,0
2,5
3,0
ψ_{ex} (Ws/kg m)
4,0
3,0
2,0
1,0
0
-10
0
10
20
30
Slope (%)

FIG. 16.16

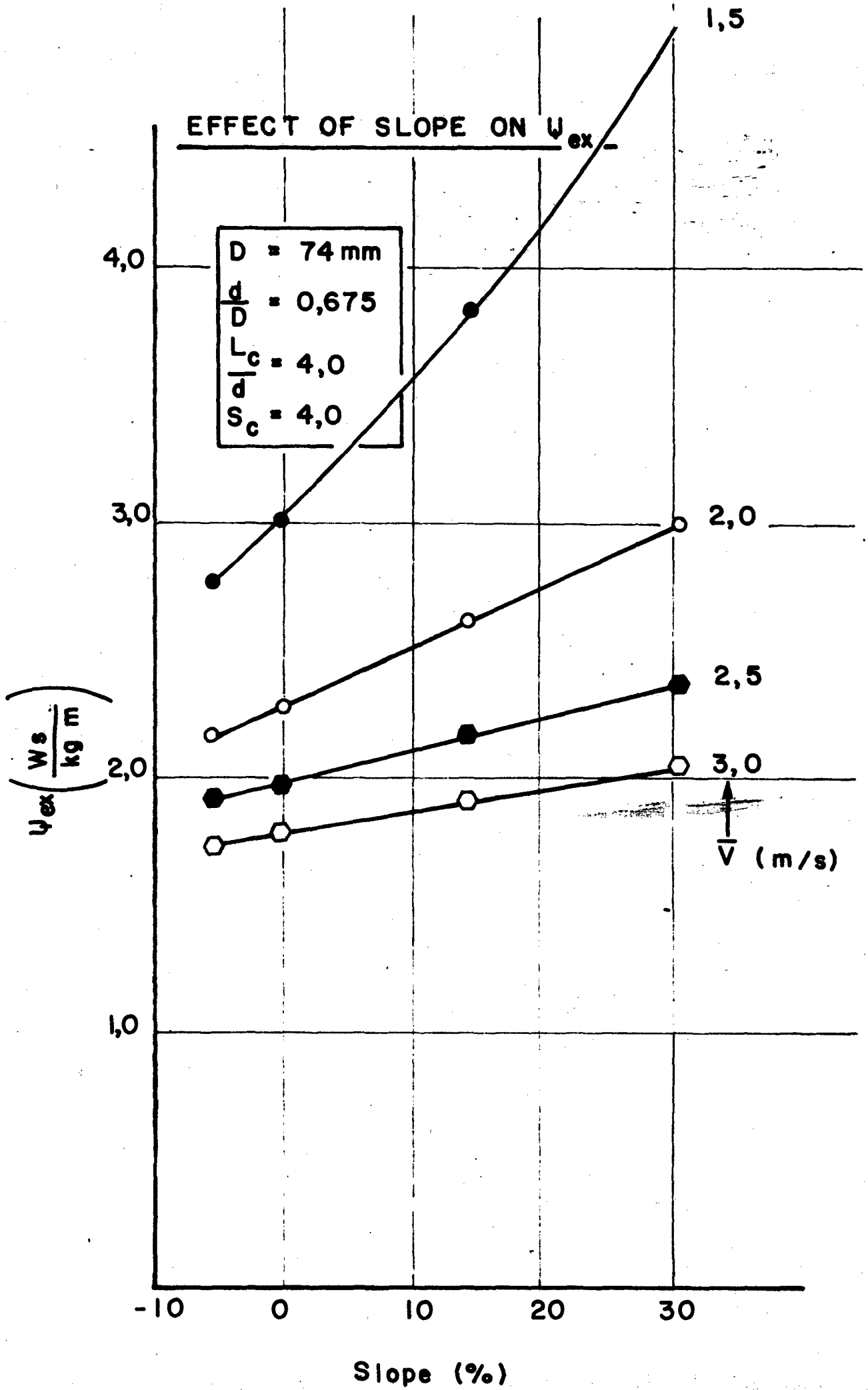
EFFECT OF SLOPE ON ψ_{ex}
D = 74 mm
d/D = 0,675
Lc/d = 4,0
Sc = 4,0
1,5
2,0
2,5
3,0
V̄ (m/s)
4,0
3,0
2,0
1,0
$\psi_{ex}\left(\frac{Ws}{kg}\right)$
-10
0
10
20
30
Slope (%)

FIG. 16.17

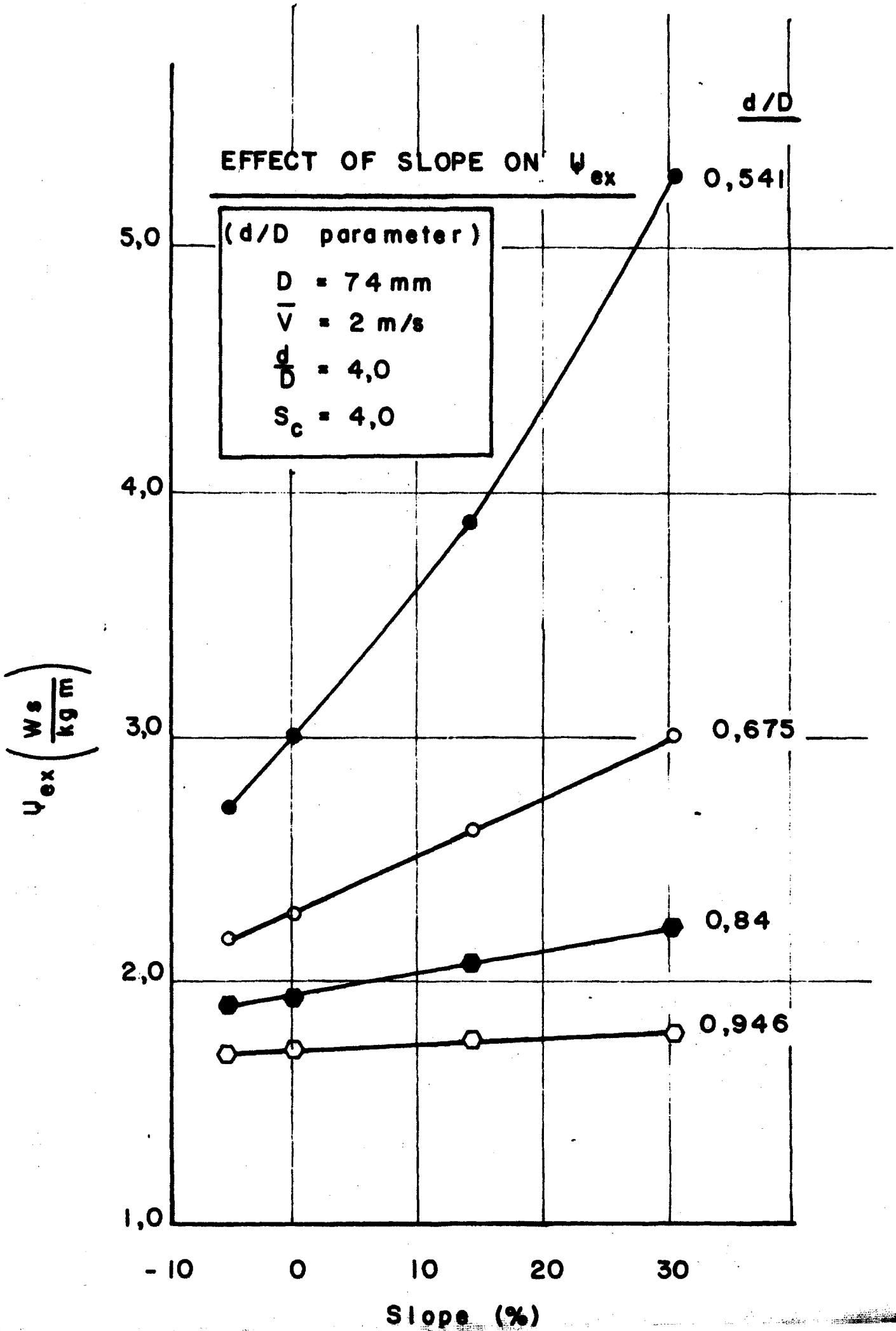
EFFECT OF SLOPE ON ψ_{ex}
(d/D parameter)
D = 74 mm
$\bar{V}$ = 2 m/s
d/D = 4,0
S_c = 4,0
d/D
0,541
0,675
0,84
0,946
5,0
4,0
3,0
2,0
1,0
ψ_{ex} $\left(\frac{Ws}{kg\,E}\right)$
-10
0
10
20
30
Slope (%)

since $L_c = M_c V_c/\theta$

where M_c = capsule mass. And this causes an increase in the excess power (P_{ex}) or ψ_{ex}.

As slope increases sin ϕ naturally increases and the subtractive term in the bracket of equation (16.12) increases. As was discussed in Chapter 15 (on the empirical correlation) the excess head loss for a horizontal pipe can be closely approximated by the excess head loss in a sloping pipe $(\Delta H_c)'_s$ minus the term C_2 sin ϕ (where $C_2 = (d/D)^2 L_c|S_c-1|$). Therefore, since $\Delta P_{ex} \propto 1/L_s$, ΔP_{ex} increases with slope increase.

From Figure 16.17 it is clear that the increase occurs at all diameter ratios, and the rate of increase rises with diameter ratio reduction.

This is because the capsule velocity reduction with slope increase is more pronounced at low diameter ratios, and hence the increase in centre to centre capsule spacing (L_s) becomes more pronounced.

Figure 16.18 shows how the centre to centre spacing (L_s) decreases with slope with d/D as parameter, and the percentage decrease, in the value of L_s, increases as diameter ratio is dimished.

8. Power requirements at incipience

It is clear from figures such as 16.1 that the total power dissipation (in, say, a horizontal pipe) increases above and below the velocity for minimum power requirement, and the total power required for starting a capsule laden pipe from rest is different from the minimum operating power and, indeed, may be greater than the optimum operating power.

A major factor in the design of a capsule transportation system is to ensure that the energy and power available is sufficient for starting up a capsule laden pipe from rest should the pipeline be shut down temporarily.

Excess head losses and mean water velocities at startup can be calculated from incipient values as discussed in Chapter 7.

FIG. 16.18

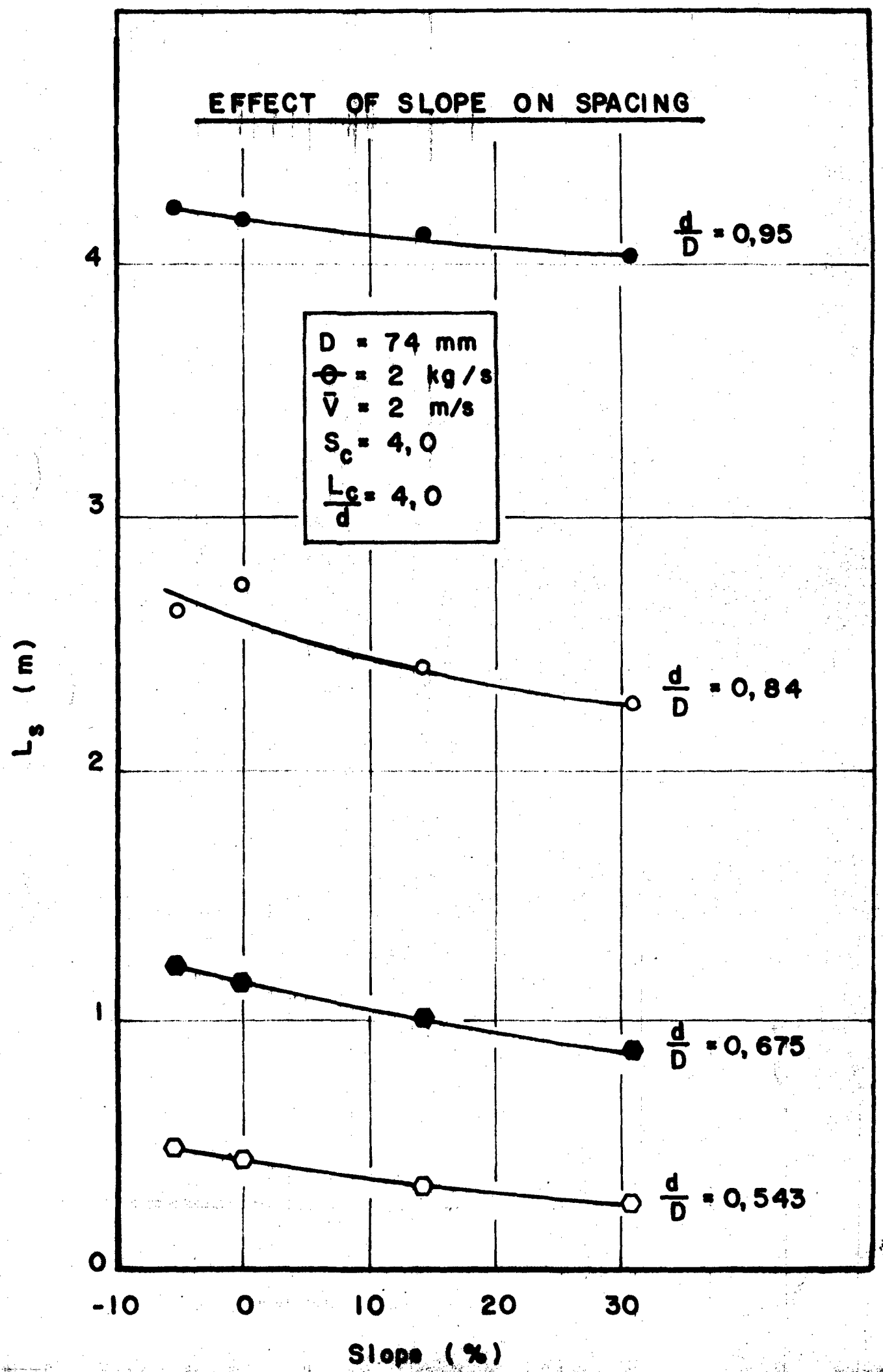
EFFECT OF SLOPE ON SPACING
D = 74 mm
Q = 2 kg/s
V̄ = 2 m/s
Sc = 4,0
Lc/d = 4,0
d/D = 0,95
d/D = 0,84
d/D = 0,675
d/D = 0,543
Ls (m)
0
1
2
3
4
-10
0
10
20
30
Slope (%)

This section is devoted to power requirements for the re-establishment of capsule motion from rest and the startup power is a function of the capsule geometry, pipe size, pipe slope, specific gravity of capsule and the centre to centre spacing. These independent variables are used for calculating or measuring the dependent variables, capsule velocity (V_i) and excess head loss $(\Delta H_c)_i$ at incipience, from which the startup power can be derived.

8.1 Definitions

The forces acting on a capsule at rest in a pipeline of slope less than the angle corresponding to the coefficient of solid to solid static friction are the fluid drag forces (form and skin friction drag) tending to initiate movement, and the forces tending to oppose motion. These are, the solid to solid friction force plus the component of weight acting down the slope (in an upward sloping pipeline).

The total power at incipient capsule motion $(P_i)_T$ per unit length is defined as:

$$(P_i)_T = \frac{w\pi D^2}{4} \overline{V}_i \left[\frac{h_f}{L} + \frac{(\Delta H_c)_{is}}{L_s} + \sin \phi\right] \qquad (16.14)$$

This is the gross pumping power required per unit length of pipe at incipience.

Also:

$$P_i = \frac{w\pi D^2}{4} \overline{V}_i \left[\frac{h_f}{L} + \frac{(\Delta H_c)_{is}}{L_s} - (d/D)^2 |S_c - 1| \frac{L_c}{L_s} \sin \phi\right] \qquad (16.15)$$

And P_i is the total power dissipated at incipience per unit length of pipe.

$$(P_i)_{ex} = \frac{w\pi D^2}{4} \overline{V}_i \left[\frac{(\Delta H_c)_{is}}{L_s} - (d/D)^2 |S_c - 1| \frac{L_c}{L_s} \sin \phi\right] \qquad (16.16)$$

$(P_i)_{ex}$ is the excess power dissipated (due to the existence of the capsule only) at incipience per unit length of pipe.

Equation (16.16) reduces to

$$(P_i)_{ex} = w\pi D^2 \overline{V}_i(\Delta H_c)_i/(4L_s) \qquad (16.17)$$

in a horizontal pipeline.

The second term on the right hand side of equation (16.14) represents the elevational plus dissipated power required for lifting the capsule, and the third term on the right hand side of equation (16.14) represents the elevational power required for lifting the water.

8.2 Effect of capsule spacing

Since $(P_i)_{ex} \propto 1/L_s$, it is apparent that the excess power increases linearly as the spacing length decreases or as the linear concentration (C_L) increases. This is clearly seen on Figure 16.19 at various specific gravities and $d/D = 0,85$. Figure 16.19 represents the situation where stationary capsules are uniformly spaced and resting on the bottom of the pipe and are just about to move.

Figure 16.20 shows the total head loss along a train of stationary capsules and it is clear that at a linear concentration of about 70% the total head loss reaches a maximum, and then starts to drop so that the total head loss for 100% linear concentration is less than for high concentrations. The reason for this is that as the concentration increases above about 70% the capsules interfere with one another so that the full exit head loss is not reached by the time the next capsule is encountered, and also the inlet head loss for a succeeding capsule is not able to attain the full value. Although the latter phenomenon will only appear at even higher concentrations than the former since the outlet head loss requires a longer length of pipe to reach its maximum value. The value at 100% linear concentration is calculated from pressure flow in annuli of unit eccentricity.

Figure 16.21 is a similar diagram for the 44 mm diameter pipe,

FIG. 16.19

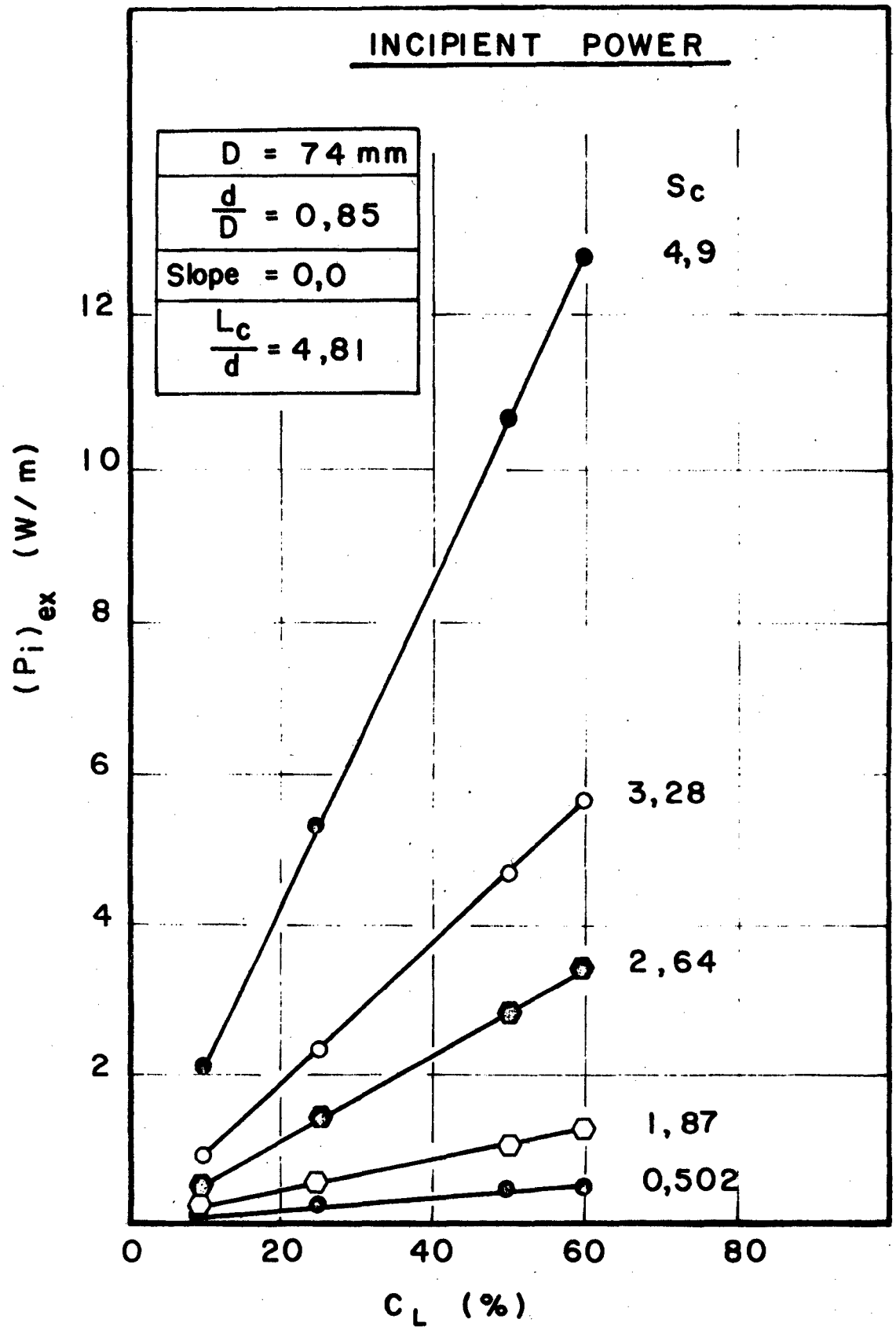
INCIPIENT POWER
D = 74 mm
d/D = 0,85
Slope = 0,0
Lc/d = 4,81
Sc
4,9
3,28
2,64
1,87
0,502
(Pi)ex (W/m)
12
10
8
6
4
2
0
20
40
60
80
CL (%)

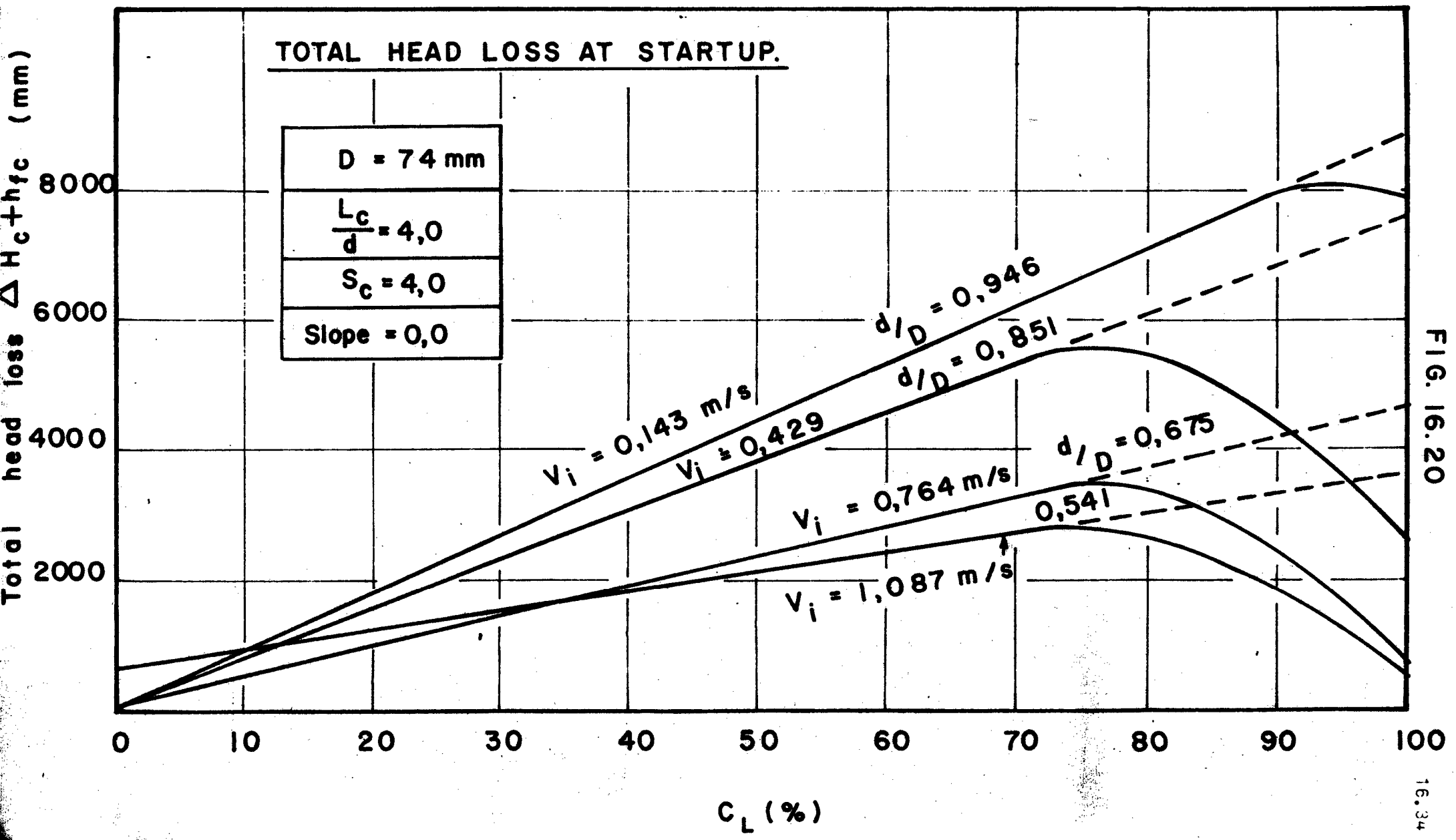
TOTAL HEAD LOSS AT STARTUP.
D = 74 mm
$\frac{L_c}{d}$ = 4,0
S_c = 4,0
Slope = 0,0
Total head loss $\Delta H_c + h_{fc}$ (mm)
8000
6000
4000
2000
0
10
20
30
40
50
60
70
80
90
100
C_L (%)
V_i = 0,143 m/s
V_i = 0,429
V_i = 0,764 m/s
V_i = 1,087 m/s
d/D = 0,946
d/D = 0,851
d/D = 0,675
0,541

FIG. 16.20

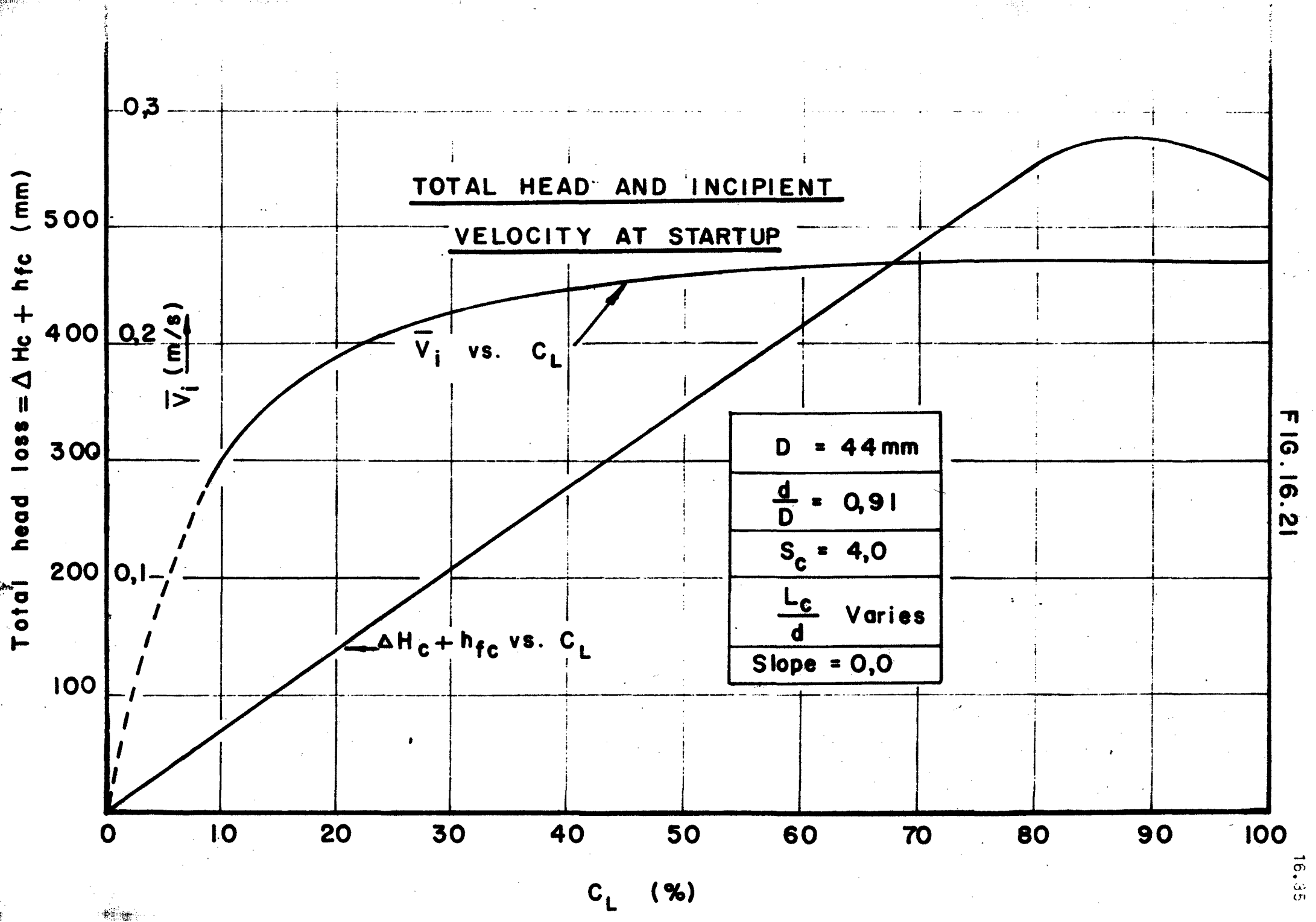
TOTAL HEAD AND INCIPIENT
VELOCITY AT STARTUP
Total head loss = Δ Hc + hfc (mm)
$\overline{V}_i$ (m/s)
$\overline{V}_i$ vs. C_L
ΔHc + hfc vs. C_L
D = 44mm
d/D = 0,91
Sc = 4,0
Lc/d Varies
Slope = 0,0
0,3
0,2
0,1
500
400
300
200
100
0
10
20
30
40
50
60
70
80
90
100
C_L (%)

FIG. 16.21

except that in this case the linear concentration was obtained by considering different capsule lengths (L_c) in the same length of pipeline (L_s). Again the linear concentration at 100% was obtained from pressure flow in the fully eccentric annulus.

The capsules represented on Figure 16.20 are of constant L_c/d for a particular diameter ratio, consequently the incipient velocity has a fixed value at a constant diameter ratio. In Figure 16.21 varying L_c/d to obtain the different linear concentrations implies a change in the start-up velocity which can be calculated (see Chapter 7). The change of incipient velocity with linear concentration in this case is shown in Figure 16.21. The reason for the increase in the value of $\overline{V}_i$ with L_c/d has been discussed in Chapter 14.

8.3 The effect of diameter ratio

Figure 16.22 shows the effect of diameter ratio on the excess power at incipient capsule motion. It is evident that a maximum excess power for startup is reached at a diameter ratio of $d/D = \sim 0{,}7$ in both 44 and 74 mm diameter pipes.

From equation (16.17)

$$(P_i)_{ex} \propto \overline{V}_i \, (\Delta H_c)_i$$

for a fixed pipe diameter and linear concentration. As the diameter ratio is increased $\overline{V}_i$ decreases and $(\Delta H_c)_i$ increases.

Figure 16.23 shows how these effects result in a maximum value of the product $\overline{V}_i \, (\Delta H_c)_i$.

Figure 16.24 is a diagram of excess incipient power as a function of incipient velocity and the dotted curves show that, for a capsule with a constant specific gravity, decreasing the diameter ratio gives an increase in the value of $(P_i)_{ex}$ while the incipient velocity increases.

The diameter ratio requiring maximum excess power to initiate motion

FIG. 16.22

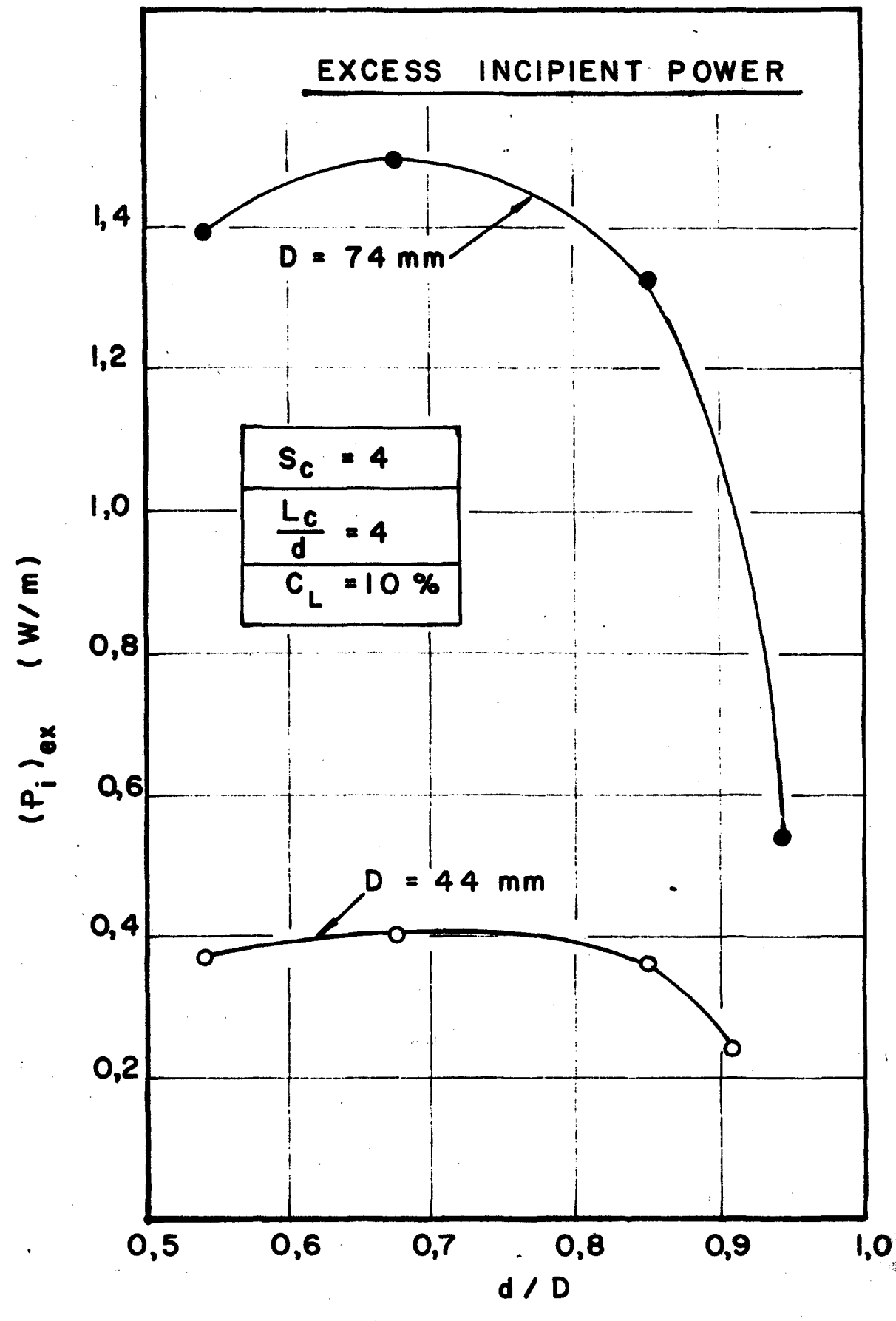
EXCESS INCIPIENT POWER
D = 74 mm
D = 44 mm
S_c = 4
$\frac{L_c}{d}$ = 4
C_L = 10 %
$(P_i)_{ex}$ (W/m)
1,4
1,2
1,0
0,8
0,6
0,4
0,2
0,5
0,6
0,7
0,8
0,9
1,0
d / D

FIG. 16.23

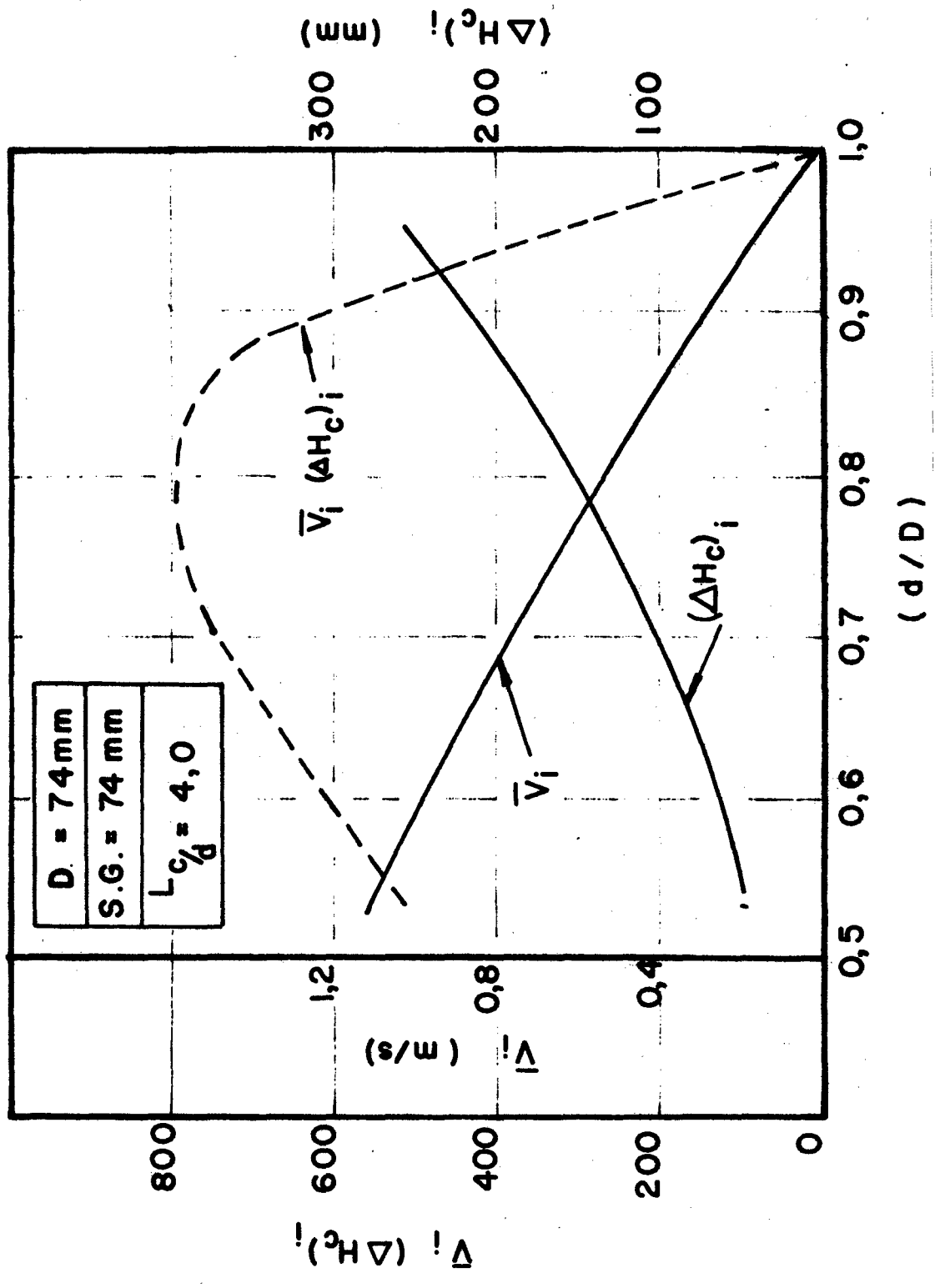
(mm) !(ΔHc)!
300
200
100
1,0
0,9
0,8
0,7
0,6
0,5
(d/D)
$\bar{V}_i$ $(\Delta H_c)_i$
$(\Delta H_c)_i$
$\bar{V}_i$
D = 74mm
S.G. = 74 mm
$L_{c/d}$ = 4,0
1,2
0,8
0,4
$\bar{V}_i$ (m/s)
800
600
400
200
0
$\bar{V}_i$!(ΔHc)!

FIG. 16.24

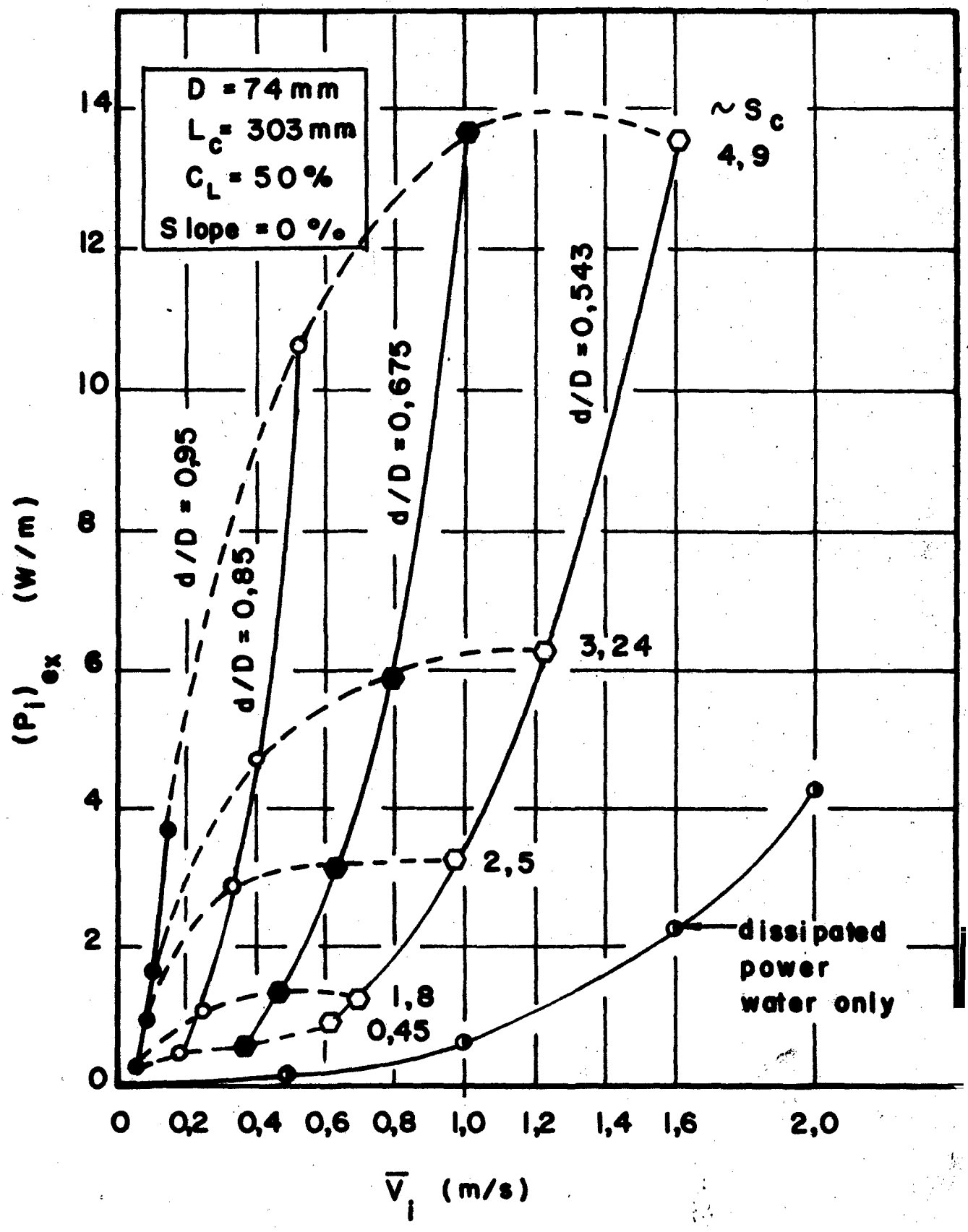
D = 74 mm
L_c = 303 mm
C_L = 50 %
Slope = 0 %
$\sim S_c$
4,9
d/D = 0,95
d/D = 0,85
d/D = 0,675
d/D = 0,543
3,24
2,5
1,8
0,45
dissipated power water only
$(P_i)_{ex}$ (W/m)
$\bar{V}_i$ (m/s)
0
2
4
6
8
10
12
14
0,2
0,4
0,6
0,8
1,0
1,2
1,4
1,6
2,0

is of the order of $d/D = 0,7$ irrespective of the specific gravity of the capsule (from Figure 16.24). For capsules of diameter ratio less than $d/D \doteqdot 0,7$ the value of $(P_i)_{ex}$ becomes less as diameter ratio decreases and incipient velocity increases. For diameter ratios greater than 0,7 the excess incipient power decreases rapidly as diameter ratio increases.

In general a decrease in diameter ratio down to $d/D \doteqdot 0,7$ means a higher excess power at startup, and most certainly a higher total dissipated power if the water only curve shown on Figure 16.24 is superimposed on the excess power. The trend is not apparent for the lowest SG.

8.4 Effect of capsule SG

The solid lines on Figure 16.24 indicate the rapidity of increase in the value of the incipient excess power at a fixed capsule geometry and linear concentration for varying values of capsule specific gravity. Even though capsules of high specific gravity need far more excess power at startup, the increase in incipient velocity is of the order of 45% for $d/D = 0,95$ reducing to 30% at $d/D = 0,54$ for specific gravity increases from 1,8 to 4,9. The excess power at incipience for these specific gravity increases is of the order of 11-fold for the 2,7-fold specific gravity increases, irrespective of the diameter ratio.

From equation (16.17)

$$(P_i)_{ex} \propto \overline{V}_i \, (\Delta H_c)_i / (L_s)$$

and L_s is fixed at capsule startup depending on the spacing at shutdown.

$$\therefore \quad (P_i)_{ex} \propto \overline{V}_i \, (\Delta H_c)_i$$

All other factors being equal, both the incipient velocity $(\overline{V}_i)$ and the excess head loss at incipience $(\Delta H_c)_i$ are dependent variables, which increase with capsule specific gravity. It has been shown (Section 17, Chapter 7) that

$$(\Delta H_c)_i \propto |S_c - 1|$$

and from equation (7.133)

$$\overline{V}_i \propto \text{function } |S_c - 1|^n$$

where n is an index from the solution of equation (7.133).

The excess power at incipience is related to the capsule specific gravity thus:

$$(P_i)_{ex} = \text{function } |S_c - 1|^{1+n}$$

In the correct functional relation $(P_i)_{ex}$ is related to $|S_c - 1|$ by a power which is of the order of 1,5, (i.e. as $|S_c - 1|$ increases from 0,8 to 3,9 there is a 4,9-fold increase for an 11-fold increase in $(P_i)_{ex}$).

This is verified on Figure 16.25 which is a log plot of $(P_i)_{ex}$ as a function of submerged specific gravity ($|S_c - 1|$) for capsule numbers 1 to 24.

8.5 Effect of capsule length

Figure 16.26 shows excess power at startup $(P_i)_{ex}$ as a function of incipient velocity $\overline{V}_i$ with diameter ratio (d/D) and length to diameter ratio (L_c/d) as parameter.

As (L_c/d) increases from 2,0 to 16,0 (i.e. an 8-fold increase) the increase in the value of $(P_i)_{ex}$ and $\overline{V}_i$ is greater for the smaller diameter ratios. That is, at d/D = 0,91 the value of $(P_i)_{ex}$ increases by 59% whilst $\overline{V}_i$ increases by 54%, whereas at d/D = 0,543 the value of $(P_i)_{ex}$ is greater by 180% and $\overline{V}_i$ increases by 140% for an eightfold increase in length to diameter ratio.

The increase in the value of $(P_i)_{ex}$ as (L_c/d) increases can clearly be seen from Figure 16.27. It is apparent that the higher the length to diameter ratio the greater the excess power at startup. And

FIG. 16.25

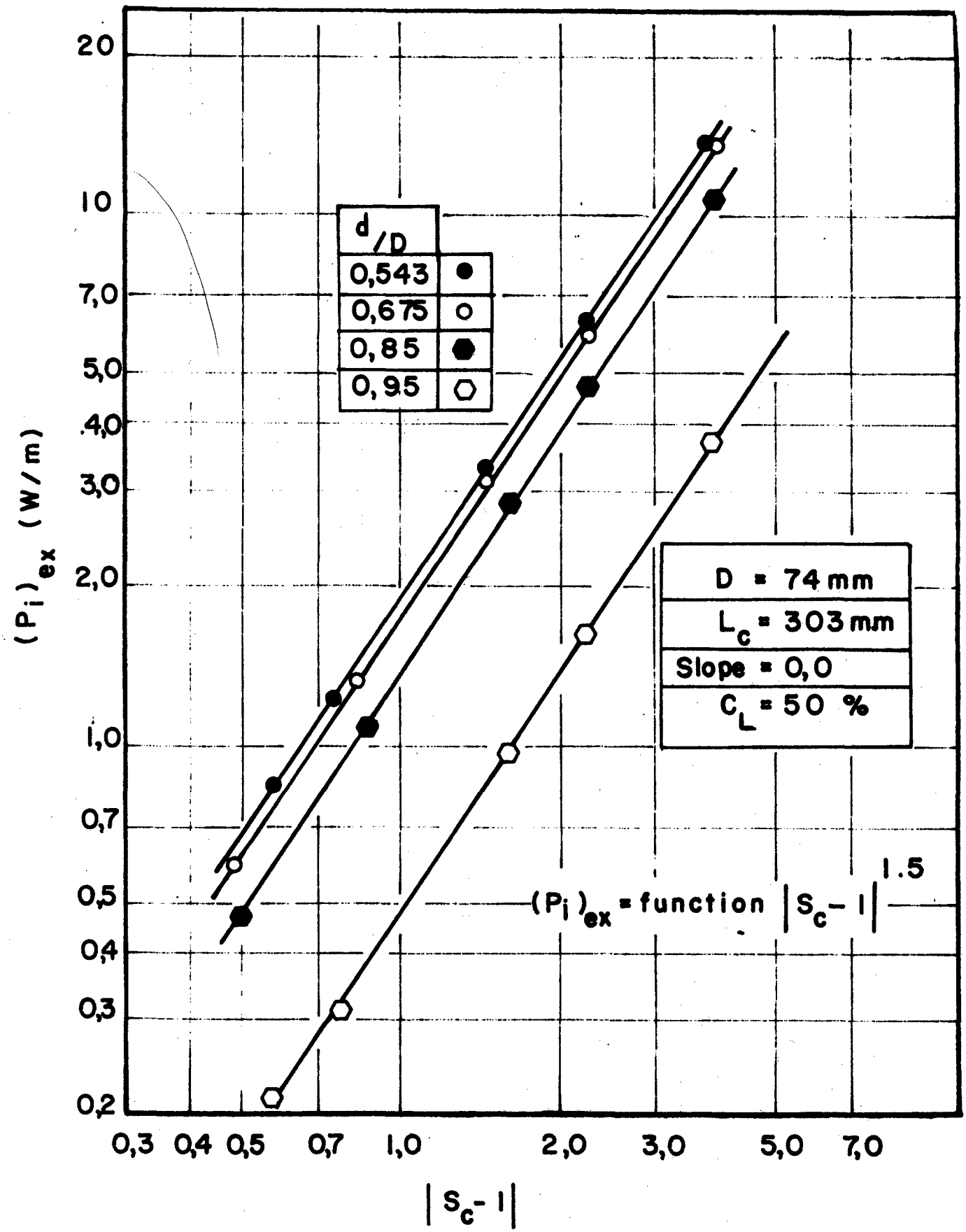
20
10
7,0
5,0
4,0
3,0
2,0
1,0
0,7
0,5
0,4
0,3
0,2
$(P_i)_{ex}$ (W/m)
0,3 0,4 0,5 0,7 1,0 2,0 3,0 5,0 7,0
$|S_c - 1|$
d/D
0,543
0,675
0,85
0,95
D = 74 mm
L_c = 303 mm
Slope = 0,0
C_L = 50 %
$(P_i)_{ex}$ = function $|S_c - 1|^{1.5}$

FIG. 16.26

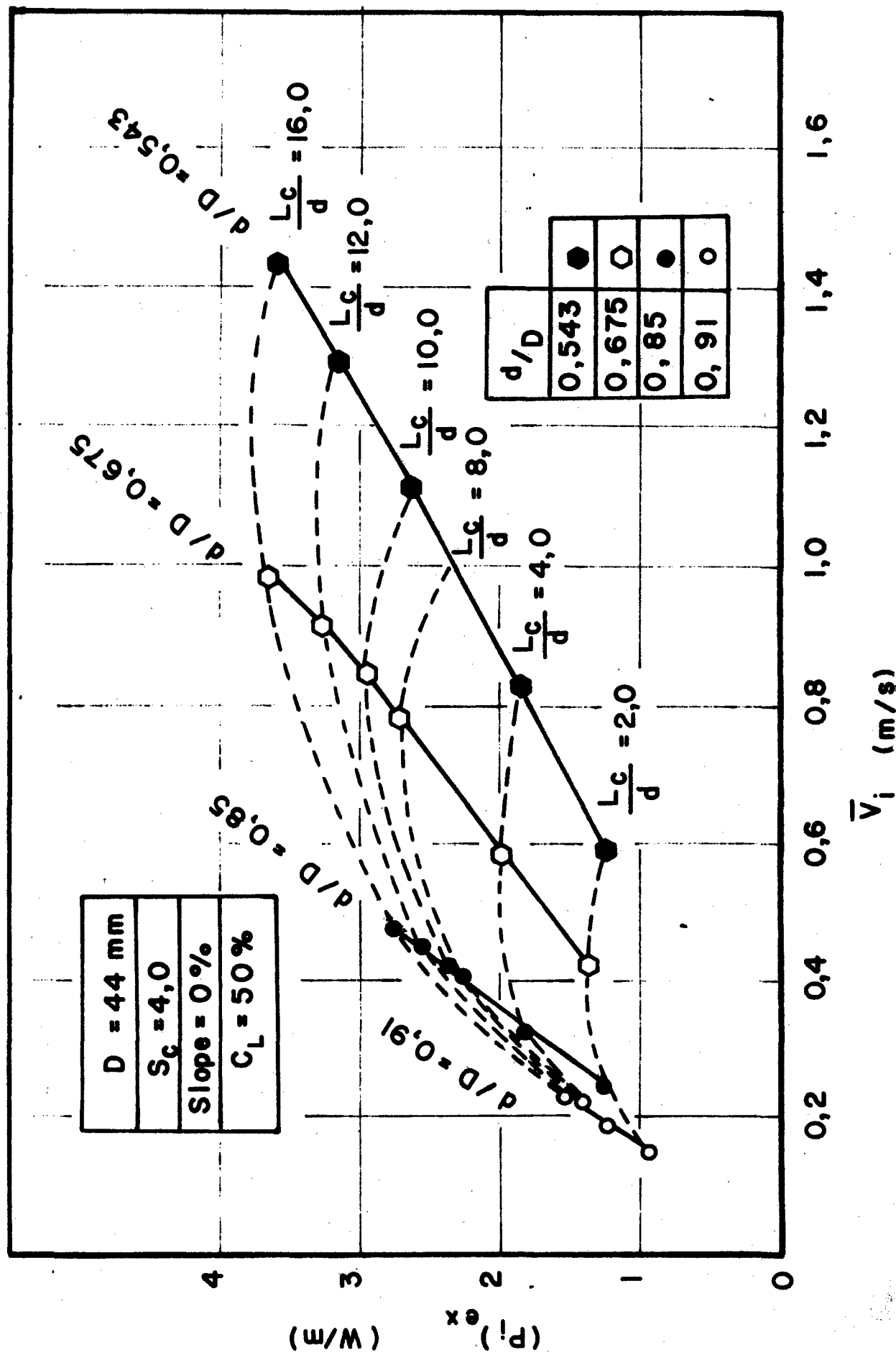
D = 44 mm
S_c = 4,0
Slope = 0%
C_L = 50%
d/D = 0,543
d/D = 0,675
d/D = 0,85
d/D = 0,91
$\frac{L_c}{d}$ = 16,0
$\frac{L_c}{d}$ = 12,0
$\frac{L_c}{d}$ = 10,0
$\frac{L_c}{d}$ = 8,0
$\frac{L_c}{d}$ = 4,0
$\frac{L_c}{d}$ = 2,0
$(P_i)_{ex}$ (W/m)
$\bar{V}_i$ (m/s)
0
1
2
3
4
0,2
0,4
0,6
0,8
1,0
1,2
1,4
1,6

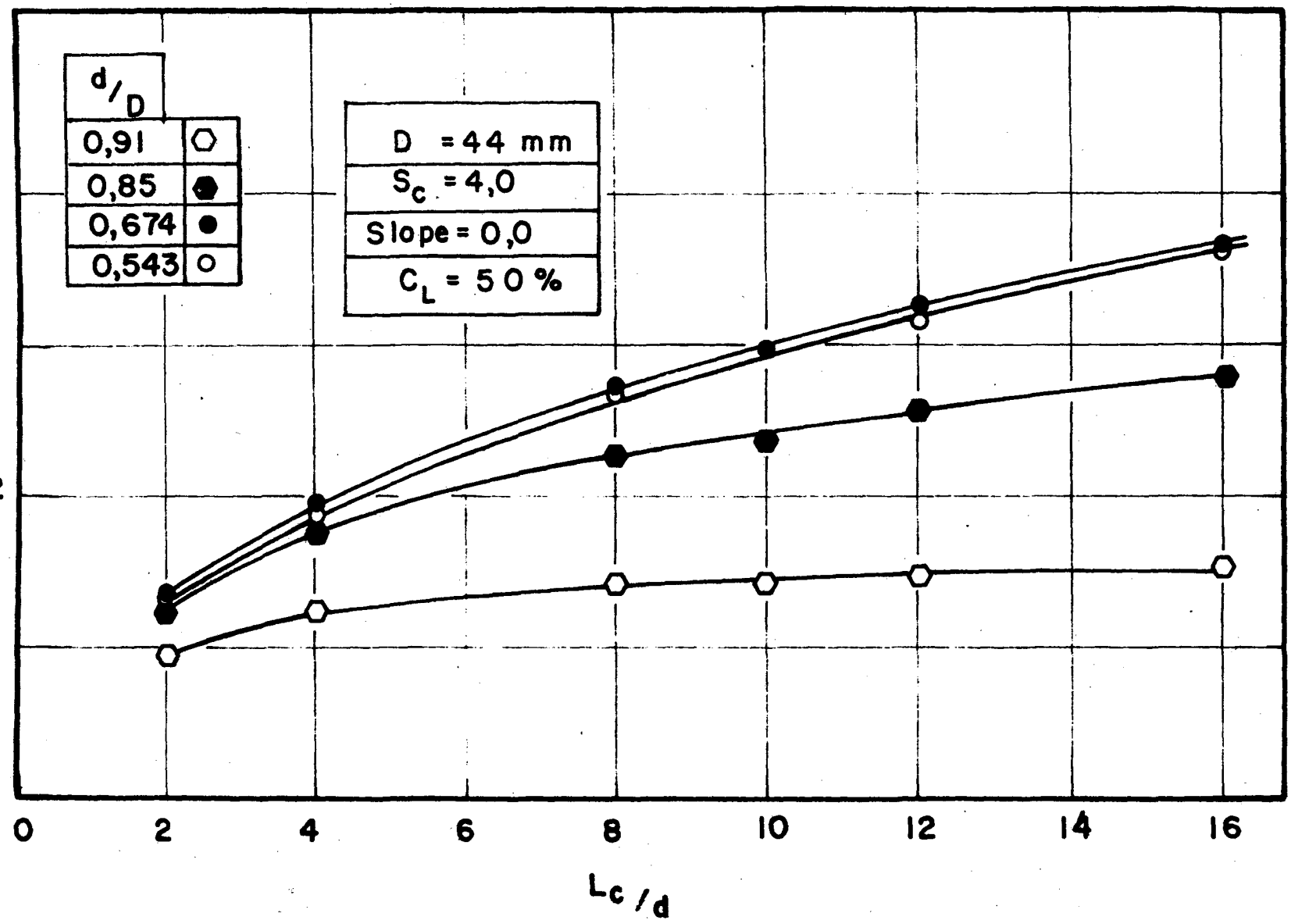
d/D
0,91
0,85
0,674
0,543
D = 44 mm
S_c = 4,0
Slope = 0,0
C_L = 50 %
$(P_i)_{ex}$ (W/m)
1
2
3
4
0
2
4
6
8
10
12
14
16
L_c/d

FIG. 16.27

the excess power increases more rapidly (with (L_c/d) increase) at the lower diameter ratios.

8.6 Effect of pipe slope

Figure 16.28 shows excess power at incipience $(P_i)_{ex}$ as a function of incipient velocity $(\overline{V}_i)$ with diameter ratio and pipeline slope as parameters.

As slope increases in a positive upward direction, capsules of a particular geometry and fixed linear concentration in the pipe need more excess power for startup and at the same time the incipient velocity is higher.

The excess power at incipience on the slope has been shown (equation (16.16)) to be a function of the incipient velocity, and the excess head loss across the capsule after the slope component term has been subtracted, all other variables remaining constant. In Chapter 14 it was shown how the incipient excess head loss on a slope could be correlated by means of the subtractive term $\lambda = (d/D)^2|S_c-1|\ L_c \sin\phi$. Hence $(P_i)_{ex}$ = function $(\overline{V}_i)$ and $(\Delta H_c)_{is}$. It is clear from Figure 16.28 that there is a relation between $(P_i)_{ex}$ and $\overline{V}_i$, which is almost linear for a fixed diameter ratio as slope varies, although the relation of $(P_i)_{ex}$ to slope is not quite linear as can be seen from Figure 16.29.

Increasing the slope from zero to 30,8% implies an increase in $\overline{V}_i$ of slightly more than 50% with a corresponding increase in $(P_i)_{ex}$ of slightly under 50% at $d/D = 0,95$. At $d/D = 0,543$ increasing the slope from 0 to 30,8% gives slightly less than 38% $\overline{V}_i$ increase and slightly more than 38% $(P_i)_{ex}$ increase.

Thus increasing the slope implies a percentage increase of incipient velocity which is of the same order as the percentage increase in the excess incipient power. Although the percentage increase, decreases as diameter ratio is reduced.

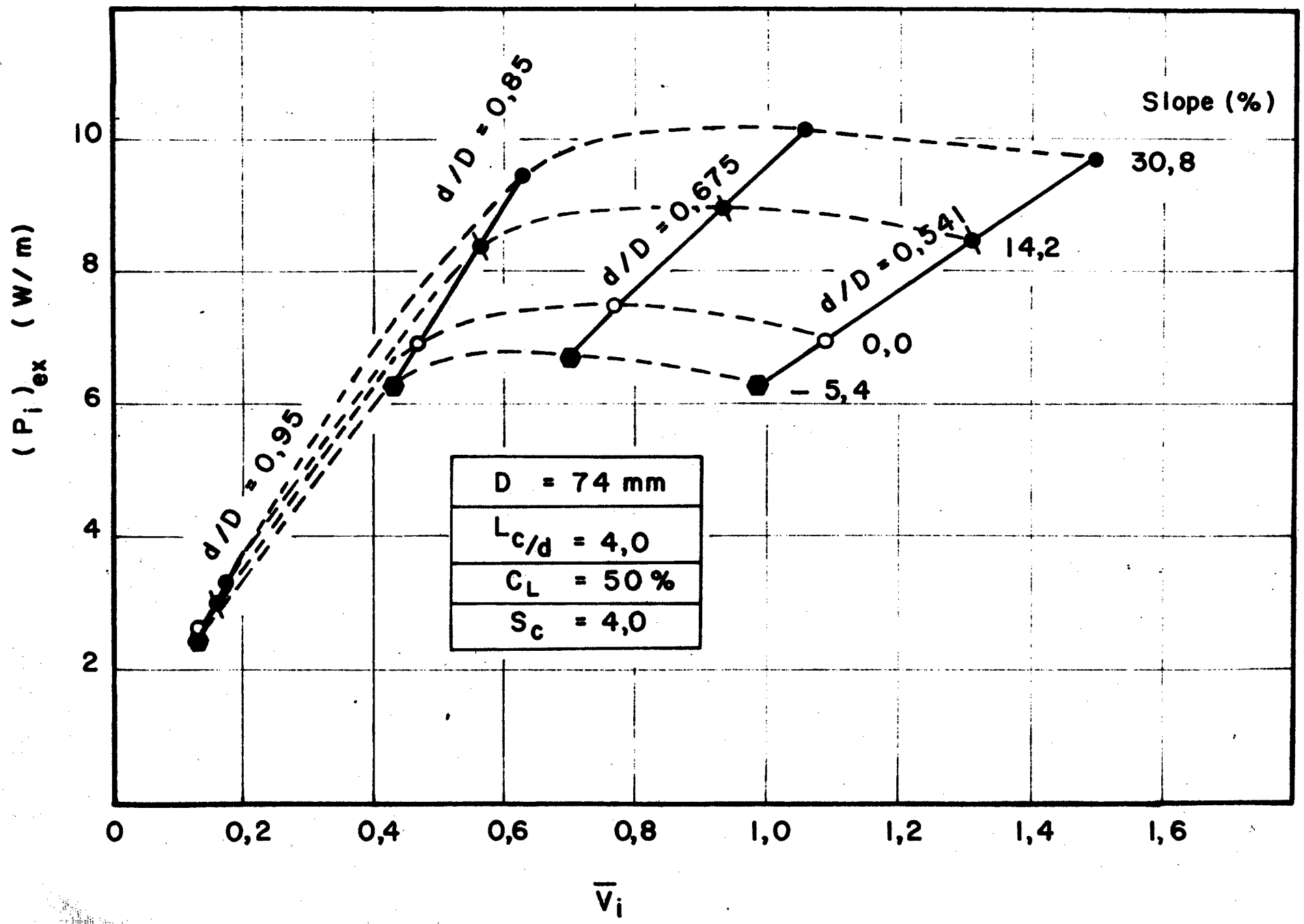
Slope (%)
30,8
14,2
0,0
- 5,4
d/D = 0,85
d/D = 0,675
d/D = 0,541
d/D = 0,95
D = 74 mm
$L_{c/d}$ = 4,0
C_L = 50 %
S_c = 4,0
$(P_i)_{ex}$ (W/m)
$\overline{V}_i$
0
0,2
0,4
0,6
0,8
1,0
1,2
1,4
1,6
2
4
6
8
10

FIG. 16. 28

FIG. 16.29

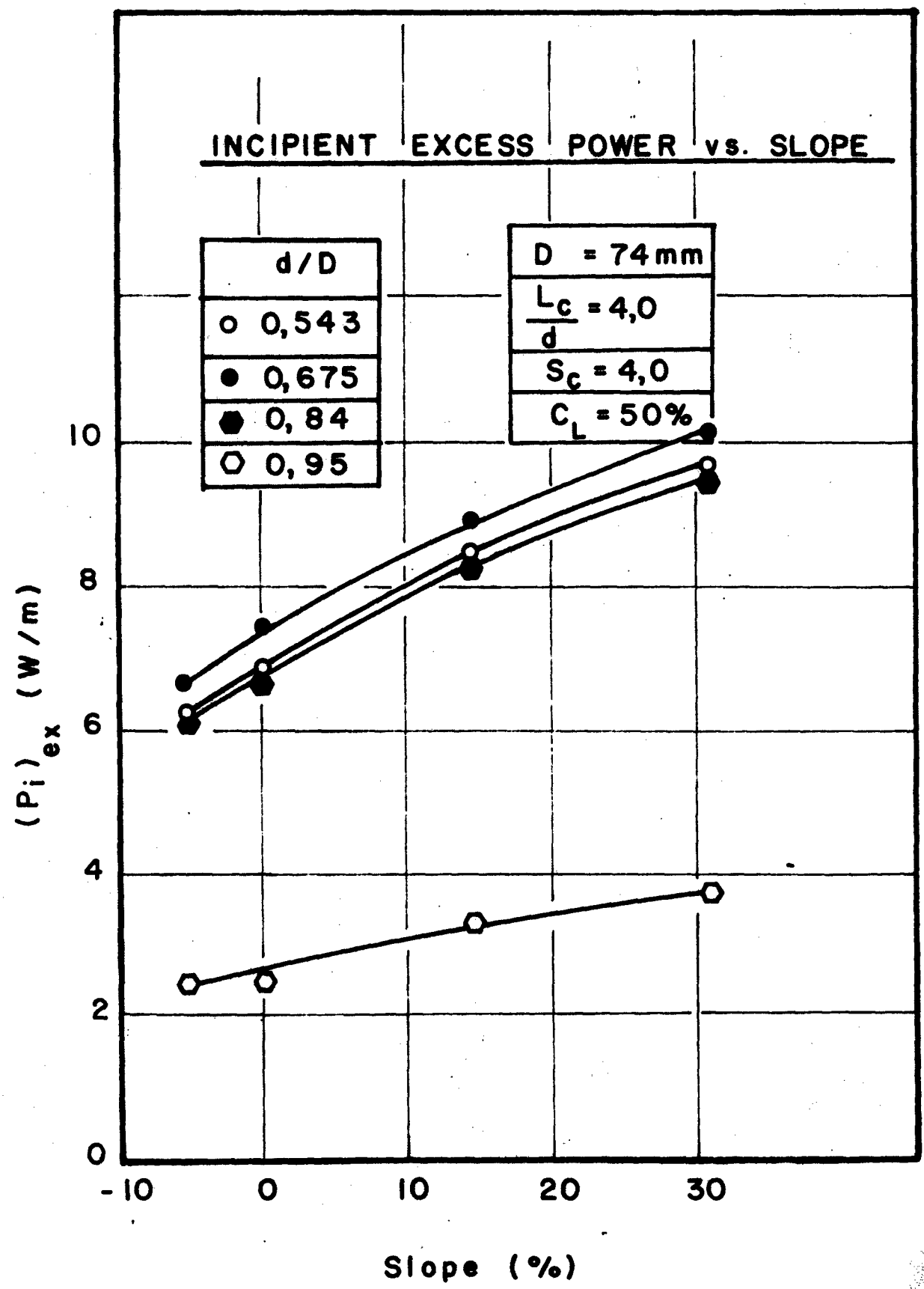
INCIPIENT EXCESS POWER vs. SLOPE
d/D
o 0,543
● 0,675
⬢ 0,84
⬡ 0,95
D = 74mm
Lc/d = 4,0
Sc = 4,0
CL = 50%
(Pi)ex (W/m)
0
2
4
6
8
10
-10
0
10
20
30
Slope (%)

The total power requirement at incipient capsule motion $(P_i)_T$ has been defined by equation (16.14), and Figure 16.30 shows the total power requirement at startup as a function of slope with diameter ratio as parameter, and a constant linear concentration, specific gravity of capsule and length to diameter ratio.

The most significant feature illustrated by this figure is the large increase in startup power as diameter ratio is decreased, particularly at the higher slopes.

9. The relation between startup power and minimum mobile power requirements

Figure 16.31 shows the gross power requirement for mobile capsules as a function of mean water velocity for 10 kg/s delivery rate ($0{,}3 \times 10^6$ tonnes per year). For a range of pipe slopes from -5,4% to 30,8%. The centre to centre spacing length at the various slopes is also shown as a function of mean water velocity, and the cut off point at $C_L = 100\%$ is indicated. The velocity $(\overline{V})$ for minimum power requirement is about 2 m/s. Now Figure 16.32 shows the gross power as a function of slope as well as linear concentration (C_L) as a function of slope at $\overline{V} = 2$ m/s.

At an upward pipeline slope of, say, 10% the linear concentration is about $C_L = 50\%$ (for $d/D = 0{,}85$) and 43 W/m total power is required to transport the load of 10 kg/s. Now referring to Figure 16.30 the total power required for startup at a slope of 10% and linear concentration $C_L = 50\%$ is 12,5 W/m. So that nearly 30% of the running power is required at capsule incipience in such a case.

For a horizontal pipeline the ratio of startup power to minimum running power, for all other variables held constant drops slightly, to about 27%.

Returning to the 10% slope, the incipient power required occurs at a mean water velocity $\overline{V}_i = 0{,}54$ m/s (see Figure 16.30) and, although in Figure 16.31 the power increases for $\overline{V}$ values below 2 m/s, the

FIG. 16.30

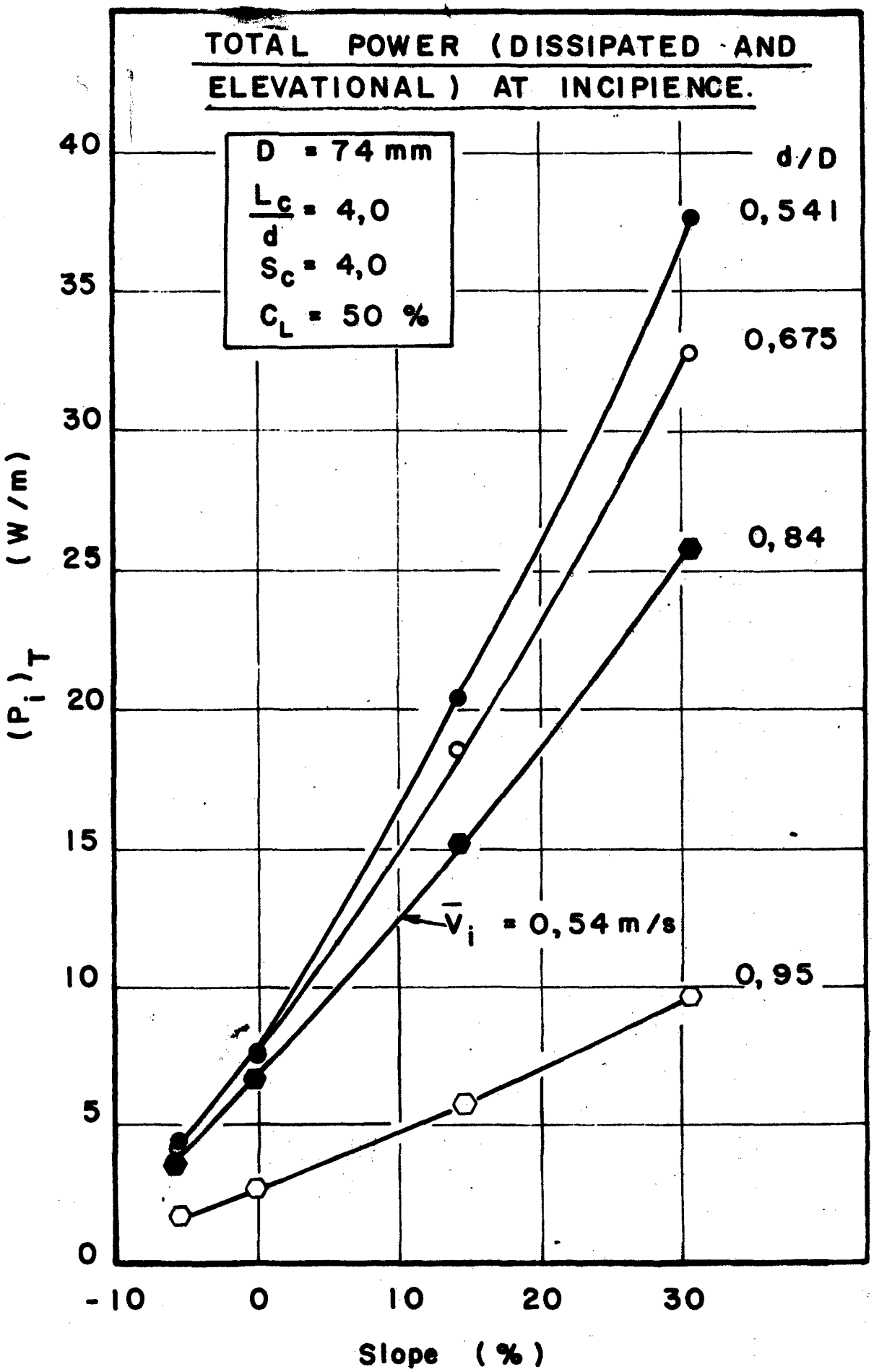
TOTAL POWER (DISSIPATED AND ELEVATIONAL) AT INCIPIENCE.
D = 74 mm
Lc/d = 4,0
Sc = 4,0
CL = 50 %
d/D
0,541
0,675
0,84
0,95
V̄i = 0,54 m/s
(Pi)T (W/m)
40
35
30
25
20
15
10
5
0
-10
0
10
20
30
Slope (%)

FIG. 16.31

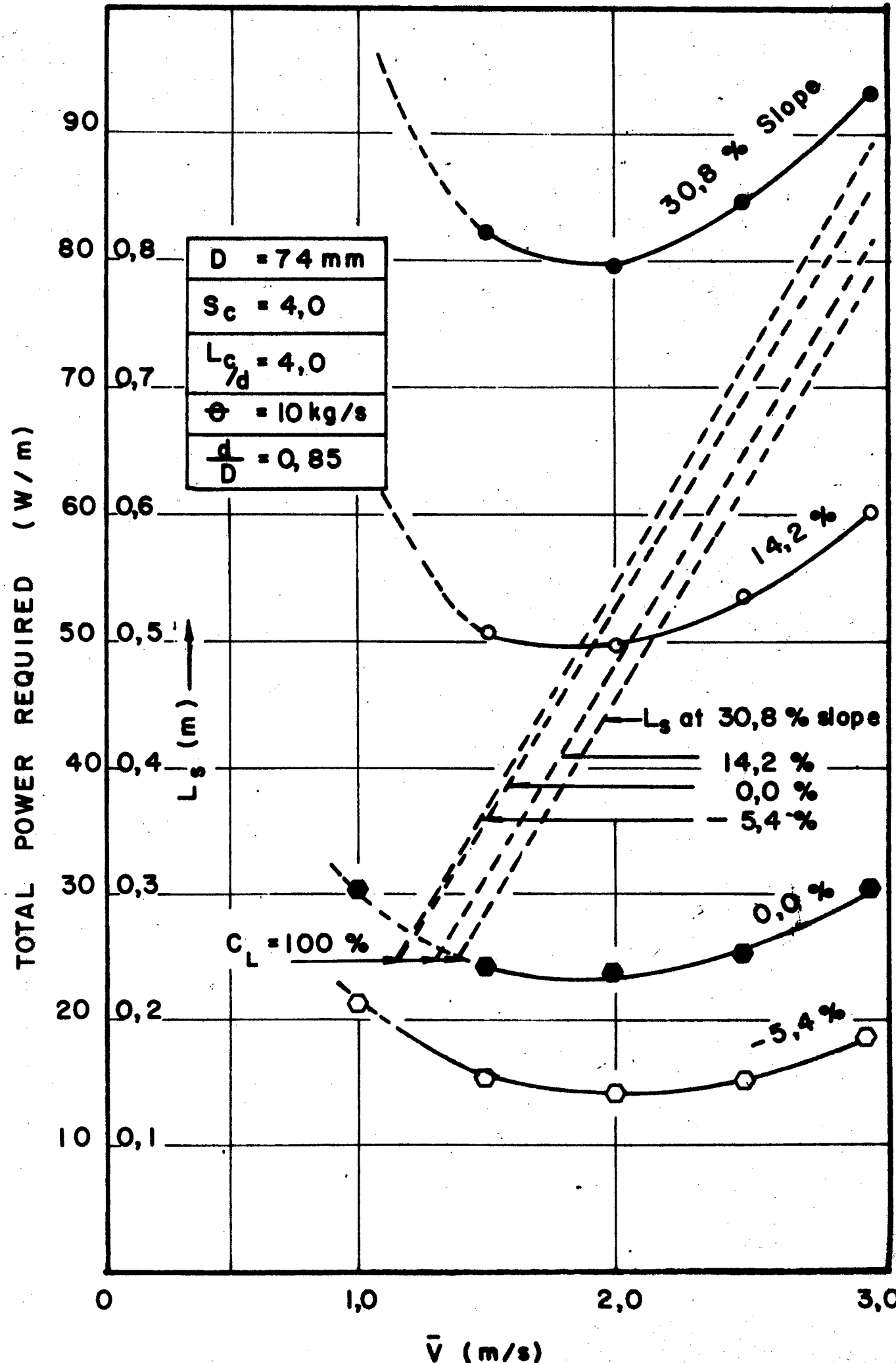
TOTAL POWER REQUIRED (W/m)
90
80
70
60
50
40
30
20
10
0,8
0,7
0,6
0,5
0,4
0,3
0,2
0,1
L_s (m)
D = 74 mm
S_c = 4,0
L_c/d = 4,0
Θ = 10 kg/s
$\frac{d}{D}$ = 0,85
30,8 % Slope
14,2 %
0,0 %
-5,4 %
C_L = 100 %
L_s at 30,8 % slope
14,2 %
0,0 %
- 5,4 %
0
1,0
2,0
3,0
$\bar{V}$ (m/s)

FIG. 16.32

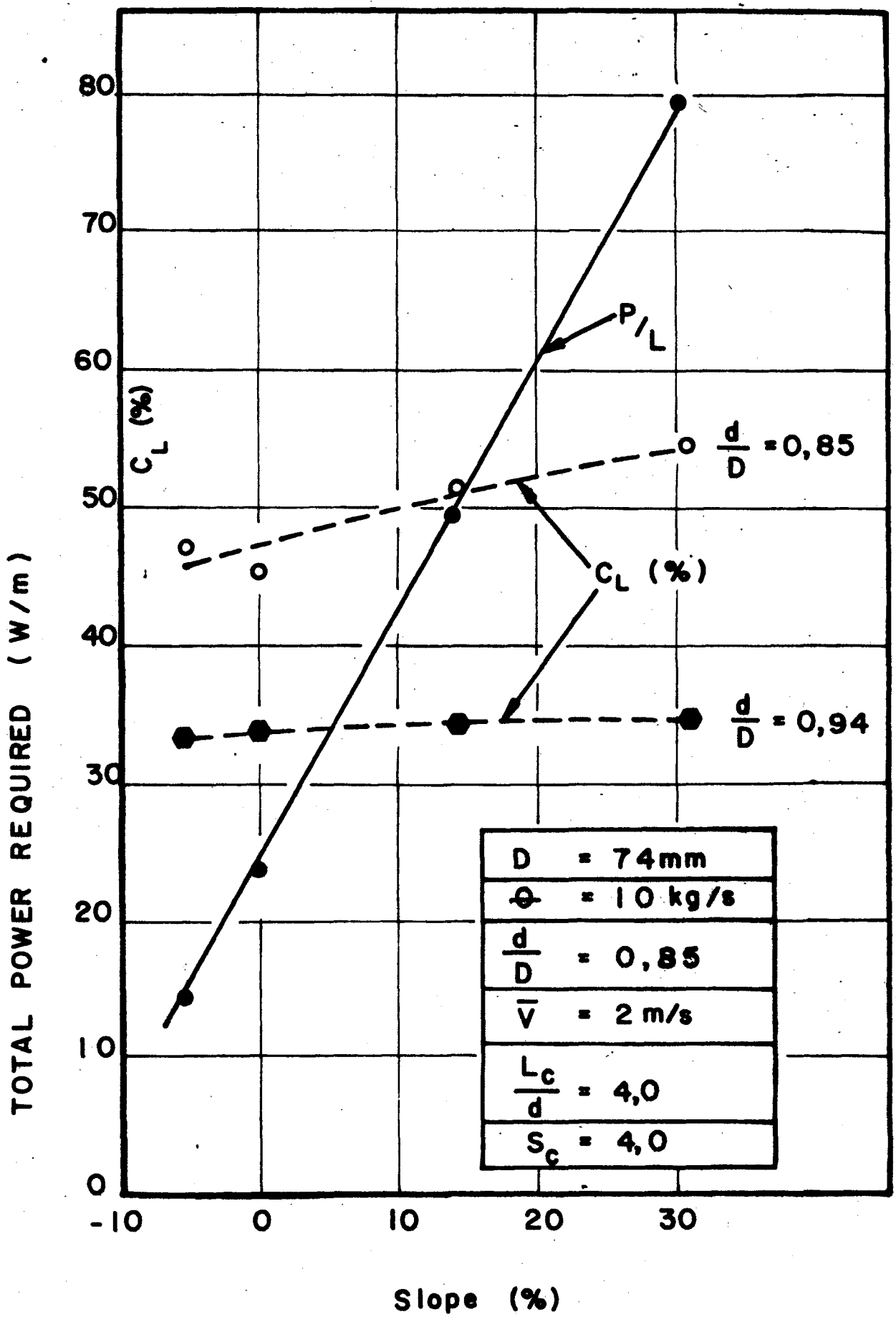
TOTAL POWER REQUIRED (W/m)
Slope (%)
80
70
60
50
40
30
20
10
0
-10
0
10
20
30
P/L
C_L (%)
$\frac{d}{D}$ = 0,85
C_L (%)
$\frac{d}{D}$ = 0,94
D = 74mm
Φ = 10 kg/s
$\frac{d}{D}$ = 0,85
$\bar{V}$ = 2 m/s
$\frac{L_c}{d}$ = 4,0
S_c = 4,0

associated linear concentration (C_L) also increases for the same delivery rate (θ = 10 kg/s) as can be seen from the dotted lines. Thus the incipient power is less than the running power.

CHAPTER 17

OPTIMISATION OF A CAPSULE TRANSPORTATION SYSTEM

In this Chapter no attempt will be made to give a completely generalised optimisation procedure. This can only be done for a particular scheme if the costs of all the dependent variables determining the total cost are known, such as the cost of encapsulation, or sintering, as the case may be, pipeline costs, injection costs, recovery costs, capital cost of booster pumps, labour costs, etc.

The object in this Chapter is to answer the following questions: given certain specifications (such as delivery rate (kg/s) and specific gravity of material to be transported), what is the optimum capsule geometry, pipe size and injection rate and what is the velocity of transport and the power requirements for the optimum situation? Only when these variables have been determined, can the designer of a capsule transportation scheme compare this system with alternative methods of transportation. In order to deal with the above problem, a brief outline is first given of some of the economic criteria involved to show that the problems dealt with in this Chapter do not comprise the whole story which can only be considered for a specific installation.

1. Economics of capsule transportation

The choice of any transport system is usually an economic one. This means minimum energy and labour costs as well as minimum capital and other operating costs. It may not be possible, however, to achieve simultaneous minima.

The capital cost of a surface pipeline is roughly proportional to the diameter, but the capacity is proportional to diameter squared.

The larger the output, the greater the distance required for the pipe

to become increasingly economical. The longer the pipeline, the lower the cost per kilogramme of material transported per metre length. This is because preparation, injection and recovery costs are independent of pipeline length. The costs involved in a capsule transportation system can be listed as follows:

1.1 Investment costs

These are fixed costs and are independent of pipeline operation. They may be divided into:

1.1.1 Installed cost of pipeline or pipelines.

1.1.2 Installed cost of the pump station.

1.1.3 Installed cost of the preparation, injection and terminal plant.

1.2 Overhead costs

1.2.1 Labour for maintenance.

1.2.2 Material for maintenance.

1.2.3 Rent of plant for maintenance.

1.2.4 Insurance of equipment.

1.2.5 Property tax.

1.2.6 Depreciation of plant, pipeline, pumps, etc.

1.3 Operating Costs

1.3.1 Energy costs.

1.3.2 Labour running costs.

1.3.3 Preparation (e.g. encapsulation or moulding) and injection costs.

1.3.4 Retrieval and recovery costs.

1.3.5 Water treatment, if this is required.

1.3.6 Water purchase; if the water has a realizable value at delivery, this is a negative cost.

2. Analysis

If all the costs can be related to the quantity of solids transported and the conveying distance, the cost of moving 1 kilogramme of solids through a distance of 1 metre is the basis for comparison.

For example:

If x_1 = installed cost of the pipeline, i.e. the cost per kg m of the initial pipeline investment including labour, trenching, piping material and fittings,

then x_1 can be represented as a function of variables thus:

Let $x_1 = f(D, C, R_1, \text{etc.})$

where C = capital recovery factor, which represents interest charged on capital investment or amortization cost.

R_1 = rate of installed pipeline per mm diameter per metre length.

Let x_2 = installed cost of the pumping stations, including controls, where x_2 is a function of such variables as the cost of the pump station and controls per unit power installed, the solids delivery rate, the flow, the specific gravity and geometry of capsules, the efficiency of the pumps and motors, etc.

An attempt can be made to list all the costs mentioned in Section 1 as functions of independent variables or as fixed costs.

The total cost (x_t) is then:

$$x_t = x_1 + x_2 + x_3 \ldots\ldots\ldots\ldots$$

where $x_1, x_2 \ldots\ldots\ldots$ depend on several variables.

Holding all other variables constant, except, say, the pipe diameter and linear concentration of capsules, the objective function (x_t) can be optimised by partially differentiating x_t with respect to pipe diameter (D) and linear concentration (C_L) and equating to zero. This leads to

simultaneous equations which have to be solved. The optimisation is given in Section 4.

The above brief description shows why it is impossible to formulate a generalised optimisation procedure.

3. Definitions

3.1 Capsule mass delivery rate

The mass output or capsule mass delivery rate (θ) can be defined as the mass of capsules delivered per second.

$$\theta = I \times M_c \qquad (17.1)$$

where I = injection rate = ejection rate (in capsules/s) = V_c/L_s

M_c = mass of each capsule (kg)

$$\theta = (\pi d^2/4)\, L_c\, \rho\, S_c\, V_c/L_s \qquad (17.2)$$

If this expression were presented graphically it could prove useful for determining different combinations of capsule geometry (d and L_c), SG, capsule velocity and capsule spacing to yield a prescribed delivery rate (θ).

Figure 17.1 shows the capsule diameter (d) as a function of injection rate with V_c as parameter and d as a function of θ also with V_c as parameter. To present all the variables, different graphs such as this could be drawn for values of SG and values of L_s. There appear to be too many variables to include on a single conventional graph.

Recourse was made to a double square nomogram (see Figure 17.2) and all the variables in equation (17.2) are successfully represented. Two perpendicular lines drawn on a transparent flat sheet (such as perspex) are necessary for solving the nomogram, and different values of the variables d, L_c, S_c, V_c and L_s can be tried to yield θ. In the example shown the required value of θ is 10×10^6 tonnes p.a. This value is

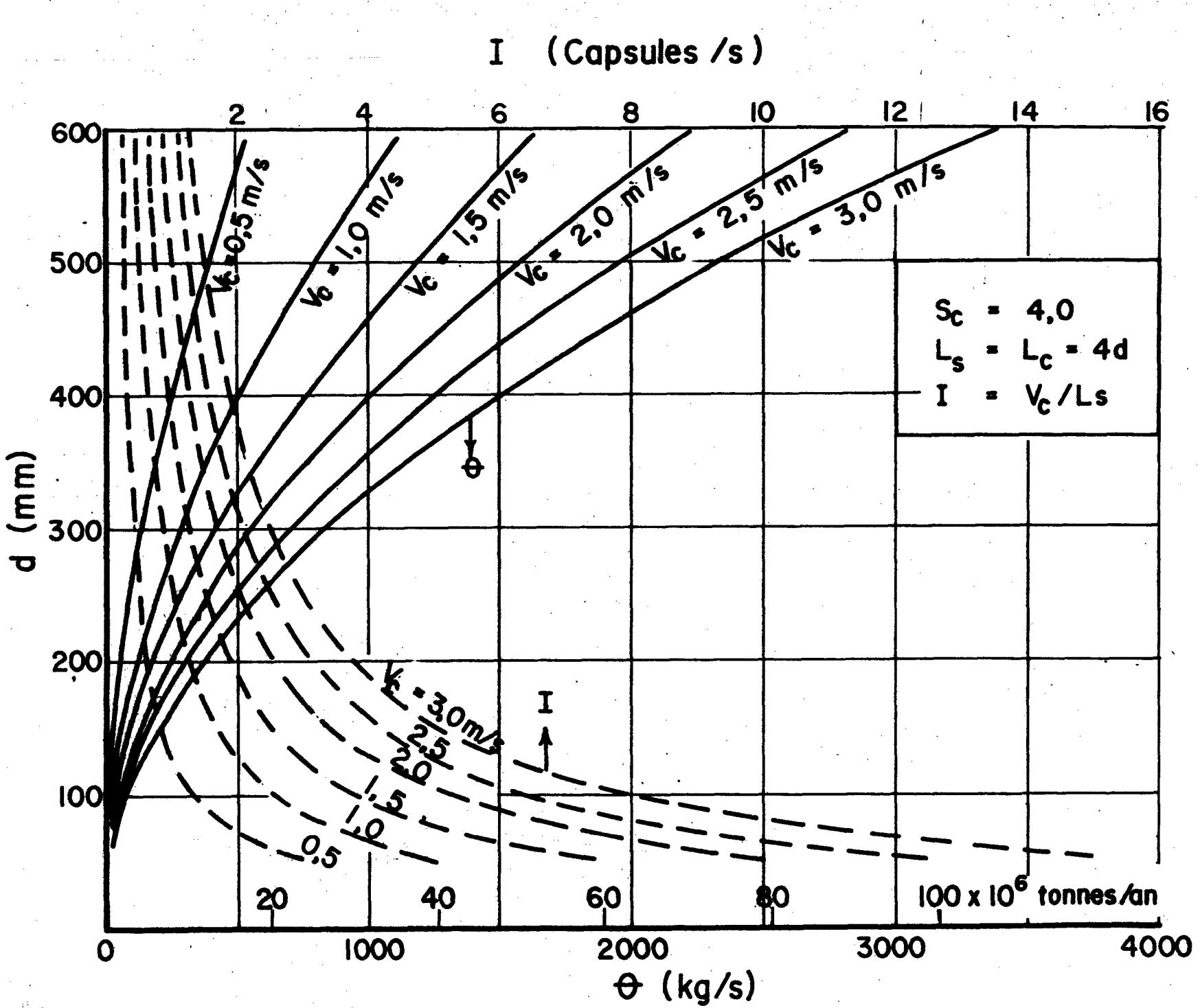
I (Capsules /s)
2
4
6
8
10
12
14
16
600
500
400
300
200
100
d (mm)
Vc = 0,5 m/s
Vc = 1,0 m/s
Vc = 1,5 m/s
Vc = 2,0 m/s
Vc = 2,5 m/s
Vc = 3,0 m/s
Sc = 4,0
Ls = Lc = 4d
I = Vc/Ls
θ
I
Vc = 3,0 m/s
2,5
2,0
1,5
1,0
0,5
20
40
60
80
100 x 10^6 tonnes/an
0
1000
2000
3000
4000
θ (kg/s)

FIG. 17.1

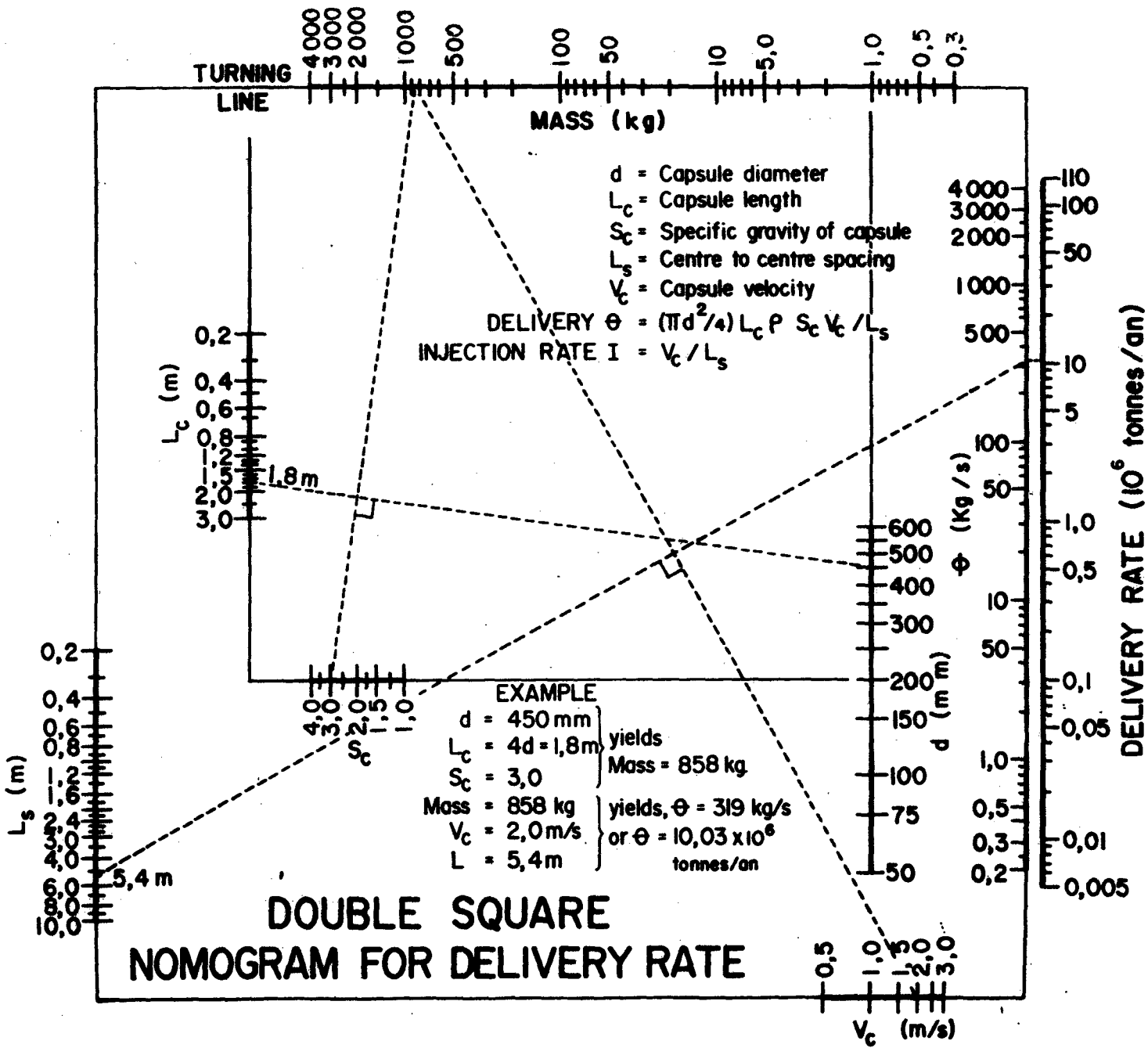
TURNING LINE
MASS (kg)
4000
3000
2000
1000
500
100
50
10
5,0
1,0
0,5
0,3
d = Capsule diameter
L_c = Capsule length
S_c = Specific gravity of capsule
L_s = Centre to centre spacing
V_c = Capsule velocity
DELIVERY $\Theta = (\pi d^2/4) L_c \rho S_c V_c / L_s$
INJECTION RATE $I = V_c / L_s$
L_c (m)
0,2
0,4
0,6
0,8
1,2
1,6
2,0
3,0
1,8 m
S_c
4,0
3,5
3,0
2,5
2,0
1,5
1,0
L_s (m)
0,2
0,4
0,6
0,8
1,2
1,6
2,4
3,0
4,0
6,0
8,0
10,0
5,4 m
EXAMPLE
d = 450 mm
L_c = 4d = 1,8m
S_c = 3,0
yields Mass = 858 kg
Mass = 858 kg
V_c = 2,0 m/s
L = 5,4 m
yields, Θ = 319 kg/s
or Θ = 10,03 x 10^6 tonnes/an
4000
3000
2000
1000
500
100
50
10
5
1,0
0,5
0,3
0,2
Φ (Kg/s)
600
500
400
300
200
150
100
75
50
d (mm)
110
100
50
10
5
1,0
0,5
0,1
0,05
0,01
0,005
DELIVERY RATE (10^6 tonnes/an)
0,5
1,0
2,0
3,0
V_c (m/s)
DOUBLE SQUARE
NOMOGRAM FOR DELIVERY RATE

FIG. 17.2

projected horizontally to give θ (in kg/s) and a square alignment to the selected values of L_s and V_c yields the capsule mass. A second square alignment from the mass to a selected value of S_c yields combinations of L_c and d.

3.2 <u>ψ-parameter</u>

The ψ-parameter represents the power requirement per unit length of pipeline divided by the capsule mass flow delivery rate. Thus:

$$\psi = \frac{w\, Q_w \Delta H_p}{I\, M_c\, L_p} \qquad (17.3)$$

where $w\Delta H_p$ = total pressure loss in a pipeline of length L_p

L_p = total length of pipeline.

$$\frac{\Delta H_p}{L_p} = \sum_{j=1}^{n} \left[\frac{\Delta H_c}{L_p} + \left(\frac{d}{D}\right)^2 \frac{L_c}{L_p} |S_c - 1| \sin\phi \right] + i + \sin\phi \qquad (17.4)$$

where n = number of capsules in the length of line L_p

$= L_p\, I/V_c$

and i = hydraulic gradient in the capsule-free pipe.

$$\therefore \quad \psi = \frac{\rho\, g\, D^2\, \overline{V} \Delta H_p}{\frac{V_c}{L_s}\, \rho_c\, d^2 L_c L_p}$$

where $L_s = \frac{V_c}{I}$ = spacing length between capsule centres.

$$\text{and} \quad \Delta H_p \frac{L_s}{L_p} = L_s \left[n \left[\frac{\Delta H_c}{L_p} + \left(\frac{d}{D}\right)^2 \frac{L_c}{L_p} |S_c - 1| \sin\phi \right] + \frac{h_f}{L_p} + \sin\phi \right]$$

$$= (\Delta H_c)'_s + iL_s + L_s \sin\phi$$

For horizontal pipes:

$$\psi = \frac{g}{S_c} \left(\frac{D}{d}\right)^2 \frac{\overline{V}}{V_c} \left[\frac{iL_s + \Delta H_c}{L_c} \right] \qquad (17.5)$$

In order to make this expression non-dimensional, the weight of capsule

material delivered per second can be substituted for the mass flow per second thus:

$$\psi_W = \frac{1}{S_c} \left(\frac{D}{d}\right)^2 \left(\frac{\overline{V}}{V_c}\right) \left(\frac{iL_s + \Delta H_c}{L_c}\right) \qquad (17.6)$$

3.3 Efficiency

The inverse of ψ can be thought of as a type of efficiency since it represents the power required to deliver a certain mass of capsules. This is a fictitious efficiency in the horizontal pipe since no useful work is done. Power is expended in dissipating energy.

In a sloping pipe the efficiency can be defined as

$$\eta = \frac{I\, W_c\, L_p \sin \phi}{w\, Q_w\, \Delta H_p} \qquad (17.7)$$

and this is a real efficiency.

However, concern is essentially with power dissipated since capsules on a slope mean that the solids to be transported have to be raised or lowered through a certain elevational distance, and this is true of any transportation system. Thus the ψ value is best thought of as a useful comparative parameter and not as an inverted efficiency. Equation (17.7) is thus rejected in favour of the expression for the ψ inverse without $\sin \phi$ in the numerator of equation (17.7).

3.4 Injection Power

When considering an entire pipeline the power is not only that required for dissipating energy and increasing potential. There is, in addition, a certain amount of power needed for injection of the capsules into the pipeline, particularly under pressure. If the pipe pressure at the injection point is (P_{in}) then:

$$\text{Power required at injector} = (P_{in})Q_c$$

This injector does no useful work but power is expended due to the

exchange of equal volume of capsule for water at high pressure. As a capsule moves into position in the pipeline the volume of water that it displaces must be forced along the pipeline.

4. Optimisation of flow velocity and power requirement

If the capsule mass delivery rate (θ) is given then the pipe diameter (D), the diameter ratio (d/D), the injection rate (I) as well as the capsule velocity (V_c) and mean water velocity ($\overline{V}$) can be determined for optimising the power requirements.

Thus of all the costs given in Section 1, the only one considered in this context is 1.3.1 (i.e. energy costs).

The ψ-parameter represents energy required per kilogram metre (Ws/kg m) and the most economic system from the viewpoint of fuel costs is that which has a minimum ψ-parameter.

ψ is a function of dependent and independent variables thus:

$$\psi = f(\overline{V}, V_c, g, D, d, \rho_c, h_f, \theta, \Delta H_c, \mu, \rho, \phi, L_c, L_s) \qquad (17.8)$$

In order to optimise the ψ-parameter, it should be a minimum with respect to all the variables given in the above equation. It will be shown below that this expression can be reduced to:

$$\psi = f(S_c, d, D, \overline{V}, \phi, L_c, L_s)$$

4.1 The optimum mean water velocity ($\overline{V}$)

From curves such as those shown in Figure 16.1, it is clear that there is an optimum $\overline{V}$ at which minimum power occurs for a particular value of θ.

It has been shown in Section 3.2 that the ψ-parameter can be expressed as:

$$\psi = \frac{g}{S_c}\left(\frac{D}{d}\right)^2\left(\frac{\overline{V}}{V_c}\right)\left[\frac{\Delta H_c}{L_c} + \frac{iL_s}{L_c} + \sin\phi\left(\frac{d}{D}\right)^2|S_c - 1| + \sin\phi(L_s/L_c)\right]$$

Expressions have been obtained in earlier Chapters (10 and 15) enabling

ψ to be expressed in terms of capsule and pipe characteristics as well as theoretical or empirical considerations, thus:

$$V_c = m(\overline{V} - \overline{V}_i)$$

where $\overline{V}_i$ is obtained analytically as discussed earlier (Chapter 7) and

$$m = 1,2 - 0,8\,(\frac{d}{D} - 0,5)^2 \qquad \text{(from Chapter 10)}$$

Also from Chapter 15

$$\frac{\Delta H_c}{L_c} = \frac{h_f}{L}\,(\frac{d}{D})^2\,\frac{25}{\overline{V}^2}\,gD\,|S_c - 1|$$

From empirical relations for smooth pipes (e.g. Blasius),

$$i = \frac{h_f}{L} = C\overline{V}^n$$

$$\therefore \qquad \frac{\Delta H_c}{L_c} = \frac{C\overline{V}^n}{\overline{V}^2}\,(\frac{d}{D})^2\,25\,gD|S_c - 1|$$

$$= \gamma\,\overline{V}^{n-2}$$

Thus

$$\psi = \alpha\,\frac{\overline{V}}{\overline{V} - \overline{V}_i}\,\left[\beta\,\overline{V}^2 + \gamma(\overline{V})^{n-2} + \delta\right] \qquad (17.9)$$

where

$$\alpha = \frac{g}{S_c}\,(\frac{D}{d})^2\,\frac{1}{m} \qquad (17.10)$$

$$\beta = C\,\frac{L_s}{L_c} \qquad (17.11)$$

$$\delta = \sin\phi\{(\frac{d}{D})^2\,|S_c - 1|\} + \sin\phi(L_s/L_c) \qquad (17.12)$$

and

$$\gamma = 25C\,(\frac{d}{D})^2\,gD|S_c - 1| \qquad (17.13)$$

To find the minimum of ψ with respect of velocity, ψ can be partially differentiated with respect to $\overline{V}$, keeping all other variables constant. θ is, of course, varying.

$$\left[\frac{\partial\psi}{\partial\bar{V}}\right]_{d,D,L_c,L_s,S_c,\phi} = \{(\alpha\beta(n+1)(\bar{V})^n + \alpha\gamma(n-1)(\bar{V})^{n-2} + \alpha\delta)(\bar{V}-\bar{V}_i)-(\alpha\beta(\bar{V})^{n+1}+\alpha\gamma(\bar{V})^{n-1}+\alpha\delta\bar{V})\}/(\bar{V}-\bar{V}_i)^2 \quad (17.14)$$

Equating to zero and simplifying yields:

$$\alpha\beta\left[n(\bar{V})^{n+1}-(n+1)(\bar{V})^n(\bar{V}_i)\right]+\alpha\gamma\left[(n-2)(\bar{V})^{n-1}-(n-1)(\bar{V})^{n-2}(\bar{V}_i)\right]-\alpha\delta\,\bar{V}_i=0 \quad (17.15)$$

The value of the mean water velocity ($\bar{V}_{min}$) for a minimum value of the ψ-parameter can be found from the above equation

i.e. $\bar{V}_{min}$ = function ($\bar{V}_i$, δ, α, β, γ, n, L_s)

where $\bar{V}_i$ = function (d, D, S_c, ϕ, L_c)

4.2 Complete optimisation of ψ-parameter

In order to carry out a complete economical analysis of the objective function (ψ), this parameter is partially differentiated with respect to each of the variables, holding the others constant and equating to zero. Thus:

$$\left[\frac{\partial\psi}{\partial d}\right]_{D,L_c,L_s,S_c,\phi,\bar{V}} = 0$$

$$\left[\frac{\partial\psi}{\partial D}\right]_{d,L_c,L_s,S_c,\phi,\bar{V}} = 0 \qquad \text{etc.}$$

followed by the solution of the resulting simultaneous equations.

Such a procedure yields optimum values. The analysis is, however, extremely laborious and recourse is made to the digital computer in order to avoid many man-hours of work.

4.3 Constraints

Optimum values of pipe diameter (D) and linear concentration (C_L) may represent a pipe diameter which is not commercially available or a C_L value which is too high and not feasible for the injector. Therefore constraints have to be built into the equations: e.g. C_L and D as

well as other variables may have to be limited (or constrained) within upper and lower limits.

4.4 Optimum capsule diameter

It has already been shown in Chapter 16 that the optimum diameter ratio is of the order $d/D \approx 0,85$. The question is; what is the optimum pipe (or capsule) size and linear concentration (or capsule spacing)? Assume that the diameter ratio $(d/D = 0,85)$, the length to diameter ratio $(L_c/d = 4,0)$ and the capsule density $(S_c = 4,0)$ are fixed. Figure 17.3 depicts ψ as a function of linear concentration with capsule diameter (d) as parameter for a delivery rate of 2,0 kg/s. It is clear that the envelope of ψ_{min} is fairly flat giving a range of capsule diameters and associated linear concentrations.

From Figure 17.3, the pipe diameter for minimum energy/kg m is of the order of 50 mm for a capsule mass delivery rate $(\theta) = 2$ kg/s.

Figure 17.4 shows how the mean velocity and the capsule velocity vary to yield $\theta = 2$ kg/s at different linear concentrations for $d = 50$ mm, i.e. tracing the $d = 50$ mm curve of Figure 17.3. Also shown on Figure 17.4 are curves of V_c and $\overline{V}$ as a function of C_L in order to yield ψ_{min} if θ varies. The curves cross where there is a minimum value of ψ at $\theta = 2$ kg/s and the relevant capsule and mean water velocities can be read off the graph at $C_L = 0,2$ (20% linefill).

Figure 17.5 shows the ψ-parameter as a function of linear concentration for θ constant and for θ varying to give ψ_{min}. Also shown (dotted) is a graph of θ as a function of C_L. The two solid curves are tangential at $C_L = 0,2$ for $\theta = 2$ kg/s. This gives the optimum value of linear concentration for $d = 50$ mm and $\theta = 2$ kg/s.

If θ is increased to 10 kg/s (see Figure 17.6) a similar pattern emerges to that shown on Figure 17.3, and if the curve for the 50 mm

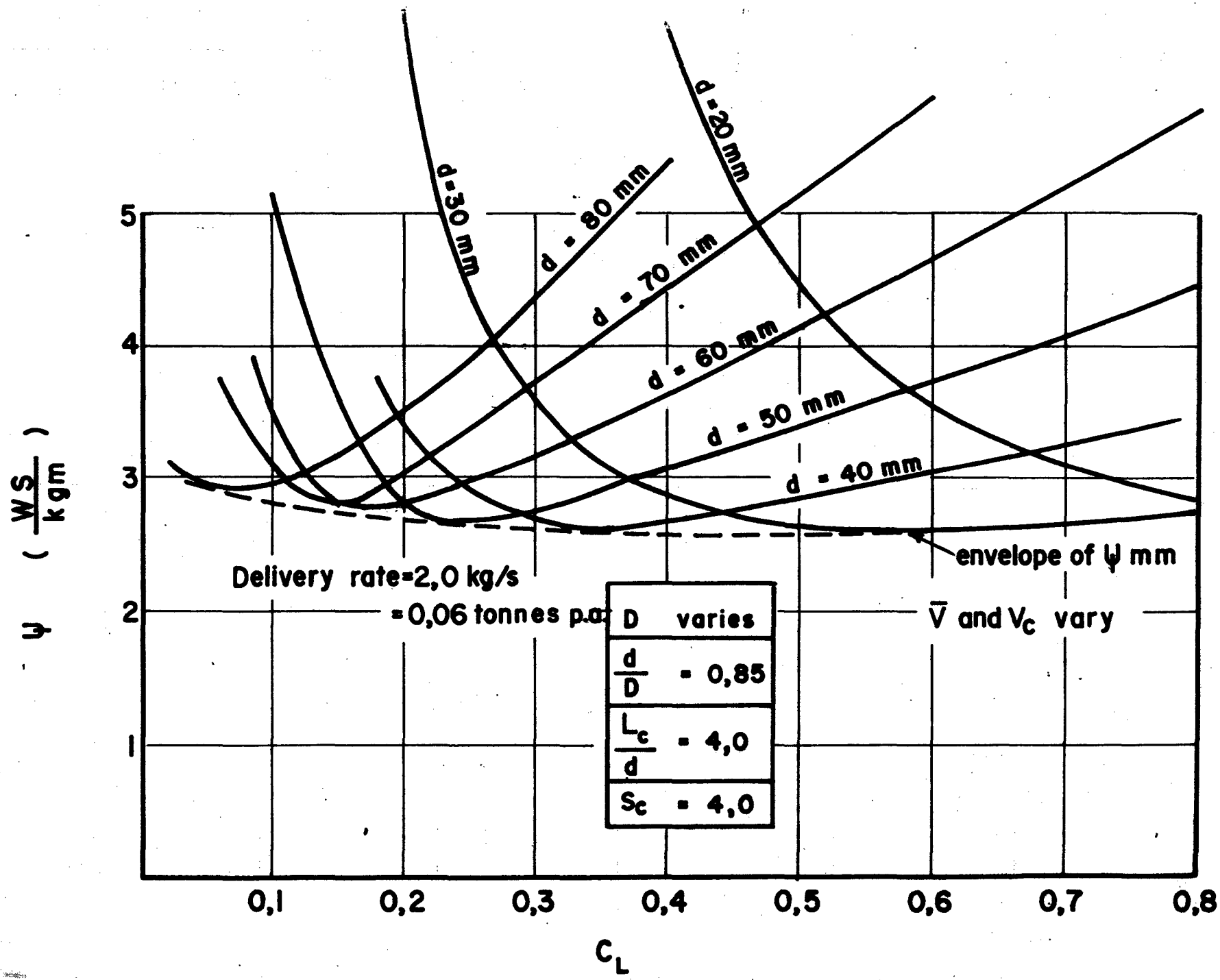
d = 30 mm
d = 80 mm
d = 70 mm
d = 60 mm
d = 50 mm
d = 40 mm
d = 20 mm
envelope of ψ mm
Delivery rate=2,0 kg/s
=0,06 tonnes p.a.
V̄ and Vc vary
D varies
d/D = 0,85
Lc/d = 4,0
Sc = 4,0
ψ (WS/kgm)
CL
1
2
3
4
5
0,1
0,2
0,3
0,4
0,5
0,6
0,7
0,8

FIG. 17.3

FIG. 17.4

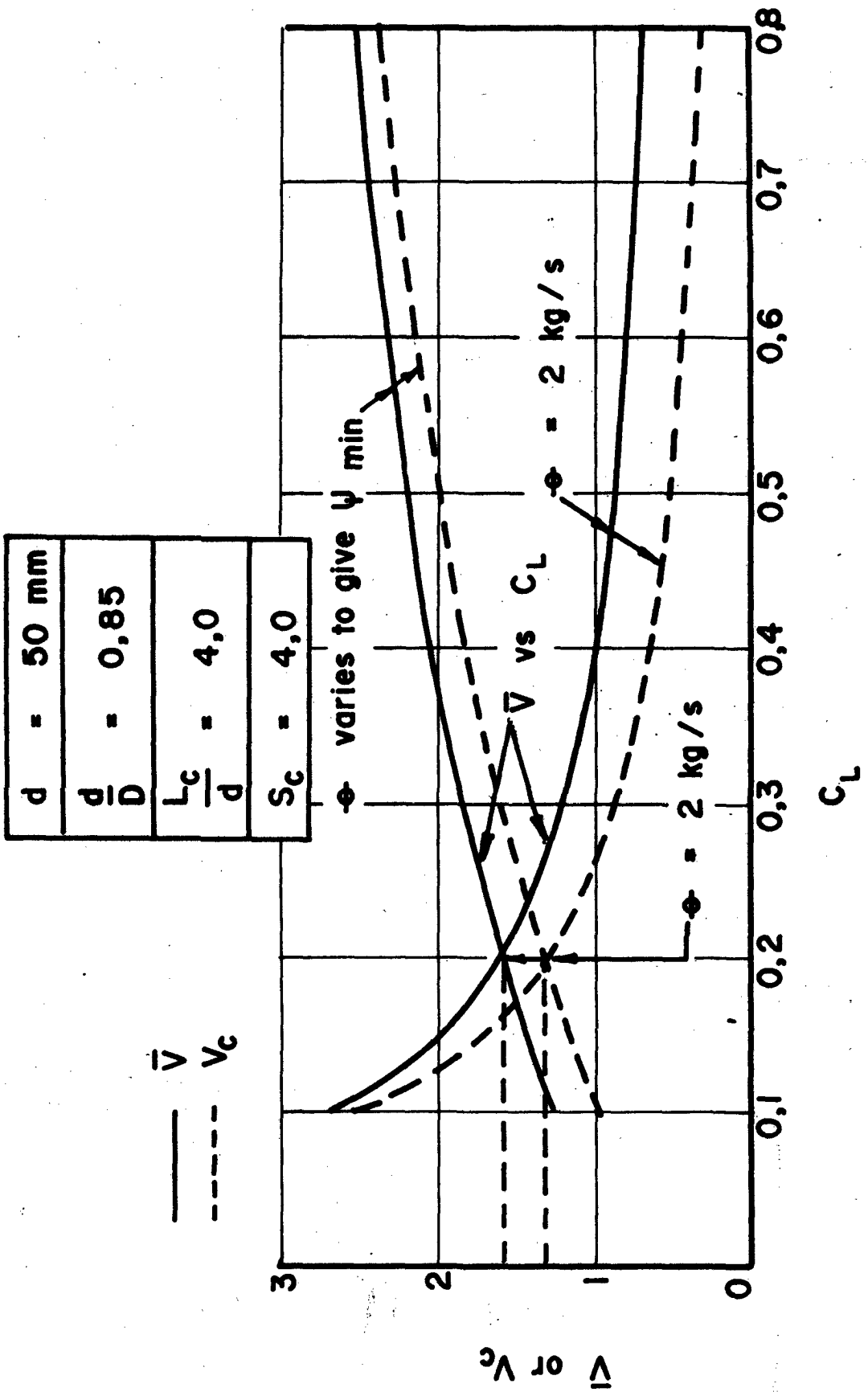
d = 50 mm
d/D = 0,85
Lc/d = 4,0
Sc = 4,0
φ varies to give ψ min
V̄ vs CL
φ = 2 kg/s
φ = 2 kg/s
V̄ > Vc
V̄ or Vc
CL
0
1
2
3
0,1
0,2
0,3
0,4
0,5
0,6
0,7
0,8

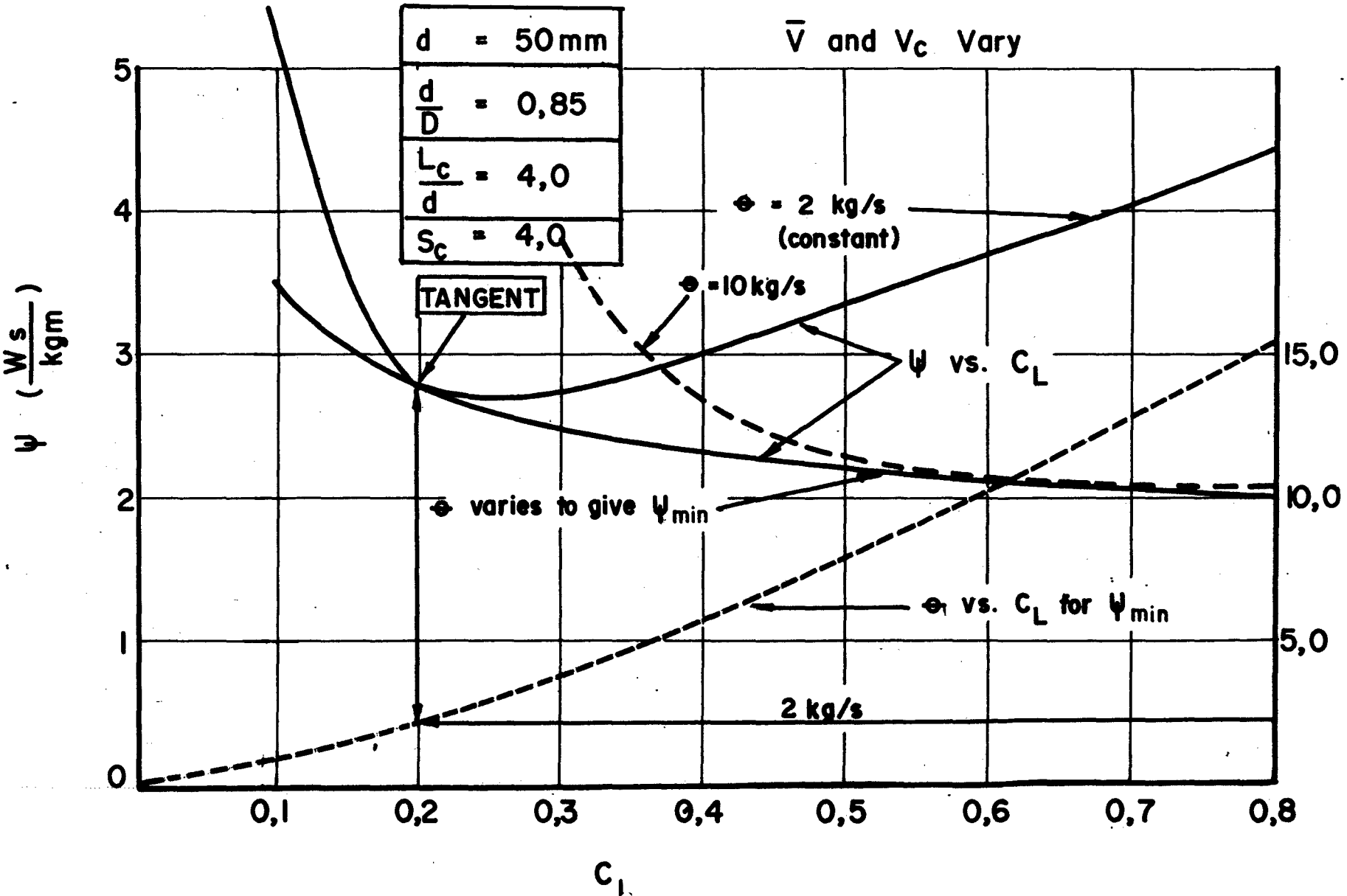
d = 50mm
d/D = 0,85
Lc/d = 4,0
Sc = 4,0
V̄ and Vc Vary
TANGENT
Φ = 2 kg/s (constant)
Φ = 10 kg/s
ψ vs. CL
Φ varies to give ψmin
Φ1 vs. CL for ψmin
2 kg/s
ψ (Ws/kgm)
Φ (kg/s)
CL
0
1
2
3
4
5
0,1
0,2
0,3
0,4
0,5
0,6
0,7
0,8
5,0
10,0
15,0

FIG. 17.5

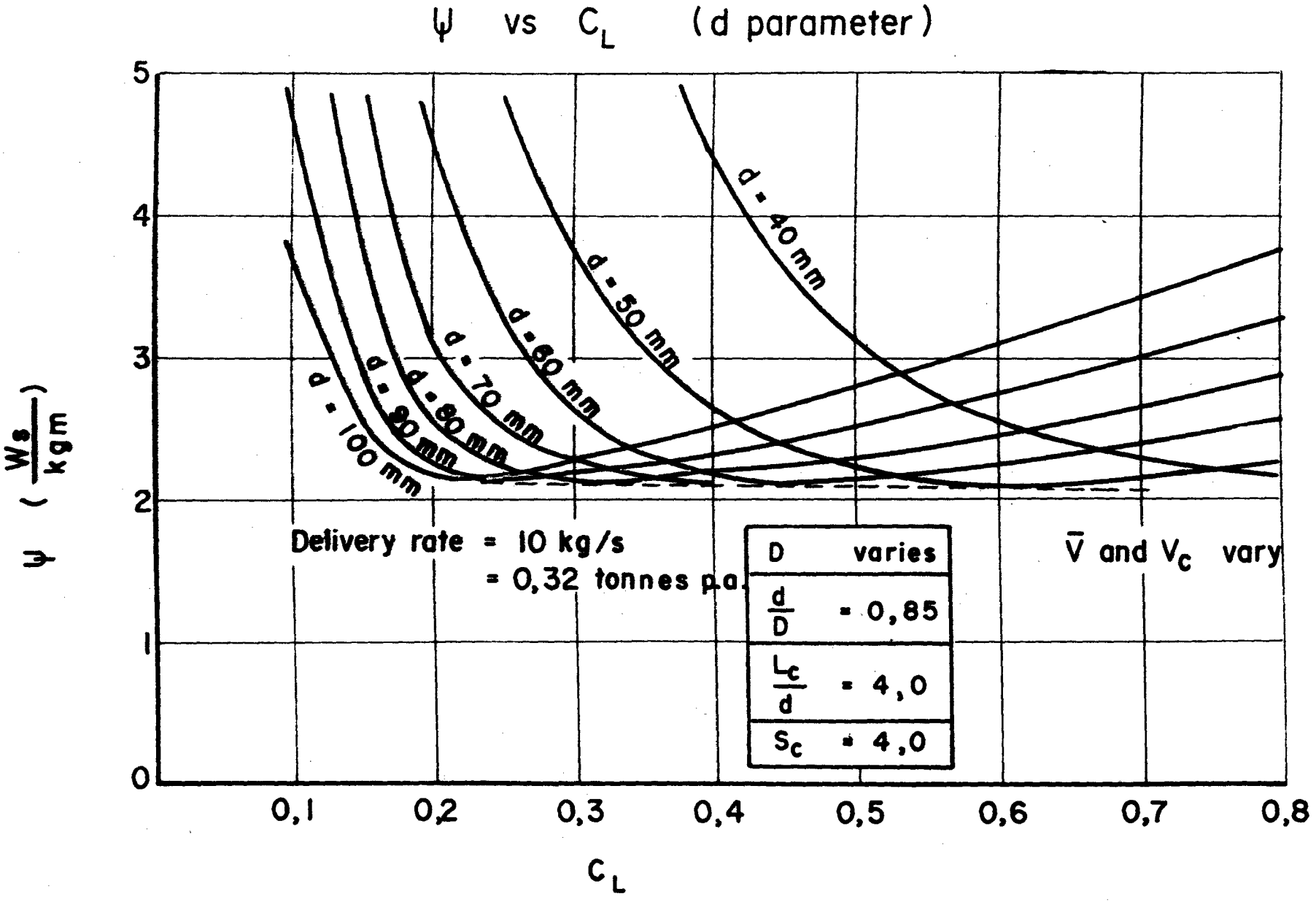
ψ vs C_L (d parameter)
ψ ($\frac{Ws}{kgm}$)
C_L
d = 40 mm
d = 50 mm
d = 60 mm
d = 70 mm
d = 80 mm
d = 90 mm
d = 100 mm
Delivery rate = 10 kg/s
= 0,32 tonnes p.a.
$\bar{V}$ and V_c vary
D varies
$\frac{d}{D}$ = 0,85
$\frac{L_c}{d}$ = 4,0
S_c = 4,0
0
1
2
3
4
5
0,1
0,2
0,3
0,4
0,5
0,6
0,7
0,8

FIG. 17.6

diameter capsule is superimposed on Figure 17.5, then the tangent occurs at $C_L = 0,6$ indicating the optimum concentration for a specific $d = 50$ mm and $\theta = 10$ kg/s.

Since every point on graphs such as Figure 17.3 and 17.6 represents a value of ψ (for a particular capsule diameter and linear concentration), the minimum points of the ψ curves represent optimum C_L values for each capsule diameter. The situation can be summarised as follows:

1. d constant; each minimum value of a curve is a minimum value of ψ, i.e. ψ_{min}.
2. The minimum value of the envelope represents a doubly minimum value of ψ. This will be designated the optimum value of ψ, i.e. (ψ_{opt}). The diameter ratio, length to diameter ratio and SG are fixed with d and C_L varying.

For large capsule diameters the linear concentration for (ψ_{min}) becomes sparse, (i.e. $d = 80$ mm and $C_L = 0,055$). Conversely, small diameters are associated with high concentrations, which may be difficult to achieve due to injector limitations.

It is obvious that as small a pipe diameter as possible should be used unless the ψ-parameter becomes too high. Actually the ψ-parameter, which is an energy term per kg of capsule mass transported per unit length (Ws/kg m) can be represented as a cost per kg m, and if the pipe diameter is to be optimised then the curve of pipeline costs and energy costs may be represented as in Figure 17.7.

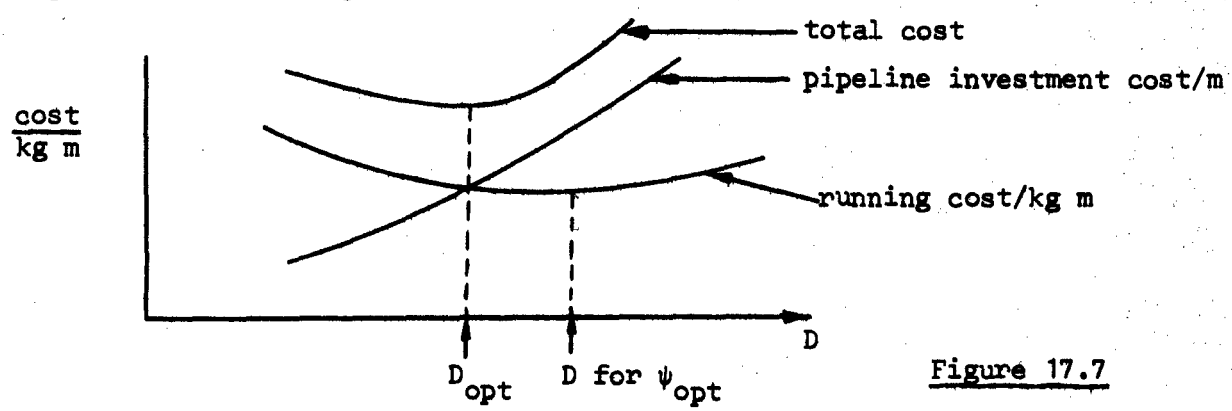

Figure 17.7

A computer programme was written for evaluating the value of ψ_{min} from equations (17.9) and (17.15).

Breifly, the programme solves for the value of $\bar{V}$ to yield ψ_{min} for a chosen linear concentration. This yields a delivery rate which corresponds to ψ_{min} but which may not be the desired delivery rate. The programme then adjusts the linear concentration by halving the error successively to achieve a delivery rate which corresponds to the prescribed value. This process converges usually within about 8 iterations. Every time it goes through an iteration the value for ψ_{min} is calculated by a further iterative process (see Appendix II).

The programme was extended to calculate the value of capsule diameter for ψ_{opt}. However, this part of the programme was not very valuable because of (a) the flatness of the ψ versus d curves and (b) the fact that the optimum value of d need not necessarily be at ψ_{opt} (see Figure 17.7).

Figure 17.8 shows the optimisation of the ψ-parameter as a function of capsule diameter (d) and pipe diameter (D) with the delivery rate (θ) as parameter.

As θ decreases the optimum ψ-parameter increases. This is because the denominator of ψ is θ. As $\theta \to 0$, $\psi \to \infty$. A capsule transportation system thus becomes, from this point of view, more economical as the capsule mass flow delivery rate increases.

As θ decreases, the rate of diameter (d) increase, to achieve ψ_{min} values, increases markedly. And at $\theta = 3000$ kg/s there is very little change in the ψ_{min} value as d increases.

A further point of note in Figure 17.8 is that, as diameter (d) increases at a particular θ value, the capsule velocity decreases. Every point on a fixed θ curve is associated with a different capsule velocity.

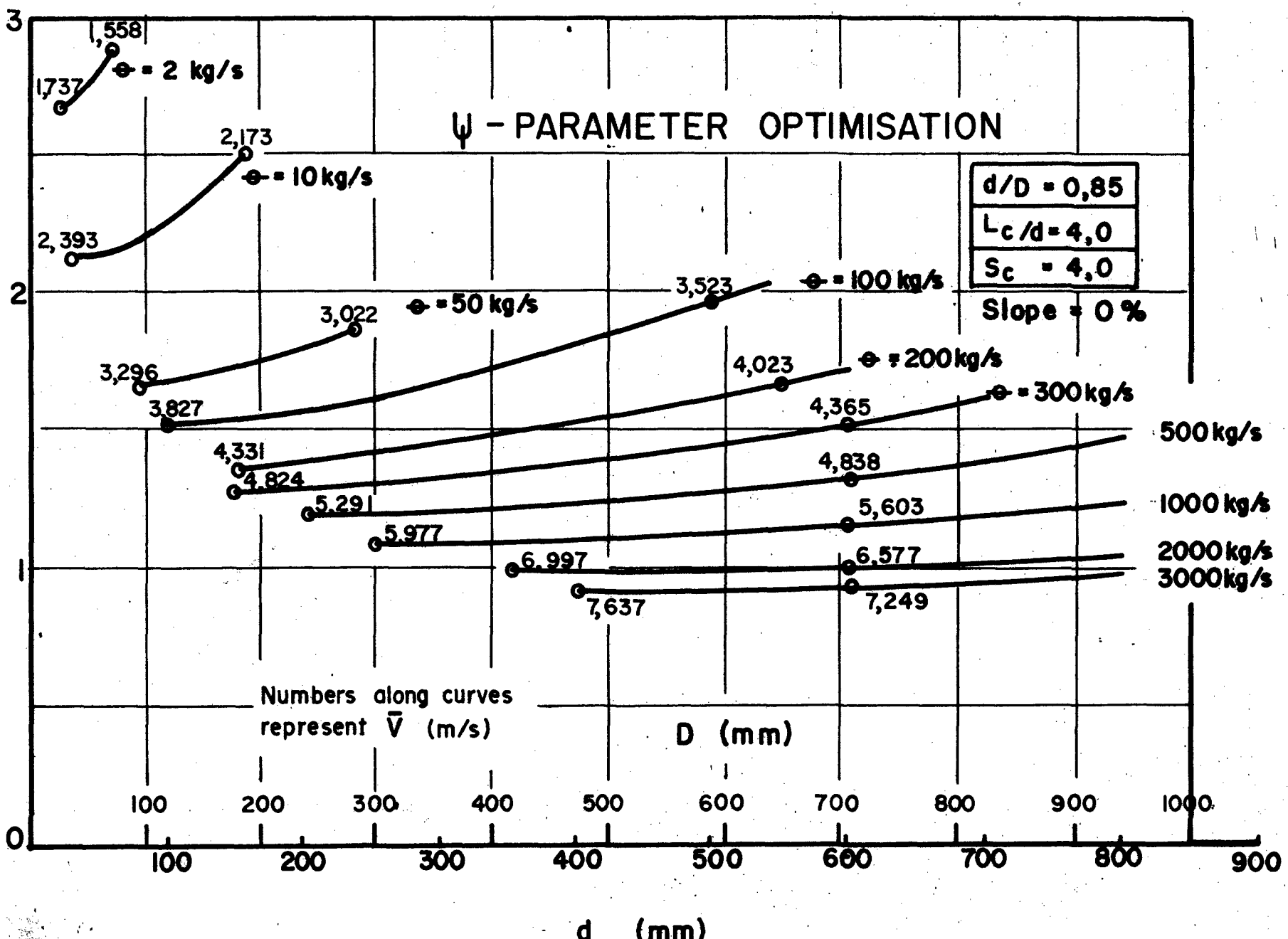
Ψ - PARAMETER OPTIMISATION
d/D = 0,85
Lc/d = 4,0
Sc = 4,0
Slope = 0 %
= 2 kg/s
= 10 kg/s
= 50 kg/s
= 100 kg/s
= 200 kg/s
= 300 kg/s
500 kg/s
1000 kg/s
2000 kg/s
3000 kg/s
1,558
1,737
2,173
2,393
3,022
3,296
3,523
3,827
4,023
4,331
4,365
4,824
4,838
5,291
5,603
5,977
6,577
6,997
7,249
7,637
Numbers along curves represent V̄ (m/s)
D (mm)
d (mm)
Ψmin (Ws/kgm)
0
1
2
3
100
200
300
400
500
600
700
800
900
1000

FIG. 17.8

To give a quantitative idea as to velocity change along the θ curves, values of $\overline{V}$ are shown. It is clear that the velocity variation is slight.

For a fixed capsule diameter the capsule velocity increases as θ increases. To increase the mass flow delivery rate, the capsules, naturally have to travel faster.

Each point on Figure 17.8 is also associated with a different value of the linear concentration (C_L).

Figure 17.9 shows how ψ varies with d if C_L is kept constant and the minimum values of curves such as these (at different linear concentrations) are coincident with the curves on Figure 17.8.

At a particular capsule mass delivery rate (θ) the value of C_L to yield minimum ψ-values increases as diameter (d) decreases.

This is best shown on Figure 17.10 which represents the optimum ψ-parameter as a function of linear concentration (C_L) for capsules of fixed diameter ratio, SG and length to diameter ratio.

The dotted curves represent contours of constant capsule diameters. It is apparent that decreasing the linear concentration results in an increase in the value of ψ_{min} and the trend is accentuated as θ decreases.

The obvious conclusion is that C_L should be as large as is practicable. Packing the capsules close together results in a smaller pipeline diameter as well as less energy per kg m of capsule mass transported. The maximum linear concentration is solely dependent on the injection technique.

Figures 17.11 and 17.12 are similar to Figures 17.8 and 17.10 except that the SG is halved. These curves are drawn in order to illustrate the effect of packing capsules with material of an SG of (say) 4,0 with a void ratio (e) of 1,0. This will be discussed in the next Chapter.

FIG. 17.9

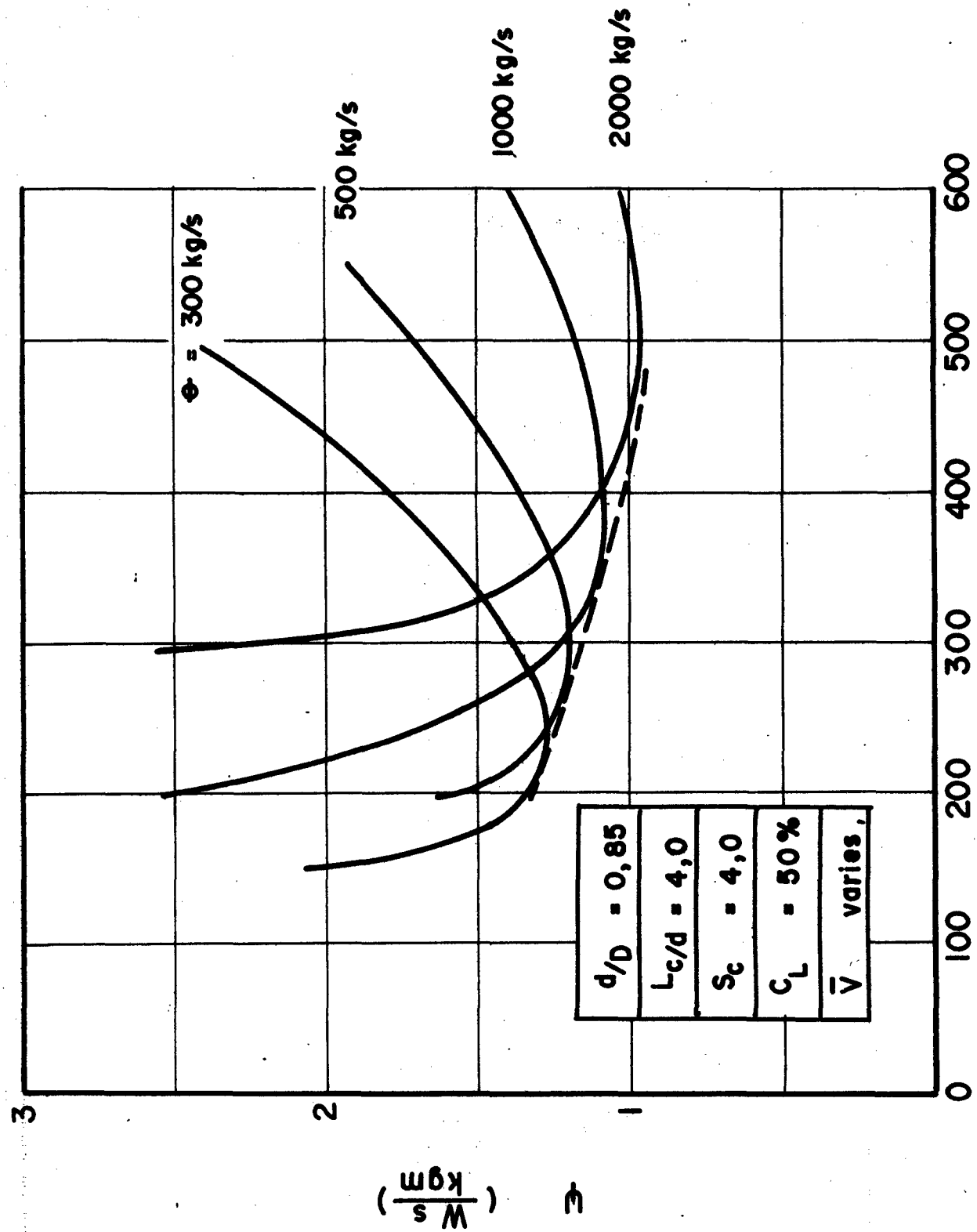
Φ = 300 kg/s
500 kg/s
1000 kg/s
2000 kg/s
d/D = 0,85
Lc/d = 4,0
Sc = 4,0
CL = 50%
V̄ varies.
3
2
1
0
100
200
300
400
500
600
d
ε (Ws/kgm)

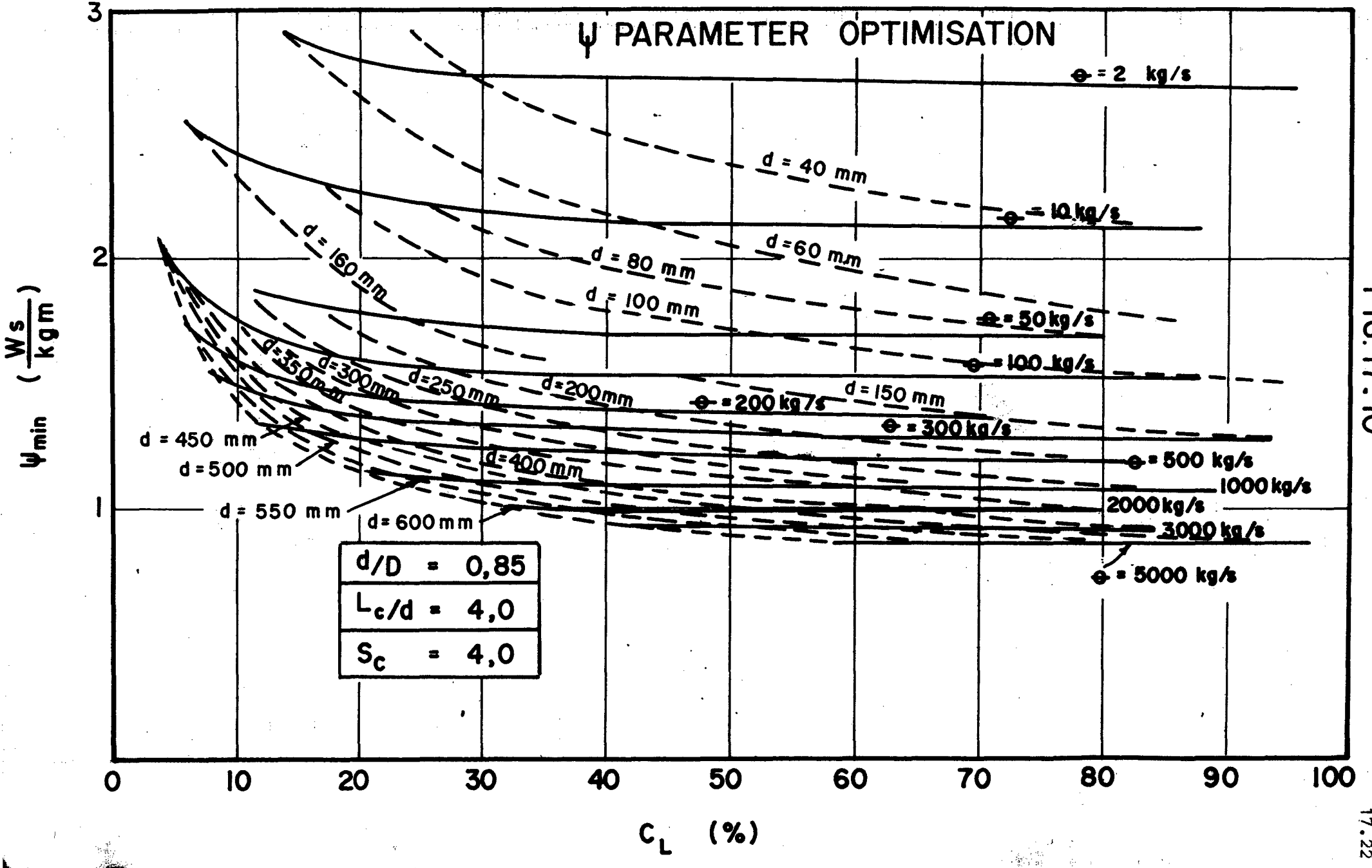
ψ PARAMETER OPTIMISATION
ψ_{min} $(\frac{Ws}{kgm})$
C_L (%)
d = 40 mm
d = 60 mm
d = 80 mm
d = 100 mm
d = 150 mm
d = 160 mm
d = 200mm
d = 250mm
d = 300mm
d = 350mm
d = 400mm
d = 450 mm
d = 500 mm
d = 550 mm
d = 600mm
= 2 kg/s
= 10 kg/s
= 50 kg/s
= 100 kg/s
= 200 kg/s
= 300 kg/s
= 500 kg/s
1000 kg/s
2000 kg/s
3000 kg/s
= 5000 kg/s
d/D = 0,85
L_c/d = 4,0
S_c = 4,0

FIG. 17.10

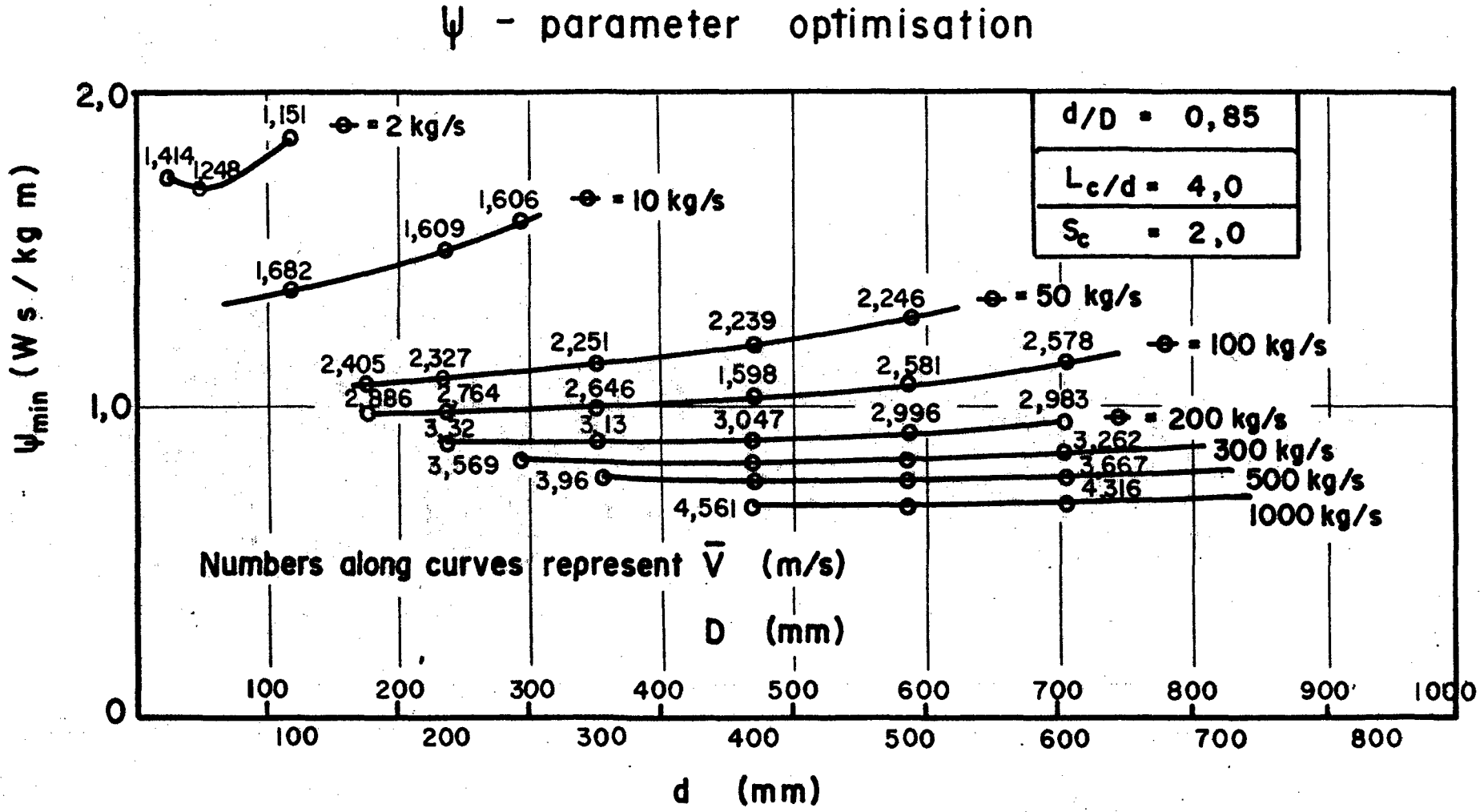

FIG. 17.11

17.23

ψ PARAMETER OPTIMISATION

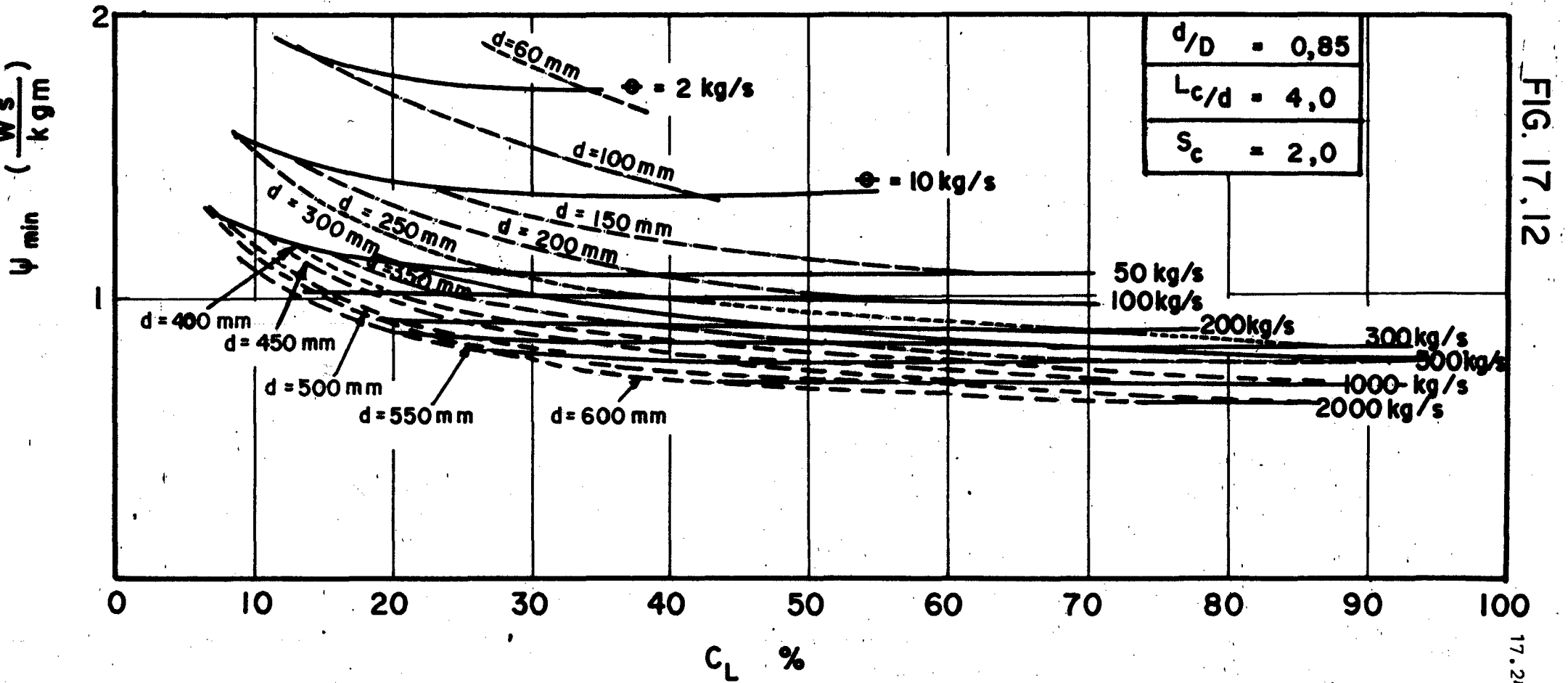

FIG. 17.12

Curves such as 17.10 and 17.11 are adequate for design purposes. Given the capsule mass delivery rate it is possible to determine the optimum ψ value as well as the pipe diameter and mean water velocity for a particular concentration.

Capsule geometries can be selected from Figure 17.2 or fed into the program (Appendix II) to yield curves such as Figure 17.10 and 17.11.

An example of the use of these curves is given in the next Chapter.

CHAPTER 18

A COMPARISON OF SUSPENDED SEDIMENT FLOW AND CAPSULE TRANSPORTATION IN PIPELINES

The excess energy and power requirements for heterogeneous as well as homogeneous suspended sediment transport systems are compared with capsule transportation.

The capsules considered may be formed, of the material to be transported (coal has already been formed into "paste slugs"), as well as containers filled with solid material having a void ratio.

1. Flow Regimes

Various regimes may exist in the two phase flow of solid liquid mixtures. These are conveniently classified in Figure 18.1. Both homogeneous and heterogeneous regimes are considered feasible when transporting solids in pipelines. The regime change depends on the velocity, solids concentration and particle size as well as pipeline properties such as size, roughness and slope, and fluid properties such as viscosity, density and velocity. Flow regimes vary from highly concentrated suspensions of minute particles moving slowly to fast moving mixtures of large particles in fairly sparse suspensions.

The main regimes are as follows.

2. Homogeneous flow

Homogeneous flow exists when velocities are high and equivalent particle diameters are small. Solid particles are more or less uniformly distributed over the cross-section of the pipe during flow. The solids are in full suspension. Homogeneous flow can arise in two ways:

2.1 Non-Newtonian flow.

Non-settling mixtures always result in homogeneous flow if conditions

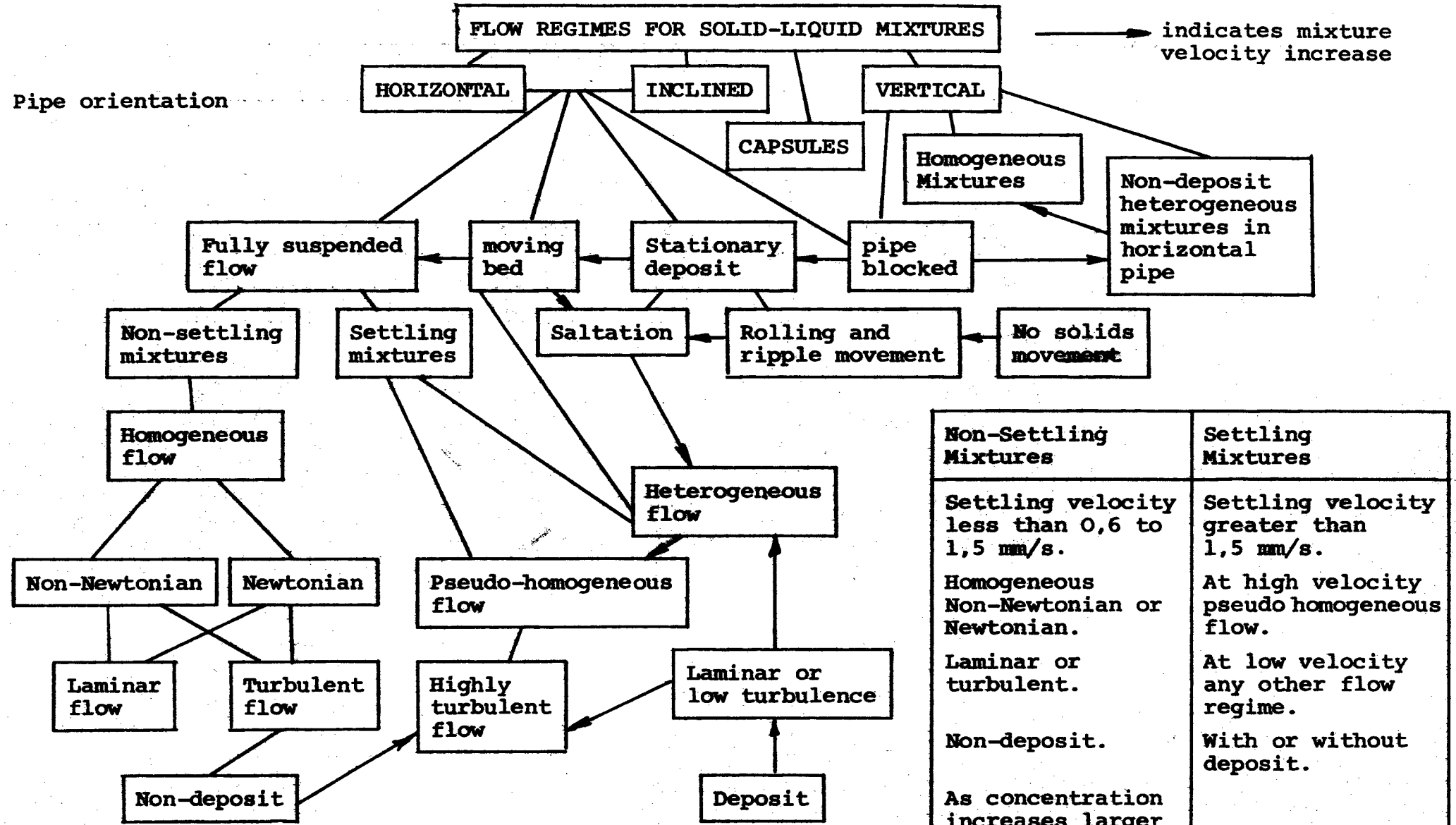

Non-Settling Mixtures	Settling Mixtures
Settling velocity less than 0,6 to 1,5 mm/s.	Settling velocity greater than 1,5 mm/s.
Homogeneous Non-Newtonian or Newtonian.	At high velocity pseudo homogeneous flow.
Laminar or turbulent.	At low velocity any other flow regime.
Non-deposit.	With or without deposit.
As concentration increases larger particles form non-settling mixtures.	

FIGURE 18.1 Flow regimes for solid - liquid mixtures.

are such that there is slight turbulence, or, if the particles are extremely small and truly non-settling then the flow will be homogeneous even when laminar.

Non-settling homogeneous flows are usually non-Newtonian. Non-Newtonian fluids are materials which do not exhibit a direct proportionality between shear stress and shear rate. The limiting condition depends on particle size, concentration, size distribution and specific gravity.

Time independent non-Newtonian fluids have been classified into fluids having a yield stress (Bingham plastics) and fluids without a yield stress (pseudo plastics). A detailed description is given in Metzner and Reed (reference 39) and most mixtures in laminar and turbulent flow in smooth pipes, can be correlated by means of Figure 18.2, where the generalised Reynolds number is given as:

$$R_{e,gen} = \frac{D^{n'} V_m^{2-n'} \rho}{K' 8^{n'-1}} \qquad (18.1)$$

where n' = a type of flow behaviour index which indicates the degree of non-Newtonian behaviour

K' = measure of the consistency of the fluid; larger values of K' mean "thicker" or "more viscous" fluids

V_m = mean velocity of flow mixture

ρ = density of non-Newtonian fluid

D = pipe diameter

and f = the conventional friction factor in Darcy's equation.

For pseudo-plastic, power law fluids;

$$\tau = K (dv/dy)^n \qquad (18.2)$$

where $\tau = \Delta P_f D/(4L)$

ΔP_f = pressure drop for the mixture.

FIG. 18.2

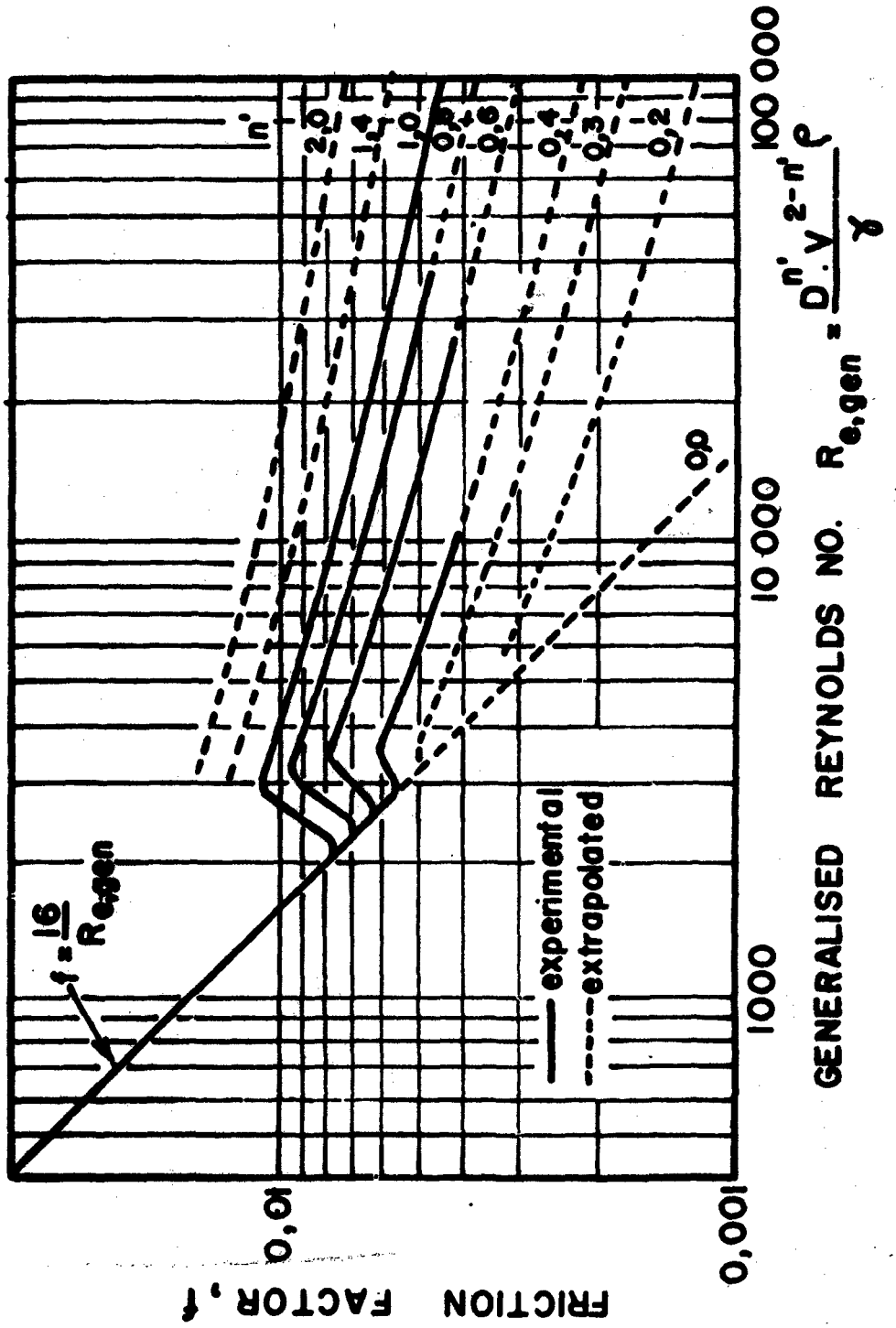
FRICTION FACTOR, f
0,01
0,001
1000
10 000
100 000
GENERALISED REYNOLDS NO. $R_{e,gen} = \frac{D^{n'} V^{2-n'} \rho}{\gamma}$
$f = \frac{16}{R_{e,gen}}$
experimental
extrapolated
n'
2,0
1,0
0,8
0,6
0,4
0,3
0,2
0,0

For Newtonian fluids $\tau = \mu(dv/dr)$

and for laminar flow

$$\mu = \Delta PD^2/(32LV_m) \tag{18.3}$$

It is thus possible to define a "nominal velocity gradient" for laminar flow of Newtonian fluids based on the mean flow velocity (V_m) and the shear stress at the wall.

$$(dV/dr)_{nom} = \tau_o/\mu = \Delta PD/(4L\mu)$$

from equation (18.3);

$$(dV/dr)_{nom} = 8V_m/D$$

The relation between shear stress and nominal velocity gradient for a pseudo plastic substance may be written as

$$\Delta PD/(4L) = K'(8V_m/D)^{n'} \tag{18.4}$$

In the general case K' and n' are not constants but vary with $8\bar{V}/D$.

Now $f = \dfrac{\tau_o}{\frac{1}{2}\rho\bar{V}^2}$ and

substituting in equation (18.2) gives:

$$f = \frac{K'(8V_m/D)^{n'}}{(\rho\bar{V}^2/2)}$$

$$= \frac{16\ K'\ 8^{n'-1}}{D^{n'}\ \bar{V}^{2-n'}\rho} \tag{18.5}$$

From the analogy between Newtonian fluids ($f = 16/R_e$) and equation (18.5) we get equation (18.1).

Metzner and Reed proposed using K' and n', as determined for laminar flow, in turbulent flow. Just as the viscosity of a Newtonian fluid is defined under laminar conditions but used in both laminar and turbulent regions.

Dodge and Metzenr (reference 13) also showed that the diagram on Figure 18.2 could be used for non-power low fluids providing K' and n'

are obtained from the point on the laminar curve of $D\Delta P_f/4L$ versus $8\bar{V}/D$ which has as ordinate the particular value of $D\Delta P_f/4L$ prevailing under the actual turbulent conditions.

2.2 Pseudo homogeneous flow

Settling mixtures, in which the flow rate and particle size are such that there is no settlement, result in homogeneous flow. This regime is pseudo-homogeneous since any particle size can be maintained in full suspension if the flow velocity and resulting turbulence are high enough.

The basic mechanism by which sediment particles are maintained in suspension is turbulence. This means that fluid containing a greater sediment concentration at a lower level is exchanged with fluid containing less sediment concentration at a higher level to offset the downward movement due to gravity. This is done by means of turbulent mixing.

The equation for homogeneous flow has been derived by Newitt et al (reference 41) and given by other authors as:

$$\frac{i_m - i_w}{C_v i_w} = \phi = |S_s - 1| \qquad (18.6)$$

where i_m = hydraulic gradient for the mixture measured in units of water

i_w = hydraulic gradient for water in units of water

C_v = delivered volumetric concentration

S_s = specific gravity of dry solids.

3. Heterogeneous flow

There is a concentration of solid particles increasing towards the bed, that is, a concentration gradient is established. The eddying movement is no longer sufficient to keep the mixture homogeneous and gravity tends to cause deposition. The particles are generally coarse, or of large density or the mean velocity of flow is low enough to allow partial

separation of particles from fluid.

The chief method of supporting particles, at least near the point of incipient deposition, is intergranular and granoperipheral collisions as well as (to a lesser extent than homogeneous flow) turbulent mixing.

The concentration gradient disappears with higher velocities and tends to a homogeneous regime.

An empirical equation for heterogeneous flow has been presented by Durand (reference 14) as:

$$\phi = 85\left[gD\frac{(S_s-1)}{V_m^2}\ \frac{1}{\sqrt{C_D}}\right]^{1,5} \tag{18.7}$$

where V_m = mixture velocity

and C_D = particle drag coefficient.

Equation (18.7) can be written in the form

$$\phi = 68,5\left[gD\ \frac{(S_s-1)}{V_m^2}\ \frac{V_t}{\sqrt{gd_p(S_s-1)}}\right]^{1,5}$$

where V_t = terminal settling velocity of solids in still water

d_p = equivalent diameter of particle.

Equation (18.7) can be combined with equation (18.6) to yield a criterion for distinguishing between homogeneous and heterogeneous flow:

$$V_m = 4,4\ gD\ C_D^{-0,25}\ (S_s-1)^{1/6} \tag{18.8}$$

where C_D = drag coefficient for the particles.

Equation (18.7) is valid above the "limit deposit velocity." This velocity is defined as the velocity below which suspended particles begin to settle and are moved along the bottom of the pipe as bed load.

Durand gives the following equation for the limit deposit velocity (V_L)

$$V_L = F_L\sqrt{2gD(S_s-1)} \tag{18.9}$$

where F_L is a function of C_V and the mean particle diameter (d_p). With fine material C_V and d_p increases the value of F_L. For $d_p > 1$ mm, the C_V and d values lose significance and $F_L = 1{,}34$ in this range.

Different values for the constant and power in equation (18.7) have been given by different authors (e.g. Bonninton (reference 4), (Condolios and Chapus (reference 11) and Zandi (reference 67)). However, most of the work was carried out by Durand, his equation is generally considered to be the most reliable, and equation (18.7) is the one used in this Chapter.

4. The deposit regimes

Most investigators consider the regimes, towards the right in Figure 18.1, to be uneconomical. A stationary bed exists with rolling and ripple movement or with saltation. This regime is, however, not necessarily uneconomic since the power requirement may decrease for velocities below the limit deposit velocity.

Nonetheless, it may be an unsafe region in which to operate because there is imminent danger of pipe blockage.

One equation is that obtained by Newitt et al (reference 41) and modified by Babcock (reference 1)

$$\left[i_m - i_w\right] \Big/ (C_v\, i_w) = 60{,}6\ (S_s - 1)\ gD/V_m^2 \qquad (18.10)$$

The excess head losses and power requirements for capsule transportation will be compared with pseudo-homogeneous, heterogeneous and non-Newtonian flow.

5. Volumetric concentration and voids ratio for capsules

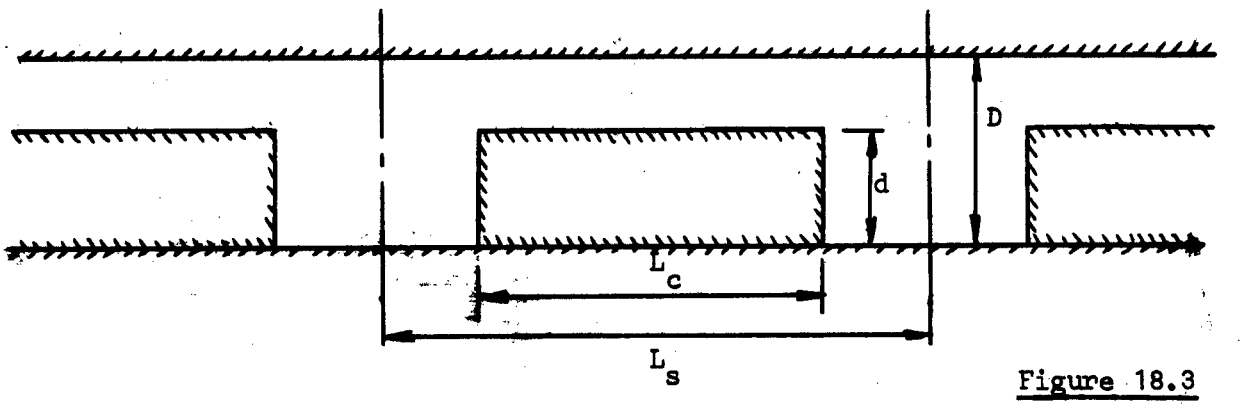

Figure 18.3

Referring to Figure 18.3, the transport or spatial volumetric concentration $(C_{vt})_c$ for capsules in the pipe can be defined as the volume occupied by the capsules divided by the total volume occupied by capsules and water

$$\therefore \quad (C_{vt})_c = (d/D)^2 \, L_c/L_s \tag{18.11}$$

For n capsules in a length of pipe (L_p)

$$\Delta H_p = \Sigma \Delta H_c = n\Delta H_c = (L_p/L_s)\Delta H_c \tag{18.12}$$

From equation (15.15)

$$\Delta H_c/L_c = (d/D)^2 |S_c - 1| \; 25(2f) \tag{18.13}$$

Combining equations (18.11), (18.12) and (18.13) yields:

$$n\Delta H_c/L_p = (C_{vt})_c \; |S_c - 1| \; 25(2f)$$

i.e.
$$\Delta H_p/L_p = (C_{vt})_c \; |S_c - 1| \; 25(2f) \tag{18.14}$$

= total excess head loss due to capsules in length L_p.

The delivered volumetric concentration $(C_{vd})_c$ can be defined as the volume of capsules delivered per unit time divided by the delivered volume of capsules and water

$$\therefore \quad (C_{vd})_c = (d/D)^2 (L_c/L_s)(V_c/\overline{V}) \tag{18.15}$$

and $(C_{vd})_c = (C_{vt})_c$ when there is no slip, i.e. when $V_c = \overline{V}$.

The void ratio (e) is defined as the volume of voids/volume of solid.

Consider a capsule containing a unit volume of solid material of speci-

fic gravity (S_s) and volume (e) of voids. The transport volumetric concentration of solid in the capsule ($(C_{vt})_{sc}$) is:

$$(C_{vt})_{sc} = (d/D)^2(L_c/L_s)(1/(1+e)) \qquad (18.16)$$

where $S_c = S_s/(1+e)$

and $$(C_{vd})_{sc} = (d/D)^2(L_c/L_s)(V_c/\overline{V})(1/(1+e)) \qquad (18.17)$$

where $(C_{vd})_{sc}$ = delivered volumetric concentration of solids in the capsule.

Equation (18.14) becomes:

$$\frac{n\Delta H_c}{L_p} = (i_m - i_w)_c = (1+e)\frac{\overline{V}}{V_c}(C_{vd})_{sc}\{(\frac{S_s}{1+e}) - 1\}\ 25(2f)$$

and $$\phi_c = \left[\frac{i_m - i_w}{C_{vd} i_w}\right]_{sc} = \frac{\overline{V}}{V_c}\ \frac{25(2f)}{i_w}(S_s - 1 + e) \qquad (18.18)$$

where i_m = head loss per unit length due to solid capsules plus water

i_w = head loss per unit length of pipeline due to water only.

6. Comparison of capsule transportation with homogeneous suspension

For homogeneous suspensions it is assumed that no slip occurs and $C_{vd} = C_{vt}$ (these are delivered and transport volumetric concentrations for solid particles in suspension).

Case I - no voids in capsule

The capsules are formed of the solid material to be transported.

Assume that $V_c = \overline{V}$ and $e = 0$

$$\therefore \quad \phi_c = \frac{25(2f)}{i_w}(S_s - 1) \qquad (18.19)$$

If $\phi_c < \phi$ (from equation (18.6)), then the capsule transportation system requires less excess head than the homogeneous suspension, and the following inequality must be satisfied:

$$25(2f)\ \overline{V}/V_c < i_w \qquad (18.20)$$

or $$D < \overline{V}\ V_c/(25g)$$

If the capsules travel at the same velocity as the water then

$$D < \overline{V}^2/(25g) \qquad (18.21)$$

The upper left of the curve on Figure 18.4 indicates the region where excess energy losses are less for homogeneous flow than for capsules.

The implication is that high velocities and small pipe diameters are required to render excess energy due to capsules less than for homogeneous suspensions.

By equating equations (18.8) and inequality (18.21), the particle diameter, can be found, below which homogeneous flow is feasible,

$$C_D < 0,6\ (S_c-1)^{2/3}(gD)^2 \qquad (18.21)$$

Also $$V_t = \sqrt{\frac{4}{3}\frac{gd_p}{C_D}(S_s-1)}$$

For particles of SG = 4,0 (say), the critical velocity below which homogeneous flow is sustained is given as follows.

From $C_D < 1,25\ (gD)^2$

$\therefore$ $C_D < 10,8$ for $D = 300$ mm (say)

From the standard C_D versus Reynolds number diagram for spherical particles, the Reynolds number for the particle $(R_e)_p$ is given by Allen's law:

$$C_D = 18,5/(R_e)_p^{0,6}$$

$\therefore$ $$(R_e)_p = 12,45 = V_t d_p/\nu$$

$\therefore$ $$d_p = 118\ \mu m$$

and $$V_t = 20,8\ mm/s$$

$$d_p = 0,493\ mm \text{ (at } S_s = 1,6 \text{ and } D = 300\ mm)$$

Each point on the curve on Figure 18.4 corresponds to a particular value of d_p for a fixed SG.

At the pipe diameter (300 mm) and velocity (V_m) where excess energy just becomes less for capsules, the particles have to be fairly finely ground to maintain homogeneous flow (for iron ore $d_p \simeq 118\ \mu m$). If the material is lighter $(S_s = 1,6)$ then particles do not have to be ground quite so

FIG. 18.4

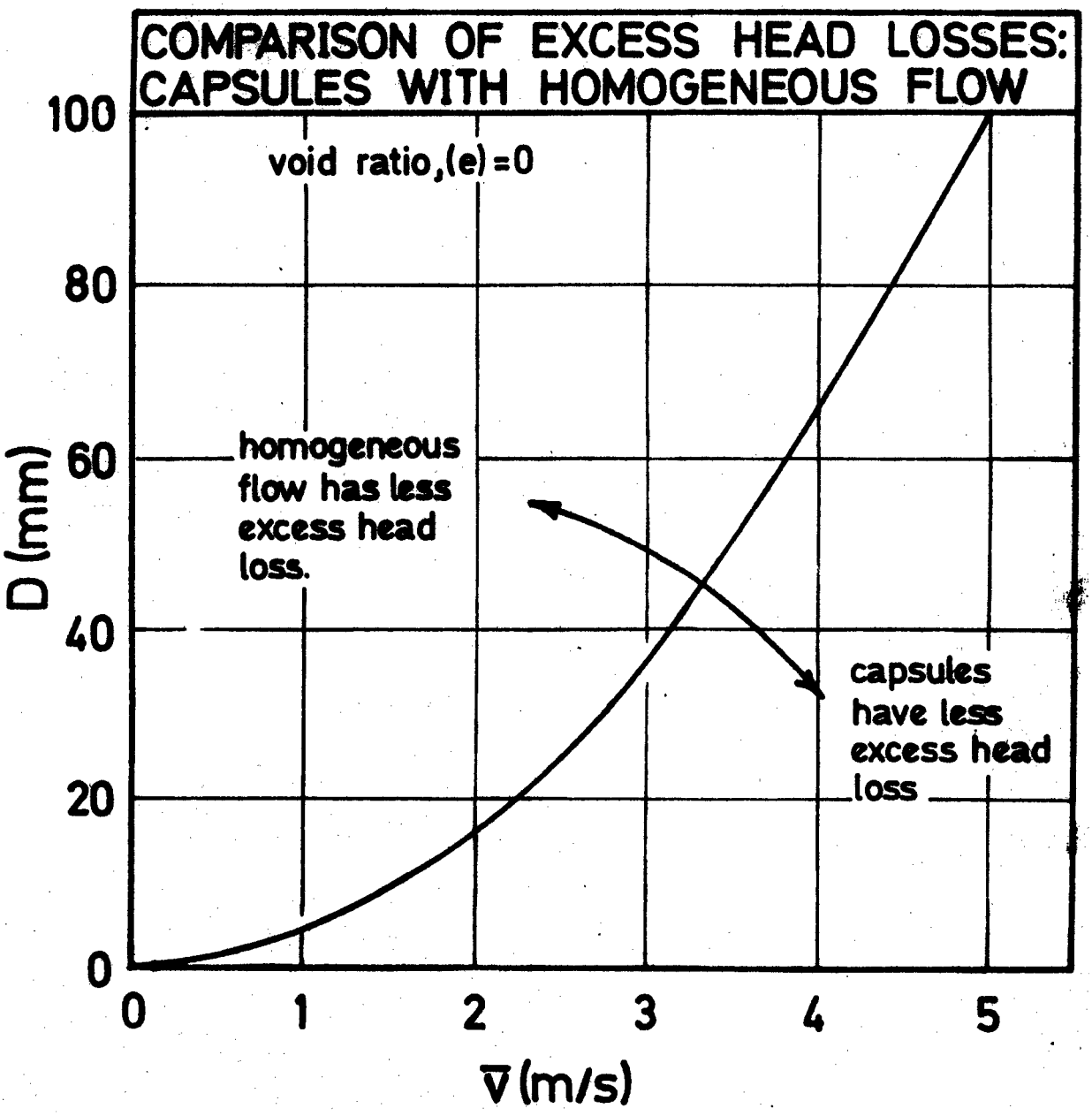
COMPARISON OF EXCESS HEAD LOSSES:
CAPSULES WITH HOMOGENEOUS FLOW
void ratio,(e)=0
homogeneous flow has less excess head loss.
capsules have less excess head loss
D (mm)
100
80
60
40
20
0
0
1
2
3
4
5
$\bar{V}$ (m/s)

fine ($d_p \approx 0{,}493$mm) to be maintained in suspension for homogeneous flow.

If capsule densities, diameter ratios and velocities are such, as to cause V_c to be greater than $\bar{V}$, then the region, where excess energy for homogeneous flow is less than for capsules, is somewhat more restricted.

Case II - voids present in the capsule

In the above case the same specific gravity was assumed for the capsule and sediment. If the solids are to be stored in the capsule the specific gravity of the capsule is lower than for the solid load because of the void ratio. However, the volumetric concentration of capsules has to be higher to achieve the same solids delivery rate. In this situation the capsules have to be lighter to achieve the same solids delivery rate. The capsules are considered as containers to be packed with the material to be transported.

The excess energy dissipation across capsules is less than for homogeneous flow if $\phi_c < \phi$, i.e. from equations (18.6) and (18.18)

$$D < \frac{\bar{V}\, V_c}{g} \frac{(S_s-1)}{(S_s-1-e)} \frac{1}{25} \qquad (18.22)$$

The following assumptions are made:

(a) The void ratio (e) for the solids packed in containers is assumed constant. A typical mined sample of iron ore (Haematite from Sishen in the Northern Cape) yielded a bulk specific gravity of about 2,2. The SG of the iron ore being about 4,4. This gives a void ratio (e) of 1,0; which is a fairly reasonable value for mined material. Although it was found that larger particles with less fines gave even higher void ratios up to about $e \approx 1{,}7$.

(b) The mass of the container itself is disregarded compared with the mass of the stored solids.

(c) The capsule velocity is assumed to be equal to the mean water

velocity. It has already been shown (Chapter 16) that a diameter ratio of $d/D = 0,85$ is about the most economical and for this diameter ratio the assumption of $V_c = \overline{V}$ is valid within about 6% above $\overline{V} = 2,0$ m/s (see Figure 10.7) for a range of capsule SG's from 0,50 to 3,28. Thus the assumption of $V_c = \overline{V}$ does not, greatly, affect the graphs that follow.

(d) The mean transport velocity in the homogeneous flow regime is equal to $\overline{V}$.

Figure 18.5 shows the pipe diameter (D) as a function of $(\overline{V})$ from the inequality (18.22). To the left and above the curves for different solid specific gravities (S_s), the homogeneous flow regime requires less excess head.

As specific gravity of solids to be transported decreases, the pipe diameter for the capsule transportation system to have less head loss than for homogeneous flow occurs at a decreasing velocity $(\overline{V})$.

When the SG is $S_s = 2,0$ for a void ratio (e) of 1,0 then the excess head required for the capsule transportation system is zero. This is because the capsules are effectively neutrally buoyant, in which case the capsule velocity is always greater than the mean water velocity.

If the grading of mined material yields a wide distribution of sizes, then it may be possible to achieve a void ratio (e) of 0,5 and Figure 18.6 shows the comparison of homogeneous flow and capsule transportation for the reduced void ratio. As the void ratio is decreased the pipe diameter, at which excess energy losses for homogeneous flow are less than for capsules, decreases, at a fixed velocity and SG.

In this case $(e = 0,5)$ the excess head loss for a solid of SG = 1,5 (coal, for example) is zero.

FIG. 18.5

COMPARISON OF EXCESS HEAD LOSSES CAPSULES WITH HOMOGENEOUS FLOW

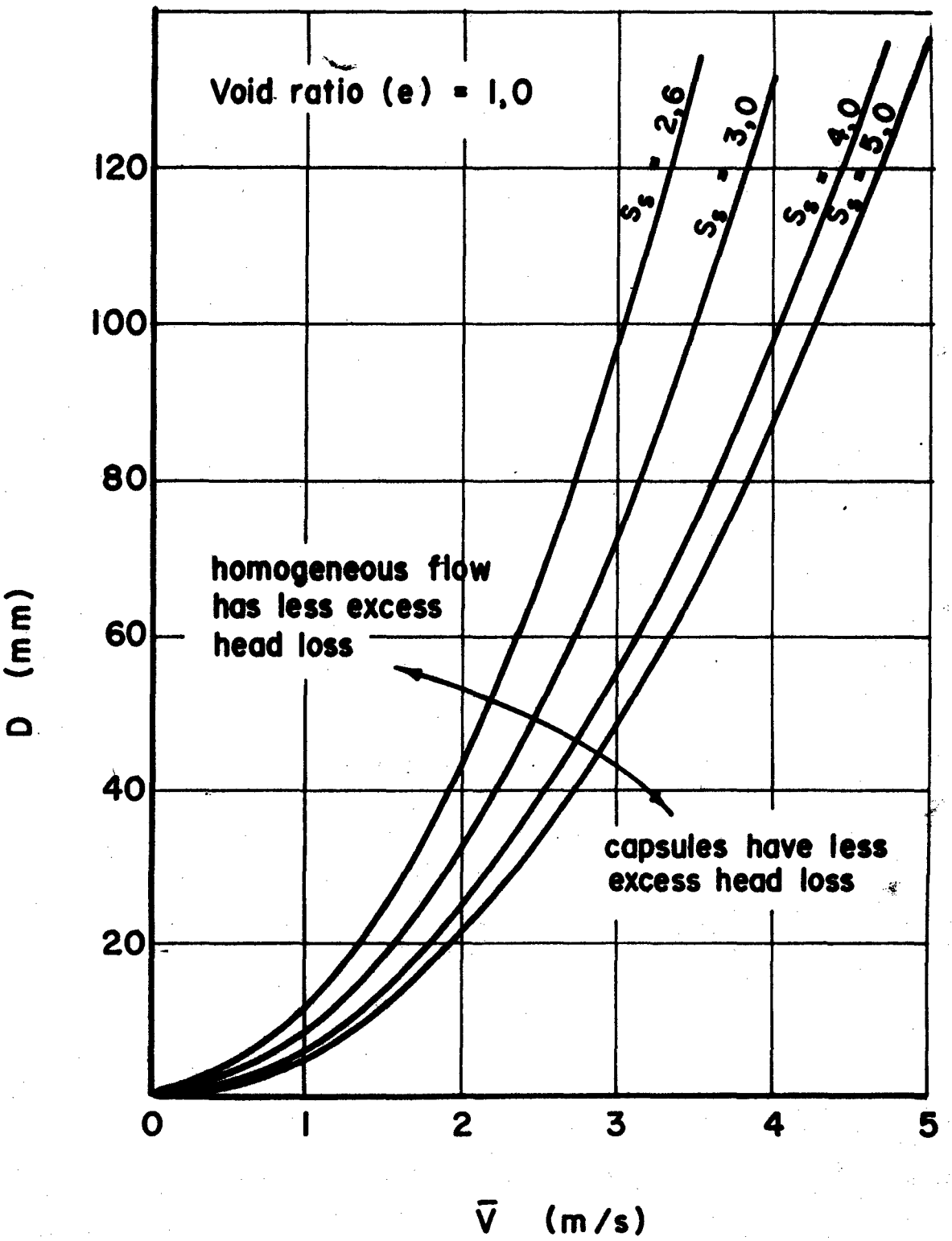

FIG. 18.6

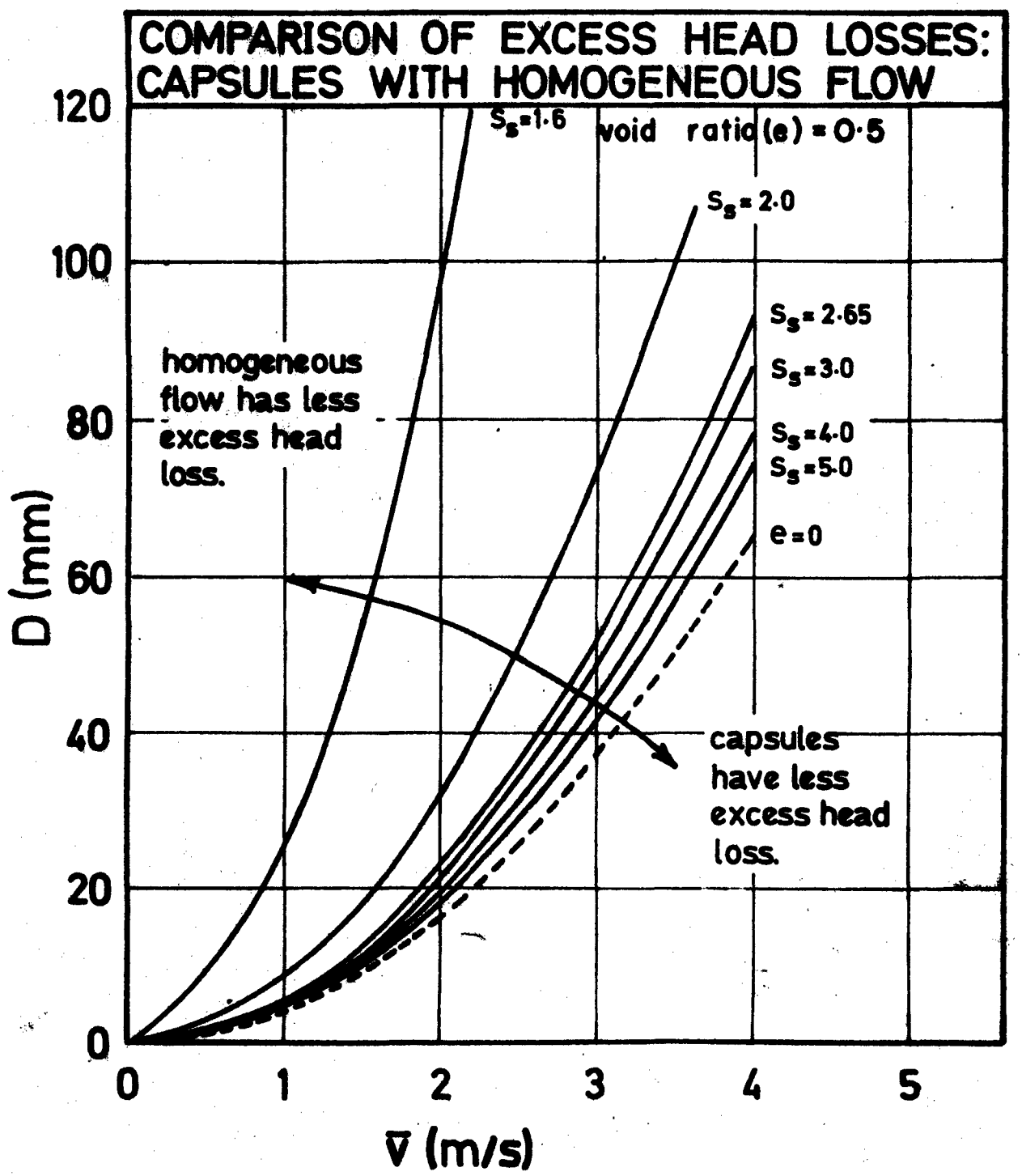
COMPARISON OF EXCESS HEAD LOSSES:
CAPSULES WITH HOMOGENEOUS FLOW
S_s=1·6
void ratio (e) = 0·5
S_s= 2·0
S_s= 2·65
S_s=3·0
S_s=4·0
S_s=5·0
e=0
homogeneous flow has less excess head loss.
capsules have less excess head loss.
D (mm)
$\bar{V}$ (m/s)
0
20
40
60
80
100
120
0
1
2
3
4
5

7. Comparison of capsule transportation with heterogeneous suspension

For capsules to have less excess head loss than flow in the heterogeneous regime then:

$$\phi_c < \phi$$

$$\therefore \frac{\bar{V}}{V_c} \frac{50f}{i_w} (S_s-1-e) < 85\left[\frac{gD(S_s-1)}{V_m^2} \frac{1}{\sqrt{C_D}}\right]^{1,5} \tag{18.23}$$

$$\therefore D > (25/85)^2 (\bar{V}^4/V_c^2)(C_D^{1,5}/g) \frac{(S_s-1-e)^2}{(S_s-1)^3} \tag{18.24}$$

Case III - no voids

Assume: (1) the "no-slip" condition for large diameter ratio capsules (say $d/D > 0,85$) i.e. $V_c = \bar{V}$, with little error, as discussed before

(2) for particle Reynolds numbers > 1000 and equivalent particle diameters $d_p > 2$ mm the drag coefficient for spherical particles is $C_D = 0,44$

(3) if the capsules are formed of the material to be transported then $S_s = S_c$ and $e = 0$.

Equation (18.24) becomes

$$D > \frac{0,00882\ \bar{V}^2\ C_D^{1,5}}{(S_c - 1)} \tag{18.25}$$

and

$$D > \frac{2,58\ \bar{V}^2\ 10^{-3}}{(S_c - 1)} \tag{18.26}$$

for $C_D = 0,44$

The inequality expressed by this equation is represented graphically on Figure 18.7. Above and to the left of the curves for different specific

FIG. 18.7

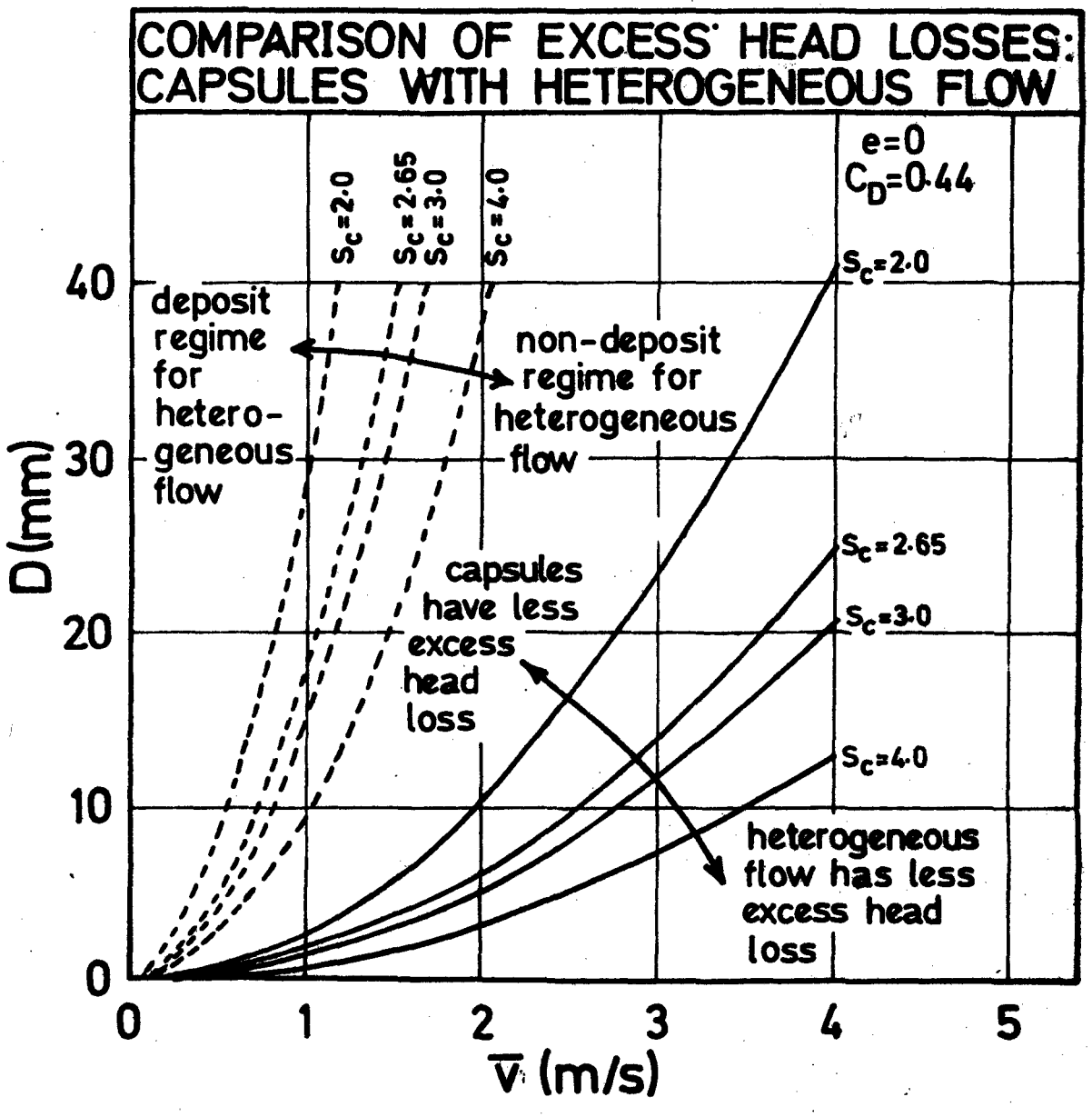
COMPARISON OF EXCESS HEAD LOSSES: CAPSULES WITH HETEROGENEOUS FLOW
e=0
C_D=0.44
S_c=2.0
S_c=2.65
S_c=3.0
S_c=4.0
deposit regime for hetero-geneous flow
non-deposit regime for heterogeneous flow
capsules have less excess head loss
heterogeneous flow has less excess head loss
D(mm)
$\bar{V}$ (m/s)
0
10
20
30
40
0
1
2
3
4
5

gravity capsules, the capsulesrequire less excess pressure head than the heterogeneous flow regime.

For a constant velocity the zone, for favourable capsule operation as regards excess head loss, occurs at decreasing pipe diameters as the solids specific gravity increases.

Also shown on Figure 18.7 are minimum deposit velocity curves which are obtained from $V_L = 1,34\sqrt{2gD(S_s-1)}$. These curves are the loci of points representing minimum excess head requirements in heterogeneous flow which coincide with the initiation of sediment deposit. Thus the most economical operating situation from the viewpoint of minimum excess energy requirements for the heterogeneous flow regime always occurs where the excess head losses are less for capsules than for heterogeneous flow.

The drag coefficient (C_D) for spherical particles is 0,44. However Bonnington (reference 4) gives $C_D = 0,9$ for irregular shaped particles of the type more likely to be transported in heterogeneous flow regimes. The effect of increasing C_D from 0,44 to 0,9 would be to increase the value of D required for less capsule excess pressure by $(0,9/0,44)^{1,5} = 2,92$. In no instance would the curves on the graph (Figure 18.7) reach the limit deposit curve considered by many authors to give the most economical transport velocity.

Case IV - voids present in the capsule

It is more likely that solids which would be transported as a heterogeneous flow suspension may actually be packed in capsules rather than formed into capsules.

Assume that, for such a situation, the voids ratio, e = 1,0. Equation 18.24 applies thus:

$$D > 2,58\ \bar{V}^2\ \frac{(S_s-2)^2}{(S_s-1)^3}\ 10^3$$

for $C_D = 0,44$

A fairly high value for C_D, for irregular particles, is $C_D = 0,9$ and:

$$D > 7,54\ \bar{V}^2\ \frac{(S_s-2)^2}{(S_s-1)^3}\ 10^3$$

Even for the reasonably high discharge coefficient chosen; $C_D = 0,9$, the curves, for minimum excess head losses for heterogeneous flow (shown dotted on Figure 18.8), are well into the region where capsules require less excess head loss.

Figure 18.9 is a similar curve at a lower void ratio and with this dense packing the capsule regime is still favourable. If $C_D = 0,44$ then the dividing curves yield even lower pipe diameters in which capsule transportation is favourable.

A coal filled capsule, of SG = 1,5 and void ratio $e = 0,5$ when packed, has the same density as water and thus acts as a neutrally buoyant capsule requiring zero excess energy. Iron ore with a specific gravity $S_s = 4,0$ to 5,0 is still more favourably transported in capsules than as a heterogeneous suspension.

Figure 18.10 shows $\phi = (i_m - i_w)/(C_v i_w)$ as a function of $V_m^2/gD(S_c-1)$ for capsules, heterogeneous flow and homogeneous flow. In the case of heterogeneous flow the drag coefficient (C_D) is assumed to be $C_D = 1,0$ in order to compare the equations graphically in this manner. The figure gives an idea as to what extent capsules require less excess head loss than heterogeneous or homogeneous suspensions as compared with previous figures which show regions of operation where capsule excess head losses are less than for homogeneous or heterogeneous flow.

It is clear from Figure 18.10 that capsules, containing material with a void ratio, have much lower values of ϕ_c than sintered capsules, formed of the material to be transported. However, more capsules are required

FIG. 18.8

COMPARISON OF EXCESS HEAD LOSSES CAPSULES WITH HETEROGENEOUS FLOW

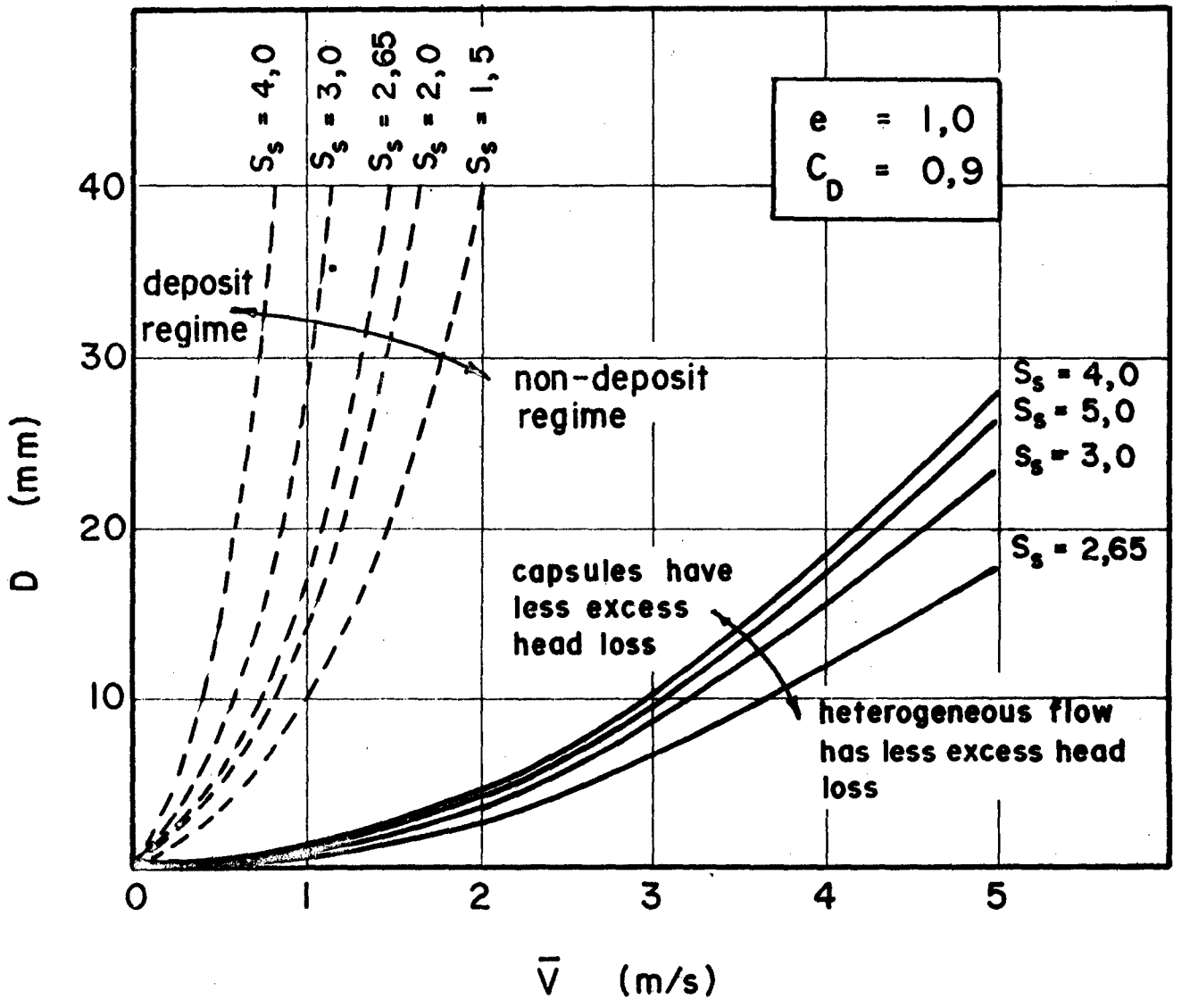

FIG. 18.9

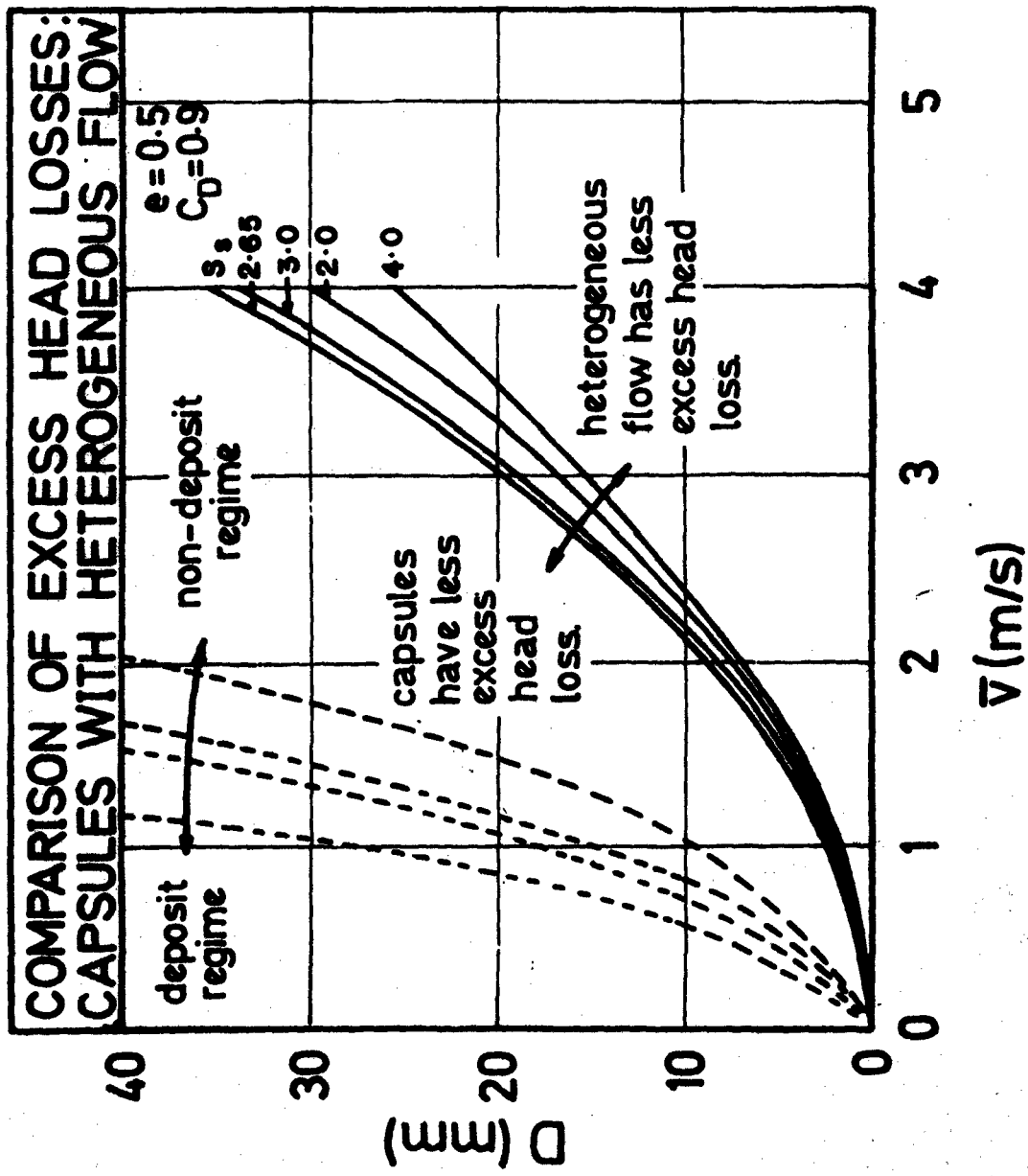
COMPARISON OF EXCESS HEAD LOSSES: CAPSULES WITH HETEROGENEOUS FLOW
e = 0.5
C_D = 0.9
s = 2·65
3·0
2·0
4·0
deposit regime
non-deposit regime
capsules have less excess head loss.
heterogeneous flow has less excess head loss.
D (mm)
40
30
20
10
0
0
1
2
3
4
5
$\bar{v}$ (m/s)

FIG. 18.10

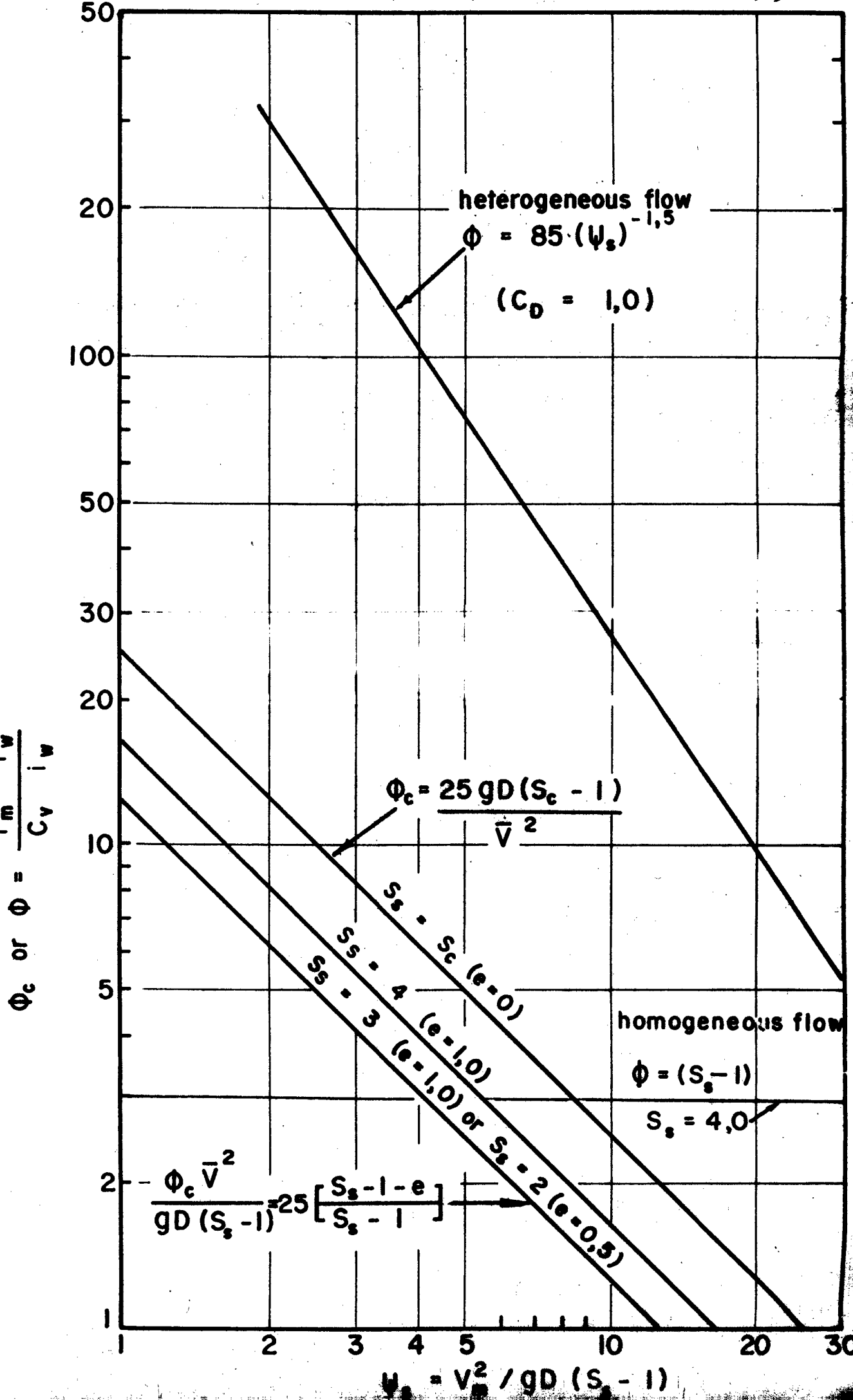
heterogeneous flow
$\Phi = 85\,(\psi_s)^{-1,5}$
$(C_D = 1,0)$
$\Phi_c = \frac{25\,gD\,(S_s - 1)}{\bar{V}^2}$
$S_s = S_c$ $(e=0)$
$S_s = 4$ $(e=1,0)$
$S_s = 3$ $(e=1,0)$ or $S_s = 2$ $(e=0,5)$
homogeneous flow
$\Phi = (S_s - 1)$
$S_s = 4,0$
$\frac{\Phi_c \bar{V}^2}{gD\,(S_s - 1)} = 25\left[\frac{S_s - 1 - e}{S_s - 1}\right]$
Φ_c or $\Phi = \frac{i_m - i_w}{C_v\, i_w}$
$\psi_s = V_m^2 / gD\,(S_s - 1)$
50
20
100
50
30
20
10
5
2
1
1
2
3
4
5
10
20
30

for the same volumetric concentration of solids.

8. Comparison of capsule transportation with non-Newtonian flow

It is difficult to generalise the comparison in this case since the rheogram varies for different materials in suspension and for different concentrations. However in the example given below, capsule transportation is compared with heterogeneous, homogeneous and non-Newtonian flow.

For a rough comparison, of excess energy requirements for non-Newtonian flow, with capsules, equation (18.22) (for homogeneous flow) is a fair approximation. The applicability of this equation increases as the flow behaviour index (n') approaches unity. And in this case i_m for homogeneous flow approaches the value for non-Newtonian flow (particularly as $K' \rightarrow \mu$).

There is no doubt that homogeneous non-Newtonian flow is a most economical method of hydraulic transportation.

Zandi (reference 68), Stepanoff (reference 64) and others have shown that homogeneous flow with very fine sediments may exhibit energy gradient suppressing action. However, Stepanoff, for example, considers the head loss in units of mixture.

9. An example of a numerical comparison of hydraulic transportation of iron ore encapsulated and in suspension

A scheme is envisaged for transporting iron ore from Sishen to Saldanha Bay in the Cape Province.

It is required to transport 10 million metric tonnes per annum of iron ore of specific gravity 4,0 a distance of 600 km in a horizontal pipeline. Assume 100% load factor.

The actual pipe from Sishen to Saldanha Bay would not be horizontal but would have an average fall of about 1 in 700 which reduces the power requirements for capsule transportation very slightly as compared with

the various forms of sediment transport.

In order to carry out a feasibility study different schemes were considered.

The following assumptions were made: Pipe diameter D = 300 mm.

This diameter was chosen fairly arbitrarily. The pipe was assumed to be hydraulically smooth.

The equations given in Sections 2 and 3 were used for evaluating the total power per unit length ($w\, i_m\, Q_m$) in the heterogeneous, pseudo homogeneous and non-Newtonian regimes, and the equations given in Chapters 16 and 17 were used for capsule transportation.

The rheological properties of iron ore, in a non-Newtonian suspension, as determined by means of a capillary tube viscometer 2,89 mm diameter and 155,4 mm long are given on Figure 18.11 (Linford and Saunders (reference 35)).

A sieve analysis of the iron ore yields;

screen opening (mm)	cum. % passing
0,211	99,9
0,152	99,4
0,104	98,0
0,076	92,4
0,053	73,7

The rheograms at the desired concentrations were interpolated.

Figure 18.12 shows the approximate power required per unit length of pipeline as a function of mean water velocity for a fixed pipe diameter (D = 300 mm), solids mass flow delivery rate (θ = 300 kg/s) and specific

FIGURE 18.11

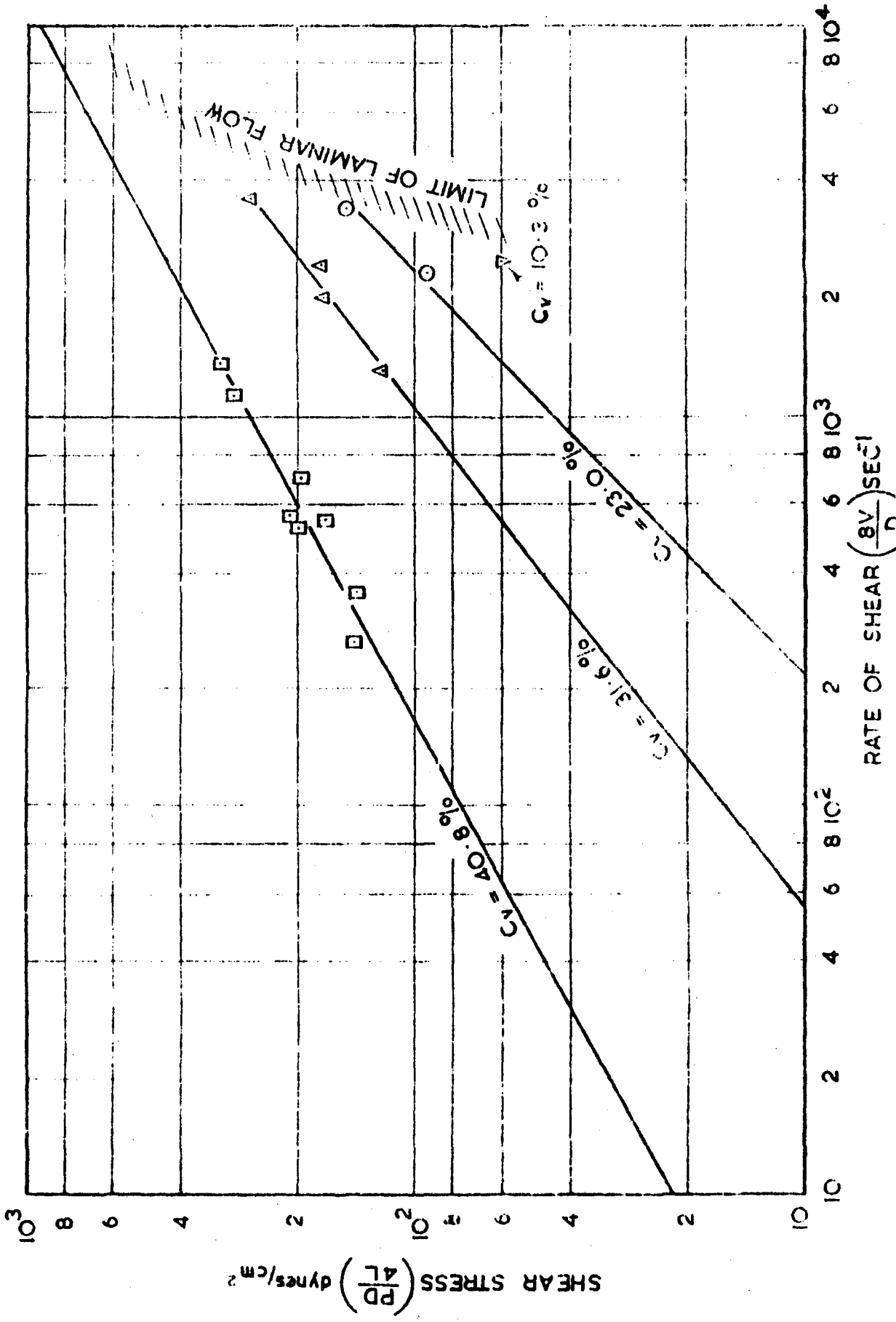
LIMIT OF LAMINAR FLOW
C_v = 10·3 %
C_v = 23·0 %
C_v = 31·6 %
C_v = 40·8 %
SHEAR STRESS $\left(\frac{PD}{4L}\right)$ dynes/cm²
RATE OF SHEAR $\left(\frac{8V}{D}\right)$ SEC⁻¹
10³ 8 6 4 2 10² 8 6 4 2 10
10 2 4 6 8 10² 2 4 6 8 10³ 2 4 6 8 10⁴

FIG. 18.12

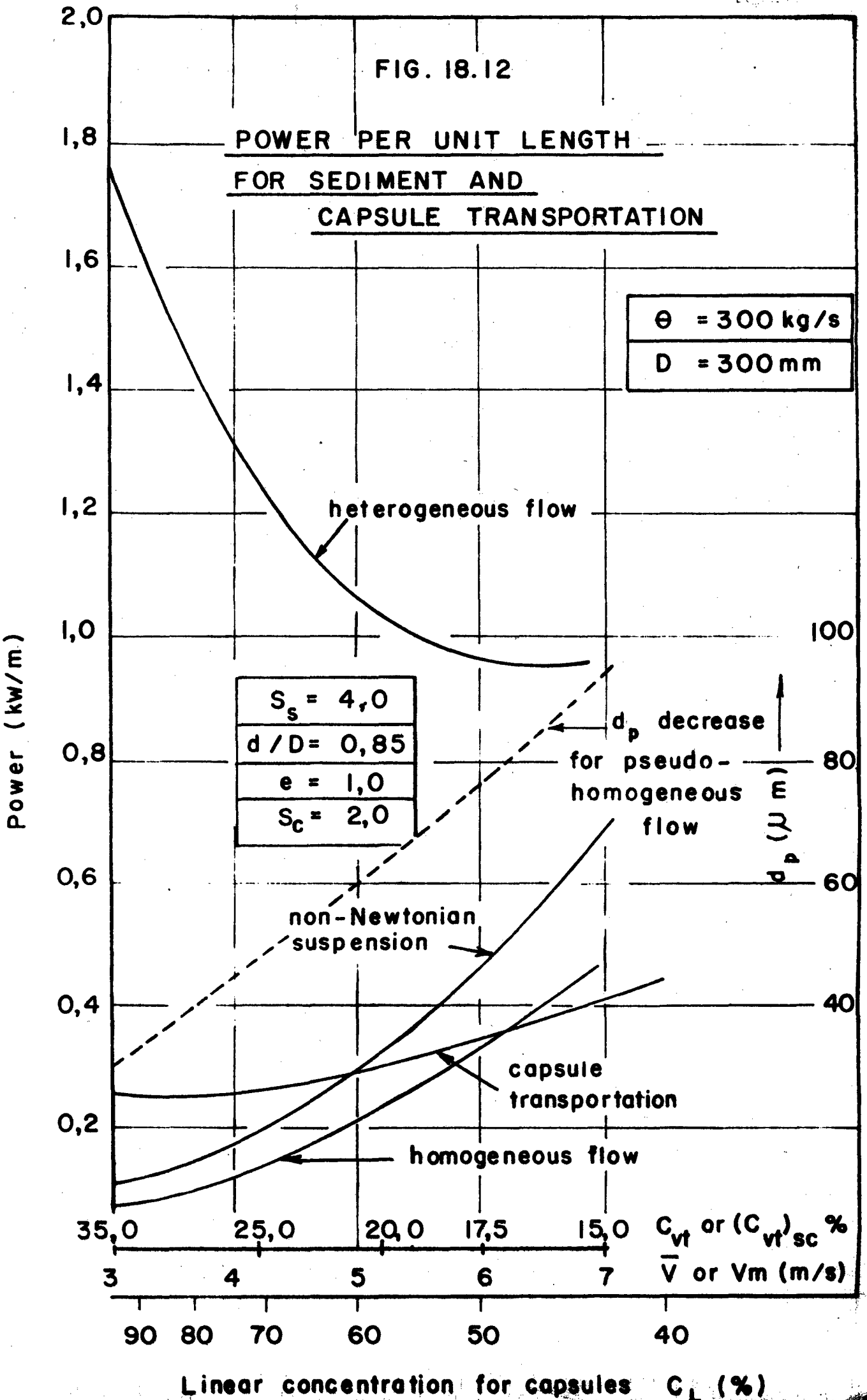
POWER PER UNIT LENGTH
FOR SEDIMENT AND
CAPSULE TRANSPORTATION
θ = 300 kg/s
D = 300 mm
heterogeneous flow
S_s = 4,0
d / D = 0,85
e = 1,0
S_c = 2,0
d_p decrease
for pseudo-
homogeneous
flow
non-Newtonian
suspension
capsule
transportation
homogeneous flow
Power (kW/m)
$\frac{\bar{E}}{d_p}$ (Ω)
2,0
1,8
1,6
1,4
1,2
1,0
0,8
0,6
0,4
0,2
100
80
60
40
35,0
25,0
20,0
17,5
15,0
C_{vt} or $(C_{vt})_{sc}$ %
3
4
5
6
7
$\bar{V}$ or Vm (m/s)
90
80
70
60
50
40
Linear concentration for capsules C_L (%)

gravity of solids ($S_s = 4{,}0$). The way in which the concentrations, (C_{vt}) or $(C_{vt})_{sc}$ and (C_L) vary with velocity is also indicated on the diagram.

A complete economic study, for a fixed solids delivery rate, would involve diagrams similar to Figure 18.12 in conjunction with diagrams showing capital cost of the pipelines (such as Figure 17.7).

For the homogeneous and heterogeneous regimes, particle size decreases with decreasing mean velocity (in Figure 18.12) in order to maintain the particles in suspension.

At the lower end of the velocity scale it is unlikely that pseudo homogeneous flow can occur. It is more probable that the rheology will yield a non-Newtonian suspension.

For example, in the non-Newtonian regime $d_{80} = 56\mu m$ and below $V_m = 5$ m/s, $d_p < 60\mu m$ for the pseudo homogeneous flow.

The graph starts at V_m or $\overline{V} = 3$ m/s since it is very difficult to achieve solids volumetric concentration higher than about 20% to 30%.

The packing of material in capsules may be varied to yield any desired void ratio (in fact large particles with few fines were found to give higher void ratios than $e = 1$, even when fully packed).

A comparison of capsules with sediment transportation at equal volumetric concentrations for various void ratios is best carried out by means of diagrams such as those shown on Figures 18.5 and 18.8 (for homogeneous and heterogeneous flow).

When maintaining a constant volumetric concentration $((C_{vt})_{sc})$, increasing the void ratio means that a larger pipe is required for the same solid mass delivery rate. This results in decreasing power requirements for capsules as well as sediment transport. Consequently, the solids have to be ground even finer. Naturally in capsule transportation the

ore is packed almost as mined.

If concentrations are increased the velocity has to be increased to avoid deposit in heterogeneous flow, or to maintain pseudo homogeneous or non-Newtonian flow with the same size particles. In the case of non-Newtonian flow increasing the volumetric concentration results in different rheological properties (see Figure 18.11). The yield stress increases as does the flow behaviour index. Thus the consequence of increasing volumetric concentration results in increased power requirements for all systems, including capsules.

The void ratio (e) required to yield lower excess energy, for capsules, than conventional two phase flow, can be found from equation (18.22) for homogeneous flow and equation (18.24) for heterogeneous flow.

Concern in this Chapter has been solely with excess energy. Other factors such as pipe wear and contamination of the transported material also have to be considered.

There are many commodities which could not be transported by pipeline, other than in capsules.

C H A P T E R 1 9

CONCLUSIONS

Part I

1. The advantages and disadvantages of sediment transportation have been discussed and many of the difficulties inherent in this method of transportation can be overcome by encapsulation.

The problems of contamination, abrasion of the pipe, attrition of the solid load and the expense of grinding and dewatering can be avoided by transporting solids in capsule form.

There are, in turn, certain disadvantages to the system such as encapsulation costs and the relatively undeveloped state of the technology.

One other disadvantage in the design of a sediment system is that the equations available are purely empirical and tend to be somewhat unreliable since different experimenters have found different coefficients (for example, shape of particles is not really accounted for in any of the available equations).

The equations for design purposes and methods of optimisation presented in this thesis enable a capsule transportation system to be designed at least as reliably as a sediment system.

2. Certain aspects of the technology of capsule transportation have been investigated and workable methods of capsule injection, retrieval and pumping of capsule water mixtures have been proposed.

The pumps and injector were used in the experimental investigations and were found to operate satisfactorily. Various methods of encapsulating solids as well as alternative pipe layout systems were also discussed.

Part II

3. The experimental investigation resulted in the establishment of two systems designated the "closed" and "open" system depending on whether capsules travelled intermittently or continuously. The merits and disadvantages of both systems were discussed and after much trial and error measuring equipment, capable of detecting the transient phenomena involved, was incorporated.

The measuring devices were an electromagnetic flow meter and a differential pressure transducer both of which were associated with rapid response recorders and calibrated in situ. Phototransducers and a digital timer with associated relays as well as electromagnetic solid state proximity switches were used for measuring capsule velocity.

A differential transformer was utilised for measuring capsule to pipe wall clearance.

All the measuring instruments, although subject to "teething" troubles, eventually worked satisfactorily and the procedure for carrying out experiments as well as the ultimate errors involved have been dealt with.

Part III

4. The two phase flow of capsule water mixtures was shown to be an eleventh order problem in the fluid mechanics of closed conduit flow.

The flow in the annulus of a mobile capsule water system was assumed to have two components; a pressure and a Couette component.

The flow in an eccentric annulus was analysed by considering quasi concentric annular slices and sub-slices.

5. The excess head loss was defined as consisting of inlet, outlet and annular losses.

6. Laminar flow in the annulus of a mobile capsule system was analysed and the mean velocity in the annulus was found to consist of pressure and Couette components of velocity and shear stress.

Turbulent Couette flow between two parallel flat plates was examined and agreement with existing literature was obtained. Using the assumption of parallel walls in the quasi concentric annulus it was possible to analyse the Couette flow component in an eccentric annulus. A finite element method of analysis enabled shear stresses on capsule and pipe walls due to laminar and turbulent Couette flow to be calculated.

The relation between flow in the annulus due to the Couette component and capsule velocity, as a function of diameter ratio, was expressed as a third order polynomial.

7. The general case of the fluid mechanics of two phase capsule water flow was analysed by the finite element method assuming that the annular head loss could be attributed to pressure flow in the annulus and by the "gross" method assuming the pressure loss in the annulus to consist of two components arising from shear on the capsule and pipe walls

separately. The various forces acting on static and mobile capsules were discussed.

8. The form drag coefficient was shown to be far greater for a capsule in a pipe than in an infinite medium.

9. The skin friction on the capsule wall due to Couette flow is greater than on the pipe wall and increases around the perimeter in an eccentric annulus, reaching a maximum where the gap between capsule and pipe wall is smallest.

10. Couette flow becomes turbulent at decreasing angles around the perimeter as capsule velocity increases and the transition from laminar to turbulent flow occurs over a wider shear stress range as velocity increases.

The effect of eccentricity on shear stress distribution around the capsule, due to Couette flow, is considerable.

11. The average shear stress on the capsule, due to Couette flow, increases as eccentricity and capsule velocity increase and complete turbulence in the annulus occurs at lower eccentricities as capsule velocity decreases.

12. As diameter ratio decreases laminar Couette flow is maintained to a greater extent around the capsule perimeter. The average Couette shear stress on the capsule increases as diameter ratio is increased, tending towards an infinite asymptote as diameter ratio approaches unity. The average shear stress on the capsule due to Couette flow increases as pipe diameter is decreased, at a fixed diameter ratio.

13. The shear on the capsule due to pressure flow always imposes a forward drag.

The ratio shear force on the pipe to shear force on the capsule, due to pressure flow, decreases as diameter ratio increases and as eccentricity increases. The ratio is also greater for turbulent than laminar pressure flow.

There is a substantial circumferential variation of shear stress due to pressure flow with the largest shear occurring at the widest gap and the shear stress increases with the pressure flow component of velocity all the way round the circumference.

At unit eccentricity, the change from laminar to turbulent pressure flow occurs further around the circumference as velocity ($\overline{V}_{ap}$) decreases. A 55% velocity reduction causes a 30% increase in the amount of circumference in laminar flow.

14. The circumferential variation, of shear stress around the capsule due to pressure flow, increases substantially as eccentricity increases.

15. The shear force on the capsule due to pressure flow decreases slightly as eccentricity increases at a constant annular head loss.

16. There is a substantial increase in shear stress, due to pressure flow, at all points around the circumference as diameter ratio decreases. Also less of the annulus is in laminar flow as diameter ratio decreases.

17. The form drag on a capsule drops steadily with capsule

velocity tending to level off at high velocities and eventually increasing with further velocity increase. This effect is accentuated as capsule density decreases.

18. The average shear stress on the capsule, due to Couette and pressure flow, increases while the capsule is stationary but as soon as the capsule starts to move a reversal of shear stress on the capsule wall is initiated and the net shear stress on the capsule increases, with velocity, in a backward direction retarding capsule motion. If the capsule starts to lift, the Couette component of shear decreases due to eccentricity reduction and another reversal of shear stress is initiated at a higher velocity.

19. The net shear stress distribution around the capsule perimeter due to pressure and Couette components indicates that the local stress acts in a forward direction and is turbulent around most of the annulus. Nonetheless, the net average shear stress on the capsule acts backwards. The Couette component in the laminar region towards the bottom of the annulus completely dominates the pressure component.

20. Solid friction drag on the capsule decreases as capsule velocity is increased. This is due to an increasing lift force as the capsule velocity increases.

21. The form drag and solid friction drag are predominant at low capsule velocities and the skin friction drag becomes appreciable at high capsule velocities. The lighter the capsule of a fixed geometry, the sooner the solid friction drag

decreases to be replaced by skin friction drag, due to Couette flow, as the main retarding force.

22. The mechanisms of capsule lift were discussed and were hypothesised to be due to streamline curvature, end effects, secondary flow, the lubricating film effect and circulation.

23. Capsules were found to travel in different modes depending on capsule velocity and density; that is, in contact with the pipe bottom, completely suspended (nose up) or travelling nose up with the rear end in contact with the pipe bottom.

The interaction of forces on the capsule were discussed for each mode of travel.

Part IV

24. Inlet head losses for eccentrically orientated annuli of static capsules were formulated with a power law

$$\frac{\Delta h_i}{\bar{V}^2/2g} = 22\left[\frac{d}{D}\right]^6$$

No simple correlation was found for concentric inlets and a polynomial of degree four expresses the inlet head losses for concentric annuli (see equation (7.114)).

25. Outlet losses for static capsules were found to be less pronounced than at the inlet. The outlet losses were found to have a similar formulation to that derived from the conventional pipe formula. The outlet head loss for concentric capsules is 15% higher and for eccentric capsules

32% lower than the sudden expansion loss derived from the conventional pipe formula.

26. Annular head losses in static capsules can be determined using a pseudo hydraulic mean radius.

The method of finite elements in quasi concentric annuli yields excellent agreement with experiment in eccentric annuli and fair agreement with concentric annuli.

27. Capsules were found to accelerate to a steady state velocity within a surprisingly short distance depending on their density, diameter ratio and ultimate velocity. The lengths of pipelines used in the experiments were ample from this point of view.

28. The effect of increasing water velocity is to increase the capsule velocity in all cases (above incipience).

29. The capsule velocity ultimately reaches a constant fraction of the mean water velocity as the latter is increased. This occurs sooner for increasing diameter ratios and decreasing capsule density.

30. High density capsules generally travel slower than lighter ones.

31. Neutrally buoyant capsule velocities are always greater than the mean water velocity and the capsule velocity increases as diameter ratio decreases.

32. The effect of submerged specific gravity of capsules is more apparent as diameter ratio decreases. The capsule velocity of low diameter ratio capsules changes by a greater amount at a fixed water velocity as the SG varies, than the larger diameter ratios.

33. The kinematic correlation, to take into account a wide range of capsule densities, was achieved by plotting $\overline{V}/\sqrt{g\ D|S_c-1|}$ as a function of $V_c/\sqrt{g\ D|S_c-1|}$.

34. The capsule velocity can be expressed as a function of the mean water velocity thus:

$$V_c = m(\overline{V} - \overline{V}_i)$$

where $\overline{V}_i$ can be determined analytically making use of experimental coefficients and m can be determined from empirical equation (10.6).

As the diameter ratio decreases, all other variables remaining constant, the velocity ratio $(V_c/\overline{V})$ also decreases. However, the low diameter ratio capsules eventually reach a velocity in excess of the high diameter ratios at very high mean water velocities.

35. As length to diameter ratio decreases capsule velocity increases, at a fixed mean water velocity. This situation tends to reversal at high mean water velocities.

36. The effect, of varying the length to diameter ratio, diminishes as diameter ratio increases and is undetectable at very high diameter ratios.

37. The greater the slope of the pipeline the greater the difference in capsule velocity at a particular mean water velocity as the diameter ratio varies. There is a reversal of this trend at high mean water velocities and there is a tendency for small diameter ratio capsules to catch up with the larger diameter ratios as the mean water velocity increases. This reversal occurs at higher mean water velocities as slope increases. As diameter ratio increases the effect of slope is minimised.

38. Well balanced capsules do not travel concentrically in a vertical pipe and tend to nutate at incipience.

39. Rough capsules generally travel slightly faster than smooth capsules although the evidence is inconclusive.

40. Increasing the linear concentration of capsules in the pipe has a very slight effect on the capsule velocity at a fixed mean water velocity. However, there is a slight decrease in capsule velocity as linear concentration increases for sparsely spaced capsules ($C_L < 20\%$). The linear concentration has less effect on capsule velocity as the mean water velocity decreases.

For more closely spaced capsules ($C_L \sim 50\%$) the train of spaced capsules travels faster than a solitary capsule and even faster than a solitary capsule of the same equivalent length as the sum of lengths of the spaced capsules.

41. Dimensionally similar capsules travel faster in small diameter compared with large diameter pipes. The effect of

different pipe diameters can be absorbed by dividing $\bar{V}$ and V_c by $\sqrt{D}$.

42. The excess energy dissipated across a mobile capsule (ΔH_c) decreases as the mean water velocity increases.

For a constant diameter ratio the decrease is most noticeable at high capsule densities.

The excess energy dissipated (ΔH_c) increases as SG increases at a fixed velocity ($\bar{V}$) and the increase is more pronounced at lower velocities.

43. As diameter ratio decreases, the difference between excess energy losses for high and low specific gravity capsules, also decreases.

44. As diameter ratio increases, all other variables remaining constant, the excess energy loss (ΔH_c) also increases and this increase is greater for low than high velocities.

45. The device of plotting the ratio ($\Delta H_c/L_c$) as a function of $\bar{V}$ successfully absorbs variations in capsule length.

46. The total excess head loss across capsules in a sloping pipe $(\Delta H_c)'_s$ decreases with increasing velocities. And the rate of decrease with velocity increase diminishes as slope increases.

47. The increase of $(\Delta H_c)'_s$ as diameter ratio is increased at a fixed mean water velocity becomes more prominent as slope increases.

48. The effect of slope can be successfully correlated by subtracting the term $\left[\left[\frac{d}{D}\right]^2 L_c \ |S_c-1| \ \text{Sin}\ \phi\right]$ from $(\Delta H_c)'_s$.

49. The results of net excess head losses across capsules in vertical pipes was inconclusive due to the energy requirement for lifting the capsules being of the same order of magnitude as the total excess head loss.

50. The roughening of capsule and pipe wall surfaces has little effect on the excess head loss. If anything the experiment showed slightly greater values of ΔH_c for smooth capsules.

51. Linear concentration does not have a great effect on excess head loss across capsules. Although the trend is that at very high concentrations the excess head loss per capsule tends to decrease since inlet and outlet head losses are not fully developed before the preceding or succeeding capsule is encountered.

52. At increasingly high velocities capsules were found to lift off the pipe bottom. The nose lifts first and the capsules generally travel with a nose up orientation. The capsules eventually reach a position beyond which increasing the velocity does not result in any more lift. In general this velocity corresponds to the velocity when $V_c/\overline{V}$ = constant.

53. The capsule velocity for incipient lift increases as diameter ratio decreases below $^d/_D \approx 0,95$ and as diameter ratio increases above $^d/_D \approx 0,95$.

The minimum capsule velocity for incipient lift occurs at a diameter ratio of about 0,95 regardless of the capsule SG (for $L_c/d = 4,0$).

The capsule velocity for incipient lift increases as capsule density increases and the effect of capsule density is increasingly evident as $^{d}/D \rightarrow 0,95$.

54. The maximum clearance achieved by a capsule decreases as SG increases at a fixed diameter ratio.

If capsule density is held constant, the maximum clearance occurs at about $^{d}/D = 0,85$ (for $S_c = 1,1$) and increasing or decreasing the diameter ratio above or below this value results in less maximum clearance. As SG increases the diameter ratio, at which maximum lift occurs, increases above $\frac{d}{D} \approx 0.85$.

Part V

55. When analysing laminar flow in stationary eccentric annuli, quasi-concentric polar co-ordinates yielded results in good agreement with bi-polar co-ordinates particularly at high diameter ratios.

56. The highest Reynolds number in the stationary eccentric annulus for which flow is completely laminar is much lower than has been assumed by other investigators and this resolves certain hitherto unexplained discrepancies, in "laminar" flow, between experiment and analysis. It is likely that in the experiments of previous investigators the flow was not completely laminar.

57. The analysis of incipient capsule motion was found to agree well with experimental results.

58. As length to diameter ratio increases there is a large increase in the excess head loss at incipience particularly at high diameter ratios. The incipient velocity correspondingly increases as length to diameter ratio is increased and the effect is, in this case, accentuated as diameter ratio decreases.

59. The excess head loss at incipience is highly dependent on capsule density at high diameter ratio, but the dependence decreases as diameter ratio decreases. Absolute values of the incipient velocity are affected more by capsule density as diameter ratio decreases.

60. As pipeline slope increases the total excess head loss at incipience increases rapidly particularly at high diameter ratios and in terms of absolute values, the incipient velocity is more profoundly affected by slope as diameter ratio decreases.

61. All the results at incipience could be correlated by means of an equation of the form $\Gamma = K/\chi^q$ with virtually no scatter. This equation with K = 33 and q = 1,85 accommodated a wide range of variables, i.e. capsule density, length to diameter ratio, diameter ratio, pipeline slope and pipe diameter (D = 44 mm to D = 150 mm).

62. The excess head loss across a mobile capsule can be calculated from the capsule characteristics as well as the mean water velocity, capsule velocity and pipeline slope.

63. Small changes in the measured or calculated value of

capsule velocity have a large effect on the excess head loss across mobile capsules.

64. In most instances, agreement between analytical results using the finite element analysis and experimental results were well within the experimental scatter. The capsule velocity is semi-empirically derived from the mean water velocity and the variables that have to be injected into the computer for calculating ΔH_c as a function of mean water velocity are the capsule and pipeline characteristics as well as the coefficient of solid to solid friction.

65. Determining the capsule velocity, analytically, from an experimental value of excess head loss yields better agreement with experiment than when the excess head loss is determined.

66. In some instances the "gross" method of analysis, although simpler and less precise than the finite element analysis, yields results of comparable accuracy, although the finite element analysis is more generally applicable.

67. The individual components of excess head losses were discussed separately and this indicated reasons for the large effect on excess head loss of small variations in capsule velocity.

68. The finite element analysis, although yielding results in fairly good agreement with experiment, is complicated and requires a large computer for solution. This necessitated the establishment of an empirical correlation for design purposes.

69. The equation for correlating results from mobile capsule experiments for a wide range of capsule densities, diameter ratios, length to diameter ratios, pipeline slopes and pipe diameters is:

$$\Gamma = 25/\chi^2$$

or $$\Delta H_c = L_c \left(d/D\right)^2 |S_c - 1| \; 50f$$

Slope was accounted for by subtracting the term
$\lambda = \left(\frac{d}{D}\right)^2 L_c |S_c - 1| \sin \phi$ from $(\Delta H_c)'_s$.

70. Other methods of correlating excess head loss were tried but none proved to be as successful as the equation finally adopted.

71. The form of empirical equations, for correlating excess head loss across incipient and mobile capsules, was the same.

72. The form of the equation was justified by considering ratios of forces acting on the capsules.

Part VI

73. For a particular mass flow delivery rate the total power dissipated per unit length of pipeline decreases to a minimum value and then increases as velocity increases.

74. Less power is dissipated as diameter ratio increases, for the same capsule mass delivery rate.

75. Also as the bulk density of individual capsules is decreased, the power decreases. So that many sparsely packed

capsules are more economically transported (from the power dissipation view point) than fewer densely packed capsules. Conversely more capsules are required for the same load.

76. As slope increases the excess power dissipated also increases due to capsule velocity reduction. The rate of increase is more rapid at lower diameter ratios.

77. The maximum excess incipient power at incipience depends on the diameter ratio (d/D) and reaches a maximum value at a diameter ratio of $^{d}/_{D} \approx 0,7$ irrespective of the capsule density.

78. The excess power at incipience is related to the capsule density as a function of $|S_c-1|^{1,5}$.

79. As length to diameter ratio increases the excess power at incipience also increases and the effect is accentuated at lower diameter ratios.

80. As slope increases in a positive upward direction, capsules of a particular geometry and fixed linear concentration in the pipe need more excess power for start-up. The effect is increased at lower diameter ratios.

81. The incipient power is less than the running power.

82. A complete economical optimisation can only be carried out if all the costs involved are known. In this thesis only power requirements are optimised and an outline is given of other economic criteria involved.

83. The ψ-parameter is introduced representing the power requirement per unit length of pipeline divided by the capsule mass flow delivery rate.

84. The ψ parameter is minimised, for a particular capsule mass flow delivery rate, to yield a minimum ψ value at a particular capsule geometry. The minimum value is associated with a specific linear concentration.

85. The optimum value of the ψ-parameter indicates that as θ increases a wide range of capsule or pipe diameters (at a fixed diameter ratio) yield similar minimum ψ values. At lower values of θ, the ψ-parameter, when optimised, yields an optimum value which shows ψ_{min} increasing as d increases. But below the value of d for optimum ψ, although ψ again increases, the concentration also increases to such an extent that the situation is physically unviable. It is thus expedient to transport capsules in as small a diameter pipe (at a fixed diameter ratio) as possible, providing the linear concentration is not impracticable depending on the injection technique.

Typical design curves are presented in Chapter 17.

86. Capsule transportation is compared with homogeneous and heterogeneous suspended sediment flow which is classified into various regimes.

87. The zones in which excess energy dissipation for capsule transportation is less than for pseudo homogeneous and heterogeneous flow are indicated on graphs of pipe diameter versus mean water velocity.

88. For homogeneous flow, decreasing pipe diameter as well as increasing the mean mixture velocity enables the zone of favourable capsule transportation to be reached for capsules of zero void ratio.

89. As the void ratio of material in capsules is increased and the specific gravity of the solids to be transported is decreased, the velocity, at a fixed pipe diameter, for favourable capsule operation,compared with homogeneous flow, decreases.

90. For heterogeneous flow, capsules always have less excess head loss, in the zone where incipient deposit occurs (i.e. the minimum head loss zone for heterogeneous flow). As the void ratio is increased, capsule transportation becomes increasingly favourable as far as energy dissipation is concerned.

91. A particular scheme is considered for comparing the power requirements, of various two phase flow regimes, with capsule transportation. On a basis of equal volumetric concentration, for the same solids delivery rate, capsules require less power than heterogeneous flow and have comparable power requirements with pseudo homogeneous and non-Newtonian flow.

92. This thesis is an extensive investigation into the hydraulics of transporting solid capsules in pipelines.

The analysis, experimental investigations, empirical correlations and technology at laboratory scale is advanced to the extent of enabling a pilot scale scheme to be attempted with confidence.

APPENDIX I

The following curves were determined for clear water in the four pipelines used in the experiments.

The friction head loss (h_f) was obtained from open tube air over water manometers and the average flow velocity ($\overline{V}$) was determined from the Veriflux magnetic detector, supplemented by gravimetric measurement.

When plotted on the universal pipe friction versus Reynolds number graph the curves for the 44 mm and 74 mm diameter perspex pipes were found to lie slightly above the curve for smooth pipes. The asbestos cement pipe yielded a relative roughness (k/D) slightly above k/D = 0,00005 and the 150 mm diameter P.V.C. pipe had a relative roughness of about k/D = 0,0002.

FIG. AI.1

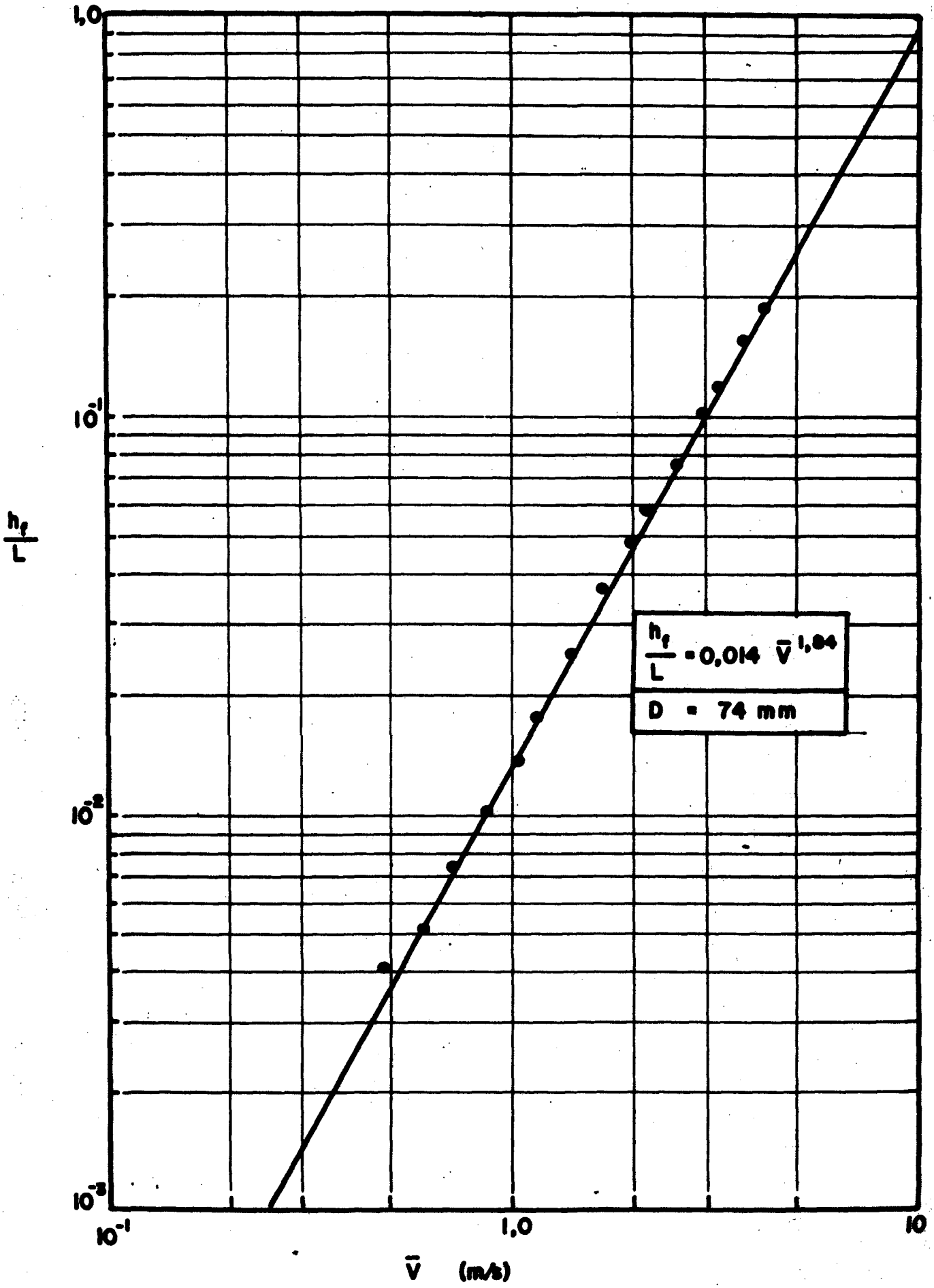
1,0
10^{-1}
10^{-2}
10^{-3}
$\frac{h_f}{L}$
$\frac{h_f}{L} = 0{,}014\ \bar{V}^{1{,}84}$
D = 74 mm
10^{-1}
1,0
10
$\bar{V}$ (m/s)

FIG. AI.2.

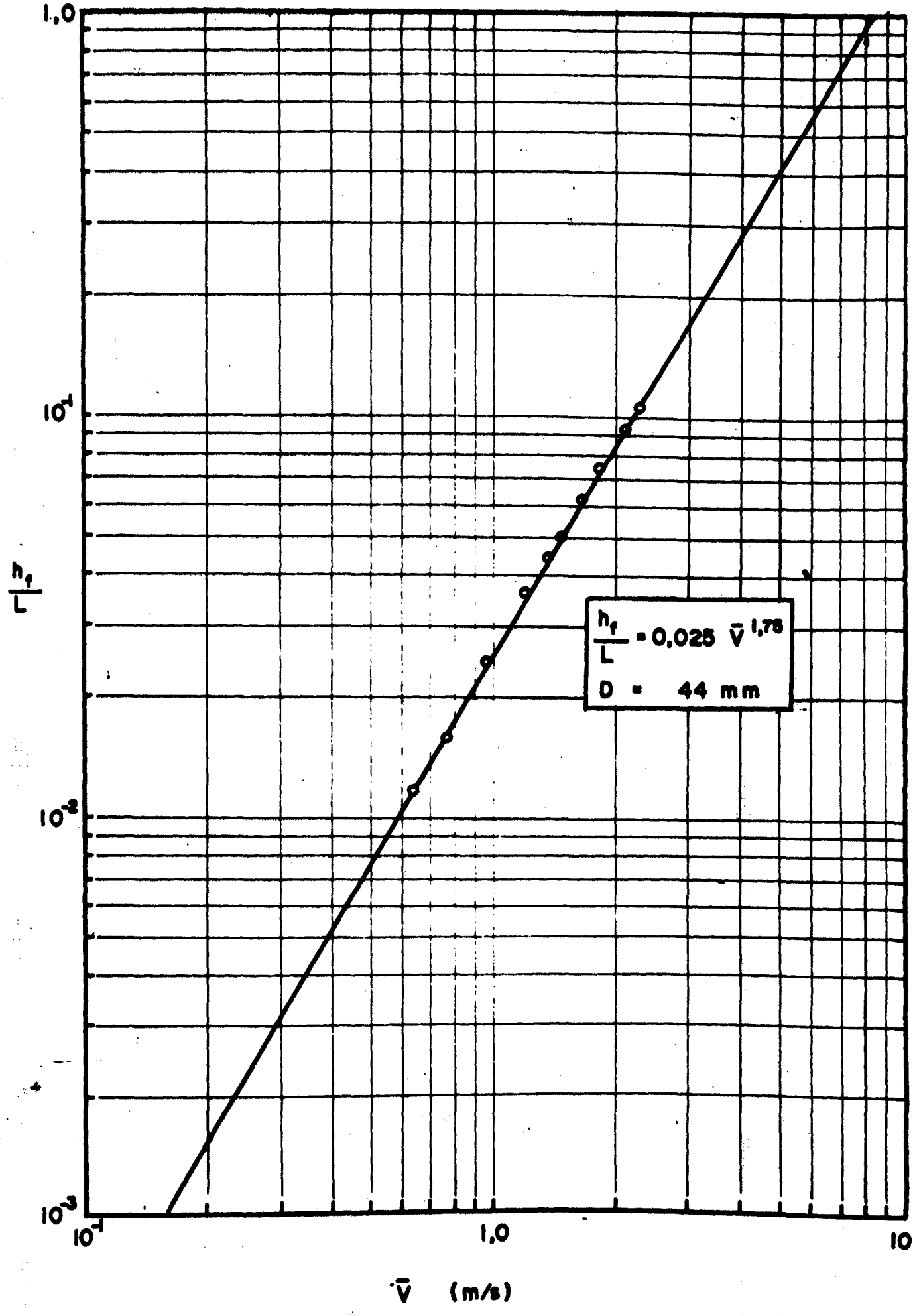
1,0
10^{-1}
10^{-2}
10^{-3}
$\frac{h_f}{L}$
$\frac{h_f}{L} = 0{,}025\ \bar{V}^{1,78}$
D = 44 mm
10^{-1}
1,0
10
$\bar{V}$ (m/s)

FIG. A I.3

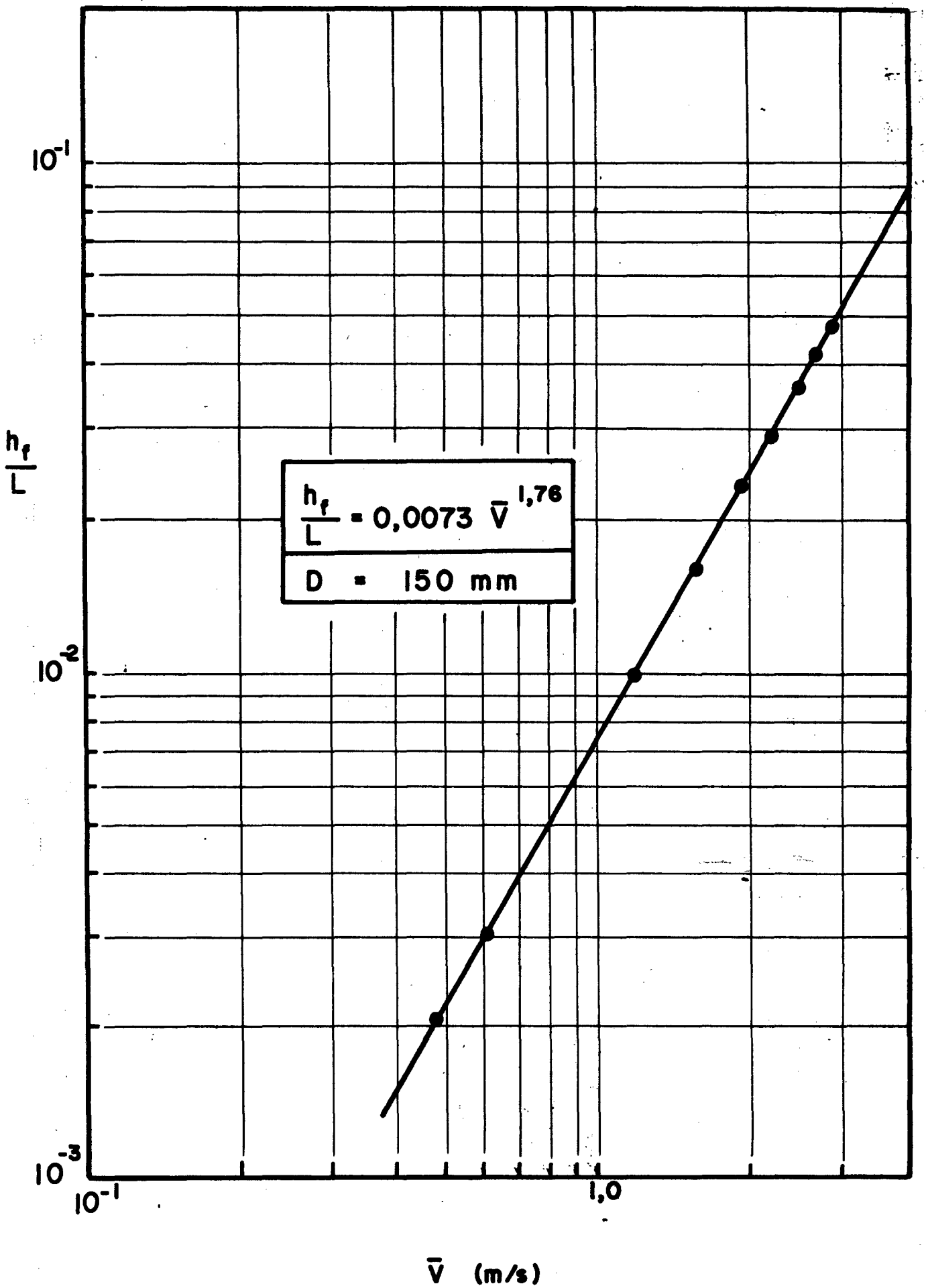
10^{-1}
10^{-2}
10^{-3}
$\frac{h_f}{L}$
$\frac{h_f}{L} = 0{,}0073\ \bar{V}^{1{,}76}$
D = 150 mm
10^{-1}
1,0
$\bar{V}$ (m/s)

FIG. AI.4

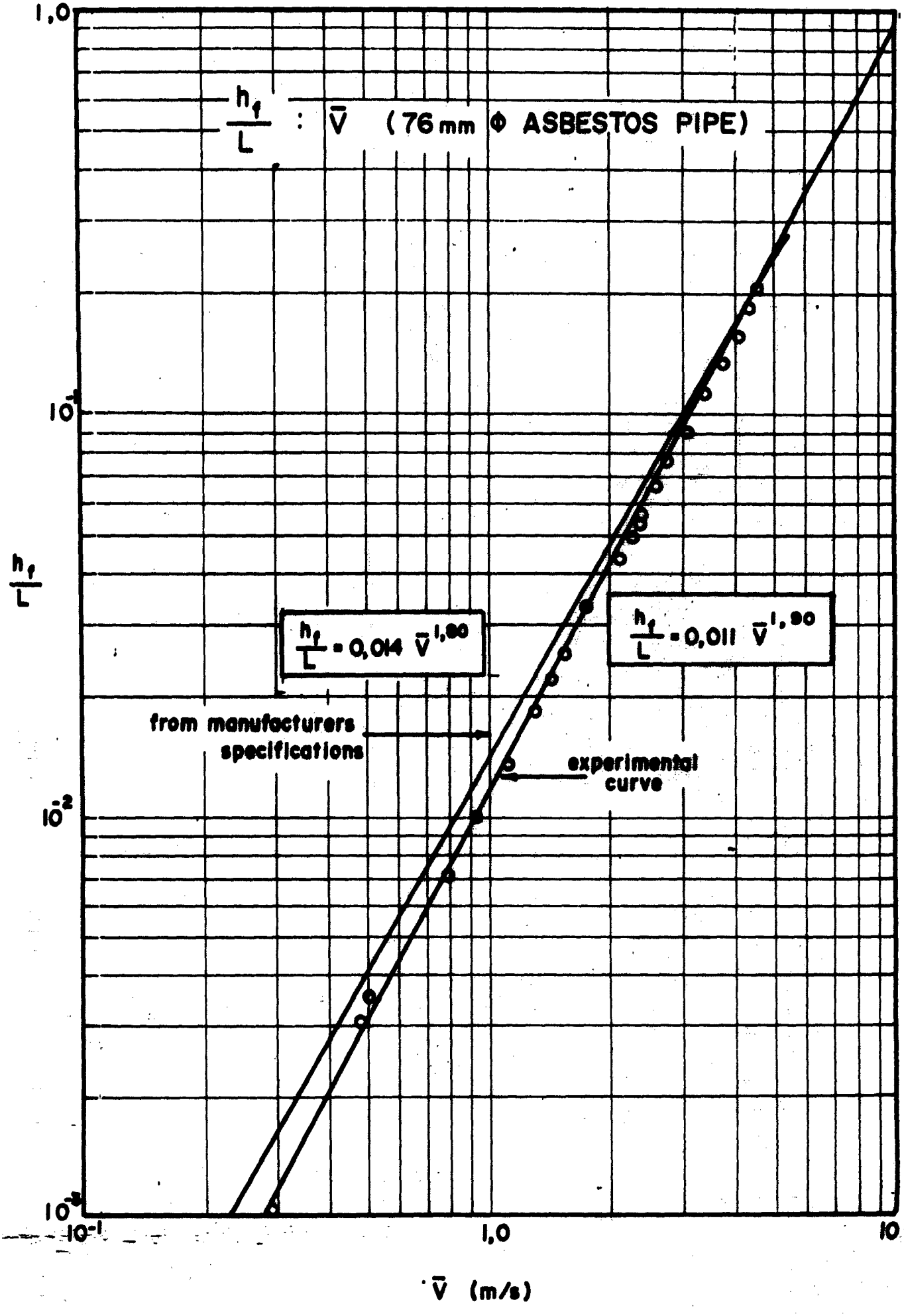
$\frac{h_f}{L}$: $\bar{V}$ (76 mm Φ ASBESTOS PIPE)
$\frac{h_f}{L} = 0{,}014\ \bar{V}^{1{,}80}$
$\frac{h_f}{L} = 0{,}011\ \bar{V}^{1{,}90}$
from manufacturers specifications
experimental curve
$\frac{h_f}{L}$
10^{-1}
10^{-2}
10^{-3}
1,0
10
$\bar{V}$ (m/s)

A P P E N D I X I I

SOME COMPUTER PROGRAMMES

During the course of this project many computer programmes were written both for the I.B.M. 1130 and Univac 1106.

In the initial stages of the investigation the programmes were directed towards the evaluation of data and determining correlating parameters. These programmes are not described herein since they are relatively straight forward. Three of the main programmes used for analysis are given, GROSS HEAD, MAIN 1 and OPTIMUM POWER. All the programmes are written in Fortran V language. The three programmes are listed and before each listing is a detailed description of the meaning of the most relevant statements.

The variable names are shown in capital letters enclosed in { } brackets.

GROSS HEAD is a programme for calculating the excess head loss across mobile capsules, using the "gross" method described in Chapters 7 and 15.

The programme calculates the head loss due to shear on the capsule wall as a function of V_r and the pipe wall as a function of $\overline{V}_{am}$. These values are added to the inlet and outlet head losses across mobile capsules.

A similar programme to this one (not listed) calculates the capsule velocity to yield the measured value of ΔH_c within a prescribed limit.

MAIN 1 is a programme using the finite element analysis for determining the excess head loss across mobile capsules as well as the components of force discussed in Chapter 8.

There are five subroutines; COUETTE determines the flow in the annulus due to the Couette component (V_c) and calls on subroutines GEOM and AREA for evaluating the geometry of the eccentric annulus and areas of slices and sub-slices. Subroutine PRESS calculates the pressure component of flow in the annulus and calls on internal subroutines GEOM and AREA as well as external subroutine FBAL which is the force balance calculation for determining the radius of maximum velocity in each quasi concentric slice of annulus.

The programme first calculates the incipient excess head loss and velocity using a Newton Raphson iteration and then calculates the mobile excess head loss calling the relevant subroutines when needed.

A brief description of the calculations is given at the end of Chapter 7 and a full description precedes the listing.

OPTIMUM POWER is used for evaluating the equations given in Chapter 17 and 18. The programme calculates the incipient power, the actual power (for a fixed linear concentration) and the minimum power for various capsule geometries and capsule mass flow delivery rates. A complete description precedes the listing.

Programme GROSS HEAD

This programme calculates the excess head loss across mobile capsules from the shear on capsule and pipe walls as functions of V_r and V_{am} respectively plus inlet and outlet losses.

Note: Fortran symbols shown thus - {CAPSL}.

14* Read capsule designation {CAPSL}, capsule diameter {DCAPS}, pipe diameter {DPIPE}, capsule length {LCAPS}, specific gravity {SG} and slope of pipeline {SLOPE}. Also included in this statement are some remnants from an old programme.

21* Read experimental excess head loss across mobile capsules at fixed $\overline{V}$ values {HCAP(I)}.

23* Read experimental capsule velocities {VCAP(I)}.

25* - 26* Carry out the entire calculation for each value of $\overline{V}$ from $\overline{V}$ = 0,5 m/s to 3,0 m/s.

28* - 30* Calculate the friction head loss per unit length of capsule free pipe, depending on the pipe diameter for which the experimental data is relevant.

33* {VAM} = mean velocity in the annulus of the mobile capsule ($\overline{V}_{am}$).

34* {RENA} = Reynolds number in the annulus based on ($\overline{V}_{am}$) using the pseudo-hydraulic mean radius concept.

35* Test for {RENA} < 2000.

36* - 37* Calculate the friction factor {FAW} and head loss in the annulus based on $\{\overline{V}_{am}\}$. The head loss {HA} is not used in the calculation.

38* {TOAD} = shear stress on pipe wall in vicinity of the capsule based on $\overline{V}_{am}$ and multiplied by the pipe diameter (D).

41* {VR} = velocity in the annulus relative to the capsule (V_r).

42* {RENC} = Reynolds number in the annulus based on (V_r).

43* Test for {RENC} < 2000.

44* {FAC} = friction factor in the annulus based on (V_r).

45* {TCD} = net shear stress on capsule wall based on (V_r) multiplied by the capsule diameter (d).

49* - 54* Calculation of inlet and outlet head loss $\Delta h_i + \Delta h_o$ = {HIHO}.

59* - 61* {HI} = inlet head loss (Δh_i) and {HO} = outlet head loss (Δh_o).

62* - 63* Head loss in annulus due to shear on pipe wall {SHEARP} and due to shear on capsule wall {SHEARC}.

64* {HC11} = excess head loss across mobile capsule.

70* Print out results of calculation.

73* Go back to beginning and read next card.

Note there are a number of remnants from old programmes which have unfortunately been left in. These have not been discussed.

Programme MAIN 1

This is the programme for calculations based in the finite element method using quasi concentric polar co-ordinates.

4* Read values of capsule designation {CAPSL} capsule diameter {DCAPS}, pipe diameter {DPIPE}, capsule length {LCAPS}, specific gravity of capsule {SG} and pipeline slope {SLOPE}.

7* Read 6 values of ΔH_c at $\bar{V}$ = 0,5 to 3,0 in 0,5 m/s increments ΔH_c = {HCAP(I)}.

9* Read 6 values of V_c at above values of $\bar{V}$, V_c = {VCAP(I)}.

15* Solid to solid friction factor (μ_f) μ_f = {UF}.

22* - 33* Establish constants for use in equation (7.133) for calculating incipient velocity $\bar{V}_i$ = {V}.

37* - 48* Solve equation (7.133) by Newton Raphson iteration to calculate incipient velocity.

49* - 51* Establish relations for head loss in open pipe from impirical equations.

52* - 56* Calculate excess head loss at incipience $(\Delta H_c)_i$ = {DHCI}.

57* - 61* Check $(\Delta H_c)_i$.

62* - 63* Calculate the area of pipe times the specific weight of water {APW} and the area of capsule times w{ACW}.

64* - 66* Calculate the volume {VOL}, mass {MASS} and submerged weight of capsule {WDASH}.

67* - 70* Calculate the friction drag at incipience {DFRICI}, the form drag at incipience {DFORMI} and the skin friction drag due to pressure flow at incipience {DSFPI} as well as the total drag {DTOTAL}.

71* - 80* Write values read and calculated on a new page.

81* - 82* Do calculations for 6 selected values of $\overline{V}$ {VBAR(I)} to end of programme, statement no. 411. Subscript (I) varies from 1 to 6 giving $\overline{V}$ values from 0,5 to 3,0 m/s in 0,5 m/s increments.

88* Initialise value of (m) for calculating (m) in finite element analysis, where $m = V_c / (\overline{V} - V_i)$; m = {MM}, to ensure experimental value of ΔH_c is maintained within 2,0 mm.

90* - 92* Establish clear pipe head loss laws for mobile capsule case.

98* {HCIM} = impirical value of ΔH_c.

99* Let ΔH_c be equal to the impirical value of ΔH_c, if experimental value not available.

100* Calculate capsule velocity {VC}.

102* Calculate the velocity in the annulus of the mobile capsule $\bar{V}_{am} = (\bar{V} - V_c(d/D)^2)/(1 - (d/D)^2)$. $\bar{V}_{am}$ = {VAM}.

106* Calculate the Couette component of the annular flow velocity from the empirical polynomial for $\bar{V}_{ac}$ as a function of (d/D). $\bar{V}_{ac}$ = {VAC}.

107* The pressure flow component in the annulus of a mobile capsule is $\bar{V}_{ap} = \bar{V}_{am} - \bar{V}_{ac}$. V_{ap} = {VAP}.

111* - 112* Test for negative value of $\bar{V}_{ap}$.

116* Test for laminar value of pressure flow velocity component.

117* - 118* Calculate the annular head loss due to pressure flow Δh_{fa} = {HFAP}.

119* - 121* Calculate inlet {HI} and outlet {HO} head losses for mobile capsule.

122* Calculate excess head loss across mobile capsule $\Delta H_c = \Delta h_{fa} + \Delta h_i + \Delta h_o - h_{fc}$ where (ΔH_c) calculated = {DELHC}.

123* - 127* Compare calculated and experimental value of ΔH_c. If this value is not within the prescribed limit adjust the value of m, i.e. {MM} and repeat calculation from statement no. 36.

131* Initialise JJJ as indicator of first round calculation.

132* - 133* Initialise eccentricity (ϵ) = {ECC} and GO TO statement 66 at 157*.

157* Establish the capsule velocity from the calculated value for insertion into the Couette flow subroutine.

161* Call subroutine Couette carrying over pipe diameter (D), capsule diameter (d), capsule length (L_c) and the eccentricity (ϵ) and returning with the gap between pipe and capsule at the lowest point {GAP}, the mean shear stress on the capsule wall due to Couette flow ($\bar{\tau}_{cc}$) = {TCC}, the mean shear stress at the pipe wall due to Couette flow ($\bar{\tau}_{pc}$) = {TPC} and the Couette forces on the pipe and capsule wall respectively.

163* Go to statement 1200 at 170*.

170* - 174* Calculate values for insertion into pressure flow subroutine.

178* Call subroutine PRESSure transferring values for the pipe and capsule radius, the calculated head loss in the annulus due to pressure flow, the eccentricity, and the coefficient of viscosity (μ). Return with the force on capsule due to pressure flow {SUMC}, the force on the pipe due to pressure flow {SUMP} and the velocity in the annulus due to pressure flow {VPRESS}.

179* - 182* Calculate inlet head loss {H1}, outlet head loss {H2} and excess head loss across mobile capsule DELHC1

187* - 189* Calculate the excess head loss across the capsule due to total shear on water at the pipe wall {XHCSP} from the shear at the pipe wall due to pressure flow ($\bar{\tau}_{pp}$) = {TPPAV} and the shear at the pipe wall due to Couette flow ($\bar{\tau}_{pc}$) = {TPCAV}.

190* - 193* Test the difference between the calculated value of (ΔH_c), or, in this case, the measured value, and the value calculated from total shear stress at the pipe wall. If the difference {HCDEL} is less than a prescribed value or positive, go to statement 63. If negative, go to 61.

197* - 198* Statement 61 reduces the eccentricity by a prescribed amount. Return to statement 66 and repeat the whole calculation until {HCDEL} is positive or less than a prescribed value.

199* Statement 63 calculates $\mu_f(1-L_r)$, i.e. {UFCL} for positive values of {HCDEL} and, incidentally, zero values.

203* The lift ratio (L_r) = {CL} is now calculated for positive values of {HCDEL}.

204* Shear stress on capsule due to pressure flow in annulus ($\bar{\tau}_{cp}$) = {TCPAV}.

205* - 210* Calculate the friction drag {DFRIC}, the form drag {DFORM}, the skin friction drag due to pressure flow {DSFP}, the skin friction drag due to Couette flow {DSFC} and the total drag {DTOT} on the capsule.

211* - 216* Calculate the various force ratios for use in Chapter 15.

217* - 221* Write the various calculated drag and force ratio values.

223* - 228* Write values of mean velocity in the annulus ($\bar{V}_{am}$) = {VAM}, mean velocity in the annulus due to Couette flow from impirical polynomial equation $\bar{V}_{ac}$ = {VAC} mean velocity in annulus due to Couette flow from finite element analysis ($\bar{V}_{ac}$) = {VCOUET}, eccentricity ϵ = {ECC}, gap, head loss due to shear at pipe wall {XHCSP} and the calculated values {UFCL}, {CL}, shear stress on capsule due to Couette flow ($\bar{\tau}_{cc}$) = {TCMEAN} and ($\bar{\tau}_{cp}$) = {TCPAV}.

233* Return to statement 1010 to write values of V_c, h_{fc}, Δh_{fa}, Δh_i, Δh_o, (ΔH_c) calculated, (ΔH_c) experimental, m, and Reynolds number in annulus due to pressure flow component. This first round is termed 'Couette m'.

143* - 144* If no value read for V_c then use empirical value and skip second round. Otherwise go to statement no. 42 for second round using experimental value of V_c.

152* - 153* Calculate values of $\bar{V}_{am}$ and $\bar{V}_{ac}$ as before.

154* Initialise eccentricity as before.

155* Set JJJ = 0 for second and subsequent round.

156* Set {VCAPSL} = VCAP(I), i.e. experimental value for

insertion into Couette flow subroutine.

161* - 242* Carry out calculation as before except {HCDEL} = {DELHC1} - {XHCSP} using calculated value of (ΔH_c), i.e. {DELHCI} from experimental V_c. This round is designated 'Experimental m'.

247* - 249* Set {MMM} = 1 as a marker for third round and calculate m = {M} from empirical equation. Return to statement no. 43 and repeat entire calculation.

234* Go to statement no. 41 for third round print out.

250* - 254* Print out values as before. This round designated 'empirical m'.

259* Go back to beginning and read the next card.

Subroutine COUETTE

Subroutine for calculating Couette flow in annulus.

19* {RP} = pipe radius.

20* {RC} = capsule radius.

21* {DR} = diameter ratio.

22* {P} = half distance between capsule and pipe centre.

23* Call subroutine GEOM for geometrical values in eccentric annulus.

27* Calculate average velocity in annular slice due to Couette flow, i.e. VAVC{L} where subscript L

denotes the slice under consideration and L varies from 1 to J where J is the total number of slices.

{CR(N,L)} = quasi concentric pipe radius at slice L and the first subscript N denotes pipe radius where N = J + 1. The two dimensional array is necessary for turbulent flow and will be used later when sub-slices are considered. The subscript N = J + 1 is used because there is one more boundary than sub-slice.

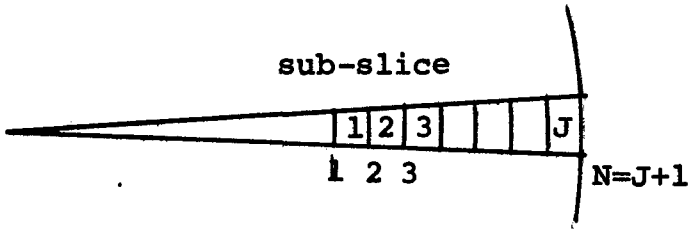

Slice

{CR(1,L)} = quasi concentric capsule radius at slice L.

29* {REC(L)} = Reynolds number at slice L for laminar Couette flow (R_{ec}).

30* If $R_{ec} > 2400$ go to statement no. 5.

31* If $R_{ec} < 2400$, JI = L. {JI} = {L} at the point where Couette flow becomes turbulent.

32* If the number of slices tested {L} is less than the total number of slices around the pipe semi-circle{J}, then return to statement no. 4 where L = L + 1.

33* Statement 5 can be reached from 30*, establishing JI as the criterion between laminar and turbulent

flow or from 32* if the entire Couette flow is laminar.

34* Call subroutine AREA.

38* - 40* Initialise {SUMQ}, i.e. total flow up to section considered; {SUMFC}, i.e. total shear force on capsule wall up to section considered and {SUMFP}, i.e. total shear force on pipe wall up to section considered.

41* Repeat calculations for each slice from 1 to J.

42* If turbulent flow exists in the slice go to statement no. 11.

43* - 55* Laminar flow calculation.

43* Calculate the velocity in slice (L) for laminar flow.

45* - 46* Calculate the flow in slice (L) and the total flow up to slice (L) in laminar flow.

47* - 48* Calculate the velocity gradient at the pipe and capsule wall $\left[\frac{du}{dr}\right]_p$ = {DUDRP} and $\left[\frac{du}{dr}\right]_c$ = {DUDRC} in laminar flow at slice (L).

49* - 50* Calculate the shear stress at pipe and capsule wall in Couette flow.

τ_{cc} = {TC} and τ_{pc} = {TP} in laminar flow at slice (L).

51* - 52* Calculate the total force on the capsule and pipe

wall up to slice (L).

53* - 54* Set b_p = {BP(L)} and b_c = {BC(L)} equal to zero in order to prevent carry over of these values from last calculation. These values are not required for laminar flow.

56* - 114* Turbulent flow calculation.

60* $A = \sqrt{\Delta S_p / \Delta S_c}$ from equation 7.171.
{SP(L)} = ΔS_p.
{SC(L)} = ΔS_c.
These are elemental lengths of perimeter around the capsule and pipe wall.

61* As a first trial in the Newton Raphson calculation for finding b_c where the local velocity equals half of the capsule velocity at slice (L) set b_{c1}, i.e. {BC(L)} equal to $b_{\ell/2}$, i.e. {B(L)/2}.

62* Set JJ = 0 as a counter for number of trials in Newton Raphson.

64* Solve equation 7.173 where $F(b_c)$ = {FBC}, i.e.
function $(b_c) = b_c^A + \left[\frac{V_c}{2\nu}\right]^{1-A} b_c - \left[\frac{V_c}{2\nu}\right]^{1-A} b_c = 0$.

65* Equation for $F'(b_c)$.

66* Correction term for $b_{c\ell}$.

67* Counter for Newton Raphson.

68* Logical IF statement to check if $b_{c\ell}$ is solved within a prescribed value.

70* If solution not satisfactory repeat calculation.

71* Calculate b_p at slice (L), i.e. {BP(L)}.

75* - 76* Calculate R'_{ecc} and R'_{ecp} and hence V_{*c} and V_{*p} for turbulent Couette flow.

79* - 84* Calculate shear stress on pipe and capsule wall due to turbulent Couette flow,

i.e. $\tau_{cc} = \rho\, u^2_{*c}$ = {TC}

$\tau_{pc} = \rho\, u^2_{*p}$ = {TP}

hence obtain the total force on the capsule and pipe wall due to turbulent Couette flow up to slice (L), i.e. {SUMFC} and {SUMFP} and the average shear stresses, i.e. {TCMEAN} = $\overline{\tau}_{cc}$ = average shear stress on capsule wall due to Couette flow, and {TPMEAN} = $\overline{\tau}_{pc}$ = average shear stress on pipe wall due to Couette flow.

85* {SUMQQ} = 0; initialise the flow in sub slices.

86* - 111* Calculate the flow in a slice by summing the flow in each sub slice.

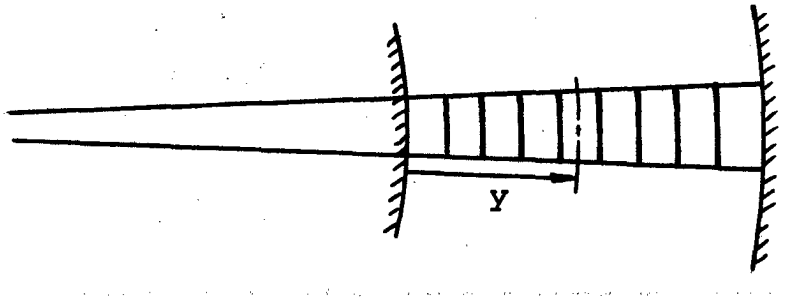

87* {y} = distance from capsule wall to the centre of a sub slice.

88* If y is greater than b_c the value is to be measured from the pipe wall rather than capsule wall.

89* Calculate y_c^+.

90* - 97* Calculate the local velocity in a quasi-concentric sub-slice (M) of slice (L) depending on whether the turbulent flow velocity distribution is in the laminar, transition or turbulent zone.

99* - 109* Calculate $b_{p\ell}$ and y, i.e. {YI} if $y > b_{c\ell}$. Hence calculate the local velocity in a sub slice (M) of slice (L) depending on the velocity distribution law applicable.

110* - 111* Calculate the total flow {SUMQQ} in a quasi concentric slice, by summing the flows in the relevant sub slices.

112* - 113* Calculate the total flow {SUMQ} in the annulus due to the Couette component, by summing the flows in the slices for turbulent and laminar conditions.

114* Calculate the average velocity per slice {V(L)},

115* The Reynolds number per slice {REC(L)},

116* The average velocity in the annulus due to Couette flow, and

117* The gap between the bottom of the capsule and the pipe {GAP}.

118* Return to the main programme.

Subroutine GEOMetry

This subroutine calculates geometrical values of the eccentric annulus as described in Chapter 7, Section 2.

8* Carry out the calculation for each slice (L) from 1 to J.

9* {A} = angle to middle of slice.

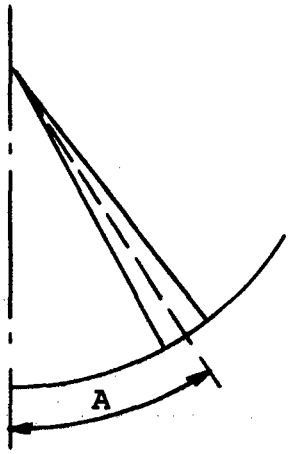

10* - 11* Calculate value of ϕ_c and θ_c see fig. 7.6 from trigonometry. {PHIC} = ϕ_c and {THETAC} = θ_c.

12* {CR(1,L)} = quasi concentric capsule radius at slice (L).

13* - 14* Calculate ϕ_p (i.e. {PHIP}) and θ_p (i.e. {THETAP}) from trigonometry.

15* - 16* {CR(N,L)} = quasi concentric pipe radius at slice (L) where N = J + 1 (i.e. one more boundary than sub-slice) and the number of sub slices is made equal to the number of slices.
B(L) = distance from pipe wall to capsule wall at slice (L) along a quasi concentric radius.

17* Carry out calculation for each sub slice

{CR(M,L)} = radius to sub slice (M) at slice (L) = $b(L) * \left[\frac{M-1}{J}\right] + CR(1,L)$

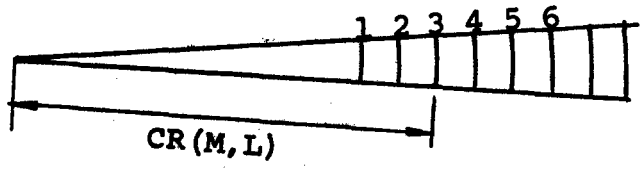

23* CRMID(M,L) = quasi concentric radius to the midpoint of a sub slice = $CR(1,L) + B(L) * \left[\frac{M-0.5}{J}\right]$.

25* - 29* Calculate $\theta(L)$, $\phi_c(L)$, $\theta_c(L)$, $\phi_p(L)$, i.e. the end values for each slice as opposed to the midpoint values calculated earlier.

30* - 35* Calculate the capsule and pipe arc lengths ΔS_c = {SC(L)} and ΔS_p = {SP(L)} .

37* Return to Couette subroutine.

Subroutine AREA

Subroutine for calculating areas and sub-areas.

-6* Repeat calculations for each slice.

7* If slice (L) greater than that in which laminar flow occurs go to statement no. 41 for calculating sub-areas. If only laminar flow occurs in a slice (L) then continue since sub-areas are not necessary

for laminar flow.

12* Calculate area of slice (L)

$$DELA(L) = \frac{\theta(L)-\theta(L-1)}{2} * (CR(N,L)^2 - CR(1,L)^2)$$

where N = J + 1.

17* Initialise sum of areas of sub slices.

21* For each slice (L) carry out the calculation for each sub-area (M,L).

23* Sub-area = $DELAA(M,L) = \frac{\theta(L)-\theta(L-1)}{2} * (CR(M,L)^2 - CR(M-1,L)^2)$.

27* Sum each sub-area.

29* Sum area of each slice.

30* Check total area of annulus (AREAA).

31* RETURN to Subroutine Couette.

Subroutine PRESS

Subroutine for pressure flow in the annulus.

10* {INDEX} = number of sub-slices per slice.

11* {J} = number of slices.

12* - 13* {KARD} = 8.
{I PRINT} = 5.
These are the relevant read and printout numbers for the Univac.

14* - 15* Calculate the centre to centre displacement between capsule and pipe DISPL = 2*P.

16* {PG} = pressure gradient from annular head loss due to pressure flow component.

20* - 23* Initialise {SUM} = total value of flow up to section under consideration, {FRICT} = total shear force on capsule and pipe wall due to pressure flow, {SUMP} = total shear force on pipe wall up to section under consideration and {SUMC} = total value of shear force on capsule wall up to section under consideration.

29* - 32* Calculate A and B values in velocity profile equations in transition zone.

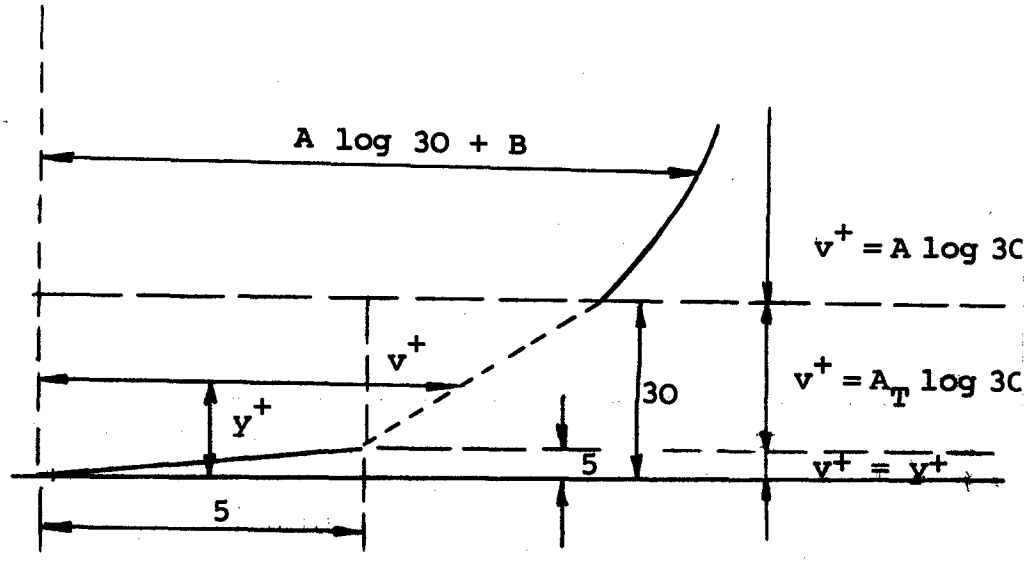

$$\frac{A \log 30 + B - 5}{\log 30 - \log 5} = \frac{v^+ - 5}{\log y^+ - \log 5}$$

$$\therefore v^+ = \frac{(A \log 30 + B - 5)}{\log 6} (\log y^+ - \log 5) + 5$$

$$= \left[\frac{A \log 30 + B - 5}{\log 6}\right] \log y^+ - \log 5 \left[\frac{A \log 30 + B - 5}{\log 6}\right] + 5$$

$$\therefore A_{Tp} = \frac{A \log 30 + B - 5}{\log 6}$$

$$B_{Tp} = 5 - \log 5 * A_T$$

A_{Tp} = {ATPIP} = A value for transition zone adjacent to pipe.

A_{Tc} = {ATCOR} = A value for core (or capsule) zone.

B_{Tp} = {BTPIP} = B value for transition zone adjacent to pipe.

B_{Tc} = {BTCOR} = B value for core (or capsule) zone.

A_{Tc} and B_{Tc} are calculated in a similar manner to A_{Tp} and B_{Tp}.

36* Test if concentric or eccentric.

40* - 47* Concentric laminar pressure flow.

41* - 42* Calculate average velocity in annulus for concentric laminar pressure flow and Reynolds number in the annulus.

43* Test for laminar or turbulent flow.

44* Calculate the flow for concentric laminar pressure flow.

45* - 46* Calculate shear on pipe wall (τ_{pp}) and capsule wall (τ_{cp}) due to laminar pressure flow.

51* - 66* Concentric turbulent pressure flow.
This calculation is carried out if {REP} > 2400.
{CR(1,1)} = {RC} = capsule radius.
{CR(INDEX + 1,1)} = {RP} = pipe radius.
DIFF 1 is used for calculating intermediate {CR} values. Subroutine FBAL (i.e. force balance) is called which works out the total flow (Q) in the annulus, the index {KRMAX} of maximum velocity, the pipe shear stress in turbulent pressure flow {TPP} and the capsule shear stress {TPC}. Also calculated are the total forces on the pipe and capsule walls, i.e. {SUMP} and {SUMC}.

70* - 98* Calculation for laminar pressure flow in the eccentric annulus. In this case there are J slices (instead of 1 as in the concentric case). The subroutine GEOM is called to calculate the geometry of the eccentric annulus.
The average velocity {VAVE} is calculated for each slice and the Reynolds number {REP} is calculated and tested for each slice to determine whether the flow is laminar or turbulent.

82* - 92* If laminar, the flow in each slice {Q}, as well as the pipe and capsule, shear stress values are calculated followed by the total flow up to the slice considered {SUM} and the shear force on pipe and capsule walls.

93* {LT} = {I} : The variable {I} in the DO loop is placed equal to {LT} at the slice where the flow changes from laminar to turbulent.

102* - 116* If turbulent pressure flow exists at all in the annulus, the following section of the calculation is carried out.

Subroutine AREA is called to work out the area of each sub slice. Subroutine FBAL is called; the flow (Q) calculated, and added to {SUM}. At the end of the iterations SUM is half of the total flow in the annulus.

118* - 127* The variables SUM, FRICT, SUMP and SUMC are multiplied by two to give the values for the whole annulus.

The average velocity due to pressure flow {VBAR}, the total Reynolds number {REP}, the conventional friction factor {F} and the multiple {FTREP} (i.e. $f \times R_e$) are calculated.

Finally, the return is made to the main programme.

Subroutine AREA

This is an internal subroutine and there are many more arguments than are specified in the argument list. They must appear in the main programme (which is in this case subroutine PRESS) under the same name.

136* Since subroutine AREA is internal the same symbols, if inadvertently used in the main programme, could cause confusion. The variables specified in a REAL statement have been allocated a unique word memory in core by the computer.

140* {DIFF} = radial distance between each sub slice.

145* Calculate area of sub slice no. 1.

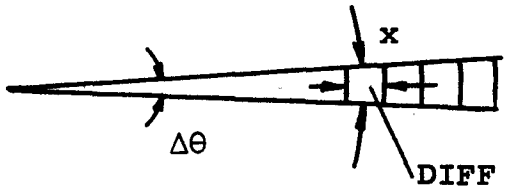

$\Delta a = x * DIFF$

$x = TETA*(CR(1,L)+0.5*DIFF)$

$\Delta\theta = \{TETA\}$

146* Calculate area of slice (L).

147* If turbulent go to 151* or if laminar go to 154*.

151* {INCR1) = constant increment in area,

i.e. DELAA(2,L) - DELAA(1,L) = DELAA(3,L) - DELAA(2,L)

$= \Delta\theta*(CRMID(3,L) * DIFF - CRMID(2,L) * DIFF)$

$= \Delta\theta*DIFF\ (CRMID(3,L) - CRMID(2,L))$

$= \Delta\theta*DIFF*DIFF = \frac{\pi}{J}*DIFF*DIFF$

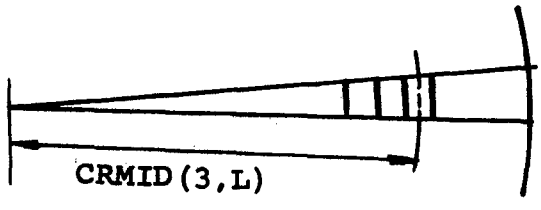

$INCR1 = \frac{\pi}{J} * DIFF * DIFF$

152* - 153* Calculate all sub-areas from K = 2 to INDEX.

155* RETURN to subroutine PRESSure.

Subroutine GEOMetry

This is an internal subroutine and precautions have to be taken as before.

168* - 172* If p is zero (i.e. concentric annulus) Control goes to statement 5 (169*) where CR(1,1) is set equal to the capsule radius {RC} and {CR(INDEX + 1,1)} is set equal to the pipe radius {RP}. Also {J} is set equal to 1.

174* If annulus is eccentric {INCR} (i.e. the angular increment per slice in radians) is calculated.

175* - 179* A = -0.5*INCR. The average angle turned through in radians at each slice is set so that the first time round it will be +0.5*INCR in the loop.
{TCL} and {TPL} are initialised at the same value for reasons which will be appreciated further on in the programme.
{CR} values calculated by trigonometry.
{B(L)} values calculated by trigonometry.

180* - 188* The following values are calculated from trigonometry:
{CR(1,L)}, CR(INDEX + 1,L), B(L), {DIFF} (radial distance between each sub slice and hence CRMID(1,L).

189* - 192* If INDEX > 1 there are many sub-areas present (i.e. eccentric case), then each {CR(M,L)} and {CRMID(M,L)} is calculated.

198* - 202* SC(L) and SP(L) are calculated from the product of the appropriate radius and change of {THETC} in radians since the last slice. {TCL} and {TPL} are now made equal to {THETC} and {THETP} and it is now evident why TCL and TPL were initialised earlier. If L < J return to statement no. 10 (178*).

203* - 205* J is compared with 1 to test whether the annulus is concentric. If so, SC(1) and SP(1) are redefined.

206* RETURN to subroutine PRESSure.

Note: The reason for departing from the conventional DO loop is the transfer into the loop at 173* (GO TO 6). This is not allowed in a 'DO' loop.

Subroutine FBAL

The purpose of this subroutine is to perform a force balance on a slice of annulus in pressure flow to find the radius of maximum velocity, the maximum velocity and the shear stress on pipe and capsule walls, returning to subroutine PRESSure with the total flow in the slice under consideration.

14* {DLAST} has been given a very large number to ensure that the force balance will not end after only one iteration.

15* {DIFF} = distance between each sub slice.

16* {INCR} = constant increment in area as discussed in internal subroutine AREA.

20* {RMAX} = radius of maximum velocity for laminar pressure flow (first approximation).

21* {KRMAX} = subscript for radius of maximum velocity, i.e. CRMID (KRMAX) = radius of maximum velocity. If there are 100 sub-areas per slice (INDEX = 100) and maximum velocity occurs at 55% of the distance between capsule and pipe wall (measured from capsule wall) then {KRMAX} = 55.

22* {AC} = annular area between capsule wall and radius of maximum velocity

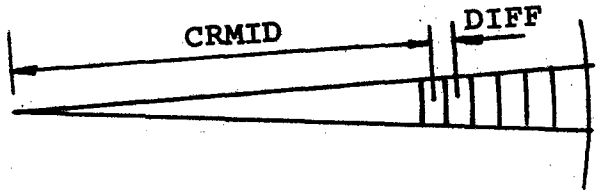

$$AC = \sum_{I=1}^{KRMAX} DELAA\ (I)$$

= DELAA(1) + DELAA(2) ..... DELAA (KRMAX)

= DELAA(1) + (DELAA(1) + INCR) + (DELAA(1) + 2*INCR)
+ ..... + (DELAA(1) + (KRMAX -1) * INCR)

= KRMAX * (DELAA(1) + 0.5* (KRMAX -1) * INCR)

Since INCR * (1 + 2 + 3 + ... + (KRMAX -1))

= 0.5 * KRMAX * (KRMAX -1) * INCR

Note that this is quicker than summing 50 or more values of DELAA.

23* {AP} = area in annulus from radius of maximum velocity to pipe wall = DELA - AC.

24* - 47* TPP, VASTP, TPC, VASTC, UC, YP, VPIPE and VCORE are calculated

{TPP}, {TPC} = shear stress on pipe and capsule wall respectively, for a slice.

{VASTP}, {VASTC} = shear velocity relative to pipe and capsule wall.

{YP}, {YC} = distances from pipe and capsule wall respectively.

{VPIPE}, {VCORE} = fluid velocities calculated from pipe and capsule (core) wall according to the law

$v^+ = A \log Y^+ + B.$

{DELTA} = discrepancy between velocities calculated from the capsule and pipe wall respectively. If VCORE < VPIPE then DELTA is positive and hence to statement no. 6 (39*) where KRMAX is incremented by 1. AC is then incremented by{DELAA (KRMAX)} and then at statement no. 7 a comparison is made to see whether DELTA is increasing or decreasing. If DELTA is smaller than the previous value {DLAST}, the approximation is improved and a further iteration is performed by going back to statement no. 9. First DELTA is preserved as DLAST for the following iteration. If DELTA is larger than DLAST (i.e. the previous value of DELTA) any further iterations will only make the analysis worse. In this case the sequence is continued at

64* - 86* Velocities are calculated for each zone.

87* - 88* The flows in each sub-area are summed to give the resultant flow in the slice.

89* Return to subroutine PRESSure.

Note that {CR} and {DELAA} have been given single dimensions in this subroutine although they can be two dimensional arrays elsewhere.
This is because when the subroutine is called, the slice is fixed.

Programme OPTIMUM POWER

Programme to calculate startup power and ψ_i, as well as power from empirical relations and minimum power for a given delivery rate.

7* READ {DELIV} = required delivery rate in kg/s.
{SG} = specific gravity of capsule.
{DRTIO} = diameter ratio (d/D).
{LRTIO} = length to diameter ratio $\left[\frac{L_c}{d}\right]$
{SLOPE} = slope of pipeline.

10* - 11* Insert DATA
{RHO} = density of conveying medium (ρ).
{MU} = dynamic viscosity (μ).
{NU} = kinematic viscosity (ν).
{PI} = π .

{UF} = coefficient of solid to solid static friction (μ_f).

{PERC 1} = one percent of delivery rate.

17* Calculate delivery rate in tons/an.

20* Initial value of capsule diameter {DCAPS}.

21* - 22* Iterations for trying different capsule diameters.

23* Store present value of capsule diameter {DCAP(I)}.

24* - 26* Calculate capsule length {LCAPS}, pipe diameter {DPIPE} and capsule mass {MASS}.

30* - 86* Calculate incipient velocity {V} and hence excess head loss at incipience {DHCI2}, startup power {POWI} and ψ_i {PSII}.

30* - 46* Calculate constants for solving equation 7.133 in order to calculate incipient velocity.

48* First trial for incipient velocity in Newton Raphson iteration.

49* - 50* Solve equation 17.15 given by the function {FX} and if the absolute value of FX is less than a prescribed value (e.g. FX < 0.001) GO TO statement no. 120 with the solution. If FX > 0.001 calculate the first differential of {FX} (i.e. {FDASHX}).

53* Set a limit for the number of iterations performed.

54* Adjust the value of incipient velocity by F(x)/F'(x).

59* Calculate pipe diameter (metres).

60* - 61* Calculate friction factor {F} in capsule free pipe from Blasius equation and hence calculate the friction head lost per unit length {HFL}.

62* - 65* Calculate $\left[\frac{4_T}{wD}\right]$, i.e. {T4WD}.

66* Calculate the excess head loss at incipience {DHCI}.

67* - 70* Calculate the Reynolds number for static capsule annulus {RES} using the pseudo hydraulic mean radius and hence the friction factor in the static capsule annulus and the annular head loss {DHAS}.

71* Check calculation of excess head loss at incipience {DHCI2} from $\Delta H_{ci} = \Delta h_{fa} + \Delta h_i + \Delta h_o - h_{fc}$.

72* DO loop to statement no. 3 for different {J} increments where J is the index for linear concentration.

78* Set linear concentration C_L as a constant times J {CL} = C_L.

79* {CV} = volumetric concentration = $C_L \left[\frac{d}{D}\right]^2$.

80* {SPACE} = centre to centre capsule spacing = L_c/C_L.

81* Store Jth {SPACE} value.

82* - 84* Calculate incipient power {POWI} and ψ_i value {PSII}.

87* {VC} = capsule velocity (V_c).

88* - 89* If $V_c > 5$ m/s or $V_c < 0.2$ m/s do not proceed.

95* {INJECT} = injection rate {I} in capsules/s.

96* - 97* {M} = m in empirical equation a function of d/D for calculating {VBAR} = $\bar{V}$ as a function of V_c and $\bar{V}_i$.

98* {F} = friction factor (f) from Blasius equation.

99* {HFL} = friction head loss per unit length of capsule free pipe.

100* {C} = constant to be used later.

101* {HCIM} = empirical value of excess energy loss across mobile capsule.

102* {PSI} = ψ - parameter.

103* Store ψ - parameter in array corresponding to appropriate capsule diameter {I} and centre to centre spacing {J}.

104* {POW} = power requirement for mobile capsule water system.

110* Calculate constant (α) {ALPHA} from equation 17.10.

112* - 114* Initialise values of {FACTR}, {SAVE} and {CHANGE} to be discussed later.

119* Initialise an arbitrary value for capsule spacing {SPACE}.

120* - 122* Calculate constants β {BETA}, γ {GAMMA} and δ {DELTA} from equations (17.11) to (17.13).

123* Commence iterative calculation. Set counter

{KONT} at zero to determine number of iterations for calculating the value of $\overline{V}$ from equation (17.15) to yield ψ min, i.e. $\overline{V}$ = {X} = {VMN}.

124* - 125* Arbitrarily initialise value of {X} = 5,0 and the differential of f(X) = 2,5.

126* Calculate f(X) from equation (17.15).

129* - 133* IF f(X) < a small value (0,001) then solution for ($\overline{V}$) is obtained, i.e. {VMN}= $\overline{V}$ value at ψ min. IF f(X) < 0, then add the increment f'(X) to X, if f(X) > 0, subtract the increment and if f(X) = 0, emerge with VMN.

134* Halve the value of f'(X).

135* - 137* If convergence is not reached within 100 iterations, then printout. Otherwise go to statement no. 53 and repeat the calculation.

139* Calculate the friction factor {F} from the Blasius equation for VMN.

140* - 149* Calculate the friction head loss in the capsule free pipe {HFL}, the excess head loss at {VMN} i.e. {HCMN} from the empirical equation, the power {POWMN} and the excess power {XPWMN}, the capsule velocity at ψ min i.e. {VCMN} and the value of ψ min {PSIMN}.

148* Calculate the delivery rate {DELVMN} corresponding to the above values of V_c and L_s.

149* - 155* If DELVMN corresponds to the required delivery rate (DELIV) within 1% (PERC1) go to statement no. 9. If not, go to statement 5 or 6 and adjust the factor (FACTR) by which the original value of (SPACE) (i.e. (SAVE)) must be multiplied. (FACTR) is adjusted by adding or subtracting (CHANGE).

151* The value of (CHANGE) is halved for each iteration.

153*, 156* and 157* If convergence is not reached within 100 iterations, then printout.

158* Calculate the required delivery rate in tons/an.

159* - 160* Calculate the injection rate INJECM and the linear concentration for ψ min, i.e. (CLMIN).

161* - 171* Printout and return statements.

172* - 182* Calculate the optimum ψ-value from the stored values of (PSI) and determine the capsule diameter and spacing to achieve this ψ-value.

183* Return to statement no. 4 and read the next card.

$HDS BELONGS TO J H LAZARUS DELHC FROM THEORY NO 40 GROSS HEAD

```
      C  ***************************************************************************
      C  CALCULATES DELHC FROM ACTUAL VC
      C  ***************************************************************************
         REAL LCAPS,LRTIO
         DIMENSION VBAR(6),        HCAP(6),VCAP(6)
         L=0
       4 CONTINUE
       5 WRITE(5,9)
       9 FORMAT(1H1)
       6 DO 41 K=1,3
         WRITE(5,10)
      10 FORMAT(///' CAPSL  DCAPS  DPIPE  LCAPS   SG     VI     FVI    DRTIO
        1  LRTIO  SL)PE')
         READ(8,15)CAPSL,DCAPS,DPIPE,LCAPS,SG,VI,FVI,DRTIC,LRTIC,SLOPE,L
      15 FORMAT(4F7.1,2F7.4,F7.5,2F7.3,F7.5,I1)
         WRITE(5,25)CAPSL,DCAPS,DPIPE,LCAPS,SG,VI,FVI,DRTIO,LRTIO,SLOPE
      25 FORMAT(4F7.1,2F7.3,F7.4,3F7.3)
         WRITE(5,30)
      30 FORMAT(/'    VBAR   VCAP    HCAP HCAPTH         HI          HO     SHEA
        1RP     SHEAR)          VR        VAM                              HA')
         READ(8,32)(HCAP(I),I=1,6)
      32 FORMAT(6F5.1)
         READ(8,33)(VCAP(I),I=1,6)
      33 FORMAT(6F5.3)
         DO 41 I=1,6
         VBAR(I)=0.5*I
         Y=VBAR(I)/SQRT(9.81*DPIPE/1000.0*ABS(SG-1.0))
         IF(DPIPE.GT.43.0.AND.DPIPE.LT.45.0) HFLD=0.025*VBAR(I)**1.75
         IF(DPIPE.GT.73.0.AND.DPIPE.LT.75.0) HFLD=0.014*VBAR(I)**1.84
         IF(DPIPE.GT.149.0.AND.DPIPE.LT.151.) HFLD=0.0073*VBAR(I)**1.76
         RAT=(DCAPS/DPIPE)**2.0*ABS(SG-1.0)
         DRAT=(DCAPS/DPIPE)**2
         VAM=(VBAR(I)-VCAP(I)*DRAT)/(1-DRAT)
         RENA=1.25*(DPIPE-DCAPS)*VAM*1000.0/0.96
         IF(ABS(RENA).LE.2000.0) GO TO 98
         FAW=0.079/(ABS(RENA))**0.25
         HA=FAW*LCAPS*(VAM**2.)*1000./(DPIPE-DCAPS)/6.14
         TOAD=(FAW*1.0000*DPIPE*VAM**2.0/2.5)
         GO TO 99
      98 TOAD=0.0
      99 VR=VAM-VCAP(I)
         RENC=1.25*(DPIPE-DCAPS)*VR *1000.0/0.96
         IF(ABS(RENC).LE.2000.0) GO TO 100
         FAC=0.079/(ABS(RENC))**0.25
         TCD=(FAC*1.0000*DCAPS*VR **2./2.5)
         TC1=(FAW*1.0000*DCAPS*VAM**2./2.5)
         GO TO 101
     100 TCD=0.
     101 A1=1-DRAT
         A4=22.0*(DCAPS/DPIPE)**6.0
         A5=1.0/A1-1.0
         A6=0.68*A5**2
         C2=(A4+A6)/19.6
         HIHO=C2*(VBAR(I)-VCAP(I))**2.0
         CL4DW=4.0*LCAPS/(DPIPE**2.-DCAPS**2.)/9.8
         SHEAR=(TOAD*VAM/VBAR(I)+TCD*(VAM-VCAP(I))/VBAR(I))*CL4DW
         HFC=HFLD*LCAPS/1000.0
         HC1=(SHEAR*HIHO -HFC)*1000.0
         VSQ2G=(VBAR(I)-VCAP(I))**2.0/19.6
         HI=A4*VSQ2G*1000.0
         HO=A6*VSQ2G*1000.0
         SHEARP=TOAD     *CL4DW*1000.0
         SHEARC=TCD              *CL4DW*1000.0
         HC11=SHEARP+SHEARC+HI+HO-HFC*1000.0
         SHEAR1=TC1*CL4DW*1000.
         HC12=SHEAR1+SHEARC+HI+HO-HFC*1000.0
         DIF=HCAP(I)-HC1
         DIFL=DIF/LRTIO
         DIFLD=DIFL/(DPIPE-DCAPS)
      41 WRITE(5,40)VBAR(I),VCAP(I),HCAP(I),HC11,HI,HO,SHEARP,SHEARC,VR,VAM
        1,SHEAR1,HC12,HA
      40 FORMAT(1X,F7.1,F7.3,2F7.1,10F10.3)
         GO TO 4
      90 CALL EXIT
         END
```

```
@FOR,IS LAZARUS.MAIN1,,MAIN1
FOR S310-04/12/72-13:09:11 (,0)

   MAIN PROGRAM

  1*            REAL LCAPS,MU,NU,M,MM,MMMP
  2*            DIMENSION VBAR(6),HCAP(6),VCAP(6),DEL(1000)
  3*          8 CONTINUE
  4*            READ(8,15)CAPSL,DCAPS,DPIPE,LCAPS,SG,SLOPE
  5*         15 FORMAT(4F7.1,2F7.4)
  6*            IF(CAPSL.LT.1.) GO TO 90
  7*            READ(8,32)(HCAP(I),I=1,6)
  8*         32 FORMAT(6F5.1)
  9*            READ(8,33)(VCAP(I),I=1,6)
 10*         33 FORMAT(6F5.3)
 11*            DATA RHO,MU,NU,PI,J/1000.0,0.0010,0.00000100,3.1416,100/
 12*      C-------------------------------------------------------------------
 13*      C  CALCULATE INCIPIENT VELOCITY AND INCIPIENT DELHC
 14*      C-------------------------------------------------------------------
 15*            UF=0.32
 16*            IF(DPIPE.GT.140.) UF=0.38
 17*            HYPOT=SQRT(SLOPE**2.0+10000.0)
 18*            SINPH=SLOPE/HYPOT
 19*            COSPH=100.0/HYPOT
 20*            RAT=(DCAPS/DPIPE)**2.0*ABS(SG-1.0)
 21*            DRAT=(DCAPS/DPIPE)**2
 22*            A1=1-DRAT
 23*            A2=A1**1.75
 24*            A3=((DPIPE-DCAPS)/1000.0)**1.25
 25*            B=DCAPS/DPIPE
 26*            C1=0.239*(LCAPS/1000.0)*B*NU**0.25/A3/A2/19.6
 27*            A4=22.0*(DCAPS/DPIPE)**6.0
 28*            A5=(1.0/A1)-1.0
 29*            A6=0.68*A5**2.0
 30*            C2=(A4+A6)/19.6
 31*            C8=UF*B**2.0*ABS(SG-1.0)*LCAPS/1000.0
 32*            COMP=(C8/UF)*SINPH
 33*            C3=C8*COSPH+COMP
 34*      C-------------------------------------------------------------------
 35*      C  NEWTON RAPHSON ITERATION FOR INCIPIENT VELOCITY
 36*      C-------------------------------------------------------------------
 37*            KOUNT=0
 38*            V=1.0
 39*         16 FX=C1*V**1.75+C2*V**2-C3
 40*            IF(ABS(FX)-.001)120,120,110
 41*        110 FDASHX=1.75*C1*V**.75+2.0*C2*V
 42*            KOUNT=KOUNT+1
 43*            IF(KOUNT-100)160,160,130
 44*        150 V=V-FX/FDASHX
 45*            GO TO 16
 46*        130 WRITE(5,2001)
 47*       2002 FORMAT(1H ,'CONVERGENCE NOT REACHED - REF 2')
 48*        120 CONTINUE
 49*            IF(DPIPE.GT.73.0.AND.DPIPE.LT.75.0) HFL =0.018*V       **1.84
 50*            IF(DPIPE.GT.43.0.AND.DPIPE.LT.45.0) HFL =0.025*V       **1.75
 51*            IF(DPIPE.GT.149.0.AND.DPIPE.LT.151.) HFL =0.0073*V       **1.76
 52*            A9=(DPIPE-DCAPS)/DPIPE
 53*            C7=C1*1000.0/B/LCAPS
 54*            C9=C7*A9
 55*            TAWD=C9*V**1.75
 56*            DHCI=(C3*1000.0/LCAPS+TAWD-HFL)*LCAPS
 57*            VAS=V/(1.0-DRAT)
 58*            RES=VAS*1.25*(DPIPE-DCAPS)*1000.0/0.96
 59*            FS=0.079/RES**0.25
 60*            DHAS=FS*LCAPS*VAS**2.0/6.14/(DPIPE-DCAPS)
 61*            DHCI2=(DHAS+C2*V**2.0)*1000.0-HFL*LCAPS
 62*            APW=9.806*3.1415*DPIPE**2/4000.
 63*            ACW=APW*DRAT
 64*            VOL=PI*DCAPS**2*LCAPS/4000000000.
 65*            MASS=VOL*1000.*SG
 66*            WDASH=VOL*9.806*1000.*(SG-1.)
 67*            DFRICI=WDASH*UF
 68*            DFORMI=(C2*V**2/DRAT+DHAS) *ACW
 69*            DSFPI=TAWD*PI*9.806*DPIPE*DCAPS*LCAPS/4000000.
 70*            DTOTAL=DFORMI+DSFPI-DFRICI
 71*          5 WRITE(5,9)
 72*          9 FORMAT(1H1)
 73*            WRITE(5,10)
 74*         10 FORMAT(///'  CAPSL   DCAPS   DPIPE   LCAPS    SG      SLOPE       VI
```

```
     1   DELHITH  RTIO    MASS   WDASH   DFRIC   DFCRP   DSFPI  DTCTAL*)
      WRITE(5,25)CAPSL,DCAPS,DPIPE,LCAPS,SG,SLOPE,V,DHCI,DHCI2,B,MASS,
     1WDASH,DFRICI,DFORMI,DSFPI,DTOTAL
   25 FORMAT(4F7.1,3F7.3,2F7.1,7F8.3,/*----------
     1----------
     2----------*)
      DO 11  I = 1 , 6
      VBAR(I)=0.5*I
C-----------------------------------------------------------------------
C  MM = VALUE OF M FOR (DELHC-HCAP(I)) LESS THAN 2  FROM FINITE
C  ELEMENT ANALYSIS
C  N = SUBSCRIPT FOR DEL(N) = ABS (DELHC-HCAP(I))
C-----------------------------------------------------------------------
      MM=0.9
      N=0
      IF(DPIPE.GT.73.0.AND.DPIPE.LT.75.0) HFLD=0.014*VBAR(I)**1.84
      IF(DPIPE.GT.43.0.AND.DPIPE.LT.45.0) HFLD=0.025*VBAR(I)**1.75
      IF(DPIPE.GT.149.0.AND.DPIPE.LT.151.) HFLD=0.0073*VBAR(I)**1.76
C-----------------------------------------------------------------------
C  HFC = FRICTION HEAD LOSS PER UNIT LENGTH LCAPS IN CAPSULE
C  FREE  LENGTH OF PIPE
C-----------------------------------------------------------------------
      HFC=HFLD*LCAPS
      HCIM=RAT*HFC*25.*9.8*(DPIPE/1000.)/(VBAR(I)**2)
      IF(HCAP(I).LT.0.0001) HCAP(I)=HCIM
   36 VC=MM*(VBAR(I)-V)
      N=N+1
   38 VAM=(VBAR(I)-VC     *DRAT)/(1-DRAT)
C-----------------------------------------------------------------------
C  POLYNOMIAL FOR VAC = FUNCTION (DCAPS/DPIPE)
C-----------------------------------------------------------------------
      VAC=(.098214+1.471571*B-2.231679*B*B+1.165949*B*B*B)*VC
      VAP=VAM-VAC
C-----------------------------------------------------------------------
C  TEST FOR NEGATIVE VAP
C-----------------------------------------------------------------------
      IF(VAP.LT.0.0)PRINT 2001
 2001 FORMAT(1H ,'VAP NEGATIVE')
      DDIF=DPIPE-DCAPS
      MMM=0
      REP=VAP*1.25*DDIF/1000./NU
      IF(ABS(REP).LT.2000.) GO TO 51
      FAP=0.079/(REP**0.25)
      HFAP=1000.*FAP*LCAPS*(VAP**2.)*4./19.6/1.25/DDIF
      VSQ2G=(VBAR(I)-VC      )**2.0/19.6
      HI=A4*VSQ2G*1000.
      HO=A6*VSQ2G*1000.
      DELHC=HFAP+HI+HO-HFC
      DEL(N)=ABS(DELHC-HCAP(I))
      IF(DEL(N).LT.2.)GO TO 51
      MM=MM+0.005
      IF(N.EQ.1) GO TO 36
      IF(DEL(N).LT.DEL(N-1)) GO TO 36
C-----------------------------------------------------------------------
C  JJJ = 1 FOR FINITE ELEMENT ANALYSIS FOR DEL(N) LESS THAN 2,FIRST ROUND
C-----------------------------------------------------------------------
   51 JJJ=1
      ECC=1.0
      GO TO 66
 1010 WRITE(5,30)
   30 FORMAT('    VBAR      VC     HFC    HFAP      HI      HO  DELHC HCAP(I)
     1    MM     REP')
      WRITE(5,50)VBAR(I),VC,HFC,HFAP,HI,HO,DELHC,HCAP(I),MM,REP
   50 FORMAT(1X,F7.1,F7.3,6F7.1,F7.3,F10.1,' COUETTE M',/'      ---------
     1----------*)
C-----------------------------------------------------------------------
C  IF NO VALUE READ FOR VCAP USE IMPIRICAL VALUE AND SKIP 2ND ROUND
C-----------------------------------------------------------------------
      IF(VCAP(I).LT.0.000001) GO TO 43
      GO TO 42
C-----------------------------------------------------------------------
C  THIRD ROUND USING IMPIRICAL VALUE OF VC
C-----------------------------------------------------------------------
   43 VCAP(I)=M*(VBAR(I)-V)
C-----------------------------------------------------------------------
C  SECOND ROUND USING EXPERIMENTAL VALUE OF VC
C-----------------------------------------------------------------------
   42 VAM=(VBAR(I)-VCAP(I)*DRAT)/(1-DRAT)
      VAC=(.098214+1.471571*B-2.231679*B*B+1.165949*B*B*B)*VCAP(I)
```

```
233*            IF(JJJ.EQ.1)GO TO 1010
234*            IF(MMM.EQ.1) GO TO 41
235*            MMMM=VCAP(I)/(VBAR(I)-V)
236*            PRINT 900
237*       900  FORMAT (*          VCAP          HFA1      H1      H2   DELHC1
238*           1 MMMM     RE>*)
239*            WRITE(5,40)VCAP(I),HFA1,H1,H2,DELHC1,MMMM,REP,HCIM
240*         40 FORMAT(8X,F7.3,7X,4F7.1,F14.3,F10.1,*EXPERIMENTAL M  DELHCIM=*,F10
241*           1.1,/*     ----------------------------------------------------
242*           1----------*)
243*       C-------------------------------------------------------------------
244*       C  GO TO 43 FOR THIRD ROUND USING IMPIRICAL VALUES OF VC AND CALCULATED
245*       C  VALUES OF DELHC FROM FINITE ELEMENT ANALYSIS
246*       C-------------------------------------------------------------------
247*          44 MMM=1
248*             M=1.2-0.8*((DCAPS/DPIPE)-0.5)**2.0
249*             GO TO 43
250*       41    PRINT 800
251*       800   FORMAT(    *          VCAPIM          HFAP     HI      HO  DELHC
252*             1      MM       REP*)
253*        411  WRITE(5,60)VCAP(I),HFA1,H1,H2,DELHC1,M,REP
254*          60 FORMAT(8X,F7.3,7X,4F7.1,F14.3,F10.1,* EMPIRICAL M*,/*----------
255*            1-----------------------------------------------------------
256*            2----------*,/*----------
257*            2-----------------------------------------------------------
258*            3----------*)
259*             GO TO 4                                                    JML
260*          90 CALL EXIT
261*             END

END OF COMPILATION:        NO  DIAGNOSTICS.
```

```
 1*             SUBROUTINE COUETT( DCA>S,DPIPE,LCAPS,VCAPSL,VCOUET,GAP,TCMEAN,
 2*            1   TPMEAN , SUMFC,SUMFP,ECC    )
 3*       C-----------------------------------------------
 4*       C  MAIN PROGRAM TO CALCULATE COUETTE FLOW IN ANNULUS
 5*       C-----------------------------------------------------
 6*             REAL MU,NU,LCAPS
 7*             DIMENSION          CR(101,101),B(100),VAVC(100),REC(100),
 8*            1V(100),Q(100),DELA(100),BC(100),UC(10000),SP(100),SC(100),BP(100),
 9*            1          REC1P(100),CRMID(100,100),DELAA(100,100),REC1C(100),THET
10*            1A(100),PHP(100),PHC(100),THETP(100),THETC(100)
11*             DATA RHO,MU,NU,PI,J/1000.0,0.0010,0.00000100,3.1416,100/
12*             N=J+1
13*          3  CONTINUE
14*           6 CONTINUE
15*             JI=0
16*       C-----------------------------------------------------
17*       C   JI = L  AT THE POINT WHERE COUETTE FLOW BECOMES TURBULENT
18*       C-----------------------------------------------------
19*             RP = DPIPE/2000.
20*             RC = DCAPS/2000.
21*             DR = DCAPS/DPIPE
22*             P = ECC     *(RP-RC)/2.
23*               CALL      GEOM(J,PI,CR,CRMID,PHC,THETC,THETA,PHP,THETP,SC,SP,RC,R
24*            1P,B,P,N)
25*             L = 0
26*           4 L = L +1
27*             VAVC(L) = VCAPSL*(1.5/ALOG(CR(N,L)/CR(1,L))-(CR(1,L))**2./((CR(N,L
28*            1))**2.-(CR(1,L))**2.))
29*             REC(L) = VAVC(L)*2.*B(L)/NU
30*             IF (REC(L).GT.2400.)GO TO 5
31*             JI=L
32*             IF (L-J)4,5,5
33*           5 JI = L
34*              CALL       AREA (J,PI,CR,DELA,THETA,DELAA,RP,RC,JI,AREAA,N)
35*       C-----------------------------------------------------
36*       C  CALCULATE FLOW IN ANNULUS FOR LAMINAR COUETTE FLOW
37*       C-----------------------------------------------------
38*             SUMQ = 0.
39*             SUMFC=0.
40*             SUMFP=0.
41*             DO 10 L = 1,J
42*             IF (L.GT.JI) GO TO 11
43*             V(L) = VCAPSL*(1.5/ALOG(CR(N,L)/CR(1,L))-(CR(1,L))**2./((CR(N,L))*
44*            1*2.-(CR(1,L)**2.)))
```

```
      Q(L) = V(L)*DELA(L)
      SUMQ = SUMQ+Q(L)
      DUDRP=VCAPSL/CR(N,L)/ALOG(CR(N,L)/CR(1,L))
      DUDRC=DUDRP*CR(N,L)/CR(1,L)
      TC=DUDRC*MU
      TP=DUDRP*MU
      SUMFC=(SUMFC+TC*SC(L))
      SUMFP=(SUMFP+TP*SP(L))
      BP(L)=0.
      BC(L)=0.
      GO TO 10
   11 CONTINUE
C-----------------------------------------------------------
C  CALCULATE BC(L) WHERE UC(N)=VCAPSL/2. IN TURB FLOW BY NEWTON RAPHSON
C-----------------------------------------------------------------------
      A = SQRT(SP(L)/SC(L))
      BC(L) = B(L)/2.
      JJ = 0
      C1 = (VCAPSL/2./NU)**(1.-A)
   15 FBC = BC(L)**A+C1*BC(L)-C1*B(L)
      FBC1 = A*BC(L)**(A-1.)+C1
      BC1 = BC(L)-FBC/FBC1
      JJ = JJ+1
      IF (ABS(BC1 - BC(L)).LE.1.E-6) GO TO 16
      BC(L) = BC1
      GO TO15
   16 BP (L) = B(_)-BC(L)
C-----------------------------------------------------------
C   VELOCITY  IN TURBULENT COUETTE FLOW AROUND CAPSULE
C-----------------------------------------------------------
      REC1C(L)=(VCAPSL/2.)*BC(L)/NU
      REC1P(L)=REC1C(L)*BP(L)/BC(L)
      UASTC=(VCAPSL/2.)*0.19/ALOG10(REC1C(L))
      UASTP=(VCAPSL/2.)*0.19/ALOG10(REC1P(L))
      TC=RHO*UASTC**2
      TP=RHO*UASTP**2
      SUMFC=(SUMFC+TC*SC(L))
      SUMFP=(SUMFP+TP*SP(L))
      TCMEAN=SUMFC/PI/RC
      TPMEAN=SUMFP/PI/RP
      SUMQQ=0.
      DO  7 M=1,J
      Y=CRMID(M,L)-CR(1,L)
      IF(Y.GT.BC(L)) GO TO 21
      YPLUSC=Y*UASTC/NU
      IF(YPLUSC.GT.10.) GO TO 18
      UC(M)=VCAPSL-UASTC*YPLUSC
      GO TO 17
   18 IF (Y/BC(L).GT.0.4) GO TO 19
      UC(M)=VCAPSL-5.6*UASTC*(1.+ALOG10(YPLUSC))
      GO TO 17
   19 UC(M)=VCAPSL-(VCAPSL/2.)+4.1*UASTC*(1.-(Y/BC(L)))
      GO TO 17
   21 JJ=M
      BP(L) = B(L)-BC(L)
      Y1 = CR(N,L)-CRMID(M,L)
      IF (Y1.GT.BP(L)) GO TO 10
      YPLUSP = Y1*UASTP/NU
      IF (YPLUSP.GT.10.) GO TO 23
      UC(M) = UASTP*YPLUSP
      GO TO 17
   23 IF (Y1/BP(L).GT.0.4) GO TO 24
      UC(M) = 5.6*UASTP*(1.+ALOG10(YPLUSP))
      GO TO 17
   24 UC(M) = (VCAPSL/2.0)-4.1*UASTP*(1.-(Y1/BP(L)))
   17 DELQQ =       UC(M)*DELAA(M,L)
    7 SUMQQ = SUMQQ+DELQQ
      Q(L)=SUMQQ
      SUMQ = SUMQ+SUMQQ
      V(L)=SUMQQ/DELA(L)
   10 REC(L)=V(L)*2.*B(L)/NU
      VCOUET=SUMQ/AREAA
      GAP = (RP-(RC*2.*P))*1000.
      RETURN
      END

END OF COMPILATION:        N)  DIAGNOSTICS.
```

```
      SUBROUTINE GEOM(J,PI,CR,CRMID,PHC,THETC,THETA,PHP,THETP,SC,SP,RC,R
     1P,B,P,N)
      DIMENSION CR(N,N),B(J),CRMID(J,J),PHC(J)        ,THETA(J),PHP(J),T
     1HETP(J),SC(J),SP(J),THETC(J)
C-------------------------------------------------------
C SUBROUTINE TO CALCULATE GEOMERICAL VALUES
C-------------------------------------------
      DO 30 L = 1,J
      A = (FLOAT(L)-0.5)*PI/FLOAT(J)
      PHIC = ASIN(P*SIN(A)/RC)
      THETAC = PHIC+A
      CR(1,L) = (P/SIN(PHIC))*SIN(THETAC)
      PHIP = ASIN(P*SIN(A)/RP)
      THETAP = A-PHIP
      CR(N,L) = (P/SIN(PHIP))*SIN(THETAP)
      B(L) =  CR(N,L)-(CR(1,L))
      DO 31 M = 1,N
      IF (M.EQ.1 ) GO TO32
      CR(M,L)=B(L)*(FLOAT(M-1)/FLOAT(J))+CR(1,L)
      GO TO 39
   32 CR(M,L) = CR(1,L)
   39 AN=FLOAT(M)-0.5
      CRMID(M,L)=(B(L)*AN/FLOAT(J))+CR(1,L)
   31 CONTINUE
      THETA(L)=FLOAT(L)*PI/FLOAT(J)
      PHC(L) = ASIN(P*SIN(THETA(L))/RC)
      THETC(L) = PHC(L)+THETA(L)
      PHP(L) = ASIN(P*SIN(THETA(L))/RP)
      THETP(L)= THETA(L)-PHP(L)
      IF (L.EQ.1) GO TO 33
      SC(L) = (THETC(L)-THETC(L-1))*RC
      SP(L) = (THETP(L)-THETP(L-1))*RP
      GO TO 30
   33 SC(1) = THETC(1)*RC
      SP(1) = THETP(1)*RP
   30 CONTINUE
      RETURN
      END
```

END OF COMPILATION: NO DIAGNOSTICS.

```
      SUBROUTINE AREA (J,PI,CR,DELA,THETA,DELAA,RP,RC,JI,AREAA,N)
      DIMENSION DELA(J),THETA(J),CR(N,N),DELAA(J,J)
      SUMA = 0.
C  SUBROUTINE TO CALCULATE INCREMENTAL AREAS DELA(L) AND SUB AREAS DELAA(M,L)
C-------------------------------------------------------------------------
      DO 43 L = 1,J
      IF (L.GT.JI) GO TO 41
C  -----------------------------------------------------------
C  CALCULATE AREAS DELA(L) IN LAMINAR FLOW
C-----------------------------------------
      IF (L.EQ.1 ) GO TO42
      DELA(L) = ((THETA(L)-THETA(L-1))/2.)*((CR(N,L))**2.-(CR(1,L))**2.)
      GO TO 43
   42       DELA(L) = (THETA(1)/2.)*((CR(N,1))**2.-(CR(1,1))**2.)
      GO TO 43
   41 CONTINUE
      SUMAA=0.
C  -----------------------------------------------------------
C  FIND SUB AREAS DELAA(M,L) AND AREAS DELA(L) FOR TURBULENT FLOW
C -----------------------------------------------------------
      DO 45 M = 1,N
      IF (M.EQ.1 ) GO TO 44
      DELAA(M,L)=((THETA(L)-THETA(L-1))/2.)*((CR(M,L))**2.-(CR(M-1,L))**
     U2.)
      GO TO 45
   44 DELAA (M,L) = 0.
   45 SUMAA=SUMAA+DELAA(M,L)
      DELA(L)=SUMAA
   43 SUMA = SUMA+DELA(L)
      AREAA= PI*((RP**2.0)-(RC**2.))/2.
      RETURN
      END
```

END OF COMPILATION: NO DIAGNOSTICS.

```
      SUBROUTINE FRESS  (RP,RC,ECC,HLOSS,MU,SUMP,SUMC,VPRESS,RHO)
C-----------------------------------------------------------------------
C  SUBROUTINE FOR PRESSURE FLOW IN ANNULUS
C-----------------------------------------------------------------------
      REAL MU,NU
      DIMENSION DELAA(100,100),B(100),CRMID(100,100),SC(100),SP(100),CR(
     1 101,100),DELA(100)           ,VPROF(100)
      DATA APIPE,BPIPE,ACORE,BCORE/6.1,3.,4.4,6.2/
      DATA PI /3.1415927/
      INDEX=100
      J = 100
      KARD=8
      IPRNT=5
      DISPL=ECC*(RP-RC)
      P=DISPL/2.0
      PG = 9.801 * RHO * HLOSS
      ARYA=PI*(RP*RP-RC*RC)
      D1=180.0/FLOAT(J)
      DEGR=0.0
      SUM=0.0
      FRICT=0.0
      SUMP=0.0
      SUMC=0.0
      RATIO = RC / RP
      NU=MU/RHO
C-----------------------------------------------------------------------
C  CALCULATE A AND B VALUES FOR TRANSITION ZONE FROM BOUNDARY CONDITIONS
C-----------------------------------------------------------------------
      ATPIP=(ALOG10(30.0)*APIPE+BPIPE-5.0)/ALOG10(6.0)
      BTPIP=5.0-ALOG10(5.0)*ATPIP
      ATCOR = (ALOG10(30.)*ACORE+BCORE-5)/ALOG10(6.)
      BTCOR = 5-ALOG10(5.)*ATCOR
C-----------------------------------------------------------------------
C IF CONCENTRIC GO TO 7 --- IF ECCENTRIC GO TO 6
C-----------------------------------------------------------------------
      IF  (DISPL)   6,7,6
C-----------------------------------------------------------------------
C SHEAR STRESS AND AVERAGE VELOCITY IN CONCENTRIC LAMINAR PRESS FLOW
C-----------------------------------------------------------------------
7     F1 = .5*(RC*RC-RP*RP)/ALOG(RATIO)
      VAVE=.25*PG*(.5*(RP*RP+RC*RC)-F1)/MU
      REP=2.0*VAVE*(RP-RC)/NU
      IF(REP-2400.0)11,12,12
   11 SUM=VAVE*ARYA
      TPP=.5*PG*(RP-F1/RP)
      TPC=.5*PG*(F1/RC-RC)
      GO TO 13
C-----------------------------------------------------------------------
C SHEAR STRESS FORCE AND VELOCITY IN CONCENTRIC TURBULENT PRESS FLOW
C-----------------------------------------------------------------------
12    CR(1,1) = RC
      CR(INDEX+1,1)=RP
      B(1)=RP-RC
      DIFF1=B(1)/INDEX
      DO 1002 KK=2,INDEX
 1002 CR(KK,1)=CR(KK-1,1)+DIFF1
      CALL AREA(1,0,DUMMY)
   61 CALL FBAL (APIPE,BPIPE,ATPIP,BTPIP,(PI*RP)
     1 ,(PI*RC),CR,(RP-RC),DELA(1),DELAA(1,1),RHO,MU,NU,PG,1,INDEX,KRMAX
     2,Q,VPIPE,TPP,TPC,VPROF(100))
      SUM=2.0*Q
      YC=KRMAX*(RP-RC)/INDEX
   13 SUMP=TPP*PI*2.0*RP
      SUMC=TPC*PI*2.0*RC
      FRICT=  SUMP+SUMC
      GO TO 30
C-----------------------------------------------------------------------
C  FLOW IN ECCENTRIC ANNULUS
C-----------------------------------------------------------------------
6     CALL GEOM
40    DO 20 I = 1 , J
      RP1 = CR(INDEX+1,I) ** 2
      RC1 = CR (1,I) ** 2
      F1 = (RP1-RC1) / ALOG(RP1/RC1)
      VAVE = .25*PG*(.5*(RP1+RC1) - F1) /MU
      DEGR = DEGR + D1
      REP = 2*VAVE*B(I)/NU
      IF(REP-2400.0)14,15,15
```

```
C-----------------------------------------------------------------
C ECCENTRIC LAMINAR PRESS FLOW
C-----------------------------------------------------------------
14      DELA(I) = (PI/J)*B(I)*(CR(1,I)+.5*B(I)  )
        Q = VAVE * DELA(I)
        TPP=.5*PG*(CR(INDEX+1,I)-F1/CR(INDEX+1,I))
        TPC=.5*PG*(F1/CR(1,I)-CR(1,I))
        SUM=SUM+Q
        PFRIC=TPP*SP(I)
        SUMP=SUMP+PFRIC
        CFRIC=TPC*SC(I)
        SUMC=SUMC+CFRIC
900     FORMAT  ( 3F30.10)
   20 FRICT=FRICT+PFRIC+CFRIC
   15 LT=I
      KOUNT=I
      IF  (LT-J)  17 , 16 , 16
   16 WRITE(IPRNT,208)
  208 FORMAT(1H ,'FLOW LAMINAR THROUGHOUT')
      GO TO 31
C-----------------------------------------------------------------
C ECCENTRIC TURBULENT PRESS FLOW
C-----------------------------------------------------------------
17      CALL AREA   (J,LT,DUMMY)
   19 DO 18 I=LT,J
      DEGR=DEGR+01
      CALL FBAL  (APIPE,BPIPE,ATPIP,BTPIP,ACORE,BCORE,ATCOR,BTCOR,SP(I),
     1 SC(I),CR(1,I),B(I),DELA(I),DELAA(1,I),RHO,MU,NU,PG,J,INDEX,KRMAX,
     2 Q,VPIPE,TPP,TPC,VPROF)
      IF(KOUNT-J/2)58,51,51
   51 KOUNT=KOUNT-J/2
   58 KOUNT=KOUNT+1
      SUM=SUM+Q
      PFRIC=TPP*SP(I)
      SUMP=SUMP+PFRIC
      CFRIC=TPC*SC(I)
      SUMC=SUMC+CFRIC
      FRICT=FRICT+PFRIC+CFRIC
18      YC=CRMID(KRMAX,I)-CR(1,I)
   31 SUM=2.0*SUM
      FRICT=2.0*FRICT
      SUMP=2.0*SUMP
      SUMC=SUMC*2.0
   30 VBAR=SUM/ARYA
      VPRESS = VBAR
      REP=2.0*VBAR*(RP-RC)  /NU
      F=PG*(RP-RC)/(VBAR*VBAR*RHO)
      FTREP=F*REP**.25
      RETURN
      SUBROUTINE AREA(J,LT,AREAA)
C-----------------------------------------------------------------
C  SUBROUTINE TO FIND AREAS AND SUB AREAS IF TURBULENT
C  J IS NO OF SLICES PER HALF REVOLUTION
C  INDEX IS NO OF SUB-AREAS PER SLICE
C  LT IS SLICE NO AT WHICH FLOW BECOMES TURBULENT
C-----------------------------------------------------------------
      INTEGER L,K,J,LT
      REAL INCR1,DIFF,TETA,AREAA
      TETA=PI/FLOAT(J)
      AREAA=.5*PI*(RP*RP-RC*RC)
      DO 43 L=1,J
      DIFF=B(L)/INDEX
C-----------------------------------------------------------------
C  DIFF IS INCREMENTAL RADIUS PER SUB SLICE
C  INCR1 IS INCREMENT IN AREA PER SUB SLICE
C-----------------------------------------------------------------
      DELAA(1,L)=TETA*DIFF*(CR(1,L)+.5*DIFF)
      DELA(L)=TETA*B(L)*(CR(1,L)+.5*B(L))
      IF(L-LT)43,1,1
C-----------------------------------------------------------------
C  IF TURBULENT GO TO 1 ,OTHERWISE CONTINUE
C-----------------------------------------------------------------
    1 INCR1=TETA*DIFF*DIFF
      DO 44 K=2,INDEX
   44 DELAA(K,L)=DELAA(K-1,L)+INCR1
   43 CONTINUE
      RETURN
      SUBROUTINE GEOM
      INTEGER L,M
      REAL INCR ,PHIP,TCL,THETC,A,THETP,DIFF,PHIC,TPL
```

```
C-----------------------------------------------------------------------
C  SUBROUTINE TO WORK OUT GEOMETRY OF ECCENTRIC ANNULI BY QUASI CONSENTRIC
C       METHOD
C  DISPLACEMENT OF CORE CENTRE FROM PIPE CENTRE = 2*P
C  J IS NO OF SLICES PER HALF REVOLUTION
C  INCR IS ANGULAR INCREMENT PER SLICE IN RADIANS
C  AIS SET AT -.5*INCR SO FIRST A = .5*INCR
C-----------------------------------------------------------------------
      L=0
      IF(P)4,5,4
    5 CR(1,1)=RC
      CR(INDEX+1,1)=RP
      L=1
      J=1
      GO TO 6
    4 INCR=PI/J
      A=-.5*INCR
      TCL=A
      TPL=A
   10 L=L+1
      A=A+INCR
      PHIC=ASIN(P*SIN(A)/RC)
      THETC=PHIC+A
      CR(1,L)=(P/SIN(PHIC))*SIN(THETC)
      PHIP=ASIN(P*SIN(A)/RP)
      THETP=A-PHIP
      CR(INDEX+1,L)=(P/SIN (PHIP))*SIN(THETP)
    6 B(L)=CR(INDEX+1,L)-CR(1,L)
      DIFF=B(L)/INDEX
      CRMID(1,L)=CR(1,L)+.5*DIFF
      IF(INDEX-1)1,1,2
    2 DO 3 M=2,INDEX
      CR(M,L)=CR(M-1,L)+DIFF
    3 CRMID(M,L)=CRMID(M-1,L)+DIFF
C-----------------------------------------------------------------------
C  WORK OUT WALL LENGTH OF PIPE(SP) AND CORE(SC)
C  PUT TCL=THETC SO NEXT TIME ROUND (THETC-TCL) REPRESENTS INCREASE IN THETC
C  DITTO FOR TPL
C-----------------------------------------------------------------------
    1 SC(L)=(THETC-TCL)*RC
      SP(L)=(THETP-TPL)*RP
      TCL=THETC
      TPL=THETP
      IF(L-J)10,11,11
   11 IF(J-1)8,9,8
    9 SC(1)=PI*RC
      SP(1)=PI*RP
    8 RETURN
      END
```

END OF COMPILATION: NO DIAGNOSTICS.

```
C-----------------------------------------------------------------------
C  SUBROUTINE FORCE BALANCE EQUATION FOR CALCULATING RMAX
C-----------------------------------------------------------------------
      SUBROUTINE FBAL(APIPE,BPIPE,ATPIP,BTPIP,ACORE,BCORE,ATCOR,BTCOR,SP
     1 ,SC,CR,B,DELA,DELAA,RHO,MU,NU,PG,J,INDEX,RMAX,Q,VPIPE,TPP,TPC,
     2 VPROF)
      REAL INCR ,MU,NU
      DIMENSION CR(1),DELAA(1) ,VPROF(1)
      DATA PI /3.1415927/
C-----------------------------------------------------------------------
C  DLAST INITIALISED AT VERY LARGE NUMBER TO ENSURE MORE
C  THAN ONE ITERATION
C-----------------------------------------------------------------------
      DLAST=10.0E30
      DIFF=B/INDEX
      INCR=PI*DIFF*DIFF/J
```

BELONGS TO J H LAZARUS NO 51 OPTIMUM POWER

```
1*          DIMENSION DCAP(100),SPC(100),PSII(100,100)
2*      C*****************************************************************
3*      C*INCIPIENT POWER, POWER AND MINIMUM POWER FOR GIVEN DELIVERY RATE  *
4*      C*****************************************************************
5*          REAL LCAPS,LRTIO,NU,MU,MASS,M,INJECT,INJECP,MIN
6*        4 CONTINUE
7*          READ(8,1) DELIV,SG,DRTIO,LRTIO,SLOPE
8*        1 FORMAT(5F8.1)
9*          IF(DELIV.LT.0.0001) GO TO90
10*         DATA RHO,MU,NU,PI,UF/1000.0,0.0010,0.00000100,3.1416,0.32/
11*         PERC1=DELIV/100.
12*         WRITE(5,8)
13*       8 FORMAT(///'          DELIVERY          SG       DRTIO    LRTIO
14*        1 SLOPE')
15*         WRITE(5,20)
16*      20 FORMAT('       KG/S  MIL T/AN  ')
17*         DELIVT = DELIV*0.03155
18*         WRITE(5,7)DELIV,DELIVT,SG,DRTIO,LRTIO,SLOPE
19*       7 FORMAT(1X,6F10.2)
20*         DCAPS=275.
21*         DO 3 I = 1,12
22*         DCAPS=DCAPS+25.
23*         DCAP(I)=DCAPS
24*         LCAPS = LRTIO*DCAPS
25*         DPIPE = DCAPS/DRTIO
26*         MASS = PI*(DCAPS**2)*LCAPS*RHO*SG/4./1000000000.
27*     C*****************************************************************
28*     C* CALCULATE INCIPIENT VELOCITY ,INCIPIENT EXCESS HEAD ,PSII AND POWI *
29*     C*****************************************************************
30*         HYPOT=SQRT(SLOPE**2.0+10000.0)
31*         SINPH=SLOPE/HYPOT
32*         COSPH=100.0/HYPOT
33*         RAT=(DCAPS/DPIPE)**2.0*ABS(SG-1.0)
34*         DRAT=(DCAPS/DPIPE)**2
35*         A1=1-DRAT
36*         A2=A1**1.75
37*         A3=((DPIPE-DCAPS)/1000.0)**1.25
38*         B=DCAPS/DPIPE
39*         C1=0.239*(LCAPS/1000.0)*B*NU**0.25/A3/A2/19.6
40*         A4=22.0*(DCAPS/DPIPE)**6.0
41*         A5=(1.0/A1)-1.0
42*         A6=0.68*A5**2.0
43*         C2=(A4+A6)/19.6
44*         C8=UF*8**2.0*ABS(SG-1.0)*LCAPS/1000.0
45*         COMP=(C8/UF)*SINPH
46*         C3=C8*COSPH+COMP
47*         KOUNT=0
48*         V=1.0
49*      16 FX=C1*V**1.75+C2*V**2-C3
50*         IF(ABS(FX)-.001)120,120,110
51*     110 FDASHX=1.75*C1*V**.75+2.0*C2*V
52*         KOUNT=KOUNT+1
53*         IF(KOUNT-100)160,160,130
54*     160 V=V-FX/FDASHX
55*         GO TO 16
56*     130 WRITE(5,2001)
57*    2001 FORMAT(1H ,'CONVERGENCE NOT REACHED - REF 2')
58*     120 CONTINUE
59*         DPIPM=DPIPE/1000.
60*         F = 0.079/((V    *DPIPM/NU)**0.25)
61*         HFL=2.*F*(V    **2)/9.8/DPIPM
62*         A9=(DPIPE-DCAPS)/DPIPE
63*         C7=C1*1000.0/B/LCAPS
64*         C9=C7*A9
65*         T4WD=C9*V**1.75
66*         DHCI=(C3*1000.0/LCAPS+T4WD-HFL)*LCAPS
67*         VAS=V/(1.0-DRAT)
68*         RES=VAS*1.25*(DPIPE-DCAPS)*1000.0/0.95
69*         FS=0.079/RES**0.25
70*         DHAS=FS*LCAPS*VAS**2.0/6.14/(DPIPE-DCAPS)
71*         DHCI2=(DHAS+C2*V**2.0)*1000.0-HFL*LCAPS
72*         DO 3 J = 1,1
73*         WRITE(5,200)
74*     200 FORMAT(///)
75*         WRITE(5,13)
76*      13 FORMAT('       DCAPS      DPIPE      LCAPS      SPACE          CL
77*        1 CV          VI       DHCIS       POWI       PSII')
78*         CL = FLOAT(J)*0.5
79*         CV = CL*DRAT
80*         SPACE = LCAPS/CL/1000.0
```

```
81*           SPC(J)=SPACE
82*           POWI =9810.0*(3.146/4.0)*(DPIPE/1000.0)**2.0*V*(HFL*DHCI/1000.0/SP
83*          1ACE-COMP/SPACE)
84*           PSII = POWI/DELIV
85*           WRITE(5,40)DCAPS,DPIPE,LCAPS,SPACE,CL,CV,V,DHCI2,POWI,PSII
86*        40 FORMAT(1X,10F10.3)
87*           VC = DELIV*SPACE/MASS
88*           IF (VC.GT.80.)GO TO 11
89*           IF(VC.LT.0.2) GO TO 12
90*           WRITE(5,201)
91*       201 FORMAT(///)
92*           WRITE(5,14)
93*        14 FORMAT('       VBAR        VC       HCIM       PSI        POW      IN
94*          1JECT      DELIV     DELIVT')
95*           INJECT = VC/SPACE
96*           M = 1.2-0.8*(B-0.5)**2
97*           VBAR = VC/M*V
98*           F = 0.079/((VBAR*DPIPM/NU)**0.25)
99*           HFL = 2.*F*(VBAR**2)/9.8/DPIPM
100*          C = HFL/(VBAR**1.75)
101*          HCIM = RAT*HFL*25.00*9.8*DPIPM/(VBAR**2)*LCAPS/1000.
102*          PSI = 9.8*VBAR/SG/DRAT/VC*(HFL*SPACE+HCIM)*1000./LCAPS
103*          PSIM(I,J)=PSI
104*          POW = PSI*DELIV
105*          WRITE(5,50) VBAR,VC,HCIM,PSI,POW,INJECT,DELIV,DELIVT
106*       50 FORMAT(1X,8F10.3,'    EMPIRICAL')
107*     C*****************************************************************
108*     C* CALCULATE PSIMN ALSO VCMN,VMIN AND DELIVMIN IE OPTIMUM DELIVERY FOR CL
109*     C*****************************************************************
110*          ALPHA=9.80/SG/DRAT/M
111*          KONT1=0
112*          FACTR=8.0
113*          SAVE=SPACE
114*          CHANGE=8.0
115*          GO TO 10
116*        5 FACTR=FACTR-CHANGE
117*          GO TO 10
118*        6 FACTR=FACTR+CHANGE
119*       10 SPACE=SAVE*FACTR
120*          BETA=C*1000.*SPACE/LCAPS
121*          GAMA = RAT * DPIPE * C*25.00*9.8/1000.0
122*          DELTA=SINPH*(RAT+1.0)
123*          KONT=0
124*          X=5.0
125*          FDASH=2.5
126*       53 FX = ALPHA*BETA*(1.75*X**2.75-2.75*X**1.75*V)-ALPHA*GAMA*(0.25*X*
127*          1*0.75+0.75*X**(-0.25)*V)-DELTA*ALPHA*V
128*          KONT=KONT+1
129*          IF(ABS(FX)-.001)82,82,1000
130*     1000 IF(FX)1001,82,1002
131*     1001 X=X+FDASH
132*          GO TO 1003
133*     1002 X=X-FDASH
134*     1003 FDASH=FDASH/2.0
135*          IF(KONT-100)53,53,1004
136*     1004 WRITE(5,2000)
137*     2000 FORMAT(1H ,'CONVERGENCE NOT REACHED - REF 1')
138*       82 VMN=X
139*          F = 0.079/((VMN *DPIPM/NU)**0.25)
140*          HFL = 2.*F*(VMN **2)/9.8/DPIPM
141*          HCMN = RAT*HFL*25.00*9.8*DPIPM/(VMN **2)*LCAPS/1000.
142*          POWMN=9810.0*(3.146/4.0)*(DPIPE/1000.)**2.0*VMN*(HFL  *(HCMN/SPACE
143*         1))
144*          XPWMN=9810.0*(3.146/4.0)*(DPIPE/1000.)**2.0*VMN*(     (HCMN/SPACE
145*         1))
146*          VCMN=M*(VMN-V)
147*          PSIMN=9.81*VMN/SG/DRAT/VCMN*(HFL  *SPACE+HCMN)/LCAPS*1000.0
148*          DELVMN = VCMN*MASS/SPACE
149*          DEL=ABS(DELVMN-DELIV)
150*          IF(DEL.LT.PERC1) GO TO 9
151*          CHANGE=CHANGE/2.0
152*          KONT1=KONT1+1
153*          IF(KONT1-100)1020,1020,1021
154*     1020 IF(DELVMN.LT.DELIV) GO TO 5
155*          IF(DELVMN.GT.DELIV) GO TO 6
156*     1021 WRITE(5,2002)
157*     2002 FORMAT(1H ,'CONVERGENCE NOT REACHED - REF 3')
158*        9 DELVMT = DELVMN+0.03155
159*          INJECM = VCMN/SPACE
160*          CLMIN=LCAPS/1000./SPACE
161*          WRITE(5,51)VMN,VCMN,HCMN,PSIMN,POWMN,INJECM,DELVMN,DELVMT,SPACE
162*          WRITE(5,52)CLMIN
163*       52 FORMAT(84X,'CLMIN=',F8.4)
164*       51 FORMAT(1X,8F10.3,'    MINIMUM   SPACE=',  F8.3)
165*          GO TO 7
```

```
166*          11 WRITE(5,17) VC
167*             GO TO 3
168*          12 WRITE(5,18) VC
169*          17 FORMAT(  /* VC GREATER THAN 3.0 M/S,VC=*,2X,F8.3)
170*          18 FORMAT(//* VC LESS THAN 0.5 M/S,VC=*,2X,F8.3)
171*           3 CONTINUE
172*             MIN=2.E20
173*             DO 21 K=1,I
174*             DO 21 L=1,J

175*             IF(PSIM(K,L).LT.0.001) GO TO 21
176*             IF(PSIM(K,L)-MIN)22,21,21
177*          22 MIN=PSIM(K,L)
178*             KK=K
179*             LL=L
180*          21 CONTINUE
181*          23 WRITE(5,24) MIN,DCAP(KK),SPC(LL)
182*          24 FORMAT(1X,3E10.3)
183*             GO TO 4
184*          90 CALL EXIT
185*             END

END OF COMPILATION:        NO  DIAGNOSTICS.
```

B I B L I O G R A P H Y

1. BABCOCK, H.A. — *"The sliding bed flow regime".* Hydrotransport I First Int. Conf. on Hyd. Trans. of solids in pipes pp H1-1-16 (Sept 1970).

2. BENTWICH, M., KELLEY, D.A. and EPSTEIN, N. — *"Two phase eccentric inter-phase laminar pipeline flow".* J. Basic Eng. Trans. ASME pp 32-36 (Mar 1970).

3. BERKOWITZ, N., BROWN, R.A.S. and JENSEN, E.J. — *"The Pipeline flow of paste slugs - Part I".* Can. J. of Chem. Eng. pp 280-285 (Dec 1965).

4. BONNINGTON, S.T. — *"Estimation of pipe friction involved in pumping solid material".* B.H.R.A. Research report TN708 (Dec 61).

5. BOURNE, E,E, FIGUEIREDO, O. and CHARLES, M.E. — *"Laminar and turbulent flow in annuli of unit eccentricity".* Can. J. Chem. Eng. Vol. 46, pp 289-93 (Oct 1968).

6. BOWDEN, F.P. and TABOR, D. — *"Friction and Lubrication".* Surface physics, Cavendish Laboratory, University of Cambridge. Methuen and Co. Ltd. (1967).

7. BRIGHTON, J.A. and JONES, J.B. — *"Fully developed turbulent flow in annuli".* Trans. ASME J. of Basic Eng. pp 835-844 (Dec 1964).

8. BROWN, R.A.S. and JENSEN, E.J. — *"The pipeline flow of paste slugs. Part II. Pressure gradients and velocities of trains of slugs".* Can. J. of Chem. Eng. pp 157-161 Vol. 46 (June 1968).

9. CALDWELL, J. — *"The hydraulic mean depth as a basis for form comparison in the flow of fluids in pipes".* J. of Royal Tech. Coll. Glasgow Vol. 2 Part 2 pp 203-220 (1930).

10. CHARLES, M.E. — *"The pipeline flow of capsules Part 2: Theoretical Analysis of the concentric flow of cylindrical forms".* Can. J. Chem. Eng. pp 46-51 (April 1963).

11. CONDOLIOS, E. and CHAPUS, E.E. — *"Transporting solid materials in pipelines".* Chem. Eng. Vol. 70 No. 13 (June 24, 1963).

12. COUETTE, M. — *"Etudes sur le frottement des liquides".* Ann. de Chemie et de Physique. Ser 6 Vol. 21 pp 433-510 (1890).

13. DODGE, D.W. and METZNER, A.B. — *"Turbulent flow of Non-Newtonian systems".* A.I.Ch.E. Journal. Vol. 5 No. 2 pp 189-204 (June 1959).

14. DURAND, R. — *"Basic Relationships of the transportation of solids in pipes - experimental research".* pp 89-102. Minn. Int. Hydr. Conv. (Sept. 1953).

15. ELLIS, H.S. — *"The pipeline flow of capsules. Part 3: An experimental investigation of the transport by water of single cylindrical and spherical capsules with density equal to that of the water".* Can. J. Chem. Eng. pp 1-8 (Feb 1964).

16. ELLIS, H.S. — *"The pipeline flow of capsules. Part 4: An experimental investigation of the transport in water of single cylindrical capsules with density greater than that of the water".* Can. J. Chem. Eng. pp 69-76 (Apr 1964).

17. ELLIS, H.S. — *"The pipeline flow of capsules. Part 5: An experimental investigation of the transport by water of single spherical capsules with density greater than that of water".* Can. J. Chem. Eng. pp 155-160 (Aug 1964).

18. ELLIS, H.S. and BOLT, L.H. — *"The pipeline flow of capsules. Part 7: An experimental investigation of the transport by two oils of single cylindrical and spherical capsules with density equal to that of the oil".* Can. J. Chem. Eng. pp 201-206 (Oct 1964).

19. ELLIS, H.S. and KRUYER, J.
"The pipeline flow of capsules. Part 10: Empirical pressure and velocity correlations for cylindrical capsules conveyed in pipelines up to 4 inches in diameter".
Hydrotransport I First Int. Conf. on Hyd. Trans. of Solids in pipes. (Sept 1970).

20. HEYDA, J.F.
"A Green's function solution for the case of laminar incompressible flow between non-concentric circular cylinders".
Jour. Franklin Inst. Vol. 267 pp 25-34 (Jan 1959).

21. HODGSON, G.W. and CHARLES, M.E.
"The pipeline flow of capsules. Part I: The concept of capsule pipelining".
Can. J. Chem. Eng. pp 43-45 (April 1963).

22. HODGSON, G.W., KRUYER, J., ROEHL, A.A. ROUND, G.F. and ELLIS, H.S.
"A practical projection of capsule pipelining: Edmonton-Hardisty trunkline test".
Paper to Annual meeting of the Can. Inst. Min. Met., Toronto, Ont. (March 1965).

23. JENSEN, E.J. and BRUCE, J.G.
"Capsule pipelining - a feasibility assessment".
Paper C1 - Hydrotransport I. First Int. Conf. on the Hyd. Trans. of Solids in pipes. (Sept 1970).

24. JONSSON, V.K. and SPARROW, E.M.
"Results of laminar flow analysis and turbulent flow experiments for eccentric annular ducts".
A.I.Ch.E. Vol. 11 No. 6 pp 1143-1145 (Nov 1965).

25. JONSSON, V.K. and SPARROW, E.M.
"Experiments on turbulent flow phenomena in eccentric annular ducts".
J. Fluid Mech. Vol. 25, Part I, pp 65-86, (1966).

26. KNUDSEN, J.G. and KATZ, D.L.
"Fluid dynamics and heat transfer".
McGraw Hill (1958).

27. KRUYER, J. and ELLIS, H.S.
"The pipeline flow of capsules, Part II".
Unpublished paper (July 1970).

28. KRUYER, J.
REDBERGER, P.J. and
ELLIS, H.S.
"The pipeline flow of capsules. Part 9".
J. Fluid Mech. Vol. 30 Part 3
pp 513-531 (Mar 1967).

29. LAMB, H.
"Hydrodynamics".
Camb. Univ. Press (1932).

30. LAZARUS, J.H.
"The future of hydraulic transport of solids in pipelines".
Proc. S.A. Inst. of Civil Eng.
Western Cape Regional Convention.
pp 38-47 (Sept 1971).

31. LAZARUS, J.H. and
KILNER, F.A.
"Incipient motion of Solid capsules in pipelines".
Hydrotransport I. First Int.
Conf. on Hyd. Trans. of Solids
in pipes. B.H.R.A. (Sept 1970).

32. LEUTHEUSSER, H.J. and
CHU, V.H.
"Experiments on plane Couette flow".
Proc. A.S.C.E. Vol. 97 Hy9.
pp 1269-1283 (Sept 1971).

33. LEVY, J.
"Model tests on shear stresses in circular pipes".
B.Sc. undergraduate thesis.
Univ. of Cape Town (1971).

34. LEVY, S.
"Turbulent flow in an annulus".
Trans. ASME Vol. 89C pp 25-31
J. of Heat Trans. (Feb 1967).

35. LINFORD, A. and
SAUNDERS, D.H.
"Hydraulic transport of iron ore".
B.H.R.A. R.R. 1015 (July 1969).

36. MALAIKA, J.
"Flow in non-circular conduits".
Proc. A.S.C.E. Vol. 88, HY6,
pp 1-30, Paper 3310 (Nov 1962).

37. MACAGNO, E.O. and
McDOUGALL, D.W.
"Turbulent flow in annular pipes".
A.I.Ch.E. Vol. 12 No. 3 pp 437-444
(May 1966).

38. METER, D.M. and
BIRD, R.B.
"Turbulent Newtonian flow in annuli
A.I.Ch.E. Vol. 7 No. 1 pp 41-45
(Mar 1961).

39. METZNER, A.B. and
REED, J.C.
"Flow of Non-Newtonian fluids - Correlation of the laminar, transition and turbulent regions".
A.I.Ch.E. pp 434-440 (Dec 1955).

40. NELSON, A.R. and
ROBERTSON, J.M.
"Analytical Studies of turbulent friction in annular conduits".
T. & A.M. Report No. 321. University of Illinois (Nov 1968).

41. NEWITT, D.M.
RICHARDSON, J.F.
ABBOTT, M. and
TURTLE, R.B.

"Hydraulic conveying of solids in horizontal pipes".
Trans. Inst. Chem. Engrs. Vol. 33 pp 93-112 (1955).

42. NEWTON, R.,
REDBERGER, P.J. and
ROUND, G.F.

"The pipeline flow of capsules. Part 6: Numerical Analysis of some variables determining free flow".
Can. J. Chem. Eng. pp 168-173 (Aug 1964).

43. NOLAN, H.G.B. and
DRUST, T.A.

"Long distance iron ore and coal slurry transportation with particular reference to South Africa".
Hydrotransport I First Int. Conf. on Hyd. Trans. of Solids in pipes ppA4 -37-56 (Sept 1970).

44. OWEN, W.M.

"Experimental study of water flow in annular pipes".
Proc. A.S.C.E. Sep No. 88 Vol. 77 (Sept 1951).

45. PRANDTL, L.

"Fluid Dynamics".
Blackie and Son Ltd. (1952).

46. QUARMBY, A.

"An experimental study of turbulent flow through concentric annuli".
Int. J. Mech. Sci. Vol. 9 pp 205-221 (1967).

47. RANDHAVA, S.S.

"An analysis of turbulent flow in concentric annuli".
A.I.Ch.E.J. pp 132-3 (Jan 1969).

48. RATKOWSKY, D.A.

"Fluid friction and heat transfer in plain concentric annuli".
Can. J. of Chem. Eng. pp 8-12 (Feb 1966).

49. REDBERGER, P.J. and
CHARLES, M.E.

"Axial laminar flow in a circular pipe containing a fixed eccentric core".
Can. J. of Chem. Eng. Vol. 40 pp 147-151 (Aug 1962).

50. REICHARDT, H.

"Ueber die Geschwindigkeitsverteilung in einer gradlinigen turbulenten Couettestromung".
ZAMM Sonderheft, Vol. 36, pps 26-29 (1956).

51. ROBERTSON, J.M. — *"On turbulent plane Couette flow".* pp169-182 Proc. of 6th An. Conf. on Fl. Mech. Texas (Sept 1959).

52. ROBERTSON, J.M. — *"Turbulent friction in eccentric annular conduits".* T. & A.M. Report No. 310 University of Illinois (Mar 1968).

53. ROBERTSON, J.M. and JOHNSON, H.F. — *"Turbulence structure in plane Couette flow".* J. Eng. Mech. Div. Proc. A.S.C.E. EM6 pp1171-1182 (Dec 1970).

54. ROSS, D. — *"A new analysis of Nikaradse's Experiments of Turbulent flow in Smooth Pipes".* Proc. of 3rd Midwest Conf. on Fl. Mech. pp 651-667 (1953).

55. ROTHFUS, R.R., MONRAD, C.C. and SENECAL, V.E. — *"Velocity Distribution and fluid friction in smooth concentric annuli".* Ind. and Eng. Chem. Vol. 42, No. 12 pp 2511-2520 (Dec 1950).

56. ROTHFUS, R.R. SARTORY, W.K. and KERMODE, R.I. — *"Flow in concentric annuli at high Reynolds number".* A.I.Ch.E.J. Vol. 12 No. 6 pp 1086-1091 (Nov 1966).

57. ROTHFUS, R.R. WALKER, J.E. and WHAN, G.A. — *"Correlation of local Velocities in tubes, Annuli and Parallel plates".* A.I.Ch.E. Vol. 4 No. 2 pp 240-245 (Jun 1958).

58. ROUND, G.F. and BOLT, L.H. — *"The pipeline flow of capsules. Part 8: An experimental investigation of the transport in oil of single, denser-than-oil spherical and cylindrical capsules".* Can J. Chem. Eng. pp 197-205 (Aug 1965).

59. ROUSE, H. — *"Engineering Hydraulics".* John Wiley and Sons, New York (1950).

60. SCHLICHLING, H. — *"Boundary Layer Theory".* McGraw-Hill (1960).

61. SNYDER, W.T. and GOLDSTEIN, G.A. — *"Analysis of fully developed laminar flow in an eccentric annulus"*. A.I.Ch.E. Vol. 11 No. 3 pp 462-467 (May 1965).

62. SPARROW, E.M. ECKERT, E.R.G. and MINKOWYCZ, W.J. — *"Heat transfer and skin friction for turbulent boundary layer flow longitudinal to a circular Cylinder"*. Trans. A.S.M.E. J. of App. Mech. pp 37-43 (Mar 1963).

63. SQUIRE , H.B. — *"Reconstruction of the theory of free turbulent flow"*. Phil. Mag. Vol. 39 No. 7 pp 1 - 20 (Jan 1948).

64. STEPANOFF, A.J. — *"Pumps and blowers - Two phase flow"*. John Wiley and Sons (1965).

65. WALKER, J.E. WHAN, G.A. and ROTHFUS, R.R. — *"Fluid friction in non-circular ducts"*. A.I.Ch.E.Vol.3 No.4 pp 484-489 (Dec 1957)

66. WOLFFE, R.A. and CLUMP, C.W. — *"The maximum velocity locus for axial turbulent flow in an eccentric annulus"*. A.I.Ch.E. Vol 9 No. 3 pp 424-5 (May 1963).

67. ZANDI, I. and GOVATOS, G. — *"Heterogeneous flow of solids in pipelines"*. A.S.C.E. Vol. 93 Hy3 Proc. Paper 5344 pp 145-159 (May 1967).

68. ZANDI, I. — *"Decreased head losses in raw water conduits"*. J. Am. W.W. Ass. Vol. 58 No. 2 pp 213-224 (1965).